

Programme & Book of Abstracts

24th IAEA Fusion Energy Conference

San Diego, USA

October 8–13, 2012

Version: September 28, 2012

Colophon

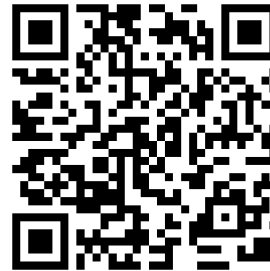
This book has been assembled from the L^AT_EX source files submitted by the contributing authors. Layout, editing, and customized T_EX & L^AT_EX macros used to typeset the book were developed by Dr P. Knowles, University of Fribourg, Switzerland & Dr F. Mulhauser, IAEA, Austria.

QR Codes for Smartphone Conference App

Scan relevant QR to download the conference app



QR code for Android



QR code for iPhone

The **Conference4me** application provides a digital, mobile copy of the conference agenda and timetables, venue information, social network updates, and more. Download **Conference4me** from the Android Play Store or from iTunes, run the application and choose the *24th IAEA Fusion Energy Conference* from the list of conferences available for download. For more information about Conference4me, including QR codes for direct downloads, please see the official Conference4me website: <http://Conference4me.psnc.pl>

Thanks to PSNC for integrating this conference into the Conference4me smartphone conference application.

Conference Secretariat

IAEA Scientific Secretaries:

Mr Ralf Kaiser

Mr Richard Kamendje

Division of Physical and Chemical Sciences

International Atomic Energy Agency

Vienna International Centre, PO Box 100

1400 Vienna, Austria

tel: +43 1 2600 21756

physics@iaea.org

IAEA Administration and Organization:

Ms Karen Morrison

Division of Conference and Document Services

International Atomic Energy Agency

Vienna International Centre, PO Box 100

1400 Vienna, Austria

tel: +43 1 2600 21317

fax: +41 (0)26 300 97 47

K.Morrison@iaea.org

Local Organization

Host Government Official:

Mr Edmund Synakowski

Associate Director

Office of Science for Fusion Energy Sciences

US Department of Energy, USA

ed.synakowski@science.doe.gov

Conference Site Issues:

Ms Michelle Bartolone, CMP

24th IAEA FEC Event Coordinator

Meeting Sites Pro, Inc., USA

michelle@meetingsitespro.com

tel: +1 858 560 4677

Ms Anastasia Nycum

24th IAEA FEC Secretariat

General Atomics

San Diego California, USA

fec2012@fusion.gat.com

tel: +1 858 455 2493

Conference Location

Hilton San Diego Bayfront Hotel

www.hiltonsandiegobayfront.com

1 Park Blvd.

San Diego, USA

Satellite Meetings

Satellite meetings will be held in Indigo rooms 202A, 202B, 204A, 204B, or 206. Deadline to reserve a meeting room is 8 September 2012.

To reserve a meeting room/time, contact:

Punit Gohil

fec2012@fusion.gat.com

Working Language & Resolution

Working Language: English

Resolution: No resolutions may be submitted for consideration on any subject; no votes will be taken

Participation in an IAEA Scientific Meeting

Governments of Member States and those organizations whose activities are relevant to the meeting subject matter are invited to designate participants in the IAEA scientific conferences and symposia. In addition, the IAEA itself may invite a limited number of scientists as invited speakers. Only participants designated or invited in this way are entitled to present papers and take part in the discussions.

Representatives of the press, radio, television or other information media and members of the public, the latter as “observers”, may also be authorized to attend, but without the right to take part in the proceedings.

Scientists interested in participating in any of the IAEA meetings should request information from the Government authorities of their own countries, in most cases the Ministry of Foreign Affairs or national atomic energy authority.

IAEA Publications

All IAEA publications may be ordered from the
Sales and Promotion Unit,
International Atomic Energy Agency,
P.O. Box 100, A-1400 Vienna, Austria
Fax: (+43 1) 2600-29302
sales.publications@iaea.org
www.iaea.org/Publications/index.html

Name	Country/International Organization
Chair: Paul Thomas	ITER
Boyd Blackwell	Australia
Xuru Duan	China
Lorne Horton	European Commission
Gabriella Saibene	European Commission
André Grosman	France
Ulrich Stroth	Germany
Arun K. Chakraborty	India
Katsumi Ida	Japan
Yutaka Kamada	Japan
Atsushi Fukuyama	Japan
Keishi Sakamoto	Japan
Hiroyuki Shiraga	Japan
Yeong-Kook Oh	Korea, Republic of
Julio Emilio Herrera-Velázquez	Mexico
Sergei Lebedev	Russian Federation
Boris V. Kuteev	Russian Federation
Francisco Castejón	Spain
Martin O'Brien	United Kingdom
Boris Breizman	United States of America
James W. Van Dam	United States of America
Charles Greenfield	United States of America
Rajesh Maingi	United States of America
Mordecai Rosen	United States of America

This book contains all abstracts accepted by the FEC programme committee. Note that abstracts have been edited for style uniformity.

Overview of Contributions

1	Keynote presentation
23	Overview talks
78	Regular talks
10	Rapporteured papers
7	Overview poster presentations
608	Regular poster presentations
2	Post deadline talks
3	Post deadline poster presentations
5	Summary talks

Overview posters will be exhibited during the entire conference. All oral presentations will also be displayed as posters according to the programme.

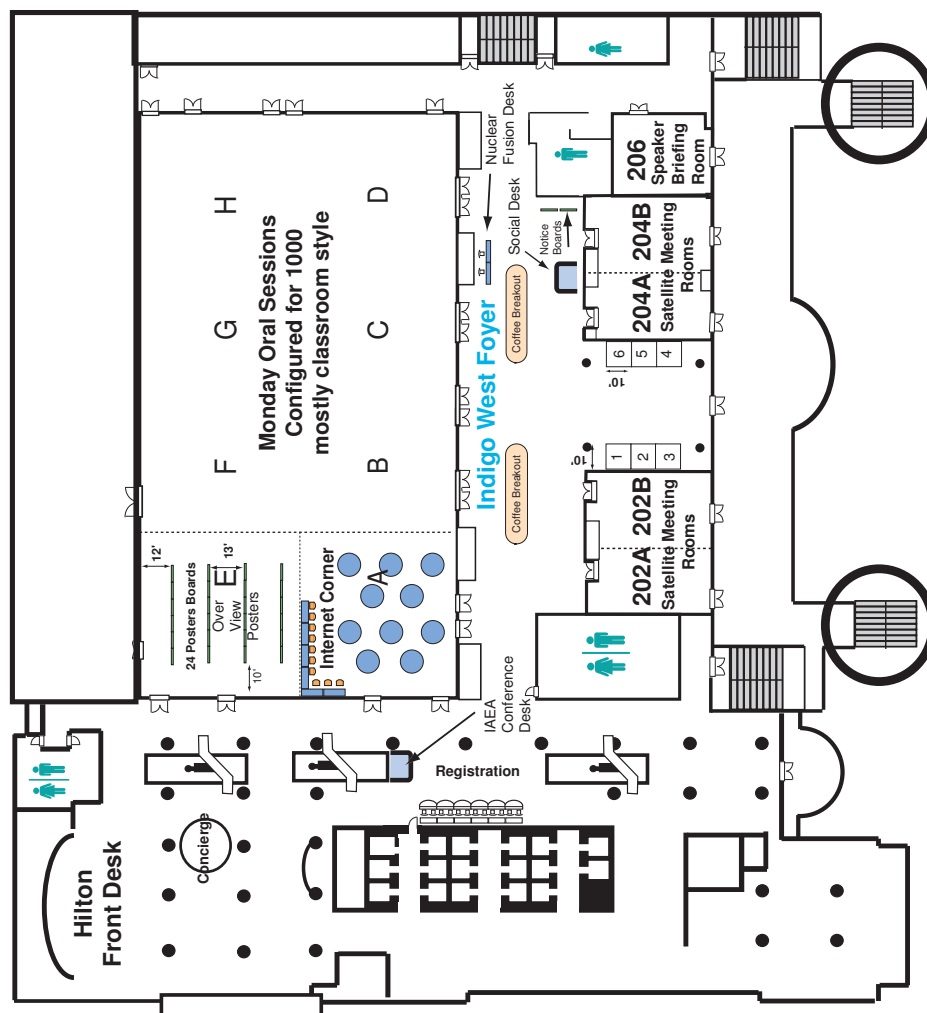
The duration of oral presentations indicated in the programme already includes discussion time. Speakers are requested to make available the following times for discussions:

- 4' for overview presentation (total 25')
- 3' for regular oral presentation (total 20')

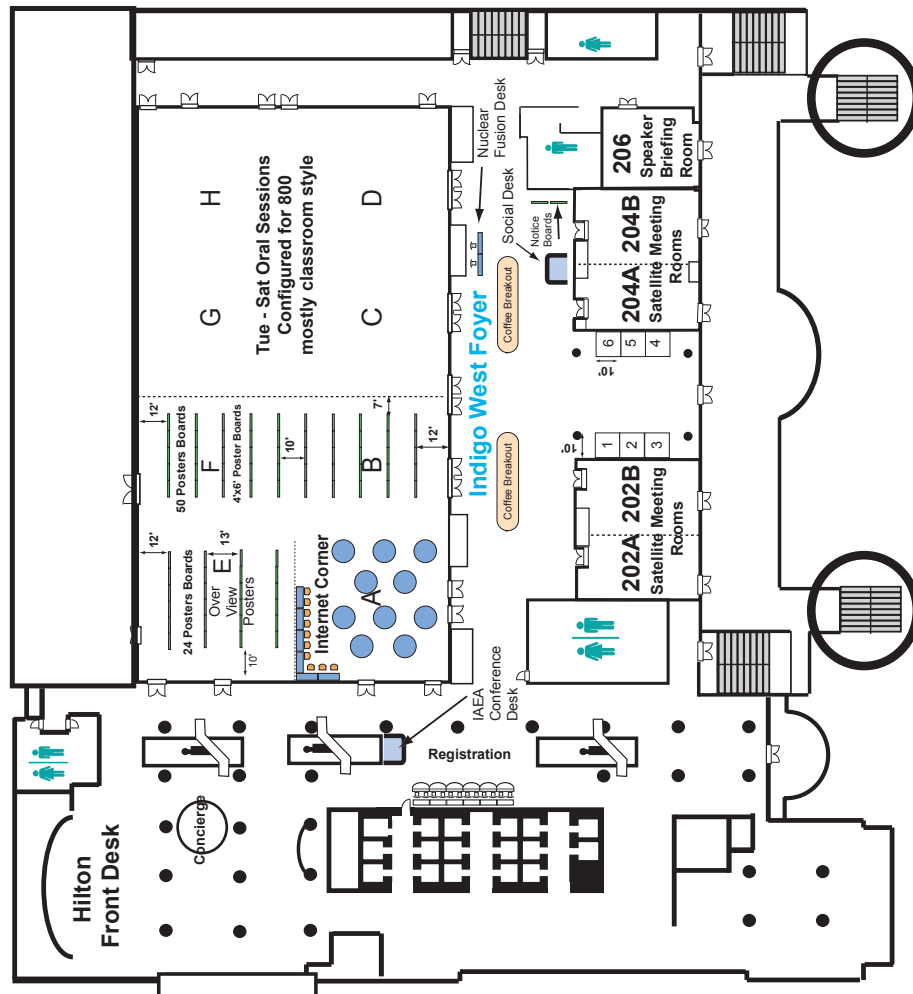
Rapporteur papers are identified by the letter “a” after the paper number. Rapporteured papers are identified by the letters “b” or “c” after the paper number.

Explanation of Abbreviations

OV	Overviews
EX	Magnetic Confinement Experiments
TH	Magnetic Confinement Theory and Modelling
	For both EX and TH , subdivisions are:
	<i>C: Confinement</i>
	<i>S: Stability</i>
	<i>W: Wave-plasma interactions, current drive, heating, and energetic particles</i>
	<i>D: Plasma-material interactions, divertors, limiters, and scrape-off layer</i>
ITR	ITER Activities
IFE	Inertial Fusion Experiments and Theory
ICC	Innovative Confinement Concepts
FTP	Fusion Technology and Power Plant Design
SEE	Safety, Environmental and Economic Aspects of Fusion
PD	Post-Deadline abstracts



Floor plan: Sunday and Monday



Floor plan: Tuesday to Saturday

Day Date	Monday Oct. 8, 2012	Tuesday Oct. 9, 2012	Wednesday Oct. 10, 2012	Thursday Oct. 11, 2012	Friday Oct. 12, 2012	Saturday Oct. 13, 2012
08:30 – 10:15	Opening & Keynote Presentation p. xii	OV/3 Overview: Magnetic Fusion p. xvi	OV/5 Overview: Inertial & Magnetic Fusion p. xxviii	IFE/1 Inertial Fusion Experiments and Theory p. xl	EX/8-TH/7 3D Equilibrium & High Beta Physics p. lv	EX/10-TH/8 Turbulence, Zonal Flows & GAMs p. lxviii
			Coffee Break			
10:45 – 12:30	OV/1 Overview: Inertial & Magnetic Fusion p. xii	EX/1 Plasma Scenarios p. xvi	EX/3-TH/2 Pedestal Stability & Control I p. xxviii	EX/5-TH/4 Waves & Energetic Particles p. xl	EX/9-PD Disruptions & Post- Deadline Papers p. lv	EX/11-ICC/1 Turbulence, Innovative Confinement Concepts and ELMs p. lxix
			Lunch			
14:00 – 16:10	OV/2 Overview: Magnetic Fusion p. xiii	OV/4 Overview: Inertial & Magnetic Fusion p. xxii	EX/4-TH/3 Plasma-Wall Interactions p. xxxiv	EX/6-TH/5 Pedestal Stability & Control II p. xlvi	FTP/3-SEE/1 Fusion Development p. lxiii	Summary p. lxx
			Coffee Break			
16:40 – 18:45	ITR/1-FTP/1 ITER Physics, Scenarios and Heating & Current Drive Technology p. xiii	EX/2-TH/1 Transport p. xxiii	ITR/2-FTP/2 Diagnostics, Main Systems Design & Construction p. xxxiv	EX/7-TH/6 Transport and Turbulence p. xlvi	FTP/4 Fusion Materials and Neutron Sources p. lxiv	Summary p. lxx
19:30 – 22:00	Reception	ITER Event		Banquet		

Programme

IFRC Meeting — Upon Invitation Only — *Room 204 (A+B)*

(09:30 – 15:00)

Conference Registration — *Hilton San Diego Bayfront Hotel Entrance, Indigo Level*

(16:00 – 19:00)

Conference Registration — *Hilton San Diego Bayfront Hotel Entrance, Indigo Level*
(07:30 – 18:30)

Opening:

Chair: T. Taylor (USA)

Indigo Ball Room (08:30 – 10:15)

Time	Id	Presenter		Title
08:30	O/1	IAEA Repre-	IAEA	Opening Address
		sentative		
08:40	O/2	Host	USA	Welcome Address
		Government		
		Representa-		
		tive		
09:20	O/3	IAEA Repre-	IAEA	Nuclear Fusion Prize Award
		sentative		
09:30	O/4	Chen, Francis	USA	Fusion Energy: For Now, and Forever

Coffee Break (10:15 – 10:45)

OV/1: Inertial & Magnetic Fusion I

Chair: A. Krasilnikov (Russian Fed.)

Indigo Ball Room (10:45 – 12:30)

Time	Id	Presenter		Title
10:45	OV/1-1	Hill, David	USA	DIII-D Overview — Research toward Resolving Key Issues for ITER and Steady-State Tokamaks
11:10	OV/1-2	Motojima, Osamu	ITER	The Status of the ITER Project
11:35	OV/1-3	Romanelli, Francesco	EU	Overview of the JET Results with the ITER-like Wall
12:00	OV/1-4	Moses, Edward	USA	The National Ignition Campaign: Status and Progress

Lunch Break (12:30 – 14:00)

OV/2: Magnetic Fusion I

Chair: Y. Liu (China)

Indigo Ball Room (14:00 – 16:10)

Time	Id	Presenter		Title
14:00	OV/2-1	Kaneko, Osamu	Japan	Extension of Operation Regimes and Investigation of Three-dimensional Current-less Plasmas in the Large Helical Device
14:25	OV/2-2	Stroth, Ulrich	Germany	Overview of ASDEX Upgrade Results
14:50	OV/2-3	Greenwald, Martin	USA	Overview of Experimental Results and Code Validation Activities at Alcator C-Mod
15:15	OV/2-4	Kwak, Jong-Gu	Korea, Rep.	Overview of KSTAR Results
15:40	OV/2-5	Wan, Baonian	China	Progress of Long Pulse and H-mode Experiments on EAST

Coffee Break (16:10 – 16:40)**ITR/1 and FTP/1: ITER Physics, Scenarios and Heating & Current Drive Technology**

Chair: M. Mori (Japan)

Indigo Ball Room (16:40 – 18:45)

Time	Id	Presenter		Title
16:40	ITR/1-1	Eich, Thomas	Germany	Scaling of the Tokamak near Scrape-off Layer H-mode Power Width and Implications for ITER
17:00	ITR/1-2	Loarte, Alberto	ITER	Progress on the Application of ELM Control Schemes to ITER
17:20	FTP/1-1	Wukitch, Stephen	USA	Evaluation of Optimized ICRF and LHRF Antennas in Alcator C-Mod
17:40	ITR/1-3	Sonato, Piergiorgio	Italy	Design of the MITICA Neutral Beam Injector: From Physics Analysis to Engineering Design
18:00	FTP/1-2	Inoue, Takashi	Japan	Acceleration of 1 MeV H ⁻ Ion Beams at ITER NB-relevant High Current Density
18:20	ITR/1-4Ra	Litvak, Alexander	Russian Fed.	Development in Russia of Megawatt Power Gyrotrons for Fusion
	FTP/1-3Rb			Progress on the Development of High Power Long Pulse Gyrotron and Related Technologies

These posters will be displayed throughout the conference

Overview Posters OVP

Poster Room: Area E (14:00 – 18:45)

Id	Presenter		Title
OV/1-1	Hill, David	USA	DIID-D Overview — Research toward Resolving Key Issues for ITER and Steady-State Tokamaks
OV/1-2	Motojima, Osamu	ITER	The Status of the ITER Project
OV/1-3	Romanelli, Francesco	EU	Overview of the JET Results with the ITER-like Wall
OV/1-4	Moses, Edward	USA	The National Ignition Campaign: Status and Progress
OV/2-1	Kaneko, Osamu	Japan	Extension of Operation Regimes and Investigation of Three-dimensional Current-less Plasmas in the Large Helical Device
OV/2-2	Stroth, Ulrich	Germany	Overview of ASDEX Upgrade Results
OV/2-3	Greenwald, Martin	USA	Overview of Experimental Results and Code Validation Activities at Alcator C-Mod
OV/2-4	Kwak, Jong-Gu	Korea, Rep.	Overview of KSTAR Results
OV/2-5	Wan, Baonian	China	Progress of Long Pulse and H-mode Experiments on EAST
OV/3-1	Sabbagh, Steven	USA	Overview of Physics Results from the National Spherical Torus Experiment
OV/3-2	Meyer, Hendrik	UK	Overview of Physics Results from MAST towards ITER/DEMO and the Upgrade
OV/3-3	Duan, Xuru	China	Overview of HL-2A Recent Experiments
OV/3-4	Ida, Katsumi	Japan	Towards an Emerging Understanding of Non-local Transport
OV/4-1	Kamada, Yutaka	Japan	Progress of the JT-60SA Project
OV/4-2	Azechi, Hiroshi	Japan	Present Status of Fast Ignition Realization Experiment (FIREX) and Inertial Fusion Energy Development
OV/4-3	Sharapov, Sergei	UK	Energetic Particle Instabilities in Fusion Plasmas
OV/4-4	Coda, Stefano	Switzerland	Overview of Recent and Current Research on the TCV Tokamak

Id	Presenter	Title
OV/4-5	Becoulet, France Alain	Science and Technology Research & Development in Support to ITER and the Broader Approach
OV/5-1	Sanchez, Spain Joaquin	Dynamics of Flows and Confinement in the TJ-II Stellarator
OV/5-2Ra	Sarff, John USA	Overview of Results from the MST Reversed Field Pinch Experiment
OV/5-2Rb	Martin, Italy Piero	Overview of the RFX Fusion Science Program
OV/5-3	Betti, USA Riccardo	Theory of Ignition, Burn and Hydro-equivalency for Inertial Confinement Fusion Implosions
OV/5-4	Zinkle, USA Steven	Multimodal Options for Materials Research to Advance the Basis for Fusion Energy in the ITER Era
OV/P-01	Buratti, Italy Paolo	Overview of FTU Results
OV/P-02	Coppi, Italy Bruno	New Developments, Plasma Physics Regimes and Issues for the Ignitor Experiment
OV/P-03	Diamond, Korea, Rep. Patrick	On the Physics of Intrinsic Torque in Toroidal Plasmas
OV/P-05	Nakajima, Japan Noriyoshi	Overview of IFERC Project in Broader Approach Activities
OV/P-06	Zhuang, Ge China	The Recent Research Work on the J-TEXT Tokamak
OV/P-07	Kruglyakov, Russian Edward Fed.	Fusion Prospects of Axisymmetric Magnetic Mirror Systems
OV/P-08	Fernandes, Portugal Horácio João	20 Years of ISTTOK Tokamak Scientific Activity

OV/3: Magnetic Fusion II

Chair: P.K. Kaw (India)

Indigo Ball Room (08:30 – 10:15)

TUE	Time	Id	Presenter		Title
	08:30	OV/3-1	Sabbagh, Steven	USA	Overview of Physics Results from the National Spherical Torus Experiment
	08:55	OV/3-2	Meyer, Hendrik	UK	Overview of Physics Results from MAST towards ITER/DEMO and the Upgrade
	09:20	OV/3-3	Duan, Xuru	China	Overview of HL-2A Recent Experiments
	09:45	OV/3-4	Ida, Katsumi	Japan	Towards an Emerging Understanding of Nonlocal Transport

Coffee Break (10:15 – 10:45)**EX/1: Plasma Scenarios**

Chair: N. Ivanov (Russian Fed.)

Indigo Ball Room (10:45 – 12:30)

Time	Id	Presenter		Title
10:45	EX/1-1	Joffrin, Emmanuel	France	Scenarios Development at JET with the New ITER-like Wall
11:05	EX/1-2	Duval, Basil	Switzerland	Real time ELM, NTM and Sawtooth Control on TCV
11:25	EX/1-3	Hubbard, Amanda	USA	Progress in Performance and Understanding of Steady ELM-free I-modes on Alcator C-Mod
11:45	EX/1-4	Stober, Joerg	Germany	Dominant ECR Heating of H-mode Plasmas on ASDEX Upgrade Using the Upgraded ECRH System and Comparison to Dominant NBI or ICR Heating
12:05	EX/1-5	Holcomb, Christopher	USA	Fully Noninductive Scenario Development in DIII-D Using New Off-Axis Neutral Beam Injection

Poster Session: P1

Poster Room: Area F-B (08:30 – 12:30)

Id	Presenter		Title
ITR/1-1	Eich, Thomas	Germany	Scaling of the Tokamak near Scrape-off Layer H-mode Power Width and Implications for ITER
ITR/1-2	Loarte, Alberto	ITER	Progress on the Application of ELM Control Schemes to ITER
FTP/1-1	Wukitch, Stephen	USA	Evaluation of Optimized ICRF and LHRF Antennas in Alcator C-Mod
ITR/1-3	Sonato, Piergiorgio	Italy	Design of the MITICA Neutral Beam Injector: From Physics Analysis to Engineering Design
FTP/1-2	Inoue, Takashi	Japan	Acceleration of 1 MeV H^- Ion Beams at ITER NB-relevant High Current Density
ITR/1-4Ra	Litvak, Alexander	Russian Fed.	Development in Russia of Megawatt Power Gyrotrons for Fusion
FTP/1-3Rb	Kajiwarra, Ken	Japan	Progress on the Development of High Power Long Pulse Gyrotron and Related Technologies
ITR/P1-01	Franzen, Peter	Germany	Commissioning and First Results of the ITER-Relevant Negative Ion Beam Test Facility ELISE
ITR/P1-02	Sato, Satoshi	Japan	Nuclear Analyses for ITER NB System
ITR/P1-03	Schunke, Beatrix	ITER	Status of the Negative Ion Based Diagnostic Neutral Beam for ITER
ITR/P1-04	Masiello, Antonio	EU	EU Development of the ITER Neutral Beam Injector and Test Facility
ITR/P1-05	Takahashi, Koji	Japan	Development of ITER Equatorial EC Launcher
ITR/P1-06	Henderson, Mark	ITER	Optimization of the EC Heating and Current Drive Capabilities
ITR/P1-07	Dumortier, Pierre	Belgium	Validation of the RF Properties and Control of the ITER ICRF Antenna
ITR/P1-08	Durodié, Frédéric	Belgium	RF Optimization of the Port Plug Layout and Performance Assessment of the ITER ICRF Antenna
ITR/P1-09	Tuccillo, Angelo	Italy	On the Use of Lower Hybrid Waves at ITER Relevant Density

TUE

Id	Presenter		Title
TUE ITR/P1-10	Parail, Vassili	UK	Self-consistent Simulation of Plasma Scenarios for ITER Using a Combination of 1.5D Transport Codes and Free Boundary Equilibrium Codes
ITR/P1-11	Sips, Adrianus	EU	Demonstrating the ITER Baseline Operation at $q_{95} = 3$
ITR/P1-12	Bandyopadhy- ay, Indranil	India	Modelling of ITER Plasma Shutdown with Runaway Mitigation Using TSC
ITR/P1-13	Kim, Sun Hee	ITER	CORSICA Modelling of ITER Hybrid Mode Operation Scenarios
ITR/P1-14	Sugihara, Masayoshi	ITER	Disruption Impacts and their Mitigation Target Values
ITR/P1-15	Casper, Thomas	ITER	Development of ITER Scenarios for Pre-DT Operations
ITR/P1-16	Cavinato, Mario	EU	ITER Plasma Position Control System and Scenario Optimization
ITR/P1-17	Na, Yong-Su	Korea, Rep.	Integrated Modelling of ITER Hybrid Scenarios Including Momentum Transport, NTMs, and ELMs in Preparation for Active Control
ITR/P1-18	Campbell, David	ITER	Challenges in Burning Plasma Physics: the ITER Research Plan
ITR/P1-19	Tala, Tuomas	Finland	Tokamak Experiments to Study the Parametric Dependences of Momentum Transport
ITR/P1-20	Moreau, Didier	France	Integrated Magnetic and Kinetic Control of Advanced Tokamak Scenarios Based on Data-Driven Models
ITR/P1-21	Poli, Francesca	USA	Stability and Performance of ITER Steady State Scenarios with ITBs
ITR/P1-22	Huijsmans, Guido	ITER	Non-linear MHD Modelling of ELM Triggering by Pellet Injection in DIII-D and Implications for ITER
ITR/P1-23	Huijsmans, Guido	ITER	Non-linear MHD Simulation of ELM Energy Deposition
ITR/P1-24	Schmitz, Oliver	Germany	Three-dimensional Fluid Modeling of Plasma Edge Transport and Divertor Fluxes during RMP ELM Control at ITER
ITR/P1-25	Evans, Todd	USA	3D Vacuum Magnetic Field Modeling of the ITER ELM Control Coils during Standard Operating Scenarios

Id	Presenter	Title
ITR/P1-26	Bazylev, Boris Germany	Analysis of Tungsten Dust Generation under Powerful Plasma Impacts Simulating ITER ELMs and Disruptions
ITR/P1-27	Pacher, Horst ITER	Narrow Heat Flux Widths and Tungsten: SOLPS Studies of the Possible Impact on ITER Divertor Operation
ITR/P1-28	Kallenbach, Arne Germany	Multi-machine Comparisons of Divertor Heat Flux Mitigation by Radiative Cooling
ITR/P1-29	Budny, Robert USA	PTRANSP Tests of TGLF and Predictions for ITER
ITR/P1-30	Petty, Craig USA	ITER Implications of the Beta Scaling of Energy Confinement
ITR/P1-31	Chapman, Ian UK	Assessing the Power Requirements for Sawtooth Control in ITER through Modelling and Joint Experiments
ITR/P1-32	Kramer, Gerrit USA	Observation of Localized Fast-Ion Induced Heat Loads in Test Blanket Module Simulation Experiments on DIII-D
ITR/P1-33	Kurki-Suonio, Taina Finland	Fast Ion Power Loads on ITER First Wall Structures in the Presence of ELM-mitigation Coils and MHD Modes
ITR/P1-34	Könies, Axel Germany	Benchmark of Gyrokinetic, Kinetic MHD and Gyrofluid Codes for the Linear Calculation of Fast Particle Driven TAE Dynamics
ITR/P1-35	Oikawa, Toshihiro ITER	Effects of ELM Control Coil on Fast Ion Confinement in ITER H-mode Scenarios
ITR/P1-36	Gohil, Punit USA	Assessment of the H-mode Power Threshold Requirements for ITER
ITR/P1-37	Singh, Raghvendra India	A Model for the Power Required to Access the H-mode in Tokamaks and Projections for ITER
ITR/P1-38	Konovalov, Sergey Russian Fed.	Studying the Capabilities of Be Pellet Injection to Mitigate ITER Disruptions
ITR/P1-39	Bazylev, Boris Germany	Modelling of Material Damage and High Energy Impacts on Tokamak PFCs during Transient Loads
ITR/P1-40	Sen, Amiya USA	Control of Major Disruptions in ITER
FTP/P1-01	Tazhibayeva, Irina Kazakhstan	Investigation and Testing of KTM Divertor Model on Basis of Lithium CPS

TUE	Id	Presenter		Title
	FTP/P1-02	Lore, Jeremy	USA	Heat Flux and Design Calculations for the W7-X Divertor Scraper Element
	FTP/P1-03	Hong, Suk-Ho	Korea, Rep.	Temporal and Spatial Evolution of In-vessel Dust Characteristics in KSTAR and Dust Removal Experiments in TReD
	FTP/P1-04	Khirwadkar, Samir	India	Tungsten Divertor Target Technology and Test Facilities Development
	FTP/P1-05	Kreter, Arkadi	Germany	Comparative Study of Chemical Methods for Fuel Removal
	FTP/P1-06	Duan, Xuru	China	Analysis of Establishment and MHD Stability of a Free Curve-Surface Flow for Liquid Metal PFCs
	FTP/P1-07	Crisanti, Flavio	Italy	"Snow Flake" Divertor and 10 MA Scenarios in FAST
	FTP/P1-08	Chaudhari, Vilas	India	Preliminary Safety Analysis of the Indian Lead Lithium Cooled Ceramic Breeder Test Blanket Module System in ITER
	FTP/P1-09	Day, Christian	Germany	Technology Gaps for the Fuel Cycle of a Fusion Power Plant
	FTP/P1-10	Kikuchi, Yusuke	Japan	Simulation Experiments of ELM-like Transient Heat and Particle Loads Using a Magnetized Coaxial Plasma Gun
	FTP/P1-11	Nakashima, Yousuke	Japan	Plasma Characteristics of the End-cell of the GAMMA 10 Tandem Mirror for the Divertor Simulation Experiment
	FTP/P1-12	Liu, Xiang	China	Progress of High Heat Flux Component Manufacture and Heat Load Experiments in China
	FTP/P1-13	Feng, Kaiming	China	Super-X Divertor Simulation for HCSB-DEMO
	ICC/P1-01	Minaev, Vladimir	Russian Fed.	Magnetic System for the Upgraded Spherical Tokamak Globus-M2
	FTP/P1-14	Ono, Masayuki	Japan	Recent Progress in the NSTX/NSTX-U Lithium Program and Prospects for Reactor-relevant Liquid-lithium Based Divertor Development
	FTP/P1-15	Uchimura, Hiromichi	Japan	Effects of the lithium concentration on tritium release behaviors from advanced tritium breeding material $\text{Li}_{2+x}\text{TiO}_3$

Id	Presenter	Title
FTP/P1-16	Isayama, Akihiko Japan	Progress in the Development of the ECRF System for JT-60SA
FTP/P1-17	Fantz, Ursel Germany	Feasibility and R Needs of a Negative Ion Based Neutral Beam System for DEMO
FTP/P1-18	Hanada, Masaya Japan	Progress in the Development of Long Pulse Neutral Beam Injectors for JT-60SA
FTP/P1-19	Fonck, Raymond USA	Local Current Injector System for Non-solenoidal Startup in a Low Aspect Ratio Tokamak
FTP/P1-20	Minami, Ryutaro Japan	Development of MW Gyrotrons for Fusion Devices by University of Tsukuba
FTP/P1-21	Yang, Hyung Yeol Korea, Rep.	Status and Plan of the Key Actuators for KSTAR Operation
FTP/P1-22	Wallace, Gregory USA	Advances in Lower Hybrid Current Drive Technology on Alcator C-Mod
FTP/P1-23	Wolf, Robert Germany	Preparation of Steady State Operation of the Wendelstein 7-X Stellarator
FTP/P1-24	Minea, Tiberiu France	3D Particle Simulation of Neutral Beam Injector, from Extraction to Tokamak Injection
FTP/P1-25	Jeong, Jin Hyun Korea, Rep.	ECH-assisted Startup Using ITER Prototype of 170 GHz Gyrotron in KSTAR
FTP/P1-26	Surrey, Elizabeth UK	The Influence on System Design of the Application of Neutral Beam Injection to a Demonstration Fusion Power Plant
FTP/P1-27	Wendel, Mark USA	Fusion Material Irradiation Test Facility at SNS
FTP/P1-28	Sergis, Antonis UK	Potential for Improvement in High Heat Flux HyperVapotron Element Performance Using Nanofluids
FTP/P1-29	Bayetti, Pascal France	Overview on CEA Contributions to the Broader Approach Projects
FTP/P1-30	Wong, Clement USA	Fusion Technology Facility — Key Attributes and Interfaces to Technology and Materials
FTP/P1-31	Bogatu, Ioan-Niculae USA	Plasma Jets for Runaway Electron Beam Suppression
FTP/P1-32	Salvador, Max Mexico	Advances in the Electrical, Control Systems, General Analysis of the Coils Design in the Mexican Tokamak Experimental Facility
FTP/P1-33	Rapp, Juergen USA	An Advanced Plasma-material Test Station for R on Materials in a Fusion Environment

TUE	Id	Presenter		Title
	FTP/P1-34	Cara, Philippe	EU	Overview and Status of the Linear IFMIF Prototype Accelerator
	FTP/P1-35	Heidinger, Roland	EU	IFMIF: Overview of the Validation Activities

Lunch Break (12:30 – 14:00)

OV/4: Inertial & Magnetic Fusion II

Chair: R. Fonck (USA)

Indigo Ball Room (14:00 – 16:10)

Time	Id	Presenter		Title
14:00	OV/4-1	Kamada, Yutaka	Japan	Progress of the JT-60SA Project
14:25	OV/4-2	Azechi, Hiroshi	Japan	Present Status of Fast Ignition Realization EXperiment and Inertial Fusion Energy Development
14:50	OV/4-3	Sharapov, Sergei	UK	Energetic Particle Instabilities in Fusion Plasmas
15:15	OV/4-4	Coda, Stefano	Switzerland	Overview of Recent and Current Research on the TCV Tokamak
15:40	OV/4-5	Becoulet, Alain	France	Science and Technology Research & Development in Support to ITER and the Broader Approach

Coffee Break (16:10 – 16:40)

EX/2 and TH/1: Transport

Chair: M. Kwon (Korea, Rep.)

Indigo Ball Room (16:40 – 18:45)

Time	Id	Presenter		Title
16:40	EX/2-1	McDermott, Rachael	Germany	Connections Between Intrinsic Toroidal Rotation, Density Peaking and Plasma Turbulence Regimes in ASDEX Upgrade
17:00	EX/2-2	Rice, John	USA	A Unified Explanation of Rotation Reversals, Confinement Saturation and Non-Diffusive Heat Transport in C-Mod Ohmic Plasmas
17:20	TH/1-1	Murakami, Sadayoshi	Japan	Study of Toroidal Flow Generation by the ICRF Minority Heating in the Alcator C-Mod Plasma
17:40	EX/2-3	Shi, Yuejiang	Korea, Rep.	ECRH Effects on Toroidal Rotation: KSTAR Experiments and Gyrokinetic Simulations of Intrinsic Torque at ITG-TEM Transitions
18:00	EX/2-4	Urano, Hajime	Japan	Dependence of Heat Transport and Confinement on Isotopic Composition in Conventional H-mode Plasmas in JT-60U
18:20	EX/2-5	Takahashi, Hiromi	Japan	Extension of Operational Regime in High-Temperature Plasmas and the Dynamic-Transport Characteristics in the LHD

TUE

Poster Session: P2*Poster Room: Area F-B (14:00 – 18:45)*

TUE	Id	Presenter		Title
	EX/1-1	Joffrin, Emmanuel	France	Scenarios Development at JET with the New ITER-like Wall
	EX/1-2	Duval, Basil	Switzerland	Real time ELM, NTM and Sawtooth Control on TCV
	EX/1-3	Hubbard, Amanda	USA	Progress in Performance and Understanding of Steady ELM-free I-modes on Alcator C-Mod
	EX/1-4	Stober, Joerg	Germany	Dominant ECR Heating of H-mode Plasmas on ASDEX Upgrade Using the Upgraded ECRH System and Comparison to Dominant NBI or ICR Heating
	EX/1-5	Holcomb, Christopher	USA	Fully Noninductive Scenario Development in DIII-D Using New Off-Axis Neutral Beam Injection
	EX/P2-01	Solomon, Wayne	USA	Access and Sustained High Performance in Advanced Inductive Discharges with ITER-Relevant Low Torque
	EX/P2-02	Kessel, Charles	USA	ITER Demonstration Discharges on Alcator C-Mod in Support of ITER
	EX/P2-03	Schweitzer, Josef	Germany	Overview of ASDEX Upgrade “Improved H-mode” Scenario Developments
	EX/P2-04	Ma, Yunxing	USA	Study of H-mode Access in the Alcator C-Mod Tokamak: Density, Toroidal Field and Divertor Geometry Dependence
	EX/P2-05	Dong, Jiaqi	China	Toroidal Rotation in L-I-H Confinement Transition in HL-2A Experiments
	EX/P2-06	Gong, Xianzu	China	Integrated Operation Scenarios for Long Pulse Discharges in EAST
	EX/P2-07	Park, Young-Seok	USA	Investigation of Plasma Rotation Alteration and MHD Stability in the Expanded H-mode Operation of KSTAR
	EX/P2-08	Jackson, Gary	USA	Long-pulse Stability Limits of ITER Baseline Scenario Plasmas in DIII-D
	EX/P2-09	Barton, Justin	USA	First-Principles Model-based Closed-loop Control of the Current Profile Dynamic Evolution on DIII-D
	EX/P2-10	Raman, Roger	USA	Non-inductive Plasma Start-up in NSTX Using Transient CHI

Id	Presenter	Title	TUE
EX/P2-11	Takase, Yuichi Japan	Non-inductive Plasma Initiation and Plasma Current Ramp-up on the TST-2 Spherical Tokamak	
EX/P2-12	Mutoh, Takashi Japan	Steady State Operation Using Improved ICH and ECH for High Performance Plasma in LHD	
EX/P2-13	Park, Jin Myung USA	Validation of Off-axis Neutral Beam Current Drive Physics in the DIII-D Tokamak	
EX/P2-14	Zushi, Hideki Japan	Non-inductive Current Start-up and Plasma Equilibrium with an Inboard Poloidal Field Null by Means of Electron Cyclotron Waves in QUEST	
EX/P2-15	Song, Xianming China	ECRH Pre-ionization and Assisted Startup in HL-2A Tokamaks	
EX/P2-16	Shiraiwa, Syun'ichi USA	Progress toward Steady-state Regimes in Alcator C-Mod	
EX/P2-17	Kulkarni, Sanjay India	Resonant and Non-resonant Type Pre-ionization and Current Ramp-up Experiments on Tokamak ADITYA in the Ion Cyclotron Frequency Range	
TH/P2-01	Kalupin, Denis EU	The European Transport Solver: an Integrated Approach for Transport Simulations in the Plasma Core	
TH/P2-02	Shumlak, Uri USA	Progress in the Plasma Science and Innovation Center	
TH/P2-03	Giruzzi, Gerardo France	Model Validation and Integrated Modelling Simulations for the JT-60SA Tokamak	
TH/P2-04	Mynick, Harry USA	Turbulent Optimization in Stellarators & Tokamaks via Shaping	
TH/P2-05	Litaudon, Xavier France	Modelling of Hybrid Scenario: from Present-day Experiments toward ITER	
TH/P2-06	Spineanu, Florin Romania	The Role of Convective Structures in the Poloidal and Toroidal Rotation in Tokamak	
TH/P2-08	Kritz, Arnold USA	Fusion Power Production in Baseline ITER H-mode Discharges	
TH/P2-09	Wang, Lu Korea, Rep.	New Results in the Theory of Non-Diffusive Heat Transport and Anomalous Electron-Ion Energy Coupling	
TH/P2-10	Carmody, Daniel USA	Microtearing Mode Fluctuations in Reversed Field Pinch Plasmas	

	Id	Presenter		Title
TUE	TH/P2-11	Leonov, Vladimir	Russian Fed.	Tokamak Discharges with Electron Thermal Conductivity Closed to the Neoclassical One
	TH/P2-12	Gurcan, Ozgur	France	Indications of Nonlocality of Plasma Turbulence
	TH/P2-13	Rafiq, Tariq	USA	Physics Basis and Validation of MMM7.1 Anomalous Transport Module
	TH/P2-14	Honda, Mitsuru	Japan	Predictive Transport Simulations Consistent with Rotation and Radial Electric Field Using TOPICS with OFMC
	TH/P2-15	Schoepf, Klaus	Austria	Impact of Fusion Alpha Driven Current on the Magnetic Configuration of a Tokamak
	TH/P2-16	Cappello, Susanna	Italy	Nonlinear Modeling for Helical Configurations in Toroidal Pinch Systems
	TH/P2-17	Weisen, Henri	EU	Non-diffusive Momentum Transport in JET H-mode Regimes: Modeling and Experiment
	TH/P2-18	Escande, Dominique	France	New Technique for the Calculation of Transport Profiles in Modulation Experiments
	TH/P2-19	Budny, Robert	USA	Evolution of Ion Heat Diffusivity and Toroidal Momentum Diffusivity during Spontaneous ITB Development in HL-2A
	TH/P2-21	Angioni, Clemente	Germany	Progress in the Theoretical Description and the Experimental Characterization of Impurity Transport at ASDEX Upgrade
	TH/P2-22	Toda, Shinichiro	Japan	Transport Analysis of Oscillatory State for Plasma Dynamics in Helical Plasmas
	TH/P2-23	Ishizawa, Akihiro	Japan	Turbulent Transport due to Kinetic Ballooning Modes in High- β Toroidal Plasmas
	TH/P2-24	Satake, Shinsuke	Japan	Drift-kinetic Simulation Studies on Neoclassical Toroidal Viscosity in Tokamaks with Small Magnetic Perturbations
	TH/P2-25	Falchetto, Gloria	France	The European Integrated Tokamak Modelling Effort: Achievements and First Physics Results
	TH/P2-26	Coppi, Bruno	USA	Advanced Confinement Regimes and their Signatures
	TH/P2-27	Kim, Kimin	USA	Study of Neoclassical Toroidal Viscosity in Tokamaks with a δf Particle Code and Resonant Nature of Magnetic Braking
	TH/P2-28	Herrera-Velázquez, Julio	Mexico	Use of the 3D-MAPTOR Code in the Study of Magnetic Surfaces Break-up due to External Non-Axisymmetric Coils

Id	Presenter	Title
TH/P2-29	Del-Castillo- Negrete, Diego	Anisotropic Heat Transport in Integrable and Chaotic 3D Magnetic Fields
TH/P2-30	Salewski, Mirko	Tomography of 2D Velocity-space Distributions from Combined Synthetic Fast-ion Diagnostics at ASDEX Upgrade

TUE

OV/5: Inertial & Magnetic Fusion III

Chair: S. Guenter (Germany)

Indigo Ball Room (08:30 – 10:15)

Time	Id	Presenter		Title
08:30	OV/5-1	Sanchez, Joaquin	Spain	Dynamics of Flows and Confinement in the TJ-II Stellarator
08:55	OV/5-2Ra	Sarff, John	USA	Overview of Results from the MST Reversed Field Pinch Experiment
	OV/5-2Rb			Overview of the RFX Fusion Science Program
09:20	OV/5-3	Betti, Riccardo	USA	Theory of Ignition, Burn and Hydro-equivalency for Inertial Confinement Fusion Implosions
09:45	OV/5-4	Zinkle, Steven	USA	Multimodal Options for Materials Research to Advance the Basis for Fusion Energy in the ITER Era

Coffee Break (10:15 – 10:45)**EX/3 and TH/2: Pedestal Stability & Control I**

Chair: F. Waelbroeck (USA)

Indigo Ball Room (10:45 – 12:30)

Time	Id	Presenter		Title
10:45	EX/3-1	Wade, Mickey	USA	Advances in the Physics Understanding of ELM Suppression Using Resonant Magnetic Perturbations in DIII-D
11:05	EX/3-2	Kirk, Andrew	UK	Understanding ELM Mitigation by Resonant Magnetic Perturbations on MAST
11:25	TH/2-1	Becoulet, Marina	France	Non-linear MHD Modelling of Rotating Plasma Response to Resonant Magnetic Perturbations
11:45	EX/3-3	Jeon, Young Mu	Korea, Rep.	ELM Control in Application of Non-Axisymmetric Magnetic Perturbations in KSTAR
12:05	EX/3-4	Suttrop, Wolfgang	Germany	Mitigation of Edge Localised Modes with Small Non-axisymmetric Magnetic Perturbations in ASDEX Upgrade

Poster Session: P3

Poster Room: Area F-B (08:30 – 12:30)

Id	Presenter		Title
EX/2-1	McDermott, Rachael	Germany	Connections Between Intrinsic Toroidal Rotation, Density Peaking and Plasma Turbulence Regimes in ASDEX Upgrade
EX/2-2	Rice, John	USA	A Unified Explanation of Rotation Reversals, Confinement Saturation and Non-Diffusive Heat Transport in C-Mod Ohmic Plasmas
TH/1-1	Murakami, Sadayoshi	Japan	Study of Toroidal Flow Generation by the ICRF Minority Heating in the Alcator C-Mod Plasma
EX/2-3	Shi, Yuejiang	Korea, Rep.	ECRH Effects on Toroidal Rotation: KSTAR Experiments and Gyrokinetic Simulations of Intrinsic Torque at ITG-TEM Transitions
EX/2-4	Urano, Hajime	Japan	Dependence of Heat Transport and Confinement on Isotopic Composition in Conventional H-mode Plasmas in JT-60U
EX/2-5	Takahashi, Hiromi	Japan	Extension of Operational Regime in High-Temperature Plasmas and the Dynamic-Transport Characteristics in the LHD
EX/P3-01	Reinke, Matthew	USA	Poloidal Variation of High-Z Impurity Density due to Hydrogen Minority ICRH on Alcator C-Mod
EX/P3-02	Podesta, Mario	USA	Measurements of Core Lithium Concentration in Diverted H-mode Plasmas of NSTX
EX/P3-03	Yoshikawa, Masayuki	Japan	Potential Fluctuation Study from the Core Plasma to End Region in the GAMMA 10 Tandem Mirror
EX/P3-04	Carraro, Lorella	Italy	High Current Plasmas in RFX-mod Reversed Field Pinch
EX/P3-05	Kirneva, Natalia	Russian Fed.	Experimental Investigation of Plasma Confinement in Reactor Relevant Conditions in TCV Plasmas with Dominant Electron Heating
EX/P3-06	Zurro, Bernardo	Spain	Suprathermal Ion Studies in ECRH and NBI Phases of the TJ-II Stellarator
EX/P3-07	Mizuuchi, Tohru	Japan	Study of Fueling Control for Confinement Experiments in Heliotron J
EX/P3-08	Ding, Weixing	USA	Magnetic Fluctuation-Driven Intrinsic Flow in a Toroidal Plasma

WED

Id	Presenter		Title
EX/P3-09	Sun, Hongjuan	Korea, Rep.	Understanding the Dynamics of Cold Pulse Nonlocality Phenomena
EX/P3-10	Kirneva, Natalia	Russian Fed.	Collisionality Dependence of Confinement in T-10 L-Mode Plasmas
EX/P3-11	Valisa, Marco	Italy	The Value of Flexibility: the Contribution of RFX to the International TOKAMAK and STELLARATOR Programme
EX/P3-12	Felici, Federico	Netherlands	Real-time Model-based Reconstruction and Control of Tokamak Plasma Profiles
EX/P3-13	Porkolab, Miklos	USA	Turbulent Transport and Gyrokinetic Analysis in Alcator C-Mod Ohmic Plasmas
EX/P3-14	Dinklage, Andreas	Germany	Inter-Machine Validation Study of Neoclassical Transport Modelling in Medium- to High-Density Stellarator-Heliotron Plasmas
EX/P3-15	Pütterich, Thomas	Germany	Tungsten Screening and Impurity Control in JET
EX/P3-16	Anderson, Jay	USA	Classical Confinement of Impurity Ions and NBI-born Fast Ions in the Reversed Field Pinch
EX/P3-17	Den Hartog, Daniel	USA	Measurement and Simulation of Electron Thermal Transport in the MST Reversed-Field Pinch
EX/P3-18	Luce, Timothy	USA	Experimental Tests of Stiffness in the Electron and Ion Energy Transport in the DIII-D Tokamak
EX/P3-19	Grierson, Brian	USA	Measurement of Deuterium Ion Toroidal Rotation and Comparison to Neoclassical Theory in the DIII-D Tokamak
EX/P3-20	Zhong, Wulu	China	Observation of ELM-Free H-mode in the HL-2A Tokamak
EX/P3-21	Duan, Xuru	China	Enhancement of Edge Impurity Transport with ECRH in HL-2A Tokamak
EX/P3-22	Hidalgo, Carlos	Spain	Dynamical Coupling Between Gradients and Transport in Tokamaks and Stellarators
EX/P3-23	Howard, Nathan	USA	Quantitative Comparison of Experimental and Gyrokinetic Simulated ICRH and I_p Dependent Impurity Transport
EX/P3-24	Ding, Siye	China	Observation of Electron Energy Pinch in HT-7 ICRF Heated Plasmas
EX/P3-25	Gao, Xiang	China	Survey of Density Modulation Experiments on the HT-7 Tokamak

Id	Presenter		Title
EX/P3-26	Doyle, Edward	USA	Particle Transport Results from Collisionality Scans and Perturbative Experiments on DIII-D
EX/P3-27	Kitajima, Sumio	Japan	Transition of Poloidal Viscosity by Electrode Biasing in the Large Helical Device
EX/P3-28	Fiore, Catherine	USA	Production of Internal Transport Barriers by Intrinsic Flow Drive in Alcator C-Mod
EX/P3-29	Burdakov, Aleksandr	Russian Fed.	Experiments on GOL-3 Multiple Mirror Trap for Fusion Program
EX/P3-30	Anderson, David	USA	Comparison of Plasma Flows and Currents in HSX to Neoclassical Theory
EX/P3-31	Nave, Maria Filomena	Portugal	Scalings of Spontaneous Rotation in the JET Tokamak
EX/P3-32	Lee, Sang Gon	Korea, Rep.	Toroidal Rotation Characteristics in KSTAR Plasmas
EX/P3-33	Verdoolaege, Geert	Belgium	Modeling Fusion Data in Probabilistic Metric Spaces for the Identification of Confinement Regimes and Scaling Laws
EX/P3-34	Scotti, Filippo	USA	Study of Carbon and Lithium Neoclassical Impurity Transport in ELM-Free H-mode Discharges in NSTX
EX/P3-35	Gao, Xiang	China	Development of Microwave Diagnostics in EAST Tokamak
ICC/P3-01	Ii, Toru	Japan	Stability and Confinement Improvement of Oblate Field-Reversed Configuration by Neutral Beam Injection
ICC/P3-02	Binderbauer, Michl	USA	A New High Performance Field Reversed Configuration Regime Through Edge Biasing and Neutral Beam Injection
TH/P3-01	Strauss, Henry	USA	Sideways Wall Force Produced during Disruptions
TH/P3-02	Lazarus, Edward	USA	An Investigation of Coupling of the Internal Kink Mode to Error Field Correction Coils in Tokamaks
TH/P3-03	Zhu, Ping	USA	Stabilizing Regimes of Edge Current Density for Pedestal Instabilities

Id	Presenter		Title
TH/P3-04	Jardin, Stephen	USA	Simulation of Sawteeth and other Global Macroscopic Dynamics of Tokamak Plasmas on the Transport Timescale
TH/P3-05	Moradi, Sara	Sweden	Impurity Transport due to Electromagnetic Drift Wave Turbulence
TH/P3-06	Kleiber, Ralf	Germany	Application of Particle-In-Cell Methods for Stellarators
TH/P3-07	Fitzpatrick, Richard	USA	Nonlinear Error-Field Penetration in Low Density Ohmically Heated Tokamak Plasmas
TH/P3-08	Sovinec, Carl	USA	Coupling of Current and Flow Relaxation in Reversed-Field Pinches due to Two-Fluid Effects
TH/P3-09	Hirota, Makoto	Japan	Nonlinear Acceleration Mechanism of Collisionless Magnetic Reconnection
TH/P3-10	Saarelma, Samuli	UK	Pedestal Modelling Based on Ideal MHD and Gyrokinetic Stability Analyses on JET and ITER Plasmas
TH/P3-11	Kruger, Scott	USA	Coupled Simulations of RF Effects on Tearing Modes
TH/P3-12	Katanuma, Isao	Japan	A Flute Instability in an Open System and the Line Tying Effect on it
TH/P3-13	Izzo, Valerie	USA	Impurity Mixing in Massive-Gas-Injection Simulations of DIII-D
TH/P3-14	Ichiguchi, Katsuji	Japan	Multi-Scale MHD Analysis of Heliotron Plasma in Change of Background Field
TH/P3-16	Pustovitov, Vladimir	Russian Fed.	Rotational Stabilization of the Resistive Wall Modes in Tokamaks
TH/P3-17	Snyder, Philip	USA	The EPED Pedestal Model: Extensions, Application to ELM-Suppressed Regimes, and ITER Predictions
TH/P3-18	Xiao, Yong	China	Convective Electron Motion in Low Frequency Collisionless Trapped Electron Turbulence
TH/P3-19	Shiraishi, Junya	Japan	Stabilization of Resistive Wall Modes by Magnetohydrodynamic Equilibrium Change Induced by Plasma Toroidal Rotation
TH/P3-20	Sen, Abhijit	India	Tearing Mode Stability in a Toroidally Flowing Plasma
TH/P3-21	Nicolas, Timoth��	France	Interplay between MHD and Particle Transport during Sawteeth

Id	Presenter	Title
TH/P3-22	Ivanov, Russian Nikolay Fed.	Magnetic Island Dynamics under External Magnetic Perturbation in Rotating Resistive Tokamak Plasma
TH/P3-23	Zheng, Linjin USA	Behavior of Magnetohydrodynamics Modes of Infernal Type at H-mode Pedestal with Plasma Rotation
TH/P3-24	Sun, Youwen China	Intrinsic Plasma Rotation Determined by Neo-classical Toroidal Plasma Viscosity in Tokamaks
TH/P3-25	Sato, Japan Masahiko	Characteristics of MHD Stability of High- β Plasmas in LHD
TH/P3-26	Mizuguchi, Japan Naoki	Numerical Modeling of Formation of Helical Structures in Reversed-Field-Pinch Plasma
TH/P3-27	Hao, China Guangzhou	Influence of Off-axis Neutral Beam Injection on Resistive Wall Mode Stability
TH/P3-28	Zakharov, USA Leonid	Current Sharing between Plasma and Walls in Tokamak Disruptions
TH/P3-29	Ilgisonis, Russian Victor Fed.	Continuum Modes of Arbitrary Rotating Tokamak Plasma
TH/P3-30	Gates, David USA	On the Origin of Tokamak Density Limit Scalings
TH/P3-31	Dong, Jiaqi China	Kinetic Shear Alfvén Wave Instability in the Presence of Impurity Ions in Tokamak Plasmas
TH/P3-32	He, Hongda China	Study of Trapped Energetic Electron Driven Fishbone Instability with Second Stable Regime in Tokamak Plasmas
TH/P3-34	Pinches, UK Simon	Development of a Predictive Capability for Fast Ion Behaviour in MAST

Lunch Break (12:30 – 14:00)

EX/4 and TH/3: Plasma-Wall Interactions

Chair: J. Li, (China)

Indigo Ball Room (14:00 – 16:10)

Time	Id	Presenter		Title
14:00	EX/4-1	Brezinsek, Sebastijan	Germany	Fuel Retention Studies with the ITER-like Wall in JET
14:20	EX/4-2	de Vries, Peter	Netherlands	Comparison of Plasma Breakdown with a Carbon and ITER-like Wall
14:40	TH/3-1	Groth, Mathias	Finland	Impact of Carbon and Tungsten as Divertor Materials on the Scrape-off Layer Conditions in JET
15:00	EX/4-3	Mayoral, Marie-Line	UK	On the Challenge of Plasma Heating with the JET Metallic Wall
15:20	TH/3-2	Krasheninnikov, Sergei	USA	On Edge Plasma, First Wall, and Dust Issues in Fusion Devices
15:40	EX/4-4	Kobayashi, Masahiro	Japan	Control of 3D Edge Radiation Structure with Resonant Magnetic Perturbation Fields Applied to Stochastic Layer and Stabilization of Radiative Divertor Plasma in LHD

Coffee Break (16:10 – 16:40)**ITR/2 and FTP/2: Diagnostics, Main System Design & Construction**

Chair: D. Stork (UK)

Indigo Ball Room (16:40 – 18:45)

Time	Id	Presenter		Title
16:40	ITR/2-1	Johnson, David	USA	ITER Diagnostics — Technology and Integration Challenges
17:00	ITR/2-2Ra	Travere, Jean-Marcel	France	Imaging Challenges for the ITER Plasma Facing Components Protection
	FTP/2-1Rb			Be Tile Power Handling and Main Wall Protection
17:20	ITR/2-3	Lorenzetto, Patrick	EU	Technology R&D Activities for the ITER Full-tungsten Divertor
17:40	ITR/2-4	Nakajima, Hideo	Japan	ITER Magnet Systems — from Qualification to Full Scale Construction
18:00	ITR/2-5	Bruzzzone, Pierluigi	Switzerland	Test Results of ITER Conductors in the SULTAN Facility
18:20	ITR/2-6	Raffray, René	ITER	The ITER Blanket System Design Challenge

Poster Session: P4

Poster Room: Area F-B (14:00 – 18:45)

Id	Presenter		Title
EX/3-1	Wade, Mickey	USA	Advances in the Physics Understanding of ELM Suppression Using Resonant Magnetic Perturbations in DIII-D
EX/3-2	Kirk, Andrew	UK	Understanding ELM Mitigation by Resonant Magnetic Perturbations on MAST
TH/2-1	Becoulet, Marina	France	Non-linear MHD Modelling of Rotating Plasma Response to Resonant Magnetic Perturbations
EX/3-3	Jeon, Young Mu	Korea, Rep.	ELM Control in Application of Non-Axisymmetric Magnetic Perturbations in KSTAR
EX/3-4	Suttrop, Wolfgang	Germany	Mitigation of Edge Localised Modes with Small Non-axisymmetric Magnetic Perturbations in ASDEX Upgrade
TH/P4-01	Leconte, Michael	Korea, Rep.	Impact of Resonant Magnetic Perturbations on Zonal Modes, Drift-Wave Turbulence and the L-H Transition Threshold
TH/P4-02	Diamond, Patrick	USA	Spatio-Temporal Evolution of the L-H and H-L Transitions
TH/P4-03	Dorf, Mikhail	USA	Numerical Modeling of Neoclassical Transport and Geodesic Acoustic Mode Relaxation in a Tokamak Edge
TH/P4-04	Shaing, Kerchung	USA	Transport Theory for Error Fields and in the Pedestal Region for Tokamaks
TH/P4-05	Papp, Gergely	Hungary	Spatio-temporal Distribution of Runaway Electron Wall Loads in ITER due to Resonant Magnetic Perturbations
TH/P4-06	Belli, Emily	USA	Eulerian Simulations of Neoclassical Flows and Transport in the Tokamak Plasma Edge and Outer Core
TH/P4-07	Pankin, Alexei	USA	Integrated Approach to the H-mode Pedestal Dynamics: Effects of Bootstrap Current and Resonant Magnetic Perturbations on ELMs
TH/P4-08	Sun, Youwen	China	Rotation Breaking Induced by ELMs on EAST
TH/P4-09	Fuhr, Guillaume	France	Penetration of Resonant Magnetic Perturbations in Turbulent Edge Plasmas with Transport Barrier

WED

Id	Presenter		Title
TH/P4-10	Hakim, Ammar	USA	Integrated Fusion Simulations of Core-Edge-Wall Thermal and Particle Transport Using the FACETS Code
TH/P4-11	Schoepf, Klaus	Austria	Modelling of the Effect of Externally Applied Resonant Magnetic Perturbations on α -particle Dynamics in Tokamak Plasmas
TH/P4-12	Chang, Choong Seock	Korea, Rep.	New Bootstrap Current Formula Valid for Edge Pedestal, and Gyrokinetic Study of its Implication to Pedestal Stability
TH/P4-13	Aydemir, Ahmet	USA	Edge Electric Fields in the Pfirsch-Schlüter Regime and their Effect on the L-H Transition Power Threshold
TH/P4-14	Ricci, Paolo	Switzerland	Progressive Steps towards Global Validated Simulation of Edge Plasma Turbulence
TH/P4-15	Singh, Raghvendra	India	Theory of Rapid Formation of Pedestal and Pedestal width due to Anomalous Particle Pinch in the Edge of H-mode Discharges
TH/P4-16	Tang, Xianzhu	USA	Parallel Transport and Profile of Boundary Plasma with a Low Recycling Wall
TH/P4-17	Zagorski, Roman	Poland	Simulations with COREDIV Code of DEMO Discharges
TH/P4-18	Ryutov, Dmitri	USA	Theory and Simulations of ELM Control with a Snowflake Divertor
TH/P4-19	Goldston, Robert	USA	Drift-based Model for Power Scrape-off Width in Low-Gas-Puff H-mode Plasmas: Theory and Implications
TH/P4-20	Callen, James	USA	RMP-Flutter-Induced Pedestal Plasma Transport
TH/P4-21	Ferraro, Nathaniel	USA	Edge Plasma Response to Non-Axisymmetric Fields in Tokamaks
TH/P4-22	Marandet, Yannick	France	Coarse Grained Transport Model for Neutrals in Turbulent SOL Plasmas
TH/P4-23	Myra, James	USA	Edge Sheared Flows and Blob Dynamics
TH/P4-24	Jiquan, Li	Japan	Effects of Collisionality on the Nonlinear Characteristics of Boundary Turbulence and Blob/hole Transport in Tokamak Plasmas
TH/P4-25	Daybelge, Umur	Turkey	Spatiotemporal Oscillations in Tokamak Edge Layer and their Generation by Various Mechanisms

Id	Presenter		Title
TH/P4-26	Ghendrih, Philippe	France	Impact on Divertor Operation of the Pattern of Edge and SOL Flows Induced by Particle Sources and Sinks
TH/P4-27	Cahyna, Pavel	Czech Rep.	Modelling of Plasma Response to Resonant Magnetic Perturbations and its Influence on Divertor Strike Points
TH/P4-28	Park, Gun Young	Korea, Rep.	Self-consistent Kinetic Simulation of RMP-driven Transport: Collisionality and Rotation Effects on RMP Penetration and Transport
EX/P4-01	Lang, Peter Thomas	Germany	Pellet Induced High Density Phases during ELM Suppression in ASDEX Upgrade
EX/P4-02	Schneider, Philip	Germany	Analysis of Temperature and Density Pedestal in a Multi-machine Database
EX/P4-03	Ryter, François	Germany	L-H Transition, Pedestal Development and I-mode Studies in the ASDEX Upgrade Tokamak
EX/P4-04	Diallo, Ahmed	USA	The Evolution of the Edge Pedestal Structure and Turbulence Spatial Scale during the ELM Cycle on NSTX
EX/P4-05	Wang, Liang	China	Observation of Current Structures at Type-III ELM Onset on EAST
EX/P4-06	Xu, Guosheng	China	New Edge Localized Modes at Marginal Input Power with Dominant RF-heating and Lithium-wall Conditioning in EAST
EX/P4-07	Classen, Ivo	Netherlands	Characterization of Temperature Fluctuations during Type-I and Type-II Edge Localized Modes at ASDEX Upgrade
EX/P4-08	Burrell, Keith	USA	Reactor-relevant Quiescent H-mode Operation Using Torque from Non-axisymmetric, Non-resonant Magnetic Fields
EX/P4-09	Reimerdes, Holger	Switzerland	Rotation Braking and Error Field Correction of the Test Blanket Module Induced Magnetic Field Error in ITER
EX/P4-10	Toi, Kazuo	Japan	Mitigation of Large Amplitude Edge-Localized-Modes by Resonant Magnetic Perturbations on the Large Helical Device
EX/P4-11	Yu, Deliang	China	Study of the High-efficiency Fuelling Features of Supersonic Molecular Beam Injection on HL-2A Tokamak

WED

Id	Presenter	Title
EX/P4-12	Bak, Jun-Gyo Korea, Rep.	ELM and Pedestal Structure Studies in KSTAR H-mode Plasmas
EX/P4-13	Jakubowski, Marcin Germany	Influence of the Resonant Magnetic Perturbations on Particle Transport in LHD
EX/P4-14	Delgado-Aparicio, Luis USA	On the Formation and Stability of Impurity-generated “Snakes” in Alcator C-Mod
EX/P4-15	Hughes, Jerry USA	Pedestal Stability and Transport on the Alcator C-Mod Tokamak: Experiments in Support of Developing Predictive Capability
EX/P4-17	Ohshima, Shinsuke Japan	Edge Plasma Response to Beam-driven MHD Instability in Heliotron J
EX/P4-18	López-Bruna, Daniel Spain	MHD Events and Transport Barriers in TJ-II Plasmas
EX/P4-19	Levesque, Jeffrey USA	High Resolution Detection and 3D Magnetic Control of the Helical Boundary of a Wall-Stabilized Tokamak Plasma
EX/P4-20	Nowak, Silvana Italy	Control of Sawteeth Periods by Pulsed ECH and ECCD in FTU Tokamak
EX/P4-21	Frassinetti, Lorenzo Sweden	Experimental Studies of the Plasma Response to Applied Nonaxisymmetric External Magnetic Perturbations in EXTRAP T2R
EX/P4-22	Lin, Yijun USA	Characterization of Neo-classical Tearing Modes in High-performance I-Mode Plasmas with ICRF Mode Conversion Flow Drive on Alcator C-Mod
EX/P4-23	Liang, Yunfeng Germany	Mitigation of Type-I ELMs with $n = 2$ Fields on JET
EX/P4-24	Masamune, Sadao Japan	Direct Observation of Soft-X Ray Filament Structure and High Current Operation in Low-Aspect-Ratio RFP
EX/P4-25	Ji, Xiaoquan China	Triggering of Neoclassical Tearing Modes by Mode Coupling in HL-2A
EX/P4-26	Xiao, Chijin Canada	Modification of Toroidal Flow in the STOR-M Tokamak
EX/P4-27	Hanson, Jeremy USA	Probing Resistive Wall Mode Stability Using Off-axis NBI
EX/P4-28	Kolemen, Egemen USA	Vertical Stability of NSTX and NSTX-U

Id	Presenter	Title
EX/P4-29	Huang, Yuan China	Perturbation Features of Intrinsic and Pellet Induced ELMs on HL-2A
EX/P4-30	Sakakibara, Satoru Japan	Response of MHD Stability to Resonant Magnetic Perturbation in the Large Helical Device
EX/P4-31	Buttery, Richard USA	Addressing New Challenges for Error Field Correction
EX/P4-32	Lazzaro, Enzo Italy	Triggerless Onset and Effect of “Natural” Rotation on Neoclassical Tearing Modes in the TCV Tokamak
EX/P4-33	Park, Jong-Kyu USA	Observation of Edge Harmonic Oscillation in NSTX and Theoretical Study of its Active Control Using HHFW Antenna at Audio Frequencies
EX/P4-34	Savrukhn, Petr Russian Fed.	Fast-scale Magnetic Perturbations and Onset of the Energy Quench during Disruption Instability in the T-10 Tokamak
EX/P4-35	Romero, Jesús Antonio Spain	Current Profile Control Using the Ohmic Heating Coil in TCV
EX/P4-36	Redd, Aaron USA	Local Helicity Injection Startup and Edge Stability Studies in the Pegasus Toroidal Experiment

WED

IFE/1: Inertial Fusion Experiments and Theory

Chair: K. Mima (Japan)

Indigo Ball Room (08:30 – 10:15)

Time	Id	Presenter		Title
08:30	IFE/1-1	Frenje,	USA	Diagnosing Implosion Performance at the National Ignition Facility by Means of Advanced Neutron-Spectrometry and Neutron-Imaging Techniques
		Johan		
08:50	IFE/1-2	McCrory,	USA	Progress toward Polar-Drive Ignition for the NIF
		Robert		
09:10	IFE/1-3	Shiraga,	Japan	Fast Ignition Integrated Experiments with Gekko-XII and LFEX Lasers
		Hiroyuki		
09:30	IFE/1-4	Sethian,	USA	Inertial Fusion Energy with Direct Drive and Krypton Fluoride Lasers
		John		
09:50	IFE/1-5	Perlado,	Spain	Approach to Power Plant Physics and Technology in Laser Fusion Energy Systems under Repetitive Operation
		José Manuel		

Coffee Break (10:15 – 10:45)**EX/5 and TH/4: Waves & Energetic Particles**

Chair: E. Fredrickson (USA)

Indigo Ball Room (10:45 – 12:30)

Time	Id	Presenter		Title
10:45	EX/5-1	Matsunaga,	Japan	Dynamics of Energetic Particle Driven Modes and MHD Modes in Wall-stabilized High- β Plasmas on JT-60U and DIII-D
		Go		
11:05	TH/4-1	Berk,	USA	Energetic Particle Long Range Frequency Sweeping and Quasilinear Relaxation
		Herbert		
11:25	EX/5-2	Yamamoto,	Japan	Studies of Energetic-ion-driven MHD Instabilities in Helical Plasmas with Low Magnetic Shear
		Satoshi		
11:45	TH/4-2	Zonca, Fulvio	Italy	Nonlinear Excitations of Zonal Structures by Toroidal Alfvén Eigenmodes
12:05	EX/5-3	Chen, Wei	China	Observation of GAM Induced by Energetic Electrons and NL Interactions among GAM, BAEs and Tearing Modes on the HL-2A Tokamak

Poster Session: P5

Poster Room: Area F-B (08:30 – 12:30)

Id	Presenter		Title
EX/4-1	Brezinsek, Sebastijan	UK	Fuel Retention Studies with the ITER-like Wall in JET
EX/4-2	de Vries, Peter	Netherlands	Comparison of Plasma Breakdown with a Carbon and ITER-like Wall
TH/3-1	Groth, Matthias	Finland	Impact of Carbon and Tungsten as Divertor Materials on the Scrape-off Layer Conditions in JET
EX/4-3	Mayoral, Marie-Line	UK	On the Challenge of Plasma Heating with the JET Metallic Wall
TH/3-2	Krasheninnikov, Sergei	USA	On Edge Plasma, First Wall, and Dust Issues in Fusion Devices
EX/4-4	Kobayashi, Masahiro	Japan	Control of 3D Edge Radiation Structure with Resonant Magnetic Perturbation Fields Applied to Stochastic Layer and Stabilization of Radiative Divertor Plasma in LHD
ITR/2-1	Johnson, David	USA	ITER Diagnostics-Technology and Integration Challenges
ITR/2-2Ra	Travere, Jean-Marcel	France	Imaging Challenges for the ITER Plasma Facing Components Protection
FTP/2-1Rb	Ferreira Nunes, Isabel	EU	Be Tile Power Handling and Main Wall Protection
ITR/2-3	Lorenzetto, Patrick	EU	Technology R&D Activities for the ITER Full-tungsten Divertor
ITR/2-4	Nakajima, Hideo	Japan	ITER Magnet Systems-from Qualification to Full Scale Construction
ITR/2-5	Bruzzzone, Pierluigi	Switzerland	Test Results of ITER Conductors in the SULTAN Facility
ITR/2-6	Raffray, René	ITER	The ITER Blanket System Design Challenge
EX/P5-01	Puiatti, Maria Ester	Italy	Wall Conditioning and Density Control in the Reversed Field Pinch RFX-mod
EX/P5-02	Zhang, Ling	China	Effect of Lithium Coating on Edge Particle Recycling in EAST H-mode Discharge
EX/P5-03	Wright, Graham	USA	Assessment of Tungsten Nano-tendrils Growth in the Alcator C-Mod Divertor

THU

Id	Presenter		Title
EX/P5-04	Coenen, Jan Willem	Germany	Longterm Evolution of the Impurity Composition and Transient Impurity Events with the ITER-like Wall at JET
EX/P5-05	van Rooij, Gerard	Netherlands	Characterization of Tungsten Sputtering in the JET Divertor
EX/P5-06	Takamura, Shuichi	Japan	Cooling Characteristics and Mitigation of He-Defected Tungsten with Nanostructure Formation
EX/P5-07	Tsitrone, Emmanuelle	France	In Vessel Fuel Inventory Build-up in Tokamaks: Lessons Learnt from Tore Supra
EX/P5-08	Kajita, Shin	Japan	Impact of Arcing on Carbon and Tungsten: from the Observations in JT-60U, LHD, and NAGDIS-II
EX/P5-09	Douai, David	France	Overview of the International Research on Ion Cyclotron Wall Conditioning
EX/P5-10	Philipps, Volker	Germany	Efficiency of Fuel Removal: Overview of Techniques Tested on Plasma-Facing Components from the TEXTOR Tokamak
EX/P5-11	Rudakov, Dmitry	USA	Measurements of Net versus Gross Erosion of Molybdenum Divertor Surface in DIII-D
EX/P5-12	Petrie, Thomas	USA	Effect of Changes in Separatrix Magnetic Geometry on Divertor Behavior in DIII-D
EX/P5-13	Wang, Liang	China	Characterization of Particle and Power Loads on Divertor Targets for Type-I, Type-III, and Mossy ELMy H-modes in EAST Superconducting Tokamak
EX/P5-14	Philipps, Volker	Germany	Development of Laser Based Techniques for In-situ Characterization of the First Wall in ITER and Future Fusion Devices
EX/P5-15	Guo, Houyang	China	Approaches towards Steady-State Advanced Divertor Operations on EAST by Active Control of Plasma-Wall Interactions
EX/P5-16	Makowski, Michael	USA	Scaling of the Divertor Heat Flux Width in the DIII-D Tokamak
EX/P5-17	Fishpool, Geoff	UK	MAST Contributions to the Exhaust Challenge, Including Testing of Super-X
EX/P5-18	Morita, Shigeru	Japan	Low Concentration of Iron as First Wall Material in LHD Plasmas with Edge Ergodic Layer

Id	Presenter	Title	THU
EX/P5-19	Bobkov, Volodymyr	Germany	
EX/P5-21	Soukhanov- skii, Vsevolod	USA	
EX/P5-22	Vijvers, Wouter	Switzerland	
EX/P5-23	Koubiti, Mohammed	France	
EX/P5-24	Mertens, Philippe	Germany	
EX/P5-25	Mirnov, Sergey	Russian Fed.	
EX/P5-26	Monier- Garbet, Pascale	France	
EX/P5-27	Gray, Travis	USA	
EX/P5-28	Battaglia, Devon	USA	
EX/P5-29	Morisaki, Tomohiro	Japan	
EX/P5-30	Giroud, Carine	UK	
ICC/P5-01	Majeski, Richard	USA	
EX/P5-31	Jaworski, Michael	USA	
EX/P5-32	Koga, Kazunori	Japan	
EX/P5-33	Ahn, Joon-Wook	USA	

Id	Presenter		Title
EX/P5-34	Wischmeier, Marco	Germany	Symmetries and Asymmetries in the Divertor Detachment in ASDEX Upgrade
EX/P5-35	Juhn, June-Woo	Korea, Rep.	A Global Particle-balance Model for Wall Interaction Analysis Associated with Open- and Closed-loop Density Control Experiments in KSTAR
EX/P5-36	Tabares, Francisco	Spain	Studies of Plasma-Lithium Interactions in TJ-II
EX/P5-37	Arnoux, Gilles	UK	Scrape-off Layer Properties of ITER-like Limiter Start-up Plasmas at JET
EX/P5-38	Marrelli, Lionello	Italy	Development of MHD Active Control in the RFX-mod RFP
EX/P5-39	Terry, James	USA	The Fine-scale Structure of the Radial Electric Field in the Scrape-Off-Layer during ICRF Heating in Alcator C-Mod
EX/P5-40	Perkins, Rory	USA	Fast Wave Power Flow along SOL Field Lines in NSTX
ITR/P5-01	Sa, Jeong-Woo	Korea, Rep.	Progress on Manufacturing of the ITER Vacuum Vessel Equatorial and Lower Ports in Korea
ITR/P5-02	Duchateau, Jean-Luc	France	Quench Detection in ITER Superconducting Magnet Systems
ITR/P5-03	Belyakov, Valery	Russian Fed.	Simulation of Eddy Current and Electromagnetic Loads in ITER Conducting Structures
ITR/P5-04	Ulrickson, Michael	USA	Transient Electromagnetic Analysis of the ITER Blanket System
ITR/P5-05	Matsui, Kunihiro	Japan	Results of ITER TF Coil Sub and Full Scale Trials Performed in Japan
ITR/P5-06	Seki, Yohji	Japan	Progress of Manufacturing and Quality Testing of the ITER Divertor Outer Vertical Target in Japan
ITR/P5-07	Bucallosi, Jérôme	France	Developments toward Fully Metallic Actively Cooled Plasma Facing Components for ITER divertor
ITR/P5-08	Escourbiac, Frédéric	ITER	Effort on Design of a Full Tungsten Divertor for ITER
ITR/P5-09	Kupriyanov, Igor	Russian Fed.	Experimental Simulation of Beryllium Armour Damage Under ITER-like Intense Transient Plasma Loads

Id	Presenter	Title
ITR/P5-10	Li, Pengyuan China	Status & Progress of the R&D Work for ITER Magnet Supports
ITR/P5-11	Alejaldre, Carlos ITER	Feedback of the Licensing Process of the First Nuclear Installation in Fusion, ITER
ITR/P5-12	Blackler, Ken ITER	ITER Machine Assembly — Challenges and Progress
ITR/P5-14	Danani, Chandan India	Activation Analyses of Lead Lithium Cooled Ceramic Breeder Test Blanket Module in ITER
ITR/P5-15	Atchutuni, Sarada Sree India	Preliminary Corrosion Studies on Structural Materials in Lead-Lithium for Indian LLCB TBM
ITR/P5-16	Panayotov, Dobromir EU	Progress in the EU Test Blanket Systems Safety Studies
ITR/P5-18	Zhou, Zhiwei China	Transient Thermal-hydraulic Modeling and Analysis of Chinese HCSB TBM
ITR/P5-22	Eskhult, Jonas Sweden	Experimental Assessment of Materials Exposed to Coolant Water under ITER Relevant Operational Conditions
ITR/P5-23	Combs, Stephen USA	Development and Testing of Plasma Disruption Mitigation Systems Applicable for ITER
ITR/P5-24	Maruyama, So ITER	ITER Fuelling and Glow Discharge Cleaning System Overview
ITR/P5-25	Simrock, Stefan ITER	Scientific Computing for Real Time Data Processing and Archiving for ITER Operation
ITR/P5-26	Le Guern, Frédéric EU	Status of R&D on In-Vessel Dust & Tritium Management in ITER
ITR/P5-27	Grosman, André France	Challenges of Integrating a Typical Diagnostics Port Plug in ITER
ITR/P5-28	Feder, Russell USA	Assessing the Nuclear Environment for ITER Port Plugs and Port-based Diagnostics
ITR/P5-29	Gribov, Yury ITER	Error Fields Expected in ITER and their Correction
ITR/P5-30	Mukhin, Evgenii Russian Fed.	Status of Thomson Scattering in ITER Divertor
ITR/P5-31	Arshad, Shakeib EU	System-Level Optimization of ITER Magnetic Diagnostics: Preliminary Results
ITR/P5-32	Mirnov, Vladimir USA	Electron Kinetic Effects on Interferometry, Polarimetry and Thomson Scattering in Burning Plasmas

THU

Id	Presenter		Title
ITR/P5-33	Conway, Garrard	Germany	ITPA Assessment of ITER Microwave Diagnostic Design Issues
ITR/P5-34	Razdobarin, Alexey	Russian Fed.	Mirrors for ITER Optical Diagnostics
ITR/P5-35	Kawano, Yasunori	Japan	Progress on Design and R&D for ITER Diagnostic Systems in Japan Domestic Agency
ITR/P5-36	Shevelev, Alexander	Russian Fed.	Reconstruction of Distribution Functions of Fast Ions and Runaway Electrons in ITER Plasmas Using Gamma-Ray Spectrometry
ITR/P5-37	Walsh, Michael	ITER	Evolution of the ITER Diagnostic Set Specifications
ITR/P5-38	Imazawa, Ryota	Japan	Analysis of Current Profile Measurement Capability on ITER
ITR/P5-39	Gin, Dmitry	Russian Fed.	ITER High Resolution Gamma Spectrometry
ITR/P5-40	Park, Hyeon Keo	Korea, Rep.	Overview of the ITPA R&D Activities for Optimizing ITER Diagnostic Performance
ITR/P5-41	Austin, Max	USA	Exploring Measurement Capabilities of ITER ECE System
ITR/P5-42	Litnovsky, Andrey	Germany	First Studies of ITER Diagnostic Mirrors in a Tokamak with All-metal Interior: Results of First Mirror Test in ASDEX Upgrade
ITR/P5-43	Chakraborty, Arun Kumar	India	Exploring the Engineering Performance Limits of DNB
ITR/P5-44	Kukushkin, Alexander	Russian Fed.	Theoretical Issues of High Resolution H- α Spectroscopy Measurements in ITER

Lunch Break (12:30 – 14:00)

EX/6 and TH/5: Pedestal Stability & Control II

Chair: G. Saibene (EU)

Indigo Ball Room (14:00 – 16:10)

Time	Id	Presenter		Title
14:00	TH/5-1	Roach, Colin	UK	Gyrokinetic Instabilities in an Evolving Tokamak H-mode Pedestal
14:20	EX/6-1	de la Luna, Elena	EU	The Effect of ELM Mitigation Methods on the Access to High H-mode Confinement ($H_{98} \sim 1$)
14:40	TH/5-2Ra	Xia, Tianyang	China	Five-field Peeling-Ballooning Modes Simulation with BOUT++
	TH/5-2Rb			Theory and Gyro-fluid Simulations of Edge-Localized-Modes
15:00	EX/6-2	Baylor, Larry	USA	Experimental Demonstration of High Frequency ELM Pacing by Pellet Injection on DIII-D and Extrapolation to ITER
15:20	TH/5-3	Hayashi, Nobuhiko	Japan	Reduction of ELM Energy Loss by Pellet Injection for ELM Pacing
15:40	EX/6-3Ra	Xiao, Weiwen	China	ELM Mitigation by Supersonic Molecular Beam Injection: KSTAR and HL-2A Experiments and Theory
	EX/6-3Rb			ELM Mitigation with SMBI & CJI Fueling in HL-2A H-mode Plasmas

THU

Coffee Break (16:10 – 16:40)

EX/7 and TH/6: Transport and Turbulence

Chair: C. Hidalgo (Spain)

Indigo Ball Room (16:40 – 18:45)

Time	Id	Presenter		Title
16:40	EX/7-1	Kaye, Stanley	USA	The Dependence of H-mode Energy Confinement and Transport on Collisionality in NSTX
17:00	TH/6-1	Guttenfelder, Walter	USA	Progress in Simulating Turbulent Electron Thermal Transport in NSTX
17:20	TH/6-2	Jhang, Hogun	Korea, Rep.	Role of External Torque and Toroidal Momentum Transport in the Dynamics of Heat Transport in Internal Transport Barriers
17:40	TH/6-3	Gusakov, Evgeniy	Russian Fed.	Multi-Scale Drift Turbulence Dynamics in Ohmic Discharge as Measured at the FT-2 Tokamak and Modeled by Full- <i>f</i> Gyrokinetic ELMFIRE-code
18:00	TH/6-4	Jenko, Frank	Germany	Global Gyrokinetic Simulations of High-performance Discharges in View of ITER
18:20	EX/7-2Ra	Zhao, Kaijun	China	New Meso-scale Electric Fluctuations Interacting with Magnetic Islands and Turbulence in Edge Plasmas of HL-2A
	EX/7-2Rb			Turbulent Eddy-mediated Particle, Momentum, and Vorticity Transport in the Edge of HL-2A Tokamak Plasma

Poster Session: P6

Poster Room: Area F-B (14:00 – 18:45)

Id	Presenter		Title
IFE/1-1	Frenje, Johan	USA	Diagnosing Implosion Performance at the National Ignition Facility by Means of Advanced Neutron-Spectrometry and Neutron-Imaging Techniques
IFE/1-2	McCrory, Robert	USA	Progress toward Polar-Drive Ignition for the NIF
IFE/1-3	Shiraga, Hiroyuki	Japan	Fast Ignition Integrated Experiments with Gekko-XII and LFEX Lasers
IFE/1-4	Sethian, John	USA	Inertial Fusion Energy with Direct Drive and Krypton Fluoride Lasers
IFE/1-5	Perlado, José Manuel	Spain	Approach to Power Plant Physics and Technology in Laser Fusion Energy Systems under Repetitive Operation
IFE/P6-01	More, Richard	USA	Particle Simulation of Fusion Ignition
IFE/P6-02	Wang, Yi-Ming	USA	Application of Radiative Cooling to ICF Ignition
IFE/P6-03	Hora, Heinrich	Australia	Shock Studies in Nonlinear Force Driven Laser Fusion with Ultrahigh Plasma Block Acceleration
IFE/P6-04	Patel, Pravesh	USA	Status of Fast Ignition Point Design
IFE/P6-05	Nagatomo, Hideo	Japan	Computational Study of the Strong Magnetic Field Generation in Non-Spherical Cone-Guided Implosion
IFE/P6-06	Wei, Mingsheng	USA	Study of Fast Electron Generation and Transport for Fast Ignition
IFE/P6-07	Qiao, Bin	USA	Self-consistent Integrated Modeling for Proton Fast Ignition
IFE/P6-08	Beg, Farhat	USA	Focusing Protons Beams for Fast Ignition
IFE/P6-09	Khaydarov, Rajabbay	Uzbekistan	Improvement of Characteristics of Laser Source of Ions by Changing the Interaction Angle of Laser Radiation
IFE/P6-10	Li, Chikang	USA	Proton Imaging of Hohlraum Plasma Stagnation in Inertial Confinement Fusion Experiments
IFE/P6-11	Arikawa, Yasunobu	Japan	Study on the Energy Transfer Efficiency in the Fast Ignition Experiment

THU

Id	Presenter		Title
IFE/P6-12	Kitagawa, Yoneyoshi	Japan	Fast Ignition Scheme Fusion Using High-Repetition-Rate Laser
IFE/P6-13	Mori, Yoshitaka	Japan	10-J Green DPSSL-pumped Laser System HAMA for High-repetitive Counter Irradiation Fast Heating Fusion Demonstration
IFE/P6-14	Kong, Hong Jin	Korea, Rep.	Highly Repetitive Laser Inertial fusion driver with Tiled Coherent Beam Combination Laser Using Stimulated Brillouin Scattering Phase Conjugation Mirrors
IFE/P6-15	Kalal, Milan	Czech Rep.	Overview and Latest Proposals in SBS PCM Based IFE Technology Featuring Self-navigation of Lasers on Injected Direct Drive Pellets
IFE/P6-16	Kwan, Joe	USA	Summary of Progress in US Heavy Ion Fusion Science Research
IFE/P6-17	Gourdain, Pierre-Alexandre	USA	Axial Magnetic Field Compression Studies Using Gas Puff Z-pinchs and Thin Liners on COBRA
IFE/P6-18	Iwamoto, Akifumi	Japan	FIREX Foam Cryogenic Target Development: Attempt of Residual Voids Reduction with Solid Hydrogen Refractive Index Measurement
IFE/P6-19	Alexander, Neil	USA	Mass-Fabrication of Targets for Inertial Fusion Energy
EX/5-1	Matsunaga, Go	Japan	Dynamics of Energetic Particle Driven Modes and MHD Modes in Wall-stabilized High- β Plasmas on JT-60U and DIII-D
TH/4-1	Berk, Herbert	USA	Energetic Particle Long Range Frequency Sweeping and Quasilinear Relaxation
EX/5-2	Yamamoto, Satoshi	Japan	Studies of Energetic-ion-driven MHD Instabilities in Helical Plasmas with Low Magnetic Shear
TH/4-2	Zonca, Fulvio	Italy	Nonlinear Excitations of Zonal Structures by Toroidal Alfvén Eigenmodes
EX/5-3	Chen, Wei	China	Observation of GAM Induced by Energetic Electrons and NL Interactions among GAM, BAEs and Tearing Modes on the HL-2A Tokamak
ICC/P6-01	Kurt, Erol	Turkey	The Finite Element Analysis of an Inertial Electrostatic Confinement Unit

Id	Presenter		Title
ICC/P6-02	Degnan, James	USA	Recent Magneto — Inertial Fusion Experiments on FRCHX
EX/P6-01	Chapman, Brett	USA	Direct Diagnosis and Parametric Dependence of 3D Helical Equilibrium in the MST RFP
EX/P6-02	Crocker, Neal	USA	Internal Amplitude, Structure and Identification of CAEs and GAEs in NSTX
EX/P6-03	Garcia-Munoz, Manuel	Germany	Fast-ion Redistribution and Loss due to Edge Perturbations in the ASDEX Upgrade, DIII-D and KSTAR Tokamaks
EX/P6-04	Sozzi, Carlo	Italy	First Operations of the Real-Time ECRH/ECCD System for Control of Magnetohydrodynamics Instabilities in the FTU Tokamak
EX/P6-05	Fredrickson, Eric	USA	Fast-ion Energy Loss during TAE Avalanches in the National Spherical Torus Experiment
EX/P6-06	Turnyanskiy, Mikhail	UK	Measurement and Optimisation of the Fast Ion Distribution on MAST
EX/P6-07	Dubuit, Nicolas	France	Electron Fishbones in LHCD Plasmas on FTU and Tore Supra
EX/P6-08	Goodman, Timothy	Switzerland	Development of Electron Cyclotron Wave Absorption Measurement for Real-Time Polarization Optimization and Studies of Quasilinear Effects
EX/P6-09	Hole, Matthew	Australia	Analysis of Alfvén Wave Activity in KSTAR Plasmas
EX/P6-10	Hoang, Tuong	France	Physics and Technology in the Ion-cyclotron Range of Frequency on Tore Supra and TITAN Test Facility: Implication for ITER
EX/P6-11	Lebedev, Sergei	Russian Fed.	Study of Fast Ion Confinement in the TUMAN-3M
EX/P6-12	Liu, Yi	China	Investigation of the Role of Energetic Particle in the Driving of Long-lived Saturated Internal Mode on HL-2A Tokamak
EX/P6-13	Liu, Yi	China	Nonlinear features of the Alfvénic wave-particle interaction in auxiliary heated HL-2A plasma
EX/P6-14	Yu, Liming	China	Frequency Jump Phenomena of e -Fishbone during High Power ECRH on HL-2A Tokamak
EX/P6-15	Ding, Xuantong	China	Coexistence of Alfvénic Modes Induced by Energetic Electrons with ECRH on HL-2A

THU

Id	Presenter		Title
EX/P6-16	Yoshimura, Yasuo	Japan	Electron Bernstein Wave Heating and Electron Cyclotron Current Drive by Use of Upgraded ECH System in LHD
EX/P6-17	Idei, Hiroshi	Japan	Electron Bernstein Wave Heating and Current Drive Effects in QUEST
EX/P6-18	Uchida, Masaki	Japan	Noninductive Formation of Spherical Tokamak at 7 Times the Plasma Cutoff Density by Electron Bernstein Wave Heating and Current Drive on LATE
EX/P6-19	Lu, Bo	China	Plasma Rotation Behavior under Lower Hybrid Current Drive and Ion Cyclotron Range of Frequency Heating on EAST
EX/P6-20	Ichimura, Makoto	Japan	Coupling of ICRF Waves and Axial Transport of High-Energy Ions Owing to Spontaneously Excited Waves in the GAMMA 10 Tandem Mirror
EX/P6-21	Ding, Bojiang	China	Investigations of LHW-plasma Coupling and Current Drive in H-mode Experiments in EAST
EX/P6-22	Heidbrink, William	USA	Fast Ion Physics Enabled by Off-Axis Neutral Beam Injection
EX/P6-23	Blackwell, Boyd	Australia	MHD Activity in the Alfvén Range of Frequencies in the H-1NF Helic
EX/P6-24	Hillairet, Julien	France	Recent Progress on Lower Hybrid Current Drive and Implications for ITER
EX/P6-25	Qin, Cheng Ming	China	Recent Results from Ion Cyclotron Resonance Heating Experiments in HT-7 and EAST Tokamak
EX/P6-26	Gao, Zhe	China	Experimental Study of Low Frequency Wave Current Drive in the SUNIST Spherical Tokamak
EX/P6-27	Kim, Sun-Ho	Korea, Rep.	Analysis of High Energy Neutral Particles Measured by CNPA and Comparison with Synthesized Fast Neutral Spectrum Based on TRANSP/FIDA for the NB Heated Plasmas in KSTAR
EX/P6-28	Fasoli, Ambrogio	Switzerland	Basic Investigations of Electrostatic Turbulence and its Interaction with Plasma and Suprathermal Ions in a Simple Magnetized Toroidal Plasma

Id	Presenter	Title	THU
EX/P6-29	Cesario, Roberto Italy	Spectral Broadening and Lower Hybrid Current Drive in High Density Tokamak Plasmas	
TH/P6-01	Marchenko, Victor Ukraine	Frequency Chirping during a Fishbone Burst	
TH/P6-02	Petrov, Yuri USA	Finite Orbit Width Features in the CQL3D Code	
TH/P6-03	Vlad, Gregorio Italy	Electron Fishbone Simulations in FTU-like Equilibria Using XHMG	
TH/P6-04	Farengo, Ricardo Argentina	Alpha Particle Redistribution in Sawteeth	
TH/P6-05	Peysson, Yves France	Effect of Density Fluctuations on LHCD and ECCD and Implications for ITER	
TH/P6-06	Bass, Eric USA	Fully Gyrokinetic Modeling of Beam-driven Alfvén Eigenmodes in DIII-D Using GYRO	
TH/P6-08	Harvey, Robert USA	Differences Between QL and Exact Ion Cyclotron Resonant Diffusion	
TH/P6-09	Zonca, Fulvio Italy	Theoretical and Numerical Studies of Wavepacket Propagation in Tokamak Plasmas	
TH/P6-10	Zonca, Fulvio Italy	Global Theories of Geodesic Acoustic Modes: Excitation by Energetic Particles and Drift Wave Turbulences	
TH/P6-11	Bonoli, Paul USA	Integrated Plasma Simulation of Lower Hybrid Current Profile Control in Tokamaks	
TH/P6-12	Vdovin, Victor Russian Fed.	Advanced ICRF Scenarios and Antennae for Large Fusion Machines from JET to DEMO	
TH/P6-13	Fukuyama, Atsushi Japan	Kinetic Integrated Modeling of Burning Plasmas in Tokamaks	
TH/P6-14	Lesur, Maxime Korea, Rep.	Subcritical Growth of Coherent Phase-space Structures	
TH/P6-16	Belova, Elena USA	Numerical Simulations of NBI-driven GAE modes in L-mode and H-mode Discharges in NSTX	
TH/P6-17	Bierwage, Andreas Japan	Nonlinear Simulation of Energetic Particle Modes in JT-60U	
TH/P6-18	Popov, Alexey Russian Fed.	Low Threshold Parametric Decay Instabilities at ECRH in Toroidal Devices Leading to Anomalous Absorption Phenomena	

Id	Presenter		Title
TH/P6-19	Spong, Donald	USA	Application and Development of the Gyro-Landau Fluid Model for Energetic-particle Instabilities
TH/P6-20	Todo, Yasushi	Japan	Linear Properties and Nonlinear Frequency Chirping of Energetic Particle Driven Geodesic Acoustic Mode in LHD
TH/P6-21	Di Troia, Claudio	Italy	Simulation of EPM Dynamics in FAST Plasmas Heated by ICRH and NNBI
TH/P6-22	Fu, Guo Yong	USA	Nonlinear Simulations of Beam-driven Geodesic Acoustic Mode in a DIII-D Plasma
TH/P6-23	Chen, Liu	China	Nonlinear Studies of β Induced Alfvén Eigenmode Driven by Energetic Particles in Fusion Plasmas
TH/P6-24	Xiang, Nong	China	PIC Simulations of the Ion Flow Induced by Radio Frequency Waves in Ion Cyclotron Frequency Range
TH/P6-25	Minashin, Pavel	Russian Fed.	Benchmarking of Codes for Spatial Profiles of Electron Cyclotron Losses with Account of Plasma Equilibrium in Tokamak Reactors
TH/P6-26	Gao, Zhe	China	Nonlinear Ponderomotive Forces with the Consideration of the Spatial Variation of Wave Fields during the Resonant Interaction
TH/P6-27	Zhao, Aihui	China	Parameter Study of Parametric Instabilities during Lower Hybrid Waves Injection into Tokamaks
TH/P6-28	Shyshkin, Oleg	Ukraine	Numerical Simulations for Fusion Reactivity Enhancement in D- ³ He and D-T Plasmas due to ³ He and T Minorities Heating
TH/P6-29	Ram, Abhay	USA	Scattering of Radio Frequency Waves by Edge Density Blobs and Fluctuations in Tokamak Plasmas
TH/P6-30	Ganesh, Rajaraman	India	Effect of Microturbulence on the Energetic Ions in Tokamaks

EX/8 and TH/7: 3D Equilibrium & High Beta Physics

Chair: A. Komori (Japan)

Indigo Ball Room (08:30 – 10:15)

Time	Id	Presenter		Title
08:30	EX/8-1	Suzuki, Yasuhiro	Japan	3D Plasma Response to Magnetic Field Structure in the Large Helical Device
08:50	TH/7-1	Cooper, Wilfred	Switzerland	Bifurcated Helical Core Equilibrium States in Tokamaks
09:10	EX/8-2	Ono, Yasushi	Japan	High Power Heating of Magnetic Reconnection for High- β ST formation in TS-3 and UTST ST Merging Experiments
09:30	TH/7-2	Hanson, James	USA	Non-Axisymmetric Equilibrium Reconstruction for Stellarators, Reversed Field Pinches and Tokamaks
09:50	EX/8-3	Gusev, Vasily	Russian Fed.	From Globus-M Results toward Compact Spherical Tokamak with Enhanced Parameters, Globus-M2

FRI

Coffee Break (10:15 – 10:45)**EX/9 and PD: Disruptions & Post-Deadline Papers**

Chair: A. Sen (India)

Indigo Ball Room (10:45 – 12:30)

Time	Id	Presenter		Title
10:45	EX/9-1	Lehnen, Michael	Germany	Impact and Mitigation of Disruptions with the ITER-like Wall in JET
11:05	EX/9-2	Hollmann, Eric	USA	Control and Dissipation of Runaway Electron Beams Created during Rapid Shutdown Experiments in DIII-D
11:25	EX/9-3	Gerhardt, Stefan	USA	Disruptions in the High- β Spherical Torus NSTX
11:45	PD/1-1			TBD
12:05	PD/1-2			TBD

Poster Session: P7*Poster Room: Area F-B (08:30 – 12:30)*

Id	Presenter		Title
TH/5-1	Roach, Colin	UK	Gyrokinetic Instabilities in an Evolving Tokamak H-mode Pedestal
EX/6-1	de la Luna, Elena	EU	The Effect of ELM Mitigation Methods on the Access to High H-mode Confinement ($H_{98} \sim 1$) on JET
TH/5-2Ra	Xia, Tianyang	China	Five-field Peeling-Ballooning Modes Simulation with BOUT++
TH/5-2Rb	Xu, Xueqiao	USA	Theory and Gyro-fluid Simulations of Edge-Localized-Modes
EX/6-2	Baylor, Larry	USA	Experimental Demonstration of High Frequency ELM Pacing by Pellet Injection on DIII-D and Extrapolation to ITER
TH/5-3	Hayashi, Nobuhiko	Japan	Reduction of ELM Energy Loss by Pellet Injection for ELM Pacing
EX/6-3Ra	Xiao, Weiwen	China	ELM Mitigation by Supersonic Molecular Beam Injection: KSTAR and HL-2A Experiments and Theory
EX/6-3Rb	Chen, Chengyuan	China	ELM Mitigation with SMBI & CJI Fuelling in HL-2A H-mode Plasmas
EX/7-1	Kaye, Stanley	USA	The Dependence of H-mode Energy Confinement and Transport on Collisionality in NSTX
TH/6-1	Guttenfelder, Walter	USA	Progress in Simulating Turbulent Electron Thermal Transport in NSTX
TH/6-2	Jhang, Hogun	Korea, Rep.	Role of External Torque and Toroidal Momentum Transport in the Dynamics of Heat Transport in Internal Transport Barriers
TH/6-3	Gusakov, Evgeniy	Russian Fed.	Multi-Scale Drift Turbulence Dynamics in Ohmic Discharge as Measured at the FT-2 Tokamak and Modeled by Full- f Gyrokinetic ELMFIRE code
TH/6-4	Jenko, Frank	Germany	Global Gyrokinetic Simulations of High-performance Discharges in View of ITER
EX/7-2Ra	Zhao, Kaijun	China	New Meso-scale Electric Fluctuations Interacting with Magnetic Islands and Turbulence in Edge Plasmas of HL-2A
EX/7-2Rb	Xu, Min	China	Turbulent Eddy-mediated Particle, Momentum, and Vorticity Transport in the Edge of HL-2A Tokamak Plasma

Id	Presenter		Title
EX/P7-01	Field, Anthony	UK	Characterisation of Ion-scale Turbulence in MAST
EX/P7-02	Ren, Yang	USA	Response of Electron-scale Turbulence and Thermal Transport to Continuous $E \times B$ Shear Ramping-up in NSTX
EX/P7-03	Tanaka, Kenji	Japan	Characteristics of Microturbulence in H-mode Plasma of LHD
EX/P7-04	Kosolapova, Natalia	France	Turbulence Wave Number Spectra Reconstruction from Radial Correlation Reflectometry Data at Tore Supra and FT-2 Tokamaks
EX/P7-05	Yan, Zheng	USA	Relating the L-H Power Threshold Scaling to Edge Turbulence Dynamics
EX/P7-06	McKee, George	USA	Turbulence and Transport Response to Resonant Magnetic Perturbations in ELM-Suppressed Plasmas
EX/P7-07	Dong, Jiaqi	China	Generation of Large Scale Coherent Structures by Turbulence in Edge Plasmas of HL-2A Tokamak
EX/P7-08	Huang, Yuan	China	Investigation of L-I-H Transitions Facilitated by Supersonic Molecular Beam Injection and Pellet Fuelling on the HL-2A Tokamak
EX/P7-09	Holland, Christopher	USA	Validation Studies of Gyrofluid and Gyrokinetic Predictions of Transport and Turbulence Stiffness Using the DIII-D Tokamak
EX/P7-10	Carter, Troy	USA	Studies of Turbulence, Transport and Flow in the Large Plasma Device
EX/P7-11	Liu, Zixi	China	Study of ELMy H-mode Plasmas and BOUT++ Simulation on EAST
EX/P7-12	Vershkov, Vladimir	Russian Fed.	Plasma Diffusion and Turbulence Studies in T-10 Tokamak
EX/P7-13	Shi, Zhongbing	China	Correlations of the Turbulent Structures during Nonlocal Effect Caused by SMBI on the HL-2A Tokamak
EX/P7-14	Wan, Baonian	China	The Observation of Dual-peak Geodesic Acoustic Modes in the Edge Plasma on Tokamaks
EX/P7-16	Canik, John	USA	Edge Plasma Transport and Microstability Analysis with Lithium-coated Plasma-facing Components in NSTX

Id	Presenter		Title
EX/P7-17	Schmitz, Lothar	USA	The Role of Zonal Flows and Predator-Prey Oscillations in the Formation of Core and Edge Transport Barriers
EX/P7-18	Smith, David	USA	Parametric Dependencies of Low- k Turbulence in NSTX H-mode Pedestals
EX/P7-19	Na, Yong-Su	Korea, Rep.	L to H-mode Power Threshold and Confinement Characteristics of H-modes in KSTAR
EX/P7-20	Beurskens, Marc	UK	L-H Power Threshold, Pedestal Stability and Confinement in JET with a Metallic Wall
EX/P7-21	Kubota, Shigeyuki	USA	Evolution of the Turbulence Radial Wavenumber Spectrum near the L-H Transition in NSTX Ohmic Discharges
EX/P7-22	Scannell, Rory	UK	Dynamics of the Plasma Edge during the L-H Transition and H-mode in MAST
EX/P7-23	Kocan, Martin	Germany	Far-reaching Impact of Intermittent Transport across the Scrape-off Layer: Latest Results from ASDEX Upgrade
EX/P7-24	Cheng, Jun	China	Time-resolved Evolution of Low Frequency Electrostatic Fluctuations during Slow L-H Transition at the Boundary Plasma of HL-2A Tokamak
TH/P7-01	Strand, Par	Sweden	Particle Transport in Ion and Electron Scale Turbulence
TH/P7-02	Kosuga, Yusuke	USA	Progress on Theoretical Issues in Modelling Turbulent Transport
TH/P7-03	Holod, Ihor	USA	Gyrokinetic Particle Simulation of Microturbulence in Tokamak Plasmas
TH/P7-04	Anderson, Johan	USA	High Frequency Geodesic Acoustic Modes in Electron Scale Turbulence
TH/P7-05	Janhunen, Salomon	Finland	Gyrokinetic Total Distribution Simulations of Drift-wave Turbulence and Neo-classical Dynamics in Tokamaks with Elmfire
TH/P7-06	Zhu, Jian-Zhou	China	Electrostatic Gyrokinetic Absolute Equilibria: Calculation, Simulation and Physics Relevant to Fusion Plasmas Turbulence
TH/P7-07	Nakata, Motoki	Japan	Plasma Size and Collisionality Scaling of Ion Temperature Gradient Driven Turbulent transport

Id	Presenter	Title
TH/P7-08	Terry, Paul USA	Interaction of Stable Modes and Zonal Flows in ITG Turbulence
TH/P7-09	Sarazin, Yanick France	Towards Turbulence Control via EGAM Excitation & Vorticity Injection
TH/P7-10	Hallatschek, Klaus Germany	Theory of External Geodesic Acoustic Mode Excitation
TH/P7-11	Kim, Chang-Bae Korea, Rep.	Advective Flux in Turbulent Plasmas Due to Noise
TH/P7-12	Hahm, Taik Soo Korea, Rep.	$\mathbf{E} \times \mathbf{B}$ Shear Suppression of Turbulence in Diverted H-mode Plasmas; Role of Edge Magnetic Shear
TH/P7-13	Ku, Seung-Hoe USA	Flux-driven Full- f Gyrokinetic Studies of the Influence of Edge Dynamics in Diverted Geometry on Tokamak Core Confinement
TH/P7-14	Wang, Wei Xing USA	Turbulence Generated Non-inductive Current and Flow Shear Driven Turbulent Transport in Tokamaks
TH/P7-15	Ganesh, Rajaraman India	Steady State Particle-In-Cell Simulations of Microturbulence in Tokamaks
FTP/3-1	Bosch, Hans-Stephan Germany	Technical Challenges in the Construction of the Steady-State Stellarator Wendelstein 7-X
FTP/3-2	Pradhan, Subrata India	SST-1 Tokamak Integration & Commissioning
SEE/1-1	Neilson, George USA	International Perspectives on a Path to MFE DEMO
FTP/3-3	Zohm, Hartmut Germany	On the Physics Guidelines for a Tokamak DEMO
FTP/3-4	Menard, Jonathan USA	Progress on Developing the Spherical Tokamak for Fusion Applications
FTP/3-5	Ruzic, David USA	Lithium-Metal Infused Trenches (LiMIT): A New Way to Remove Divertor Heat Flux
FTP/4-1	Hatano, Yuji Japan	Hydrogen Isotope Trapping at Defects Created with Neutron- and Ion-Irradiation in Tungsten
FTP/4-2	Gilbert, Mark UK	Integrated Computational study of Material Lifetime in a Fusion Reactor Environment
FTP/4-3	Kondo, Hiroo Japan	Initial Results of the Large Liquid Lithium Test Loop for the IFMIF Target

Id	Presenter		Title
FTP/4-4Ra	Rajendraku-mar, Ellappan	India	Status of LLCB TBM R&D Activities in India
FTP/4-4Rb	Aiello, Giacomo	France	Activities on the Helium Cooled Lithium Lead Test Blanket Module for ITER
FTP/4-4Rc	Feng, Kaiming	China	Current Progress of Chinese Solid Breeder TBM
FTP/4-5Ra	Fikar, Jan	Switzerland	Optimisation of a Nanostructured ODS Ferritic Steel Fabrication towards Improvement of its Plasticity
FTP/4-5Rb	Chernov, Viacheslav	Russian Fed.	Low Activation Vanadium Alloys for Fusion Power Reactors — the RF Results
FTP/4-6	Azizov, Englen	Russian Fed.	Development of Magnetic Fusion Neutron Sources and Fusion-Fission Hybrid Systems in Russia
SEE/P7-01	Chang, Hansoo	Korea, Rep.	The Long-term Impact of the Fukushima on the Prospect of the Fusion Power in Korea: TIMES Model Approach for the Electricity Sector
SEE/P7-02	Yamazaki, Kozo	Japan	Economic, CO ₂ Emission and Energy Assessments of Fusion Reactors
FTP/P7-01	Kammash, Terry	USA	Feasibility of a Fusion Hybrid Reactor Based on the Gasdynamic Mirror
FTP/P7-02	Simonen, Thomas	USA	A 14 MeV Fusion Neutron Source for Material and Blanket Development and Fission Fuel Production
FTP/P7-03	Sahin, Sümer	Turkey	Radiation Damage Studies on a Laser Fusion Reactor
FTP/P7-04	Kim, Myung Hyun	Korea, Rep.	A Feasibility Study on a Clean Power Fusion Fission Hybrid Reactor
FTP/P7-05	Şahin, Hacı	Turkey	Neutronic Calculation of Radiation Damage in First Wall of a Fusion-Fission Reactor
FTP/P7-06	Zhou, Zhiwei	China	Neutronic Analysis of a Thorium-uranium Fueled Fusion-fission Hybrid Energy System
FTP/P7-07	Kuteev, Boris	Russian Fed.	Conceptual Design Requirements and Solutions for MW-Range Fusion Neutron Source FNS-ST

Id	Presenter	Title
FTP/P7-08	Kotschenreuther, Mike	Deterministically Safe Highly Sub-Critical Fission-Fusion Hybrid Reactors
FTP/P7-09	Shikama, Tatsuo	Behaviors of Hydrogen Isotopes in Silicon Carbide for Evaluation of Hydrogen Permeability and Retention in Nuclear Fusion Systems
FTP/P7-10	Hino, Tomoaki	Performances of Helium, Neon and Argon Glow Discharges for Reduction of Fuel Hydrogen Retention in Tungsten, Stainless Steel and Graphite
FTP/P7-11	Tran, Minh Quang	Development of W Based Materials for Fusion Power Reactors
FTP/P7-12	Borovikov, Valery	Self-healing of Radiation Damage by Coupled Motion of Grain Boundaries in Tungsten Divertor Plates under Reactor Conditions
FTP/P7-14	Muroga, Takeo	Research on Tritium/Heat Transfer and Irradiation Synergism for First Wall and Blanket in the TITAN Project
FTP/P7-15	Wakai, Eiichi	Development of Small Specimen Test Techniques for the IFMIF Test Cell
FTP/P7-16	Chen, Jiming	Research of Low Activation Structural Material for Fusion Reactor in SWIP
FTP/P7-17	Tanigawa, Hiroyasu	Research and Development Status of Reduced Activation Ferritic/Martensitic Steels Corresponding to DEMO Design Requirement
FTP/P7-18	Troev, Troyo	Simulation of Defects in Fusion Materials Containing Hydrogen and Helium
FTP/P7-19	Fischer, Ulrich	KIT Fusion Neutronics R&D Activities and Related Design Applications
FTP/P7-20	Sakasai, Akira	Manufacturing and Development of JT-60SA Vacuum Vessel and Divertor
FTP/P7-21	Panchapakesan, Srinivasan	Radiological Dose Rate Mapping of D-D/D-T Neutron Generator Facilities
FTP/P7-22	Ide, Shunsuke	Optimization of JT-60SA Plasma Operational Scenario with Capabilities of Installed Actuators
FTP/P7-23	Sharma, Aashoo	SST-1 Magnet System Progress towards Device Assembly
FTP/P7-24	Li, Jiangang	Lessons Learned from EAST's Failures

Id	Presenter		Title
FTP/P7-25	Velasquez, Carlos Eduardo	Brazil	Neutronic Evaluation of a Power Plant Conceptual Study considering Different Modelings
FTP/P7-26	Gryaznevich, Mikhail	UK	First Results from Tests of High Temperature Superconductor Magnets on Tokamak
FTP/P7-27	Uspuras, Eugenijus	Lithuania	Analysis of Consequences in the Loss-of-coolant Accident in Wendelstein 7-X Experimental Nuclear Fusion Facility
FTP/P7-28	Brown, Thomas	USA	Progress in Developing a High-Availability Advanced Tokamak Pilot Plant
FTP/P7-29	Kemp, Richard	UK	Benchmarking Reactor Systems Studies by Comparison of EU and Japanese System Code Results for Different DEMO Concepts
FTP/P7-30	Orsitto, Francesco	Italy	Steady State versus Pulsed Tokamak DEMO
FTP/P7-31	Utoh, Hiroyasu	Japan	Critical Design Factors for Sector Transport Maintenance in DEMO
FTP/P7-32	Asakura, Nobuyuki	Japan	Divertor Design and Physics Issues of Huge Power Handling for SlimCS Demo Reactor
FTP/P7-33	Someya, Youji	Japan	A Feasible DEMO Blanket Concept Based on Water Cooled Solid Breeder
FTP/P7-34	Miyazawa, Junichi	Japan	Multifarious Physics Analyses of the Core Plasma Properties in a Helical DEMO Reactor FFHR-d1
FTP/P7-35	Garofalo, Andrea	USA	A Fast-Track Path to DEMO Enabled by ITER and FNSF-AT
FTP/P7-36	Tanaka, Teruya	Japan	Neutronics Design of Helical Type DEMO Reactor FFHR-d1
FTP/P7-37	Yanagi, Nagato	Japan	Divertor Heat Flux Reduction by Resonant Magnetic Perturbations in the LHD-Type Helical DEMO Reactor

Lunch Break (12:30 – 14:00)

FTP/3 and SEE/1: Fusion Development

Chair: D. Campbell (ITER)

Indigo Ball Room (14:00 – 16:10)

Time	Id	Presenter		Title
14:00	FTP/3-1	Bosch,	Germany	Technical Challenges in the Construction of the Steady-State Stellarator Wendelstein 7-X
14:20	FTP/3-2	Pradhan, Subrata	India	SST-1 Tokamak Integration & Commissioning
14:40	SEE/1-1	Neilson, George	USA	International Perspectives on a Path to a Magnetic Fusion Energy DEMO
15:00	FTP/3-3	Zohm, Hartmut	Germany	On the Physics Guidelines for a Tokamak DEMO
15:20	FTP/3-4	Menard, Jonathan	USA	Progress on Developing the Spherical Tokamak for Fusion Applications
15:40	FTP/3-5	Ruzic, David	USA	Lithium-Metal Infused Trenches: A New Way to Remove Divertor Heat Flux

FRI

Coffee Break (16:10 – 16:40)

FTP/4: Fusion Materials and Neutron Sources

Chair: G. Marbach (France)

Indigo Ball Room (16:40 – 18:45)

Time	Id	Presenter		Title
16:40	FTP/4-1	Hatano, Yuji	Japan	Hydrogen Isotope Trapping at Defects Created with Neutron- and Ion-Irradiation in Tungsten
17:00	FTP/4-2	Gilbert, Mark	UK	Integrated Computational study of Material Lifetime in a Fusion Reactor Environment
17:20	FTP/4-3	Kondo, Hiroo	Japan	Initial Results of the Large Liquid Lithium Test Loop for the IFMIF Target
17:40	FTP/4-4Ra	Rajendrakumar, Ellappan	India	Status of LLCB TBM R Activities in India
	FTP/4-4Rb			Activities on the Helium Cooled Lithium Lead Test Blanket Module for ITE
	FTP/4-4Rc			Current Progress of Chinese Solid Breeder TBM
18:00	FTP/4-5Ra	Fikar, Jan	Switzerland	Optimisation of a Nanostructured ODS Ferritic Steel Fabrication towards Improvement of its Plasticity
	FTP/4-5Rb			Low Activation Vanadium Alloys for Fusion Power Reactors — the RF Results
18:20	FTP/4-6	Azizov, Englen	Russian Fed.	Development of Magnetic Fusion Neutron Sources and Fusion-Fission Hybrid Systems in Russia

Poster Session: P8*Poster Room: Area F-B (14:00 – 18:45)*

Id	Presenter		Title
EX/8-1	Suzuki, Yasuhiro	Japan	3D Plasma Response to Magnetic Field Structure in the Large Helical Device
TH/7-1	Cooper, Wilfred	Switzerland	Bifurcated Helical Core Equilibrium States in Tokamaks
EX/8-2	Ono, Yasushi	Japan	High Power Heating of Magnetic Reconnection for High- β ST formation in TS-3 and UTST ST Merging Experiments
TH/7-2	Hanson, James	USA	Non-Axisymmetric Equilibrium Reconstruction for Stellarators, Reversed Field Pinches and Tokamaks
EX/8-3	Gusev, Vasily	Russian Fed.	From Globus-M Results toward Compact Spherical Tokamak with Enhanced Parameters, Globus-M2
EX/9-1	Lehnen, Michael	Germany	Impact and Mitigation of Disruptions with the ITER-like Wall in JET
EX/9-2	Hollmann, Eric	USA	Control and Dissipation of Runaway Electron Beams Created during Rapid Shutdown Experiments in DIII-D
EX/9-3	Gerhardt, Stefan	USA	Disruptions in the High- β Spherical Torus NSTX
EX/10-1	Inagaki, Shigeru	Japan	Is Turbulence Determined by Local Temperature Gradient?
EX/10-2	Estrada, Teresa	Spain	Spatiotemporal Structure of the Turbulence-flow Interaction at the L-H Transition in TJ-II Plasma
TH/8-1	Watanabe, Tomo-Hiko	Japan	Turbulence Spectra, Transport, and $E \times B$ Flows in Helical Plasmas
TH/8-2	Staebler, Gary	USA	A New Paradigm for $E \times B$ Velocity Shear Suppression of Gyro-kinetic Turbulence and the Momentum Pinch
EX/10-3	Tynan, George	USA	Zonal Flows as the Trigger Event for the L-H Transition
EX/11-1	Xu, Guosheng	China	Evidence of Zonal-Flow-Driven Limit-Cycle Oscillations during L-H Transition and at H-mode Pedestal of a New Small-ELM Regime in EAST
ICC/1-1Ra	Jarboe, Thomas	USA	Progress on HIT-SI and Imposed Dynamo Current Drive

Id	Presenter		Title
ICC/1-1Rb	Nagata, Masayoshi	Japan	Flow and Magnetic Field Profiles in the HIST Spherical Torus Plasmas Sustained by Double Pulsing Coaxial Helicity Injection
ICC/P8-01	Bellan, Paul	USA	Dynamics of Open-field-line MHD Experimental Configurations and Theoretical Investigation of Action Integrals as Effective Hamiltonians
ICC/P8-02	Saitoh, Haruhiko	Japan	Observation of Magnetic Fluctuations and Disruption of Magnetospheric Plasma in RT-1
EX/11-2	Maingi, Rajesh	USA	The Nearly Continuous Improvement of Discharge Characteristics and Edge Stability with Increasing Lithium Coatings in NSTX
EX/11-3	Park, Hyeon Keo	Korea, Rep.	Visualization of ELM Dynamics and its Response from External Perturbations via 2D Electron Cyclotron Emission Imaging in KSTAR
EX/11-4	Groebner, Richard	USA	Improved Understanding of Physics Processes in Pedestal Structure, Leading to Improved Predictive Capability for ITER
EX/P8-01	Khorshid, Pejman	Iran	Overview of Resonant Helical Magnetic Field Experiments on the IR-T1 Tokamak
EX/P8-02	Vianello, Nicola	Italy	3D Effects on RFX-mod Helical Boundary Region
EX/P8-03	Pucella, Gianluca	Italy	Density Limit Experiments on FTU
EX/P8-04	Murari, Andrea	Italy	Latest Developments in Data Analysis Tools for Disruption Prediction and for the Exploration of Multimachine Operational Spaces
EX/P8-05	Plyusnin, Vladislav	Portugal	Latest Progress in Studies of Runaway Electrons in JET
EX/P8-06	Saint-Laurent, François	France	Overview of Runaway Electrons Control and Mitigation Experiments on Tore Supra and Lessons Learned in View of ITER
EX/P8-07	Berkery, John	USA	Global Mode Control and Stabilization for Disruption Avoidance in High- β NSTX Plasmas

Id	Presenter		Title
EX/P8-08	Volpe, Francesco	USA	Stabilization of Disruptive Locked Modes by Magnetic Perturbations and Electron Cyclotron Current Drive at DIII-D
EX/P8-09	Granetz, Robert	USA	Disruption Mitigation Experiments with Two Gas Jets on Alcator C-Mod
EX/P8-10	Nagasaki, Kazunobu	Japan	Stabilization of Energetic-Ion-Driven MHD Mode by ECCD in Heliotron J
EX/P8-11	Seol, Jaechun	Korea, Rep.	Effects of RF-Heating Induced MHD Activities on the Toroidal Rotation in Tokamaks
EX/P8-12	Pautasso, Gabriella	Germany	Towards the Density Required for Runaway Electron Suppression in ITER
EX/P8-13	Na, Yong-Su	Korea, Rep.	Experiment for Stabilization of Tearing Mode in KSTAR
EX/P8-14	Kim, Junghee	Korea, Rep.	The Effect of Toroidal Plasma Rotation on Sawtooth Activity in KSTAR
EX/P8-15	Duan, Xuru	China	Study of Runaway Electron Generation in Synergetic ECRH & SMBI Plasma and during Major Disruptions in the HL-2A Tokamak
PD/1-1			TBD
PD/1-2			TBD
PD/P8-01			TBD
PD/P8-02			TBD
PD/P8-03			TBD

EX/10 and TH/8: Turbulence, Zonal Flows & GAMs

Chair: B. Blackwell (Australia)

Indigo Ball Room (08:30 – 10:15)

Time	Id	Presenter		Title
08:30	EX/10-1	Inagaki, Shigeru	Japan	Is Turbulence Determined by Local Temperature Gradient?
08:50	EX/10-2	Estrada, Teresa	Spain	Spatiotemporal Structure of the Turbulence-flow Interaction at the L–H Transition in TJ–II Plasma
09:10	TH/8-1	Watanabe, Tomo-Hiko	Japan	Turbulence Spectra, Transport, and $E \times B$ Flows in Helical Plasmas
09:30	TH/8-2	Staebler, Gary	USA	A New Paradigm for $E \times B$ Velocity Shear Suppression of Gyro-kinetic Turbulence and the Momentum Pinch
09:50	EX/10-3	Tynan, George	USA	Zonal Flows as the Trigger Event for the L–H Transition

SAT

Coffee Break (10:15 – 10:45)

EX/11 and ICC/1: Turbulence, Innovative Confinement Concepts & ELMs
 Chair: J. Herrera-Velázquez (Mexico) *Indigo Ball Room (10:45 – 12:30)*

Time	Id	Presenter		Title
10:45	EX/11-1	Xu, Guosheng	China	Evidence of Zonal-Flow-Driven Limit-Cycle Oscillations during L-H Transition and at H-mode Pedestal of a New Small-ELM Regime in EAST
11:05	ICC/1-1Ra ICC/1-1Rb	Jarboe, Thomas	USA	Progress on HIT-SI and Imposed Dynamo Current Drive Flow and Magnetic Field Profiles in the HIST Spherical Torus Plasmas Sustained by Double Pulsing Coaxial Helicity Injection
11:25	EX/11-2	Maingi, Rajesh	USA	The Nearly Continuous Improvement of Discharge Characteristics and Edge Stability with Increasing Lithium Coatings in NSTX
11:45	EX/11-3	Park, Hyeon Keo	Korea, Rep.	Visualization of ELM Dynamics and its Response from External Perturbations via 2D Electron Cyclotron Emission Imaging in KSTAR
12:05	EX/11-4	Groebner, Richard	USA	Improved Understanding of Physics Processes in Pedestal Structure, Leading to Improved Predictive Capability for ITER

SAT

Lunch Break (12:30 – 14:00)

S/1: Summary

Chair: G.S. Lee (Korea, Rep.)

Indigo Ball Room (14:00 – 16:10)

Time	Id	Presenter		Title
14:00	S/1-0	IAEA Representative & Prize Winners	IAEA	Nuclear Fusion Prize Winners' Statements
14:20	S/1-1	Morris, William	UK	Summary EX/C and ICC
14:50	S/1-2	Yamada, Hiroshi	Japan	Summary EX/S, EX/W and EX/D
15:20	S/1-3	Hahm, Taik Soo	Korea, Rep.	Summary Theory

SAT

Coffee Break (16:10 – 16:40)**S/2: Summary**

Chair: P. Thomas (ITER)

Indigo Ball Room (16:40–18:00)

Time	Id	Presenter		Title
16:30	S/2-1	Hinkel, Denise	USA	Summary Inertial Fusion Experiments and Theory
17:00	S/2-2	Milora, Stanley	USA	Summary FTP, ITR and SEE
17:30	S/2-3	IAEA Representative	IAEA	Closing

Contents

Conference Secretariat	iii
FEC Programme Committee	vi
List of Contributions	vii
Explanation of Abbreviations	vii
Floor Plan: Sunday & Monday	viii
Floor Plan: Tuesday to Saturday	ix
Overview Timetable	x
Programme	xi
Sunday October 7, 2012	xi
Monday October 8, 2012	xii
Tuesday October 9, 2012	xvi
Wednesday October 10, 2012	xxviii
Thursday October 11, 2012	xl
Friday October 12, 2012	lv
Saturday October 13, 2012	lxviii
OV: Overviews	1
OV/1-1 D. N. Hill	
DIII-D Overview — Research Toward Resolving Key Issues for ITER and Steady-State Tokamaks	2
OV/1-2 O. Motojima	
The Status of the ITER Project	3
OV/1-3 F. Romanelli	
Overview of the JET Results with the ITER-like Wall	4
OV/1-4 E. Moses	
The National Ignition Campaign: Status and Progress	5
OV/2-1 O. Kaneko	
Extension of Operation Regimes and Investigation of Three-dimensional Current-less Plasmas in the Large Helical Device	6
OV/2-2 U. Stroth	
Overview of ASDEX Upgrade Results	7
OV/2-3 M. Greenwald	
Overview of Experimental Results and Code Validation Activities at Al- cator C-Mod	8
OV/2-4 J. G. Kwak	
Overview of KSTAR Results	9
OV/2-5 B. Wan	
Progress of Long Pulse and H-mode Experiments on EAST	10

OV/3-1	S. A. Sabbagh	
	Overview of Physics Results from the National Spherical Torus Experiment	11
OV/3-2	H. Meyer	
	Overview of Physics Results from MAST towards ITER/DEMO and the Upgrade	12
OV/3-3	X. Duan	
	Overview of HL-2A Recent Experiments	13
OV/3-4	K. Ida	
	Towards an Emerging Understanding of Nonlocal Transport	14
OV/4-1	Y. Kamada	
	Progress of the JT-60SA Project	15
OV/4-2	H. Azechi	
	Present Status of Fast Ignition Realization EXperiment and Inertial Fusion Energy Development	16
OV/4-3	S. Sharapov	
	Energetic Particle Instabilities in Fusion Plasmas	17
OV/4-4	S. Coda	
	Overview of Recent and Current Research on the TCV Tokamak	19
OV/4-5	A. Becoulet	
	Science and Technology Research & Development in Support to ITER and the Broader Approach	20
OV/5-1	J. Sanchez	
	Dynamics of Flows and Confinement in the TJ-II Stellarator	21
OV/5-2Ra	J. Sarff	
	Overview of Results from the MST Reversed Field Pinch Experiment	22
OV/5-2Rb	P. Martin	
	Overview of the RFX Fusion Science Program	23
OV/5-3	R. Betti	
	Theory of Ignition, Burn and Hydro-equivalency for Inertial Confinement Fusion Implosions	24
OV/5-4	S. Zinkle	
	Multimodal Options for Materials Research to Advance the Basis for Fusion Energy in the ITER Era	25
OV/P-01	P. Buratti	
	Overview of FTU Results	26
OV/P-02	B. Coppi	
	New Developments, Plasma Physics Regimes and Issues for the Ignitor Experiment	27
OV/P-03	P. H. Diamond	
	On the Physics of Intrinsic Torque in Toroidal Plasmas	28
OV/P-05	N. Nakajima	
	Overview of IFERC Project in Broader Approach Activities	29
OV/P-06	G. Zhuang	
	The Recent Research Work on the J-TEXT Tokamak	30
OV/P-07	E. Kruglyakov	
	Fusion Prospects of Axisymmetric Magnetic Mirror Systems	31

OV/P-08 H. J. Fernandes	
20 Years of ISTTOK Tokamak Scientific Activity	32
EX: Magnetic Confinement Experiments	33
EX/1-1 E. Joffrin	
Scenarios Development at JET with the New ITER-like Wall	34
EX/1-2 B. Duval	
Real time ELM, NTM and Sawtooth Control on TCV	35
EX/1-3 A. Hubbard	
Progress in Performance and Understanding of Steady ELM-free I-modes on Alcator C-Mod	36
EX/1-4 J. Stober	
Dominant ECR Heating of H-mode Plasmas on ASDEX Upgrade Using the Upgraded ECRH System and Comparison to Dominant NBI or ICR Heating	37
EX/1-5 C. T. Holcomb	
Fully Noninductive Scenario Development in DIII-D Using New Off-Axis Neutral Beam Injection	38
EX/2-1 R. McDermott	
Connections Between Intrinsic Toroidal Rotation, Density Peaking and Plasma Turbulence Regimes in ASDEX Upgrade	39
EX/2-2 J. Rice	
A Unified Explanation of Rotation Reversals, Confinement Saturation and Non-Diffusive Heat Transport in C-Mod Ohmic Plasmas	40
EX/2-3 Y. Shi	
ECRH Effects on Toroidal Rotation: KSTAR Experiments and Gyroki- netic Simulations of Intrinsic Torque at ITG-TEM Transitions	41
EX/2-4 H. Urano	
Dependence of Heat Transport and Confinement on Isotopic Composition in Conventional H-mode Plasmas in JT-60U	42
EX/2-5 H. Takahashi	
Extension of Operational Regime in High-Temperature Plasmas and the Dynamic-Transport Characteristics in the LHD	43
EX/3-1 M. R. Wade	
Advances in the Physics Understanding of ELM Suppression Using Reso- nant Magnetic Perturbations in DIII-D	44
EX/3-2 A. Kirk	
Understanding ELM Mitigation by Resonant Magnetic Perturbations on MAST	45
EX/3-3 Y. M. Jeon	
ELM Control in Application of Non-Axisymmetric Magnetic Perturbations in KSTAR	46
EX/3-4 W. Suttrop	
Mitigation of Edge Localised Modes with Small Non-axisymmetric Mag- netic Perturbations in ASDEX Upgrade	47

EX/4-1	S. Brezinsek	
	Fuel Retention Studies with the ITER-like Wall in JET	48
EX/4-2	P. C. de Vries	
	Comparison of Plasma Breakdown with a Carbon and ITER-like Wall . .	49
EX/4-3	M. L. Mayoral	
	On the Challenge of Plasma Heating with the JET Metallic Wall	50
EX/4-4	M. Kobayashi	
	Control of 3D Edge Radiation Structure with Resonant Magnetic Pertur- bation Fields Applied to Stochastic Layer and Stabilization of Radiative Divertor Plasma in LHD	51
EX/5-1	G. Matsunaga	
	Dynamics of Energetic Particle Driven Modes and MHD Modes in Wall- stabilized High- β Plasmas on JT-60U and DIII-D	52
EX/5-2	S. Yamamoto	
	Studies of Energetic-ion-driven MHD Instabilities in Helical Plasmas with Low Magnetic Shear	53
EX/5-3	W. Chen	
	Observation of GAM Induced by Energetic Electrons and NL Interactions among GAM, BAEs and Tearing Modes on the HL-2A Tokamak	54
EX/6-1	E. de la Luna	
	The Effect of ELM Mitigation Methods on the Access to High H-mode Confinement ($H_{98} \sim 1$) on JET	55
EX/6-2	L. R. Baylor	
	Experimental Demonstration of High Frequency ELM Pacing by Pellet Injection on DIII-D and Extrapolation to ITER	56
EX/6-3Ra	W. W. Xiao	
	ELM Mitigation by Supersonic Molecular Beam Injection: KSTAR and HL-2A Experiments and Theory	57
EX/6-3Rb	C. Y. Chen	
	ELM Mitigation with SMBI & CJI Fuelling in HL-2A H-mode Plasmas .	58
EX/7-1	S. M. Kaye	
	The Dependence of H-mode Energy Confinement and Transport on Col- lisionality in NSTX	59
EX/7-2Ra	K. J. Zhao	
	New Meso-scale Electric Fluctuations Interacting with Magnetic Islands and Turbulence in Edge Plasmas of HL-2A	60
EX/7-2Rb	M. Xu	
	Turbulent Eddy-mediated Particle, Momentum, and Vorticity Transport in the Edge of HL-2A Tokamak Plasma	61
EX/8-1	Y. Suzuki	
	3D Plasma Response to Magnetic Field Structure in the Large Helical Device	62
EX/8-2	Y. Ono	
	High Power Heating of Magnetic Reconnection for High-Beta ST formation in TS-3 and UTST ST Merging Experiments	63

EX/8-3	V. K. Gusev	
	From Globus-M Results Toward Compact Spherical Tokamak with Enhanced Parameters, Globus-M2	64
EX/9-1	M. Lehnen	
	Impact and Mitigation of Disruptions with the ITER-like Wall in JET	65
EX/9-2	E. M. Hollmann	
	Control and Dissipation of Runaway Electron Beams Created during Rapid Shutdown Experiments in DIII-D	66
EX/9-3	S. P. Gerhardt	
	Disruptions in the High- β Spherical Torus NSTX	67
EX/10-1	S. Inagaki	
	Is Turbulence Determined by Local Temperature Gradient?	68
EX/10-2	T. Estrada	
	Spatiotemporal Structure of the Turbulence-flow Interaction at the L-H Transition in TJ-II Plasma	69
EX/10-3	G. Tynan	
	Zonal Flows as the Trigger Event for the L-H Transition	70
EX/11-1	G. Xu	
	Evidence of Zonal-Flow-Driven Limit-Cycle Oscillations during L-H Transition and at H-mode Pedestal of a New Small-ELM Regime in EAST	71
EX/11-2	R. Maingi	
	The Nearly Continuous Improvement of Discharge Characteristics and Edge Stability with Increasing Lithium Coatings in NSTX	72
EX/11-3	H. K. Park	
	Visualization of ELM Dynamics and its Response from External Perturbations via 2D Electron Cyclotron Emission Imaging in KSTAR	73
EX/11-4	R. Groebner	
	Improved Understanding of Physics Processes in Pedestal Structure, Leading to Improved Predictive Capability for ITER	74
EX/P2-01	W. M. Solomon	
	Access and Sustained High Performance in Advanced Inductive Discharges with ITER-Relevant Low Torque	75
EX/P2-02	C. Kessel	
	ITER Demonstration Discharges on Alcator C-Mod in Support of ITER	76
EX/P2-03	J. Schweinzer	
	Overview of ASDEX Upgrade “Improved H-mode” Scenario Developments	77
EX/P2-04	Y. Ma	
	Study of H-mode Access in the Alcator C-Mod Tokamak: Density, Toroidal Field and Divertor Geometry Dependence	78
EX/P2-05	A. Sun	
	Toroidal Rotation in L-I-H Confinement Transition in HL-2A Experiments	79
EX/P2-06	X. Gong	
	Integrated Operation Scenarios for Long Pulse Discharges in EAST	80
EX/P2-07	Y. S. Park	
	Investigation of Plasma Rotation Alteration and MHD Stability in the Expanded H-mode Operation of KSTAR	81

EX/P2-08	G. L. Jackson	
	Long-pulse Stability Limits of ITER Baseline Scenario Plasmas in DIII-D	82
EX/P2-09	J. E. Barton	
	First-Principles Model-based Closed-loop Control of the Current Profile Dynamic Evolution on DIII-D	83
EX/P2-10	R. Raman	
	Non-inductive Plasma Start-up in NSTX Using Transient CHI	84
EX/P2-11	Y. Takase	
	Non-inductive Plasma Initiation and Plasma Current Ramp-up on the TST-2 Spherical Tokamak	85
EX/P2-12	T. Mutoh	
	Steady State Operation Using Improved ICH and ECH for High Perfor- mance Plasma in LHD	86
EX/P2-13	J. M. Park	
	Validation of Off-axis Neutral Beam Current Drive Physics in the DIII-D Tokamak	87
EX/P2-14	H. Zushi	
	Non-inductive Current Start-up and Plasma Equilibrium with an Inboard Poloidal Field Null by Means of Electron Cyclotron Waves in QUEST	88
EX/P2-15	X. Song	
	ECRH Pre-ionization and Assisted Startup in HL-2A Tokamaks	89
EX/P2-16	S. Shiraiwa	
	Progress toward Steady-state Regimes in Alcator C-Mod	90
EX/P2-17	S. Kulkarni	
	Resonant and Non-resonant type Pre-ionization and Current Ramp-up Experiments on Tokamak ADITYA in the Ion Cyclotron Frequency Range	91
EX/P3-01	M. Reinke	
	Poloidal Variation of High-Z Impurity Density due to Hydrogen Minority ICRH on Alcator C-Mod	92
EX/P3-02	M. Podesta	
	Measurements of Core Lithium Concentration in Diverted H-Mode Plas- mas of NSTX	93
EX/P3-03	M. Yoshikawa	
	Potential Fluctuation Study from the Core Plasma to End Region in the GAMMA 10 Tandem Mirror	94
EX/P3-04	L. Carraro	
	High Current Plasmas in RFX-mod Reversed Field Pinch	95
EX/P3-05	N. Kirneva	
	Experimental Investigation of Plasma Confinement in Reactor Relevant Conditions in TCV Plasmas with Dominant Electron Heating	96
EX/P3-06	B. Zurro	
	Suprathermal Ion Studies in ECRH and NBI Phases of the TJ-II Stellarator	97
EX/P3-07	T. Mizuuchi	
	Study of Fueling Control for Confinement Experiments in Heliotron J	98
EX/P3-08	W. X. Ding	
	Magnetic Fluctuation-Driven Intrinsic Flow in a Toroidal Plasma	99

EX/P3-09	H. J. Sun	Understanding the Dynamics of Cold Pulse Nonlocality Phenomena	100
EX/P3-10	V. Trukhin	Collisionality Dependence of Confinement in T-10 L-Mode Plasmas	101
EX/P3-11	M. Valisa	The Value of Flexibility: the Contribution of RFX to the International TOKAMAK and STELLARATOR Programme	102
EX/P3-12	F. Felici	Real-time Model-based Reconstruction and Control of Tokamak Plasma Profiles	103
EX/P3-13	M. Porkolab	Turbulent Transport and Gyrokinetic Analysis in Alcator C-Mod Ohmic Plasmas	104
EX/P3-14	A. Dinklage	Inter-Machine Validation Study of Neoclassical Transport Modelling in Medium-to High-Density Stellarator-Heliotron Plasmas	105
EX/P3-15	T. Pütterich	Tungsten Screening and Impurity Control in JET	106
EX/P3-16	J. Anderson	Classical Confinement of Impurity Ions and NBI-born Fast Ions in the Reversed Field Pinch	107
EX/P3-17	D. Den Hartog	Measurement and Simulation of Electron Thermal Transport in the MST Reversed-Field Pinch	108
EX/P3-18	T. C. Luce	Experimental Tests of Stiffness in the Electron and Ion Energy Transport in the DIII-D Tokamak	109
EX/P3-19	B. Grierson	Measurement of Deuterium Ion Toroidal Rotation and Comparison to Neo- classical Theory in the DIII-D Tokamak	110
EX/P3-20	W. Zhong	Observation of ELM-Free H-Mode in the HL-2A Tokamak	111
EX/P3-21	Z. Cui	Enhancement of Edge Impurity Transport with ECRH in HL-2A Tokamak	112
EX/P3-22	C. Hidalgo	Dynamical Coupling Between Gradients and Transport in Tokamaks and Stellarators	113
EX/P3-23	N. Howard	Quantitative Comparison of Experimental and Gyrokinetic Simulated ICRH and I_p Dependent Impurity Transport	114
EX/P3-24	S. Ding	Observation of Electron Energy Pinch in HT-7 ICRF Heated Plasmas . .	115
EX/P3-25	X. Gao	Survey of Density Modulation Experiments on the HT-7 Tokamak	116

EX/P3-26	E. J. Doyle	Particle Transport Results from Collisionality Scans and Perturbative Experiments on DIII-D	117
EX/P3-27	S. Kitajima	Transition of Poloidal Viscosity by Electrode Biasing in the Large Helical Device	118
EX/P3-28	C. Fiore	Production of Internal Transport Barriers by Intrinsic Flow Drive in Alcator C-Mod	119
EX/P3-29	A. Burdakov	Experiments on GOL-3 Multiple Mirror Trap for Fusion Program	120
EX/P3-30	D. T. Anderson	Comparison of Plasma Flows and Currents in HSX to Neoclassical Theory	121
EX/P3-31	M. F. Nave	Scalings of Spontaneous Rotation in the JET Tokamak	122
EX/P3-32	S. G. Lee	Toroidal Rotation Characteristics in KSTAR Plasmas	123
EX/P3-33	G. Verdoolaege	Modeling Fusion Data in Probabilistic Metric Spaces for the Identification of Confinement Regimes and Scaling Laws	124
EX/P3-34	F. Scotti	Study of Carbon and Lithium Neoclassical Impurity Transport in ELM-Free H-Mode Discharges in NSTX	125
EX/P3-35	B. Ling	Development of Microwave Diagnostics in EAST Tokamak	126
EX/P4-01	P. Lang	Pellet Induced High Density Phases during ELM Suppression in ASDEX Upgrade	127
EX/P4-02	P. A. Schneider	Analysis of Temperature and Density Pedestal in a Multi-machine Database	128
EX/P4-03	F. Ryter	L-H Transition, Pedestal Development and I-mode Studies in the ASDEX Upgrade Tokamak	129
EX/P4-04	A. Diallo	The Evolution of the Edge Pedestal Structure and Turbulence Spatial Scale during the ELM Cycle on NSTX	130
EX/P4-05	N. Yan	Observation of Current Structures at Type-III ELM Onset on EAST . . .	131
EX/P4-06	H. Wang	New Edge Localized Modes at Marginal Input Power with Dominant RF-heating and Lithium-wall Conditioning in EAST	132
EX/P4-07	I. Classen	Characterization of Temperature Fluctuations during Type-I and Type-II Edge Localized Modes at ASDEX Upgrade	133

EX/P4-08	K. H. Burrell	Reactor-relevant Quiescent H-mode Operation Using Torque from Non-axisymmetric, Non-resonant Magnetic Fields	134
EX/P4-09	H. Reimerdes	Rotation Braking and Error Field Correction of the Test Blanket Module Induced Magnetic Field Error in ITER	135
EX/P4-10	K. Toi	Mitigation of Large Amplitude Edge-Localized-Modes by Resonant Magnetic Perturbations on the Large Helical Device	136
EX/P4-11	D. Yu	Study of the High-efficiency Fuelling Features of Supersonic Molecular Beam Injection on HL-2A Tokamak	137
EX/P4-12	J. G. Bak	ELM and Pedestal Structure Studies in KSTAR H-mode Plasmas	138
EX/P4-13	M. Jakubowski	Influence of the Resonant Magnetic Perturbations on Particle Transport in LHD	139
EX/P4-14	L. F. Delgado-Aparicio	On the Formation and Stability of Impurity-generated “Snakes” in Alcator C-Mod	140
EX/P4-15	J. Hughes	Pedestal Stability and Transport on the Alcator C-Mod Tokamak: Experiments in Support of Developing Predictive Capability	141
EX/P4-17	S. Ohshima	Edge Plasma Response to Beam-driven MHD Instability in Heliotron J	142
EX/P4-18	D. López-Bruna	MHD Events and Transport Barriers in TJ-II Plasmas	143
EX/P4-19	J. Levesque	High Resolution Detection and 3D Magnetic Control of the Helical Boundary of a Wall-Stabilized Tokamak Plasma	144
EX/P4-20	S. Nowak	Control of Sawteeth Periods by Pulsed ECH and ECCD in FTU Tokamak	145
EX/P4-21	L. Frassinetti	Experimental Studies of the Plasma Response to Applied Nonaxisymmetric External Magnetic Perturbations in EXTRAP T2R	146
EX/P4-22	Y. Lin	Characterization of Neo-classical Tearing Modes in High-performance I-Mode Plasmas with ICRF Mode Conversion Flow Drive on Alcator C-Mod	147
EX/P4-23	Y. Liang	Mitigation of Type-I ELMs with $n = 2$ Fields on JET	148
EX/P4-24	S. Masamune	Direct Observation of Soft-X Ray Filament Structure and High Current Operation in Low-Aspect-Ratio RFP	149
EX/P4-25	X. Ji	Triggering of Neoclassical Tearing Modes by Mode Coupling in HL-2A	150

EX/P4-26	C. Xiao	
	Modification of Toroidal Flow in the STOR-M Tokamak	151
EX/P4-27	J. Hanson	
	Probing Resistive Wall Mode Stability Using Off-axis NBI	152
EX/P4-28	E. Kolemen	
	Vertical Stability of NSTX and NSTX-U	153
EX/P4-29	Y. Huang	
	Perturbation Features of Intrinsic and Pellet Induced ELMs on HL-2A . .	154
EX/P4-30	S. Sakakibara	
	Response of MHD Stability to Resonant Magnetic Perturbation in the Large Helical Device	155
EX/P4-31	R. J. Buttery	
	Addressing New Challenges for Error Field Correction	156
EX/P4-32	E. Lazzaro	
	Triggerless Onset and Effect of “Natural” Rotation on Neoclassical Tearing Modes in the TCV Tokamak	157
EX/P4-33	J. K. Park	
	Observation of Edge Harmonic Oscillation in NSTX and Theoretical Study of its Active Control Using HHFW Antenna at Audio Frequencies	158
EX/P4-34	P. Savrukhin	
	Fast-scale Magnetic Perturbations and Onset of the Energy Quench during Disruption Instability in the T-10 tokamak	159
EX/P4-35	J. A. Romero	
	Current Profile Control Using the Ohmic Heating Coil in TCV	160
EX/P4-36	A. Redd	
	Local Helicity Injection Startup and Edge Stability Studies in the Pegasus Toroidal Experiment	161
EX/P5-01	M. E. Puiatti	
	Wall Conditioning and Density Control in the Reversed Field Pinch RFX- mod	162
EX/P5-02	L. Zhang	
	Effect of Lithium Coating on Edge Particle Recycling in EAST H-mode Discharge	163
EX/P5-03	G. Wright	
	Assessment of Tungsten Nano-tendril Growth in the Alcator C-Mod Divertor	164
EX/P5-04	J. W. Coenen	
	Longterm Evolution of the Impurity Composition and Transient Impurity Events with the ITER-like Wall at JET	165
EX/P5-05	G. van Rooij	
	Characterization of Tungsten Sputtering in the JET Divertor	166
EX/P5-06	S. Takamura	
	Cooling Characteristics and Mitigation of He-Defected Tungsten with Nanos- tructure Formation	167
EX/P5-07	E. Tsitrone	
	In Vessel Fuel Inventory Build-up in Tokamaks: Lessons Learnt from Tore Supra	168

EX/P5-08	S. Kajita	
	Impact of Arcing on Carbon and Tungsten: from the Observations in JT-60U, LHD, and NAGDIS-II	169
EX/P5-09	D. Douai	
	Overview of the International Research on Ion Cyclotron Wall Conditioning	170
EX/P5-10	M. Rubel	
	Efficiency of Fuel Removal: Overview of Techniques Tested on Plasma-Facing Components from the TEXTOR Tokamak	171
EX/P5-11	D. L. Rudakov	
	Measurements of Net versus Gross Erosion of Molybdenum Divertor Surface in DIII-D	172
EX/P5-12	T. W. Petrie	
	Effect of Changes in Separatrix Magnetic Geometry on Divertor Behavior in DIII-D	173
EX/P5-13	L. Wang	
	Characterization of Particle and Power Loads on Divertor Targets for Type-I, Type-III, and Mossy ELMy H-modes in EAST Superconducting Tokamak	174
EX/P5-14	V. P. Philipps	
	Development of Laser Based Techniques for In-situ Characterization of the First Wall in ITER and Future Fusion Devices	175
EX/P5-15	H. Guo	
	Approaches towards Steady-State Advanced Divertor Operations on EAST by Active Control of Plasma-Wall Interactions	176
EX/P5-16	M. A. Makowski	
	Scaling of the Divertor Heat Flux Width in the DIII-D Tokamak	177
EX/P5-17	G. Fishpool	
	MAST Contributions to the Exhaust Challenge, Including Testing of Super-X	178
EX/P5-18	S. Morita	
	Low Concentration of Iron as First Wall Material in LHD Plasmas with Edge Ergodic Layer	179
EX/P5-19	V. Bobkov	
	ICRF Operation with Improved Antennas in a Full W-wall ASDEX Upgrade, Status and Developments	180
EX/P5-21	V. Soukhanovskii	
	Snowflake Divertor as Plasma-Material Interface for Future High Power Density Fusion Devices	181
EX/P5-22	W. A. J. Vijvers	
	Reduction of Peak Wall Power Loads in L- and H-mode Tokamak Plasmas in TCV with the Snowflake Divertor	182
EX/P5-23	M. Koubiti	
	Improvement of the Spectroscopic Investigation of Pellet Ablation Clouds	183
EX/P5-24	P. Mertens	
	Power Handling of the Tungsten Divertor in JET	184

EX/P5-25	S. Mirnov	
	Recent achievements of the T-11M lithium program	185
EX/P5-26	P. Monier-Garbet	
	Tore Supra Contribution to Experimental Prediction of the Power Flux to the Limiter in the ITER Start-up Mode	186
EX/P5-27	T. Gray	
	The Effects of Increasing Lithium Deposition on the Power Exhaust Chan- nel in NSTX	187
EX/P5-28	D. Battaglia	
	Dependence of the L-H Power Threshold on X-point Geometry	188
EX/P5-29	T. Morisaki	
	First Results of Closed Helical Divertor Experiment in LHD	189
EX/P5-30	C. Giroud	
	Nitrogen Seeding for Heat Load Control in JET ELMy H-mode Plasmas and its Compatibility with ILW Materials	190
EX/P5-31	M. Jaworski	
	Liquid Lithium Divertor Characteristics and Plasma-Material Interactions in NSTX High-Performance Plasmas	191
EX/P5-32	K. Koga	
	Control of Dust Flux in LHD and in a Divertor Simulator	192
EX/P5-33	J. W. Ahn	
	Toroidal Asymmetry of Divertor Heat Deposition during the ELM and 3-D Field Application in NSTX	193
EX/P5-34	M. Wischmeier	
	Symmetries and Asymmetries in the Divertor Detachment in ASDEX Up- grade	194
EX/P5-35	J. W. Juhn	
	A Global Particle-balance Model for Wall Interaction Analysis Associated with Open- and Closed-loop Density Control Experiments in KSTAR . . .	195
EX/P5-36	F. Tabares	
	Studies of Plasma-Lithium Interactions in TJ-II	196
EX/P5-37	G. Arnoux	
	Scrape-off Layer Properties of ITER-like Limiter Start-up Plasmas at JET	197
EX/P5-38	L. Marrelli	
	Development of MHD Active Control in the RFX-mod RFP	198
EX/P5-39	J. Terry	
	The Fine-scale Structure of the Radial Electric Field in the Scrape-Off- Layer during ICRF Heating in Alcator C-Mod	199
EX/P5-40	R. Perkins	
	Fast Wave Power Flow along SOL Field Lines in NSTX	200
EX/P6-01	B. Chapman	
	Direct Diagnosis and Parametric Dependence of 3D Helical Equilibrium in the MST RFP	201
EX/P6-02	N. Crocker	
	Internal Amplitude, Structure and Identification of CAEs and GAEs in NSTX	202

EX/P6-03	M. Garcia-Munoz	Fast-ion Redistribution and Loss due to Edge Perturbations in the ASDEX Upgrade, DIII-D and KSTAR Tokamaks	203
EX/P6-04	C. Sozzi	First Operations of the Real-Time ECRH/ECCD System for Control of Magnetohydrodynamics Instabilities in the FTU Tokamak	204
EX/P6-05	E. Fredrickson	Fast-ion Energy Loss during TAE Avalanches in the National Spherical Torus Experiment	205
EX/P6-06	M. Turnyanskiy	Measurement and Optimisation of the Fast Ion Distribution on MAST . .	206
EX/P6-07	Z. O. Guimarães-Filho	Electron Fishbones in LHCD Plasmas on FTU and Tore Supra	207
EX/P6-08	T. Goodman	Development of Electron Cyclotron Wave Absorption Measurement for Real-Time Polarization Optimization and Studies of Quasilinear Effects .	208
EX/P6-09	M. J. Hole	Analysis of Alfvén Wave Activity in KSTAR Plasmas	209
EX/P6-10	T. Hoang	Physics and Technology in the Ion-cyclotron Range of Frequency on Tore Supra and TITAN Test Facility: Implication for ITER	210
EX/P6-11	S. Lebedev	Study of Fast Ion Confinement in the TUMAN-3M	211
EX/P6-12	W. Deng	Investigation of the Role of Energetic Particle in the Driving of Long-lived Saturated Internal Mode on HL-2A Tokamak	212
EX/P6-13	Y. Liu	Nonlinear Features of the Alfvénic Wave-particle Interaction in Auxiliary Heated HL-2A Plasma	213
EX/P6-14	L. Yu	Frequency Jump Phenomena of e -Fishbone during High Power ECRH on HL-2A Tokamak	214
EX/P6-15	X. Ding	Coexistence of Alfvénic Modes Induced by Energetic Electrons with ECRH on HL-2A	215
EX/P6-16	Y. Yoshimura	Electron Bernstein Wave Heating and Electron Cyclotron Current Drive by Use of Upgraded ECH System in LHD	216
EX/P6-17	H. Idei	Electron Bernstein Wave Heating and Current Drive Effects in QUEST .	217
EX/P6-18	M. Uchida	Noninductive Formation of Spherical Tokamak at $7\times$ the Plasma Cutoff Density by Electron Bernstein Wave Heating and Current Drive on LATE	218
EX/P6-19	B. Lu	Plasma Rotation Behavior under Lower Hybrid Current Drive and Ion Cyclotron Range of Frequency Heating on EAST	219

EX/P6-20	M. Ichimura	
	Coupling of ICRF Waves and Axial Transport of High-Energy Ions Owing to Spontaneously Excited Waves in the GAMMA 10 Tandem Mirror . . .	220
EX/P6-21	B. Ding	
	Investigations of LHW-plasma Coupling and Current Drive in H-mode Experiments in EAST	221
EX/P6-22	W. W. Heidbrink	
	Fast Ion Physics Enabled by Off-Axis Neutral Beam Injection	222
EX/P6-23	B. Blackwell	
	MHD Activity in the Alfvén Range of Frequencies in the H-1NF Helic . .	223
EX/P6-24	J. Hillairet	
	Recent Progress on Lower Hybrid Current Drive and Implications for ITER	224
EX/P6-25	C. Qin	
	Recent Results from Ion Cyclotron Resonance Heating Experiments in HT-7 and EAST Tokamak	225
EX/P6-26	Y. Tan	
	Experimental Study of Low Frequency Wave Current Drive in the SUNIST Spherical Tokamak	226
EX/P6-27	S. H. Kim	
	Analysis of High Energy Neutral Particles Measured by CNPA and Comparison with Synthesized Fast Neutral Spectrum Based on TRANSP/FIDA for the NB Heated Plasmas in KSTAR	227
EX/P6-28	A. Fasoli	
	Basic Investigations of Electrostatic Turbulence and its Interaction with Plasma and Suprathermal Ions in a Simple Magnetized Toroidal Plasma .	228
EX/P6-29	R. Cesario	
	Spectral Broadening and Lower Hybrid Current Drive in High Density Tokamak Plasmas	229
EX/P7-01	A. Field	
	Characterisation of Ion-scale Turbulence in MAST	230
EX/P7-02	Y. Ren	
	Response of Electron-scale Turbulence and Thermal Transport to Continuous $\mathbf{E} \times \mathbf{B}$ Shear Ramping-up in NSTX	231
EX/P7-03	K. Tanaka	
	Characteristics of Microturbulence in H-mode Plasma of LHD	232
EX/P7-04	N. Kosolapova	
	Turbulence Wave Number Spectra Reconstruction from Radial Correlation Reflectometry Data at Tore Supra and FT-2 Tokamaks	233
EX/P7-05	Z. Yan	
	Relating the L-H Power Threshold Scaling to Edge Turbulence Dynamics	234
EX/P7-06	G. R. McKee	
	Turbulence and Transport Response to Resonant Magnetic Perturbations in ELM-Suppressed Plasmas	235
EX/P7-07	J. Dong	
	Generation of Large Scale Coherent Structures by Turbulence in Edge Plasmas of HL-2A Tokamak	236

EX/P7-08	C. Liu	Investigation of L-I-H Transitions Facilitated by Supersonic Molecular Beam Injection and Pellet Fuelling on the HL-2A Tokamak	237
EX/P7-09	C. Holland	Validation Studies of Gyrofluid and Gyrokinetic Predictions of Transport and Turbulence Stiffness Using the DIII-D Tokamak	238
EX/P7-10	T. Carter	Studies of Turbulence, Transport and Flow in the Large Plasma Device . .	239
EX/P7-11	Z. Liu	Study of ELMy H-mode Plasmas and BOUT++ Simulation on EAST . .	240
EX/P7-12	V. Vershkov	Plasma Diffusion and Turbulence Studies in T-10 Tokamak	241
EX/P7-13	Z. Shi	Correlations of the Turbulent Structures during Nonlocal Effect Caused by SMBI on the HL-2A Tokamak	242
EX/P7-14	D. Kong	The Observation of Dual-peak Geodesic Acoustic Modes in the Edge Plasma on Tokamaks	243
EX/P7-16	J. Canik	Edge Plasma Transport and Microstability Analysis with Lithium-coated Plasma-facing Components in NSTX	244
EX/P7-17	L. Schmitz	The Role of Zonal Flows and Predator-Prey Oscillations in the Formation of Core and Edge Transport Barriers	245
EX/P7-18	D. Smith	Parametric Dependencies of Low- k Turbulence in NSTX H-mode Pedestals	246
EX/P7-19	H. S. Kim	L to H-mode Power Threshold and Confinement Characteristics of H-modes in KSTAR	247
EX/P7-20	M. Beurskens	L-H Power Threshold, Pedestal Stability and Confinement in JET with a Metallic Wall	248
EX/P7-21	S. Kubota	Evolution of the Turbulence Radial Wavenumber Spectrum near the L-H Transition in NSTX Ohmic Discharges	249
EX/P7-22	R. Scannell	Dynamics of the Plasma Edge during the L-H Transition and H-mode in MAST	250
EX/P7-23	M. Kocan	Far-reaching Impact of Intermittent Transport across the Scrape-off Layer: Latest Results from ASDEX Upgrade	251
EX/P7-24	J. Cheng	Time-resolved Evolution of Low Frequency Electrostatic Fluctuations during Slow L-H Transition at the Boundary Plasma of HL-2A Tokamak . .	252

EX/P8-01	P. Khorshid	
	Overview of Resonant Helical Magnetic Field Experiments on the IR-T1 Tokamak	253
EX/P8-02	N. Vianello	
	3D Effects on RFX-mod Helical Boundary Region	254
EX/P8-03	G. Pucella	
	Density Limit Experiments on FTU	255
EX/P8-04	A. Murari	
	Latest Developments in Data Analysis Tools for Disruption Prediction and for the Exploration of Multimachine Operational Spaces	256
EX/P8-05	V. V. Plyusnin	
	Latest Progress in Studies of Runaway Electrons in JET	257
EX/P8-06	F. Saint-Laurent	
	Overview of Runaway Electrons Control and Mitigation Experiments on Tore Supra and Lessons Learned in View of ITER	258
EX/P8-07	J. Berkery	
	Global Mode Control and Stabilization for Disruption Avoidance in High- β NSTX Plasmas	259
EX/P8-08	F. A. Volpe	
	Stabilization of Disruptive Locked Modes by Magnetic Perturbations and Electron Cyclotron Current Drive at DIII-D	260
EX/P8-09	R. Granetz	
	Disruption Mitigation Experiments with Two Gas Jets on Alcator C-Mod	261
EX/P8-10	K. Nagasaki	
	Stabilization of Energetic-Ion-Driven MHD Mode by ECCD in Heliotron J	262
EX/P8-11	J. Seol	
	Effects of RF-Heating Induced MHD Activities on the Toroidal Rotation in Tokamaks	263
EX/P8-12	G. Pautasso	
	Towards the Density Required for Runaway Electron Suppression in ITER	264
EX/P8-13	K. Kim	
	Experiment for Stabilization of Tearing Mode in KSTAR	265
EX/P8-14	J. Kim	
	The Effect of Toroidal Plasma Rotation on Sawtooth Activity in KSTAR	266
EX/P8-15	Y. Zhang	
	Study of Runaway Electron Generation in Synergetic ECRH & SMBI Plasma and during Major Disruptions in the HL-2A Tokamak	267
TH: Magnetic Confinement Theory and Modelling		269
TH/1-1	S. Murakami	
	Study of Toroidal Flow Generation by the ICRF Minority Heating in the Alcator C-Mod Plasma	270
TH/2-1	M. Becoulet	
	Non-linear MHD Modelling of Rotating Plasma Response to Resonant Magnetic Perturbations	271

TH/3-1	M. Groth	
	Impact of Carbon and Tungsten as Divertor Materials on the Scrape-off Layer Conditions in JET	272
TH/3-2	S. Krasheninnikov	
	On Edge Plasma, First Wall, and Dust Issues in Fusion Devices	273
TH/4-1	H. Berk	
	Energetic Particle Long Range Frequency Sweeping and Quasilinear Relaxation	274
TH/4-2	F. Zonca	
	Nonlinear Excitations of Zonal Structures by Toroidal Alfvén Eigenmodes	275
TH/5-1	C. Roach	
	Gyrokinetic Instabilities in an Evolving Tokamak H-mode Pedestal	276
TH/5-2Ra	T. Xia	
	Five-field Peeling-Ballooning Modes Simulation with BOUT++	277
TH/5-2Rb	X. Xu	
	Theory and Gyro-fluid Simulations of Edge-Localized-Modes	278
TH/5-3	N. Hayashi	
	Reduction of ELM Energy Loss by Pellet Injection for ELM Pacing	279
TH/6-1	W. Guttenfelder	
	Progress in Simulating Turbulent Electron Thermal Transport in NSTX .	280
TH/6-2	H. Jhang	
	Role of External Torque and Toroidal Momentum Transport in the Dynamics of Heat Transport in Internal Transport Barriers	281
TH/6-3	E. Gusakov	
	Multi-Scale Drift Turbulence Dynamics in Ohmic Discharge as Measured at the FT-2 Tokamak and Modeled by Full- f Gyrokinetic ELMFIRE-code	282
TH/6-4	F. Jenko	
	Global Gyrokinetic Simulations of High-performance Discharges in View of ITER	283
TH/7-1	W. Cooper	
	Bifurcated Helical Core Equilibrium States in Tokamaks	284
TH/7-2	J. Hanson	
	Non-Axisymmetric Equilibrium Reconstruction for Stellarators, Reversed Field Pinches and Tokamaks	285
TH/8-1	T. H. Watanabe	
	Turbulence Spectra, Transport, and $E \times B$ Flows in Helical Plasmas . . .	286
TH/8-2	G. M. Staebler	
	A New Paradigm for $E \times B$ Velocity Shear Suppression of Gyro-kinetic Turbulence and the Momentum Pinch	287
TH/P2-01	D. Kalupin	
	The European Transport Solver: an Integrated Approach for Transport Simulations in the Plasma Core	288
TH/P2-02	U. Shumlak	
	Progress in the Plasma Science and Innovation Center	289

TH/P2-03	G. Giruzzi	
	Model Validation and Integrated Modelling Simulations for the JT-60SA Tokamak	290
TH/P2-04	H. Mynick	
	Turbulent Optimization in Stellarators & Tokamaks via Shaping	291
TH/P2-05	X. Litaudon	
	Modelling of Hybrid Scenario: from Present-day Experiments toward ITER	292
TH/P2-06	F. Spineanu	
	The Role of Convective Structures in the Poloidal and Toroidal Rotation in Tokamak	293
TH/P2-08	A. Kritz	
	Fusion Power Production in Baseline ITER H-Mode Discharges	294
TH/P2-09	L. Wang	
	New Results in the Theory of Non-Diffusive Heat Transport and Anomalous Electron-Ion Energy Coupling	295
TH/P2-10	D. Carmody	
	Microtearing Mode Fluctuations in Reversed Field Pinch Plasmas	296
TH/P2-11	V. Leonov	
	Tokamak Discharges with Electron Thermal Conductivity Closed to the Neoclassical One	297
TH/P2-12	Ö. Gürçan	
	Indications of Nonlocality of Plasma Turbulence	298
TH/P2-13	T. Rafiq	
	Physics Basis and Validation of MMM7.1 Anomalous Transport Module	299
TH/P2-14	M. Honda	
	Predictive Transport Simulations Consistent with Rotation and Radial Electric Field Using TOPICS with OFMC	300
TH/P2-15	V. Yavorskiy	
	Impact of Fusion Alpha Driven Current on the Magnetic Configuration of a Tokamak	301
TH/P2-16	S. Cappello	
	Nonlinear Modeling for Helical Configurations in Toroidal Pinch Systems	302
TH/P2-17	H. Weisen	
	Non-diffusive Momentum Transport in JET H-mode Regimes: Modeling and Experiment	303
TH/P2-18	D. Escande	
	New Technique for the Calculation of Transport Profiles in Modulation Experiments	304
TH/P2-19	Q. Gao	
	Evolution of Ion Heat Diffusivity and Toroidal Momentum Diffusivity during Spontaneous ITB Development in HL-2A	305
TH/P2-21	C. Angioni	
	Progress in the Theoretical Description and the Experimental Characterization of Impurity Transport at ASDEX Upgrade	306

TH/P2-22	S. Toda	Transport Analysis of Oscillatory State for Plasma Dynamics in Helical Plasmas	307
TH/P2-23	A. Ishizawa	Turbulent Transport due to Kinetic Ballooning Modes in High- β Toroidal Plasmas	308
TH/P2-24	S. Satake	Drift-kinetic Simulation Studies on Neoclassical Toroidal Viscosity in Tokamaks with Small Magnetic Perturbations	309
TH/P2-25	G. Falchetto	The European Integrated Tokamak Modelling Effort: Achievements and First Physics Results	310
TH/P2-26	B. Coppi	Advanced Confinement Regimes and Their Signatures	311
TH/P2-27	K. Kim	Study of Neoclassical Toroidal Viscosity in Tokamaks with a δf Particle Code and Resonant Nature of Magnetic Braking	312
TH/P2-28	J. Herrera-Velázquez	Use of the 3D-MAPTOR Code in the Study of Magnetic Surfaces Break-up due to External Non-Axisymmetric Coils	313
TH/P2-29	D. del-Castillo-Negrete	Anisotropic Heat Transport in Integrable and Chaotic 3-D Magnetic Fields	314
TH/P2-30	M. Salewski	Tomography of 2D Velocity-space Distributions from Combined Synthetic Fast-ion Diagnostics at ASDEX Upgrade	315
TH/P3-01	H. Strauss	Sideways Wall Force Produced during Disruptions	316
TH/P3-02	E. Lazarus	An Investigation of Coupling of the Internal Kink Mode to Error Field Correction Coils in Tokamaks	317
TH/P3-03	P. Zhu	Stabilizing Regimes of Edge Current Density for Pedestal Instabilities . . .	318
TH/P3-04	S. C. Jardin	Simulation of Sawteeth and other Global Macroscopic Dynamics of Tokamak Plasmas on the Transport Timescale	319
TH/P3-05	S. Moradi	Impurity Transport due to Electromagnetic Drift Wave Turbulence	320
TH/P3-06	R. Kleiber	Application of Particle-In-Cell Methods for Stellarators	321
TH/P3-07	R. Fitzpatrick	Nonlinear Error-Field Penetration in Low Density Ohmically Heated Tokamak Plasmas	322
TH/P3-08	C. Sovinec	Coupling of Current and Flow Relaxation in Reversed-Field Pinches due to Two-Fluid Effects	323

TH/P3-09	M. Hirota	
	Nonlinear Acceleration Mechanism of Collisionless Magnetic Reconnection	324
TH/P3-10	S. Saarelma	
	Pedestal Modelling Based on Ideal MHD and Gyrokinetic Stability Analyses on JET And ITER Plasmas	325
TH/P3-11	S. Kruger	
	Coupled Simulations of RF Effects on Tearing Modes	326
TH/P3-12	I. Katanuma	
	A Flute Instability in an Open System and the Line Tying Effect on it	327
TH/P3-13	V. A. Izzo	
	Impurity Mixing in Massive-Gas-Injection Simulations of DIII-D	328
TH/P3-14	K. Ichiguchi	
	Multi-Scale MHD Analysis of Heliotron Plasma in Change of Background Field	329
TH/P3-16	V. Pustovitov	
	Rotational Stabilization of the Resistive Wall Modes in Tokamaks	330
TH/P3-17	P. B. Snyder	
	The EPED Pedestal Model: Extensions, Application to ELM-Suppressed Regimes, and ITER Predictions	331
TH/P3-18	Y. Xiao	
	Convective Electron Motion in Low Frequency Collisionless Trapped Electron Turbulence	332
TH/P3-19	J. Shiraishi	
	Stabilization of Resistive Wall Modes by Magnetohydrodynamic Equilibrium Change Induced by Plasma Toroidal Rotation	333
TH/P3-20	A. Sen	
	Tearing Mode Stability in a Toroidally Flowing Plasma	334
TH/P3-21	X. Garbet	
	Interplay between MHD and Particle Transport during Sawteeth	335
TH/P3-22	N. Ivanov	
	Magnetic Island Dynamics under External Magnetic Perturbation in Rotating Resistive Tokamak Plasma	336
TH/P3-23	L. Zheng	
	Behavior of Magnetohydrodynamics Modes of Infernal Type at H-mode Pedestal with Plasma Rotation	337
TH/P3-24	Y. Sun	
	Intrinsic Plasma Rotation Determined by Neoclassical Toroidal Plasma Viscosity in Tokamaks	338
TH/P3-25	M. Sato	
	Characteristics of MHD Stability of High Beta Plasmas in LHD	339
TH/P3-26	N. Mizuguchi	
	Numerical Modeling of Formation of Helical Structures in Reversed-Field-Pinch Plasma	340
TH/P3-27	G. Hao	
	Influence of Off-axis Neutral Beam Injection on Resistive Wall Mode Stability	341

TH/P3-28	L. Zakharov	
	Current Sharing between Plasma and Walls in Tokamak Disruptions . . .	342
TH/P3-29	V. Ilgisonis	
	Continuum Modes of Arbitrary Rotating Tokamak Plasma	343
TH/P3-30	D. Gates	
	On the Origin of Tokamak Density Limit Scalings	344
TH/P3-31	G. Lu	
	Kinetic Shear Alfvén Wave Instability in the Presence of Impurity Ions in Tokamak Plasmas	345
TH/P3-32	H. He	
	Study of Trapped Energetic Electron Driven Fishbone Instability with Second Stable Regime in Tokamak Plasmas	346
TH/P3-34	S. Pinches	
	Development of a Predictive Capability for Fast Ion Behaviour in MAST .	347
TH/P4-01	M. Leconte	
	Impact of Resonant Magnetic Perturbations on Zonal Modes, Drift-Wave Turbulence and the L-H Transition Threshold	348
TH/P4-02	P. H. Diamond	
	Spatio-Temporal Evolution of the L-H and H-L Transitions	349
TH/P4-03	M. A. Dorf	
	Numerical Modeling of Neoclassical Transport and Geodesic Acoustic Mode Relaxation in a Tokamak Edge	350
TH/P4-04	K. C. Shaing	
	Transport Theory for Error Fields and in the Pedestal Region for Tokamaks	351
TH/P4-05	G. Papp	
	Spatio-temporal Distribution of Runaway Electron Wall Loads in ITER due to Resonant Magnetic Perturbations	352
TH/P4-06	E. A. Belli	
	Eulerian Simulations of Neoclassical Flows and Transport in the Tokamak Plasma Edge and Outer Core	353
TH/P4-07	A. Pankin	
	Integrated Approach to the H-mode Pedestal Dynamics: Effects of Bootstrap Current and Resonant Magnetic Perturbations on ELMs	354
TH/P4-08	H. Xiong	
	Rotation Breaking Induced by ELMs on EAST	355
TH/P4-09	G. Fuhr	
	Penetration of Resonant Magnetic Perturbations in Turbulent Edge Plasmas with Transport Barrier	356
TH/P4-10	A. Hakim	
	Integrated Fusion Simulations of Core-Edge-Wall Thermal and Particle Transport Using the FACETS Code	357
TH/P4-11	Y. Moskvitina	
	Modelling of the Effect of Externally Applied Resonant Magnetic Perturbations on α -particle Dynamics in Tokamak Plasmas	358

TH/P4-12	C. S. Chang	
	New Bootstrap Current Formula Valid for Edge Pedestal, and Gyrokinetic Study of its Implication to Pedestal Stability	359
TH/P4-13	A. Aydemir	
	Edge Electric Fields in the Pfirsch-Schlüter Regime and their Effect on the L-H Transition Power Threshold	360
TH/P4-14	P. Ricci	
	Progressive Steps towards Global Validated Simulation of Edge Plasma Turbulence	361
TH/P4-15	P. K. Kaw	
	Theory of Rapid Formation of Pedestal and Pedestal width due to Anomalous Particle Pinch in the Edge of H-mode Discharges	362
TH/P4-16	X. Tang	
	Parallel Transport and Profile of Boundary Plasma with a Low Recycling Wall	363
TH/P4-17	R. Zagorski	
	Simulations with COREDIV Code of DEMO Discharges	364
TH/P4-18	D. Ryutov	
	Theory and Simulations of ELM Control with a Snowflake Divertor	365
TH/P4-19	R. Goldston	
	Drift-based Model for Power Scrape-off Width in Low-Gas-Puff H-mode Plasmas: Theory and Implications	366
TH/P4-20	J. D. Callen	
	RMP-Flutter-Induced Pedestal Plasma Transport	367
TH/P4-21	N. M. Ferraro	
	Edge Plasma Response to Non-Axisymmetric Fields in Tokamaks	368
TH/P4-22	Y. Marandet	
	Coarse Grained Transport Model for Neutrals in Turbulent SOL Plasmas	369
TH/P4-23	J. Myra	
	Edge Sheared Flows and Blob Dynamics	370
TH/P4-24	J. Li	
	Effects of Collisionality on the Nonlinear Characteristics of Boundary Turbulence and Blob/hole Transport in Tokamak Plasmas	371
TH/P4-25	U. Daybelge	
	Spatiotemporal Oscillations in Tokamak Edge Layer and their Generation by Various Mechanisms	372
TH/P4-26	P. Ghendrih	
	Impact on Divertor Operation of the Pattern of Edge and SOL Flows Induced by Particle Sources and Sinks	373
TH/P4-27	P. Cahyna	
	Modelling of Plasma Response to Resonant Magnetic Perturbations and its Influence on Divertor Strike Points	374
TH/P4-28	G. Park	
	Self-consistent Kinetic Simulation of RMP-driven Transport: Collisionality and Rotation Effects on RMP Penetration and Transport	375

TH/P6-01	V. Marchenko	
	Frequency Chirping during a Fishbone Burst	376
TH/P6-02	Y. V. Petrov	
	Finite Orbit Width Features in the CQL3D Code	377
TH/P6-03	G. Vlad	
	Electron Fishbone Simulations in FTU-like Equilibria Using XHMGC . . .	378
TH/P6-04	R. Farengo	
	Alpha Particle Redistribution in Sawteeth	379
TH/P6-05	Y. Peysson	
	Effect of Density Fluctuations on LHCD and ECCD and Implications for ITER	380
TH/P6-06	E. M. Bass	
	Fully Gyrokinetic Modeling of Beam-driven Alfvén Eigenmodes in DIII-D Using GYRO	381
TH/P6-08	R. W. Harvey	
	Differences Between QL and Exact Ion Cyclotron Resonant Diffusion . . .	382
TH/P6-09	Z. Lu	
	Theoretical and Numerical Studies of Wave-packet Propagation in Toka- mak Plasmas	383
TH/P6-10	Z. Qiu	
	Global Theories of Geodesic Acoustic Modes: Excitation by Energetic Particles and Drift Wave Turbulences	384
TH/P6-11	P. Bonoli	
	Integrated Plasma Simulation of Lower Hybrid Current Profile Control in Tokamaks	385
TH/P6-12	V. Vdovin	
	Advanced ICRF Scenarios and Antennae for Large Fusion Machines from JET to DEMO	386
TH/P6-13	A. Fukuyama	
	Kinetic Integrated Modeling of Burning Plasmas in Tokamaks	387
TH/P6-14	M. Lesur	
	Subcritical Growth of Coherent Phase-space Structures	388
TH/P6-16	E. Belova	
	Numerical Simulations of NBI-driven GAE modes in L-mode and H-mode Discharges in NSTX	389
TH/P6-17	A. Bierwage	
	Nonlinear Simulation of Energetic Particle Modes in JT-60U	390
TH/P6-18	A. Popov	
	Low Threshold Parametric Decay Instabilities at ECRH in Toroidal De- vices Leading to Anomalous Absorption Phenomena	391
TH/P6-19	D. Spong	
	Application and Development of the Gyro-Landau Fluid Model for Energetic- particle Instabilities	392
TH/P6-20	H. Wang	
	Linear Properties and Nonlinear Frequency Chirping of Energetic Particle Driven Geodesic Acoustic Mode in LHD	393

TH/P6-21	C. Di Troia	
	Simulation of EPM Dynamics in FAST Plasmas Heated by ICRH and NNBI	394
TH/P6-22	G. Fu	
	Nonlinear Simulations of Beam-driven Geodesic Acoustic Mode in a DIII-D Plasma	395
TH/P6-23	X. Wang	
	Nonlinear Studies of β -Induced Alfvén Eigenmode Driven by Energetic Particles in Fusion Plasmas	396
TH/P6-24	N. Xiang	
	PIC Simulations of the Ion Flow Induced by Radio Frequency Waves in Ion Cyclotron Frequency Range	397
TH/P6-25	A. Kukushkin	
	Benchmarking of Codes for Spatial Profiles of Electron Cyclotron Losses with Account of Plasma Equilibrium in Tokamak Reactors	398
TH/P6-26	Z. Gao	
	Nonlinear Ponderomotive Forces with the Consideration of the Spatial Variation of Wave Fields during the Resonant Interaction	399
TH/P6-27	A. Zhao	
	Parameter Study of Parametric Instabilities during Lower Hybrid Waves Injection into Tokamaks	400
TH/P6-28	O. Shyshkin	
	Numerical Simulations for Fusion Reactivity Enhancement in D- ³ He and D-T Plasmas due to ³ He and T Minorities Heating	401
TH/P6-29	A. Ram	
	Scattering of Radio Frequency Waves by Edge Density Blobs and Fluctuations in Tokamak Plasmas	402
TH/P6-30	J. Chowdhury	
	Effect of Microturbulence on the Energetic Ions in Tokamaks	403
TH/P7-01	A. Skyman	
	Particle Transport in Ion and Electron Scale Turbulence	404
TH/P7-02	Y. Kosuga	
	Progress on Theoretical Issues in Modelling Turbulent Transport	405
TH/P7-03	I. Holod	
	Gyrokinetic Particle Simulation of Microturbulence in Tokamak Plasmas	406
TH/P7-04	J. Anderson	
	High Frequency Geodesic Acoustic Modes in Electron Scale Turbulence	407
TH/P7-05	J. S. Janhunen	
	Gyrokinetic Total Distribution Simulations of Drift-wave Turbulence and Neo-classical Dynamics in Tokamaks with Elmfire	408
TH/P7-06	J. Z. Zhu	
	Electrostatic Gyrokinetic Absolute Equilibria: Calculation, Simulation and Physics Relevant to Fusion Plasmas Turbulence	409
TH/P7-07	M. Nakata	
	Plasma Size and Collisionality Scaling of Ion Temperature Gradient Driven Turbulent transport	410

TH/P7-08	P. Terry	
	Interaction of Stable Modes and Zonal Flows in ITG Turbulence	411
TH/P7-09	Y. Sarazin	
	Towards Turbulence Control via EGAM Excitation & Vorticity Injection .	412
TH/P7-10	K. Hallatschek	
	Theory of External Geodesic Acoustic Mode Excitation	413
TH/P7-11	C.-B. Kim	
	Advective Flux in Turbulent Plasmas Due to Noise	414
TH/P7-12	T. S. Hahm	
	$E \times B$ Shear Suppression of Turbulence in Diverted H-mode Plasmas; Role of Edge Magnetic Shear	415
TH/P7-13	S. H. Ku	
	Flux-driven Full- f Gyrokinetic Studies of the Influence of Edge Dynamics in Diverted Geometry on Tokamak Core Confinement	416
TH/P7-14	W. W. Wang	
	Turbulence Generated Non-inductive Current and Flow Shear Driven Tur- bulent Transport in Tokamaks	417
TH/P7-15	R. Ganesh	
	Steady State Particle-In-Cell Simulations of Microturbulence in Tokamaks	418
FTP: Fusion Technology and Power Plant Design		419
FTP/1-1	S. Wukitch	
	Evaluation of Optimized ICRF and LHRF Antennas in Alcator C-Mod .	420
FTP/1-2	T. Inoue	
	Acceleration of 1 MeV H^- Ion Beams at ITER NB-relevant High Current Density	421
FTP/1-3Rb	K. Kajiwara	
	Progress on the Development of High Power Long Pulse Gyrotron and Related Technologies	422
FTP/2-1Rb	I. M. Ferreira Nunes	
	Be Tile Power Handling and Main Wall Protection	423
FTP/3-1	H.-S. Bosch	
	Technical Challenges in the Construction of the Steady-State Stellarator Wendelstein 7-X	424
FTP/3-2	S. Pradhan	
	SST-1 Tokamak Integration & Commissioning	425
FTP/3-3	H. Zohm	
	On the Physics Guidelines for a Tokamak DEMO	426
FTP/3-4	J. Menard	
	Progress on Developing the Spherical Tokamak for Fusion Applications .	427
FTP/3-5	D. Ruzic	
	Lithium-Metal Infused Trenches: A New Way to Remove Divertor Heat Flux	428
FTP/4-1	Y. Hatano	
	Hydrogen Isotope Trapping at Defects Created with Neutron- and Ion- Irradiation in Tungsten	429

FTP/4-2	M. Gilbert	
	Integrated Computational study of Material Lifetime in a Fusion Reactor Environment	430
FTP/4-3	H. Kondo	
	Initial Results of the Large Liquid Lithium Test Loop for the IFMIF Target	431
FTP/4-4Ra	E. Rajendrakumar	
	Status of LLCB TBM R&D Activities in India	432
FTP/4-4Rb	G. Aiello	
	Activities on the Helium Cooled Lithium Lead Test Blanket Module for ITER	433
FTP/4-4Rc	K. Feng	
	Current Progress of Chinese Solid Breeder TBM	434
FTP/4-5Ra	P. Unifantowicz	
	Optimisation of a Nanostructured ODS Ferritic Steel Fabrication towards Improvement of its Plasticity	435
FTP/4-5Rb	V. Chernov	
	Low Activation Vanadium Alloys for Fusion Power Reactors — the RF Results	436
FTP/4-6	E. Azizov	
	Development of Magnetic Fusion Neutron Sources and Fusion-Fission Hybrid Systems in Russia	437
FTP/P1-01	I. Tazhibayeva	
	Investigation and Testing of KTM Divertor Model on Basis of Lithium CPS	438
FTP/P1-02	J. Lore	
	Heat Flux and Design Calculations for the W7-X Divertor Scraper Element	439
FTP/P1-03	S. H. Hong	
	Temporal and Spatial Evolution of In-vessel Dust Characteristics in KSTAR and Dust Removal Experiments in TReD	440
FTP/P1-04	S. Khirwadkar	
	Tungsten Divertor Target Technology and Test Facilities Development . .	441
FTP/P1-05	A. Kreter	
	Comparative Study of Chemical Methods for Fuel Removal	442
FTP/P1-06	Z. Xu	
	Analysis of Establishment and MHD Stability of a Free Curve-Surface Flow for Liquid Metal PFCs	443
FTP/P1-07	F. Crisanti	
	“Snow Flakes” Divertor and 10 MA Scenarios in FAST	444
FTP/P1-08	V. Chaudhari	
	Preliminary Safety Analysis of the Indian Lead Lithium Cooled Ceramic Breeder Test Blanket Module System in ITER	445
FTP/P1-09	C. Day	
	Technology Gaps for the Fuel Cycle of a Fusion Power Plant	446
FTP/P1-10	Y. Kikuchi	
	Simulation Experiments of ELM-like Transient Heat and Particle Loads using a Magnetized Coaxial Plasma Gun	447

FTP/P1-11	Y. Nakashima	Plasma Characteristics of the End-cell of the GAMMA 10 Tandem Mirror for the Divertor Simulation Experiment	448
FTP/P1-12	X. Liu	Progress of High Heat Flux Component Manufacture and Heat Load Experiments in China	449
FTP/P1-13	G. Zheng	Super-X Divertor Simulation for HCSB-DEMO	450
FTP/P1-14	M. Ono	Recent Progress in the NSTX/NSTX-U Lithium Program and Prospects for Reactor-relevant Liquid-lithium Based Divertor Development	451
FTP/P1-15	H. Uchimura	Effects of the Lithium Concentration on Tritium Release Behaviors from Advanced Tritium Breeding Material $\text{Li}_{2+x}\text{TiO}_3$	452
FTP/P1-16	A. Isayama	Progress in the Development of the ECRF System for JT-60SA	453
FTP/P1-17	U. Fantz	Feasibility and R&D Needs of a Negative Ion Based Neutral Beam System for DEMO	454
FTP/P1-18	M. Hanada	Progress in the Development of Long Pulse Neutral Beam Injectors for JT-60SA	455
FTP/P1-19	R. Fonck	Local Current Injector System for Nonsolenoidal Startup in a Low Aspect Ratio Tokamak	456
FTP/P1-20	R. Minami	Development of MW Gyrotrons for Fusion Devices by University of Tsukuba	457
FTP/P1-21	H. Y. Yang	Status and Plan of the Key Actuators for KSTAR Operation	458
FTP/P1-22	G. Wallace	Advances in Lower Hybrid Current Drive Technology on Alcator C-Mod .	459
FTP/P1-23	R. Wolf	Preparation of Steady State Operation of the Wendelstein 7-X Stellarator	460
FTP/P1-24	T. Minea	3D Particle Simulation of Neutral Beam Injector, from Extraction to Tokamak Injection	461
FTP/P1-25	J. Jeong	ECH-assisted Startup using ITER Prototype of 170 GHz Gyrotron in KSTAR	462
FTP/P1-26	E. Surrey	The Influence on System Design of the Application of Neutral Beam Injection to a Demonstration Fusion Power Plant	463
FTP/P1-27	M. Wendel	Fusion Material Irradiation Test Facility at SNS	464

FTP/P1-28	A. Sergis	Potential for Improvement in High Heat Flux HyperVapotron Element Performance Using Nanofluids	465
FTP/P1-29	P. Bayetti	Overview on CEA Contributions to the Broader Approach Projects	466
FTP/P1-30	C. P. Wong	Fusion Technology Facility — Key Attributes and Interfaces to Technology and Materials	467
FTP/P1-31	I.-N. Bogatu	Plasma Jets for Runaway Electron Beam Suppression	468
FTP/P1-32	M. Salvador	Advances in the Electrical , Control Systems, General Analysis of the Coils Design in the Mexican Tokamak Experimental Facility	469
FTP/P1-33	J. Rapp	An Advanced Plasma-material Test Station for R&D on Materials in a Fusion Environment	470
FTP/P1-34	P. Cara	Overview and Status of the Linear IFMIF Prototype Accelerator	471
FTP/P1-35	R. Heidinger	IFMIF: Overview of the Validation Activities	472
FTP/P7-01	T. Kammash	Feasibility of a Fusion Hybrid Reactor Based on the Gasdynamic Mirror .	473
FTP/P7-02	T. Simonen	A 14 MeV Fusion Neutron Source for Material and Blanket Development and Fission Fuel Production	474
FTP/P7-03	S. Sahin	Radiation Damage Studies on a Laser Fusion Reactor	475
FTP/P7-04	T. Siddique	A Feasibility Study on a Clean Power Fusion Fission Hybrid Reactor . . .	476
FTP/P7-05	H. Şahin	Neutronic Calculation of Radiation Damage in First Wall of a Fusion-Fission Reactor	477
FTP/P7-06	S. Xiao	Neutronic Analysis of a Thorium-uranium Fueled Fusion-fission Hybrid Energy System	478
FTP/P7-07	B. Kuteev	Conceptual Design Requirements and Solutions for MW-Range Fusion Neutron Source FNS-ST	479
FTP/P7-08	M. Kotschenreuther	Deterministically Safe Highly Sub-Critical Fission-Fusion Hybrid Reactors	480
FTP/P7-09	S. Nagata	Behaviors of Hydrogen Isotopes in Silicon Carbide for Evaluation of Hydrogen Permeability and Retention in Nuclear Fusion Systems	481
FTP/P7-10	T. Hino	Performances of Helium, Neon and Argon Glow Discharges for Reduction of Fuel Hydrogen Retention in Tungsten, Stainless Steel and Graphite . .	482

FTP/P7-11	M. Battabyal	
	Development of W Based Materials for Fusion Power Reactors	483
FTP/P7-12	V. Borovikov	
	Self-healing of Radiation Damage by Coupled Motion of Grain Boundaries in Tungsten Divertor Plates under Reactor Conditions	484
FTP/P7-14	T. Muroga	
	Research on Tritium/Heat Transfer and Irradiation Synergism for First Wall and Blanket in the TITAN Project	485
FTP/P7-15	E. Wakai	
	Development of Small Specimen Test Techniques for the IFMIF Test Cell	486
FTP/P7-16	J. Chen	
	Research of Low Activation Structural Material for Fusion Reactor in SWIP	487
FTP/P7-17	H. Tanigawa	
	Research and Development Status of Reduced Activation Ferritic/Mar- tensitic Steels Corresponding to DEMO Design Requirement	488
FTP/P7-18	T. Troev	
	Simulation of Defects in Fusion Materials Containing Hydrogen and Helium	489
FTP/P7-19	U. Fischer	
	KIT Fusion Neutronics R&D Activities and Related Design Applications .	490
FTP/P7-20	A. Sakasai	
	Manufacturing and Development of JT-60SA Vacuum Vessel and Divertor	491
FTP/P7-21	S. Panchapakesan	
	Radiological Dose Rate Mapping of D-D/D-T Neutron Generator Facilities	492
FTP/P7-22	S. Ide	
	Optimization of JT-60SA Plasma Operational Scenario with Capabilities of Installed Actuators	493
FTP/P7-23	A. Sharma	
	SST-1 Magnet System Progress Towards Device Assembly	494
FTP/P7-24	J. Li	
	Lessons Learned from EAST's Failures	495
FTP/P7-25	C. E. Velasquez	
	Neutronic Evaluation of a Power Plant Conceptual Study considering Dif- ferent Modelings	496
FTP/P7-26	M. Gryaznevich	
	First Results from Tests of High Temperature Superconductor Magnets on Tokamak	497
FTP/P7-27	E. Uspuras	
	Analysis of Consequences in the Loss-of-Coolant Accident in Wendelstein 7-X Experimental Nuclear Fusion Facility	498
FTP/P7-28	T. Brown	
	Progress in Developing a High-Availability Advanced Tokamak Pilot Plant	499
FTP/P7-29	R. Kemp	
	Benchmarking Reactor Systems Studies by Comparison of EU and Japanese System Code Results for Different DEMO Concepts	500
FTP/P7-30	F. P. Orsitto	
	Steady State versus Pulsed Tokamak DEMO	501

FTP/P7-31	H. Utoh	
	Critical Design Factors for Sector Transport Maintenance in DEMO . . .	502
FTP/P7-32	N. Asakura	
	Divertor Design and Physics Issues of Huge Power Handling for SlimCS Demo Reactor	503
FTP/P7-33	Y. Someya	
	A Feasible DEMO Blanket Concept Based on Water Cooled Solid Breeder	504
FTP/P7-34	J. Miyazawa	
	Multifarious Physics Analyses of the Core Plasma Properties in a Helical DEMO Reactor FFHR-d1	505
FTP/P7-35	A. M. Garofalo	
	A Fast-Track Path to DEMO Enabled by ITER and FNSF-AT	506
FTP/P7-36	T. Tanaka	
	Neutronics Design of Helical Type DEMO Reactor FFHR-d1	507
FTP/P7-37	N. Yanagi	
	Divertor Heat Flux Reduction by Resonant Magnetic Perturbations in the LHD-Type Helical DEMO Reactor	508
ICC: Innovative Confinement Concepts		509
ICC/1-1Ra	T. Jarboe	
	Progress on HIT-SI and Imposed Dynamo Current Drive	510
ICC/1-1Rb	M. Nagata	
	Flow and Magnetic Field Profiles in the HIST Spherical Torus Plasmas Sustained by Double Pulsing Coaxial Helicity Injection	511
ICC/P1-01	V. B. Minaev	
	Magnetic System for the Upgraded Spherical Tokamak Globus-M2	512
ICC/P3-01	T. Ii	
	Stability and Confinement Improvement of Oblate Field-Reversed Config- uration by Neutral Beam Injection	513
ICC/P3-02	M. Binderbauer	
	A New High Performance Field Reversed Configuration Regime Through Edge Biasing and Neutral Beam Injection	514
ICC/P5-01	R. Majeski	
	Results from LTX with Lithium-Coated Walls	515
ICC/P6-01	E. Kurt	
	The Finite Element Analysis of an Inertial Electrostatic Confinement Unit	516
ICC/P6-02	J. Degnan	
	Recent Magneto — Inertial Fusion Experiments on FRCHX	517
ICC/P8-01	P. Bellan	
	Dynamics of Open-field-line MHD Experimental Configurations and The- oretical Investigation of Action Integrals as Effective Hamiltonians	518
ICC/P8-02	H. Saitoh	
	Observation of Magnetic Fluctuations and Disruption of Magnetospheric Plasma in RT-1	519

IFE: Inertial Fusion Experiments and Theory	521
IFE/1-1 J. Frenje Diagnosing Implosion Performance at the National Ignition Facility by Means of Advanced Neutron-Spectrometry and Neutron-Imaging Techniques	522
IFE/1-2 R. L. McCrory Progress toward Polar-Drive Ignition for the NIF	523
IFE/1-3 H. Shiraga Fast Ignition Integrated Experiments with Gekko-XII and LFEX Lasers .	524
IFE/1-4 J. Sethian Inertial Fusion Energy with Direct Drive and Krypton Fluoride Lasers . .	525
IFE/1-5 J. M. Perlado Approach to Power Plant Physics and Technology in Laser Fusion Energy Systems under Repetitive Operation	526
IFE/P6-01 R. More Particle Simulation of Fusion Ignition	527
IFE/P6-02 Y.-M. Wang Application of Radiative Cooling to ICF Ignition	528
IFE/P6-03 H. Hora Shock Studies in Nonlinear Force Driven Laser Fusion with Ultrahigh Plasma Block Acceleration	529
IFE/P6-04 P. Patel Status of Fast Ignition Point Design	530
IFE/P6-05 H. Nagatomo Computational Study of the Strong Magnetic Field Generation in Non- Spherical Cone-Guided Implosion	531
IFE/P6-06 M. Wei Study of Fast Electron Generation and Transport for Fast Ignition	532
IFE/P6-07 B. Qiao Self-consistent Integrated Modeling for Proton Fast Ignition	533
IFE/P6-08 C. McGuffey Focusing Protons Beams for Fast Ignition	534
IFE/P6-09 R. Khaydarov Improvement of Characteristics of Laser Source of Ions by Changing the Interaction Angle of Laser Radiation	535
IFE/P6-10 C. Li Proton Imaging of Hohlraum Plasma Stagnation in Inertial Confinement Fusion Experiments	536
IFE/P6-11 Y. Arikawa Study on the Energy Transfer Efficiency in the Fast Ignition Experiment .	537
IFE/P6-12 Y. Kitagawa Fast Ignition Scheme Fusion Using High-Repetition-Rate Laser	538
IFE/P6-13 Y. Mori 10-J Green DPSSL-pumped Laser System HAMA for High-repetitive Counter Irradiation Fast Heating Fusion Demonstration	539

IFE/P6-14	H. J. Kong	
	Highly Repetitive Laser Inertial fusion driver with Tiled Coherent Beam Combination Laser using Stimulated Brillouin Scattering Phase Conjugation Mirrors	540
IFE/P6-15	M. Kalal	
	Overview and Latest Proposals in SBS PCM Based IFE Technology Featuring Self-navigation of Lasers on Injected Direct Drive Pellets	541
IFE/P6-16	J. Kwan	
	Summary of Progress in US Heavy Ion Fusion Science Research	542
IFE/P6-17	P. Gourdain	
	Axial Magnetic Field Compression Studies Using Gas Puff Z-pinches and Thin Liners on COBRA	543
IFE/P6-18	A. Iwamoto	
	FIREX Foam Cryogenic Target Development: Attempt of Residual Voids Reduction with Solid Hydrogen Refractive Index Measurement	544
IFE/P6-19	N. B. Alexander	
	Mass-Fabrication of Targets for Inertial Fusion Energy	545
ITR: ITER Activities		547
ITR/1-1	T. Eich	
	Scaling of the Tokamak near Scrape-off Layer H-mode Power Width and Implications for ITER	548
ITR/1-2	A. Loarte	
	Progress on the Application of ELM Control Schemes to ITER	549
ITR/1-3	P. Sonato	
	Design of the MITICA Neutral Beam Injector: From Physics Analysis to Engineering Design	550
ITR/1-4Ra	A. Litvak	
	Development in Russia of Megawatt Power Gyrotrons for Fusion	551
ITR/2-1	D. Johnson	
	ITER Diagnostics — Technology and Integration Challenges	552
ITR/2-2Ra	J.-M. Traverre	
	Imaging Challenges for the ITER Plasma Facing Components Protection	553
ITR/2-3	P. Lorenzetto	
	Technology R&D Activities for the ITER Full-tungsten Divertor	554
ITR/2-4	H. Nakajima	
	ITER Magnet Systems — from Qualification to Full Scale Construction	555
ITR/2-5	P. Bruzzone	
	Test Results of ITER Conductors in the SULTAN Facility	556
ITR/2-6	A. R. Raffray	
	The ITER Blanket System Design Challenge	557
ITR/P1-01	P. Franzen	
	Commissioning and First Results of the ITER-Relevant Negative Ion Beam Test Facility ELISE	558
ITR/P1-02	S. Sato	
	Nuclear Analyses For ITER NB System	559

ITR/P1-03	B. Schunke	Status of the Negative Ion Based Diagnostic Neutral Beam for ITER . . .	560
ITR/P1-04	A. Masiello	EU Development of the ITER Neutral Beam Injector and Test Facility . .	561
ITR/P1-05	K. Takahashi	Development of ITER Equatorial EC Launcher	562
ITR/P1-06	M. Henderson	Optimization of the EC Heating and Current Drive Capabilities	563
ITR/P1-07	P. Dumortier	Validation of the RF Properties and Control of the ITER ICRF Antenna	564
ITR/P1-08	F. Durodié	RF Optimization of the Port Plug Layout and Performance Assessment of the ITER ICRF Antenna	565
ITR/P1-09	A. A. Tuccillo	On the Use of Lower Hybrid Waves at ITER Relevant Density	566
ITR/P1-10	V. Parail	Self-consistent Simulation of Plasma Scenarios for ITER Using a Combi- nation of 1.5 D Transport Codes and Free Boundary Equilibrium Codes .	567
ITR/P1-11	A. C. C. Sips	Demonstrating the ITER Baseline Operation at $q_{95} = 3$	568
ITR/P1-12	I. Bandyopadhyay	Modelling of ITER Plasma Shutdown with Runaway Mitigation Using TSC	569
ITR/P1-13	S. H. Kim	CORSICA Modelling of ITER Hybrid Mode Operation Scenarios	570
ITR/P1-14	M. Sugihara	Disruption Impacts and their Mitigation Target Values	571
ITR/P1-15	T. Casper	Development of ITER Scenarios for Pre-DT Operations	572
ITR/P1-16	M. Cavinato	ITER Plasma Position Control System and Scenario Optimization	573
ITR/P1-17	Y. S. Na	Integrated Modelling of ITER Hybrid Scenarios Including Momentum Transport, NTMs, and ELMs in Preparation for Active Control	574
ITR/P1-18	D. Campbell	Challenges in Burning Plasma Physics: the ITER Research Plan	575
ITR/P1-19	T. Tala	Tokamak Experiments to Study the Parametric Dependences of Momen- tum Transport	576
ITR/P1-20	D. Moreau	Integrated Magnetic and Kinetic Control of Advanced Tokamak Scenarios Based on Data-Driven Models	577
ITR/P1-21	F. Poli	Stability and Performance of ITER Steady State Scenarios with ITBs . .	578
ITR/P1-22	S. Futatani	Non-linear MHD Modelling of ELM Triggering by Pellet Injection in DIII- D and Implications for ITER	579

ITR/P1-23	G. Huijsmans	
	Non-linear MHD Simulation of ELM Energy Deposition	580
ITR/P1-24	O. Schmitz	
	Three-dimensional Fluid Modeling of Plasma Edge Transport and Divertor Fluxes during RMP ELM Control at ITER	581
ITR/P1-25	T. E. Evans	
	3D Vacuum Magnetic Field Modeling of the ITER ELM Control Coils during Standard Operating Scenarios	582
ITR/P1-26	I. Garkusha	
	Analysis of Tungsten Dust Generation under Powerful Plasma Impacts Simulating ITER ELMs and Disruptions	583
ITR/P1-27	A. S. Kukushkin	
	Narrow Heat Flux Widths and Tungsten: SOLPS Studies of the Possible Impact on ITER Divertor Operation	584
ITR/P1-28	A. Kallenbach	
	Multi-machine Comparisons of Divertor Heat Flux Mitigation by Radiative Cooling	585
ITR/P1-29	R. Budny	
	PTRANSP Tests of TGLF and Predictions for ITER	586
ITR/P1-30	C. C. Petty	
	ITER Implications of the Beta Scaling of Energy Confinement	587
ITR/P1-31	I. Chapman	
	Assessing the Power Requirements for Sawtooth Control in ITER through Modelling and Joint Experiments	588
ITR/P1-32	G. J. Kramer	
	Observation of Localized Fast-Ion Induced Heat Loads in Test Blanket Module Simulation Experiments on DIII-D	589
ITR/P1-33	T. Kurki-Suonio	
	Fast Ion Power Loads on ITER First Wall Structures in the Presence of ELM-mitigation Coils and MHD Modes	590
ITR/P1-34	A. Könies	
	Benchmark of Gyrokinetic, Kinetic MHD and Gyrofluid Codes for the Linear Calculation of Fast Particle Driven TAE Dynamics	591
ITR/P1-35	T. Oikawa	
	Effects of ELM Control Coil on Fast Ion Confinement in ITER H-mode Scenarios	592
ITR/P1-36	P. Gohil	
	Assessment of the H-mode Power Threshold Requirements for ITER . . .	593
ITR/P1-37	R. Singh	
	A Model for the Power Required to Access the H-mode in Tokamaks and Projections for ITER	594
ITR/P1-38	S. Kononov	
	Studying the Capabilities of Be Pellet Injection to Mitigate ITER Disrup- tions	595

ITR/P1-39	B. Bazylev	
	Modelling of Material Damage and High Energy Impacts on Tokamak PFCs during Transient Loads	596
ITR/P1-40	A. Sen	
	Control of Major Disruptions in ITER	597
ITR/P5-01	J. W. Sa	
	Progress on Manufacturing of the ITER Vacuum Vessel Equatorial and Lower Ports in Korea	598
ITR/P5-02	J. L. Duchateau	
	Quench Detection in ITER Superconducting Magnet Systems	599
ITR/P5-03	V. Belyakov	
	Simulation of Eddy Current and Electromagnetic Loads in ITER Con- ducting Structures	600
ITR/P5-04	M. Ulrickson	
	Transient Electromagnetic Analysis of the ITER Blanket System	601
ITR/P5-05	K. Matsui	
	Results of ITER TF Coil Sub and Full Scale Trials Performed in Japan	602
ITR/P5-06	Y. Seki	
	Progress of Manufacturing and Quality Testing of the ITER Divertor Outer Vertical Target in Japan	603
ITR/P5-07	X. Courtois	
	Developments Toward Fully Metallic Actively Cooled Plasma Facing Com- ponents for ITER divertor	604
ITR/P5-08	F. Escourbiac	
	Effort on Design of a Full Tungsten Divertor for ITER	605
ITR/P5-09	I. Kupriyanov	
	Experimental Simulation of Beryllium Armour Damage Under ITER-like Intense Transient Plasma Loads	606
ITR/P5-10	P. Li	
	Status & Progress of the R&D Work for ITER Magnet Supports	607
ITR/P5-11	C. Alejaldre	
	Feedback of the Licensing Process of the First Nuclear Installation in Fu- sion, ITER	608
ITR/P5-12	K. Blackler	
	ITER Machine Assembly — Challenges and Progress	609
ITR/P5-14	C. Danani	
	Activation Analyses of Lead Lithium Cooled Ceramic Breeder Test Blan- ket Module in ITER	610
ITR/P5-15	S. S. Atchutuni	
	Preliminary Corrosion Studies on Structural Materials in Lead-Lithium for Indian LLCB TBM	611
ITR/P5-16	D. Panayotov	
	Progress in the EU Test Blanket Systems Safety Studies	612
ITR/P5-18	Y. Zhang	
	Transient Thermal-hydraulic Modeling and Analysis of Chinese HCSB TBM	613

ITR/P5-22	S. Wikman	Experimental Assessment of Materials Exposed to Coolant Water under ITER Relevant Operational Conditions	614
ITR/P5-23	S. Combs	Development and Testing of Plasma Disruption Mitigation Systems Applicable for ITER	615
ITR/P5-24	S. Maruyama	ITER Fuelling and Glow Discharge Cleaning System Overview	616
ITR/P5-25	S. Simrock	Scientific Computing for Real Time Data Processing and Archiving for ITER Operation	617
ITR/P5-26	F. Le Guern	Status of R&D on In-Vessel Dust&Tritium Management in ITER	618
ITR/P5-27	S. Salasca	Challenges of Integrating a Typical Diagnostics Port Plug in ITER	619
ITR/P5-28	R. Feder	Assessing the Nuclear Environment for ITER Port Plugs and Port-based Diagnostics	620
ITR/P5-29	Y. Gribov	Error Fields Expected in ITER and their Correction	621
ITR/P5-30	E. Mukhin	Status of Thomson Scattering in ITER Divertor	622
ITR/P5-31	G. Ambrosino	System-Level Optimization of ITER Magnetic Diagnostics: Preliminary Results	623
ITR/P5-32	V. Mirnov	Electron Kinetic Effects on Interferometry, Polarimetry and Thomson Scattering in Burning Plasmas	624
ITR/P5-33	G. Conway	ITPA Assessment of ITER Microwave Diagnostic Design Issues	625
ITR/P5-34	A. Razdobarin	Mirrors for ITER Optical Diagnostics	626
ITR/P5-35	Y. Kawano	Progress on Design and R&D for ITER Diagnostic Systems in Japan Domestic Agency	627
ITR/P5-36	A. Shevelev	Reconstruction of Distribution Functions of Fast Ions and Runaway Electrons in ITER Plasmas Using Gamma-Ray Spectrometry	628
ITR/P5-37	G. Vayakis	Evolution of the ITER Diagnostic Set Specifications	629
ITR/P5-38	R. Imazawa	Analysis of Current Profile Measurement Capability on ITER	630
ITR/P5-39	D. Gin	ITER High Resolution Gamma Spectrometry	631

ITR/P5-40	H. K. Park	
	Overview of the ITPA R&D Activities for Optimizing ITER Diagnostic Performance	632
ITR/P5-41	V. Udintsev	
	Exploring Measurement Capabilities of ITER ECE System	633
ITR/P5-42	A. Litnovsky	
	First Studies of ITER Diagnostic Mirrors in a Tokamak with All-metal Interior: Results of First Mirror Test in ASDEX Upgrade	634
ITR/P5-43	C. Rotti	
	Exploring the Engineering Performance Limits of DNB	635
ITR/P5-44	A. B. Kukushkin	
	Theoretical Issues of High Resolution H- α Spectroscopy Measurements in ITER	636
SEE: Safety, Environmental and Economic Aspects of Fusion		637
SEE/1-1	G. Neilson	
	International Perspectives on a Path to a Magnetic Fusion Energy DEMO	638
SEE/P7-01	H. Chang	
	The Long-term Impact of the Fukushima on the Prospect of the Fusion Power in Korea: TIMES Model Approach for the Electricity Sector	639
SEE/P7-02	K. Yamazaki	
	Economic, CO ₂ Emission and Energy Assessments of Fusion Reactors . . .	640
Index by contribution number		641
Index by author		645

Overviews



DIII-D Overview — Research Toward Resolving Key Issues for ITER and Steady-State Tokamaks

D. N. Hill¹ and DIII-D Team¹

¹*Lawrence Livermore National Laboratory, Livermore, USA*

Corresponding Author: hilldn@fusion.gat.com

The DIII-D Research Program has made significant advances in the physics understanding of key ITER issues and operating regimes important for ITER and future steady-state fusion tokamaks. Edge localized mode (ELM) suppression with resonant magnetic perturbations (RMP) has been now demonstrated in the ITER baseline scenario at $q_{95} = 3.1$ by controlling the poloidal mode spectrum of $n = 3$ RMP. Temporal modulation of the $n = 2$ and $n = 3$ RMP toroidal phase reveals a complex plasma response that includes an island-like modulation in T_e consistent with recent theory that predicts such island formation can inhibit the pedestal expansion. Pellet pacing experiments with injection geometry similar to that planned for ITER produced a ten-fold increase in the ELM frequency and a strong reduction in ELM divertor energy deposition. Disruption experiments producing reproducible runaway electron beams ($I_{RE} \sim 300$ kA with 300 ms lifetimes) reveal RE dissipation rates $\sim 2\times$ faster than expected and demonstrate the possibility of full RE ramp down with feedback control. Long-duration ELM-free QH-mode discharges have been produced with co-current NBI by using $n = 3$ coils to generate sufficient counter- I_P torque. With electron cyclotron heating, ITER baseline discharges at $\beta_N = 2$ and scaled neutral beam injection torque have been maintained in stationary conditions for more than 4 resistive times. Successful modification of a neutral beam line to provide 5 MW of adjustable off-axis injection has enabled sustained operation at $\beta_N \sim 3$ with minimum safety factors well above 2 accompanied by broader current and pressure profiles than previously observed. With q_{min} above 1.5, stationary discharges with $\beta_N = 3.5$ have been extended to $2\tau_R$, limited only by available beam energy (power and pulse length).

This work was supported by the US Department of Energy under DE-AC52-07NA27344 and DE-FC02-04ER54698.

The Status of the ITER Project

O. Motojima¹

¹ITER Organisation, St-Paul-lez-Durance, France

Corresponding Author: osamu.motojima@iter.org

Over the last 2 years, ITER has made the transition from building up the infrastructure (ITER Organisation (IO) staff, Domestic Agencies (DAs)) and completing the design to become a real project. A new management structure was introduced in 2010 and several new communication channels were established with the DAs. To date 69 Procurement Arrangements have been signed with the DAs, representing 75% of the total value to be procured in kind. Thus, a large percentage of the work is now performed in the DAs and in the industry of the ITER members. The work performed by the IO is changing during this transition to oversight of the work performed in the DAs and industry. A Strategic Management Plan (SMP) is used to status the project performance and to flag issues and delays. With the SMP and the matching Detailed Work Schedule, ITER is now in the position to develop recovery plans and to tackle delays at an early stage.

Construction is progressing rapidly in Cadarache and factories in Members have begun manufacturing the components: Over 4 years, 300 tons of advanced Nb3Sn for the TF coils have been produced; manufacturing facilities for conductors and magnets have been set up; and full-scale TF radial plate, case and sub-scale winding mock-ups have been manufactured, together with relevant mock-ups of the vacuum vessel, divertor and blanket. The base mat and seismic pads on which the tokamak building will rest are under construction; the electrical yard is close to be finished and the ITER HQ building too. A decision has been taken to start operation with an all W divertor. The main technical reason is to learn to deal with the issues of melt layers and potential flaking in the non-nuclear phase of the operation. Elimination of the CFC/W divertor results in a considerable cost saving which is used to pay for deferred items.

ITER is presently well into the construction phase and is facing the problems to be expected in such phases. However, it has a more complex organization and procurement scheme than other large science projects and so the solution of problems tends to be more complicated. The achievements over the last 2 years have shown that an international cooperation such as ITER can work successfully and that it is able to deal with the usual problems which arise in large and technically ambitious construction projects.

OV

Overview of the JET Results with the ITER-like Wall

F. Romanelli¹

¹ *JET-EFDA, Culham Science Centre, Abingdon, UK*

Corresponding Author: francesco.romanelli@jet.efda.org

The JET programme is strongly focussed on the consolidation of the ITER design choices and the preparation of ITER operation. To this aim, during the last two years the materials of the plasma facing components (PFCs) have been replaced with the same combination foreseen in ITER, namely a combination of Be for the main wall and W for the divertor. The installation of the ILW required more than 3000 tiles to be fitted by remote handling manipulators and interfaces. In addition to the new wall, JET has installed several upgrades to active protection systems and diagnostics, vertical stability control and on heating capability with an increase of the routinely-available neutral beam power from 20 MW up to 30 MW. The JET programme in the first set of campaigns after the shutdown was devoted to the development of operational scenarios with the new plasma facing materials and the investigation of the retention properties. In particular, validation of the predictions for ITER in retention levels, breakdown at low voltage, H-mode threshold, confinement level and erosion rates are part of the on-going studies and results obtained so far demonstrate agreement with initial expectations.

OV

The National Ignition Campaign: Status and Progress

E. Moses¹, J. Lindl¹, and NIC Team¹

¹*Lawrence Livermore National Laboratory, Livermore, USA*

Corresponding Author: moses1@llnl.gov

Since the completion of the National Ignition Facility (NIF) construction project in March 2009, a wide variety of experiments have been completed in support of NIF's mission areas: national security, fundamental science, and fusion energy. NIF capabilities and infrastructure are in place with over 50 X-ray, optical and nuclear diagnostic systems and the ability to shoot cryogenic DT layered capsules. NIF, a Nd:Glass laser facility, has operated routinely at 1.45–1.6 MJ of 3ω light with very high reliability since September 2011 and is on track to reach its design goal of 1.8 MJ and 500 TW of ultraviolet light in 2012. The National Ignition Campaign (NIC), an international effort with the goal of demonstrating thermonuclear burn in the laboratory, is making steady progress toward achieving ignition. Experiments in 2011 demonstrated the ability to achieve densities over 500 g/cm² utilizing precision pulse shaping, along with neutron yields within a factor of 5–6 of those required for entering the regime of strong alpha particle heating. Experiments in 2012 are being carried to further optimize this performance. Other experiments have been completed in support of high-energy-density science, materials equation of state, and materials strength. In all cases, records of extreme temperatures and pressures, highest neutron yield and highest energy densities have been achieved. This paper will provide status update of the unprecedented experimental capabilities of the NIF and describe the progress achieved so far on the path toward ignition.

OV

Extension of Operation Regimes and Investigation of Three-dimensional Current-less Plasmas in the Large Helical Device

O. Kaneko¹, LHD Experiment Group¹

¹ *National Institute for Fusion Science, Toki, Japan*

Corresponding Author: kosamu@nifs.ac.jp

Progress in parameter improvement as well as physical understanding of three-dimensional net-current free plasmas in LHD is overviewed.

Efficient ion heating by the upgraded low energy NBI and improvement in ion transport have led to the central ion temperature of 7 keV at the density of $1.5 \times 10^{19} \text{ m}^{-3}$. The pre-wall conditioning by ICRF is effective to achieve high ion temperature. The volume averaged beta value has reached 5.1% and the high beta state over 4.5% has been maintained for longer than 100 energy confinement times. A new dipole antenna has been installed for ICRF heating, which can control toroidal phasing and excite the fast wave with large wavenumbers. It shows better heating efficiency at higher density than the conventional monopole antenna as expected. Two of ten sections of inboard side helical divertor were modified to a baffled structure as a pilot, and neutral compression of more than 10 times was demonstrated, which agrees with the prediction of 3D Monte Carlo simulation.

A resonant magnetic perturbation (RMP) with $m/n = 1/1$, which has resonance at the plasma periphery, has been applied to the experiments of divertor detachment, ELM mitigation and penetration of perturbed field. The RMP has a stabilizing effect on detached plasmas by changing the radiation pattern in the edge. A radiating plasma with reduced divertor heat load by a factor of 3–10 can be sustained stably. The RMP has reduced the ELM amplitude and increased the ELM frequency. It is noted that ELMs of LHD are thought to be induced by interchange modes destabilized at the edge while peeling ballooning modes cause ELMs in tokamaks. Two types of intrinsic toroidal rotation have been identified in LHD. One is intrinsic rotation in the counter direction driven by the positive radial electric field near the plasma periphery, and the other is that in the co-direction driven by the ion temperature gradient at half of the plasma minor radius. The existence of non-linearity in the latter rotation strongly suggests that the driving mechanism is Reynolds stress due to turbulence, not neoclassical viscosity. The dynamic response of micro-turbulence to ECH modulation has been studied in terms of the long distance radial correlation of turbulence, which is expected to be the most possible candidate for causing non-local transport.

Overview of ASDEX Upgrade Results

U. Stroth¹, ASDEX Upgrade Team¹

¹ *Max-Planck-Institut für Plasmaphysik, EURATOM Association, Garching, Germany*

Corresponding Author: stroth@ipp.mpg.de

The medium size divertor tokamak ASDEX Upgrade possesses flexible shaping capability and versatile heating and current drive systems. Recently the technical capabilities were extended by increasing the ECRH power and by installing 2×8 internal magnetic perturbation coils. Using these coils, reliable suppression of large type I ELMs could be demonstrated in a wide operational window, which opens up above a critical plasma density. The edge plasma parameters are little affected. Nevertheless, the ELMs are replaced by repetitive small scale events, which cause lower energy losses but are sufficient to keep the tungsten concentration in the core plasma at a low level. The temperature in the outer divertor rises moderately during ELM mitigation but the inner divertor remains detached at all times. The pellet fuelling efficiency was observed to increase which opened a path to H-mode discharges with peaked density profiles at line densities clearly exceeding the empirical Greenwald limit. With a maximum total heating of 23 MW, high P/R H-modes with moderate divertor peak power loads below 5 MW/m^2 were achieved by feedback-controlled radiation cooling.

Owing to the increased ECRH power to 4 MW, H-mode discharges could be studied in regimes with dominant electron heating and low plasma rotation velocities, i.e., under conditions particularly relevant for ITER. At low densities the roles of electron and ion temperatures in the L-H transition could be disentangled. It is found that transitions appear at a critical value of the ion pressure gradient, pointing to the neoclassical radial electric field and the related flow shear as important parameters for the transition. Reynolds stress as additional source of flow shear was investigated by means of Doppler reflectometry. ECRH was used to shape the electron temperature profile and to switch between ITG and TEM dominated turbulence regimes. The relation of the dominant instability with particle, momentum, ion and electron heat transport was assessed in detail. Using probes in the SOL, for the first time electron temperature fluctuations were measured and excellent agreement of the turbulent statistics with GEMR simulations is found. Using a retarding field analyser, fluctuating and average ion temperatures were measured in the far SOL which allows assessing the power flux on the first wall.

OV

Overview of Experimental Results and Code Validation Activities at Alcator C-Mod

M. Greenwald¹, Alcator C-Mod Team¹

¹MIT, Plasma Science and Fusion Center, Cambridge, USA

Corresponding Author: mjgreen@mit.edu

Recent research on the Alcator C-Mod tokamak has focused on a broad range of scientific issues with particular emphasis on ITER needs and on detailed comparisons between experimental measurements and predictive models. It was possible for the first time to demonstrate quantitative, simultaneous agreement between nonlinear gyrokinetic calculations (GYRO) of impurity transport fluxes and experimental observations for impurity diffusion, convection and ion heat flux. Experiments into self-generated rotation in torque-free C-Mod discharges, found an unexpected connection between momentum and energy transport in which spontaneous flow reversal was observed at a critical density, identical to the transition density between LOC and SOC regimes. It was shown for the first time that ITBs could be created with the aid of self-generated $\mathbf{E} \times \mathbf{B}$ shear flow. Research on ICRF heating focused on understanding and mitigating production of metallic impurities. 3D finite-element antenna modeling predicts significantly reduced parallel electric fields if the antenna were aligned to the total magnetic field. A novel field-aligned antenna has been recently installed and has demonstrated sharply reduced impurity generation. LHCD experiments have shown efficient current drive and creation of electron internal transports barrier via modification of magnetic shear. At higher densities, experiments and modeling with ray tracing and full-wave codes suggest that excessive wave interaction in outer regions of the plasma combined with low single-pass absorption are responsible for markedly lower efficiency. Experiments with I-mode have increased the operating window for this promising ELM-free regime. Extrapolation to ITER suggests that $Q \sim 10$ could be possible in ITER. H-mode studies have measured pedestal widths consistent with KBM-like instabilities, while the pedestal heights quantitatively match the EPED predictions. Investigations into the physics and scaling of the heat-flux footprint showed a scaling proportional to $T_e^{3/2}$. The width was found to be independent of conducted power, B_T or q_{95} and insensitive to the SOL connection length. As at the midplane, I_P is the dominant control parameter. At the same time, heat flux can be reduced to about 10% of the total input power via impurity seeding, while maintaining good H-mode energy confinement even with power close to threshold.

Overview of KSTAR Results

J. G. Kwak¹, KSTAR Team¹

¹*National Fusion Research Institute, Daejeon, Republic of Korea*

Corresponding Author: jgkwak@nfri.re.kr

After the first H-mode discharge in 2010, the H-mode has been sustained longer and the operational regime of plasma parameters has been significantly extended. Due to the proper tuning of equilibrium configuration and plasma control, values of $\beta_N = 1.9$ and $W_{\text{tot}} = 340$ kJ have been achieved with energy confinement time $\tau_E = 171$ ms. Typical H-mode discharges were operated with the plasma current of 600 kA at the toroidal magnetic field $B_T = 2$ T. L-H transition was obtained with 0.8 – 1.5 MW of PNBI in double null (DN) configuration and the H-mode lasted up to 5 sec. The measured power threshold as a function of density shows a roll-over with the minimum value of ~ 0.8 MW at $\bar{n}_e \sim 2 \times 10^{19} \text{ m}^{-3}$. Based on the achievement of high beta H-mode, various methods of ELM control has been implemented including RMP (Resonant Magnetic Perturbation), SMBI (Supersonic Molecular Beam Injection), vertical jogging and ECCD injection on the pedestal.

We observed various ELM responses, i.e., suppression, mitigation and mode locking depending on the relative phases of the IVC coils. During ELMs suppression by 90 degree phase $n = 1$ RMP, ELMs were completely suppressed. ELM pace making by fast vertical jogging of the plasma column has been also demonstrated. A newly installed SMBI system was also utilized for ELM control and a state of mitigated ELMs for a few tens of ELM periods has been sustained by the optimized repetitive SMBI pulses. A simple cellular automata (Sand-pile) model predicts that shallow deposition near the pedestal foot induced small-sized high-frequency ELMs mitigating large natural ELMs. In addition to the ELM control experiments mentioned above, various physics topics were explored focusing on ITER related physics issues such as the intrinsic rotation driven by RF power injection and sawtooth physics in H-mode.

In 2012, goal of the machine performance is the long pulse H-mode over 10 s which would be the first step for validating the physics issues at the normal conductor tokamak.

OV

Progress of Long Pulse and H-mode Experiments on EAST

B. Wan¹, H. Guo¹, Y. Liang¹, G. Xu¹, X. Gong¹, J. Li¹, and EAST Team¹

¹*Institute of Plasma Physics, Chinese Academy of Sciences, Hefei, China*

Corresponding Author: bnwan@ipp.ac.cn

Significant experimental progress has been made since last IAEA FEC towards improved confinement and high plasma performance regimes under long pulse conditions. In particular, the following key results have been achieved with a combination of RF and LHCD under a very low recycling wall condition: 1 MA plasma current, fully steady long pulse diverted plasma entirely driven by LHCD over 100 s, and a new type of stationary H-mode discharges lasted much longer than several ten times the energy confinement time. Experiments have been performed to identify the key role that zonal flows play in mediating the L-H transition and sustaining H-mode confinement. This leads to many new advances in H-mode physics, including the observations of a new limit-cycle oscillation preceding the L-H transition at marginal input power and the kinetic energy transfer between shear flows and ambient turbulences, as well as modulations of a high-frequency broad-band turbulence by oscillating zonal flows in a new small-ELM regime, etc. In addition, clear current filaments have been observed only in the far SOL where the voltage difference of plasma sheath between two divertor plates connected by a filament is large. Furthermore, an initial acceleration of the central toroidal rotation has been observed before the L-H transition, with rotation breaking over a longer time scale, accompanied by momentum loss, at the edge during every type III ELM event. Detailed analysis shows that the magnitude of the edge NTV torque that is needed for rotation breaking is roughly in accord with the experimental observations. This paper presents these recent advances and characteristics of and means to control different H-modes. New advances and issues with enhanced capabilities in present campaign that may arise will also be presented.

Overview of Physics Results from the National Spherical Torus Experiment

S. A. Sabbagh^{1,2}, NSTX Research Team^{1,2}

¹*Department of Applied Physics, Columbia University, New York, USA*

²*Princeton Plasma Physics Laboratory, Princeton University, Princeton, USA*

Corresponding Author: sabbagh@pppl.gov

Research on the National Spherical Torus Experiment, NSTX, targets physics understanding needed for extrapolation to a steady-state ST Fusion Nuclear Science Facility, pilot plant, or DEMO. The unique ST operational space is leveraged to test physics theories for next-step tokamak operation, including ITER. Present research also examines implications for the coming device upgrade, NSTX-U. Energy confinement increases as collisionality is reduced by lithium (Li) wall conditioning. Nonlinear microtearing simulations match experimental electron diffusivity quantitatively and predict reduced electron heat transport at lower collisionality. Measured high- k turbulence is reduced in H-mode. Beam-emission spectroscopy measurements indicate that the poloidal correlation length of pedestal turbulence increases at higher electron density and gradient, and decreases at higher T_i . Plasma characteristics change nearly continuously with increasing Li evaporation, and ELMs stabilize due to edge density gradient alteration. Global mode stability studies show stabilizing resonant kinetic effects are enhanced at lower collisionality. Combined radial and poloidal field sensor feedback controlled $n = 1$ perturbations and improved stability. The disruption probability due to unstable RWMs is reduced at high $\beta_N/l_i > 11$. Greater instability seen at lower β_N is consistent with decreased kinetic RWM stabilization. A model-based RWM state-space controller produced long-pulse discharges exceeding $\beta_N = 6.4$ and $\beta_N/l_i = 13$. Precursor analysis shows 99% of disruptions can be predicted with 10 ms warning and a false positive rate of only 4%. Disruption halo currents rotate toroidally and can have significant toroidal asymmetry. Global kinks cause measured fast ion redistribution. Full-orbit calculations show redistribution from the core outward and toward $V_{||}/V = 1$. The snowflake divertor configuration enhanced by radiative detachment shows large reductions in steady-state and ELM heat fluxes (peak values down from 7 MW/m² to less than 1 MW/m²). Non-inductive current fraction (NICF) up to 65% is reached experimentally. NSTX-U scenario development calculations project 100% NICF at $I_p = 1$ MA. Coaxial helicity injection has reduced the inductive startup flux, with L-mode plasmas ramped to 1 MA requiring 35% less inductive flux.

Supported in part by US DOE Contract DE-AC02-09CH11466.

Overview of Physics Results from MAST towards ITER/DEMO and the Upgrade

H. Meyer¹, MAST Team¹

¹EURATOM/CCFE Fusion Association, Culham Science Centre, Abingdon, UK

Corresponding Author: hendrik.meyer@ccfe.ac.uk

New diagnostic, modelling and plant capability on MAST have delivered important results in key areas for ITER/DEMO and the upgrade. Linear gyro-kinetic calculations highlight the interplay of kinetic ballooning and micro tearing modes in setting the pedestal width. Using the upgraded 18 coil ELM control array ELM mitigation by resonant magnetic perturbations (RMP) has now been demonstrated with $n = 3, 4$ and 6 proving the importance of the alignment of the perturbation to the magnetic field lines with the unique phasing capability. Already a 2D equilibrium deformation consistent with lobe structures at the X-point, only observed when the RMPs affect the plasma, destabilises the ELM despite the lower pressure gradient. The interplay of edge flow shear and turbulence at the L-H transition measured by a new 50 kHz Doppler spectroscopy diagnostic shows limit-cycle like dynamics during 4–5 kHz H-mode dithers. Further insight into dn/dr , j and v may be provided by a novel 3D electron Bernstein emission imaging system. For the first time ELM resolved scrape-off-layer T_i profiles have been characterised simultaneously in the divertor and mid-plane with retarding field analysers. Divertor design is aided by ELM resolved data on the n_e and I_p dependence of target heat flux profiles. Under conditions foreseen for the upgrade (off-axis NBI, $q_{\min} > 1.3$, $I_p > 0.8$ MA) measurements of profiles of the neutron and fast ion D_α emission indicate a substantial reduction of the fast-ion redistribution compared to on-axis injection. To model the fast-ion redistribution due to the wave particle interaction driven by the super Alfvénic beam ions accurately dynamic friction is now included into the modelling recovering the observed non-linear mode behaviour well. Low-k turbulence, measured using a new 2D beam emission spectroscopy diagnostic, shows L-mode turbulence at $r/a > 0.7$ propagating in the ion diamagnetic direction with respect to the local $\mathbf{E} \times \mathbf{B}$ flow and reduced turbulence levels in H-mode. Using in detail event triggering on NTMs the T_e perturbation due to the 2/1 island has been measured allowing detailed assessment of the NTM stability. Further studies of disruption mitigation with massive gas injection compared different gas mixtures and injection locations including a newly developed controllable high-field-side valve.

Work supported by UK EPSRC and EURATOM.

Overview of HL-2A Recent Experiments

X. Duan¹, L. Yan¹, X. Ding¹, J. Dong¹, Y. Liu¹, and HL-2A Team¹

¹*Southwestern Institute of Physics, Chengdu, China*

Corresponding Author: duanxr@swip.ac.cn

Since the last FEC, the experiments on HL-2A tokamak have been focused on the investigations on H-mode related physics including ELM mitigation, energetic particle physics, transport including nonlocality and edge impurities, MHD instabilities, turbulence and zonal flow physics, etc. In particular, it's demonstrated for the first time that the supersonic molecular beam injection (SMBI) and cluster jet injection (CJI) can convert large ELMs into a series of small ELMs in HL-2A. After SMBI or CJI, the ELM frequency rises by a factor of 2 to 3 on average and its amplitude decreases by about 50%. With high power ECRH, the energetic particle induced modes have been observed in different frequency ranges. The high frequency (200–350 kHz) modes with relatively small amplitude are close to the gap frequency of toroidicity induced Alfvén eigenmode (TAE). The coexistent multi-mode magnetic structures in the high temperature and low collision plasma will affect the plasma transport greatly. The L-I-H transition has been studied in pure NBI-heating deuterium plasmas. For the first time, the absolute rate of nonlinear energy transfer between turbulence and zonal flows was measured and the secondary mode competition between low frequency zonal flows (LFZFs) and geodesic acoustic modes (GAMs) was identified in experiments, which demonstrated that the energy transfer is large enough to affect the turbulence saturation level and its dynamics and that zonal flows play an important role in the low to high (L-H) plasma confinement transition. The increasing turbulent energy at 30–60 kHz, the spontaneous $\mathbf{E} \times \mathbf{B}$ flow shear are identified to be responsible for the generation of LSCSs, which is in agreement with the theoretical prediction and provides unambiguous experimental evidences for LSCS generation mechanism in tokamak edge plasmas. New meso-scale electric potential fluctuations (MSEFs) at frequency $f \sim 10.5$ kHz with two components of $n = 0$ and $m/n = 6/2$ are identified in the edge plasmas for the first time. The MSEFs coexist and interact with the magnetic islands of $m/n = 6/2$, turbulence and LFZFs. These results benefitted from the substantial improvement of the hardware such as 3 MW ECRH and 1.5 MW NBI as well as diagnostics, and have significantly contributed to the understanding of the underlying physics.

OV

Towards an Emerging Understanding of Nonlocal Transport

K. Ida¹, Z. Shi², H. Sun³, S. Inagaki⁴, K. Kamiya⁵, J. Rice⁶, N. Tamura¹,
P. H. Diamond³, T. Estrada⁷, C. Hidalgo⁷, X. L. Zou⁸, G. Dif-Pradalier⁸,
T. S. Hahm⁹, U. Stroth¹⁰, A. Field¹¹, K. Itoh¹, X. Ding², J. Dong², S. I. Itoh⁴,
Y. Sakamoto⁵, and S. Oldenb rger¹²

¹National Institute for Fusion Science, Toki, Japan

²Southwestern Institute of Physics, Chengdu, China

³WCI Center for Fusion Theory, National Fusion Research Institute, Daejeon, Republic of Korea

⁴Research Institute for Applied Mechanics, Kyushu University, Kasuga, Japan

⁵Japan Atomic Energy Agency, Naka, Japan

⁶MIT Plasma Science and Fusion Center, Cambridge, USA

⁷Laboratorio Nacional de Fusion, Asociacion EURATOM-CIEMAT, Madrid, Spain

⁸Association Euratom-CEA, CEA/IRFM, Saint Paul-lez-Durance, France

⁹Seoul National University, Seoul, Republic of Korea

¹⁰Max-Planck-Institut f r Plasmaphysik, Garching, Germany

¹¹Culham Centre for Fusion Energy, Abingdon, UK

¹²Itoh Research Center for Plasma Turbulence, Kyushu University, Kasuga, Japan

Corresponding Author: ida@nifs.ac.jp

In this overview, recent progress on the experimental analysis and theoretical models for non-local transport (non-Fickian fluxes in real space) are overviewed. The non-locality in the heat and momentum transport observed in the plasma, the departures from linear flux-gradient proportionality and the spontaneously and externally triggered non-local transport phenomena will be described in both L-mode and improved-mode plasmas in various devices (LHD, JT-60U, HL-2A, Alcator C-mod, KSTAR, etc.). Non-locality of transport has been observed in the response to perturbations, such as a core temperature rise associated with the cooling at edge by pellet injection, sustainment of the core temperature increase for repetitive perturbations by supersonic molecular beam injection (SMBI), strong coupling of transport at different radii as seen in the curvature transition of ITB, and spatial propagation of ITB regions.

The probability distribution function (PDF) analysis for differences in temperature gradient from steady state values, studies of the fluctuation response during “non-locality events”, and micro-meso scale turbulence coupling studies are discussed as new approaches to investigate the mechanism of non-local transport. The experimental observation of meso-scale fluctuation with long range correlation during non-local phenomena is reviewed as a possible agent causing the non-locality of transport. The turbulence with long correlation, which is one of the strong candidates for causing the non-locality of the transport, was confirmed experimentally and the coupling between the different turbulence scales has also been identified in various devices (LHD, HL-2A, TJ-II, TJ-K, PANTA, etc.).

Theoretical models of non-locality fall into two categories, namely models which are intrinsically local but which support fast front propagation (e.g., for turbulence spreading, barrier propagation etc.) and those which are intrinsically non-local (i.e., relate heat flux to temperature gradient by a non-local kernel). The intrinsically non-local models link the Kernal scale to the interval between steps in the “staircase” zonal flow pattern. Radial propagation of turbulence and barrier fronts models have had some success in explaining phenomena such as fast response to cold-pulses and profile rigidity in response to off-axis heating perturbations.

Progress of the JT-60SA Project

Y. Kamada¹, P. Barabaschi², S. Ishida³, and JT-60SA Team³

¹*Japan Atomic Energy Agency, Naka, Japan*

²*JT-60SA EU Home Team, Fusion for Energy, Garching, Germany*

³*JT-60SA Project Team, Naka, Japan*

Corresponding Author: kamada.yutaka@jaea.go.jp

The shared procurement and construction of the JT-60SA device by Japan and EU is progressing well, including preparation of the plan for key research and development. The JT-60SA device has been designed in order to complement ITER in all areas of fusion plasma development necessary to decide DEMO construction. Detailed studies to predict plasma performance have confirmed these capabilities. The tokamak construction will start in Dec 2012. JT-60SA enables explorations in ITER- and DEMO-relevant plasma regimes in terms of the non-dimensional parameters (β , the normalized poloidal gyro radius, the normalized collisionality, the fast ion β etc.) under ITER- and DEMO-relevant heating conditions (such as dominant electron heating and low central fuelling, and low external torque input). Detailed studies of plasma performance prediction support these capabilities. Under these conditions, heat/particle/momentum transport, L-H transition, ELM/RMP/Grassy-ELM characteristics, the pedestal structure, high energy ion behaviors and the divertor plasma controllability can be quantified. By integrating these studies, the project provides “simultaneous & steady-state sustainment of the key performance characteristics required for DEMO” with integrated control scenario development. Assuming $H_H = 1.3 - 1.4$, the expected I_p for high $\beta_N = 4.3$, high bootstrap fraction (70 – 80%) full non-inductive current drive is 2.1 – 2.3 MA at the Greenwald density ratio $n_G = 1$. The central reference of DEMO for JT-60SA is a compact steady-state reactor. However, the JT-60SA research project has to treat the “DEMO regime” as a spectrum spreading around the reference design, and has to assess reliable DEMO design targets.

OV

Present Status of Fast Ignition Realization EXperiment and Inertial Fusion Energy Development

H. Azechi¹, T. Jitsuno¹, T. Johzaki¹, M. Key², R. Kodama³, M. Koga¹, K. Kondo⁴, J. Kawanaka¹, K. Mima¹, N. Miyanaga¹, M. Murakami¹, H. Nagatomo¹, K. Nagai¹, M. Nakai¹, H. Nakamura¹, T. Nakamura¹, T. Nakazato¹, Y. Nakao⁵, K. Nishihara¹, H. Nishimura¹, T. Norimatsu¹, P. Norreys⁶, T. Ozaki⁷, J. Pasley⁸, H. Sakagami⁷, Y. Sakawa¹, N. Sarukura¹, K. Shigemori¹, T. Shimizu¹, H. Shiraga¹, A. Sunahara¹, T. Taguchi⁹, K. Tanaka⁵, K. Tsubakimoto¹, Y. Fujimoto¹, S. Fujioka¹, H. Homma¹, and A. Iwamoto⁷

¹*Institute of Laser Engineering, Osaka University, Osaka, Japan*

²*Lawrence Livermore National Laboratory, Livermore, USA*

³*Graduate School of Engineering, Osaka University, Osaka, Japan*

⁴*Kansai Photon Science Institute, Osaka, Japan*

⁵*Graduate School of Engineering, Kyushu University, Japan*

⁶*Rutherford Appleton Laboratory, UK*

⁷*National Institute for Fusion Science, Aomori, Japan*

⁸*University of York, York, UK*

⁹*Graduate School of Engineering, Setsunan University, Japan*

Corresponding Author: azechi@ile.osaka-u.ac.jp

Controlled thermonuclear ignition and subsequent burn will be demonstrated in a couple of years on the central ignition scheme. Fast ignition has the high potential to ignite a fuel using only about one tenth of laser energy necessary to the central ignition. This compactness may largely accelerate inertial fusion energy development. One of the most advanced fast ignition programs is the Fast Ignition Realization Experiment (FIREX). The goal of its first phase is to demonstrate ignition temperature of 5 keV, followed by the second phase to demonstrate ignition-and-burn. The second series experiment of FIREX-I from late 2010 to early 2011 has demonstrated a high ($\sim 20\%$) coupling efficiency from laser to thermal energy of the compressed core, suggesting that one can achieve the ignition temperature at the laser energy below 10 kJ. Given the demonstrations of the ignition temperature at FIREX-I and the ignition-and-burn at the National Ignition Facility, the inertial fusion research would then shift from the plasma physics era to power generation era.

Energetic Particle Instabilities in Fusion Plasmas

S. Sharapov¹, B. Alper¹, H. Berk², D. Borba³, B. Breizman², C. Challis¹, I. Classen⁴,
E. Jacob⁵, A. Fasoli⁶, E. Fredrickson⁷, G. Y. Fu⁷, M. Garcia-Munoz⁸, T. Gassner⁹,
K. Ghantous⁷, V. Goloborodko⁹, N. Gorelenkov⁷, M. Gryaznevich¹, S. Hacquin¹⁰,
B. Heidbrink¹¹, C. Hellesen⁵, V. Kiptily¹, G. Kramer⁷, P. Lauber⁸, M. Lilley¹²,
M. Lisak¹³, F. Nabais³, R. Nazikian⁷, R. Nyqvist¹³, C. Perez von Thun¹⁴, S. Pinches¹,
M. Podesta⁷, M. Porkolab¹⁵, K. Shinohara¹⁶, K. Schoep⁹, Y. Todo¹⁷, K. Toi⁷,
M. van Zeeland¹⁸, I. Voitsekhovitch¹, and V. Yavorskij⁹

¹Euratom/CCFE Fusion Association, Culham Science Centre, Abingdon, UK

²Institute Fusion Studies, University of Texas at Austin, Austin, USA

³Euratom/IST Fusion Association, Centro de Fusão Nuclear, Lisboa, Portugal

⁴FOM Institute DIFFER - Association Euratom-FOM, Nieuwegein, The Netherlands

⁵Euratom/VR Fusion Association, Uppsala University, Sweden

⁶CRPP/EPFL, Association Euratom-Confédération Suisse, Lausanne, Switzerland

⁷Princeton Plasma Physics Laboratory, Princeton, USA

⁸Max Planck Institute für Plasmaphysik, Euratom Association, Garching, Germany

⁹Euratom/ÖAW Fusion Association, University of Innsbruck, Austria

¹⁰CEA, IRFM, Association Euratom-CEA, St Paul Lez Durance, France

¹¹University of California, Irvine, USA

¹²Imperial College, London, UK

¹³Euratom/VR Fusion Association, Chalmers University of Technology, Göteborg, Sweden

¹⁴JET-EFDA Close Support Unit, Culham Science Centre, Abingdon, UK

¹⁵PSFC, Massachusetts Institute of Technology, Cambridge, USA

¹⁶JAEA, Naka, Japan

¹⁷NIFS, Aomori, Japan

¹⁸General Atomics, San Diego, USA

Corresponding Author: sergei.sharapov@ccfe.ac.uk

A remarkable progress was made in diagnosing energetic particle instabilities on present-day machines and in establishing a theoretical framework for describing them. This overview presents a point-by-point comparison between the much improved diagnostics of Alfvén Eigenmodes (AEs) and modelling tools developed world-wide, and outlines progress in interpreting the observed phenomena. A multi-machine comparison is presented giving a fair idea on the performance of both diagnostics and modelling tools for different plasma conditions. On JET equipped with 2D gamma-ray camera and interferometry, core-localised TAEs were detected causing redistribution of fast ions from inside the $q = 1$ radius to outer plasma region followed by monster sawtooth crashes. TAE modelling using the HAGIS code showed a good agreement with the measured re-distribution and its effect on sawteeth. On DIII-D and AUG, ECE-imaging provides detailed measurements of amplitude and structure of AEs. A successful modelling was performed using the ORBIT code for reproducing the anomalously flat beam profiles on DIII-D. In AUG, a monitoring of the fast-ion redistribution and losses with an array of scintillators and fast-ion D-alpha spectroscopy has shown how a radial chain of overlapping AEs enables the transport of fast-ions from the core to the fast-ion loss detector. On NSTX, beam-driven AEs were observed in the form of “avalanche” consisting of coupled modes with strong frequency chirp. These modes caused 10% drops in the neutron rate explained by effects of decrease in the beam energy and beam losses resulting from the interaction with TAE. A nonlinear model for near-threshold beam-driven instabilities has successfully encompassed many of the temporal characteristics of AEs seen in experiments. A steady-state nonlinear mode saturation and bursts of mode activity were found to be associated with both the strength and type of relaxation process in the phase-space region surrounding the resonance of the distribution function. An extension of the model to modes with a frequency sweep comparable to the starting frequency opened the opportunity

for understanding the chirping modes in DIII-D, MAST, NSTX, START, and LHD. Finally, this presentation will outline expectations for ITER based on our present knowledge.

This work was funded by the RCUK Energy programme and EURATOM.

Overview of Recent and Current Research on the TCV Tokamak

S. Coda¹

¹ *École Polytechnique Fédérale de Lausanne, Centre de Recherches en Physique des Plasmas,
Association EURATOM-Confédération Suisse, Switzerland*

Corresponding Author: stefano.coda@epfl.ch

Through a diverse research program, TCV addresses physics issues and develops tools for ITER and for the longer-term goals of nuclear fusion, relying especially on its extreme plasma shaping and ECRH launching flexibility and preparing for an ECRH and NBI power upgrade. Localized edge heating was unexpectedly found to decrease the period and relative energy loss of ELMs. Successful ELM pacing has been demonstrated by following individual ELM detection with an ECRH power cut before turning the power back on to trigger the next ELM, the duration of the cut determining the ELM frequency. In a parallel study, negative triangularity was also seen to reduce the ELM energy release. Both stabilizing and destabilizing agents (ECCD on or inside the $q = 1$ surface, respectively) were used in a similar scheme to pace sawtooth oscillations, permitting precise control of their period. Locking of the sawtooth period to a pre-defined ECRH modulation period has also been demonstrated. In parallel with fundamental investigations of NTM seed island formation by sawtooth crashes, sawtooth control has permitted nearly failsafe NTM prevention when combined with backup NTM stabilization by ECRH. Additional work has addressed the destabilization of NTMs in the absence of a sawtooth trigger, and particularly its relation to plasma rotation. Further real-time control developments include the demonstration of joint current and internal inductance control using the Ohmic transformer and the validation of an ECRH power absorption observer based on transmitted stray radiation, for eventual polarization control. A new profile control methodology was also introduced, relying on real-time modelling to supplement diagnostic information; the RAPTOR current transport code in particular has been employed for joint control of the internal inductance and temperature profile. H-mode studies have focused on the L-H threshold dependence on the main ion species and on the divertor leg length. In L-mode, a systematic scan of the auxiliary power deposition profile, with no effect on confinement, has ruled it out as the cause of confinement degradation. Both L- and H-modes have been explored in the snowflake regime with emphasis on edge measurements, revealing that the heat flux to the strike points on the secondary separatrix increases as the X-points approach each other, well before they coalesce.

OV

Science and Technology Research & Development in Support to ITER and the Broader Approach

A. Becoulet¹, CEA-IRFM Team¹

¹CEA, IRFM, St-Paul-Lez-Durance, France

Corresponding Author: alain.becoulet@cea.fr

Magnetic Fusion Energy has now entered its development era that steers the activities of traditional fusion laboratories. Recent achievements in fusion science and technology in support to both the ITER and the Broader Approach (BA) projects are reported here. On top of the direct contribution to ITER and JT-60SA procurement packages, many scientific activities, aiming at reducing risks in operation of ITER and BA, have been carried out using the CEA dedicated in-house facilities (Tore Supra tokamak, ICRH test facility for ITER, remote operated diagnostics, actively cooled PFC qualification, cryogenics test facilities from strand to sub size superconducting conductors characterization, etc).

The paper reviews the research and development actions taken in the past two years by CEA in this context, in order to ensure an ITER safe operation (quench detection, disruption mitigation, surface monitoring of plasma facing components), qualify the long pulse RF Heating and Current Drive systems, and progress in MHD, turbulence and transport first principle simulations.

A fully documented project, turning Tore Supra into a long pulse actively cooled diverted plasma test facility, is now being proposed to the ITER partners. This evolution allows the R&D and commissioning tests of actual ITER actively cooled tungsten divertor elements under ITER-relevant edge plasma conditions, during the ITER procurement phase, and targets its risk reduction.

In parallel, the contribution to the Broader Approach projects is shown to be complemented by an ambitious programme on integrated modeling of the main scenarios and an assessment of EC power needed for NTM stabilization.

Dynamics of Flows and Confinement in the TJ-II Stellarator

J. Sanchez¹, F. Castejón¹, and TJ-II Team²

¹Laboratorio Nacional de Fusión, Asociación EURATOM/CIEMAT, Madrid, Spain

²NSC KIPT, Ukraine; RNC Kurchatov Institute, Moscow, Russian Federation; Ioffe Physical Technical Institute, St Petersburg, Russian Federation; Russian Academy of Sciences, Moscow, Russian Federation; IPFN, Lisbon, Portugal; Universidad Carlos III, Madrid, Spain; BIFI, Zaragoza, Spain

Corresponding Author: joaquin.sanchez@ciemat.es

Operation with Li coated wall is the basis for a significant improvement in the performance of TJ-II, and lies behind the findings in this overview, related to the role of flows in confinement improvement. Specific progress has been performed in the use of Li as alternative to solid plasma facing materials for future fusion devices. Recently a liquid lithium limiter (LLL) based on the Capillary Porous System (CPS) has been installed in TJ-II and first results will be reported.

Although TJ-II presents a strong damping, the simulations predict that the presence of an ambipolar radial electric field as well as turbulence driven flows provide driving mechanisms for mean and fluctuating flows that will cause long range toroidal correlation whose typical frequencies are in agreement with the experiment. The transitions to improved confinement are accompanied by an amplification of long-range correlation in the plasma potential, which is a footprint of zonal flows. The amplitude of these structures have been seen to modulate the particle transport into the SOL for the first time. We also investigate the relation between the zonal flows and the turbulent flux of particles and momentum via the Reynolds and Maxwell stresses as well as suprathermal particles. Suprathermal ion can contribute with significant energy content, with poloidal rotation up to 2 – 5 times higher than the thermal component even the ECRH regime.

Taking advantage of the flexibility of TJ-II, low order rationals are introduced in the plasma, which helps to transit from L to H mode. The influence of the so developed MHD modes on transport is investigated showing a bursty behaviour and evidence of radially propagating events. During L-H transitions, an oscillating low frequency non-damped sheared flow appears in the edge prior to the change to H mode, which presents a predator-pray relation with the turbulence. The spatial evolution of this turbulence-flow shows both radial outward and inward propagations. These results show the need to study L-H transition within a 1D spatio-temporal framework.

The dynamical coupling between density gradients and particle transport has been investigated and compared in the plasma boundary of different tokamaks (JET, ISTTOK) and stellarator (TJ-II), showing that the size of turbulent events is minimum in the proximity of the most probable density gradient.

OV

Overview of Results from the MST Reversed Field Pinch Experiment

J. Sarff¹, A. Almagri¹, J. Anderson¹, F. Auriemma², M. Borchardt¹, W. Bergerson³, D. Brower³, D. Carmody¹, S. Cappello², K. J. Caspary¹, B. Chapman¹, D. Craig⁴, V. I. Davydenko⁵, P. Deichuli⁵, D. Demers⁶, D. Den Hartog¹, W. Ding³, J. Duff¹, S. Eilerman¹, A. Falkowski¹, P. Fimognari⁶, C. Forest¹, P. Franz², J. Goetz¹, R. W. Harvey⁷, D. Holly¹, P. Innocente², A. Ivanov⁵, J. Kim¹, J. King¹, J. Ko¹, J. J. Koliner¹, S. Kumar¹, J. D. Lee¹, L. Lin³, D. Liu¹, R. Lorenzini², R. Magee¹, E. Martinez², K. McCollam¹, M. McGarry¹, V. Mirnov¹, B. Momo², P. Nonn¹, M. Nornberg¹, S. Oliva¹, E. Parke¹, P. Piovesan², S. V. Polosatkin⁵, M. E. Puia², J. Reusch¹, A. Seltzman¹, C. Sovinec¹, M. Spolaore², D. Spong⁸, H. Stephens¹, D. Stone¹, N. Stupishin⁵, D. Terranova², P. Terry¹, J. Titus⁹, M. Thomas¹, D. Thuecks¹, J. Triana¹, J. Waksman¹, and P. Zanca²

¹University of Wisconsin, Madison, USA

²Consorzio RFX, Associazione EURATOM-ENEA sulla Fusione, Padova, Italy

³The University of California at Los Angeles, Los Angeles, USA

⁴Wheaton College, Wheaton, USA

⁵Budker Institute of Nuclear Physics, Novosibirsk, Russian Federation

⁶Xantho Technologies, Madison, Wisconsin, USA

⁷CompX, Del Mar, California, USA

⁸Oak Ridge National Laboratory, Oak Ridge, USA

⁹Florida A&M University, Tallahassee, USA

Corresponding Author: jssarff@wisc.edu

This overview of results from the MST program summarizes physics important for the advancement of the RFP as well as for improved understanding of toroidal magnetic confinement in general. Evidence for the classical confinement of ions in the RFP is provided by analysis of impurity ion transport. With inductive current profile control, the test-particle diffusivity for ions in a stochastic magnetic field is reduced below the classical transport level. (The neoclassical enhancement of radial transport is negligible in the RFP.) Carbon impurity measured by CHERS reveals a hollow profile and outward particle convection. Modeling of classical transport agrees with the profile evolution, and temperature screening explains the hollow profile. Classical confinement is also observed for energetic ions created by 1 MW NBI. The energetic ion confinement is consistent with classical slowing-down and ion loss by charge-exchange. The first appearance of Alfvén eigenmodes and energetic particle modes by NBI in a RFP plasma are obtained. MST plasmas robustly access the quasi-single-helicity state that has commonalities to the stellarator and “snake” formation in tokamaks. The dominant mode grows to 8% of the axisymmetric field strength, while the remaining modes are reduced. Energy confinement is improved as a result. Predictive capability for tearing mode behavior has been improved through nonlinear, 3D, resistive MHD computation using the measured resistivity profile and Lundquist number, which reproduces the sawtooth cycle dynamics. New two-fluid analysis that includes Hall physics and gyro-viscosity has established a new basis for understanding physics beyond a single-fluid model. Nonlinear two-fluid (NIMROD) computation reveals coupling of parallel momentum transport and current profile relaxation. Large Reynolds and Maxwell stresses, plus separately measured kinetic stress, indicate an intricate momentum balance and possible origin for MST’s intrinsic plasma rotation. Microturbulence from drift-wave-like instabilities might be important in the RFP when magnetic fluctuations are reduced. New gyrokinetic analysis indicates that micro-tearing modes can be unstable at high beta, with a critical gradient for the electron temperature that is larger than for tokamak plasmas by roughly the aspect ratio.

Supported by US DoE and NSF.

Overview of the RFX Fusion Science Program

P. Martin¹, M. E. Puiatti¹, and RFX-mod Team¹

¹ *Consorzio RFX, Associazione EURATOM-ENEA sulla Fusione, Padova, Italy*

Corresponding Author: piero.martin@igi.cnr.it

With a program well-balanced among the goal of exploring the fusion potential of the reversed field pinch (RFP) and that of contributing to the solution of key science and technology problems in the roadmap to ITER, the European RFX-mod device has produced a set of high-quality results since the last 2010 Fusion Energy Conference. RFX-mod is a 2 MA RFP, which can also be operated as a tokamak and where advanced confinement states have 3D features studied with stellarator tools. Self-organized equilibria with a single helical axis and improved confinement (SHAx) have been deeply investigated and a more profound understanding of their physics has been achieved. First wall conditioning with Lithium provides a tool to operate RFX at higher density than before, and application of helical magnetic boundary conditions favour stationary SHAx states. The correlation between the quality of helical states and the reduction of magnetic field errors acting as seed of magnetic chaos has been robustly proven. Helical states provide a unique test-bed for numerical codes conceived to deal with 3D effects in all magnetic configurations. In particular the stellarator equilibrium codes VMEC and V3FIT have been successfully adapted to reconstruct RFX-mod equilibria with diagnostic input. The border of knowledge has been significantly expanded also in the area of feedback control of MHD stability. Non-linear dynamics of tearing modes and their control has been modelled, allowing for optimization of feedback models. An integrated dynamic model of the RWM control system has been developed integrating the plasma response to multiple RWMs with active and passive conducting structures (CarMa model) and with a complete representation of the control system. RFX has been operated as a tokamak with safety factor kept below 2, with complete active stabilization of the (2, 1) Resistive Wall Mode (RWM). This opens the exploration of a broad and interesting operational range otherwise excluded to standard tokamaks. Control experiments and modelling led to the design of a significant upgrade of the RFX-mod feedback control system to dramatically enhance computing power and reduce system latency. The possibility of producing D-shaped plasmas is being explored.

OV

Theory of Ignition, Burn and Hydro-equivalency for Inertial Confinement Fusion Implosions

R. Betti¹, K. Anderson¹, T. Boehly¹, T. Collins¹, S. Craxton¹, J. Delettrez¹,
D. Edgell¹, R. Epstein¹, D. Froula¹, M. Lafon¹, V. Glebov¹, V. Goncharov¹,
D. Harding¹, M. Hohenberger¹, S. Hu¹, I. Igumenshev¹, J. Knauer¹, S. Loucks¹,
J. Marozas¹, F. Marshall¹, R. L. McCrory¹, P. McKenty¹, D. Meyerhofer¹, P. Nilson¹,
P. Radha¹, S. Regan¹, T. Sangster¹, W. Seka¹, R. Short¹, D. Shvarts¹, A. Shvydky¹,
S. Skupsky¹, J. Soures¹, C. Stoeckl¹, W. Theobald¹, B. Yaakobi¹, R. Nora¹, J. Frenje²,
D. Casey², C. Li², R. Petrasso², F. Séguin², A. Casner³, J. Perkins⁴, X. Ribeyre⁵, and
G. Schurtz⁵

¹Laboratory for Laser Energetics, University of Rochester, New York, USA

²Massachusetts Institute of Technology, Cambridge, USA

³CEA-DAM-DIF, Arpajon, France

⁴Lawrence Livermore National Laboratory, Livermore, USA

⁵Université Bordeaux CELIA, Talence, France

Corresponding Author: betti@lle.rochester.edu

OV

Recent advances in the theory of ignition and burn for inertial confinement fusion are presented and related to the experimental observables of the current indirect-drive ignition campaign on the National Ignition Facility (NIF) and the direct-drive implosion campaign on the OMEGA laser. The performance parameter currently used for the ignition campaign (the Experimental Ignition Threshold Factor or ITFX) is related to the well-known Lawson criterion. Hydro-equivalent curves are derived and used to extrapolate current results from OMEGA to future direct-drive ignition experiments on the NIF. The impact of laser-plasma instabilities, hot electron and radiation preheat on the hydrodynamic scaling is discussed. Remedies to mitigate the detrimental effects of laser-plasma and hydrodynamic instabilities are presented. It is also shown that ignition through a late shock launched at the end of the laser pulse (shock ignition) may be possible on the NIF at sub-megajoule energies.

Multimodal Options for Materials Research to Advance the Basis for Fusion Energy in the ITER Era

S. Zinkle¹, A. Möslang², T. Muroga³, and H. Tanigawa⁴

¹*Nuclear Science & Engineering Directorate, Oak Ridge National Laboratory, Oak Ridge, USA*

²*Karlsruhe Institute of Technology, Eggenstein-Leopoldshafen, Germany*

³*National Institute for Fusion Science, Toki, Japan*

⁴*Japan Atomic Energy Agency, Aomori, Japan*

Corresponding Author: zinklesj@ornl.gov

Sustained worldwide efforts on fusion energy research have led to substantial improvements in understanding of plasma physics and fusion technology issues. Several options with varying degrees of technological risk are being contemplated for the next major fusion energy device that will be constructed after ITER begins operation. These options include a variety of plasma confinement configurations, coolants, tritium breeding materials, power conversion systems, and operating temperatures. In many cases, variations in the aggressiveness of the design parameters for next-step devices are associated with uncertainties in the performance of the materials systems to be used in the divertor, first wall and breeding blanket, and tritium extraction and power conversion systems. In order to reduce some of these uncertainties and to assist in the selection of the most appropriate design concept(s) that meet national needs, well-coordinated international fusion materials research on multiple fundamental feasibility issues can serve an important role during the next ten years.

There are two inter-related overarching objectives of fusion materials research to be performed in the next decade:

1. Understanding materials science phenomena in the demanding DT fusion energy environment,
2. Using this improved understanding to develop and qualify materials to provide the basis for next-step facility construction authorization by funding agencies and public safety licensing authorities.

There are several important fundamental materials questions that should be resolved soon due to their potential major impact on next-step fusion reactor designs, including radiation effects on mechanical properties, structural stability and tritium permeation and trapping. An overview will be given of the current state-of-the-art of major materials systems that are candidates for next-step fusion reactors, including a summary of existing knowledge regarding operating temperature and neutron irradiation fluence limits due to high temperature strength and radiation damage considerations, coolant compatibility information, and current industrial manufacturing capabilities. The critical issues and prospects for development of high performance fusion materials will be discussed along with recent research results and planned activities of the international materials research community.

Overview of FTU Results

P. Buratti¹, FTU Team¹, ECRH Team², and Z. O. Guimarães-Filho³

¹Associazione EURATOM-ENEA, Frascati, Italy

²Associazione EURATOM-ENEA, Milano, Italy

³Aix-Marseille University, IIFS-PIIM, Marseille, France

Corresponding Author: paolo.buratti@enea.it

Since the 2010 IAEA-FEC Conference, FTU has exploited improvements in cleaning procedures and in the density control system to complete a systematic exploration of access to high-density conditions in a wide range of plasma currents and magnetic fields. The line-averaged densities at the disruptive limit increased more than linearly with the toroidal field, while no dependence on plasma current was found, in fact the maximum density of $4.3 \times 10^{20} \text{ m}^{-3}$ was reached at $B = 8 \text{ T}$ even at the minimum current of 0.5 MA, corresponding to twice the Greenwald limit. The lack of plasma current dependence is due to the increase of density peaking with the safety factor.

Experiments with the 140 GHz ECRH system were focused on the sawtooth period control and on the commissioning of the new launcher with real-time-steering capability that will act as the front-end actuator of a real time system for sawtooth period control and tearing modes stabilization. Various ECRH and ECCD modulation schemes have been used; with the fastest one, the sawtooth period synchronized with the 8 ms modulation period. The observed period variations were simulated using the JETTO code with a critical shear model for the crash trigger. The new launcher is of the plug-in type, allowing quick insertion and connection to the transmission line. Both beam characteristics and steering speed were in line with design expectation.

Experimental results on the connection between improved coupling of lower hybrid waves in high-density plasmas and the reduction of spectral broadening of the injected wave have been compared with the results of fully kinetic non-linear model calculations.

The effect of wall conditioning by lithium on MHD activities has been studied by comparing discharges with and without lithium conditioning at low- q_a and at the density limit. In both cases lithium conditioning has the same effect of reducing MHD modes associated with edge cooling by light impurities as a careful wall preparation. Experiments with the liquid lithium limiter inserted in the SOL, which have shown the formation of a radiative belt that acts as a virtual toroidal limiter, have been interpreted by the edge code TECXY as an effect of strong radiation from Li^+ ions in non-coronal equilibrium.

New Developments, Plasma Physics Regimes and Issues for the Ignitor Experiment

B. Coppi¹, A. Airoidi², R. Albanese², F. Bombarda³, A. Cardinali³, G. Cenacchi², E. Costa⁴, P. Detragiache³, A. DeVellis³, G. Faelli⁵, A. Ferrari⁵, A. Frattolillo³, P. Frosi³, F. Giammanco⁶, G. Grasso⁷, S. Mantovani⁵, S. Migliori³, S. Pierattini³, G. Ramogida³, G. Rubinacci², M. Sassi⁵, M. Tavani⁴, A. Tumino⁷, and F. Villone²

¹ *MIUR, Italy*

² *Consorzio CREATE, Naples, Italy*

³ *ENEA, Italy*

⁴ *INAF, Rome, Italy*

⁵ *CIFS, Turin, Italy*

⁶ *Università di Pisa, Pisa, Italy*

⁷ *Columbus Superconductors, Genoa, Italy*

Corresponding Author: coppi@mit.edu

The IGNIR collaboration between Italy and Russia is centered on the construction of the core of the Ignitor machine in Italy and its installation and operation within the Trinita site (Troitsk, Russia). The scientific goal of the experiment is to approach for the first time, the ignition conditions of a magnetically confined D-T plasma. A parallel initiative has developed that integrates this program, involving the study of plasmas in which a high energy population is present, with ongoing research in high-energy astrophysics and with a theory effort involving the National Institute for High Mathematics and the Inter University Space Physics Consortium, CIFS. Innovations in the adopted diagnostic systems are expected from the collaboration with INAF, the National Institute for Astrophysics (X-ray diagnostics), with INFN (nuclear diagnostics), and with the University of Pisa. The Ignitor core construction has been fully funded by the Italian government. Meanwhile, considerable attention has been devoted toward identifying the industrial groups with the facilities necessary to build the main machine components. An important step for the Ignitor program is the adoption of the superconducting material MgB₂ for the largest poloidal field coils (P14) that is compatible with the He gas cooling system designed for the entire machine. The progress made for the construction of these coils is described. The main physics issues that the Ignitor experiment is expected to face are analyzed considering the most recent developments in both experimental observations and theory of weakly collisional magnetically confined plasmas. Of special interest is the I-Regime that has been investigated in depth only recently and combines advanced confinement properties with a high degree of plasma purity. This is a promising alternative to the high density L-Regime that had been observed by the Alcator program and had motivated the Ignitor project. The provisions that are incorporated in the machine design in order to prevent the development of macroscopic instabilities with deleterious amplitudes are presented.

On the Physics of Intrinsic Torque in Toroidal Plasmas

P. H. Diamond^{1,2}, T. Hahm³, Ö. Gürcan⁴, C. McDevitt⁵, Y. Kosuga², N. Fedorczak²,
W. Wang⁶, H. Jhang¹, J. Kwon¹, S. Kim¹, S. Ku⁶, G. Dif-Pradalier⁷, J. Abiteboul⁷,
Y. Sarazin⁷, J. Rice⁸, K. Ida⁹, W. Solomon⁶, S. Yi¹, T. Rhee¹, C. Chang⁶, and
R. Singh¹⁰

¹WCI Center for Fusion Theory, NFRI, Republic of Korea

²CMTFO, UCSD, La Jolla, USA

³Seoul National University, Seoul, Republic of Korea

⁴LPP Ecole Polytechnique, Palaiseau, France

⁵LANL, Los Alamos, USA

⁶Princeton Plasma Physics Laboratory, Princeton, USA

⁷CEA, Cadarache, France

⁸PSFC, MIT, Cambridge, USA

⁹NIFS, Aomori, Japan

¹⁰ITER, IPR, Gujarat, India

Corresponding Author: diamondph@gmail.com

OV-P-03

Intrinsic rotation is a critical physics issue for ITER, both for resistive wall mode mitigation and for confinement optimization. Rotation control requires predictive understanding of intrinsic rotation, and so this goal has stimulated a great deal of research on intrinsic torque, driven by the non-diffusive fluctuation-induced residual stress[1]. In this OV, we discuss recent theoretical, simulation and experimental progress which elucidates the important physics of intrinsic torque. In contrast to recent OV's on rotation, here we focus on intrinsic torque rather than on the momentum pinch[2]. We present important new results on the critical role of boundary stresses in intrinsic torque. The heat flux-driven character of intrinsic torque is emphasized throughout.

Specifically, we present a novel, unifying theory of intrinsic rotation in terms of fluctuation entropy balance. We then discuss various symmetry breaking mechanisms and their underlying microphysical structure. Applications of the theory to MFE phenomenology are discussed in detail. Novel results on symmetry breaking effects at the boundary, which reveal boundary-specific intrinsic torques, are discussed. We also consider RMP effects on intrinsic rotation.

References

- [1] P. H. Diamond, *et al.*, NF (2009).
- [2] A. Peeters, *et al.*, FEC (2010), C. Angioni, *et al.*, H-Mode Workshop (2011).

Overview of IFERC Project in Broader Approach Activities

N. Nakajima¹, IFERC Project Team¹, IFERC-Home Team, JA¹, and
IFERC-Home Team, EU¹

¹*National Institute for Fusion Science, Aomori, Japan*

Corresponding Author: nakajima@nifs.ac.jp

In order to contribute to ITER and to an early realization of the DEMO reactor, International Fusion Energy Research Centre (IFERC) started the activity from 2007/7/1 with 10 years period under the Broader Approach (BA) framework and now implements the three sub-projects; DEMO Design and R&D Coordination Centre (DDA & R&D), Computational Simulation Centre (CSC), and ITER Remote Experimentation Centre (REC). DDA & R&D: The DEMO Design Activity (DDA) in 2011 covered the studies on system codes, divertor, in Vessel Components, operation modes and maintenance. After benchmark test of the system codes by EU and JA, the codes were used to investigate an $R = 8.5$ m steady-state device and an $R = 10$ m pulsed device. In addition, comparison between steady-state and pulsed was done from engineering points of view. Maintenance study was another important issue and the various schemes were compared to review the features. These works will provide the databases toward conceptual designs planned in the period from 2015. As for R&D, preparation of facilities, installation of equipment, and preliminary R&Ds have been performed in 5 tasks (T1-T5). R&D activities are now being upgraded both in EU and JA for T1 (lifetime and off-axial mechanical properties and electrical properties of SiC_f/SiC composites), T2 (tritium accountancy etc. in Tritium technology), T3 (production and characterization of reduced activation ferritic/martensitic steel in Materials engineering), and T4/ T5 (mass production technology of Be-Ti intermetallic compounds for neutron multiplier as well as Li₂SiO₄ and Li₂TiO₃ for tritium breeders). CSC: The mission of CSC is to exploit high-performance and large-scale magnetically confined fusion (MCF) simulations. The Light House Project was carried out by using codes with a good scalability, in order to show MCF simulations could exploit a new research field or a frontier research. For example, particle-fluid hybrid simulations on energetic particle-driven instability and alpha particle transport have been performed in an ITER steady state scenario plasma, and it is found out that saturation level of multiple TAE modes with medium toroidal mode numbers is so low that the confinement of alpha particles is not degraded. REC: The mission of REC is to prepare ITER remote experiments and verify the functions. The overall plan of REC will be created in 2012.

The Recent Research Work on the J-TEXT Tokamak

G. Zhuang¹, K. Gentle², Y. Pan¹, X. Hu¹, Z. Chen¹, Z. Wang¹, Y. Ding¹, M. Zhang¹,
L. Gao¹, Z. Yang¹, Z. Chen¹, Z. Cheng¹, X. Zhang¹, and H. Huang¹

¹College of Electrical and Electronic Engineering, Huazhong University of Science and Technology, Wuhan Hubei, China

²Institute for Fusion Studies, University of Texas at Austin, Austin, USA

Corresponding Author: ge.zhuang@mail.hust.edu.cn

The main results from the J-TEXT tokamak in the last two years, which emphasized the observation and analysis of MHD activity, are summarized and presented in this meeting.

Static resonant magnetic perturbations generated by saddle coil currents are applied to J-TEXT Ohmic plasmas in order to study their influence on MHD instabilities. With sufficiently large RMPs, the $m/n = 2/1$ (m and n are the poloidal and toroidal mode numbers) mode locking is easily obtained. The analysis of the mode locking thresholds varied by scanning of the spatial phase of RMPs shows that the $m/n = 2/1$ component of intrinsic error field of the J-TEXT tokamak is about 0.4 Gs. In addition to normal mode locking events, the (partial) stabilization of the $m/n = 2/1$ tearing mode by moderate magnetic perturbation amplitude is observed experimentally. With experimental parameters as input, both the mode locking and mode stabilization by RMPs are also obtained from nonlinear numerical modeling based on reduced MHD equations. It is found that the suppression of the tearing mode by RMPs of moderate amplitude is possible for a sufficiently high plasma rotation frequency and low Alfvén velocity. Gas puffing is also used to affect the MHD activity in J-TEXT. For example, neon gas injection can cause inverse sawtooth-like activity that spreads from the $q = 1$ surface to the axis; in particular, small amplitude $m/n = 1/1$ mode oscillations superimposed on the inverse sawtooth waveform around the $q = 1$ surface are observed after the impurity injection. Nevertheless, other impurities such as helium and argon impurities can't trigger such events. In addition, gas puffing can also be applied to mitigate disruptions, especially on the current quench phase. It is found that no runaway current generation occurs in intentionally provoked disruptions when the toroidal magnetic field is lower than 2.2 T. The runaway currents can be suppressed by the intensive gas puffing of H₂.

To meet the requirement of charactering the MHD activity, a far-infrared polarimeter-interferometer has been developed to measure the current density profile, while a tangential X-ray imaging crystal spectrometer (XICS) provides ion temperature and toroidal rotation velocity measurements. First results are obtained with observation of perturbations associated with sawtooth and MHD activities. The details will be given in this meeting.

Fusion Prospects of Axisymmetric Magnetic Mirror Systems

E. Kruglyakov¹, A. Burdakov¹, and A. Ivanov¹

¹*Budker Institute of Nuclear Physics SB RAS, Novosibirsk, Russian Federation*

Corresponding Author: e.p.kruglyakov@inp.nsk.su

Studies of the magnetic mirrors have been started in 50–60 s of the last century. Very soon it was found out that axially symmetric mirrors suffer from the curvature-driven instabilities which results in unacceptable plasma losses. Introduction of non-axisymmetric (quadrupole) configurations with min- B magnetic field improved plasma confinement significantly. Then, plasma losses associated with less destructive kinetic instabilities become dominative. Later on, the methods of suppression of the kinetic instabilities were successfully developed and confinement was further improved. However, it was recognized that even the axial plasma losses determined by classical binary collisions appear to be too high for practical application of the mirrors. In the 70s, some ideas emerged how to reduce these losses. These ideas are briefly reviewed in [1] and in the references therein. Another advance in magnetic mirror studies was invention of axisymmetric mirrors with improved longitudinal and transverse plasma confinement. Several techniques for achieving MHD stabilization of the axisymmetric mirrors are considered in [2]. These versions of the mirror systems are of particular interest as neutron sources, fusion-fission hybrids, and pure fusion reactors. At present, two versions of the advanced magnetic mirrors, namely a gas dynamic trap (GDT) and multi mirror confinement system are studied in the Budker Institute.

References

- [1] A. V. Burdakov, A. A. Ivanov, E. P. Kruglyakov, *Plasma Phys. Cont. Fus.*, **52** 124026 (2010).
- [2] D. D. Ryutov, H. L. Berk, B. I. Cohen, A. W. Molvik, T. C. Simonen, *Phys. Plasmas* **18** 092301 (2011).

20 Years of ISTTOK Tokamak Scientific Activity

H. J. Fernandes¹, J. Cabral¹, C. A. F. Varandas¹, and C. Silva¹

¹*Associação Euratom/IST, Instituto de Plasma e Fusão Nuclear, Instituto Superior Técnico, Universidade Técnica de Lisboa, Portugal*

Corresponding Author: hf@ipfn.ist.utl.pt

The ISTTOK tokamak commissioning began in January 1990, after the establishment operating coincidentally with the signing of the EURATOM association agreement established with Instituto Superior in 1990 on the field of controlled nuclear fusion. In 1991 the first article have been issue in the Portuguese journal “Gazeta de Física” and the firsts scientific reports were mentioned to the international community on the 17th Symposium on Fusion Technology, Rome 1992.

This communication aims to present an overview of ISTTOK scientific activity since its commissioning in the main areas of its activity, namely

1. Plasma diagnostics an in particular the Heavy Ion Beam (HIBD),
2. AC current operations,
3. plasma control,
4. liquid metal limiters,
5. plasma fluctuation studies and
6. study of fusion relevant materials.

The ISTTOK achievements demonstrate that small tokamaks can play an important role in the fusion plasma physics community as a result of their flexibility, high availability and good opportunity for the development of sophisticated diagnostics and technology tools.

Magnetic Confinement Experiments

EX

Scenarios Development at JET with the New ITER-like Wall

E. Joffrin¹, J. Bucalossi¹, P. Lomas², F. Rimini², R. Neu³, I. M. Ferreira Nunes⁴, M. Baruzzo⁵, M. Beurskens², C. Bourdelle¹, S. Brezinsek⁶, G. Calabro⁵, C. Challis², M. Clever⁶, J. Coenen⁶, R. Dux³, E. de la Luna⁷, P. de Vries⁸, L. Frassinetti⁹, C. Giroud², M. Groth¹⁰, J. Hobirk³, G. Maddison², J. Mailloux², C. Maggi³, G. Matthews², M. Mayoral², T. Pütterich³, M. Sertoli³, B. Sieglin³, G. Sips⁴, and G. van Rooij⁸

¹CEA, IRFM, Centre de Cadarache, Saint-Paul-lez-Durance, France

²Euratom/CCFE Fusion Association, Culham Science Centre, Abingdon, UK

³Max-Planck-Institut für Plasmaphysik, Euratom Association, Garching, Germany

⁴JET-EFDA-CSU, Culham Science Centre, Abingdon, UK

⁵Associazione EURATOM-ENEA sulla Fusione, C.R. Frascati, Italy

⁶Association Euratom/Forschungszentrum, Jülich, Germany

⁷Laboratorio Nacional de Fusion, Asociacion Euratom-CIEMAT, Madrid, Spain

⁸Association Euratom/DIFFER, Rijnhuizen, Nieuwegein, Netherlands

⁹Association VTR, KT, Stockholm, Sweden

¹⁰Association Euratom-Tekes, VTT, Finland

Corresponding Author: emmanuel.joffrin@jet.efda.org

EX

In the recent JET experimental campaigns with the new ITER-like Wall (ILW), major progress has been achieved in the characterisation of the H-mode regime:

1. Plasma breakdown and L-mode operation have been recovered in a few days of operation.
2. Stable type I ELMy H-modes with $H_{98}(y, 2)$ close to 1 and $\beta_N \sim 1.6$ have been achieved in high triangularity ITER-like shape plasmas on the bulk divertor tungsten tile.
3. It has been shown that the ELM frequency is a determining factor for the control of the core radiation level from metallic impurity.
4. In comparison to carbon equivalent discharges, total radiation is similar but the edge radiation is lower and the plasma core radiation higher.

The maximisation of confinement, the control of metallic impurity sources and heat loads are the main challenges facing the development of the ITER scenarios in JET in the ILW environment at higher current and toroidal which will get closer to dimensionless ITER parameters in terms of ρ^* and ν^* . This paper reviews the major physics and operational achievements and challenges that JET has to face to produce stable plasma scenarios (baseline and hybrid scenarios) with maximised performances with the ILW in support of ITER future operation.

Real time ELM, NTM and Sawtooth Control on TCV

B. Duval¹, F. Felici², T. Goodman¹, J. Rossel¹, G. Canal¹, S. Coda¹, J. M. Moret¹,
and O. Sauter¹

¹*Ecole Polytechnique Fédérale de Lausanne, Centre des Recherches en Physique des Plasmas,
Association Euratom-Confédération Suisse, Lausanne, Switzerland*

²*Eindhoven University of Technology, Mechanical Engineering Department, Control
Systems Technology Laboratory, Eindhoven, Netherlands*

Corresponding Author: basil.duval@epfl.ch

TCV's real-time (RT) control system uses a range of diagnostic signals to detect plasma events and react with programmable, controllable actuators such as orientable ECH power and Tokamak control actuators. Three examples of MHD phenomena control are presented with RT recognition of temporal and/or spatial extents of events controlled by synchronous modulation of the power or heating position displacement.

ELM energy release changed with ECH in the plasma edge. Although these ELMs satisfy the Type I designation, their frequency increases, the relative energy loss per ELM decreases, although the coupled power decreases. ELM pacing was achieved by cutting the heating power at the ELM event for a given time before turning the power back on to trigger the arrival of the next ELM. The delay before the ELM appearance is found consistent with type-I ELM frequency vs average power scaling.

At sufficiently high beta, ST crashes of sufficient amplitude generate NTM seed islands that grow. NTMs can be avoided by destabilising ST (the foreseen ITER strategy), or be stabilised altering the current distribution inside an island i.e., "healed" by localised ECH or current drive (ECCD). NTMs may be mitigated with continuous pre-emptive ECCD in the expected region, predictive ECCD if the generating ST crash time is known, and/or reactive ECCD when a NTM is observed.

Stabilising individual STs was demonstrated on TCV by applying ECCD near the $q = 1$ surface for a set duration after a ST crash. A new ST event is triggered a short, and relatively constant, time after the ECCD is then removed. Using the RT system, the ST period was changed on a crash to crash basis by varying the stabilising ECCD injection period. Pacing through destabilisation was also achieved by applying ECCD inside the $q = 1$ surface with opposite phasing.

Longer ST, that trigger NTMs, can now be generated. A second gyrotron providing ECCD at the $q = 3/2$ surface just before the ST demonstrated efficient pre-emptive NTM stabilisation. An integrated control system simultaneously controls the ST period, preempts NTM formation and suppresses any NTMs that appear. The combination of RT identification and multi-actuator reaction has been demonstrated on TCV using a combination of targeted ECH and ECCD to efficiently pact, pre-empt and/or "heal" MHD modes.

EX

Progress in Performance and Understanding of Steady ELM-free I-modes on Alcator C-Mod

A. Hubbard¹, D. Whyte¹, A. Dominguez¹, M. Greenwald¹, N. Howard¹, J. Hughes¹, C. Kessel², B. LaBombard¹, L. Bruce¹, M. Reinke¹, J. Rice¹, P. Snyder³, J. Terry¹, A. White¹, Y. Lin¹, and S. Wukitch¹

¹*Massachusetts Institute of Technology, Plasma Science and Fusion Center, Cambridge, USA*

²*Princeton Plasma Physics Laboratory, Princeton, USA*

³*General Atomics, San Diego, USA*

Corresponding Author: hubbard@psfc.mit.edu

The I-mode regime of operation has been extended in recent Alcator C-Mod campaigns in duration and robustness, over a wide range of parameters. This attractive regime features an edge thermal barrier, and H-mode like energy transport, in combination with L-mode like density profiles and particle transport. This prevents accumulation of impurities, and means that ELMs are not needed to expel them. I-modes are now routinely maintained in stationary conditions for over $10\tau_E$. They are usually ELM free, a key advantage given the concern over divertor heat pulses on ITER. Instead, a continuous pedestal fluctuation appears to enhance selectively particle over thermal transport [2]. High performance I-modes are usually obtained with unfavourable ion drift direction. They have been produced in both upper and lower null plasmas, with $q_{95} = 2.5 - 5.3$ and extending to low ν^* . τ_E is in the range of H-mode, with $H_{98}(y, 2)$ up to 1.2, and exhibits less degradation with power ($W \sim P^{0.7}$). Power thresholds for I-mode are somewhat higher than typical L-H scalings, and increase with I_p as well as with density. The widest power range for I-mode, nearly a factor of two above the L-I threshold, has been obtained in reversed field, lower null discharges at moderate n_e . Detailed measurements have been made of profiles and turbulence in the edge pedestal region, aiming to understand the separation of particle and energy transport. At the L-I transition, broadband turbulence in the 50 – 150 kHz range decreases. A pedestal-localized weakly coherent mode at $\sim 200 - 250$ kHz is observed on density, magnetic and T_e diagnostics [3]. Stability analysis using ELITE shows that the pedestal is deeply stable to peeling-ballooning modes, consistent with the lack of ELMs. Initial assessments of the potential application of the I-mode regime on ITER, extrapolating from C-Mod results, indicate that an attractive operating scenario is possible, if issues of operation in the unfavourable drift configuration can be addressed. The L-I transition should be accessible at low density, and $Q = 10$ is projected at $n_{e,\psi 95} = 5 \times 10^{19} \text{ m}^{-3}$. This exercise also highlights some of the key issues remaining to be addressed, on C-Mod and in joint experiments.

References

- [1] D.G. Whyte *et al.*, Nucl. Fusion **50** (2010) 105005.
- [2] A.E. Hubbard *et al.*, Phys. Plasmas **18** (2011) 056115.
- [3] A.E. White *et al.*, Nucl. Fusion **51** (2011) 113005.

Dominant ECR Heating of H-mode Plasmas on ASDEX Upgrade Using the Upgraded ECRH System and Comparison to Dominant NBI or ICR Heating

J. Stober¹, F. Sommer¹, C. Angioni¹, L. Barrera¹, V. Bobkov¹, E. Fable¹, R. Fischer¹,
C. Hopf¹, B. Kurzan¹, F. Leuterer¹, R. McDermott¹, A. Mlynek¹, F. Monaco¹,
S. Mueller¹, M. Muenich¹, S. Rathgeber¹, F. Ryter¹, M. Schubert¹, H. Schuetz¹,
E. Viezzer¹, D. Wagner¹, and H. Zohm¹

¹Max-Planck-Institut für Plasmaphysik, EURATOM-Association, Garching, Germany

Corresponding Author: joerg.stober@t-online.de

In contrast to ITER and future fusion reactors, plasmas used today for preparational or fundamental studies are often heated dominantly via the ion channel and with strong concurrent momentum input. This is due to the dominance of NBI heating systems, which are widely used because of their reliability and universal applicability. The potential danger of this approach is an over-estimation of the scaled fusion performance, which depends on T_i and not T_e , but the ratio of these temperatures may depend on the heating mix. Even worse, an increasing value of T_e/T_i is expected to increase the ITG dominated turbulent transport in the ion channel reducing T_i further. Additionally, the significantly reduced torque of future NBI-systems may increase transport due to a reduction of rotational shear.

To clarify above mentioned uncertainties it is important to study the effect of dominant electron heating with a minimum of momentum input. At ASDEX Upgrade such studies have been started using the upgraded ECRH system which delivers 4 MW of ECRH to the plasma, exceeding the minimum H-mode power threshold for typical high I_p , B_t conditions by a factor of two. Additionally, 6 MW of ICRH and 20 MW of NBI are installed at AUG. This contribution reports on the upgrade of the ECRH system and its application in studying H-mode plasmas in which the heating mix between the three available systems is varied while keeping the total heating power constant. This was done for several different levels of total heating powers.

Kinetic profiles (n, T, v, E) are measured using the recently upgraded suite of diagnostics in the core and, with high spatial resolution, in the pedestal region. Transport analysis and comparisons to predictions based on stability of drift modes (GS2) are presented. The major findings are: no effect of the heating mix on pedestal pressure although plasma rotation varies significantly, no direct correlation of the rotational shear with the shape of density or temperature profiles, and a significant increase of T_e/T_i as the fraction of electron heating exceeds a certain threshold. The cases analysed so far were all at high collisionality. These studies will be continued towards higher heating powers and lower collisionality.

EX

Fully Noninductive Scenario Development in DIII-D Using New Off-Axis Neutral Beam Injection

C. T. Holcomb¹, J. R. Ferron², F. Turco³, T. C. Luce², P. A. Politzer², M. J. Lanctot¹, M. Okabayashi⁴, Y. In⁵, J. M. Hanson³, T. W. Petrie², R. J. La Haye², A. W. Hyatt², T. H. Osborne², L. Zeng⁶, E. J. Doyle⁶, T. L. Rhodes⁶, J. M. Park⁷, and Y. Zhu⁸

¹*Lawrence Livermore National Laboratory, Livermore, USA*

²*General Atomics, San Diego, USA*

³*Columbia University, New York, USA*

⁴*Princeton Plasma Physics Laboratory, Princeton, USA*

⁵*FAR-TECH, Inc., San Diego, USA*

⁶*University of California Los Angeles, Los Angeles, USA*

⁷*Oak Ridge National Laboratory, Oak Ridge, USA*

⁸*University of California Irvine, Irvine, USA*

Corresponding Author: holcomb@fusion.gat.com

New off-axis neutral beam injection (NBI) capability on DIII-D has expanded the range of achievable and sustainable current and pressure profiles of interest for developing the physics basis of steady-state scenarios in future tokamaks. Fully noninductive (NI) scenarios are envisioned to have broad current and pressure profiles with elevated minimum safety factors (q_{\min}), high normalized beta (β_N), and a large fraction of the plasma current I_p sustained by the bootstrap current. Using off-axis NBI, plasmas have been produced with q_{\min} between ~ 1.3 and ~ 2.5 to evaluate the suitability for steady-state operation ($f_{\text{NI}} \equiv I_{\text{NI}}/I_p = 1$). Nearly stationary plasmas were sustained for two current profile relaxation timescales ($2\tau_R = 3$ s), with $q_{\min} = 1.5$, $\beta_N = 3.5$, $f_{\text{NI}} = 70\%$, and performance that projects to $Q = 5$ in an ITER-size machine. The duration of the high β_N phase is limited only by the available NBI energy. Low-order tearing modes are absent and the predicted ideal-wall $n = 1$ kink β_N limit is > 4 . To achieve higher f_{NI} , higher β_N is needed to increase the bootstrap current, and higher q_{\min} will decrease the required external current drive near the axis. Experiments to produce plasmas with $q_{\min} > 2$ showed that the use of off-axis NBI results in higher sustained q_{\min} , with q_{\min} at a larger radius (i.e., a broader current profile), and a broader pressure profile. These changes increased the predicted ideal-wall $n = 1$ kink mode β_N limit from below to above $\beta_N = 4$. These plasmas achieved a maximum $\beta_N = 3.2$ limited by the available NBI power and reduced confinement ($H_{98} \sim 1$) relative to similar plasmas with lower q_{\min} . $\beta_N = 4$ with $q_{\min} > 1.5$ was transiently obtained albeit with only 2 out of 5 MW of off-axis NBI available. Off-axis fishbones and low-order tearing modes were observed in the course of the q -profile scan. These studies indicate that obtaining a sustained, high performance, $f_{\text{NI}} = 1$ scenario involves a number of trade-offs related to the choice of q -profile.

This work was supported by the US Department of Energy under DE-AC52-07NA27348, DE-FC02-04ER54698, DE-FG02-04ER54761, DE-AC02-09CH11466, DE-FG02-08ER85195, DE-FG02-08ER549874, DE-AC05-00OR22725, and SC0G804302.

Connections Between Intrinsic Toroidal Rotation, Density Peaking and Plasma Turbulence Regimes in ASDEX Upgrade

R. McDermott¹, F. Casson¹, R. Dux¹, E. Fable¹, T. Pütterich¹, F. Ryter¹, E. Viezzer¹, and C. Angioni¹

¹Max Planck Institut für Plasmaphysik, Garching, Germany

Corresponding Author: rachael.mcdermott@ipp.mpg.de

Recently, ASDEX Upgrade has made significant contributions to momentum transport studies thanks to the upgrade of the core charge exchange recombination spectroscopy system, which now produces much higher quality ion temperature and toroidal rotation profiles. This upgrade enabled the development of an intrinsic rotation database that contains over 200 observations. The edge rotation on AUG is always co-current, while the core rotation can be either co- or counter-current directed. The latter results in a null point in the profile at finite rotation gradient, which is clear evidence of a localized residual stress momentum flux. Moreover, the Mach number in the center of the plasma appears to be determined largely by the normalized gradient of the toroidal rotation at mid-radius, u' . This correlation holds for all of the observations regardless of plasma confinement regime or type of auxiliary heating. Further examination of the database reveals that u' exhibits the strongest correlation with the local logarithmic electron density gradient, R/L_{ne} : hollow rotation profiles coincide with peaked n_e profiles, while co-current rotation corresponds to low R/L_{ne} . The known relationship between density peaking and plasma turbulence suggests a connection between the turbulence and the intrinsic rotation behavior as well. A study based on local linear gyro-kinetic calculations found good quantitative agreement between the predicted and measured values of u' through the imposition of a finite tilting angle of -0.3 radians on the turbulent mode structure. The mechanism expected to produce such a tilting is a combination of $\mathbf{E} \times \mathbf{B}$ and profile shearing residual stress. These database results are also consistent with observations of residual stress in non-intrinsic rotation scenarios. Flat to hollow rotation profiles are observed concomitant with peaked electron density profiles when sufficient ECRH power is added to NBI heated H-modes causing the turbulent regime to transition from ITG to TEM. Momentum transport analyzes of these plasmas show that the observations can only be explained by the presence of a core localized, counter-current directed, residual stress induced torque of the same order of magnitude as the applied NBI. These results have important implications for torque modulation experiments, which often assume that the residual stress is negligibly small.

EX

A Unified Explanation of Rotation Reversals, Confinement Saturation and Non-Diffusive Heat Transport in C-Mod Ohmic Plasmas

J. Rice¹, M. Reinke¹, N. Howard¹, H. Sun², P. H. Diamond³, C. Gao¹, M. Greenwald¹,
A. Hubbard¹, Y. Podpaly¹, J. Terry¹, I. Cziegler³, L. F. Delgado-Aparicio⁴,
P. Ennever¹, D. Ernst¹, J. Hughes¹, E. Marmar¹, M. Porkolab¹, W. Rowan⁵, and
S. Wolfe¹

¹*Plasma Science and Fusion Center, MIT, Cambridge, USA*

²*National Fusion Research Institute, Daejeon, Republic of Korea*

³*CMTFO UCSD, San Diego, USA*

⁴*Princeton Plasma Physics Laboratory, Princeton, USA*

⁵*IFS, University of Texas at Austin, Austin, USA*

Corresponding Author: rice@psfc.mit.edu

Recently, the connection among rotation reversals, energy confinement saturation (the transition between the LOC and saturated Ohmic confinement, SOC, regimes) and changes in underlying turbulence has been demonstrated. Examination of the rotation reversal results and a large body of confinement saturation observations suggests that there is a critical value of the collisionality where these effects transpire. Also occurring with the rotation reversals and the LOC/SOC transition is a saturation of the electron density profile peaking. These results may be unified with the following ansatz: at low collisionality in the LOC regime, the underlying turbulence is dominated by trapped electron modes and the rotation is directed co-current; at high collisionality in the SOC regime, ion temperature gradient modes prevail, the rotation is counter-current and the density profile peaking saturates. There are two other phenomena which appear to be related and occur at the LOC/SOC transition: a transformation from non-diffusive to diffusive heat transport and a change from symmetric up/down edge impurity density profiles to up/down asymmetric. Heat transport was investigated by means of rapid edge cooling from impurity injection by laser blow-off, and following the electron temperature profile evolution from electron cyclotron emission. In the high density in the SOC regime, there is “normal” diffusive heat transport, with a drop in the core temperature lagging the edge cooling by about an energy confinement time. Also with SOC, the core rotation is counter-current, and there is a significant up/down edge impurity density asymmetry. At low density in the LOC regime, the core electron temperature increases (on a faster time scale) following the edge cooling, indicating the workings of a convective heat pinch or transient ITB. The core rotation with LOC is co-current and the edge impurity density profile is up/down symmetric. Rotation reversal, the transformation from non-diffusive to diffusive heat transport, the switch of edge impurity density profiles from up/down symmetric to asymmetric and changes in turbulence have all been observed dynamically during a single discharge with a density ramp to change the collisionality. These empirical results unify a large body of previously seemingly unrelated phenomena.

EX

ECRH Effects on Toroidal Rotation: KSTAR Experiments and Gyrokinetic Simulations of Intrinsic Torque at ITG–TEM Transitions

Y. Shi¹, J. Kwon², S. Lee¹, W. Ko¹, T. Rhee², P. H. Diamond^{2,3}, S. Yi², K. Ida⁴, L. Terzolo¹, S. Yoon¹, J. Lee¹, K. Lee¹, Y. Nam¹, Y. Bae¹, M. Bitter⁵, and K. Hill⁵

¹National Fusion Research Institute, Daejeon, Republic of Korea

²WCI Center for Fusion Theory, National Fusion Research Institute, Daejeon, Republic of Korea

³CMTFO and CASS, University of California, San Diego, USA

⁴National Institute for Fusion Science, Toki, Japan

⁵Princeton Plasma Physics Laboratory, Princeton, USA

Corresponding Author: yjshi@nfri.re.kr

Toroidal rotation is important for control of stability and transport in tokamaks. Intrinsic rotation is self-generated by ambient turbulence via the non-diffusive residual stress, which motivates the question of how macroscopic rotation profiles will evolve in response to changes in the ambient micro-turbulence. One “control knob” for the micro-turbulence population is the heating mix of NBI and ECRH. The change in rotation to counter-direction by ECH in KSTAR is explained by the turbulence change from ITG to CTEM. We investigate the effect of ECRH heating on NBI-driven toroidal rotation profiles in L-mode and H-mode discharges in KSTAR tokamak. 1.3 MW of NBI is injected in the co-current direction and 350 kW of ECRH are applied. The ion temperature and toroidal rotation are measured with high resolution XICS and CES. NBI in the co-current direction drives peaked rotation profiles with (H-mode) and without (L-mode) a pedestal. Dramatic decreases in the core toroidal rotation values are observed when on-axis ECRH is added to H-mode. These increments $\Delta V_\phi/V_\phi \sim -30\%$ indicate the presence of on ECH-induced counter-current torque acting in the discharge core. We note that, for steady state with same external torque and boundary condition, the change of the radial gradient of plasma rotation implies the change of residual stress. Interestingly, edge and pedestal rotation velocities in H-mode are nearly unchanged. We explore the viability of the ITG–TEM transition as an explanation of the observed change in the sign of the core intrinsic torque. The global gyrokinetic code gKPSP was used for the study. We performed ITG and TEM simulations at values of $\eta_i = 3.1$ (i.e., ITG) and $\eta_i = 1.0$ (i.e., TEM), respectively. Note that the low value of η_i for the CTEM case is qualitatively consistent with the reduction in core ∇T_i observed with ECRH in KSTAR. Results show that the residual stress changes sign as ITG–TEM transition occurs, indicating a change in the direction of the net wave energy density flux. Direct simulations also reveal a mean macroscopic profile reversal at ITG–TEM transition, thus confirming the overall consistency of the argument. Also we will perform nonlinear gyrokinetic simulations to calculate the strength of intrinsic torque reversal at ITG–TEM transition and compare the simulation results with experiments.

EX

Dependence of Heat Transport and Confinement on Isotopic Composition in Conventional H-mode Plasmas in JT-60U

H. Urano¹, T. Takizuka², T. Nakano¹, T. Fujita¹, N. Oyama¹, Y. Kamada¹, and
N. Hayashi¹

¹*Japan Atomic Energy Agency, Naka, Japan*

²*Osaka University, Suita, Osaka, Japan*

Corresponding Author: urano.hajime@jaea.go.jp

Dependence of heat transport on isotopic composition is investigated in conventional H-mode plasmas for the application to ITER. The identical profiles of electron density, electron temperature and ion temperature are obtained for hydrogen and deuterium plasmas while the required power becomes clearly larger for hydrogen, resulting in the reduction of the heat diffusivity for deuterium.

The result of the identical temperature profiles in spite of different heating power suggests that the characteristics of heat conduction differs essentially between hydrogen and deuterium even at the same scale length of temperature gradient. On the other hand, the edge stability is improved by increased total poloidal beta regardless of the difference of the isotopic composition.

EX

Extension of Operational Regime in High-Temperature Plasmas and the Dynamic-Transport Characteristics in the LHD

H. Takahashi¹, M. Osakabe¹, K. Nagaoka¹, S. Murakami², I. Yamada¹, Y. Takeiri¹, M. Yokoyama¹, L. Hyungho³, K. Ida¹, R. Seki¹, C. Suzuki¹, M. Yoshinuma¹, T. Ido¹, A. Shimizu¹, M. Goto¹, S. Morita¹, T. Shimoizuma¹, S. Kubo¹, S. Satake¹, S. Matsuoka¹, N. Tamura¹, H. Tsuchiya¹, K. Tanaka¹, M. Nunami¹, A. Wakasa², K. Tsumori¹, K. Ikeda¹, H. Nakano¹, M. Kasaki¹, Y. Yoshimura¹, M. Nishiura¹, H. Igami¹, T. Seki¹, H. Kasahara¹, K. Saito¹, R. Kumazawa¹, S. Muto¹, K. Narihara¹, T. Mutoh¹, O. Kaneko¹, and H. Yamada¹

¹National Institute for Fusion Science, Toki, Japan

²Department of Nuclear Engineering, Kyoto University, Kyoto, Japan

³Department of Nuclear Fusion and Plasma Science, University of Science and Technology, Daejeon, Republic of Korea

Corresponding Author: takahashi.hiromi@lhd.nifs.ac.jp

Realization of high- T_i plasmas is one of the most important issues in helical plasmas, which have an advantage for steady-state operation comparison with tokamak plasmas. Since 2010, newly installed perpendicular-NBI with the beam energy of 40 keV has been operational in the Large Helical Device (LHD) and the total-heating power of perpendicular-NBIs increased from 6 MW to 12 MW. Such low-energy NBIs are effective for ion heating and enabled us to achieve a higher T_i than that obtained previously. In the last experimental campaign, ICRF-discharge cleaning was adopted to reduce particle recycling from the wall. As a result, NBI-heating-power profile became peaked and the density-normalized ion heating power in the core region increased by 18% and the central T_i of 7 keV, which is the world's highest value for helical devices, was successfully achieved as the new record in the LHD.

In the LHD, high- T_i plasmas have been realized in combination with a carbon pellet. The kinetic-energy confinement was improved by a factor of 1.5 after the pellet injection. In the high- T_i phase, a flat or hollow profile in the electron density has been observed. This is the different characteristics from PEP mode investigated in Tokamaks. After the pellet injection, the central T_i , the gradient of T_i and that of the toroidal-flow velocity at the core region clearly increased indicating the formation of the ion-internal-transport barrier. In the high- T_i phase, reduction of the thermal diffusivity over the wide region was observed. In the core region, the time constant of the improvement of the ion-heat transport was found to be larger than that in the peripheral region. The toroidal-momentum transport was also improved accompanied with the reduction of the thermal diffusivity and the Prandtl number ignoring the intrinsic torque was close to unity. However, the confinement improvement was temporal and the gradient of T_i gradually decreased. Similarly, the toroidal-momentum transport went back to the low-confinement state in the latter phase of the discharge. Decrease of the negative radial electric field and increase of the density fluctuation were also observed in the phase.

EX

Advances in the Physics Understanding of ELM Suppression Using Resonant Magnetic Perturbations in DIII-D

M. R. Wade¹, R. Nazikian², R. J. Buttery¹, J. S. de Grassie¹, T. E. Evans¹,
N. M. Ferraro¹, G. R. McKee³, R. A. Moyer⁴, D. M. Orlov⁴, O. Schmitz⁵,
P. B. Snyder¹, and L. Zeng⁶

¹General Atomics, San Diego, USA

²Princeton Plasma Physics Laboratory, Princeton, USA

³University of Wisconsin-Madison, Madison, USA

⁴University of California San Diego, USA

⁵Forschungszentrum Jülich, Jülich, Germany

⁶University of California Los Angeles, Los Angeles, USA

Corresponding Author: wade@fusion.gat.com

Recent experiments on DIII-D have increased confidence in the ability to suppress edge localized modes (ELMs) using edge-resonant magnetic perturbations (RMPs) in ITER, including an improved physics basis of the edge response to RMPs as well as expansion of RMP ELM suppression to more ITER-like conditions. Experiments aimed at an improved physics understanding have revealed a complex plasma response in the edge region that combines aspects of ideal MHD, vacuum field penetration, and direct turbulent response to the applied RMP. New observations include RMP-induced helical displacements near the separatrix that increase with q_{95} , a displacement inversion layer in the edge temperature profile response when a rational surface associated with the largest applied RMP poloidal harmonics ($m = 10 - 12$, $n = 3$ or $m = 9 - 11$, $n = 2$) is located near the pedestal top, and nearly instantaneous changes in density fluctuations throughout the pedestal region to $n = 3$ RMP amplitude variations. This complex response results in transport modifications near the q_{95} window for edge localized mode (ELM) suppression that result in ~30% narrower pedestal width than observed without the RMP applied. These experiments have taken advantage of DIII-D's unique capability to vary the RMP spectrum ($n = 3$ from one or two internal coils, $n = 2$) as well as toroidal phase variations of $n = 3$ and $n = 2$ RMPs for enhanced diagnostic fidelity, all done at the pedestal collisionality levels expected in ITER. In addition, RMP ELM suppression has been expanded to include the use of $n = 2$ RMPs and has been robustly obtained in the ITER baseline scenario ($q_{95} = 3.1$) using a single-row $n = 3$ RMP.

Work supported by the US DOE under DE-FC02-04ER54698, DE-AC02-09CH11466, DE-FG02-89ER53296, DE-FG02-08ER54999, DE-FG02-07ER54917, and DE-FG02-08ER54984.

Understanding ELM Mitigation by Resonant Magnetic Perturbations on MAST

A. Kirk¹, I. Chapman¹, Y. Liu¹, P. Cahyna², J. Harrison¹, P. Denner¹, G. Fishpool¹,
Y. Liang³, E. Nardon⁴, S. Saarelma¹, R. Scannell¹, and A. Thornton¹

¹EURATOM/CCFE Fusion Association, Abingdon, UK

²Institute of Plasma Physics AS CR, Prague, Czech Republic

³EURATOM-FZ Jülich, Jülich, Germany

⁴Association Euratom/CEA, St. Paul-lez-Durance, France

Corresponding Author: andrew.kirk@ccfe.ac.uk

MAST is equipped with 18 coils (6 in the upper row and 12 in the lower row) for use in Resonant Magnetic Perturbation (RMP) ELM control experiments. These coils give considerable flexibility since they allow a range of toroidal mode numbers (up to $n = 6$) but also allow improved alignment of the magnetic perturbations with the plasma equilibrium by allowing the phase of the applied field to be varied during the shot. In addition, mixed spectra (e.g., $n = 3$ and $n = 4$) can be applied. ELM suppression has not been achieved on MAST but ELM mitigation has been established in a range of plasmas using RMPs with toroidal mode numbers of $n = 3, 4$ or 6 . The RMPs produce an increase in the ELM frequency of up to a factor of 5 with a comparable decrease of the ELM size. Coincident with the effect on the ELMs, for the first time, clear lobe-like structures are observed near to the X-point. These lobes or manifold structures, that were predicted previously, have been observed for the first time in a range of discharges and their appearance is correlated with the effect of RMPs on the plasma i.e., they only appear above a threshold when a density pump out is observed or when the ELM frequency is increased. They appear to be correlated with the RMPs penetrating the plasma and may be important in explaining why the ELM frequency increases. The number and location of the structures observed can be well described using vacuum modelling. Differences in radial extent and poloidal width from vacuum modelling are likely to be due to a combination of transport effects and plasma screening.

Broader pedestal widths are observed during the ELM mitigated phase, resulting in lower pressure gradients which would normally suggest improved stability. The 2D separatrix has been modified to include several lobe structures in the X-point region. These equilibria have then been used as input to ELITE stability calculations, which show that such structures can destabilise ballooning modes, consistent with the increase in ELM frequency observed. In addition, a quasi-linear code, MARS-Q code has been used to investigate the effects of the penetration process and plasma response on the observed structures. These computations quantify several factors affecting the dynamics of the RMP field penetration.

Work supported by the RCUK Energy Programme and EURATOM.

EX

ELM Control in Application of Non-Axisymmetric Magnetic Perturbations in KSTAR

Y. M. Jeon¹, J. K. Park², S. Yoon¹, K. D. Lee¹, J. G. Bak¹, Y. Nam¹, W. Ko¹,
S. G. Lee¹, W. Kim¹, Y. K. Oh¹, J. G. Kwak¹, K. Lee¹, H. Kim¹, H. Y. Yang¹, and
G. Yun³

¹*National Fusion Research Institute, Daejeon, Republic of Korea*

²*Princeton Plasma Physics Laboratory, Princeton, USA*

³*Pohang University of Science and Technology, Pohang, Republic of Korea*

Corresponding Author: ymjeon@nfri.re.kr

In 2011 KSTAR campaign, we successfully demonstrated an ELM suppression by applying small non-axisymmetric magnetic perturbations, which is the first achievement by using $n = 1$ magnetic perturbations (MPs) [1] while DIII-D did by using $n = 3$ MPs [2]. The ELM-suppressed MP discharges show several unique features such as two step ELM responses (intensification and then suppression) and a gradual increase of density in the ELM-suppressed phase. Also, there were several interesting phenomena caused by the applied MPs found:

1. A saturation of T_e pedestal evolution suggesting an enhanced electron thermal transport in the pedestal.
2. An abrupt change of floating potential on divertor plate depending on the applied magnetic spectra suggesting a distinctive change of pedestal particle transport.
3. A characteristic broadband change of magnetic fluctuations depending on the magnetic spectra showing a correlation with the edge T_e evolution.

Also it was validated that the ELMs can be intensified (increased size and reduced frequency) by applying a particular $n = 1$ MP, which is another important ELM response for further understanding of ELM-MP physics mechanism. Furthermore a variety of ELM responses to different magnetic spectra has been observed such as a strong mitigation and a direct H/L back-transition by $n = 1$ MPs, and even a triggering by $n = 2$ MP. It reveals out the importance of understanding the underlying ELM-RMP physics mechanism and of optimizing the magnetic spectra on ELM control.

References

- [1] Y. M. Jeon, *et al.*, submitted to Phys. Rev. Lett. (2011)
- [2] T. E. Evans, *et al.*, Phys. Rev. Lett. **92**, (2004) 235003

Mitigation of Edge Localised Modes with Small Non-axisymmetric Magnetic Perturbations in ASDEX Upgrade

W. Suttrop¹, L. Barrera Orte¹, T. Eich¹, R. Fischer¹, J. C. Fuchs¹, M. Kocan¹,
T. Lunt¹, R. McDermott¹, T. Pütterich¹, S. Rathgeber¹, M. Rott¹, F. Ryter¹,
T. Vierle¹, E. Viezzer¹, and E. Wolfrum¹

¹ *Max-Planck-Institut für Plasmaphysik, Garching, Germany*

Corresponding Author: wolfgang.suttrop@ipp.mpg.de

The ASDEX Upgrade tokamak is currently being enhanced with a set of in-vessel saddle coils to study the effects of non-axisymmetric magnetic perturbations. One of the most pronounced phenomena is the mitigation of Edge Localised Modes (ELMs) when $n = 2$ perturbation fields are applied in High-confinement mode. In addition, the effects on the H-mode transition threshold, pellet injection, scrape-off-layer transport, plasma rotation, radial electrical field, divertor target power deposition, and edge gradients in the H-mode transport barrier region are studied in recent experiments.

ELM mitigation appears as a distinct transition from type-I ELMs to a type of small ELMs with much reduced divertor power load. Stored energy, plasma density and pedestal pressure in the mitigated phase remain close to unmitigated type-I ELMy phases. H-mode edge barrier gradients do not change significantly as ELMs become mitigated, however the H-mode pedestal top density increases slightly due to increased particle confinement with coil currents on. The edge pedestal top electron pressure remains virtually unchanged. Effective ion charge, Z_{eff} , and tungsten concentration typically drop as ELMs become mitigated. A main requirement for ELM mitigation is the plasma edge density exceeding a threshold which depends on plasma current and can be described as a fixed fraction of the Greenwald density, $f_{\text{GW}} = 0.65$. So far, “density pump-out” has been observed at lower plasma density, but not above the ELM mitigation threshold.

Access to ELM mitigation does not seem to depend on whether the applied perturbation field is aligned with the equilibrium magnetic field (“resonant”) or not. This is tested by changing the parity of upper and lower coil currents, which yields a variation of the resonant field component by a factor of five. However, the coil current threshold for ELM mitigation is found to be unchanged.

Effects of the non-axisymmetric field perturbation are observed at the plasma boundary however in the plasma core no effect on plasma rotation and no interaction with pre-existing neoclassical tearing mode islands are detected. This indicates that the resonant perturbation field amplitude is effectively shielded in the plasma interior.

EX

Fuel Retention Studies with the ITER-like Wall in JET

S. Brezinsek¹, T. Loarer², V. P. Philipps¹, H. G. Esser¹, S. Grünhagen³, R. Smith³,
R. Felton³, U. Samm¹, J. W. Coenen¹, M. Groth⁴, M. Stamp³, J. Banks³,
G. Matthews³, A. Boboc³, S. Knipe³, D. Douai², M. Clever¹, U. Kruezi¹,
M. Fresinger¹, A. Huber¹, J. Bucalossi², S. Vartagnian², R. Neu⁵, J. Hobirk⁵, P. Belo⁶,
I. Nunes⁶, M. F. Nave⁶, D. Frigione⁷, S. Jachmich⁸, A. Meigs³, and I. Coffey⁹

¹*Institute of Energy- and Climate Research, Forschungszentrum Jülich, Association EURATOM-FZJ, Germany*

²*CEA, IRFM, Saint-Paul-lez-Durance, France*

³*EURATOM/CCFE Fusion Association, Culham Science Centre, Abingdon, UK*

⁴*Aalto University, Espoo, Finland*

⁵*Max-Planck-Institut für Plasmaphysik, Garching, Germany*

⁶*Institute of Plasmas and Nuclear Fusion, Association EURATOM-IST, Lisbon, Portugal*

⁷*Associazione EURATOM-ENEA sulla Fusione, Frascati, Rome, Italy*

⁸*Association Euratom-Etat Belge, ERM-KMS, Brussels, Belgium*

⁹*Queen's University Belfast, Belfast, UK*

Corresponding Author: s.brezinsek@fz-juelich.de

JET underwent a transformation from a full carbon-dominated device with all Plasma-Facing Components (PFCs) made of Carbon-Fibre Composites (CFC) to a full metallic device with Be PFCs in the main chamber, bulk W at the outer target plate, and W-coated CFC elsewhere in the divertor. The ITER-Like Wall (ILW) experiment at JET provides an ideal test bed for the ITER material choice in the DT phase and shall demonstrate as primary goals the plasma compatibility with the new metallic wall and the expected reduction in fuel retention. We report on a set of experiments ($I_p = 2.0$ MA, $B_t = 2.4$ T) in different plasma conditions (ohmic, L- and H-mode) with global gas balance demonstrating a strong reduction of the long term fuel retention with the ILW by a factor ten with respect to previously performed CFC references. All experiments have been executed in series of identical plasma discharges in order to achieve a maximum of plasma duration until the analysis limit for the Active Gas Handling System has been reached. The composition analysis shows high purity of the recovered gas, typically 99% D, with a reduction of residual hydrocarbons with operational time. For typical L-mode discharges (0.5 MW RF heating) and type III ELMy H-mode plasmas (5.0 MW NBI heating) in high triangularity a drop of the retention rate from 1.27×10^{21} D/s and 1.37×10^{21} D/s to values down to 4.8×10^{19} D/s and 7.2×10^{19} D/s, respectively, has been measured. The retention rate is normalised to the integral divertor time which amounts 440 s for the L-mode and 317 s for the H-mode plasmas. The dynamic retention increases in the limiter phase with the Be first wall in comparison with CFC, but also the outgassing after the discharge has risen in the same manner and compensates this transient retention.

The main retention mechanism for the long term retention is the co-deposition of fuel with Be eroded from the main chamber, whereas the fuel content in the Be layers is potentially reduced by one order in comparison with carbon layers as laboratory experiments suggested. The lower retention is also in line with the reduction of the C flux in the same order in the plasma edge layer measured by optical spectroscopy. The reduction is fully supportive in the ITER material choice and widens the operational space without active cleaning and is in line with retention predictions by J. Roth [1].

References

[1] J. Roth, J. Nucl. Mater. **390** (2009).

Comparison of Plasma Breakdown with a Carbon and ITER-like Wall

P. C. de Vries¹, A. C. C. Sips^{2,3}, H. T. Kim^{4,5}, P. J. Lomas⁴, F. Mavigilia⁵,
R. Albanese⁶, I. Coffey⁴, E. Joffrin⁷, M. Lehnen³, M. O'Mulane⁴, I. Nunes^{2,9},
G. van Rooij¹, F. Rimini⁴, and M. Stamp⁴

¹*FOM DIFFER, Nieuwegein, Netherlands*

²*JET-EFDA, Culham Science Centre, Abingdon, UK*

³*European Commission, Brussels, Belgium*

⁴*CCFE/Fusion Association, Culham Science Centre, Abingdon, UK*

⁵*Department of Physics, Imperial College London, London, UK*

⁶*Associazione EURATOM-ENEA-CREATE, Univ. di Napoli Federico II, Napoli, Italy*

⁷*CEA-IRFM, Association Euratom-CEA, Cadarache, France*

⁸*Institut für Energie- und Klimaforschung-IEK-4, Forschungszentrum Jülich, EURATOM Association, Jülich, Germany*

⁹*Associação EURATOM-IST, Instituto de Plasmas e Fusão Nuclear, Lisboa, Portugal*

Corresponding Author: p.c.devries@diff.nl

The standard method to initiate plasma in a tokamak is, to ionize pre-filled gas by applying a toroidal electric field via transformer action from poloidal coils. For ITER the available electric field will be limited to low values of 0.33 V/m, raising considerable interest to understand and optimise the plasma breakdown process. At JET un-assisted breakdown has previously been achieved at electric fields as low as 0.23 V/m though with carbon plasma-facing components. It is well-known that impurities can have a impact on the breakdown process. The recent installation of a full metal, ITER-like, first wall provided the opportunity to study the impact of the plasma-facing materials on breakdown. This study will present for the first time a full experimental characterisation of tokamak breakdown at JET, using all discharges since 2008, covering both operations with a main chamber carbon and beryllium ITER-like wall.

It was found that the avalanche phase was unaffected by the change in wall material. However, the large reduction in carbon levels resulted in significant lower radiation during the burn-through phase of the breakdown process. Breakdown failures, that usually developed with a carbon wall during the burn-through phase (especially after disruptions) were absent with the ITER-like wall.

A new model of plasma burn-through including plasma-surface interaction effects has been developed. The simulations show that chemical sputtering of carbon is the determining factor for the impurity content, and hence the radiation, during the burn-through phase for operations with a carbon wall. For a beryllium wall, the plasma surface effects do not raise the radiation levels much above those obtained with pure deuterium plasmas, similar as seen in the experimental study discussed above.

EX

On the Challenge of Plasma Heating with the JET Metallic Wall

M. L. Mayoral¹, O. Asunta², V. Bobkov³, C. Challis¹, D. Ciric¹, J. W. Coenen⁴,
L. Colas⁵, A. Czarnecka⁶, I. Day¹, A. Ekedahl⁵, C. Giroud¹, M. Garcia-Munoz³,
M. Goniche⁵, M. Graham¹, P. Jacquet¹, I. Jenkins¹, E. Joffrin⁵, T. Jones¹, D. King¹,
R. King¹, V. Kiptily¹, K. Kirov¹, C. Klepper⁷, E. Lerche⁸, C. Maggi³, J. Mailloux¹,
F. Marcotte⁹, G. Matthews¹, D. Milanese¹⁰, I. Monakhov¹, M. Nightingale¹, R. Neu³,
J. Ongena⁸, T. Pütterich³, V. Riccardo¹, F. Rimini¹, J. Strachan¹¹, E. Surrey¹,
V. Thompson¹, D. Van Eester⁸, and G. van Rooij¹²

¹Association EURATOM-CCFE, Culham Science Centre, Abingdon, UK

²Aalto University, Association EURATOM-Tekes, Aalto, Finland

³Max-Planck-Institut für Plasmaphysik, Garching, Germany

⁴Forschungszentrum Jülich, Jülich, Germany

⁵CEA, St-Paul-Lez-Durance, France

⁶Association Euratom-IPPLM, Warsaw, Poland

⁷Oak Ridge National Laboratory, Oak Ridge, USA

⁸Association "EURATOM - Belgian State", Brussels, Belgium

⁹École Nationale des Ponts et Chaussées, Marne-la-Vallée, France

¹⁰Associazione EURATOM-ENEA sulla Fusione, Politecnico di Torino, Italy

¹¹Princeton University, Princeton, USA

¹²DIFER, Association EURATOM-FOM, Nieuwegein, Netherlands

EX

Corresponding Author: marie-line.mayoral@ccfe.ac.uk

In this contribution, the major aspects linked to the use of the JET heating systems: NBI, ICRF and LHCD, in an ITER-like wall will be presented. We will show that although each system had its own issues, efficient and safe plasma heating was obtained with still room on each system for higher power. For the NBI up to 21 MW was safely coupled, issues that had to be tackled were for example the beam shine through and the beam "re-ionisation". For the ICRF system, that has coupled 5 MW in L-mode and 3 MW H-mode, the main area of concern was linked to acceleration of ions in the sheath rectified voltages created by the residual parallel electric field on the antenna structure and related heat loads and impurities production. For the LH, arcing and generation of fast electron beams in front of the launcher that can lead to high heat loads were the keys issues but 2.5 MW were delivered without problems. For each system, an overview will be given of their compatibility with the new Be/W first wall, of the main modifications implemented to be able to use them in a metallic environment and a review of differences in behavior compared with the previously installed first wall in C, with special emphasis on impurity content in the plasma and heat loads on the first wall. When relevant, the JET experience will be put in the context of ITER.

Control of 3D Edge Radiation Structure with Resonant Magnetic Perturbation Fields Applied to Stochastic Layer and Stabilization of Radiative Divertor Plasma in LHD

M. Kobayashi¹, S. Masuzaki¹, I. Yamada¹, N. Tamura¹, N. Ohno², B. J. Peterson¹,
K. Tanaka¹, Y. Narushima¹, T. Akiyama¹, K. Sato¹, M. Goto¹, S. Morita¹, and
Y. Feng³

¹*National Institute for Fusion Science, Tokyo, Japan*

²*Nagoya University, Nagoya, Japan*

³*Max-Planck-Institute für Plasmaphysik, Greifswald, Germany*

Corresponding Author: kobayashi.masahiro@lhd.nifs.ac.jp

It is found that resonant magnetic perturbation (RMP) fields has stabilizing effect on radiating edge plasma, realizing stable sustainment of radiative divertor (RD) operation in the Large Helical Device (LHD). Without RMP, otherwise, thermal instability leads to radiative collapse. Divertor power load is reduced by a factor of 3 – 10 during the RMP assisted RD phase. RMP has $m/n = 1/1$ mode, which has resonance layer in the edge stochastic region, and creates remnant island. 3D edge transport simulation result, which is consistent with the radiation profile measurement, show radiation condensation around X-point of the island, where the code predicts $n_e > 10^{20} \text{ m}^{-3}$ and $T_e \sim \text{a few eV}$. The well structured edge radiation with RMP such as the selective cooling around X-point is considered to provide stabilization effect by holding the intense radiation there and thus avoids it penetrating inward. It has also been demonstrated that RMP fields itself can onset transition to RD operation by increasing perturbation strength while density and input power are kept constant. The results show a possibility of new control knob for divertor power load in 3D magnetic field configuration. Operation range of RMP assisted RD is identified in terms of RMP strength and radial location of resonance layer of RMP.

EX

Dynamics of Energetic Particle Driven Modes and MHD Modes in Wall-stabilized High- β Plasmas on JT-60U and DIII-D

G. Matsunaga¹, M. Okabayashi², K. Shinohara¹, N. Aiba¹, J. R. Ferron³,
W. W. Heidbrink⁴, C. T. Holcomb⁵, G. L. Jackson³, Y. In⁶, T. C. Luce³,
W. M. Solomon², E. J. Strait³, and Y. Q. Liu⁷

¹*Japan Atomic Energy Agency, Japan*

²*Princeton Plasma Physics Laboratory, Princeton, USA*

³*General Atomics, San Diego, USA*

⁴*University of California-Irvine, Irvine, USA*

⁵*Lawrence Livermore National Laboratory, Livermore, USA*

⁶*FAR-TECH, Inc., General Atomics, San Diego, USA*

⁷*Euratom/CCFE Fusion Association, Culham Science Centre, Abingdon, UK*

Corresponding Author: matsunaga.go@jaea.go.jp

In the wall-stabilized high- β plasmas in JT-60U and DIII-D, interesting interactions of energetic particle (EP) driven modes and MHD modes have been observed. First, EP-driven modes trigger resistive wall modes (RWMs) and edge localized modes (ELMs).

In both devices, EP-driven modes have been observed in the high- β plasmas above the no-wall β limit; these modes are called “Energetic particle driven Wall Mode (EWM)” in JT-60U and “Off-axis Fishbone Mode (OFM)” in DIII-D. The triggering of ELM by the EWM/OFM is found to correlate with EP transport induced by the EWM/OFM. Moreover, the triggering of RWM by the EWM/OFM is thought to be due to reduction of the EP stabilization effect on the RWM stability. Second, a slow $n = 1$ magnetic oscillation has been observed together with an ELM. This $n = 1$ magnetic oscillation seems to occur due to ELM before the RWM onset, thus, the RWM stability is becoming marginal. Since the time scale of this oscillation is comparable to the marginal RWM time scale, this is considered to be the ELM-impacted RWM.

EX

Studies of Energetic-ion-driven MHD Instabilities in Helical Plasmas with Low Magnetic Shear

S. Yamamoto¹, E. Ascasíbar², R. Jiménez-Gómez², S. Kobayashi¹, S. Ohshima¹,
K. Yasuda³, K. Nagaoka⁴, D. Spong⁵, D. Pretty⁶, K. Nagasaki¹, T. Mizuuchi¹,
H. Okada¹, T. Minami¹, Y. Nakamura³, K. Hanatani¹, S. Konoshima¹, T. Estrada²,
K. Mukai³, H. Y. Lee³, L. Zang³, F. Sano¹, and B. Blackwell⁶

¹*Institute of Advanced Energy, Kyoto University, Kyoto, Japan*

²*National Laboratory for Magnetic Fusion, CIEMAT, Madrid, Spain*

³*Graduate School of Energy Science, Kyoto University, Kyoto, Japan*

⁴*National Institute for Fusion Science, Toki, Japan*

⁵*Oak Ridge National Laboratory, Oak Ridge, USA*

⁶*Plasma Research Laboratory, The Australian National University, Canberra, Australia*

Corresponding Author: syama@iae.kyoto-u.ac.jp

We discuss the features of energetic-ion-driven MHD instabilities such as Alfvén eigenmodes (AEs) in three-dimensional magnetic configuration with low magnetic shear and low toroidal field period number (N_p) that are characteristic of advanced helical plasmas. Comparison of experimental and numerical studies in Heliotron J with those in TJ-II indicates that the most unstable AE is global AE (GAE) in the low rotational transform (ι) configuration and helicity-induced AE (HAE) in the high ι configuration.

EX

Observation of GAM Induced by Energetic Electrons and NL Interactions among GAM, BAEs and Tearing Modes on the HL-2A Tokamak

W. Chen¹, X. T. Ding¹, L. M. Yu¹, X. Q. Ji¹, J. Q. Dong¹, Q. W. Yang¹, Y. Liu¹,
M. Isobe², L. W. Yan², S. Y. Chen³, J. Cheng¹, Y. Zhou¹, W. Li¹, Z. W. Xia¹,
X. M. Song¹, Z. B. Shi¹, Y. Huang¹, and X. R. Duan¹

¹*Southwestern Institute of Physics, Chengdu, China*

²*National Institute for Fusion Science, Toki, Japan*

³*College of Physical Science and Technology, Sichuan University, Chengdu, China*

Corresponding Author: chenw@swip.ac.cn

The very low-frequency (LF) Alfvénic and acoustic fluctuations, such as beta-induced Alfvén eigenmode (BAE), and geodesic acoustic mode (GAM), are presently of considerable interest in the present-day fusion and future burning plasmas. The low-frequency waves can significantly affect the plasma performance, and induce the particle losses and reduce the plasma self-heating. These LF instabilities can play a key role in turbulence and anomalous transport regulation, especially, while there is significant fraction of high energy particles in plasma. They can be used as energy channels to transfer the fusion-born-alpha-particle energy to the thermonuclear plasma, i.e., GAM/BAE channeling.

The energetic-electron and magnetic-island induced BAEs had been observed and investigated on HL-2A in the previous works. In the present paper, we will present our further works about the LF Alfvénic and acoustic modes, and it is reported that the first experimental results are associated with the GAM induced by energetic-electrons (termed eEGAM) in HL-2A Ohmic plasma. The energetic-electrons are generated by parallel electric fields during magnetic reconnection associated with tearing mode (TM). The energy spectra, which detected by Cadmium-telluride (CdTe) scintillators, indicate that the energetic electrons redistribute during strong TM. The magnetic fluctuation spectrogram indicates that the eEGAM is always accompanied by TM and BAEs. The eEGAM is not observed in the absence of strong TM and BAEs, and its mode frequency always complies with

$$f_{\text{GAM}} = f_{\text{BAE2}} - f_{\text{TM}}, \quad f_{\text{GAM}} = f_{\text{BAE1}} + f_{\text{TM}} \quad (1)$$

as well as

$$f_{\text{GAM}} = \frac{f_{\text{BAE1}} + f_{\text{BAE2}}}{2}. \quad (2)$$

The eEGAM localizes in the core plasma, i.e., in the vicinity of $q = 2$ surface where the ion Landau damping γ_i is larger than the edge due to $\gamma_i \propto \exp(-q^2)$, and is very different from that excited by the drift-wave turbulence in the edge plasma. The analysis indicated that the eEGAM is provided with the magnetic components, whose intensities depend on the poloidal angles, and its mode numbers are $|m/n| = 2/0$ which are consistent with the theoretical prediction. The new findings give a deep insight into the underlying physics mechanism for the excitation of the LF Alfvénic/acoustic fluctuation and zonal flows (ZFs).

The Effect of ELM Mitigation Methods on the Access to High H-mode Confinement ($H_{98} \sim 1$) on JET

E. de la Luna^{1,2}, R. Sartori³, G. Saibene³, P. Lomas⁴, V. Parail⁴, M. N. A. Beurskens⁴,
E. Delabie⁵, D. Dodt⁶, C. Giroud⁴, D. Harting⁷, N. Hawkes⁴, F. Koechl⁸, C. Maggi⁶,
D. McDonald⁴, F. Rimini⁴, A. Loarte⁹, and E. R. Solano²

¹EFDA-CSU, Culham Science Centre, Abingdon, UK

²Laboratorio Nacional de Fusion, Asociacion EURATOM-CIEMAT, Madrid, Spain

³Fusion for Energy, Joint Undertaking, Barcelona, Spain

⁴EURATOM/CCFE Fusion Association, Culham Science Centre, Abingdon, UK

⁵Dutch Institute for Fundamental Energy Research, Nieuwegein, Netherlands

⁶MPI für Plasmaphysik, EURATOM Association, Garching, Germany

⁷Institute for Energy Research-Plasma Physics, Forschungszentrum Jülich, Association EURATOM, Jülich, Germany

⁸Association EURATOM-ÖAW/ATI, Atominstitut, TU Wien, Austria

⁹ITER Organization, St. Paul Lez Durance, France

Corresponding Author: elena.de.la.luna@jet.efda.org

Since ITER is expected to operate at powers close to the H-mode threshold power scaling, it is important for ITER predictions to investigate the confinement and plasma dynamics in H-modes for heating powers marginally above the H-mode threshold power (P_{L-H}). The JET experience is that such operation leads to a transient behavior of the H-mode, with transitions from Type I ELMs to Type III or L-mode. One question relevant to the extrapolation to ITER is to which extent this transient behavior is related to the ELM dynamics (loss power in between ELMs, ELM crash) and therefore if it can be changed, and how, with ELM amelioration methods.

This paper describes experiments carried out in JET before the installation of the ITER-like wall to investigate the influence of ELM amelioration on the power requirements to obtain and maintain target H-mode confinement ($H_{98}(y) \sim 1$) in stationary conditions. Two ELM mitigation methods were used in these experiments: edge magnetic perturbations (static, $n = 2$) produced by Error Field Correction coils (EFCCs) and ELM pacing by fast vertical movements of the plasma column ("vertical kicks").

Experiments have shown that the power needed to access the stationary type I ELMy H-mode regime was reduced by $\sim 40\%$ (in high triangularity plasmas) with the use of vertical kicks without loss of confinement. On the other hand, applying edge magnetic perturbations in H-modes with P_{loss} close to P_{L-H} leads to a behavior of the H-mode normally associated with even lower P_{loss} (i.e., a Type I ELMy H-mode reverts to low ELM frequency regime). A set of experiments using slow NBI ramps during the application of EFCCs showed that while the P_{L-H} decreases in pulses with $I_{EFCC} = 2 - 3$ kA, the power required to achieve stationary conditions with regular type I ELMs in the same pulses increases, suggesting that different mechanisms are at play. The results obtained with both mitigation methods suggest that the power threshold for the type I ELM regime (with $H_{98}(y) \sim 1$ in stationary conditions) is not simply proportional to the power above P_{L-H} and other mechanism such as the ELM dynamics also plays a role. Analysis of the local plasma edge conditions leading to the H-mode and the plasma evolution after the L-H mode transition, will be presented and directions for future work discussed.

EX

Experimental Demonstration of High Frequency ELM Pacing by Pellet Injection on DIII-D and Extrapolation to ITER

L. R. Baylor¹, T. C. Jernigan¹, N. Commaux¹, S. K. Combs¹, S. J. Meitner¹,
N. H. Brooks², T. E. Evans², M. E. Fenstermacher³, C. J. Lasnier³, R. A. Moyer⁴,
T. H. Osborne², P. B. Parks², E. J. Strait², E. A. Unterberg¹, and A. Loarte⁵

¹*Oak Ridge National Laboratory, Oak Ridge, USA*

²*General Atomics, San Diego, USA*

³*Lawrence Livermore National Laboratory, Livermore, USA*

⁴*University of California, San Diego, USA*

⁵*ITER Organization, St Paul Lez Durance Cedex, France*

Corresponding Author: baylorlr@ornl.gov

Pellet pacing of edge localized modes (ELMs), which is the triggering of rapid small ELMs by pellet injection, has been proposed as a method to prevent large ELMs that can erode the ITER plasma facing components [1]. D₂ pellet injection has been used on the DIII-D tokamak to successfully demonstrate for the first time the pacing of ELMs at a 10× higher rate than natural ELMs. The demonstration of ELM pacing on DIII-D was made by injecting slow (< 200 m/s) 1.3 mm D₂ pellets at 60 Hz from the low field side in an ITER shaped plasma with a low natural ELM frequency of 5 Hz, $q_{95} = 3.5$, $\beta_N = 1.8$, and normalized energy confinement factor $H_{98} = 1.1$, with the input power only slightly above the H-mode threshold. The non-pellet similar discharges have ELM energy losses up to 50 kJ (~ 8% of total stored energy), while the case with pellets was able to demonstrate 60 Hz ELMs with an average ELM energy loss less than 5 kJ (< 1% of the total). Total divertor heat flux from the ELMs is reduced by more than a factor of 10 as measured by a fast framing IR camera. Central impurity accumulation of Ni is significantly reduced by the application of the 60 Hz pellets. No significant increase in density or decrease in energy confinement with the pellets was observed.

Experimental details have shown that the ELMs are triggered before the pellets reach the top of the H-mode pressure pedestal, implying that very small shallow penetrating pellets would be sufficient to trigger ELMs. Fast camera images of the pellets entering the plasma from the low field side show a local triggering phenomenon. A single plasma filament becomes visible near the pellet cloud and strikes the outer vessel wall within 200 μs followed by additional ejected filaments. The implications of these results for possible pellet ELM pacing on ITER will be discussed.

References

[1] P. T. Lang *et al.*, Nucl. Fusion **44** (2004) 665.

Work supported by the US Department of Energy under DE-AC05-00OR22725, DE-FC02-04ER54698, DE-AC52-07NA27344, and DE-FG02-07ER54917.

ELM Mitigation by Supersonic Molecular Beam Injection: KSTAR and HL-2A Experiments and Theory

W. W. Xiao^{1,2}, P. H. Diamond^{1,3}, W. C. Kim¹, L. H. Yao², S. W. Yoon¹, X. T. Ding²,
J. Kim¹, S. H. Hahn¹, M. Xu¹, G. S. Yun⁴, B. B. Feng², C. Y. Chen², W. L. Zhong²,
Z. B. Shi², J. Cheng², J. G. Bak¹, Y. U. Nam¹, J. W. Ahn⁵, H. K. Kim¹, H. T. Kim¹,
K. P. Kim¹, X. L. Zou⁶, H. K. Park⁷, G. H. Choe⁴, M. J. Choi⁴, J. I. Song¹,
S. G. Lee¹, T. Rhee¹, J. M. Kwon¹, D. L. Yu², K. D. Lee¹, W. H. Ko¹, S. I. Park¹,
M. Jung¹, Y. S. Bae¹, Y. K. Oh¹, J. G. Kwak¹, L. W. Yan², and J. Q. Dong²

¹National Fusion Research Institute, Daejeon, Republic of Korea

²Southwestern Institute of Physics, Chengdu, China

³University of California, San Diego, La Jolla, USA

⁴Pohang Univ. of Science and Technology, Pohang, Republic of Korea

⁵Oak Ridge National Laboratory, Oak Ridge, USA

⁶CEA, IRFM, Saint-Paul-lez-Durance, France

⁷Pohang University of Science and Technology, Pohang, Republic of Korea

Corresponding Author: xiaoww123@nfri.re.kr

New experimental results of ELM mitigation by supersonic molecular beam injection (SMBI) are report in HL-2A and KSTAR. The experiments show that ELM frequency increase

$$\frac{f_{\text{ELM}}^{\text{SMBI}}}{f_{\text{ELM}}^0} \sim 2 - 3.5, \quad (1)$$

and an ELM amplitude decrease for a finite duration period during an SMBI influence time, τ_I . Pedestal density profiles were relaxed by SMBI and recovered gradually during τ_I . This indicates that the degradation of pedestal particle confinement. Also, a slight changes of stored energy and toroidal rotation during τ_I was observed. A change in the spectrum of edge particle flux was observed in both devices. It shows that the in low frequency region is reduced while the high frequency component increases. This suggests that SMBI inhibits the formation of large (low frequency) avalanches or transport events, while triggering more small (high frequency) avalanches. A bi-stable sandpile model reproduces features of these experiments, showing a low frequency large scale transport event is break up into high frequency small scale events by particle injection inside the pedestal. Our experimental observations show that shallow injection, just inside the pedestal foot, will be enough to mitigate ELMs, indicating that the ITER requirement for low field side pellet injection to reach the pedestal top may be overly conservative.

EX

ELM Mitigation with SMBI & CJI Fuelling in HL-2A H-mode Plasmas

C. Y. Chen¹, L. H. Yao¹, B. B. Feng¹, Z. H. Shi¹, W. J. Zhong¹, J. Cheng¹, D. L. Yu¹,
Y. Zhou¹, Q. W. Yang¹, and X. R. Duan¹

¹*Southwestern Institute of Physics, Chengdu, China*

Corresponding Author: cheny@swip.ac.cn

For a tokamak fusion reactor, the mitigation of Edge Localized Mode (ELM) is likely a mandatory requirement to avoid excessive erosion of the divertor targets and yet exploit the benefits of high confinement mode operation. It is reported that pellets could trigger ELM when injected in type-I ELMy H-mode and ELM pacing has been accomplished with small multi-pellets injection. Resonant Magnetic Perturbation (RMP) is another effective method to ELM mitigation that full ELM suppression has been achieved on DIII-D and AUG. Recently, ELM amplitude decrease and frequency increase for a finite duration are observed after the Supersonic Molecular Beam Injection (SMBI) fuelling into H-mode plasmas on HL-2A. The same phenomenon is observed even more significantly after the Cluster Jet Injection (CJI) fuelling.

EX

The Dependence of H-mode Energy Confinement and Transport on Collisionality in NSTX

S. M. Kaye¹, S. Gerhardt¹, R. E. Bell¹, A. Diallo¹, W. Guttenfelder¹, B. P. LeBlanc¹,
and R. Maingi²

¹*Princeton Plasma Physics Laboratory, Princeton University, Princeton, USA*

²*Oak Ridge National Laboratory, Oak Ridge, USA*

Corresponding Author: kaye@pppl.gov

Understanding the dependence of confinement on collisionality in tokamaks is important for the design of next-step devices, which will operate at collisionalities at least one order of magnitude lower than in present generation. A wide range of collisionality has been obtained in the National Spherical Torus Experiment (NSTX) by employing two different wall conditioning techniques one with boronization and between-shot helium glow discharge conditioning, and one using lithium evaporation. Discharges with lithium conditioning generally achieved lower collisionality. The data from experiments using these different techniques differed in terms of their confinement dependence on dimensional, engineering variables; data from unlithiated discharges had a strong, nearly linear dependence on B_T , with a weaker dependence on I_p . The lithiated discharges, on the other hand, tended to follow the ITER 98(y,2) scaling. These different sets of data, however, were unified by an underlying dependence on collisionality, exhibiting a strong increase of normalized confinement time with decreasing collisionality, holding other dimensionless variables as fixed as possible. This result is consistent with gyrokinetic calculations that show microtearing and Electron Temperature Gradient modes to be more stable at lower collisionality.

This work was supported by U.S. Dept. of Energy Contract Nos. DE-AC02-09CH11466 and DE-AC05-00OR22725.

EX

New Meso-scale Electric Fluctuations Interacting with Magnetic Islands and Turbulence in Edge Plasmas of HL-2A

K. J. Zhao¹, J. Dong^{1,2}, L. W. Yan¹, P. H. Diamond^{3,4}, M. Xu³, G. R. Tynan³,
Z. X. Wang⁵, L. Wei⁵, K. Itoh⁶, A. Fujisawa⁷, Y. Nagashima⁷, S. Inagaki⁷,
W. Y. Hong¹, J. Cheng¹, Z. H. Huang¹, Q. Li¹, X. Q. Ji¹, Y. Huang¹, Y. Liu¹,
Q. W. Yang¹, X. T. Ding⁷, X. R. Duan¹, and S. I. Itoh⁷

¹*Southwestern Institute of Physics, Chengdu, China*

²*Institute for Fusion Theory and Simulation, Zhejiang University, Hangzhou, China*

³*Center for Momentum Transport and Flow Organization, University of California, San Diego, USA*

⁴*WCI Center for Fusion Theory, NRFI, Daejeon, Republic of Korea*

⁵*School of Physics and Optoelectronic Technology, Dalian University of Technology, Dalian, China*

⁶*National Institute for Fusion Science, Toki, Japan*

⁷*Research Institute for Applied mechanics, Kyushu University, Kasuga, Japan*

Corresponding Author: kjzhao@swip.ac.cn

New meso-scale electric fluctuations (MSEFs), having two components of $n = 0$ and $m/n = 6/2$ potential fluctuations, are first identified in the edge plasmas of a tokamak. The MSEFs coexist and interact with the magnetic fluctuations with two components of $n = 0$ and $m/n = 6/2$ (magnetic islands). The MSEFs also coexist and interplay with turbulence and low frequency zonal flow. The MSEFs mainly modulate the turbulence of frequencies higher than 100 kHz and lower than 200 kHz.

EX

Turbulent Eddy-mediated Particle, Momentum, and Vorticity Transport in the Edge of HL-2A Tokamak Plasma

M. Xu^{1,2}, G. R. Tynan¹, P. H. Diamond^{1,3,4}, K. J. Zhao², J. Q. Dong², J. Cheng²,
C. Holland¹, P. Manz¹, N. Fedorczak¹, S. Chakraborty Thakur¹, J. H. Yu¹,
W. J. Hong², L. W. Yan², Q. W. Yang², Y. Huang², X. M. SONG², L. Z. Cai²,
W. L. Zhong², Z. B. Shi², X. T. Ding², X. R. Duan², and Y. Liu²

¹*CMTFO & CER & MAE Department, University of California, San Diego, USA*

²*Southwestern Institute of Physics, Chengdu, China*

³*WCI Center for Fusion Theory, NFRI, Daejeon, Republic of Korea*

⁴*CASS & Department of Physics, La Jolla, USA*

Corresponding Author: minxu.min@gmail.com

We report the first experimental evidence that turbulent eddies mediate the particle, momentum and vorticity transport at the edge of a tokamak plasma so as to amplify the shear layer at the last closed flux surface (LCFS). We find that turbulent eddies with relative negative vorticity (opposite to B field) and positive azimuthal momentum (electron-diamagnetic drift direction) are drawn from both sides of and move towards the location $r - r_{\text{LCFS}} = -1$ cm ; while eddies with relative positive vorticity (i.e., parallel to the B field) and negative azimuthal momentum (ion-diamagnetic drift direction) propagate away from this location towards to the core and scrape-off layer (SOL) plasma regions. Thus negative vortices act to concentrate positive momentum into the region just inside the LCFS, and plasma in this region acquires a $\mathbf{E} \times \mathbf{B}$ drift in the electron drift direction while plasma deeper within and out in the SOL has an $\mathbf{E} \times \mathbf{B}$ drift in the ion diamagnetic direction. This turbulent eddy-mediated particle, momentum, and polarization charge transport process is shown in figure 1 by the conditionally averaged quantities inferred by using vorticity as the reference. Notice that eddies with positive and negative vorticity are associated with different signs of density fluctuation and transport in different directions inside the LCFS at $r - r_{\text{LCFS}} = -2$ cm and in the SOL at $r - r_{\text{LCFS}} = 1$ cm .

EX

3D Plasma Response to Magnetic Field Structure in the Large Helical Device

Y. Suzuki¹, S. Sakakibara¹, K. Nagasaki², K. Ida¹, M. Yoshinuma¹, K. Kamiya³,
K. Watanabe¹, S. Ohdachi¹, Y. Takemura⁴, R. Seki¹, K. Nagaoka¹, K. Ogawa⁵,
Y. Narushima¹, H. Yamada¹, and S. Inagaki⁶

¹*National Institute for Fusion Science, Toki, Japan*

²*Institute of Advanced Energy, Kyoto University, Uji, Japan*

³*Japan Atomic Energy Agency, Naka Fusion Institute, Naka, Japan*

⁴*Graduate University for Advanced Studies, Sokendai, Japan*

⁵*Department of Energy Engineering and Science, Nagoya University, Toki, Japan*

⁶*Research Institute for Applied Mechanics, Kyushu University, Kasuga, Japan*

Corresponding Author: suzuki.yasuhiro@lhd.nifs.ac.jp

In the LHD experiments, the volume averaged beta value was achieved to 5% in the quasi-steady state. For such high-beta plasmas, the change of the magnetic field structure is expected. Since the magnetic field of the LHD is intrinsically 3D structure, the plasma current flowing along 3D field lines drives perturbed field to break nested flux surfaces for the vacuum field, so-called the “3D plasma response”. This is an important and critical issue in stellarator and heliotron researches. Understanding of the nature of stochastic field lines is also a critical issue for application of the Resonant Magnetic Perturbation in tokamaks. To study theoretically the impact of 3D plasma response to the magnetic field, 3D MHD equilibrium was studied using a 3D MHD equilibrium calculation code without assumption of nested flux surfaces. In that study, magnetic field lines in the peripheral region become stochastic and expanding due to increasing beta then the plasma volume in the inside of the last closed flux surface shrinks. However, the connection length of stochastic field lines is still longer than the electron mean free path. That means the change of the effective plasma boundary by the 3D plasma response. To study the 3D plasma response, the radial electric field, E_r , is measured in the peripheral region. The positive electric field appears in the region and that suggests the boundary between opened and closed field lines. The position of appearing positive E_r is the outside of the vacuum boundary. A 3D MHD modeling predicts the expanding of the effective plasma boundary by the 3D plasma response. The position of appearing strong E_r is almost comparable to expanded plasma boundary of the modeling. That is, the 3D plasma response is identified in the LHD experiments.

EX

High Power Heating of Magnetic Reconnection for High-Beta ST formation in TS-3 and UTST ST Merging Experiments

Y. Ono¹, H. Tanabe¹, Y. Kamino¹, K. Yamasaki¹, K. Kadowaki¹, Y. Hayashi¹, and T. Yamada¹

¹*Graduate School of Frontier Sciences, University of Tokyo, Tokyo, Japan*

Corresponding Author: ono@k.u-tokyo.ac.jp

The high-power reconnection heating of spherical tokamak (ST) has been studied in TS-3 merging experiment as a promising solenoid (CS)-less startup and also as a new type of efficient heating method. Our 2-D measurements of plasma flow, magnetic field, ion temperature T_i and electron density has first verified the mechanism of merging formation of the high-beta ST with significant ion heating of magnetic reconnection. When two ST plasmas merge axially together, the produced reconnection (X) point transforms inflows of their private magnetic fluxes into outflows of common flux of the produced new ST. The reconnection outflow accelerates plasma ions quickly up to the order of Alfvén speed. Our 2-D Mach probe measurement clearly shows that the bi-directional inflow is transformed into the fast bi-directional outflow and also that the outflow velocity abruptly decreases to 1/3 at the down-stream where the ion temperature peaks. Our 1-D Doppler probe, electrostatic probe and magnetic probe measurements indicate that both of electron density and magnetic field strength change abruptly at two downstream positions where the outflow velocity damps. Their damping ratios $\sim 2 - 3$ almost satisfy the Rankine-Hugoniot relation. Those facts indicate that the accelerated ions are thermalized at the two downstream areas with the fast shock. The fast shock and/or viscosity damping of those ions probably forms two hot spots in the downstream. Unlike the reconnection heating caused by current-driven instabilities, the thermalized ions are confined by a thick layer of reconnected magnetic flux surrounding the X-point, forming a high-beta ST often with absolute minimum- B profile. After the fast shock forms the hollow magnetic field profile during the reconnection, this absolute min- B profile is often maintained after the merging/ reconnection. The series of our experiments indicate that ion temperature (thermal energy) increment is proportional to the square of the reconnecting poloidal magnetic field B_p . Since the ion outflow velocity close to Alfvén speed scales with B_p , the T_i (and ion thermal energy) increment scales with its square. The reconnection outflow and fast shock damping quickly produce MW-class ion heating power (< 30 MW in TS-3) based on the square scaling of B_p , forming the absolute min- B profile quickly.

EX

From Globus–M Results Toward Compact Spherical Tokamak with Enhanced Parameters, Globus–M2

V. K. Gusev¹, V. V. Bulanin², F. V. Chernyshev¹, I. N. Chugunov¹, V. V. Dyachenko¹,
M. A. Irzak¹, G. S. Kurskiev¹, S. A. Khitrov¹, N. A. Khromov¹, A. D. Melnik¹,
V. B. Minaev¹, A. B. Mineev³, M. I. Mironov¹, I. V. Miroshnikov³,
A. N. Novokhatsky¹, A. A. Panasenkov⁴, M. I. Patrov¹, M. P. Petrov¹, Yu. V. Petrov¹,
V. A. Rozhansky², A. N. Saveliev¹, N. V. Sakharov¹, O. N. Shcherbinin¹,
I. Yu. Senichenkov², A. E. Shevelev¹, S. Yu. Tolstyakov¹, V. I. Varfolomeev¹,
A. V. Voronin¹, A. Yu. Yashin², F. Wagner², and E. G. Zhilin⁵

¹*A. F. Ioffe Physico-Technical Institute, Russian Academy of Sciences, St. Petersburg, Russian Federation*

²*Saint Petersburg State Polytechnical University, St. Petersburg, Russian Federation*

³*D. V. Efremov Institutes of Electrophysical Apparatus, St. Petersburg, Russian Federation*

⁴*IPT RRC “Kurchatov Institute”, Moscow, Russian Federation*

⁵*Ioffe Fusion Technologies Ltd, St. Petersburg, Russian Federation*

Corresponding Author: vasily.gusev@mail.ioffe.ru

The spherical tokamak Globus-M has largely reached its projected parameters. Some of the deficiencies, which do not allow to cross the present operational range have been identified. The experimental basis and the recognition of the reasons for limitations form the basis for the parameter definition of the next step, Globus M2. In this paper we report on the major findings on Globus-M including recent results and we present the design parameters of Globus-M2.

The summary of the main results obtained on Globus-M with neutral beam auxiliary heating and ion cyclotron heating is presented. The transport analysis of both L and H-mode and ITB discharges together with investigation of fast ion behavior in Globus-M created the basement for predictive numerical simulations in the conditions of magnetic field and plasma current increasing to 1 T and 0.5 MA correspondingly. The plasma column dimensions remain unchanged in the new machine named Globus-M2. The results show that at the density of $\sim 10^{20} \text{ m}^{-3}$ plasma in Globus-M2 is heated up to the temperature of over 1 keV range and the energy stored in plasma is 3 – 5 times over the achieved level. The prospects on RF plasma heating and quasistationary noninductive current drive by means of ion cyclotron range waves and lower hybrid waves as well as the data of numerical simulations are discussed.

EX

Impact and Mitigation of Disruptions with the ITER-like Wall in JET

M. Lehnen¹, G. Arnoux², N. Baumgarten¹, S. Brezinsek¹, J. Flanagan²,
S. N. Gerasimov², T. C. Hender², A. Huber¹, S. Jachmich³, U. Kruezi¹,
G. F. Matthews², J. Morris², V. V. Plyusnin⁴, C. Reux⁵, V. Riccardo¹, B. Sieglin⁶, and
P. de Vries⁷

¹*Institute for Energy Research – Plasma Physics, Forschungszentrum Jülich, Association EURATOM-FZJ, Trilateral Euregio Cluster, Jülich, Germany*

²*Euratom/CCFE Association, Culham Science Centre, Abingdon, UK*

³*Laboratoire de Physique des Plasmas-Laboratorium voor Plasmafysica, Association EURATOM-Belgian State, ERM/KMS, Brussels, Belgium*

⁴*Instituto de Plasmas e Fusão Nuclear/IST, Associacao EURATOM-IST, Lisbon, Portugal*

⁵*École Polytechnique, LPP, CNRS, Palaiseau, France*

⁶*IPP Garching, Germany*

⁷*FOM Inst. Differ, Netherlands*

Corresponding Author: m.lehnen@fz-juelich.de

Disruptions are a critical issue for ITER because of the high thermal and magnetic energies that are released on short time scales, which results in extreme forces and heat loads. This contribution reports on disruption properties with the new ITER-like wall (ILW) in JET. It is shown that the material of the plasma-facing components (PFC) has significant impact on the disruption loads. The most important impact of the ILW is the absence of radiating impurities during the disruption. This has significant implications:

1. Low radiation during the current quench phase.
2. A hot current quench plasma.
3. Long current decay times (often limited by vertical displacement).
4. High heat loads caused by conduction of magnetic energy to PFC.
5. Higher halo current fractions in non-VDE disruptions.

The fraction of radiated energy has dropped from 40 – 50% of the total (magnetic and thermal) energy with carbon wall to about 20% on average and even below 10% for VDE. The lack of radiation results in hot current quench plasmas of up to 1 keV and consequently long current decay times. With carbon wall about 80% of all unmitigated disruptions had a linear current quench time below 6 ms/m², whereas with the ITER-like wall only 15% are that fast and 20% have a very long current quench well above 20 ms/m². The slow current quench times facilitate vertical displacement during the current quench and the halo current fraction is increased.

The heat fluxes to first wall components have dramatically increased with the ILW, because of the low radiation. Temperatures close to the melting limit have been locally observed on upper first wall structures during deliberate VDE and even at plasma currents as low as 1.5 MA and thermal energy of about 1.5 MJ only. Local melting has been detected on these structures by regular video inspection.

A high radiation fraction can be regained by massive injection of a mixture of 10%Ar with 90% D₂, ensuring a fast current quench and, by this, reducing the halo current fraction below 10%, the vertical vessel forces by up to 50% and the sideways forces virtually to zero. Because of the high radiation, the temperature of PFC stays below 400°C. Non-sustained breakdowns in the pulses following the injection of D₂ mixtures as observed with carbon wall are absent with the ILW.

Work supported by EURATOM and carried out under EFDA.

Control and Dissipation of Runaway Electron Beams Created during Rapid Shutdown Experiments in DIII-D

E. M. Hollmann¹, M. E. Austin², J. A. Boedo¹, N. H. Brooks³, N. Commaux⁴,
N. W. Eidietis³, T. E. Evans³, D. A. Humphreys³, V. A. Izzo¹, A. N. James⁵,
T. C. Jernigan⁴, A. Loarte⁶, J. R. Martin-Solis⁷, R. A. Moyer¹, J. M. Munoz-Burgos⁸,
P. B. Parks³, D. L. Rudakov¹, E. J. Strait³, M. A. Van Zeeland³, J. C. Wesley³,
J. H. Yu¹, and C. Tsui⁹

¹University of California San Diego, La Jolla, USA

²University of Texas at Austin, Austin, USA

³General Atomics, San Diego, USA

⁴Oak Ridge National Laboratory, Oak Ridge, USA

⁵Lawrence Livermore National Laboratory, Livermore, USA

⁶ITER Organization, St Paul Lez Durance, France

⁷Universidad Carlos III, Leganés, Spain

⁸Oak Ridge Associated Universities, Oak Ridge, USA

⁹Institute for Aerospace Studies, University of Toronto, Toronto, Canada

Corresponding Author: ehollmann@ucsd.edu

High-current (multi-MA) runaway electron (RE) beams could form in ITER during disruptions or rapid shutdowns. To avoid localized wall damage, it is crucial to understand how these RE beams are lost and how they can be controlled and dissipated. DIII-D dedicated experiments on rapid shutdown REs have improved understanding of the processes involved in RE formation, control, dissipation, and final impact with the vessel wall. Improvements in RE beam feedback control enabled stable confinement of RE beams out to the volt-s limit of the ohmic coil, as well as enabled a rampdown to zero current [1]. Collisional dissipation of RE beam current was studied by massive gas injection of different impurities into RE beams. RE current dissipation is shown to be more rapid than expected from avalanche theory [2,3] — this anomalous dissipation appears to be linked to the presence of high-Z impurity ions in plasma. It is not clear if the anomalous dissipation is due to radial diffusion of REs into the wall or an anomalously large collisional drag on the REs. Evidence for radial diffusion of REs is seen with diagnostic pellets, which show diffuse REs well outside the main RE beam [4]. Evidence for anomalous collisional drag on REs is seen in the RE energy distribution function, which shows a large increase in electrons at low energies, when compared with avalanche theory. Final RE-wall impact studies show that the REs are lost to the wall rapidly and with significant toroidal asymmetry once the beam radius touches the wall [5]. Significant ($\sim 10\times$) apparent conversion of RE magnetic energy to kinetic energy [6] is observed in the final RE-wall impact for sufficiently slow impacts; for rapid impacts, the RE magnetic energy appears to go mostly into wall currents and ohmic plasma current.

References

- [1] N. W. Eidietis, *et al.*, “Control of post-disruption runaway electron beams in DIII-D”, submitted to Phys. Plasmas (2012).
- [2] M. N. Rosenbluth and S. V. Putvinski, Nucl. Fusion **37** (1997) 1355.
- [3] E. M. Hollmann, *et al.*, Nucl. Fusion **51** (2011) 103026.
- [4] A. James, *et al.*, J. Nucl. Mater. **415** (2011) S849.
- [5] A. James, *et al.*, Nucl. Fusion **52** (2012) 013007.
- [6] A. Loarte, *et al.*, Nucl. Fusion **51** (2011) 073004.

Work supported in part by the US DOE under DE-FG02-07ER54917, DE-FG03-97ER54415, DE-FC02-04ER54698, DE-AC05-00OR22725, DE-AC52-07NA27344, and DE-AC05-06OR23100.

Disruptions in the High- β Spherical Torus NSTX

S. P. Gerhardt¹, R. Bell¹, M. Bell¹, J. Berkery², A. Boozer², E. Fredrickson¹,
E. Kolemen¹, B. P. LeBlanc¹, R. Maingi³, J. Manickam¹, A. McLean⁴, J. Menard¹,
D. Mueller¹, R. Raman⁵, S. Sabbagh², V. Soukhanovskii⁴, and H. Yuh⁶

¹*Princeton Plasma Physics Laboratory, Princeton, USA*

²*Dept. of Appl. Phys., Columbia University, New York, USA*

³*Oak Ridge National Laboratory, Oak Ridge, USA*

⁴*Lawrence Livermore National Laboratory, Livermore, USA*

⁵*University of Washington, Washington, USA*

⁶*Nova Photonics, Princeton, USA*

Corresponding Author: sgerhard@pppl.gov

Disruptions in next-step tokamak devices, whether at conventional or low aspect ratio, must be rare, predictable, and have minimal consequences for the plant. This paper addresses these issues using data the National Spherical Torus Experiment (NSTX). The disruptivity increases rapidly for $q^* < 2.5$, but does not show a strong dependence on β_N ; more complicated physics such as kinetic stabilization plays a role in determining the disruptive β_N limit. The lowest disruptivity is at higher- β_N , where the large bootstrap current prevents the current profile from evolving to a kink/tearing unstable state. Many disruption precursors have been investigated from a database of > 2100 disruptions, including direct measurement of MHD signals, confinement indicators, and parameters of the equilibrium evolution. Disruptive thresholds on these quantities have been defined, often using physics based 0-D models of the plasma behavior. Compound disruption warnings are formed from the weighted sum of binary threshold tests. These compound tests can be used to detect $\sim 99\%$ of disruptions with at least 10 ms warning time, with a false-positive rate of $\sim 8\%$. Missed disruptions are often driven by resistive wall modes, while the false positive count is dominated by modes that slow and often lock, but do not disrupt. Once a disruption begins, the NSTX plasma typically becomes vertically unstable, and halo currents are observed to flow. Halo current fractions > 30% have been observed, with the largest currents typically in Ohmic and L-mode plasmas; large halo currents often occur in cases with the largest current quench rates. Both the final disruption onset and the growth of large halo currents typically correspond to the edge q dropping to 2, although some currents are observed during the phase of the VDE with higher edge- q . The halo current patterns are not toroidally symmetric, and the non-axisymmetry is observed to rotate toroidally up to 7 times, with typical rotation frequencies of 0.5 – 2 kHz, although the rotation is often non-steady. The rotation frequency is anti-correlated with the halo current amplitude. The non-axisymmetric part of the halo current typically decays before the $n = 0$ part, and modeling indicates that the loss of the $n \neq 0$ current corresponds to the time when the last closed magnetic surface vanishes.

This work was supported by the US DOE.

EX

Is Turbulence Determined by Local Temperature Gradient?

S. Inagaki¹, T. Tokuzawa², N. Tamura², S. I. Itoh¹, K. Ida², T. Shimoizuma², S. Kubo²,
K. Tanaka², T. Ido², A. Shimizu², H. Tsuchiya², N. Kasuya², Y. Nagayama²,
K. Kawahata², S. Sudo², H. Yamada², A. Fujisawa¹, K. Itoh², and T. Kobayashi³

¹*Research Institute for Applied Mechanics, Kyushu University, Kasuga, Japan*

²*National Institute for Fusion Science, Toki, Japan*

³*Interdisciplinary Graduate School of Engineering Sciences, Kyushu University, Kasuga, Japan*
Corresponding Author: inagaki@riam.kyushu-u.ac.jp

Here we report dynamic response of micro-fluctuations and turbulent flux to a low frequency heat wave induced by the ECH modulation and development of observation of low frequency fluctuation with long distance radial correlation length comparable to the plasma radius (long-range mode) in LHD. A low frequency global wave is excited by central ECH power modulation at 25 Hz. The typical low-density L-mode NBI plasmas are chosen as targets. Density fluctuation is measured with an O-mode reflectometer and time evolutions of temperature and temperature gradient are measured with a 28-channel radiometer. Experimental observations show that

1. The responses of heat flux and micro-fluctuation amplitudes to the change in temperature gradient have hysteresis characteristics.
2. The long-range mode is a possible candidate to explain a correlation between micro-fluctuations at distant positions.

These results deny the local transport model, where turbulence is determined by local temperature gradient, and strongly suggest that turbulence should be determined by global interactions within the radial correlation length.

This study pioneers research of the following fundamental processes for turbulence transport, i.e.,

1. Dynamics of micro-fluctuations.
2. Relations between turbulent flux, fluctuation amplitude and local temperature gradient.
3. Comprehensive observations of low frequency long-range modes.

These results will open the way to understand physical mechanics of turbulence transport. This is beneficial for turbulence control in future burning plasmas.

EX

Spatiotemporal Structure of the Turbulence-flow Interaction at the L-H Transition in TJ-II Plasma

T. Estrada¹, C. Hidalgo¹, E. Blanco¹, E. Ascasíbar¹, and T. Happel²

¹*Laboratorio Nacional de Fusión, Euratom-CIEMAT, Spain*

²*Max-Planck-Institut für Plasmaphysik, Garching, Germany*

Corresponding Author: teresa.estrada@ciemat.es

The spatiotemporal behaviour of the interaction between turbulence and flows has been studied close to the L-H transition threshold conditions in the edge region of TJ-II plasmas. The temporal dynamics of the interaction displays an oscillatory behaviour with a characteristic predator-prey relationship. This intermediate oscillatory transient stage has been seen in L-H transition experiments in some other devices. However, in those experiments, as in the Kim & Diamond predator-prey theory model, only the temporal dynamics of the turbulence-flow interaction is studied. In TJ-II, dedicated experiments have been carried out to study the spatial evolution of the turbulence-flow oscillation pattern. Radial outward and inward propagation velocities of the turbulence-flow front are found. As the turbulence-flow front propagates outwards, the turbulence-flow events generate a dual shear layer and thus enhance the formation of the radial electric field well. A possible explanation for the spatiotemporal evolution of the oscillation-pattern could be linked to the radial spreading of the plasma turbulence from the plasma core to the edge barrier. As the turbulence propagates towards the barrier, the associated turbulence driven flow generates the inner shear layer which in turn regulates the turbulence level. The observations could be also figured out in terms of turbulent bursts propagating toward the plasma edge. These turbulent bursts could be generated in the plasma interior due to instabilities linked, for instance, to the magnetic topology. A reversal in the front propagation velocity is observed in some particular cases after a quiet period without oscillations. In those cases the oscillation-pattern arises at the outer shear layer position and propagates towards the plasma interior. The results indicate that the edge shear flow linked to the L-H transition can behave either as a slowing-down, damping mechanism of outward propagating turbulent-flow oscillating structures, or as a source of inward propagating turbulence-flow events. These results show the need of approaching L-H transition studies within a 1-D spatiotemporal framework.

EX

Zonal Flows as the Trigger Event for the L–H Transition

G. Tynan¹, J. A. Boedo¹, I. Cziegler¹, P. H. Diamond¹, N. Fedorczak¹, C. Holland¹,
P. Manz¹, S. Mueller¹, S. Thakur¹, G. Xu², B. Wan², H. Wang², H. Guo², J. Dong²,
K. Zhou², J. Cheng², W. Hong², L. Yan², and M. Xu²

¹ *University of California San Diego, San Diego, USA*

² *Southwestern Institute of Physics, Chengdu, China*

Corresponding Author: gtynan@ucsd.edu

The kinetic energy transfer between shear flows and the ambient turbulence is measured for the first time in the EAST, DIII-D and HL-2A tokamaks. In EAST as the plasma is heated and approaches the L-H transition, the rate of energy transfer from the turbulence into the zonal flow increases. Finally, when this rate becomes comparable to the energy input rate into the turbulence, the transition into the H-mode occurs. Work in DIII-D focuses on turbulence-zonal flow energetics during intermediate confinement regime characterized by a limit cycle behavior of the turbulence energy and zonal flow and shows, for the first time, modulation in turbulent Reynolds stress and nonlinear energy transfer into the modulated zonal flow. Finally, in HL-2A as ECH heating power is increased in L-mode we observe an increase in the nonlinear coupling of turbulence energy to the zonal flow found at the plasma edge. Taken together the results show the key role that zonal flows play in mediating the transition into H-mode, and provide a route to a physics-based understanding of the L-H transition and of the macroscopic scaling of the transition power threshold.

EX

Evidence of Zonal-Flow-Driven Limit-Cycle Oscillations during L–H Transition and at H–mode Pedestal of a New Small-ELM Regime in EAST

G. Xu¹, H. Wang¹, H. Guo¹, B. Wan¹, V. Naulin², P. Diamond³, G. Tynan³, M. Xu³,
and H. Zhao⁴

¹*Institute of Plasma Physics, Chinese Academy of Sciences, Hefei, China*

²*Association Euratom-RisøDTU, Roskilde, Denmark*

³*University of California San Diego, San Diego, USA*

⁴*Department of Modern Physics, USTC, Hefei, China*

Corresponding Author: gsxu@ipp.ac.cn

Small-amplitude edge localized oscillations have been observed, for the first time, in EAST preceding the L-H transition at marginal input power, which manifest themselves as dithering in the divertor D_α signals at a frequency under 4 kHz, much lower than the GAM frequency. Detailed measurements using two toroidally separated reciprocating probes inside the separatrix demonstrate a periodic turbulence suppression accompanied by an oscillation in E_r as the shearing rate transiently exceeds the turbulence decorrelation rate. Wavelet bicoherence analysis shows a strong three-wave coupling between edge turbulence in the range of 30 – 100 kHz and low-frequency E_r oscillations. Just prior to the L-H transition, the E_r oscillations often evolve into intermittent negative E_r spikes. The E_r oscillations, as well as the E_r spikes, are strongly correlated with the turbulence driven Reynolds stress, thus providing a direct evidence of the zonal flows for the L-H transition at marginal input power. Furthermore, near the transition threshold sawtooth heat pulses appear to periodically enhance the dithering, finally triggering the L-H transition after a big sawtooth crash. The zonal flow induced limit-cycle oscillations were observed not only prior to the L-H transition but also at the H-mode pedestal following the transition, or in the inter-ELM phase. In addition, a high-frequency-broadband (50 – 500 kHz) turbulence has been observed in the steep-gradient region of the H-mode pedestal in EAST, which exhibits an initial growth phase with small-amplitude axisymmetric magnetic perturbations. This high-frequency turbulence is modulated by the low-frequency zonal flows, resulting in small-ELM-like transport events. Good confinement ($H_{98} \sim 1$) is achieved in such a “small-ELM” regime, even with heating power close to the L-H transition threshold. The growth, saturation and disappearance of the zonal flows are correlated with those of the high-frequency turbulence, with the energy gain of the zonal flows being of the same order as the energy loss of the high-frequency turbulence, thus strongly suggesting a causal link between them. A novel predator-prey model, incorporating the evolution of zonal flows, pressure gradient and turbulences at two different frequency ranges, has been developed and successfully reproduced the key features of this newly observed small-ELM regime.

EX

The Nearly Continuous Improvement of Discharge Characteristics and Edge Stability with Increasing Lithium Coatings in NSTX

R. Maingi¹, D. P. Boyle², J. Canik¹, S. Kaye², T. Osborne³, C. Skinner², M. Bell²,
 R. Bell², A. Diallo², S. Gerhardt², T. Gray¹, W. Guttenfelder², M. Jaworski²,
 R. Kaita², H. Kugel², B. LeBlanc², J. Manickam², D. Mansfield², J. Menard²,
 M. Ono², M. Podesta², R. Raman³, Y. Ren², L. Roquemore², S. Sabbagh⁴, P. Snyder⁵,
 and V. Soukhanovskii⁶

¹*Oak Ridge National Laboratory, Oak Ridge, USA*

²*Princeton Plasma Physics Laboratory, Princeton, USA*

³*University of Washington, Seattle, USA*

⁴*Columbia University, New York, USA*

⁵*General Atomics, San Diego, USA*

⁶*Lawrence Livermore National Laboratory, Livermore, USA*

Corresponding Author: maingir@ornl.gov

The understanding of regimes with:

1. High pressure at the top of the H-mode pedestal.
2. Devoid of large ELMs is important for scenario optimization of ITER and future devices.

EX

Lithium wall coatings have been shown to both improve energy confinement and eliminate ELMs in NSTX. Here, we present analysis of variable pre-discharge lithium evaporation from multiple experiments, for more insight into the pedestal expansion and ELM suppression physics. First, a nearly continuous improvement of a number of discharge characteristics, e.g., reduced recycling, ELM frequency, and edge electron transport, with increasing pre-discharge lithium evaporation has been identified. These correlations ran contrary to initial expectations that the beneficial effects would saturate at much lower evaporation amounts than used in experiments. Profile and stability analysis clarified the mechanism responsible for ELM avoidance and the role of lithium: lithium coatings reduce recycling and core fueling; thus the density and its gradient near the separatrix are reduced. The temperature gradient near the separatrix is unaffected; hence the pressure gradient and bootstrap current near the separatrix are reduced, leading to stabilization of kink/peeling modes thought to be responsible for the NSTX ELMs. Thus, the enhanced edge stability with lithium coatings is correlated with the reduction of the pressure and its gradient near the separatrix. The key ingredient for ELM avoidance is control of the particle channel independent of the thermal channel at the edge: the density profile is continuously manipulated via the amount of lithium evaporation and resulting recycling control, leading to reduced neutral fueling. The surprising and beneficial facet of the NSTX data, however, is the continued growth of the edge transport barrier width in these circumstances, leading to 100% higher plasma pressure at the approximate top of the n_e profile barrier with high pre-discharge evaporation. Analysis shows enhanced edge transport; coupled with the heating power reduction to stay below the global beta limit, the pressure gradient and associated bootstrap current are maintained below the edge stability limit, thus avoiding ELMs. This allows the H-mode edge transport barrier to expand further and in such a way that peeling stability improves as a result of the inward shift of the bootstrap current.

Visualization of ELM Dynamics and its Response from External Perturbations via 2D Electron Cyclotron Emission Imaging in KSTAR

H. K. Park¹, M. Choi¹, J. Lee¹, W. Lee¹, G. Yun¹, Y. Bae², Y. Jeon², S. Yoon²,
C. Domier³, N. Luhmann³, A. Donné^{4,5}, and W. Xiao^{2,6}

¹*Postech, Pohang, Republic of Korea*

²*National Fusion Research Institute, Daejeon, Republic of Korea*

³*University of California, Davis, USA*

⁴*FOM-Institute, DIFFER, Nieuwegein, Netherlands*

⁵*Eindhoven University of Technology, Department of Applied Physics, Netherlands*

⁶*Southwestern Institute of Physics, Chengdu, China*

Corresponding Author: hyeonpark@postech.ac.kr

The nature of the Edge Localized Mode (ELM) in the H-mode regime in toroidal plasmas is complex and therefore requires advanced diagnostic tools in order to enhance the understanding of the physical dynamics. It is particularly important to find a comprehensive way to eliminate or suppress this instability which is a critical issue for H-mode operation in ITER and DEMO. There have been numerous studies on the nature of this instability as well as its control by external means whereas the control attempts have thus far been largely empirical. A high resolution (spatial and temporal) 2-D ECEI system successfully characterized the real time dynamics of the entire evolution of the ELM in KSTAR campaigns (2010 and 2011). This includes the growth, saturation and bursting process of this instability. In the 2011 KSTAR campaign, the external actuators such as Resonant Magnetic Perturbation (RMP) coils with an $n = 1$ structure, Supersonic Molecular Beam Injection (SMBI) and Electron Cyclotron Heating/Current Drive (ECH/ECCD) were introduced and the detailed temporal and spatial responses of the ELMs to the actuators were visualized. In RMP experiment, the mode number was changed from high to low m/n numbers with the increase in size and intensity before complete suppression. During SMBI experiment, the mode number was changed from low to high m/n numbers with the decrease in size and intensity. When ECH/ECCD power was applied to the edge, there was no clear response.

EX

Improved Understanding of Physics Processes in Pedestal Structure, Leading to Improved Predictive Capability for ITER

R. Groebner¹, C. S. Chang², J. W. Hughes³, R. Maingi⁴, P. B. Snyder¹, and X. Q. Xu⁵

¹General Atomics, San Diego, USA

²Princeton Plasma Physics Laboratory, Princeton, USA

³Massachusetts Institute of Technology, Cambridge, USA

⁴Oak Ridge National Laboratory, Oak Ridge, USA

⁵Lawrence Livermore National Laboratory, Livermore, USA

Corresponding Author: groebner@fusion.gat.com

Joint experiment/theory/modeling research has led to increased confidence in predictions of the pedestal height in ITER. This work was performed as part of a US DOE Joint Research Target in FY2011 to identify physics processes to control the H mode pedestal structure. This work included experiments on C-Mod, DIII-D and NSTX as well as interpretation of experimental data with theory-based modeling codes. The research provides new benchmarking of physics components in the EPED model, used to predict the height of the ITER pedestal. Validation studies performed with BOUT++ and ELITE increase confidence that the pedestals in the 3 machines reach the predicted peeling/ballooning limit at the onset of Type-I ELMs. Kinetic calculations with XGC0 and NEO, using realistic collision operators, show that analytic models of bootstrap current are accurate to $\sim 10 - 15\%$ for C-Mod and DIII-D and to $\sim 40\%$ in NSTX. Studies in all 3 devices show that the pedestal width scales approximately as expected if the pedestal p' is limited by KBMs. The proposed KBM width scaling data quantitatively agrees with DIII-D and C-Mod data within $\sim 20\%$. These benchmarking studies improve confidence in the models for P-B modes, bootstrap current and KBMs used by the EPED model, which predicts values of pedestal pressure height and width that agree within $\sim 20\%$ of measurements in Type I ELMy discharges on C-Mod and DIII-D. The JRT research included studies of other physics processes proposed to be important for pedestal structure. Studies of models for neo-classical and paleoclassical transport find that these mechanisms may be significant, but that additional transport is needed to describe the fully developed pedestal. Benchmarking of the electromagnetic gyrokinetic codes, GYRO, GEM and GTC for one DIII-D pedestal predict that electron drift modes and KBMs were linearly unstable within the pedestal and ion temperature gradient modes were unstable on the pedestal top. Experimental and modeling results suggest that electron temperature gradient modes may play a role in the pedestal structure of all 3 machines. Experimental and modeling evidence suggest that both atomic physics and a pinch play a role in controlling the density pedestal in all 3 devices.

This work supported in part by the US DOE under DE-FC02-04ER54698, DE-AC02-09CH11466, DE-FC02-99ER54512, DE-AC05-00OR22725 and DEAC52-07NA27344.

Access and Sustained High Performance in Advanced Inductive Discharges with ITER-Relevant Low Torque

W. M. Solomon¹, P. A. Politzer², R. J. Buttery², J. R. Ferron², A. M. Garofalo²,
J. M. Hanson³, Y. In⁴, G. L. Jackson², C. T. Holcomb⁵, R. J. La Haye²,
M. J. Lanctot⁵, T. C. Luce², M. Okabayashi¹, C. C. Petty², F. Turco³, and
A. S. Welande²

¹*Princeton Plasma Physics Laboratory, Princeton, USA*

²*General Atomics, San Diego, USA*

³*Columbia University, New York, USA*

⁴*FAR-TECH, San Diego, USA*

⁵*Lawrence Livermore National Laboratory, Livermore, USA*

Corresponding Author: solomon@fusion.gat.com

Recent experiments on DIII-D have demonstrated that advanced inductive discharges with high normalized fusion gain approaching levels consistent with ITER $Q = 10$ operation can be accessed and sustained with very low amounts (~ 1 Nm) of externally driven torque. This level of torque is anticipated to drive a similar amount of rotation as the beams on ITER, via simple consideration of the scaling of the moment of inertia and confinement time. These discharges have achieved $\beta_N \sim 3.1$ with $H_{98} \sim 1$ at $q_{95} \sim 4$, and have been sustained for the maximum duration of the counter neutral beams (NBs). In addition, plasmas using zero net neutral beam torque from the startup all the way through to the high beta phase have also been created. Advanced inductive discharges are found to become increasingly susceptible to 2/1 neoclassical tearing modes as the torque is decreased, which if left unmitigated, generally slow and lock, terminating the high performance phase of the discharge. Access is not notably different whether one ramps the torque down at high β_N , or ramps the β_N up at low torque. The use of electron cyclotron heating (ECH) has proven to be an effective method of avoiding such modes, allowing stable operation at high beta and low torque, a portion of phase space that has otherwise been inaccessible. In many cases, the ECH has been aimed to drive current near the $q = 2$ surface, although this does not appear to be a critical element in order to gain the benefits of the ECH. Indeed, high $\beta_N \sim 3$ discharges at low torque have been sustained using ECH without current drive, and deposited significantly inside of the $q = 2$ surface. The insensitivity to the deposition position, together with the lack of need for current drive, suggests that the EC assists stability in a different way than the simply replacing the bootstrap current caused by the flattening of the pressure profile in the island. These advanced inductive discharges are measured to have significant levels of intrinsic torque at the edge, consistent with a previously determined empirical scaling considering the role of the turbulent Reynolds stress and thermal ion orbit loss.

This work was supported by the US Department of Energy under DE-AC02-09CH11466, DE-FC02-04ER54698, DE-FG02-04ER54761, DE-FG02-08ER85195, and DE-AC52-07NA27344.

EX-P

ITER Demonstration Discharges on Alcator C-Mod in Support of ITER

C. Kessel¹, S. M. Wolfe², I. H. Hutchinson², J. W. Hughes², Y. Lin², Y. Ma²,
D. R. Mikkelsen¹, F. Poli¹, M. L. Reinke², and S. J. Wukitch²

¹*Princeton Plasma Physics Laboratory, Princeton, USA*

²*MIT Plasma Science and Fusion Center, Cambridge, USA*

Corresponding Author: ckessel@pppl.gov

Alcator C-Mod is providing discharges that match several simultaneous parameters expected in ITER in the rampup, flattop and rampdown phases, and simulations of these discharges with time-dependent transport evolution codes. Discharges have been produced at both $B = 5.4$ T and 2.7 T, utilizing H-minority heating fundamental and 2nd harmonic, respectively. Discharges with rampup durations appropriate to ITER's show that ICRF heating obtains V-s savings with only weak effects on the current profile, in spite of strong modifications of the central electron temperature. Significant V-s savings in ohmic rampup by utilizing lower densities appears only to be effective at very low density, $n/n_{Gr} \sim 0.08$. Injection of lower hybrid during the rampup is effective for saving V-s, again only at similarly low densities. Simulations of C-Mod rampup discharges have been performed with the Tokamak Simulation Code (TSC), utilizing TORIC full wave calculation of the ICRF deposition, and using the Current Diffusive Ballooning (CDBM), Bohm-gyro Bohm, Coppi-Tang, and modified GLF23 (enhanced thermal diffusivity near plasma edge) transport models showing that they are not reproducing the temperature profile evolution, and consequently do not reproduce the experimental internal self-inductance or the V-s. Discharges which obtained EDA H-modes during flattop, with $B = 2.7$ T and $I_p = 0.65$ MA, obtain parameter values between $(\beta_N, n/n_{Gr}, H_{98}) = (1.9, 0.60, 1.0)$ to $(1.5, 0.8, 0.67)$. The lower n/n_{Gr} values are associated with the higher H_{98} and β_N . Discharges showed a degradation of the energy confinement as the higher densities were approached, but also an increasing H_{98} with net power to the plasma

$$P_{\text{net}} = P_{\text{ICRF}}^{\text{abs}} + P_{OH} - \frac{dW}{dt} - P_{\text{rad}}. \quad (1)$$

For these discharges up to 3 MW was injected, while intrinsic impurities (B, Mo) provided radiated power fractions ($P_{\text{rad}}/P_{\text{in}}$) of 25–37%, typical of those required in ITER. Experiments at 5.4 T have demonstrated the plasma can remain in H-mode as the rampdown phase is entered with at least 0.75 MW of ICRF injection, the back transition occurring when the net power reaches 1 MW, and the density will decrease at the same rate as I_p when in H-mode, maintaining the flattop n/n_{Gr} value. Maintaining the H-mode longer into the rampdown and ramping the plasma current down faster can mitigate the OH coil over-current associated with the back transition.

Overview of ASDEX Upgrade “Improved H-mode” Scenario Developments

J. Schweinzer¹, J. Hobirk¹, J. Stober¹, A. Kallenbach¹, R. McDermott¹, C. Hopf¹,
E. Fable¹, and G. Tardini¹

¹Max-Planck-Institut für Plasmaphysik, Euratom Association, Garching, Germany

Corresponding Author: josef.schweinzer@ipp.mpg.de

“Improved H-mode” discharges in ASDEX Upgrade (AUG) are characterized by enhanced confinement factors, high β and a q -profile with almost zero shear in the core of the plasma at $q(0)$ around 1.

First attempts to reach high performance in the all-tungsten AUG relied on the observation that energy confinement was most improved when nitrogen (N) was puffed. In such plasmas the achieved confinement factors H_{98} turned out to be as good as, or even better than, the values obtained in the carbon dominated AUG when discharges at the same values of F_{GW} are compared. The improved confinement of N seeded discharges is an effect of higher pedestal temperatures which extend to the plasma core via profile stiffness. Further developments of the N seeded scenario aim to extend the duration of the high performance phase to a few seconds and also to increase the triangularity. The latter step helps to extend the operational window towards higher F_{GW} values.

By introducing the so called current over-shoot technique significantly improved confinement with H_{98} around 1.3 was reached in the carbon walled era at JET. This technique has now been applied to the all-W AUG where “improved H-modes” with $\beta_N = 4$ and H-factors of 2.5 have been produced transiently. The scenario at AUG uses a fast plasma current ramp up to 1.2 MA with NBI heating starting with the X-point formation and ending at the time of maximum I_p . Then an ohmic phase with a current ramp down to 1 MA modifies the edge part of the q -profile. In the consecutive heating power ramp to about 10 MW many parameters, e.g., stored energy and electron density, but also the radiation, increase strongly. The most stable pulses so far utilise also on-axis ECRH for impurity control and off-axis ECCD to stabilise an occurring (2, 1) mode in the periphery of the plasma. With small modifications (gas puff rate, timing of pre-heat in I_p ramp-up) and in particular with less aggressive heating the stability and duration of the high performance phase has been extended.

This paper will deal with the present status of AUG plasma operation of “improved H-Mode” scenarios at optimized performance reporting on improvements of the nitrogen seeded as well as the current overshoot scenario. For the latter experimental results will be accompanied by TGLF calculations.

EX-P

Study of H-mode Access in the Alcator C-Mod Tokamak: Density, Toroidal Field and Divertor Geometry Dependence

Y. Ma¹, J. Hughes¹, B. LaBombard¹, A. Hubbard¹, R. Churchill¹, J. Terry¹,
S. Zweben², and E. Marmar¹

¹MIT Plasma Science and Fusion Center, Cambridge, USA

²Princeton Plasma Physics Laboratory, Princeton, USA

Corresponding Author: yma@psfc.mit.edu

Knowing the conditions for H-mode access is important for ITER high performance plasma operation. The experimental study carried out on Alcator C-Mod in support of this research primarily focused on:

1. Determining optimum global and local plasma conditions for promoting H-mode access.
2. Characterizing plasma behaviors before L-H transition at low density.
3. Demonstrating a strong ($> 50\%$) reduction in H-mode threshold power (P_{th}) with modified divertor geometry.

It is known that “hidden” variables other than those indicated by the multi-machine scaling law can also have a great impact on P_{th} . In C-Mod, we observed a strong reduction in P_{th} at medium and high densities with slot divertor operation. A minimum P_{th} of 0.7 MW appears at $1.5 \times 10^{20} \text{ m}^{-3}$ in this configuration, which is only 40% of the scaling law prediction. Interestingly, the edge T_e and n_e profiles prior to L-H transition are not apparently affected by divertor geometry. This result is promising and of particular interest for H-mode access at reduced power.

H-mode access at low density is a potential concern for ITER H-mode operation. This issue has been studied in dedicated C-Mod experiments operated at two different B_T (5.4 T and 3.5 T). At 5.4 T, both P_{th} and $T_{e,95}$ (T_e at $\psi = 0.95$) preceding L-H transition rise considerably for density below $1.0 \times 10^{20} \text{ m}^{-3}$. The ion and electron temperature near the pedestal top remain well equilibrated in the low-density regime, which contrasts the AUG result. The few plasmas with very low density ($< 0.8 \times 10^{20} \text{ m}^{-3}$) show an edge T_e pedestal formed well before L-H transition, however, no clear edge n_e or T_i pedestal emerged until after L-H transition. Another significant finding is that the low density limit for H-mode access moves to lower values of density when B_T is reduced.

Scaling of P_{th} and local plasma edge conditions for H-mode access was examined over a wide range of plasma parameters in C-Mod divertor plasmas with ion ∇B drift in the favorable direction for H-mode access. The obtained local conditions were employed to test the L-H transition models based on the suppression of resistive-ballooning mode and drift-Alfvén wave turbulence. A new model developed recently to predict H-mode access power was also tested

Toroidal Rotation in L–I–H Confinement Transition in HL–2A Experiments

A. Sun¹, X. Han¹, and J. Dong¹

¹*Southwestern Institute of Physics, Chengdu, China*

Corresponding Author: apsun@swip.ac.cn

The toroidal rotation is studied on HL-2A in recent co-current direction NBI experiments and charge exchange recombination spectroscopy (CXRS) is used to measure its velocity profiles. Three cases with co-NBI are studied in this paper. Case I is H-mode discharges, case II is I-phase of H-mode discharges, and case III is ECH H-mode discharges. In H-mode discharges, it is found that the toroidal rotation velocities increase significantly from L-mode to H-mode discharge, the direction of edge toroidal rotation is reversed at the L-H transition, and both core and edge toroidal rotation decrease at the H-L back transition. However, it is larger in the L-mode phase after H-L transition than that before the L-H transition. In I-phase of H-mode discharges, the results of the experiments show that the toroidal rotation velocities in I-phase are lower than those in H-phase. The effect of ECH on toroidal rotation is studied in ECH H-mode discharges. It is found that the rotation velocity will go up in the edge plasma before ECH, and increases in the core plasma and its direction is reversed in the edge plasma after ECH beginning. The toroidal momentum diffusivity is analyzed with ONETWO code and the result shows that their distributions are different at different stages. The toroidal rotation experiment with NBI is also simulated with tokamak transport code ONETWO and anomalous transport model GLF23. The simulation results show reasonable agreement with the experiment.

EX-P

Integrated Operation Scenarios for Long Pulse Discharges in EAST

X. Gong¹, J. Qian¹, B. Wan¹, and J. Li¹

¹*Institute of Plasma Physics, Chinese Academy of Sciences, Hefei, China*

Corresponding Author: xz.gong@ipp.ac.cn

The Experimental Advanced Superconducting Tokamak (EAST) is a fully superconducting tokamak with a flexible poloidal field system to accommodate both single null (SN) and double null (DN) divertor configurations, and its main mission is to establish steady-state high performance plasma and study related physics and technologies. Development of PFMs and improvements of the actively water-cooled PFCs and other in-vessel components have been carried out in the past few years to have the highest priority suitable for long pulse operation. With LHCD assistance and advance plasma control, Integrated Operation Scenarios were focused on superconducting tokamak, which are including low loop voltage startup and plasma ramp up/down with active internal inductance and shaping control to avoid the huge thermal energy impact on the first wall. Slow sweeping strike points by plasma configuration control spread heat load on divertor plates during long pulse operation. A series of wall-conditioning technologies in superconducting machines (RF-DC, HF_GDC) are explored, which will make unique contributions and produce results of significance for ITER in the future. Lithium wall conditioning proved to be an effective tool to reduce recycling and control the density during the last campaign. As a result, long pulse diverted plasma operations up to 100 s were realized by LHCD of 1.0 MW and reliable plasma operation with $I_p = 1.0$ MA was obtained in the last experimental campaign on 2010. Stationary H-mode plasma discharges combined auxiliary heating of ICRF and LHCD, have been achieved and sustained up to 6.5 s. Actively ELMs controls are expected to be implemented by RMP coils, pellet injection and SMBI. With available LHCD (4.0 MW at 2.45 GHz) and ICRH (4.5 MW at 25 – 110 MHz) system upgrade, more long pulse and high performance plasma operation for ITER-relevant advanced regimes will be validated in this EAST campaign on 2012.

EX-P

Investigation of Plasma Rotation Alteration and MHD Stability in the Expanded H-mode Operation of KSTAR

Y. S. Park¹, S. Sabbagh¹, J. Berkery¹, J. Bialek¹, S. Lee², W. Ko², Y. Jeon², J. Park³,
S. Hahn², J. Kim², S. Yoon², K. I. You², K. Lee², G. Yun⁴, H. Park⁴, Y. Bae²,
W. C. Kim², Y. Oh², and J. Kwak²

¹*Department of Applied Physics, Columbia University, New York, USA*

²*National Fusion Research Institute, Daejeon, Republic of Korea*

³*Princeton Plasma Physics Laboratory, Princeton, USA*

⁴*Pohang University of Science and Technology, Pohang, Republic of Korea*

Corresponding Author: ypark@pppl.gov

Initial H-mode operation of the KSTAR has been expanded to higher normalized β , β_N , and lower plasma internal inductance, l_i , moving toward design target operation. As a key supporting device for ITER, an important goal for KSTAR is to produce physics understanding of MHD instabilities at long pulse with steady-state profiles, at high β_N and over a wide range of plasma rotation profiles. Instability characteristics in the present expanded H-mode operational space, the influence of varied plasma rotation, and methods to access ITER-relevant low plasma rotation are presently investigated. Equilibria have reached new maximum values in key parameters $\beta_N = 1.9$, stored energy of 340 kJ with an energy confinement time of 171 ms in 2011. These results mark substantial progress toward the $n = 1$ ideal no-wall stability limit, most closely positioned at $\beta_N = 2.5$, $l_i = 0.7$. Rotating MHD modes are observed with perturbations having tearing parity as determined by Mirnov and ECE measurements. Modes with $m/n = 3/2$ are triggered during the H-mode phase at $0.5 < \beta_N < 1$ but do not substantially reduce plasma stored energy. In contrast, 2/1 modes to date are only observed when both the confinement and plasma rotation profiles are lowered after H-L back-transition, and mode locking creates a repetitive crash of β_N by more than 50%. A correlation is found between the 2/1 amplitude and local rotation shear from an X-ray imaging crystal spectrometer, and additionally, 2/1 modes appear to onset only below $\sim 1,200$ km/s/m of local rotation shear. Plasma rotation alteration by applied $n = 1, 2$ fields and the associated neoclassical toroidal viscosity (NTV) induced torque can be used as a rotation profile alteration tool, but also to study the collisionality dependence and steady-state behavior of NTV. Initial success in non-resonant alteration of the H-mode rotation profile in KSTAR were made by using an $n = 2$ applied field. Analysis is pending to determine if the observed stronger rotation damping by $n = 1$ braking is resonant or non-resonant. The implications of kinetic RWM stability using the measured KSTAR rotation profiles and their variations are presently being evaluated using the MISK code to further examine the initial theoretical guidance that showed unfavorable RWM stability for projected device target plasmas using projected rotation profiles.

EX-P

Long-pulse Stability Limits of ITER Baseline Scenario Plasmas in DIII-D

G. L. Jackson¹, F. Turco³, T. C. Luce¹, R. J. Buttery¹, A. W. Hyatt¹, E. J. Doyle⁴, J. R. Ferron¹, R. J. La Haye¹, P. A. Politzer¹, W. M. Solomon², and M. R. Wade¹

¹General Atomics, San Diego, USA

²Princeton Plasma Physics Laboratory, Princeton, USA

³Columbia University, New York, USA

⁴University of California Los Angeles, Los Angeles, USA

Corresponding Author: jackson@fusion.gat.com

Long duration plasmas, stable to $m/n = 2/1$ tearing modes (TM), with an ITER similar shape and an ITER similar value of I_p/aB_T have been demonstrated in DIII-D, evolving to stationary conditions with the most stable operating point at β_N approximately 2. Lower β_N , corresponding to an ITER baseline scenario 2 value of 1.8, led to a higher probability of $m/n = 2/1$ tearing modes, which is the opposite of predictions from neoclassical tearing mode theory. These plasmas ($\Delta t_{\text{duration}} \leq 7.5$ s and $\leq 11\tau_R$), without electron cyclotron current drive (ECCD) for TM mitigation, have extended shorter pulse experiments in which the internal inductance was continually evolving [1] often until rotating $m/n = 2/1$ TMs or locked modes occurred, which are a concern for ITER operation.

Although long-pulse plasmas have reached stationary conditions, in some cases with similar programming $m/n = 2/1$ TMs and locked modes limited the duration, indicating operation near stability limits. In addition to the plasmas described above, the use of ECCD, broadly deposited near $q = 3/2$, allowed stable operation in plasmas with reduced torque which were otherwise found to be $2/1$ TM unstable. We note that direct stabilization of $2/1$ TMs was not attempted in these experiments.

With one toroidal row of the DIII-D internal coil set ($n = 3$ configuration) and broad ECCD for $2/1$ TM mitigation, edge localized mode suppression with periods up to 1 s was observed ($q_{95} = 3.15$) in plasmas with an ITER similar shape.

References

[1] F. Turco and T. C. Luce, Nucl. Fusion **50** (2010) 095010.

This work was supported by the US Department of Energy under DE-FC02-04ER54698, DE-AC02-09CH11466, DE-FG02-04ER54761, and DE-FG02-08ER54984.

First-Principles Model-based Closed-loop Control of the Current Profile Dynamic Evolution on DIII-D

J. E. Barton¹, M. D. Boyer¹, W. Shi¹, W. P. Wehner¹, E. Schuster¹, T. C. Luce², J. R. Ferron², M. L. Walker², D. A. Humphreys², B. G. Penaflor², and R. D. Johnson²

¹*Lehigh University, Bethlehem, USA*

²*General Atomics, San Diego, USA*

Corresponding Author: justin.barton@lehigh.edu

Recent DIII-D experiments represent the first successful use of first-principles, model-based, full magnetic profile control in a tokamak. For ITER to be capable of operating in advanced tokamak operating regimes, characterized by a high fusion gain, good plasma confinement, magnetohydrodynamic stability, and a noninductively driven plasma current, for extended periods of time, several challenging control problems still need to be solved. For instance, setting up a suitable toroidal current density profile is key for one possible advanced operating scenario characterized by noninductive sustainment of the plasma current and steady-state operation. The control approach at the DIII-D tokamak is to create the desired current profile during the ramp-up and early flat-top phases of the plasma discharge and then actively maintain this target profile for the remainder of the discharge. The evolution in time of the current profile in tokamaks is related to the evolution of the poloidal magnetic flux profile, which is modeled in normalized cylindrical coordinates using a nonlinear dynamic partial differential equation referred to as the magnetic diffusion equation. This first-principles control-oriented model of the current density profile evolution in response to auxiliary heating and current drive systems [Neutral Beam Injection (NBI)], line-averaged density, and electric field due to induction, was developed and used to synthesize a combined feedforward + feedback control scheme to drive the current profile to a desired target profile. The model combines the magnetic diffusion equation with empirical correlations obtained at DIII-D for the temperature and noninductive current. Static and dynamic plasma response models were integrated into the design of the feedback controllers by employing robust, optimal, and backstepping control theories. A general framework for real-time feedforward + feedback control of magnetic and kinetic plasma profiles was implemented in the DIII-D Plasma Control System. Experimental results are presented to demonstrate the ability of the first-principles model-based feedback controllers to control the toroidal current density profile.

EX-P

This work was supported by the NSF CAREER award program (ECCS-0645086) and the US DOE under DE-FG02-09ER55064, DE-FG02-92ER54141 and DE-FC02-04ER54698.

Non-inductive Plasma Start-up in NSTX Using Transient CHI

R. Raman¹, D. Mueller², S. Jardin², T. Jarboe¹, B. Nelson¹, M. Bell¹, S. Gerhardt², E. Hooper³, S. Kaye², C. Kessel², J. Menard², M. Ono², and V. Soukhanovskii³

¹*University of Washington, Seattle, USA*

²*Princeton Plasma Physics Laboratory, Princeton, USA*

³*Lawrence Livermore National Laboratory, Livermore, USA*

Corresponding Author: raman@aa.washington.edu

Transient Coaxial Helicity Injection (CHI) in the National Spherical Torus Experiment (NSTX) has generated toroidal current on closed flux surfaces without the use of the central solenoid. When induction from the solenoid was added, CHI initiated discharges in NSTX achieved 1 MA of plasma current using 65% of the solenoid flux of standard induction-only discharges. In addition, they have lower density, which is difficult to achieve by other means in NSTX, and a low normalized internal plasma inductance of 0.35, which is consistent with broad current profiles expected for high performance NSTX-U discharges. The Tokamak Simulation Code (TSC) has now been used to understand the scaling of CHI generated toroidal current with variations in the external toroidal field and injector flux. These simulations show favorable scaling of the CHI start-up process with increasing machine size. Tokamaks and spherical tokamaks have generally relied on a central solenoid to generate the initial plasma current. The inclusion of a central solenoid in a steady-state tokamak to provide plasma startup limits the minimum aspect ratio and increases the device complexity. For reactors based on the ST concept, elimination of the central solenoid is essential, making alternate methods for plasma start-up necessary. CHI is implemented in NSTX by driving current from an external source along field lines that connect the inner and outer lower divertor plates. The NSTX is now undergoing a major upgrade (NSTX-U) to increase the capabilities of its toroidal and poloidal field coils and to add a second neutral beam line. Analysis of the NSTX results shows that the amount of closed-flux current generated by CHI is closely related to the initially applied injector flux. On NSTX-U the available injector flux is about 340 mWb, considerably exceeding the 80 mWb in NSTX. Simulations with the TSC projects that it should be possible to generate 500 kA of closed-flux current with CHI in NSTX-U. At this current, the second more tangentially injecting neutral beam should be capable of providing sufficient current drive to ramp-up the plasma current. The results from TSC simulations show that CHI could be an important tool for non-inductive start-up in next-step STs.

This work was supported by U.S. DOE contracts DE-FG02-99ER54519 and DE-AC02-09CH11466.

Non-inductive Plasma Initiation and Plasma Current Ramp-up on the TST-2 Spherical Tokamak

Y. Takase¹, A. Ejiri¹, H. Kakuda¹, T. Oosako¹, T. Wakatsuki¹, O. Watanabe¹,
T. Ambo¹, H. Furui¹, T. Hashimoto¹, J. Hiratsuka¹, H. Kasahara², K. Kato¹,
R. Kumazawa², C. Moeller³, T. Mutoh², Y. Nagashima⁴, K. Saito², T. Sakamoto¹,
T. Seki², T. Shinya¹, M. Sonehara¹, R. Shino¹, and T. Yamaguchi¹

¹University of Tokyo, Kashiwa, Japan

²National Institute for Fusion Science, Toki, Japan

³General Atomics, San Diego, USA

⁴Research Institute for Applied Mechanics, Kyushu University, Kasuga, Japan

Corresponding Author: takase@k.u-tokyo.ac.jp

To realize a compact spherical tokamak (ST) reactor, operation without the central solenoid must be demonstrated. In particular plasma current ramp-up from zero to a level required for fusion burn is crucial. Plasma initiation and current ramp-up in ST by waves in the lower-hybrid (LH) frequency range were demonstrated for the first time on TST-2. A combline antenna was used to inject RF power of ~ 100 kW at 200 MHz. Formation of a low current (~ 1 kA, mainly driven by pressure gradient) ST configuration can be accomplished by waves in a broad frequency range (21 MHz – 8.2 GHz in TST-2). However, further current ramp-up (to ~ 10 kA, mainly driven by RF) is most efficient with a uni-directional traveling wave in the LH frequency range. Sufficient RF power must be supplied and the vertical field must be ramped up to maintain equilibrium. Plasma current ramp-up to 15 kA was achieved with 60 kW of net RF power. Soft X-ray emission in the direction of electron acceleration by RF wave was enhanced more strongly in the co-drive case (acceleration in the direction to increase the plasma current) compared to the counter-drive case. Hard X-ray spectral measurements showed that the photon flux is an order of magnitude higher and the photon temperature is higher in the co-current-drive direction than in the counter-current-drive direction (60 keV vs. 40 keV). These observations are consistent with acceleration of electrons by a uni-directional RF wave. The combline antenna excites vertical electric fields which match the polarization of the fast wave. There is evidence that the LH wave is excited nonlinearly, based on the frequency spectra measured by magnetic probes in the plasma edge region. While the pump wave at 200 MHz has a stronger toroidal component (fast wave polarization), the lower sideband has a stronger poloidal component (LH wave polarization). The time evolution indicates the tendency of the pump wave toroidal component to weaken when both sideband poloidal and toroidal components intensify. It is expected that the effectiveness of current drive would improve if the LH wave could be excited directly by the antenna. Two types of traveling-wave LH wave antennas will be tested on TST-2, a dielectric-loaded waveguide array, and an array of mutually coupled structure with the electric field polarized in the toroidal direction.

EX-P

Steady State Operation Using Improved ICH and ECH for High Performance Plasma in LHD

T. Mutoh¹, T. Seki¹, R. Kumazawa¹, K. Saito¹, H. Kasahara¹, S. Kubo¹,
T. Shimozuma¹, Y. Yoshimura¹, H. Igami¹, H. Takahashi¹, Y. Nakamura¹,
M. Tokitani¹, S. Mauzaki¹, H. Idei², Y. Takeri¹, H. Yamada¹, O. Kaneko¹, and
A. Komori¹

¹National Institute for Fusion Science, Toki, Japan

²Research Institute for Applied Mechanics, Kyusyu University, Kasuga, Japan

Corresponding Author: mutoh@nifs.ac.jp

The steady state operation (SSO) of high-performance plasma in LHD [1] has progressed since the last IAEA conference by means of a newly installed ICH antenna (HAS antenna [2], HAnd Shake type) and an improved ECH system. HAS antenna could control the launched parallel wave number and heated a core plasma efficiently. The heating power of steady state ICH and ECH exceeded 1 MW and 500 kW, respectively, and the higher-density helium plasma with minority hydrogen ions was sustained. Plasma performance improved; e.g., an electron temperature of more than 2 keV at a density of more than $2 \times 10^{19} \text{ m}^{-3}$ became possible for more than 1 min. Dipole phasing operation of the HAS antenna is better than that of monopole operation, and the monopole operation gives almost the same performance with the poloidal array antenna [1]. Three 77 GHz high-power gyrotrons were also installed for high-power ECH in LHD [3]. The frequency of 77 GHz is selected to heat the plasma core region for the wider plasma operation condition, and to increase sustainable plasma density to mitigate the high energetic ion population produced by ICRF wave.

The injected power to plasma is finally absorbed by divertor plates, antenna side protectors and the chamber wall. The ratios of heat flow through various channels are estimated and about half of the heat flow goes to the divertor plates, and around 10% is goes to the ICRF antenna protectors. The non-uniform heat flow to the chamber wall decreased from 30% to 15% as the density increased.

The particle balance during SSO was also analyzed. The ratio of the total supplied particles (helium and hydrogen) to the externally pumped particles is around 20, which indicates that wall pumping is a dominant particle sink during the SSO of 320 sec. The vacuum chamber works as a large particle sink in LHD. In the case of 54 min plasma operation in 2006 [1], the LHD chamber wall also worked as a particle sink even after the very long operation time.

These experiences of steady state operation give us useful information for ITER and future fusion devices.

References

- [1] T. Mutoh, R. Kumazawa, T. Seki, *et al.*, Nuclear Fusion **47** (2007) pp 1250-1257
- [2] H. Kasahara, K. Saito, *et al.*, Plasma and Fusion Research, **5**, (2010), 2090-1-5
- [3] T. Shimozuma, *et al.*, Fusion Science and Technology, **58**, 2010, pp530-538

Validation of Off-axis Neutral Beam Current Drive Physics in the DIII-D Tokamak

J. M. Park¹, M. Murakami¹, C. C. Petty², W. W. Heidbrink³, M. A. Van Zeeland²,
D. C. Pace⁴, R. Prater², J. R. Ferron², T. H. Osborne², C. T. Holcomb⁴,
G. J. Jackson², and T. W. Petrie²

¹*Oak Ridge National Laboratory, Oak Ridge, USA*

²*General Atomics, San Diego, California*

³*University of California, Irvine, USA*

⁴*Oak Ridge Institute for Science Education, Oak Ridge, USA*

⁵*Lawrence Livermore National Laboratory, Livermore, USA*

Corresponding Author: parkjm@ornl.gov

DIII-D experiments on neutral beam current drive (NBCD) using the new tilted beamline have clearly demonstrated off-axis NBCD in agreement with modeling. Two of the eight neutral beam sources have been modified for downward vertical steering to provide significant off-axis current drive for AT scenario development. For validation of off-axis NBCD physics, the local NBCD profile was measured in H-mode plasma and compared with modeling under a range of beam injection and discharge conditions. The full radial profile of NBCD measured by the magnetic pitch angles from the motional Stark effect (MSE) diagnostic shows a clear hollow NBCD with the peak NBCD location at $\rho \sim 0.45$, which is in good agreement with the classical model calculation using the Monte-Carlo beam ion slowing down code, NUBEAM. Time evolution of the MSE signals is consistent with transport simulation with realistic current drive sources. The beam-stored energy estimated by equilibrium reconstruction and neutron emission data do not show any noticeable anomalous losses of NBCD and fast ions. The measured magnitude of off-axis NBCD is very sensitive with the toroidal magnetic field direction that modifies the alignment of the off-axis beam injection to the local helical pitch of the magnetic field lines. If the signs of the toroidal magnetic field and the plasma current yield the proper helicity, both measurement and calculation indicate that the efficiency is as good as on-axis NBCD because the increased fraction of trapped electrons reduces the electron shielding of the injected ion current. This dependency of the off-axis NBCD efficiency on the toroidal field direction is crucial to optimum use of the off-axis beams not only for DIII-D but also for ITER. A detailed NB and Electron Cyclotron Heating (ECH) power scan with variation of the ratio of beam injection energy to electron temperature (E_b/T_e) at fixed β and with variation of β at fixed E_b/T_e , around the anticipated ITER parameters, implies that ITER is not likely to suffer from the loss of NBCD efficiency due to additional transport from microturbulence.

This work supported in part by U.S. Department of Energy under DE-AC05-00OR22725, DE-FC02-04ER54698, SC-G903402, DE-AC05-06OR23100 and DE-AC52-07NA27344.

EX-P

Non-inductive Current Start-up and Plasma Equilibrium with an Inboard Poloidal Field Null by Means of Electron Cyclotron Waves in QUEST

H. Zushi¹, S. Tashima², M. Ishiguro², and M. Hasegawa¹

¹*Riam Kyushu University, Fukuoka, Japan*

²*AEES Kyushu University, Fukuoka, Japan*

Corresponding Author: zushi@triam.kyushu-u.ac.jp

ECW Start-up scenarios in QUEST: Non-inductive current start-up using ECW ($f = 8.2$ GHz, $P_{\text{rf}} < 140$ kW, O-mode, $N_{\parallel 0} < 0.4$) has been investigated from a view point of multiple ECR interaction, large up-shift and auto resonance condition ($N_{\parallel \sim 1}$) in QUEST. Due to large up-shift of N_{\parallel} at R_{1ce} , ECCD with mildly relativistic electrons moving in the wave momentum direction can be expected. The start-up rate dI_p/dt of $0.3 - 0.5$ MA/sec was achieved within 0.2 s after rf injection. During this phase rapid build up of the energy spectrum of mildly relativistic electrons is observed. This fact strongly supports the ECR current drive scenario based on the relativistic resonance interaction.

Equilibrium with an inboard poloidal field null: MHD equilibrium state with an inboard poloidal field null is characterized by high β_p . Parameters are $a = 0.27$ m, $R_0 = 0.79$ m, $\Delta/a = 0.4$ and $\varepsilon\beta_p = 1.5$, respectively. Here Δ denotes the Shafranov shift. The R_s locates at ~ 0.5 m. During the flattop phase, I_p reached to 25 kA with a positive dependence of B_ν and could be sustained for ~ 10 s. Loop voltage was less than 10 mV, the line density $0.5 \times 10^{18} \text{ m}^{-3}$ ($<$ the cutoff density) and T_e was measured < 100 eV by Thomson scattering. The value of $\beta_p + L_i/2$, the Shafranov lambda, was kept ~ 5 . Using observed HX temperature of ~ 50 keV and assumed density of the energetic electrons of $\sim 10\%$ of density β_p (= phot/poloidal magnetic pressure) due to energetic electrons is consistent with that in MHD equilibrium.

Relaxation oscillations of this equilibrium: High β_p equilibrium oscillates at the frequency of ~ 20 Hz under some conditions for $10 - 20$ kA. The slow rise and sharp drop in I_p are correlated to changes in density, R_s , shift and the HX energy spectrum emitted from the current carrying electrons. The out-of-phase relation in two energy windows ($20 - 100$ keV and $200 - 400$ keV) of HXs suggests that electrons are preferably accelerated against the induced return electric field (~ 20 mV/m) during the I_p rise. Thus, confinement of the energetic electrons affects the stability of this equilibrium.

EX-P

ECRH Pre-ionization and Assisted Startup in HL-2A Tokamaks

X. Song¹, L. Chen¹, J. Zhang¹, J. Rao¹, J. Zhou¹, and J. Li¹

¹*Southwestern Institute of Physics, Chengdu, China*

Corresponding Author: songxm@swip.ac.cn

ECRH pre-ionization and assisted startup is foreseen in ITER, because the electric field applied for ionization and ramp-up of plasma current is limited to a very low value about 0.3 V/m. Many data for ECRH pre-ionization and assisted startup have been obtained from C-Mod, ASDEX Upgrade, DIII-D, JT-60U, JET and KSTAR. This paper presents the experiment results in HL-2A Tokamak from 2010 to 2012, with emphasis on the following two new and better results.

1. The minimum loop voltage for successful plasma establishment is reduced up to 1 V, corresponding toroidal electric field of 0.1 V/m, which is $3\times$ smaller than the ITER value of 0.3 V/m, and smaller than the best value of 0.15 V/m ever obtained from DIII-D.
2. Plasma can be established successfully with ECRH second harmonic X mode (X2) switching on before or after application of the reduced loop voltage, which presents important experiment data to the answer of the open issue addressed in ITPA joint experiment IOS-2.3.

IOS-2.3 focuses on the breakdown-assist experiment results with X2 mode ECRH when ECRH power is launched after application of the reduced loop voltage, which is the situation operating in ITER during its commissioning phase, and so far never performed before. In HL-2A experiments, ECW with the fundamental O mode (O1) or X2 is launched, and the toroidal injection angle can be changed from 0° to 200° in the equatorial plane. During 2010-2011 HL-2A experiment campaigns, the loop voltage can be reduced to 3 V by O1 and X2 mode ECW, with minimum power 200 kW and 600 kW, respectively. The effects of toroidal inclination, prefill pressure, wall conditioning and poloidal field null structure on X2 mode pre-ionization and assisted startup have been studied. During 2012 HL-2A experiment campaigns, the breakdown condition can be greatly improved with siliconization and lithiumization, and good results have been obtained. The loop voltage for successful plasma establishment is reduced up to 1 V, and plasma can be established readily with X2 mode ECRH switching on 30 ms before or 30 ms after application the reduced loop voltage. The minimum ECRH power is about 500 kW. The minimum loop voltage for successful pure ohmic breakdown is also presented, which is 3.4 V.

EX-P

Progress toward Steady-state Regimes in Alcator C-Mod

S. Shiraiwa¹, P. Bonoli¹, O. Meneghini^{1,2}, R. R. Parker¹, G. M. Wallace¹,
J. R. Wilson³, S. G. Baek¹, I. C. Faust¹, R. W. Harvey⁴, A. P. Smirnov⁵, and
A. Hubbard¹

¹*Plasma Science and Fusion Center, MIT, Cambridge, USA*

²*General Atomics, San Diego, USA*

³*Princeton Plasma Physics Laboratory, Princeton, USA*

⁴*CompX, Del Mar, USA*

⁵*M. V. Lomonosov Moscow State University, Moscow, Russian Federation*

Corresponding Author: shiraiwa@psfc.mit.edu

Over 1 MW of RF power in the lower hybrid (LH) frequency range (4.6 GHz) has been injected into C-Mod plasmas. Fully non-inductive discharges were sustained for 2 – 3 current relaxation time with $n_e = 0.5 \times 10^{20} \text{ m}^{-3}$, $I_p = 0.5 \text{ MA}$ and $B_T = 5.4 \text{ T}$. Sawteeth are completely suppressed and modestly reversed shear plasmas, with $q_0 \sim 2$ and $q_{\min} \sim 1.5$, were obtained. CD efficiency is in the range of $2.0 - 2.5 \times 10^{19} \text{ A/Wm}^2$, consistent with what is assumed in ITER. Also, spontaneous formation of an ITB was observed during these discharges after the current profile relaxed. Accessing ITER-relevant steady-state regimes with $f_{\text{BS}} \sim 50\%$ in C-Mod requires increasing the density to $\sim 1.5 \times 10^{20} \text{ m}^{-3}$ with $T_{e0} \sim 5 \text{ keV}$ [1]. Target plasmas with these parameters have been produced in C-Mod both by mode-converted ICRF heating as well as in I-Mode [2]. However, in low temperature ($T_{e0} \sim 2 \text{ keV}$) Ohmically heated plasmas, LHCD efficiency drops precipitously as the density is increased above $\sim 5 \times 10^{19} \text{ m}^{-3}$ even though this density is well below conventional limits set by either accessibility or parametric decay [3,4]. This falloff with density has been explored with two newly developed and independent simulations, ray-tracing and fullwave codes coupled with 3D Fokker-planck codes [5,6]. Both simulations indicate that wave interactions in edge plasmas including SOL can lead to the observed loss in efficiency, either by direct collisional absorption and/or by causing an up-shift in the parallel refractive index. The simulations also indicate that the loss in efficiency can be recovered by increasing the first-pass absorption. Experiments aimed at verifying this result have been carried out in mode-converted ICRF-heated He discharges with high T_{e0} (up to 5.3 keV). Good agreement with the simulations is found, verifying that low parasitic absorption occurs with stronger absorption. Based on this result, additional launcher was design to aim maximizing the velocity space synergy between two launchers. Implications for realizing steady-state regimes in C-Mod will be discussed.

References

- [1] P. T. Bonoli *et al.*, **40** (2000) 1251.
- [2] D. G. Whyte *et al.*, **50** (2010) 105005.
- [3] G. M. Wallace *et al.*, **17** (2010) 082508.
- [4] G. M. Wallace *et al.*, **51** (2011) 083032.
- [5] O. Meneghini *et al.*, **16** (2009) 090701.
- [6] S. Shiraiwa *et al.*, **18** (2011) 080705.

Resonant and Non-resonant type Pre-ionization and Current Ramp-up Experiments on Tokamak ADITYA in the Ion Cyclotron Frequency Range

S. Kulkarni¹, K. Mishra¹, S. Kumar¹, Y. Srinivas¹, H. M. Jadav¹, K. Parmar¹,
B. R. Kadia¹, A. Varia¹, R. Joshi¹, M. Parihar¹, M. K. Gupta¹, N. Ramaiya¹,
J. Ghosh¹, P. Atrey¹, R. Jha¹, S. Joisa¹, R. Tanna¹, S. B. Bhatt¹, C. N. Gupta¹, and
P. K. Kaw¹

¹*Institute for Plasma Research, Bhat, India*

Corresponding Author: kulkarni@ipr.res.in

Here we report the pre-ionization experiments carried out in ICRF range using poloidal type fast wave antenna, and 200 kW RF system at 24.8 MHz frequency which corresponds to the second harmonic resonance layer at the center of the vacuum vessel of tokamak ADITYA at 0.825 T. The experiments are carried out in different phases like only RF plasma, RF plasma in presence of toroidal magnetic field, RF pre-ionization with higher loop voltages and then at lower loop voltages by decreasing current and then at lower loop voltages with constant volts-seconds. In last phase the current ramp-up is carried out at lower loop voltages as well as with slow rise time to simulate the requirements of steady state tokamaks like SST-1. The toroidal magnetic field is varied from 0.825 T to 0.075 T, pressure is varied from 3×10^{-5} torr to 8.0×10^{-4} torr and RF power is varied from 20 W to 120 kW. The diagnostics used are Langmuir probes, visible camera, spectroscopy, soft and hard X-ray detection techniques, diamagnetic loop and microwave diagnostics like interferometer and reflectometer. After plasma production at different magnetic fields, the pre-ionization experiments are carried out at different loop voltages to ramp up the current and we could ramp up current at all available loop voltages starting from 22 V to 8 V of the ohmic loop voltage to get normal plasma discharge of 90 kA and 90 ms duration.

There exists a minimum value of the toroidal magnetic field (0.09 T) below which no plasma spread is observed and also below 20 kW RF power we did not observe pre-ionization. It is observed that at lower loop voltages the current ramp-up is possible only in presence of pre-ionization.

EX-P

Poloidal Variation of High-Z Impurity Density due to Hydrogen Minority ICRH on Alcator C-Mod

M. Reinke¹, J. Rice¹, Y. Lin¹, I. H. Hutchinson¹, N. Howard¹, A. Bader¹, S. Wukitch¹, P. David¹, A. Hubbard¹, J. Hughes¹, and Y. Podpaly¹

¹*MIT Plasma Science and Fusion Center, Cambridge, USA*

Corresponding Author: mlreinke@psfc.mit.edu

In the Alcator C-Mod tokamak, strong, steady-state variations of molybdenum density within a flux surface are routinely observed in plasmas using hydrogen minority ion cyclotron resonant heating. In/out asymmetries, up to a factor of 2, occur with either inboard or outboard accumulation depending on the major radius of the minority resonance layer. Quantitative comparisons between existing parallel high-Z impurity transport theories and experimental results show good agreement when the resonance layer is on the high-field side (HFS) of the tokamak but disagree substantially for low-field side (LFS) heating. Impurity accumulation on the LFS of a flux surface can be explained by the centrifugal force, and is the first observation of intrinsic rotation generating an in/out asymmetries. The accumulation of impurity density on the HFS of a flux surface is shown to be driven by a poloidal potential variation sustained by magnetically trapped non-thermal, cyclotron heated minority ions. Parallel impurity transport theory is extended to account for these fast-ion effects and shown to agree with experimentally measured impurity density asymmetries.

EX-P

Measurements of Core Lithium Concentration in Diverted H-Mode Plasmas of NSTX

M. Podesta¹, R. E. Bell¹, A. Diallo¹, B. P. LeBlanc¹, and F. Scotti¹

¹*Princeton Plasma Physics Laboratory, Princeton, USA*

Corresponding Author: mpodesta@pppl.gov

The National Spherical Torus Experiment (NSTX) is investigating the use of lithium as a candidate plasma-facing material to handle the large power flux to the wall of fusion devices. To investigate the possible contamination of the core plasma caused by lithium influx from the plasma boundary, measurements of core lithium concentration, $n_{\text{Li}}(R)$, have been performed in diverted H-mode plasmas of NSTX. Various experimental scenarios, representative of the NSTX operating space, are explored from the 2010 NSTX experimental campaign, during which a total of ~ 1.3 kg of lithium was evaporated into the vessel. It is found that, in spite of the large amount of lithium (hundreds of milligrams) introduced in the vessel either before or during a discharge, n_{Li} remains insignificant, typically $\ll 0.1$ % of the electron density. The measured n_{Li} is rather insensitive to variations of plasma current, toroidal field, divertor conditions and of the specific technique utilized for lithium conditioning of the vessel wall. These results enable projections to the higher field and current and longer pulse length of the NSTX Upgrade (NSTX-U), suggesting that lithium contamination will remain negligible compared to other impurities such as carbon.

Work supported by U.S. DOE Contract DE-AC02-09CH11466.

EX-P

Potential Fluctuation Study from the Core Plasma to End Region in the GAMMA 10 Tandem Mirror

M. Yoshikawa¹, M. Sakamoto¹, Y. Miyata², M. Aoyama¹, M. Mizuguchi¹, M. Hirata¹,
M. Ichimura¹, T. Imai¹, T. Kariya¹, I. Katanuma¹, J. Kohagura¹, R. Minami¹,
Y. Nakashima¹, T. Numakura¹, R. Ikezoe¹, H. Nakanishi³, and Y. Nagayama³

¹*Plasma Research Center, University of Tsukuba, Tsukuba, Japan*

²*Japan Atomic Energy Agency, Naka, Japan*

³*National Institute for Fusion Science, Toki, Japan*

Corresponding Author: yosikawa@prc.tsukuba.ac.jp

Correlation between the drift type fluctuation and anomalous radial transport was observed in GAMMA 10 and these fluctuations were suppressed by electron cyclotron heating (ECH) driven radial electric field. We have developed new diagnostics to investigate for these studies, which are a simultaneous two points measuring gold neutral beam probe (GNBP) for the radial electric field and potential fluctuation and a high speed end plate potential fluctuation measurement system. The radial electric field and its fluctuation successfully obtained by using simultaneous two point measurements. The potential fluctuation phase difference between the two measuring positions in a single plasma shot was obtained for fluctuation analysis. The coherency of the drift type potential fluctuations between the core plasma by GNBP and that of the end plate measurement was clearly observed. By using end plate system with the GNBP, we can study detailed potential fluctuations in the core plasma without ECH. It is found that these potential and electric field fluctuations are clearly suppressed by the positive electric fields. We have obtained the strong tools for investigating the correlation of the radial electric field and the potential fluctuations between core and edge plasmas.

EX-P

High Current Plasmas in RFX-mod Reversed Field Pinch

L. Carraro¹, P. Innocente¹

¹ *Consorzio RFX, Associazione EURATOM-ENEA sulla fusione, Padova, Italy*

Corresponding Author: lorella.carraro@igi.cnr.it

High current (I_p up to 2 MA) operations in RFX-mod access the Single Helical Axis (SHAx) regime, during which the magnetic dynamics is dominated by the innermost resonant mode ($m = 1, n = -7$): the magnetic chaos level is reduced and internal magnetic field configuration is close to a pure helix. The best plasma performances at high I_p with pure SHAx states featuring electron transport barriers have been reached with shallow values of the reversal parameter $F = B_t(a)/\langle B_t \rangle$ ($-0.05 < F < 0$).

The SHAx states show back transitions to Multiple Helicity (MH) regime; at $I_p > 1.5$ MA their total persistence is greater than 90% of the plasma current flat-top. During the SHAx state strong electron temperature (T_e) gradients can show up, identifying an electron transport barrier. The dynamics of the thermal structure has been characterized with a new high time resolution T_e profile diagnostic, SXR double-filter multichord system. The high T_e gradients last up to 10 – 15 ms, more than the energy confinement time.

The strongest barriers in the central helical region are achieved at the lowest total amplitudes of the $m = 1$ secondary modes. Improvements of error field control capability has been recently identified in the correction of systematic errors in the edge field measurements and of the fields induced by the presence of a conductive wall with 3D structures.

The T_e profile measured inside the barrier is flat; to describe the transport in this region, electrostatic turbulence and subsequent vortical drift have been taken into account in a simplified model, in alternative, the residual $m = 2$ mode activity has been considered as the source of the magnetic chaos.

In the region of the T_e gradients, the main gas diffusion coefficient is one order of magnitude lower than the MH case and the convection term is negligible, in agreement with the removal of the stochastic transport.

The large plasma volume external to the barrier is crucial to improve the global confinement. The T_e gradients in the region $0.7 < r/a < 0.95$ increase at lower amplitudes of the $m = 0$ modes, likely connected to a lower edge turbulence. Lithium wall conditioning experiments are ongoing aiming at producing higher edge temperature and temperature gradients through a reduced radiation and recycling: promising experiments with more peaked density profiles and good density control up to $n/n_G = 0.5$ have been produced.

EX-P

Experimental Investigation of Plasma Confinement in Reactor Relevant Conditions in TCV Plasmas with Dominant Electron Heating

N. Kirneva¹, A. Pochelon², R. Behn², S. Coda², B. P. Duval², T. P. Goodman²,
B. Labit², A. Karpushov², O. Sauter², and M. Silva²

¹*Institute of Physics of Tokamaks, National Research Center “Kurchatov Institute”, Moscow, Russian Federation*

²*Ecole Polytechnique Fédérale de Lausanne (EPFL), Centre de Recherches en Physique des Plasmas, Association Euratom-Confédération Suisse, Lausanne, Switzerland*

Corresponding Author: kirneva@nfi.kiae.ru

This paper reports on recent TCV experiments performed to investigate the confinement of electron-heated discharges simulating reactor relevant conditions with dominant electron heating. The dependence of the L-mode confinement properties on the electron heating power density profile width has been analyzed for the first time. Discharges with on-axis peaked ECR heating profiles with half-width varying between 15 and 40% of the minor radius have been performed in the range of heating power 0.5 – 2 MW and at line-averaged density $2 \times 10^{19} \text{ m}^{-3} = 0.15 n_{Gw}$. A scenario with off-axis heating peaked at $\rho \sim 0.7$ but the same total heating power has also been studied for comparison. The following features have been found [1]:

1. The confinement is largely independent of the power deposition profile width, provided a significant fraction occurs inside the $q = 1$ radius.
2. The energy confinement time scales with the heating power as $\tau_E \sim P_{\text{tot}}^{-0.73}$, independent of the heating profile width, when the power is peaked on-axis.
3. Off-axis heating results in stronger confinement degradation ($\tau_E \sim P_{\text{tot}}^{-0.9}$). An investigation of the plasma confinement in high-density discharges has also been performed.

A limit density close to and even exceeding the Greenwald limit $\bar{n}_e \sim (0.6 - 1.1) \times n_{Gw}$ has been achieved in ohmically heated plasmas, depending on the q -edge value.

References

- [1] N.A. Kirneva, K.A. Razumova, A. Pochelon *et al.*, Plasma Physics Control. Fusion **54** (2012) 015011.

Suprathermal Ion Studies in ECRH and NBI Phases of the TJ-II Stellarator

B. Zurro¹, A. Baciero¹, M. Liniers¹, and A. Cappa¹

¹*Laboratorio Nacional de Fusion, Asociacion EURATOM-CIEMAT, Madrid, Spain*

Corresponding Author: b.zurro@ciemat.es

In TJ-II we have been able to detect suprathermal ions by passive spectroscopy in the plasma interior and by means of a luminescent probe for those escaping from the confinement region. We have measured their temporal evolution in both cases and with several vision cords in the first system. The luminescent probe has very high sensitivity and it was operated in a height pulse analysis regime. Its data was processed by an ad hoc digital pulse algorithm which has made possible to determine its ion energy distribution function in ECRH and NBI regimes. We have been studying, not only with protons but also in some selected impurity ions, temperatures and population of these suprathermal ions as well as its flow and rotation velocity when the available photon statistics permit it. We have attained several conclusions:

1. The typical temperatures of the suprathermal ions is a factor 4 higher than the thermal one in the case of protons.
2. In many cases the ion energy content of this suprathermal component is comparable to the energy content of the thermal one with relevant implications for the TJ-II energy balance.
3. The suprathermal rotation measured in a poloidal plane can be a factor between 2.5 and 5 higher than the rotation of the thermal component.

All these results represent a true challenge for theories capable of explaining its generation, like in the case of ECRH phase, and its rotation: suprathermal particles constitute an excellent probe of physical mechanisms inside a high temperature plasma complementary of thermal ones. Its time behavior in transient situations has made possible to realize that the confinement time is lower as the energy of the selected population is higher, and this fact suggests that the deconfinement mechanisms of suprathermal ions cannot be explained solely by Coulomb collisions, but rather well intrinsic properties of the TJ-II magnetic configuration, like magnetic ripple, magnetic configuration, etc., must be invoked even to understand qualitatively this behavior within the stellarator field.

EX-P

Study of Fueling Control for Confinement Experiments in Heliotron J

T. Mizuuchi¹, F. Sano¹, K. Nagasaki¹, H. Okada¹, T. Minami¹, S. Kobayashi¹,
S. Yamamoto¹, S. Oshima², K. Mukai³, H. Lee³, L. Zang³, M. Takeuchi¹,
K. Yamamoto³, S. Arai³, T. Kagawa³, K. Mizuno³, T. Minami³, Y. Wada³,
H. Watada³, H. Yashiro³, N. Nishino⁴, Y. Nakashima⁵, S. Kado⁶, K. Hanatani¹,
Y. Nakamura², and S. Konoshima¹

¹*Institute of Advanced Energy, Kyoto University, Gokasho, Uji, Japan*

²*Graduate School of Energy Science, Kyoto University, Uji, Japan*

³*Kyoto University Pioneering Research Unit for Next Generation, Uji, Japan*

⁴*Graduate School of Engineering, Hiroshima University, Higashi-Hiroshima, Japan*

⁵*Plasma Research Center, University of Tsukuba, Tsukuba, Japan*

⁶*School of Engineering, The University of Tokyo, Bunkyo, Japan*

Corresponding Author: mizuuchi@iae.kyoto-u.ac.jp

This paper discusses the effects of fueling control on plasma performance in Heliotron J, a helical-axis heliotron device with an $L/M = 1/4$ helical coil ($R_0 = 1.2$ m, $\langle a_p \rangle = 0.12 - 0.17$ m, $\langle B_0 \rangle \leq 1.5$ T). Here, L and M are the pole number of the helical coil and its helical pitch number, respectively. Based on recent installation/improvement of diagnostics, which give us plasma profile database for detailed transport analyses, the confinement study has been accelerated. Here fueling and recycling control is not only one of the key issues for high density and high performance plasma but also plays important roles in diagnostics. Effectiveness of supersonic molecular beam injection (SMBI) fueling has been studied based on profile data. A peaked density profile is realized by SMBI in NBI plasma, while a conventional gas puff (GP) fueling results in rather flat profile for the same heating condition. This is qualitatively consistent with the edge density profile reconstructed from an AM microwave reflectometer data. Since the amount of gas to obtain the same increment of the line-averaged density is about 30 – 40% higher in GP compared to SMBI, the expected difference in the neutral density outside the plasma after SMBI or GP might contribute to make the observed different density profile at ~ 20 ms after the fueling. SMBI can also affect plasma fluctuations. Fast camera observation for filament structure in the edge turbulence has revealed that SMBI can change its rotation direction and/or speed. Similar change is observed at L-H transition in Heliotron J. In addition, recent density fluctuation measurement at different radial positions with a beam-emission spectroscopy (BES) system suggests SMBI affects the fluctuation inside the last-closed flux surface. Here, the observed fluctuation may be some MHD mode relating to high-energy ions. During about 10 ms after SMBI, the fluctuation is not observed in BES data and the Mirnov-coil signal is decreased, suggesting change of excitation condition of the mode. These observations suggest more preferable control scenario of NBI deposition profile toward core heating through $n_e(r)$ modification caused by SMBI.

Magnetic Fluctuation-Driven Intrinsic Flow in a Toroidal Plasma

W. X. Ding¹, L. Lin¹, D. L. Brower¹, A. F. Almagri², D. J. Den Hartog², G. Fiksel³,
and J. Sarff²

¹ *University of California, Los Angeles, USA*

² *University of Wisconsin-Madison, Madison, USA*

³ *University of Rochester, New York, USA*

Corresponding Author: wding@ucla.edu

Magnetic fluctuations have been long observed in various magnetic confinement configurations. These perturbations may arise naturally from plasma instabilities such as tearing modes and energetic particle driven modes, but they can also be externally imposed by error fields or external magnetic coils. It is commonly observed that large MHD modes lead to plasma locking (no rotation) due to torque produced by eddy currents on the wall, and it is predicted that stochastic field induces flow damping where the radial electric field is reduced. Flow generation is of great importance to fusion plasma research, especially low-torque devices like ITER, as it can act to improve performance. Here we describe new measurements in the MST reversed field pinch (RFP) showing that the coherent interaction of magnetic and particle density fluctuations can produce a turbulent fluctuation-induced kinetic force that acts to drive spontaneous plasma rotation. Key observations include:

1. The average kinetic force, $\sim 0.5 \text{ N/m}^3$, is comparable to the intrinsic flow acceleration.
2. Between sawtooth crashes, the spatial distribution of the kinetic force is directed to create a sheared parallel flow profile that is consistent with the measured flow profile, suggesting the kinetic force could be responsible for intrinsic plasma rotation.

EX-P

Understanding the Dynamics of Cold Pulse Nonlocality Phenomena

H. J. Sun^{1,2}, P. H. Diamond^{1,3}, Z. Shi², G. M. D. Hogewey⁴, J. Citrin⁴, Z. Wang², C. Chen², L. Yao², X. Ding², S. Yoon¹, S. G. Lee¹, B. Feng², X. Huang², Y. Zhou², J. Zhou², X. Song², W. C. Kim¹, and J. G. Kwak¹

¹*NFRI, Daejeon, Republic of Korea*

²*Southwestern Institute of Physics, Chengdu, China*

³*CMTFO, University of California San Diego, La Jolla, USA*

⁴*DIFFER, Nieuwegein, Netherlands*

Corresponding Author: asufish@gmail.com

Resolving the long standing question of whether tokamak transport is local or non-local is crucial for successful predictive modeling of ITER. Though most theoretical and modeling schemes are based on the local Fickian formulation, there are many conspicuous experimental results suggesting otherwise. Most notable of these is the cold pulse nonlocality in which edge cooling produces a central temperature rise on a time scale drastically shorter than the bulk confinement time. In this paper, we present experimental and theoretical results which illuminate the enigma of the cold pulse and support the hypothesis that the associated central temperature rise is due to the formation of a transient thermal barrier structure. We present fluctuation measurements which support this conclusion. Experiments show that Supersonic Molecular Beam Injection (SMBI) into a LOC plasma results in fast edge cooling and the subsequent central heating. Sequential SMBI sustains the elevated core temperature if the interval between SMBI pulses is shorter than one confinement time. Microwave reflectometry studies of the response of core turbulent density fluctuations to SMBI show that small scale, high frequency fluctuations are reduced in this state with sustained increase of $T_e(0)$. Theoretical studies have focused on the elucidation of the origin of the rapid profile response to the peripheral cooling. Studies of model simulations of cold pulse experiments recover all of the elements of non-locality — i.e., the inversion, a transient thermal barrier due to the self-consistent shearing and a fast response. Further studies reveal that the key to the inversion and transient thermal barrier is diamagnetic shearing, self-consistently produced in response to dynamic profile perturbations. Thus, we propose that the long standing mystery of turbulent nonlocality phenomena is ultimately rooted in a simple but strongly nonlinear feedback loops in the transport dynamics, and that dynamic shearing can produce the transient barrier structures required to explain the cold pulse phenomenology.

Collisionality Dependence of Confinement in T-10 L-Mode Plasmas

V. Trukhin¹, N. Kirneva¹, A. Borschegovskij¹, E. Gorbunov¹, L. Kluchnikov¹,
S. Krylov¹, V. Krupin¹, S. Maltsev¹, T. Myalton¹, Y. Pavlov¹, I. Roy¹, D. Sergeev¹,
D. Shelukhin¹, A. Sushkov¹, E. Trukhina¹, and V. Vershkov¹

¹*Institute of Physics of Tokamaks, National Research Center "Kurchatov Institute", Moscow, Russian Federation*

Corresponding Author: trukhin@gmail.com

Investigation aimed at the understanding of a general origin of the thermal and particle transport has been carried out in regimes with the dominant electron heating in the T-10 tokamak. ECR heating with the power of 0.25-3 MW has been used. Two scans have been summarized for the analysis: density scan at the constant EC heating power value, ($P_{EC} = 0.9$ MW, $P_{tot} = 1$ MW), and recently obtained EC heating power scan at the fixed density $n_e = 1.8 \times 10^{19} \text{ m}^{-3} = 0.25 n_{GW}$. The value of the effective collisionality was changed in the range $\nu_{eff} \sim 0.1 - 10$. For the first time it was shown that the main regularities of the energy and particle confinement do not depend of the method of collisionality modification. These features are the following:

1. energy confinement time increase with collisionality and saturates at $\nu_{eff} \sim 1 - 2$;
2. the density peaking increases with collisionality and goes to higher level at the same ν_{eff} value, $\nu_{eff} \sim 1 - 2$;
3. the density profile flattening becomes stronger with collisionality increase in the ECR heated discharges in comparison with the ohmically heated discharges taken at the same collisionality.

EX-P

The Value of Flexibility: the Contribution of RFX to the International TOKAMAK and STELLARATOR Programme

M. Valisa¹

¹ *Consorzio RFX, Associazione EURATOM-ENEA sulla Fusione, Padova, Italy*

Corresponding Author: valisa@igi.cnr.it

RFX-mod embodies the characteristics of flexibility of an experiment where cross-configuration studies can be carried out. Such condition has aroused lively interest and has led to important collaborations with laboratories worldwide (JT60-SA, DIII-D, AUG, PPFL, PPPL, Auburn University, ORNL). As a Reversed Field Pinch (RFP), RFX-mod addresses many basic physics issues that are common to both Tokamak and Stellarators, just in a different region of the parameters space of a hot plasma, characterized by low magnetic fields. In addition RFX-mod can be run directly as a low current, ohmic, circular Tokamak and apply to it its state-of-the-art system for active MHD feedback control and investigate, for instance, Resistive Wall Modes and Resonant Field Amplification processes. The control of the (2,1) mode has allowed exploring equilibria down to $q(a) = 1.6$, showing the importance of correctly treating the aliasing of the sidebands generated by the correction coils. A high triangularity plasma with double x-point has also been produced. Entering an ohmic H mode would open the way to further important studies such as ELM's control.

The bridge with the Stellarator community has been established because the RFP helical states can provide a good test-bed for numerical codes conceived to deal with 3D effects. The equilibrium codes VMEC and V3FIT developed for the Stellarator have been successfully adapted to reconstruct RFX-mod equilibria with diagnostics. Such equilibria show a good agreement with the results of the RFP equilibrium reconstruction code SHEq, providing the additional information on the role of pressure. The resulting q profiles show a non monotonic radial shape and the presence of a maximum where usually a strong thermal barrier develops.

The contribution of coherent structures to the transport of particles and energy at the plasma edge has been studied on RFX-mod with direct observations of current density filaments in the edge region both in the RFP configuration — where drift kinetic Alfvén structures have been identified — and in the Tokamak configuration, where small scales current filaments have been found. These results are compared with the findings in the TORPEX experiment, those obtained in the AUG experiments during type one ELM's, and with those in the TJ-II Stellarator device where similar investigations are in progress.

EX-P

Real-time Model-based Reconstruction and Control of Tokamak Plasma Profiles

F. Felici¹, O. Sauter², M. De Baar^{1,3}, S. Coda², B. Duval², T. Goodman²,
G. Hommen³, J. M. Moret², M. Steinbuch¹, and R. Voorhoeve¹

¹*Eindhoven University of Technology, Eindhoven, Netherlands*

²*École Polytechnique Fédérale de Lausanne, Centre de Recherches en Physique des Plasmas,
Lausanne, Switzerland*

³*TU Eindhoven/FOM-DIFFER association Euratom-FOM, Nieuwegein, Netherlands*

Corresponding Author: f.felici@tue.nl

A new paradigm for real-time plasma profile reconstruction is demonstrated in the TCV tokamak. Predictions based on physics models are merged with available real-time diagnostic data to construct a self-consistent profile state estimate compatible with a time-dependent model of transport processes in the plasma. This is enabled by a new Rapid Plasma Transport simulator (RAPTOR), implemented in the new TCV real-time control system. RAPTOR simulates the radial current diffusion including the ohmic coil transformer voltage and non-inductive sources in real-time, while the plasma physically evolves in the tokamak. This makes available an extensive set of quantities which are normally not known in real-time such as the bootstrap current fraction, safety factor, magnetic shear and loop voltage profiles. This approach represents a generalization of existing approaches for real-time equilibrium reconstruction with measurement-constrained current density profile, as transport physics knowledge is now included in the reconstruction.

The same rapid transport code is also used in predictive mode, including a model of the electron temperature evolution, for off-line studies of optimal actuator trajectories during plasma ramp-up scenarios. Constraints are included in the optimization to reflect realistic operational limits. These studies show that a plasma current overshoot combined with appropriately timed heating are beneficial for rapidly reaching a stationary q profile with flat central shear. The demonstration of this new paradigm paves the way for further integration of real-time tokamak plasma simulations for prediction, scenario monitoring, disruption avoidance and feedback control.

This work was supported in part by the Swiss National Science Foundation.

EX-P

Turbulent Transport and Gyrokinetic Analysis in Alcator C-Mod Ohmic Plasmas

M. Porkolab¹, J. Dorris², P. Ennever¹, D. Ernst¹, C. Fiore¹, M. Greenwald¹,
A. Hubbard¹, E. Marmar¹, Y. Ma¹, Y. Podpaly¹, M. Reinke¹, J. Rice¹, J. C. Rost¹,
N. Tsujii¹, J. Candy³, G. Staebler³, and R. Waltz³

¹*MIT Science and Fusion Center, Cambridge, USA*

²*Fisker Automotive, Anaheim, USA*

³*General Atomics, San Diego, USA*

Corresponding Author: porkolab@psfc.mit.edu

Transport in ohmically heated plasmas in Alcator C-Mod was studied in both the linear (LOC) and saturated (SOC) confinement regimes and the importance of turbulent transport was established with gyrokinetic analysis. The presence of turbulence was measured with an absolutely calibrated phase contrast imaging (PCI) method and was compared with theoretical predictions. While in the SOC regime the measured electron and ion transport coefficients were comparable in magnitude and in agreement with GYRO predictions due to the dominance of ITG turbulence, in the LOC regime the measured transport coefficients disagreed with predictions [1]. Importantly, in the experiments electron transport was dominant, whereas GYRO found dominant ion transport due to prevailing ITG turbulence. After extensive analysis with TGLF and GYRO, in the present work it is found that in the LOC regime using an effective impurity ion species with $Z_i \leq 8$, and moderately high Z_{eff} (2.0 – 5.6), in agreement with experimental measurements as the density was decreased) electron transport became dominant due to excitation of dominant TEM/ETG turbulence [2,3]. The key ingredient in the present results is the observation that dilution of the main ion species (deuterium) by impurity ion species of moderate charge state ($Z_i \approx 8$) results in the onset of TEM/ETG dominated turbulence. The turbulent spectrum measured with the Phase Contrast Imaging (PCI) diagnostic is in good agreement with predictions of a synthetic PCI diagnostic installed in global GYRO as long as the Doppler shift due to the measured $\mathbf{E}_r \times \mathbf{B}$ is included. However, the measured flow shear is too weak to impact the stability of TEM or ITG modes in a significant way. Experiments are underway where low- Z_i impurities are injected into C-Mod plasmas to test the impact of ion dilution.

References

- [1] L. Lin, *et al.*, Plasma Physics Contr. Fusion **51** (2009) 065006.
- [2] M. Porkolab, *et al.*, 38th EPS Conference on Plasma Phys. Strasbourg (2011).
- [3] M. Porkolab, *et al.*, Bull. Am. Phys. Soc. **56** (2011) 139.

Work supported by the US DOE.

Inter-Machine Validation Study of Neoclassical Transport Modelling in Medium-to High-Density Stellarator-Heliotron Plasmas

A. Dinklage¹, M. Yokoyama², A. Wakasa³, K. Tanaka², S. Murakami³, R. Seki²,
T. Morisaki², K. Ida², M. Yoshinuma², C. Suzuki², Y. Suzuki², H. Yamada²,
J. L. Velasco⁴, D. López-Bruna⁴, A. López-Fraguas⁴, E. Ascasíbar⁴, J. Arevalo⁴,
J. Baldzuhn¹, C. Beidler¹, Y. Feng¹, J. Geiger¹, M. Jakubowski¹, H. Maassberg¹,
Y. Turkin¹, and R. Wolf¹

¹Max-Planck-Institut für Plasmaphysik, Garching, Germany

²National Institute for Fusion Science, Toki, Japan

³Department of Nuclear Engineering, Kyoto University, Kyoto, Japan

⁴The National Fusion Laboratory, CIEMAT, Madrid, Spain

Corresponding Author: dinklage@ipp.mpg.de

Stellarator-Heliotrons (S-H) offer an alternative route to steady-state fusion reactors and one mission of the largest S-H devices is to provide a physics basis for burning S-H plasmas. The S-H devices closest to reactor conditions play key-roles: the Large Helical Device and Wendelstein 7-X (under construction). In contrast to tokamaks, 3D magnetic fields in S-H lead even in the plasma core to localized, trapped particles significantly enhancing the radial neoclassical (NC) transport for reactor-relevant conditions (long-mean-free-path (lmfp), $T_e \sim T_i$, high $nT\tau$). In order to test a recently concluded benchmarking of calculations of NC transport coefficients, this study compares experimental findings with NC predictions for medium- to high-density S-H plasmas.

The focus of this study is put on recent experiments conducted in LHD and TJ-II also involving findings from Wendelstein 7-AS. This experimental inter-machine study was to test NC transport models in the transition from medium- to high-density, lmfp S-H (3D) plasmas at high heating power. In 3D magnetic configurations, radial electric fields (E_r) must arise to satisfy the ambipolarity condition which is not intrinsically satisfied as in axisymmetric tokamaks. In the plasma core, E_r complies with predictions for LHD and W7-AS, differences are found for TJ-II operating at lower densities. Steady-state energy balance analyses were performed using the integrated transport code, TASK3D for LHD discharges, and by ASTRA in TJ-II. For W7-AS, the experimentally determined particle and energy fluxes were compared to NC fluxes with transport coefficients from DKES and found to be consistent with NC theory up to 2/3 of the minor radius under lmfp, high $nT\tau$ conditions. Cases with similar findings can be reported from LHD, but depend sensitively on the shift of the major plasma axis.

The inter-machine dataset obtained a variety of magnetic configurations will be comprehensively analyzed to assess the ranges of validity of NC transport predictions. This study is providing quantitative tests of the NC theory employed in the optimization of W7-X and to allow assessment of NC transport in the reactor-relevant regime of S-H devices. Moreover, the coupling of NC energy and particle transport is highly relevant for the discharge scenario development for large S-H devices in view of reactor operation scenarios.

The work has been done as a joint effort within the International Stellarator-Heliotron Profile Database (Coordinated Working Group) collaboration. This initiative works within the IEA Implementing Agreement for Cooperation in Development of the Stellarator-Heliotron Concept (2.10.1992).

EX-P

Tungsten Screening and Impurity Control in JET

T. Pütterich¹, R. Dux¹, M. Beurskens², V. Bobkov¹, S. Brezinsek³, J. Bucalossi⁴,
J. W. Coenen³, I. Coffey⁵, A. Czarnecka⁶, E. Joffrin⁴, K. Lawson², M. Lehnen³,
E. de la Luna⁷, J. Mailloux², S. Marsen¹, M. L. Mayoral², A. Meigs², R. Neu¹,
F. Rimini², M. Sertoli¹, M. Stamp², S. Wiesen³, and G. van Rooij⁸

¹*Max-Planck-Institut für Plasmaphysik, Garching, Germany*

²*EURATOM CCFE Fusion Assoc., Culham Science Centre, Abingdon, UK*

³*Institute of Energy- and Climate Research, Forschungszentrum Jülich, Jülich, Germany*

⁴*CEA, Assoc. EURATOM-CEA, IRFM, Saint Paul Lez Durance, France*

⁵*Queen's University Belfast, Belfast, UK*

⁶*EURATOM, Inst Plasma Physics & Laser Microfusion, Warsaw, Poland*

⁷*EURATOM CIEMAT, Madrid, Spain*

⁸*DIFFER, Nieuwegein, Netherlands*

Corresponding Author: thomas.puetterich@ipp.mpg.de

For the ITER-like wall at JET, the screening of the divertor W-source is investigated along with possibilities to influence the central metal transport. From visible spectroscopy the erosion fluxes of W are determined at the outer strike line, which intersects the horizontal, solid tungsten target tile. The W-fluxes as determined by visible spectroscopy are related to the W-content in the main plasma, which is derived from VUV spectroscopy, in order to obtain an effective W confinement time τ_W .

EX-P

The investigations have been performed in low- and high-triangularity H-mode discharges at 2.0 MA and 2.5 MA, while a deuterium fuelling gas puff has been varied from shot to shot. Both the W-erosion in the divertor and the W-screening behave beneficial for increasing gas puff, i.e., the erosion decreases and τ_W decreases. Thus, an increasing gas puff leads to a strong reduction of the W-content in all investigated H-mode plasmas. Important players for this behaviour are the divertor electron temperature, the SOL and plasma edge transport and the ELM frequency. While the absolute numbers for the W-concentrations are very low (a few 10^{-6}), impurity accumulation is observed for cases without any gas puff. This behaviour is discussed also considering the influence of other metal impurities. Independent of the radiating species, it is explored to what extent central wave heating (ICRH and LH) and impurity avoidance strategies, i.e., gas puffing and ELM-pace-making, help to avoid impurity accumulation.

Classical Confinement of Impurity Ions and NBI-born Fast Ions in the Reversed Field Pinch

J. Anderson¹, A. F. Almagri¹, K. J. Caspary¹, B. E. Chapman¹, D. Craig²,
V. I. Davydenko³, D. J. Den Hartog¹, W. Ding⁴, S. Eilerman¹, G. Fiksel^{1,5},
C. B. Forest¹, A. Ivanov³, J. J. Koliner¹, S. T. A. Kumar¹, L. Lin⁴, D. Liu¹,
V. V. Mirnov¹, M. D. Nornberg¹, S. V. Polosatkin³, J. S. Sarff¹, D. A. Spong⁶,
N. Stupishin³, and J. Waksman¹

¹ *University of Wisconsin, Madison, USA*

² *Wheaton College, Wheaton, USA*

³ *Budker Institute of Nuclear Physics, Novosibirsk, Russian Federation*

⁴ *University of California, Los Angeles, USA*

⁵ *University of Rochester Laboratory for Laser Energetics, New York, USA*

⁶ *Oak Ridge National Laboratory, Oak Ridge, USA*

Corresponding Author: jkanders@wisc.edu

Classical behavior of two types of ions (impurity and NBI-born fast bulk) has recently been observed in the MST RFP plasma. Both have positive implications, as NBI-born fast ions (with normalized Larmor radius similar to that of fusion alphas in a reactor-sized plasma) are well confined and transfer their energy to the background plasma. Classical transport of impurities in this specific collisionality regime leads to a decrease in core impurity density thereby reducing bremsstrahlung losses in the dense core plasma. The confinement time and radial transport properties of carbon impurity ions are determined by classical theory during periods of suppressed magnetic turbulence in MST. The measured density of fully stripped carbon rapidly evolves to a hollow profile due to outward convection, consistent with the temperature screening mechanism in classical transport modeling.

A confinement time is deduced from the decay of core carbon ions sourced by methane pellet injection and agrees with classical modeling. Classical behavior of NBI-born fast ions is also observed. A new 1 MW injector sources 25 kV hydrogen (and roughly 3% deuterium) atoms in the core of MST. The measured fast H distribution and time decay of beam-target neutron flux both indicate classical slowing without enhanced radial transport, even in a stochastic magnetic field. This leads to a substantial population of fast ions and has several effects on the bulk plasma including enhanced rotation, electron heating, and stabilization of the core resonant tearing mode. Beam driven instabilities in the RFP are observed for the first time, as both continuum energetic particle modes and discrete toroidal Alfvén eigenmodes are excited by inverse Landau damping.

Work supported by USDOE.

EX-P

Measurement and Simulation of Electron Thermal Transport in the MST Reversed-Field Pinch

D. Den Hartog¹, J. Reusch¹, J. Anderson¹, F. Ebrahimi^{1,2}, C. Forest^{1,2}, D. Schnack¹,
and H. Stephens^{1,2}

¹*University of Wisconsin-Madison, Madison, USA*

²*The Center for Magnetic Self-Organization in Laboratory and Astrophysical Plasmas,
Madison, USA*

Corresponding Author: djdenhar@wisc.edu

Comparison of measurements made in the MST Reversed-Field Pinch (RFP) to the results from extensive single-fluid nonlinear resistive MHD simulations provides two key observations. First, thermal diffusion from parallel streaming in a stochastic magnetic field is reduced by particle trapping in the magnetic mirror associated with the toroidal equilibrium. Second, the structure and evolution of long-wavelength temperature fluctuations measured in MST shows remarkable qualitative similarity to fluctuations appearing in a finite-pressure nonlinear MHD simulation. New high-time-resolution measurements of the evolution of the electron temperature profile $[T_e(r, t)]$ through a sawtooth event in high-current RFP discharges have been made using the recently enhanced capabilities of the multi-point, multi-pulse Thomson scattering diagnostic on MST. Thermal diffusion is calculated by performing a low resolution fit of the χ_e profile to the electron temperature data via the energy conservation equation, assuming Fourier's law $q_e = -n_e \chi_e \Delta T_e$. These measurements are then compared directly to simulations using the nonlinear, single-fluid MHD code DEBS, run at parameters matching the RFP discharges in MST. These simulations display MHD activity and sawtooth behavior similar to that seen in MST. In a zero β simulation, the measured χ_e is compared to the thermal diffusion due to parallel losses along diffusing magnetic field lines, $\nu_{\parallel} D_{\text{mag}}$, where D_{mag} is determined from the simulation by tracing magnetic field lines.

Agreement within uncertainties is only found if the reduction in thermal diffusion due to electron trapping is taken into account. In a second simulation, the pressure field was evolved self consistently assuming Ohmic heating and anisotropic thermal conduction. Although these pressure-evolved simulation results need further confirmation, the fluctuations in the simulated temperature are very similar in character and time evolution to temperature fluctuations measured in MST.

EX-P

Experimental Tests of Stiffness in the Electron and Ion Energy Transport in the DIII-D Tokamak

T. C. Luce¹, K. H. Burrell¹, J. C. DeBoo¹, J. E. Kinsey¹, A. Marinoni², C. C. Petty¹,
E. J. Doyle³, C. Holland⁴, G. R. McKee⁵, J. C. Rost², S. P. Smith¹, P. B. Snyder¹,
W. M. Solomon⁶, G. M. Staebler¹, A. E. White², Z. Yan⁵, and L. Zeng³

¹*General Atomics, San Diego, USA*

²*Massachusetts Institute of Technology, Cambridge, USA*

³*University of California Los Angeles, Los Angeles, USA*

⁴*University of California San Diego, La Jolla, USA*

⁵*University of Wisconsin-Madison, Madison, USA*

⁶*Princeton Plasma Physics Laboratory, Princeton, USA*

Corresponding Author: luce@fusion.gat.com

Drift wave theories (ion or electron temperature gradient modes) have an onset threshold in gradient beyond which the flux transported is predicted to increase very rapidly. For fixed boundary condition, this type of behavior would manifest itself as a strong resistance to change in the temperature profiles or “stiffness”. A new series of experiments exploiting the unique tools available in the DIII-D tokamak have explored this concept of stiffness in the electron channel in L-mode plasmas and in the ion channel in H-mode plasmas, specifically as a function of applied torque. In L mode, the electron temperature scale length in a narrow region was varied by a factor of 4 by changing the deposition location of the electron cyclotron heating (ECH) and changing the electron heat flux by a factor of 10. The response of the temperature profile is not dependent on the applied torque, as seen by self-similar response of the profile with balanced, co-current, and counter-current injection of neutral beams (NBI). One ECH source was also modulated to probe the flux/gradient relationship dynamically. The response is consistent with a threshold in gradient or scale length at quite low values, which is exceeded for virtually all cases with auxiliary heating in DIII-D. A similar tool for variation of the ion heat deposition is not available in DIII-D. However, the majority of the NBI heating power is deposited in the ions, so the response of the ion temperature profile to a power scan in H mode with low and high torque was obtained. The ion temperature scale length increases significantly with heating power at a normalized radius of 0.4 for both low and high torque. The change in the ion temperature scale length decreases strongly at increasing radius. The scale length is virtually constant at low torque input at a normalized radius of 0.7. This dependence on applied torque is in contrast to the electron profile results in L mode, which show little correlation with the applied torque.

Work supported by the US DOE under DE-FC02-04ER54698, DE-FG02-04ER54762, DE-FG02-08ER54984, DE-FG02-07ER54917, DE-FG02-89ER53296, DE-FG02-08ER54999, DE-AC02-09-CH11466, and DE-FC02-99ER54512.

EX-P

Measurement of Deuterium Ion Toroidal Rotation and Comparison to Neoclassical Theory in the DIII-D Tokamak

B. Grierson¹, K. H. Burrell², W. W. Heidbrink³, N. A. Pablant¹, and W. M. Solomon¹

¹*Princeton Plasma Physics Laboratory, Princeton, USA*

²*General Atomics, San Diego, USA*

³*University of California-Irvine, Irvine, USA*

Corresponding Author: bgrierson@pppl.gov

Recent experimental comparisons of the bulk deuterium ion toroidal rotation to neoclassical theory have revealed a significant discrepancy with neoclassically predicted bulk ion toroidal rotation. Performance of ITER plasmas will depend strongly on the level of main-ion toroidal rotation achieved due to the beneficial effects of rotation for stabilization of MHD as well as the toroidal rotation contribution to the radial electric field and associated $\mathbf{E} \times \mathbf{B}$ shear stabilization of turbulence. Recent measurements of the main-ion toroidal rotation in deuterium plasmas have been made through new spectroscopic capabilities and integrated modeling.

Neoclassically the main-ion species is generally predicted to rotate faster in the co-current direction than impurity ions. However, recent measurements of carbon and deuterium ion toroidal rotation in ECH dominated H-mode conditions have revealed that the main-ions rotate slower than carbon in the co-current direction, opposite to the neoclassical predictions, and similar to previous measurements in helium plasmas. The discrepancy lies in the neoclassical prediction of the main-ion poloidal rotation. We compute the main-ion poloidal rotation from our direct measurements and find that the deuterium ion poloidal flow velocity is significantly larger than neoclassical theory from NCLASS predicts. In low toroidal rotation ITER scenarios the performance will depend on the E_r shear stabilization of turbulence through toroidal rotation, poloidal rotation and pressure gradient contributions to the total radial electric field. The modeling of ITER performance displays a strong dependence on the predicted levels of toroidal rotation obtained by fixing the ratio of $\chi_\psi \chi_i$, however this ratio is poorly understood, and our current experimental databases of this scaling are based on measurements of impurity ions. As toroidal rotation approaches zero, E_r will be dominated by the pressure and poloidal rotation contributions; hence an accurate determination of the poloidal flow is required in plasmas with low toroidal rotation.

This work supported in part by the U.S. Department of Energy under DE-AC02-09CH11466, DE-FC02-04ER54698 and SC-G903402.

Observation of ELM-Free H-Mode in the HL-2A Tokamak

W. Zhong¹, X. Zou², X. Duan¹, X. Ding¹, J. Dong¹, W. Xiao^{1,3}, Z. Shi¹, X. Song¹,
F. Xia¹, X. Huang¹, Y. Dong¹, Z. Liu¹, X. Ji¹, J. Cheng¹, Y. Zhou¹, W. Chen^{1,4},
D. Yu¹, X. Han¹, Z. Cui¹, Y. Zhang¹, Y. Xu¹, J. Li¹, G. Lei¹, J. Cao¹, J. Rao¹,
J. Zhou¹, M. Huang¹, Y. Huang¹, L. Chen¹, Y. Liu¹, L. Yan¹, Q. Yang¹, and Y. Liu¹

¹*Southwestern Institute of Physics, Chengdu, China*

²*CEA, IRFM, Saint-Paul-lez-Durance, France*

³*WCI Center for Fusion Theory, National Fusion Research Institute, Daejeon, Republic of Korea*

⁴*National Institute for Fusion Science, Toki, Japan*

Corresponding Author: zhongwl@swip.ac.cn

For the first time, a high performance ELM-free H-mode was observed in the HL-2A tokamak. It was realized with Electron Cyclotron Resonance Heating (ECRH) and co-current Neutral Beam Injection (NBI) heating. The $H_{98}(y, 2)$ factor increased by about 40 – 50% compared with the one before the transition. This regime is triggered by a minor disruption via the edge current change, where the temperature profile undergoes a sudden contraction. The mechanism leading to this regime is investigated.

During the ELM-free phase, the edge particle transport barrier is formed with peaked central density, and the edge turbulence is significantly reduced. An EHO mode has been identified in the ELM-free H-mode plasmas. It propagates poloidally in the direction of the electron diamagnetic drift velocity and toroidally in the direction of the plasma current and NBI. The edge particle transport is enhanced with EHO which locates near the q_{95} surface. Interesting, the EHO/ELM transition during the plasma current ramp phase has been observed with a transient phase where the EHO and grassy ELM coexist. And each burst of the grassy ELM tends to stabilize the EHO. Thus the amplitude of the EHO becomes more fluctuant in the case of mixture of EHO and grassy ELM. During this phase, the EHO amplitude is decreasing and then it is completely disappeared, and ELMs appear with increasing density. It is likely that these transitions are governed by the edge current profile and the pedestal gradient.

EX-P

Enhancement of Edge Impurity Transport with ECRH in HL-2A Tokamak

Z. Cui¹, H. Zhou¹, Y. Gao¹, Y. Xu¹, P. Sun¹, X. Huang¹, Z. Shi¹, J. Cheng¹, Y. Li¹, B. Feng¹, L. Yan¹, Q. Yang¹, X. Duan¹, M. Kobayashi², X. Ding¹, and S. Morita²

¹*Southwestern Institute of Physics, Chengdu, China*

²*National Institute for Fusion Science, Toki, Japan*

Corresponding Author: cuizy@swip.ac.cn

In next-generation fusion devices reduction of impurity concentration is of great importance for mitigating the radiation losses and the fusion fuel dilution to achieve a high confinement and high density plasma with a high radiation loss fraction at the edge for divertor compatibility. In HL-2A tokamak electron cyclotron resonance heating (ECRH) has been extensively carried out for the particle and impurity transport studies.

The flattening of impurity density profile is frequently observed during the ECRH phase, while the interaction of plasma facing components with edge plasma and nonthermal electrons usually becomes stronger during ECRH phase. Radial profiles of impurity ions have been observed with a space-resolved vacuum ultra-violet (VUV) spectrometer recently developed in HL-2A, of which the intensity is absolutely calibrated using bremsstrahlung continuum. The impurity transport has been studied with this spectrometer in both edge and core plasmas for the ohmic discharges with ECRH using carbon emissions of CIII to CV.

A quick decrease against the electron density in the ratio of CV to CIV with ECRH is observed, but a gradual decrease of the ratio is obtained in Ohmic plasmas. The dependence of CV/CIV on n_e in Ohmic plasmas can be explained by the change in the edge density where the CIV is located. However, the quick decrease of CV/CIV with ECRH is caused by a change of the transport of C⁴⁺ ions in the core plasma.

The effect of electron temperature on CV emission is small. Based on the analysis of the radial profile of CV with a 1D impurity transport code an outward flux to carbon ions in the ECRH plasma and an inward flux in the Ohmic plasmas have been obtained in the core plasma. In the SOL region, the C²⁺ ions are moved upstream because the increased ion temperature gradient along magnetic field transfers impurity ions upstream, while the density gradient along the magnetic field transfers them downstream. The carbon transport in the SOL is enhanced for both the Ohmic and ECRH plasmas and radiation loss from carbon ions is increased in the SOL. The effect of impurity screening is reduced.

The results indicate that ECRH puts out the impurity from the core plasma and enhances the radiation in the edge plasma, suggesting a favorable condition to next-generation fusion devices.

Dynamical Coupling Between Gradients and Transport in Tokamaks and Stellarators

C. Hidalgo¹, C. Silva², B. Carreras³, B. van Milligen¹, H. Figueiredo², L. García⁴,
M. A. Pedrosa¹, B. Gonçalves¹, and A. Alonso¹

¹*CIEMAT, Madrid, Spain*

²*EURATOM-IST, Lisbon, Portugal*

³*Alaska University, Fairbanks, USA*

⁴*Universidad Carlos III, Madrid, Spain*

Corresponding Author: carlos.hidalgo@ciemat.es

Understanding the relation between free energy sources and transport is a fundamental issue in systems far from thermal equilibrium that has been debated for years. Instabilities governed by a gradient will typically produce transport events at all scales connecting different regions of plasma. In the case of a critical gradient mechanism, the functional dependence between the transport flux and the gradient is expected to show a sharp increase as the system crosses the instability threshold and finite background transport below the threshold, implying a non-linear relation between gradients and turbulent transport [1]. It is well known that edge turbulent transport is strongly bursty and that a significant part is caused by few large transport events [2]; this is possibly reflecting the fact that systems out of thermal equilibrium are dynamically exploring different accessible states.

In this paper, the dynamical coupling between gradients and transport has been investigated in the plasma boundary of different tokamak (JET, ISTTOK) and stellarator (TJ-II) devices, showing that the size of turbulent events is minimum in the proximity of the most probable gradient. The local system relaxes to the most probable state in a time comparable to the auto-correlation time of turbulence.

Experimental results were found to be consistent with results from two very different models [3,4] of plasma turbulence and transport, where non-local effects play an important role. These non-local effects are resulting from a series of feedback mechanisms at different radial locations where at a given point in the plasma the local gradients drive the turbulence and turbulence controls the transport.

These observations [5] provide a guideline for further developments in plasma diagnostics, transport modelling and data processing to characterize transport and gradients in terms of joint probability distribution functions.

References

- [1] F. Ryter *et al.*, Phys. Rev. Lett. **86** (2001) 2325.
- [2] M. Endler *et al.*, Nuclear Fusion **35** (1995) 1307.
- [3] L. Garcia *et al.*, Phys. Plasmas **9** (2002) 841.
- [4] L. Garcia *et al.*, Phys. Plasmas **8** (2001) 4111.
- [5] C. Hidalgo *et al.*, Phys. Rev. Lett **108** (2012) 065001.

Quantitative Comparison of Experimental and Gyrokinetic Simulated ICRH and I_p Dependent Impurity Transport

N. Howard¹, M. Greenwald¹, D. Mikkelsen², A. White¹, D. Ernst¹, M. Reinke¹,
Y. Podpaly¹, and J. Candy³

¹*MIT Plasma Science and Fusion Center, Cambridge, USA*

²*Princeton Plasma Physics Lab, Princeton, USA*

³*General Atomics, San Diego, USA*

Corresponding Author: ntoward@psfc.mit.edu

For the first time, quantitative comparison of nonlinear gyrokinetic simulation and experiment is found to demonstrate simultaneous agreement in the ion heat and impurity transport channels. Linear and nonlinear simulation was used to interpret changes in measured transport as changes in turbulence drive and suppression terms.

Extensive sensitivity analysis of the GYRO predicted impurity transport to uncertainty in experimental measurement was performed to assess quantitative agreement or disagreement between simulation and experiment. The modification of measured and gyrokinetic simulated impurity transport in response to changes in plasma current (I_p) and Ion Cyclotron Resonance Heating (ICRH) were also studied for the first time in the core of Alcator C-Mod. Utilization of a novel multi-pulse laser blow-off system coupled with the unique measurements provided by a high resolution x-ray crystal spectrometer allows for precise characterization of the spatial and temporal behavior of the full, time-evolving profile of the He-like calcium charge state. Changes in the experimental impurity transport coefficients have been determined during scans of ICRH (1.0-3.3 MW) and $I_p = 0.6 - 1.2$ MA using a synthetic diagnostic developed around the impurity transport code STRAHL.

At fixed values of a/L_{Te} , a/L_n , and \hat{s} , increasing ICRH input power is observed to reduce the drive for Ion Temperature Gradient (ITG) turbulence. Linear stability analysis performed using the gyrokinetic code GYRO suggests that the character of the core plasma turbulence transitions from ITG to Trapped Electron Mode (TEM) dominated during the power scan.

Measured changes in the experimental transport coefficients with input power have been compared with qualitative predictions of quasi-linear theory. During the I_p scan, significant modification of the measured impurity confinement time and the parameters a/L_n and \hat{s} is observed. Analysis using high fidelity, global ($0.29 < r/a < 0.62$), nonlinear GYRO simulations predict a decrease in the inward impurity pinch and diffusion with increasing plasma current which is both quantitatively and qualitatively consistent with experimental observations. Physical interpretation of I_p and ICRH driven changes in turbulent impurity transport as well as critical comparison of code predictions with measured transport will be presented.

Observation of Electron Energy Pinch in HT-7 ICRF Heated Plasmas

S. Ding¹, B. Wan¹, X. Zhang¹, J. Qian¹, Z. Liu¹, and Y. Duan¹

¹*Institute of Plasma Physics, Chinese Academy of Sciences, Hefei, China*

Corresponding Author: archangel@ipp.ac.cn

Inward energy pinch in electron channel is observed in HT-7 superconducting tokamak using off-axis ion cyclotron resonance frequency (ICRF) heating. The experimental results and power balance transport analysis by TRANSP code are presented in this article. With the aids of GLF23 transport model, which predicts energy diffusivity in experimental condition, the estimation of electron pinch velocity is obtained by experimental data and is reasonably similar to the results in previous study, such as Song in Tore Supra. The parametric dependence of pinch velocity and the benchmarks between HT-7 experiment and existent theories will be performed soon.

Survey of Density Modulation Experiments on the HT-7 Tokamak

X. Gao¹, Y. Jie¹, H. Liu¹, K. Tanaka², W. Liao¹, J. Shen¹, Z. Liu¹, L. Zeng¹, X. Han¹,
and Y. Yang¹

¹*Institute of Plasma Physics, Chinese Academy of Sciences, Hefei, China*

²*National Institute for Fusion Science, Toki, Japan*

Corresponding Author: xgao@ipp.ac.cn

The particle diffusion coefficient and the convection velocity have been studied by means of the density modulation using pulsed deuterium gas puffing on the HT-7 tokamak. It was observed in AC plasmas that the particle transport coefficient and confinement time of the positive current plasma is different from that of the negative current plasma [1] on HT-7 tokamak. New experimental result improved our understanding in AC plasma operation on HT-7 tokamak. It was found that the particle confinement time becomes much higher when the directions of plasma current and toroidal field are uniform. Recently, the density modulation experiments are carried out with advanced liquid lithium limiter on HT-7 tokamak. The interesting results are compared and discussed in detail with previous results under the graphite limiter on HT-7 tokamak.

References

- [1] Gao X. *et al.* Nucl. Fusion **48** (2008) 035009.

Particle Transport Results from Collisionality Scans and Perturbative Experiments on DIII-D

E. J. Doyle¹, L. Zeng¹, T. E. Evans², G. R. McKee³, S. Mordijck⁴, R. A. Moyer⁵,
W. A. Peebles¹, C. C. Petty², T. L. Rhodes¹, and G. M. Staebler²

¹University of California-Los Angeles, Los Angeles, USA

²General Atomics, San Diego, USA

³University of Wisconsin-Madison, Madison, USA

⁴College of William and Mary, Williamsburg, USA

⁵University of California San Diego, La Jolla, USA

Corresponding Author: edoyle@ucla.edu

Recent GYRO simulations predict that particle flux, as a function purely of collisionality, should show a strong increase at low collisionality, but with little change above a critical value, $\nu^* \sim 0.01$. In an L-mode experiment in which collisionality was varied from $\nu^* \sim 0.01$ to 0.05, little change was observed in the density profile, profile peaking, measured D , V , (obtained using perturbative techniques), or measured fluctuation levels, in agreement with the GYRO predictions made prior to the experiment. This experiment was performed using similarity techniques to vary the collisionality; i.e., the magnetic field B_T was changed from 2.1 to 1.65 T, and heating power was also varied, while matching key dimensionless parameters such as relative gyroradius, β and safety factor. TGLF and GYRO simulations of the actual experimental discharges are underway.

In a second set of experiments, perturbative transport techniques using oscillating gas puffs were utilized to measure D and V in multiple operating regimes, including conventional ELMing H mode, ELM-suppressed operation obtained using resonant magnetic perturbations (RMPs), QH-mode, and L-mode. These experiments provide the first direct measurement confirming an increase in D and decrease in V with RMP application. One important feature of the measurements is that the changes in D and V with RMP application extend deep into the plasma core, past the edge region where the applied RMP fields are expected to directly impact the magnetic field topology. In the plasma core, clear increases in plasma turbulence levels are observed, consistent with TGLF modeling, while $\mathbf{E} \times \mathbf{B}$ shear decreases to a level below the linear growth rate.

This work was supported in part by the US Department of Energy under DE-FG02-08ER54984, DE-FC02-04ER54698, DE-FG02-89ER53296, DE-FG02-08ER54999, DE-FG02-05ER54809 and DE-FG02-07ER54917.

EX-P

Transition of Poloidal Viscosity by Electrode Biasing in the Large Helical Device

S. Kitajima¹, H. Takahashi², K. Ishii¹, Y. Sato¹, M. Kanno¹, J. Tachibana¹,
A. Okamoto¹, M. Sasao¹, S. Inagaki³, M. Takayama⁴, S. Masuzaki², M. Shoji²,
N. Ashikawa², M. Tokitani², M. Yokoyama², Y. Suzuki², S. Satake², T. Ido²,
A. Shimizu², Y. Nagayama², T. Tokuzawa², K. Nishimura², and T. Morisaki²

¹*Department of Quantum Science and Energy Engineering, Tohoku University, Sendai, Japan*

²*National Institute for Fusion Science, Toki, Japan*

³*Kyushu University, Hakozaki, Fukuoka, Japan*

⁴*Akita Prefectural University, Honjo, Akita, Japan*

Corresponding Author: sumio.kitajima@qse.tohoku.ac.jp

The transitions to the improved confinement mode, which were accompanied with bifurcation phenomena characterized by a negative resistance, were clearly observed in various magnetic configurations on the Large Helical Device (LHD) by the electrode biasing. The configuration dependence of the transition condition and the radial resistivity qualitatively agreed with neo-classical theories.

The effects of the ion viscosity maximum on the transition to an improved confinement mode were experimentally investigated by the externally controlled $\mathbf{J} \times \mathbf{B}$ driving force for a poloidal rotation using the hot cathode biasing in Tohoku University Heliac (TU-Heliac) [1, 2]. Here, J and B are a biasing electrode current and a magnetic field. In steady state the $\mathbf{J} \times \mathbf{B}$ driving force balances with the ion viscous damping force and the friction to neutral particles. Then the local maximum in ion viscosity can be evaluated experimentally from the external driving force at the transition. The remaining problems in the biasing experiments on TU-Heliac were:

1. To spread a ripple component in magnetic configuration.
2. To improve a target plasma to a high-performance region.

In LHD the effective helical ripple and viscosity maxima have wider region than those in TU-Heliac. The relation between a poloidal Mach number and ion viscosities in LHD predicted by the neoclassical theory [3] shows that viscosity maxima change drastically depending on the position of the magnetic axis that mainly changes the effective helical ripple. LHD can produce higher temperature plasmas at higher field than the plasma in TU-Heliac. We tried the biasing experiment in LHD, and reported the first observation of transition phenomena [4]. In this paper we report the difference of the transition condition in three configurations by the electrode biasing experiments in LHD and the radial electric field and the viscosity estimated from the neoclassical transport code FORTEC-3D [5] for a non-axisymmetric system.

References

- [1] H. Takahashi *et al.*, Plasma Phys. Control. Fusion **48** (2006) 39.
- [2] S. Kitajima *et al.*, Nucl. Fusion **46** (2006) 200.
- [3] K. C. Shaing: Phys. Rev. Lett. **76** (1996) 4364.
- [4] S. Kitajima *et al.*, Nucl. Fusion **51** (2011) 083029.
- [5] S. Satake *et al.*, PPCF, **53** (2011) 054018.

Production of Internal Transport Barriers by Intrinsic Flow Drive in Alcator C-Mod

C. Fiore¹, D. R. Ernst¹, Y. Podpaly¹, D. Mikkelsen², N. T. Howard¹, J. Lee¹,
M. L. Reinke¹, J. E. Rice³, J. W. Hughes¹, Y. Ma¹, W. L. Rowan³, and
I. Bespamyatnov³

¹*Massachusetts Institute of Technology, Cambridge, USA*

²*Princeton Plasma Physics Laboratory, Princeton, USA*

³*IFS, University of Texas, Austin, USA*

Corresponding Author: fiore@psfc.mit.edu

New results suggest that changes observed in the intrinsic toroidal rotation influence the internal transport barrier (ITB) formation in the Alcator C-Mod tokamak. Detailed plasma rotation and ion temperature profile measurements are combined with linear and non-linear gyrokinetic simulation to examine the effects of the self-generated rotational shear on the transport changes that occur in C-Mod ITB plasmas. These arise when the resonance for ICRF minority heating is positioned off-axis at or outside of the plasma half-radius.

These ITBs form in a reactor relevant regime, without particle or momentum injection, with $T_i \approx T_e$, and with monotonic q profiles ($q_{\min} < 1$). C-Mod H-mode plasmas exhibit strong intrinsic co-current rotation that increases with increasing stored energy without external drive. When the resonance position is moved off-axis, the rotation decreases in the center of the plasma resulting in a radial toroidal rotation profile with a central well which deepens and moves farther off-axis when the ICRF resonance location reaches the plasma half-radius. This profile results in strong $\mathbf{E} \times \mathbf{B}$ shear ($> 1.5 \times 10^5$ Rad/s) in the region where the ITB foot is observed.

Gyrokinetic analyses indicate that this spontaneous shearing rate is comparable to the linear ion temperature gradient (ITG) growth rate at the ITB location and is sufficient to reduce the turbulent particle and energy transport. The newly available detailed measurement of the ion temperature demonstrates that the radial profile flattens as the ICRF resonance position moves off axis, decreasing the drive for ITG the instability as well. These results are the first evidence that intrinsic rotation can affect confinement in ITB plasmas, and suggest that this regime could be achievable in ITER and in future reactor experiments.

EX-P

Experiments on GOL-3 Multiple Mirror Trap for Fusion Program

A. Burdakov¹, A. P. Avrorov¹, and A. Arzhannikov²

¹*Budker Institute of Nuclear Physics, Novosibirsk, Russian Federation*

²*Novosibirsk State University, Novosibirsk, Russian Federation*

Corresponding Author: a.v.burdakov@inp.nsk.su

The GOL-3 Multiple Mirror Trap is an 11 m-long solenoid with axially-periodical (corrugated) magnetic field. In the basic operation regime the solenoid consists of 52 magnetic corrugation cells with $B_{\max}/B_{\min} = 4.8/3.2$ T. Deuterium plasma of $10^{20} - 10^{22} \text{ m}^{-3}$ density is heated up to ~ 2 keV ion temperatures (at $\sim 10^{21} \text{ m}^{-3}$ density and confinement time ~ 1 ms) by a high power relativistic electron beam. Main conclusion from data is that plasma heating and confinement in the multiple mirror traps are of essentially turbulent nature.

In general, achieved plasma parameters support our vision of a multiple mirror trap as the alternative path to a fusion reactor with $\beta \sim 1$ and $10^{21} - 10^{22} \text{ m}^{-3}$ plasma density. Project of a new linear trap with multiple mirror plugs is in progress in Novosibirsk BINP. Several new experiments in support of the fusion program based on linear machines are presented.

An intense electron beam source of a new type, based on a gaseous arc plasma emitter, was developed and first experiments with this beam are carried out; the new data on plasma rotation and electromagnetic radiation in the GOL-3 will be presented.

EX-P

Comparison of Plasma Flows and Currents in HSX to Neoclassical Theory

D. T. Anderson¹, A. R. Briesemeister¹, J. C. Schmitt², F. S. B. Anderson¹,
K. M. Likin¹, J. N. Talmadge¹, G. M. Weir¹, and K. Zhai¹

¹*HSX Plasma Laboratory, University of Wisconsin-Madison, Madison, USA*

²*Princeton Plasma Physics Laboratory, Princeton, USA*

Corresponding Author: dtanders@wisc.edu

The Helically Symmetric Experiment (HSX) was designed to have an axis of symmetry in the helical direction, reduced neoclassical transport and small equilibrium currents due to the high effective transform. Unlike other stellarators in which $\|B\|$ varies in all directions on a flux surface, plasmas in HSX are free to rotate in the direction of quasihelical symmetry. In this paper we will present measurements with Charge Exchange Recombination Spectroscopy (CXRS) that demonstrate for the first time that intrinsic plasma flows with a velocity up to 20 km/s are predominantly in the direction of symmetry. Whereas previous neoclassical calculations did not conserve momentum, we show that the experimental results agree better with recent modifications to neoclassical theory that do conserve momentum. Also, we present for the first time a 3D equilibrium reconstruction of the plasma pressure and current profile based on a set of magnetic flux loops. Early in time, the magnetic signals indicate that, because of the absence of toroidal curvature, a helical Pfirsch-Schlüter current develops. Later in time, the bootstrap current evolves over a time scale longer than the plasma discharge and is modeled using a 3D suseptance matrix method. The reconstructed pressure profile agrees well with the experimental measurements. The reconstructed current profile agrees well with the neoclassical calculations of the bootstrap current including momentum conservation. However, a wide range of current profiles also show reasonable agreement with the data, indicating that the measured edge magnetic signals are not that sensitive to the small bootstrap current, especially in the plasma core and additional constraints are needed for core current profile reconstruction.

EX-P

Scalings of Spontaneous Rotation in the JET Tokamak

M. F. Nave¹, L. G. Eriksson², C. Giroud³, J. S. de Grassie⁴, T. Hellsten⁵, T. Johnson⁵,
K. Kirov³, Y. Lin⁶, J. Mailloux³, P. Mantica¹¹, M. L. Mayoral³, F. I. Parra⁶,
J. Ongena⁷, T. Tala⁸, A. Salmi⁸, J. H. F. Severo⁹, and P. de Vries¹⁰

¹*Instituto de Plasmas e Fusão Nuclear, Instituto Superior Técnico, Lisbon, Portugal*

²*European Commission, Research Directorate General, Brussels, Belgium*

³*CCFE/Euratom Fusion Association, Abingdon, UK*

⁴*General Atomics, San Diego, USA*

⁵*Association EURATOM - VR, Fusion Plasma Physics, EES, KTH, Stockholm, Sweden*

⁶*Plasma Science and Fusion Center, Massachusetts Institute of Technology, Cambridge, USA*

⁷*ERM-KMS, Association EURATOM-Belgian State, Brussels, Belgium*

⁸*Association Euratom-Tekes, VTT, Finland*

⁹*Institute of Physics, University of Sao Paulo, Sao Paulo, Brazil*

¹⁰*FOM Institute DIFFER, Association EURATOM-FOM, Netherlands*

¹¹*Instituto di Fisica del Plasma, CNR-EURATOM, Milano, Italy*

Corresponding Author: mfn@ipfn.ist.utl.pt

Intrinsic rotation levels measured in JET plasmas are generally lower than expected from scaling laws that predict that rotation increases with normalised beta. Several factors have been observed to influence intrinsic rotation, such as fast ion losses and toroidal field (TF) ripple, suggesting that different physics mechanisms are at play to drive intrinsic rotation and that these should be taken into consideration when extrapolating to future devices. TF ripple, in particular, was found to have a significant effect on the rotation of plasmas without momentum input. JET results suggest that ITER intrinsic rotation may be substantially less than what was predicted by the multi-machine rotation scaling of Ref. [1].

The JET intrinsic rotation database includes plasmas with Ohmic heating, ion-cyclotron radio-frequency (ICRF) heating (in two scenarios: minority heating and mode conversion) and, lower hybrid current drive. Typical C6 toroidal velocities are less than 30 km/s. JET data from ELMy H-modes not previously included in a multi-machine database were compared with a scaling for the Alfvén-Mach number, and a scaling for the velocity change from L-mode into H-mode [1]. These two scalings do not reproduce well the JET data, where rotation can be lower for the same beta normalized. At JET no significant difference between H-mode and L-mode rotation is observed. In either L-mode or in H-mode, core counter-rotation is a common observation in JET plasmas. Velocity profiles often change sign from co-rotation in the edge to counter-rotation in the core. Factors clearly influencing the direction of rotation are heating details, such as ICRF resonance position, plasma current and MHD activity. In view of models of turbulent momentum transport that predict that changes in rotation might be correlated to gradients of bulk plasma parameters, the possible correlation of JET core rotation with electron and ion temperatures and plasma density has been investigated. The effect of TF ripple on intrinsic rotation was studied by varying the ripple from 0.08% to 1.5% in Ohmic and in ICRF heated plasmas. In both cases ripple causes counter rotation, indicating a strong torque due to non-ambipolar transport of thermal ions and in the case of ICRF also fast ions. At ITER relevant ripple levels of 0.5% JET plasmas were hardly rotating.

References

[1] J. Rice *et al.*, Nucl. Fusion **47** (2007) 1618.

Toroidal Rotation Characteristics in KSTAR Plasmas

S. G. Lee¹, Y. Shi¹, Y. S. Na², L. Terzolo¹, J. W. Yoo¹, Y. S. Kim¹, W. H. Ko¹,
J. M. Kwon¹, H. H. Lee¹, Y. K. Oh¹, J. G. Kwak¹, M. Bitter³, and K. Hill³

¹*National Fusion Research Institute, Daejeon, Republic of Korea*

²*Dep. of Energy System Engineering, Seoul National University, Seoul, Republic of Korea*

³*Princeton Plasma Physics Laboratory, Princeton, USA*

Corresponding Author: slee@nfri.re.kr

Investigation of the toroidal rotation is one of the most important topics for the magnetically confined fusion plasma researches since it is essential for the stabilization of resistive wall modes (RWMs) and its shear plays an important role to improve plasma confinement by suppressing turbulent transport. Impurity toroidal rotation has been observed in the core region of KSTAR plasmas from the Doppler shift of helium-like argon x-ray lines with various plasma discharges including pure ohmic heating, electron cyclotron resonance heating (ECRH), and neutral beam injection (NBI). The direction of the impurity rotation in the KSTAR ohmic plasma discharges is the same as that of the electrons, opposite to the plasma current, and the magnitude of the core toroidal rotation velocity is consistent with that of the ECEI measurement. In NBI heated plasmas, the toroidal rotation, V_ϕ , is co-current direction and the speed is increased up to 200 km/s. The core toroidal rotation velocity directly changed when large type-I edge localized modes occurred in the H-mode discharge. This paper will describe the experimental results of impurity toroidal rotation characteristics with ohmic plasmas as well as plasmas with ECRH, and NBI heating in KSTAR plasmas.

EX-P

Modeling Fusion Data in Probabilistic Metric Spaces for the Identification of Confinement Regimes and Scaling Laws

G. Verdoolaege¹, G. Van Oost¹

¹ *Ghent University, Ghent, Belgium*

Corresponding Author: geert.verdoolaege@ugent.be

Any measurement is in essence a sample from a latent probability distribution. Hence, measurement uncertainty is an intrinsic property, rather than a side-effect, of the measurement process, and it should be taken advantage of. In this contribution we show that an inherent probabilistic description of fusion confinement data drastically improves the capability to discriminate between confinement regimes and considerably reduces the prediction error for scaling laws for the energy confinement time. We model measurements of physical variables from the International Global H-Mode Confinement Database by independent Gaussian probability density functions (PDFs) using information on the respective error bars. In the framework of information geometry a family of PDFs forms a Riemannian manifold with the Fisher information serving as the metric tensor. We map the confinement data on a probabilistic Gaussian product manifold and we use the geodesic distance (GD) as a natural similarity measure between the PDFs. Via multidimensional scaling (MDS) we next carry out a projection of the confinement data into a lower-dimensional Euclidean space. The projection respects the distance geometry on the original manifold, hence allowing a faithful visualization of the confinement data. Cluster structure can be observed in the data corresponding to confinement regimes. This is confirmed in a k -nearest neighbor classification task, yielding an excellent discrimination capability between confinement regimes. In comparison, the Euclidean distance, which neglects the inherent probabilistic structure of the data, performs significantly worse with respect to visualization and classification.

Our observation that information on the measurement uncertainties is most valuable for the classification task, is the starting point for a regression analysis using data projected via MDS into a Euclidean space. We show that, compared to the Euclidean distance, using the GD in the original space leads to significantly reduced discrepancies between the predicted and experimental energy confinement time. This inherent probabilistic derivation of scaling laws will be further explored in future work.

Study of Carbon and Lithium Neoclassical Impurity Transport in ELM-Free H-Mode Discharges in NSTX

F. Scotti¹, V. A. Soukhanovskii², S. Kaye¹, S. Gerhardt¹, R. Andre¹,
W. Guttenfelder¹, R. E. Bell¹, B. P. LeBlanc¹, and R. Kaita¹

¹*Princeton Plasma Physics Laboratory, Princeton, USA*

²*Lawrence Livermore National Laboratory, Livermore, USA*

Corresponding Author: fscotti@pppl.gov

Intrinsic impurity (carbon and lithium) neoclassical transport is analyzed for H-mode discharges in the National Spherical Torus eXperiment (NSTX). The application of lithium coatings on boronized graphite plasma facing components led to high performance H-mode discharges with edge localized modes (ELMs) suppression but affected by core carbon accumulation (core inventory increased by up to 3–4×). Lithium ions instead, did not accumulate and had densities (n_{Li}) only up to 1% of carbon densities (n_{C}) [1]. Carbon influxes from main wall and divertor did not increase, indicating an increase in core impurity confinement. Core transport codes TRANSP, NCLASS and MIST are used to assess the impact of lithium conditioning on impurity transport. In NSTX H-mode discharges, ion particle transport is close to neoclassical due to the suppression of anomalous ion transport [2]. Changes in neoclassical transport due to modifications in main ion temperature (T_D) and density (n_D) profiles, together with the disappearance of ELMs, can explain the core carbon accumulation. The reduction in edge carbon collisionality leads to reduced carbon diffusivities ($D_{\text{C}} < 1 \text{ m}^2/\text{s}$) for $\rho > 0.8$. The increase in ∇n_D results in an increase in both edge and core inward convective velocity ($\nu_{\text{C}} \sim (-10) \text{ m/s}$ at $\rho \sim 0.8$) while the reduction in edge ∇T_D reduces the ν_{C} temperature screening component. These changes are consistent with the observed early formation of a hollow n_{C} profile and slower core accumulation. The enhancement in lithium particle diffusivities ($D_{\text{Li}} \sim 5 \text{ m}^2/\text{s}$ at $\rho \sim 0.8$) due to the presence of a strong impurity (carbon) can account for the low lithium core contamination. MIST code modeling shows that the high D_{Li} results in n_{Li} of the order of 1 – 10% of n_{C} (assuming the same source for the two impurities).

References

- [1] M. G. Bell, *et al.*, Plasma Phys. Control. Fusion **51** (2009) 12.
- [2] L. Delgado-Aparicio, *et al.*, Nucl. Fusion, **49** (2009) 085028.

Work supported by U.S. DOE Contract DE-AC02-09CH11466 and DE-AC52-07NA27344.

Development of Microwave Diagnostics in EAST Tokamak

B. Ling¹, Y. Liu¹, A. Ti¹, S. Zhang¹, X. Han¹, Y. Wang¹, T. Zhang¹, J. Bu¹, E. Li¹, X. Gao¹, L. Hu¹, C. Domier², N. Luhmann², P. Phillips³, H. Huang³, and G. Taylor⁴

¹*Institute of Plasma Physics, Chinese Academy of Sciences, Hefei, China*

²*University of California, Davis, USA*

³*Fusion Research Center, Austin, USA*

⁴*Princeton Plasma Physics Laboratory, Princeton, USA*

Corresponding Author: ling@ipp.ac.cn

EAST is a fully superconducting tokamak aimed at high performance plasma under steady-state condition. EAST program is moving rapidly toward exploring the physics and technologies associated with long-pulse, high-performance plasmas in superconducting tokamak. Several critical microwave diagnostics are under development for the research program of EAST.

There is a set of heterodyne radiometer containing 16 channels, covering 98.5 to 126.5 GHz frequency range installed on EAST.

In order to cover the most range of EAST plasma, a set of new ECE system including 32 channels has been developed in collaboration with UC Davis, whose frequency range is from 104 GHz to 168 GHz. A grating polychromator system, transferred from PPPL, is under commission on EAST, which can cover the whole operation range of toroidal magnetic field up to 3.5 T. In order to investigate the H-mode physics and pedestal structure on EAST, frequency modulated reflectometer is being under construction. Progress of these critical microwave diagnostics will be presented in this article. Observation on plasma instability phenomena in EAST will be elucidated.

EX-P

Pellet Induced High Density Phases during ELM Suppression in ASDEX Upgrade

P. Lang¹, C. Angioni¹, R. McDermott¹, R. Fischer¹, J. C. Fuchs¹, O. J. Kardaun¹,
B. Kurzan¹, G. Kocsis², M. Maraschek¹, A. Mlynek¹, W. Suttrop¹, T. Szepesi²,
G. Tardini¹, and H. Zohm¹

¹Max Planck Institut für Plasmaphysik, Garching, Germany

²WIGNER RCP RMKI, Budapest, Hungary

Corresponding Author: ptl@ipp.mpg.de

Magnetic perturbations (MP) with $n = 2$ have been found in ASDEX Upgrade to result in reproducible and robust ELM mitigation in a wide heating power and safety factor range. ELM mitigation is established for peripheral densities above a critical threshold. Pellets injected into mitigation phases do not trigger type-I ELM like events unlike when launched into unmitigated type-I ELMy plasmas. The absence of ELMs results in an improved pellet fuelling efficiency and persistent density build up, mostly eliminating the need for strong gas puff. No deleterious impact was found on MHD activity, plasma rotation or impurity transport. Notably, the pedestal density, temperature, pressure and rotation profiles remain virtually unchanged. Reliable and reproducible operation at line averaged densities from 0.75 up to $1.5 \times n_{Gw}$ (core densities of up to $1.6 \times n_{Gw}$) has been demonstrated using pellets, no upper density limit for the ELM-mitigated regime has been encountered so far. There is no confinement improvement in the density regime above about $n/n_{Gw} = 0.85$ as predicted by the IPB98(y,2) energy confinement scaling; at best the confinement can be kept at the initial level. A prolonged train of pellets with repetition time t_P produces an enhanced plasma particle inventory which exhibits a maximum just after the pellet arrives, and which drops with a decay time τ_P towards a minimum just before the next pellet. For $t_P > \tau_P$, an approximately linear relationship exists between the pellet flux and the time averaged plasma density. In parallel, a mild reversible plasma energy reduction takes place. This behaviour is already known from previous pellet fuelling studies performed under ELMy H-mode conditions; the achieved quasi steady-state operational boundaries can be well explained by additional pellet-driven convective losses. In the ELM suppressed regime, however, enhancing the pellet flux by reducing τ_P , below the initial value of τ_P resulted in a strong sudden density enhancement. Furthermore, no further significant energy reduction takes place. The behaviour is caused by an increasing τ_P , attributed mainly to changing transport properties. Usually, fuelling performance improvement can be gained solely by deeper pellet particle deposition, which results in a slightly enhanced pellet particle persistence time.

EX-P

Analysis of Temperature and Density Pedestal in a Multi-machine Database

P. A. Schneider¹, E. Wolfrum¹, R. Groebner², T. Osborne², M. Beurskens³,
M. Dunne⁴, S. Günter¹, B. Kurzan¹, K. Lackner¹, P. B. Snyder², and H. Zohm¹

¹*Max-Planck-Institut für Plasmaphysik, Garching, Germany*

²*General Atomics, San Diego, USA*

³*EURATOM /CCFE Fusion Association, Culham Science Centre, Abingdon, UK*

⁴*Department of Physics, University College Cork, Association Euratom-DCU, Cork, Ireland*

Corresponding Author: philip.schneider@ipp.mpg.de

A pedestal database was built using data from type-I ELMy H-modes of ASDEX Upgrade, DIII-D and JET. Edge data from high resolution diagnostics was analysed directly before an ELM crash. In this phase reproducible conditions are expected which lead to the type-I ELM crash. The pedestal is characterized in terms of pedestal top, width and gradient. These parameters are determined with the same procedure for all three machines. For the analysis a database approach was chosen where discharges from all machines were collected to cover a wide range of plasma current, magnetic field, plasma pressure and shape.

Three main topics are addressed with the database: the pedestal width of electron temperature and electron density; the pedestal top of the electron pressure; and the gradient lengths of temperature L_{Te} and density L_{ne} , including their ratio $\eta_e = L_{ne}/L_{Te}$.

The pedestal width of temperature and density scale differently in the presented database. The scalings predict that in ITER the temperature pedestal will be appreciably wider than the density pedestal. The pedestal top of the electron pressure shows a linear correlation with the pedestal pressure gradient in real space.

The gradient length ratio η_e in the pedestal was found to vary systematically from around 1 at high to over 2 for low collisionality. At low triangularity L_{Te} in the pedestal can be changed with variation of the heating power, independently of the density gradient length. For high collisionality η_e approaches unity regardless of the applied heating power.

This work was supported in part by EURATOM and carried out within the framework of the European Fusion Development Agreement. The views and opinions expressed herein do not necessarily reflect those of the European Commission. This work was supported in part by the U.S. Department of Energy under DE-FC02-04ER54698 and DE-FG02-95ER54309.

L–H Transition, Pedestal Development and I–mode Studies in the ASDEX Upgrade Tokamak

F. Ryter¹, P. Sauter¹, W. Suttrop¹, E. Viezzer¹, M. Willensdorfer², E. Wolfrum¹, M. Bernert¹, M. Burckhart¹, G. Conway¹, R. Fischer¹, S. DaGraca³, B. Kurzan¹, R. McDermott¹, S. Potzel¹, T. Pütterich¹, S. Rathgeber¹, and J. Vicente³

¹Max-Planck-Institut für Plasmaphysik, EURATOM Association, Garching, Germany

²Institute of Applied Physics, Vienna University of Technology, Vienna, Austria

³Instituto de Plasmas e Fusão Nuclear, Instituto Superior Técnico/UTL, Lisboa, Portugal

Corresponding Author: ryter@ipp.mpg.de

Investigations of the L-H transition in situations with a high power threshold, such as low density, unfavorable ion ∇B drift or application of magnetic perturbations widen the knowledge on transition and pedestal physics. At ASDEX Upgrade, such studies yield the following results.

H-modes achieved with ECRH at low density allowed to decouple the electron and ion channels. The analysis reveals the key role of the ions reflected by a constant values of the minimum radial electric field well (E_r) over a wide range of density and T_e/T_i . This also explains the increase of H-mode threshold power (P_{thr}) towards low density.

Discharges with L-H transitions induced at different densities by ECRH exhibit very different reaction of the edge electron temperature and density at the transition. While T_e almost does not respond to the L-H transition, n_e increases abruptly, reflecting a strong transport change. The density increase depends mainly on the neutral gas pressure in the divertor region prior to the L-H transition. In line with the peeling-ballooning theory, the first ELM occurs at a given value of the pedestal pressure. The H-L back-transition following the ECRH turn-off happens at the same pedestal pressure, which is also that at the L-H transition.

The magnetic perturbations (MPs) used to mitigate ELMs also influence the L-H transition. At low density, the MPs do not affect P_{thr} , while at high density P_{thr} is 2 times above its usual value. For intermediate densities, the L-H transition is followed by mitigated ELMs and requires only 20% more power than the usual P_{thr} . The first analysis of edge profiles points towards a reduction of the ion pressure gradient induced by the MPs.

The I-mode emerges gradually from L-mode as power is increased in cases with high P_{thr} . It is characterized by a pedestal in both T_e and T_i , while the density profile keeps L-mode characteristics. The pedestal development suggests a self-amplification between increasing E_r shearing and turbulence reduction. Plasmas heated by ECRH or NBI at different densities indicate that the ion channel plays a key role in this process. Overall, the formation of a temperature pedestal with increasing power seems to be universal property of divertor tokamak plasmas, generally masked by the transition to H-mode.

EX-P

The Evolution of the Edge Pedestal Structure and Turbulence Spatial Scale during the ELM Cycle on NSTX

A. Diallo¹, R. Maingi², G. J. Kramer¹, D. Smith³, T. Osborne⁴, W. Guttenfelder¹,
R. Bell¹, C. S. Chang¹, S. H. Ku¹, B. LeBlanc¹, and M. Podesta¹

¹*Princeton Plasma Physics Laboratory, Princeton, USA*

²*Oak Ridge National Laboratory, Oak Ridge, USA*

³*University of Wisconsin, Madison, USA*

⁴*General Atomics, San Diego, USA*

Corresponding Author: adiallo@pppl.gov

Characterizations of the pedestal parameter dynamics and microturbulence in the pedestal region throughout the edge localized modes (ELM) cycles are performed on the National Spherical Torus Experiment (NSTX). First, a clear buildup of the pedestal height is observed between ELMs for three different plasma currents, and this buildup tends to saturate prior to the onset of ELM at low and medium plasma current. The pedestal parameter evolutions during the ELM cycle are found to be qualitatively consistent with the peeling ballooning description of the ELM cycle. Second, using the beam emission spectroscopy systems probing the pedestal top, we report first measurements of the spatial structure of turbulence fluctuations during an ELM cycle in the pedestal region. Measurements show spatial structure $k_{\theta}\rho_i$ ranging from 0.1 to 0.2 propagating in the ion diamagnetic drift direction. These propagating spatial scales are found to have a large poloidal extent ($\sim \beta^{\text{ped}}$) and are consistent with ion-scale microturbulence of the type ion temperature gradient (ITG), ITG-trapped electron mode, and/or kinetic ballooning modes (KBM). Preliminary simulations during the last part of the ELM cycle, using XGC1 code in a fully nonlinear regime, show poloidal correlation around $9\beta^{\text{ped}}$ smaller than experimental observations. Characterization of the microturbulence in the pedestal region represents a first step in unraveling the role of microturbulence in limiting the pedestal gradient, which is critical for ITER and next-step devices.

EX-P

Observation of Current Structures at Type-III ELM Onset on EAST

N. Yan^{1,2,3}, V. Naulin^{1,2}, G. Xu³, H. Xiong³, H. Wang³, M. Jiang³, P. Liu³, L. Wang³,
S. Liu³, W. Zhang³, L. Shao³, and B. Wan³

¹*Department of Physics, Technical University of Denmark, Roskilde, Denmark*

²*Sino-Danish Center for Education and Research, Aarhus, Denmark*

³*Institute of Plasma Physics, Chinese Academy of Sciences, Hefei, China*

Corresponding Author: yann@fysik.dtu.dk

In far scrape-off layer (SOL), alternating negative and positive burst structures in ion saturation current were detected at the onset of each type-III edge localized mode (ELM) on EAST. Different from the fast streaming phenomenon reported previously, one subsequent positive burst structure appears every time in the early phase of ELM. It seems like a quick transitional stage between edge localized mode (MHD) phase and transport phase during the ELM. A pronounced sinusoidal pattern has been observed on the radial magnetic induction signal by Langmuir - magnetic probe, corresponding with almost a single peak mode on the poloidal induction signal in this transitional phase. As a local diagnostic, the floating potential arises abruptly in this phase, indicating the emergence or passage of polarized plasma structure. Further more, the ELM crash enter into another phase after this sudden burst structure. To verify the current characteristic of this structure, a mono-polar current filaments model was involved, which can reproduce same pattern commendably. Thus, current transport may dominant in transitional stage and plays an important role in the nonlinear development phase of ELM exhaustive crash. As current structure can only be observed in far SOL region of EAST, it maybe conceivable to consider the current origin from local condition rather than release from inside of the pedestal. Our observation may potentially provide support evidence for the recent theory prediction that the error field generated by scrape-off layer current can ultimately trigger the ELM through the coupling with MHD modes inside the separatrix.

EX-P

New Edge Localized Modes at Marginal Input Power with Dominant RF-heating and Lithium-wall Conditioning in EAST

H. Wang¹, G. Xu¹, H. Guo^{1,2}, B. Wan¹, V. Naulin³, S. Ding¹, N. Yan¹, W. Zhang¹,
L. Wang¹, S. Liu¹, R. Chen¹, L. Shao¹, H. Xiong¹, P. Liu¹, and M. Jiang¹

¹*Institute of Plasma Physics, Chinese Academy of Sciences, Hefei, China*

²*Tri Alpha Energy, Rancho Santa Margarita, USA*

³*Association Euratom-Riso, Roskilde, Denmark*

Corresponding Author: hqwang@ipp.ac.cn

The EAST tokamak has achieved, for the first time, the ELMy H-mode at a confinement improvement factor $H_{\text{ITER89-P}} \sim 1.7$, with dominant RF heating and active wall conditioning by lithium evaporation and real-time injection of Li powder. During the H-mode phase, a new small-ELM regime has been observed with the power threshold of the L-H transition close to the prediction by the international tokamak scaling. The small-ELM regime is manifested as sinusoidal-like oscillations on edge plasma measurements with frequencies ranging from several hundred Hz to 3 kHz, which exhibits an initial growth phase and can last over 1 s. In contrast to the usual type-III ELMy regime, both plasma density and stored energy increase almost linearly with time during the small-ELM phase. Heat fluxes at the divertor target plates during the small ELMs are much smaller than those for the type-III ELMs by one order of magnitude. Magnetic measurements show small-amplitude oscillations during the small ELMs with the poloidal mode number $m = 1$, and the toroidal mode number $n = 0$.

Detailed measurements from the reciprocating probes near the separatrix reveal that the oscillations on the floating potential and ion saturation current of small ELMs are much smaller than those of type-III ELMs. Further study of the floating potential inside the separatrix shows modulation interactions and strong three-wave coupling between the small ELMs and high-frequency-broadband (80 – 500 kHz) turbulences that emerge after the L-H transition or in the inter-ELM phase. The fluctuations of the floating potential at different toroidal, poloidal and radial locations are strongly correlated with each other, with nearly no phase differences poloidally and toroidally, but with finite phase difference radially, thus providing strong evidence for the presence of zonal flows. New observations have also been made on the type-III ELMs. Measurements from Mach probes have demonstrated a decreasing co-current rotation during type-III ELMs. These suggest that the type-III ELMs may transport substantial particles, energy and momentum out of the plasma. Each type-III ELMy crash enhances the radial electric field E_r and turbulence driven Reynolds stress. Furthermore, the filament-like structure of type-III ELMs has clearly been identified as multiple peaks on the ion saturation and floating potential measurements.

EX-P

Characterization of Temperature Fluctuations during Type-I and Type-II Edge Localized Modes at ASDEX Upgrade

I. Classen¹, J. Boom¹, A. Bogomolov¹, E. Wolfrum², M. Maraschek², W. Suttrop², P. de Vries¹, T. Donne^{1,3}, B. Tobias⁴, C. Domier⁵, N. Luhmann⁵, and H. Park⁶

¹*FOM Institute DIFFER, Nieuwegein, Netherlands*

²*Max-Planck-Institut für Plasmaphysik, Garching, Germany*

³*Eindhoven University of Technology, Eindhoven, Netherlands*

⁴*Princeton Plasma Physics Laboratory, Princeton, USA*

⁵*University of California, Davis, USA*

⁶*POSTECH, Gyeongbuk, Republic of Korea*

Corresponding Author: i.g.j.classen@diffier.nl

The application of a 2D temperature diagnostic, ECE-Imaging, at ASDEX Upgrade revealed a variety of temperature fluctuations associated with type-I and type-II edge localized modes (ELMs). The characteristics and dynamics of the various modes, and their role in the ELM cycle, are presented.

During type-I ELMs, different phases of distinct mode activity have been identified. Prior to the onset of the ELM crash, a short lived mode is observed in the pedestal region that rotates in the electron diamagnetic drift direction. The poloidal mode number, estimated around $m = 75$, is seen to increase towards the ELM crash, simultaneously with a poloidal velocity increase. This speeding up of the mode is followed by the actual ELM crash phase. As the crash develops, multiple filamentary structures are observed just outside the separatrix. Most of these filaments are observed to rotate in the electron diamagnetic drift direction, although often the first few filaments move in the opposite direction. A third type of fluctuation is often observed in between ELM crashes. This mode shows a pronounced poloidal amplitude asymmetry. On the plasma mid-plane the mode amplitude has a minimum. The occurrence of this mode tends to lengthen the ELM period, suggesting it regulates the stability of the pedestal.

In type-II ELMs (large) temperature crashes are absent and a continuous broadband fluctuation in the 20–60 kHz range is observed, flattening the T_e profile at the top of the pedestal. This mode rotates in the electron diamagnetic direction and has a poloidal mode number $m \sim 100$. As with the mode observed between type-I ELM crashes, also the time averaged 2D mode amplitude of the type-II ELM mode shows a pronounced minimum at the plasma mid-plane. The similarities between the characteristics of these two modes suggest that it is the same instability. In type-I ELMs it delays the next crash, in type-II ELMs it might be responsible for the complete absence of crash events. A more detailed investigation of this mode shows beat-wave-like behavior in both space and time, indicating that it actually consists of multiple simultaneous modes that are alternately interfering destructively and constructively.

EX-P

Reactor-relevant Quiescent H-mode Operation Using Torque from Non-axisymmetric, Non-resonant Magnetic Fields

K. H. Burrell¹, A. M. Garofalo¹, W. M. Solomon², M. E. Fenstermacher³,
T. H. Osborne¹, J. K. Park², M. J. Schaffer¹, and P. B. Snyder¹

¹General Atomics, San Diego, USA

²Princeton Plasma Physics Laboratory, Princeton, USA

³Lawrence Livermore National Laboratory, Livermore, USA

Corresponding Author: burrell@fusion.gat.com

Recent DIII-D results demonstrate that quiescent H-mode (QH-mode) sustained by magnetic torque is a promising operating mode for future burning plasmas. We have produced steady, edge localized mode (ELM)-free, QH-mode plasmas with co I_p neutral beam torque at reactor relevant levels. This was achieved by replacing the counter- I_p torque from neutral beam injection (NBI) with the torque due to neoclassical toroidal viscosity [1] produced by non-axisymmetric, non-resonant external magnetic fields. In addition, QH-mode plasmas have simultaneously demonstrated the reactor requirements of steady operation at the maximum stable pedestal pressure, ELM-free operation and rapid particle transport for helium exhaust in discharges which operate with constant density and radiated power [2]. Using $n = 3$ non-resonant magnetic fields (NRMF) from two sets of non-axisymmetric coils, recent experiments have achieved long duration QH-modes with co I_p NBI torque up to 1 – 1.3 Nm. Scaling from ITER, this co I_p torque is 3 to 4 times the NBI torque that ITER will have [1]. These experiments utilized an ITER-relevant lower single-null plasma shape and were done with ITER-relevant values of $\nu_{ped}^* \sim 0.1$ and $\beta_T^{ped} \sim 1\%$. The discharges exhibited confinement quality $H_{98}(y, 2) = 1.3$, in the range required for ITER. In preliminary experiments only using $n = 3$ fields from a coil outside the toroidal coil, QH-mode plasmas with low $q_{95} = 3.4$ have reached normalized fusion gain values of $G = \beta_N H_{89}/q_{95}^2 = 0.4$, which is the desired value for ITER. Shots with the same coil configuration also operated with net zero NBI torque. The limits on G and co I_p torque have not yet been established for this coil configuration. Peeling-ballooning stability calculations utilizing the EPED1 model predict that the H-mode edge pedestal in ITER will be in the stability region required for QH-mode operation [3].

References

- [1] A. M. Garofalo, *et al.*, Nucl. Fusion **51** (2011) 083018.
- [2] K. H. Burrell, *et al.*, Phys. Plasmas **12** (2005) 056121.
- [3] K. H. Burrell, *et al.*, Phys. Plasmas **19** (2012) to be published.

Work supported by the US Department of Energy under DE-FC02-04ER54698, DE-AC02-09ER54698 and DE-AC02-09CH11466.

Rotation Braking and Error Field Correction of the Test Blanket Module Induced Magnetic Field Error in ITER

H. Reimerdes¹, J. M. Hanson², Y. In³, M. Okabayashi⁴, N. Oyama⁵, J. K. Park⁴, A. Salmi⁶, M. J. Schaffer⁷, J. A. Snipes⁸, W. Solomon⁴, E. J. Strait⁷, and T. Tala⁶

¹*Ecole Polytechnique Fédérale de Lausanne (EPFL), CRPP, Lausanne, Switzerland*

²*Columbia University, New York, USA*

³*FAR-TECH, San Diego, USA*

⁴*Princeton Plasma Physics Laboratory, Princeton, USA*

⁵*JAEA, Mukouyama, Ibaraki, Japan*

⁶*Association EURATOM-Tekes, VTT, Finland*

⁷*General Atomics, San Diego, USA*

⁸*ITER Organization, Route de Vinon sur Verdon, Saint Paul Lez Durance, France*

Corresponding Author: holger.reimerdes@epfl.ch

Experiments on DIII-D confirm that the tritium breeding test blanket modules (TBMs) in ITER will lead to a decrease of the plasma rotation in H-modes [1]. Moreover, they suggest that long-wavelength correction fields applied with non-axisymmetric saddle coils will only be able to ameliorate a fraction of such a rotation reduction. The new finding obtained in rotating H-modes contrasts previous experiments, which showed that saddle coils are very effective in restoring resilience to locked modes in L-mode plasmas. The experiments use a TBM mock-up coil that has been especially designed to simulate the error field induced by the ferromagnetic steel of a pair of TBMs in one of ITER port. The TBM field is applied in rotating H-mode plasmas with shape, β and safety factor similar to the ITER baseline scenario. The $n = 1$ error field correction (EFC) is applied with a set of non-axisymmetric saddle coils (I-coil), whose currents are optimized in the presence of the TBM mock-up field using a newly developed non-disruptive technique that maximizes the plasma rotation. However, a test of the effectiveness of the TBM EFC yields that the optimized EFC can only recover approximately a quarter of the 30% rotation decrease attributed to the TBM error field. An alternative criterion to evaluate the “goodness” of an EFC has been its effectiveness in canceling the $n = 1$ plasma response to the error field. Plasma response measurements in the TBM experiment show that the I-coil can indeed cancel the magnetic measurements of the $n = 1$ plasma response to the TBM mock-up field. The required currents are consistent with ideal MHD predictions using the IPEC code, but differ significantly from the currents that maximize the plasma rotation. The contrast between the limited effectiveness of $n = 1$ EFC in rotating H-modes and their ability to recover a low locking density in L-mode plasmas shows that the components of the non-axisymmetric field that braking the plasma at high rotation differ from the components that are responsible for the field penetration. However the observation that the $n = 1$ currents that minimize the $n = 1$ plasma response do not correspond to the $n = 1$ currents that maximize the rotation challenge our understanding of error field correction.

References

- [1] M. J. Schaffer, *et al.*, Nucl. Fusion **51** (2011) 103028.

Mitigation of Large Amplitude Edge-Localized-Modes by Resonant Magnetic Perturbations on the Large Helical Device

K. Toi¹, S. Ohdachi¹, Y. Suzuki¹, F. Watanabe², K. Tanaka¹, S. Sakakibara¹, K. Ogawa³, M. Isobe¹, X. Du⁴, T. Akiyama¹, M. Goto¹, K. Ida¹, S. Masuzaki¹, T. Morisaki¹, S. Morita¹, K. Narihara¹, Y. Narushima¹, T. Tokuzawa¹, I. Yamada¹, R. Yasuhara¹, M. Yoshinuma¹, K. Kawahata¹, and H. Yamada¹

¹*National Institute for Fusion Science, Toki, Japan*

²*Faculty of Energy Science, Kyoto University, Kyoto, Japan*

³*Faculty of Engineering, Nagoya University, Nagoya, Japan*

⁴*Department of Fusion Science, The Graduate University for Advanced Study, Toki, Japan*

Corresponding Author: toi@lhd.nifs.ac.jp

The Large Helical Device (LHD) produces H-mode plasmas with large amplitude edge-localized-modes (ELMs). The ELMs are induced by interchange modes destabilized at the $\iota = 1$ rational surface in the stochastic field region just outside the last closed flux surface. These large amplitude ELMs expel large amount of plasma stored energy from the edge transport barrier (ETB) region, that is, up to 20% of the stored energy (W_p). Resonant magnetic perturbations (RMPs) with dominant $m = 1/n = 1$ component have clearly reduced the ELM amplitude and increased the ELM frequency. In this mitigated case, the energy loss by an ELM pulse is reduced less than 5% of W_p . The RMPs have reduced edge electron density preferentially, without modifying electron and ion temperature profiles noticeably. The RMPs slightly reduced the confinement improvement factor H averaged over ELMing phase for the ISS04 stellarator scaling having gyro-Bohm character.

EX-P

Study of the High-efficiency Fuelling Features of Supersonic Molecular Beam Injection on HL-2A Tokamak

D. Yu¹, C. Chen¹, L. Yao¹, J. Dong^{1,2}, B. Feng¹, Y. Zhou¹, Z. Shi¹, J. Zhou¹, X. Han¹, W. Zhong¹, C. Cui¹, Y. Huang¹, Z. Cao¹, Y. Liu¹, L. Yan¹, Q. Yang¹, X. Duan¹, and Y. Liu¹

¹*Southwestern Institute of Physics, Chengdu, China*

²*Institute for Fusion Theory and Simulation, Zhejiang University, Hangzhou, China*

Corresponding Author: yudl@swip.ac.cn

Features of high fuelling efficiency of supersonic molecular beam injection (SMBI) have been studied on HL-2A tokamak. Normalized by fuel inventory, the D_α emission induced by SMBI is about 50% higher than that of gas puffing (GP), indicating that SMBI can send the fuel to the plasma edge more efficiently. And strong particle convection (inward pinch) is observed both by hydrogen cyanide (HCN) interferometer as the densities from core channels increasing whereas the edge channels decreasing during the post-fuelling phase and by the microwave reflectometry (MWR). By comparing the SMBI pulses with and without electron cyclotron resonance heating (ECRH), the pinch may be driven by the enhancement of normalized electron temperature gradient. It is observed that higher enhancement (up to twice) of normalized electron temperature gradient for SMBI than that for GP, and this may be another mechanism for higher fuelling efficiency of SMBI.

EX-P

ELM and Pedestal Structure Studies in KSTAR H-mode Plasmas

J. G. Bak¹, J. W. Ahn², H. Kim³, J. Lee³, S. Yoon¹, R. Maingi², Y. Jeon¹,
A. England¹, Y. Park⁴, S. Sabbagh⁴, Y. Bae¹, S. Hahn¹, D. Hillis², H. Han¹, J. Kim¹,
W. Kim¹, W. Ko¹, H. Lee¹, K. Ida⁵, J. Kwak¹, K. Lee¹, Y. Na³, Y. Oh¹, S. Park¹, and
Y. Nam¹

¹*National Fusion Research Institute, Daejeon, Republic of Korea*

²*Oak Ridge National Laboratory, Oak Ridge, USA*

³*Seoul National University, Seoul, Republic of Korea*

⁴*Columbia University, New York, USA*

⁵*National Institute for Fusion Science, Toki, Japan*

Corresponding Author: jgbak@nfri.re.kr

The ELM and pedestal structure are studied in Korea Superconducting Tokamak Advanced Research (KSTAR) ELMy H-mode plasmas. KSTAR H-mode plasmas have three distinctive types of ELMs; large type-I ELMs with low ELM frequency ($f_{\text{ELM}} = 10 - 50$ Hz) and good confinement ($H_{98}(y, 2) = 0.9 - 1$), intermediate, possibly type-III, ELMs with high ELM frequency ($f_{\text{ELM}} = 50 - 250$ Hz) at a reduced confinement ($H_{98}(y, 2) = 0.7 - 0.8$), and a mixed, large and small, ELM regime with good confinement ($H_{98}(y, 2) \sim 1$). The NBI power scan shows that ELM frequency is increased with increasing input power for large ELMs, which is a typical behavior of type-I ELMs. Type-I ELMs are appeared in a wide range of NBI power, $0.8 \leq P_{\text{NBI}} \leq 1.5$ MW, but in a limited density range ($0.35 \leq n_e/n_G \leq 0.45$). Intermediate ELMs are observed in a wider density range, $0.35 \leq n_e/n_G \leq 0.55$, than for type-I ELMs and we suspect that these ELMs might be type-III considering that the confinement quality is degraded compared to type-I ELMs and the relatively lower n_e/n_G value compared to the type-II ELMs. Mixed ELMs often occur in late H-mode and the density range is also wider, $0.38 \leq n_e/n_G \leq 0.57$, than that of type-I ELMs. Pedestal profiles of electron temperature (T_e) from the ECE measurement and toroidal velocity (V_t) from the charge exchange spectroscopy (CES) measurement show continuous build up on the low field side (LFS) during the inter-ELM period for type-I ELMy H-mode. However, the recovery of T_i pedestal from the CES after the ELM crash does not occur until it finally rises back up at the last stage of the inter-ELM period, i.e., $> 80\%$ of the ELM cycle. The estimated electron pedestal collisionality,

$$\nu_e^* = q_{95} R \varepsilon^{-1.5} \lambda_{ee}^{-1}, \quad (1)$$

is quite low, $\nu_e^* \sim 0.2 - 0.5$, for the type-I ELMy H-mode. An ideal MHD stability analysis for ELMy H-mode plasmas is also carried out by the ELITE code in order to investigate unstable domains for the ELM occurrence, as well as its sensitivity to a range of estimated/measured profiles. In this work, the experimental investigations of the characteristics of the ELM and the pedestal structure during the ELM in the KSTAR H-mode plasmas will be reported, and the preliminary results from the ideal MHD analysis for ELMy H-mode plasmas will be presented.

Influence of the Resonant Magnetic Perturbations on Particle Transport in LHD

M. Jakubowski¹, P. Drewelow¹, S. Masuzaki², T. Akiyama², S. Bozhenkov¹,
M. Kobayashi², T. Morisaki², Y. Narushima², K. Tanaka², R. Wolf¹, and H. Yamada²

¹*Max-Planck-Institut für Plasmaphysik, Garching, Germany*

²*National Institute for Fusion Science, Toki, Japan*

Corresponding Author: marcin.jakubowski@ipp.mpg.de

Resonant Magnetic Perturbations (RMPs) recently became a very popular tool to control plasma exhaust in tokamaks following the results obtained on DIII-D. So called pump-out results from a pitch resonant coupling of the external field to the internal magnetic field. Large Helical Device (LHD) due to three-dimensional nature of the magnetic equilibrium a stochastic region is formed at the plasma edge. In spite of different origins stochastic boundary has similar features in tokamaks and helical devices, which results from heterogeneous open field lines region at the plasma boundary. Additionally at LHD, so called LID coils create perturbation with $m/n = 1/1$ and $2/1$ components. Depending on plasma conditions either enhance or heal $m/n = 1/1$ magnetic island. In the first case there is rather significant reduction on the confinement, caused mostly by enhanced heat and particle transport across the island. In the latter one there is rather a small drop of beta increasing with increasing LID current. These changes coincide with increasing width of open stochastic volume at the plasma edge near the X-point. With increasing amplitude of magnetic perturbation field lines with very long connection length ($L_c > 400$ m) are replaced by laminar flux tubes with $L_c \sim 100$ m. We also performed experiments where we changed the amplitude of the perturbation linearly with I_{LID} in the range of 0 – 2.7 kA. We have realized two cases: first, where the discharge is ignited with external perturbation already superimposed to equilibrium magnetic fields (which cannot be realized in tokamaks) and second, where the external perturbation is applied to the plasma already ignited (typical case of tokamaks with RMPs). There is a clear difference in size of $1/1$ island and dependence of n_e and T_e on LID current showing screening of external field in the latter case with a threshold in penetration of order of 600 A. Above 2 kA we observe global reduction of T_e and n_e profiles. In the case of pre-existing magnetic perturbation the threshold of 600 A is not present and for the same LID current island width is larger when compared to the case with magnetic perturbation applied after plasma ignition. As a result particle transport and confinement are affected much stronger in the discharges with pre-existing magnetic perturbation.

EX-P

On the Formation and Stability of Impurity-generated “Snakes” in Alcator C-Mod

L. F. Delgado-Aparicio^{1,2}, R. Granetz², L. Sugiyama³, J. Rice², Y. Podpaly²,
M. L. Reinke², D. Gates¹, M. Bitter¹, S. Wolfe², M. Greenwald², K. Hill¹,
A. Hubbard², E. Marmar², N. Pablant¹, S. Scott¹, R. Wilson¹, and S. Wukitch²

¹*Princeton Plasma Physics Laboratory, Princeton, USA*

²*MIT, Plasma Science and Fusion Center, Cambridge, USA*

³*MIT, Laboratory for Nuclear Science, Cambridge, USA*

Corresponding Author: ldelgado@pppl.gov

A suite of novel spectroscopic imaging diagnostics have facilitated the determination of the perturbed radiated power and impurity density inside the (1,1) “snakes” with unprecedented temporal and spatial resolution, and made it possible to infer, for the first time, the perturbed profiles of the impurity density, plasma pressure, Z_{eff} , and resistivity at the center of these helical modes. The observations show that in the early phase of C-Mod Ohmic discharges, snakes typically form as a growing, kink-like 1/1 helical impurity density structure with a nearly circular cross section. The circular kink structure then makes a seamless transition to a crescent-like impurity density structure that resembles the 1/1 magnetic island formed by a resistive internal kink and endures for the life of the snake. Periodic sawtooth crashes are observed during both phases. We thus offer a novel explanation for the formation of impurity-induced “snakes” which is not in agreement with the widely accepted model developed by Wesson, which explains the formation of these modes by a plasma current density perturbation from a localized temperature loss at the $q = 1$ rational surface. In particular, the conditions for finding a saturated island cannot be inferred from an extended Modified Rutherford formalism as assumed up to now, but by considering an enhanced impurity density, plasma pressure and resistivity at the center of the island as the main stabilizing effects in agreement with 3D non-linear MHD models. Although the formation mechanism of these impurity-induced “snakes” is different than the ones which are induced by pellet-injection, our experimental result and interpretation may also explain the increased stability of pellet-induced “snakes” which have been observed in fusion devices such as conventional tokamaks, spherical tori and reversed field pinches.

This work was performed under US DoE contracts DE-FC02-99ER54512 at MIT and DE-AC02-09CH11466 at PPPL.

Pedestal Stability and Transport on the Alcator C-Mod Tokamak: Experiments in Support of Developing Predictive Capability

J. Hughes¹, P. Snyder², X. Xu³, J. Walk¹, E. Davis¹, R. Churchill¹, R. Groebner²,
A. Hubbard¹, B. Lipschultz¹, T. Osborne¹, S. Wolfe¹, and D. Whyte¹

¹*Massachusetts Institute of Technology, Plasma Science and Fusion Center, Cambridge, USA*

²*General Atomics, San Diego, USA*

³*Lawrence Livermore National Laboratory, Livermore, USA*

Corresponding Author: jwhughes@psfc.mit.edu

New experimental data on the Alcator C-Mod tokamak are used to benchmark predictive modeling of the edge pedestal in various high-confinement regimes, contributing to a greater confidence in projection of pedestal height and width in ITER and reactors. Measurements in conventional Type-I ELMy H-mode have been used to test the theory of peeling-ballooning (PB) stability and pedestal structure predictions from the EPED model, which extends these theoretical comparisons to the highest pressure pedestals of any existing tokamak. Calculations with the ELITE code confirm that C-Mod ELMy H-modes operate near stability limits for ideal PB modes. Experimental C-Mod studies have provided supporting evidence for pedestal width scaling as the square root of poloidal beta at the pedestal top. This is the dependence that would be expected from theory if KBMs were responsible for limiting the pedestal width. The EPED model has been tested across an extended data on C-Mod, reproducing pedestal height and width reasonably well, and extending the tested range of EPED to within a factor of 3 of the absolute pedestal pressure targeted for ITER.

In addition, C-Mod offers access to two regimes, enhanced D-alpha (EDA) H-mode and I-mode, that have high pedestals but in which large ELM activity is naturally suppressed and, instead, particle and impurity transport are regulated continuously. Significant progress has been made in both measuring and modeling pedestal fluctuations, transport and stability in these regimes. Pedestals of EDA H-mode and I-mode discharges are found to be ideal MHD stable, consistent with the general absence of ELM activity. Like ELITE, the BOUT++ code finds the EDA pedestal to be stable to ideal modes. However, it does identify finite growth rates for edge modes when realistic values of resistivity and diamagnetism are included. The result is consistent with the interpretation of the quasi-coherent mode (QCM), which is omnipresent in the EDA pedestal, as a resistive ballooning mode, which could act to regulate the pedestal pressure profile in the same manner that KBMs are predicted to regulate collisionless pedestals. Full non-linear dynamics in BOUT++ are being used to simulate edge potential and density fluctuations, and the transport they drive in the EDA pedestal. Similar investigations are being initiated for I-mode.

EX-P

Edge Plasma Response to Beam-driven MHD Instability in Heliotron J

S. Ohshima¹, K. Hashimoto², S. Kobayashi³, S. Yamamoto³, K. Nagasaki³,
T. Mizuuchi³, H. Okada³, T. Minami³, K. Hanatani³, S. Konoshima³, K. Mukai²,
H. Y. Lee², L. Zang², M. Takeuchi⁴, and F. Sano³

¹*Kyoto University Pioneering Research Unit for Next Generation, Gokasho, Japan*

²*Graduate School of Energy Science, Kyoto University, Gokasho, Japan*

³*Institute of Advanced Energy, Kyoto University, Gokasho, Japan*

⁴*Japan Atomic Energy Agency, Mukoyama, Japan*

Corresponding Author: ohshima@iae.kyoto-u.ac.jp

Nonlinear behavior of broad-band fluctuation and dynamical potential change, associated with beam-driven MHD phenomenon, are observed around edge region in a medium-sized helical device, Heliotron J. Nonlinear phase relationship between the MHD and broad-band fluctuation is demonstrated as a result of bicoherence and envelope analyses applied to floating potential signals measured with multiple Langmuir probes (LPs) in neutral beam injection (NBI) heated plasmas. Also, structural potential profile change synchronized with the cyclic MHD burst is discovered. These experimental observations suggest that such MHD fluctuations can have influence on the confinement property of bulk plasma through nonlinear process and/or change of electric field structure.

EX-P

MHD Events and Transport Barriers in TJ-II Plasmas

D. López-Bruna¹, M. A. Ochando¹, A. López-Fraguas¹, and E. Ascasíbar¹

¹CIEMAT, Madrid, Spain

Corresponding Author: daniel.lopezbruna@ciemat.es

The physics of hot plasmas in toroidal sheared magnetic fields is common to tokamaks and stellarators and there are good reasons to believe that so is the physics of spontaneous formation of transport barriers. Both types of device have found relationships between the presence of magnetic resonances and the onset of transport barriers. In particular, the TJ-II stellarator, a Helic device that can operate at different values of the vacuum rotational transform ($\iota \sim 1$) at low magnetic shear, has permitted the identification of a cause-effect relationship between a proper location of magnetic resonant layers and the L-H transition. To stress the importance of the magnetic structure, here we study MHD events that generate in the plasma bulk and propagate until they reach a resonant layer. Depending on the plasma conditions (e.g., collisionality and order of the rational ι) the avalanche may traverse the resonant layer, get stopped at its location, or trigger the formation of either an internal or edge transport barrier depending on the location of the magnetic resonance. Since external control on the location and magnitude of resonant layers is technically feasible, these studies suggest a harmless means of transport control including transport barriers in toroidal plasmas for magnetic confinement fusion.

High Resolution Detection and 3D Magnetic Control of the Helical Boundary of a Wall-Stabilized Tokamak Plasma

J. Levesque¹, S. Angelini¹, J. Bialek¹, P. Byrne¹, B. DeBono¹, P. Hughes¹, M. Mauel¹,
G. A. Navratil¹, Q. Peng¹, N. Rath¹, D. Rhodes¹, D. Shiraki¹, and C. Stoafer¹

¹*Department of Applied Physics & Applied Mathematics, Columbia University, New York, USA*

Corresponding Author: jpl2131@columbia.edu

We report high-resolution detection of the time-evolving, three-dimensional (3D) plasma magnetic structure of wall-stabilized tokamak discharges in the HBT-EP device. Measurements and control experiments are conducted using a newly-installed adjustable conducting wall made up of 20 independent, movable, wall segments that have been precision located and equipped with 120 modular control coils and 216 poloidal and radial magnetic sensors. The control coils are energized with high-power solid-state amplifiers, and massively-parallel, high-throughput real-time feedback control experiments can be performed using low-latency connections between input and output CompactPCI modules and a GPU processor. The time evolution of unstable and saturated wall-stabilized external kink modes are studied in detail with and without applying magnetic perturbations with the control coils. The 3D dynamic structure of the magnetic field surrounding the entire plasma is defined with biorthogonal decomposition using the full set of magnetic sensors without the need to fit either a Fourier or a model-based basis. Naturally occurring external kinks are composed of independent helical modes, frequently having $m/n = 3/1$ and $6/2$ helicity, that are seen to modulate each other in time. When magnetic perturbations are applied by energizing the control coils, the resonant magnetic response can be either linear, saturated, or disruptive depending upon the amplitude of the applied perturbation and on plasma's current profile and rotation rate. Active feedback experiments have been conducted using 40 magnetic sensors and 40 control coils, and initial results show the closed-loop plasma response as a function of gain and phase.

EX-P

Control of Sawteeth Periods by Pulsed ECH and ECCD in FTU Tokamak

S. Nowak¹, S. Cirant¹, P. Buratti², B. Esposito², G. Granucci¹, A. Tuccillo²,
D. Marocco², and A. Romano²

¹*Istituto di Fisica del Plasma, IFP-CNR, Associazione EURATOM-ENEA-CNR sulla Fusione, Milan, Italy*

²*Centro Ricerche di Frascati, Associazione EURATOM-ENEA, Rome, Italy*

Corresponding Author: nowak@ifp.cnr.it

The neoclassical tearing modes (NTMs) are resistive instabilities degrading the high β plasma confinement with loss of plasma energy. As the NTMs can be triggered by long sawteeth crashes, the control of the sawteeth periods (τ_{ST}) is a key physics issue in fusion devices: the τ_{ST} shortening can avoid the NTMs onset allowing to achieve high plasma performances. A powerful tool for the sawteeth control is the highly localized electron cyclotron heating (ECH) and current drive (ECCD) capable to modify the plasma current density with effect on sawteeth period. In FTU tokamak EC power modulation has been investigated as trigger of sawtooth crashes to test conditions for an a-priori constant τ_{ST} using 1 – 2 gyrotrons up to 0.8 MW in view of the real time EC system working soon. ECH/ECCD modulations at 20 Hz (20% , 80% d.c.) and 125 Hz (50% d.c.) were performed in plasma with magnetic field ramp to move the EC deposition from inside to outside the minor inversion radius r_{inv} at $q = 1$ surface. Irregular τ_{ST} , smaller than 6.4 ms ohmic value, have been obtained, as expected, by ECH & co-ECCD 20 Hz modulation at $r < r_{inv}$. Conversely, a new interesting evidence was found inside $q = 1$ using 125 Hz 50% d.c. modulation: for EC_{on} phase of 4 ms less than the ohmic 6.4 ms the τ_{ST} increases up to 8 ms EC pulse period with unforeseen sawteeth stabilization remaining quite constant in the EC absorption location $0.4 < r_{dep}/r_{inv} < 0.6$. This coupling between modulation and sawtooth crashes suggests an interesting strategy to set an a-priori constant and further reduced τ_{ST} using faster EC pulses, as 500 Hz/1 kHz. Transport calculations have been carried out to simulate these behaviours by using the JETTO code where the crashes are described by the model based on the change of magnetic shear. A predictive analysis is in progress to confirm the coupling between faster modulations (> 125 Hz) and constant τ_{ST} .

EX-P

Experimental Studies of the Plasma Response to Applied Nonaxisymmetric External Magnetic Perturbations in EXTRAP T2R

L. Frassinetti¹, E. Olofsson¹, S. Menmuir¹, W. Khan¹, P. Brunzell¹, and J. Drake¹

¹*KTH, Royal Institute of Technology, Stockholm, Sweden*

Corresponding Author: lorenzo.frassinetti@ee.kth.se

The EXTRAP T2R resistive wall mode feedback control system, along with new control algorithms has enabled experimental studies of the interaction of external magnetic perturbations with the plasma. Application of low amplitude transient, broad-spectrum magnetic perturbations in parallel with feedback stabilization enables non-destructive measurement of RWM growth rates. It is found that the obtained eigenmode spectrum compares well with cylindrical ideal MHD thin resistive wall theory. Resonant external magnetic perturbations have been applied to study the interaction with magnetic islands. A stationary perturbation leads to braking of the magnetic island rotation and locking of the island position. When the magnetic island is close to complete locking, regular phase flips are seen correlated with large island amplitude variations. Stationary resonant magnetic perturbations have been applied to study how local electromagnetic torques at the resonant surface brakes the plasma rotation. The electromagnetic torque affects first the rotation at the resonant surface, and then the effect propagates across the rotation profile. Non-resonant magnetic perturbations may affect the plasma rotation through neoclassical toroidal viscosity. Application of a non-resonant external perturbation shows reduction of the fluid velocity over the core region, demonstrating a non-local braking effect. The capabilities of the control coils have been utilized for studying the role of varying perturbation harmonic. Resonant magnetic perturbation penetration into the plasma may be reduced by plasma flow screening. This effect is studied by generating a RMP that interacts with a tearing mode (TM), while the flow velocity is changed by applying a second perturbation that is non-resonant, thus producing a flow reduction without perturbing significantly other parameters. By modifying the amplitude of the non-RMP, the degree of RMP penetration has been studied at varying plasma flow velocity.

EX-P

Characterization of Neo-classical Tearing Modes in High-performance I-Mode Plasmas with ICRF Mode Conversion Flow Drive on Alcator C-Mod

Y. Lin¹, R. Granetz¹, M. Reinke¹, J. Rice¹, S. Wolfe¹, and S. Wukitch¹

¹MIT Plasma Science and Fusion Center, Cambridge, USA

Corresponding Author: ylin@psfc.mit.edu

Neo-classical tearing modes (NTMs) have been observed definitely for the first time on Alcator C-Mod. The NTMs occur in high performance I-mode plasmas that are heated by a combination of ICRF D(H) minority heating at 80 MHz and D(³He) mode conversion (MC) heating at 50 MHz. I-mode plasmas have confinement as good as H-mode but lower collisionality [1]. Due to the stabilizing effect by the energetic minority hydrogen ions, long sawtooth (≥ 40 ms) and large sawtooth crashes ($\Delta T_{e0} \geq 3$ keV) are produced in these hot ($T_{e0} \leq 9$ keV) plasmas. A typical case is that soon after the plasma enters I-mode, a ($m = 4, n = 3$) mode ($f = 40 - 60$ kHz) appears following a large sawtooth crash, and then a (3,2) mode (20 - 40 kHz) appears later at slightly higher β_N . The (3,2) mode can also occur without a preceding (4,3) mode. In some plasmas, a (2,1) mode may appear simultaneously with the (3,2) mode, and lead to disruption. The onset criterion of the (3,2) NTMs approximately follows that obtained from DIII-D and ASDEX Upgrade [2]. The onset parameters are $\beta_p \sim 0.4 - 0.7$, $\beta_N \sim 1.0 - 1.4$, $\beta_N/\rho_i^* \sim 200 - 350$, $\nu_{q=3/2} \sim 0.04 - 0.25$. The saturated magnetic island width of the (4,3) mode is typically $\omega_{\text{sat}} \sim 0.4 - 0.6$ cm, and the mode usually has an insignificant effect on confinement. For the (3,2) mode, $W_{\text{sat}} \sim 0.8 - 1$ cm, which is $3 - 4 \times$ the ion banana width, and the mode can cause small confinement degradation ($\Delta\beta/\beta \sim$ a few percent). The NTMs have a strong effect on plasma rotation. MC flow drive generates large toroidal rotation above 100 km/sec in L-mode [3], and when the plasma enters I-mode, plasma rotation is expected to increase significantly due to the additional intrinsic rotation torque from the edge T_e pedestal. However, the rotation almost always stops rising after the onset of the NTM(s). The appearance of the (3,2) mode usually rapidly reduces the rotation speed, and the (2,1) mode, if occurs, would completely halt the rotation. We will discuss the prospect of NTM avoidance and control using ICRF to modify sawtooth plus using lower hybrid waves to modify the local current profile.

References

- [1] D. G. Whyte *et al.*, Nucl. Fusion **50** (2010) 105005.
- [2] R. J. La Haye, Physics of Plasmas **7** (2000) 3349.
- [3] Y. Lin *et al.*, Nucl. Fusion **51** (2011) 063002.

Work supported by US DoE Cooperative Agreement DE-FC02-99ER54512.

EX-P

Mitigation of Type-I ELMs with $n = 2$ Fields on JET

Y. Liang¹, P. Lomas², I. Nunes², M. Gryaznevich², M. N. A. Beurskens², S. Brezinsek¹,
J. Coenen¹, P. Denner¹, T. Eich³, L. Frassinetti⁴, S. Gerasimov², D. Harting¹,
S. Jachmich⁵, A. Meigs², J. Pearson¹, M. Rack¹, S. Saarelma², B. Sieglin³, Y. Yang¹,
and L. Zeng¹

¹*Forschungszentrum Jülich GmbH, Jülich, Germany*

²*EURATOM/CCFE Fusion Association, Culham Science Centre, Abingdon, UK*

³*Max-Planck-Institut für Plasmaphysik, EURATOM-Assoziation, Garching, Germany*

⁴*Association EURATOM-VR, Fusion Plasma Physics, EES, KTH, Stockholm, Sweden*

⁵*Association EURATOM-Belgian State, Koninklijke Militaire School - Ecole Royale Militaire, Brussels, Belgium*

Corresponding Author: y.liang@fz-juelich.de

Recently, strong mitigation of Type-I Edge Localized Modes (ELMs) has been observed with application of the $n = 2$ field in high collisionality ($\nu_e^* = 2.0$) H-mode plasma on JET tokamak with ITER-like wall. In this experiment, the EFCC power supply system has been enhanced with a coil current up to 88 kAt (twice than before). With an $n = 2$ field, the large type-I ELMs with frequency of ~ 45 Hz was replaced by the high frequency (few hundreds Hz) small ELMs. No density pump-out was observed during an application of the $n = 2$ field. The influence of the $n = 2$ field on the core and the pedestal electron pressure profiles is within the error bar and it can be neglected.

During the normal type-I ELM H-mode phase, the maximal surface temperature (T_{\max}) on the outer divertor plate was overall increasing and associated with large periodical variation due to the type-I ELMs. However, during an application of the $n = 2$ field, T_{\max} was saturated and has only small variation in few degrees due to the small mitigated ELMs. Splitting of the outer strike point has been observed during the strong mitigation of the type-I ELMs.

EX-P

Direct Observation of Soft-X Ray Filament Structure and High Current Operation in Low-Aspect-Ratio RFP

S. Masamune¹, A. Sanpei¹, K. Oki¹, D. Fukahori¹, K. Deguchi¹, S. Nakaki¹,
H. Himura¹, N. Mizuguchi², T. Akiyama², K. Kawahata², A. Ejiri³, R. Paccagnella⁴,
and D. Den Hartog⁵

¹*Kyoto Institute of Technology, Kyoto, Japan*

²*National Institute for Fusion Science, Toki, Japan*

³*University of Tokyo, Kashiwa, Japan*

⁴*Consorzio RFX, Padova, Italy*

⁵*University of Wisconsin, Madison, USA*

Corresponding Author: masamune@kit.ac.jp

An equilibrium analysis has shown that the aspect ratio $A(= R/a)$ is an important parameter for optimization of the RFP configuration because the q profile is closely connected to A in the self-organized state. Furthermore, some theories show that the pressure-driven bootstrap current increases as A is lowered to less than 2. RELAX is a RFP machine ($R = 0.5 \text{ m}/a = 0.25 \text{ m}$; $A = R/a = 2$) to explore the plasma characteristics in low- A regime. In shallow reversal plasmas, the discharge tends to transit to the QSH state, or helical Ohmic equilibrium state. Experimental internal field profiles showed good agreement with the theoretical helical Ohmic equilibrium state. Recent progress in high-speed soft-X ray (SXR) imaging diagnostic has made it possible to identify a simple helical SXR filament structure. The helically deformed core with higher SXR emissivity is rotating at a speed of $\sim 1.6 \times 10^4 \text{ rad/s}$, the same as that of the dominant $m = 1/n = 4$ mode. A Poincare plot of the reconstructed magnetic field lines in a poloidal cross section during the QSH phase has shown the helically deformed nested flux surfaces in the core region. These results are consistent with our previous SXR emissivity profile measurement which suggested improved confinement in the helically deformed core. The easier access to the helical state in RELAX may result from the characteristic q profile in low- A RFP where wider space without major resonance allows the island to grow without interacting neighboring mode. The MHD behavior of RELAX plasmas has been studied in detail in the current region from 40 kA to 80 kA, where two possible improved confinement regions were suggested: QSH-dominated shallow-reversal region and deep-reversal region with low magnetic fluctuation level. In both regions, further improvement of plasma performance can be expected with higher S because quality of the QSH is improved more at higher S , and magnetic fluctuation level decreases with increasing S in the RFP. In order to improve plasma performance we have started optimization of higher current operation. Optimized 100 kA discharge has shown that the discharge resistance decreases with increasing the plasma current. It indicates the possibilities of improved performance of low- A RFP plasma at higher current regions.

EX-P

Triggering of Neoclassical Tearing Modes by Mode Coupling in HL-2A

X. Ji¹, Y. Liu¹, Q. Yang¹, J. Q. Wang², X. Wang³, B. Feng¹, Y. Xu¹, T. Sun¹,
Y. Dong¹, W. Deng¹, W. Chen¹, and B. Yuan¹

¹*Southwestern Institute of Physics, Chengdu, China*

²*College of Physical Science and Technology, Sichuan University, Chengdu, China*

³*State Key Laboratory of Nuclear Physics & Technology and School of Physics, Peking University, Beijing, China*

Corresponding Author: jixq@swip.ac.cn

The onset of neoclassical tearing modes (NTMs) for previous theories requires a seed island, whose width need exceed the critical value. Such seed islands are often provided by sawtooth activities, fishbones, or edge localized modes (ELMs). However, the mechanism for seed island formation is not well understood up to now. In this paper, NTMs triggered by two mode toroidal coupling and preliminary modeling results on HL-2A are presented.

In HL-2A, the m/n NTMs can be driven unstable by toroidal mode coupling with the central MHD activities ($m - 1/n$) and also the external classical tearing modes ($m + 1/n$). For understanding the experimental results, preliminary modeling has been carried out based on the forced reconnection by toroidal mode coupling. In toroidal geometry, a perturbation with the mode number m/n , have the $m \pm 1/n$ components. Which can induce the forced reconnection on the $q = m \pm 1/n$ rational surface, and provide seed island for metastable $q = m \pm 1/n$ NTM. In HL-2A, 2/1 coupled with 1/1, 3/2 coupled with 2/1 or 4/2 have been experimentally observed. Considering this driven effect, we calculate the temporal evolution of the NTM island. It is found that the results are in good agreements with the experiment data.

Modification of Toroidal Flow in the STOR-M Tokamak

C. Xiao¹, S. Elgriw¹, Y. Liu¹, T. Onchi¹, M. Dreval², M. Hubeny¹, Y. Ding¹, T. Asai³,
and A. Hirose¹

¹*University of Saskatchewan, Saskatoon, Canada*

²*Institute of Plasma Physics, Kharkov, Ukraine*

³*Nihon University, Tokyo, Japan*

Corresponding Author: chijin.xiao@usask.ca

Flow measurements using ion Doppler spectroscopy (IDS) have been recently used to study toroidal flow velocities of impurity ions. By selecting ion species, such as a CIII line (464.7 nm) with emission intensity peaking at the radial location near $r = 7$ cm, an OV line (650.0 nm) at, and CVI line (529.0 nm) near the plasma core, an estimated radial resolution of flow velocities can be achieved through a single line of sight along the tangential direction of the torus. During nominal ohmic discharges, the toroidal flow is in the counter-current direction in the core region at $r \sim 0$ cm (CVI line) and $r = 4$ cm (OV line) and changes to co-current direction towards the edge at $r = 7$ cm (CIII line). In the extreme edge and scrape-off-layer (SOL), the flow is also in the co-current direction as measured by a movable Mach probe. Resonant magnetic perturbations (RMP) using a set of resonant helical coils in the $m/n = 2/1$ configuration [1] or tangential compact torus injection [2] changes the flow towards the co-current direction in all regions, while during the improved confinement phase triggered by fast gas puffing, the flow changes towards the counter-current direction.

References

- [1] Elgriw S., Liu D., Asao T., Hirose A., Xiao C., Nucl. Fusion **51** (2011) 113008.
- [2] Xiao C., Sen S., Hirose A., Phys. Plasmas **11** (2004) 4041.

Probing Resistive Wall Mode Stability Using Off-axis NBI

J. Hanson¹, M. J. Lanctot², H. Reimerdes³, I. T. Chapman⁴, Y. In⁵, R. J. La Haye⁶,
Y. Liu⁴, G. A. Navratil¹, M. Okabayashi⁷, E. J. Strait⁶, W. M. Solomon⁷, and
F. Turco¹

¹*Columbia University, New York, USA*

²*Lawrence Livermore National Laboratory, Livermore, USA*

³*École Polytechnique Fédérale de Lausanne, Lausanne, Switzerland*

⁴*EURATOM/CCFE Fusion Association, Culham Science Centre, Abingdon, UK*

⁵*FAR-TECH, San Diego, USA*

⁶*General Atomics, San Diego, USA*

⁷*Princeton Plasma Physics Laboratory, Princeton, USA*

Corresponding Author: jmh2130@columbia.edu

EX-P
DIII-D experiments with off-axis neutral beam injection (NBI) yield evidence of modifications to resistive wall mode (RWM) stability. Measurements of the plasma response to slowly rotating, applied $n = 1$ perturbations decrease in amplitude as the fractional mix of off-axis NBI power is increased at constant normalized β . This reduction of the plasma response amplitude due to the off-axis injection is observed in repeatable plasmas over a range of plasma rotation values, and is correlated with increased pitch-alignment of the fast ion slowing-down distribution. Present day tokamaks are routinely able to operate above the ideal MHD no-wall β -limit predicted for $n = 1$ external kink instabilities, and a theory incorporating kinetic modifications to the ideal MHD RWM dispersion relation is consistent with the parametric dependencies of experimental stability measurements. The present theory features several mechanisms that lead to an exchange of energy between the RWM and kinetic particle populations, including resonances between trapped thermal ions and the bulk plasma rotation, a generic stabilizing influence of trapped energetic ions independent of plasma rotation, and damping due to passing ions near rational flux surfaces. Recent experiments exploited the new off-axis NBI capability on DIII-D to investigate the impact of changing the fractional off-axis NBI power and torque on RWM stability at constant normalized β and plasma internal inductance. Transport simulations based on reconstructions of the experimental equilibria indicate increased pitch-alignment of the fast ion slowing-down distribution and a decreased trapped fraction as the off-axis NBI power is increased. The observed increase in RWM damping due to off-axis NBI provides a new test for passive stability models needed to predict performance limits in ITER and future burning plasma devices.

This work was supported in part by the US Department of Energy under DE-FG02-04ER54761, DE-AC52-07NA27344, DE-FG02-08ER85195, DE-FC02-04ER54698, and DE-AC02-09CH11466.

Vertical Stability of NSTX and NSTX-U

E. Kolemen¹, M. Walker², D. Gates¹, D. Mueller¹, A. S. Welander², J. Menard¹,
D. Humphreys², and S. Gerhardt¹

¹*Princeton Plasma Physics Laboratory, Princeton, USA*

²*General Atomics, San Diego, USA*

Corresponding Author: ekolemen@pppl.gov

This paper studies the vertical stability of NSTX and NSTX-U, and explains some of the upgrades to the control capabilities that have been implemented and under investigation for NSTX-U that can stabilize Vertical Displacement Events (VDEs). In this study we use NSTX experimental data and $n = 0$ stability simulations via gspert, a nonrigid plasma response model based on the linearized Grad-Shafranov equation, and Corsica, a free-boundary equilibrium and transport code. On NSTX, it is shown experimentally and by simulations that the growth rate, γ , accelerates as the plasma moved away from the center. Also, it is shown via experimental data and the simulations that γ increases as an increase in aspect ratio. Acceleration in the γ as the plasma drifts leads to the prioritization of early detection and faster control over more control power. With these considerations in mind, there are currently three improvements for the NSTX-U. First, a new, more sophisticated vertical position estimator will enable early and more accurate detection. Second, RWM coils, which are much faster than the poloidal field coils, were put in the vertical control loop, which will reduce control action delay against VDEs. Improvements to the control algorithm are also under development.

EX-P

Perturbation Features of Intrinsic and Pellet Induced ELMs on HL-2A

Y. Huang¹, C. Liu¹, L. Nie¹, X. Ji¹, Z. Feng¹, K. Yao¹, D. Yu¹, X. Song¹, G. Zhu¹, J. Cao¹, J. Zhou¹, Z. Cui¹, Y. Liu¹, Q. Yang¹, L. Yan¹, Q. Wang¹, X. Ding¹, J. Dong¹, X. Duan¹, and Y. Liu¹

¹*Southwestern Institute of Physics, Chengdu, China*

Corresponding Author: yhuang@swip.ac.cn

The H-mode discharge is generally accompanied by quasiperiodic edge localized mode (ELM) events. Many efforts have been spent worldwide on the understanding, mitigation and control of the ELMs, in order to eventually suppress the most destructive ELMs to meet the lifetime requirements on ITER target plates. The pellet pacing ELM mitigation concept is being tested in many tokamaks, but the mechanism of a pellet triggering an ELM is yet partly understood. In HL-2A tokamak, ELMy H-mode operation is routinely performed and small type-III ELMs with high repetition rate and some type-I (or possibly large type-III) ELM events are observed. Pellet injection experiments are performed in ELMy H-mode and ELM-free H-mode as well as L-mode plasmas to study the physics of pellet triggering ELM. The analysis and comparison of magnetic perturbation spectra and the toroidal mode number of pellet-triggered ELM events with those of spontaneous ELMs in H-mode plasmas, are presented in this article.

EX-P

Response of MHD Stability to Resonant Magnetic Perturbation in the Large Helical Device

S. Sakakibara¹, Y. Takemura², M. Okamoto³, K. Watanabe¹, Y. Suzuki¹,
Y. Narushima¹, S. Ohdachi¹, K. Ida¹, M. Yoshinuma¹, K. Tanaka¹, T. Tokuzawa¹,
K. Narihara¹, I. Yamada¹, and H. Yamada¹

¹*National Institute for Fusion Science, Toki, Japan*

²*The Graduate University for Advanced Studies, Toki, Japan*

³*Ishikawa National College Technology, Ishikawa, Japan*

Corresponding Author: sakakis@lhd.nifs.ac.jp

Penetration of a Resonant Magnetic Perturbation (RMP) and its effect on MHD stability have been investigated in the Large Helical Device (LHD). The existence of an error field is one of the common problems in magnetic confinement systems because it may degrade plasma confinement and trigger MHD instabilities. The RMP experiments have been done in many tokamaks and RFPs to identify the threshold of error field penetration, which is required for estimating the tolerance to the error field in ITER [1]. Here we have investigated the threshold of the perturbation field strength by changing the RMP field in varying magnetic shear and magnetic hill of LHD so as to find the common physics of the effect of an error field in both tokamaks and helical devices. Previous experiments in LHD showed that the $m/n = 1/1$ static island abruptly grows and leads to a minor collapse during a discharge [2]. The threshold of the appearance of the island clearly decreases with the magnetic shear reduced by controlling external coils and/or driving the plasma current. The spatial structure of the island is consistent with that of natural magnetic island as confirmed by electron beam mapping [3]. While these experiments are equivalent to those in the constant RMP (natural error field) condition, the threshold of the RMP strength to the penetration has been investigated in different magnetic shear configurations as the next step. As a result, the mode penetration is prevented by an enhancement of the magnetic shear and/or reduction of the magnetic hill in addition to the plasma flow effects. The penetration is accelerated as the plasma approaches the unstable regime against interchange modes. The experiment cancelling the ambient error field shows that the rotation of the $m/n = 1/1$ mode is locked and leads to minor collapse in such an unstable regime. The mode has an interchange type radial structure, at least, before the locking.

References

- [1] T. C.Hender *et al.*, Nuclear Fusion **47** (2007) S128.
- [2] S. Sakakibara *et al.*, Fusion Science and Technology **50** (2006) 177.
- [3] T. Morisaki *et al.*, Fusion Science and Technology **50** (2010) 465.

Addressing New Challenges for Error Field Correction

R. J. Buttery¹, A. H. Boozer², Y. Liu³, J. K. Park⁴, N. M. Ferraro¹, V. Amoskov⁵,
Y. Gribov⁶, R. J. La Haye¹, E. Lamzin⁵, J. Menard⁴, M. J. Schaffer¹, and E. J. Strait¹

¹General Atomics, San Diego, USA

²Columbia University, New York, USA

³EURATOM/CCFE Fusion Association, Culham Science Centre, Abingdon, UK

⁴Princeton Plasma Physics Laboratory, Princeton, USA

⁵D. V. Efremov Scientific Research Institute of Electrophysical Apparatus, St. Petersburg,
Russian Federation

⁶ITER Organization, St Paul Lez Durance, France

Corresponding Author: buttery@fusion.gat.com

The correction of error fields in ITER is found to be far more challenging than previously thought due to the effects of a multi-component response to such fields at multiple surfaces in the plasma. This situation is exacerbated by an amplification of error fields in H-modes, where a developing resistive response is observed, with fields found to brake plasma rotation and destabilize intrinsic $m = 2, n = 1$ tearing instabilities. New scalings of mode-trigger thresholds were obtained from this process, and are compared with new Monte Carlo calculations of the error fields expected in ITER, updated for the ideal-response formalism by which the error fields couple to the plasma. These indicate that correction will need to reduce error fields by $\sim 50\%$ to avoid instability in the ITER baseline. This is comparable to the best levels of correction presently achievable in devices around the world. Obtaining this level of correction typically requires well-optimized dual toroidal array dual arrays, usually located close to the plasma. Experiments have explored this physics using large amplitude proxy error fields with a known controllable field structure. These confirm the limitations and indicate that they arise within $n = 1$ field components, rather than higher toroidal mode number, or inherent stability or control limits. This indicates that the fields must couple to the plasma through multiple ideal mode, and that once in the plasma, must interact at more than one resonant surface or non-resonantly. Modeling with the IPEC code favors the latter interpretation with a decrease in resonant fields being accompanied by an increase in NTV damping. Further results using an optimized “ideal-mode” structured correction field, yield little improvement over standard error field correction, also favoring a non-resonant interpretation of the residual field effects. These results indicate that ITER needs to have sufficient harmonic flexibility to adapt to the underlying error field, cancelling it at more than one surface in the plasma, and preferably near its source. Thus it should consider a multi-harmonic error field correction strategy, and may need to additionally deploy its ELM control coils for error correction, to ensure disruption free operation.

Supported in part by the US DOE under DE-FC02-04ER54698, DE-FG02-04ER54761, DE-AC02-09CH11466, and DE-AC05-06OR23100.

Triggerless Onset and Effect of “Natural” Rotation on Neoclassical Tearing Modes in the TCV Tokamak

E. Lazzaro¹, S. Nowak¹, O. Sauter², B. Duval², L. Federspiel², A. Karpushov²,
D. Kim², H. Reimerdes², J. Rossel², D. Wagner², and G. Canal²

¹*Istituto di Fisica del Plasma IFP-CNR, Associazione EURATOM-ENEA-CNR sulla Fusione, Milano, Italy*

²*École Polytechnique Fédérale de Lausanne, Lausanne, Switzerland*

Corresponding Author: e.lazzaro@alice.it

Plasma rotation affects significantly the performance and stability of tokamak plasmas and is a major object of research both for first principles physics and applications. In the TCV tokamak spontaneous plasma toroidal rotation in absence of external momentum is observed and it is found experimentally that central electron cyclotron heating (ECH) and current drive (ECCD) can modify the rotation profile. The presence of MHD modes is known to produce magnetic viscosity that flattens the toroidal rotation profile over the whole central region, up to the rational surface of the corresponding mode. This work presents new experimental evidence of the interplay of plasma rotation and the onset of $m/n = 3/2$ and $2/1$ tearing instabilities in the neoclassical regime in absence of sawteeth or other trigger event, such as ELMs and fishbones. The evolution of these modes seems to be characterized, initially, by a conventional growth rate, driven by the ECH induced modification of the plasma current density profile followed by an NTV flattening of the core rotation profile, and then, by a neoclassical behaviour during the EC power ramp. During this stage the rotation is forced below the ion diamagnetic velocity and it may change the sign of the ion polarization current. This genuinely triggerless mechanism for NTM onset is investigated here experimentally for the first time with obvious relevance to ITER. The experiments, carried out on the TCV tokamak, give a direct measurement of the association of the change of the plasma rotation frequency and NTM onset in absence of other trigger events, which can be compared with theoretical expectations and related to the instability tearing parameter and other terms in the modified Rutherford equation.

EX-P

Observation of Edge Harmonic Oscillation in NSTX and Theoretical Study of its Active Control Using HHFW Antenna at Audio Frequencies

J. K. Park¹, R. Goldston¹, N. Crocker², E. Fredrickson¹, M. Bell¹, R. Maingi³, K. Tritz⁴, M. Jaworski¹, M. Ono¹, J. Menard¹, R. Bell¹, B. LeBlanc¹, and S. Kubota²

¹*Princeton Plasma Physics Laboratory, Princeton, USA*

²*University of California Los Angeles, Los Angeles, USA*

³*Oak Ridge National Laboratory, Oak Ridge, USA*

⁴*Johns-Hopkins University, Baltimore, USA*

Corresponding Author: jpark@pppl.gov

Edge localized modes (ELMs) can generate unacceptable heat loads to plasma facing components in a reactor scale tokamak or spherical torus, and therefore ELM control is a critical issue in ITER. ELM control using non-axisymmetric (3D) fields is a promising concept, but the 3D coil requirements are demanding in cost and engineering. An alternative means may be to use internally driven 3D field oscillations such as edge harmonic oscillations (EHOs), but the relevant operational window is possibly more limited than the external 3D field applications. The disadvantages of each approach can be mitigated if the external and the internal drive of 3D fields can be constructively combined. This paper presents two important topics for this vision: Experimental observations of edge harmonic oscillations in NSTX (not necessarily the same as EHOs in DIII-D), and theoretical study of its audio-frequency drive using the high harmonic fast wave (HHFW) antenna as 3D field coils. Edge harmonic oscillations were observed particularly well in NSTX ELM-free operation with low $n = 1$ core modes, with various diagnostics confirming $n = 4 - 6$ coherent oscillations in 2 - 8 kHz frequency range. These oscillations, which share some characteristics with the $n = 1$ dominated modes observed in small-ELM regimes in NSTX [1], seem to have a favored operational window in rotational shear, similarly to EHOs in DIII-D QH modes. However, in NSTX, they are not observed to provide particle or impurity control, possibly due to their weak amplitudes, of a few mm displacements, as measured by reflectometry. The external drive of these modes has been proposed in NSTX, by utilizing audio-frequency currents in the HHFW antenna straps [2]. Analysis shows that the HHFW straps can be optimized to maximize $n = 4 - 6$ while minimizing $n = 1 - 3$. Also, IPEC calculations show that the optimized configuration with only 1 kAt current can produce twice larger displacements than the observed internal modes, ~ 6 mm vs. 3 mm. The possibility of implementing a drive system will be examined in NSTX-U first, and successful application may provide a pathway for future devices, including ITER.

References

- [1] A. C. Sontag, J. M. Canik, R. Maingi *et al.*, Nucl. Fusion **51** (2011) 103022
- [2] J. K. Park, R. J. Goldston, Presented at the 16th MHD Mode Control Workshop (2011)

This research was supported by U.S. DOE contracts #DE-AC02-09CH11466.

Fast-scale Magnetic Perturbations and Onset of the Energy Quench during Disruption Instability in the T-10 tokamak

P. Savrukhin¹, E. Shestakov¹, S. Grashin¹, A. Sushkov¹, and D. Sarichev¹

¹*NRC “Kurchatov Institute”, Moscow, Russian Federation*

Corresponding Author: psavrukhin@nfi.kiae.ru

Avoidance of the plasma disruptions is an ultimate goal of a reliable future thermonuclear reactor. Present studies in the T-10 tokamak are clarifying trigger conditions of the fast transition to energy quench from moderate growth of the MHD perturbations at the initial stage of the disruption. New magnetic probe system is installed on the T-10 tokamak to investigate fast-scale magnetic perturbations (f up to 2 MHz). The system is based on vertical and horizontal magnetic probes made by nickel wire in glass enamel isolation (effective area 20 – 250 cm²) separated from the support structures by ceramic spacers (5 – 10 mm). The probe system is mounted on the top of movable rode allowing positioning along vertical axis close to the plasma boundary at the low field side of the torus. Additional positioning system allows rotation of the probes around the vertical axis on pulse to pulse basis. The probes are directly connected to the ADC module (acquisition rate 60 MHz) through short (~ 4 m) coaxial cables. The system allowed identification of the fast-scale magnetic oscillations (0.2–0.5 MHz) during energy quench phase of the disruption instability in plasma with high density. Amplitude of the fast-scale magnetic oscillations decays with distance from the plasma boundary 2 – 10 \times faster than one of the standard magnetohydrodynamic (MHD) modes. The fast-scale magnetic oscillations are observed sometimes simultaneously with bursts of the nonthermal ($E \sim 50 - 150$ keV) x-ray radiation. This could indicate indirectly connection of the oscillations with nonthermal electrons generated during initial stage of the disruption. Analysis indicated that the oscillations could be connected with spark effect initiated in the plasma core in presence of the large-scale MHD modes. While mechanism of the oscillations is still not clear at the moment they can be used as trigger of the disruption feedback stabilization system. The trigger is used in the T-10 experiments with quasi-stable plasma recovery by ECRH after initial minor disruption.

EX-P

The work is supported by ROSATOM (H.4f.45.90.11.1021) and RFBR (Grant 11-02-01344).

Current Profile Control Using the Ohmic Heating Coil in TCV

J. A. Romero¹, S. Coda², F. Felici², J. M. Moret², J. Paley², G. Sevillano³, I. Garrido³,
and H. B. Le³

¹*CIEMAT, Madrid, Spain*

²*CRPP-EPFL, Lausanne, Switzerland*

³*EHU, Bilbao, Spain*

Corresponding Author: jesus.romero@ciemat.es

The economy of future tokamaks may have to rely on having large bootstrap current fractions and/or pulsed operation, with limited power available from non inductive current drive actuators. The transformer primary coil can assist in reducing the power requirements of the non inductive current drive sources needed for current profile control, since the general shape of the current profile can be easily manipulated by the transformer, at least transiently. Thus, a natural extension of the existing magnetic control systems (plasma current, shape and position control using the PF coil system) is to add the control of the magnetic field structure inside the plasma using the transformer primary coil. The scheme will be particularly useful for the start up and termination phases of future pulsed reactors such as ITER, of ignition designs relying on a fast plasma current ramp, such as Ignitor, as well as of present day tokamak research facilities.

To test these ideas, we have designed and developed a control system on TCV. Two main objectives have guided the design. First the wish to regulate or control the plasma current, inductance or any other current profile related variable with a control law as independent as possible of the machine model parameters, so the design can easily be applied to any tokamak. Second, the possibility to use the full capability of the OH coil power supplies using a switching control law. We have used a non-linear control strategy known as sliding mode control because it fulfils these two main requirements.

First system tests have been very encouraging; internal inductance has been controlled for the whole pulse by acting directly on the OH coil voltage, starting from as early as 30 ms after plasma breakdown.

The resulting control architecture is simple enough to be implemented in any present or future reactor with a standard set of magnetic sensors, so it has the potential to become a routine and standard control system with the same rank as plasma current, position or shape control.

Local Helicity Injection Startup and Edge Stability Studies in the Pegasus Toroidal Experiment

A. Redd¹, J. Barr¹, M. Bongard¹, M. G. Burke¹, R. Fonck¹, E. Hinson¹,
D. Schlossberg¹, and K. Thome¹

¹ *University of Wisconsin-Madison, Madison, USA*

Corresponding Author: aredd@wisc.edu

Studies on the Pegasus ultralow aspect ratio tokamak are exploring: nonsolenoidal startup using localized helicity injection via edge current injection; and edge peeling mode stability and dynamics. The helicity injection operating space is constrained by helicity injection and dissipation rates and a geometric limit on plasma current. Extrapolation of this technique to other devices requires understanding of the dissipation mechanisms and development of appropriate operating scenarios. To address these issues, the Pegasus program is focused on extending helicity injection startup and growth to ~ 0.3 MA plasma currents and relatively long pulse lengths. In addition to using plasma arc current sources, recent experiments demonstrate the feasibility of using passive electrodes to grow discharges for relatively long pulse lengths. Shaped electrodes serving as current and helicity sources can be optimized with respect to both helicity and relaxation constraints. Bursts of MHD activity are observed during helicity injection, and correlate with rapid equilibrium changes, including inward motion of the magnetic axis and redistribution of the toroidal current. Internal magnetic measurements show the creation of a poloidal null prior to the formation of a tokamak-like equilibrium, and the redistribution of current into the core region as the plasma evolves. The MHD activity results in strong ion heating, with ion temperatures ~ 1 keV observed. The plasma arc injector impedance is consistent with a double-layer sheath at the extraction aperture. The increasing understanding developed in these studies support scalability of the helicity injection technique to large devices. Operation at near-unity aspect ratio with high plasma current relative to the toroidal field allows study of peeling modes, a cause of Edge Localized Modes (ELMs) in larger devices. Peeling modes in Pegasus appear as coherent edge-localized electromagnetic activity with low toroidal mode numbers and high poloidal mode numbers. Internal magnetics and fast framing images show the formation of current-carrying field-following filamentary structures, which briefly accelerate radially, detach from the plasma, and propagate radially at a constant velocity. The filaments acceleration and propagation velocity all correspond to the predictions of electromagnetic blob theory.

EX-P

Wall Conditioning and Density Control in the Reversed Field Pinch RFX-mod

M. E. Puiatti¹, S. Dal Bello¹

¹*Consorzio RFX, Padova, Italy*

Corresponding Author: mariaester.puiatti@igi.cnr.it

In the Reversed Field Pinch RFX-mod at the highest plasma current of 2 MA, when error fields are not effectively feedback controlled, localized thermal loads up to tenths of MW/m² can be produced. To withstand such high power loads, the first wall is covered by graphite tiles. As a drawback, due to the high H retention of the graphite, the density control is extremely difficult. Consequently, various wall conditioning techniques have been optimized in the last campaigns and are discussed in the present contribution, including wall lithization and boronization in combination with He Glow Discharge Cleaning (GDC). The cleaning procedure by GDC has been optimized with dedicated experiments, identifying the conditions of better uniformity and effectiveness. Wall boronisation has been carried out by diborane glow discharges of different duration with samples exposed and analyzed to study the uniformity, thickness, erosion and redeposition of Boron. A relevant carbon content has been found in the redeposited layer, consistent with an only halved carbon influx after boronization. Lithium conditioning has been applied; the total amount of evaporated Li is about 15 g. Main results are:

1. with a lithized wall a much better density control is obtained and recycling is lowered;
2. impurity influxes do not show significant differences when comparing discharges after GDC wall conditioning and after lithization, consistently with a low impurity content in all conditions;
3. at Greenwald fraction less than 0.2 density profiles with lithized wall are more peaked than with carbon wall;
4. higher densities up to $n/n_G \approx 0.5$ can be produced in a controlled way with a lithized wall, but with a very high rate of feeding, resulting in hollow density profiles;
5. Li evaporation is effective in covering about one half of the machine surface. In the next future, lithization experiments by a multipellet injector are planned, aiming at a more uniform Li deposition.

In summary, lithization has clear operational advantages, but requires long pre-treatments to extract the H saturating the graphite. On this basis, an activity is in progress to study the possibility of changing the present carbon wall with a metallic (W) one.

Effect of Lithium Coating on Edge Particle Recycling in EAST H-mode Discharge

L. Zhang¹, G. Xu¹, W. Gao¹, Z. Sun¹, Y. Li¹, J. Li¹, M. Jiang¹, Z. Wu¹, J. Hu¹,
X. Gong¹, L. Hu¹, and H. Guo¹

¹*Institute of Plasma Physics, Chinese Academy of Sciences, Hefei, China*

Corresponding Author: zhangling@ipp.ac.cn

During the last EAST campaign, the lithium coating on the graphite plasma facing components (PFC) became a routine wall conditioning technique, which was applied by evaporation assisted by helium or deuterium glow-discharge cleaning (GDC) or ion cyclotron radio frequency (ICRF), and real-time lithium powder injection. Two ovens were used to thermally evaporate nearly 1 kg of lithium in EAST over a significant fraction of the PFC, and about 40 g lithium powder were injected into the plasma by a lithium dropper. From the late-mid period of this campaign, the lithium evaporation was performed everyday with amount of about 13 g. With progressively increasing lithium coating, the gas puffing rate was gradually increased because of the strong pumping capacity of the lithium coating. As a result, the ratio of hydrogen to deuterium concentrations $H/(D+H)$ was gradually reduced approximately from 40% to 5% with deuterium gas fuelling until the amount of deposited lithium accumulated to 50 g, which greatly improved the ICRF heating efficiency. Note that the lowest hydrogen concentration achieved previously without lithium coating was about 15% in helium discharges.

An absolutely calibrated photodiode array (PDA) with D_α filter viewing the lower divertor was used to investigate the neutral particle flux profile and estimate the neutral density. It was found that just prior to the L-H transition and during the H mode, the recycling peaked at the strike point, which showed that the neutral particle recycling predominately arose from the ion flux at the divertor plate. With increasing lithium accumulation, the neutral deuterium density near the lower X-point was reduced by a factor of 4 (from $\sim 20 \times 10^{16} \text{ m}^{-3}$ to $\sim 5 \times 10^{16} \text{ m}^{-3}$), and this was correlated with a gradual reduction in the low hybrid wave (LHW) heating power needed to access the H mode, i.e., down to $\sim 0.4 \text{ MW}$ for the shots with only LHW as auxiliary heating. It appears, hence, that the neutral particle density near the lower X-point might play a key role on the L-H transition. It is postulated that wall conditioning may affect confinement, e.g., via neutral-ion charge-exchange momentum losses, which may affect radial electric field and turbulent transport. The effect of lithium coating on edge recycling (such as by forming LiD) and its impact on plasma confinement will be further investigated in the future.

EX-P

Assessment of Tungsten Nano-tendrils Growth in the Alcator C-Mod Divertor

G. Wright¹, D. Brunner¹, M. Baldwin², R. Doerner², B. LaBombard¹, B. Lipschultz¹, J. Terry¹, and D. Whyte¹

¹MIT, Cambridge, USA

²University of California San Diego, La Jolla, USA

Corresponding Author: wright@psfc.mit.edu

The conditions for the growth of tungsten (W) or molybdenum (Mo) nano-tendrils have been well defined in linear plasma devices (helium plasma, $T_s > 1000\text{K}$, $E_{\text{He}^+} > 20\text{ eV}$). We have exploited the high power density in Alcator C-Mod to successfully grow W nano-tendrils on a Langmuir probe (ramped approximately 11 degrees into the parallel plasma flux) in the lower divertor during a single run day, demonstrating for the first time that these nano-tendril structures can be grown in a tokamak divertor. Scanning electron microscopy and focused ion beam cross-sectioning shows a $600 \pm 150\text{ nm}$ thick nano-tendril layer on the surface of the W Langmuir probe after approximately 15 seconds of accumulated growth time. This layer thickness is in agreement with calculations using a preliminary empirical growth formula proposed by Baldwin *et al.*[1]. The W nano-tendrils show no sign of melting despite receiving surface heat fluxes of approximately 35 MW/m^2 and three full current (900 kA) plasma disruptions during the growth sequence. There is also no indication of unipolar arcing from the nano-tendrils. Sputtering calculations show that sputtering is playing a minor role in nano-tendril growth on the W surfaces. However, strong sputtering is likely inhibiting nano-tendril growth on nearby Mo surfaces that received heat fluxes of 10 MW/m^2 and achieved surface temperatures $> 1000\text{ K}$ but showed no indications of nano-tendril growth. Having shown that these nano-tendrils can form in a tokamak divertor and given that the key growth conditions are met in an all-W ITER divertor during operation in He or the DT phase, there is a strong need to understand how other plasma conditions not re-created in this work, such as ELMs and impurity seeding, can affect growth and how these nano-tendril layers can impact plasma-material interactions and tokamak operations.

References

[1] M. J. Baldwin, R. P. Doerner, Nucl. Fusion **48** (2008) 035001.

This work is supported by US DOE award DE-SC00-02060 and US DOE contract DE-FC02-99ER54512.

Longterm Evolution of the Impurity Composition and Transient Impurity Events with the ITER-like Wall at JET

J. W. Coenen¹, S. Brezinsek¹, M. Clever¹, I. Coffey², R. Dux³, M. Groth⁴, A. Huber¹, D. Ivanova⁵, K. Krieger³, K. Lawson⁶, S. Marsen³, A. Meigs⁶, R. Neu³, G. van Rooij⁵, M. Sertoli³, and M. Stamp⁶

¹*Forschungszentrum Jülich GmbH, Jülich, Germany*

²*Astrophysics Research Centre, Queen's University, Belfast, UK*

³*Max-Planck Institut für Plasmaphysik, Garching, Germany*

⁴*Aalto University, Espoo, Finland*

⁵*Royal Institute of Technology, Stockholm, Sweden*

⁶*Culham Center for Fusion Energy, Abingdon, UK*

Corresponding Author: j.w.coenen@fz-juelich.de

In ITER a beryllium (Be) first-wall and a tungsten (W) divertor withstanding high heat-flux area are planned to be used. This contribution focuses on the evolution of impurities during the recent campaigns in JET with the ITER-like wall (ILW) their sources as well as material migration and possible implication for plasma operation due to spurious impurity events. The evolution of Be, W and carbon (C) as well as other trace elements was investigated by in-situ measurements with optical spectroscopy.

For Be experimental results confirm the generally observed migration pattern in devices with lower single null configuration characterized by the main chamber wall and outer divertor as areas subject to net erosion of plasma exposed surfaces and migration of eroded material predominantly to the inner divertor. The characteristic time scale for the main wall Be source reaching steady state was found to be ~ 100 s.

The C influx from the divertor decreased by a factor 4 in the first 2000 plasmas seconds, and stayed almost constant since then in comparable weekly performed monitoring discharges. Dedicated CFC/ILW comparison discharges in L-mode revealed a reduction of the CII emission in the outer divertor leg of about a factor 5 – 10. Trace impurities such as oxygen (O) and argon (Ar) are mainly observed via high ionization stages in the main plasma as local spectroscopy shows O and Ar only in minor quantities. Oxygen was observed to be decreasing significantly (factor ~ 7) during the initial operation (120 pulses) while long breaks such as weekends lead to a re-appearance, which is overcome after ~ 3 plasma discharges reaching a low steady state level. Compared to the CFC operation of JET the steady oxygen levels decreased by a factor of 3 – 10 due to Be acting as an oxygen getter. Dedicated experiments on W sputtering have been performed during ICRH heated L-modes as well as low-power H-Modes. The W erosion flux is determined by spectroscopy of W/W^+ evolving along timescales comparable to Be.

Initially irregular impurity events occurred during all plasma scenarios, but the frequency decreased strongly with operational time. These events, probably small particles or dust, occur with a typically rise time of ms and lead to a long lasting increase ($\sim s$) in radiated power. The observed radiation is mainly due to iron, nickel and tungsten.

EX-P

Characterization of Tungsten Sputtering in the JET Divertor

G. van Rooij¹, J. W. Coenen², M. Beurskens⁵, S. Brezinsek², M. Clever², R. Dux³,
C. Giroud⁵, M. Groth⁴, K. Krieger³, S. Marsen³, G. Matthews⁵, G. Maddison⁵,
A. Meigs⁵, R. Neu³, T. Pütterich³, G. Sips⁶, M. Stamp⁵, W. Vijvers⁷, and P. de Vries¹

¹*Dutch Institute for Fundamental Energy Research, Nijmegen, Netherlands*

²*Forschungszentrum Jülich GmbH, Jülich, Germany*

³*Max-Planck-Institut für Plasmaphysik, EURATOM Association, Garching, Germany*

⁴*Aalto University, Espoo, Finland*

⁵*CCFE, Abingdon, UK*

⁶*European Commission, Brussels, Belgium*

⁷*École Polytechnique Fédérale de Lausanne, Lausanne, Switzerland*

Corresponding Author: g.j.vanrooij@diffier.nl

The current design of ITER projects tungsten (W) as plasma-facing components (PFCs) in the divertor for its active phase. The physical sputtering of W by impurities is an important issue, in particular when extrinsic impurities are seeded. It may compromise the life time of the PFCs as well as cause deterioration of the fusion performance by radiation due to unduly high W concentrations in the centre. In this contribution, we utilize the present ITER-like Wall (ILW) at JET to gain insight into ITER-relevant aspects of divertor W erosion such as impurity flux density, charge state and impact energy. A systematic spectroscopic study of L-mode and H-mode discharges with auxiliary heating by RF or NBI was performed using various W and W⁺ spectral lines to quantify the W source strength at the solid tungsten outer divertor target subject to the local plasma conditions. The results demonstrate that Be is the main sputtering species for unseeded discharges and causes in L-mode at divertor temperatures between 20 and 40 eV a total W sputtering flux in the range of $1 - 5 \times 10^{-18} \text{ s}^{-1}$ in the outer divertor. The inter ELM sputtering in H-mode was in the same range but (based on an example with 13 MW NBI heating, $7.5 \times 10^{-19} \text{ m}^{-3}$ line averaged density, 10 Hz ELMs) typically more than a factor of 5 lower than the sputtering due to ELMs. Sawteeth were observed to increase the divertor Be content and therewith the W sputtering by up to an order of magnitude. The W sputtering decreased to below the detection limit ($\sim 1 \times 10^{-17} \text{ s}^{-1}$) at semi-detached conditions.

Cooling Characteristics and Mitigation of He-Defected Tungsten with Nanostructure Formation

S. Takamura¹, T. Miyamoto¹, and N. Ohno²

¹*Faculty of Engineering, Aichi Institute of Technology, Toyota, Japan*

²*Graduate School of Engineering, Nagoya University, Nagoya, Japan*

Corresponding Author: takamura@aitech.ac.jp

The surface cooling mechanisms (mainly, decrease in secondary electron emission (SEE) and increase in radiation emissivity) of nanostructured tungsten (W) are summarized comprehensively. Recovery of He-defected W towards flat surface is demonstrated as well as the suppression of nanostructure formation by covering the surface with carbon thin film. The key factor for physical mechanism of nanostructure formation is given by comparing the surface temperature ranges for W (1000 – 1500K) and tantalum (Ta) (< 900K).

In Vessel Fuel Inventory Build-up in Tokamaks: Lessons Learnt from Tore Supra

E. Tsitrone¹, B. Pégourié¹, S. Panayotis¹, Y. Marandet², C. Brosset¹, J. Bucalossi¹,
T. Dittmar¹, E. Gauthier¹, P. Languille¹, F. Linez³, T. Loarer¹, J. Y. Pascal¹,
C. Martin², and P. Roubin²

¹CEA, IRFM, Saint-Paul-lez-Durance, France

²CNRS/Université de Provence, Centre de St-Jérôme, Marseille, France

³CNRS/Université de Provence, Orléans, France

Corresponding Author: emmanuelle.tsitrone@cea.fr

For next step fusion devices, fuel retention by the vessel walls is a crucial issue, as the tritium inventory will be limited for safety reasons. The rate at which the in vessel fuel inventory builds up will have a strong impact on the device operation, as it determines the number of discharges allowed before reaching the tritium safety limit and the frequency of shutdowns eventually needed for plasma facing components (PFC) detritiation processes. Extensive studies performed on Tore Supra have allowed to gain a global view on these issues, taking advantage of the long pulse capability of the device to cumulate ITER relevant particle fluence on PFC within a reasonable operation time. This paper presents an overview of the results obtained in terms of fuel retention under long pulse operation in Tore Supra, showing a consolidated carbon and deuterium balance. In particular, the critical importance of taking into account long term outgassing between discharges when assessing fuel inventory build up over long periods is outlined. This result is based on the recent extension of the analysis carried out in terms of fuel retention and carbon balance for a dedicated wall inventory campaign in 2007 to the full period preceding the extraction of in vessel samples for post mortem analysis (2001-2007). Special care was taken to assess the amount of deuterium outgassed during the nights and weekends of the experimental campaigns and during vents. In particular, dedicated experiments have been performed during the last Tore Supra vent to estimate the deuterium recovered during the process. While the impact of vents is rather moderate, it is shown that the outgassing during nights and weekends is the main process that reconciles both the post mortem and gas balance estimates of fuel retention as well as the coupled carbon-deuterium balance. Results from Tore Supra and present day devices are extrapolated to derive estimates of the fuel inventory build up in ITER over an experimental campaign, for different wall materials options and taking into account different operational scenario. In particular, the potential impact of long term outgassing on the fuel inventory build up is assessed, showing that it remains modest for high fuel uptake during plasma/high repetition rate of discharges, while it can play a significant role for lower fuel uptake/lower repetition rate.

Impact of Arcing on Carbon and Tungsten: from the Observations in JT-60U, LHD, and NAGDIS-II

S. Kajita¹, M. Tokitani², M. Fukumoto³, T. Nakano³, S. Masuzaki², N. Ohno⁴,
S. Takamura⁵, N. Yoshida⁶, and Y. Ueda⁷

¹*EcoTopia Science Institute, Nagoya University, Nagoya, Japan*

²*National Institute for Fusion Science, Toki, Japan*

³*JAEA, Ibaraki, Japan*

⁴*Graduate School of Engineering, Nagoya University, Nagoya, Japan*

⁵*Aichi Institute of Technology, Toyota, Japan*

⁶*Research Institute for Applied Mechanics, Kyushu University, Fukuoka, Japan*

⁷*Graduate School of Engineering, Osaka University, Osaka, Japan*

Corresponding Author: kajita@ees.nagoya-u.ac.jp

Arcing is a long standing plasma-surface interaction issue, and the issue is being revived recently. This paper gives warning on the impact of arcing in fusion devices based on the observations in JT-60U, LHD, and the linear divertor simulator NAGDIS-II. From the analysis of arc trails on carbon baffle plate of JT-60U using a laser scanning microscope, it was found that eroded depth was several tens of micrometers in some parts, where the deposited layer seemed to be peeled off. Comparing the erosion by arcing to that by sputtering, it was thought that the arcing cannot surpass the sputtering for carbon based material unless arcing is initiated very frequently. In NAGDIS-II, the demonstration experiments of arcing/unipolar arcing have been conducted. In future fusion devices including ITER, materials are exposed to helium ions. In NAGDIS-II, the nanostructure tungsten exposed to helium plasma was used for the experiments. A pulsed laser ($\lambda = 694.7$ nm) was used to mimic the transient heat load while the sample was exposed to the helium plasma. The pulse width was approximately 0.5 ms, which was similar to the Type-I ELMs. From the experiments in NAGDIS-II, the necessary averaged laser pulse energy to ignite arcing was approximately 0.01 MJm^{-2} when the nanostructure was formed on the surface by the helium plasma irradiation. Even taking into account the spikes of the laser pulse, the necessary energy to ignite arcing seemed more than one order of magnitude lower than the mitigated type-I ELMs in ITER such as 0.5 MJm^{-2} . Thus, it raises a concern that the arcing is also triggered by small plasma heat load due to the type-II or type-III ELMs in ITER if the nanostructures are formed on the surface. The nanostructured tungsten, which was fabricated in NAGDIS, was exposed to the LHD divertor plasma for 2 s. After the exposure to the LHD plasma, interestingly, the arcing was initiated even without any transient events, supporting the view that the arcing is easily initiated on the nanostructured tungsten surface. The erosion of tungsten by arcing will become an important issue in a fusion reactor, where helium fluence is significantly increased.

EX-P

Overview of the International Research on Ion Cyclotron Wall Conditioning

D. Douai¹, T. Wauters², A. Lysoivan², V. Philipps³, V. Rohde⁴, S. H. Hong⁵, N. Ashikawa⁶, V. Bobkov⁴, S. Brémond¹, S. Brezinsek³, M. Graham⁷, E. Joffrin¹, G. Lombard¹, S. H. Kim⁵, A. Kreter³, M. L. Mayoral⁷, J. M. Noterdaeme^{4,8}, J. Ongena², B. Pégourié¹, R. Pitts⁹, G. Sergienko³, M. Shimada⁹, and S. J. Wang⁵

¹CEA, IRFM, St. Paul lez Durance, France

²LPP-ERM/KMS, Association Euratom-Belgian State, Brussels, Belgium

³FZJ/ Institut für Energieforschung - Plasmaphysik, Jülich, Germany

⁴Max-Planck-Institut für Plasmaphysik, Garching, Germany

⁵National Fusion Research Institute, Daejeon, Republic of Korea

⁶National Institute for Fusion Science, Toki, Japan

⁷CCFE, Culham Science Centre, Abingdon, UK

⁸Gent University, EESA Department, Gent, Belgium

⁹ITER Organization, St. Paul lez Durance, France

Corresponding Author: david.douai@cea.fr

This paper gives an overview of the experimental and modeling activity on Ion Cyclotron Wall Conditioning (ICWC), which is currently coordinated by the ITPA Scrape-Off-Layer & Divertor Topical Group, in order to assess the applicability of this technique for ITER for recovery from disruptions, vent or air leak, recycling control and mitigation of the tritium inventory build-up. Experimental results obtained on TORE SUPRA, TEXTOR, ASDEX-Upgrade, JET, KSTAR and LHD are presented. The conditions for safely producing RF plasmas with conventional ICRH antennas have been carefully investigated. Discharge homogeneity has been improved by adding a small poloidal component to the toroidal field. The use of pulsed discharges allows mitigating re-implantation of wall desorbed particles reionized in the ICWC discharge. A 0-D model of ICWC plasmas in He and H₂ has been developed which reproduces wall density, neutral and ion fluxes determined experimentally. Experimental observations in carbon devices and modelling seem to indicate that ICWC plasmas interact preferentially with transient reservoirs in carbon rather than in co-deposited layers. The found fuel removal rates are extrapolated to ITER, but it is pointed that efficiency will decrease with ICWC operation time.

Efficiency of Fuel Removal: Overview of Techniques Tested on Plasma-Facing Components from the TEXTOR Tokamak

M. Rubel¹, V. Philipps², A. Huber², D. Ivanova¹, P. Petersson¹, B. Schweer², and M. Zlobinski²

¹*Royal Institute of Technology (KTH), Association EURATOM-VR, Stockholm, Sweden*

²*Forschungszentrum Jülich, Association Euratom - FZJ, Jülich, Germany*

Corresponding Author: rubel@kth.se

Curtailing of long-term fuel inventory in plasma-facing components (PFC) is one of the most critical and challenging issues to be resolved in order to ensure safe and economically viable operation of a reactor, especially if the use of carbon target plates is considered. This paper provides an overview of results obtained with thermal, photonic, oxidative and plasma-assisted fuel removal processes studied on PFC and probes from the TEXTOR tokamak: graphite and metal (steel or tungsten) substrates. Comparative experiments were also carried out in laboratory devices. Three aspects have been taken into account in the assessment of each approach: efficiency of removal of fuel and co-deposits, effect on the surface condition of the PFC and dust formation caused by destruction and disintegration of co-deposits. To control the gas phase and surface morphology during subsequent stages of treatment a set of analysis techniques was used: e.g., thermal desorption spectrometry, optical and X-ray spectroscopy, ion beam analysis and microscopy. The main results are:

1. Oxidative methods remove fuel and carbon but the rate strongly depends on the overall film composition; the presence of non-volatile impurities (B, Si, metals) slows the process.
2. Nitrogen-assisted discharges do not lead to a noticeable fuel removal.
3. Desorption at 623K, i.e., at the maximum baking temperature of the ITER divertor, removes only 15% of hydrogenic species. Effective fuel release requires heating above 850 – 900K, but baking at such conditions results in cracking and peeling-off of co-deposits thus leading to the dust formation. The same is observed under oxidation at that temperature level.
4. Laser-induced ablation generates large amount of dust which may still contain substantial amount of fuel. The irradiation may result in substrate damage.
5. Efficient local fuel release from C layers occurs with low-power laser-induced desorption.

The ongoing study shows that no single method alone would provide solution to efficient fuel removal especially from shadowed regions in a reactor. The whole activity indicates that hybrid scenario, involving mechanical methods and hovering of dust, would be needed to reduce fuel inventory. Fuel re-absorption by depleted layers is also now examined.

EX-P

Measurements of Net versus Gross Erosion of Molybdenum Divertor Surface in DIII-D

D. L. Rudakov¹, P. C. Stangeby², N. H. Brooks³, W. R. Wampler⁴, J. N. Brooks⁵,
D. N. Buchenauer⁶, J. D. Elder², M. Fenstermacher⁷, C. J. Lasnier⁷, A. W. Leonard³,
A. G. McLean⁷, R. A. Moyer¹, A. Okamoto⁸, J. G. Watkins⁴, and C. P. Wong³

¹ *University of California San Diego, La Jolla, USA*

² *University of Toronto Institute for Aerospace Studies, Toronto, Canada*

³ *General Atomics, San Diego, USA*

⁴ *Sandia National Laboratories, Albuquerque, USA*

⁵ *Purdue University, West Lafayette, USA*

⁶ *Sandia National Laboratories, Livermore, USA*

⁷ *Lawrence Livermore National Laboratory, Livermore, USA*

⁸ *Tohoku University, Sendai, Japan*

Corresponding Author: rudakov@fusion.gat.com

EX-P

We report the first measurements of post-exposure net erosion and in-situ gross erosion of molybdenum under controlled, well-diagnosed plasma conditions in a tokamak divertor. Net erosion rate of 0.40 ± 0.04 nm/s was measured on a molybdenum sample exposed to the divertor plasma in the DIII-D tokamak using the Divertor Material Evaluation System (DiMES). A silicon disk 1 cm in diameter coated with a 24 nm thick film of Mo and mounted in a graphite DiMES holder in the lower divertor of DIII D was exposed in a series of 7 reproducible lower single null L-mode plasma discharges. The exposure was performed near the attached outer strike point (OSP) for a total flattop time of ~ 28 s. The plasma density and temperature near the OSP, measured by the divertor Langmuir probes, were $n_e = 1.3 - 1.5 \times 10^{19} \text{ m}^{-3}$, $T_e = 25 - 30$ eV. An upper bound estimate of the average gross erosion rate of 3.75 nm/s was inferred from spectroscopic measurements using an absolutely calibrated CCD camera with MoI filter centered around 390 nm and having a bandwidth of ~ 10 nm. Net erosion of Mo was measured by comparing the Mo layer thickness measured by Rutherford backscattering (RBS) before and after the exposure. The reduction of Mo thickness was 11 ± 1 nm, corresponding to an average net erosion rate of 0.40 ± 0.04 nm/s i.e., significantly smaller than the gross erosion rate measured by the camera. This result is consistent with theory/computational expectations of high local redeposition. The distribution of Mo redeposited on the graphite holder was measured by RBS. As expected, Mo deposits were concentrated near the Mo-coated sample edge, with an e-folding length of ~ 2 mm. The total amount of Mo found on the holder was only $\sim 20\%$ of the net amount of Mo eroded from the sample, possibly due to high re-sputtering and further transport of deposited Mo from the graphite surface. Plasma density and temperature profiles from divertor Langmuir probes around the radial location of the sample are used as input to detailed modeling of erosion/redeposition using the REDEP/WBC code package + OEDGE code combination, currently in progress.

This work was supported in part by the US Department of Energy under DE-FG02-07ER54917, DE-FC02-04ER54698, DE-AC04-94AL85000 and DE-AC52-07NA27344.

Effect of Changes in Separatrix Magnetic Geometry on Divertor Behavior in DIII-D

T. W. Petrie¹, J. Canik², A. W. Leonard¹, M. A. Mahdavi¹, J. G. Watkins³,
R. J. Buttery¹, M. E. Fenstermacher⁴, J. R. Ferron¹, R. J. Groebner¹, D. N. Hill⁴,
A. W. Hyatt¹, C. T. Holcomb⁴, C. J. Lasnier⁴, T. C. Luce¹, R. A. Moyer⁵, and
P. C. Stangeby⁶

¹General Atomics, San Diego, USA

²Oak Ridge National Laboratory, Oak Ridge, USA

³Sandia National Laboratories, Albuquerque, USA

⁴Lawrence Livermore National Laboratory, Livermore, USA

⁵University of California San Diego, La Jolla, USA

⁶University of Toronto, Toronto, USA

Corresponding Author: petrie@fusion.gat.com

We report results and interpretation of recent experiments on DIII-D designed to evaluate divertor geometries favorable for radiative heat dispersal. Two approaches studied involved lengthening the parallel connection in the scrape-off layer (SOL), L_{\parallel} , and increasing the radius of outer divertor target, R_{TAR} , with the goal of reducing target temperature, T_{TAR} , and increasing n_{TAR} . Based on 1-D two-point modeling:

$$n_{\text{TAR}} \propto [R_{\text{TAR}}]^2 [L_{\parallel}]^{6/7} [n_{\text{SEP}}]^3 \quad (1)$$

and

$$T_{\text{TAR}} \propto [R_{\text{TAR}}]^{-2} [L_{\parallel}]^{-4/7} [n_{\text{SEP}}]^{-2}, \quad (2)$$

where n_{SEP} is the midplane separatrix density. These scalings suggest that conditions conducive to a radiative divertor solution can be achieved at low n_{SEP} by increasing either R_{TAR} or L_{\parallel} . While our data are consistent with the above L_{\parallel} scalings, the observed scalings on R_{TAR} displayed a more complex behavior, under certain conditions deviating from the above scalings. Our analysis indicates that deviations from the R_{TAR} scaling were due to the presence of convected heat flux, driven by escaping neutrals, in the more open configurations of the larger R_{TAR} cases. Modeling with the SOLPS code support the postulate that even small differences in the divertor geometry can change the divertor neutral trapping sufficiently to explain some of the discrepancy between experiment and two-point model predictions. When similar recycling conditions were maintained, as during a sweep over a more limited range, much of the expected dependence of and on was largely recovered. Our results also show that a significant fraction of the radiated power can be dissipated along the extended, outer divertor leg at higher density when the leg was attached, e.g., $P_{\text{RAD,OD}}/P_{\text{RAD,TOT}} \approx 0.3 - 0.4$ with $q_{95} = 4 - 5$. Our study includes both L-mode and H-mode plasmas. The ion $\mathbf{B} \times \nabla \mathbf{B}$ drift is directed toward the X-point for both cases, and the collisionalities in the SOL straddle the conduction and sheath-limited regimes. Variation in poloidal length of the outer divertor leg was 25 – 75 cm and variation in radial placement of the outer divertor separatrix was 1.2 m to 1.7 m. The results of this study are relevant to some key tenets of divertor configurations with extended outer divertor legs, e.g., the isolated divertor.

This work was supported by the US DOE under DE-FC02-04ER54698, DE-AC05-00OR22725, DE-AC04-94AL85000, DE-AC52-07NA27344, and DE-FG02-07ER54917.

Characterization of Particle and Power Loads on Divertor Targets for Type-I, Type-III, and Mossy ELMy H-modes in EAST Superconducting Tokamak

L. Wang¹, G. Xu¹, H. Guo¹, B. Wan¹, X. Gong¹, S. Liu¹, H. Wang¹, K. Gan¹,
F. Wang¹, N. Yan^{1,2}, W. Zhang¹, M. Jiang¹, P. Liu¹, L. Chen¹, R. Chen¹, H. Xiong³,
L. Shao¹, D. S. Wang^{1,3}, X. Gao¹, Z. Wu¹, and G. Luo³

¹*Institute of Plasma Physics, Chinese Academy of Sciences (ASIPP), Hefei, China*

²*Association Euratom-Risø DTU, Roskilde, Denmark*

³*Department of Modern Physics, USTC, Hefei, China*

Corresponding Author: wliang@ipp.ac.cn

The ELM-resolved particle and power loads on divertor targets were studied in a wide range of discharge conditions in the EAST superconducting tokamak, mainly using divertor triple Langmuir probe (DTLP) arrays embedded in the target plates, along with infrared (IR) camera and other key divertor diagnostics. The target particle and power loads for type-I, type-III and mossy ELMy H-mode plasmas are investigated, respectively. The experiments were performed with lower hybrid current drive (LHCD) alone or combined with ion cyclotron resonance heating (ICRH), with Lithium wall coatings. For a typical type-I ELM in EAST, the divertor heat load is about 10% the plasma stored energy, while it is about 1–2% for a typical type-III ELM in EAST. The mossy ELMs induce even less change to the plasma stored energy, i.e., $\sim 0.1\%$. The peak heat fluxes on the divertor targets for mossy, type-III and type-I ELMs are characteristically $\sim 0.1 \text{ MW/m}^2$, $\sim 2 \text{ MW/m}^2$ and $\sim 10 \text{ MW/m}^2$, respectively. The mossy ELMy H-mode in EAST may provide a potential scenario for ITER. In the present ongoing campaign of EAST, mossy ELMy H-mode duration has been lengthened to 1 s with LHCD+ICRH, which is only limited by ICRH pulse length and may be readily extended to longer values. In an ELM-free period, the power deposition obtained from DTLPs was compared to that from IR camera, which is not ELM-resolved at present. And the results of the two cross diagnostics are comparable. Statistically, the frequencies for mossy, type-III, and type-I ELMs are 1–2 kHz, 200–800 Hz, and $< 100 \text{ Hz}$. During both type-I and type-III ELM phases, the SOL width and plasma-wetted area on divertor targets broaden insignificantly, compared to that between ELMs. This insignificant broadening is independent of the auxiliary heating technique. The mid-plane SOL width for type-III ELMs in EAST is $\sim 8–15 \text{ mm}$, being different to that during type-I ELMs. The divertor in-out asymmetry during both type-III and type-I ELMs has also been studied. For type-III ELMs, divertor plasmas favor the outboard target in LSN, which exhibits an even stronger in-out divertor asymmetry in DN. Also in the ongoing campaign the fine structure of ELMs, i. e., ELM filaments were observed by DTLPs. The typical interval time between adjacent ELM filaments for type-III ones in EAST is $\sim 150–250 \mu\text{s}$.

Development of Laser Based Techniques for In-situ Characterization of the First Wall in ITER and Future Fusion Devices

V. P. Philipps¹, A. Malaquias², A. Hakola³, G. Maddaluno⁴, P. Gasior⁵, M. Laan⁶,
H. van der Meiden⁷, M. Rubel⁸, S. Almagia⁹, L. Caneve⁹, F. Colao⁹, A. Czarnecka⁵,
N. Gierse¹, A. Huber¹, M. Kubkowska⁵, P. Petersson⁸, B. Schweer¹, and M. Zlobinski¹

¹*Forschungszentrum Jülich, Jülich, Germany*

²*EFDA-CSU/EURATOM-IST, Lisboa, Portugal*

³*EURATOM-TEKES, VTT, Finland*

⁴*EURATOM-ENEA, Roma, Italy*

⁵*EURATOM-IPPLM, Warsaw, Poland*

⁶*EURATOM-TEKES, Tartu, Estonia*

⁷*EURATOM-FOM, Nieuwegein, Netherlands*

⁸*EURATOM-VR, Stockholm, Sweden*

⁹*ENEA UTAPRAD-DIM, Roma, Italy*

Corresponding Author: v.philipps@fz-juelich.de

In situ methods to measure the fuel retention and characterize the material deposition on the wall are highly important for ITER and future fusion devices. Laser-based methods are the most promising candidates (for non-invasive applications) and are being investigated in a cooperative undertaking in various European associations under EFDA coordination.

The work concentrates on laser techniques by which the laser light is guided from outside the biological shield by a mirror system through a window onto special wall areas and on three different laser methods:

1. Laser induced desorption spectroscopy (LIDS) in which ms laser pulses thermally desorb the retained fuel from a wall area of about 1 cm² and the desorbed fuel is spectroscopically detected in the edge of a running plasma.
2. Laser induced ablation spectroscopy (LIAS) in which ns laser pulses ablate a small wall spot and the ablated material together with the incorporated fuel is detected in a similar way as for LIDS.
3. Laser induced breakdown spectroscopy (LIBS) in which ns (or even ps) laser pulses produce a plasma plume which (in proper conditions) emits line radiation being a fingerprint of the chemical composition of the ablated materials in front of the irradiated wall spot.

The aims are to compare the pros and cons of the methods and find an optimized solution for ITER. LIDS and LIAS have been developed to a prototype-like status for ITER application in the TEXTOR tokamak. LIBS has been investigated in several EU associations in dedicated lab experiments with a focus on the particular conditions in ITER, including pilot experiments in the TEXTOR tokamak. To enable a clear and fair quantification of the methods, standard deposits of diamond like carbon (DLC) and mixed W/Al/C (Al mimic Be here) with thicknesses of 2 – 3 μm deposited on rough and polished W substrates with a known D inventory have been prepared by magnetron sputtering and vacuum arc deposition and used as standard samples in these observations.

Approaches towards Steady-State Advanced Divertor Operations on EAST by Active Control of Plasma-Wall Interactions

H. Guo¹, J. Li¹, B. Wan¹, Y. Liang¹, and G. Xu¹

¹*Institute of Plasma Physics, Chinese Academy of Sciences, Hefei, China*

Corresponding Author: hyguo@ipp.ac.cn

EAST will be one of the world's first magnetic confinement devices that must address Plasma-Wall Interaction (PWI) issues facing high power steady-state operations. EAST has recently significantly augmented its RF heating capabilities up to 10 MW, including LHCD and ICRH. It has also undertaken an extensive upgrade during the recent shutdown to replace the carbon tiles on the main chamber wall and divertor surface by the Mo tiles, except those near the strike points, allowing baking up to 250°C, with active water cooling. The divertor tiles will further be upgraded to monoblock Tungsten, as to be used in ITER, to address PWI issues for ITER and DEMO.

EAST demonstrated long pulse operation over 100 s, entirely driven by LHCD during the last experimental campaign. In order to achieve this, the following major means were applied to EAST to actively control PWI interactions:

1. Active divertor pumping using an in-vessel large capacity cryopump for facilitating density control.
2. Advanced wall conditioning with Lithium (Li) evaporation and real-time, in-situ Li powder injection for controlling neutral recycling.
3. Localized divertor gas puffing for reducing peak heat fluxes near the strike points.
4. Strike point sweeping to spread the heat loads on the divertor target plates.

In addition, highly radiative impurity Ar was injected into the divertor to further reduce the peak divertor heat fluxes and mitigate the in-out divertor plasma asymmetries in EAST. Despite the injection of Ar, Z_{eff} in the core plasma was little affected, suggesting strong divertor screening. Ar seeding has also been explored in the newly achieved H-modes in EAST, significantly increasing the frequency and decreasing the amplitude of ELMs, thus reducing the particle and heat loads on the divertor target plates. These first results are very promising, and will further be investigated in EAST for high power, long pulse operations.

EAST has now just started a new experimental campaign with significantly augmented auxiliary heating power and new Mo wall, which will lead to increasing PWI challenges. It will therefore require developing advanced scenarios for divertor heat flux control at high performance in a high- Z metal wall and long pulse operation environment. New advances and issues that may arise will also be presented.

Scaling of the Divertor Heat Flux Width in the DIII-D Tokamak

M. A. Makowski¹, A. W. Leonard², D. Elder³, C. J. Lasnier¹, T. H. Osborne², and P. C. Stangeby³

¹*Lawrence Livermore National Laboratory, Livermore, USA*

²*General Atomics, San Diego, USA*

³*University of Toronto Institute for Aerospace Studies, Toronto, Canada*

Corresponding Author: makowski@fusion.gat.com

DIII-D measurements indicate a systematic narrowing of the divertor heat flux width λ_q with plasma current in H-mode plasmas and significantly weaker dependence on other parameters. Comparisons of λ_q with upstream SOL profiles indicate a similar variation, consistent with expectations from flux-limited transport. The inverse dependence of λ_q on plasma current suggests that physics solutions for heat flux control may be more essential in next step devices to reduce the local heat flux below the maximum steady-state heat load sustainable by material surfaces of $\sim 10 \text{ MW/m}^2$. We find that the heat flux profile is well fit by a two-parameter function with one parameter (λ_{pvt}) characterizing the profile in the private flux region and the second (λ_{sol}) characterizing the SOL. The heat flux integral width (integral of the profile divided by its peak value) of this function is a weighted linear sum of these two parameters. The integral width scales inversely with I_p , and has weaker dependencies on other parameters. However, λ_{sol} is found to have a much simpler scaling, depending only on I_p (or equivalently, the poloidal magnetic field B_p). Measurements of upstream n_e and T_e profiles with an upgraded Thomson scattering diagnostic has made it possible to test parallel and radial transport models. The SOL profiles exhibit a narrowing n_e with increasing I_p consistent with the measured divertor heat flux and a flux-limited parallel transport model. The strong dependence of λ_q on B_p suggests two possible physics mechanisms setting the heat flux width. A semi-empirical model based on ion orbit drifts is consistent with the measured heat flux width and the dependence of the SOL n_e profile. A critical pressure gradient model was also tested finding the SOL pressure profile width scaling consistently with a calculation of the ideal ballooning stability limit. A density scan from a low density attached state to a high density detached divertor state revealed SOL profile scale lengths related to the heat flux width for attached conditions. This suggests that the upstream profiles can be used to make inferences about radial transport under detached conditions where the divertor heat flux profile no longer represents the upstream SOL transport.

This work was supported by the US DOE under DE-FC02-04ER54698 and DE-AC52-07NA27344.

EX-P

MAST Contributions to the Exhaust Challenge, Including Testing of Super-X

G. Fishpool¹, S. Allan¹, J. Canik², S. Elmore^{1,3}, W. Fundamenski¹, A. Kirk¹, J. Harrison¹, E. Havlickova¹, F. Militello¹, P. Molchanov⁴, V. Rozhansky⁴, and A. Thornton¹

¹*EURATOM/CCFE Fusion Association, Culham Science Centre, Abingdon, UK*

²*Oak Ridge National Laboratory, Oak Ridge, USA*

³*Department of Electrical Engineering and Electronics, University of Liverpool, Liverpool, UK*

⁴*St. Petersburg State Polytechnical University, St. Petersburg, Russia*

Corresponding Author: geoff.fishpool@ccfe.ac.uk

Developing an effective technical solution for handling plasma exhaust is a key part of designing DEMO. Over the last two years, the exhaust has been actively studied in MAST experiments, and in the analysis and design work for the upgrade project. This paper reports on recent experiments, and on the design of the upgraded divertor; with its capability of exploring the Super-X configuration.

The upgrade features great flexibility in the length and expansion of the low-field-side divertor legs, within chambers that are well closed off from the main chamber. The recent experiments have extended the characterisation of the present, open, MAST divertor, for direct comparison with results from the upgrade. Target profiles are measured with Langmuir probes and IR thermography. The density limit has been explored as a function of fuelling location and plasma current. Detachment of the inner leg of a single null configuration has been studied.

For the first time, a fixed retarding field energy analyser has been used to measure the ion temperatures in the divertor of a tokamak. A similar device has been exposed to the upstream plasma. These measurements are used to constrain SOLPS modelling.

A series of experiments has investigated the ability of massive gas injection to control the transient heat loads to the divertor during disruptions. An upgrade to the disruption mitigation valve system has been used with a selection of gases to study the effects of impurity mass and injection quantity. Investigation has shown that the most effective mitigation is seen for high mass ($Z > 4$) impurities which reduce the divertor heat load to 40% of the total stored energy.

Detailed analysis has refined the design of the divertor for the upgrade of MAST. Operational flexibility has been assessed in terms of connection length and flux expansion, thereby specifying the power supply currents, voltages and accuracy of control. Studies have refined the shape of the entrance to the divertor and indicated the potential of Super-X-like geometries. Improvements have been made in the divertor chambers — for active pumping and diagnostic access. Prospects for the experimental programme will be discussed in the paper.

Work supported by the RCUK Energy Programme and EURATOM.

Low Concentration of Iron as First Wall Material in LHD Plasmas with Edge Ergodic Layer

S. Morita^{1,2}, C. Dong¹, M. Kobayashi^{1,2}, M. Goto^{1,2}, I. Murakami¹, E. Wang², N. Ashikawa¹, Z. Cui³, K. Fujii⁴, M. Hasuo⁴, D. Kato¹, F. Koike⁵, S. Masuzaki^{1,2}, H. Sakaue¹, T. Shikama⁴, C. Suzuki¹, N. Yamaguchi⁶, N. Yamamoto⁷, and H. Zhou³

¹National Institute for Fusion Science, Toki, Japan

²Dept. of Fusion Science, Graduate Univ. for Advanced Studies, Toki, Japan

³Southwestern Institute of Physics, Chengdu, China

⁴Dept. of Mechanical Engineering and Science, Kyoto University, Kyoto, Japan

⁵Physics Lab., School of Medicine, Kitasato Univ., Kanagawa, Japan

⁶Physics Lab., Graduate School of Medicine and Pharmaceutical Sciences, Univ. of Toyama, Toyama, Japan

⁷Center of ASSER, Chubu University, Aichi, Japan

Corresponding Author: morita@nifs.ac.jp

Experiments of Large Helical Device (LHD) have been successfully conducted during past 14 years, based on the first wall fully covered with rectangular protection plates made of stainless steel, basically having no serious impurity problem. The impurity behavior of iron has been quantitatively studied with a spectroscopic system newly developed for measuring two-dimensional distribution of extreme-ultraviolet (EUV) impurity lines. The iron density in core plasmas is found to be fairly low, at least five orders of magnitude smaller than the electron density. The highest density of iron is observed during impurity accumulation triggered by pellet injection. The central density of Fe²³⁺ ions analyzed from FeXXIV profile reaches $2.6 \times 10^9 \text{ cm}^{-3}$ during the impurity accumulation phase with appearance of a large inward convective velocity of $V = -6 \text{ m/s}$, whereas it is only $3 \times 10^8 \text{ cm}^{-3}$ before the accumulation occurs. No accumulation is observed for light impurities. The accumulation is mainly caused by the density gradient. These results are very similar to tokamak ones, but only the value of the iron density is different between tokamaks and LHD. The stochastic magnetic field layer of LHD can effectively fulfill its function as the impurity screening in collisional regime of $10 < L_K/L_{ee} < 100$, where L_K is the Kolmogorov length and L_{ee} the electron mean free path. In 3D edge transport simulation the impurity screening is observed in the edge boundary region, where the L_K is nearly 10 m. The iron with slower velocity is ionized at outer region of the stochastic layer where the parallel thermal gradient (i.e., thermal force) is smaller. Therefore, larger values of L_K/L_{ee} for heavier ions like iron enhance the friction force along magnetic field, leading to an efficient impurity screening. In LHD the radiation loss from iron is smaller than 1 MW in usual discharges ($P_{\text{NBI}} = 20\text{--}30 \text{ MW}$), which is often comparable to radiation from carbon originated in divertor plates. These transport processes interacted with magnetic field structure are of primal reason why the density of iron impurity is fairly low in LHD. The screening effect developed in edge stochastic layer intrinsically existing in LHD works well for materials of the first wall. The present result strongly suggests tolerant use of high- Z materials to the first wall of LHD-type reactor.

EX-P

ICRF Operation with Improved Antennas in a Full W-wall ASDEX Upgrade, Status and Developments

V. Bobkov¹, F. Braun¹, R. Dux¹, A. Herrmann¹, H. Faugel¹, H. Fünfgelder¹,
L. Giannone¹, A. Kallenbach¹, M. Kocan¹, H. W. Müller¹, R. Neu¹,
J. M. Noterdaeme^{1,2}, T. Pütterich¹, G. Siegl¹, F. Zeus¹, and H. Zohm¹

¹Max-Planck-Institute für Plasma Physics, Garching, Germany

²Ghent University, EESA Department, Ghent, Belgium

Corresponding Author: bobkov@ipp.mpg.de

Operation of ICRF (Ion Cyclotron Range of Frequencies) antennas in many magnetic fusion experiments is often accompanied by enhanced plasma-wall interactions. These become more problematic in high-Z machines, such as the full tungsten (W) ASDEX Upgrade (AUG), where the W released from the wall during the ICRF operation contributes to radiation losses from the plasma. A significant part of the ICRF-specific plasma-wall interactions in AUG can be attributed to the existence of the parallel component of RF electrical field near antenna E_{\parallel} . This field contributes to elevated sheath potentials which can directly influence the W sputtering. It can also affect as well as depend on the plasma convection in the scrape-off-layer. In AUG, two strategies to establish the compatibility of ICRF antennas with the W wall are being pursued.

The first, long term strategy is based on reduction of the E_{\parallel} field by following the guidelines on antenna design elaborated with the help of finite-elements EM calculations. The experiments with the modified 2-strap antenna have been conducted in 2011. During single antenna ICRF operation at low deuterium injection rates, the modified antenna showed better balance between the central heating and the W source. However, an uncertainty exists whether the observed improvement is caused by the reduced E_{\parallel} , or by influence of the limiter shape on geometry of magnetic field line connections. In order to help to resolve this, a new retarding field analyser was installed in AUG to measure the plasma potential on the field lines connected to the modified antenna. After 2012, two new 3-strap antennas compatible with the 3 dB splitter scheme for ELM-resilient ICRF operation will be installed. The design of these antennas follows the guideline on reduction of E_{\parallel} that utilizes the balance between the π -phased contributions of the image RF currents.

The second, short term strategy on extending the ICRF operational space with the W wall to the low gas injection rate conditions in AUG, makes use of low-Z materials in the vicinity of ICRF antennas. For the coming 2012 experimental campaign, two antennas have thus been equipped with the boron-coated side limiters (50 μm thick coating), which have been previously characterized as the most important W sources during ICRF operation.

Snowflake Divertor as Plasma-Material Interface for Future High Power Density Fusion Devices

V. Soukhanovskii¹, R. E. Bell², S. P. Gerhardt², S. Kaye², E. Kolemen²,
B. P. LeBlanc², E. Meier¹, J. E. Menard², A. G. McLean¹, S. F. Paul²,
T. D. Rognlien¹, D. D. Ryutov¹, F. Scotti², M. V. Umansky¹, D. Battaglia²,
A. Diallo², R. Kaita², R. Maingi³, D. Mueller², M. Podesta², R. Raman⁴, and
A. L. Roquemore²

¹*Lawrence Livermore National Laboratory, Livermore, USA*

²*Princeton Plasma Physics Laboratory, Princeton, USA*

³*Oak Ridge National Laboratory, Oak Ridge, USA*

⁴*University of Washington, Seattle, USA*

Corresponding Author: vlad@llnl.gov

Recent NSTX results demonstrate that the snowflake divertor (SFD) configuration may provide a promising solution for mitigating steady-state and transient divertor heat loads and target plate erosion, and project favorably to future fusion devices. In NSTX, a medium-size spherical tokamak with high divertor heat flux ($q_{\text{peak}} \leq 15 \text{ MW/m}^2$, $q_{\parallel} \leq 200 \text{ MW/m}^2$), steady-state SFD configurations lasting up to 0.6 s ($\leq 10\tau_E$) in 4 MW NBI-heated H-mode discharges. In agreement with theory, the SFD geometry increased the plasma-wetted area, the X-point connection length, and the divertor volume. The SFD formation led to a stable partial detachment of the outer strike point otherwise inaccessible in the standard divertor at $P_{\text{SOL}} = 3 \text{ MW}$ in NSTX. Peak divertor heat flux was reduced from 3–7 MW/m² to 0.5–1 MW/m², while radiated power and recombination rate increased. Additional seeding of deuterated methane increased divertor radiation further. Heat fluxes from Type I ELMs ($\Delta W/W = 7 - 10\%$) were also significantly dissipated: peak target temperatures measured at peak ELM times reached 1000–1200°C in the standard divertor phase and only 300–500°C in the SFD phase. H-mode core confinement was maintained albeit the radiative detachment, while core carbon concentration was reduced by up to 50%. To project SFD properties to future devices, a two-dimensional multi-fluid edge transport model based on the UEDGE code is developed, and initial simulations indicate large reductions in T_e, T_i , particle and heat fluxes due to the SFD geometry effects. In the planned NSTX Upgrade, two up-down symmetric sets of four divertor coils will be used to test the SFD for handling the projected steady-state 20–30 MW/m² peak divertor heat fluxes in 2 MA discharges up to 5 s long with up to 12 MW NBI heating.

EX-P

Supported by the U.S. DOE under Contracts DE-AC52-07NA27344, DE-AC02-09CH11466, DE-AC05-00OR22725, and DEFG02-99ER54519.

Reduction of Peak Wall Power Loads in L- and H-mode Tokamak Plasmas in TCV with the Snowflake Divertor

W. A. J. Vijvers¹, G. Canal¹, B. Labit¹, H. Reimerdes¹, S. Coda¹, B. Duval¹, F. Piras¹, T. Rognlien², D. Ryutov², B. Tal³, G. de Temmerman⁴, and J. Zielinski⁴

¹*Ecole Polytechnique Fédérale de Lausanne (EPFL), CRPP, Lausanne, Switzerland*

²*Lawrence Livermore National Laboratory, Livermore, USA*

³*WIGNER RCP, RMKI, Budapest, Hungary*

⁴*FOM Institute DIFFER, Nieuwegein, Netherlands*

Corresponding Author: wouter.vijvers@epfl.ch

This paper presents experimental evidence, obtained on the TCV tokamak, for the feasibility of using the snowflake (SF) divertor for lowering the steady-state and transient heat fluxes to the plasma facing components in both L- and H-mode tokamak plasmas. The SF, characterized by a second-order poloidal field null, features a hexagonal magnetic field structure in the null-region and hence four divertor legs. A systematic study of the physics behind the power redistribution towards the two secondary strike points (SPs) was made by gradually changing the configuration from a standard single null to the SF. The power reaching the strike points was measured with Langmuir probe arrays and fast framing infrared cameras. L-mode experiments were performed with Ohmic heating only, while H-mode experiments had up to 2 MW of ECRH. The parameter sigma, defined as the distance between the two X-points normalized to the plasma minor radius, characterizes the proximity to the ideal SF and was varied between 3 and 0.25, while retaining the main plasma shape. This scan showed that in L-mode most of the exhaust power reaches the primary SPs and that P_{SP1} decreases linearly with decreasing sigma (by $\sim 20\%$ at $\sigma = 0.25$). A significant part of the redistributed power reaches the secondary SP at the bottom of TCV (SP3). No significant power reaches SP3 at $\sigma \geq 0.6$ in both L- and H-mode. Upon decreasing sigma in H-mode, we observe a sharp drop in peak power to the primary strike point and a strong increase in power to SP3 at $\sigma \sim 0.6$. The power to SP1 during the ELMs keeps dropping as sigma decreases, as in L-mode, while the peak P_{SP3} remains approximately constant for the remainder of the scan. This behavior is in qualitative agreement with the model described in [1], which explains strong power redistribution during ELMs by strong convection in the null region, triggered by a high local poloidal β . The validity of the model and its correspondence with the experimental data is studied. Measurements of the plasma properties at SP4 are in preparation. Further studies include the analysis of filament transport using coherently averaged images from a fast visible camera. Both radial movement of blobs and significant flux-tube squeezing were observed.

References

- [1] D. D. Ryutov *et al.*, APS DPP, Salt Lake City, **9** (2011) 00104.

Improvement of the Spectroscopic Investigation of Pellet Ablation Clouds

M. Koubiti¹, M. Goto², S. Morita², S. Ferri¹, L. Godbert-Mouret¹, Y. Marandet¹, J. Rosato¹, and R. Stamm¹

¹PIIM, UMR Université d'Aix-Marseille / CNRS, Centre de St. Jérôme, Marseille, France

²National Institute for Fusion Science, Toki, Japan

Corresponding Author: mohammed.koubiti@univ-amu.fr

In magnetic fusion devices, pellet injection is seen as a major technique for deep fuelling and plasma control by mitigating edge instabilities like ELMs or triggering ITBs. Owing to its high efficiency in burning plasmas compared to gas fuelling, pellet injection will be the primary core fuelling system for ITER. Usually H/D pellets are used to extend the operational regimes to higher densities without deteriorating the quality of the plasma confinement. In parallel, pellets made from other materials like C, Al and Ti are used for other purposes like impurity transport studies. During the pellet ablation process (~ 3 ms), a high-density plasma forms around the pellet core (the so-called ablation cloud) and emits a strong line radiation. In this context, spectroscopy helps in understanding the ablation physics. For instance, one can obtain the pellet penetration depth from spectroscopic measurements. Line intensities are used to extract population densities of excited levels which are compared to theoretical values calculated at LTE. Except for H/D pellets, line emission is due to ions at different ionization stages. For carbon pellets injected in LHD, the radiation from the ablation cloud which is dominated by C II and C III lines, is used to determine its parameters. The ablation cloud temperatures are obtained assuming LTE for both ions while the electron densities are determined from the Stark broadening and the optical thickness of the C II 723 nm and C III 117 nm lines. A two-layer model is assumed for the ablation cloud: a small high-density layer surrounded by a larger and lower density layer. Up to now, the density of the high-density layer, was determined by fitting C II 723 nm spectra whose shapes are dominated by Stark effect. Although all splitting and broadening effects have been included in the line profiles used for fitting, the calculated profiles will be improved in this work by using more accurate Zeeman-Stark profiles calculated with the PPP line shape code. Such calculations are justified by more recent measurements in which both Zeeman splitting and Stark broadening were visible on the spectra of the C II 723 nm line. This will increase the accuracy of the deduced pellet ablation cloud parameters. The link between the ablation cloud characteristics of pellets and those of the main plasma in which they are injected will be discussed.

EX-P

Power Handling of the Tungsten Divertor in JET

P. Mertens¹, G. Arnoux², S. Brezinsek¹, M. Clever^{1,2}, J. W. Coenen¹, S. Devaux³,
T. Eich³, M. Groth⁴, A. Huber¹, S. Jachmich⁵, M. Lehnen¹, P. J. Lomas²,
G. Maddaluno⁶, H. Maier³, S. Marsen³, G. F. Matthews², R. Neu³, V. Riccardo²,
G. van Rooij⁷, C. Ruset⁸, and B. Sieglin³

¹*Forschungszentrum Jülich, EURATOM-Association, Jülich, Germany*

²*Culham Centre for Fusion Energy, Abingdon, UK*

³*Max-Planck-Institut für Plasmaphysik, Garching, Germany*

⁴*Aalto University, Aalto, Finland*

⁵*LPP-ERM/KMS, Association EURATOM-Belgian State, Brussels, Belgium*

⁶*Association EURATOM-ENEA sulla Fusione, C.R. Frascati, Roma, Italy*

⁷*FOM Institute Differ, Nieuwegein, Netherlands*

⁸*LPRP, EURATOM-MEDC Association, Bucharest, Romania*

Corresponding Author: ph.mertens@fz-juelich.de

With incident power densities of 5 – 10 MW/m² or locally even higher, divertor target plates of large tokamaks are driven close to the material limits. The power handling performance is essential to their characterisation. The thermal performance of tungsten is critical to the decision as to whether to start ITER with an all tungsten divertor. In the new ITER-like Wall in JET, the divertor tiles consist of carbon-fibre composites coated with tungsten except for a specific row within the range of the outer strike point where bulk tungsten is used.

The multilayer coating (Mo/W) is 12 – 25 µm thick depending on the poloidal position. Ion beam tests have shown that the risk of delamination is low (< 1% area) as long as the coating is maintained below 1200°C and carbidisation is negligible. The tiles are coated by combined magnetron sputtering and ion implantation (CMSII-discharges in argon). The resulting Ar content of the layers (< 2% at.) is seen in spectroscopic traces. W-radiation events were spectroscopically observed which correspond to particles penetrating the main plasma (equivalent diameters around 100 µm). The number of events has decreased with time. Regular inspections have not revealed any definitive evidence of delamination.

The bulk tungsten row consists of 48 tile assemblies. Each one is made of two sets of four stacks of 24 lamellae. The stacks are aligned with the toroidal direction. To minimise the risk of fracture, the brittle tungsten is subjected by the clamping to compression forces only. The surface temperature is currently limited to 1200°C to avoid appreciable grain growth and possible thermo-mechanical fatigue ($T_{\text{observed}} < 900^\circ\text{C}$ at the time of writing). Later, the upper bound will be set to 2200°C (a limit on the power density) and, for the deposited energy density per pulse, to 54 MJ/m². Taking advantage of the segmentation of the tiles, sweeping over two stacks is effective for spreading out the load down to acceptable levels.

Loads in the order of 25 MJ/m² were reached so far. The modelled temperature rise of the plasma-facing tungsten shows a fair agreement with the records of thermocouples and of infrared cameras and pyrometers which are sensitively dependent on the emissivity (0.18 – 0.6). The experimental behaviour is close to design values in a wide range of operational parameters.

Recent achievements of the T-11M lithium program

S. Mirnov¹, V. Lazarev¹, E. Azizov¹, N. Djigailo¹, V. Nesterenko¹, I. Lyublinski², and A. Vertkov²

¹*GSC TRINITI, Moscow, Russian Federation*

²*JSC "Red Star", Moscow, Russian Federation*

Corresponding Author: mirnov@triniti.ru

The main subject of T-11M tokamak lithium research is solution of the technological problems, connected with creation of the plasma facing components (PFC) of a steady-state tokamak reactor, which can be used as a fusion neutron source (FNS). The idea of liquid lithium as material of steady-state limiter was tested in early T-11M experiments by using of the lithium capillary porous system (CPS). The recent lithium activity in tokamak T-11M had three main directions: investigations of long-term interaction of a lithium limiter with hydrogen plasma, investigations of different schemes of lithium collection and development of new kind CPS limiters, namely a vertical rail limiter on the low B-field side. For the long-term investigations the T-11M tokamak was transformed into the test stand with steady-state deuterium glow discharge (DGD) for exposing of PFC. Series of alternated DGD exposures and ordinary shots of T-11M operation were used for test of lithium emission of limiter surface and evolution of deuterium recycling after long-term deuterium plasma interaction. The measurements showed that the effect of "lithium poisoning by deuterium bombardment" is small enough and the Li-limiter can be used successfully during the long-term tokamak operations as a Li-emitter. For the investigation of different schemes of lithium collection the additional ring R limiter-collector in the shadow of the main rail limiter was placed in the T-11M vessel. The combination of the results of this experiment with measurements of lithium distribution in the limiter SOL by the method of recombination target allowed an estimation of absolute values of the lithium flux into plasma column from the hot zone of the rail limiter during an ordinary T-11M discharge. This estimation and measurements of lithium deposition on the cold (lateral) sides of T-11M limiters (R+rail) allowed us to reconstruct the lithium flux distributions close to the plasma boundary and first wall. The vertical CPS limiter was designed for increasing of the circulating part of lithium emission. This limiter was installed and successfully tested in the T-11M during operating modes. It allowed the twice increasing of the "cold" collector area as compared to the previous rail limiter. The new vertical lithium limiter allowed us to find the ohmic limiter H-mode with plasma density increase up to Greenwald limit.

EX-P

Tore Supra Contribution to Experimental Prediction of the Power Flux to the Limiter in the ITER Start-up Mode

P. Monier-Garbet¹, R. Dachicourt¹, J. P. Gunn¹, J. Bucalossi¹, F. Clairet¹, L. Colas¹,
Y. Corre¹, R. Dejarnac², P. Devynck¹, and N. Fedorczak³

¹CEA, IRFM, Saint-Paul Lez Durance, France

²Association EURATOM-IPP.CR, Prague, Czech Republic

³Center for Momentum Transport and Flow Organization, USCD, San Diego, USA

Corresponding Author: pascale.monier-garbet@cea.fr

This paper reports on the experimental programme run on Tore Supra, taking advantage of its limiter plasma edge, to gain more confidence in the prediction of the power flux to the start-up limiter in ITER. A scaling law for the value of parallel power flux q_{\parallel} at the last closed flux surface, and its e-folding length λ_q in the scrape-off layer is proposed in limiter configuration. It finds a different dependence on macroscopic plasma parameters than the scaling presently used for ITER tile shaping. For example, at constant power flowing into the scrape-off layer the measured λ_q decreases with density, whereas the ITER scaling law predicts the opposite behaviour. The method that is used combines Langmuir probe, retarding field analyzer measurements, and power balance analysis. Using this method, it is found that strong secondary electron emission dominates the physics of power transmission to the wall. It results that the ion power flux is much smaller than expected, most of the power being carried by electrons. Nonetheless, the power decay length scaling found using this method is similar to standard Langmuir probe analysis because q_{\parallel} is dominated by the J_{\parallel} profile. In addition to this, for very high electron densities (up to a factor 1.4 above the Greenwald value) a steady-state highly radiating regime is observed, minimising the heat load on the limiter. This regime is investigated through a dedicated set of edge diagnostics, including Langmuir probes and spatially resolved VUV spectroscopy on the limiter.

The Effects of Increasing Lithium Deposition on the Power Exhaust Channel in NSTX

T. Gray¹, J. Canik¹, A. McLean², R. Maingi¹, J. W. Ahn¹, M. Jaworski³, R. Kaita³,
T. Osborne⁴, S. Paul³, F. Scotti³, and V. Soukhanovskii⁴

¹*Oak Ridge National Laboratory, Oak Ridge, USA*

²*Lawrence Livermore National Laboratory, Livermore, USA*

³*Princeton Plasma Physics Laboratory, Princeton, USA*

⁴*General Atomics, San Diego, USA*

Corresponding Author: tkgray@pppl.gov

Previous measurements on the National Spherical Torus Experiment (NSTX) demonstrated peak, perpendicular heat fluxes, $q_{\text{dep,pk}} \leq 15 \text{ MW/m}^2$ with an inter-ELM integral heat flux width, $\lambda_{q,\text{int}} \sim 3 - 7 \text{ mm}$ during high performance, high power operation (plasma current, $I_p = 1.2 \text{ MA}$ and injected neutral beam power, $P_{\text{NBI}} = 6 \text{ MW}$) when magnetically mapped to the outer midplane. Analysis indicates that $\lambda_{q,\text{int}}$ scales approximately as I_p^{-1} [1]. The extrapolation of the divertor heat flux and λ_q for NSTX-U are predicted to be upwards of 24 MW/m^2 and 3 mm respectively assuming a high magnetic flux expansion, $f_{\text{exp}} \sim 30$, $P_{\text{NBI}} = 10 \text{ MW}$, balance double null operation and boronized wall conditioning.

While the divertor heat flux has been shown to be mitigated through increased magnetic flux expansion [1], impurity gas puffing [2], and innovative divertor configurations [3] on NSTX, the application of evaporative lithium coatings in NSTX has shown reduced peak heat flux from 5 to 2 MW/m^2 during similar operation with 150 and 300 mg of pre-discharge lithium evaporation respectively. Measurement of divertor surface temperatures in lithiated NSTX discharges is achieved with a unique dual-band IR thermography system [4,5] to mitigate the variable surface emissivity introduced by evaporative lithium coatings. This results in a relative increase divertor radiation as measured by the divertor bolometry system. SOLPS [6] modeling of heavy lithium evaporation discharges will be presented to elucidate divertor operation in this scenario. While the measure divertor heat flux is reduced with heavy lithium evaporation, λ_q contracts to $3-6 \text{ mm}$ at low I_p but remains constant as I_p is increased to 1.2 MA yielding λ_q comparable to no lithium discharges at high I_p . Implications for NSTX-U operation with heavy lithium coatings in the divertor will be discussed.

References

- [1] T. K. Gray, *et al.*, J. Nucl. Mater. **415** (2011) S360-S364.
- [2] V. A. Soukhanovskii, *et al.*, Phys. Plasmas **16** (2009) 022501.
- [3] V. A. Soukhanovskii, *et al.*, Nucl. Fusion **51** (2010) 012001.
- [4] J. W. Ahn, *et al.*, Rev. Sci. Instrum. **81** (2010) 023501.
- [5] A. G. McLean, *et al.*, submitted to Rev. Sci. Instrum. (2011).
- [6] J. M. Canik, *et al.*, Phys. Plasmas **18** (2011) 056118.

Work supported by U.S. Department of Energy contracts: DE-AC05-00OR22725, DE-AC52-07NA27344 and DE-AC02-09CH11466

Dependence of the L-H Power Threshold on X-point Geometry

D. Battaglia¹, C. S. Chang¹, S. Kaye¹, S. H. Ku¹, R. Maingi², R. Bell¹, A. Diallo¹,
S. Gerhardt¹, B. LeBlanc¹, and J. Menard¹

¹*Princeton Plasma Physics Laboratory, Princeton, USA*

²*Oak Ridge National Laboratory, Oak Ridge, USA*

Corresponding Author: dbattagl@pppl.gov

The L-H power threshold (P_{LH}) on the National Spherical Torus Experiment decreases with larger X-point radius (R_x) and the amount of lithium evaporated on the divertor surfaces. The edge T_e (where $T_e \sim T_i$ in the L-mode edge) at the L-H transition decreases 30–40% with larger R_x , but is fairly independent of the edge density, neutral fueling rate and lithium conditioning. These observations are consistent with the X-transport theory, which predicts that the edge radial electric field (E_r) just inside the plasma separatrix must become more negative as T_i or R_x are increased in order to counteract non-ambipolar neoclassical ion orbit loss in a diverted plasma. Consequently, the $\mathbf{E} \times \mathbf{B}$ shearing rate, which is predicted to be favorable for triggering and sustaining H-mode, increases with both T_i and R_x . Self-consistent E_r calculations using the XGC0 code provide insight into the dependence of the shearing rate on the magnetic geometry and edge T_i . For example, the shearing rate remains constant as R_x is reduced from 0.64 m to 0.47 m only if the edge T_i profile is increased by 25%. Increasing the neutral recycling rate does not significantly alter the T_i profile needed to maintain the same shearing rate, but does require more core heating to maintain the critical edge temperature. This is consistent with the experimental observations that P_{LH} varies with R_x and divertor recycling, while T_e at the L-H transition only depends on R_x . This agreement between theory and experiment provides a valuable tool for interpreting the hidden variables in the empirical P_{LH} scaling relationships and for optimizing the heating requirements for ITER and other advanced tokamaks. XGC0 simulations are used to examine other known P_{LH} dependences, including the ion ∇B drift direction, X-point height, ion species and plasma current.

Supported by US DOE contracts DE-AC02-09CH11466 and DE-AC05-00OR22725.

First Results of Closed Helical Divertor Experiment in LHD

T. Morisaki¹, S. Masuzaki¹, M. Kobayashi¹, M. Shoji¹, J. Miyazawa¹, R. Sakamoto¹,
G. Motojima¹, M. Goto¹, H. Funaba¹, H. Tanaka¹, K. Tanaka¹, I. Yamada¹,
S. Ohdachi¹, H. Yamada¹, and A. Komori¹

¹National Institute for Fusion Science, Toki, Japan

Corresponding Author: morisaki@nifs.ac.jp

The edge plasma control with divertor is a crucial issue for fusion research. Especially in reactors, excess neutrals including helium ash and impurities have to be pumped out efficiently to sustain the edge pedestal and burning plasma in steady-state. In addition, sufficient cooling for plasma before reaching target plates is strongly required from the engineering point of view. Thus it is prerequisite for efficient pumping to increase neutral pressure in the divertor region with closed configurations. In helical devices, closed divertor experiments have been conducted using magnetic islands surrounding the plasma, e.g., local island divertor (LID) in LHD. However, due to the small wetted area of LID, it cannot accommodate steady-state and/or high power operations. Hence the helical divertor (HD) which is intrinsically built in the heliotron configuration is a solution to prospect future helical devices.

The baffle-structured closed HD is being constructed in LHD. The closed HD consists of ten discrete modules which are partially installed on the inboard side of the torus, where $\sim 88\%$ of diverted particles flow into. Each module consists of a pair of vertical target plates and a “dome” structure. At this stage, two of ten modules have been installed. The geometrical optimization of the target plates and the dome was carried out with numerical simulations to maximize the neutral compression in the closed HD region. It was demonstrated that the neutral pressure in closed HD can be increased $\sim 13\times$ higher than that in open HD.

Experiments were carried out with neutral beam (NB) heated hydrogen discharges. Neutral pressures in open and closed HDs were measured with ASDEX-style fast ion gauges installed under the dome. During the discharge with continuous gas puffing, neutral pressures in both open and closed HDs increased monotonically with increase in electron density. It was clearly observed that neutral pressure in closed HD was more than $10\times$ higher than that in open HD. This result agrees quantitatively well with that obtained with numerical simulations. Consequent increase of recycling flux was also observed in Langmuir probes measurements in closed HD, while little difference in global plasma parameters could be seen with present two closed HD modules. Active pumping in closed HD is planned in the near future.

EX-P

Nitrogen Seeding for Heat Load Control in JET ELMy H-mode Plasmas and its Compatibility with ILW Materials

C. Giroud¹, M. Oberkofler², D. Douai³, G. Maddison¹, M. Beurskens¹, S. Brezinsek⁴, J. W. Coenen⁴, T. Dittmar⁵, A. Drenik⁶, L. Frassinetti⁷, S. Jachmich⁸, E. Joffrin³, R. Neu², F. Rimini¹, G. van Rooij⁹, A. C. C. Sips¹⁰, P. Tabares¹¹, P. de Vries⁹, G. Arnoux¹, A. Martin-Rojo¹¹, P. da Silva Aresta Belo¹², M. Brix¹, G. Calabro¹³, M. Clever⁴, I. Coffey¹⁴, S. Devaux², T. Eich², A. Huber⁴, M. Kempenaars¹, U. Kruezi⁴, K. Lawson¹, M. Lehnen⁴, P. Lomas¹, S. Marsen², A. Meigs¹, I. M. Ferreira Nunes¹², B. Sieglin², A. Sirinelli¹, M. Stamp¹, and S. Wiesen⁴

¹EURATOM/CCFE Fusion Association, Culham Science Centre, Abingdon, UK

²Max-Planck-Institut für Plasmaphysik, Garching, Germany

³CEA, IRFM, Association Euratom-CEA, St Paul lez Durance, France

⁴Forschungszentrum Jülich, Association EURATOM-FZJ, Jülich, Germany

⁵UCSD, PISCES Lab, San Diego, USA

⁶Jozef Stefan Institute, Ljubljana, Slovenia

⁷Association EURATOM-VR, Department of Physics, Stockholm, Sweden

⁸Association Euratom-Etat Belge, ERM-KMS, Brussels Belgium

⁹FOM Institute Differ, Nieuwegein, Netherlands

¹⁰JET-EFDA/CSU, Culham Science Centre, Abingdon, UK

¹¹CIEMAT, Madrid, Spain

¹²IPFN, EURATOM-IST, Lisbon, Portugal

¹³Associazione Euratom/ENEA sulla Fusione, Rome, Italy

¹⁴Astrophysics Research Centre, Queen's University, Belfast, Northern Ireland, UK

Corresponding Author: carine.giroud@ccfe.ac.uk

The challenge of achieving a scenario with sufficient energy confinement ($H_{98}(y, 2) \sim 1$), at high density ($f_{GDL} \sim 0.85$) and compatible with the material selection of the DT phase of ITER is being addressed at JET with bulk beryllium (Be) main-chamber limiters and a full tungsten (W) divertor. This contribution investigates three aspects: reduction of inter-ELM power load to the divertor without significant degradation of the energy confinement via impurity seeding (Ne or N₂); limitation of impurity production from the new plasma-facing materials; compatibility of the extrinsic impurities with the ILW materials. Being chemically reactive, N₂ can modify the chemical state of material surfaces which could change the fuel retention properties. An increase in gas retention has been measured in JET ILW seeded discharges. It is likely that this increase is not actually due to wall retention but linked to the formation of ammonia (ND₃). An estimate of the rate of ND₃ production will be given. Experiments at JET with the Carbon-Fibre Composite (CFC) wall explored the reduction of the inter-ELM power load in an ELMy H-mode scenario at high density ($H_{98}(y, 2) \sim 1$, $f_{GDL} \sim 0.8$) with a mix of D₂ with either Ne or N₂, constant input power and close the type I to III ELMs boundary. The same discharges were repeated in JET ILW, so far with D₂ fuelling only, with the aim to characterize the difference between the two wall materials. A striking difference in the ELM type domain has been observed: type I ELMs now exists in the type III ELMs domain of the CFC wall. The possible absence of a transition in ELM regime close to the $H_{98}(y, 2) \sim 1$ could be an advantage in achieving a stationary highly radiative scenario. A first exploration of N₂ seeding shows a clear reduction in the nitrogen legacy in ILW in comparison with the CFC wall.

This work was funded by the RCUK Energy programme and EURATOM. The work was carried out within the framework of EFDA.

Liquid Lithium Divertor Characteristics and Plasma-Material Interactions in NSTX High-Performance Plasmas

M. Jaworski¹, T. Abrams¹, J. P. Allain², M. Bell¹, R. Bell¹, A. Diallo¹, T. Gray³,
S. Gerhardt¹, B. Heim², R. Kaita¹, J. Kallman^{1,4}, H. Kugel¹, B. LeBlanc¹, R. Maingi³,
A. McLean⁴, J. Menard¹, R. Nygren⁵, M. Ono¹, S. Paul¹, M. Podesta¹,
L. Roquemore¹, S. Sabbagh⁶, F. Scotti¹, C. Skinner¹, V. Soukhanovskii⁴, D. Stotler¹,
and C. Taylor²

¹Princeton Plasma Physics Laboratory, Princeton, USA

²Purdue University, West Lafayette, USA

³Oak Ridge National Laboratory, Oak Ridge, USA

⁴Lawrence Livermore National Laboratory, Livermore, USA

⁵Sandia National Laboratories, Albuquerque, USA

⁶Columbia University, New York, USA

Corresponding Author: mjaworsk@pppl.gov

ITER and future fusion experiments are hampered by erosion and degradation of plasma-facing components, forcing regular replacement. The conventional approach has been the use of high-Z walls (e.g., W) which can undergo permanent modification due to erosion and melting. One novel approach to solving these issues in the tokamak edge is the usage of liquid metal plasma facing components.

The National Spherical Torus Experiments (NSTX) is the only US confinement device operating a liquid metal divertor target to examine the technological and scientific aspects of this innovative approach. The Liquid Lithium Divertor (LLD) module formed a nearly toroidally continuous surface in the outer, lower divertor. NSTX H-mode discharges were repeatedly run with the outer strike-point directly on the LLD plates. Peak heat fluxes of $\sim 5 \text{ MW/m}^2$ were regularly applied to the LLD surfaces alongside significant ion fluxes. No molybdenum line radiation was observed in these plasma [3] indicating protection of the substrate material.

During these experiments, no macroscopic ejection was observed from the LLD contrary to experiments conducted in the DIII-D tokamak, where lithium ejection exposed the substrate [4]. Quiescent scrape-off layer current (SOLC) densities were $\sim 10 \text{ kA/m}^2$, with peak SOLCs $> 100 \text{ kA/m}^2$. Stability analyses for the liquid metal layers show that despite the large current densities, capillary and viscous forces are effective at reducing motion demonstrating stable operation of the liquid metal PFC.

The strong chemical reactivity of lithium results in the steady accumulation of impurities in the PFC material, mitigating the low-Z benefits of the lithium. Eroded material from the carbon PFCs in NSTX can redeposit onto the LLD, and background vacuum gases are also gettering onto the surface. Flowing systems are under study and are designed to allow one to obtain a low-Z, replenishable PFC by removing gettering materials and eliminating the accumulation effect.

References

- [1] P. C. Stangeby, J. Nucl. Mater. **415** (2011) S278.
- [2] J. W. Coenen, J. Nucl. Mater. **415** (2011) S92.
- [3] H. W. Kugel, *et al.*, Fusion Eng. Des. 2011 in press.
- [4] D. Whyte, *et al.*, Fusion Eng. Des. **74** (2004) 133.

This work supported by USDOE contracts DE-AC02-09CH11466 (PPPL), DE-AC05-00OR22725, DE-AC52-07NA27344, DE-FG02-99ER54524, DE-FG02-08ER54990, and DE-AC04-94AL85000.

Control of Dust Flux in LHD and in a Divertor Simulator

K. Koga¹, K. Nishiyama¹, Y. Morita¹, D. Yamashita¹, K. Kamataki¹, G. Uchida¹,
H. Seo¹, N. Itagaki^{1,2}, M. Shiratani¹, N. Ashikawa³, S. Masuzaki³, K. Nishimura³, and
S. Akio³

¹*Department of Electronics, Kyushu University, Motoooka Nishi-ku Fukuoka, Japan*

²*PRESTO JST, Tokyo, Japan*

³*NIFS, Toki, Japan*

Corresponding Author: koga@ed.kyushu-u.ac.jp

Much attention has recently directed to the study of dust in fusion devices mainly because dust can pose safety issues related to its chemical activity, tritium retention and radioactive content [1]. Therefore, it is important to invent a dust removal method. Effects of a local bias potential on the flux of dust particles have been studied by dust collections in a divertor simulator [2]. The collected dust particles can be classified into three kinds: spherical particles, agglomerates, and flakes. Spherical dust particles are below about 500 nm in size. Agglomerates are 50 – 600 nm in size and composed of small spherical primary particles of around 10 nm in size. Flakes have the size above 1 μm and are irregular in shape. The spherical dust flux increases exponentially by 2 orders of magnitude with increasing the local bias potential from negative to positive, while the fluxes of agglomerates and flakes are irrelevant to the bias voltages. Based on the results for spherical dust particles, the effect of local bias potential on the dust removal in fusion devices has been studied by dust collection experiment in the LHD. The major composition of the dust particles is carbon, which is the primary component of the divertor plates in LHD (IG-430), whereas flakes contain Fe and Cr, which are the main components of its first wall (SS316). Agglomerates in LHD are rare. The particle and mass fluxes of carbon and metal dust collected on the substrates increases exponentially by 1 – 1.5 orders of magnitude with increasing the local bias potential. The results indicate that collection of dust flux using the local biasing is useful to remove dust particles at the shadow area in fusion devices.

References

- [1] S. I. Krasheninnikov, *et al.*, Plasma Phys. Control. Fus. **50** (2008) 124054.
- [2] S. Iwashita, *et al.*, J. Plasma Fusion Res. **8** (2009) 308.

Toroidal Asymmetry of Divertor Heat Deposition during the ELM and 3-D Field Application in NSTX

J. W. Ahn¹, K. Gan², F. Scotti³, R. Maingi¹, J. Canik¹, T. Gray¹, J. Lore¹,
A. McLean⁴, L. Roquemore³, and V. Soukhanovskii⁴

¹*Oak Ridge National Laboratory, Oak Ridge, USA*

²*Institute of Plasma Physics, Chinese Academy of Sciences, Hefei, China*

³*Princeton Plasma Physics Laboratory, Princeton, USA*

⁴*Lawrence Livermore National Laboratory, Livermore, USA*

Corresponding Author: jahn@pppl.gov

Non-axisymmetric divertor heat and particle depositions often occur in tokamaks either for steady imposed perturbations or from transient events. Such asymmetries will make divertor heat flux management more challenging in ITER and next step devices because the tile design and cooling requirement are usually based on a 2-D axisymmetric calculation. In NSTX, 2-D heat flux data calculated by a 3-D heat conduction solver allowed for the evaluation of peak heat flux (q_{peak}) and heat flux width (λ_q) for each toroidal angle, which generates a toroidal array of q_{peak} and λ_q at each time slice. Then the toroidal degree of asymmetry (DoA) of q_{peak} and λ_q as a function of time was defined as

$$DoA(q_{\text{peak}}) = \sigma_{q_{\text{peak}}} / \bar{q}_{\text{peak}} \quad (1)$$

and

$$DoA(\lambda_q) = \sigma_{\lambda_q} / \bar{\lambda}_q. \quad (2)$$

σ is the standard deviation of q_{peak} and λ_q over data in the toroidal array and is normalized respectively by mean values of q_{peak} and λ_q to produce DoA at each time slice. In case of ELMs and 3-D field application, the helical heat deposition produces additional scatter of data around mean values to the background scatter level without these events and it raises DoA for both q_{peak} and λ_q . Both values of $DoA(q_{\text{peak}})$ and $DoA(\lambda_q)$ are highest at the ELM peak times, while they become lower toward the later stage of the inter-ELM period. The correlation between $DoA(q_{\text{peak}})$ and $DoA(\lambda_q)$ is the strongest at the ELM peak times and becomes weaker later in the ELM cycle. A wide angle, 2-D fast visible camera with capability of viewing nearly full divertor surface is also being used to study the toroidal and radial structure of the divertor flux profile. The 2-D data is remapped to the (r, ϕ) plane and facilitates comparison with modeling. The divertor heat flux profile during the ELMs triggered by the applied 3-D fields are found to have the same spatial structure (in both r and ϕ directions) as that for the profile during the inter-ELM period in the presence of applied 3-D fields. Data for the intrinsic and applied 3-D fields as well as for the triggered and natural ELM filaments from different ELM types have been obtained. EMC3-Eirene modeling showed that the observed asymmetric divertor flux is qualitatively reproduced.

This work was supported by the US Department of Energy, contract numbers DE-AC05-00OR22725, DE-AC02-09CH11466, and DE-AC52-07NA27344.

EX-P

Symmetries and Asymmetries in the Divertor Detachment in ASDEX Upgrade

M. Wischmeier¹, S. Potzel¹, L. Aho-Mantila², M. Bernert¹, D. Coster¹, H. W. Müller¹, F. Reimold¹, and ASDEX Upgrade Team¹

¹IPP Garching, Garching, Germany

²Association Euratom-Tekes, VTT, Finland

Corresponding Author: marco.wischmeier@ipp.mpg.de

Large burning plasma fusion devices such as ITER and DEMO require divertor detachment to not exceed the tolerable power load densities ($< 5 \text{ MW/m}^2$) for long pulse operation. The understanding of the processes leading to divertor detachment is currently incomplete and a reliable prediction for future large scale devices out of reach. In ASDEX Upgrade divertor detachment has been studied for Ohmic and L-mode density ramp discharges with deuterium and hydrogen as a fuelling species and both toroidal field directions. The effect of seeding nitrogen has been tested. Prior to the detachment of the outer divertor a fluctuating detachment state appears in the SOL of the inner divertor, characterized by strong radiative fluctuations close to the X-point. Simultaneously a region with high n_e appears in the inner far SOL and X-point regions. Once these radiative fluctuations disappear detachment occurs along the entire inner target plate and the outer divertor reaches a state of complete detachment. The integrated ion flux at the inner target reaches its peak value at an only $\sim 10 - 20\%$ lower line averaged density than for the outer divertor target. However, the maximum of the integrated ion flux to the inner target remains well below what is observed at the outer target.

Numerical transport code packages, such as SOLPS 5.0, contain an as complete as possible model of our current understanding of the basic processes present in the Scrape Off Layer. Under common assumptions for the model it is found that the roll over of the ion flux at the inner and outer targets occurs at a similar n^{sep} . Contrary to experimental findings the simulated peak values remain comparable for both target plates and no strong reduction of the ion flux density is seen for the inner divertor. The experimental observation of the high n_e in the far SOL during the fluctuating phase indicates that plasma is transported outward into the far SOL and/or strong radiation spontaneously sets in over a large volume in the far SOL. Based on these observations various levels of perpendicular transport in the X-point region of the inner divertor are assumed and recycling impurities such as oxygen and nitrogen are included. This leads to a shift of the simulated peak ion flux into the far inner SOL and a reduction of its peak value at the roll over by more than a factor of 3.

A Global Particle-balance Model for Wall Interaction Analysis Associated with Open- and Closed-loop Density Control Experiments in KSTAR

J. W. Juhn¹, Y. S. Hwang¹, S. H. Hong², S. H. Hahn², Y. U. Nam², and Y. Yu²

¹*Seoul National University, Seoul, Republic of Korea*

²*National Fusion Research Institute, Daejeon, Republic of Korea*

Corresponding Author: jwjuhn@nfri.re.kr

Based on successful experiments of open- and closed-loop density control in 300 kA circular Ohmic discharges in KSTAR 2011, a 0-D global particle model has been developed. Starting from the Maddison's multi-reservoir model with the parameters for KSTAR, an outgassing-like term was added into the wall inventory equation so that the particular behaviors of KSTAR plasmas can be reproduced. The model enables quantifying the particle confinement time τ_i and external fuelling efficiency f_{ex} from the particular discharges with fuelling modulation. The total recycling coefficient R can be also determined by the model. The value was roughly from 0.97 to 0.99 in the particular low density plasmas of up to $2.5 \times 10^{19} \text{ m}^{-3}$, which seems reasonable in this full carbon machine. Furthermore the particle flux to the main chamber was calculated as $1 - 3 \times 10^{22} \text{ D/s}$ and to limiter was estimated as $0.5 - 1.5 \times 10^{22} \text{ D/s}$ during the particular period in the discharges of interest. Again these values are very reasonable comparing with other carbon devices such as TEXTOR (1×10^{22} for limiter), Tore Supra (1×10^{22} for limiter) and JET ($1 - 3 \times 10^{22}$ for main chamber). The other obtained parameters (τ_i , f_{ex} and others) were further applied to the density feedback experiments and the calculated density by the multi-reservoir model is in great agreement with the measured density. In these first feedback control experiments, only proportional gains were applied in order to avoid any unexpected risk due to slow response of the integral gains and to focus on the assessment of the integrated density control system that was quite successful. However, as expected, this simple controller led to clear undershoots of the density from the reference target. While the undershoots will be compensated by the integral gains in future experiment, it enabled quantifying the recycling coefficient R quite accurately by a solution of simple balance equation adjoined with the fuelling formula. In the particular feedback experiment, R was determined as 0.97 which is similar value obtained by the model in the open-loop experiment. The whole experimental scheme will be expanded to the other discharges such as H-modes.

EX-P

Studies of Plasma-Lithium Interactions in TJ-II

F. Tabares¹, D. Tafalla¹, E. Oyarzabal¹, A. B. Martin-Rojo¹, M. A. Ochando¹,
E. Ascasíbar¹, J. A. Ferreira², A. Vertkov³, and V. Balakirev³

¹CIEMAT, Madrid, Spain

²TE/VSC CERN, Geneva, Switzerland

³Red Star Public Corporation, Moscow, Russian Federation

Corresponding Author: tabares@ciemat.es

In the present work, three different experiments concerning the specific features of plasma-lithium interactions will be addressed.

First, a solid bar of lithium with biasing and displacement capabilities has been exposed to the plasma edge in TJ-II under lithiated wall conditions. Heating powers up to 0.8 MW (ECRH and NBI) were injected into the plasma, leading to unmitigated power densities at the bar tip up to 30 MW/m². Edge parameters were characterized by a supersonic He beam diagnostic and Li I, Li II and H α emissions at the bar and its proximity were recorded.

Secondly, we have performed a search for other characteristic effects of lithium surfaces, other than the well-known low recycling. We recorded the I-V characteristics and Li emission signal of lithium covered metallic electrodes in H and He Glow Discharge plasmas. The plasma parameters and electron energy distribution were obtained from the analysis of a Langmuir probe signal and from the measurement of the 728/706 (singlet to triplet) emission lines of He in the corresponding discharges. At small negative potentials of the electrode, an apparent excess of ion current is driven, which is well correlated with the presence of secondary electron emission from the surface upon suprathermal electron bombardment, but with enhanced yields over the bibliographic values.

Finally, a liquid lithium limiter (LLL) based on the Capillary Porous System (CPS) has been installed and tested in TJ-II [4]. The movable limiter has Langmuir Probes and thermocouples for diagnostic as well as biasing capabilities. Upon exposure to the plasma, the limiter can be fully outgassed under vacuum in order to assess the hydrogen retention characteristics and its dependence on operation temperature.

Scrape-off Layer Properties of ITER-like Limiter Start-up Plasmas at JET

G. Arnoux¹, C. Silva², M. Brix¹, H. Bufferand³, S. Devaux⁴, T. Farley⁵, M. Firdaouss⁶,
D. Frigione⁷, M. Groth⁸, J. Gunn⁶, J. Horacek⁹, S. Jachmich¹⁰, P. Lomas¹,
S. Marsen¹¹, G. Matthews¹, R. Pitts¹², M. Stamp¹, and P. Tamain⁶

¹CCFE, Abingdon, UK

²Associação EURATOM/IST, Instituto de Plasmas e Fusão Nuclear, Lisbon, Portugal

³CNRS Aix-Marseille Université, École Centrale, Marseille, France

⁴Max-Planck-Institut für Plasmaphysik, EURATOM-Assoziation, Garching, Germany

⁵University of Bristol, Bristol, UK

⁶Association EURATOM-CEA, CEA/DSM/IRFM, Saint Paul Lez Durance, France

⁷Associazione EURATOM-ENEA sulla fusione, C.R. Frascati, Roma, Italy

⁸Aalto University, Aalto, Finland

⁹Association EURATOM-IPP.CR, Institute of Plasma Physics, Praha, Czech Republic

¹⁰Ecole Royale Militaire, Brussels, Belgium

¹¹Max-Planck-Institut für Plasmaphysik, EURATOM Assoziation, Greifswald, Germany

¹²ITER Organisation, Saint Paul Lez Durance, France

Corresponding Author: gilles.arnoux@ccfe.ac.uk

The scrape-off layer (SOL) power decay length, λ_q , in the limiter phase of ITER as well as the overall power balance are critical parameters for optimization of the wall geometry and thereby determining the power handling limits of the beryllium clad wall modules in ITER. Historically, an L-mode divertor SOL scaling has been used to estimate the ITER width, but recent measurement in limiter configuration on a variety of tokamaks, including those described here from JET, are showing that this is not a valid approach and that a new scaling is required. One issue associated with this new database is that it is almost exclusively constructed from power decay length measurements made using reciprocating Langmuir probes in the main SOL, usually far from the limiters. The power loads on the limiters are usually predicted by projecting the upstream power density along the field line (cross-field transport or poloidal asymmetry are neglected). It has been long known that the sink action of the limiter can locally enhance the radial plasma flux, especially when the last closed flux surface is close enough to the limiter and when the field lines come at a grazing angle. In dedicated limiter experiments with the new ITER like wall at JET (beryllium first wall and tungsten divertor) IR thermography data show that the peak power load at the limiter can be underestimated by a factor 2 if local action of the limiter is not taken into account. In this contribution, we characterise the conditions at which the limiter plays a significant role. When it does not play a role, the λ_q measured at the limiter matches probe measurements. For ohmic plasmas, λ_q scales inversely to the heating power, in line with the scaling found on Tore Supra. Beam heated plasmas do not follow this trend.

EX-P

Development of MHD Active Control in the RFX-mod RFP

L. Marrelli¹

¹ *Consorzio RFX, Associazione Euratom-ENEA sulla Fusione, Padova, Italy*

Corresponding Author: lionello.marrelli@igi.cnr.it

In the last two years many efforts have been dedicated to develop and implement new MHD control approaches in RFX-mod, to optimize the existing schemes based on refined physical models and to design an upgrade of the real-time control system.

In particular the study of the transition to a helical state with $m = 1$, $n = -7$ helicity has been extended to high plasma currents up to 2 MA. These experiments have been performed with a real time version of the modal dynamic decoupler, with significant reduction of $m = 0$, $n = 7$ and $m = 1$, $n = 7$ harmonics.

The control of the edge field due to the Tearing Mode harmonic composing the helical state, namely the $m = 1$, $n = 7$ one, has been simulated by means of the improved RFXlocking code, allowing to perform parametric scans of different feedback schemes based on different magnetic sensors. Experiments with gains determined by the model are on going in order to verify model prediction.

The improved RFXlocking code (including digital feedback) shows that further reduction of the helical field at the plasma edge is possible by reducing significantly the latency of the control system. This motivated the design and realization of a new real-time control system based on a new architecture. The new system, which merges the MHD and equilibrium control, is supervised by the MARTe software framework, developed at JET and currently used for the JET vertical stabilization and in other fusion devices.

As far as the capability of stabilizing Resistive Wall Modes is concerned, an integrated dynamic model of the system was developed integrating the plasma response in the presence of active and passive conducting structures (CarMa model) and a complete representation of the control system. An enriched version of the plasma response model has been developed including multiple RWMs with $abs(n) = 2, 3, 4, 5, 6$. This is required in order to analyse the effect of the a reduced set of coils on stabilization, since it allows the simultaneous study of modes which could be amplified by the low n order sidebands. Dedicated experiments were run by destabilizing otherwise marginally stable modes applying negative proportional gains in the control loop, in order to compare the experimental unstable mode growth rates with the model.

The Fine-scale Structure of the Radial Electric Field in the Scrape-Off-Layer during ICRF Heating in Alcator C-Mod

J. Terry¹, I. Cziegler², S. Wukitch¹, M. Garrett¹, C. Lau¹, Y. Lin¹, R. Ochoukov¹,
D. Whyte¹, and S. Zweben³

¹MIT Plasma Science and Fusion Center, Cambridge, USA

²University of California San Diego, La Jolla, USA

³Princeton Plasma Physics Laboratory, Princeton, USA

Corresponding Author: terry@psfc.mit.edu

By observing the radial structure in the poloidal dynamics of the SOL turbulence during the application of ICRF power ($P_{\text{RF}} > 0.3$ MW), we find a fine-scale radial structure in the poloidal phase velocities (V_{pol}) of the broadband turbulence. The radial profiles are very different from typical profiles in Ohmic plasmas. Since $V_{\text{pol}}(r)$ in the SOL is dominated by $V_{\mathbf{E} \times \mathbf{B}}$, this structure implies that a fine-scale E_r profile is formed in the presence of the ICRF. This profile extends to regions well separated toroidally from the ICRF antennas (~ 2 m). The $\|V_{\text{pol}}\|$ values in the far SOL imply an E_r as large as 25 kV/m. The size-scale of the structure in this radial profile is much smaller than the fast wave perpendicular wavelength (~ 10 cm). The observed velocity fields are consistent with the presence of potential structures arising as a consequence of sheath rectification of the ICRF waves, and potentials as large as 350 V are implied. Such E_r profiles and potentials may help to explain the increased impurity content observed with ICRF heating, as a consequence of both enhanced sputtering and enhanced transport/penetration across the SOL. This effect will be important for impurity generation and SOL transport in regions well away from the antennas. Using 2D Gas-Puff-Imaging we find that, in the ~ 3 cm region outside the separatrix, the steady-state dominant propagation direction for V_{pol} reverses up to three times; i.e., in some configurations, $V_{\text{pol}}(r)$ varies from downward ($E_r > 0$) in the ~ 1 cm outside the separatrix, and then alternates from upward ($E_r < 0$), to downward ($E_r > 0$), to upward ($E_r < 0$) in the next ~ 2 cm. The local maxima in radial profiles of the potential occur on the field-lines just grazing active antennas. Thus the fine scale structure is a consequence of different antennas mapping to different SOL radii at the GPI view. The dependence of the implied potentials upon launched power follows the theoretically predicted trend ($\sim P_{\text{RF}}^{1/2}$). However, the potential structures are found to be significantly broadened compared to the basic theoretical expectation, having a radial width that is $\sim 5 \times \delta_e$, where δ_e is the skin depth for RF waves in the C-Mod SOL. The observed radial width also exhibits a power-dependence.

EX-P

Work supported by USDoE awards DE-FC02-99ER54512 & DE-AC02-09CH11466.

Fast Wave Power Flow along SOL Field Lines in NSTX

R. Perkins¹, J. W. Ahn², R. Bell¹, A. Diallo¹, S. Gerhardt¹, T. Gray², D. Green²,
E. F. Jaeger², J. Hosea¹, M. Jaworski¹, B. LeBlanc¹, G. Kramer¹, A. McLean²,
R. Maingi², C. Phillips¹, P. Ryan², S. Sabbagh³, G. Taylor¹, J. Wilson¹, and
L. Roquemore³

¹*Princeton Plasma Physics Laboratory, Princeton, USA*

²*Oak Ridge National Laboratory, Oak Ridge, USA*

³*Columbia University, New York, USA*

Corresponding Author: rperkins@pppl.gov

The efficiency of fast wave (FW) heating and current drive can be reduced by a myriad of edge RF power loss processes in the vicinity of the antenna and in the scrape off layer (SOL), prior to the RF power reaching the core plasma inside the last closed flux surface (LCFS). These processes include sheath dissipation by near fields on and in the vicinity of the antenna, propagation of power on open field lines to the divertor regions, and possibly others. These edge losses subtract directly from the power RF power deposited inside the LCFS and must be minimized in order to optimize fast wave performance generally. On NSTX up to 60% of the HHFW power coupled from the antenna can be lost to the SOL regions [1, 2]. A large part of this edge power loss is deposited in bright spirals on the divertor floor and ceiling and can deliver up to ~ 2 MW/m² of heat for ~ 2 MW of coupled antenna power [2]. In this paper, magnetic field mapping with the SPIRAL code shows that the spirals are caused by HHFW power flowing along open field lines that originate at radii between the antenna and the LCFS. The spiralled geometry occurs because the field lines strike the divertor regions further around toroidally and further inward in major radius as the radii of the lines at the antenna midplane approach the LCFS. Magnetic pitch scans show that the spirals move inward in major radius in the divertor regions at a given toroidal location with increasing pitch, as observed with cameras, tile currents, and Langmuir probes. The magnetic mappings track this behavior quite well. This one-to-one mapping of edge power flow from the SOL in front of the antenna to the divertor region should validate advanced RF codes for the SOL (e.g., [3]) against power flow along the field lines. Such codes then can be used to understand this edge power loss process and to assure minimization of RF heat deposition and erosion in the divertor on ITER.

References

- [1] J. C. Hosea *et al.*, AIP Conf Proceedings **1187** (2009) 105.
- [2] G. Taylor *et al.*, Physics of Plasmas **17** (2010) 056114.
- [3] D. L. Green *et al.*, Physical Review Letters **107** (2011) 145001.

This work was supported by DOE Contract No. DE-AC02-09CH11466.

Direct Diagnosis and Parametric Dependence of 3D Helical Equilibrium in the MST RFP

B. Chapman¹, F. Auriemma², W. Bergerson³, D. Brower³, S. Cappello²,
D. Den Hartog¹, W. Ding³, P. Franz², S. Kumar¹, P. Innocente², J. H. Kim¹, L. Lin³,
R. Lorenzini², E. Martines², K. McCollam¹, B. Momo², M. Nornberg¹, E. Parke¹,
P. Piovesan², M. E. Puiatti², J. Reusch¹, J. Sarff¹, M. Spolaore², D. Terranova²,
P. Terry¹, and P. Zanca²

¹University of Wisconsin-Madison, Madison, USA

²Consorzio RFX, Padova, Italy

³UCLA, Los Angeles, USA

Corresponding Author: bchapman@wisc.edu

Helical (stellarator-like) equilibria can occur in the core of nominally axisymmetric tokamak and RFP plasmas, including the “snake” in JET [1], planned hybrid-scenario plasmas in ITER [2], and the “single-helical-axis” (SHAx) state in RFX-mod [3]. Here we report for the first time the emergence of the SHAx state in MST, and we report the first direct measurement of the internal magnetic field evolution associated with such a helical equilibrium [4]. Both the probability of the SHAx state’s emergence and its duration increase strongly with I_p in MST and RFX-mod, but the required I_p in MST is lower than in RFX-mod. However, due to differences in other plasmas parameters as well, the two devices share a common range of the dimensionless Lundquist number, thus better unifying the results. This state is still not entirely understood [5], but recent theoretical work analogizing the helical structure to a coherent turbulent vortex predicts that the structure’s ability to sustain itself increases as I_p^2 [6].

References

- [1] A. Weller *et al.*, Phys. Rev. Lett. **59** (1987) 2303.
- [2] W. A. Cooper *et al.*, Plasma Phys. Controlled Fusion **53** (2011) 024002.
- [3] R. Lorenzini *et al.*, Nature Phys. **5** (2009) 570.
- [4] W. F. Bergerson *et al.*, Phys. Rev. Lett. **107** (2011) 255001.
- [5] S. Cappello *et al.*, Nucl. Fusion **51** (2011) 103012.
- [6] J. H. Kim and P. W. Terry, paper to be submitted.

Internal Amplitude, Structure and Identification of CAEs and GAEs in NSTX

N. Crocker¹, E. D. Fredrickson², N. N. Gorelenkov², W. A. Peebles¹, S. Kubota¹,
R. E. Bell², B. P. LeBlanc², J. E. Menard², M. Podesta², K. Tritz³, and H. Yuh⁴

¹*University of California Los Angeles, Los Angeles, USA*

²*Princeton Plasma Physics Laboratory, Princeton, USA*

³*The Johns Hopkins University, Baltimore, USA*

⁴*Nova Photonics, Princeton, USA*

Corresponding Author: ncrocker@physics.ucla.edu

Fast-ions (e.g., fusion alphas and neutral beam ions) will excite a wide range of instabilities in ITER or a Fusion Nuclear Science Facility device. Among the possible instabilities are high frequency Alfvén eigenmodes (AE) excited through Doppler-shifted cyclotron resonance with beam ions [1]. High frequency AEs cause fast-ion transport [2,3,4], correlate with electron thermal transport [5] and are postulated to contribute to ion heating [6]. These high frequency modes have historically been identified variously as compressional (CAE) or global (GAE) Alfvén eigenmodes, but the identification has not proven conclusive. Identification is essential to understanding the extent of their effect, since the two types of modes have very different effects on resonant particle orbits. The effect on plasma performance of high frequency AEs is investigated in NSTX. This is facilitated by a recently upgraded array of 16 fixed-frequency quadrature reflectometers. Detailed measurements of high frequency AE amplitude and eigenmode structure were obtained in a high power (6 MW), beam-heated H-mode plasma (shot 141398) [7] very similar to those discussed in Ref. [5]. These measurements, which extend from the plasma edge to deep in the core, can be used in modeling the effects of the modes on electron thermal transport. The observed modes are identified by comparison of their frequency and measured toroidal mode numbers with local Alfvén dispersion relations [7]. The modes identified as CAEs have higher frequencies and smaller toroidal mode numbers than the GAEs. Also, they are strongly core localized, in contrast with the GAEs, which also peak toward the plasma center but have much broader radial extent.

References

- [1] W. W. Heidbrink, *et al.*, Nucl. Fusion **46** (2006) 324.
- [2] E. D. Fredrickson, *et al.*, Phys. Plasmas **11** (2004) 3653.
- [3] E. D. Fredrickson, *et al.*, Europhys. Conf. Abstracts 35G, **2** (2011) 119.
- [4] E. D. Fredrickson, *et al.*, Proc. of 23rd IAEA FEC, Daejeon, Korea, (2010), EXW/P7-06.
- [5] D. Stutman, *et al.*, Phys. Rev. Lett. **102** (2009) 115002.
- [6] D. Gates, *et al.*, Phys. Rev. Lett. **87** (2001) 205003.
- [7] N. A. Crocker, *et al.*, Plasma Phys. Contr. Fusion **15** (2011) 105001.

Work supported by U.S. DOE Contracts DE-FG02-99ER54527 and DE-AC02-09CH11466.

Fast-ion Redistribution and Loss due to Edge Perturbations in the ASDEX Upgrade, DIII-D and KSTAR Tokamaks

M. Garcia-Munoz¹, S. Äkäslopolo², O. Asunta², J. Boom³, X. Chen⁴,
I. G. J. Classen³, G. D. Conway¹, R. K. Fisher⁵, B. Geiger¹, T. Happel¹,
W. W. Heidbrink⁴, V. Igochine¹, J. Kim⁶, J. Y. Kim^{6,7}, T. Kurki-Suonio²,
N. Lazanyi⁸, N. Luhmann⁹, T. Lunt¹, M. Maraschek¹, M. A. Van Zeeland⁵,
W. Suttrop¹, H. Park¹⁰, T. L. Rhodes¹¹, G. I. Pokol⁸, D. Pace⁵, K. Shinohara¹²,
M. Willensdorfer¹³, and E. Wolfrum¹

¹Max-Planck Institute for Plasma Physics, Garching, Germany

²Aalto University, Aalto, Finland

³FOM Institute DIFFER, Nieuwegein, Netherlands

⁴University of California Irvine, Irvine, USA

⁵General Atomics, San Diego, USA

⁶National Fusion Research Institute, Daejeon, Republic of Korea

⁷University of Science and Technology, Daejeon, Republic of Korea

⁸Budapest University of Technology, Budapest, Hungary

⁹University of California-Davis, Davis, USA

¹⁰POSTECH, Pohang, Republic of Korea

¹¹University of California-Los Angeles, Los Angeles, USA

¹²JAEA, Naka, Japan

¹³Technische Universität Wien, Vienna, Austria

Corresponding Author: manuel.garcia-munoz@ipp.mpg.de

The impact of Edge Localized Modes (ELMs) and externally applied resonant and non-resonant Magnetic Perturbations (MPs) on fast-ion confinement/transport has been investigated in the ASDEX Upgrade, DIII-D and KSTAR tokamaks. These studies were enabled by coordinated multi-machine experiments and new diagnostic capabilities that provide detailed experimental results of the interaction between energetic particles and instabilities in particle phase-space. New findings include: bursts of fast-ion losses induced by ELMs dominate the losses in H-mode plasmas as measured by fast-ion loss detectors (FILDs) at different toroidal and poloidal positions; in low-collisionality H-modes, ELM and inter-ELM fluctuations in fast-ion losses appear often strongly connected with main ELM properties and edge flows; filamentary fast-ion losses are observed during ELMs suggesting a strong interaction between fast-ions and the instabilities concomitant to the ELM blobs and filaments; large changes in escaping-ion phase-space are observed within single ELMs; during the mitigation/suppression of type-I ELMs by externally applied MPs, the large fast-ion blobs/filaments observed during ELMs are replaced by a loss of fast-ions with a broad-band frequency and an amplitude of up to 6 times higher than the NBI prompt loss signal without MPs; a clear synergy in the overall fast-ion transport is observed between edge perturbations and internal MHD fluctuations such as Alfvén Eigenmodes (AEs) and sawteeth. Measured fast-ion losses are typically on banana orbits that explore the entire pedestal / Scrape-Off-Layer (SOL). A systematic study of the observed fast-ion losses induced ELMs (mitigated and not-mitigated) and MPs as a function of the MP configuration and magnitude will be presented together with F3D-OFMC and ASCOT simulations of the MP induced fast-ion losses.

EX-P

First Operations of the Real-Time ECRH/ECCD System for Control of Magnetohydrodynamics Instabilities in the FTU Tokamak

C. Sozzi¹, E. Alessi¹, L. Boncagni², C. Galperti¹, C. Marchetto¹, S. Nowak¹, W. Bin¹, A. Botrugno², A. Bruschi¹, S. Cirant¹, G. D'Antona³, O. D'Arcangelo¹, D. Farina¹, L. Figini¹, R. Ferrero³, S. Garavaglia¹, G. Gustavo¹, A. Grosso², F. Iannone², E. Lazzaro¹, A. Moro¹, V. Mellerà¹, D. Minelli¹, M. Panella², P. Platania¹, G. Ramponi¹, A. Simonetto¹, B. Tilia², V. Vitale², and O. Tudisco²

¹*Istituto di Fisica del Plasma CNR, Associazione EURATOM-ENEA, Milano, Italy*

²*C.R. Frascati, Associazione EURATOM-ENEA, Padova, Italy*

³*Dipartimento di Elettrotecnica, Politecnico di Milano, Milano, Italy*

Corresponding Author: sozzi@ifp.cnr.it

Time-controlled injection of powerful Electron Cyclotron (EC) waves is an effective way to reduce the tearing instabilities that can develop close to low rational m/n (poloidal/toroidal mode numbers) magnetic surfaces in tokamak operations at high β (plasma/magnetic pressure). A Real Time Control (RTC) system including fast data acquisition/elaboration and actuator's control is being implemented in FTU tokamak. Most of the elements of the control chain of the prototype system have been successfully tested in plasma operations. Main objectives are the detection and control of $m/n = 3/2$ and $2/1$ NTM, and of the sawtooth activity. The actuator is the newly installed fast (poloidal angular velocity = $1^\circ/0.01$ s) steerable two-beam (2×0.4 MW $\times 0.5$ s) 140 GHz EC launcher. The RTC system uses signals from standard diagnostics: electron temperature from 12-channels ECE (EC Emission) grating polychromator, 2×8 magnetic from the Mirnov coils and 2 ECRH power monitors. This set of signals undergoes a two-stage elaboration through the control chain. Main task of the first stage is MHD activity detection and location. In the second stage the controller provides time and space references for the EC power injection. The diagnostics codes act in a timescale ($1 - 50 \mu\text{s}$) significantly shorter than the time step of the controller (1 ms). The architecture of the system allows taking advantage of available a-priori information about the probable location of the unstable perturbation. A fast magnetic equilibrium reconstruction and a fast EC ray tracing codes have been implemented for these purposes. The main algorithms blocks in the detection stage are ECE-ECE, ECE-Mirnov and ECE-ECRH cross-correlation in the time domain, and SVD (Single Value Decomposition) of Mirnov signals in time and space domain. The cross-correlation algorithms are used to locate the magnetic island and SVD provides an independent marker of the instability through its frequency detection. The control system is implemented with the open-source framework MARTe (Multi-threaded Application Real-Time executor) on Linux/RTAI real-time operating system. The capabilities of effective detection, false positive resilience, and mode number discrimination are discussed through the application to actual plasma data. The process of validation of RT tools by comparison with off-line analysis is also described.

Fast-ion Energy Loss during TAE Avalanches in the National Spherical Torus Experiment

E. Fredrickson¹, D. Darrow¹, N. Gorelenkov¹, G. Kramer¹, M. Podesta¹, S. Gerhardt¹, R. Bell¹, A. Diallo¹, B. LeBlanc¹, R. White¹, N. Crocker², S. Kubota², A. Bortolon³, F. Levinton⁴, and H. Yuh⁴

¹*Princeton Plasma Physics Laboratory, Princeton, USA*

²*UCLA, Los Angeles, USA*

³*UCI, Irvine, USA*

⁴*Nova Photonics, Princeton, USA*

Corresponding Author: efredrickson@pppl.gov

Strong TAE avalanches on the National Spherical Torus Experiment are typically correlated with drops in the neutron rate in the range of 5 – 15%. In previous studies of avalanches in L-mode plasmas, these neutron drops were shown to be consistent with modeled losses of fast ions due to the strong, multi-mode TAE bursts. In this study, TAE avalanches in an NSTX H-mode plasma were studied. At the measured TAE mode amplitudes, simulations with the ORBIT code found that fast ion losses were negligible. However, the ORBIT simulations predicted that the TAE would scatter the fast ions in energy, resulting in a significant drop in fast ion β , even in the absence of fast ion losses. Convoluting the fast ion distribution with the energy dependence of the D-D fusion cross-section rate found that this drop in fast ion beta was consistent with the measured drop in neutron rate. Further, the estimated change in the fast ion energy is comparable to the estimated energy in the TAE wave-field.

Work supported by U.S. DOE Contract DE-AC02-09CH11466, DE-FG02-06ER54867, and DE-FG02-99ER54527.

EX-P

Measurement and Optimisation of the Fast Ion Distribution on MAST

M. Turnyanskiy¹, C. Challis¹, R. Akers¹, M. Cecconello², A. Kirk¹, S. Pinches¹,
S. Sangaroon¹, and I. Wodniak²

¹*EURATOM/CCFE Fusion Association, Culham Science Centre, Abingdon, UK*

²*Dept. of Physics and Astronomy, Uppsala University, Uppsala, Sweden*

Corresponding Author: mikhail.turnyanskiy@ccfe.ac.uk

A key tool to control the q -profile and provide heating and non inductive current drive is Neutral Beam Injection (NBI), which relies on good Fast Ion (FI) confinement. Driving current by Neutral Beam Current Drive (NBCD) scheme is particularly important in STs due to the limited applicability of other non-inductive current drive schemes and because of the limited space available for neutron shielding of a solenoid. Operations with high NBI power and increased FI pressure pose an additional risk of destabilising low- n FI driven instabilities potentially degrading the FI confinement and leading to the loss of core heating and current drive.

Previous results from MAST and other tokamaks indicate the presence of anomalous fast ion redistribution which increases with beam power. In this paper we present a quantification of this effect on the FI population by utilising new diagnostic capabilities for monitoring of the fast ions on MAST such as recently commissioned scanning Neutron Camera (NC) and Fast Ion D $_{\alpha}$ Emission (FIDA) diagnostics. The observed anomalous FI diffusivity correlates with the amplitude of $n = 1$ energetic particle modes, indicating that they are the probable cause of the anomaly in MAST. Finally it will be demonstrated that broadening the fast ion pressure profile by the application of NBI in an off-axis location can mitigate the growth of these modes and result in a dramatic reduction in the anomalous fast ion redistribution.

Results show the value of neutron profile measurements, not only for diagnosing the fast ion density profile to quantify the effects of instabilities on the FI distribution, but also to allow the optimisation of plasma scenarios and even machine design to maximise the effectiveness of heating and current drive systems. Further modelling work is ongoing to describe these FI driven mode-plasma interactions in more detail. The achieved reduction in anomalous FI transport by controlling the FI distribution is predicted significantly improve NBCD efficiency together with the potential for current profile control and providing encouraging prospects for the use of off-axis NB injection in future tokamak devices.

This work was funded by the RCUK Energy programme and EURATOM.

Electron Fishbones in LHCD Plasmas on FTU and Tore Supra

Z. O. Guimarães-Filho¹, N. Dubuit¹, S. Benkadda¹, A. Botrugno², P. Buratti²,
G. Calabro², J. Decker³, D. Elbeze³, X. Garbet³, P. Maget³, A. Merle³, G. Pucella²,
R. Sabot³, A. A. Tuccillo², and F. Zonca²

¹*Aix Marseille University, Marseille, France*

²*Associazione Euratom-ENEA sulla Fusione, Roma, Italy*

³*CEA, IRFM, Saint-Paul-Lez-Durance, France*

Corresponding Author: zwinglio.guimaraes@yahoo.com.br

Usually, Electron driven fishbone modes are observed in Electron Cyclotron Resonant Heating (ECRH) plasmas [1,2]. The fast electrons produced by Lower Hybrid Current Drive (LHCD) systems often help destabilizing these modes when using a combination of ECRH and LHCD [2], but in most machines LHCD alone is unable to destabilize *e*-fishbones [1,2]. However, in FTU and Tore Supra *e*-fishbones were recently observed in shots with LHCD only [3,4].

The evolutions of the mode radial position and frequency were determined from the ECE measurements using the procedure presented in [5]. In a second step, the energy of the resonant electrons was estimated based on the expression of the precession drift frequency [3].

In FTU, two regimes of *e*-fishbones (with and without bursts) can be obtained depending on the LH power [3], while in Tore Supra, only near stationary evolutions are observed. On the other hand, frequency jumps between modes with different mode wave numbers can be observed only in Tore Supra [4].

The relative trend of the mode frequency and position in FTU depends on the fishbone regime: the evolution in the regime without bursts is much slower than in the burst regime [6]. Moreover, the frequency evolution during the bursts is consistent with a nonadiabatic downward frequency chirping produced by mode particle pumping [6].

In Tore Supra, the mode position evolves continuously even during the frequency jumps. Moreover, the mode position evolution agrees with the *q*-profile evolution and corresponds to an inverse cascade in mode wave numbers starting by an 4/4 mode and finishing in a 1/1.

In both tokamaks, the energy of the resonant electrons was found to be close to the thermal energy if the pitch angle correction is neglected. Moreover, recent theoretical works [7] have shown that the passing electrons may also contribute to the drive of *e* fishbones. The dispersion relation in this case allows solutions with the mode frequency much lower than the precessional drift frequency [7], in agreement with these observations.

References

- [1] K. L. Wong Phys.Rev.Lett. **85** (2000) 996
- [2] X. T. Ding Nucl. Fusion **42** (2009) 491.
- [3] F. Zonca Nucl. Fusion **47** (2007) 1588.
- [4] A. Macor Phys.Rev.Lett. **102** (2009) 155005.
- [5] Z. O. Guimarães-Filho Plasma Phys. Control. Fusion **53** (2011) 074012.
- [6] Z. O. Guimarães-Filho submitted to Nucl. Fusion
- [7] A. Merle, 12th IAEA, Austin (USA), 2011

EX-P

Development of Electron Cyclotron Wave Absorption Measurement for Real-Time Polarization Optimization and Studies of Quasilinear Effects

T. Goodman¹, J. Decker², S. Coda¹, F. Felici³, and M. Silva¹

¹*EPFL-CRPP, Lausanne, Switzerland*

²*CEA, IRFM, St Paul-Lez-Durance, France*

³*Eindhoven University of Technology, Eindhoven, Netherlands*

Corresponding Author: timothy.goodman@epfl.ch

Electron Cyclotron Resonance Heating (ECRH) and current drive (ECCD) is in widespread use in today's tokamaks and is planned for ITER, from plasma breakdown through the current ramp-down. The ITER control system must avoid coupling to the first-harmonic X mode (X1) at full field since any polarization mismatch of O1 at the plasma surface will be immediately reflected from the X-cutoff, which is close to the plasma edge, and the power from the focused beams will strike the wall and cause localized heating during the long pulse length in ITER. Accurate knowledge of the power absorption efficiency is also clearly beneficial to an intelligent application of these techniques but is notoriously difficult to obtain. A promising candidate is the measurement of stray power escaping the plasma using microwave radiation detectors.

To this end, fast polarizers on TCV are used on a receiver antenna while one launching antenna acts as a transmitter of short perturbation pulses, and additional antennas heat the plasma. Non-absorbed launched power is reflected off the inner wall and is incident on the receiver permitting a two-pass-transmission measurement. These experiments can provide a detailed check of ray-tracing, absorption and transmitted polarization calculations, and of the maximization routine to be used with the fast polarizers to determine that polarization, in the presence of scattered power. The key point here is that the transmitted signal (determined by the input polarization) to noise (scattering from blobs, plasma surface, various MHD modes, etc.) ratio in the undesired mode can be varied intentionally from shot-to-shot using the input polarizers. The TCV experiments provide input data for designing a protection system and quantify the measurable lower power limits that can be expected using ITER relevant polarizers.

Once characterized, the double-pass transmission and stray radiation measurements will also be used during experiments on TCV to quantify the quasilinear (QL) effects in ECRH absorption and compare them with theory. In conditions where the optical thickness is ~ 0.6 , we explore the transition region where QL flattening should show up in the total absorption. A power scan should reveal a decreasing fraction of power absorption with increasing power.

This work was supported in part by the Swiss National Science Foundation.

Analysis of Alfvén Wave Activity in KSTAR Plasmas

M. J. Hole¹, C. M. Ryu², Y. M. Hao², K. Toi³, J. Kim⁴, and J. G. Bak³

¹*Plasma Research Laboratory, Australian National University, Canberra, Australia*

²*POSTECH, Pohang, Republic of Korea*

³*National Institute for Fusion Science, Toki, Japan*

⁴*National Fusion Research Institute, Daejeon, Republic of Korea*

Corresponding Author: matthew.hole@anu.edu.au

We report on evidence of neutral beam driven wave activity in KSTAR plasmas. In 2010 and 2011 campaigns KSTAR plasmas included 1MW of neutral beam heating, which provided drive for Alfvénic wave activity modes. Data from the 2010 campaign, which was fully analysed during 2011, identifies the 40 kHz magnetic fluctuations as a β -induced Alfvén eigenmode resonant with the $q = 1$ surface. Evidence is multiple fold: a Fourier mode analysis identifies the mode as $n = 1$. Electron cyclotron emission chords identify the $q = 1$ inversion radius. These constrain equilibrium reconstruction, and permit detailed MHD calculations using the global MHD stability code MISHKA. A scan of mode frequency near the $q = 1$ minimum of the continuum identifies a core localised $n = 1$ mode separated from the continuum. A complementary kinetic analysis, when coupled with ion and electron temperature measurements ratios obtain from crystallography, enables calculation of the frequency evolution - which is in agreement with observations.

In 2011 a series of experiments were conducted to scope Alfvén excitation using NBI and ECRH heating as a function of field strength and plasma current. In these experiments plasmas with toroidal current up to 600 kA were generated with 1.5 MW of NBI heating and up to 120 kW of co or counter ECRH, and the field strength varied from 1.7 T to 2 T. Spectral and mode number analysis of the magnetics data identifies 150 – 250 kHz coherent activity with a toroidal mode number of $n = 1$. Assuming a poloidal mode number of $m = 1$, we have computed the evolution of the toroidal Alfvén eigenmode (TAE) middle of the gap frequency, and compared the frequency evolution to magnetic spectrograms. While the frequency of the mode is above the Nyquist frequency, the aliased frequency tracks the observations to within 20%, providing some confidence of a TAE interpretation. Finally, we also report evidence of ion fishbone activity.

EX-P

Physics and Technology in the Ion-cyclotron Range of Frequency on Tore Supra and TITAN Test Facility: Implication for ITER

T. Hoang¹, X. Litaudon¹, J. M. Bernard¹, L. Colas¹, R. Dumont¹, J. Jacquot¹, A. Argouarch¹, H. Bottollier-Curtet¹, S. Brémond¹, S. Champeaux², Y. Corre¹, P. Dumortier³, M. Firdaouss¹, D. Guilhem¹, J. Gunn¹, P. Gouard¹, C. Klepper⁴, M. Kubic¹, G. Lombard¹, D. Milanese⁵, A. Messiaen³, P. Mollard¹, O. Meyer¹, and D. Zarzoso¹

¹CEA, IRFM, St-Paul-Lez-Durance, France

²CEA, DAM, DIF, Arpajon, France

³Association EURATOM-Belgian State, TEC, Royal Military Academy, Brussels, Belgium

⁴Oak Ridge National Laboratory, Oak Ridge, USA

⁵Department of Electronics, Politecnico di Torino, Torino, Italy

Corresponding Author: tuong.hoang@cea.fr

The ITER ion-cyclotron range of frequency (ICRF) heating system, required to couple 20 MW of power to the plasmas in continuous wave (CW), have provide robust coupling for a variety of plasma scenarios with edge localized modes. To support the design of this system and to mitigate risks of operation in ITER, CEA has initiated some R&D programs accompanied by experiments together with modeling efforts. This paper reports recent results, including:

1. Test of a new Faraday screen (FS) concept electrically characterized by a slotted frame and cantilevered horizontal rods, on Tore Supra. RF sheath rectification is now better understood and included self-consistently in the ITER antenna physics design.
2. First operation of CW test bed facility TITAN. This consists in qualifying the Tore Supra ICRH antenna in long duration operation of 1000 s.
3. R&D of high permittivity materials for the load test of the antenna under ITER plasma conditions.

In addition, results of the design of ITER ICRH scenarios using the full wave code EVE are reported, particularly the current drive efficiency calculation. In ITER, due to the simultaneous presence of multiple species there is no pure fast wave current drive configuration unlike present day experiments. Nevertheless, a current of ± 200 kA in DT, or ± 100 kA in DT(³He) could be driven on axis with 10 MW of power.

Study of Fast Ion Confinement in the TUMAN-3M

S. Lebedev¹, L. Askinazi¹, A. Barsukov², F. V. Chernyshev¹, V. Kornev¹,
S. Krikunov¹, A. D. Melnik¹, A. Panasenkov², D. Razumenko¹, V. Rozhdestvensky¹,
G. Tilinin², A. Tukachinsky¹, M. Vildjunas¹, and N. Zhubr¹

¹*Ioffe Physical-Technical Institute, St. Petersburg, Russian Federation*

²*NRC "Kurchatov Institute", Moscow, Russian Federation*

Corresponding Author: sergei.lebedev@mail.ioffe.ru

Confinement of NBI produced fast ions (FI) in the TUMAN-3M tokamak was studied using neutron flux detectors (NFD) and neutral particle analyzer. Two NFDs measured flux of 2.45 MeV DD neutrons. They are calibrated to account for total radiated neutron flux I_n . Since ion temperature in the device is below 0.5 keV neutrons are produced by beam-plasma reactions and thus their flux is very sensitive to FI amount. NPA measured spectra of thermal and slowing down ions in the range of 0.2 – 30 keV.

In the experiments deuterium NB with $E_b = 19 - 25$ keV was injected in co-current direction tangentially to surface with $R_{inc} = 0.42$ m (plasma major radius R_0 is 0.53 m and minor radius a_l is 0.22 m; working gas is deuterium). Recently performed upgrade of power supply allowed to increase toroidal field B_t and plasma current I_p in the NBI phase from 0.68 to 1.0 T and from 140 to 190 kA, correspondingly. With higher B_t & I_p an improvement of target plasma performance was observed. In particular, increase in the central electron temperature $T_e(0)$ from 0.4 – 0.5 up to 0.65 – 0.75 keV and two-fold decrease of effective charge increment ΔZ_{eff} during NBI application were found. The increase of $T_e(0)$ resulted in longer FI slowing down time. Decrease of ΔZ_{eff} is clear indication of substantial reduction of first orbit losses.

Increases in B_t & I_p resulted in growth of I_n at similar E_b and n_e indicating enhanced capture of FI. Two-fold increase in I_n with increasing B_t & I_p was found. Factor of 1.2 of the I_n increase is explained by increased deuterium content in the bulk plasma due to Z_{eff} decrease. Some 20% of the I_n increase is evidently caused by enhanced capture of FI. Remaining 45% of the flux increase might be understood if longer FI slowing down time τ_s at higher B_t & I_p is assumed. The assumption is in line with the expectation of τ_s increase with T_e rise ($\sim T_e^{3/2}$).

To examine an existence of FI losses exceeding Coulomb deceleration the characteristic time of I_n decay after NBI switch-off τ_n was measured. Measured τ_n appeared to be by a factor of 1.1 – 1.2 shorter than the one calculated from classical collision theory. This was explained by charge-exchange losses and by FI redistribution induced by beam instabilities. Measured by NPA enhancement in the ion tail is in agreement with simulations of NB capture efficiency and neutron flux measurements.

EX-P

Investigation of the Role of Energetic Particle in the Driving of Long-lived Saturated Internal Mode on HL-2A Tokamak

W. Deng¹, Y. Liu¹, X. Q. Wang², W. Chen¹, Y. B. Dong¹, S. Ohdachi³, X. Q. Ji¹, Y. Shen¹, J. Y. Cao¹, J. Zhou¹, B. B. Feng¹, Y. G. Li¹, X. L. Huang¹, J. M. Gao¹, X. Y. Han¹, Z. W. Xia¹, M. Huang¹, H. Wang¹, X. R. Duan¹, and X. G. Wang⁴

¹*Southwestern Institute of Physics, Chengdu, China*

²*School of Physics and Optoelectronic Technology, Dalian, China*

³*National Institute for Fusion Science, Toki, Japan*

⁴*School of Physics and State Key Lab of Nuclear Physics & Technology, Beijing, China*

Corresponding Author: dengw@swip.ac.cn

Long-lived saturated internal mode (LLM) in HL-2A tokamak, observed during neutral beam injection (NBI) with weakly reversed or broad low magnetic shear, is considered as a pressure-gradient driven MHD mode triggered by energetic particles. When the LLM occurs, a reduction in the electron density and the plasma stored energy, and fast ion losses are usually observed. The observed LLM appears with the safety factor profile has a weak shear in a broad range with q_{\min} around unity. The ideal interchange can become marginal stable due to the weak magnetic shear if $\Delta q = 1 - q_{\min}$ reaches a critical value, then it can be excited by the energetic particles during NBI. In HL-2A experiments, it is observed that LLMs can be suppressed by electron cyclotron resonant heating (ECRH), and by applying supersonic molecular beam injection (SMBI) or cluster jet injection (CJI) effectively. The control of LLMs may also be related to the change of Δq or the pressure profile induced by the local heating or fuelling.

EX-P

Nonlinear Features of the Alfvénic Wave-particle Interaction in Auxiliary Heated HL-2A Plasma

Y. Liu¹, X. Peng¹, X. Ji¹, Y. Dong¹, L. Yu¹, W. Chen¹, Y. Zhang¹, M. Isobe², and X. Duan¹

¹*Southwestern Institute of Physics, Chengdu, China*

²*National Institute for Fusion Science, Toki, Japan*

Corresponding Author: yiliu@swip.ac.cn

The physics of Alfvénic gap modes and their interaction with energetic particles is of interest in both magnetic fusion and nonlinear physics. Alfvénic gap modes may eject energetic particles from the plasma and impair reactor performance. Alfvénic modes can also provide a paradigm-testing case for nonlinear wave-particle interaction physics. Phenomena related to wave-particle interaction are identified in the tokamak plasma of the HL-2A, where the beta-induced Alfvén acoustic eigen mode (BAAE) are triggered by energetic ions produced by neutral beam heating while β -Induced Alfvén Eigenmode (BAE) is driven by fast electrons. The experimental signatures of the nonlinear regime include frequency splitting, chirping and spectral broadening. These phenomena are found to be consistent with a general nonlinear theory of kinetic instabilities near stability threshold developed by Berk.

In this paper, we report the first experimental identification of the strongly nonlinear regime in the interaction of Alfvénic wave on energetic particles in HL-2A. First, a clear splitting was firstly observed for BAAE. Second, pitch-fork splitting is also observed for BAE. At last, an e-BAE can transform into three branches with a feature of broadband rather than discrete in frequency. The nonlinear BERK-Breizman model is used to interpret the phenomena over a wide parameter range. A Vlasov code is used to solve the BERK-Breizman model numerically with the parameters of HL-2A plasma, taking into account a collision term that represents particle annihilation and injection processes, and an external wave damping accounting for background dissipative mechanisms. To compare theory and experiment simulated signal is constructed, using typical HL-2A values to return from normalized time to real time. The phenomena can now be explained in terms of BERK-Breizman theory in the sideband formation, chirping regime or chaotic regime. The experimental data presented here identify for the first time a fast-ion-driven BAAE activity and a fast-electron-driven BAE instability in the nonlinear regime. The observed features agree with predictions of the Berk-Breizman-Pekker model, including rapid, nonperiodic variation in mode amplitudes. Characterizing the non-linear states of the BAAE, BAE yielded information about the fast particle population and the diffusion induced by NBI or ECRH.

EX-P

Frequency Jump Phenomena of e -Fishbone during High Power ECRH on HL-2A Tokamak

L. Yu¹, X. Ding¹, S. Chen², W. Chen¹, Y. Dong¹, J. Dong¹, X. Ji¹, Z. Shi¹, Q. Yang¹,
Y. Zhou¹, X. Song¹, J. Zhou¹, J. Rao¹, M. Huang¹, B. Feng¹, Y. Huang¹, Y. Liu¹,
L. Yan¹, and X. Duan¹

¹Southwestern Institute of Physics, Chengdu, China

²College of Physical Science and Technology, Sichuan University, Chengdu, China

Corresponding Author: yulm@swip.ac.cn

It is important to carry out the experimental studies for the fishbone instabilities, which are relevant for understanding alpha particle dynamics in burning plasmas. The e -fishbone frequency jump related to the redistribution of the energetic electrons has been observed on Tore Supra with LHCD, which is important for the energetic particle losses. In this paper, the e -fishbone frequency jump phenomena with high power on axis ECRH on HL-2A will be reported. The new results are different from the phenomena on Tore-Supra, because the trapped particle is dominated in this case.

The frequency spectra of the soft x-ray shows that the frequency of the fluctuations is about 5 kHz in the low ECRH power and increases to about 8 kHz when the power increases to 1.2 MW. The chirping mode during ECRH has been identified as the fishbone instability induced by energetic electrons in the previous investigation in the device. It is interested to study the nature of the frequency jump phenomena in the high power ECRH. The frequency jump can be observed, when ECRH power increases to about 0.7 MW. The frequency jump phenomena appear within about 25 ms periodically. The frequency jumps between 8 kHz and 15 kHz, when the power is 1.2 MW. The evidence of the changes of poloidal wave number can be obtained by the results of the tomography of two soft x ray arrays. The results show that the modes are located $q = 1$ surface and poloidal wave numbers are $m = 1$ or 2. That means the mode changes between $m/n = 1/1$ and $m/n = 2/2$.

It is very important to understand the mechanism driven by both the passing particles and trapped particles, comparing with the e -fishbone features during LHCD. And it is also very important to study the instability with high power electron heating and the confinement of the energetic particles.

Coexistence of Alfvénic Modes Induced by Energetic Electrons with ECRH on HL-2A

X. Ding¹, L. Yu¹, S. Chen², W. Chen¹, X. Ji¹, J. Dong¹, Z. Shi¹, Q. Yang¹, X. Song¹,
J. Zhou¹, J. Rao¹, M. Huang¹, Y. Zhou¹, B. Feng¹, Y. Huang¹, Y. Liu¹, L. Yan¹, and
X. Duan¹

¹*Southwestern Institute of Physics, Chengdu, China*

²*Sichuan University, Chengdu, China*

Corresponding Author: dingxt@swip.ac.cn

The MHD instabilities driven by energetic-particle are of particular importance for future burning plasma devices, where energetic particles will be produced by high power heating and fusion reaction. The energetic electron behaviors in present devices can provide a contribution for burning plasma research, because their effect on low-frequency MHD modes in the former has the analogous effect of the fast ions in the latter. In this paper, the new experimental results about coexistence of the low frequency multi-modes driven by energetic electrons with high ECRH power are presented.

The evolution of the magnetic fluctuations during ECRH has been observed by means of Mirnov coils and soft x-ray arrays. Experimental results show that the multi-mode coexistence phenomena occur during the high power ECRH both with on-axis and off-axis deposition. With the low ECRH, only one mode can be observed, which has been identified as *e*-BAE. When the power is over about 600 kW, two or three peaks appear in the spectra of the magnetic fluctuation. The modes located outside of 20 cm of the minor radius. These modes are proved to be related with the energetic electrons strongly and disappear when the plasma density increase during gas puffing.

To obtain the detail features of the modes, the mode numbers, the power density spectra and the correlation spectra both toroidally and poloidally have been analyzed. The toroidal mode numbers of the modes are $n = 1$ or 2 . The frequencies of the modes are proportional to Alfvén frequency, but much lower than it. The statistical curves for frequency of the three modes versus the $Bn_e^{-1/2}$ have been obtained with the magnetic field from 1.2 T to 1.4 T and the density from $0.3 \times 10^{13} \text{ cm}^{-3}$ to $1.4 \times 10^{13} \text{ cm}^{-3}$, indicating that all of them are related with low frequency Alfvén modes. The frequency spectra are broadening and overlap each other, when the ECRH power high enough. No clear nonlinear interaction between the modes and the other low frequency MHD mode occurs in high power ECRH plasma from the bicoherence spectra analysis.

The multi-mode coexistence phenomena driven by energetic electrons with high ECRH power are observed for the first time. This evolution should be very important for the ITER, because the multi-modes coexistent magnetic structure in the high temperature plasma will affect the plasma transport greatly.

EX-P

Electron Bernstein Wave Heating and Electron Cyclotron Current Drive by Use of Upgraded ECH System in LHD

Y. Yoshimura¹, H. Igami¹, S. Kubo¹, T. Shimozuma¹, H. Takahashi¹, M. Nishiura¹, S. Ohdachi¹, S. Sakakibara¹, G. Motojima¹, K. Tanaka¹, K. Ida¹, M. Yoshinuma¹, C. Suzuki¹, S. Ogasawara², R. Makino², H. Idei³, R. Kumazawa¹, T. Mutoh¹, and H. Yamada¹

¹*National Institute for Fusion Science, Toki, Japan*

²*Nagoya University, Nagoya, Japan*

³*Research Institute for Applied Mechanics, Kyusyu University, Kasuga, Japan*

Corresponding Author: yoshimu@ms.nifs.ac.jp

In LHD, electron Bernstein wave (EBW) heating was successfully demonstrated by two ways of mode conversion to EBWs from injected EC-waves, by so-called slow-XB and OXB techniques. To realize the excitation of EBWs by the slow-XB technique, EC-waves in X-mode polarization should be injected to plasmas from high magnetic field side (HFS). In LHD, newly installed inner-vessel mirror close to a helical coil is used for the HFS injection. Evident increases in T_e at the plasma core region and W_p were caused by the HFS injection with 0.18 s pulse width to a plasma with $n_e(0)$ of $24 \times 10^{19} \text{ m}^{-3}$, that is, 3.3 times higher than the plasma cut-off density for O-mode waves, and 1.6× higher than the left-hand cut-off density of $14.7 \times 10^{19} \text{ m}^{-3}$ for slow-X-mode waves. Thus, the heating effects especially the increase in T_e at the plasma core region should be attributed to the mode-converted EBWs, not to the X- or O-mode waves.

For excitation of EBWs by the OXB technique, O-mode waves should be injected from the low magnetic field side toward the so-called “mode conversion window”. Two pulses of 77 GHz, 1.05 MW EC-wave (0.1 s pulse width each with a 0.1 s interval) in O-mode polarization were injected to an NB-sustained plasma, aiming at the mode conversion window calculated in advance. With both of the two ECH pulses, increases in W_p and mitigations of decreasing trend in T_e measured with ECE are recognized. The line average electron density continuously increased during the ECH pulse injection. At the start timing of the 1st pulse, $n_e(0)$ was equal to the O-mode cut-off density, $7.35 \times 10^{19} \text{ m}^{-3}$, and $n_e(0)$ gradually increased to $7.7 \times 10^{19} \text{ m}^{-3}$ at the end of the 2nd pulse. The heating efficiency $P_{\text{abs}}/P_{\text{ech}}$ is evaluated as $\sim 15\%$.

Using the high-power, long-pulse 77 GHz ECH system, 2nd harmonic on-axis ECCD experiments with 775 kW injection power and the line average electron density of $0.3 \times 10^{19} \text{ m}^{-3}$ were conducted. At optimum beam directions, maximum EC-driven currents up to 40 kA in both the co- and counter-ECCD directions were achieved. Also, recent experiment indicated that ECCD could affect the formation of an electron internal transport barrier (e-ITB). The powerful ECCD is expected to be an effective tool to control the MHD activity and the formation of e-ITB through the modification of current and rotational transform profiles.

Electron Bernstein Wave Heating and Current Drive Effects in QUEST

H. Idei¹, K. Hanada¹, H. Zushi¹, and E. Kalinnikova¹

¹*Research Institute for Applied Mechanics, Kyushu University, Fukuoka, Japan*

Corresponding Author: idei@triam.kyushu-u.ac.jp

Electron Bernstein Wave Heating and Current Drive (EBWH/CD) effects have been first observed in over dense plasmas using the developed phased-array antenna system in QUEST. Good focusing and steering properties tested in the low power facilities were confirmed with a high power level in the QUEST device. The new operational window to sustain the plasma current was observed in the RF-sustained high-density plasmas at the higher incident RF power. Increment and decrement of the plasma current and the loop voltage were observed in the over dense ohmic plasma by the RF injection respectively, indicating the EBWH/CD effects.

Noninductive Formation of Spherical Tokamak at $7\times$ the Plasma Cutoff Density by Electron Bernstein Wave Heating and Current Drive on LATE

M. Uchida¹, T. Maekawa¹, H. Tanaka¹, F. Watanabe¹, Y. Noguchi¹, K. Kengoh¹, S. Omi¹, R. Hayashi¹, T. Fukunaga¹, H. Mizogami¹, T. Kanemitsu¹, and J. Katsuma¹

¹Graduate School of Energy Science, Kyoto University, Kyoto, Japan

Corresponding Author: m-uchida@energy.kyoto-u.ac.jp

We report on an experiment of spherical tokamak formation by electron Bernstein (EB) waves in the Low Aspect ratio Torus Experiment device, in which the current reaches 10 kA and the density reaches $7\times$ the plasma cutoff density. Thus an extremely overdense torus plasma has been for the first time produced and maintained solely by EB waves. In the LATE device it was shown that EB waves can rapidly ramp up the plasma current as fast as 260 kA/s, comparable to the lower hybrid ramp-up rate. Another important capability of EB waves for production and heating of extremely overdense torus plasma has been shown in this paper.

The microwaves at 2.45 GHz from four magnetrons are injected from midplane four launchers with an oblique angle in the form of O-mode. When a microwave power of $P_{\text{inj}} = 10$ kW is injected under a weak vertical field of $B_v = 18$ G, a plasma current is initiated and increases up to 2 kA, resulting in the formation of closed flux surfaces. Next, the plasma current ramps up with ramps of the microwave power and B_v , and finally reaches 9.3 kA, after which the plasma is kept steady by $P_{\text{inj}} = 40$ kW under $B_v = 100$ G for 40 ms until the end of microwave pulse (The current reaches 11 kA when $P_{\text{inj}} = 58$ kW and $B_v = 120$ G.). The forward X-ray develops both in energy range and photon counts as I_p increases, indicating that the current is carried by EB-wave driven fast electron tail. The four chords measurement of line integrated density shows that the density reaches extremely overdense regime in the final steady phase. The final line averaged density reaches $n_e = 5.2 \times 10^{17} \text{ m}^{-3}$, that is $7\times$ the plasma cutoff density.

The upper hybrid resonance (UHR) layer is estimated to lie to higher field side of the 2^{nd} ECR layer. Then EB waves mode converted from the incident electromagnetic waves at the UHR layer propagate in their first propagation band toward the fundamental ECR layer and may heat the bulk electrons as well as the fast electrons at the plasma core. Extreme ultraviolet emission signals from the vertical chords crossing the ECR layer on midplane show a large increase towards the final steady phase. In addition, impurity line radiations at higher excitation energies such as CV (304 eV) and OV (72 eV) appear and strongly increase toward the final stage, suggesting that the electron temperature also increase.

Plasma Rotation Behavior under Lower Hybrid Current Drive and Ion Cyclotron Range of Frequency Heating on EAST

B. Lu¹, F. Wang¹, Y. Shi^{1,3}, G. Xu¹, B. Wan¹, M. Bitter², K. Hill², S. Lee³, Y. Li¹,
and J. Fu³

¹*Institute of Plasma Physics, Chinese Academy of Sciences, Hefei, China*

²*Princeton Plasma Physics Laboratory, Princeton, USA*

³*National Fusion Research Institute, Daejeon, Republic of Korea*

Corresponding Author: blu@ipp.ac.cn

Radio frequency (RF) wave driven plasma rotation has been considered to a potential method to provide the sufficient rotation for the steady operations of ITER or future reactor-scale devices. While substantial rotations have been observed on many devices with various auxiliary RF heating schemes, the variation among the observations requires more experimental studies. Experimental rotation observations from the tangential X-ray crystal spectrometer on EAST for both low and high confinement mode plasmas under lower hybrid current driven (LHCD) and ion cyclotron resonance frequency heating (ICRF) are presented. It was found that lower hybrid wave induces co-current core rotation change individually or combined with ICRF for both low and high confinement discharges. Rotation in H-mode plasmas scales consistently with Rice scaling. For ELMy H-modes, core rotation decreases during the ELM burst phase before reaching steady state. The change in core rotation is consistent with edge rotation change for ELM phase. It was also observed that rotation decreases or even reverses its sign for some ohmic and LHCD plasmas when impurities accumulates in the core region.

EX-P

Coupling of ICRF Waves and Axial Transport of High-Energy Ions Owing to Spontaneously Excited Waves in the GAMMA 10 Tandem Mirror

M. Ichimura¹, R. Ikezoe¹, M. Hirata¹, T. Iwai¹, T. Yokoyama¹, Y. Ugajin¹, T. Sato¹,
T. Iimura¹, Y. K. Saito¹, M. Yoshikawa¹, J. Kohagura¹, Y. Shima¹, and T. Imai¹

¹*Plasma Research Center, University of Tsukuba, Ibaraki, Japan*

Corresponding Author: ichimura@prc.tsukuba.ac.jp

Ion cyclotron range of frequency (ICRF) waves have been used for plasma production, heating and sustaining MHD stability in the GAMMA 10 tandem mirror. Maximum ion temperature has reached 10 keV and the temperature anisotropy (which is defined as the temperature ratio of perpendicular to parallel to the magnetic field line) becomes more than 10. In such high performance plasmas with the strong anisotropy, high-frequency fluctuations, so-called Alfvén-ion-cyclotron (AIC) waves, are spontaneously excited. The AIC waves are excited as eigenmodes and have several discrete peaks in the frequency spectrum. In addition to magnetic probes installed in the peripheral region, a microwave reflectometer system is introduced for the measurement of spatial structure of density fluctuations owing to the ICRF waves in the core region. Couplings between the ICRF waves for heating and the excited AIC waves are clearly observed in the central cell of GAMMA 10 with the reflectometer for the first time. Parametric decay of the heating ICRF waves to the AIC waves and low-frequency waves are discussed. Waves which have differential frequencies between discrete peaks of the AIC waves are also observed in the region around 0.1 MHz. To evaluate wave-particle interactions, the behaviors of high-energy ions with energies more than 5 keV are measured with semiconductor detectors installed in the central cell and in the east end. Ions escaped across the magnetic field line are detected in the central cell and ions along the field line are detected in the east end. The fluctuations around 0.1 MHz are detected only on the signal of the semiconductor detector installed in the east end. Pitch angle scattering of high-energy ions owing to those low-frequency waves are clearly indicated. Considerable energy transport to the ends owing to the AIC waves is suggested theoretically. Energy flow along the magnetic field line is one of the important subjects when the ICRF power is injected in the perpendicular direction to magnetic field line.

This work is partly supported by Grant-in-Aid for Scientific Research under the Ministry of Education, Culture, Sports, Science and Technology, Japan (No.21540506) and also by the bidirectional collaborative research program of National Institute for Fusion Science, Japan (NIFS09KUGM040).

Investigations of LHW-plasma Coupling and Current Drive in H-mode Experiments in EAST

B. Ding¹, E. H. Kong¹, M. H. Li¹, L. Zhang², W. Wei¹, M. Wang¹, H. D. Xu¹,
G. S. Xu¹, X. F. Han¹, L. M. Zhao¹, H. C. Hu¹, Y. Yang¹, L. Liu¹, A. Ekedahl²,
Y. Peysson², J. Decker², V. Basiuk², P. Huynh², J. F. Artaud², F. Imbeaux²,
J. F. Shan¹, F. K. Liu¹, Y. P. Zhao¹, X. Z. Gong¹, L. Q. Hu¹, X. Gao¹, H. Y. Guo¹,
B. N. Wan¹, and J. G. Li¹

¹*Institute of Plasma Physics, Chinese Academy of Sciences, Hefei, China*

²*CEA, IRFM, St. Paul-lez-Durance, France*

Corresponding Author: bjding@ipp.ac.cn

Aimed at high confinement (H-mode) plasma in EAST, the LHW-plasma coupling and current drive experiments were continued since last IAEA conference, by optimizing the plasma configuration and the distance between plasma and LHW antenna. A local gas puffing pipe near LHW antenna is installed to improve LHW-plasma coupling so as to sustain H-mode plasma. In the H-mode experiment without gas puffing shows that plasma-wave coupling deteriorates as the transition from low to high (L-H) confinement occurs, due to the steep gradient density profile in H-mode, which lowers the density at the grill mouth. The density is then recovered slowly until the H-L transition occurs. The plasma radiation has a correspondingly periodic characteristic behaviour during L-H and H-L transition. Such multiple L-H-L transition is mainly due to the changes of radiation power and coupled LHW power, suggesting that the coupled LHW power for H-mode plasma is marginal.

Using lithium coating and gas puffing near LHW antenna, an example of H-mode plasma up to 3.5 is sustained by LHCD alone. It is seen that there is no obvious change in RC from L-H phase due to gas puffing and coupling deteriorates after switching off gas puffing, thus leading to H-L transition. H-mode plasma is obtained by LHCD with a wide range of parameters: $I_p = 0.4 \sim 0.8$ MA, $B_t = 1.35 \sim 1.81$ T, $n_e = 1.5 \sim 2.5 \times 10^{19} \text{ m}^{-3}$, $P_{\text{LHW}} \geq 0.5$ MW. LHW power deposition and driven current profile with C3PO/LUKE are calculated with the experimental parameters. Simulation shows that the H-mode can be obtained in a wide range of power deposition, implying that central and large driven current seems not a necessary condition for the H-mode plasma. For typical H-mode discharge, particularly the power can not propagate into the core region due to high density during the H-mode phase. As a result, driven current decreases and loop voltage increases. This can be also seen from driven current profile predicted by the CRONOS, from which H-mode is reproduced with the initial equilibrium from EFIT and density from experiments. Floating potential measured by reciprocating Langmuir probe suggests that edge fluctuation is suppressed after L-H transition. This is possibly due to that LHW drives poloidal flow which can suppress fluctuation effectively. Though the CRONOS results are preliminary, it offers an effective tool to guide and interpret experiment for EAST.

EX-P

Fast Ion Physics Enabled by Off-Axis Neutral Beam Injection

W. W. Heidbrink¹

¹ *University of California Irvine, Irvine, USA*

Corresponding Author: heidbrink@fusion.gat.com

Off-axis injection of neutral beams into DIII-D has provided new insights into fast-ion instabilities that may impact alpha-particle and neutral-beam confinement in ITER. Off-axis injection alters the stability of reversed shear Alfvén eigenmodes (RSAE). The enhanced stability for off-axis injection is attributed to flattening of the fast-ion gradient that drives the modes unstable. Beam deposition for the off-axis beams peaks near the mode location so switching between on-axis sources that inject at the midplane and off-axis sources that aim below the midplane has a large local effect on the gradient. In contrast, at larger minor radius, the fast-ion gradient is similar for on- and off-axis injection. As a result, switching between on/off-axis beams has little effect on the stability of TAEs that appear in the outer portion of the plasma. Surprisingly, even though the gradient is flattened and the mode frequencies change, switching the vertical angle of injection also has little effect on the stability of β -induced Alfvén-acoustic eigenmodes that are unstable near the magnetic axis. Two-dimensional measurements of RSAE mode structure show that the phase of the eigenfunction varies with radius [1]. This phase variation is not present in the ideal MHD model but does appear in gyrokinetic and gyrofluid calculations. The phase variation was originally attributed to symmetry breaking associated with the fast-ion gradient [1] but the recent comparisons show that hypothesis is incorrect.

Separate control of the gradient and of the trapped/passing fraction, which depends sensitively on the magnetic field pitch, is a powerful tool in fast-ion instability studies. This capability is used to explore the stability of off-axis fishbones that are driven unstable by resonance with the precessional motion of trapped fast ions [2]. These modes expel fast ions in a “beacon” that is measured by seven types of loss detectors. The new capability is also used to study transport of fast ions by microturbulence. Preliminary analysis suggests that departures from classical confinement are observed in some H-mode plasmas.

References

- [1] B. J. Tobias, *et al.*, Phys. Rev. Lett. **106** (2011) 075003.
- [2] W. W. Heidbrink, *et al.*, Plasma Phys. Cont. Fusion **53** (2011) 085028.

Work supported by the US DOE under SC-G903402 and DE-FC02-04ER54698.

MHD Activity in the Alfvén Range of Frequencies in the H-1NF Helic

B. Blackwell¹, J. Howard¹, S. Haskey¹, D. Pretty¹, J. Bertram¹, N. Thapar¹, J. Read¹,
M. J. Hole¹, J. Brotankova¹, C. Nührenberg², R. Dewar¹, A. Könies², M. Fitzgerald¹,
and S. Ma¹

¹*Australian National University, Canberra, Australia*

²*Max-Planck-Institut für Plasmaphysik, Greifswald, Germany*

Corresponding Author: boyd.blackwell@anu.edu.au

The H-1 flexible heliac with its wide range of magnetic configurations is an ideal device for studying instabilities in the low to mid Alfvénic range-low to hundreds of kHz, in H/He RF produced plasma around 0.5 T. More than 80 magnetic probes in three arrays, and several optical imaging diagnostics provide data on poloidal, helical and radial mode structures. In addition to spontaneously excited modes, excitation is provided through a phased pair of loops close to the plasma, and a recent upgrade has facilitated scans of the dependence on magnetic field. Sensitive multi channel interferometry, framing cameras synchronised with the mode, and gas puff illumination techniques provide density fluctuation data in two dimensions. The vast data set acquired shows very clear dependences on transform and density, made possible by the low shear and precise control of configuration. Data are compared with predictions of several codes, notably CAS3D, and CONTI, and show both Alfvénic GAE-like and/or acoustic-like (BAE) behaviour in different regimes. The relationship to these modes and GAMs is discussed. Investigation of the influence of magnetic islands on plasma has shown several interesting effects, including a local enhancement of confinement under some conditions. Mapping and probe results will be presented, along with n_e fluctuation profiles from a new, high sensitivity multi-chord interferometer, and results from Alfvén mode excitation experiments.

EX-P

Recent Progress on Lower Hybrid Current Drive and Implications for ITER

J. Hillairet¹, Y. Peysson¹, A. Ekedahl¹, M. Goniche¹, J. Achard¹, Y. S. Bae², S. I. Park², E. Corbel¹, X. Litaudon¹, T. Hoang¹, J. Decker¹, R. Magne³, M. Preynas¹, M. Prou¹, L. Delpech¹, J. Belo³, W. Namkung⁴, P. Sharma⁵, and D. Guilhem¹

¹CEA, IRFM, St-Paul-Lez-Durance, France

²National Fusion Research Institute, Daejeon, Republic of Korea

³Euratom-IST, Universidade Técnica de Lisboa, Lisboa, Portugal

⁴Dept. of Physics, Pohang Univ. of Science and Technology, Pohang, Republic of Korea

⁵Institute for Plasma Research, Bhat, Gandhinagar, Gujarat, India

Corresponding Author: julien.hillairet@cea.fr

The demonstration that a sustainable production of energy is achievable from nuclear fusion in a tokamak requires controlling non-inductive current drive plasmas in steady state conditions. Following the ITER Science and Technology Advisory Committee recommendation, LHCD is now considered for a future upgrade of its heating and current drive (H&CD) capability. Preparing the ITER steady state operations not only requires the development of ITER operating scenarios or burning plasma physics, but also to master the LHCD auxiliaries. The achievement of stationary plasmas sustained by LHCD, i.e., zero loop voltage discharges over durations much longer than the resistive time scale and the total thermalisation time scale of the tokamak components, obliges to address a number of technological and physical challenges: development of high power Continuous Wave (CW) radiofrequency (RF) sources, actively cooled transmission lines with low RF power loss, antennas with high coupling efficiency, real time control systems and diagnostics and LH current deposition modeling. In order to minimize the operational risks for ITER, all of these items - from the RF sources to the current deposition calculations - must have a high reliability and efficiency.

In order to address these steady-state operational issues, eighteen klystrons have been validated routinely at ~ 620 kW/CW in relevant Tore Supra plasma conditions. The Passive-Active Multijunction (PAM) is an ITER-relevant concept whose capabilities to address long pulse operation issues has been demonstrated in Tore Supra. A general framework for modeling the current drive by coupling the ray tracing calculations and Fokker-Planck solver has been developed. This scheme reproduces efficiently the HXR signal of Tore Supra steady state discharges and can be used as a predictive tool for the design of next-generation LH launchers.

Based on the latest LHCD results obtained in the Tore Supra tokamak, a re-design of the 20 MW LH system for ITER has been conducted through an international collaborative task, coordinated by CEA/IRFM under the EFDA organization. In 2011, a 5 GHz mode converter has been successfully tested at low power. Furthermore, a 5 GHz window will be tested at high power in collaboration with the National Fusion Research Institute (NFRI) in Republic of Korea in 2012.

Recent Results from Ion Cyclotron Resonance Heating Experiments in HT-7 and EAST Tokamak

C. Qin¹, X. Zhang¹, Y. Zhao¹, B. Wan¹, X. Gong¹, Y. Mao¹, S. Yuan¹, D. Xue¹,
L. Wang¹, S. Ju¹, Y. Chen¹, H. Wang¹, Y. Lin², J. Qian¹, L. Hu¹, J. Li¹, Y. Song¹,
S. Wukitch², J. M. Noterdaeme^{3,4}, R. Kumazawa⁵, T. Seki⁵, K. Satio⁵, and
H. Kasahara⁵

¹*Institute of Plasma Physics Chinese Academy of Sciences, Hefei, China*

²*MIT Plasma Science and Fusion Center, Cambridge, USA*

³*Max-Planck Institute for Plasma Physics, Garching, Germany*

⁴*University of Ghent, Ghent, Belgium*

⁵*National Institute for Fusion Science, Toki, Japan*

Corresponding Author: chmq@ipp.ac.cn

Recent ICRF heating experiment in HT-7 and EAST tokamak devices is given. Experimental results in HT-7 show efficient ion and electron heating have been achieved. In the mode conversion case, direct ion heating by the mode converted ion Bernstein waves (MC IBW) was observed. Experimental evidence and numerical simulation show that the interaction between the MC IBW and ⁷Li ions at the first ion cyclotron harmonic resonance of ⁷Li is the main mechanism for RF power deposition. In the EAST tokamak, the RF heating is found to depend strongly on plasma preheating. In combination with LHW, the ICRF heating efficiency is even higher than the one of ICRF only. With 1.0 MW of ICRF power injected at a line-averaged electron density of $4.0 \times 10^{19} \text{ m}^{-3}$, the electron temperature increases from 1.0 keV to above 2.0 keV and the loop voltage drops. An increase of the stored energy by 30 kJ was obtained. Density pump-out was observed during L-mode discharges at a high electron density of $4.0 \times 10^{19} \text{ m}^{-3}$. In these discharges, re-attachment of the plasma was observed when ICRF power was applied. Combined operation of ICRF and LH at EAST often resulted in a degradation of the LH wave coupling due to RF sheaths induced local density modification by ICRF antenna. The potential measurements with two Langmuir probes confirmed the presence of an enhanced sheath with ICRF when the probe is connected to the active antenna. Moreover, the modification of plasma potential dependence on antenna phase, RF power and plasma-antenna distance was observed.

EX-P

Experimental Study of Low Frequency Wave Current Drive in the SUNIST Spherical Tokamak

Y. Tan¹, Z. Gao¹, W. Wang¹, L. Wang², X. Yang², C. Feng², L. Xie¹, H. Xie¹, and Y. Liu¹

¹*Department of Engineering Physics, Tsinghua University, Beijing, China*

²*Institute of Physics, Chinese Academy of Sciences, Beijing, China*

Corresponding Author: tanyi@sunist.org

Alfvén wave is one of the waves that can overcome the density limit and reach the interior of spherical tokamak (ST) plasmas. Therefore, it may be possible to drive plasma current by low frequency waves through Alfvén resonance in STs. This method has been tested in the SUNIST spherical tokamak ($R/a = 0.3 \text{ m}/0.23 \text{ m}$; $B_{T0} = 0.15 \text{ T}$; $I_P = 30 - 50 \text{ kA}$; $n_e \sim 1 \times 10^{-19} \text{ m}^{-3}$; pulse length: 4–25 ms). Four pairs of antennas, which are made by poloidal folded stainless steel straps, have been installed in the equatorial plane of the vacuum vessel with a uniform toroidal spacing angle of 90 degree. Two pairs of the antennas are protected by side limiters (consist of boron nitride plates) but the two pairs left are not protected by anything. The antenna system is powered by a four phases outputs radio frequency (RF) generator (0.4 – 1 MHz, < 100 kW per output). The most obvious observation after injecting RF waves from bare antennas was the increased intensity of impurity lines (carbon and oxygen). The boron nitride plates protected antennas have better performance on impurities. The experimentally measured impedance of the antenna system has the similar characteristics as theoretical one-dimension MHD calculations. Since the antenna system was fed in π phasing, both $N = \pm 1$ and $M = \pm 1$ vacuum modes are excited. From the experimental impedance curve, it seems that the plasma may have responded to both two modes. When the RF waves ($\sim 40 \text{ kW}$ for each phase) were applied to lower density ($n_e < 8 \times 10^{-18} \text{ m}^{-3}$) and lower current ($I_P \sim 30 \text{ kA}$) plasmas by bare antennas, we often observe an enhancement of runaway electrons. Hard X ray measurements by CdTe detectors support this observation. However, when the RF waves were applied to the discharges with normal density ($n_e > 1 \times 10^{-19} \text{ m}^{-3}$) and normal plasma current ($I_P \sim 40 \text{ kA}$), no obvious differences could be found compared to discharges without RF waves.

Analysis of High Energy Neutral Particles Measured by CNPA and Comparison with Synthesized Fast Neutral Spectrum Based on TRANSP/FIDA for the NB Heated Plasmas in KSTAR

S. H. Kim¹, S. J. Wang¹, C. K. Hwang¹, S. K. Kim¹, M. Park¹, L. Terzolo²,
A. England², Y. S. Lee², and J. W. Yoo²

¹*Korea Atomic Energy Research Institute, Daejeon, Republic of Korea*

²*NFRI, Daejeon, Republic of Korea*

Corresponding Author: shkim95@kaeri.re.kr

It is important to measure the fast ions accurately in tokamak plasmas since it represents the ion heating by NB/ICRF and it is a basis for the evaluation of the fast ion induced instabilities, transport, and neutron generation. A CNPA (Compact Neutral Particle Analyzer) based on Si-diode is an effective way to infer the fast ion distribution function by comparing with synthetic diagnostic data. TRANSP code with NUBEAM module can generate fast ion distribution function by using measured plasma parameters such as density, temperature profiles. FIDA/NPA code can synthesize the fast neutral particle spectrum through Monte Carlo (MC) simulation by using the output of TRANSP. In this study, the high energy neutral particle spectrum is analyzed for NB heated plasmas in KSTAR and compared with the numerical result by using the TRANSP /FIDA codes.

EX-P

Basic Investigations of Electrostatic Turbulence and its Interaction with Plasma and Suprathermal Ions in a Simple Magnetized Toroidal Plasma

A. Fasoli¹, F. Avino¹, A. Bovet¹, I. Furno¹, K. Gustafson¹, J. Loizu¹, P. Ricci¹, and C. Theiler¹

¹CRPP-EPFL, Lausanne, Switzerland

Corresponding Author: ambrogio.fasoli@epfl.ch

Progress in basic understanding of turbulence, from unstable electrostatic modes to the formation of blobs, and its influence on the transport both of the plasma bulk and of suprathermal components, is achieved in the TORPEX simple magnetized torus (SMT). This configuration combines a microwave plasma production scheme with a quasi-equilibrium generated by a toroidal magnetic field, onto which a small vertical component is superimposed, and represents a simplified paradigm of the tokamak scrape-off-layer. After having clarified the formation of blobs in ideal interchange turbulence, TORPEX experiments elucidated the mechanisms behind the blob motion, with a general scaling law relating their size and speed. Such analytical scaling is verified over a wide range of parameters in TORPEX data, as well as in the results of 2D fluid numerical simulations. The parallel currents associated with the blobs, responsible for the damping of the charge separation that develops inside them, hence determining their cross-field velocity, have been measured. Methods to control the blob dynamics are now devised, based on creating convective cells using biased electrodes, arranged in an array on a metal limiter. Measurements reveal the formation of convective cells, fairly uniform along the magnetic field. Depending on the biasing scheme, radial and vertical blob velocities can be varied. Suprathermal ion transport in small-scale turbulence is another area in which TORPEX experiments can contribute to understand basic burning plasma physics concepts. Suprathermal ions are generated up to 1 keV by a miniaturized lithium source, and are detected using a movable double-gridded energy analyzer. We characterize vertical and radial spreading of the ion beam, associated with the ideal interchange-dominated plasma turbulence, as a function of the suprathermal ion energy and the plasma temperature. Experimental results are in good agreement with global fluid simulations. A closed field line configuration is being implemented on TORPEX using a current carrying filament suspended in the centre of the chamber. This system will allow investigations of the interaction of plasma and suprathermal particles with instabilities and turbulence in magnetic configurations of increasing complexity. This work was partly supported by the Fond National Suisse pour la Recherche Scientifique.

EX-P

Spectral Broadening and Lower Hybrid Current Drive in High Density Tokamak Plasmas

R. Cesario¹, L. Amicucci², A. Cardinali¹, C. Castaldo¹, A. Galli², F. Napoli³,
G. Schettini³, and A. Tuccillo¹

¹ *Associazione EURATOM/ENEA sulla Fusione, Frascati, Italy*

² *Università di Roma Sapienza, Dipartimento Ingegneria Elettronica, Rome, Italy*

³ *Università di Roma Tre, Dipartimento Ingegneria Elettronica, Rome, Italy*

Corresponding Author: roberto.cesario@enea.it

To control the plasma current profile represents one of the most important problems of the research of nuclear fusion energy based on the tokamak concept, as its solution would allow satisfying the necessary conditions of stability and confinement of plasma column. This problem can be solved by using the lower hybrid current drive (LHCD) effect, which was demonstrated to occur also at reactor grade high plasma densities, provided that a proper method, assessed on FTU (Frascati Tokamak Upgrade), should be utilised.

It was predicted by theory that operations with relatively high temperature in the plasma periphery are useful for diminishing the parametric instability (PI)-produced spectral broadening and, consequently, enabling the coupled lower hybrid (LH) to penetrate into the bulk at reactor grade high plasma density and producing current drive effects. Experiments of Frascati Tokamak Upgrade (FTU) confirmed these predictions indeed.

We show here results obtained by a fully kinetic plasma model that describes the non-linear evolution of the spectral broadening phenomenology. The previous perturbative limit has been removed by completely solving the non linear coupled equations of the modes involved in the instability, utilising a fully kinetic plasma model. The LH sideband waves can be now properly considered also when their amplitude is well above the noise level, as occurs indeed in the data provided by radiofrequency probes available from experiments. A comparison of the LH spectral broadening obtained by modeling and experiment is presented, and the impact on the LH wave propagation and damping is discussed.

Considering the FTU method and assuming reasonably high electron temperature at the edge, the PI-produced spectral broadening is expected to be mitigated in ITER, thus enabling the penetration of the coupled LH power in the main plasma.

By successful LHCD effect, the control of the plasma current profile at normalised minor radius of about $r/a = 0.8$ would be possible, with much higher efficiency than that obtainable by other tools. A useful reinforce of bootstrap current effects would be thus possible by LHCD in ITER.

Characterisation of Ion-scale Turbulence in MAST

A. Field¹, R. Akers¹, D. Dunai², Y. C. Ghim^{1,3}, P. Hill⁴, B. McMillan⁴, C. Michael¹,
S. Saarelma¹, and C. Roach⁴

¹EURATOM/CCFE Fusion Association, Culham Science Centre, Abingdon, UK

²KFKI RMKI, Association EURATOM, Budapest, Hungary

³Rudolf Peierls Centre for Theoretical Physics, University of Oxford, Oxfordshire, UK

⁴Centre for Fusion, Space and Astrophysics, Warwick University, Coventry, UK

Corresponding Author: anthony.field@ccfe.ac.uk

Ion thermal transport in spherical tokamaks is often observed to be close to the neo-classical level, which is consistent with the suppression of anomalous transport due to ion-scale turbulence by strong NBI-driven flow shear. In order to test this conjecture a 2D BES diagnostic has been implemented on MAST to image the low- k ($< 1.6 \text{ cm}^{-1}$) density turbulence. Initial investigations have focused on characterization of the turbulence in L- and H-mode discharges. The BES data exhibits both broad-band turbulence as well as coherent, global MHD modes, which complicates the analysis. The poloidal motion of the fluctuations is found to be dominated by the local $\mathbf{E} \times \mathbf{B}$ drift, with smaller diamagnetic contributions in either the ion- or electron drift directions depending on the dominant branch of turbulence, e.g., ITG or TEM. Calculation of the spectral density $S(f, k)$ using a maximum entropy technique allows the localised turbulence to be distinguished from the global modes. In the periphery of L-mode plasmas the dominant turbulence appears to propagate in the ion-diamagnetic direction relative to the local $\mathbf{E} \times \mathbf{B}$ velocity but weaker turbulence observed in H-mode propagates in the electron diamagnetic direction. The BES turbulence observations have been compared with synthetic data generated from non-linear, gyro-kinetic simulations performed using the ORB5 and GS2 codes. Initial comparisons, based on global ORB5 simulations both with and without sheared flow, reproduce some important characteristics of the turbulence, e.g., flow-shear preventing spreading of the turbulence from an unstable peripheral region into the plasma core, although significant differences are apparent, the observed turbulence exhibiting shorter “eddy” lifetimes and correlation lengths in the outer regions and hence being “stronger” than the simulated turbulence.

Work funded by the RCUK Energy Programme, EURATOM and HAS.

Response of Electron-scale Turbulence and Thermal Transport to Continuous $\mathbf{E} \times \mathbf{B}$ Shear Ramping-up in NSTX

Y. Ren¹, W. Guttenfelder¹, S. Kaye¹, E. Mazzucato¹, K. Lee², and C. Domier²

¹*Princeton Plasma Physics Laboratory, Princeton, USA*

²*University of California at Davis, Davis, USA*

Corresponding Author: yren@pppl.gov

Microturbulence is considered to be a major candidate in driving anomalous transport in fusion plasmas, and the equilibrium $\mathbf{E} \times \mathbf{B}$ shear generated by externally driven flow can be a powerful tool to control microturbulence in future fusion devices such as FNSF and ITER. Here we present the first observation of the change in electron-scale turbulence wavenumber spectrum (measured by a high- k scattering system) and thermal transport responding to continuous $\mathbf{E} \times \mathbf{B}$ shear ramping-up in an NSTX center-stack limited and NBI-heated L-mode plasma. It is found that while linear stability analysis shows that the maximum ETG mode linear growth rate far exceeds the observed $\mathbf{E} \times \mathbf{B}$ shearing rate in the measurement region of the high- k scattering system, the unstable ITG modes are susceptible to $\mathbf{E} \times \mathbf{B}$ shear stabilization. We observed that as the $\mathbf{E} \times \mathbf{B}$ shearing rate is continuously ramped up in the high- k measurement region, the ratio between the $\mathbf{E} \times \mathbf{B}$ shearing rate and the maximum ITG mode growth rate continuously increases (from about 0.2 to 0.7) and the maximum power of the measured electron-scale turbulence wavenumber spectra decreases. Meanwhile, both the electron and ion thermal transports are also reduced as long as MHD activities are not important. These observations are found to be consistent with $\mathbf{E} \times \mathbf{B}$ shear stabilization of the ion-scale turbulence.

EX-P

Characteristics of Microturbulence in H-mode Plasma of LHD

K. Tanaka¹, T. Kobayashi², K. Toi¹, S. Inagaki¹, C. Michael³, L. Vyacheslavov⁴,
D. Mikkelsen⁵, J. Baumgaertel⁵, G. Hammett⁵, W. Guttenfelder⁵, Y. Takemura⁶,
S. Sakakibara¹, Y. Suzuki¹, M. Yokoyama¹, K. Ida¹, Y. Ichihara¹, R. Yasuhara¹,
K. Narihara¹, T. Akiyama¹, T. Tokuzawa¹, and K. Kawahata¹

¹National Institute for Fusion Science, Toki, Japan

²Kyushu University, Kasuga, Japan

³Culham Centre for Fusion Energy, Abingdon, UK

⁴Budker Institute of Nuclear Physics, Novosibirsk, Russian Federation

⁵Princeton Plasma Physics Laboratory, Princeton, USA

⁶The Graduate School of Advanced Science, Toki, Japan

Corresponding Author: ktanaka@nifs.ac.jp

In LHD, an H-mode transition was achieved after ELM suppression. The main plasma of LHD is surrounded by a thick ergodic layer, of width around 30% of the minor radius. This ergodic layer consists of $m/n = 10/10$ and $m/n = 20/22$ magnetic islands. This three dimensional structure of the edge magnetic field is similar to resonant magnetic perturbations (RMP) in tokamaks, so these results may be relevant to ELM suppressed RMP experiments in tokamaks. H-mode transition was found with constant heating (5 MW NBI) and fueling. This outwardly shifted configuration has $R_{\text{axis}} = 3.9$ m, $B_t = 0.9$ T. Small ELMs were visible, then dithering took place, and finally, dithering disappeared and the H-mode transition occurred.

After transition, both electron and ion temperature profiles were almost unchanged, while density profile changed significantly. This indicates that confinement improvement occurs only for particles. Density profiles before and after H-mode transition are hollow, but in H-phase the edge density gradient increased and the highest density points shifts from $r/a = 0.7$ in L phase to $r/a = 0.9$ in H-phase, implying that a transport barrier was formed at $r/a > 0.9$. Turbulence was measured by two dimensional phase contrast imaging (2D-PCI) with frequencies of 20 – 500 kHz and wavenumbers of $0.1 - 1 \text{ mm}^{-1}$. The fluctuation amplitude dropped suddenly at the transition timing suggesting that the reduction of turbulence is linked to the improvement of particle transport. 2D-PCI showed the fluctuation velocity had two propagation components. One moves in the electron diamagnetic (e-dia.) direction in the lab. frame at $r/a < 1.2$, the other moves in the ion diamagnetic (i-dia.) direction in laboratory frame at $r/a = 1.3$. After the transition, fluctuation amplitudes dropped for $r/a = 0.5 - 1.0$, in addition, the fluctuation's spatial structure changed significantly. After the transition, the e-dia. component at $r/a < 1.2$ splits into two parts and the phase velocity of fluctuation at $r/a = 0.9$ increased from 3 km/s in L phase to 7 km/s in H-phase resulting in the formation of velocity shear around transport barrier. Simultaneous measurements of $\mathbf{E} \times \mathbf{B}$ poloidal rotation velocity did not show clear change, thus, the phase velocity is due to the change of fluctuation phase velocity. The formation of velocity shear around the transport barrier can play important role in particle confinement improvement.

Turbulence Wave Number Spectra Reconstruction from Radial Correlation Reflectometry Data at Tore Supra and FT-2 Tokamaks

N. Kosolapova^{1,2}, E. Gusakov², S. Heuraux², A. Altukhov¹, A. Gurchenko¹,
F. Clairet³, and R. Sabot³

¹*Ioffe Physical-Technical Institute of Russian Academy of Science, St. Petersburg, Russian Federation*

²*Institute Jean Lamour, Université Henri Poincaré, Nancy, France*

³*CEA Cadarache, Saint Paul Les Durance, France*

Corresponding Author: n.kosolapova@mail.ioffe.ru

Radial correlation reflectometry (RCR) [1] is a microwave scattering technique for measuring the properties of electron density fluctuations in tokamaks. The coherence decay of two scattering signals with growing difference of probing frequencies is studied by the diagnostic to determine the turbulence radial wave number spectrum and the turbulence correlation length.

As it was shown already in 1D numerical computations performed in Born approximation [2], the scattering signal cross correlation function (CCF) decays spatially much more gradually than the turbulence CCF. This slow decay of RCR CCF was attributed to the contribution of small angle scattering off very long scale fluctuations. Later this observation was confirmed also in 2D analytical study [3] and in full-wave 1D numerical modeling [4] for small level of turbulent density fluctuations. Recently a new theoretical approach [5] shows that in the case of linear density profile the turbulence spectrum can be expressed in terms of the ordinary mode RCR CCF using the integral transformation.

In the present work we perform the results of the proposed theoretical method application to extract turbulence characteristics from experimental data obtained at Tore Supra and FT-2 tokamaks. The radial wave number spectrum and its correlation length as well as spatial turbulence correlation function have been successfully determined. The quality of reconstruction has been proved by numerical simulations for various spectra in conditions relevant to experiment (see also [6]). We also discuss the limitations of the method, and possible application to ITER.

References

- [1] N. Bretz, *Physical Fluids* **4** (1992) 2414.
- [2] H. Hutchinson, *Plasma Phys. Control. Fusion* **34** (1992) 1225. [3] E. Z. Gusakov and B. O. Yakovlev, *Plasma Phys. Control. Fusion* **44** (2002) 2525.
- [4] G. Leclert *et al.*, *Plasma Phys. Control. Fusion* **48** (2006) 1389.
- [5] E. Z. Gusakov and N. V. Kosolapova, *Plasma Phys. Control. Fusion* **53** (2011) 045012.
- [6] N. V. Kosolapova, E. Z. Gusakov and S. Heuraux, *Plasma Phys. Control. Fusion* **54** (2011) 035008.

Relating the L–H Power Threshold Scaling to Edge Turbulence Dynamics

Z. Yan¹, G. R. McKee¹, J. A. Boedo², D. L. Rudakov², P. H. Diamond², R. J. Fonck¹,
R. J. Groebner³, T. H. Osborne³, and P. Gohil³

¹*University of Wisconsin-Madison, Madison, USA*

²*University of California San Diego, La Jolla, USA*

³*General Atomics, San Diego, USA*

Corresponding Author: yanz@fusion.gat.com

Understanding the physics of the L-H transition power threshold scaling dependencies on toroidal field and density [1] is critical to operating and optimizing the performance of ITER. Measurements of long-wavelength ($k_{\perp}\rho_I < 1$) turbulent eddy dynamics, characteristics, flows, and flow shear in the near edge region of DIII-D plasmas have been obtained during an ion gyro-radius scan (varying toroidal field and current) and density scan in a favorable geometry (ion ∇B drifts towards the X-point), demonstrating the underlying mechanisms that influence the macroscopic L-H power threshold scaling relations. It is found the integrated long wavelength density fluctuation amplitudes scale with ρ^* approaching the L-H transition, suggesting stronger drive of zonal flows for more favorable condition at lower toroidal field. Turbulence poloidal flow spectrum evolves from Geodesic Acoustic Mode (GAM) dominant at lower power to Low-Frequency Zonal Flow (LFZF) dominant near the L-H transition, and the effective shearing rate correspondingly increases. An inferred Reynolds Stress, $\langle \tilde{v}_r(t) \tilde{v}_\theta(t) \rangle$, from BES velocimetry measurements [2] is found to increase near the L-H transition. Similar observations were made by the Langmuir probe measurements. At lower density, a clear increase of the LFZF is observed prior to the L-H transition, which is not evident at higher density. Taken together, these results are qualitatively/semi-quantitatively consistent with the density and toroidal field scaling of the L-H transition power threshold.

References

- [1] E. J. Doyle, *et al.*, Nucl. Fusion **47** (2007) S18.
- [2] G. R. McKee, *et al.*, Rev. Sci. Instrum. **75** (2004) 3490.

This work was supported in part by the US Department of Energy under DE-FG02-89ER53296, DE-FG02-08ER54999, DE-FG02-07ER54917, DE-FC02-04ER54698, and DE-FG02-08ER54984.

Turbulence and Transport Response to Resonant Magnetic Perturbations in ELM-Suppressed Plasmas

G. R. McKee¹, R. J. Buttery², T. E. Evans², C. Holland³, R. A. Moyer³, S. Mordijk⁴,
R. Nazikian⁵, T. L. Rhodes⁶, O. Schmitz⁷, M. R. Wade³, and Z. Yan¹

¹ *University of Wisconsin-Madison, Madison, USA*

² *General Atomics, San Diego, USA*

³ *University of California San Diego, La Jolla, USA*

⁴ *College of William & Mary, Williamsburg, USA*

⁵ *Princeton Plasma Physics Laboratory, Princeton, USA*

⁶ *University of California Los Angeles, Los Angeles, USA*

⁷ *Forschungszentrum Jülich, Jülich, Germany*

Corresponding Author: mckee@fusion.gat.com

Long wavelength turbulence increases dramatically in the outer regions of DIII-D plasmas with the application of radial resonant magnetic field perturbations (RMP) to suppress edge-localized modes (ELMs). Correspondingly, transport increases and global energy confinement decreases in these low collisionality RMP-ELM suppressed discharges. This process is evident through a sharp reduction in core and pedestal density, while ion and electron temperatures may change only slightly. Low wavenumber density turbulence ($k_{\perp}\rho_i < 1$) in the range of 60 – 300 kHz, measured with beam emission spectroscopy (BES), is modified and generally increases throughout the outer region ($0.6 < \rho < 1.0$) of the plasma in response to RMPs over a range of q_{95} values; ELM suppression, in contrast, occurs for a narrower range in q_{95} . This turbulence has radial and poloidal correlation lengths on the scale of a few cm. Radial magnetic field modulation experiments indicate that these turbulence modifications occur on a time scale of a few milliseconds or less near $\rho = 0.85 - 0.95$, significantly faster than transport time-scales and faster than the local pressure gradients and shearing rates evolve at these locations. As the internal coil current is varied from 3.2 to 4.2 kA, the turbulence magnitude varies in phase by 30% or more, while local density changes by only a few percent. This dynamical behavior suggests that the turbulence is directly affected by the RMP, which may partially or largely explain the resulting increased transport and stabilization of the pedestal against peeling-ballooning instabilities that are thought to drive ELMs. Zonal flow damping by the RMP is a mechanism being investigated as a potential causal agent. Understanding this transport process will be crucial to extrapolating and optimizing the RMP ELM-suppression technique in ITER.

This work was supported in part by the US Department of Energy under DE-FG02-89ER53296, DE-FG02-08ER54999, DE-FC02-04ER54698, DE-FG02-07ER54917, DE-AC02-09CH11466, and DE-FG02-08ER54984.

EX-P

Generation of Large Scale Coherent Structures by Turbulence in Edge Plasmas of HL-2A Tokamak

J. Dong^{1,2}, J. Cheng¹, L. Yan¹, K. Itoh³, K. Zhao¹, W. Hong¹, Z. Huang¹, D. Kong⁴, M. Xu⁵, P. H. Diamond^{5,6}, G. R. Tynan⁵, Q. Yang¹, X. Ding¹, X. Duan¹, and Y. Liu¹

¹*Southwestern Institute of Physics, Chengdu, China*

²*Institute for Fusion Theory and Simulation, Zhejiang University, Hangzhou, China*

³*National Institute for Fusion Science, Toki, Japan*

⁴*Department of Modern Physics, USTC, Hefei, China*

⁵*University of California at San Diego, La Jolla, USA*

⁶*National Fusion Research Institute, Daejeon, Republic of Korea*

Corresponding Author: jiaqi@swip.ac.cn

The generation mechanisms as well as the spatial and spectral characteristics of three dimensional large-scale coherent structures (LSCSs) in the form of blobs or filaments, stretching along magnetic field lines in the edge plasmas of the HL-2A tokamak are investigated using 10-tip poloidal and 8-tip radial probe arrays toroidally separated by 2100 mm [1,2]. The LSCSs in frequency range of 15 – 100 kHz, with radial and poloidal size of about 20 – 30 μm to 10 – 15 mm and finite parallel wave vector have been experimentally observed with high spatial and temporal resolutions. The turbulence energy from 30 to 60 kHz is found to contribute significantly to the growth of the turbulent eddies of broad spectrum. The latter gradually increase, following the increasing turbulence energy of 30 – 60 kHz, and then break up into LSCSs with dipolar potential fluctuations at the inner side of the LCFS, where the Reynolds stress driven $\mathbf{E} \times \mathbf{B}$ flow is strong, the flow shearing rate has a maximum and the flow shearing time is close to the LSCS generation time. The LSCSs are then ejected by the $\mathbf{E} \times \mathbf{B}$ flow shear across the LCFS and into the SOL, the back reaction of the ejection on the turbulence is also observed and may result in intermittent behaviors of the LSCS generation. Thus, the increasing turbulent energy, the spontaneous $\mathbf{E} \times \mathbf{B}$ flow shear are identified responsible for the generation of LSCSs, which is in agreement with the theoretical prediction and provides unambiguous experimental evidences for LSCS generation mechanism in tokamak edge plasmas for the first time. The correlation between the sheared flow and Reynolds stress is demonstrated. The evidence for the back-reaction of LSCS ejection on turbulence is also presented. Furthermore, the particle and energy transports induced by the LSCSs and the ambient turbulence are estimated and analyzed in detail.

References

- [1] J. Cheng *et al.*, Plasma Phys. Control Fusion **52** (2010) 055003.
- [2] L. W. Yan *et al.*, Journal of Nuclear Materials **415** (2011) S475-S478.

Investigation of L-I-H Transitions Facilitated by Supersonic Molecular Beam Injection and Pellet Fuelling on the HL-2A Tokamak

C. Liu¹, Y. Huang¹, Y. Liu¹, L. Yao¹, J. Dong¹, G. Zhu¹, Z. Shi¹, D. Yu¹, Y. Zhou¹, C. Chen¹, B. Feng¹, W. Zhong¹, H. Xu¹, J. Cao¹, L. Nie¹, K. Yao¹, Z. Feng¹, L. Yan¹, X. Ding¹, X. Duan¹, and Y. Liu¹

¹Southwestern Institute of Physics, Chengdu, China

Corresponding Author: liuchunhua@swip.ac.cn

H-mode operation is extremely important and has been chosen as the standard operation scenario for ITER to meet its objectives, but the physical mechanism of H-mode access has not been fully understood and the power threshold for the L- H transition remains uncertainty. L-H transition induced by pellet injection has been studied on DIII-D, in which process the intermediate phase (I-phase) is recognized with quasi-periodic oscillations and turbulent instability bursts. Besides spontaneous slow L-H transitions, L-I-H transitions are facilitated on the HL-2A tokamak at lower neutral beam heating power by pulsed intense edge fuelling such as pellet and supersonic molecular beam injection (SMBI) ,which give us high opportunity to investigate the underlying mechanisms of the L-I-H transitions and the influence of fuelling on the transitions as well.

Because the edge pressure is initially adiabatic to pellet or SMB ablation, the plasma density increases much and the edge electron temperature drops. Then density remains at high level, the edge is re-heated and the temperature rises gradually, thus a delay time is needed for the edge pressure gradient is sufficient to induce the I-phase. The plasma remains in I-phase for about 20 ms and is heated further towards edge pressure highly enough to cause an H-mode transition. The phenomenon is consistent with the scaling of power threshold (P_{th}) versus line-averaged density in low density branch, where P_{th} decreases with density increasing.

The edge density and thus edge pressure are higher in I-phase than that in L-mode, but lower than that in H-mode. In I-phase, the energy confinement is better than in L-mode but worse than in H-mode. The density pedestal formation process with SMBI is similar with pellet fuelling. At high density plasma, SMBI is found usually to kill a spontaneous I-phase and stop the potential L-H transition. The radial electrical field and shear flow at edge region, mainly driven by edge pressure gradient, are also presented to investigate the L-I-H transition.

EX-P

Validation Studies of Gyrofluid and Gyrokinetic Predictions of Transport and Turbulence Stiffness Using the DIII-D Tokamak

C. Holland¹, J. E. Kinsey², J. C. DeBoo², K. H. Burrell², C. C. Petty², A. E. White³, T. L. Rhodes⁴, L. Schmitz⁴, E. J. Doyle⁴, J. C. Hillesheim⁴, G. R. McKee⁵, Z. Yan⁵, S. P. Smith², G. Wang⁴, L. Zeng⁴, P. B. Snyder², R. E. Waltz², G. M. Staebler², and J. Candy²

¹University of California San Diego, La Jolla, USA

²General Atomics, San Diego, USA

³Massachusetts Institute of Technology, Cambridge, USA

⁴University of California Los Angeles, Los Angeles, USA

⁵University of Wisconsin-Madison, Madison, USA

Corresponding Author: cholland@ucsd.edu

A series of carefully designed validation experiments have been conducted on DIII-D to rigorously test gyrofluid and gyrokinetic predictions of transport and turbulence stiffness in both the ion and electron channels. In the first experiment, the ratio of the volume-averaged electron temperature profile to its value at $\rho = 0.84$ was found to be essentially invariant with increased heating over a factor of 3 variation in neutral beam injection (NBI) heating in H-mode plasmas with constant pedestal conditions, while a small increase was observed in the ion temperature ratio. The TGLF [1] transport model reproduces the profile measurements and trends with increased NBI heating, providing significant additional support for the fidelity of TGLF in H-modes. Building off these global studies, experiments that quantified local electron stiffness by varying the deposition of electron cyclotron heating (ECH) about a specified reference radius were performed. Applying this technique to L-mode plasmas with no other external heating, a critical inverse temperature gradient scale length $a/L_{Te,crit} = 2.0 \pm 0.3$ ($1/L_{Te} = -\nabla T_e/T_e$, $a = 0.6$ m) has been identified for the first time in DIII-D. Both TGLF and nonlinear GYRO [2] simulations predict similar levels of near-zero turbulence and transport at or below the experimental critical gradient and experimentally relevant levels above it, and a similar transition is observed in linear growth rate calculations. However, both codes also underpredict the power balance calculations of the electron and ion heat fluxes Q_e and Q_i , and increases to both a/L_{Te} and a/L_{Ti} larger than experimental uncertainties are needed to match the power balance results. These results build upon previous validation studies [3] of electron transport at DIII-D, for which new gyrokinetic modeling results will be reported.

References

- [1] G. M. Staebler, *et al.*, Phys. Plasmas **14** (2007) 055909.
- [2] J. Candy and R. E. Waltz, Phys. Rev. Lett. **91** (2003) 45001.
- [3] J. C. DeBoo *et al.*, Phys. Plasmas **17** (2010) 056105.

Work supported by the US DOE under DE-FG02-07ER54917, DE-FG02-06ER54871, DE-FC02-04ER54698, DE-FC02-99ER54512, DE-FG02-08ER54984, DE-FG02-89ER53296 and DE-FG02-08ER54999.

Studies of Turbulence, Transport and Flow in the Large Plasma Device

T. Carter¹, D. Schaffner¹, B. Friedman¹, and M. Umansky²

¹*University of California, Los Angeles, USA*

²*Lawrence Livermore National Laboratory, Livermore, USA*

Corresponding Author: tcarter@physics.ucla.edu

The edge and scrape-off-layer region of tokamaks has a direct and important impact on overall performance of these devices: e.g., because of stiffness in core transport, the pedestal pressure directly impacts fusion power in burning plasma experiments. Developing first-principles understanding of and a predictive capability for processes in the edge region is critically important to ensure the success of future experiments like ITER. In this paper, we describe studies of an important edge-physics related process, the interaction of flow and flow shear with turbulence and efforts to validate two-fluid models of turbulent transport against LAPD data. LAPD is a 17 m long, 60 cm diameter magnetized plasma column with typical plasma parameters $n_e \sim 10^{12} \text{ cm}^{-3}$, $T_e \sim 10 \text{ eV}$, and $B \sim 1 \text{ kg}$. Broadband, fully-developed turbulence is observed in the edge of the LAPD plasma along with spontaneously driven azimuthal flows. Recently, the capability to continuously vary the edge flow and flow shear has been developed in LAPD using biasing of an annular limiter. Spontaneous flow is observed in the ion diamagnetic direction (IDD), biasing tends to drive flow in the opposite direction, allowing a continuous variation of flow from the IDD to the electron diamagnetic direction, with a near-zero flow and flow shear state achieved along the way. Enhanced confinement and density profile steepening is observed with increasing shearing rate; degraded confinement is observed when spontaneous flow is nulled-out and near-zero shear is achieved. Particle flux and radial correlation length are observed to decrease with increasing shear; consistency with theoretical models of shear suppression is found. The decrease occurs with shearing rates which are comparable to the inverse turbulent autocorrelation time in the zero flow state. The control over edge flows and flow shear and extensive measurement capability in LAPD provides an opportunity to validate edge turbulence models. LAPD turbulence has been modeled using the 3D Braginskii fluid turbulence code BOUT++. Good qualitative and semi-quantitative agreement is found between BOUT++ simulations and LAPD experimental measurements in low flow regimes.

EX-P

Study of ELMy H-mode Plasmas and BOUT++ Simulation on EAST

Z. Liu¹, X. Gao¹, X. Xu², and J. Li¹

¹*Institute of Plasma Physics, Chinese Academy of Sciences, Hefei, China*

²*Lawrence Livermore National Laboratory, Livermore, USA*

Corresponding Author: zxliu316@ipp.ac.cn

Stationary edge localized modes (ELM) H-mode plasmas have been achieved on Experimental Advanced Superconducting Tokamak (EAST) by Low Hybrid Wave ($P_{LHW} \sim 1$ MW at 2.45 GHz) in 2010. This kind of ELMy H-mode has been studied. Threshold power increases with plasma density, and decreases with the distance between the X-point and the divertor surface on EAST. The minimum threshold power is about 0.9 MW at $2 \times 10^{19} \text{ m}^{-3}$. Experimental energy confinement time during H-mode discharges is much higher than L-mode discharges, and the H-factor in H-mode is between 0.5 and 1. EAST experiment results including magnetic geometry data, experimentally measured pressure and calculated current from the pressure are used to investigate the physics of ELM with BOUT++ simulation code. The linear simulation results show that the ELMs in EAST are dominated by resistive ballooning mode. When the Lundquist Number (dimensionless ratio of the resistive diffusion time to the Alfvén time) is equal or less 10^7 , it is resistive unstable in the ELMy H-mode.

EX-P

Plasma Diffusion and Turbulence Studies in T-10 Tokamak

V. Vershkov¹, D. Shelukhin¹, Y. Dnestronskii¹, M. Borisov¹, G. Subbotin¹,
A. Danilov¹, M. Buldakov¹, M. Isaev¹, E. Gorbunov¹, D. Sergeev¹, S. Grashin¹,
V. Krupin¹, L. Kluchnikov¹, K. Korobov¹, S. Krylov¹, E. Kuleshin¹, T. Myalton¹,
D. Ryjakov¹, Y. Skosyrev¹, N. Timchenko¹, V. Trukhin¹, V. Chistiakov¹, and
S. Cherkasov¹

¹*Institute of Tokamak Physics, National Research Center "Kurchatov Institute", Moscow,
Russian Federation*

Corresponding Author: vershkov@nfi.kiae.ru

Two approaches for plasma diffusion studies were compared: low perturbation technique of periodic puff ($dn/n_e = 0.3\%$) and strong puff ($dn/n_e < 50\%$). Core density perturbations can be described in the model with constant in time-constant diffusion coefficients and pinch velocities, while at the edge this model failed. Three phases were distinguished in discharges with strong gas puff. Enhanced electron heat conductivity and lower turbulence frequencies were observed during density ramp up and down, while low electron heat conductivity and higher turbulence frequencies are typical for the intermediate phase. Density profile variation in this phase can be described in the model with constant in time coefficients. The increase of the low frequencies in turbulence spectra was also found in the "density pump out" phase during central ECRH.

Correlations of the Turbulent Structures during Nonlocal Effect Caused by SMBI on the HL-2A Tokamak

Z. Shi¹, H. Sun^{1,2}, X. Ding¹, X. Huang¹, Y. Dong¹, Y. Liu¹, W. Zhong¹, J. Zhou¹,
Y. Zhou¹, J. Rao¹, Q. Yang¹, and X. Duan¹

¹*Southwestern Institute of Physics, Chengdu, China*

²*WCI Center for Fusion Theory, National Fusion Research Institute, Daejeon, Republic of Korea*

Corresponding Author: shizb@swip.ac.cn

Experiments with nonlocal effect have been performed by using supersonic molecular beam injection (SMBI) in the case of the low density operation on the HL-2A tokamak. The increase in central electron temperature by the perturbations can be prolonged to about 100 ms by using repetitive SMBI with density control. A nearly relation between the central temperature rise and the edge perturbation caused by SMBI has been observed. The nonlocal effect becomes strong as the edge perturbation increases. The rise of the central temperature becomes small as the density increases, and it is saturated in the high density plasma. The cutoff density for nonlocal has been found. There is an upper density limit to induce non-local transport and the value corresponds to about 40% of the Greenwald density limit. The correlations of the fluctuations are measured by using a correlation reflectometer, which has the capability to measure the fluctuations both in the poloidal and radial directions. The low frequency fluctuation rise and the high frequency fluctuation suppression are observed after SMBI injection. It is found that the radial correlation of the fluctuation decreases, while the poloidal correlation of the fluctuation increases compared without nonlocal effect. This suggests that the low frequency fluctuation has a poloidal structure rather than a radial structure. So, the low frequency fluctuation rise can be considered as the enhancement of the poloidal elongated structures. The high frequency fluctuation can be suppressed by these poloidal elongated structures.

The Observation of Dual-peak Geodesic Acoustic Modes in the Edge Plasma on Tokamaks

D. Kong¹, J. Cheng², A. Liu¹, T. Lan¹, H. Zhao¹, H. Shen¹, M. Xu³, L. Yan²,
J. Dong², W. Hong², W. Zhang⁴, R. Chen⁴, G. Xu⁴, B. Wan⁴, H. Li¹, W. Liu¹, and
C. Yu¹

¹University of Science and Technology of China, Hefei, China

²Southwestern Institute of Physics, Chengdu, China

³University of California at San Diego, La Jolla, USA

⁴Institute of Plasma Physics, Hefei, China

Corresponding Author: dfkong@mail.ustc.edu.cn

In low density (HL-2A) and lithium wall condition (HT-7) two coherent modes are discovered of the GAM frequency range only on potential signals, i.e., at 11 kHz and 18 kHz, which are symmetric for their poloidal and toroidal mode number $n = m = 0$. So we can conclude that both two coherent modes are GAMs, named LFGAM and HFGAM respectively.

The results show that the amplitudes of LFZF and HFGAM decrease in outward direction. For LFGAM, the amplitude reach maximum value at $r - a = -1$ cm and then decrease with radial outward. In the mean time, the peak frequencies for dual GAMs remain the same of the range $\rho > 0.93$, while the theoretical predict frequencies calculated from the local plasma temperatures increase with radial inward. The radial wave number for HFGAM increases in radial outward direction and keep positive, where the positive sign means outward. These characteristics of GAM are consistent with the kinetic GAM theory after considering the finite Larmor radius effect. For LFGAM, experiment results indicate that the phase velocity of LFGAM propagates outward in the range of $r - a > -0.8$ cm and inward in the rest range.

To study the nonlinear coupling among LFGAM, HFGAM and ambient turbulence, the envelope analysis are used. There are strong nonlinear coupling between the dual GAMs and AT. Moreover, the cross phase at LFGAM and HFGAM frequencies are near π and $\pi/2$, respectively. It reveals that the LFGAM modulates AT with amplitude modulation, which means LFGAM is generated locally. For HFGAM, the AT is modulated with phase modulation, which means HFGAM is generated in deeper radial position and modulates local AT.

EX-P

Edge Plasma Transport and Microstability Analysis with Lithium-coated Plasma-facing Components in NSTX

J. Canik¹, W. Guttenfelder², R. Maingi¹, T. Osborne³, S. Kubota⁴, Y. Ren², R. Bell², H. Kugel², B. LeBlanc², and V. Soukhanovskii⁵

¹*Oak Ridge National Laboratory, Oak Ridge, USA*

²*Princeton Plasma Physics Laboratory, Princeton, USA*

³*General Atomics, San Diego, USA*

⁴*UCLA, Los Angeles, USA*

⁵*Lawrence Livermore National Laboratory, Livermore, USA*

Corresponding Author: canikjm@ornl.gov

The application of lithium coatings to the plasma-facing components (PFCs) of the National Spherical Torus Experiment (NSTX) has been shown to strongly impact plasma performance, improving energy confinement and eliminating ELMs. The pedestal structure is strongly affected by lithium: in discharges with lithium coatings, the density pedestal widens, and the electron temperature (T_e) gradient increases inside a radius of $\Psi_N \sim 0.95$, but is unchanged for $\Psi_N > 0.95$. Interpretive 2-D plasma/neutrals modeling has been performed for pre-lithium and with-lithium discharges. The modeling indicates that the application of lithium to the PFC surfaces reduces R from $\sim 0.98 - 0.9$. The inferred effective electron thermal χ_e^{eff} and particle D_e^{eff} profiles reflect the profile changes: χ_e^{eff} is similar in the near-separatrix region, and is reduced in the region $\Psi_N < 0.95$ in the with-lithium case. The (D_e^{eff}) profile shows a broadening of the region with low diffusivity with lithium, while the minimum value within the steep gradient region is comparable in the two cases. The linear microstability properties in the near-separatrix and pedestal-top regions have been analyzed. At $\Psi_N = 0.88$, low- k ($k_{\theta}\rho_s < 1$) microinstabilities are unstable, with the dominant modes being ITG-like in the pre-lithium case and TEM-like with lithium. The radial electric field shearing rate at this location increases with lithium, becoming significant compared to the maximum linear growth rate. In the region $\Psi_N > 0.95$, both the pre- and with-lithium cases are calculated to be strongly unstable to ETG modes, and are also both found to lie near the onset for kinetic ballooning modes.

The Role of Zonal Flows and Predator-Prey Oscillations in the Formation of Core and Edge Transport Barriers

L. Schmitz¹, L. Zeng¹, T. L. Rhodes¹, J. C. Hillesheim², W. A. Peebles²,
R. J. Groebner², K. H. Burrell², E. J. Doyle¹, W. M. Solomon³, and G. Wang¹

¹*University of California Los Angeles, Los Angeles, USA*

²*General Atomics, San Diego, USA*

³*Princeton Plasma Physics Laboratory, Princeton, USA*

Corresponding Author: lschmitz@ucla.edu

Understanding the formation dynamics of core and edge transport barriers is crucial for extrapolating present tokamak performance to burning plasma regimes. We present here direct evidence of low frequency Zonal Flows (ZF) reducing electron-scale turbulence in an electron internal transport barrier (ITB) at the $q = 2$ rational surface, and periodically suppressing ITG-scale turbulence via a predator-prey cycle near the separatrix, triggering edge barrier formation. Multi-channel Doppler Backscattering (DBS) has revealed strong similarity of the radial structure of the ZF-induced double shear layer, the ratio of $\mathbf{E} \times \mathbf{B}$ shearing rate $\omega_{\mathbf{E} \times \mathbf{B}}$ to turbulence decorrelation rate $\Delta\omega_D$, and the phase shift between turbulence envelope and time-dependent flow shear in both barrier types. Electron-scale $k_\theta, \rho_s \sim 3$ turbulence suppression by localized ZF shear $\Delta r \sim 4\rho_s \sim 1.5 - 2$ cm has been directly observed for the first time in an electron ITB. Both steady-state and oscillating ZF components with a broad frequency spectrum $f_{ZF} \leq 5$ kHz are found; ZF shear and density fluctuation amplitude are anticorrelated. In plasmas near the L-H transition threshold power, ZFs are observed to trigger edge barrier formation via limit cycle oscillations at/inside the separatrix, with a 90° phase lag of the ZF with respect to the density fluctuation envelope, characteristic of predator-prey oscillations. These observations are in qualitative agreement with a 0-D Lotka-Volterra model. Turbulence reduction due to ZF shearing is first observed when the turbulence decorrelation rate decreases sharply at or before ZF onset and the increasing ZF shearing rate locally surpasses the decorrelation rate. Above threshold, ZFs are observed as short transients preceding the transition, and executing only part of one limit cycle period. The “final” transition to H-mode with sustained turbulence/transport reduction is shown to be linked to increasing equilibrium flow shear due to the increasing ion pressure gradient. Limit cycle oscillations during the H-L back-transition, recently observed in DIII-D, are potentially important for ITER as a tool for controlled reduction of β_θ during current ramp-down.

EX-P

This work was supported in part by the U.S. Department of Energy under DE-FG02-08ER54984, DE-FG03-01ER54615, DE-FC02-04ER54698 and DE-AC02-09CH11466.

Parametric Dependencies of Low- k Turbulence in NSTX H-mode Pedestals

D. Smith¹, R. Fonck¹, G. R. McKee¹, R. Bell², A. Diallo², S. Kaye², B. LeBlanc²,
R. Maingi³, and B. Stratton³

¹*University of Wisconsin-Madison, Madison, USA*

²*Princeton Plasma Physics Laboratory, Princeton, USA*

³*Oak Ridge National Laboratory, Oak Ridge, USA*

Corresponding Author: drsmith@engr.wisc.edu

Validating predictive models of pedestal turbulence is critical for ITER and next-step devices. Here, we characterize the poloidal correlation length and decorrelation time of low- k pedestal turbulence in NSTX ELM-free, MHD-quiescent H-mode plasmas, plus we identify parametric dependencies that influence pedestal turbulence quantities. Poloidal correlation lengths in the pedestal are typically 10 – 20 cm and about $10\rho_i$. The parametric dependence with toroidal flow shear is consistent with enhanced confinement at higher flow shear, and parametric dependencies with density gradient and electron temperature inverse scale length are consistent with low- k drift-wave turbulence. Also, parametric dependencies with collisionality provide insight into turbulence mediation by zonal flows. The measurements and analysis presented here broadly characterize pedestal turbulence in high-performance spherical torus plasmas and establish validation benchmarks for pedestal and edge simulations in the challenging spherical torus parameter regime.

EX-P

L to H-mode Power Threshold and Confinement Characteristics of H-modes in KSTAR

H. S. Kim¹, Y. S. Na¹, J. W. Ahn², Y. M. Jeon³, S. W. Yoon³, K. D. Lee³, W. H. Ko³,
Y. S. Bae³, W. C. Kim³, and J. G. Kwak³

¹*Seoul National University, Seoul, Republic of Korea*

²*Oak Ridge National Laboratory, Oak Ridge, USA*

³*National Fusion Research Institute, Daejeon, Republic of Korea*

Corresponding Author: ftwalker.hyuns@gmail.com

Since KSTAR has obtained the H-mode in 2010 campaign, H-mode plasmas were routinely obtained with combined heating of NBI with maximum power of 1.5 MW and ECRH with maximum power of ~ 0.3 MW and ~ 0.6 MW for 110 GHz and 170 GHz, respectively. The L- to H-mode power threshold and confinement properties of KSTAR H-modes are investigated in this work. Firstly, the L- to H-mode power threshold and the power loss to the separatrix are calculated by power balance analysis for about collected 400 shots. As a result, a trend of roll-over is observed in the power threshold of KSTAR H-mode compared with the multi-machine power threshold scaling in the low density regime. Dependence of the power threshold on other parameters are also investigated such as the X-point position and shaping parameters like as triangularity and elongation. In addition, the reason of reduction of power threshold in 2011 campaign compared with that in 2010 is addressed. Secondly, the confinement enhancement factors are calculated to evaluate the performance of KSTAR H-modes. The calculated H_{89-p} and $H_{98}(y, 2)$ represent that the confinement is enhanced in most KSTAR H-mode discharges. Interestingly, even in L-mode phases, confinement is observed to be enhanced against the multi-machine scalings. H_{exp} factor is newly introduced to evaluate the amount of confinement improvement in the H-mode phase compared with the L-mode phase in a single discharge. H_{exp} exhibits that the global energy confinement time of the H-mode phase is improved about 1.3–2.0 times compared with that of the L-mode phase. Finally, interpretive and predictive numerical simulations are carried out using the ASTRA code for typical KSTAR H-mode discharges. The Weiland model and the GLF23 model are employed for calculating the anomalous contributions of both electron and ion heat transport in predictive simulations. For the H-mode phase, the Weiland model reproduces the experiment well. The results presented here are expected to support establishment of ITER H-mode plasmas.

EX-P

L–H Power Threshold, Pedestal Stability and Confinement in JET with a Metallic Wall

M. Beurskens¹, L. Frassinetti², C. Maggi³, G. Calabro⁴, B. Alper¹, C. Bourdelle⁵, C. Angioni³, S. Brezinsek⁶, P. Buratti⁴, C. Challis¹, J. Flanagan¹, E. Giovannozzi⁴, C. Giroud¹, M. Groth⁷, J. Hobirk³, E. Joffrin⁵, M. Leyland⁸, P. Lomas¹, E. de la Luna⁹, M. Kempenaars¹, P. Mantica¹⁰, M. Maslov¹, G. Matthews¹, M. L. Mayoral¹, R. Neu³, P. B. Snyder¹, I. Nunes¹¹, T. Osborne¹², S. Saarelma¹, and P. de Vries¹³

¹EURATOM /CCFE Fusion Association, Culham Science Centre, Abingdon, UK

²Division of Fusion Plasma Physics, Association EURATOM-VR, Stockholm, Sweden

³IPP Garching, Garching, Germany

⁴Associazione EURATOM-ENEA sulla Fusione, Frascati, Italy

⁵Association Euratom-CEA, IRFM, St-Paul-Lez-Durance, France

⁶Forschungszentrum Jülich, Jülich, Germany

⁷Association EURATOM/Helsinki University of Technology, Espoo, Finland

⁸Department of Physics, University of York, Heslington, York, UK

⁹Ciemat, Madrid, Spain

¹⁰Istituto di Fisica del Plasma “P. Caldirola”, Milano, Italy

¹¹Centro de Fusao Nuclear, Associacao EURATOM-IST, Lisboa, Portugal

¹²General Atomics, San Diego, USA

¹³FOM DIFFER, Nieuwegein, Netherlands

Corresponding Author: marc.beurskens@ccfe.ac.uk

After the change-over from the Carbon-Fibre Composite (CFC) wall to an ITER-like metallic wall (ILW) the baseline type I ELMy H-mode scenario has been re-established in JET with the new plasma-facing materials Be and W. A key finding for ITER is that the power required to enter H-mode has reduced with respect to that in JET with the CFC wall. In JET with the ILW the power threshold to enter H-mode (P_{L-H}) is below the international L-H power threshold scaling $P_{Martin-08}$. The minimum threshold is $P_{L-H} = 1.8$ MW compared to $P_{Martin-08} = 4$ MW with a pedestal density of $n_{ped} = 2 \times 10^{19} \text{ m}^{-3}$ in plasmas with $I_p = 2.0$ MA, $B_t = 2.4$ T. However the threshold depends strongly on density; using slow ion cyclotron heating (ICRH) power ramps P_{L-H} varies from 1.8 to 4.5 MW in a range of lower and upper plasma triangularity ($\delta_L = 0.32 - 0.4$, $\delta_U = 0.19 - 0.38$).

Stationary Type I ELMy H-mode operation has been re-established at both low and high triangularity with $I_p \leq 2.5$ MA, $q_{95} = 2.8 - 3.6$ and $H_{98} \leq 1$. The achieved plasma collisionality is relatively high, in the range of $1 < \nu_{eff} < 4$ due to the required strong gas dosing. Stability analysis with the linear MHD stability code ELITE show that the pedestal is marginally unstable with respect to the Peeling Ballooning boundary. Due to the stabilising effect of the global pressure β_N on the pedestal stability, a strong coupling between core and edge confinement is expected. Indeed in an H-mode profile database comparison with 119 CFC- ($0.1 < \nu_{eff} < 1$) and 40 ILW-H-modes a strong coupling of the core versus edge confinement is found, independent of wall material. In addition, the pedestal predictions using the EPED predictive pedestal code coincide with the measured pedestal height over a wide range of normalised pressure $1.5 < \beta_N < 3.5$.

Due to the strong core-edge coupling, beneficial effects of core profile peaking on confinement are weak in the database comparison. However, differences in the individual temperature and density profile peaking occur across the database. When collisionality is increased from $\nu_{eff} = 0.1$ to 4, the density peaking decreases from $R/L_{ne} = 4$ to 0.5 but is compensated by an increase in temperature peaking from $R/L_{Ti} = 5$ up to 8, offering a challenge for micro turbulence-transport models.

Evolution of the Turbulence Radial Wavenumber Spectrum near the L–H Transition in NSTX Ohmic Discharges

S. Kubota¹, C. E. Bush², R. Maingi², S. J. Zweben³, R. Bell³, N. Crocker¹, A. Diallo³,
S. Kaye³, B. P. LeBlanc³, R. J. Maqueda⁴, J. K. Park³, W. A. Peebles¹, R. Raman⁵,
and Y. Ren³

¹*UCLA, Los Angeles, USA*

²*Oak Ridge National Laboratory, Oak Ridge, USA*

³*Princeton Plasma Physics Laboratory, Princeton University, Princeton, USA*

⁴*Nova Photonics, Princeton, USA*

⁵*University of Washington, Seattle, USA*

Corresponding Author: skubota@ucla.edu

The measurement of radially extended meso-scale structures such as zonal flows and streamers, as well as the underlying microinstabilities driving them, is critical for understanding turbulence-driven transport in plasma devices [1]. In particular, the shape and evolution of the radial wavenumber spectrum indicate details of the nonlinear spectral energy transfer [2], the spreading of turbulence [3], as well as the formation of transport barriers [4]. In the National Spherical Torus Experiment (NSTX), the FMCW backscattering diagnostic [5] is used to probe the turbulence radial wavenumber spectrum ($k_r = 0 - 22 \text{ cm}^{-1}$) across the outboard minor radius near the L- to H-mode transition in Ohmic discharges. During the L-mode phase, a broad spectral component ($k_r \sim 2 - 10 \text{ cm}^{-1}$) extends over a significant portion of the edge-core from $R = 120$ to 155 cm ($\rho = 0.4 - 0.95$). At the L-H transition, turbulence is quenched across the measurable k_r range at the ETB location, where the radial correlation length drops from $\sim 1.5 - 0.5 \text{ cm}$. The k_r spectrum away from the ETB location is modified on a time scale of tens of microseconds, indicating that nonlocal turbulence dynamics are playing a strong role. Close to the L-H transition, oscillations in the density gradient and edge turbulence quenching become highly correlated. These oscillations are also present in Ohmic discharges without an L-H transition, but are far less frequent. Similar behavior is also seen near the L-H transition in NB-heated discharges.

References

- [1] A. Fujisawa *et al.*, Plasma Phys. Control. Fusion **53** (2011) 124015.
- [2] J. Li and Y. Kishimoto, Phys. Plasmas **17** (2010) 072304.
- [3] T. S. Hahm *et al.*, Plasma Phys. Control. Fusion **46** (2004) A323.
- [4] W. X. Wang *et al.*, Phys. Plasmas **14** (2007) 072306.
- [5] S. Kubota *et al.*, 53rd Meeting of the APS Division of Plasma Physics, **4** (2012) 00003.

Work supported by U.S. DOE Contracts DE-FG02-99-ER54527 and DE-AC02-09CH11466.

EX-P

Dynamics of the Plasma Edge during the L–H Transition and H–mode in MAST

R. Scannell¹, H. Meyer¹, D. Dunai², G. Cunningham¹, A. Field¹, A. Kirk¹, S. Samuli¹,
A. Patel¹, and S. Zoletnik²

¹*EURATOM /CCFE Fusion Association, Culham Science Centre, Abingdon, UK*

²*KFKI-RMKI, EURATOM Association, Budapest, Hungary*

Corresponding Author: rory.scannell@ccfe.ac.uk

The evolution of the MAST plasma during the L-H transition has been studied in the density range $1.5 - 3.0 \times 10^{19} \text{ m}^{-3}$. A dithering transition phase, the duration of which depends on the plasma density, is observed before the transition to ELMy or ELM free H-mode. A range of new diagnostic data has been taken during these periods, showing a spin-up of the perpendicular He^+ flow correlated with changes in the D_α emission. In this density range the power threshold increases with increasing density. As well as the expected power threshold dependency on absolute density, the threshold power is observed to depend on the density evolution prior to the transition. Small changes in fuelling location, plasma current, toroidal field and plasma shape can lead to changes in the power threshold by a factor of two, significantly larger than those predicted by the scaling. The pedestal evolution between typical type I ELMs in connected double null configuration on MAST show increasing pedestal pressure and width as function time through the ELM cycle. This results in an expanding high pressure gradient region with little increase in peak pressure gradient within this region. It has been shown that the triggering of these ELMs is caused by decreasing stability limit as the transport barrier moves inwards. Application of $n = 6$ resonant magnetic perturbations to the plasma causes ELM mitigation, with smaller but much more frequent ELMs. The pressure gradients in this mitigated period are significantly less than those observed during non-mitigated type I ELMs. This reduction in pressure gradient, which indicates a different stability limit, results from both a decrease in pedestal height and increase in pedestal width.

Work supported by the RCUK Energy Programme and EURATOM.

Far-reaching Impact of Intermittent Transport across the Scrape-off Layer: Latest Results from ASDEX Upgrade

M. Kocan¹, W. Müller¹, J. Adámek², G. Conway¹, P. de Marné¹, T. Eich¹,
R. Fischer¹, C. Fuchs¹, F. Gennrich³, A. Herrmann¹, J. Horacek², Z. Huang⁴,
C. Ionita¹, A. Kallenbach¹, M. Komm², T. Lunt¹, M. Maraschek¹, C. Maszl³,
F. Mehlmann³, S. Müller¹, B. Nold¹, T. Ribeiro¹, V. Rohde¹, R. Schrittwieser³,
B. Scott¹, U. Stroth¹, W. Suttrop¹, and E. Wolftrum¹

¹Max-Planck-Institut für Plasmaphysik, EURATOM Association, Garching, Germany

²Association EURATOM-IPP.CR, Prague, Czech Republic

³Institute for Ion Physics and Applied Physics, Association Euratom-ÖAW, Austria

⁴Institut für Plasmaforschung, Universität Stuttgart, Stuttgart, Germany

Corresponding Author: martin.kocan@ipp.mpg.de

Latest research of intermittent transport in the scrape-off layer (SOL) of the ASDEX Upgrade tokamak is presented. Near the separatrix the fluctuations of the plasma and the floating potentials, measured by various Langmuir probes (LPs), are found to be anti-correlated due to fluctuations of the electron temperature. This indicates that, in contrast to a widely used experimental practice, a free exchange of both potentials is unjustified and can lead to significant error. Measurements of ion energies in turbulent L-mode and ELM filaments were carried out using a retarding field analyzer. In L-mode plasma, the filament ion temperature measured at 2 cm outside the separatrix is 80 – 110 eV, i.e., 3 – 4× the background ion temperature. Turbulent filaments also convect plasma to the wall with larger density than the background plasma density. Qualitatively similar observations were obtained during inter-ELM periods. Such enhanced particle and energy fluxes can potentially raise the erosion of the first wall in ITER. The ion temperature averaged over an ELM measured 35 – 60 mm outside the separatrix is in the range of 20 – 200 eV (5 – 50% of the pedestal top ion temperature). This demonstrates that ELM filaments carry hot ions over large radial distances in the SOL, which, in turn, can lead to enhanced sputtering from the first wall in future tokamaks. Lowest ion energies are observed during ELMs mitigated by in-vessel magnetic perturbations (MPs). The ELM ion temperature in the far SOL is found to increase with the ELM energy, indicating that on average the filaments in large ELMs propagate faster radially. The filamentary structure of the ion current density measured by LPs at the outboard mid-plane during mitigated ELMs is qualitatively similar to that observed during type I ELMs. The amplitude of the ion current density decreases only slightly when ELMs are mitigated, but, in contrast to type I ELMs, bursts of the ion current are observed throughout the ELM cycle including inter-ELM periods. This shows again that ELM mitigation replaces type I ELMs by more continuous transport events. In H-mode, MPs modify the SOL transport (intermittency decreases, time-averaged ion current rises) even if the plasma density is below the empirical ELM mitigation threshold. In the low density L-mode, MPs are associated with the decrease of the fluctuation level in the SOL.

EX-P

Time-resolved Evolution of Low Frequency Electrostatic Fluctuations during Slow L–H Transition at the Boundary Plasma of HL-2A Tokamak

J. Cheng¹, Z. H. Huang², L. W. Yan², J. Q. Dong², W. Y. Hong², D. F. Kong²,
M. Xu³, K. J. Zhao¹, T. Lan², A. D. Liu², Y. G. Li¹, X. M. Song¹, Q. W. Yang¹,
X. T. Ding¹, X. R. Duan¹, and Y. Liu¹

¹*Southwestern Institute of Physics, Chengdu, China*

²*Southwestern Institute of Physics, Hefei, China*

³*CMTFO & CER & MAE Department, UCSD, La Jolla, USA*

Corresponding Author: chengj@swip.ac.cn

A quasi-period electrostatic oscillation with 2 – 3 kHz is observed using Langmuir probe array during slow L-H transition in edge plasma of HL-2A Tokamak. This low frequency oscillation radially propagates inwards with 0.3 – 0.6 km/s inside the separatrix about 3 – 8 mm, and it appears on potential, density, electron pressure and Reynolds stress gradients. The dP_e/dr fluctuation amplitude can reach 30 – 40%. The dR_s/dr is prior to E_r fluctuation about $\pi/2$, indicating the existence of nonlinear interaction between them. In near SOL, this low frequency oscillation also appears in potentials, E_r and density fluctuation, suggesting a significant correlation among them at edge and near SOL plasma. This quasi-period oscillation might be correlated with mean flow or low frequency zonal flow, and the latter might set a condition for the former developing, implying a competitive process between them. The competition characterized by a quasi-period oscillation seems to determine the L-H transition.

EX-P

Overview of Resonant Helical Magnetic Field Experiments on the IR-T1 Tokamak

P. Khorshid¹, M. Ghoranneviss¹, A. Lahazi¹, H. Bolourian¹, R. Arvin²,
S. Mohammadi², and A. Nikmohammadi²

¹Islamic Azad University, Mashhad Branch, Mashhad, Iran

²Plasma Physics Research Center, Islamic Azad University, Tehran, Iran

Corresponding Author: pkhorshid@gmail.com

The Experimental studies during externally applied resonant helical magnetic field (RHF) perturbation in IR-T1 tokamak have been investigated. The experiments have been done in various directions of plasma current and toroidal magnetic field to finding the role of I_p and B_t direction in RHF application. The Morlet wavelet spectra, Fourier coefficient decomposition (FCD) and Singular value decomposition (SVD) analysis have been used to perform time-frequency and spatial-wave number harmonics analyses on the measured MHD fluctuations. The profiles of electron temperature, floating potential, radial electric field, poloidal and toroidal rotation velocity have been measured in the edge of plasma by using of a movable Langmuir probes, Rake probe and Mach probe. In RHF application during $L = 2/n = 1$ and $q_a = 3.7$, the $m = 2$ MHD mode oscillations amplified and $m = 3$ mode suppressed. Also by applying $L = 3/n = 1$ the $m = 2$ MHD mode oscillations has been disappeared. The toroidal velocity changes after a short delay time of about $t_d = 1 - 1.5$ ms during RHF application while poloidal velocity changes just after RHF. Results of visible line emissions of O(II), C(III) impurities and H_α radiation with and without RHF $L = 2$ show that the addition of a relatively small amount of resonant magnetic helical field could be effective for improving the quality of the discharge by reducing of light impurities radiation and possible suppressing major disruptions. The resonant field induced a phase with reduced H_α radiation level.

EX-P

3D Effects on RFX-mod Helical Boundary Region

N. Vianello¹, E. Martines¹

¹ *Consorzio RFX, Associazione Euratom-ENEA sulla Fusione, Padova, Italy*

Corresponding Author: nicola.vianello@igi.cnr.it

In present fusion research strong effort is devoted to the studies of the effects of non-axisymmetric magnetic perturbation or magnetic field ergodization on the external region of the plasma. On this topic interesting results can be drawn from the helical configuration observed in high-current regimes in RFPs where a helical core is surrounded by an almost quasi-symmetric boundary and the small residual helical ripple is sufficient to modulate all the kinetic properties of the plasma and the plasma wall interaction. This contribution presents the most recent experimental results and physical interpretation of the phenomena observed in the edge region of the RFX-mod Reversed Field Pinch experiment, with a strong emphasis on the effects of helical deformation. Experimental observations indicate that plasma pressure and floating potential are found to oscillate in phase with the oscillation of helical radial displacement with increasing values of pressure and pressure gradient and more negative values of floating potential corresponding to more protruding plasma. Helical flow is observed at the edge, with the same periodicity of the dominant mode. This flow pattern is interpreted in terms of modulation of ion to electron diffusion rate, which is further complicated by the fact that the shift of the dominant mode causes radial displacement of the $m = 0$ islands which resonate at the reversal surface and are found to deeply influence particle transport in this region. The ambipolar electric field arising in order to ensure quasi-neutrality indeed correctly takes into account the observed flow pattern, interpretation corroborated by comparison with the hamiltonian guiding center code ORBIT. Strong effort will be devoted to the determination of the actual phase relation between magnetic perturbation and velocity perturbation, and its dependence on plasma collisionality. Finally helical ripple is found to influence also turbulence characteristics at the edge with the observation of a ripple of the radial correlation length of short-wavelength fluctuations. Further observation of the effects on blobs will be provided.

EX-P

Density Limit Experiments on FTU

G. Pucella¹, O. Tudisco¹, M. L. Apicella¹, G. Apruzzese¹, G. Artaserse¹, F. Belli¹,
W. Bin², L. Boncagni¹, A. Botrugno¹, P. Buratti¹, G. Calabro¹, C. Castaldo¹,
C. Cianfarani¹, V. Cocilovo¹, L. Dimatteo¹, B. Esposito¹, D. Frigione¹, L. Gabellieri¹,
E. Giovannozzi¹, G. Granucci², M. Marinucci¹, D. Marocco¹, E. Martines³,
G. Mazzitelli¹, C. Mazzotta¹, S. Nowak², G. Ramogida¹, A. Romano¹, A. A. Tuccillo¹,
L. Zeng⁴, and M. Zuin³

¹ENEA, Associazione Euratom-ENEA, Frascati, Rome, Italy

²IFP-CNR, Associazione Euratom-ENEA, Milano, Italy

³Consorzio RFX, Associazione Euratom-ENEA, Padova, Italy

⁴Institute of Plasma Physics, Chinese Academy of Sciences, Hefei, China

Corresponding Author: gianluca.pucella@enea.it

One of the main problems in tokamak fusion devices concerns the capability to operate at high plasma density, that is observed to be limited by the appearance of catastrophic events causing loss of plasma confinement. The commonly used empirical scaling law for the density limit is the Greenwald limit, predicting that the maximum achievable line averaged density along a central chord depends only on the average plasma current. The aim of this work is to present the results of dedicated density limit experiments performed on the Frascati Tokamak Upgrade (FTU) in which the high density domain was explored in a wide range of values of plasma current ($I = 500 - 900$ kA) and toroidal magnetic field ($B = 4 - 8$ T). These experiments confirm the edge nature of the density limit as a Greenwald like scaling holds for the maximum achievable line averaged density along a peripheral chord. However, when the central line-averaged is considered, the dependence of the density peaking on the edge safety factor, associated to the presence of MARFEs, give rise to a new density limit scaling law in which the central line-averaged density is solely dependent on the toroidal magnetic field. The behaviour of the density limit with the magnetic field in presence of pellet injection and with strong lithium coated wall will be studied in FTU in the next future, possibly including lower magnetic field discharges.

EX-P

Latest Developments in Data Analysis Tools for Disruption Prediction and for the Exploration of Multimachine Operational Spaces

A. Murari¹, J. Vega², B. Cannas³, S. Dormido-Canto⁴, A. Fanni³, A. Pau³,
S. Giuliana³, J. M. Ramirez⁴, J. Mlynar⁵, and M. Odstrcil⁵

¹*Consorzio RFX Padova, Padova, Italy*

²*CIEMAT, Madrid, Spain*

³*Electrical and Electronic Engineering Department, University of Cagliari, Italy*

⁴*Dpto. Informática y Automática, UNED, Madrid, Spain*

⁵*Association EURATOM-IPP.CR, Faculty of Nuclear Sciences and Physical Engineering CTU, Prague, Czech Republic*

Corresponding Author: andrea.murari@igi.cnr.it

Disruptions are unavoidable in current Tokamaks and accurate and reliable predictions are a prerequisite to any mitigation strategy. Therefore the most recent efforts in data analysis and machine learning have concentrate on the one hand on improving the success rate of predictors and on the other hand on developing tools which can help in the understanding of disruption physics. The best performing predictor for JET is APODIS, which has been trained and tested, in a 24 dimensional space of features (all available in real time), using hundred of shots selected among more than 8400 discharges analysed using high performance computation tools. In the campaigns (C24, C25, C27a) with good quality signals and without the use of magnetic perturbation for ELM mitigation, not included in the training set, the success rate of the predictor is higher than 90%, 35 ms before the disruption (for a rate of false alarms of a few percent). The following developments of this line of research will involve the optimisation of the learning rate.

The prediction of the type of disruption is in its turn a fundamental aspect to optimise mitigation strategies. The predictors of the complexity of APODIS can reach very good performance but their results are quite difficult to relate to physical theories of disruptions. Tools of higher interpretability are required to explore the operational space and investigate the physics (even at the price of reduced performance in terms of prediction accuracy). The adopted data driven approach consists of trying to determine whether the relevant information lies on an embedded, possibly non-linear, manifold within the higher-dimensional space. If this proved feasible, the data could be represented well in a low-dimensional subspace and more effectively analysed to extract information about the physics of the disruptions and their precursors. To this end, recently, dimensionality reduction and manifold learning methods have been successfully investigated, using various tools ranging from Data Tours to Principal Component Analysis and Self Organising Maps (SOM). In particular using SOM it has been possible to map seven non dimensional parameters in a way that the disruptive and non disruptive regions of the operational space are quite separate. This is quite promising for the understanding of disruptions and cross machine comparison.

Latest Progress in Studies of Runaway Electrons in JET

V. V. Plyusnin¹, V. Kiptily², B. Bazylev³, A. Shevelev⁴, E. Khilkevich⁴, J. Mlynar⁵,
M. Lehnen⁶, G. Arnoux², T. Hender², A. Huber⁶, S. Jachmich⁷, U. Kruezi⁶,
R. Pereira¹, C. Reux⁸, A. Fernandes¹, V. Riccardo², P. de Vries⁹, and
JET EFDA Contributors¹⁰

¹*Instituto de Plasmas e Fusão Nuclear, Associação EURATOM-IST, Instituto Superior
Tecnico, Lisboa, Portugal*

²*Euratom/CCFE Association, Culham Science Centre, Abingdon, UK*

³*Karlsruhe Institute of Technology, Karlsruhe, Germany*

⁴*A. F. Ioffe Institute of the Russian Academy of Sciences, St. Petersburg, Russia*

⁵*Association EURATOM/IPP.CR, IPP AS CR, Prague, Czech Republic*

⁶*Institute for Energy Research-Plasma Physics, Forschungszentrum Jülich, Jülich, Germany*

⁷*Laboratoire de Physique des Plasmas-Laboratorium voor Plasmafysica, Brussels, Belgium*

⁸*CEA, IRFM, Saint-Paul-lez-Durance, France*

⁹*FOM DIFFER, Nieuwegein, Netherlands*

¹⁰*JET-EFDA, Culham Science Centre, Abingdon, UK*

Corresponding Author: vladislav.plyusnin@ipfn.ist.utl.pt

Latest disruption experiments in JET with carbon-fibre composite (CFC) in plasma facing components (PFC) have been carried out using either Massive Gas Injection or constant puff. These studies provided new data and further update of the database on disruption generated runaway electrons (RE). Temporal and spatial dynamics of RE beams have been studied using inverse reconstruction of the measured hard and soft X-rays emission during RE plateaux. Energy spectra of RE have been measured. Data is used in modelling of RE generation in the presence of spatial dynamics of current carrying channel and in simulations of interaction of RE beams with PFC in JET. First operations of JET with ITER-like Wall (ILW) showed that disruptions in new all-metal environment do not favour to runaway process. More than 10 times slower plasma current quenches that in experiments with CFC and electron temperatures about 100 eV have been measured. However, many RE generation events have been detected by HXR diagnostics during steady-state stages of discharges in JET with ILW. Modelling of the evolution of these discharges using simulation tool JETTO confirmed the possibility for significant RE generation.

EX-P

JET EFDA Contributors: See the Appendix of F. Romanelli *et al.*, Proceedings of the 23rd IAEA Fusion Energy Conference 2010, Daejeon, Republic of Korea.

Overview of Runaway Electrons Control and Mitigation Experiments on Tore Supra and Lessons Learned in View of ITER

F. Saint-Laurent¹, G. Martin¹, S. Putvinski², J. Bucalossi¹, S. Brémond¹, and P. Moreau¹

¹CEA, IRFM, Saint-Paul-lez-Durance, France

²ITER Organization, Saint-Paul-lez-Durance, France

Corresponding Author: francois.saint-laurent@cea.fr

Runaway electrons (RE) generated during disruption are identified as a major issue for ITER. Mitigation techniques are thus mandatory to suppress RE formation or/and reduce their heat loads. Two ways are explored on Tore Supra:

- Suppress the RE beam formation and avalanche amplification by multiple gas jet injections at current quench (CQ).
- Control the RE beam when it is formed and increase the collisionnality to slow down relativistic electrons.

A RE deconfinement at CQ before their exponential amplification might be achieved by ultra-fast supersonic gas injection. Thus a new concept of injector has been developed and tested on Tore Supra. A high pressure gas cartridge (150 bars), is open by rupture of a bursting disk. Neon or helium gas injections (240 Pam³) were triggered at CQ of disruptive plasma. The propagation of the neutral gas burst in the plasma is followed using a fast camera. The cold gas front travels through the plasma and penetrates at half of gas velocity in vacuum. Despite these observations, no robust perturbations on the current decay and on the loop voltage are recorded. The expected RE suppression has not been observed yet. Moreover, neither indication of an increase of MHD activity nor RE destabilization is observed.

RE beams (hundreds of kA) lasting several seconds are observed on Tore Supra. Such a plateau formation is eased with circular plasma in limiter configuration and develops only when the CFC first wall is depleted of deuterium. Mastering the RE plateau regime is a key to deploy mitigation techniques. Associated to a position control, a several hundred milliseconds RE current control was demonstrated on Tore Supra. Massive gas injection (MGI) was triggered on such a controlled RE plateau to increase the electron collisionnality. A subsequent reduction of high electron energy tail is observed, attributed to a beginning of thermalization. These results are very encouraging for mastering the RE beam regime towards a full thermalization.

The suppression of the avalanching process is the only way to guaranty that RE effects are mastered. Because a reliable suppression technique is not available yet and is still an issue for ITER, RE beam control experiments must be pursued. The aim of a collisionnal thermalization of RE seems feasible but is not achieved yet.

Global Mode Control and Stabilization for Disruption Avoidance in High- β NSTX Plasmas

J. Berkery¹, S. Sabbagh¹, R. Bell², R. Betti³, J. Bialek¹, A. Diallo², D. Gates²,
S. Gerhardt², O. Katsuro-Hopkins¹, B. LeBlanc², J. Manickam², J. Menard²,
Y. S. Park¹, M. Podesta², and H. Yuh⁴

¹*Department of Applied Physics & Applied Mathematics, Columbia University, New York, USA*

²*Princeton Plasma Physics Laboratory, Princeton, USA*

³*Laboratory for Laser Energetics, University of Rochester, Rochester, USA*

⁴*Nova Photonics, Princeton, USA*

Corresponding Author: jberkery@pppl.gov

Global MHD instabilities may disrupt operation of ITER and other future tokamaks. The National Spherical Torus Experiment (NSTX) has previously investigated passive stabilization and demonstrated active control of resistive wall modes (RWMs), accessing high $\beta_N = 7.2$. Current research focuses on greater understanding of the stabilization physics, projection to future devices, quantitative comparison to experiment, and demonstration of improved active control techniques that can aid the goal of disruption avoidance in ITER. Combined radial and poloidal field sensor feedback gain and phase used in NSTX experiments produced a greater than three times reduction in disruption probability. Time domain analysis with the VALEN code reproduces the dynamics of the mode amplitude as a function of feedback phase and determines the optimal gain. Additionally, a new model-based RWM state space controller proposed for ITER, which includes a 3D model that compensates for plasma and mode-induced wall currents, was used. Open-loop comparisons between sensor measurements and the state space control model showed agreement with a sufficient number of states and when details of the 3D wall model were added. The state space controller was demonstrated to sustain long pulse, high β_N discharges, and reduce $n = 1$ applied fields that normally disrupt the plasma. Present calculations of kinetic stability using the MISK code show improved quantitative agreement with NSTX experimental marginal stability points and emphasize the importance of the plasma rotation profile. Collisions have competing effects: they both dissipate the mode energy and damp the stabilizing kinetic effects. The low collisionality of future machines can improve RWM stability, but only if the plasma rotation is in a favorable resonance. Energetic particles have been shown to be generally stabilizing, and scaling of the model to ITER high performance discharges indicates that the stabilizing effects of alpha particles may be required to maintain a stable RWM at the expected plasma rotation profile. Alterations to the theory now focus on improved agreement with experiment over the entire database. One such alteration is the inclusion of anisotropic distribution functions for energetic particles from neutral beam injection.

EX-P

Supported by US DOE Contracts DE-FG02-99ER54524, DE-AC02-09CH11466, and DE-FG02-93ER54215.

Stabilization of Disruptive Locked Modes by Magnetic Perturbations and Electron Cyclotron Current Drive at DIII-D

F. A. Volpe¹, R. J. La Haye², M. J. Lanctot³, S. Mao⁴, R. Prater², E. J. Strait², and A. S. Welander²

¹*Columbia University, New York, USA*

²*General Atomics, San Diego, USA*

³*Lawrence Livermore National Laboratory, Livermore, USA*

⁴*University of Wisconsin-Madison, Madison, USA*

Corresponding Author: fv2168@columbia.edu

Magnetic perturbations were used to control the rotation and toroidal phase of locked modes (LMs) and of their rotating precursors, when present, thus enabling the first full suppression of locked modes by modulated or continuous Electron Cyclotron Current Drive (ECCD). In a first set of experiments the applied perturbations were static and caused the rotating precursor to directly lock in a position such that its O-point was accessible to localized, continuous ECCD. ECCD in the O-point rapidly and completely stabilized the LM and avoided a disruption. Higher ECCD power was more stabilizing, as expected, and ECCD was more efficient than simple EC heating in the O-point, also as expected. For ECCD in the X-point the LM was increased in amplitude. For ECCD at intermediate toroidal locations it grew slower and the disruption was delayed, but not avoided. LM suppression permitted disruption-free operation at β_N as high as 2.5 in discharges which otherwise disrupted at β_N as low as 1.7. The confinement was also improved and the H-mode never lost, as a result of LM suppression. Complete LM stabilization was observed in slowly rotating plasmas, for balanced Neutral Beam Injection (NBI). For unbalanced NBI, instead, the LM was often unlocked and accelerated by the NBI torque before being completely suppressed by the ECCD. In other experiments, rapidly rotating magnetic perturbations were used to unlock the island or catch it when still rotating, and sustain its rotation at up to 100 Hz. At the same time the ECCD was modulated synchronously with the driven rotation of the island. The island amplitude was reduced when ECCD was selectively applied in the island O-point, while current drive at the X-point increased the island size. Detailed data on ECCD in intermediate toroidal positions were collected by adopting slightly different frequencies for the ECCD modulation and island rotation, which was equivalent to slowly scanning the relative toroidal phase. The mode amplitude was observed to decrease as the rotation rate increased.

This work was supported by the US Department of Energy under DE-FG03-97ER544156, DE-SC0006415, DE-FC02-04ER54698, and DE-AC52-07NA27344.

Disruption Mitigation Experiments with Two Gas Jets on Alcator C-Mod

R. Granetz¹, G. Olynyk¹, M. Reinke², D. Whyte¹, and S. Combs²

¹*MIT Plasma Science & Fusion Center, Cambridge, USA*

²*Oak Ridge National Laboratory, Oak Ridge, USA*

Corresponding Author: granetz@mit.edu

Massive gas injection (MGI) disruption mitigation experiments have shown that this technique can quickly convert a large fraction of plasma thermal and magnetic energy into radiated power. To date, gas has been injected from a single spatial location, and bolometric measurements have shown that the resulting radiated power is often toroidally asymmetric, which could cause melting of beryllium first wall surfaces in ITER. Therefore, the ITER MGI system proposes multiple gas jets distributed around the torus.

On Alcator C-Mod, a 2nd gas jet has been installed 154 degrees around the torus from the existing gas jet. The hardware components of both gas jets are nominally identical. A pair of AXUV photodiode arrays viewing the plasma midplane is used to measure the $n = 1$ component of the toroidal asymmetry, and a toroidally-distributed set of six individual detectors, each viewing a collimated slice of the plasma, provides toroidal resolution higher than $n = 1$ and is used to calculate the toroidal peaking factor (TPF) of the radiated power.

Experiments have begun to characterise the effect of using two jets on the radiation TPF, varying the relative timing between the firing of the gas jets from shot-to-shot. It is observed that the TPF depends on the phase of the disruption. During the pre-TQ, when the gas is cooling the plasma edge, the TPF varies reproducibly with the relative gas jet timing. However, during the thermal quench (TQ) and current quench (CQ), when most of the plasma energy is radiated, the results are more complicated. At large positive delay times (i.e., jet #2 fires well after jet #1) the TPF is seen to be variable and often high, agreeing with earlier results using only this jet. However, at large negative delay times (jet #2 fires well before jet #1), the TPF is significantly lower and more reproducible. This may indicate that slight differences in hardware and/or geometry between the two gas jet systems are important. The growth of $n = 1$ MHD modes may also be playing a role.

Observations of the radiation asymmetry during the TQ and CQ phases, as well as the effectiveness of two gas jets with respect to mitigation of thermal deposition in the divertor, halo currents, runaways, etcetera, will also be presented.

Stabilization of Energetic-Ion-Driven MHD Mode by ECCD in Heliotron J

K. Nagasaki¹, T. Mizuuchi¹, Y. Yoshimura², T. Estrada³, F. Sano¹, S. Yamamoto¹, S. Kobayashi¹, K. Sakamoto¹, H. Okada¹, K. Hanatani¹, T. Minami¹, K. Masuda¹, S. Konoshima¹, S. Ohshima¹, Y. Nakamura⁴, K. Mukai⁴, H. Y. Lee⁴, L. Zang⁴, T. Kagawa⁴, T. Minami⁴, K. Mizuno⁴, Y. Nakamura⁴, Y. Nagae⁴, G. Motojima², N. Marushchenko⁵, and Y. Turkin⁵

¹*Institute of Advanced Energy, Kyoto University, Kyoto, Japan*

²*National Institute for Fusion Science, Toki, Japan*

³*CIEMAT, Madrid, Spain*

⁴*Graduate School of Energy Science, Kyoto University, Kyoto, Japan*

⁵*Max Planck Institut für Plasmaphysik, EURATOM Association, Greifswald, Germany*

Corresponding Author: nagasaki@iae.kyoto-u.ac.jp

Second harmonic electron cyclotron current drive (ECCD) has been applied in the Stellarator/Heliotron device, Heliotron J, to control rotational transform profile. Localized EC driven current at central region changes the rotational transform, making a high magnetic shear. An energetic-ion-driven MHD mode of 80 kHz has been completely stabilized when the counter EC current of more than 2 kA is driven. An experiment of scanning the EC driven current shows that there is a threshold in magnetic shear to stabilize the energetic-ion-driven MHD mode.

EX-P

Effects of RF-Heating Induced MHD Activities on the Toroidal Rotation in Tokamaks

J. Seol¹, S. G. Lee¹, B. H. Park¹, K. I. You¹, K. C. Shaing^{2,3}, H. Lee¹, L. Terzolo¹,
K. Ida⁴, J. W. Yoo⁴, G. S. Yun⁵, W. H. Ko¹, K. D. Lee¹, Y. Shi¹, S. J. Wang⁶,
S. Park¹, J. Y. Kim¹, and Y. K. Oh¹

¹*National Fusion Research Institute, Daejeon, Republic of Korea*

²*University of Wisconsin, Madison, USA*

³*National Cheng Kung University, Tainan, Taiwan, China*

⁴*National Institute for Fusion Science, Toki, Japan*

⁵*POSTECH, Pohang, Japan*

⁶*Korea Atomic Energy Research Institute, Daejeon, Republic of Korea*

Corresponding Author: jseol@nfri.re.kr

The magnitude of toroidal rotation velocity is reduced by electron cyclotron resonance heating (ECRH) or ion cyclotron resonance frequency (ICRF) regardless of the direction of toroidal rotation. This can be explained by the neoclassical toroidal viscosity (NTV) by MHD activities. Toroidal rotation changes due to ECRH have been observed in many devices such as DIII-D, JT-60U and ASDEX-Upgrade. However, there is no widely accepted explanation for the effects of ECRH on the toroidal rotation. The results from various experiments are very complicated and indicate no clear tendency. In this paper, we introduce the results from KSTAR on the rotation changes due to radiofrequency heating. The rotation was reduced when ECRH and ICRF were injected in the central region both in H-mode and L-mode. It was found that central ECRH induces the MHD instabilities inside $q = 1$ surface. The magnetic field perturbation driven by the MHD instabilities causes the NTV, which is otherwise assumed to be negligible. Thus, the toroidal rotation can be damped by the NTV. In this research, we calculate the ECRH-driven torque density from the rotation profile. The NTV torque density also is estimated from δB to give a comparison with the ECRH-driven torque density.

EX-P

Towards the Density Required for Runaway Electron Suppression in ITER

G. Pautasso¹, M. Bernert¹, K. Gal¹, K. Mank¹, A. Mlynek¹, and A. Herrmann¹

¹IPP, Garching, Germany

Corresponding Author: gap@ipp.mpg.de

Experiments of massive gas injection (MGI) in existing tokamaks have shown that this technique is suitable for disruption mitigation. A reduction of the localized heat load on the divertor is easily achieved by increasing the fraction of radiated energy with impurity injection. A reduction of the vertical force on the vessel is accomplished when the current quench duration is reduced with respect to the vertical displacement time constant. With the choice of gas type and quantity, the current quench evolution can be tailored to avoid the formation of runaway electrons (REs). Experiments with valves close to the plasma are showing that the large critical density (n_c), which assures the collisional suppression of REs, is reachable in mid-sized tokamaks. The MGI method is the prime candidate for an ITER disruption mitigation system but its application to such a large tokamak is not entirely straightforward. The fueling efficiency (F_{eff}) of the injected gas, for example, is a big unknown in the ITER MGI system design: It can vary from a few % to over 50% across different devices and experimental conditions; in addition, numerical models for the evaluation of the ion/electron source within the plasma do not exist yet. The mitigation system at ASDEX Upgrade has evolved in the last decade from electromagnetic valves located outside the vessel to valves located in the vessel first on the low (LFS) and more recently on the high field side (HFS). The valves close to the plasma exhibit a larger F_{eff} than the valves located further-away. The F_{eff} of MGI from the HFS ranges between 35 and 55% for moderate amounts of injected neon and helium, which is a factor of two larger than the F_{eff} reached with the fast valve close to the plasma located on the LFS. The improved performance of the HFS with respect to the LFS MGI motivated the installation of a second valve behind the heat shield during the 2011 Summer break. The three valves presently installed in the vessel should allow the attainment of an effective density close to n_c in dedicated experiments planned for Spring 2012.

EX-P

Experiment for Stabilization of Tearing Mode in KSTAR

K. Kim¹, Y. S. Na¹, D. Na¹, M. G. Yoo¹, H. S. Kim¹, M. Choi², G. Yun², Y. S. Park³,
Y. M. Jeon⁴, S. Park⁴, K. D. Lee⁴, and L. Terzolo⁴

¹*Seoul National University, Seoul, Republic of Korea*

²*POSTECH, Pohang, Republic of Korea*

³*Columbia University, New York, USA*

⁴*National Fusion Research Institute, Daejeon, Republic of Korea*

Corresponding Author: lecllexa@snu.ac.kr

Tearing mode (TM), a type of current-driven resistive instability was observed in L-mode plasmas during 2011 campaign of KSTAR. It was usually observed in discharges with the magnetic perturbation (MP) intended to suppress edge localized mode (ELM). When with $n = 1$ MP, TM was appeared just after ramping down of the MP coil current. There are two electron cyclotron heating and current drive (ECH/CD) systems available in 2011 campaign equipped with movable launchers which can change the poloidal and the toroidal angle in between shots for control of MHD activities operating at power of ~ 0.3 MW and ~ 0.6 MW for 110 GHz and 170 GHz, respectively. The island position can be estimated by electron cyclotron emission imaging (ECEI) as well as ECE diagnostics in KSTAR. In 2011 campaign, based on the collected information of the (2, 1) island position, a discharge is designed for suppression of the (2, 1) mode by adjusting the EC launcher angles to the estimated island position for suppression of the mode assuming that the plasma condition is similar to other shots with the (2, 1) mode.

In this work, the experiment for stabilization of (2, 1) tearing mode, shot # 6272, is analysed by experimental observations and simulations. Particularly, the effect of ECH to suppression of the mode is investigated by simulations with ECH effects [1] newly included to the modified Rutherford equation (MRE) [2]. Mirnov coil (MC) arrays and ECE are mainly used for analysis of the island width and location as well as the mode number. ASTRA, coupled with the MRE solver [3] with ECH effects is used for integrated simulations of plasma equilibrium, transport, heating and current drive, and magnetic island evolution, in a self-consistent way. The results will be expected to contribute to prepare a feedback controller of NTMs for high performance plasmas in KSTAR.

References

- [1] D. De Lazzari, *et al.*, Nucl. Fusion, Vol. **49** (2009) 075002.
- [2] R. J. LaHaye, *et al.*, Nucl. Fusion, Vol. **46** (2006) 451.
- [3] Yong-Su Na, *et al.*, 23th IAEA FEC (2010).

The Effect of Toroidal Plasma Rotation on Sawtooth Activity in KSTAR

J. Kim¹, S. W. Yoon¹, J. W. Yoo^{1,2}, S. G. Lee¹, H. S. Han¹, and K. I. You¹

¹*National Fusion Research Institute, Daejeon, Republic of Korea*

²*Department of Nuclear Fusion and Plasma Science, University of Science and Technology, Daejeon, Republic of Korea*

Corresponding Author: kimju@nfri.re.kr

It has been found that toroidally rotating plasmas exhibit beneficial effects such as suppression or reformation of magnetohydrodynamic (MHD) instabilities. In KSTAR plasmas, it is found that sawtooth period lengthens significantly as the toroidal rotation speed increases. Stability analysis reveals the critical rotation speed to reach the marginal stability, suppressing the growth of the ideal internal kink instability. This means sufficiently fast toroidal rotation gives a complete stabilization of $n = 1$ internal kink mode as well as suppression of the sawtooth with the condition of q_0 below than unity.

Study of Runaway Electron Generation in Synergetic ECRH & SMBI Plasma and during Major Disruptions in the HL-2A Tokamak

Y. Zhang¹, Y. Liu¹, G. Yuan¹, J. Yang¹, X. Song¹, J. Zhou¹, L. Yao¹, B. Feng¹,
C. Chen¹, X. Song¹, X. Li¹, X. Ding¹, L. Yan¹, Q. Yang¹, and X. Duan¹

¹*Southwestern Institute of Physics, Chengdu, China*

Corresponding Author: zhangyp@swip.ac.cn

Runaway electron (RE) is a crucial issue in achieving safe tokamak operation due to its severe threat to tokamak machines when they hit the first wall, especially during disruptions. Therefore, investigations on the behaviour of REs and the evolution of disruption generated RE beam have been a very active area during the past decades. Anomalous RE enhancement has been recently observed in synergetic ECRH and supersonic molecular beam injection (SMBI) experiments in the HL-2A tokamak. With the aid of the soft X-ray cameras, the detailed time and space resolved images of the long-lived RE beam in flight during major disruptions have been observed and these allow a detailed analysis of the generation and evolution of the disruption generated RE beam in a major disruption. In this paper, the RE generation in synergetic ECRH & SMBI plasma and during major disruptions in the HL-2A tokamak will be demonstrated and discussed.

EX-P

Magnetic Confinement Theory and Modelling



Study of Toroidal Flow Generation by the ICRF Minority Heating in the Alcator C-Mod Plasma

S. Murakami¹, K. Itoh², L. Zheng³, J. Van Dam³, P. Bonoli⁴, J. Rice³, C. Fiore³, and A. Fukuyama⁴

¹*Departement Nuclear Engineering, Kyoto University, Kyoto, Japan*

²*National Institute for Fusion Science, Toki, Japan*

³*University of Texas at Austin, Texas, USA*

⁴*Massachusetts Institute of Technology, Cambridge, USA*

Corresponding Author: murakami@nucleng.kyoto-u.ac.jp

Important role of the plasma flow and its shear in the transport improvement is suggested by many experimental observations. The spontaneous toroidal flow has been observed during ICRF heating with no direct momentum input in many devices. Especially, in the Alcator C-Mod plasma, the spontaneous toroidal flow and ITB formation have been investigated intensively in the ICRF heating plasma and they found that the ITB plasma (ITB foot is located near $r/a = 0.5$) was obtained when the ICRF resonance location was placed at well off the magnetic axis, near $\|r/a\| = 0.5$.

We study the toroidal flow generation by the ICRF minority heating in the Alcator C-Mod plasma using GNET code, which can solve a linearized drift kinetic equation for minority ions including complicated orbits of accelerated energetic particles. The obtained steady state distribution of energetic minority ions is analyzed and the radial profile of the averaged toroidal flow of minority ions is evaluated. In our previous study we have found that a co-directional toroidal flow, which direction is consistent with experimental observations, is generated outside of the RF wave power absorption region and that the toroidal precession motion of energetic tail ions plays an important role in generating the averaged toroidal flow.

In order to make clear the relation between the ICRF driven flow and the ITB formation we investigate the resonance location dependence of the toroidal flow profile changing the resonance location from $r/a = -0.6$ to $+0.6$ on the equatorial plane. It is found that a co-directional toroidal flow of the minority ion is generated outside of the RF wave power absorption region and that the maximum averaged velocity of the minority ion reaches about 300 km/s, which is more than five times bigger than the experimentally observed bulk velocity. We consider that the energetic minority ion can drive the toroidal flow of the bulk plasma to the observed velocity level. When we shift the resonance location to the out side of $\|r/a\| = 0.5$ the opposite direction toroidal flow is enhanced near the central region and the velocity shear is increased. This suggests a role of the ICRF driven flow on the experimentally observed ITB formation during ICRF heating in the Alcator C-Mod plasma.

HL

Non-linear MHD Modelling of Rotating Plasma Response to Resonant Magnetic Perturbations

M. Becoulet¹, F. Orain¹, G. Huijsmans², P. Maget¹, N. Mellet¹, G. Dif-Pradalier¹,
G. Latu¹, C. Passeron¹, E. Nardon¹, V. Grandgirard¹, and A. Ratnani¹

¹Association Euratom-CEA, CEA/DSM/IRFM, Centre de Cadarache, St-Paul-lez-Durance, France

²ITER Organization, St-Paul-lez-Durance, France

Corresponding Author: marina.becoulet@cea.fr

The application of Resonant Magnetic Perturbations (RMPs) demonstrated the possibility of total Type I ELM suppression or strong mitigation of the ELM size in many experiments motivating to use this method on ITER, where Type I ELMs represent a particular danger for Plasma Facing Components (PFC) and divertor materials. In the present work the rotating plasma response to RMPs was studied using the non-linear resistive reduced MHD codes: RMHD in cylindrical geometry and JOEKE in toroidal geometry including X-point and Scrape Off Layer (SOL). For this purpose the RMHD and JOEKE codes were further developed to include RMPs physic, toroidal rotation source, neoclassical poloidal viscosity to describe poloidal rotation dynamics and, finally, two fluid diamagnetic effects. The equilibrium plasma flows, essential for RMP screening, were studied in toroidal geometry with X-point using JOEKE code. It was demonstrated that in toroidal plasma the parallel equilibrium flow is mostly constrained by the toroidal rotation source in the core region. However in the SOL and near the separatrix equilibrium flows result essentially from the combination of sheath boundary conditions for parallel velocity on the divertor plates, toroidal curvature effects, X-point configuration, neoclassical poloidal viscosity and diamagnetic and drifts. Usually screening of central islands induced by static RMPs was obtained both in cylindrical and toroidal geometry in plasma with flows. However, at certain plasma parameters or due to the non-linear evolution of the radial electric field produced by RMPs, the poloidal rotation can be compensated by the electron diamagnetic rotation locally. In this case RMPs can penetrate. At certain plasma parameters coupling of RMPs to the intrinsic MHD mode localized at the plasma edge was observed in modeling in toroidal geometry with X-point. Typical JET-like equilibrium, plasma parameters and RMP spectrum generated by external EFCC at $n = 2$, 40 kAt were used in JOEKE modelling. Initial modelling results of RMPs with non-linear MHD rotating plasma response will be presented for ITER parameters.

TH

Impact of Carbon and Tungsten as Divertor Materials on the Scrape-off Layer Conditions in JET

M. Groth¹, S. Brezinsek², P. da Silva Aresta Belo³, M. N. A. Beurskens⁴, M. Brix⁴,
M. Clever², J. W. Coenen², G. Corrigan⁴, T. Eich⁵, J. Flanagan⁴, C. Giroud⁴,
D. Harting², A. Huber², S. Jachmich⁶, M. Lehnen², C. Lowry⁷, C. F. Maggi⁸,
S. Marsen⁵, A. Meigs⁴, G. Sergienko², B. Sieglin⁵, C. Silva³, A. Sirinelli⁴,
M. F. Stamp⁴, G. van Rooij⁸, and S. Wiesen²

¹Aalto University, Association EURATOM-Tekes, Espoo, Finland

²Institute of Energy and Climate Research, EURATOM Association, Jülich, Germany

³Institute of Plasmas and Nuclear Fusion, Association EURATOM/IST, Lisbon, Portugal

⁴Culham Centre for Fusion Energy, Association EURATOM-CCFE, Abingdon, UK

⁵Max-Planck Institute for Plasma Physics, EURATOM Association, Garching, Germany

⁶Association "EURATOM Belgium State", Laboratory for Plasma Physics, Brussels, Belgium

⁷EFDA Close Support Unit, Culham Science Centre, Abingdon, UK

⁸DIFFER, Association EURATOM-FOM, Nieuwegein, Netherlands

Corresponding Author: mathias.groth@aalto.fi

In detached divertor conditions, a five-fold stronger reduction of the ion current to the low-field side target plate and a 30% increase in the density limit were observed in neutral-beam heated, low-confinement mode plasmas with the ITER-like Wall compared to the previous carbon wall. These significant differences occurred at higher core densities despite the fact that nearly identical scrape-off layer parameters were measured in attached divertor conditions. When attached, the magnitude and distribution of radiative power as well as the total ion currents to the divertor target plates were measured the same for a range of divertor plasma geometries, including configurations with the high field side strike point on the vertical plate and the low field side strike point on the horizontal plate, and configurations with both strike points on the vertical plates. The 5-to-10-fold reduction of the scrape-off layer carbon content as inferred from low charge state carbon emission, and the fact that both beryllium and tungsten have a low radiation potential in the scrape-off layer, would indicate that the deuterium emission was and still is the dominating radiator. Simulations of deuterium gas fuelling scans with the fluid edge code EDGE2/EIRENE show that replacing carbon with beryllium and tungsten as wall materials leads to reduced impurity radiation, as expected, and translates into an increase in the power conducted to the plates. The ion currents to the plates, however, are predicted to be similar in both materials configurations. Saturation of the ion currents is predicted at the highest achievable density; the simulations do not predict the reduction of the currents close to the density limit as observed in the experiments. Since the JET ITER-like wall constitutes the same materials and their poloidal distribution as foreseen for the nuclear phase of ITER, understanding the observed differences in the SOL conditions between the two materials configuration, and clarifying the discrepancy between the experimental data and simulations are instrumental for erosion and power handling in ITER.

HL

On Edge Plasma, First Wall, and Dust Issues in Fusion Devices

S. Krasheninnikov¹, J. R. Angus¹, J. Guterl¹, A. Y. Pigarov¹, R. D. Smirnov¹,
R. P. Doerner¹, M. Umansky², T. Rognlien², D. K. Mansfield³, A. L. Roquemore³,
C. H. Skinner³, E. D. Marenkov⁴, and A. A. Pisarev⁴

¹*University of California at San Diego, La Jolla, USA*

²*Lawrence Livermore National Laboratory, Livermore, USA*

³*Princeton Plasma Physics Laboratory, Princeton, USA*

⁴*Nuclear Research National University MEPhI, Moscow, Russian Federation*

Corresponding Author: skrash@mae.ucsd.edu

The processes in the edge plasma and first wall play crucial role in both performance and design of any fusion reactor. Here we address some major issues related to the physics of the edge plasma, first wall, and dust in fusion devices: We present the results of 3D modeling of mesoscale-structures (blobs and ELM filaments) with BOUT++ code. We show that the onset of resistive drift wave turbulence can significantly alter ballistic propagation of mesoscale-structures; We report on the UEDGE modeling of intermittent edge plasma transport with novel approach which is based on self-consistent modeling of a sequence of macro-blobs appropriately launched from the core/edge interface and propagating through the edge and SOL; We present the results of the simulation of hydrogen retention in Be, performed with the codes WallPSI and FACE. We found a good agreement of the simulation results with available experimental data on hydrogen retention in Be and penetration depth of hydrogen into bulk of material for different sample temperatures; We report on the impact of the hydrogen retention in the first wall on the H-mode pedestal recovery. We show that for some parameter range the pedestal recovery can be controlled by hydrogen outgassing processes; We present the results of the simulation of the impact of dust on the performance of edge plasma with coupled DUSTT/UEDGE package for both NSTX and ITER. We demonstrate that dust injection into divertor can effectively reduce heat load to divertor plate due to radiative power dissipation without the onset of thermal instability. However, for other dust injection locations at relatively high dust injection rate (~ 10 g/s for ITER-like plasmas) thermal instability develops shortly after the onset of divertor detachment causing discharge termination.

HT

Energetic Particle Long Range Frequency Sweeping and Quasilinear Relaxation

H. Berk¹, G. Wang¹, N. Gorelenkov², B. Breizman¹, K. Ghantous², M. Lilley³,
R. Nyqvist⁴, and M. van Zeeland⁵

¹*University of Texas at Austin, Austin, USA*

²*Princeton Plasma Physics Laboratory, Princeton, USA*

³*Imperial College, London, UK*

⁴*Chalmers University, Göteborg, Sweden*

⁵*General Atomics, San Diego, USA*

Corresponding Author: hberk@mail.utexas.edu

Investigating the relaxation of energetic particles (EP) with MHD modes is an area where ideal and kinetic theories need to be investigated to enable credible planning for future self-sustained burning plasmas. These theories need to be tested with predictions of present day experiments. Here we discuss two aspects to the relaxation.

1. The effect of frequently observed long-range frequency sweeping events attributed to the formation of clump and hole phase space structures.
2. Progress of modified quasi-linear theories for including the validation of a simple quasi-linear of EP relaxation in a comparison with experimental data.

Long-range frequency sweeping, within the purview of adiabatic theory, requires an intrinsic improvement in the description of the background plasma response far from the mode's linear frequency which causes change in the mode structure. Improved adiabatic descriptions, which will be presented, enables an accurate efficient tool for study of the consequences of chirping in energetic particle relaxation. Quasilinear (QL) Theory is studied with two different models. In one we report on a truncated phase space model that is reduced to 1.5 dimensions and has produced predictions that correlate well with the experimental data on DIII-D, even though the predicted relaxed EP distribution function is not fully resolved. In a more complete second QL model we report on the progress of a full QL phase space code that is able to bridge the gap between isolated mode interactions to the typical QL theory where mode overlap is intrinsically assumed.

HL

Nonlinear Excitations of Zonal Structures by Toroidal Alfvén Eigenmodes

F. Zonca^{1,2}, L. Chen²

¹*Associazione EURATOM-ENEA sulla Fusione, Rome, Italy*

²*Institute for Fusion Theory and Simulation, Zhejiang University, Hangzhou, China*

Corresponding Author: fulvio.zonca@enea.it

Zonal flows and, more generally, zonal structures are known to play important self-regulatory roles in the dynamics of microscopic drift-wave type turbulences. Since Toroidal Alfvén Eigenmode (TAE) plays crucial roles in the Alfvén wave instabilities in burning fusion plasmas, it is, thus, important to understand and assess the possible roles of zonal flow/structures on the nonlinear dynamics of TAE. It is shown that zonal flow/structure spontaneous excitation is possible only near the lower accumulation point of the shear Alfvén wave continuous spectrum, including the proper trapped ion responses, causing the zonal structure to be dominated by the zonal current instead of the usual zonal flow. This work shows that including kinetic thermal ion treatment in the nonlinear simulations of Alfvénic modes is an important ingredient for realistic comparisons with experimental measurements, where the existence of zonal currents has been clearly observed.

Gyrokinetic Instabilities in an Evolving Tokamak H-mode Pedestal

C. Roach¹, D. Dickinson^{1,2}, S. Saarelma¹, R. Scannell¹, A. Kirk¹, and H. Wilson²

¹*Culham Centre for Fusion Energy, Abingdon, UK*

²*York Plasma Institute, Department of Physics, University of York, York, UK*

Corresponding Author: colin.m.roach@ccfe.ac.uk

Plasma equilibria reconstructed from the spherical tokamak MAST, have sufficient resolution to capture plasma evolution during the short period between edge-localised-modes (ELMs). Immediately after the ELM steep gradients in pressure, P , and density, n_e , form a pedestal close to the separatrix, and then expand into the core. Local gyrokinetic analysis over the ELM cycle reveals the dominant microinstabilities, and suggests a new physical picture for the formation and arrest of this pedestal: in the pedestal dP/dr and dn_e/dr are limited by kinetic ballooning modes (KBMs), consistent with the hypothesis of the EPED pedestal model; in the core close to the pedestal KBMs are absent, but higher perpendicular wavenumber microtearing modes (MTMs) dominate and limit the electron temperature gradient; the pressure pedestal propagates into the core because increasing dn_e/dr and dP/dr stabilises the MTMs until they are supplanted by KBMs at higher dP/dr ; deeper inside the core dP/dr is lower and MTMs become more virulent over the ELM cycle with rising local β ; when the pedestal is almost fully developed, the pressure gradient transition region is close to an instability threshold where MTMs and KBMs become simultaneously unstable with large growth rates over a broad spectral range. Above this threshold the dominant modes change from KBMs at lower wavenumber, to MTMs above a toroidal mode number $n \sim 25$ ($n = 25$ is within the observed range for ELM filaments in MAST). The breaching of this limit may trigger a significant change in edge transport. Recent measurements from the pedestal region between ELMs in DIII-D find high and low frequency bands of turbulence propagating in the electron and ion drift directions respectively, broadly consistent with the properties of the MTMs and KBMs reported here. Further analysis to deepen our understanding of these physical processes is underway and will be reported.

HL

Five-field Peeling-Ballooning Modes Simulation with BOUT++

T. Xia¹, X. Xu², Z. Liu¹, S. Liu¹, B. Gui^{1,2}, and J. Li²

¹*Institute of Plasma Physics, Chinese Academy of Sciences, Hefei, China*

²*Lawrence Livermore National Laboratory, Livermore, USA*

Corresponding Author: xiaty@ipp.ac.cn

In this paper we report the simulations on ELMs with 5-field peeling-ballooning model using BOUT++ code. A minimum set of three-field two-fluid equations based on the peeling-ballooning (P-B) model with non-ideal physics effects is found to simulate pedestal collapse when using the BOUT++ simulation code [1]. Based on this 3-field model, we investigate the effects of perturbed parallel velocity first. The perturbed parallel velocity can decrease the growth rate by 20.0%, and the energy loss caused by ELMs is decreased by 12.1%. After this work, in order to study the particle and energy transport at the pedestal region, we extend the previous two-fluid 3-field model of the pedestal collapse by separating the pressure into ion density, ion and electron temperature equations. Through the simulation, we find that the equilibrium density n_{i0} does not affect the normalized linear growth rate in the ideal MHD model because the dispersion relationship for normalized growth rate has nothing to do with density. With diamagnetic effects, the growth rate is inversely proportional to n_{i0} . The reason is that the diamagnetic effects, which are inversely proportional to n_{i0} , increase the threshold of the growth of perturbation. For the same pressure profile, constant T_0 cases increase the growth rate by 6.2% compared with constant n_{i0} cases in ideal MHD model. With diamagnetic effects, the growth rate is increased by 31.43% for toroidal mode number $n = 15$. This is because that the gradient of n_{i0} introduces the cross term in the vorticity equation. This cross term has the destabilizing effect on peeling-ballooning mode. For the nonlinear simulation, the gradient of n_{i0} in the pedestal region can increase the energy loss of ELMs and drive the perturbation to go into the core region. In order to simulate the recovering phase of ELMs, the edge transport barrier (ETB) is necessary. Therefore, besides the parallel viscosity, the parallel thermal conductivities of ions and electrons are also implemented into this 5-field model. The effects of thermal conductivity by employing flux limited expression will stabilize the growth of the turbulence and decrease the energy loss in the pedestal region. The more details will be discussed in this paper. This model can successfully be used for EAST tokamak. The simulations of EAST will be reported.

References

- [1] Phys. Rev. Lett. **105** (2010)175005.

TH

Theory and Gyro-fluid Simulations of Edge-Localized-Modes

X. Xu¹, P. Xi^{1,2}, A. Dimits¹, I. Joseph¹, M. V. Umansky¹, T. Xia^{1,3}, B. Gui^{1,3}, S. Kim⁴, S. Tokunaga⁴, G. Park⁴, T. Rhee⁴, H. Jhang⁴, P. Diamond^{4,5}, B. Dudson⁶, and P. Snyder⁷

¹*Lawrence Livermore National Laboratory, Livermore, USA*

²*School of Physics, Peking University, Beijing, China*

³*Institute of Plasma Physics, Chinese Academy of Sciences, Hefei, China*

⁴*WCI Center for Fusion Theory, National Fusion Research Institute, Daejeon, Republic of Korea*

⁵*University of California San Diego, La Jolla, USA*

⁶*University of York, Heslington, York, UK*

⁷*General Atomics, San Diego, USA*

Corresponding Author: xxu@llnl.gov

This paper reports the theoretical and simulation results of a gyro-Landau-fluid (GLF) extension of the BOUT++ code which contributes to increasing the physics understanding of edge-localized-modes (ELMs). Large ELMs with low-to-intermediate- n peeling-ballooning (P-B) modes are significantly suppressed due to finite Larmor radius (FLR) effects when the ion temperature increases. However, small ELMs with an island of instability at intermediate n values are driven unstable due to:

1. The ion drift wave resonance with a branch of the drift acoustic wave in a two-fluid model.
2. The Landau wave-particle resonances with thermal passing ions in a gyro-fluid model.

HL

This result is good news for high ion temperatures in ITER due to the large stabilizing effects of FLR. The simulation results are shown to be consistent with the two-fluid model including the ion diamagnetic drift for type-I ELMs, which retains the first-order FLR correction. The maximum growth rate is inversely proportional to T_i because the FLR effect is proportional to T_i . The FLR effect is also proportional to toroidal mode number n , so for high n cases, the P-B mode is stabilized by FLR effects. Nonlinear gyro-fluid simulations show results that are similar to those from the two-fluid model, namely that the P-B modes trigger magnetic reconnection, which drives the collapse of the pedestal pressure. Hyper-resistivity is found to limit the radial spreading of ELMs by facilitating magnetic reconnection. Due to the additional FLR-corrected nonlinear $\mathbf{E} \times \mathbf{B}$ convection of the ion gyro-center density, the gyro-fluid model further limits the radial spreading of ELMs. Zonal magnetic fields are shown to arise from an ELM event and finite β drift-wave turbulence when electron inertia effects are included. These lead to current generation and self-consistent current transport as a result of $\mathbf{E} \times \mathbf{B}$ convection in the generalized Ohm's law. Because edge plasmas have significant spatial inhomogeneities and complicated boundary conditions, we have developed a fast non-Fourier method for the computation of Landau-fluid closure terms based on an accurate and tunable approximation. The accuracy and the fast computational scaling of the method have been demonstrated.

This work supported in part by the US DOE under DE-AC52-07NA27344, LLNL LDRD project 12-ERD-022 and LDRD project 11-ERD-058. LLNL-ABS-527551.

Reduction of ELM Energy Loss by Pellet Injection for ELM Pacing

N. Hayashi¹, N. Aiba¹, T. Takizuka², and N. Oyama¹

¹*Japan Atomic Energy Agency, Ibaraki, Japan*

²*Osaka University, Suita, Japan*

Corresponding Author: hayashi.nobuhiko@jaea.go.jp

The reduction of ELM energy loss by the pellet injection for ELM pacing has been studied by an integrated core/scrape-off-layer/divertor transport code TOPICS-IB with a MHD stability code and a pellet model. In the ELM pacing, ELMs with the reduced energy loss should be reliably triggered by small pellets to minimize fueling and the impact on the target pedestal plasma. It is found that the energy loss can be reduced by a pellet, which penetrates deeply into the pedestal and triggers high- n ballooning modes with localized eigenfunctions near the pedestal top, where n is the toroidal mode number. This reduction is realized by a small pellet injected from the low-field-side (LFS), while the high-field-side injection triggers lower- n modes with wide eigenfunctions before the pellet penetrates deeply into the pedestal. Early injection on the natural ELM cycle reduces the energy loss because the high magnetic shear prevents the onset of lower- n modes, but leads to the reduction of target pedestal pressure and the enlargement of pellet size to trigger the ELM. On the other hand, the late injection induces the large energy loss comparable to the natural ELM. The LFS pellet injection to the pedestal plasma equivalent to that at the middle timing on the natural ELM cycle is suitable for ELM pacing.

TH

Progress in Simulating Turbulent Electron Thermal Transport in NSTX

W. Guttenfelder¹, J. L. Peterson², J. Candy³, S. Kaye¹, Y. Ren¹, R. Bell¹, E. A. Belli³,
G. Hammett¹, B. LeBlanc¹, D. Mikkelsen¹, W. Nevins², G. Staebler³, and H. Yuh⁴

¹*Princeton Plasma Physics Laboratory, Princeton, USA*

²*Lawrence Livermore National Laboratory, Livermore, USA*

³*General Atomics, San Diego, USA*

⁴*Nova Photonics, Princeton, USA*

Corresponding Author: wgutten@pppl.gov

Nonlinear simulations have progressed for multiple NSTX discharge scenarios to:

- Validate with experimental turbulence and transport data.
- Help differentiate unique instability mechanisms.
- Improve confidence in predictive modeling for future low aspect ratio fusion devices.

First nonlinear gyrokinetic simulations of microtearing turbulence in a high- β NSTX H-mode discharge predict experimental levels of transport that are dominated by magnetic flutter and increase with collisionality. This dependence is roughly consistent with energy confinement times in dimensionless collisionality scaling experiments providing evidence for the importance of microtearing modes in high- β NSTX plasmas. In lower β H-mode plasmas from a second collisionality scaling experiment microtearing modes are predicted to be stable. Instead, nonlinear simulations predict that ETG turbulence provides a significant fraction of the experimental transport, although the predicted transport is insensitive to variation in collisionality. ETG transport has also been predicted to be important in RF heated L-mode plasmas that exhibit electron internal transport barriers (e -ITBs) with strong negative magnetic shear ($s < -0.5$). Non-local simulations verify that at the base of the e -ITB the predicted ETG flux reaches experimental levels, but turbulence cannot propagate inward due to a nonlinear stabilizing effect from negative magnetic shear that occurs in the absence of strong $\mathbf{E} \times \mathbf{B}$ shear. Small differences in many parameters influence the microstability properties, and likely confinement scalings, to varying degree. For example, additional linear and nonlinear simulations predict that microtearing growth rates and transport increase with β , s/q (for positive shear, $s > 0$), and possibly even Z_{eff} . On the other hand, ETG turbulence is often weakly dependent or stabilized with β , and tends to be stabilized by increasing s/q (for $s > 0$) and Z_{eff} . Furthermore, both ETG and microtearing can be stabilized with sufficiently strong density gradient, while microtearing alone can be strongly suppressed with experimental levels of flow shear. In an effort to move towards predictive capability, first tests of the TGLF model for NSTX discharges have begun.

This work is supported by US DOE contracts DE-AC02-09CH11466, DE-FG03-95ER54309, DE-AC52-07NA27344 and DE-AC05-00OR22725.

HL

Role of External Torque and Toroidal Momentum Transport in the Dynamics of Heat Transport in Internal Transport Barriers

H. Jhang¹, S. S. Kim¹, S. Tokunaga¹, and P. H. Diamond^{1,2}

¹*National Fusion Research Institute, Daejeon, Republic of Korea*

²*Center for Astrophysics and Space Sciences and Department of Physics, University of California San Diego, La Jolla, USA*

Corresponding Author: hgjhang@nfri.re.kr

We study the coupling of intrinsic rotation and toroidal momentum transport to the dynamics of internal transport barriers (ITB). In particular, we

1. Elucidate the role of external torque in ITB formation and ion temperature de-stiffening
2. Analyze the interplay between intrinsic rotation and ITB dynamics.
3. Characterize the heat transport in steady state ITB plasmas.

First, we find an external torque can either facilitate or hamper bifurcation in heat flux driven plasmas depending on its sign relative to the direction of intrinsic torque. The ratio between the radially integrated momentum density to power input is shown to be a key control parameter governing the characteristics of bifurcation. Second, we find that intrinsic rotation is closely coupled to ITB dynamics via dynamic change of Reynolds stress. In particular, we show that the excitation of parallel shear flow instability causes a Reynolds stress change and drives a momentum redistribution, which significantly influences ITB dynamics. Finally, we show that highly non-diffusive transport processes prevail in ITB plasmas (depending on the degree of turbulence suppression) from a statistical analysis of heat transport in steady state ITBs obtained from a long time flux-driven gyrofluid simulations.

TH

Multi-Scale Drift Turbulence Dynamics in Ohmic Discharge as Measured at the FT-2 Tokamak and Modeled by Full- f Gyrokinetic ELMFIRE-code

E. Gusakov¹, V. V. Bulanin², A. Gurchenko¹, S. Leerink³, A. Altukhov¹, L. Esipov¹, J. Heikkinen⁴, S. Janhunen³, M. Kantor¹, T. Kiviniemi³, T. Korpilo³, D. Kuprienko¹, S. Lashkul¹, and A. Petrov²

¹*Ioffe Physical-Technical Institute of Russian Academy of Science, St. Petersburg, Russian Federation*

²*St. Petersburg State Polytechnical University, St. Petersburg, Russian Federation*

³*Euratom-Tekes Association, Aalto University, Aalto, Finland*

⁴*Euratom-Tekes Association, VTT, Finland*

Corresponding Author: evgeniy.gusakov@mail.ioffe.ru

The complex interaction between large-scale mean flows, meso-scale zonal flows and fine-scale micro-turbulence excited due to specific profiles of plasma parameters and leading to anomalous transport is an important area of experimental and theoretical research in magnetically confined plasmas. Recent progress in massively parallelized simulations of the electron and ion gyrokinetic particle distribution function and the electromagnetic field has paved the way for several global gyrokinetic code development projects making first principal based investigations of this complex interplay possible, as all the above mentioned processes are simultaneously incorporated into one simulation.

In the present paper direct measurements of micro, meso, and macro-scale transport phenomena in the FT-2 tokamak are shown to be quantitatively reproduced by Elmfire global full- f nonlinear gyrokinetic particle-in-cell simulation predictions. A detailed agreement with mean equilibrium flows, oscillating fine-scale zonal flows and turbulence spectra observed by a set of sophisticated microwave back-scattering techniques as well as a good fit of the thermal diffusivity data are demonstrated. Both the shift and the broadening of the power spectrum of synthetic and experimental Doppler reflectometry diagnostics have been found to overlap perfectly at various radial positions, indicating similar rotation and spreading of the selected density fluctuations. At the same time similar radial electric field dynamics have been observed by comparisons of the probability distribution function, the standard deviation and the dominant frequency of the simulated and experimentally measured radial electric field fluctuations, identifying the turbulent driven geodesic acoustic mode as a key contributor to the observed burstiness of the radial electric field. A clear influence of the impurity ions on the fluctuating radial electric field is observed.

HL

Global Gyrokinetic Simulations of High-performance Discharges in View of ITER

F. Jenko¹, H. Doerk¹, T. Goerler¹, D. Hatch¹, J. Hobirk¹, J. Schweinzer¹, G. Tardini¹,
D. Told¹, A. Volk¹, E. Wolfrum¹, T. Dannert², T. Bird³, P. Xanthopoulos³,
S. Brunner⁴, O. Sauter⁴, L. Villard⁴, A. Banon Navarro⁵, D. Carati⁵, P. Morel⁵,
C. Hegna⁶, M. Pueschel⁶, P. Terry⁶, J. Citrin⁷, P. Mantica⁸, and M. Barnes⁹

¹Max Planck Institute for Plasma Physics, Garching, Germany

²Rechenzentrum Garching, Garching, Germany

³IPP, Greifswald, Germany

⁴EPFL, Lausanne, Switzerland

⁵ULB, Brussels, Belgium

⁶University of Wisconsin at Madison, Madison, USA

⁷FOM, Nieuwegein, Netherlands

⁸IFP-Istituto di Fisica del Plasma, Milano, Italy

⁹MIT, Cambridge, USA

Corresponding Author: fsj@ipp.mpg.de

One of the key challenges for plasma theory and simulation in view of ITER is to enhance the understanding and predictive capability concerning high-performance discharges. The goal of this contribution is to shed light on central open issues by means of physically comprehensive ab initio simulations with the global gyrokinetic code GENE (including electromagnetic effects, collisions, and real MHD equilibria), applied to discharges in TCV, AUG, and JET — with direct relevance to ITER.

First, we address the nature of anomalous transport in high- β plasmas. GENE simulations of AUG H-mode discharges reveal that microtearing modes tend to be unstable over the outer half of the plasma, inducing magnetic electron heat diffusivities up to several m^2/s . Moreover, ITG turbulence is able to excite linearly stable microtearing modes, which may in turn dominate the electron heat transport at high β .

Second, we present new investigations regarding the stiffness of ion temperature profiles in standard and improved H-modes in AUG and JET, in particular in relation to nitrogen seeding and toroidal rotation. According to nonlinear GENE simulations, the former effect tends to be small in the plasma core, confirming the conjecture that the main effect is coming from the edge region. Triggered by recent JET results, studies of the effect of toroidal rotation on profile stiffness are performed, examining the competition between (stabilizing) perpendicular and (destabilizing) parallel flow shear physics under realistic conditions, showing that conventional attempts to model flow shear effects need to be somewhat revised.

Third, we investigate what determines the residual anomalous transport in barriers. Global GENE simulations of electron-ITB discharges in the TCV tokamak exhibit a strong profile effects on the TEM turbulence. Meanwhile, ETG turbulence generally carries a large fraction of the overall heat flux and seems to help determine the properties of the established barrier. A related investigation regarding the pedestals of AUG H-mode discharges confirms this scenario. Moreover, by means of the recently developed flux-surface global version of GENE, the influence of resonant magnetic perturbations on the edge turbulence is studied, including effects mediated by subtle changes in the MHD equilibrium.

TH

Bifurcated Helical Core Equilibrium States in Tokamaks

W. Cooper¹, J. P. Graves¹, H. Reimerdes¹, O. Sauter¹, M. Albergante¹, D. Brunetti¹,
F. Halpern¹, D. Pfefferlé², T. M. Tran¹, J. Rossel¹, A. Pochelon¹, S. Coda¹,
B. P. Duval¹, B. Labit¹, O. Schmitz², I. T. Chapman³, L. L. Lao⁴, A. D. Turnbull⁴,
T. E. Evans⁴, R. J. Buttery⁴, J. R. Ferron⁴, M. van Zeeland⁴, E. Lazarus⁵, A. J. Cole⁶,
and B. Tobias⁷

¹*École Polytechnique Fédérale de Lausanne, Association Euratom-Suisse, Centre de
Recherches en Physique des Plasmas, Lausanne, Switzerland*

²*Forschungszentrum Jülich, Jülich, Germany*

³*CCFE, Abingdon, UK*

⁴*General Atomics, San Diego, USA*

⁵*Oak Ridge National Laboratory, Oak Ridge, USA*

⁶*University of Wisconsin, Madison, USA*

⁷*Princeton Plasma Physics Laboratory, Princeton, USA*

Corresponding Author: wilfred.cooper@epfl.ch

Tokamaks with weak to moderate reversed central magnetic shear in which the minimum of the inverse rotational transform q_{\min} is in the neighbourhood of unity can trigger bifurcated MagnetoHydroDynamic (MHD) equilibrium states. In addition to the standard axisymmetric branch that can be obtained with standard Grad-Shafranov solvers, a novel branch with a three-dimensional (3D) helical core has been computed with the ANIMEC code [1], an anisotropic pressure extension of the VMEC code [2]. The solutions have imposed nested magnetic flux surfaces and are similar to saturated ideal internal kink modes.

The difference in energy between both possible branches is very small. Plasma elongation, current and β enhance the susceptibility for bifurcations to occur. An initial value nonlinear ideal MHD evolution of the axisymmetric branch compares favourably with the helical core equilibrium structures calculated.

Peaked prescribed pressure profiles reproduce the “snake” structures observed in many tokamaks which has led to a new explanation of the snake as a bifurcated helical equilibrium state that results from a saturated ideal internal kink in which pellets or impurities induce a hollow current profile. Snake equilibrium structures are computed in free boundary TCV tokamak simulations. Magnetic field ripple and resonant magnetic perturbations in MAST free boundary calculations do not alter the helical core deformation in a significant manner when q_{\min} is near unity. These bifurcated solutions constitute a paradigm shift that motivates the application of tools developed for stellarator research in tokamak physics investigations. The examination of fast ion confinement in this class of equilibria is performed with the VENUS code [3] in which a coordinate independent noncanonical phase-space Lagrangian formulation of guiding centre drift orbit theory has been implemented.

References

- [1] W. A. Cooper *et al.*, Comput. Phys. Commun. **180** (2009) 1524.
- [2] S. P. Hirshman *et al.*, Comput. Phys. Commun. **43** (1986) 143.
- [3] M. Jucker *et al.*, Comput. Phys. Commun. **182** (2011) 912.

This work was supported in part by the Swiss National Science Foundation. We thank S. P. Hirshman for his invaluable contributions.

Non-Axisymmetric Equilibrium Reconstruction for Stellarators, Reversed Field Pinches and Tokamaks

J. Hanson¹, S. Lazerson², D. Anderson³, D. Franz⁴, D. Gates², J. Harris⁵, S. Hirshman⁵, K. Ida⁶, S. Knowlton¹, L. L. Lao⁷, E. Lazarus⁵, L. Marrelli⁴, N. Pablant², S. Sakakibara⁶, J. Schmitt³, A. Sontag⁵, B. Stevenson¹, Y. Suzuki⁶, and D. Terranova⁴

¹ *Auburn University, Auburn, USA*

² *Princeton Plasma Physics Laboratory, Princeton, USA*

³ *University of Wisconsin, Madison, USA*

⁴ *Consorzio RFX, EURATOM-ENEA Association, Padova, Italy*

⁵ *Oak Ridge National Laboratory, Oak Ridge, USA*

⁶ *National Institute for Fusion Science, Toki, Japan*

⁷ *General Atomics, San Diego, USA*

Corresponding Author: jdhanson@auburn.edu

Equilibrium reconstruction is the process of minimizing the mismatch between modeled and observed signals by changing the parameters that specify the equilibrium. While stellarator equilibria are inherently non-axisymmetric, non-axisymmetric effects are also crucial for understanding stability and confinement of high-performance reversed field pinch and tokamak plasmas. Therefore, two-dimensional reconstruction tools are not adequate for fully exploring 3D plasmas.

The V3FIT and STELLOPT codes are 3D equilibrium reconstruction codes, both based on the VMEC 3D equilibrium code. VMEC models field-period symmetric 3D flux surface geometry but does not treat magnetic islands and chaotic regions. VMEC requires the specification of the pressure and either rotational transform or toroidal current profiles, as functions of either the toroidal or poloidal flux. VMEC can treat both axisymmetric and non-axisymmetric configurations, both free- and fixed-boundary equilibria, and both stellarator-symmetric and non-stellarator-symmetric equilibria.

Both V3FIT and STELLOPT can utilize signals from magnetic diagnostics, soft X-rays (SXR), Thomson scattering, and geometrical information from plasma limiters. STELLOPT can also utilize Motional Stark Effect (MSE) signals. Both calculate a finite difference approximation to a Jacobian for the signal-mismatch minimization. V3FIT and STELLOPT differ in the details of their minimization algorithms, their utilization of auxiliary profiles (like electron density and soft x-ray emissivity), and in their computation of model signals.

V3FIT is currently in use on stellarators (HSX, CTH), reversed field pinches (RFX-mod) and tokamaks (DIII-D) for a wide variety of studies: interpretation of Pfirsch-Schlüter and bootstrap currents, design of new magnetic diagnostics, magnetic island generation, vertical instabilities, density-limit disruption activity, conformance of multiple data sources to a single set of flux surfaces, quasi-single helicity states in reversed field pinches, and error-field effects on nominally axisymmetric tokamak plasmas. STELLOPT is currently in use on stellarators (LHD) and tokamaks (DIII-D) providing detailed profile reconstructions for transport calculations and diagnostic inversions. Examples of equilibrium reconstruction are shown.

TH

Turbulence Spectra, Transport, and $\mathbf{E} \times \mathbf{B}$ Flows in Helical Plasmas

T. H. Watanabe^{1,2}, M. Nunami^{1,2}, H. Sugama^{1,2}, S. Satake^{1,2}, S. Matsuoka¹,
A. Ishizawa¹, S. Maeyama³, and K. Tanaka¹

¹*National Institute for Fusion Science, Toki, Japan*

²*Graduate University for Advanced Studies, Toki, Japan*

³*Tokyo Institute of Technology, Tokyo, Japan*

Corresponding Author: watanabe.tomohiko@nifs.ac.jp

Turbulence spectra and transport in helical plasmas are investigated by the gyrokinetic simulations of ion temperature gradient (ITG) turbulence interacting with microscopic $\mathbf{E} \times \mathbf{B}$ zonal flows (ZFs) and by the neoclassical transport analysis of macroscopic $\mathbf{E} \times \mathbf{B}$ flows. Our recent kinetic simulations enable us quantitative evaluation of the turbulent transport level and the macroscopic radial electric field (E_r) relevant to the Large Helical Device (LHD) experiments. The gyrokinetic simulations with the GKV-X code clarify the spectral transfer of potential fluctuations toward stable modes with higher radial wavenumbers through ZF-turbulence interactions, and elucidate the regulation of turbulent transport due to ZFs in the neoclassically-optimized magnetic configuration. The radial electric field E_r with an equilibrium-scale length, which is evaluated by the neoclassical transport code, FORTEC-3D, including the finite-orbit-width effects, leads to further enhancement of the ZF response. Thus, turbulent transport processes are significantly influenced by neoclassical processes in helical systems through the effects of the magnetic configuration and macroscopic E_r on microscopic ZFs. The “flux-tube bundle” model is constructed for the multi-scale simulation studies on turbulence, ZFs, and E_r , and is confirmed to reproduce the same E_r effect on the ZF response as that obtained by the poloidally-global simulation.

HL

A New Paradigm for $\mathbf{E} \times \mathbf{B}$ Velocity Shear Suppression of Gyro-kinetic Turbulence and the Momentum Pinch

G. M. Staebler¹, R. E. Waltz¹, J. E. Kinsey¹, and W. Solomon²

¹*General Atomics, San Diego, USA*

²*Princeton Plasma Physics Laboratory, Princeton, USA*

Corresponding Author: staebler@fusion.gat.com

The toroidal Reynolds stress due to the shear in the $\mathbf{E} \times \mathbf{B}$ velocity Doppler shift acts like a momentum pinch [1] against the parallel velocity shear contribution to the stress. This momentum pinch cannot be computed with the quench rule paradigm [2]. This is because the quench rule only reduces the amplitude of the turbulence and does break the parity of the linear eigenfunctions [1]. Detailed studies of the nonlinear radial wavenumber spectrum of electric potential fluctuations in gyro-kinetic plasma turbulence simulations with GYRO have lead to a new paradigm [3] that is capable of computing the momentum pinch. It is found that shear in the $\mathbf{E} \times \mathbf{B}$ velocity Doppler shift suppresses turbulence by inducing a shift in the peak of the radial wavenumber spectrum and a reduction in the amplitude. An analytic model of the process is used to understand the roles of the sheared velocity and the nonlinear mode coupling. The analytic model leads to a simple formula for the nonlinear spectrum that is used in the quasilinear Trapped Gyro-Landau Fluid (TGLF) model to compute the transport. The TGLF model accurately reproduces the suppression of energy transport and the toroidal Reynolds stress driven by the Doppler shear using the new model fit to the GYRO simulations. The toroidal Reynolds stress is directly due to the finite radial wavenumber of the linear eigenmodes breaking of the mode parity. This new “spectral shift” model is the first to identify the shift in the radial wavenumber spectrum as the central mechanism by which $\mathbf{E} \times \mathbf{B}$ velocity shear suppresses turbulence. Verification of the spectral shift model with GYRO scans over plasma parameters will be presented. Simulation of DIII-D high and low torque discharges using the TGLF model will also be shown.

References

- [1] G. M. Staebler, *et al.*, Phys. Plasmas **18** (2011) 056106.
- [2] R. E. Waltz, *et al.*, Phys. Plasmas **2** (1995) 2408.
- [3] G. M. Staebler, *et al.*, “A new paradigm for the suppression of gyro-kinetic turbulence by velocity shear”, submitted to Phys. Rev. Lett. (2012).

This work was supported by the US Department of Energy under DE-FG02-95ER54309 and DE-AC02-09CH11466.

TH

The European Transport Solver: an Integrated Approach for Transport Simulations in the Plasma Core

D. Kalupin¹, V. Basiuk², D. Coster³, P. Huynh², L. Alves⁴, T. Aniel², J. F. Artaud², J. Bizarro⁴, R. Coelho⁴, D. Farina⁵, J. Ferreira⁴, A. Figueiredo⁴, L. Figini⁵, K. Gal⁶, L. Garzotti⁷, F. Imbeaux², I. Ivanova-Stanik⁸, T. Jonsson⁹, C. Konz³, S. Nowak⁵, G. Pereverzev³, O. Sauter¹⁰, B. Scott³, M. Schneider², R. Stankiewicz⁸, P. Strand¹¹, and I. Voitsekhovitch⁷

¹EFDA-CSU Garching, Garching, Germany

²CEA, IRFM, Saint-Paul-lez-Durance, France

³Max-Planck-Institut für Plasmaphysik, EURATOM-IPP Association, Garching, Germany

⁴Associação EURATOM/IST, Instituto de Plasmas e Fusão Nuclear - Laboratório Associado, Instituto Superior Técnico, Lisboa, Portugal

⁵Istituto di Fisica del Plasma CNR, Euratom-ENEA-CNR Association, Milano, Italy

⁶KFKI RMKI, EURATOM Association, Budapest, Hungary

⁷JET-EFDA, Culham Science Centre, Abingdon, UK

⁸Institute of Plasma Physics and Laser Microfusion, EURATOM Association, Warsaw, Poland

⁹Royal Institute of Technology, VR-Euratom Association, Stockholm, Sweden

¹⁰Ecole Polytechnique Fédérale de Lausanne, Centre de Recherches en Physique des Plasmas, Association Euratom-Confédération Suisse, Lausanne, Switzerland

¹¹Euratom-VR, Chalmers University of Technology, Göteborg, Sweden

Corresponding Author: denis.kalupin@efda.org

TH-P

The “European Transport Solver” (ETS) is the new modular package for scenario simulations developed within the EFDA Integrated Tokamak Modelling (ITM) Task Force. It solves 1-D transport equations to which the geometry (2D equilibrium), the transport coefficients and the sources are provided by stand alone modules coupled in a self consistent way to the transport solver through generalized data structures. It uses the KEPLER collaborative software environment to compose and manage the scientific workflows, where physics modules are built into the ETS workflows as precompiled “actors”. The high level of modularity of KEPLER allows one to have several complex workflows solving similar problems (for instance, those can either solve for the electron density or the ion density). This paper presents the status of the ETS developments, the results on verification and validation of the package and its first physics applications.

Progress in the Plasma Science and Innovation Center

U. Shumlak¹, A. Glasser¹, C. Hansen¹, E. Held², T. Jarboe¹, J. Y. Ji², C. Kim¹,
W. Lowrie¹, V. Lukin⁴, E. Meier¹, R. Milroy¹, J. O'Bryan³, B. Nelson¹, C. Sovinec³,
and C. Akcay¹

¹University of Washington, Seattle, USA

²Utah State University, Logan, USA

³University of Wisconsin, Madison, USA

⁴Naval Research Laboratory, Washington D.C., USA

Corresponding Author: shumlak@uw.edu

Highlights of recent progress in the Plasma Science and Innovation (PSI) Center include adding reacting neutrals in the MHD model, providing capability for CAD description to grid generation to MHD simulation, incorporating energetic particles in extended MHD modeling, simulating 3D physics with Hall MHD, such as rotating magnetic field (RMF) current drive and inductive asymmetric current drive. The PSI Center is a collaborative effort to refine existing computational tools with the goal of improving computational predictability. The Center collaborates with experimental research groups to test the codes and to support the experiments. The Center refines primarily NIMROD and HiFi to have sufficient physics, boundary conditions, and geometry to be calibrated with experiments to achieve predictive capabilities. This paper describes some of the recent code advances, applications to experimental devices, and comparison to experimental data. The HIT-SI bow tie spheromak uses geometrically asymmetric injectors to inject helicity. From experimental data and Hall-MHD NIMROD simulations, the spheromak is formed and sustained by a combination of reconnection and quiescent dynamo drive. The HiFi code uses a 3D finite element spatial discretization that uses a multi-block grid, imported from a CAD description from the experimental design. The grid quality is determined using an a priori error estimator that identifies regions that need improved grid resolution. The TCSU field reversed configuration (FRC) investigates RMF current drive to generate and sustain an FRC. Three-dimensional Hall-MHD NIMROD simulations using experimental parameters show the generation of an FRC with toroidal magnetic field and size that compare well with experimental results. A reacting plasma model, which has a singly ionized plasma and a dynamic, neutral gas, that undergo ionization, recombination, and charge exchange reactions, has been implemented in HiFi and used to simulate the ELF experiment of an FRC plasma drifting through a background of initially static neutral gas. The FRC leading edge ionizes and imparts momentum to the neutral gas. By collaborating with a variety of experiments, the PSI Center is able to focus efforts on adding appropriate physics capabilities to existing fluid codes and thereby provide computational support and eventually predictive capability for experiments.

Model Validation and Integrated Modelling Simulations for the JT-60SA Tokamak

G. Giruzzi¹, J. Garcia¹, M. Schneider¹, N. Hayashi², J. F. Artaud¹, M. Baruzzo³, T. Bolzonella³, D. Farina⁴, C. Sozzi⁴, L. Figini⁴, S. Nowak⁴, E. Joffrin¹, X. Litaudon¹, T. Fujita², S. Ide², A. Fukuyama⁵, Y. Sakamoto², H. Urano², and T. Suzuki²

¹CEA, IRFM, 13108 Saint-Paul-lez-Durance, France

²JAEA, Naka City, Japan

³RFX/Padova, Padova, Italy

⁴IFP, Milano, Italy

⁵Kyoto University, Kyoto, Japan

Corresponding Author: gerardo.giruzzi@cea.fr

JT-60SA will be at the forefront of the international fusion programme for many years, both before and during the D-T phase of the ITER operation. The preparation of its scientific programme is now progressing in the framework of a Japan-EU collaboration and integrate advances coming both from experiments on other tokamaks and theoretical developments. As for ITER and DEMO, integrated modelling of full discharges will be the main ingredient to perform this preparation effectively and on a rational and coherent basis. To this end, a coordinated Japan-EU modelling activity has started with the ambitious goal of providing predictive simulations of the main JT-60SA scenarios.

The first milestone of this activity is the critical comparison and benchmark of Japanese and EU models and codes used for integrated tokamak modelling. The benchmark of the H&CD codes, in particular of NBI codes for the complex injector configuration of the JT-60SA machine will be discussed.

The second milestone is the validation of the main models and simulation framework used in both Japanese and EU integrated modelling suites of codes. These include, e.g., energy and particle transport models, pedestal models, rotation sources and transport, synthetic diagnostics. It is assumed that simulations of JT-60SA scenarios should be based at least on experimental results of the two machines that are the most similar, for size and configuration: JT-60U and JET. On this basis, a validation exercise has been undertaken, involving: data exchange of reference JT-60U and JET shots, representing the main scenarios (H-mode, hybrid, advanced); predictive simulations of the reference shots with both Japanese and EU codes and models, with the aim of finding a unified modelling framework that works for both machines: this should give the maximum confidence for prediction of JT-60SA.

The first results of this comparison will be presented and discussed, with particular emphasis on the transport model comparison.

The third milestone is the predictive modelling of JT-60 SA scenario, logically to be carried out after the previous steps are completed. Nevertheless, preparation of this activity has been done by simpler models, both 0-D and 0.5-D. These results and the methods used to obtain them will be presented and discussed.

Turbulent Optimization in Stellarators & Tokamaks via Shaping

H. Mynick¹, N. Pomphrey¹, P. Xanthopoulos², and M. Lucia¹

¹*Princeton Plasma Physics Laboratory, Princeton, USA*

²*MPG/IPP, Greifswald, Germany*

Corresponding Author: mynick@pppl.gov

A method[1,2] has recently been developed for evolving toroidal configurations to ones with reduced turbulent transport, using the STELLOPT optimization code and the GENE gyrokinetic code. The potential for this method is now being explored and extended. The growing body of results has found that the effectiveness of the current “proxy” figure of merit Q_{prox} used by STELLOPT to estimate transport levels depends on the class of toroidal device considered. The present proxy works well for quasi-axisymmetric stellarators and tokamaks, and modestly for quasi-helically symmetric designs, but not for the W7X quasi-omnigenous/quasi-isodynamic design. We are exploring the origin of this variation, and improving the dependence of the proxy on key geometric factors, extending it to apply to transport channels other than the ITG turbulence it was originally developed for. We are also examining incorporating GENE directly into STELLOPT to improve the turbulent Q_{prox} , and the relative effectiveness of different search algorithms. To aid in these efforts, we have adapted STELLOPT to provide a new capability for mapping the topography of the cost function in the search space.

References

- [1] H. E. Mynick, N. Pomphrey, P. Xanthopoulos, Phys. Rev. Letters, **105** (2010) 095004.
- [2] H. E. Mynick, N. Pomphrey, P. Xanthopoulos, Phys. Plasmas, **18** (2011) 056101.

Modelling of Hybrid Scenario: from Present-day Experiments toward ITER

X. Litaudon¹, I. Voitsekhovitch², J. F. Artaud¹, P. Belo³, J. Bizarro³, T. Casper⁴, J. Citrin⁵, E. Fable⁶, J. Ferreira³, J. Garcia¹, L. Garzotti², J. Hobirk⁶, G. Hogewij⁵, F. Imbeaux¹, E. Joffrin¹, F. Koechl⁷, J. Lönroth⁸, F. Liu¹, D. Moreau¹, V. Parail², P. Snyder⁹, and M. Schneider¹

¹CEA, IRFM, Saint Paul lez Durance, France

²EURATOM/CCFE Fusion Association, Culham Science Centre, Abingdon, UK

³Associação EURATOM-IST, Instituto de Plasmas e Fusão Nuclear, Lisbon, Portugal

⁴ITER Organization, Saint Paul lez Durance, France

⁵FOM Institute DIFFER, Association EURATOM-FOM, Nieuwegein, Netherlands

⁶Max-Planck-Institut für Plasmaphysik, Garching, Germany

⁷Association EURATOM-ÖAW/ATI, Atominstitut, TU Wien, Vienna, Austria

⁸Helsinki University of Technology, Helsinki, Finland

⁹General Atomics, San Diego, USA

Corresponding Author: xavier.litaudon@cea.fr

An attractive operating scenario for ITER has recently emerged that combines long plasma duration similar to the steady-state scenario, together with the reliability of the reference H-mode regime: the so-called “hybrid” scenario. Worldwide a significant experimental effort has been devoted to explore the operating space in present day tokamaks. This paper is an overview of the recent European modelling effort carried out within the Integrated Scenario Modelling group which aims at

1. Understanding the underlying physics of the hybrid regime in ASDEX-Upgrade and JET.
2. Extrapolating them toward ITER.

Six JET and two ASDEX-Upgrade hybrid scenarios performed under different experimental conditions have been simulated in an interpretative and predictive way in order to address the current profile dynamics and its link with core confinement, the relative importance of magnetic shear, s , and $\mathbf{E} \times \mathbf{B}$ flow shear on the core turbulence, pedestal stability and H-L transition. The correlation of the improved confinement with an increased s/q at outer radii observed in JET and ASDEX-Upgrade discharges is consistent with the predictions based on the GLF23 model applied in the simulations of the ion and electron kinetic profiles.

Projections to ITER hybrid scenarios have been carried out focusing on optimization of the heating/current drive schemes to reach and ultimately control the desired q -profile with the ITER actuators and constraints. Firstly, access condition to the hybrid-like q -profiles during the current ramp-up phase has been investigated. Secondly, from the interpreted role of the s/q ratio, ITER hybrid scenario flat-top performance has been optimized through tailoring the q -profile shape and pedestal conditions. EPED predictions of pedestal pressure and width have been used as constraints in the interpretative modelling while the core heat transport is predicted by GLF23. Finally, model based approach for real-time control of advanced tokamak scenarios has been applied to ITER hybrid regime for simultaneous magnetic and kinetic profile control.

The Role of Convective Structures in the Poloidal and Toroidal Rotation in Tokamak

F. Spineanu¹, M. O. Vlad¹

¹ *Association EURATOM - MEdC Romania, National Institute of Laser, Plasma and Radiation Physics, Bucharest, Romania*

Corresponding Author: spineanu@nipne.ro

Mixed regimes consisting of coexistence large scale flows (H-mode, Internal Transport Barriers) and turbulence are expected to be the current state in ITER. The rotation, either spontaneous or induced, will play a major role in the quality of the confinement. We investigate the influence of the poloidal rotation on the toroidal flow. The efficiency of the sheared poloidal rotation to control the instabilities is considerably higher than that of the toroidal rotation but it is usually assumed that the poloidal rotation should be at the neoclassical level due to the damping induced by magnetic pumping. This is true if the drive of the poloidal rotation relies on the Reynold stress of a poloidally quasi-symmetric turbulence. Much higher drive of the poloidal rotation is however provided by flows associated with the convective structures that can be generated in the plasma cross-section beyond a threshold in the plasma pressure gradient. This drive overcomes the damping due to the magnetic pumping and the poloidal rotation is sustained. Cells of convection consisting of closed, large scale flows can be spontaneously generated, triggered by streamers sustained by the baroclinic term able to generate vorticity. Similar to the Reyleigh-Benard first bifurcation (from purely conductive to convective regime), the onset is very fast and the drive exerted on the poloidal rotation leads to a fast time variation of the polarization radial electric field. This is sufficient to create a distinction between the phases (first half, second half) of bounce on a banana of trapped ions and, implicitly, leads to acceleration in the toroidal direction.

The structure consisting of cells of convection, breaking the azimuthal symmetry, is not a stationary state, mainly because they will induce magnetic perturbations. The reconfiguration of the flow due to the magnetic reconnections will reinstall the conductive state even if the gradients are still favorable to a convective response. The intermittent generation of convective structures must then be treated as a stochastic process consisting of a random sequence of events. The effect on the (toroidal) angular momentum transport will be discussed on the basis of the fluctuating drive of the Reynolds stress (a doubly random process).

TH-P

Fusion Power Production in Baseline ITER H-Mode Discharges

A. Kritz¹, T. Rafiq¹, and A. Pankin²

¹ *Lehigh University, Bethlehem, USA*

² *Tech-X Corporation, Colorado, USA*

Corresponding Author: kritz@lehigh.edu

Previous studies of ITER steady state and hybrid scenarios [1,2] are extended to studies of ITER ELMy H-mode 15 MA scenarios. Results are obtained using the PTRANSP predictive integrated modeling code with time evolved boundary conditions and the plasma shape provided by the Tokamak Simulation Code (TSC). Current is ramped to 15 MA during first 100 sec and the central density is ramped to values in the range of 0.85×10^{20} to $1.05 \times 10^{20} \text{ m}^{-3}$. Impurities are 2% Be, Argon in the range 0.12% to 0.3% and 2% He³. Variation in density and in level of Argon impurity provides insight to the sensitivity of fusion power production to variation in these parameters. The dependence of confinement and the associated fusion power production on the level and mixture of beam and RF heating as well as on the choice of RF heating mixes are examined. Components of the ITER H-mode plasma current density (ohmic, bootstrap, beam and radio frequency) are shown as functions of plasma radius along with the integrated current contained within a given plasma radius. Also shown, for various plasma conditions, are the neutron density production as a function of radius and the rate at which neutrons are produced within a given radius. Various discharge conditions are studied in which the input power is reduced once alpha power heating is underway. Pedestal pressure is varied in the range of EPED1 [3] predictions to examine the sensitivity of fusion power production to the pedestal pressure. The PTRANSP code is used to compute temperature, magnetic q and toroidal rotation profiles using either the MMM7.1 or the GLF23 anomalous transport model, combined with neoclassical transport. Verification studies are carried out repeating PTRANSP simulations using the ASTRA code. The effects of low, reverse and strong magnetic shear on internal transport barriers are explored. In the PTRANSP simulation scans the same rotation velocity boundary condition will be employed for each discharge. Simulations are carried out turning off flow shear in order to separate the flow shear and magnetic shear effects on internal transport barriers. This is an important issue for ITER since it is expected that the toroidal rotation will be small.

References

- [1] A. H. Kritz, *et al.*, Nucl. Fusion **51** (2011) 123009 .
- [2] T. Rafiq, *et al.*, Phys. Plasmas, **18** (2011) 112508.
- [3] P. B. Snyder, *et al.*, Phys. Plasmas **16** (2009) 056118.

New Results in the Theory of Non-Diffusive Heat Transport and Anomalous Electron-Ion Energy Coupling

L. Wang¹, L. Zhao², and P. Diamond²

¹ *WCI Center for Fusion Theory, Daejeon, Republic of Korea*

² *UCSD, La Jolla, USA*

Corresponding Author: wanglu.phy@gmail.com

We present new results in the theory of non-diffusive heat transport, with special emphasis on electron thermal transport. Two foci of this paper are:

1. The theory of the convective energy velocity (i.e., heat pinch) for both electrons and ions [1].
2. The theory of collisionless electron-ion energy coupling [2].

Both these topics are important for ITER, since in a burning plasma, alpha particles slow down through Coulomb collisions with the electrons. We emphasize that the heat pinch and collisionless transfer are physically distinct and independent processes, which can, in principle, co-exist in low collisionality regimes. For both ions and trapped electrons, an inward heat pinch is predicted for flat density profiles, while outward energy convection is predicted for steep density profiles. An analysis of various energy dissipation channels shows that collisionless energy transfer and the consequent ion heating will occur predominantly by quasilinear processes and through zonal flow dissipation. This implies that any putative ITER transport model must include the effect of turbulent heating and inter-species coupling, in addition to predicting the electron heat flux.

References

- [1] L. Wang and P. H. Diamond, Nucl. Fusion **51** (2011) 083006.
- [2] Lei Zhao and P. H. Diamond, U.S. Transport Task Force Workshop, San Diego, California, April 6-9, (2011).

Microtearing Mode Fluctuations in Reversed Field Pinch Plasmas

D. Carmody¹, P. Terry¹, Y. Ren², J. Sarff¹, A. Almagri¹, and M. Pueschel¹

¹*University of Wisconsin-Madison, Madison, USA*

²*Princeton Plasma Physics Laboratory, Princeton, USA*

Corresponding Author: dcarmody@wisc.edu

Improved confinement scenarios in RFP plasmas that reduce global tearing modes are expected to lead to plasmas where confinement is limited by microturbulence driven by gradients of pressure, density, and temperature. Because enhanced confinement regimes in MST yield temperature profiles with core gradients near the critical threshold for temperature-gradient driven instability, a linear analysis of temperature-gradient driven micro-instabilities in MST-like RFP equilibria is undertaken using toroidal gyrokinetics for beta values ranging from 0 to 10%. These simulations show that when the ratio of minor radius to temperature gradient scale length is greater than 3 – 4, MST plasmas are unstable to ITG at low beta and unstable to microtearing at high $\beta \sim 10\%$. The β at which microtearing dominates ITG is 5%, with ITG becoming completely stable just above 10%. Theory shows that the higher critical beta for ITG stabilization, relative to tokamaks, is associated with the shorter scale lengths for magnetic curvature. At the MST-relevant β of 10% the micro-tearing mode growth rate peaks at a poloidal wavenumber of $k_y \rho_s = 1.4$ inverse gyroradii. However, instability is strong even for low wavenumbers, where there is a growth rate 2 – 3 times that of ITG at its maximal wavenumber for zero β . The growth rate remains large even for very low collisionality, with indications that different microtearing branches are associated with low and moderate collisionalities. With these growth rate values significant transport is expected. MST has several diagnostics that will access microturbulence spatial scales, including FIR interferometry/scattering, fast Thomson scattering, heavy ion beam probe, and material probes. Work is underway to prepare these diagnostics for electrostatic and magnetic turbulence measurements for model validation in high-performance plasmas.

TH-P

Tokamak Discharges with Electron Thermal Conductivity Closed to the Neoclassical One

V. Leonov

NRC "Kurchatov Institute", Moscow, Russian Federation

Corresponding Author: leo@nfi.kiae.ru

At the development of plasma transport models it is very important to have the asymptotic transitions to the cases when transport coefficients are well described by some first principle based theories. For the ion component of tokamak plasma this is a transition to results of the neoclassical theory (in Ohmically heated high density discharges). Another stable opinion has been formed in characterizing the electron transport, as being principally anomalous. Conclusions of L. A. Artsimovich [1], who analyzed the first tokamak experiments, are contributed to this. He called the electron thermal conductivity of the minimal level as "pseudo-classical" due to "classical" behavior of its dependences on plasma parameters despite of the several times higher amplitude. This opinion was supported later by B. B. Kadomtsev [2] and by many other authors. However, these conclusions have been done as a result of simplified consideration of transport processes using only diagonal terms of transport matrix. In this work it is shown that, taking into account the off-diagonal terms of neoclassical transport coefficient matrix, one can reduce imaginary anomaly of electron thermal conductivity coefficients in tokamaks. Presented results of predictive modeling of several representative tokamak discharges with the ASTRA transport code [3] show that profiles of electron and ion temperatures measured in these experiments can be well described in the frame of the neoclassical transport theory. Contributions of different channels of energy losses from the ion and electron plasma components are investigated. So, results of the modeling of transport properties of high density discharges for some tokamaks show that electron and ion heat transport in the plasma core in these regimes can be described using the complete matrix of the neoclassical coefficients. Therefore minimal coefficients of electron heat transport in tokamaks are not "pseudo-classical" but the neoclassical ones.

References

- [1] Artsimovitch L. A., Nucl. Fus., **12** (1972) 215.
- [2] Kadomtsev B. B., Plasma Phys. Reports (Rus), **5** (1983), 938.
- [3] Pereversev, G. V., Yushmanov, P. N., Preprint IPP 5/98 (2002), Garching, Germany.

Indications of Nonlocality of Plasma Turbulence

Ö. Gürcan¹, L. Vermare¹, P. Hennequin¹, V. Berionni¹, P. Diamond^{2,3},
G. Dif-Pradalier⁴, X. Garbet⁴, P. Ghendrih⁴, V. Grandgirard⁴, C. McDevitt¹,
P. Morel¹, Y. Sarazin⁴, A. Storelli¹, and C. Bourdelle⁴

¹*LPP/École Polytechnique/CNRS, Palaiseau, France*

²*WCI Center for Fusion Theory, NFRI, Daejeon, Republic of Korea*

³*University of California San Diego, La Jolla, USA*

⁴*CEA, IRFM, Saint Paul Lez Durance, France*

Corresponding Author: ozgur.gurcan@lpp.polytechnique.fr

Nonlocality, which may manifest itself as a breaking of the favorable gyro-Bohm scaling of transport via phenomena such as avalanches or turbulence spreading and is an important threat to ITER operation has been considered and observed to various extents in simulations and experiments. Understanding of its details, is an essential challenge for the transport community. Here, we present some indications in the form of characteristic observations from experiment, such as the recent results from the Tore Supra tokamak, using detailed high-resolution fluctuation diagnostics, that show the existence of mesoscale structures (Geodesic Acoustic Modes) and their dynamics and simulation results using the GYSELA code, developed by the IRFM-CEA, a full- f , global gyrokinetic code that simulates the ion scales but can also treat neoclassical physics, momentum transport with ripple etc. and finally discuss existing simple models that help understand, and underline the important features of non-locality of plasma turbulence. We discuss possible ways of verification of such models dealing with both turbulence and transport scales and in particular the mesoscale “interface” between these two hypothetically distinct scales. Turbulence spreading, and dynamics of the turbulence intensity field is a critical ingredient of this mixed range, which is also coupled to momentum transport via residual stress generation. It is also argued that nonlocality plays a key role in the L to H transition.

Physics Basis and Validation of MMM7.1 Anomalous Transport Module

T. Rafiq¹, A. Kritz¹, R. Budny², I. Voitsekhovitch³, and A. Pankin⁴

¹*Lehigh University, Bethlehem, USA*

²*Princeton Plasma Physics Laboratory, Princeton, USA*

³*JET-EFDA, Culham Science Centre, Abingdon, UK*

⁴*Tech-X Corporation, Colorado, USA*

Corresponding Author: rafiq@lehigh.edu

The MMM7.1 anomalous transport module, recently installed in the PTRANSP code, is used to compute thermal, particle and toroidal angular momentum transport. The new MMM7.1 is documented and organized as a standalone module, which fully complies with the NTCC standards. The new transport module can be used with a standalone driver as well as within the integrated PTRANSP code and in other whole device modeling codes such as ASTRA, TSC, ONE-TWO, SWIM and FACETS. The MMM7.1 module includes a model for ITG, TE modes and MHD modes as well as a model for ETG modes and a model for drift resistive inertial ballooning modes. The model for transport driven by ITG/TE modes now includes the diffusion and radial convective pinch of toroidal angular momentum. It is found that this ITG/TE model can predict the observed intrinsic plasma rotation given a relatively small toroidal rotation at the plasma edge. The theoretical foundation of MMM7.1 is significantly advanced compared to the earlier MMM95 model. The new ITG/TE model in MMM7.1 module more accurately computes the suppression of transport at low and reverse magnetic shear. The MMM7.1 module is further improved by making better approximations to the structure of the eigenfunctions along field lines in order to include the effects of non-circular flux surfaces, finite β , and Shafranov shift. Simulations using the MMM7.1 module compute the internal transport barrier that is experimentally observed in reversed magnetic shear discharges with sufficiently large toroidal angular rotation. The fluid approach which underlies the derivation of MMM7.1, while not as complete as a kinetic approach, allows prediction of the evolution of plasma discharges on an energy transport time scale. In this study, the theory based MMM7.1 is derived and simulations of DIII-D and JET tokamak discharges are presented to illustrate how various elements of the transport model influence the evolution of the tokamak plasma discharges. The discharges simulated include Ohmic, L-mode, H-mode plasmas and plasmas with co- and counter-rotations and plasmas with internal transport barriers. Results will be presented to understand the interaction between physical processes that influence transport in magnetically confined plasmas.

TH-P

Predictive Transport Simulations Consistent with Rotation and Radial Electric Field Using TOPICS with OFMC

M. Honda¹, N. Hayashi¹, T. Takizuka², M. Yoshida¹, and T. Fujita¹

¹*Japan Atomic Energy Agency, Naka, Japan*

²*Osaka University, Osaka, Japan*

Corresponding Author: honda.mitsuru@jaea.go.jp

A toroidal momentum equation solver newly implemented in TOPICS calculates a temporal variation of a total toroidal momentum with an external torque input by OFMC. A solid scheme that can calculate parallel, poloidal and toroidal flows, and thus the radial electric field E_r is developed using the Matrix Inversion method. The coupling of the solver and the scheme with the aid of OFMC provides a means to investigate complex phenomena involving E_r and toroidal rotation. The simulations show the importance of inward pinch, the residual stress and the boundary condition for estimating toroidal rotation. Predictive capability we gained helps us seek the controllability for upcoming JT-60SA and ITER.



Impact of Fusion Alpha Driven Current on the Magnetic Configuration of a Tokamak

V. Yavorskij¹, K. Schoepf¹, T. Gassner¹, V. Goloborodko^{1,2}, A. Polevoi³, and S. Sharapov⁴

¹*Institute for Theoretical Physics, University of Innsbruck, Austria*

²*Institute for Nuclear Research, Ukrainian Academy of Sciences, Kiev, Ukraine*

³*ITER Organization, Cadarache, France*

⁴*EURATOM /CCFE Association, Culham Science Centre, Abingdon, UK*

Corresponding Author: victor.yavorskij@uibk.ac.at

The paper evaluates the influence of fusion alphas on burning plasmas in future tokamak reactors. In comparison to the relatively weak effect of charged fusion products (CFPs) in today's devices, the substantially enhanced fusion power in burning tokamak plasmas may bring on a significant impact of CFPs on the equilibrium and bulk plasma parameters. Based on 3D Fokker-Planck modelling of DT fusion alphas we analyze here their effect on the plasma current and equilibrium in basic ITER scenarios. Particularly considering the peculiarities of the velocity and spatial distributions of confined alpha particles with energies exceeding a hundreds of keV, we calculate the poloidal profiles of the total alpha induced bootstrap current as well as of the fusion power deposition to bulk plasma electrons and ions. The present study demonstrates that fusion alphas are expected to induce an additional rotational transform of the magnetic field lines in reactor size tokamak plasmas. In reversed shear plasma scenarios the impact of the alpha driven current appears to be greater. While in the ITER steady state scenario alpha particles induce a 15% reduction of the safety factor in the core area, in the 2nd ITER Scenario with positive shear the safety factor reduction in the core is < 5% according to our calculations. Nevertheless, also such an alteration may reduce the core safety factor, which in Scenario 2 is only 1.02 – 1.04, to a value below 1, the crucial value for plasma stability. It is noted that, in spite of the low intensity of the total current driven by fusion alphas, the alpha driven current can play a role of a seed current for the bootstrap tokamak reactor. Evidently, the development of advanced plasma scenarios and research programs for ITER and future tokamak reactors should account for the effects of currents driven by fusion alphas.

TH-P

Nonlinear Modeling for Helical Configurations in Toroidal Pinch Systems

S. Cappello¹, D. Bonfiglio¹, L. Chacon², G. Ciaccio¹, D. Escande³, S. Guo¹,
I. Predebon¹, F. Sattin¹, G. Spizzo¹, M. Veranda¹, and Z. Wang¹

¹*Consorzio RFX, Padova, Italy*

²*Oak Ridge National Laboratory, Oak Ridge, USA*

³*Laboratoire PIIM, Marseille Université, Marseille, France*

Corresponding Author: susanna.cappello@igi.cnr.it

We present the current status of research in nonlinear modeling studies developed about the RFX-mod experiment, where several pinch configurations can be compared ranging from the self-organized helical RFP, to circular Tokamak passing through Ultra Low q ones, thus providing a flexible experiment in view of a future validation stage for several modeling tools. We focus presently on 3D nonlinear MHD modeling and nonlinear gyrokinetic tools for studies of helical configurations in the Reversed Field Pinch regime.

We present new results of 3D nonlinear visco-resistive MHD simulations, which address the issue of stimulating by suitable helical magnetic boundary condition a helical QSH configuration with different toroidal periodicity (in particular a non resonant one) with respect to the self-organized one. On a parallel side, we present first MHD toroidal simulations with the PIXIE3D code.

Preliminary indications show that QSH state is not stationary like it was in the cylindrical case. Instead, it is interrupted by crashes which may be reminiscent of the experimental phenomenology. A discussion of the magnetic topology obtained both as a result of stimulated nonresonant QSH regimes and of toroidal geometry effect will be presented, including results of code's benchmarking of available tools like NEMATO and ORBIT.

Concerning nonlinear gyrokinetic studies, Ion temperature gradient (ITG) modes have been studied in the last years as a possible source of ion heat transport in the RFP. Such instabilities have revealed to be strongly stabilized compared to tokamak plasmas, due to the Landau damping acting in low- q configurations. However, for strongly outwardly peaked impurity profile — which is the case for RFX-mod plasmas — they can be more relevant. In this contribution, we address the nonlinear problem still in axisymmetric RFP geometries. A large set of 2-species gyrokinetic turbulence simulations with GS2 is presented, in order to compare the linear and nonlinear stability threshold. An up-shift in $a/LT_{i,c}$ is found, consistently with the picture given in tokamak plasmas (the so-called Dimits shift).

Non-diffusive Momentum Transport in JET H-mode Regimes: Modeling and Experiment

H. Weisen^{1,2}, Y. Camenen³, A. Salmi⁴, M. Gelfusa⁵, P. de Vries⁶, M. Maslov⁷,
T. Tala⁴, M. Beurskens⁷, and C. Giroud⁷

¹*Centre de Recherches en Physique des Plasmas, Association EURATOM - Confédération Suisse, Lausanne, Switzerland*

²*EFDA-CSU, Culham Science Centre, Abingdon, UK*

³*IIFS/PIIM/UMR, CNRS/Aix-Marseille Université, Marseille, France*

⁴*Association EURATOM-Tekes, VTT, Finland*

⁵*Associazione EURATOM-ENEA - University of Rome "Tor Vergata", Roma, Italy*

⁶*FOM Institute Rijnhuizen, Association, Nijmegen, Netherlands*

⁷*EURATOM/CCFE Fusion Association, Abingdon, UK*

Corresponding Author: henri.weisen@epfl.ch

A systematic comparison of theoretical predictions for momentum transport in JET with experimental results has provided detailed insight into the physics of momentum transport, in particular non-diffusive transport. For this project, 400 representative experimental samples, selected from an extensive JET profile database with more than 1000 experimental profiles obtained over the entire baseline H-mode and hybrid operating domains, were used as input for the gyrokinetic code GKW. Linear and non-linear local calculations have allowed to quantify the contributions of diffusive transport, the Coriolis pinch and residual stresses to the overall transport and predict the expected angular velocity gradient R/L_ω for each of these samples. Direct comparisons of modeled and experimental data show that overall, the predicted Coriolis pinch account for approximately 70% of the observed non-diffusive contributions to R/L_ω . First results from linear calculations indicate that the remainder is consistent in magnitude with expectations for residual stresses. The strong contribution of the Coriolis pinch is due to the fact that most of these NBI-heated plasmas are strongly rotating, with Mach numbers in the range 0.05 to 0.35. Regressions were used to determine the overall parameter dependencies, both for the experimental and the theoretical dataset. Remarkably, the experimental scaling for non-diffusive transport matches the theoretical scaling for the Coriolis pinch for the three most relevant parameters $R/L_{n,q}$ and $f_t = \sqrt{\epsilon}$, the trapped particle fraction. A scaling with T_i/T_e in the experimental database and not characteristic of the Coriolis pinch, is suggestive of a contribution by residual stresses. Residual stresses are addressed in ongoing linear and non-linear simulations.

TH-P

New Technique for the Calculation of Transport Profiles in Modulation Experiments

D. Escande¹, F. Sattin², Y. Camenen¹, A. Salmi³, and T. Tala³

¹*Laboratoire PIIM, CNRS-Aix Marseille Université, Marseille, France*

²*Consorzio RFX, Padova, Italy*

³*Association Euratom-Tekes, VTT, Finland*

Corresponding Author: dominique.escande@univ-amu.fr

Transport codes provide a classical way to infer the profile of transport coefficients in fusion plasmas: assuming given functionals for the transport coefficient profiles, the free parameters are iteratively adjusted to best reproduce the measurements. This work introduces a new technique, the matrix approach (MA), which avoids any a priori constraint of the profiles, and computes them by simply inverting a 2D matrix, which also provides the uncertainty on the reconstruction for the case of modulation experiments. This is done by a controllable smoothing of the experimental data, instead of the ad hoc regularization of the profile of transport coefficients operated by transport codes. As a preliminary check, the MA was applied to already published JET data of momentum transport corresponding to three discharges that share the same initial equilibrium state. While an analysis of the data by a transport code suggests that all three cases share nearly the same transport coefficients, the MA rules this out, since the three uncertainty domains do not overlap at the various measurement positions. This suggested performing a similar analysis involving a residual stress on top of the advective and diffusive contributions to the flux. Then a single set of transport coefficients was found to be compatible with all three cases.

Evolution of Ion Heat Diffusivity and Toroidal Momentum Diffusivity during Spontaneous ITB Development in HL-2A

Q. Gao¹, R. V. Budny²

¹*Southwestern Institute of Physics, Chengdu, China*

²*Princeton University Plasma Physics Laboratory, Princeton, USA*

Corresponding Author: qgao@swip.ac.cn

Toroidal momentum torques generating V_t (toroidal flow) affect ITB evolution and decay in TFTR, JT-60U and DIII-D, suggesting that momentum inputs could offer a means for controlling barrier dynamics. An important question is whether it is possible to produce and control an ITB with inputting toroidal momentum in a discharge. To explore the role of external inputs of toroidal momentum on the development of ITBs we model the NBI heating discharges in HL-2A ($R = 1.64$ m, $a = 0.4$ m, $B_t = 2.8$ T, $I_p = 0.48$ MA) by using TRANSP. The modeled discharge: $B_t = 2.6$ T, $I_p = 300$ kA, $\bar{n}_e = 2.4 \times 10^{19}$ m³, single null divertor, H-mode boundary. As many experiments showed that optimized q -profile is one of the essential ingredients in establishing ITB, 0.5 MW LH power in the current drive mode is injected at $t = 0.8$ s to control the current profile. Since the 2.45 GHz LH wave drives off-axis current in HL-2A, the q -profile with weak shear region extended to $\rho \sim 0.8$, $q_0 > 2.0$ and $q_a \sim 5.3$ is established after the current profile sufficiently relaxed (at $t \sim 1.1$ s). In order to control the toroidal momentum input, 3 MW NBI ($E = 45$ keV) is injected tangentially with both co- and counter-injection during $t = 0.4 - 1.8$ s. The heat and momentum transport is calculated with a physics-based model GLF23. The transport model includes turbulence suppression mechanisms of $\mathbf{E} \times \mathbf{B}$ rotation shear. With appropriate neutral beam injection the nonlinear interplay between the transport determined gradients in V_t and $T_{i,e}$ and the $\mathbf{E} \times \mathbf{B}$ flow shear (including q -profile) produces transport bifurcations, leading to a stepwise growing ITB. After its growth duration steady ITB is formed from $t \sim 1.35$ s. The ITB establishment is dependent on the toroidal momentum input. Quasi-steady ITBs can not be established unless the co-injected NBI power is in the range of 2.85 MW to 2.4 MW (correspondingly the counter-injected power is 0.15 MW to 0.6 MW respectively), which suggests that the NBI producing toroidal flow plays an important role in the ITB formation. The relationship between viscosity and ion heat transport in the ITB formation process is studied. Detailed examination of the evolution of toroidal momentum diffusivity and ion heat diffusivity in a region around the ITB development shows that the transport barrier of momentum develops more quickly and its enhanced confinement region extends further outward than that of heat.

TH-P

Progress in the Theoretical Description and the Experimental Characterization of Impurity Transport at ASDEX Upgrade

C. Angioni¹, F. Casson¹, C. Veth¹, Y. Camenen², R. Dux¹, B. Geiger¹,
R. McDermott¹, A. Peeters³, and M. Sertoli¹

¹*Max-Planck-Institut für Plasmaphysik, EURATOM Association, Garching, Germany*

²*PIIM, CNRS/Aix-Marseille-Univ., Marseille, France*

³*Faculty of Mathematics, Physics and Informatics, Universitaet Bayreuth, Bayreuth, Germany*

Corresponding Author: clemente.angioni@ipp.mpg.de

The understanding of impurity transport from the wall to the center of the plasma and the identification of reliable methods to control central impurity accumulation are essential elements toward the achievement of practical fusion energy. A combination of theoretical and experimental research is required to identify the physical mechanisms from the theoretical standpoint, and to validate their impact on the measured impurity density profiles from the experimental side. In this contribution, advances in the theoretical description of turbulent impurity transport, particularly related to the inclusion of rotational effects, are presented. An analytical fluid model, which still captures the main elements of the physics, and linear and nonlinear numerical calculations with the gyrokinetic codes GKW and GS2 are presented and compared. In particular, GKW has the unique feature for a gyrokinetic code of including also centrifugal effects on turbulent transport. The impurity transport mechanisms produced by a radial gradient of the toroidal velocity and by centrifugal effects are singled out in the analytical calculations, and identified in the numerical results. These advances allow, in particular, the consistent prediction of the two dimensional impurity density distribution over the poloidal cross section. This more comprehensive theoretical description is also applied to the modelling of ASDEX Upgrade measurements of impurity density profiles. In neutral beam injection heated H-mode plasmas, central electron cyclotron heating is observed to increase the peaking of both the electron density and the boron density profiles. An inverse correlation is observed between the peaking of the boron density profile and the plasma toroidal rotation, as well as the boron logarithmic temperature gradient. The theoretical explanation of this phenomenology relates the boron response to the reduction of plasma rotation in the presence of central electron heating.

Transport Analysis of Oscillatory State for Plasma Dynamics in Helical Plasmas

S. Toda¹, K. Itoh¹

¹*National Institute for Fusion Science, Toki, Japan*

Corresponding Author: toda@nifs.ac.jp

The formation mechanism of transport barriers is important issue to realize improved confinement modes in toroidal plasmas. In helical plasmas, two kinds of the oscillation for the plasma quantities are experimentally observed. Firstly, the limit cycle phenomena in the temporal evolution of the electrostatic potential, namely the electric pulsation, have been observed in the core region. Related with the electric pulsation, the electron internal transport barrier is observed in the electron temperature profile. Therefore, the physical mechanism, which realizes the oscillatory plasma state, is critical for the study of improved confinement modes. Secondly, the density limit oscillation in the helical device was reported. The achievable limit of the density due to the radiation collapse has been studied, because the strong degradation of the confinement occurs if the radiation collapse happens. Dynamics of the radial structure for the plasma quantities are important for the study of the density limit. The temporally self-generated oscillation of the radial electric field has been shown as a simulation result in the core region of helical plasmas. The clear transport barrier in the radial profile of the temperature is obtained in the core region, which is associated with the oscillation of the radial electric field. Dynamics of the temperature gradient are shown during the self-generated oscillation to compare the experimental results. The temporal evolution of the density profile is newly included in a simulation when the radiative loss is calculated in the edge region of helical plasmas. Two kinds of the stationary states are studied. One is dominated by the transport loss and another is dominated by the radiative loss. The dependence of the achieved density limit on the heating power is derived, when the temporal evolution of the density is calculated. The dependence of the critical density on the heating power when the temporal evolution of the density profile is included alters compared with the case with the temporally fixed density profile. The multiple solutions of the radial electric field, which satisfy the ambipolar condition, are obtained in the edge region of helical plasmas. Progress in the study of the density limit oscillation in the edge region is reported.

TH-P

Turbulent Transport due to Kinetic Ballooning Modes in High- β Toroidal Plasmas

A. Ishizawa¹, S. Maeyama², T. Watanabe¹, H. Sugama¹, and N. Nakajima²

¹*National Institute for Fusion Science, Toki, Japan*

²*Tokyo Institute of Technology, Tokyo, Japan*

Corresponding Author: ishizawa@nifs.ac.jp

Turbulent transport in high- β toroidal plasmas is investigated by means of a newly developed simulation code solving electromagnetic gyrokinetic equations combined with gyro-fluid equations for electrons. The new code allows simulations of turbulent transport at high- β with smaller computational cost and less numerical difficulty than solving gyrokinetic equations for both electrons and ions which have disparate spatio-temporal scales. The code is applicable to a model configuration of Large Helical Device (LHD) experiments as well as tokamaks, and linear calculations show that kinetic ballooning modes (KBMs) are destabilized at high- β . A nonlinear simulation for a tokamak plasma shows that heat transport due to KBM at high- β ($\beta = 2\%$) is significantly larger than that due to ion temperature gradient mode (ITG) driven turbulence at zero β because of high KBM growth rate and weak zonal flow.

Drift-kinetic Simulation Studies on Neoclassical Toroidal Viscosity in Tokamaks with Small Magnetic Perturbations

S. Satake^{1,2}, H. Sugama^{1,2}, R. Kanno^{1,2}, and J. K. Park³

¹*National Institute for Fusion Science, Toki, Japan*

²*The Graduate University for Advanced Studies, Toki, Japan*

³*Princeton Plasma Physics Laboratory, Princeton, USA*

Corresponding Author: satake@nifs.ac.jp

Effect of magnetic perturbations on neoclassical toroidal viscosity (NTV) in tokamaks is investigated by using a drift-kinetic δf simulation code, FORTEC-3D. The effect of magnetic perturbation on plasma transport and rotation is one of the important issues in recent tokamak experiments and forthcoming ITER project, in which the resonant magnetic perturbation (RMP) applied externally is a candidate to mitigate the edge localized modes. Finite NTV caused by RMPs damp the toroidal rotation, which might bring adverse effects on the other MHD instabilities such as resistive wall modes and locked modes.

We have developed the simulation code to evaluate the NTV numerically. Compared with conventional analytic formulae which adopt many approximations, FORTEC-3D solves the drift-kinetic equation by following the exact guiding-center orbits including the finite-orbit-width effect and Coulomb collisions, and the viscosity is directly evaluated from the plasma distribution function, δf .

In this paper, basic properties of NTV, such as the dependence of collisionality, $\mathbf{E} \times \mathbf{B}$ rotation speed, etc., are investigated by using the δf simulation. Benchmark tests of the code with analytic formulae of NTV are also reported. We have found some distinctive features which have not found in previous studies.

First, we have investigated the NTV in the limit of zero $\mathbf{E} \times \mathbf{B}$ rotation. Single-helicity, $(m, n) = (7, 3)$ mode small perturbation field is applied to a tokamak configuration. It is found that conventional asymptotic limit formulae for the $1/\nu$ and super-banana plateau regimes overestimate the NTV, while the combined analytic formula by J. K. Park agrees well with FORTEC-3D in a wide range of collision frequency.

Second, FORTEC-3D and Park's formula has been benchmarked in finite- $\mathbf{E} \times \mathbf{B}$ rotation cases. A reference radial electric field (E_r) was given from the force balance relation, and the dependence was studied by magnifying the reference E_r amplitude. Two calculations agree well when E_r is close to the reference value. The peak of NTV at the resonant surface shrinks in both calculations as $\|E_r\|$ becomes larger. However, as $\|E_r\|$ increases, there appear other twin peaks of NTV on the both sides of the original resonant surface only in the δf simulation. It is anticipated that the finite-orbit-width effect can cause the difference from the analytic formula.

The European Integrated Tokamak Modelling Effort: Achievements and First Physics Results

G. Falchetto¹, D. Coster², R. Coelho³, P. Strand⁴, L. G. Eriksson⁵, V. Basiuk¹,
D. Farina⁶, F. Imbeaux¹, T. Jonsson⁷, C. Konz², X. Litaudon¹, G. Manduchi⁸,
A. H. Nielsen⁹, M. Ottaviani¹, R. Paccagnella⁸, G. Pereverzev², B. Scott²,
D. Tskhakaya¹⁰, G. Vlad¹¹, I. Voitsekhovitch¹², B. Guillerminet¹, D. Kalupin¹³,
E. Giovannozzi¹¹, H. J. Klingshirn², D. Yadikin⁴, and W. Zwingmann⁵

¹CEA, IRFM, Saint-Paul-lez-Durance, France

²Max-Planck-Institut für Plasmaphysik, EURATOM-IPP Association, Garching, Germany

³Associação EURATOM/IST, Lisboa, Portugal

⁴Chalmers University of Technology, Göteborg, Sweden

⁵European Commission, Directorate-General for Research and Innovation, Brussels, Belgium

⁶Istituto di Fisica del Plasma CNR, Euratom-ENEA-CNR Association, Milano, Italy

⁷Royal Institute of Technology, VR-Euratom Association, Stockholm, Sweden

⁸Associazione EURATOM-ENEA sulla Fusione, Consorzio RFX, Padova, Italy

⁹Association EURATOM-DTU, Roskilde, Denmark

¹⁰Association EURATOM-ÖAW, University of Innsbruck, Innsbruck, Austria

¹¹Associazione Euratom-ENEA sulla Fusione, Roma, Italy

¹²JET-EFDA, Culham Science Centre, Abingdon, UK

¹³EFDA-CSU, Garching, Germany

Corresponding Author: gloria.falchetto@cea.fr

The achievements and first physics results are presented of the European Integrated Tokamak Modelling Task Force (EFDA ITM-TF) effort, aiming at providing a standardized platform and an integrated modelling suite of validated numerical codes, for the simulation and prediction of a complete plasma discharge in any tokamak.

The framework developed by the ITM-TF, based on a generic datastructure enclosing both simulated and experimental data, allowed for the development of sophisticated integrated simulations (workflows) for physics application. Those include the European Transport Solver (ETS), incorporating a sophisticated module for synergy effects between heating schemes, several equilibrium modules, pellets, impurities, neutrals, sawteeth and NTM modules, a variety of simple transport modules and neoclassical modules. The ETS workflows have been subject to an extensive verification and validation laying the foundations for the use of ETS for both predictive and interpretative transport simulations as well as scenario modeling on present devices and ITER.

The equilibrium reconstruction and linear MHD stability simulation chain is being applied for production runs on several devices. In particular, an analysis of the edge MHD stability of ASDEX Upgrade type-I ELMy H-mode discharges and ITER hybrid scenario was performed, revealing the stabilizing effect of an increased Shafranov shift on edge modes.

A successful benchmark among EC beam/ray-tracing codes (C3PO, GRAY, TORAY-FOM, TORBEAM, TRAVIS) has been performed in the ITM framework for an ITER case for different launching conditions from the Equatorial Launcher, showing good agreement of the computed absorbed power and driven current.

Simulations performed within the ITM infrastructure with the turbulence code GEM for a JET hybrid discharge and the comparison of the simulated anomalous fluxes with TRANSP are presented, addressing in particular, the effect of the $\mathbf{E} \times \mathbf{B}$ shear on the thermal and particle confinement. Finally, recent developments on the integration and validation of synthetic diagnostics (fusion products, mse and reflectometry) on the ITM platform are shown.

Advanced Confinement Regimes and Their Signatures

B. Coppi¹, T. Zhou¹

¹*MIT, Cambridge, USA*

Corresponding Author: coppi@mit.edu

A unified theory [1, 2] has been developed for the modes that are excited at the edge of the plasma column and are an important signature of the advanced confinement regimes in which magnetically confined plasmas can be driven. In particular the so-called EDA H-Regime, the Elmy H-Regime and the I-Regime are considered and the modes that are identified theoretically have characteristics that are consistent with or have anticipated those of the modes observed experimentally for each of the investigated regimes. The phase velocities, the produced transport processes, the frequencies, the wavelengths and the consistency with the direction of spontaneous rotation are the factors considered for comparison with the relevant experiments. The phase velocity is in the direction of the ion diamagnetic velocity, in the plasma reference frame, for the Quasi-Coherent Mode that is present in the EDA H-Regime and is identified as a ballooning mode at Finite Larmor Radius marginal stability involving the effects of transverse ion viscosity and other dissipative effects [2]. Both in this regime and in the Elmy H-Regime impurities are driven towards the center of the plasma column. Instead, in the I-Regime the excited “Heavy Particle” mode [1] with a phase velocity in the electron diamagnetic velocity direction is shown to expel the impurities toward the plasma edge. The modes considered for the Elmy H-Regime are of ballooning kind, driven by the combined effects of the plasma pressure gradient and the magnetic curvature, are close to the relevant non-dissipative marginal stability, involve the effects of finite magnetic diffusivity and finite electron thermal conductivity and can have phase velocities in either directions [2].

References

- [1] B. Coppi and T. Zhou, Phys. Lett. (2011) 2916 and B. Coppi and T. Zhou, Phys. Plasmas, **19** (2012) 012302.
- [2] B. Coppi and T. Zhou, MIT(LNS) Report HEP 09/04 (2011), Cambridge, MA, to be submitted to Phys. Plasmas.

Sponsored in part by the U.S. DOE.

TH-P

Study of Neoclassical Toroidal Viscosity in Tokamaks with a δf Particle Code and Resonant Nature of Magnetic Braking

K. Kim¹, J. K. Park¹, G. Kramer¹, A. Boozer², and J. Menard¹

¹*Princeton Plasma Physics Laboratory, Princeton, USA*

²*Columbia University, New York, USA*

Corresponding Author: kkim@pppl.gov

Non-axisymmetric magnetic perturbations can fundamentally change neoclassical transport in tokamaks by distorting particle orbits on deformed or broken flux surfaces. Understanding transport under non-axisymmetric magnetic perturbations is a critical issue for ITER and future fusion devices where non-axisymmetric perturbations are potentially important control elements to actively stabilize locked modes, edge localized modes, and resistive wall modes. Neoclassical transport with non-axisymmetry, often called Neoclassical Toroidal Viscosity (NTV) transport in tokamaks, is intrinsically non-ambipolar, and highly complex depending on parametric regimes. Thus a numerical approach is required to achieve its precise description. This paper reports the study of non-ambipolar transport and NTV torque with a new δf particle code, and the improved understanding of magnetic braking in perturbed tokamaks. Initial calculation of non-ambipolar particle flux clearly indicates the strong resonant nature of magnetic braking, which is typically supposed as driven by non-resonant perturbations, while bootstrap current shows resonant or non-resonant features depending on collisionality. In addition, NTV torque is directly estimated by calculating anisotropic pressures and utilizing magnetic field spectrum method. Calculation results of NTV compared with theory and experiments will be reported, and detailed analyses on magnetic braking in tokamaks such as NSTX will be discussed.



This work was supported by the US DOE Contract # DE-AC02-09CH11466.

Use of the 3D-MAPTOR Code in the Study of Magnetic Surfaces Break-up due to External Non-Axisymmetric Coils

J. Herrera-Velázquez¹, E. Chávez-Alarcon², and R. Celso³

¹*Instituto de Ciencias Nucleares, Universidad Nacional Autónoma de México, Mexico*

²*Instituto Nacional de Investigaciones Nucleares, D. F. México, México*

³*Facultad de Ingeniería Mecánica y Eléctrica, Universidad Autónoma de Nuevo León, México*

Corresponding Author: herrera@nucleares.unam.mx

We show how the outer magnetic surfaces can be broken up in a spherical tokamak, by breaking the axisymmetry using an inner tilted coil. The configuration chosen for this work is that of the MEDUSA small spherical tokamak, a small glass chamber device, which allows the introduction of such a coil. The simulation is carried out with the 3D-MAPTOR code developed by the authors. Given an initial condition for the magnetic field, it is integrated from the plasma current profile and the external currents, such as the toroidal and the vertical field. Poincaré maps along the toroidal angle and the image of the field, as seen from above can be plotted. The latter allows the identification of parameters for which the ripple effect is significant.

Anisotropic Heat Transport in Integrable and Chaotic 3-D Magnetic Fields

D. del-Castillo-Negrete¹, L. Chacon¹, and D. Blazevski²

¹*Fusion Energy Division, Oak Ridge National Laboratory, Oak Ridge, USA*

²*University of Texas at Austin, Austin, USA*

Corresponding Author: delcastillod@ornl.gov

Understanding heat transport in magnetized plasmas is a problem of fundamental interest in controlled fusion. Three issues make this problem particularly difficult:

- (a) The extreme anisotropy between the parallel (i.e., along the magnetic field), EMBED Equation.3, and the perpendicular, EMBED Equation.3 conductivities;
- (b) Magnetic field lines chaos which in general precludes the construction of magnetic field line coordinates;
- (c) Nonlocal parallel flux closures in the limit of small collisionality. Motivated by the extreme anisotropy encountered in fusion plasmas, in which the ratio EMBED Equation.3 may exceed 1010, we mainly focus on the study of purely parallel transport, i.e., EMBED Equation.3, but also report on recent extensions of the method to incorporate perpendicular transport and sources.

We propose a Lagrangian-Green's function (LG) that bypasses the need to discretize and invert the transport operators on a grid. The proposed method allows the integration of the parallel transport equation without perpendicular pollution, while preserving the positivity of the temperature field, and it is applicable to local and non-local parallel flux closures in integrable, weakly chaotic, and fully chaotic magnetic fields. We present applications of the method to:

- (1) Non-diffusive radial transport in fully chaotic magnetic fields, and fractal properties in weakly chaotic fields.
- (2) Parallel transport in the presence of internal transport barriers in reversed shear magnetic field configurations.
- (3) Finite EMBED Equation.3 anisotropic transport.

Concerning (1), we provide numerical evidence of non-diffusive effective radial transport (with both local and non-local closures) that casts doubts on the applicability of quasilinear diffusion descriptions. General conditions for the existence of non-diffusive, multivalued flux-gradient relations in the temperature evolution are derived. For (2), we focus on the study of shearless Cantori, i.e., partial transport barriers located at the minimum of q . Finally, regarding (3), we report on recent developments on the applications of the extended LG method to study transport in magnetic islands in the presence of sources with finite $\chi_{\parallel}/\chi_{\perp}$ ratios.

Tomography of 2D Velocity-space Distributions from Combined Synthetic Fast-ion Diagnostics at ASDEX Upgrade

M. Salewski¹, B. Geiger², S. K. Nielsen¹, H. Bindslev³, M. Garcia-Munoz²,
W. W. Heidbrink⁴, S. B. Korsholm¹, F. Leipold¹, F. Meo¹, D. Moseev^{2,5},
P. Michelsen¹, M. Stejner², and G. Tardini²

¹Technical University of Denmark, Roskilde, Denmark

²Max-Planck-Institut für Plasmaphysik, Garching, Germany

³Aarhus University, Aarhus, Denmark

⁴University of California, Irvine, USA

⁵FOM Institute DIFFER, EURATOM-FOM, Nieuwegein, Netherlands

Corresponding Author: msal@fysik.dtu.dk

Collective Thomson scattering (CTS) and fast-ion D α (FIDA) diagnostics measure 1D functions of the 2D fast-ion velocity distribution functions in magnetically confined plasmas. A single such 1D measurement is usually not sufficient to build accurate tomographies of 2D anisotropic fast-ion velocity distribution functions. But we can compute tomographies from several simultaneous 1D CTS and FIDA measurements. Such reconstructions contain salient features of the underlying 2D fast-ion velocity distribution functions as was shown theoretically in 2004 for two and three synthetic 1D CTS measurements. Since then FIDA measurements have been demonstrated, and several tokamaks have been equipped with multiple FIDA views. In 2012, a second CTS receiver and a second FIDA optical head have been installed on ASDEX Upgrade, so that four simultaneous 1D measurements of the 2D fast-ion distribution function are now possible if CTS and FIDA measurements are used together. We reconstruct 2D fast-ion velocity distribution functions from TRANSP/NUBEAM using combined synthetic 1D CTS and FIDA measurements. Here we develop a new reconstruction prescription that makes use of the recent idea of weight functions. In the past, reconstruction algorithms were made tractable by expansion of the 1D (synthetic) measurements as well as the 2D fast-ion velocity distribution functions into orthonormal sets of base functions. Exploiting CTS or FIDA weight functions we are lead to a simpler reconstruction prescription that is inherently tractable and obviates the use of such expansions. Our prescription is analogue to a tomography but in velocity space rather than in configuration space. Computed tomography in configuration space is widely used in medical imaging (X-ray, PET, MRI scanners) and also in nuclear fusion research. With our prescription we can build tomographies of the 2D velocity distribution function for any set of 1D fast-ion measurements obtained for any machine with multiple CTS or FIDA views or a mix of these. Applying our prescription to a set of real 1D fast-ion measurements will yield an entirely experimentally determined 2D fast-ion velocity distribution function that can be compared with simulations.

Sideways Wall Force Produced during Disruptions

H. Strauss¹, R. Paccagnella², J. Breslau³, L. Sugiyama⁴, S. Jardin³, and R. Sayer⁵

¹*HRS Fusion, West Orange, USA*

²*Consorzio RFX and Istituto Gas Ionizzati del C.N.R., Padova, Italy*

³*Princeton Plasma Physics Laboratory, Princeton, USA*

⁴*MIT, Cambridge, USA*

⁵*CS Engineering, Oak Ridge, USA*

Corresponding Author: hank@hrsfusion.com

A critical issue for the ITER device construction is to evaluate the forces produced on the surrounding conducting structures during plasma disruptions [1]. In this work we extend previous studies of vertical displacement events (VDE) combined with disruptions [2]. The emphasis is on the non axisymmetric “sideways” wall force. The disruptions are simulated using the M3D [3] code, which solves resistive MHD equations. We model an ITER scenario, starting from an ITER reference equilibrium at 15 MA, which can be unstable, in the event of control failure, to a vertical displacement event (VDE). The VDE is allowed to evolve until the plasma touches the wall. When the original separatrix poloidal flux contour passes through the wall, the last closed flux surface has approximately $q = 2$. At this point the plasma is unstable to an $(m, n) = (2, 1)$ external kink or resistive wall mode. This mode causes an $n = 1$ halo current to flow to the wall, producing the sideways force. The wall force depends strongly on the ratio of the wall penetration time to the mode growth time. When this ratio is large, the wall force asymptotes to a relatively smaller value, well below the critical value ITER is designed to withstand. The simulational parameters have been made more realistic than previous simulations [2] by increasing S more than an order of magnitude. A weak dependence of sideways force on S is found. In addition to ITER, we have studied disruptions in NSTX in order to validate our model. Simulations of axisymmetric VDEs have been carried out by using the 2D TSC code with a more detailed model of the NSTX wall than in previous studies [4]. Comparison of the axisymmetric and asymmetric VDE simulations will be presented.

References

- [1] T. Hender *et al.*, Nuclear Fusion **47** (2007) S128-202.
- [2] H. R. Strauss, R. Paccagnella, and J. Breslau, Phys. Plasmas **17** (2010) 082505.
- [3] W. Park, E. V. Belova, G. Y. Fu, X. Tang, H. R. Strauss, L. E. Sugiyama, Phys. Plasmas **6** (1999) 1796.
- [4] R. O. Sayer, Y. K. M. Peng, S. C. Jardin, A. G. Kellman, J. C. Wesley, Nuclear Fusion **33** (1993) 969.

An Investigation of Coupling of the Internal Kink Mode to Error Field Correction Coils in Tokamaks

E. Lazarus¹

¹ *Oak Ridge National Laboratory, Oak Ridge, USA*

Corresponding Author: lazarus@fusion.gat.com

The coupling of the internal kink to an external $m/n = 1/1$ perturbation is studied for profiles that are known to result in a saturated internal mode in the limit of a cylindrical tokamak. 3D equilibria are calculated with the VMEC code.

If a small $m/n = 1/1$ perturbation is applied to the boundary, it is found that for aspect ratios $A = 30$ circular plasmas and $A = 3$ elliptical shapes that the coupling is strong. That is, the magnitude of the perturbation at $q = 1$ is much larger than the edge perturbation for edge perturbations in the range $\delta R/R_0 \approx 10^{-3} - 10^{-4}$. Without the edge perturbation the saturated mode is not observed in toroidal geometry, even at very large aspect ratio.

Plasma shapes that are favorable for MHD stability tend to have large sawtooth crashes. These crashes can be problematic in that they can trigger neoclassical tearing modes, they can interfere with ELM-suppression produced by RMP, and in the most severe cases can result in a prompt loss of 15% of total stored energy beyond the last closed flux surface.

Typically, modern shaped tokamaks have error field correction coils. These coils are often needed during the plasma current ramp to prevent locked modes. However, once the nominal operating point is achieved, they are no longer needed. It is proposed that this $m/n = 1/1$ excitation could readily be applied with these error field correction coils. This should be explored as a mechanism for controlling sawtooth amplitudes in high performance tokamak discharges.

Stabilizing Regimes of Edge Current Density for Pedestal Instabilities

P. Zhu¹, C. Hegna¹, and C. Sovinec¹

¹*University of Wisconsin-Madison, Madison, USA*

Corresponding Author: pzhu@wisc.edu

Resistive MHD computations using the NIMROD code find stabilizing effects of edge current density distribution on the low- n instabilities localized in the edge pedestal region. It is widely accepted that the low- n edge localized modes can be driven unstable by increasing the edge current density. The destabilization of the edge current driven peeling modes is reproduced in our computations for a tokamak equilibrium with a modest pedestal height. However, for a higher pedestal equilibrium with sufficiently large edge current density, the q profile develops a region where the magnetic shear becomes negative. In this regime, the low- n edge instabilities are partially or fully stabilized. The stabilizing effects of edge current density in regions with reversed magnetic shear appear to be consistent with a necessary condition for peeling mode stability from analytical theory. Nonlinear simulations indicate that the stabilizing effects of edge current density on the low- n edge instabilities through reverse shear can persist throughout the nonlinear exponential growth phase. These stabilizing effects delay the subsequent nonlinear stage, during which the filament size in the radial direction exceeds the pedestal width and disconnected blob-like substructures start to develop within the filaments. The energy loss from these radially extending filaments can reach above 10% of the total energy in pedestal. We present a systematic study on the stabilizing regimes of edge current density, and use nonlinear simulations to explore how these regimes can be exploited for the control of edge localized instabilities in experiments.



Simulation of Sawteeth and other Global Macroscopic Dynamics of Tokamak Plasmas on the Transport Timescale

S. C. Jardin¹, N. Ferraro², N. Breslau¹, and J. Chen¹

¹*Princeton Plasma Physics Laboratory, Princeton, USA*

²*General Atomics, San Diego, USA*

Corresponding Author: jardin@pppl.gov

Recent advances in implicit numerical algorithms for solving the 3D extended magneto-hydrodynamic equations in strongly magnetized plasmas have enabled massively parallel simulations of the internal global dynamics of tokamaks that can use very large time steps which allow one to span the timescales of ideal MHD stability, magnetic reconnection, and particle, energy, and momentum transport. It is now possible and feasible to run these high-resolution time-dependent initial value simulations for 10^6 or more Alfvén times so as to span all relevant timescales in a single simulation. A transport model is specified by prescribing functions for the plasma resistivity, viscosity, particle diffusivity, and thermal conductivities. The calculations are then run long enough so that the system reaches either a stationary state or exhibits time-periodic behavior. We have identified different regimes that correspond to: periodic sawteeth events without precursors, stationary helical states with flow, or periodic behavior involving semi-stationary helical states (or precursors) together with sawteeth crashes. The parameter regimes for these different behaviors are mapped out and discussed for both single fluid and 2-fluid MHD.

Impurity Transport due to Electromagnetic Drift Wave Turbulence

S. Moradi¹, I. Pusztai¹, T. Fülöp¹, and A. Mollén¹

¹ *Chalmers University of Technology, Göteborg, Sweden*

Corresponding Author: sara@nephy.chalmers.se

In the view of an increasing interest in high β operation scenarios, such as hybrid scenarios for ITER the question of finite β effects on the impurity transport is a critical issue due to possible fuel dilution and radiative cooling in the core. Here, electromagnetic effects at finite β on impurity transport are studied through local linear gyrokinetic simulations with GYRO [1] in particular we investigate the parametric dependences of the impurity peaking factor (zero-flux density gradient) and the onset of the kinetic ballooning modes (KBM). Our results show that for the considered plasma parameters two possible modes can be unstable depending on the normalized electron pressure; ion temperature gradient (ITG) modes dominate in the region β_e less than 0.015, while KBM dominate for β_e greater than 0.015. The KBM instability threshold depends on the plasma parameters, particularly strongly on plasma shape. We have shown that magnetic geometry significantly influences the results, and the commonly used s-alpha model overestimates the KBM growth rates and ITG stabilization at high β . The β_e scaling of the impurity peaking factor shows two branches in connection with the two branches of the unstable modes present. We find that electromagnetic effects even at low β can have significant impact on the impurity transport. In the ITG branch the peaking factor increases with β_e with strong charge dependence and this dependence increases as β_e increases, however, for heavy impurities with lower charge to mass ratio such as tungsten, lower peaking factors with very little β_e dependence is observed. In the β range where the KBM is the dominant instability the impurity peaking factor is strongly reduced, with very little dependence on β and the impurity charge.

References

- [1] J. Candy and E. Belli, General Atomics Report GA-A26818 (2011).

Application of Particle-In-Cell Methods for Stellarators

R. Kleiber¹, M. Borchardt¹, T. Fehér¹, R. Hatzky², K. Kauffmann¹, A. Könies¹,
A. Mishchenko¹, J. Regaña¹, and O. Zacharias¹

¹*Max-Planck-Institut für Plasmaphysik, EURATOM-Association, Greifswald, Germany*

²*Max-Planck-Institut für Plasmaphysik, EURATOM-Association, Garching, Germany*

Corresponding Author: ralf.kleiber@ipp.mpg.de

Particle-in-cell methods are an efficient way of simulating the gyrokinetic equation especially in complicated three-dimensional configurations such as stellarators because they are relatively easy to implement and show a good scaling behaviour on parallel machines. It is however necessary to employ variance reduction techniques in order to decrease the noise inherent to particle methods. Especially if electromagnetic effects are included, it is necessary to use an adaptive control variate technique to overcome the, so called, cancellation problem.

The code EUTERPE is a global (full radius, full flux surface) gyrokinetic particle-in-cell code which, for three-dimensional equilibria provided by the VMEC equilibrium code, is able to simulate up to three kinetic species (ions, electrons, fast/impurities). It solves the field equations for the electrostatic and parallel vector potentials and can be used for linear and nonlinear simulations. We give an overview of recent developments and applications of this code:

- Linear simulations of electromagnetic ITG modes in a sequence of Wendelstein 7-X equilibrium configurations with β increasing from zero to 5%. It was found that electromagnetic effects lead to a significant change in the growth rate and frequency of the modes as compared with the electrostatic case.
- For three dimensional systems a new solver for the field equation including the flux surface averaged potential was developed. It allowed to simulate the relaxation towards residual zonal flows in stellarators including an external radial electric field.
- A hybrid model was developed where EUTERPE was coupled with the reduced MHD equilibrium code CKA. This allows the calculation of the energy transfer between fast particles and the MHD mode. This perturbative linear model gives an estimate of the expected growth rate induced by fast particles.
- The implementation of collisions gives the possibility of simulating neoclassical effects using the high flexibility of a Monte-Carlo method.

Nonlinear Error-Field Penetration in Low Density Ohmically Heated Tokamak Plasmas

R. Fitzpatrick¹

¹*Institute for Fusion Studies, University of Texas at Austin, Austin, USA*

Corresponding Author: rfitzp@farside.ph.utexas.edu

A theory is developed in order to predict the error-field penetration threshold in low density, ohmically heated, tokamak plasmas. The novel feature of the theory is that the response of the plasma in the vicinity of the resonant surface to the applied error-field is calculated from nonlinear drift-MHD magnetic island theory, rather than linear layer theory. Error-field penetration, and subsequent locked mode formation, is triggered when the destabilizing effect of the resonant harmonic of the error-field overcomes the stabilizing effect of the ion polarization current (caused by the rotation of the error-field-induced island chain in the local ion fluid frame). The predicted scaling of the error-field penetration threshold with engineering parameters is

$$(b_r/B_T)_{\text{crit}} = n_e \cdot B_T^{-1.8} \cdot R_0^{-0.25}, \quad (1)$$

where b_r is the resonant harmonic of the vacuum radial error-field at the resonant surface, B_T the toroidal magnetic field-strength, n_e the electron number density at the resonant surface, and R_0 the major radius of the plasma. This scaling — in particular, the linear dependence of the threshold with density — is consistent with experimental observations. When the scaling is used to extrapolate from JET to ITER, the predicted ITER error-field penetration threshold is $(b_r/B_T)_{\text{crit}} = 5 \times 10^{-5}$, which just lies within the expected capabilities of the ITER error-field correction system.

Coupling of Current and Flow Relaxation in Reversed-Field Pinches due to Two-Fluid Effects

C. Sovinec¹, J. King^{1,2}, J. Sauppe¹, V. Mirnov¹, J. Sarff¹, and W. Ding³

¹ *University of Wisconsin-Madison, Madison, USA*

² *Tech-X Corporation, Boulder, USA*

³ *University of California at Los Angeles, Los Angeles, USA*

Corresponding Author: csovinec@cae.wisc.edu

We present a computational study of the coupling between dynamo and momentum transport, motivated by findings of two-fluid effects in the Madison Symmetric Torus (MST). Laser polarimetry and magnetic probes measure correlated current-density and magnetic-field fluctuations during sawtooth events [1,2]. With ion skin depths being $0.1 - 0.2 a$, the correlation implies significant Hall dynamo effect. It also implies net Lorentz force from the fluctuations, which can act to redistribute parallel flow. Linear computations elucidate the underlying magnetic tearing and show electron-ion decoupling from kinetic-Alfvén-wave (KAW) physics when the sound gyroradius exceeds the resistive tearing width. With warm ions, results also produce a drift regime, where growth rates are smaller than in the resistive-MHD limit [3]. Analysis shows that the ion drift results from poloidal curvature and the radial variation of B , both of which are significant in pinch profiles. Nonlinear multi-helicity simulations qualitatively and semi-quantitatively reproduce the Hall dynamo and the flow profile relaxation that are observed in the laboratory [4]. The scaled magnitude of the computed Hall dynamo is comparable to the 40 V/m inferred from core-mode correlations in 400 kA MST discharges. Relaxation in our two-fluid modeling affects flows parallel to the large-scale B -field, inducing a net increase in the core and a net decrease in the edge. The orientation of this change is consistent with observations, and the magnitude is comparable to the 10 km/s in MST. Computations also reproduce competing Reynolds stress from flow fluctuations, which has been measured through Mach probes in the edge of MST [2]. The helicity of the large-scale B -field can affect the relative orientation of current-profile and flow-profile relaxation, and computational results on its influence are presented. Also, relaxation in MST starts with a net flow profile, and numerical results with and without initial flow are compared.

References

- [1] W. X. Ding, D. L. Brower, *et al.*, Phys. Plasmas **13** (2006) 112306.
- [2] A. Kuritsyn, G. Fiksel, *et al.*, Phys. Plasmas **16** (2009) 55903.
- [3] J. R. King, C. R. Sovinec, and V. V. Mirnov, Phys. Plasmas **18** (2011) 42303.
- [4] J. R. King, C. R. Sovinec, and V. V. Mirnov, accepted for publication in Phys. Plasmas.

Supported by US DOE DE-FG02-06ER5480, DE-FG02-85ER53212, and NSF PHY-0821899.

Nonlinear Acceleration Mechanism of Collisionless Magnetic Reconnection

M. Hirota¹, P. Morrison², Y. Ishii¹, M. Yagi¹, and N. Aiba¹

¹*Japan Atomic Energy Agency, Naka, Japan*

²*University of Texas at Austin, Austin, USA*

Corresponding Author: hirota.makoto@jaea.go.jp

A mechanism for fast magnetic reconnection in collisionless plasma is studied for understanding sawtooth collapse in tokamak discharges. Nonlinear growth of the tearing mode driven by electron inertia is analytically estimated by invoking the energy principle for the first time. Decrease of potential energy in the nonlinear regime (where the island width exceeds the electron skin depth) is found to be steeper than in the linear regime, resulting in acceleration of the reconnection. Release of free energy by such ideal fluid motion leads to unsteady and strong convective flow, which theoretically corroborates the inertia-driven collapse model of the sawtooth crash [1].

References

[1] D. Biskamp and J. F. Drake, Phys. Rev. Lett. **73** (1994) 971.

Pedestal Modelling Based on Ideal MHD and Gyrokinetic Stability Analyses on JET And ITER Plasmas

S. Saarelma¹, M. Beurskens¹, T. Casper², I. Chapman¹, D. Dickinson^{1,3},
L. Frassinetti⁴, G. Huijsmans², A. Kirk¹, O. Kwon⁵, M. Leyland³, J. Lee⁶, A. Loarte²,
Y. Na⁶, C. Roach¹, and H. Wilson²

¹*Euratom/CCFE Fusion Association, Culham Science Centre, Abingdon, UK*

²*ITER Organization, St. Paul Lez Durance, France*

³*York Plasma Institute, Department of Physics, University of York, York, UK*

⁴*Division of Fusion Plasma Physics, Royal Institute of Technology, Association
EURATOM-VR, Stockholm, Sweden*

⁵*Department Of Physics, Daegu University, Gyungbuk, Republic of Korea*

⁶*Department of Nuclear Engineering, Seoul National University, Seoul, Republic of Korea*

Corresponding Author: samuli.saarelma@ccfe.ac.uk

The H-mode pedestal is crucial for the good confinement of a tokamak fusion plasma. In this paper we analyze the stability of the pedestal used in ITER transport simulations and show that a pedestal temperature of 6.1 keV (corresponding to 115 kPa) is at the stability limit of a type I ELMy H-mode pedestal limited by peeling-ballooning modes. We also show that the pedestals assumed in the ramp-up and ramp-down simulations are within the stability limits.

To get further understanding at the pedestal development, we investigate ideal MHD and gyrokinetic stability in the pedestal of two well-diagnosed JET discharges. We find that both infinite- n ideal MHD ballooning and kinetic ballooning modes (KBM) are in the second stable region due to a bootstrap current peak driven by the pedestal pressure gradient. This indicates that the pedestal pressure gradient in JET is not limited by the KBMs during the inter-ELM period. The experimental observation of steady increase of the edge pressure gradient during the inter-ELM period in low fuelling plasma further confirms that the edge pressure gradient is not limited until an ELM crash that is triggered by the peeling-ballooning modes. This is in strong contrast with the earlier analysis of MAST pedestals where the entire pedestal was found KBM unstable and no increase of pressure gradient during the ELM cycle was observed [1].

The results from the gyrokinetic analysis indicate that the pedestal evolution in JET is not controlled by KBMs. It is likely that ITER pedestals with a large bootstrap current peak are also stable against KBMs.

References

- [1] Dickinson D. *et al.*, Plasma Phys. Controlled Fusion, **53** (2011) 115010.

Coupled Simulations of RF Effects on Tearing Modes

S. Kruger¹, T. Jenkins¹, E. Held², J. Ramos³, J. King¹, D. Schnack⁴, and R. Harvey⁵

¹*Tech-X Corporation, Boulder, USA*

²*Utah State University, Logan, USA*

³*Massachusetts Institute of Technology, Cambridge, USA*

⁴*University of Wisconsin-Madison, Madison, USA*

⁵*CompX Corporation, Dallas, USA*

Corresponding Author: kruger@txcorp.com

We present integrated feedback simulations of neoclassical tearing modes in tokamak plasmas. The implementation relies on the NIMROD and GENRAY codes, along with new codes for calculating a local quasilinear operator, and for performing the code coupling. The mathematical formulation relies on the formulation of a third-order electron drift-kinetic equation that captures the bootstrap current effects and is consistent with ECCD-driven kinetic distortion effects such as the Fisch-Boozer and Ohkawa current drives. Numerically solving the drift-kinetic equation relies on a new high-order continuum discretization scheme suitable for solving the equation in the presence of a macroscopic three-dimensional magnetic field. Implementing these new kinetic closures implicitly, along with the drift-kinetic terms, provides many numerical challenges and requires careful verification.



A Flute Instability in an Open System and the Line Tying Effect on it

I. Katanuma¹, S. Sato¹, and Y. Okuyama¹

¹ *University of Tsukuba, Tsukuba, Japan*

Corresponding Author: katanuma@prc.tsukuba.ac.jp

A flute instability is the most dangerous instability to an open system such as GAMMA10. A line tying is a powerful tool for stabilizing a flute instability because the magnetic field lines terminate at the conducting ends in an open system. Firstly, a particle simulation was performed to investigate a flute instability and the line tying effect on it. Here the particle code takes into account the electron inertia along a magnetic field line precisely and the code (two and half dimension) adopts the implicit method so that it can calculate the problems with large space and time scales. The particle simulation has revealed the mechanism of an appearance of the line tying in a flute instability. That is, the acceleration of electrons due to a flute instability was found to be responsible for the line tying, but not the electron thermal speed. There is not, however, a stability boundary resulting from line tying in the linear phase of a flute instability. We have newly found the nonlinear (quasilinear) stability criterion to a flute instability with conducting ends. Secondly, a reduced MHD simulation was carried out in order to investigate the line tying effect of the limiters on a flute instability in GAMMA10. There are two limiters (named MLO) at $z = 7$ m and -7 m in GAMMA10, which are inserted into the plasma, where the radius of the limiter is 0.115 m mapped at the central cell. The plasma radius is 0.18 m at the central cell, so that the plasma escaping from the central cell touches MLO. MLO is expected to have an effect of line tying on a flute instability in GAMMA10 in the light of the nonlinear (quasilinear) stability criterion found by a particle simulation. The reduced MHD code solves the time evolution of vorticity, mass density, temperature and electrostatic potential in two-dimensional cross section perpendicular to the magnetic field lines. The centrifugal acceleration of ions resulting from a magnetic field line curvature is included in the radial dependence of magnetic field line specific volume. The line tying effect of MLO is taken into account by setting the fluctuating part of vorticity being zero in $r > 0.115$ m, because the vorticity plays a role of charge density in the frame of MHD. The reduced MHD simulation has revealed that MLO has a stabilizing effect on the flute instability, which is consistent with the experimental observation.

TH-P

Impurity Mixing in Massive-Gas-Injection Simulations of DIII-D

V. A. Izzo¹, P. B. Parks²

¹*University of California San Diego, San Diego, USA*

²*General Atomics, San Diego, USA*

Corresponding Author: izzo@fusion.gat.com

Simulations of massive-gas-injection (MGI) in DIII-D have been carried out with the extended MHD code NIMROD in order to study the role of 2D and 3D plasma flows, specifically those associated with the $m = 1/n = 1$ instability, in mixing injected impurities into the core. In a simulation with poloidally and toroidally symmetric impurity injection, we find that the impurity distribution does not remain poloidally symmetric through the initial phase of the simulation, rather 2D flow patterns tend to concentrate impurities on the outboard midplane. The first MHD instabilities to appear have $q > 1$, but these modes have little effect on impurity mixing. However, the $1/1$ mode that is responsible for the final drop in core T_e during the thermal quench also produces a 3D flow pattern that pulls the outboard localized impurity blob toward the magnetic axis, producing a rapid increase in the core impurity density, and further enhancing core cooling. In further simulations, we switch to poloidally asymmetric impurity sources localized respectively on the high-field- and low-field-sides of the torus. In each case the MHD onset time following the initial edge cooling is found to be approximately the same, and the impurity mixing efficiencies for the three scenarios are compared. Finally, these mixing results are further compared with simulations in which the source is also toroidally asymmetric. The results are analyzed with goal of optimizing the efficacy of massive gas injection, particularly toward the goal of collisional suppression of runaway electrons.

TH-P

Work supported by the US DOE under DE-FG02-95ER54309.

Multi-Scale MHD Analysis of Heliotron Plasma in Change of Background Field

K. Ichiguchi¹, S. Sakakibara¹, S. Ohdachi¹, and B. A. Carreras²

¹*National Institute for Fusion Science, Toki, Japan*

²*BACV Solutions Inc., Oak Ridge, USA*

Corresponding Author: ichiguch@nifs.ac.jp

The mechanism of a partial collapse observed in the experiments with the change of the background magnetic field in the Large Helical Device (LHD) is investigated with a nonlinear MHD simulation by utilizing a multi-scale numerical scheme. It is crucial to predict the MHD stability boundary in the design of future reactors. However, systematic procedure for the prediction has not been established in heliotron configurations. In LHD, experiments were carried out to find the stability boundary as a function of the horizontal position of the vacuum magnetic axis. In these experiments, the background magnetic field is changed during each shot so that the corresponding vacuum magnetic axis position is shifted inwardly. A partial plasma temperature collapse happens during the shift of the magnetic axis. In the present work, we investigate the mechanism of this partial collapse with a numerical MHD approach. To incorporate the change of the background field, we have to treat the time evolution of the equilibrium as well as the perturbations. Since the time scale of the equilibrium change is much longer than that of the perturbations, we utilize a multi-scale numerical scheme. In the scheme, time-dependent nonlinear dynamics calculations and updates of a static equilibrium are iterated. By applying the method to the LHD plasma, we identify the collapse mechanism. In the time evolution, a nonlinear saturation occurs after the linear growth of the perturbation. In the linear phase, the growth is accelerated by the real-time enhancement of the magnetic hill due to the change of the background magnetic field. The instability has the characteristic properties of an infernal mode. At saturation, the core pressure is degraded in a short time. The degradation is caused by the vortices of the infernal mode, which corresponds to the partial collapse observed in the experiments. We also compare the time evolutions with and without the change of the background magnetic field, and obtain that the plasma with the change is more unstable than that without the change. This tendency agrees with the experiments. Further extension of this simulation can reveal the key physics of the collapse onset, which will be necessary for the prediction of the stability boundary in the reactor design.

TH-P

Rotational Stabilization of the Resistive Wall Modes in Tokamaks

V. Pustovitov¹

¹*National Research Centre “Kurchatov Institute”, Moscow, Russian Federation*

Corresponding Author: pustovit@nfi.kiae.ru

The paper is devoted to studying the combined effect of the mode rotation and energy dissipation in the resistive wall on the plasma stability. The problem is analyzed on the basis of the energy approach complementing the standard methods of the traditional MHD theory of plasma stability. The key element that makes our model different from this theory and commonly used thin-wall approaches to the stability analysis of the resistive wall modes (RWMs) is the incorporation of the skin effect. In the ideal MHD theory of plasma stability, the skin depth is, formally, zero. On the contrast, the thin-wall theory of the RWM stability assumes the skin depth much larger than the wall thickness. The presented model considers the intermediate case with a finite skin depth compared to the wall thickness. This corresponds to the modes in-between the typical RWMs and the ideal MHD modes, but the wall resistivity is still an important factor affecting the modes dynamics. It is shown that, in this region, the growth rates of the locked modes must be one-two orders larger than the calculated in the thin-wall models. On the other hand, the fast RWMs can be completely stabilized by the mode rotation above some critical level. Qualitatively, this corresponds to the rotational stabilization observed in the DIII-D tokamak and allowing the plasma operation above the no-wall stability limit [1]. This is the main result of this study which is completely analytical with all dependencies explicitly shown. In particular, the dispersion relations for the fast RWMs and the critical frequency of the mode rotation necessary for the rotational stabilization are expressed through the quantities that depend on the plasma parameters or can be experimentally found by the magnetic measurements outside the plasma. Theoretical and experimental applications of the results are also discussed.

References

- [1] E. J. Strait *et al.*, Phys. Plasmas **11** (2004) 2505.

The EPED Pedestal Model: Extensions, Application to ELM-Suppressed Regimes, and ITER Predictions

P. B. Snyder¹, T. H. Osborne¹, K. H. Burrell¹, J. Candy¹, R. J. Groebner¹,
A. W. Leonard¹, R. Nazikian², D. Orlov³, O. Schmitz⁴, M. R. Wade¹, and
H. R. Wilson⁵

¹*General Atomics, San Diego, USA*

²*Princeton Plasma Physics Laboratory, Princeton, USA*

³*University of California San Diego, La Jolla, USA*

⁴*Forschungszentrum Jülich, Jülich, Germany*

⁵*The University of York, York, USA*

Corresponding Author: snyder@fusion.gat.com

The pressure at the top of the edge transport barrier (or “pedestal height”) strongly impacts global confinement and fusion performance, while large ELMs can significantly limit component lifetimes. Hence, accurately predicting the pedestal height in ITER, as well as developing a predictive understanding of ELM suppression, are essential. The EPED model predicts the H-mode pedestal height and width based upon two fundamental and calculable constraints:

1. Onset of non-local peeling-ballooning (P-B) modes at low to intermediate mode number.
2. Onset of nearly local kinetic ballooning modes (KBM) at high mode number.

The model calculates both constraints directly with no fit parameters, using ELITE to calculate the P-B constraint, and a “BCP” technique, supplemented by gyrokinetic eigenvalue calculations with GYRO, to calculate the KBM constraint. EPED has been successfully compared to observed pedestal height for 259 cases on 5 tokamaks, finding agreement within $\sim 20\%$. Major new results are successful testing of EPED in Quiescent H-Mode discharges, and the development of a working model to understand ELM suppression by resonant magnetic perturbations (RMPs). Dynamically, the ELM crash is typically followed by a recovery, in which the pressure gradient encounters the KBM limit, but the pedestal can continue to broaden until the P-B boundary is reached, an ELM is triggered, and the cycle repeats. The ELM can be suppressed if this recovery phase is interrupted such that the width of the edge barrier is prevented from continuing to broaden. We propose an EPED-based working model for suppression of ELMs by RMPs in which the conceptual “wall” is provided by a resonant island or stochastic region that drives strong transport and prevents inward pedestal propagation. This leads to predictions of specific profile changes and ranges of q in which ELM suppression is possible, which agree with initial tests on DIII-D. EPED predictions for ITER have been made for more than 100 baseline and hybrid cases, finding a high pedestal that is further optimized at high density. Detailed predictions, including expected requirements for QH Mode and RMP ELM suppression, as well as coupling to core transport predictions, will be discussed.

Work supported in part by the US DOE under DE-FG02-95ER54309, DE-FC02-04ER54698, DE-AC02-09CH11466, and DE-FG02-07ER54917.

Convective Electron Motion in Low Frequency Collisionless Trapped Electron Turbulence

Y. Xiao¹, Z. Lin²

¹*Institute for Fusion Theory and Simulation, Zhejiang University, Hangzhou, China*

²*University of California, Irvine, USA*

Corresponding Author: yxiao@zju.edu.cn

Collisionless trapped electron mode (CTEM) is an important instability candidate for burning plasmas that leads to electron turbulent transport, since the high energy alpha particles produced by fusion reactions will first heat electrons to enhance the electron temperature. Global gyrokinetic particle simulation of CTEM turbulence in toroidal plasmas using the Gyrokinetic Toroidal Code (GTC) finds both diffusive and convective electron motion using a Lagrangian analysis of the self-consistent particle orbits. A resonance broadening model fits well the diffusive and convective electron motion. The diffusion component is mainly contributed by the deeply trapped electrons, while the convection component could be caused by either deeply or barely trapped electrons. The kinetic origin of this convective motion is identified to arise from the conservation of the second invariant when trapped electrons lose kinetic energy to the drift wave through toroidal precessional resonance. The relation between the convection velocity and kinetic energy loss of the trapped electron is predicted by analytic theory and verified by simulation quantitatively. The conservation of second invariant is found to act as a powerful constraint in low frequency turbulent transport, which can induce a convective motion by losing/gaining energy. This discovery has extensive applications in many fusion-related scenarios.

Stabilization of Resistive Wall Modes by Magnetohydrodynamic Equilibrium Change Induced by Plasma Toroidal Rotation

J. Shiraishi¹, N. Aiba², N. Miyato¹, and M. Yagi¹

¹*Japan Atomic Energy Agency, Rokkasho, Japan*

²*Japan Atomic Energy Agency, Naka, USA*

Corresponding Author: shiraishi.junya@jaea.go.jp

It is shown for the first time that magnetohydrodynamic (MHD) equilibrium change induced by plasma toroidal rotation significantly reduces the growth rates of resistive wall modes (RWMs). Moreover, the equilibrium change can open the stable window even if there is no window under the assumption that the rotation affects only the linear dynamics, which is employed in conventional numerical studies. The rotation modifies the equilibrium pressure, current density, and mass density profiles, which results in the change of the potential energy including rotational effects. To study the effect of equilibrium change, a new code has been developed. The RWMaC modules, which solve electromagnetic dynamics in vacuum and the resistive wall, have been implemented in the MINERVA code, which solves the linearized ideal MHD equations with rotation in tokamak geometry.

Tearing Mode Stability in a Toroidally Flowing Plasma

A. Sen¹, D. Chandra¹, and P. K. Kaw¹

¹*Institute for Plasma Research, Bhat, India*

Corresponding Author: senabhijit@gmail.com

We report on an analytic calculation of Δ' , the tearing mode stability index, in a toroidal tokamak geometry with an equilibrium sheared toroidal flow. A flow modified external kink equation is derived and a boundary layer formalism is adopted. The “outer” solutions of this equation, obtained analytically using a perturbation theory are matched asymptotically to the analytic ideal “inner” solutions to get a closed expression for Δ' in terms of the plasma parameters. Our calculations are a generalization of the earlier work, see Ref. [1]. In the cylindrical limit we also recover the results of Ref. [2] that shows the destabilizing effect of purely axial flows. For a purely toroidal flow the various flow dependent terms of the “inner” solutions are compared and the nature of their contributions analyzed to delineate their influence on Δ' . We also extend our results to include finite β corrections and nonlinear modifications arising from considerations of finite width of the island in the calculation of Δ' . Our analytic expressions should prove useful in providing a rigorous basis for assessing the validity of various ansatz for Δ' that are currently being used to explain experimental data and to benchmark MHD code calculations of this stability index.

References

- [1] Hegna and Callen, Phys. Plasmas **1** (1994) 2308.
- [2] Gimblett *et al.*, Phys. Plasmas **3** (1996) 3619.



Interplay between MHD and Particle Transport during Sawteeth

X. Garbet¹, T. Nicolas¹, R. Sabot¹, H. Lütjens², J. F. Luciani², F. Halpern³,
R. Guirlet¹, J. Decker¹, and A. Merle¹

¹CEA, IRFM, St-Paul-Lez-Durance, France

²Centre de Physique Théorique, École Polytechnique, Palaiseau, France

³CRPP, EPFL, Association Euratom-Suisse, Lausanne, Switzerland

Corresponding Author: xavier.garbet@cea.fr

In this contribution, the plasma density evolution in sawtooth regime on the Tore Supra tokamak is studied. The density is measured using a novel fast-sweeping X-mode reflectometry technique, which is fast enough to allow tomographic reconstructions. There is strong evidence that temperature and density are governed by different mechanisms. Postcursor oscillations sometimes lead to the formation of a density plateau, which is explained in terms of the convection cells associated with the kink mode. A crescent-shaped density structure located inside the $q = 1$ surface is often visible just after the crash and indicates that a significant part of the density withstands the crash and is reinjected inside the surface. 3D full bifluid and nonlinear MHD simulations with the XTOR-2F code recover this structure and show that it arises from the perpendicular flows emerging from the reconnection layer.

Magnetic Island Dynamics under External Magnetic Perturbation in Rotating Resistive Tokamak Plasma

N. Ivanov¹, A. Kakurin¹, and S. Konovalov¹

¹*National Research Centre “Kurchatov Institute”, Moscow, Russian Federation*

Corresponding Author: ivnick@nfi.kiae.ru

The modeling of the magnetic island evolution under RMP in rotating plasma from seed island initial generation, through appearance and development of the NTM till its locking and saturation is presented. The effects of plasma resistivity, viscosity, diamagnetic drift and the effect of the currents induced in the resistive vacuum vessel are taken into account. The calculations are carried out with the TEAR-code based on the non-linear modified Rutherford model. The dependence of the tearing mode stability index on the angular position of the mode with respect to the RMP is taken into account. It results in deviations of the magnetic island rotation velocity from the velocity of the plasma layer in the vicinity of the rational magnetic surface. The magnetic island dynamics under RMP is analyzed for different plasma parameters and mode numbers. The NTM behavior and capabilities of the NTM avoidance or suppression in ITER are discussed for cases of the seed island generation by different RMP sources including the coils for ELM mitigation.

Behavior of Magnetohydrodynamics Modes of Infernal Type at H-mode Pedestal with Plasma Rotation

L. Zheng¹, M. Kotschenreuther¹, and P. Valanju¹

¹*University of Texas at Austin, Austin, USA*

Corresponding Author: lzheng@mail.utexas.edu

Magnetohydrodynamics instabilities of high-mode (H-mode) pedestal are investigated in this paper with the inclusion of bootstrap current for equilibrium and rotation for stability. This may help clarify the physics of edge localized modes (ELMs) and edge harmonic oscillations (EHOs) or outer modes (OMs). The equilibrium of an H-mode discharge at the Jointed European Torus (JET) is reconstructed numerically using VMEC code. It is found that with bootstrap current taken into account, a safety-factor reversal or plateau can be generated near plasma edge. This confirms previous results of numerical equilibrium reconstructions using other types of codes. The low n magnetohydrodynamic instabilities, where n is toroidal mode number, are investigated numerically in this type of equilibria using the AEGIS code. It is found that infernal type harmonic can prevail at safety-factor reversal or plateau region. The toroidal plasma rotation effect related to continuum damping is investigated. The numerical results show that the frequency of marginally stable modes is close the value of rotation frequency at pedestal top, when the value of safety factor at plateau is slightly above a rational number. This mode frequency seems to coincide with experimental observation of the frequencies of edge harmonic oscillations (or outer modes) at quiescent H-mode. We also find that MHD instabilities of such a type of equilibria are sensitive to how close to a rational number the q value at q -plateau is and the distance of the q -plateau to plasma edge. Comparison with experimental observations will also be discussed.

Intrinsic Plasma Rotation Determined by Neoclassical Toroidal Plasma Viscosity in Tokamaks

Y. Sun¹, K. C. Shaing^{2,3}, and Y. Liang⁴

¹*Institute of Plasma Physics, Chinese Academy of Sciences, Hefei, China*

²*Institute for Space, Astrophysical and Plasma Sciences, National Cheng Kung University, Taiwan, Republic of China*

³*Engineering Physics Department, University of Wisconsin, Madison, USA*

⁴*Forschungszentrum Jülich GmbH, Jülich, Germany*

Corresponding Author: ywsun@ipp.ac.cn

Intrinsic steady state plasma rotation is important for plasma confinement in ITER, since the momentum input is expected to be small. It is well known that the intrinsic plasma rotation in stellarators is determined by non-ambipolar diffusion due to helical ripple. The non-ambipolar diffusion due to small 3D magnetic perturbation described by the Neoclassical Toroidal plasma Viscosity (NTV) theory may be important in determining the intrinsic plasma rotation in tokamaks, because the Non-Axisymmetric Magnetic Perturbations (NAMP) always exist. The NTV theory in different collisionality regimes has been well developed in the last few years, and it has been summarized in Ref. [1]. The numerical results showed a good agreement with the analytic solutions in different asymptotic limits [2]. The intrinsic toroidal plasma rotation determined by the NTV effect in tokamaks is investigated in this paper. It is found by searching the root of the ambipolarity constraint $\sum_{j=i,e} e_j \Gamma_j \Omega_\phi = 0$, where Ω_ϕ is the toroidal rotation, and e_j and Γ_j are the electric charge and the particle flux of the j ($i \equiv$ ions, and $e \equiv$ electrons) species. It is found that the result strongly depends on the plasma collisionality. In high collisionality case, the ion flux is dominant and the intrinsic steady state flow is in counter-current direction. It corresponds to the “ion root” named in stellarators. In low collisionality case, there are three roots. One corresponds to the ‘ion root’ in counter-current direction. The second stable one corresponds to the “electron root” in co-current direction, near which the electron flux is dominant. The third one is an unstable root. The NTV torque drives the plasma rotation towards one of the stable roots. This means that the intrinsic toroidal rotation in low collisionality case can also be possible in co-current direction. Both of these two roots scale like the diamagnetic frequency. The prediction of intrinsic rotation due to NTV on ITER will also be discussed.

References

- [1] Shaing *et al.*, Nucl. Fusion **50** (2010) 025022.
- [2] Y. Sun *et al.*, Phys. Rev. Lett. **105** (2010) 145002.

Characteristics of MHD Stability of High Beta Plasmas in LHD

M. Sato¹, N. Nakajima¹, K. Watanabe¹, Y. Todo¹, and Y. Suzuki¹

¹*National Institute for Fusion Science, Toki, Japan*

Corresponding Author: masahiko@nifs.ac.jp

In order to understand characteristics of the MHD stability of high beta plasmas obtained in the LHD experiments, full MHD simulations including the chaotic magnetic field region have been performed for the first time. Nonlinear MHD simulation is carried out by using the MIPS code (MHD Infrastructure for Plasma Simulation) which solves the full MHD equations in the cylindrical coordinates (r, ϕ, z) based on an MHD equilibrium obtained by HINT2 without assuming existence of the nested flux surfaces. The simulations have been performed for three MHD equilibria where the central beta values are 7.5, 9 and 11%, respectively. For the magnetic Reynolds number S , we have carried out the simulation for two different S cases where S are chosen to 10^5 and 10^6 . The used pressure profiles are similar to experimentally obtained ones. For the MHD equilibria used in this simulation, the Mercier unstable region shifts from core to periphery as beta increases. From the numerical results, as the beta increases, the dominant eigenmodes change from an internal ballooning mode to modes expanding into a chaotic magnetic field. This implies a chaotic magnetic field region should be included in the analysis of the high beta plasmas with unstable modes near plasma periphery. The linear growth rate decreases as the beta value and/or S increase, although beta dependence becomes weaker for lower S . Although the instabilities grow in the periphery region in the linear phase, the core region comes under the influence of the instabilities and the central pressure decreases in the nonlinear phase. However, the collapse of the central pressure strongly depends on S . As S increases, the degree of the collapse decreases, namely the saturated state strongly depends on S and the higher beta plasma can be maintained for higher S . Those results are consistent with a result that high beta LHD plasmas enter the second stable region of ideal ballooning modes as beta increases, and remaining destabilized ballooning modes are considered to be resistive type, of which characteristics will be clarified soon.

TH-P

Numerical Modeling of Formation of Helical Structures in Reversed-Field-Pinch Plasma

N. Mizuguchi^{1,2}, A. Sanpei³, K. Oki³, S. Masamune³, H. Himura³, K. Ichiguchi^{1,2}, and Y. Todo^{1,2}

¹*National Institute for Fusion Science, Toki, Japan*

²*The Graduate University for Advanced Studies, Sokendai, Japan*

³*Kyoto Institute of Technology, Kyoto, Japan*

Corresponding Author: mizu@nifs.ac.jp

A unique control method which makes use of the self-concentrating nature of the plasma perturbations into a small number of modes has been proposed both experimentally and theoretically in the reversed-field-pinch(RFP) to avoid the degradation of confinement due to the chaotizing of the field lines in the core region. Several types of such states termed QSH or SHAx have been observed. In this study nonlinear 3D MHD simulations have been executed for the low-aspect-ratio RFP plasma to reveal the physical mechanism of the formation processes of such helical structures. Time development of the MHD plasma is solved explicitly in a cylindrical full-toroidal geometry with finite difference grids by using the MIPS code. The initial conditions are the reconstructed equilibria obtained by the RELAXFit code which roughly follow the experimental data of the RELAX machine. Two cases, where the $q = 1/4$ rational surface does (Case #1) and does not (Case #2) exist, are examined. Under the condition of finite resistivity, the $n = 4$ component dominates the growth compared to the other modes for both cases. For the Case #2, the system undergoes relaxations twice before reaching to the dissipative phase. At the relaxed state, a helically twisted structure with a dominant $n = 4$ component is formed clearly. It should be noted that such an $n = 4$ structure is also formed for the Case #1. The poloidal pressure profile gradually deforms into a highly hollow bean-shaped structure for both of the cases. The formation mechanism of the hollow structure is different between the two cases. For Case #1, the resonant $m/n = 1/4$ mode grows with a large single magnetic island, showing a typical behavior of the tearing modes. The original magnetic axis shrinks gradually, whereas the created O-point of the island forms a new magnetic axis. Such a mechanism has been conventionally proposed for the model of the QSH or SHAx states. On the other hand, for Case #2, the original nested surfaces are directly deformed into a helical one by the non-resonant mode. Then, for both of the cases, the core pressure flows out along the deformed magnetic field lines, probably through a magnetic reconnection between the core and the bean-shaped field region. Such a transient concentration to the $n = 4$ mode is comparable to the experiment.

Influence of Off-axis Neutral Beam Injection on Resistive Wall Mode Stability

G. Hao¹, Y. Liu², A. Wang¹, X. Peng¹, H. He¹, Q. Chen¹, and X. Qiu¹

¹*Southwestern Institute of Physics, Chengdu, China*

²*Euratom/CCFE Fusion Association, Culham Science Centre, Abingdon, UK*

Corresponding Author: haogz@swip.ac.cn

The stabilization of the resistive wall mode (RWM) is an essential issue for future magnetic fusion reactors (e.g., ITER) aiming at long-duration steady discharges over the no-wall beta limit. The RWM has been extensively investigated during recent years, both theoretically and experimentally. However, so far the physical mechanism of the passive control of the RWM has not been investigated fully, particularly the mechanism for the interaction between the RWM and energetic particles (EPs). Recent experiments in DIII-D indicate that the increase of the off-axis neutral beam injection (NBI) power can lead to the enhancement of RWM stability, which is opposite to expectation from consideration of the trapped particles fraction reduced by off-axis NBI. In this work, we apply our previous theory model to investigate the deposition effect of trapped EPs from off-axis NBI on the RWM instability. The results show that the spatial deposition effect of trapped EPs indeed significantly affects the RWM stability, and, compared with the on-axis case, off-axis deposition of EPs can contribute more stabilization to the RWM.

Current Sharing between Plasma and Walls in Tokamak Disruptions

L. Zakharov¹, S. A. Galkin²

¹*Princeton University, PPPL, Princeton, USA*

²*FAR-TECH, San Diego, USA*

Corresponding Author: zakharov@pppl.gov

Plasma disruptions in tokamaks represent a significant obstacle in enhancing performance of the plasma regime, especially in the next step machines, such as ITER. Although, for the global forces due to disruptions on the vacuum vessel there is sufficient certainty because of explicit scalings, e.g., from JET to ITER, many important aspects of plasma interaction with the plasma facing components (localization of forces, their impulse, rotation, etc) require additional consideration.

Here, the new aspects of electric current sharing between plasma and the wall during vertical disruption events (VDE) will be presented. Recently it was understood that theory predicted currents play the major role in VDEs. Called the “Hiro” currents, they are excited in the wall by the plasma motion into the wall. Regarding them, the instability, which acts as a “current” generator, provides large currents independent of resistivity of the plasma-wall contact. The Hiro currents can flow along the tiles surface while the plasma itself shorts out the electric circuit between tiles.

The effect of the Hiro currents might be significant for the ITER plasma facing beryllium tiles. As a result, significant forces (both vertical and sideways) can be applied to the tiles themselves. Also, the edges of the tiles can be potentially damaged by significant Hiro currents flowing between tiles. Realistic numerical simulations of this effect with a presently being developed Disruption Simulation Code (DSC) will be presented. Also, the role of the counterpart of the Hiro currents (edge currents flowing in the same direction as the plasma current) during VDEs will be clarified by simulating VDE. The ESC code is appropriately modified for this purposes. These currents may suggest an alternative interpretation of the tile current measurements during VDE in contrast to the presently adopted “halo” current concept.

Continuum Modes of Arbitrary Rotating Tokamak Plasma

V. Ilgisonis^{1,2}, V. Lakhin¹, and A. Smolyakov^{1,3}

¹*Kurchatov Institute, Moscow, Russian Federation*

²*Peoples Friendship University of Russia, Moscow, Russian Federation*

³*University of Saskatchewan, Saskatoon, Canada*

Corresponding Author: vil@nfi.kiae.ru

A theory for localized low-frequency ideal MHD modes in axisymmetric toroidal systems is discussed for tokamak plasma equilibria with both toroidal and poloidal equilibrium plasma flows. The general set of equations describing the coupling of shear Alfvén and slow (sound) modes and defining the continuous spectrum of rotating plasmas in axisymmetric toroidal systems is derived in the form suitable for a standard stability analysis. The equations are applied to study the continuous spectra in large aspect ratio tokamaks. The unstable continuous modes in the case of predominantly poloidal plasma rotation with the angular velocity exceeding the sound frequency are found. Their stabilization by the shear Alfvén coupling effect is studied.

On the Origin of Tokamak Density Limit Scalings

D. Gates¹, L. F. Delgado-Aparicio¹

¹*Princeton Plasma Physics Laboratory, Princeton, USA*

Corresponding Author: dgates@pppl.gov

The onset criterion for radiation driven islands in combination with a simple cylindrical model of tokamak current channel behavior is consistent with the empirical scaling of the tokamak density limit. A number of the unexplained phenomena at the density limit are consistent with this novel physics mechanism. Issues addressed in this work include:

1. The scaling is universal, but the density limit appears associated with radiative collapse which can be complicated given the quantum nature of impurity line radiation.
2. If the physics is associated with radiative collapse, why is the density limit so weakly dependent on heating power?
3. Why is the limit only weakly dependent on the type of radiator?
4. The collapse is associated with the onset of magnetic islands, so why does the limit not depend on plasma shaping which is known to affect MHD stability)?
5. Why is the density limit power scaling different in stellarators?
6. Why are tearing modes associated with the radiative collapse?

It is hoped that given the apparent success of this simple model in explaining the observed global scalings will lead to a more comprehensive analysis of the possibility that radiation driven islands are the physics mechanism responsible for the density limit. In particular, with modern diagnostic capabilities detailed measurements of current densities, electron densities and impurity concentrations at rational surfaces should be possible, enabling verification of the mechanism described above.

Kinetic Shear Alfvén Wave Instability in the Presence of Impurity Ions in Tokamak Plasmas

G. Lu¹, J. Dong^{1,2}, Y. Shen², Z. He², and H. He²

¹*Southwestern Institute of Physics, Chengdu, China*

²*Institute for Fusion Theory and Simulation, Zhejiang University, Hangzhou, China*

Corresponding Author: gaiminlv@gmail.com

The effect of impurity ions on the temperature gradient driven instability (ITG) of kinetic shear Alfvén waves (KSAWs) in tokamak plasma is studied by means of gyrokinetic theory including the finite Larmor radius effects of the hydrogen and impurity ions. It is found that the impurity ions have a stabilizing effects on the ITG of the KSAWs if the ratio of the plasma and impurity density gradients scale lengths L_{ec} ($L_{ec} = L_{ne}/L_{nc}$, where L_{ne} and L_{nc} stand for the density gradient scale lengths of electrons and impurity ions) is of positive sign, but in the opposite case they are destabilizing or stabilizing, depending on the impurity charge concentration f_c ($f_c = Zn_c/n_0$, where Z , n_c , n_0 are impurity ion charge number, impurity density and electron density, respectively). In the latter case, for large negative L_{ec} , the growth rate first increases with the impurity concentration f_c , but decreases after reaching a maximum value. Furthermore, heavier charged impurity ions have stronger effects than the lighter charged ones. Using the quasilinear theory, the corresponding particle and energy transport is also investigated. The numerical results verify the importance of the impurity ions in the experiments.

Study of Trapped Energetic Electron Driven Fishbone Instability with Second Stable Regime in Tokamak Plasmas

H. He¹, J. Dong^{1,2}, G. Fu³, Z. He¹, X. Peng¹, G. Zheng¹, Z. Wang¹, G. Lu¹, G. Hao¹, T. Xie¹, and L. Wang¹

¹*Southwestern Institute of Physics, Chengdu, China*

²*Institute for Fusion Theory and Simulation, Zhejiang University, Hangzhou, China*

³*Princeton Plasma Physics Laboratory, Princeton, USA*

Corresponding Author: hehd@swip.ac.cn

The influence of energetic particles on plasma confinement in toroidal devices is a major concern in magnetic fusion community and, therefore, has been investigated in experiment, theory and simulations in recent decades. The fishbone modes induced by energetic particles have been observed in many tokamak experiments with auxiliary heating. The fishbone-like instability modes can result in loss of energetic particles and degrade the confinement of burning plasmas or even bring about disruption of plasma column. Accordingly, it is a main task to avoid fishbone bursts in future advanced tokamak devices. The finding of second stable regime of fishbone-like modes in the higher beta regions provides a possible method to shun these unstable modes. A more general dispersion relation for fishbone-like modes driven by trapped energetic electrons (EEs) is obtained when the spatial and pitch angle distributions of the (EEs) are taken into account. In this work, This is an extension of the study on fishbone modes excited by barely passing energetic particles. The numerical results show that the trapped energetic electrons can also drive fishbone modes into a second stable regime. The numerical results show that the diamagnetic drift correlated with the spatial density gradient of energetic particles is the driving source for the fishbone-like modes whereas the damping force resulting in the formation of second stable regime may come from the high order derivatives terms of the density distribution. It is also demonstrated that the second stable regime would only appear at rather high β_h (=pressure of EEs / toroidal magnetic pressure) when the density distribution of the EEs is not peaked enough or the magnetic shear is higher than a critical value. The first critical β -value of EEs is approximately proportional to core plasma potential whereas the second one depends on the energy of the EEs and thus the mode frequency which is approximately a linear function of β_h . The finding of the second stable regime of fishbone modes has considerable significance for avoiding the instability and improving plasma confinement in future advanced tokamaks.

Development of a Predictive Capability for Fast Ion Behaviour in MAST

S. Pinches¹, R. Akers¹, B. Breizman², M. Cecconello³, R. Lake⁴, M. Lilley⁵,
C. Michael¹, and S. Sharapov¹

¹*Euratom/CCFE Fusion Association, Culham Science Centre, Abingdon, UK*

²*The University of Texas at Austin, Austin, USA*

³*Dept. Physics & Astronomy, Uppsala Uni., Euratom-VR Association, Uppsala, Sweden*

⁴*Centre for Fusion, Space & Astrophysics, Warwick University, Coventry, UK*

⁵*Imperial College, London, UK*

Corresponding Author: simon.pinches@ccfe.ac.uk

A recent focus of the programme at MAST has been upon the development of tools to interpret and understand the fast ion driven instabilities observed with a view to developing a predictive capability for the future: In particular, which modes will be unstable, how will they behave, and what will be the consequences? The drive arises from gradients in the fast ion distribution, and the calculation of smooth high resolution 6D distributions (recently made possible using a GPU-based approach) has allowed much more realistic simulations of the wave-particle interaction taking place. For the resonant neutral beam ions in MAST, dynamical friction dominates over pitch-angle scattering and facilitates a complex nonlinear wave evolution through the formation of structures in the fast ion distribution. Dynamical friction has been captured within the HAGIS code by treating the collisional terms as a combination of drag and a phase-space dependent Krook-like relaxation rate. Since fusion-born alpha-particles are also slowing down in nature, this physics is expected to be important in describing the behaviour of alpha-driven modes in future burning plasmas. Two new fast ion diagnostics have been installed and commissioned on MAST: A 4-chord scanning neutron camera and a FIDA system with toroidal and vertical views. Experiments have quantified the changes in the fast ion distribution associated with the presence of internal $n = 1$ chirping modes. Simulations of the coherent redistribution due to these modes has been described by diffusive and convective terms. Subsequent simulations using only these transport coefficients reproduce the modifications to the fast ion profile arising from the full wave-particle simulations motivating their adoption within more global transport codes. As a further aid to experimental interpretation, synthetic forms of the MAST neutron camera and FIDA views have been developed allowing a direct comparison between the measurements and simulations, and providing confidence that the processes responsible for the fast ion redistribution are correctly understood.

This work was funded by the RCUK Energy Programme under grant EP/I501045 and the European Communities under the contract of Association between EURATOM and CCFE. The views and opinions expressed herein do not necessarily reflect those of the European Commission.

Impact of Resonant Magnetic Perturbations on Zonal Modes, Drift-Wave Turbulence and the L–H Transition Threshold

M. Leconte¹, P. H. Diamond^{1,2}, and Y. Xu³

¹*NFRI, Daejeon, Republic of Korea*

²*UCSD, La Jolla, USA*

³*Association Euratom-Belgian State, Brussels, Belgium*

Corresponding Author: mleconte@nfri.re.kr

We study the effects of Resonant Magnetic Perturbations (RMPs) on turbulence, flows and confinement in the framework of resistive drift-wave turbulence. This work was motivated by experiments reported at IAEA 2010 conference [1] that showed a decrease of long-range correlations during the application of RMPs. To elucidate the effect of the RMPs on zonal structures in drift-wave turbulence, we construct an extended Hasegawa-Wakatani model including RMP fields [2,3]. The effect of the RMPs is to induce a linear coupling between the zonal electric field and the zonal density gradient — i.e., a spatial modulation of the electron diamagnetic frequency — which drives the system to a state of electron radial force balance for large RMP amplitude. A predator-prey model coupling the primary drift-wave dynamics to the zonal mode dynamics is derived. This model has both turbulence drive and RMP amplitude as control parameters and predicts a novel type of transport bifurcation in the presence of RMPs. The novel regime has a power threshold which increases as the square of RMP amplitude. This is in qualitative agreement with experiments [4,5]. Recent results includes a description of the full L-H transition scenario with RMPs, including the mean flow, the modeling of field line stochastization by a hyper-resistivity linking zonal perturbations of potential and density in Ohm law, and the extension of the RMP-modified Hasegawa-Wakatani model to include the dynamics of parallel flow and ion temperature, to describe RMP effects on ITG turbulence.

References

- [1] Y. Xu *et al.*, Nucl. Fusion **51** (2011) 063020.
- [2] M. Leconte and P. H. Diamond, Phys. Plasmas **18** (2011) 082309.
- [3] M. Leconte and P. H. Diamond, 53rd APS DPP international conference, Salt Lake City, UT, USA, invited session CI2 http://pop.aip.org/53rd_meeting, accepted in Phys. Plasmas.
- [4] A. Kirk *et al.*, Plasma Phys. Control. Fusion **53** (2011) 065011.
- [5] F. Ryter *et al.*, Proceedings of the 13th International Workshop on H-Mode Physics, Oxford, UK (2011), accepted in Nucl. Fusion.

Spatio-Temporal Evolution of the L–H and H–L Transitions

P. H. Diamond^{1,2}, K. Miki², N. Fedorczak¹, Y. Kosuga¹, M. Malkov¹, Ö. Gürçan³,
T. S. Hahm⁴, and G. Xu⁵

¹*University of California San Diego, La Jolla, USA*

²*WCI Center for Fusion Theory, NFRI, Daejeon, Republic of Korea*

³*École Polytechnique, Palaiseau, France*

⁴*Seoul National University, Seoul, Republic of Korea*

⁵*Chinese Academy of Sciences, Hefei, China*

Corresponding Author: pdiamond@ucsd.edu

Understanding the L-H and H-L transitions is crucial to successful ITER operation. In this paper, we present novel theoretical results on:

1. The spatio-temporal dynamics of the L-H and H-L transitions.
2. The physics origin of the ∇B -drift asymmetry in the power threshold.

Special emphasis is given to the role of zonal flows (ZFs). We have significantly extended earlier transition models to develop a 5-field reduced mesoscale model which evolves turbulence intensity, zonal flow shear, pressure, and density profiles and mean poloidal mass flow in radius and time. The mean $\mathbf{E} \times \mathbf{B}$ velocity is calculated via radial force balance using density, pressure and poloidal velocity. Studies of a slow power ramp up reveal evolution from L-I (Intermediate) -H phases. The I-phase exhibits nonlinear waves (locally, a limit-cycle oscillation (LCO)) which are nucleated near the LCFS, from the L-phase pre-transition edge. As the heat flux approaches criticality, the LCO phase delay between intensity and zonal flow shear evolves, while the non-linear LCO period and amplitude increase, i.e., the cycle slows. Transition occurs when the instantaneous LCO ZF shear is driven sufficiently to quench the turbulence, thus allowing rapid growth of the mean shear which then locks in the transition.

TH-P

Numerical Modeling of Neoclassical Transport and Geodesic Acoustic Mode Relaxation in a Tokamak Edge

M. A. Dorf¹, R. H. Cohen¹, J. C. Compton¹, M. Dorr¹, J. A. Hittinger¹, T. Rognlien¹,
P. Colella², D. Martin², and P. W. McCorquodale²

¹*Lawrence Livermore National Laboratory, Livermore, USA*

²*Lawrence Berkeley National Laboratory, Berkeley, USA*

Corresponding Author: mdorf@lbl.gov

The edge of a tokamak in a high confinement (H-mode) regime is characterized by steep density gradients, and a large radial electric field. Recent analytical studies demonstrated that the presence of a strong radial electric field consistent with a subsonic pedestal equilibrium modifies the conventional results of the neoclassical formalism developed for the core region. In the present work we make use of the recently developed gyrokinetic code COGENT to numerically investigate neoclassical transport in a tokamak edge including the effects of a strong radial electric field. The results of numerical simulations are found to be in good qualitative agreement with the theoretical predictions and the quantitative discrepancy is discussed. In addition, the present work investigates the effects of a strong radial electric field on the relaxation of geodesic acoustic modes (GAMs) in a tokamak edge. We present numerical simulations demonstrating that the presence of a strong radial electric field characteristic of a tokamak pedestal can enhance the GAM decay rate, and provide the heuristic arguments elucidating this finding.

Transport Theory for Error Fields and in the Pedestal Region for Tokamaks

K. C. Shaing^{1,2}, C. T. Hsu², Y. Sun³, M. S. Chu², and S. A. Sabbagh⁴

¹*Engineering Physics Department, University of Wisconsin, Madison, USA*

²*Plasma and Space Science Center, National Cheng Kung University, Tainan, Taiwan*

³*Chinese Academy of Sciences, Hefei, China*

⁴*Columbia University, New York, USA*

Corresponding Author: kshaing@wisc.edu

Real tokamaks have error fields that break toroidal symmetry and lead to enhanced particle, energy and momentum transport. The comprehensive theory for the error field induced transport fluxes consists of several collisionality regimes resulting from the asymptotic analysis of the drift kinetic equation. An analytic theory for the superbanana plateau resonance at the phase space boundary has been developed to show that the strength of the resonance is weakened when the resonance occurs at the phase space boundary. Fusion born alpha particles are extremely sensitive to error fields. Only resonant transport mechanisms, such as superbanana plateau resonance, are important for error field induced energetic alpha particle transport. The energy loss limits the magnitude of the error fields in International Thermonuclear Experimental Reactor (ITER). Neoclassical transport theory in the pedestal region of the high confinement mode (H-mode) is also presented to show that effects of orbit squeezing and the sonic poloidal $\mathbf{E} \times \mathbf{B}$ velocity reduce the ion heat conductivity. Here, E is the electric field and B is the magnetic field. Other transport quantities, including bootstrap current, are also obtained.

This work was supported by the US Department of Energy under Grant No. DE-FG02-01ER54619 with the University of Wisconsin.

TH-P

Spatio-temporal Distribution of Runaway Electron Wall Loads in ITER due to Resonant Magnetic Perturbations

G. Papp^{1,2}, M. Drevlak³, T. Fülöp², and G. I. Pokol¹

¹*Budapest University of Technology and Economics, Budapest, Hungary*

²*Nuclear Engineering, Department of Applied Physics, Chalmers University of Technology, Association EURATOM-VR, Göteborg, Sweden*

³*Max-Planck-Institut für Plasmaphysik, Greifswald, Germany*

Corresponding Author: papp@reak.bme.hu

Disruptions in large tokamaks can lead to the generation of a relativistic runaway (RE) electron beam that may cause serious damage to the first wall. To suppress the RE beam the application of resonant magnetic perturbations (RMP) has been suggested. In this work we investigate the effect of resonant magnetic perturbations on the spatial distribution of the RE wall loads by simulating the RE drift orbits in magnetostatic perturbed fields (RMP and TF ripple) and calculating the transport and orbit losses for various particle energies and different magnetic perturbation configurations. In the simulations we use model configurations with actual (TEXTOR) and planned (ITER) RMP systems and solve the relativistic, gyro-averaged drift equations for the runaway electrons including radiation losses and collisions.

The results indicate that runaway electrons are rapidly lost from regions where the normalised perturbation amplitude $\delta B/B_i$ larger than $\sim 0.1\%$ in a properly chosen perturbation geometry, and this can affect the maximum runaway current. This applies to the region outside the radius corresponding to the normalised flux $\psi = 0.5$ in ITER, when the ELM mitigation coils are used at maximum current in their most favourable configuration.

We found that the toroidal distribution of the runaway electron wall loads becomes more localised due to the 3D perturbations. However, the loss patterns are more widespread in the poloidal direction as compared to the unperturbed case. The exact loss pattern depends on the geometric properties of the RMP configuration such as periodicity or helicity. On the other hand, the loss patterns do not depend on the particle energies and starting positions.

The results indicate that the low n mode number perturbations can increase the risk of localised RE loads. Therefore the spatial localisation of the wall loads has to be considered when designing RMP configurations for RE suppression. We suggest an RMP configuration for ITER that balances effective RMP removal of runaway electrons and localised wall loads.

Eulerian Simulations of Neoclassical Flows and Transport in the Tokamak Plasma Edge and Outer Core

E. A. Belli¹, J. A. Boedo², J. Candy¹, R. H. Cohen³, P. Colella⁴, M. A. Dorf³,
M. R. Dorr³, J. A. Hittinger³, P. W. McCorquodale⁴, T. D. Rognlien³, and
P. B. Snyder⁴

¹*General Atomics, San Diego, USA*

²*University of California San Diego, La Jolla, USA*

³*Lawrence Livermore National Laboratory, Livermore, USA*

⁴*Lawrence Berkeley National Laboratory, Berkeley, USA*

Corresponding Author: bellie@fusion.gat.com

The δf code NEO is used to study the neoclassical transport for parameters relevant in the plasma edge and outer core. NEO includes multiple ion species, general geometry, and rapid toroidal rotation. It has recently been upgraded to include the full linearized Fokker-Planck collision operator, using novel numerical schemes which can accurately treat the disparate scales that arise in the case of multi-species plasmas, thus providing an exact solution for the local neoclassical transport. Comparisons are been made between the NEO neoclassical simulations and experimental measurements of the deuterium parallel velocity profiles and carbon impurity flow profiles in the edge for DIII D-L mode discharges. Emphasis is made on understanding how the flows of the different ion species are correlated in the edge region. Extensions of these studies further into the tokamak boundary region are explored via comparisons with COGENT, a full f Eulerian code describing both closed and open field-line regions. With COGENT, the generation of intrinsic plasma flows due to neoclassical particle losses in the tokamak edge, e.g., from thermal ion orbit losses and x-point losses, are investigated. Comparisons are also made with UEDGE, a 2D fluid code with a neoclassical transport model for both closed and open field lines allowing general collisionality, to assess the adequacy of the fluid transport model and provide a target for the kinetic codes in the collisional regime. Extensions of the NEO algorithm for use in gyrokinetic stability calculations of the highly collisional plasma edge are also explored.

TH-P

This work was supported in part by the US Department of Energy under DE-FG02-95ER54309, DE-FG02-07ER54917, DE-AC52-07NA27344 and DE-AC03-76SF00098 and by the Edge Simulation Laboratory project under DE-FC02-06ER54873.

Integrated Approach to the H-mode Pedestal Dynamics: Effects of Bootstrap Current and Resonant Magnetic Perturbations on ELMs

A. Pankin¹, S. Kruger¹, T. Rognlien², E. A. Belli³, J. D. Callen⁴, J. Cary^{1,5},
C. Chang⁶, R. Groebner³, A. Hakim⁶, I. Joseph², G. Kagan⁷, A. Kritiz⁸, G. Park⁹,
T. Rafiq⁸, and P. B. Snyder³

¹*Tech-X Corporation, Boulder, USA*

²*Lawrence Livermore National Laboratory, Livermore, USA*

³*General Atomics, San Diego, USA*

⁴*University of Wisconsin, Madison, USA*

⁵*University of Colorado, Boulder, USA*

⁶*Princeton Plasma Physics Laboratory, Princeton, USA*

⁷*Los Alamos National Laboratory, Los Alamos, USA*

⁸*Lehigh University, Bethlehem, USA*

⁹*National Fusion Research Institute, Daejeon, Republic of Korea*

Corresponding Author: pankin@txcorp.com

The accurate prediction of Edge Localized Modes (ELMs) and their mitigation are critical for sustainable discharge operation. Two main research questions are elucidated in this study:

1. What are the effects of uncertainties in the bootstrap current computations on the ELM stability predictions?
2. How do the resonant magnetic perturbations (RMPs) that are introduced to mitigate ELMs change the overall plasma confinement?

In order to answer these questions, high physics fidelity codes that have been developed during the SciDAC CPES, CSWIM, and FACETS projects are used. The computation starts from an “equilibrium cloud” generated using the FACETS framework. The edge plasma profiles are advanced using kinetic neoclassical XGC0 code. The resulting plasma pressure and bootstrap current profiles are updated in the initial equilibria by the M3D-OMP code. The updated equilibrium is analyzed in the FLUXGRID component of FACETS that incorporates several bootstrap current models. The bootstrap current predictions from these models are compared with the predictions from XGC0. Conclusions about validity ranges for each model are deduced. Differences in the predictions for the ELM stability thresholds that result from uncertainties in the computations of bootstrap current are determined using ideal MHD stability codes. The core plasma profiles from updated equilibria are advanced to steady state solutions using the integrated whole-device modeling FACETS code. The edge plasma profiles are maintained using the UEDGE component of FACETS. The effect of 3D magnetic perturbations on plasma confinement is investigated in these coupled core-edge simulations. The magnetic perturbation effect has been recently implemented in UEDGE using the magnetic field line diffusivity model. The applied RMPs degrade the edge confinement by modifying plasma profiles to the MHD stable profiles. The RMP effect on overall plasma confinement is determined by comparing the energy confinement time computed with the FACETS code with the energy confinement time for the corresponding cases without RMPs. Recommendations are made for ranges of plasma parameters for ELM-free discharge scenarios with RMPs that yield optimum energy confinement. The stabilizing effect of RMPs is confirmed through MHD stability analysis with ideal MHD stability codes.

Rotation Breaking Induced by ELMs on EAST

H. Xiong¹, G. Xu¹, Y. Sun¹, B. Wan¹, V. Naulin², N. Yan², and F. Wang²

¹*Institute of Plasma Physics, Chinese Academy of Sciences, Hefei, China*

²*Association Euratom-RisøDTU, Roskilde, Denmark*

Corresponding Author: hxiong@ipp.ac.cn

Spontaneous rotation has been observed in LHCD H-mode plasmas with type III ELMs (edge localized modes) on EAST, and it revealed that type III ELMs can induce the loss of both core and edge toroidal rotation. Here we work on the breaking mechanism during the ELMs. Several large tokamaks have discovered ELMs' filamentary structures. It revealed that the ELMs are filamentary perturbations of positive density formed along the local field lines close to the LCFS. Currents flowing in the filaments induce magnetic perturbations, which break symmetry of magnetic field strength and lead to deformation of magnetic surface, thus generate NTV (neo-classical toroidal viscosity) torque that affects toroidal rotation. We adopt 1cm maximum edge magnetic surface displacement from experimental observation, and our calculation shows that the edge torque is about 0.35 N/m², and the core very small. The expected angular momentum density change is about 3.8 N/m², nearly 10 times larger than the calculation. Previous work on EAST has suggested that there is a mechanism at the edge that breaks the rotation, while the core rotation change is mostly likely related with momentum transport to the edge. In other words, NTV torque should have less impact on the core but great on edge, which corresponds with the calculation as well. In our calculation, we found that the core has little dependence on the magnetic surface displacement, while the edge relies on it heavily. The exact profile of the edge torque has uncertain that comes from the exact edge displacement profile and the accurate mode number. However, the magnitude of the edge NTV torque is still nearly 0.1 – 1 N/m², indicating it should been emphasized while considering rotation change. Further work including transport code is planned.

TH-P

Penetration of Resonant Magnetic Perturbations in Turbulent Edge Plasmas with Transport Barrier

G. Fuhr¹, O. Agullo¹, S. Benkadda¹, P. Beyer¹, M. Faganello¹, X. Garbet²,
A. Marcus¹, A. Monnier¹, M. Muraglia³, A. Poyé², F. Waelbroeck⁶, A. Sen⁴,
A. Smolyakov⁵, and W. Horton⁶

¹*Aix-Marseille University, Marseille, France*

²*Association Euratom-CEA, CEA/DSM/IRFM, Caradache, France*

³*LCP, Aix-Marseille Université, Marseille, France*

⁴*Institute for Plasma Research, Bhat, India*

⁵*Department of Physics and Engineering Physics, University of Saskatchewan, Saskatchewan, Canada*

⁶*Institute for Fusion Studies, University of Texas, Austin, USA*

Corresponding Author: guillaume.fuhr@univ-amu.fr

In the context of edge localized mode (ELM) control by resonant magnetic perturbations (RMPs), the impact of micro-turbulence on the RMP penetration process and effectiveness is an important issue. Indeed, on the one hand, theoretical investigations as well as quasi-linear and non-linear MHD modeling reveal that the magnetic perturbation is strongly screened by plasma rotation. On the other hand, micro turbulence that is unavoidably present at the plasma edge, governs transport processes and strongly interacts with sheared plasma rotation.

In this work, we study the penetration of RMPs by means of numerical simulations with different turbulence models and geometries. First, using a simplified reduced MHD model in the EMEDGE3D code, the plasma response to RMPs is studied in three-dimensional tokamak geometry with flux driven micro turbulence and a transport barrier induced by sheared plasma rotation. Second, the magnetic field penetration is studied in the framework of a two-dimensional two-fluid model including diamagnetic effects. In both models, a helical magnetic perturbation is induced at the plasma boundary and necessary numerical techniques have been developed to avoid generation of artificial courant at the boundary. In a third part of this work, we study in the frame of a two fluid model the interaction between an pre existing magnetic island and small scale turbulence propagating towards this island.

Integrated Fusion Simulations of Core-Edge-Wall Thermal and Particle Transport Using the FACETS Code

A. Hakim^{1,4}, A. Pankin¹, T. Rognlien², J. Cary^{1,6}, R. Groebner³, S. Kruger¹,
P. Alexander⁵, and S. Shasharina¹

¹*Tech-X Corporation, Boulder, USA*

²*Lawrence Livermore National Laboratory, Livermore, USA*

³*General Atomics, San Diego, USA*

⁴*Princeton Plasma Physics Laboratory, Princeton, USA*

⁵*University of California at San Diego, La Jolla, USA*

⁶*University of Colorado, Boulder, USA*

Corresponding Author: ammar@princeton.edu

We present integrated fusion simulations that couple the core-edge-wall transport into a self-consistent advance for the state of the plasma on transport time-scales. We accomplish this using the Framework Application for Core Edge Transport Simulation (FACETS), a recently developed parallel fusion simulation package incorporating the best models for each region of the tokamak. An overview of the FACETS framework and available components will be presented. We then present coupled simulation results from selected DIII-D discharges. In particular, we focus on the evolution of coupled particle and thermal transport using the TGLF model for computing core transport fluxes. Edge cross-field fluxes are interpreted from experimental data. Measured toroidal rotation profiles are used, coupled to neoclassical estimates of the poloidal flow, to provide the radial electric field needed in shear flow suppression of transport. In addition the evolution of the plasma current is also taken into account. This allows for the formation of a transport barrier that is incorporated in the core region. WallPSI modelling is used to provide boundary conditions on the wall-facing boundary of UEDGE. Another focus of this work will be to study the effect of neutral fuelling of the edge. In an experimental discharge neutrals are introduced due to wall recycling and also from gas-puffs. The effect of these sources on the development of the edge pedestal is studied using coupled simulations.

TH-P

Modelling of the Effect of Externally Applied Resonant Magnetic Perturbations on α -particle Dynamics in Tokamak Plasmas

Y. Moskvitina¹, K. Schoepf³, A. Moskvitin², V. Yavorskij^{3,4}, and O. Shyshkin²

¹*National Science Centre “Kharkov Physics and Technology Institute”, Kharkiv, Ukraine*

²*Karazin National University, Kharkiv, Ukraine*

³*Institute for Theoretical Physics, University of Innsbruck, Association EURATOM-OEAW, Austria*

⁴*Institute for Nuclear Research, Ukrainian Academy of Sciences, Kyiv, Ukraine*

Corresponding Author: yu.moskvitina@gmail.com

Resonant magnetic perturbations (RMPs) have become a powerful tool for modifying dge transport properties and for plasma stability control in present day tokamaks. The transport behaviour of charged fusion products as altered by these perturbations can be regarded as a crucial point for approving the application of RMPs in future tokamak reactors. Our present study focuses on fusion α particle losses driven by resonant magnetic perturbations which are used for mitigation or complete suppression of ELMs. For the simulation of the dynamics of an α particle ensemble we employ a Monte-Carlo approach. Resonant magnetic perturbations are shown to result only in a small enlargement of first orbit losses of charged fusion products from tokamak plasmas. On the other hand RMPs can substantially affect the confinement of partly thermalised α particles. Thus a significant impact is observed on α s with energies below 70 keV, where RMPs enhance the α loss by about 30%. The main physical mechanisms responsible for increased α particle losses are induced by reconnection of magnetic field lines and by Coulomb collisions. The formation of magnetic islands together with the stochastic magnetic layers at the plasma edge is a natural consequence of RMP excitation. It was demonstrated that, due to the formation of these resonant magnetic field structures, irregularities of the energetic α particle orbits occur, which lead to a substantial increase of α particle losses from the plasma periphery. It is noted that the enhanced α particle losses during RMPs application may be viewed as a positive phenomenon from the point of view of helium ash removal.

New Bootstrap Current Formula Valid for Edge Pedestal, and Gyrokinetic Study of its Implication to Pedestal Stability

C. S. Chang^{1,2}, S. Koh², W. Choe¹, S. Ku², S. Parker³, W. Wan³, and Y. Chen³

¹*Korea Advanced Institute of Science and Technology, Daejeon, Republic of Korea*

²*Princeton Plasma Physics Laboratory, USA*

³*University of Colorado, Boulder, USA*

Corresponding Author: cschang@pppl.gov

Previous formulas on the plasma bootstrap current have been developed for the core plasma. However, the edge plasma has an unconventional and difficult neoclassical property compared to the core plasma. There have been prevailing suspicions that the existing bootstrap current formula may not be accurate enough for pedestal physics study. Kinetic simulation based upon first-principles equations in realistic diverted geometry is needed for a more proper study of the bootstrap current in the edge pedestal. A drift-kinetic neoclassical particle code XGC0, equipped with both a mass-momentum-energy conserving linear operator and a fully-nonlinear collision operator, has been used to study the edge bootstrap current profile in realistic diverted magnetic field geometry under self-consistent radial electric field development. XGC0 is a neoclassical version of the edge gyrokinetic code XGC1 [1].

It is found that when the edge electrons are deep in the weakly collisional banana regime, surprisingly, XGC0 kinetic simulation confirms that the existing analytic expressions, represented by [2], are still valid in this unconventional radial region. However, when the pedestal electrons are in plateau-collisional regime, significant deviation of the numerical results from the existing analytic formulas is observed. In a conventional aspect ratio tokamak with $R_0/a \approx 3$ (DIII-D, etc), edge bootstrap current from kinetic simulation is less than that from existing analytic formula. When the aspect ratio is tight $R/a < 1.5$ (NSTX, etc), numerically obtained edge bootstrap current is greater than the analytic expressions.

A new analytic fitting formula, as a simple modification to the existing Sauter formula, has been developed which brings the analytic expression to a better agreement with the kinetic simulation result in the pedestal. The new formula will give a stronger foundation for the pedestal physics research. As an urgent application of the new formula, effect of the modified edge bootstrap current on the pedestal stability will also be reported using tokamak gyrokinetic codes GEM and XGC1, which will significantly augment the existing MHD studies of pedestal stability.

References

- [1] C. S. Chang, S. Ku, P. H. Diamond, *et al.*, Phys. Plasmas **16** (2009) 056108.
- [2] O. Sauter *et al.*, Phys. Plasmas **6** (1999) 056108.

Edge Electric Fields in the Pfirsch-Schlüter Regime and their Effect on the L–H Transition Power Threshold

A. Aydemir¹, B. Breizman¹, and R. Hazeltine¹

¹*The University of Texas at Austin, Institute for Fusion Studies, Austin, USA*

Corresponding Author: aydemir@mail.utexas.edu

In the collisional tokamak edge plasmas just inside the separatrix, a radial electric field can be associated with the Pfirsch-Schlüter currents, and poloidal density and temperature gradients. Building upon our previous works, this mechanism is further clarified and quantified here. Dependence of the resulting electric fields on magnetic topology, geometric factors like the upper/lower triangularity and elongation, and the relative position of the X-point(s) in the poloidal plane are examined in detail. Starting with the assumption that an initially more negative radial electric field at the edge helps lower the transition power threshold, we find that our results are in agreement with a variety of experimental observations. In particular, for a “normal” configuration of the plasma current and toroidal field we show:

1. The net radial electric field contribution by the Pfirsch-Schlüter currents at the plasma edge is negative for a lower single null (LSN) and positive for a corresponding upper single null (USN) geometry.
2. It becomes more negative as the X-point height is reduced.
3. It also becomes more negative as the X-point radius is increased. These observations are consistent with the observed changes in the L-H transition power threshold under similar changes in the experimental conditions. In addition we find that:
4. In USN with an unfavorable ion grad-B drift direction, the net radial electric field contribution is positive but decreases as the X-point radius decreases. This is consistent with the C-Mod observation that an L-I Mode transition can be triggered by increasing the upper triangularity in this configuration.
5. Locally the radial electric field is positive above the outer mid-plane and reverses sign with reversal of the toroidal field, consistent with DIII-D observations in low-power L-mode discharges. Thus, taken as a whole, the Pfirsch-Schlüter current-driven fields can explain a number of observations on the L-H or L-I transition and the required power threshold levels not captured by simple scaling laws. They may indeed be an important “hidden variable.”

Progressive Steps towards Global Validated Simulation of Edge Plasma Turbulence

P. Ricci¹, A. Fasoli¹, I. Furno¹, J. Loizu¹, S. Jolliet¹, F. Halpern¹, A. Masetto¹,
B. Rogers², and C. Theiler²

¹*CRPP-EPFL, Lausanne, Switzerland*

²*Dartmouth College, Hanover, USA*

Corresponding Author: paolo.ricci@epfl.ch

Simulations of edge turbulence are particularly challenging due to the presence of large amplitude fluctuations and to the coupling of equilibrium and fluctuating scales. While validating edge simulations is necessary to assess the accuracy of our understanding, difficulties in experimental diagnostics and the lack of a precise validation methodology have, to date, severely limited the process. The Global Braginskii Solver (GBS) code has been developed to simulate plasma turbulence in edge-relevant conditions [1]. We have initially studied relatively simple configurations of increasing complexity, linear magnetic configurations and the Simple Magnetized Torus. GBS has now reached the capabilities of performing non-linear self-consistent global three-dimensional simulations of the plasma dynamics in the Scrape-Off Layer (SOL). By solving the drift-reduced Braginskii equations, the code evolves self-consistently the plasma flux from the core, turbulent transport, and the plasma losses to the limiter plates. This gradual approach has allowed gaining a deep understanding of turbulence, from identifying the driving instabilities to estimating the turbulence saturation amplitude. In particular, we point out the need of global simulations to correctly represent the SOL dynamics, simultaneously describing both fluctuating and equilibrium quantities. A code validation development project has been conducted side by side with the GBS development [2]. A methodology to carry out experiment-simulation comparison had been established and applied to quantify the level of agreement between the GBS the TORPEX experiment.

References

- [1] P. Ricci *et al.*, Phys. Rev. Lett. **100** (2008) 225002; P. Ricci and B. N. Rogers, Phys. Rev. Lett. **104** (2010) 145001; B. N. Rogers and P. Ricci, Phys. Rev. Lett. **104** (2010) 225002.
- [2] P. Ricci *et al.*, Phys. Plasmas **16** (2009) 055703; P. Ricci *et al.*, Phys. Plasmas **18** (2011) 032109 .

This work is supported by the Swiss National Science Foundation.

Theory of Rapid Formation of Pedestal and Pedestal width due to Anomalous Particle Pinch in the Edge of H-mode Discharges

P. K. Kaw¹, R. Singh^{1,2}, H. Nordman³, X. Garbet⁴, C. Bourdelle⁴, D. Campbell², A. Loarte², and D. Bora²

¹*Institute for Plasma Research, Bhat, India*

²*ITER Organization, Saint Paul-Lez-Durance, France*

³*Chalmers Institute of Technology, Göteborg, Sweden*

⁴*CEA, Saint Paul-Lez-Durance, France*

Corresponding Author: kaw@ipr.res.in

A theory based on a turbulent particle pinch is proposed to explain the rapid formation of sharp density gradients in tokamak edge plasmas, in particular the pedestal region. The inward radial particle flux in the pedestal results from the interaction between small scale electron temperature gradient driven (ETG) turbulence and self-consistently formed “electron geodesic acoustic modes” (el-GAMs). To address this phenomenon, the el-GAM modulational instability driven by the ETG turbulence background is studied. The ETG level of fluctuations and particle pinch are estimated through the back reaction of eGAMs on ETG turbulence. It is found that the particle pinch is quite sensitive to magnetic shear, safety factor, ratio of electron to ion temperatures and atomic mass number. In the absence of particle source in the pedestal, the density gradient length scale, of the order of the pedestal width, is estimated. It is shown that it is proportional to the major radius, up to some dependence on the poloidal beta. Moreover it does not depend on the normalized gyro-radius. This scaling agrees with DIII-D and JET similarity experiments [1]. This dependence is favorable when extrapolated to the pedestal width in ITER in spite of its low normalized gyro radius. It is also shown that the density scale length becomes sharper by increasing the magnetic shear. A new H-mode pedestal pressure scaling is derived assuming that the pressure gradient is limited by the ballooning instability.

References

[1] Beurskens *et al.*, Nucl Fusion **51** (2009) 124051.

Acknowledgements: One author (R. Singh) thanks Drs. Ö. Gürçan and J. Anderson for fruitful discussions.

Parallel Transport and Profile of Boundary Plasma with a Low Recycling Wall

X. Tang¹, Z. Guo¹

¹*Los Alamos National Laboratory, Los Alamos, USA*

Corresponding Author: xtang@lanl.gov

Reduction of wall recycling by, for example, a flowing liquid surface at the divertor and first wall, holds the promise of accessing the distinct tokamak reactor operational mode with boundary plasmas of high temperature and low density. Earlier work has indicated that such a boundary plasma would reduce the temperature gradient across the entire plasma and hence remove the primary micro-instability drive responsibly for anomalous particle and energy transport. Here we present a systematic study solving the kinetic equations both analytically and numerically, with and without Coulomb collision. The distinct roles of magnetic field strength modulation and the ambipolar electric field on the electron and ion distribution functions are clarified. The resulting behavior on plasma profile and parallel heat flux, which are often surprising and counter the expectations from the collisional fluid models, on which previous work were based, are explained both intuitively and with a contrast between analytical calculation and numerical simulations.

The transport-induced plasma instabilities, and their essential role in maintaining ambipolarity, are clarified, along with the subtle effect of Coulomb collision on electron temperature and wall potential as small but finite collisionality is taken into account.

Simulations with COREDIV Code of DEMO Discharges

R. Zagorski¹, R. Stankiewicz¹, and I. Ivanova-Stanik¹

¹*Institute of Plasma Physics and Laser Microfusion, Warsaw, Poland*

Corresponding Author: roman.zagorski@ipplm.pl

The reduction of divertor target power load due to radiation of sputtered and externally seeded impurities in fusion reactor is investigated in this paper. The approach is based on integrated numerical modelling of DEMO discharges using the COREDIV code, which self-consistently solves 1D radial transport equations of plasma and impurities in the core region and 2D multifluid transport in the SOL. The model is fully self-consistent with respect to both the effects of impurities on the alpha-power level and the interaction between seeded and intrinsic impurities. The code has been already successfully benchmarked with the data from present day experiments (JET, ADEX).

Calculations have been performed for inductive DEMO scenario and DEMO Steady-State configuration with tungsten walls and Ar seeding. In case of DEMO Steady-State scenario strong increase of Z_{eff} and significant reduction of the alpha power are observed with the increase of Ar influx which is caused by the decrease of fuel ions density due to the dilution effect. It leads to the reduction of the target plate heat loads but surprisingly the radiation level remains almost constant with the increased seeding which is the result of the interplay between the energy losses and tungsten source due to sputtering processes. It has been found that the W radiation is the dominant energy loss mechanism and it accounts for 90% of all radiation losses.

In case of pulsed DEMO scenario, it appears that the helium accumulation might be a serious problem. Even without seeding the resulting Z_{eff} is very large (> 2.6) and consequently only relatively weak seeding can be applied for pulsed scenario. It is found that helium accumulation depends strongly on the transport model used for helium, if the helium diffusion is increased than the accumulation effect is mitigated.

Theory and Simulations of ELM Control with a Snowflake Divertor

D. Ryutov¹, B. Cohen¹, R. Cohen¹, E. Kolemen², M. A. Makowski¹, J. Menard¹,
T. Rognlien¹, V. Soukhanovskii¹, M. Umansky¹, and X. Xu¹

¹*Lawrence Livermore National Laboratory, Livermore, USA*

²*Princeton Plasma Physics Laboratory, Princeton, USA*

Corresponding Author: ryutov1@llnl.gov

This paper is concerned with the use of a snowflake (SF) divertor for the control and mitigation of edge localized modes (ELMs). Our research is focused on the following three issues:

1. Effect of the SF geometry on neoclassical ion orbits near the separatrix, including prompt ion losses and the related control mechanism for the electric field and plasma flow in the pedestal;
2. Influence of the thereby modified flow and of high poloidal plasma beta in the divertor region on plasma turbulence and transport in the snowflake-plus geometry;
3. Reaction of the SF divertor to type-1 ELM events. Neoclassical ion orbits in the vicinity of the SF separatrix are changed due to a much weaker poloidal field near the null and much longer particle dwell-time in this area.

This leads to an increase of the prompt ion loss, which then affects the radial electric field profile near the separatrix. The resulting $\mathbf{E} \times \mathbf{B}$ flow shear in the pedestal region affects the onset of ELMs. The electric field and velocity shear are then used as a background for two-fluid simulations of the edge plasma turbulence in a realistic geometry with the 3D BOUT code. A SF-plus geometry is chosen, so that the separatrix topology remains the same as for the standard X-point divertor, whereas the magnetic shear both inside and outside the separatrix increases dramatically. It is found that mesoscale instabilities are suppressed when the geometry is close to a perfect SF. In situations where complete suppression of ELMs is impossible, the SF divertor offers a path to reducing heat loads during ELM events to an acceptable level. Two effects, both related to the weakness of the poloidal field near the SF null, act synergistically in the same favorable direction. The first is the onset of strong, curvature-driven convection in the divertor, triggered by the increase of the poloidal pressure during the ELM and leading to the splitting of the heat flux between all four (as is the case in a SF geometry) divertor legs. The second effect is a temporal dilation of the heat pulse caused by a large connection length between the midplane and divertor plates. The net result is a more than 10-fold decrease of the divertor-surface temperature rise initiated by an ELM event.

Work performed for U.S. DoE by LLNL under Contract DE-AC52-07NA27344 and LDRD project 11-ERD-058, and by PPPL under Contract DE-AC02-09CH11466.

Drift-based Model for Power Scrape-off Width in Low-Gas-Puff H-mode Plasmas: Theory and Implications

R. Goldston¹

¹*Princeton Plasma Physics Laboratory, Princeton, USA*

Corresponding Author: rgoldston@pppl.gov

A heuristic model for the plasma scrape-off width in low-gas-puff tokamak H-mode plasmas is introduced. ∇B and curvature drifts into the scrape-off layer (SOL) are balanced against near-sonic parallel flows out of the SOL, to the divertor plates. These assumptions result in an estimated SOL width of order the poloidal gyroradius. It is next assumed that anomalous perpendicular electron thermal diffusivity is the dominant source of heat flux across the separatrix, investing the SOL width, derived above, with heat from the main plasma. The separatrix temperature is then calculated based on a two-point model balancing power input to the SOL with Spitzer-Härm parallel thermal conduction losses to the divertor. This results in a heuristic closed-form prediction for the power scrape-off width that is in quantitative agreement both in absolute magnitude and in scaling with recent experimental data. The applicability of the Spitzer-Härm model to this regime can be questioned at the lowest densities, where the presence of a sheath can raise the divertor target electron temperature. A more general two-point model including a finite ratio of divertor target to upstream electron temperature shows only a 5% effect on the SOL width with target temperature $f_T = 75\%$ of upstream, so this effect is likely negligible in experimentally relevant regimes. To achieve the near-sonic flows measured experimentally, and assumed in this model, sets requirements on the ratio of upstream to total SOL particle sources relative to the square-root of the ratio of target to upstream temperature. As a result very high recycling regimes may allow significantly wider power fluxes. The Pfisch-Schlüter model for equilibrium flows has been modified to allow near-sonic flows, appropriate for gradient scale lengths of order the poloidal gyroradius. This results in a new quadrupole flow pattern that amplifies the usual P-S flows at the outer midplane, while reducing them at the inner. The strong parallel flows and plasma charging implied by this model suggest a mechanism for H-mode transition, consistent with the observation that LSN divertors have lower power threshold and the JT-60 divertor did not accommodate H-mode. These results suggest that ITER may need to operate at least transiently in the low SOL regime presented here in order to achieve H-mode transition.

RMP-Flutter-Induced Pedestal Plasma Transport

J. D. Callen¹, C. Hegna¹, and A. J. Cole²

¹ *University of Wisconsin, Madison, USA*

² *Columbia University, New York, USA*

Corresponding Author: callen@engr.wisc.edu

Plasma toroidal rotation can prevent or limit reconnection of externally applied resonant magnetic perturbation (RMP) fields δB on rational magnetic flux surfaces. Hence, it causes the induced radial perturbations to vanish or be small there, and thereby inhibits magnetic island formation and stochasticity in the edge of high (H-mode) confinement tokamak plasmas. However, the radial component of the spatial magnetic flutter induced by RMP fields off rational surfaces causes a radial electron thermal diffusivity of $(1/2)(\delta B_\rho/B)^2$ times a magnetic-shear-influenced effective parallel electron thermal diffusivity. The resultant RMP-flutter-induced electron thermal diffusivity can be comparable to experimentally inferred values at the top of H-mode pedestals. This process also causes a factor of about 3 smaller RMP-induced electron density diffusivity there. Because this electron density transport is non-ambipolar, it produces a toroidal torque on the plasma, which is usually in the co-current direction. Kinetic-based cylindrical screw-pinch and toroidal models of these RMP-flutter-induced plasma transport effects have been developed. The RMP-induced increases in these diffusive plasma transport processes are typically spatially inhomogeneous in that they are strongly peaked near the rational surfaces in low collisionality pedestals, which may lead to resonant sensitivities to the local safety factor q . The effects can be large enough to reduce the radially averaged gradients of the electron temperature and density at the top of H-mode edge pedestals, and modify the plasma toroidal rotation and radial electric field there. At high collisionality the various effects are less strongly peaked at rational surfaces and thus less likely to exhibit RMP-induced resonant behavior. These RMP-flutter-induced plasma transport processes provide a new paradigm for developing an understanding of how RMPs modify the pedestal structure to stabilize peeling-ballooning modes and thereby mitigate or suppress edge localized modes (ELMs) in tokamak H-mode plasmas.

TH-P

Edge Plasma Response to Non-Axisymmetric Fields in Tokamaks

N. M. Ferraro¹, L. L. Lao¹, R. A. Moyer², D. M. Orlov², R. J. Buttery¹, T. E. Evans¹,
M. J. Lancot³, P. B. Snyder¹, and M. R. Wade¹

¹General Atomics, San Diego, USA

²University of California San Diego, La Jolla, USA

³Lawrence Livermore National Laboratory, Livermore, USA

Corresponding Author: ferraro@fusion.gat.com

The application of non-axisymmetric fields is found to have significant effects on the transport and stability of H-mode tokamak plasmas. These effects include dramatic changes in rotation and particle transport, and may lead to the partial or complete suppression of edge-localized modes (ELMs) under some circumstances [1]. The physical mechanism underlying these effects is presently not well understood, in large part because the response of the plasma to non-axisymmetric fields is significant and complex. Here, recent advances in modeling the plasma response to non-axisymmetric fields are discussed. Calculations using a resistive two-fluid model in diverted toroidal geometry confirm the special role of the perpendicular electron velocity in suppressing the formation of islands in the plasma [2]. The possibility that islands form near the top of the pedestal, where the zero-crossing of the perpendicular electron velocity may coincide with a mode-rational surface, is explored, and the implications for ELM suppression are discussed. Modeling results are compared with empirical data. It is shown that numerical modeling is successful in reproducing some experimentally observed effects of applied non-axisymmetric fields on the edge temperature and density profiles. The numerical model self-consistently includes the plasma, separatrix, and scrape-off layer. Rotation and diamagnetic effects are also included self-consistently. Solutions are calculated using the M3D-C1 extended-MHD code [3].

References

- [1] T. E. Evans, *et al.*, Phys. Rev. Lett. **92** (2004) 235003.
- [2] N. M. Ferraro, *et al.*, "Calculations of two-fluid linear response to non-axisymmetric fields in tokamaks", submitted to Phys. Plasmas (2011).
- [3] N. M. Ferraro, S. C. Jardin, and P. B. Snyder, Phys. Plasmas **17** (2010) 102508.

This work was supported by the US Department of Energy under DE-FG02-95ER54309, DE-FG02-07ER54917, DE-AC52-07NA27344, and DE-AC02-09CH11466.

Coarse Grained Transport Model for Neutrals in Turbulent SOL Plasmas

Y. Marandet¹, A. Mekkaoui¹, D. Reiter², P. Boerner², P. Genesio¹, J. Rosato¹,
H. Capes¹, L. Godbert-Mouret¹, M. Koubiti¹, and R. Stamm¹

¹PIIM, CNRS/Aix-Marseille University, Marseille, France

²IEK4, FZJ, Jülich, Germany

Corresponding Author: yannick.marandet@univ-amu.fr

Edge plasmas of magnetic fusion devices exhibit strong intermittent turbulence, which governs perpendicular transport of particles and heat. Turbulent fluxes result from the coarse graining procedure used to derive the transport equation, which entails time averaging of the underlying equations governing the turbulent evolution of the electron and ion fluids. In previous works, we have pointed out that this averaging is not carried out on the Boltzmann equation that describes the transport of neutral particles (atoms, molecules) in current edge code suites (such as SOLPS). Since fluctuations in the far SOL are of order unity, calculating the transport of neutral particles, hence the source terms in plasma fluid equations, in the average plasma background might lead to misleading results. In particular, retaining the effects of fluctuations could affect the estimation of the importance of main chamber recycling, hence first wall sputtering by charge exchange atoms, as well as main chamber impurity contamination and transport. In this contribution, we obtain an exact coarse-grained equation for the average neutral density, assuming that density fluctuations are described by multivariate Gamma statistics. This equation is a scattering free Boltzmann equation, where the ionization rate has been renormalized to account for fluctuations. The coarse grained transport model for neutrals has been implemented in the EIRENE code, and applications in 2D geometry with ITER relevant plasma parameters are presented. Our results open the way for the implementation of the effects of turbulent fluctuations on the transport of neutral particles in coupled plasma/neutral edge codes like B2-EIRENE.

TH-P

Edge Sheared Flows and Blob Dynamics

J. Myra¹, D. D'Ippolito¹, D. Russell¹, W. M. Davis², S. Zweben², J. Terry³, and
B. LaBombard³

¹*Lodestar Research Corporation, Boulder, USA*

²*Princeton Plasma Physics Laboratory, Princeton, USA*

³*Massachusetts Institute of Technology, Cambridge, USA*

Corresponding Author: jmyra@lodestar.com

A study of sheared flows in the edge and scrape-off layer (SOL) and their interaction with blob-filaments is presented. Edge sheared flows are believed to be important for the L-H, and H-L transitions. Blob generation and dynamics impacts both the (near-separatrix) scrape-off-layer (SOL) width critical for power handling in the divertor, and the interaction of plasma in the far SOL with plasma-facing components. These topics are critical for ITER and future devices. A fluid-based 2D curvature-interchange model embedded in the SOLT code is employed to study these issues. Sheared binormal flows both regulate the power flux crossing the separatrix and control the character of emitted turbulence structures such as blob-filaments. At a critical power level (depending on parameters) the laminar flows containing intermittent, but bound, structures give way to full-blown blob emissions signifying a transition from quasi-diffusive to convective transport. In order to diagnose sheared flows in experiments and assess their interaction with blobs, a blob-tracking algorithm has been developed and applied to both NSTX and Alcator C-Mod data. Blob motion and ellipticity can be affected by sheared flows, and are diagnosed and compared with seeded blob simulations. A picture of the interaction of blobs and sheared flows is emerging from advances in the theory and simulation of edge turbulence, combined with ever-improving capabilities for edge diagnostics and their analysis.

TH-P

Supported by the USDOE under grants DE-FG02-97ER54392, DE-FG02-02ER54678, DE-AC02-09-CH11466, DE-FC02-99ER54512, DE-AC02-09CH11466, and PPPL Subcontract S009625-F.

Effects of Collisionality on the Nonlinear Characteristics of Boundary Turbulence and Blob/hole Transport in Tokamak Plasmas

J. Li¹, J. Cheng², Y. Longwen², D. Jiaqi², and K. Yasuaki¹

¹*Kyoto University, Kyoto, Japan*

²*Southwestern Institute of Physics, Chengdu, China*

Corresponding Author: lijq@energy.kyoto-u.ac.jp

Blob/hole dynamics near tokamak separatrix is of striking importance in determining the boundary transport. Based on simulations using an extended 2-region (edge/SOL) fluid model, we found that blob/hole dynamics are sensitively influenced by the plasma collisionality, i.e., ion-electron and ion-neutral collisions. Namely, the holes are enhanced in highly collisional edge whereas the blobs are weakened at the SOL, causing larger particle convection. These blob/hole dynamics are closely correlated with potential dipoles. The trends are experimentally evidenced on the HL-2A tokamak. Moreover, as the neutral-ion collision increases, the blobs at the SOL tend to develop into streamers propagating outwards with reduced amplitude while the holes inwards are suppressed, showing a key role in nonlinear structure regulation and resultant transport suppression. Results suggest that adjusting the plasma collisionality by fueling, e.g., gas puffing, could serve as a method to nonlinearly select turbulent structures, i.e., blobs, holes or streamers, to access the control of boundary transport.

Spatiotemporal Oscillations in Tokamak Edge Layer and their Generation by Various Mechanisms

U. Daybelge¹, C. Yarim¹, and A. Nicolai²

¹*Istanbul Technical University, Istanbul, Turkey*

²*Forschungszentrum Jülich, Jülich, Germany*

Corresponding Author: daybelge@itu.edu.tr

Toroidal and poloidal rotations of plasma at the edge region of tokamak devices have long been known to play an important role, such as enhancing the confinement properties by suppressing turbulent behaviour, improving tolerance to error fields and increasing stability to neoclassical tearing modes. Hence, understanding of creation and evolution of rotation is important, since external momentum would not be enough or could not even be realized especially for future large fusion devices. In addition to the externally applied momentum, several mechanisms have been suggested to explain the reasons for spontaneous toroidal rotation of plasmas. For a tokamak edge region as found, for example, within the operational boundaries of the ASDEX upgrade, relevance of the collisional neoclassical theory was recently emphasized. In this regime gyro stresses play a considerable role in modifying the coupled flux surface averaged continuity, energy and momentum equations. Examination of the terms in these equations that are responsible for diffusion or reaction and acting as sources, can show the share of the neoclassical mechanisms to terms like intrinsic rotation, etc. Using similarities of our equations to the nonlinear reaction-diffusion equations with a susceptibility to the Turing instability and applying some robust numerical methods, we present here an approach based on the spatiotemporal simulation of the oscillations in plasma temperature, density, toroidal and poloidal rotation velocities under various perturbative effects. Present study considers a subsonic, collisional plasma in front of the magnetic separatrix. Study indicates a nonlinear, three-time-scales-coupling between the evolutions of the density, temperature and poloidal and toroidal rotation velocities. Numerical solutions of the coupled system for the vector $W = [T, N, U_\phi, U_\theta]$ were studied under various given sources such as a periodic pellet injection or loop voltage variation with chosen initial and Dirichlet or Neumann-boundary-conditions at the both ends of the radial boundary layers. Some of these effects were seen, to lead to a chaotic spatiotemporal behaviour of W , or to lead to rapidly diverging rotation velocity profiles. Steep gradients in assumed initial profiles were found in most cases, to enhance such effects.

Impact on Divertor Operation of the Pattern of Edge and SOL Flows Induced by Particle Sources and Sinks

P. Ghendrih¹, T. Auphan², B. Bensiali³, M. Bilanceri⁴, K. Bodi^{3,5}, J. Bucalossi¹,
H. Bufferand^{1,3}, G. Chiavassa³, G. Ciracolo³, R. Futtersack¹, H. Guillard⁴,
C. Guillemaut¹, Y. Marandet⁶, A. Mentrelli², D. Moulton¹, A. Paredes³, R. Pasquetti⁷,
E. Serre³, F. Schwander³, and P. Tamain¹

¹CEA-IRFM, Saint Paul-lez-Durance, France

²LATP, Technopole de Château-Gombert, Marseille, France

³M2P2, Technopole de Château-Gombert, Marseille, France

⁴INRIA, Sophia Antipolis & LJAD, Nice, France

⁵Dept. of Aerospace Engg., IIT Bombay, Mumbai, India

⁶PIIM, CNRS/Aix-Marseille Université, Marseille, France

⁷LJAD, Nice, France

Corresponding Author: philippe.ghendrih@cea.fr

The role of divertors in present device operation is to control particle sources and sinks and consequently the energy flux channels in the boundary region of magnetically confined plasmas. The ESPOIR effort is based on a set of fluid codes from 1-D parallel to 3-D micro-turbulence modelling. Due to the long range particle transport into the SOL governed by intermittent turbulent bursts, the precise location of the particle sources at the wall is required to properly address the screening of the neutral particle influx. To that end we have developed a penalisation technique that extends the simulation domain up to all the plasma facing components of interest. The penalisation technique initiated for particle and momentum sinks has been extended to the temperatures as well as to electric currents. We have used the penalisation technique in 2D simulations of the radial shift of the plasma from the low field side modular limiter to the high field side bumper limiter. Experiments of the kind were achieved in TFTR, JET and Tore Supra to investigate the particle confinement time and particle trapping in the wall. We show that the ballooned transport plays a crucial role in these experiments so that most of the core density drop is reversible. In the divertor configuration, low ionisation sources are shown to govern a supersonic solution. Simulations of such a regime exhibit weak divertor density variation as the core plasma density is ramped up, in agreement with analytical predictions. In the standard divertor regimes, we show analytically that the plasma tends to a supersonic flow when the total plasma pressure is conserved along the field lines. The back transition to the subsonic flow at the plate then takes place at the cross-over between the diffusive heat transport and the convective energy transport. Such behaviour disappears when total plasma pressure losses take place. In the case of very strong divertor screening one finds a Mach number close to zero at the X-point and that the core particle fuelling is governed by the main chamber recycling. In this limit case, we thus model the known bifurcation between the low and high screening SOL and its possible relationship to the H-mode termination and density limit physics. Edge plasma turbulence simulations will also be addressed in conjunction with the effects of volumetric sources and large scale flows.

TH-P

Modelling of Plasma Response to Resonant Magnetic Perturbations and its Influence on Divertor Strike Points

P. Cahyna¹, Y. Liu², E. Nardon³, A. Kirk², J. Harrison², A. Thornton², I. Chapman²,
M. Peterka¹, R. Panek¹, and O. Schmitz⁴

¹*Institute of Plasma Physics AS CR, Prague, Czech Republic*

²*EURATOM/CCFE Fusion Association, Culham Science Centre, Abingdon, UK*

³*Association Euratom/CEA, CEA Cadarache, St. Paul-lez-Durance, France*

⁴*Forschung Zentrum Jülich, Jülich, Germany*

Corresponding Author: cahyne@ipp.cas.cz

Resonant magnetic perturbations (RMPs) for edge localized mode (ELM) mitigation in tokamaks can be modified by the plasma response and indeed strong screening of the applied perturbation is in some cases predicted by simulations. In this contribution we investigate what effect would such screening have on the spiralling patterns (footprints) which may appear at the divertor when RMPs are applied. We use two theoretical tools for investigation of the impact of plasma response on footprints: a simple model of the assumed screening currents, which can be used to translate the screening predicted by MHD codes in a simplified geometry into the real geometry, and the MHD code MARS-F. The former consistently predicts that footprints are significantly reduced when complete screening of the resonant perturbation modes (like it is the case in ideal MHD) is assumed. This result is supported by the result of MARS-F in ideal mode for the case of the MAST tokamak. To predict observed patterns of fluxes it is necessary to take into account the deformation of the scrape-off layer, and for this we developed an approximative method based on the Melnikov integral. If the screening of perturbations indeed reduces the footprints, it would provide us with an important tool to evaluate the amount of screening in experiments, as the footprints can be easily observed. We thus present a comparison between predictions and experimental data, especially for the MAST tokamak, where a significant amount of data has been collected.

Self-consistent Kinetic Simulation of RMP-driven Transport: Collisionality and Rotation Effects on RMP Penetration and Transport

G. Park¹, C. Chang², Y. Jeon¹, and J. Kim¹

¹*NFRI, Daejeon, Republic of Korea*

²*Princeton Plasma Physics Laboratory, Princeton, USA*

Corresponding Author: gypark@nfri.re.kr

Control of the edge localized modes (ELMs) is one of the most critical issues for a more successful operation of ITER and the future tokamak fusion reactors. This paper reports ITER relevant simulation results from the XGC0 drift-kinetic code, with respect to the collisionality, plasma density, and rotation dependence of the RMP penetration and the RMP-driven transport in diverted DIII-D geometry with neutral recycling. The simulation results are consistent with the experimental results, and contribute to the physics understanding needed for more confident extrapolation of the present RMP experiments to ITER. It is found that plasma-responded stochasticity becomes weaker as the collisionality gets higher and RMP-driven transport (i.e., density pump-out) is much weaker in the high collisionality case compared with that in the low collisionality one, which is consistent with the recent experimental results on DIII-D and ASDEX-U tokamaks. As for rotation effect, low rotation is found not to affect the stochasticity much in the edge region, while high rotation significantly suppresses the RMPs in the core. The clear difference in RMP behavior between the low and high collisionality regimes can be understood by examining the perturbed current Fourier amplitude profiles within the range of resonant poloidal mode numbers ($m = 8 - 15$, $n = 3$). It can be seen that primary shielding currents are strongly concentrated around the steep pedestal region just inside the separatrix, which naturally produces very strong suppression of RMPs there, in low collisionality case. However, in high collisionality case, primary shielding currents are very weak and accumulating toward inner radii leading to the shielding of RMPs further into the plasma. Our kinetic simulation method is also applied to the modeling of RMP ELM control experiments on KSTAR tokamak and the results will be presented together.

TH-P

Frequency Chirping during a Fishbone Burst

V. Marchenko¹, S. Reznik¹

¹*Institute for Nuclear Research, Kyiv, Ukraine*

Corresponding Author: march@kinr.kiev.ua

It is shown that gradual (more than a factor of two, in some cases - down to zero in the lab frame) reduction of the mode frequency (the so called frequency chirping) can be attributed to the reactive torque exerted on the plasma during the fishbone instability burst, which slows down the plasma rotation inside the $q = 1$ surface and reduces the mode frequency in the lab frame, while frequency in the plasma frame remains constant. This torque arises due to imbalance between the power transferred to the mode by energetic ions and the power of the mode dissipation by thermal species. Estimates show that the peak value of this torque exceeds the neutral beam torque in modern tokamaks and in ITER. The line-broadened quasilinear burst model, properly adapted for the fishbone case, is capable of reproducing the key features of the bursting mode.



Finite Orbit Width Features in the CQL3D Code

Y. V. Petrov¹, R. Harvey¹

¹ *CompX, Del Mar, USA*

Corresponding Author: petrov@compxco.com

The CQL3D Fokker-Planck equation solver is being upgraded to allow for the Finite-Orbit-Width (FOW) capabilities, which will provide an accurate description for a neoclassical transport, losses to the walls, and transfer of particles, momentum, and heat to the scrape-off layer. Two different options are discussed for implementing the FOW capabilities. In one option, the Fokker-Planck equation is solved for the distribution function of orbits centered around given flux surface; in the other, the equation is solved for the local distribution function at the outer-most point of flux surface at the midplane. Both options use a fast lookup table that allows characterization of orbits without actually tracing them. The lookup table, in effect, performs mapping from the Constants-Of-Motion space onto the (R_0, u_0, θ_0) computational space on the midplane. The FOW modifications have been implemented for the formations of neutral beam source, RF quasilinear diffusion operator, particle diagnostics and collisional operator, and internal boundary conditions are being refined. Initial test runs show that in general, the FOW modifications result in a broader profiles of power absorption and RF-driven current, and accurate description of the loss cone.

Electron Fishbone Simulations in FTU-like Equilibria Using XHMGC

G. Vlad¹, S. Briguglio¹, G. Fogaccia¹, F. Zonca¹, C. Di Troia¹, V. Fusco¹, and X. Wang²

¹ *Associazione Euratom-ENEA sulla Fusione, Rome, Italy*

² *IFTS, Zhejiang University, Hangzhou, China*

Corresponding Author: gregorio.vlad@enea.it

Internal kink instabilities exhibiting fishbone like frequency chirp down have been observed in a variety of experiments where a high energy electron population was present. The relevance of the electron fishbones is primarily related to the fact that suprathermal electrons are characterized by relatively small orbit width, when compared with those of fast ions, similarly to the case of alpha particles in burning plasmas: thus, electron fishbones offer the opportunity to study the coupling between energetic particles and MHD modes in burning plasma relevant conditions even in present machines. In fact, precession resonance depends on energy, not mass; meanwhile, suprathermal electron transport perpendicular to the equilibrium magnetic field caused by fishbones can reflect some properties of fluctuation induced transport of fusion alphas due to precession resonance. The nonlinear MHD-Gyrokinetic code (HMGC) has been recently extended (from which the name XHMGC) to include new physics, including both thermal ion compressibility and diamagnetic effects, and finite parallel electric field due to parallel thermal electron pressure gradient, which enters the parallel Ohm's law and generalizes it, accounting for the kinetic thermal plasma response. Moreover, XHMGC is now able to treat up to three independent particle populations kinetically, assuming different equilibrium distribution functions (as, e.g., bulk ions, energetic (ion and/or electrons) particles accelerated by NBI, ICRH, fusion generated alpha particles, etc.). We will refer to the typical parameters of the FTU machine, where electron fishbones appearance has occurred in Lower Hybrid heated discharges. The FTU-like equilibrium corresponds to a torus with circular shape cross section, with an inverse aspect ratio ~ 0.3 . The safety factor profile has been assumed slightly reversed. Energetic electrons, described by a strongly anisotropic Maxwellian distribution function (thus, retaining resonant excitation), and the bulk ions, described by isotropic Maxwellian (in order to account for thermal ion Landau damping and finite compressibility) will be treated kinetically. A detailed study of single particle resonant frequencies during linear phase of the mode will be presented, together with nonlinear dynamics characterization of single particle motion in phase space during mode saturation.

Alpha Particle Redistribution in Sawteeth

R. Farengo¹, H. Ferrari^{1,2}, P. Garcia-Martinez^{1,2}, M. C. Firpo³, and A. Lifschitz⁴

¹*Centro Atómico Bariloche and Instituto Balseiro, Bariloche, Argentina*

²*CONICET, Bariloche, Argentina*

³*Laboratoire de Physique des Plasmas, École Polytechnique, Palaiseau, France*

⁴*Université Paris Sud, Orsay, France*

Corresponding Author: farengo@cab.cnea.gov.ar

The dynamics of alpha particles will be extremely important in ITER and future fusion reactors. Sawteeth can redistribute the alpha particles, thus modifying the power deposition profile and increasing alpha particle losses and wall loading. It is also hoped that they will help removing the helium ash. We study the effect of sawteeth on alpha particle confinement by following the trajectories of a large number of particles. The total electric and magnetic fields, sum of the equilibrium plus perturbation, are used to calculate the trajectories. Two approaches are being employed to calculate these fields. The first one uses a simple analytical equilibrium with ITER like parameters and $q_{\text{axis}} < 1$ and the experimental information regarding the space and time dependence of the displacement eigenfunction to calculate the total fields. Using ideal MHD, the perturbed magnetic field is calculated as the curl of the cross product of the displacement with the equilibrium field and the perturbed electric field is obtained from Ohm's law. The second method uses a more realistic equilibrium, solution of a nonlinear Grad-Shafranov equation, and 3D resistive MHD simulations to calculate the total fields. A "diffusion coefficient" is introduced to quantify the displacement of the particles from their initial flux surface and different particle energies and mode frequency and amplitude are employed.

Effect of Density Fluctuations on LHCD and ECCD and Implications for ITER

Y. Peysson¹, J. Decker¹, and S. Coda²

¹CEA, Saint-Paul-lez-Durance, France

²CRPP-EPFL, Lausanne, Switzerland

Corresponding Author: yves.peysson@cea.fr

The role played by electron density fluctuations near the plasma edge on rf current drive in tokamaks is assessed quantitatively. For this purpose, a general framework for incorporating density fluctuations in existing modelling tools has been developed. It is valid when rf power absorption takes place far from the fluctuating region of the plasma. The ray-tracing formalism is modified in order to take into account time-dependent perturbations of the density, while the FokkerPlanck solver remains unchanged. The evolution of the electron distribution function in time and space under the competing effects of collisions and quasilinear diffusion by rf waves is determined consistently with the time scale of fluctuations described as a statistical process.

Using the ray-tracing code C3PO and the 3D linearized relativistic bounce-averaged Fokker-Planck solver LUKE, the effect of electron density fluctuations on the current driven by the lower hybrid (LH) and the electron cyclotron (EC) waves is estimated quantitatively. A thin fluctuating layer characterized by electron drift wave turbulence at the plasma edge is considered. The effect of fluctuations on the LH wave propagation is equivalent to a random scattering process with a broadening of the poloidal mode spectrum proportional to the level of the perturbation. However, in the multipass regime, the LH current density profile remains sensitive to the ray chaotic behaviour, which is not averaged by fluctuations. The effect of large amplitude fluctuations on the EC driven current is found to be similar to an anomalous radial transport of the fast electrons. The resulting lower current drive efficiency and broader current profile are in better agreement with experimental observations. Finally, applied to the ITER ELMy H-mode regime, the model predicts a significant broadening of the EC driven current density profile with the fluctuation level, which can make the stabilization of neoclassical tearing mode potentially more challenging.

Fully Gyrokinetic Modeling of Beam-driven Alfvén Eigenmodes in DIII-D Using GYRO

E. M. Bass¹, R. E. Waltz²

¹*University of California San Diego, La Jolla, USA*

²*General Atomics, San Diego, USA*

Corresponding Author: bassem@fusion.gat.com

Linear properties of a spectrum of Alfvén eigenmodes (AEs) have been investigated in a benchmark DIII-D shear-reversed discharge using the gyrokinetic code GYRO [1]. GYRO's gyrokinetic global eigenvalue solver tracks a linearly interacting spectrum of two toroidal Alfvén eigenmodes (TAEs) and a reverse-shear Alfvén eigenmode (RSAE), all at $n = 3$, as they evolve over a short time slice of the discharge. Predicted frequencies agree well with experiment over most of the RSAE frequency sweep range. As the discharge evolves, RSAEs and TAEs are shown to exchange identity and even hybridize into modes with identifying features of both types. Observed kinetic corrections to eigenfunction structure, most notably a twist of the eigenfunction in the poloidal plane that experiments confirm [2], have likely implications for mode stability, and thus energetic particle (EP) confinement [3], in ITER and future fusion devices. Although driving EPs certainly induce the eigenfunction twist, this and other work [4] shows relative insensitivity to the EP profile for unstable modes. In experiment and present simulations, the twist direction always turns around near the first resonant surface outside the minimum in q . Most modes also exhibit some degree of EP-induced broadening of poloidal harmonics, most visible in regions of high magnetic shear. This broadening is characteristic of energetic particle modes (EPMs) [5] and illustrates a transition from parallel velocity dominance to drift orbit frequency dominance in the driving EP resonance condition across the extended mode footprint. The present results also shed light on details of the experimental spectrogram controlled by interaction of observed unstable modes and more weakly driven modes not visible in the experiment.

References

- [1] J. Candy and R. E. Waltz, Phys. Rev. Lett. **91** (2003) 045001.
- [2] B. J. Tobias, *et al.*, Phys. Rev. Lett. **106** (2011) 075003.
- [3] R. B. White, *et al.*, Phys. Plasmas **17** (2010) 056107.
- [4] B. J. Tobias, *et al.*, submitted to Nucl. Fusion (2011).
- [5] E. M. Bass and R. E. Waltz, Phys. Plasmas **17** (2010) 112319.

This work was supported by the US Department of Energy under DE-FG02-95ER54309 and DE-FC02-08ER54977.

Differences Between QL and Exact Ion Cyclotron Resonant Diffusion

R. W. Harvey¹, Y. V. Petrov¹, E. F. Jaeger², P. T. Bonoli³, and A. Bader³

¹*CompX, Del Mar, USA*

²*XCEL Engineering, Oak Ridge, USA*

³*PSFC, Massachusetts Institute of Technology, Cambridge, USA*

Corresponding Author: rwharvey@compxco.com

This work reports on some differences between ICRF quasi-linear (QL) diffusion theory and diffusion coefficients obtained with an exact orbit calculation using the DC (Diffusion Coefficient) code. The calculations model NPA experimental results for an Ion Cyclotron Resonant Heating (ICRH) C-Mod minority heating experiment. The DC results indicate a shorter rampup time for NPA fluxes than obtained using QL theory, in general agreement with the experiment.

Diffusion coefficients calculated with ICRF quasilinear(QL) theory are compared with results from exact Lorentz orbits in full-wave fields from the AORSA full-wave code. The orbit-calculations are carried out using the parallelized, DC code which calculates nonlinear RF diffusion by suitable average of RF induced changes in particle velocity by numerically integrating the ion Lorentz force equation in the combined equilibrium and RF EM fields. Inclusion of a full toroidal mode spectrum shows that most correlations cease to exist after one poloidal circuit, justifying modeling of the diffusion with the dominant $n_\phi = 10$ mode, neglecting correlations beyond the first turn. This enables faster time-dependent modeling of the minority hydrogen distribution function. The radial power absorption profiles are quite close, whether using QL theory or the full DC diffusion coefficients. However, a significant discrepancy does appear for pitch angle diffusion at near perpendicular angle in velocity space. Our working hypothesis is that this results from a finite gyro-orbit effect, which becomes important at higher energies.

The C-Mod, vertically viewing Neutral Particle Analyzer has, in separate studies by Dr. Aaron Bader, MIT, been shown to produce steady state spectra in reasonably good agreement with the coupled AORSA(QL)-CQL3D Fokker-Planck simulations. However, the NPA fluxes achieve steady state more rapidly than the QL simulations predict, and also decay significantly faster. On the other hand, the coupled, time-dependent AORSA-DC-CQL3D calculation shows that the additional pitch angle scattering, discovered with DC, provides an explanation of the more rapid NPA flux turn-on. The vertical NPA is particularly sensitive to the near perpendicular velocity fast ions populated by the additional pitch angle scattering. Simulation of the turn-off phase of the fast ion distribution is in progress.

Theoretical and Numerical Studies of Wave-packet Propagation in Tokamak Plasmas

Z. Lu^{1,2}, F. Zonca^{2,3}, and A. Cardinali²

¹*School of Physics, Peking University, Beijing, China*

²*Associazione EURATOM-ENEA sulla Fusione, Roma, Italy*

³*Institute for Fusion Theory and Simulation, Zhejiang University, Hangzhou, China*

Corresponding Author: luzhixinpku@gmail.com

Theoretical and numerical studies of wave-packet propagation are presented to analyze the time varying 2D mode structures of electrostatic fluctuations in tokamak plasmas, using general flux coordinates. Instead of solving the 2D wave equations directly, the solution of the initial value problem is obtained, following the propagation of wave-packets generated by a source and reconstructing the time varying field. As application, the 2D WKB method is applied to investigate the shaping effects (elongation and triangularity) of tokamak geometry on the lower hybrid wave propagation and absorption. Meanwhile, the mode structure decomposition (MSD) method is used to handle the boundary conditions and simplify the 2D problem, casted into two nested 1D problems. The MSD method is related to that discussed in earlier works and reduces to the well-known “ballooning formalism”, when spatial scale separation applies. This method is used to investigate the time varying 2D electrostatic ITG mode structure with a mixed WKB-full wave technique. The time varying field pattern is reconstructed and the time asymptotic structure of the wave-packet propagation gives the 2D eigenmode and the corresponding eigenvalue. As a general approach to investigate 2D mode structures in tokamak plasmas, our method also applies for electromagnetic waves with general source/sink terms, either by an internal/external antenna or nonlinear wave interaction with zonal structures.

This work is supported by the Chinese Scholarship, Euratom Communities under the contract of Association between EURATOM/ENEA, NSFC, National Basic Research Program of China (973 Program), and National ITER Program of China.

TH-P

Global Theories of Geodesic Acoustic Modes: Excitation by Energetic Particles and Drift Wave Turbulences

Z. Qiu¹, F. Zonca², and L. Chen³

¹*Institute for Fusion Theory and Simulation, Zhejiang University, Hangzhou, China*

²*Associazione EURATOM-ENEA sulla Fusione, Rome, Italy*

³*Department of Physics and Astronomy, University of California, Irvine, USA*

Corresponding Author: zyzhou@mail.ustc.edu.cn

Excitation of Geodesic Acoustic Modes (GAMs) by both energetic particles (EPs) and drift wave (DW) turbulences taking into account plasma nonuniformities are investigated in this work. The global radial mode structures of EP induced GAM (EGAM) are systematically studied and their properties are found to depend on the nonuniformities of both the GAM continuous spectrum and EP radial profile. For a radially broad EP drive, the eigenmode equation valid for arbitrary EP drift orbit width is derived, and then solved using a Fourier transformation technique. The excited EGAM is shown to strongly couple to the GAM continuous spectrum; resulting in a finite drive threshold in EP density. The cross-scale couplings between micro-, meso- and macro-scales, discussed in this work, are mediated by the EP dynamics and have many interesting similarities with complex behaviors, expected in burning plasmas of fusion interest. The excitation of GAM by DW turbulence accounting for various kinetic dispersiveness and nonuniformities is also investigated, with the paradigm of three-wave resonant parametric decay instability. Considering the scale length of linear DW eigenmode envelope is much smaller than that of particle diamagnetic drift frequency L^* , in the linear growth phase, the parametric instability is convective for typical tokamak parameters, when the finite group velocities of GAM and DW sideband are taken into account. This is a case of less practical interest. However, if we look at longer time scales, and finite L^* effects are taken into account, the convectively amplified GAM-DW wave-packet pair is reflected at the DW linear turning points, resulting in a quasi-exponentially growing absolute instability. DW turbulence spreading with the excitation of GAM is also investigated, with emphasis on quantitative understanding of the dispersiveness associated with kinetic GAM.

Integrated Plasma Simulation of Lower Hybrid Current Profile Control in Tokamaks

P. Bonoli¹, R. W. Harvey², J. C. Wright¹, J. Chen³, D. B. Batchelor⁴, A. E. Hubbard¹,
S. C. Jardin³, C. E. Kessel³, R. R. Parker¹, and S. Shiraiwa¹

¹*Massachusetts Institute of Technology, Cambridge, USA*

²*CompX Corporation, Del Mar, USA*

³*Princeton Plasma Physics Laboratory, Princeton, USA*

⁴*Oak Ridge National Laboratory, Oak Ridge, USA*

Corresponding Author: bonoli@psfc.mit.edu

Lower hybrid (LH) waves have the attractive property that they damp efficiently via Landau resonance at relatively low electron temperature on “tail electrons” at parallel phase speeds that are approximately 2.5 – 3.0 times the electron thermal speed. As a consequence they can be used to drive current in the outer half of tokamak plasmas in order to broaden the current profile and access and optimize improved energy confinement regimes. In order to assess the use of lower hybrid (LH) current profile control in present day devices and in future reactor designs we have developed a time dependent simulation capability for this type of plasma control and tested it using sawtooth modification experiments via LHCD that were performed in the Alcator C-Mod device. These experiments were initially simulated using the TSC transport code to evolve the background plasma and the Porcelli model to predict sawtooth behavior. The LHCD was calculated using the LSC code and the predicted LH current was 200 – 250 kA with a total plasma current of 450 kA.

In order to improve the physics fidelity of the LHCD calculation we have taken advantage of a parallel framework, the Integrated Plasma Simulator (IPS), where the driven LH current density profiles are computed using a ray tracing component (the GENRAY code) and a Fokker Planck component (the CQL3D code), that are iterated in a coupled time advance with TSC. The GENRAY code affords a more detailed description of the LH launcher including its poloidal extent and the CQL3D code allows for an accurate description of the 2-D velocity space effects in the wave damping; both effects of which are known to be very important for LH wave propagation and absorption.

We shall present time dependent comparisons of predicted profiles of LH current drive obtained from both coupled TSC-LSC and TSC-GENRAY-CQL3D simulations over an entire discharge simulation. The IPS framework also includes an ion cyclotron range of frequency (ICRF) component, the massively parallel TORIC solver. We will also show predictive simulations for C-Mod where LHRF power is injected into discharges that have been pre-heated using the ICRF mode conversion heating scheme in order to raise the background electron temperature and thus increase the single pass damping of the LH waves into the target plasma.

TH-P

Advanced ICRF Scenarios and Antennae for Large Fusion Machines from JET to DEMO

V. Vdovin¹

¹ *Tokamak Physics Institute NRC Kurchatov Institute, Moscow, Russian Federation*

Corresponding Author: vdov@nfi.kiae.ru

Recent JET ICRF experiments in ITER-like new Be chamber demonstrated strongly larger Tungsten content in plasma core compared with the NBI case thus evidencing remarkable waves interaction with a boundary plasma and wall. Also it was reported the remarkable Antennae loading resistance decrease for four Antennae A2 used when compared with previous datas for Carbon wall.

We have performed extensive 3D STELION code (coupled with 2D F-P solver) modeling of the Minority ions scenarios D(H), D(He³) and Heavy minority D(Be) scenario for JET, IGNITOR, ITER and DEMO plasmas. All these scenarios demonstrate the multi pass absorption regimes with multiple FW eigen modes excitation of the Toroidal resonators thus involving some power deposition to the periphery plasmas presumably being reason for impurities release. These results are supported by accurate novel analytical formula for FW optical thickness. Extremely energetic and strongly anisotropic proton tails, dragged by electrons, in D(H) or He⁴(H) scenarios are demonstrated for all above machines. The Beryllium Heavy minority scenario D(Be), proposed and modelled for JET, is better one due to Be tails absence but still suffers by multi pass absorption regime. This last scenario permits Be content determination in plasma core by experimentally identifying the D-Be ion-ion hybrid layer position.

Fortunately we have found by 3D simulations, supported by analytical formulas, that minority hydrogen second harmonic scenario crucially improves the wave absorption providing the Single Pass Absorption (SPA) regime. Higher frequencies (for JET's proposal ~ 57 MHz) from 57 to 352 MHz to new scenario for the above machines, starting from ITER (80 & 152 MHz), give a possibility to drastically increase the coupling antenna-plasma and a possibility to use resonators/waveguides types antennae which are much higher electrically strong, are compact and easily matched with RF generators. Problems with interloops mismatching for multi loops antennae, met for ILA on JET, and now designed for similar ITER antenna, are overcome. Concepts of these antennae for ITER and IGNITOR will be shown. The Hydrogen minority contents are 6% for D-T ITER and DEMO, 10% for IGNITOR and 15 – 20% for JET D-He⁴ plasmas.

Kinetic Integrated Modeling of Burning Plasmas in Tokamaks

A. Fukuyama¹, H. Nuga², D. Raburn¹, A. Wakasa¹, and S. Murakami¹

¹*Kyoto University, Kyoto, Japan*

²*Tsukuba University, Tsukuba, Japan*

Corresponding Author: fukuyama@nucleng.kyoto-u.ac.jp

In order to self-consistently describe the behavior of burning plasmas in the presence of energetic particles, we have been developing a kinetic integrated tokamak modeling code TASK3G. This modeling is based on the behavior of the momentum distribution function of each particle species. The time evolution of the momentum distribution function is described by an advanced Fokker-Planck component TASK/FP and the influence of energetic particles on global stability is studied by a full wave component TASK/WM. The start up of ITER plasmas with multi-scheme heating and current drive is studied including radial transport and fusion reaction rate calculated from the momentum distribution function. We have confirmed that the momentum dependence of the radial diffusion coefficients strongly affects the profiles of energetic ions and fusion output power. The linear stability of global eigen modes in the presence of energetic particles is also discussed.

Subcritical Growth of Coherent Phase-space Structures

M. Lesur¹, P. H. Diamond²

¹*NFRI, Daejeon, Republic of Korea*

²*CMTFO and CASS, UCSD, La Jolla, USA*

Corresponding Author: maxime.lesur@polytechnique.org

Coherent phase-space structures are an important feature of plasma turbulence. They can drive nonlinear instabilities, intermittency in drift-wave turbulence, and cause transport that departs from quasilinear predictions. Our theoretical and numerical efforts are directed toward a comprehensive understanding of turbulence, not merely as an ensemble of waves, but as a mixture of coupled waves and localized structures. This work focuses on phase-space structure dynamics and reports significant progress in this direction. We start with the Berk-Breizman model, a tractable paradigm for wave-particles interactions, in the presence of extrinsic dissipation. Despite its apparent simplicity, this model exhibits a wealth of complex nonlinear behavior, relevant to Alfvén wave experiments, the travelling wave tube quasilinear experiment with a lossy helix, or nonlinear wave-particle interaction effects on zonal flows. In this work, we present a new theory which describes the growth of coherent structures called as holes and clumps, which can in turn drive the wave by direct momentum exchange due to the dissipation. This mechanism explains the existence of nonlinear instabilities in both barely unstable and linearly stable (subcritical) regimes. In addition, theory predicts a criterion for nonlinear instability, which sets a minimum size of the seed structure. Simple expressions of the hole/clump growth rate and the initial perturbation threshold are in quantitative agreement with numerical simulations. The nonlinear instability in the barely unstable regime, which is predicted by our theory, is observed for the first time in simulation. Extending the model to multiple resonances, our simulations show that coalescing holes survive much longer than the classical quasilinear diffusion time and dominate the nonlinear evolution.

Numerical Simulations of NBI-driven GAE modes in L-mode and H-mode Discharges in NSTX

E. Belova¹, N. N. Gorelenkov¹, E. D. Fredrickson¹, H. L. Berk², G. J. Kramer¹, and S. S. Medley¹

¹*Princeton Plasma Physics Laboratory, Princeton, USA*

²*Institute for Fusion Studies University of Texas, Austin, USA*

Corresponding Author: ebelova@pppl.gov

Hybrid 3D code HYM has been used to investigate properties of beam ion driven GAE modes in NSTX. The HYM code is a nonlinear, global stability code in toroidal geometry, which includes fully kinetic ion description. Excitation of GAE modes have been studied for L-mode and H-mode NSTX discharges. Equilibrium profiles and plasma parameters have been chosen to match several of the NSTX discharge numbers profiles, and the HYM equilibrium solver has been modified to improve the equilibrium fit to the TRANSP and EFIT profiles. Numerical simulations for H-mode have been performed for the NSTX shots, where a GAE activity and related High-Energy Feature (HEF) have been observed. HYM simulations comparison with experimental results for NSTX L-mode shots, show good agreement in terms of the most unstable toroidal mode numbers, frequency, amplitude and the mode structure. It has been shown that most resonant particles have stagnant orbits, and poloidal structure of the unstable mode is relatively coincident with location of the resonant orbits. Linearized and nonlinear simulations have been performed in order to study in detail resonant wave-particle interaction in order to understand the nonlinear evolution of the instability.

Nonlinear Simulation of Energetic Particle Modes in JT-60U

A. Bierwage¹, N. Aiba², W. Deng³, M. Ishikawa², G. Matsunaga², K. Shinohara²,
Y. Todo⁴, and M. Yagi¹

¹*Japan Atomic Energy Agency, Rokkasho, Japan*

²*Japan Atomic Energy Agency, Naka, Japan*

³*University of California, Irvine, USA*

⁴*National Institute for Fusion Science, Toki, Japan*

Corresponding Author: bierwage.andreas@jaea.go.jp

Global nonlinear simulations of intermittent large-amplitude events (ALE) observed in neutral-beam-driven JT-60U plasmas are performed. For the first time, simulations of these relaxation events are performed with realistic flux surface geometry and bulk plasma pressure. Comparisons with earlier results obtained with a circular plasma model and zero bulk pressure are made. It is found that plasma shaping reduces linear growth rates and initial saturation levels by factors 2 – 2.5. In agreement with theoretical predictions, a destabilizing influence of bulk pressure and stabilizing influence of compressibility is observed. Radial mode location and frequencies are comparable in all cases and agree with experimental results. During the first burst of mode activity (within 100 microseconds), energetic ion transport is reduced by a factor 3 – 4 due to shaping and finite beta effects. The first burst is followed by complicated dynamics, which vary from case to case. Interestingly, at the end of the relaxation event (after a few 100 microseconds), the cumulative loss of energetic ions from the central core region is comparable in all cases. Since the present study deals with a tokamak plasma subject to strong drive from energetic particles, the results are relevant to burning plasma research as will be pursued in JT-60SA and ITER.

Low Threshold Parametric Decay Instabilities at ECRH in Toroidal Devices Leading to Anomalous Absorption Phenomena

A. Popov¹, E. Gusakov¹, and A. Saveliev¹

¹*Ioffe Institute, St. Petersburg, Russian Federation*

Corresponding Author: a.popov@mail.ioffe.ru

Electron cyclotron resonance heating (ECRH) at power level of up to 1 MW in a single microwave beam is often used in present day tokamak and stellarator experiments and planned for application in ITER. Parametric decay instabilities (PDI) leading to anomalous reflection and/or absorption of microwave power are believed to be deeply suppressed in MW power level heating experiments utilizing gyrotrons. However during the last decade a “critical mass” of observations has been obtained evidencing presence of anomalous phenomena that accompany ECRH experiments at toroidal devices. Among them one can mention non local electron transport accompanying ECRH in some devices, observations of the anomalous backscattering signal in the 200 – 600 kW level experiment at Textor tokamak and, finally, fast ion generation often observed in many machines during ECRH pulse. The later two phenomena were observed at the non-monotonic plasma density profile.

In the present paper it is shown that in the case of sharp enough non-monotonic density profile the low-threshold (40 kW level for TCV experimental parameters) absolute PDI of the 2nd harmonic X-mode EC wave, leading to its anomalous absorption via decay into low frequency IB wave and high frequency electron Bernstein (EB) wave, may be excited due to the EB wave trapping in 3D toroidal cavity close to equatorial plane. This PDI can be responsible both for change of the power deposition profile and ion acceleration.

The effect of the parametric decay of the X-mode pump wave into two short wave-length upper hybrid (UH) plasmons propagating in opposite directions is considered as well. We demonstrate the possibility of the 3D localization of both the UH daughter waves. Similar to the mechanism of the EB wave trapping in radial direction, the radial localization of the UH wave can be achieved in a vicinity of the density profile local maximum often observed in ECRH experiments at toroidal devices (at the discharge axis for the peaked profile, at the edge for the hollow density profile or at the O-point of the magnetic island). The poloidal and toroidal UH waves trapping can be achieved, in particular, due to the finite size of the pump beam. The two-plasmon PDI can lead to the pump wave anomalous absorption and variation of the power deposition.

TH-P

Application and Development of the Gyro-Landau Fluid Model for Energetic-particle Instabilities

D. Spong¹

¹*Oak Ridge National Laboratory, Oak Ridge, USA*

Corresponding Author: spongda@ornl.gov

Reduced dimensionality models for energetic particle (EP) instabilities [1,2] provide good computational efficiency in simulation of EP-destabilized shear Alfvén modes through the use of Landau-fluid closure methods. This allows rapid testing of profiles and parameter variations and can facilitate understanding experimental results when not all quantities are precisely measured. The recent applications of this model (TAEFL) are the topic of this paper and include: RSAE to TAE frequency up-sweep transitions [3] in DIII-D advanced tokamak (reversed q -profile) regimes, antenna-based Alfvén damping measurements in JET [4], ITPA-EP benchmark studies, and ITER alpha and beam-driven instabilities [5]. The non-perturbative nature of this model is evident in the up-down MHD parity-breaking twist of the mode structures predicted for reversed shear q -profiles. Such characteristics are now measured experimentally [4], and provide a signature of the kinetic destabilization of these modes. Techniques have also been developed to extend the TAEFL model to more general forms of fast ion velocity distribution; by including two additional moments (parallel temperature and heat flux) slowing-down distributions, anisotropic Maxwellians and distributions with hole-clump perturbations can be modeled. Two further recent improvements in the TAEFL Landau closure are the coupling of sound waves and an extension of the existing tokamak initial value solver to an eigenvalue model that can treat both axisymmetric and 3D equilibria. The acoustic coupling effects were essential for modeling up-sweeping RSAE mode frequencies.

References

- [1] D. A. Spong, B. A. Carreras, C. L. Hedrick, *Physics of Fluids B* **4** (1992) 3316.
- [2] D. A. Spong, B. A. Carreras, C. L. Hedrick, *Phys. Plasmas* **1** (1994) 1503.
- [3] B. Tobias, I. G. J. Classen, C. W. Domier, W. W. Heidbrink, N. C. Luhmann, R. Nazikian, H. K. Park, D. Spong, and M. A. Van Zeeland, *Phys. Rev. Lett.* **106** (2011) 075003.
- [4] D. Testa, D. Spong, T. Panis, P. Blanchard, A. Fasoli, *et al.*, *Nuclear Fusion* **51** (2011) 043009.
- [5] M. A. Van Zeeland, N. N. Gorelenkov, W. W. Heidbrink, G. J. Kramer, D. A. Spong, *et al.*, *Nuc. Fus.* (2012).

Acknowledgements - This work was supported by the U.S. Department of Energy under contract DE-AC05-00OR22725 with UT-Battelle, LLC, under the U.S. DOE SciDAC GSEP Center and under the contracts DE-FC02-08ER54977 and DE-FC02-04ER54698.

Linear Properties and Nonlinear Frequency Chirping of Energetic Particle Driven Geodesic Acoustic Mode in LHD

H. Wang¹, Y. Todo^{1,2}, and C. Kim³

¹*The Graduate University for Advanced Studies, Hayama, Japan*

²*National Institute for Fusion Science, Toki, Japan*

³*University of Washington, Seattle, USA*

Corresponding Author: wanghao@nifs.ac.jp

Linear properties and nonlinear evolution of energetic particle driven geodesic acoustic mode (GAM) have been investigated for the Large Helical Device (LHD) plasmas with a hybrid simulation code for energetic particles and magnetohydrodynamics (MHD). Good agreement was found for the frequency and the spatial location of GAM between the experiment and the simulation. Frequency chirping up of the GAM was observed in the experiment. We found frequency chirping takes place in the nonlinear evolution of the GAM. We analyzed the fluctuation of the energetic particle distribution function and the energy transfer rate in velocity space. It was found that two pairs of hole and clump are formed along constant magnetic moment curves in velocity space. Transit frequencies of the holes and clumps are in good agreement with the GAM frequencies in the nonlinear phase. This indicates the holes and clumps keep resonant with the GAM when the frequency chirping takes place. It is clarified with the energy transfer analysis that the GAM amplitude evolution is governed by the interaction with the resonant particles in the hole at the high energy side.

Simulation of EPM Dynamics in FAST Plasmas Heated by ICRH and NNBI

C. Di Troia¹, S. Briguglio¹, G. Fogaccia¹, G. Vlad¹, and F. Zonca¹

¹ENEA, Rome, Italy

Corresponding Author: claudio.ditroia@enea.it

The Fusion Advanced Studies Torus (FAST) has been proposed as a possible European ITER Satellite facility, aimed at preparing ITER operation scenarios and experimentally studying burning plasma physics issues in deuterium plasmas. The external heatings in the extreme H-mode scenario of FAST are supplied by NNBI (Negative Neutral Beam Injection) and ICRH (Ion Cyclotron Resonance Heating).

Energetic particles generated by NNBI and minority population from ICRH can excite meso-scale fluctuations. For this reason, FAST can investigate radial transport of energetic ions due to collective mode excitations with the same characteristics of those expected in reactor relevant conditions.

The supra-thermal minority population produced by ICRH is characterized by peaked off-axis density distribution and effective perpendicular Temperature profiles. Moreover, the minority particles move mainly on trapped orbits. The supra-thermal population from NNBI shows an average pitch angle correlated to the beam injection angle. In this latter case, most of the particles follow passing orbits, with an imbalance between co- and counter-passing orbits.

Those behaviors can be described with a recently proposed parametric equilibrium distribution function which depends only on the invariants of motion and constant parameters. These parameters are chosen to be consistent with profiles produced by FAST NNBI and ICRH systems, respectively characterized by 1 MeV beam energy with 10 MW power and antenna frequency between 80 MHz and 85 MHz with 30 MW power, typically deposited on Helium minority. The reconstructed FAST scenario is used for numerical simulation studies with XHMGC, a MHD-gyrokinetic code which allows to treat simultaneously different populations of energetic particles and describes the thermal plasma by low-beta nonlinear reduced MHD equations with circular shifted magnetic surface equilibrium.

Linear and nonlinear EPM (Energetic Particle driven Mode) behaviors are analyzed, retaining self-consistently the mutual interaction between waves and energetic particles. The roles played by fast particle characteristic frequencies and radial profiles in determining the Alfvén fluctuation spectrum are studied and illustrated by detailed synthetic diagnostics.

Nonlinear Simulations of Beam-driven Geodesic Acoustic Mode in a DIII-D Plasma

G. Fu¹, R. Nazikian¹, R. Budny¹, M. Gorelenkova¹, G. R. McKee², and
M. van Zeeland³

¹*Princeton Plasma Physics Laboratory, Princeton, USA*

²*University of Wisconsin-Madison, Madison, USA*

³*General Atomics, San Diego, USA*

Corresponding Author: fu@pppl.gov

Recent experimental observation in neutral beam-heated DIII-D plasmas indicated that energetic particles can drive an axisymmetric mode unstable with frequency comparable to that of Geodesic Acoustic Mode (GAM)[1]. The instability has been identified by linear theory as an energetic particle-induced GAM mode or EGAM [2]. In this paper, we present first results of nonlinear hybrid simulations of beam-driven EGAM in DIII-D plasmas. The mode is driven by free energy associated with velocity space gradient of beam ion distribution function via wave particle resonant interaction. The calculated linear mode structure is strongly peaked in the core of plasma with clear radial propagation. In the nonlinear stage, the mode saturates due to flattening of particle distribution function. The mode spreads out radially with a significant second harmonic in density perturbation. The calculated mode frequency, saturation amplitude and mode radial propagation agree well with the Beam Emission Spectroscopy (BES) measurement. These results have important implications for burning plasmas such as ITER where EGAM might be excited by fast beam ions in steady state scenario with elevated q -profiles. The instability can significantly modify the fast beam ion distribution and associated beam-driven current. The EGAM could also interact with plasma micro-turbulence and affect thermal confinement.

References

- [1] R. Nazikian *et al.*, Phys. Rev. Lett. **101** (2008) 185001.
- [2] G. Y. Fu, Phys. Rev. Lett. **101** (2008) 185002.

Nonlinear Studies of β -Induced Alfvén Eigenmode Driven by Energetic Particles in Fusion Plasmas

X. Wang^{1,2}, S. Briguglio², L. Chen^{1,3}, G. Fogaccia², C. Di Troia², G. Vlad², and F. Zonca^{1,2}

¹*Institute for Fusion Theory and Simulation, Zhejiang University, Hangzhou, China*

²*Associazione EURATOM-ENEA sulla Fusione, Roma, Italy*

³*Department of Physics and Astronomy, University of California, Irvine, USA*

Corresponding Author: wangxinnku@zju.edu.cn

The β -induced Alfvén eigenmodes (BAEs) driven by energetic particles (EPs) are observed in early and recent experiments, which can lead to radial redistribution of EPs and, consequently, anomalous EP transport. In the present work, we have employed the nonlinear hybrid magnetohydrodynamic gyro-kinetic code (XHMGC), and investigated the excitation and nonlinear saturation of BAE via transit resonance with slowing-down beam ions. Saturation is found to be characterized by upward frequency chirping and symmetry breaking between co- and counter-passing particles, which can be understood as the evidence of radial resonance detuning. Further investigations on the scaling of the saturation amplitude with the growth rate is also found to be consistent with radial resonance detuning due to the radial non-uniformity and mode structure.

PIC Simulations of the Ion Flow Induced by Radio Frequency Waves in Ion Cyclotron Frequency Range

N. Xiang^{1,2}, C. Gan¹, J. Chen¹, and J. R. Cary^{2,3}

¹*Institute of plasma Physics, Chinese academy of Science, Hefei, China*

²*Center for Integrated Plasma Studies, University of Colorado, Boulder, USA*

³*Tech-X Corporation, Boulder, USA*

Corresponding Author: xiangn@ipp.ac.cn

PIC simulations have been conducted to study the nonlinear interactions of plasmas and radio frequency wave in the ion cyclotron frequency range. It is found that in the presence of the mode conversion from an electromagnetic wave into an electrostatic wave (ion Bernstein wave), the ions near the lower hybrid resonance can be heated by nonlinear Landau damping via the parametric decay. As a result, the ion velocity distribution in the poloidal direction becomes asymmetric near the lower hybrid resonance and an ion poloidal flow is thus produced. The flow directions are opposite on both sides of the lower hybrid resonance. The poloidal flow is mainly produced by the nonlinear Reynolds stress and the electromagnetic force of the incident wave in the radial direction rather than poloidal direction predicted by the existing theories.

Benchmarking of Codes for Spatial Profiles of Electron Cyclotron Losses with Account of Plasma Equilibrium in Tokamak Reactors

A. Kukushkin¹, P. Minashin¹

¹*NRC Kurchatov Institute, Moscow, Russian Federation*

Corresponding Author: kuka@nfi.kiae.ru

Potential importance of electron cyclotron (EC) wave emission in the local electron power balance in the steady-state regimes of ITER operation with high temperatures and in DEMO reactor suggested accurate calculations of the local net radiated power density, $P_{EC}(\rho)$. When central electron temperature increases to ~ 30 keV the local EC power loss can become a substantial part of heating from fusion alphas and is close to the total auxiliary heating. The first benchmarking of the codes for calculating the spatial profiles of EC power losses was carried out with the codes SNECTR, CYTRAN, CYNEQ, and EXACTEC in a wide range of temperature and density profiles expected in reactor-grade tokamaks, for a homogeneous magnetic field, $B(\rho) = \text{const}$. [1]. The benchmarking has shown good agreement of results within two different tasks:

1. Specular reflection in a circular cylinder (SNECTR, EXACTEC).
2. Diffuse reflection in any geometry or any type of reflection in noncircular toroids (SNECTR, CYTRAN, CYNEQ).

Here we extend the above benchmarking to the case of an inhomogeneous profile of magnetic field, which is calculated with allowance for plasma equilibrium. This extension covers comparison of CYNEQ results with those from the RAYTEC code, for prescribed temperature and density profiles, and from CYTRAN and EXACTEC for plasma profiles, including electric current density profile, obtained in the frame of self-consistent 1.5 D transport simulations in the frame of the ASTRA and the CRONOS suit of codes, respectively. This enables us to evaluate the role of plasma equilibrium effects (Shafranov shift, 2D plasma shape) on the $P_{EC}(\rho)$ profile. The role of plasma equilibrium is analyzed also in application to the to the similarity of normalized $P_{EC}(\rho)$ profiles, formerly observed in the calculations for the case of a constant magnetic field $B(\rho) = \text{const}$. The role of this universality for an independent, additional benchmarking of the codes, and for accuracy assessment, is analyzed. The present benchmarking makes a substantial step towards practical tasks of reactor-grade tokamaks ITER and DEMO.

References

- [1] F. Albajar, M. Bornatici, F. Engelmann and A. B. Kukushkin, Fusion Science and Technology **55** (2009) 76-83.

Nonlinear Ponderomotive Forces with the Consideration of the Spatial Variation of Wave Fields during the Resonant Interaction

Z. Gao^{1,3}, J. Chen^{2,3}

¹*Department of Engineering Physics, Tsinghua University, Beijing, China*

²*Institute of Plasma Physics, Chinese Academy of Science, Hefei, China*

³*Institute of Plasma Physics, CAS, China*

Corresponding Author: gaozhe@tsinghua.edu.cn

The quasi-linear diffusion theory catches the most important process in plasma-wave interaction, that is, the resonance. Besides basic assumptions on small amplitude and sufficient phase mixing, the quasi-linear theory also requires the damping or growth should be small compared to the real frequency or the wavelength. In practice, the slowly-varying is considered but the space-variation of waves is neglected during the resonance. However, the wave propagates in the plasma and feel the kinetic damping, its amplitude will decay. This effect will induce the ponderomotive force not only on the nonresonant particles, but also on the resonant particles. On the other hand, the conventional concept of ponderomotive force is in the single particle picture. Many previous works have extended this concept to consider the rf nonlinear force on a pack of plasma both in fluid and kinetic theory. However, incomplete treatment on the stress term would result in some fake conclusions.

In this work, the generalized rf force is investigated by using the second-order rf kinetic theory. The force inside the magnetic surface, i.e., parallel and tangential force, are especially focused on. Both forces include two parts. The one is proportional to the parallel momentum input, where the relation of the momentum and energy just like a particle. The other component is related to the variation of the wave amplitude; but is also completely the resonant term. Therefore the total force inside the magnetic surface depends on the resonant mechanism. This conclusion indicates again that the quasi-linear EM force is not a good approximation to the rf force since it includes the nonresonant component and results in some fake conclusions such as nonresonant drive by helicity injection in steady status. The components of the rf force due to the spatial-variation of wave fields during the resonant interaction can be reproduced from the single particle picture and the fluid theory. The magnitudes of the forces depend on the spectrum width comparing to the wavelength, the harmonics order and other factors. Special setup may make this kind of force significant so as to drive current/flow.

This work is supported by NSFC, under Grant Nos. 10990210, 10990214 and 11175103, and MOST of China, under Contract Nos. 2009GB105002 and 2008GB717804.

Parameter Study of Parametric Instabilities during Lower Hybrid Waves Injection into Tokamaks

A. Zhao¹, Z. Gao¹

¹*Tsinghua University, Beijing, China*

Corresponding Author: zhaoaihui@sunist.org

In order to explain the density threshold problem in lower hybrid current drive (LHCD), the parametric instability (PI) of LH waves is considered especially in the scrape-off plasma layer. Many previous works are performed on this topic and some methods are proposed to diminish the PI thus enable the penetration of the coupled LH power in the core of high density plasmas. However, the dependence of the PI on local density and other parameters seems not consistent with each other, which might be due to different parameter regions or the employment of different physical model with different simplifications. Here, we will try to give a comprehensive parameter study of the nonlinear dispersion relation of the PI during the LHW injection into plasmas, and then discuss the physical mechanism involved. In this work the drift kinetic model and fluid model will be employed. The result with the coupling coefficient containing both $\mathbf{E} \times \mathbf{B}$ drift term and the E_{\parallel} coupling term, is compared to that with the coupling coefficient only including $\mathbf{E} \times \mathbf{B}$ drift term. Both numerical and analytical results show that the E_{\parallel} coupling term becomes important for lower plasma density and smaller angle δ_1 (the angle between the perpendicular wavevector of the lower sideband and the pump). Although the PI becomes most unstable at large angle δ_1 , the role of E_{\parallel} coupling term might be important since considering the smaller angle δ_1 usually corresponds to the convective loss caused by the inhomogeneity of plasmas and the pump power. The influence of other parameters such as the electron temperature and the LH pump power will be investigated in this work. Cases of the coupling to different low frequency modes, for example ion-sound and ion-cyclotron quasimodes will be discussed as well.

TH-P

Numerical Simulations for Fusion Reactivity Enhancement in D-³He and D-T Plasmas due to ³He and T Minorities Heating

O. Shyshkin¹, Y. Moskvitina¹, A. Moskvitin¹, N. Yanagi², and A. Sagara²

¹ V. N. Karazin Kharkiv National University, Kharkiv, Ukraine

² National Institute for Fusion Science, Toki, Japan

Corresponding Author: oleg.shyshkin@gmail.com

One of the possible techniques to decrease neutron load on plasma facing components and superconducting coils in fusion reactor is to use fuel cycle based on D-³He as alternative to D-T [1]. Taking into account that the thermal reactivity of D-³He is much lower than that of D-T, the approach such as ICRF catalyzed fusion should be developed. The main idea of this technique is to modify reagent distribution function in order to achieve favorable reaction rate for nuclear fusion energy production [2]. Recent experimental results show high efficiency of ICRH acceleration of ³He minority in D plasma in order to increase fusion reaction rates. From the other hand this technique could be used to achieve the favorable distribution of T ions in D plasma and hence to reduce the amount tritium needed for sustainable fusion plasma burning [3]. The effect of transition to non-Maxwellian plasma is essential for reactor aspects studies both in tokamaks and heliotrons.

The objective of present study is to clarify the effect of non-Maxwellian distribution function of plasma minorities ³He and T on fusion reactivity. This study is done by means of numerical code, based on test-particle approach [4, 5]. This code solves the guiding center equation of a general vector form. To simulate the Coulomb collisions of test-particle with the other species the discretized collision operator based on binomial distribution is used [6]. A simplified model for ICRF heating is included in code as well [7].

We simulate the possibility to increase the averaged reactivity by modification of distribution function of ³He and T minorities in D plasma due to selective ICRF heating. In our model we observe an increment of reactivity for both either D-³He due to heating on main harmonic and D-T on second harmonic heating. The increase of reactivity is an important issue for the performance of fusion reactors, which needs further detailed studies.

References

- [1] P. E. Stott Plasma Phys. Control. Fusion **47** (2005) 1305.
- [2] T. H. Stix, Nucl. Fusion **15** (1975) 737.
- [3] N. Yanagi *et al.*, Plasma and Fus. Res. **6** (2011) 2405046.
- [4] O. A. Shyshkin *et al.*, Nucl. Fusion **47** (2007).
- [5] O. A. Shyshkin *et al.*, Plasma and Fus. Res. **6** (2011) 2403064.
- [6] A. H. Boozer and Gioietta Kuo-Petravic, Phys.Fluids, **24** (1981) 851.
- [7] S. Murakami *et al.*, Nucl. Fusion **46** (2006) S425-S432.

Scattering of Radio Frequency Waves by Edge Density Blobs and Fluctuations in Tokamak Plasmas

A. Ram¹, K. Hizanidis², and Y. Kominis²

¹*Massachusetts Institute of Technology, Cambridge, USA*

²*National Technical University, Athens, Greece*

Corresponding Author: abhay@mit.edu

The density fluctuations and blobs present in the edge region of magnetic fusion devices can scatter radio frequency (RF) waves through refraction, reflection, and diffraction. This paper is on two complementary theories that study the effect of fluctuations and blobs on the propagation of RF waves. The first study is on refractive scattering using geometric optics description of wave propagation. A Fokker-Planck description of scattering from a random spatial distribution of blobs of random sizes is formulated. A detailed analysis shows that refractive scattering can diffuse geometric optics rays in configuration space and in wave-vector space. The diffusion in space can make the rays miss their intended target region, while the diffusion in wave-vector space can broaden the wave spectrum. The latter effect modifies the current profile and reduces the current drive efficiency. The second study uses a full wave scattering theory which, besides refraction, includes reflection, diffraction, shadowing, and, quite significantly, coupling to different plasma waves. For example, an externally launched electron cyclotron ordinary mode can couple power to the extraordinary mode due to scattering. The full-wave theoretical model is completely new, first of its kind, study on scattering of RF waves by density blobs. The full-wave model is not limited by the geometric optics approximation of weak density fluctuations; consistent with experimental observations, the ratio of the blob density to the background density can be arbitrary. The scattering of both electron cyclotron waves and lower hybrid waves shows interesting features that are being studied theoretically and computationally. There appear to be effects that have important consequences for ITER — the electron cyclotron waves can be sufficiently deflected by the edge fluctuations so as to miss their intended target region where current is needed to control the neoclassical tearing mode.

Effect of Microturbulence on the Energetic Ions in Tokamaks

J. Chowdhury¹, R. Ganesh¹, W. Wang², S. Ethier², and J. Manickam²

¹*Institute for Plasma Research, Bhat, India*

²*Princeton Plasma Physical Laboratory, Princeton, USA*

Corresponding Author: tojugal@gmail.com

In contrast to earlier speculations of very weak effect of microturbulence on redistribution of energetic particles, recent experimental and theoretical efforts indicated redistribution of energetic particles due to microturbulence. In this work, nonlinear global gyrokinetic studies on the interaction of energetic particles with microturbulence is addressed. It is shown that both ITG and TEM turbulence could disperse energetic ions significantly. The nature of energetic ion transport is found to change progressively from subdiffusive to diffusive regime with increasing system size. These energetic ions are found to obey different energy scalings depending on their pitch angle distribution. Poloidal transport of tracer energetic particles are also investigated. The finite larmor radius effects of energetic ions are elucidated by first considering the drift kinetic followed by a gyrokinetic. Nondiffusive transport can often be split into diffusive term and particle pinch. In that regard, the energetic ions pinch is investigated using nonlinear global gyrokinetic simulations.

TH-P

Particle Transport in Ion and Electron Scale Turbulence

A. Skyman¹, P. Strand¹, H. Nordman¹, J. Anderson¹, and R. Singh²

¹*Chalmers University of Technology, Göteborg, Sweden*

²*Institute for Plasma Research, Bhat, India*

Corresponding Author: andreas.skyman@chalmers.se

In the present work the turbulent transport of main ions and impurities in tokamaks, driven by ion scale ITG/TE modes and electron scale ETG modes, is studied. Nonlinear and quasi-linear gyrokinetic simulation results obtained with the code GENE are compared with results from a computationally efficient fluid model. In particular, the transport of particles in regions of steep density gradients, relevant to the pedestal region of H-mode plasmas, is investigated.

The main focus of the work is to obtain steady state particle profiles locally, determined from the balance between diffusive and convective fluxes in source-free regions. The sign of the convective particle velocity (pinch) and the particle density peaking, measured by the density gradient (R/L_n) for zero particle flux, is calculated. For ITG/TE mode turbulence, scalings are obtained for the particle peaking with the driving density and temperature gradients and the impurity charge number. The crucial question of helium ash removal is also investigated. For ETG mode turbulence, the main ion density gradient corresponding to zero particle flux, relevant to the formation and sustaining of the steep edge pedestal, is estimated.

Progress on Theoretical Issues in Modelling Turbulent Transport

Y. Kosuga¹, P. Diamond^{1,2}, L. Wang², and Ö. Gürcan³

¹ *University of California San Diego, San Diego, USA*

² *WCI Center for Fusion Theory, NFRI, Ibaraki, Japan*

³ *LPP, Ecole Polytechnique, Palaiseau, France*

Corresponding Author: yukosuga@physics.ucsd.edu

Predictive modelling of turbulent transport is essential to the success of ITER and DEMO. Since first principle simulations cannot yet confront the complexities of this task, some model reduction is necessary, both for utility and for understanding. Two critical issues in transport model design are:

1. The structure of mean field theory for Kubo number larger than or order of unity.
2. The nonlinear dynamics of flows, both zonal and toroidal.

Here we describe recent progress in:

- The mean field theory of drift wave turbulent transport for Kubo number larger than or order of unity.
- The calculation of fully evolved zonal flow dynamics.
- Modelling intrinsic torque which drives toroidal rotation, and calculating the efficiency of the generation process. A unifying theme of those studies is their formulation in terms of phase space density correlation evolution.

Gyrokinetic Particle Simulation of Microturbulence in Tokamak Plasmas

I. Holod¹, D. Fulton¹, and Z. Lin¹

¹ *University of California Irvine, Irvine, USA*

Corresponding Author: iholod@uci.edu

Recent progress in gyrokinetic simulations of plasma microturbulence using GTC code is reported. Several topics are covered, including anomalous transport of toroidal angular momentum, simulations in real geometry, validation and verification efforts, and extension of the simulation model to include the magnetic field perturbations.

Simulations of momentum transport driven by the ion temperature gradient (ITG) and collisionless trapped electron model (CTEM) turbulence emphasize the important role of particle flux in the momentum convection. Parameter dependence of the momentum pinch is investigated showing strong dependence on the background density gradient.

Comparison of nonlinear simulations using GTC and XGC1 code as well as GTC simulations in realistic geometry of DIII-D and HL-2A tokamaks are presented as a part of validation and verification efforts.

GTC simulations of electromagnetic effects in microturbulence are presented, which include finite- β ITG and kinetic ballooning mode simulation.

Work is supported by US DOE SciDAC GSEP Center.



High Frequency Geodesic Acoustic Modes in Electron Scale Turbulence

J. Anderson¹, H. Nordman¹, R. Singh², A. Skyman¹, and P. Kaw²

¹*Chalmers University of Technology, Göteborg, Sweden*

²*Institute for Plasma Research, Bhat, Gandhinagar, Gujarat, India*

Corresponding Author: anderson.johan@gmail.com

There has been overwhelming evidence that coherent structures such as vortices, streamers and zonal flows ($m = n = 0$, where m and n are the poloidal and toroidal modenumbers respectively) play a critical role in determining the overall transport in magnetically confined plasmas. Some of these coherent structures, so called streamers, are radially elongated structures that cause intermittent, bursty events, which can mediate significant transport of heat and particles, for instance, imposing a large heat load on container walls.

In this work the presence of a high frequency branch of the geodesic acoustic mode (GAM) driven by electron temperature gradient (ETG) modes is demonstrated. The work is based on a fluid description of the ETG mode retaining non-adiabatic ions and the dispersion relation for high frequency GAMs driven nonlinearly by ETG modes is derived. A new saturation mechanism for ETG turbulence through the interaction with high frequency GAMs is found, resulting in a significantly enhanced ETG turbulence saturation level compared to the mixing length estimate.

Gyrokinetic Total Distribution Simulations of Drift-wave Turbulence and Neo-classical Dynamics in Tokamaks with Elmfire

J. S. Janhunen¹, J. Heikkinen², T. Kiviniemi¹, T. Korpilo¹, and S. Leerink¹

¹*Aalto University School of Science, Aalto, Finland*

²*Euratom-Tekes Association, VTT, Finland*

Corresponding Author: salomon.janhunen@aalto.fi

One of the outstanding problems of transport processes in tokamaks is the L-H transition and in general transport barrier formation, explanation of which has attracted several possible hypotheses ranging from purely neo-classical (rotational runaway) to parametric instabilities between turbulent eddies and zonal flows. Total f gyrokinetic simulation allows for the investigation of all the most important transport processes simultaneously, or by distinguishing between neo-classical and turbulent mechanisms in flow generation and transport. Elmfire is a gyrokinetic 5D total distribution simulation capable of transport time scale simulations of a multi-species plasma with self-consistent evolution of microturbulence, neo-classical physics and large scale structures.

Generally gyrokinetic investigations of neo-classical processes have been obtained potential flux surface averaging, eliminating all modes except the (0,0) zonal mode in simulations. We present an improved model for gyrokinetic particle simulations of neo-classical physics. We also discuss theoretical aspects of the gyrokinetic theory which includes the polarization drift in particle equations of motion, and present conservation of total angular momentum and energy in Elmfire. The role of sampling error is investigated, and the effect of noise on long time scale evolution of the system.

Electrostatic Gyrokinetic Absolute Equilibria: Calculation, Simulation and Physics Relevant to Fusion Plasmas Turbulence

J. Z. Zhu¹, T. H. Watanabe², T. Hahm³, and P. H. Diamond^{1,3}

¹*WCI Center for Fusion theory, NFRI, Daejeon, Republic of Korea*

²*NIFS/The Graduate University for Advanced Studies, Toki, Japan*

³*Department of Nuclear Engineering, Seoul National University, Seoul, Republic of Korea*

⁴*CMTFO, UCSD, La Jolla, USA*

Corresponding Author: zhujianzhougml@gmail.com

Nonlinear gyrokinetic equations play a fundamental role in our understanding of fusion plasma turbulence and associated transport. Gyrokinetics can be Galerkin truncated to have the absolute statistical equilibrium solution to which the truncated system should ultimately relaxed and be used to study the turbulence and the relevant transports. Here, we systematically review several versions of gyrokinetic absolute equilibria (GKAE) discovered at recent subsequent stages of research, together with the comprehensive numerical results and realistic physical discussions.

Plasma Size and Collisionality Scaling of Ion Temperature Gradient Driven Turbulent transport

M. Nakata¹, Y. Idomura¹

¹ *Japan Atomic Energy Agency, Rokkasho, Japan*

Corresponding Author: nakata.motoki@jaea.go.jp

The plasma size (ρ^*) and collisionality (ν^*) scaling of toroidal ion temperature gradient driven turbulent transport is investigated by using a full- f global gyrokinetic code GT5D with fixed gradient (FG) and fixed source (FS) models. The FG model with an adaptive source/sink, which sustains a zero-toroidal-rotation and a constant temperature profile, is newly introduced so as to emulate δf like simulations, but still including the formation of mean radial electric fields (Mean- E_r) and collisional effects. First, transport dynamics is compared among FG and FS simulations at asymptotically local limit

$$\rho^* = \frac{\text{thermal gyroradius}}{\text{minor radius}} = 1/300 \quad (1)$$

and a local fluxtube (FT) simulation. It is found that all the cases shows similar characteristics in the avalanche-propagation speed and in the dependency of the propagation direction on the Mean- E_r /zonal- E_r shear. The probability density function of the radial heat flux for the FS and FG models shows similar tail-components while their frequency spectra show significant differences, i.e., the self-organized-criticality (SOC) type spectrum appearing only in the FS case. Second, three scaling experiments on the heat transport, i.e., minor-radius scan with scaled ρ^* and ν^* (normalized collisionality), ρ^* scan with fixed ν^* , and ν^* scan with fixed ρ^* , are carried out, where $\rho^* = 1/300 - 1/100$, $\nu^* = 0.0165 - 0.0495$ are examined. An enhancement from Bohm transport scaling, which has been found in the FS case [1], is found for the present FG case in the first minor-radius-scan even though they show qualitatively different transport dynamics. The second and third scans clarify the critical physical effects behind the enhancement from the Bohm transport scaling. The plasma size ρ^* effects associated with Mean E_r and equilibrium profile shear are responsible for the Bohm transport scaling, while the enhancement of the transport scaling is mainly attributed to collisional ν^* effects.

References

- [1] S. Jolliet and Y. Idomura, Nucl. Fusion **52** (2012) 023026.

Interaction of Stable Modes and Zonal Flows in ITG Turbulence

P. Terry¹, K. Makwana¹, D. Hatch², M. Pueschel¹, J. Kim¹, W. Nevins³, F. Jenko²,
and H. Doerk²

¹ *University of Wisconsin-Madison, Madison, USA*

² *Max Planck Institute for Plasma Physics, Garching, Germany*

³ *Lawrence Livermore National Laboratory, Livermore, USA*

Corresponding Author: pwterry@wisc.edu

The regulation of ion temperature gradient (ITG) turbulence by zonal flows, which reduces turbulence levels and transport, is shown to involve enhanced energy transfer from the instability to damped modes in the low wavenumber range of the instability, with zonal flows acting as a catalyst. Energy transfer is dominated by the nonlinear triplet interaction of the unstable mode, a zonal flow, and stable modes at three interacting perpendicular wavenumbers. This holds for both fluid and gyrokinetic models. In the former a highly efficient transfer, enabled by minimization of the nonlinear three-wave frequency sum, a large coupling coefficient, and large zonal flow amplitude, allows saturation at a much lower level than possible when zonal flows are removed and energy transfer to damped modes is less efficient. Zonal flow shearing is not an important aspect of this process. The interaction of the unstable mode and zonal flows excites damped modes with tearing parity. At finite beta, these make the magnetic field stochastic and drive magnetic fluctuation-induced electron thermal transport. Because the tearing component is excited through coupling with zonal flows, zonal flows have the heterodox property of enhancing transport, albeit in the electron channel through magnetic stochasticity. In the main ion thermal transport channel damped modes reduce transport levels relative to quasilinear theory. In gyrokinetic simulations of ITG turbulence, stronger damped mode excitation, leading to a larger ratio of quasilinear heat flux to true flux, occurs for weaker magnetic shear. This ratio also increases in Tore Supra at weak magnetic shear, and is associated with stronger zonal flow excitation, consistent with the interaction of damped modes and zonal flows.

TH-P

Towards Turbulence Control via EGAM Excitation & Vorticity Injection

Y. Sarazin¹, D. Zarzoso¹, A. Strugarek^{1,2}, J. Abiteboul¹, X. Garbet¹,
G. Dif-Pradalier¹, R. Dumont¹, V. Grandgirard¹, P. Ghendrih¹, G. Latu³, S. Brun⁴,
P. H. Diamond^{3,4,5}, J. M. Kwon⁵, and S. Yi⁵

¹CEA, IRFM, Saint Paul-lez-Durance, France

²CEA, IRFU, Université Paris-Diderot, Gif-sur-Yvette, France

³Center for Momentum Transport & Flow Organisation, UCSD, La Jolla, USA

⁴Center for Astrophysics and Space Sciences, UCSD, La Jolla, USA

⁵National Fusion Research Institute, Daejeon, Republic of Korea

Corresponding Author: yanick.sarazin@cea.fr

Any means towards turbulence control would be highly beneficial to fusion reactors. Experimentally, fusion plasmas can exhibit spontaneous transitions towards high confinement regimes characterized by local reduction of turbulent transport. The resulting transport barriers exhibit complex dynamics: they can expand and/or move adiabatically, but they can also experience sudden relaxations, either quasi-periodic like Edge Localized Modes or definitive. The shear of the radial electric field dE_r/dr , by tearing apart convective cells, is one of the generic mechanisms which are advocated for such transport bifurcations. However, first principle gyrokinetic models do not reproduce these experimental evidences so far. Such inherently multi-scale physical mechanisms clearly require global simulations.

In this paper, we report on important progresses in this direction obtained by means of flux-driven global gyrokinetic simulations. The 5D gyrokinetic GYSELA code is used, which evolves the entire ion distribution function coupled to quasi neutrality. Importantly, no scale separation assumption is assumed, so that equilibrium profiles and fluctuations evolve self-consistently. All electrostatic branches of the Ion Temperature Gradient (ITG) driven turbulence are modeled with adiabatic electrons.

Two experimentally relevant turbulence control mechanisms are unveiled. First of all, vorticity injection efficiently generates a sheared radial electric field, which leads to a barrier for both heat and momentum transport. Interestingly enough, this barrier exhibits an oscillatory relaxation dynamics, which bears some analogy with ELM-like events (Edge Localized Modes). Secondly, a heat source specifically designed to generate a fast particle population is found to durably excite EGAMs (Energetic Geodesic Acoustic Modes), even in the saturated turbulent regime. The resulting dE_r/dr is then shown to impact both neoclassical transport and ITG turbulence.

Theory of External Geodesic Acoustic Mode Excitation

K. Hallatschek¹, G. R. McKee²

¹*Max-Planck-Institute for Plasma Physics, Garching, Germany*

²*University of Wisconsin-Madison, Madison, USA*

Corresponding Author: klaus.hallatschek@ipp.mpg.de

It is extremely appealing to externally excite geodesic acoustic modes in a tokamak, either to artificially reduce the turbulent transport provided sufficiently large amplitude is achievable, since GAMs are theoretically expected to impact the transport, or for diagnostic purposes, since the GAM frequency is dependent on the temperature and flux surface shapes. Moreover, even when not sufficient to suppress the turbulence completely, raising the GAM amplitude may lower the LH transition threshold. It can be shown that injection of momentum by heating, neutral particle beams or various plasma waves tends to be rather inefficient. In contrast resonant excitation by magnetic perturbations by external coils is a viable and potentially efficient method. (In principle, this could already be done at present, e.g., in the DIII-D tokamak with the in-vessel ELM stabilization coils).

An elegant way to compute the action of external coil currents on the interior flux surfaces has been discovered, which allows analytical estimates and the coupling of a novel dynamic equilibrium code with a turbulence code to study the resonance in detail. To describe the induced resonance layer within the turbulence calculation it is essential to retain the radial variation of the GAM frequency throughout the computational domain, i.e., use a nonlocal framework and not rely on the flux tube/local approximation. The peaking and phase variation due to the resonance lead to strong flow shear at the resonance, and a modulation and partial suppression of the turbulence by the GAMs. The results offer several control knobs to influence the drive effectivity and aid in designing a GAM drive antenna.

For example, the ELM suppression coils (internal, or I-coils) in DIII-D can produce a perturbation field of 0.02 mT at 7 kHz, yielding a displacement of about 6 mm under good conditions according to the mentioned analytical estimates, while displacement amplitudes larger than 2 mm can be readily detected by spectroscopic imaging and Doppler measurements.

Considering all possible optimizations it is evident that generation of geodesic oscillations by external fields is an efficient, viable method with potentially far reaching impact which would allow for the first time to influence poloidal rotation on the fine radial scales relevant to the turbulence.

TH-P

Advective Flux in Turbulent Plasmas Due to Noise

C.-B. Kim¹

¹*Soongsil University, Seoul, Republic of Korea*

Corresponding Author: cbkim@ssu.ac.kr

Appearance of advective flux in the turbulent plasmas driven by noise is studied numerically. The noise is assumed to be delta-correlated in time and to have anisotropic component so that a reflection symmetry is not obeyed along \hat{y} direction. Numerical simulations are performed for a two-dimensional model of Hasegawa-Mima equation (HME). It is found that, under uv forcing, the induced flux density is anisotropic so that while it is random along \hat{y} , it is not along the perpendicular direction \hat{x} and that the flux is advective with the velocity being proportional to $k^2 \rho_s^2$.



$\mathbf{E} \times \mathbf{B}$ Shear Suppression of Turbulence in Diverted H-mode Plasmas; Role of Edge Magnetic Shear

T. S. Hahm¹, W. Lee¹, D. Na¹, J. Lee¹, J.-W. Park¹, S. S. Kim², P. H. Diamond²,
H.-S. Kim¹, Y. S. Na¹, H. Jhang², J. M. Kwon², Y. M. Jeon², and W. H. Ko²

¹*Seoul National University, Seoul, Republic of Korea*

²*National Fusion Research Institute, Daejeon, Republic of Korea*

Corresponding Author: tshahm@snu.ac.kr

KSTAR tokamak has achieved H-mode plasmas well ahead of its original schedule [1]. An interesting feature of KSTAR plasmas at the H-mode transition is an abrupt increase in its edge q value [2]. Often, this happens as the plasma becomes diverted, losing a contact with the outer limiter. Motivated by the KSTAR results, we investigate how plasma boundary shape such as x-point modifies the $\mathbf{E} \times \mathbf{B}$ shearing rate and microturbulence at the edge in this work.

The $\mathbf{E} \times \mathbf{B}$ shearing rate for an isotropic turbulent eddy in a shaped plasma is given in Ref. [3]. We can characterize the potentially beneficial effects of magnetic shear, safety factor, and elongation by adopting a simpler high aspect ratio version [4] of the $\mathbf{E} \times \mathbf{B}$ shearing rate, and a simple double-null analytic model equilibrium previously used for resistive MHD instability analyses in diverted H-mode plasmas [5]. This model exhibits a logarithmic divergence of q_{MHD} , and stronger algebraic divergence of magnetic shear. Furthermore, strong global shear at the edge is expected to reduce the radial correlation length of edge turbulence and consequently facilitate reduction of transport which leads to the H-mode transition [5].

We are currently validating this working hypothesis of the $\mathbf{E} \times \mathbf{B}$ shear suppression of turbulence further facilitated by strong magnetic shear against KSTAR H-mode data. While direct E_r measurements are not available from KSTAR, we can estimate it by using toroidal velocity measured by Charge Exchange Recombination Spectroscopy, neoclassical poloidal velocity, modeled pedestal pressure profile, and the radial force balance relation for impurity ions. Turbulence growth rate will be estimated for the modeled profiles, using the TRB gyrofluid code [6,7], and will be compared to the $\mathbf{E} \times \mathbf{B}$ shearing rate.

References

- [1] M. Kwon *et al.*, Nucl. Fusion **51** (2011) 094006
- [2] S. W. Yoon *et al.*, Nucl. Fusion **51** (2011) 113009
- [3] T. S. Hahm and K. H. Burrell, Phys. Plasmas **2** (1995) 1648
- [4] T. S. Hahm, Phys. Plasmas **1** (1994) 2940
- [5] T. S. Hahm and P. H. Diamond, Phys. Fluids **30** (1987) 133
- [6] X. Garbet *et al.*, Phys. Plasmas **8** (2001) 2793
- [7] S. S. Kim *et al.*, Nucl. Fusion **51** (2011) 073021

Flux-driven Full- f Gyrokinetic Studies of the Influence of Edge Dynamics in Diverted Geometry on Tokamak Core Confinement

S. H. Ku¹, C. S. Chang¹, P. H. Diamond^{2,3}, J. Lang¹, D. Stotler¹, G. Dif-Pradalier⁴,
and W. Tang¹

¹*Princeton Plasma Physics Laboratory, Princeton, USA*

²*NFRI, Daejeon, Republic of Korea*

³*University of California, San Diego, USA*

⁴*Association Euratom-CEA, CEA/IRFM, France*

Corresponding Author: sku@pppl.gov

A first principles-based understanding of the relationship between the ion temperature (T_i) at the pedestal top and that in the central core is critically needed to enable reliable predictions of fusion power efficiency in ITER. Utilizing petascale high-performance computers, the multi-scale (combined neoclassical, kinetic turbulence, and neutral physics scales), full-function (“full- f ”) gyrokinetic code XGC1 has produced new results showing that the ion temperature gradient driven (ITG) turbulence inter-connects the core and edge T_i through self-organized-criticality (SOC) and, thus, can account for the observed profile stiffness. The simulation domain is the entire tokamak volume, from the magnetic axis, through the separatrix, scrape-off layer and divertor, and out to the grounded material wall. Results from the XGC1 simulations are consistent with the experimentally observed rapid (much faster than diffusive) connection between T_i and the turbulence dynamics. The underlying physics is turbulence spreading through nonlinear avalanche dynamics. Smaller scale avalanches are self-regulated within a zonal flow staircase, while larger scale avalanches across the staircase are self-regulated when the zonal flow walls open up from time to time. This kind of non-diffusive, non-local behavior has also been observed in hot and cold pulse experiments as well as in other tokamak experiments. XGC1 simulations of a separate cold pulse has cross-validated these experimental physics observations. Even though the central core is forced to stay at a subcritical value of ∇T_i , our simulation results show that the outer turbulence spreads into the central core in a specific way that produces efficient heat flux. A strong $\mathbf{E} \times \mathbf{B}$ shearing layer is formed in the edge density pedestal region — with another one formed at a smaller minor radius, possibly giving rise to an internal transport barrier. The present discussion will focus on ITG and trapped electron mode turbulence, including their effects on pedestal structure and inward particle pinch physics in the presence of neutral ionization and charge exchange.

Turbulence Generated Non-inductive Current and Flow Shear Driven Turbulent Transport in Tokamaks

W. W. Wang¹, S. Ethier¹, T. S. Hahm², W. M. T. Tang³, and A. Boozer³

¹*Princeton University Plasma Physics Laboratory, Princeton, USA*

²*Seoul National University, Seoul, Republic of Korea*

³*Columbia University, New York, USA*

Corresponding Author: wwang@pppl.gov

New results obtained from global gyrokinetic simulations regarding turbulence-induced plasma current and flow shear driven turbulence and transport in tokamaks are reported in this paper.

1. These plasma self-generated non-inductive parallel currents can have a strong impact on the physics of plasma disruptions and overall plasma confinement. Specifically, their influence on key magnetohydrodynamic (MHD) instabilities such as neoclassical tearing mode (NTM) and edge localized mode (ELM), is of great importance. It is found that the collisionless trapped electron mode (CTEM) and ion temperature gradient (ITG) turbulence can drive significant, quasi-stationary parallel current. The underlying dynamics is closely related to the nonlinear plasma flow generation by turbulent residual stress. However, unlike toroidal momentum, which is mostly carried by ions, the turbulent current is mainly carried by electrons and driven by electron residual stress. The current generation by turbulence exhibits a characteristic dependence on plasma parameters that is similar to plasma flow generation. Specifically, it increases with the pressure gradient, decreases with equilibrium current I_p , and increases with the radial variation of the safety factor. Interestingly, the CTEM driven current is essentially carried by trapped electrons, unlike the neoclassical bootstrap current which is mainly carried by passing particles. It is suggested that the predicted characteristic dependence can be examined using large experimental databases, along with crosschecks with fluctuation measurements.
2. Our global nonlinear gyrokinetic simulations show that strong flow shear may drive the negative compressibility mode unstable in tokamak geometry in some experimentally relevant parameter regimes and that the associated turbulence can produce significant energy and momentum transport, including an intrinsic torque in the co-current direction. The generic nature of flow shear turbulence in tokamak plasmas is investigated in detail, including mechanisms for its nonlinear saturation and the influence of the q -profile structure.

Systematic studies with special attention paid to flow optimization for minimizing plasma transport will be reported.

TH-P

Steady State Particle-In-Cell Simulations of Microturbulence in Tokamaks

R. Ganesh¹, W.-L. Lee², S. Ethier², and J. Manickam²

¹*Institute for Plasma Research, Bhat, Gandhinagar, India*

²*Princeton Plasma Physics Laboratory, Princeton, USA*

Corresponding Author: rajaraman.ganesh@gmail.com

The use of a generalized weight-based particle simulation scheme suitable for simulating Tokamak plasmas, where the zeroth-order inhomogeneity is important is presented. The scheme which is a generalization of the perturbation schemes developed earlier for particle-in-cell (PIC) simulations, is now capable of handling the full distribution of particles. The new scheme can simulate both the perturbation (δf) and the full f within the same code. Its development is based on the concept of multi-scale expansion which separates the scale lengths of back-ground inhomogeneity from those associated with the perturbations. We will report on the simulations studies, carried out on the state-of-the-art massively parallel computers, for the Ion Temperature Gradient (ITG) instabilities in the presence of zonal flows and a constant inhomogeneity drive. The physics of the steady state transport in tokamaks will also be discussed.

Fusion Technology and Power Plant Design



Evaluation of Optimized ICRF and LHRF Antennas in Alcator C-Mod

S. Wukitch¹, Y. Lin¹, M. Reinke¹, J. Terry¹, G. Wallace¹, I. Cziegler², I. Faust¹, M. Garrett¹, J. Hillairet³, C. Lau¹, B. Lipschultz¹, O. Meneghini¹, R. Ochoukov¹, R. Parker¹, M. Preynas³, S. Shiraiwa¹, D. Whyte¹, and R. Wilson⁴

¹MIT Plasma Science and Fusion Center, Cambridge, USA

²UCSD Center for Energy Research, San Diego, USA

³CEA, IRFM, Saint Paul lez Durance, France

⁴Princeton Plasma Physics Laboratory, Princeton, USA

Corresponding Author: wukitch@psfc.mit.edu

Ion cyclotron range of frequency heating (ICRF) and lower hybrid range of frequency current drive (LHCD) are expected to be key heating and current drive actuators for future fusion reactors and devices. However, impurity contamination associated with ICRF antenna operation remains a major challenge, particularly in devices with metallic plasma facing components. For LHCD, maximizing coupled power to the plasma remains a challenge, particularly to maintain low reflection coefficient over range of plasma conditions. Here, we report on an experimental investigation to test whether a field aligned (FA) ICRF antenna can reduce the impurity contamination and SOL modification associated with antenna operation. We also report on results from a new limiter for the LH coupler designed to reduce reflection coefficients across a wider range of plasma conditions.

The unique feature of the so-called FA-antenna is that the current straps and antenna box structure are perpendicular to the total magnetic field. This alignment allows integrated E_{\parallel} (electric field along a magnetic field line) to be minimized through symmetry. Using finite element method and a cold plasma model, the FA-antenna has been found to have lower integrated E_{\parallel} relative to the previous antenna geometry.

Initial results indicate that the impurity contamination associated with the FA-antenna is lower relative to our standard ICRF antennas. Configured as a 2-strap antenna, the antenna has lower core impurity contamination and lower impurity source at the antenna at high power density ($\sim 15 \text{ MW/m}^2$). An array of core and boundary plasma diagnostics are presently being used to characterize the impurity behavior and impact on the SOL transport and SOL density profiles; the latest results will be presented.

For LHCD, reflection coefficients are very sensitive to the local density and its profile in front of the LHCD coupler. Previously the local LH coupler protection limiter was fixed to the outer wall of the vacuum vessel. The new limiter is mounted on the coupler and protrudes 0.25 mm beyond the coupler for plasma heat flux protection. The protection tiles allow the LH launcher to be moved closer to the plasma than previously possible. Initial high power ($P_{\text{net}} \sim 700 \text{ kW}$) results show lower reflection coefficients were achieved ($\Gamma^2 \sim 0.1$) as compared to the old configuration ($\Gamma^2 \sim 0.2$).

FTP

Acceleration of 1 MeV H⁻ Ion Beams at ITER NB-relevant High Current Density

T. Inoue¹, M. Taniguchi¹, M. Kashiwagi¹, N. Umeda¹, H. Tobari¹, M. Dairaku¹, J. Takemoto¹, K. Tsuchida¹, K. Watanabe¹, H. Yamanaka¹, A. Kojima¹, M. Hanada¹, and K. Sakamoto¹

¹Japan Atomic Energy Agency, Naka, Japan

Corresponding Author: inoue.takashi52@jaea.go.jp

ITER neutral beam (NB) system requires deuterium negative ion beams of 1 MeV, 40 A at the current density of 200 A/m² from a single large negative ion source and an accelerator. This paper summarizes progress in R&D with a reduced size accelerator, so-called “the MeV accelerator” at Japan Atomic Energy Agency (JAEA). In the last Fusion Energy Conference, we reported achievement of 1 MV voltage holding in vacuum for more than one hour. Physics of beamlet deflections due to their own space charges and magnetic field was also reported utilizing a sophisticated three dimensional beam trajectory analyses. The improved voltage holding and a trajectory compensation technique have been applied to the MeV accelerator.

Many discharge burn marks have been observed inside the accelerator after long pulse operation reported in the last conference. It was turned out that such discharge marks were observed at positions facing to high local electric field, such as edges, corners, and steps between grid and its support. In the present MeV accelerator, such positions have been modified, for example, by increasing radii of corners around grid supports, and increasing gap length between grids to lower the local electric concentrations to about 3 – 4 kV/mm.

For compensation of magnetic deflection, aperture offset was applied at the bottom of the EXG. Magnetic field is formed by small permanent magnets embedded in EXG between aperture lines. Since the polarities are arranged so as to be alternative in each line between apertures, aperture offset of 0.8 mm was defined in the direction against the magnetic deflection. To counteract the beamlet deflection by space charge repulsion, a field shaping plate, a metal plate to deform electric field, were installed around the aperture area for deflection of outermost beamlet inward. Position and thickness of the plate was designed by the analyses.

It should be highlighted that reduction of beam direct interception at grids has brought substantial improvement in voltage holding during beam acceleration at around 1 MV. By the improved voltage holding even under beam acceleration, H⁻ ion beams of 185 A/m² (430 mA in total) have been successfully accelerated up to 0.98 MeV. This is a world first demonstration of negative ion beams at high current, high current density and high energy close to the ITER requirements.

FTP

Progress on the Development of High Power Long Pulse Gyrotron and Related Technologies

K. Kajiwara¹, K. Sakamoto¹, Y. Oda¹, K. Hayashi¹, K. Takahashi¹, and A. Kasugai¹

¹Japan Atomic Energy Agency, Naka, Japan

Corresponding Author: kajiwara.ken@jaea.go.jp

In the development of a higher power dual-frequency gyrotron, a high order mode gyrotron, which permits to select the oscillation at 170 GHz or 137 GHz, has been fabricated and tested. Short pulse experiments (0.5 ms) were performed with 1.3 MW power output at more than 30% of the oscillation efficiency for both frequencies. In long pulse experiments, 760 kW/46%/60 s at 170 GHz and 540 kW/42%/20 s at 137 GHz are achieved. It is the first time long pulse experiments with the dual-frequency gyrotron/triode electron gun. Since the RF beam direction from the output window is designed to be almost the same for both frequencies, good power couplings to the transmission line, which are 96% for 170 GHz and 94% for 137 GHz, are obtained by using a pair of identical phase correcting mirrors. Pulse extension is underway aiming for > 1 MW at CW operation.

A 5 kHz full power modulation experiment was performed using the 170 GHz gyrotron of TE_{31,8} mode oscillation. The 5 kHz full power modulation was achieved with the full beam modulation by employing a fast voltage switching between the anode and cathode of the triode type electron gun. This satisfies the requirement of ITER. For further improvement, an advanced anode power supply system is proposed to reduce the oscillation period of adjacent mode at the start-up phase of each pulse.

FTP

Be Tile Power Handling and Main Wall Protection

I. M. Ferreira Nunes^{1,2}, V. Riccardo³, P. J. Lomas³, P. de Vries³, G. Arnoux³,
S. Devaux³, T. Farley³, M. Firdaouss⁴, G. Matthews³, C. Reux⁵, and K.-D. Zastrow³

¹*Associação EURATOM-IST, IPFN-Laboratório Associado, Lisboa, Portugal*

²*EFDA-CSU, Culham Science Centre, Abingdon, UK*

³*Culham Science Centre, EURATOM/CCFE Association, Abingdon, UK*

⁴*CEA, IRFM, Saint-Paul-lez-Durance, France*

⁵*Ecole Polytechnique, CNRS, Palaiseau, France*

Corresponding Author: isabel.nunes@jet.efda.org

In this paper we describe the design methodologies applied to JET's ITER-like Wall, many of which have been adopted by ITER, and the experimental evaluation of their effectiveness. Avoiding exposed edges over 40mm effective height and using rigorous methods to ensure true implementation good power handling, within the expected design values has been achieved. Compromises had to be made in the design of the upper dump plate, which has led to minor melting during vertical disruptions. This experience has direct relevance to the ITER plasma facing components (PFCs) where stringent criteria for exposure of edges at the castellation scale have not yet been set and penetration of field lines into areas in extreme off-normal configurations has to be considered. In addition, to prevent potential risks of melting due to tile misalignment, damage or design errors, an active protection system was put in place. The design requirements for the Be tiles includes good power handling for start-up limiter operation and the shielding of large of metallic components such as antennas and diagnostics from the high power fluxes due to high power input diverted ELMy H-modes. In the design of the tiles surface, it is assumed an exponential decay of power density with radius, the scrape-off length values of 10 mm for ohmic and L-mode plasmas and 5mm for H-mode plasmas; the scrape-off layer (SOL) surface is approximated by $2\pi R$ (where R is the SOL major radius). The limits on the surface temperature of the new Be tiles will constrain limiter operation and set the minimum gaps for diverted operation and require active protection to guard against melting. To test these limits and validate the assumptions of the design, experiments were performed with varying additional power and distance to the limiters in both L-mode and H-mode. Both shadowing and power handling depend on the field line angle as well as the plasma scrape-off length. Thus the power handling limitations will depend upon plasma scenario and is being explored experimentally. The impact on the overall performance caused by misalignments, damage and other possible non-conformances appears minimal. Real time active protection relying on near IR cameras has been used successfully for the protection of the main chamber and is close to being fully commissioned.

FTP

Technical Challenges in the Construction of the Steady-State Stellarator Wendelstein 7-X

H.-S. Bosch¹

¹*Max Planck Institute für Plasma Physics, Garching, Germany*

Corresponding Author: claudia.schoenian@ipp.mpg.de

The “fully-optimized” stellarator Wendelstein 7-X stellarator, presently under construction in Greifswald, combines a quasi-isodynamic magnetic field configuration sustained by superconducting coils with a steady-state exhaust concept, steady-state heating at high power, and a size sufficient to reach reactor-relevant $nT\tau$ -values. It is the mission of the project to demonstrate the reactor potential of the optimized stellarator line.

For the development of a credible stellarator reactor concept, steady-state operation has to be demonstrated with fully integrated discharge scenarios at high heating power with a divertor providing suitable power and particle exhaust. The development of reactor-relevant operation regimes is the chief scientific goal of Wendelstein 7-X.

The subject of steady-state operation, however, is of more general interest, as this is also of great concern and interest for future tokamak devices. Consistent with the physics requirements of steady-state plasmas must be the engineering aspects of a steady-state fusion device. We discuss these issues for the design, manufacturing, and assembly of Wendelstein 7-X.

The major components of Wendelstein 7-X have been manufactured, tested and delivered: 70 super-conducting coils, 121 superconducting bus-bars for the 7 coil current circuits, about 1000 cryo pipes, 10 half-modules of the central support structure, the plasma vessel and outer vessel, and 254 ports. The main focus of the project has in recent years shifted to the assembly process and considerable progress has been achieved.

Although in the early phases of the Wendelstein 7-X construction several schedule delays have accumulated, there have been no major project delays for more than four years and completion of the device is foreseen for mid 2014. A summary of the technological challenges that have been faced in the project and solutions found are discussed in this paper. In addition the route towards completion, commissioning, and the first operation phase is presented.

FTP

SST-1 Tokamak Integration & Commissioning

S. Pradhan¹, Z. Khan¹, V. Tanna¹, A. Sharma¹, P. Biswas¹, H. Patel¹, H. Masand¹,
A. Srivastav¹, A. Varadarajalu¹, U. Prasad¹, K. Doshi¹, D. Raval¹, T. Parekh¹,
Y. Khristi¹, N. C. Gupta¹, M. K. Gupta¹, J. Tank¹, and A. Chauhan¹

¹*Institute for Plasma Research, Bhat, Gandhinagar, India*

Corresponding Author: pradhan@ipr.res.in

Steady State Superconducting Tokamak (SST-1) commissioning attempted in 2006 was unsuccessful due to leaks being observed in magnet joints and isolators in the helium and nitrogen circuits. Additionally, 80K thermal shields remained at higher temperature and leaks were observed in vacuum vessel baking channels. After a comprehensive review, the SST-1 refurbishment has been undertaken replacing all existing joints with sub nano-ohm leak-tight joints in superconducting magnet winding packs, installing single phase LN₂ cooled bubble type thermal shields, developing and installing supercritical helium cooled 5K thermal shields on Toroidal Field (TF) magnet cases, ensuring thermal and electrical isolations between various sub-systems of SST-1, testing all SST-1 TF magnets in cold with nominal currents. Furthermore, the task of testing each of the fully assembled modules and octants of SST-1 machine shell in representative experimentally simulated scenarios, experimentally establishing the operational reliability of the SST-1 vacuum vessel baking system, time synchronizing various heterogeneous subsystems of SST-1 through a dedicated GPS networking, ensuring reliable large data storage scenarios has also been started. Currently, SST-1 machine shell is getting fully assembled and an “engineering validation” would commence with the objectives of establishing SST-1 as an appropriate calibrated UHV compatible thermo-mechanical and magnetic device prior to first plasma.

Design and engineering criticality in tokamak components that reduces functional risks, and important qualification measures that reduce the leaks in the cold operational scenarios are some of the highlights of SST-1 refurbishment. Importance of testing superconducting magnets in cold with operational currents, flow imbalance and thermal run away elimination in thermal shields, consequences of the magnetic configurations with the machine assembly being done at room temperature are some of the major lessons learnt and are useful inputs to future devices.

FTP

On the Physics Guidelines for a Tokamak DEMO

H. Zohm¹, C. Angioni¹, G. Federici², G. Gantenbein³, L. Porte⁴, O. Sauter⁴,
T. Hartmann¹, E. Poli¹, K. Lackner¹, G. Tardini¹, D. Ward⁵, and M. Wischmeier¹

¹*Max-Planck-Institut für Plasmaphysik, Garching, Germany*

²*EFDA, PPP&T, Garching, Germany*

³*KIT, Karlsruhe, Germany*

⁴*CRPP, EPFL, Lausanne, Switzerland*

⁵*CCFE, Culham, Oxfordshire, UK*

Corresponding Author: zohm@ipp.mpg.de

With ITER construction under way, the question of possible designs for a machine after ITER is receiving renewed attention. In many fusion energy roadmaps, such a step, often called DEMO, is a machine that should bridge the gap between ITER and the first commercial Fusion Power Plant (FPP). Hence, crucial elements for many DEMO designs are e.g., net electricity production or T-selfsufficiency and reasonable reliability and availability. For such a DEMO design, a consistent set of physics and technology assumptions has to be made, usually used in 0-d system codes to optimise with respect to a given set of criteria. Since DEMO is projected to run in a different regime than ITER, extrapolation using the ITER rules (so-called “ITER physics design guidelines”) is not always straightforward and the validity of model based physics assumptions has to be checked. In the frame of the EFDA PPP&T work programme, we have conducted an assessment of the physics assumptions made in present day systems codes and have critically examined the underlying physics base.

Work has mainly concentrated on so-called “DEMO Physics Issues”, defined as issues that do not have to be resolved for ITER to achieve its mission, but are critical for DEMO, in particular the areas of

1. steady state operation,
2. high density operation at $n/n_{GW} > 1$ and
3. exhaust at high P/R .

The work presented will be a first step towards establishing “DEMO physics guide lines” similar to what has been done for ITER. We also present a study of an operating scenario for DEMO based on “improved H-mode” (also termed “advanced inductive”) operation which has a firm experimental basis and may lead to acceptable steady state operation conditions, provided the total current drive efficiency, i.e., the product of efficiency in the plasma and wall plug efficiency can be made high enough.

FTP

Progress on Developing the Spherical Tokamak for Fusion Applications

J. Menard¹, T. Brown¹, J. Canik², J. Chrzanowski¹, L. Dudek¹, L. El-Guebaly³, S. Gerhardt¹, S. Kaye¹, C. Kessel¹, E. Kolemen¹, M. Kotschenreuther⁴, R. Maingi², C. Neumeyer¹, M. Ono¹, R. Raman⁵, S. Sabbagh⁶, V. Soukhanovskii⁷, T. Stevenson¹, R. Strykowski¹, P. Titus¹, P. Valanju⁴, G. Voss⁸, and A. Zolfaghari¹

¹*Princeton Plasma Physics Laboratory, Princeton, USA*

²*Oak Ridge National Laboratory, Oak Ridge, USA*

³*University of Wisconsin, Madison, USA*

⁴*University of Texas, Austin, USA*

⁵*University of Washington, Seattle, USA*

⁶*Columbia University, New York, USA*

⁷*Lawrence Livermore National Laboratory, Livermore, USA*

⁸*Culham Centre for Fusion Energy, Abingdon, UK*

Corresponding Author: jmenard@pppl.gov

A Fusion Nuclear Science Facility (FNSF) could play an important role in the development of fusion energy by providing the high neutron flux and fluence environment needed to develop fusion materials and components. The spherical tokamak (ST) is a leading candidate for an FNSF due to its compact size and modular configuration. Two activities preparing the ST for possible FNSF applications have been advanced in the U.S. during the past two years. First, a major upgrade of the National Spherical Torus eXperiment (NSTX) has been designed, approved, and initiated. Second, previous “pilot plant” studies identified key research needs and design issues for ST-based FNSF devices and motivate studies of the impact of device size on neutron wall loading, tritium breeding, and electricity production. Progress in both research activities will be described. A key research goal of NSTX Upgrade is to access 3 – 5 times lower collisionality to more fully understand transport, stability, and non-inductive start-up and sustainment in the ST. Such considerations motivate the upgrade of NSTX to double the toroidal field, plasma current, and NBI heating power, and quintuple the pulse duration. Higher toroidal field and pulse length will be achieved by fabricating and installing a new center stack (CS), and a second more tangential neutral beam injection (NBI) will be installed to increase NBI current drive efficiency by up to a factor of two, support fully non-inductive operation, enable control of the core q profile, and ramp-up the plasma current to 1MA levels. Understanding the impact of varied device size is another important ongoing ST research activity. For example, for an ST-FNSF with average neutron wall loading of 1 MW/m², the impact of increased major radius is stabilizing, but the overall fusion power and tritium consumption increases. For higher performance operation targeting net electricity production, the smallest possible ST that can achieve electricity break-even has $R = 1.6$ m assuming very high blanket thermal conversion efficiency at 0.59 as was utilized in ARIES-AT design studies. A near-term issue that will be addressed is the impact of device size on tritium breeding ratio (TBR) where smaller devices have more difficulty achieving TBR > 1 since a higher fraction of in-vessel surface area must be dedicated to auxiliary heating ports and blanket test modules.

FTP

Lithium-Metal Infused Trenches: A New Way to Remove Divertor Heat Flux

D. Ruzic¹, D. Andruczyk¹, and W. Xu¹

¹*Center for Plasma-Material Interactions, Department of Nuclear, Plasma and Radiological Engineering, University of Illinois, Urbana-Champaign, USA*

Corresponding Author: druzic@illinois.edu

As we come closer to realizing fusion as a viable power source, many machines which have made significant progress in plasma heating and power find that removing heat from the divertor region has become a challenging problem. Peak heat fluxes up to 20 MWm^{-2} are typical these days for machines and if there is an ELM event or disruption then it can be even higher. Solid plasma facing components (PFC) materials such as carbon and tungsten suffer from permanent damage due to huge thermal stresses. The alternative is to use a liquid PFC where the surface is replenished. Liquid Lithium offers such an alternative and has the added advantages that it offers a low recycling surface allowing for density control and higher confinement times.

At the University of Illinois at Urbana-Champaign (UIUC), such a system has been developed. The Lithium-Metal Infused Trenches (LiMIT) concept uses the self-driven flow of liquid lithium to cool the divertor surface. At UIUC's CPMI labs a proof-of-principle experiment has been done and it is scheduled to be used in the Chinese HT-7 tokamak in April of 2012. LiMIT uses many narrow, parallel trenches with millimeter thick gaps between them to flow the liquid lithium. The tile with the trenches runs perpendicular to the toroidal magnetic field direction. Once a temperature gradient is established between the top and bottom of the trench from the plasma hitting the lithium surface, a thermoelectric current is generated in the direction of the temperature gradient. The lithium flow is driven along the trenches in the radial direction across the plasma strike point removing heat.

Self driven flow velocities have been measured to be $0.22 \pm 0.03 \text{ ms}^{-1}$ and IR camera measurements showed clear temperature increases after the lithium had passed the area. The tile is heated via a linear electron beam which has a peak heat flux of $10.0 \pm 1.1 \text{ MWm}^{-2}$ and the temperature increase showed no significant evaporation of the lithium. The heating of the surface as well as the magnetic field strength can have an effect on the velocity and heat transport. Analytical solutions reveal that in the presence of a strong magnetic field the surface temperature and flow velocity are proportional to the square root of the surface heat flux. This has large heat transfer potential for future applications in fusion devices.

FTP

Hydrogen Isotope Trapping at Defects Created with Neutron- and Ion-Irradiation in Tungsten

Y. Hatano¹, V. Alimov¹, M. Shimada², J. Shi¹, M. Hara¹, Y. Oya³, M. Kobayashi³, K. Okuno³, T. Oda⁴, G. Cao⁵, N. Yoshida⁶, N. Futagami⁶, K. Sugiyama⁷, J. Roth⁷, B. Tyburska-Pueschel⁷, J. Dorner⁷, I. Takagi⁸, M. Hatakeyama⁹, H. Kurishita⁹, and M. Sokolov¹⁰

¹Hydrogen Isotope Research Center, University of Toyama, Japan

²Idaho National Laboratory, Idaho-Falls, USA

³Shizuoka University, Shizuoka, Japan

⁴The University of Tokyo, Tokyo, Japan

⁵The University of Wisconsin, Madison, USA

⁶Kyushu University, Fukuoka, Japan

⁷Max Planck Institut für Plasmaphysik, Garching, Germany

⁸Kyoto University, Kyoto, Japan

⁹Tohoku University, Sendai, Japan

¹⁰Oak Ridge National Laboratory, Oak Ridge, USA

Corresponding Author: hatano@ctg.u-toyama.ac.jp

Tritium (T) inventory in tungsten (W) after neutron (n) irradiation is an important safety problem because radiation defects trap hydrogen isotopes. Therefore, deuterium (D) retention in n-irradiated W has been examined in Japan/US joint project TITAN. In this project, small W disks were irradiated in High Flux Isotope Reactor, Oak Ridge National Laboratory at coolant temperature ($\sim 50^\circ\text{C}$) to 0.025 dpa and exposed to high flux D plasma at $100 - 500^\circ\text{C}$ in Idaho National Laboratory. Irradiation of 20 MeV W self-ions at room temperature to 0.5 dpa has also been performed to understand effects of displacement damages without transmutation. The ion-irradiated W specimens were exposed to low energy, low flux D atoms and D₂ gas not to modify the damaged structure near the surface at $130 - 600^\circ\text{C}$. Deuterium depth profiles and detrapping energy were examined by nuclear reaction analysis and thermal desorption spectroscopy (TDS), respectively. Both n- and ion-irradiations led to rather high D retention (0.1 – 1 atomic percent) even at high temperatures (at above 500°C) due to the presence of strong trapping sites with detrapping energy of ~ 2 eV. Those defects were thermally stable at least up to 700°C . These observations suggest that baking in vacuum at moderate temperatures could not be so effective for T removal. Nevertheless, significant D release from the ion-irradiated W was observed even at 200°C under the exposure to H atoms.

FTP

Integrated Computational study of Material Lifetime in a Fusion Reactor Environment

M. Gilbert¹, S. Dudarev¹, L. Packer¹, S. Zheng¹, and J.-C. Sublet¹

¹*EURATOM/CCFE Fusion Association, Culham Centre for Fusion Energy, Abingdon, UK*
Corresponding Author: mark.gilbert@ccfe.ac.uk

The high-energy, high-intensity neutron fluxes produced by the fusion plasma will have a significant life-limiting impact on reactor components in both experimental and commercial fusion devices. Not only do the neutrons bombarding the materials induce atomic displacement cascades, leading to the accumulation of structural defects, but they also initiate nuclear reactions, which cause transmutation of the elemental atoms. Understanding the implications associated with the resulting compositional changes is one of the key outstanding issues related to fusion energy research. Several complimentary computational techniques have been used to investigate the problem. Firstly, neutron-transport simulations, performed on a reference design for the demonstration fusion power plant (DEMO), quantify the variation in neutron irradiation conditions as a function of geometry. The resulting neutron fluxes and spectra are then used as input into inventory calculations, which allow for the compositional changes of a material to be tracked in time. These calculations reveal that the production of helium (He) gas atoms, whose presence in a material is of particular concern because it can accumulate and cause swelling and embrittlement, will vary significantly, even within the same component of a reactor.

Lastly, a density-functional-based model for He-induced grain-boundary embrittlement has been developed to predict the life-limiting consequences associated with relatively low concentrations of He in materials situated at various locations in the DEMO structure. The results suggest that some important fusion materials may be significantly more susceptible to this type of failure than others.

This work was funded by the RCUK Energy Programme under grant EP/I501045 and the European Communities under the contract of Association between EURATOM and CCFE. The views and opinions expressed herein do not necessarily reflect those of the European Commission. This work was carried out within the framework of the European Fusion Development Agreement.

FTP

Initial Results of the Large Liquid Lithium Test Loop for the IFMIF Target

H. Kondo¹, T. Furukawa¹, H. Yasushi¹, T. Kanemura¹, M. Ida¹, W. Kazuyoshi¹,
H. Horiike², N. Yamaoka², I. Matsushita³, H. Iuchi³, F. Groeschel⁴, and E. Wakai¹

¹*Japan Atomic Energy Agency, Tokyo, Japan*

²*Osaka University, Osaka, Japan*

³*Mitsubishi Heavy Industries Mechatronics Systems, Kobe, Japan*

⁴*IFMIF/EVEDA Project Team*

Corresponding Author: kondo.hiroo@jaea.go.jp

Construction and initial performance tests of EVEDA (Engineering Validation and Engineering Design Activities) Lithium Test Loop (ELTL) were completed and therefore one of the major milestones in the engineering validation toward IFMIF (International Fusion Materials Irradiation Facility) was accomplished. The ELTL, which holds 2.5-ton Li, is a prototype of a Li target facility of the IFMIF and is the largest-ever liquid lithium loop in the history of the fusion research.

Construction of the ELTL, which simulates hydraulic condition of the Li target and purification systems envisaged in the IFMIF, is a main pillar of the Japanese activities of the lithium target system in the IFMIF/EVEDA. Engineering design of the ELTL was carried out in 2009 to early 2010, and then construction was commenced in 2009 and completed in Nov. 2010 in the Japan Atomic Energy Agency.

The initial validation performance tests conducted after the construction included the following three stages:

1. Lithium ingot installation in the ELTL.
2. Basic operations (lithium charging and draining).
3. Lithium circulation tests.

In the third set of tests, the performance of each component comprising the ELTL (e.g., a lithium cooler, electro-magnetic pumps and flow meters, a cold trap and an economizer) was confirmed to meet the predefined specifications. In conclusion, it is assured that the electro-magnetic pump circulates lithium at the flow rate of 3000 l/min thorough the target assembly. In the final stage of the circulation test, stable lithium flow at a velocity of 5 m/s was successfully achieved in the target assembly at an Ar gas pressure of 0.12 MPa.

FTP

Status of LLCB TBM R&D Activities in India

E. Rajendrakumar¹

¹*Institute for Plasma Research, Bhat, Gandhinagar, India*

Corresponding Author: rajendrakumare@gmail.com

The development of Lead-Lithium Ceramic Breeder (LLCB) blanket is being performed as the primary candidate of Indian Test Blanket Module (TBM) program towards DEMO reactor. The LLCB TBM will be tested from the first phase of ITER operation (H-H phase) in one-half of a ITER port no-2. Neutronic calculations for the above design of LLCB TBM blanket have been carried out to estimate tritium production rate and radial profiles of nuclear heating in the blanket. The thermal-hydraulic analysis have been carried out for both serial flow and parallel flow of Pb-Li. Based on this analysis LLCB design has been optimized. To study the MHD effects, lab scale liquid metal MHD experiments has been performed to understand MHD phenomena in complex flow geometries and to generate relevant MHD database for validation of MHD numerical code. Safety analysis has been carried out for the safety licensing of LLCB TBM system for ITER. A set of four reference accidents has been identified for complete LLCB TBM System. An in-house customized computer code is developed and through these deterministic safety analyses the prescribed safety limits are shown to be well within limits for Indian LLCB-TBM design and it also meets overall safety goal for ITER. Lead-Lithium loop construction involves development of critical components like electromagnetic pump, heat exchanger, recuperator, cold trap, flow meter, pressure transmitters etc. Series of experiments on compatibility of Pb-Li with candidate structural materials Indian specific RAFMS have been attempted to study corrosion effects. Two parallel experiments were conducted in Pb-Li buoyancy loop and in a electromagnetic pump driven loop in the presence and absence of magnetic field. The specimens were characterized using analytical tools such as Optical microscopy, Scanning electron microscopy, energy dispersive X-ray (SEM/EDX), EPMA. Lithium Titanate development is under progress through two techniques:

1. Solid state reaction.
2. Chemical solution based technique.

FTP

Extruder Spherodization process was adopted for preparation of spherical pebbles. RAFM Steel development in India is based on the chemical composition of the conventional P91 steel is modified by substitution of highly radioactive element molybdenum by tungsten and niobium by tantalum. This paper will provide present status of TBM related R&D activities in India.

Activities on the Helium Cooled Lithium Lead Test Blanket Module for ITER

G. Aiello¹, A. Li Puma¹, J. F. Salavy¹, L. Jourdheuil², L. Cachon³, G. De Dinechin¹, L. Forest¹, F. Gabriel¹, C. Girard³, D. Keller⁴, K. Liger³, S. Madeleine³, A. Morin¹, J. Pavageau³, G. Rampal¹, P. Sardain⁴, H. Simon¹, E. Rigal², and J. Wagrez⁴

¹CEA/DEN/DANS, Gif sur Yvette, France

²CEA/DRT/GRE, Grenoble, France

³CEA/DEN/CAD, Saint-Paul-lez-Durance, France

⁴CEA/DSM/IRFM, Saint-Paul-Lez-Durance, France

Corresponding Author: giacomo.aiello@cea.fr

This paper gives an overview of the activities carried out at CEA concerning different aspects of the module and the associated systems (TBS, Test Blanket System): system engineering and configuration management, compliance with existing regulation, conceptual design, manufacturing and assembling of subcomponents, testing programme, instrumentation needs, ancillary systems, maintenance in ITER port cell and transport of irradiated waste.



Current Progress of Chinese Solid Breeder TBM

K. Feng¹, G. Zhang¹, Z. Zhao¹, Y. Chen¹, Y. Feng¹, T. Luo¹, X. Ye¹, G. Hu¹,
B. Xiang¹, L. Zhang¹, P. Wang¹, Z. Li¹, Q. Wang¹, F. Zhao¹, Q. Cao¹, F. Wang¹,
Y. Zhong¹, and M. Zhang¹

¹*Southwestern Institute of Physics, Chengdu, China*

Corresponding Author: fengkm@swip.ac.cn

The helium-cooled/solid breeder with the pebble bed concept has been adopted in Chinese ITER test blanket modules (TBM) design. The structure dimension of HCCB TBM design is based on 1/2 ITER test port divided vertically. In order to reduce the effects of magnetic field ripple, the design was updated with reduced RAFM steel mass. The arrangement of pebble beds in the sub-module is changed from the original transverse direction to the current vertical direction. In this updated design, each sub-module has cooling plates fed in parallel by high pressure Helium. Flow-rates of He coolant are controlled by the coolant bypass system between first-wall and sub-modules. Updated design were exhibited that the coolant flow of FW has been changed from the toroidal direction to the poloidal direction; and every 3 coolant channels are to form a cooling loop, and there are 9 loops in total inside the FW. Moreover, a modification for sub-module has also considered, the number of tritium breeding zone and neutron multiplier zones consist of 2 zones and 3 zones, respectively. Some test facilities including electro-magnetism test facility and helium test loop are being built in China. Relevant R&D on the key issues of the tritium system, RAFM steel structure material, function materials including the solid tritium breeder and neutron multiplier as well as the tritium permeation barriers, are being conducted in China. Chinese Low-activated Ferritic/martensitic steel, CLF-1, as TBM structural materials is developing towards industrially level. Exploration study of neutron multiplier Be pebbles fabrication technology has been done. Be pebbles are produced by the rotating electrode process (REP). The lithium orthosilicate as tritium breeding materials of HCCB TBM have been fabricated at laboratory level. The design of a test helium loop working at high pressure (8 MPa) and high temperature (550°C) prior to TBMs installation in ITER have been completed. In addition, Chinese HCCB TBM will be tested in Port #2 with the India Liquid Lithium Ceramic Breeder (LLCB) TBM simultaneously. Two TBMs and its associated ancillary systems will be integrated on the same Port as well as interfaced with ITER buildings and systems.

FTP

Optimisation of a Nanostructured ODS Ferritic Steel Fabrication towards Improvement of its Plasticity

P. Unifantowicz¹, J. Fikar¹, P. Spatig¹, Z. Oksiuta², M.-F. Maday³, C. Testani⁴,
N. Baluc¹, and M. Q. Tran¹

¹*Centre de Recherches en Physique des Plasmas, Ecole Polytechnique Fédérale de Lausanne,
Villigen PSI, Switzerland*

²*Bialystok Technical University, Faculty of Mechanical Engineering, Bialystok, Poland*

³*National Agency for New Technologies, Energy and Sustainable Economic Development —
ENEA, Rome, Italy*

⁴*Centro Sviluppo Materiali, Rome, Italy*

Corresponding Author: paulina.unifantowicz@psi.ch

In order to increase the operation temperature of the high-chromium reduced activation steels foreseen in applications of fusion reactors, ferritic steels containing 12 to 14% Cr in weight and reinforced with a dispersion of nano-oxides are being under development. The nano-oxides are incorporated into the matrix by adding Y₂O₃ or Fe-Y intermetallic particles to the initial steel powder, and by performing an intensive ball milling. In order to produce an ODS-steel with better mechanical properties, two specific actions of the production route were considered in this work to minimize the air contamination and porosity. The first one consists in using a higher purity pre-alloyed steel powder instead of mixture of elemental powders. The second one is to perform an additional densification after the hot-isostatic pressing (HIP) by hot cross rolling (HCR) the consolidated HIPed ingot.

The steel powders batches were produced by ball milling of either elemental or pre-alloyed powders with Y₂O₃ or Fe₂Y reinforcement particles in attritor, applying a hydrogen milling atmosphere at a controlled pressure and subsequent hot isostatic pressing. The influence of the type of substrate powders on the mechanical properties was studied for the ODS steels after HIP and after a thermal-mechanical treatment. HCR were applied at a temperature of 800°C.

Optical microscope observations revealed a refinement of the microstructure with smaller porosity. Transmission electron microscope observations of the HCR ODS steel samples microstructures showed mainly recovered grains but also a slight coarsening of the finest oxides particles compared with the steel after HIP. Grains elongation in the rolling plane or in the normal plane was not observed. Hot cross-rolling resulted in an increase of ultimate tensile strength and a significant decrease of the ductile to brittle transition temperature (DBTT). While a lower DBTT has been found for the ODS steels on which HCR was applied, it remains that the upper shelf energy is relatively low in comparison to conventional steel, about twice as low. Thus, more activities are required to produce a material possessing a better balance between the desired high tensile strength, low DBTT and high value of the upper fracture shelf energy. Possible modifications in the fabrication to reach that goal will be discussed.

FTP

Low Activation Vanadium Alloys for Fusion Power Reactors — the RF Results

V. Chernov¹, V. Drobyshev¹, M. Potapenko¹, D. Blokhin¹, N. Budylkin¹,
N. Degtyarev¹, E. Mironova¹, A. Tyumentsev², I. Ditenberg², B. Kardashev³,
A. Blokhin⁴, N. Loginov⁴, V. Romanov⁴, A. Sivak⁵, and P. Sivak⁵

¹*A. A. Bocvar High-technology Research Institute of Inorganic Materials, Moscow, Russian Federation*

²*Tomsk State University, Tomsk, Russian Federation*

³*A. F. Ioffe Physical-Technical Institute of the Russian Academy of Sciences, St. Petersburg, Russian Federation*

⁴*A.I. Leypunsky Institute for Physics and Power Engineering, Obninsk, Russian Federation*

⁵*NRC "Kurchatov Institute", Moscow, Russian Federation*

Corresponding Author: soptimizmom@mail.ru

The Results of development and researches of functional properties of low activation vanadium alloys (V-Ti-Cr and V-Cr-W-Zr-C systems) being developed for the cores of nuclear fusion and fission (Gen-IV, space) power reactors are presented.

Scientific and technological problems of the investigations are related with enhancement of functional properties based on:

1. Special optimized thermal (TT), thermomechanical (TMT) and thermochemical (TCT) treatments of V-4Ti-4Cr alloys.
2. Development of new (V-Cr-W-Zr-C system) vanadium alloys.

The TMT and TCT regimes ensuring the capability of significant (up to 2 times) enhancement of yield strength in the temperature range up to 800°C keeping relatively high plasticity reserve have been found for alloys.

The results of the theoretical, modeling and simulating studies of characteristics of self-point defects and dislocations, their interactions and mobility are presented. Nuclear physics characteristics (primary radiation damage, activation, transmutation, postreactor cooling) of alloys irradiated for a long time in neutron spectra of the fusion reactor DEMO-RF (15.3 dpa/year) and fast power reactor BN-600 (80 dpa/year) are calculated. The interaction characteristics of V-4Ti-4Cr alloy with hydrogen and the influence of hydrogen on mechanical properties of the alloy (impact toughness, internal friction) have been studied.

Obtained results allows one to recommend the vanadium alloys for applications in nuclear reactors at operating temperature window 300 – 800(850)°C. The planes of high-dose and high-temperature reactor tests of vanadium alloys are scheduled at material science assemblies of reactor BN-600 (2013 - 2015, doses 50 – 200 dpa, irradiation temperatures 400 – 800°C).

Development of Magnetic Fusion Neutron Sources and Fusion-Fission Hybrid Systems in Russia

E. Azizov¹, G. Gladush¹, and B. Kuteev¹

¹ National Research Center “Kurchatov Institute”, Moscow, Russian Federation

Corresponding Author: azizov@nfi.kiae.ru

Development of tokamak based fusion neutron sources and fusion-fission hybrids for nuclear fuel production and nuclear waste transmutation has been initiated in Russia to accelerate implementation of modern magnetic fusion technologies.

Various devices realizing intense DT fusion from 1 MW up to 100 MW have been considered and passed the pre-conceptual design level. Those include conventional, advanced and spherical tokamaks, helical systems and mirror machines. The nuclear fuel production and transmutations are addressed both for U-Pu and Th-U fuel cycles with different types of coolers and nuclear fuels.

For tokamaks with beam driven plasma at $Q = 0.2 - 1$ it is possible to reach neutron loadings higher than 0.2 MW/m^2 having the external wall area from 10 to 50 m^2 and fusion power from 1 to 10 MW. Tokamaks with unshielded coils, copper or beryllium, have simplest design and lowest cost. The upgrading program of Globus-M tokamak has been initiated in Russia. It will be helpful for decision making about future ST-devices. Conventional tokamaks with shielded coils were considered having Cu, HTSC and LTSC conductors. All tokamaks have problems with steady state operation, heating and current drive are as well as with plasma FW and divertor loadings, ELMs and disruptions.

The ignition conditions $Q > 30$ for plasma are planned to study within IGNITOR project. Reaching the 100 MW fusion power for a few seconds in the magnetic field of 13 T at plasma current 11 MA is the major goal. The conceptual design of the machine is completed and construction has started in Italy. The site for the device will be provided by TRINITI. Design of the FNS on mirror machine at Novosibirsk has shown possibility to reach 2 MW/m^2 neutron loadings at 2 m^2 area. Certain benefits may be provided by quasi-axisymmetric helical systems, which are disruption-free, are less sensitive to current drive requirements and have potential characteristics competitive with conventional and AT tokamaks.

The most promising applications for FNS and FFHS are pure neutron production at thermal neutron flux higher than $10^{15} \text{ n/cm}^2\text{s}$, nuclear fuel production in continuous molten salt cycles, especially in Th-U one. Within next years Russia plans to complete the engineering design of several FNS options, to make a choice and to begin construction of a demonstration FNS with fusion power up to 10 MW.

FTP

Investigation and Testing of KTM Divertor Model on Basis of Lithium CPS

I. Tazhibayeva¹, E. Kenzhin¹, G. Shapovalov¹, T. Kulsartov¹, Y. Ponkratov¹,
I. Lyublinski², E. Azizov³, P. Agostini⁴, G. Mazzitelli⁴, and A. Vertkov²

¹*Institute of Atomic Energy, National Nuclear Center RK, Almaty, Kazakhstan*

²*FSUE "Red Star", Moscow, Russian Federation*

³*NRC "Kurchatov Institute", Moscow, Russian Federation*

⁴*ENEA, Frascati and Brasimone, Rome, Italy*

Corresponding Author: anna@ntsc.kz

Lithium capillary porous system (CPS) as power divertor receivers tiles are proposed to study at the tokamak KTM. Trial start-up of KTM tokamak was done in September, 2010. The main goal of work is creation and testing the model of Li divertor (MLD) at KTM condition. As a result of project realization the Li-technology will be developed and Na-K cooling module of lithium divertor for tokamak KTM will be designed and tested. The construction of MLD, development of process for preparation, protection, clearing and rehabilitation of lithium CPS surfaces in tokamak conditions was completed. At the first stage the test MLD external systems, and test of MLD analog without temperature stabilization system are planned to be done during this year. Second stage will include the adjustment tests of demonstration models of KTM tokamak divertor using reduce plasma parameters. Research of lithium influence on the parameters of plasma discharge and specific power load on the plasma facing components; optimum operating modes definition of the lithium divertor will be done after KTM physical start-up.

In order to justify the use of lithium divertor module the experiments were carried out to study sorption characteristics of lithium CPS against hydrogen isotopes. Goal of present work is to assess parameters of hydrogen isotope interaction with lithium CPS under conditions modeling the operation of the tokamak KTM modes to regulate pre-start modes of working gases input. It is necessary to know also the influence of neutron irradiation on parameters of hydrogen isotopes interaction with Li CPS as well as tritium generation, accumulation and release by Li CPS under neutron irradiation for future Li technology application on fusion power reactor. Therefore, we carried out investigations of hydrogen isotopes interaction with Li/Li CPS under reactor conditions using reactor IVG-1M of NNC RK. The gas absorption technique was used to study hydrogen/helium isotope interaction with the samples of lithium CPS.

This work is carried out jointly Kazakhstani-Russian organizations in framework of the ISTC project K-1561 with ENEA collaboration.

Heat Flux and Design Calculations for the W7-X Divertor Scraper Element

J. Lore¹, T. Andreeva², J. Boscary², J. Canik¹, J. Geiger², J. Harris¹, A. Lumsdaine¹, D. McGinnis¹, A. Peacock², and J. Tipton³

¹*Oak Ridge National Laboratory, Oak Ridge, USA*

²*Max Planck Institut für Plasmaphysik, EURATOM-Association, Greifswald, Germany*

³*University of Evansville, Evansville, USA*

Corresponding Author: lorejd@ornl.gov

The W7-X stellarator is a high-performance optimized stellarator currently under construction in Greifswald, Germany. W7-X will operate under near steady-state conditions (~ 30 minute pulses), with high input power ($15 - 20$ MW, $8 - 10$ MW in first operational phase). The power and particle exhaust will be handled using an island divertor, in which last closed flux surface is defined by an island chain. New divertor components are being designed to protect the edges of the primary targets during the bootstrap current evolution in scenarios that deviate from the “minimum bootstrap current” configurations. These new components will have peak heat fluxes $\sim 10 - 12$ MW/m², and will be constructed using CFC (carbon fiber composite) monoblocks of the same type that has been qualified for ITER.

The heat flux distribution to the plasma facing components is calculated from field line following in a 3D magnetic field that includes the plasma contribution. The magnetic field is determined from the VMEC [1] (3D equilibrium) and Extender [2] (fields outside the last closed flux surface) codes. The heat flux and strike patterns in the 9 reference W7-X operating configurations will be presented for various values of the total bootstrap current during its evolution. The calculated heat fluxes to the scraper element are used as an input to heat transfer calculations. Several quantities which guide the scraper design are calculated, e.g., CFC surface temperature, fluid temperature rise, and fluid pressure drop. The results of both the heat flux calculations and the heat transfer model are used in a coupled optimization procedure to develop the geometry of the scraper element. The latest divertor geometry will be presented, along with results from the optimization and analysis procedures.

This research was supported by the US Department of Energy, Contracts DE-AC05-00OR22725.

References

- [1] S. P. Hirshman, W. I. van Rij, and P. Merkel, *Comp. Phys. Commun.* **43** (1986) 143.
- [2] M. Drevlak, D. Monticello, and A. Reiman, *Nucl. Fusion* **45** (2005) 731.

Temporal and Spatial Evolution of In-vessel Dust Characteristics in KSTAR and Dust Removal Experiments in TReD

S. H. Hong¹, K.-R. Kim², H. Park², S.-G. Cho³, E.-K. Park³, Y. U. Nam¹, J. Chung¹, T.-H. Lho¹, W. C. Kim¹, S.-J. Park², and K.-S. Chung²

¹*National Fusion Research Institute, Republic of Korea*

²*National Fusion Research Institute, Daejeon, Republic of Korea*

³*HanYang University, Seoul, Republic of Korea*

Corresponding Author: sukhhong@nfri.re.kr

Visible CCD images from 2010 and 2011 campaigns were analyzed by using image analysis technique. It is found that limiter machine like Tore Supra (TS) has main localized origins as well as many random dust creation events while divertor machines like ASDEX Upgrade (AUG) and KSTAR have origins localized mainly at divertor. The number of dust creation event per second (DCEs; dust creation frequency) is large in both machine configuration just after the machine restart, and decreases as a function of time during the machine conditioning. In TS, DCEs were in a range between 3 – 6 /s while that in divertor machines AUG and KSTAR are between 0.5 – 4.

Dust velocity distribution in 2010 and 2011 campaign was evaluated by using a dedicated software. Only “well defined dust trajectories” at in-board side are considered. Dust velocity is in the range of 10 – 400 m/s with peak velocities of 30 and 50 m/s respectively. It is observed that metal dusts created by runaway electron impact have much faster velocity, probably hypervelocity.

Short term (daily) and long term (campaign integrated) dust samples were collected and analyzed. Statistics on short term dust samples indicates that the dusts are getting more and more smaller and rounded as a function of time. Most of dusts collected by short term based method are carbon-based materials. Average particle flux is $\sim 1.2 \times 10^4$ part/cm²/s and it decreases slightly as a function of plasma operation time. Most of dusts have effective radius in the range between 0.075 – 3 μ m, peak at 0.115 μ m. Total mass of dusts (extrapolated with area of mid-plane) during the analyzed period is ~ 122 mg (average ~ 7 mg/day, ~ 0.072 μ g/cm²). Dusts from long term campaign integrated samples are large size broken graphite pieces, stainless steel, copper, etc. Various shapes and flake-like dusts are observed. Areal distribution of dusts is from 0.43 – 1701 μ m² (peak at ~ 2 μ m²), and average flux of ~ 3.48 part/cm²/s is obtained (~ 10 part/cm²/s in AUG). The mass difference of silicon wafer between before and after the dust collection was 0.1 ± 0.05 mg on 6.78 cm² (14.8 μ g/cm²). Extrapolate the amount of dusts using the area under the divertor (~ 3.38 m²), 497 mg would be present (~ 9.6 mg/day).

The transportation efficiency of Al₂O₃ dusts in He glow discharge in TReD machine was $\sim 10 - 15\%$ (injected vs collected). Currently, dust removal rate is obtained as ~ 10 mg/h.

Tungsten Divertor Target Technology and Test Facilities Development

S. Khirwadkar¹, K. Balasubramanian²

¹*Institute for Plasma Research, Gandhinagar, India*

²*Non-Ferrous Materials Technology Development Centre, Hyderabad, India*

Corresponding Author: sameer@ipr.res.in

Tungsten divertor target technology development is in progress at IPR for water-cooled divertors of ITER-like tokamak. Test mock-ups are fabricated using tungsten materials in macro-brush as well as mono-block fashion. Vacuum brazing technique is used for macro-brush fabrication whereas high pressure high temperature diffusion bonding technique is used for mono-block fabrication. Experimental facilities are also being set-up at IPR for Non-destructive testing and high heat flux testing of divertor targets. Present paper describes recent results on high heat flux testing of the test mock-ups and briefly mention about some of the experimental test facilities being set-up at IPR.

Comparative Study of Chemical Methods for Fuel Removal

A. Kreter¹, S. Möller¹, C. Schulz¹, D. Douai², H. G. Esser¹, A. Lysoivan³,
V. Philipps¹, U. Samm¹, G. Sergienko¹, and T. Wauters³

¹*Institute for Energy and Climate Research – Plasma Physics, Forschungszentrum Jülich,
Association EURATOM-FZJ, Trilateral Euregio Cluster, Jülich, Germany*

²*CEA, IRFM, Association Euratom-CEA, St Paul lez Durance, France*

³*LPP-ERM/KMS, Association Euratom-Belgian State, Brussels, Belgium*

Corresponding Author: a.kreter@fz-juelich.de

To extend the availability of ITER, tritium stored in the vessel has to be removed on a regular basis. The research on the fuel removal at Forschungszentrum Jülich has been concentrated in recent years on chemical methods including thermo-chemical erosion (TCE) also known as baking in reactive gases, glow-discharge conditioning (GDC) and ion-cyclotron wall conditioning (ICWC). The studies were conducted in the tokamak TEXTOR and in laboratory devices using pre-characterized samples with deuterated carbon layers. GDC, in contrast to TCE and ICWC, is not applicable in the presence of the nominal magnetic field. Our investigations showed that GDC can be operated at a magnetic field of up to 10 mT and is therefore compatible with the ferritic inserts foreseen in ITER. The TCE using oxygen as the removal gas can effectively be employed at elevated temperatures of at least 300°C. Plasma-based GDC and ICWC can also be applied at lower wall temperatures. TCE is equally efficient in cleaning from the wall surface as from the remote areas such as gaps of castellations. GDC is homogeneous along the wall surface except for small recessed areas like gaps. ICWC is typically inhomogeneous along the poloidal circumference. Applying the radial magnetic field, we were able to control the poloidal position of the main IC plasma production. Thus, some wall regions, e.g., the divertor, can selectively be exposed to ICWC. Owing to higher ion fluxes to the wall, ICWC activates a larger amount of neutrals than GDC, which then penetrate in gaps and clean gap walls efficiently. Removal rates with oxygen were typically by a factor of 3 – 10 higher than with hydrogen and ammonia and 10 – 30 than with nitrogen. The estimates using the highest removal rate for ICWC show that about 2 hours are needed to remove the layer deposited within one ITER pulse. The application of ammonia in TCE led to the peeling-off of layers, which is a potential dust production mechanism. However, it appears to be suitable for the non-oxidizing cleaning of metallic mirrors envisaged for optical diagnostics in ITER.

Analysis of Establishment and MHD Stability of a Free Curve-Surface Flow for Liquid Metal PFCs

Z. Xu¹, X. Zhang¹, C. Pan¹, X. Duan¹, and Y. Liu¹

¹*Southwestern Institute of Physics, Chengdu, China*

Corresponding Author: xuzy@swip.ac.cn

An innovation concept of three layer s guidable liquid metal free curve-surface flow is addressed and its establishment and MHD stability are also analyzed on theoretically Layer I is a basic conduction layer, layer II is a key adjust layer, layer III is the surface layer. To adjust layer I and II in suitable flowing conditions, the MHD effect stability surface layer III can be obtained. In meantime, the layer I and II can be as the heat sink and the coolant flow (it is also suitable to a flat surface flow to avoid rivulet flow). According to Newton's laws and fluid mechanical principles, the analysis results show that an MHD effect stability free curve surface flow can be established under a given curve surface in a gradient magnetic field.

FTP-P

“Snow Flakes” Divertor and 10 MA Scenarios in FAST

F. Crisanti¹, P. Martin¹, P. Mantica¹, G. Calabro¹, V. Fusco¹, V. Pericoli Ridolfini¹, M. E. Puiatti¹, L. Lauro Taroni¹, M. Valisa¹, F. Villone¹, G. Vlad¹, and R. Zagorski²

¹Associazione ENEA-Euratom sulla Fusione, Italy

²EURATOM/IPPLM Association, Warsaw, Poland

Corresponding Author: crisanti@frascati.enea.it

The overarching FAST goals lead to a more flexible design and to a research plan based on three DEMO and ITER priorities:

1. Exploring plasma wall interaction in reactor relevant conditions.
2. Testing tools and scenarios for safe and reliable tokamak operation up to the border of stability.
3. Addressing fusion plasmas with a significant population of fast particles, plus being complementary to the JT60-SA missions. Unique of the FAST approach is the capability of addressing all of them simultaneously in a single, fully integrated scenario with dimensionless physics parameters very close to DEMO and ITER.

FAST has the possibility to tackle the power exhaust problem in regimes relevant to DEMO with an actively cooled W-divertor capable to sustain loads up to 20 MW/m^{-2} with $P/R \sim 22 \text{ MW/m}$. A “Snow Flakes” divertor can be implemented in FAST with the present poloidal coils up to the reference scenario with $I_p = 6.5 \text{ MA}$. According to the 2-D plasma edge code TECXY the peak power flow along the SOL field lines can be reduced by a factor ~ 3.0 . A new FAST scenario has then been designed at $I_p = 10 \text{ MA}$, $B_T = 8.5 \text{ T}$, $q_{95} \approx 2.3$. Transport simulations by using the code JETTO and the first principle transport model GLF23 indicate that, under these conditions, FAST could achieve an equivalent $Q \sim 3.5$. FAST will be equipped with a set of feedback controlled active coils located between the first wall and the vacuum vessel ($\sim 25 \text{ cm}$ far from the plasma edge) and accessible for maintenance with the remote handling system. Preliminary studies indicate that these coils can carry currents up to 20 kA ($\sim 4 \text{ MA/m}^2$) with AC frequency up to few kHz. The coil set will produce magnetic perturbation with toroidal number $n = 1$ or $n = 2$. MHD analysis performed with the linear code MARS (both assuming the presence of a perfect conductive wall at $r/a = 1.3$ and using the exact 3D resistive wall structure) shows the possibility of the FAST conductive structures to stabilize $n = 1$ and $n = 2$ ideal modes. This leaves therefore room for active mitigation of the resistive mode (down to a characteristic time of 1 ms) for safety purposes. The main target of this experiment is the preparation of a complete and reliable low q_{95} scenario, ready to be transferred to a possible ITER scenario very close to its operational limits.

Preliminary Safety Analysis of the Indian Lead Lithium Cooled Ceramic Breeder Test Blanket Module System in ITER

V. Chaudhari¹, R. K. Singh², P. Chaudhuri¹, B. Yadav¹, C. Danani¹, and R. K. Ellappan¹

¹*Institute for Plasma Research, Bhat, Gandhinagar, India*

²*Bhabha Atomic Research Center, Mumbai, India*

Corresponding Author: vilas.ipr@gmail.com

Safety analysis has been carried out for the safety licensing of Lead Lithium cooled Ceramic Breeder (LLCB) Test Blanket Module (TBM) system; India's proposed prototype of DEMO blanket concept for testing in International Thermonuclear Experimental Reactor (ITER). A set of four reference accidents is identified for LLCB TBM System. Each accidental sequence begins with a Postulated Initiating Event (PIE) identified through Failure Modes and Effects Analysis (FMEA) at component level. The analysis address specific reactor safety concerns, such as passive removal of decay heat, pressurization of confinement buildings, vacuum vessel pressurization, release of activated products and tritium during these accidental events and hydrogen production from chemical reactions between lead-lithium liquid metal and beryllium with water. An in-house customized computer code is developed and through these deterministic safety analyses the prescribed safety limits are shown to be well within limits for Indian LLCB-TBM design and it also meets overall safety goal for ITER. This paper reports transient analysis results of the safety assessment.

Technology Gaps for the Fuel Cycle of a Fusion Power Plant

C. Day¹, B. Bornschein², D. Demange³, T. Giegerich³, M. Kovari³, B. Weyssow⁴, and R. Wolf⁵

¹*Karlsruhe Institute of Technology, Germany*

²*Karlsruhe Institute of Technology, Association EURATOM-KIT, Karlsruhe, Germany*

³*Association EURATOM-CCFE, Culham Science Centre, Abingdon, UK*

⁴*EFDA-CSU, Garching, Germany*

⁵*Max Planck Institut für Plasmaphysik, Association EURATOM-IPP, Garching, Germany*

Corresponding Author: christian.day@kit.edu

Control and management of the fuel and fusion product streams is one of the most difficult issues for fusion power plant development. This function is provided by the fusion fuel cycle and addresses the vacuum pumping systems, the fuelling systems, the tritium plant systems and the in-vessel components, especially the divertor and the breeding blankets with their associated periphery. The design of these systems decides the accumulated tritium inventories and the processing times of the unburnt fuel, which both must be absolutely minimised. As main tool to match this requirement, a simplified fuel cycle architecture has been developed based on the concept of Direct Internal Recycling (DIR) of the unburnt fuel close to the divertor. Advantages and compromises of this concept will be discussed.

In all areas where ITER does not serve as a convincing basis for technology scale-up, new technologies have to be developed. This paper is reporting results of ongoing activities in EU to assess the fuel cycle systems of DEMO. It will go through the current state of technology, address the technical readiness, identify the areas which are considered to require essential supporting R&D towards a functional system for a reactor, and propose potential solutions together with experimental information — if available — or outline R&D paths for their development.

Simulation Experiments of ELM-like Transient Heat and Particle Loads using a Magnetized Coaxial Plasma Gun

Y. Kikuchi¹, K. Shoda¹, D. Iwamoto¹, I. Sakuma¹, Y. Kitagawa¹, N. Fukumoto¹,
M. Nagata¹, Y. Ueda², and S. Suzuki³

¹*Graduate School of Engineering, University of Hyogo, Himeji, Japan*

²*Osaka University, Suita, Osaka, Japan*

³*Japan Atomic Energy Agency, Naka, Japan*

Corresponding Author: ykikuchi@eng.u-hyogo.ac.jp

A magnetized coaxial plasma gun (MCPG) device has been developed for simulation experiments of transient heat and particle loads during type I edge localized modes (ELMs) predicted in ITER. The MCPG has been recently upgraded to increase surface absorbed energy density up to $\sim 2 \text{ MJ/m}^2$ that makes it possible to investigate tungsten (W) melting behaviors. In the experiment, mono-block W samples, to be used for the ITER divertor, were exposed to repetitive pulsed hydrogen plasmas with duration of $\sim 0.2 \text{ ms}$, incident ion energy of $\sim 50 \text{ eV}$, and surface absorbed energy density of $\sim 0.7, 1.4, \text{ and } 2 \text{ MJ/m}^2$. No melting occurred on the mono-block W surface at energy density of $\sim 0.7 \text{ MJ/m}^2$, while major cracks were formed. Cracking and melting of the mono-block W surface were clearly observed at energy density of $\sim 1.4 \text{ and } 2 \text{ MJ/m}^2$. Micro-sized cracks were identified for energy density above the melting threshold.

It is considered that the micro-sized cracks were formed due to surface melting and resolidification in each plasma pulse. The mono-block W samples with pulsed plasma irradiation will be exposed to cyclic heat loads of $\sim 20 \text{ MW/m}^2$ in an electron beam facility JEBIS at JAEA in order to investigate damage of ITER divertor materials under a combination of steady-state and transient heat loads.

Moreover, we introduce a new experiment using two MCPG devices to understand vapor shielding effects of a W surface under ELM-like pulsed plasma bombardment. The second plasmoid is applied with a variable delay time after the first plasmoid. A vapor cloud layer in front of the W surface produced by the first plasmoid irradiation could shield the second pulsed plasma load on the W surface. In this upgrade, weight loss measurements of W samples after pulsed plasma exposures became possible, which is a great advantage for quantitative evaluation of vapor shielding effects on erosion of W.

Plasma Characteristics of the End-cell of the GAMMA 10 Tandem Mirror for the Divertor Simulation Experiment

Y. Nakashima¹, M. Sakamoto¹, M. Yoshikawa¹, H. Takeda¹, K. Ichimura¹, K. Hosoi¹,
M. Hirata¹, M. Ichimura¹, R. Ikezoe¹, T. Imai¹, T. Kariya¹, I. Katanuma¹,
J. Kohagura¹, R. Minami¹, T. Numakura¹, H. Ueda¹, N. Asakura², T. Furuta³,
A. Hatayama³, Y. Hirooka⁴, S. Kado⁵, S. Masuzaki⁴, H. Matsuura⁶, S. Nagata⁷,
N. Nishino⁸, N. Ohno⁹, A. Sagara⁴, T. Shikama⁷, M. Shoji⁴, M. Toma³,
A. Tonegawa¹⁰, and Y. Ueda¹¹

¹Plasma Research Center, University of Tsukuba, Tsukuba, Japan

²Japan Atomic Energy Agency, Naka, Japan

³Faculty of Science and Technology, Keio University, Japan

⁴National Institute for Fusion Science, Toki, Japan

⁵Department of Nuclear Engineering and Management, The University of Tokyo, Tokyo, Japan

⁶Radiation Research Center, Osaka Prefecture University, Osaka, Japan

⁷Institute for Material Research, Tohoku University, Japan

⁸Graduate School of Engineering, Hiroshima University, Japan

⁹Graduate School of Engineering, Nagoya University, Japan

¹⁰Graduate School of Science, Tokai University, Japan

¹¹Graduate School of Engineering, Osaka University, Japan

Corresponding Author: nakashima@prc.tsukuba.ac.jp

In this paper, detailed characteristics and controllability of plasmas emitted from the end-cell of the GAMMA 10 tandem mirror are described from the viewpoint of divertor simulation studies. In the case of only ICRF plasma, the heat flux of 0.8 MW/m² has already been achieved and proportionally increased with the ICRF power for ion heating. The energy analysis of ion flux by using end-loss ion energy analyzer (ELIEA) proved that the obtained high ion temperature (100 – 400 eV) was comparable to SOL plasma parameters in toroidal devices and was controlled by changing the ICRF power. Parallel ion temperature $T_{i\parallel}$ determined from the probe and calorimeter shows a linear relationship with the stored energy in the central-cell and agrees with the results of ELIEA. Recently additional plasma heating experiment using ICRF in the anchor-cell (RF3) was carried out in order to improve the performance. A significant enhancement of the line-density is observed and the resultant ion flux becomes two times higher than that without RF3. The particle flux is estimated to be 6.5×10^{22} particles/s m², which indicate an effectiveness of additional heating with ICRF wave in the neighboring cells toward the improved E-divertor experiments for achieving the targeted parameters of this project ($P_{\text{HEAT}} \sim 20$ MW/m², $\Gamma_i = 10^{23-24}$ /m²s).

We have started various experiments such as radiator gas injection onto the tungsten target and visible measurement of plasma-gas-material interactions with a fast camera. Numerical simulation studies have also started in the end-cell for understanding the behavior of plasmas in divertor simulation experiments. In this spring a large-sized divertor experimental module will be installed and radiative cooling experiments of the end-cell plasma are planned by using gas injection into the module for realizing the detached plasma condition.

References

- [1] Y. Nakashima, *et al.*, Fusion Eng. Design **85-6** (2010) 956-962.
- [2] Y. Nakashima, *et al.*, Trans. Fusion Sci. Technol. **59-1T** (2011) 61-66.

This work is supported by the bidirectional collaboration research program with National Institute for Fusion Science.

Progress of High Heat Flux Component Manufacture and Heat Load Experiments in China

X. Liu¹, Y. Lian¹, Z. Xu¹, J. Chen¹, L. Chen¹, Q. Wang¹, X. Duan¹, G. Luo², and Q. Yan³

¹*Southwestern Institute of Physics, Chengdu, China*

²*Institute of Plasma Physics, Chinese Academy of Sciences, Hefei, China*

³*University of Science & Technology Beijing, Beijing, China*

Corresponding Author: xliu@swip.ac.cn

High heat flux components for first wall and divertor are the key subassembly of the present fusion experiment apparatus and fusion reactors in the future. It is requested the metallurgical bonding among the plasma facing materials (PFMs), heat sink and support materials. As to PFMs, ITER grade vacuum hot pressed beryllium CN-G01 was developed in China and has been accepted as the reference material of ITER first wall. Additionally pure tungsten and tungsten alloys, as well as chemical vapor deposition (CVD) W coating are being developed for the aims of ITER divertor application and the demand of domestic fusion devices, and significant progress has been achieved. For plasma facing components (PFCs), high heat flux components used for divertor chamber are being studied according to the development program of the fusion experiment reactor of China. Two reference joining techniques of W/Cu mockups for ITER divertor chamber are being developed, one is mono-block structure by pure copper casting of tungsten surface following by hot iso-static press (HIP), and another is flat structure by brazing.

The critical acceptance criteria of high heat flux components are their high heat load performance. A 60 kW Electron-beam Material testing Scenario (EMS-60) has been constructed at Southwestern Institute of Physics (SWIP), which adopts an electron beam welding gun with maximum energy of 150 keV and $150 \times 150 \text{ mm}^2$ scanning area by maximum frame rate of 30 kHz. Furthermore, an Engineering Mockup testing Scenario (EMS-400) facility with 400 kW electron-beam melting gun is under construction and will be available by the end of this year. After that, China will have the comprehensive capability of high heat load evaluation from PFMs and small-scale mockups to engineering full scale PFCs.

A brazed W/CuCrZr mockup with $25 \times 25 \times 40 \text{ mm}^3$ in dimension was tested at EMS-60. The heating and cooling time are 10 seconds and 15 seconds, respectively. The experiment procedure is 3 MW/m^2 by 200 cycles and then 6 MW/m^2 by 1000 cycles, following by 8.5 MW/m^2 for 200 cycles and 11 MW/m^2 for 100 cycles. No off-normal surface temperature change and cracks were observed. The similar screening tests of small-scale mono-block W/CuCrZr mockups will be tested soon. Next large size brazed W/CuCrZr components will be manufactured and evaluated.

FTP-P

Super-X Divertor Simulation for HCSB-DEMO

G. Zheng¹, K. Feng¹, Y. Pan¹, H. He¹, and X. Cui¹

¹*Southwestern Institute of Physics, Chengdu, China*

Corresponding Author: zgy@swip.ac.cn

A new magnetic geometry, called Super-X divertor, is design to solve the severe heat exhaust problems in high power density for HCSB-DEMO. Super-X divertor increases the plasma-wetted area close to the separatrix by expanding the magnetic field lines with two other X-points and increases the parallel connection length by moving outer strike-point to larger R. The heat load at targets is invested by using B2.5-Eirene edge plasma transport simulation codes. The simulation results show that, with 600 MW heating power flows into SOL/divertor regions and the density at the separatrix is $3.5 \times 10^{19} / \text{m}^3$, the peak heat load at inner and outer divertor are respectively 8.9 MW/m^2 and 3.5 MW/m^2 , which are much less than that of standard divertor and below the design targets (10 MW/m^2). It is suggested that Super-X divertor be a candidate divertor for an economically competitive fusion reactor to solute the high heat load problem at divertor target.

Recent Progress in the NSTX/NSTX-U Lithium Program and Prospects for Reactor-relevant Liquid-lithium Based Divertor Development

M. Ono¹, M. Bell¹, M. Jaworski¹, R. Kaita¹, H. Kugel¹, J. W. Ahn², R. Bell¹, J. P. Allain³, J. Canik², S. Ding⁴, S. Gerhardt¹, T. Gray², S. Kaye¹, W. Guttenfelder¹, Y. Hirooka⁵, J. Kallman⁶, B. LeBlanc¹, R. Maingi¹, D. Mansfield¹, A. McLean¹, J. Menard¹, D. Mueller¹, R. Nygren⁷, S. Paul¹, M. Podesta¹, R. Raman¹, Y. Ren¹, S. Sabbagh⁸, F. Scotti¹, C. Skinner¹, V. Soukhanovskii¹, V. Surla⁹, L. Zakharov¹, C. Taylor³, and NSTX Research Team¹

¹*Princeton Plasma Physics Laboratory, Princeton, USA*

²*Oak Ridge National Laboratory, Oak Ridge, USA*

³*Purdue University, West Lafayette, USA*

⁴*Academy of Science Institute of Plasma Physics, Hefei, China*

⁵*National Institute for Fusion Science, Toki, Japan*

⁶*Lawrence Livermore National Laboratory, Livermore, USA*

⁷*Sandia National Laboratory, Albuquerque, USA*

⁸*Columbia University, New York, USA*

⁹*Center for Plasma-Materials Interactions, University of Illinois, Urbana-Champaign, USA*

Corresponding Author: mono@pppl.gov

Developing a reactor compatible divertor has been identified as a particularly challenging technology problem for magnetic confinement fusion. While tungsten has been identified as the most attractive solid divertor material, the NSTX/NSTX-U lithium (Li) program is investigating the viability of liquid lithium (LL) as a potential reactor compatible divertor plasma facing component (PFC). In the near term, operation in NSTX-U is projected to provide reactor-like divertor heat loads $\leq 40 \text{ MW/m}^2$ for 5 s. During the most recent NSTX campaign, $\sim 0.85 \text{ kg}$ (1.5 liter) of Li was evaporated onto the NSTX PFCs where a $\sim 50\%$ reduction in heat load on the LLD was observed, attributable to enhanced divertor bolometric radiation signal. This reduced divertor heat flux through radiation observed in the NSTX LLD experiment is consistent with the results from other Li experiments and calculations. These results motivate an LL-based closed radiative divertor concept proposed here for NSTX-U and fusion reactors. With an LL coating, the Li is evaporated from the divertor strike point surface due to the intense heat. The evaporated Li is readily ionized by the plasma due to its low ionization energies, and the ionized Li ions can radiate strongly, resulting in a significant reduction in the divertor heat flux. Due to the rapid plasma transport in divertor plasma, the radiation values can be significantly enhanced up to $\sim 11 \text{ MJ/cc}$ of LL. This radiative process has the desired function of spreading the focused divertor heat load to the entire divertor chamber, which facilitates the divertor heat removal. The LL divertor surface can also provide a “sacrificial” surface to protect the substrate solid material from transient high heat flux such as the ones caused by the ELMs. The closed radiative LLD concept has the advantages of providing some degree of partition in terms of plasma disruption forces on the LL, Li particle divertor retention, and strong divertor pumping action from the li-coated divertor chamber wall. By operating at a lower temperature than the first wall, the LLD can serve to purify the entire reactor chamber, as impurities generally migrate toward lower temperature Li-condensed surfaces. To maintain the LL purity, a closed LL loop system with a modest capacity (e.g., $\sim 1 \text{ liter/sec}$ for $\sim 1\%$ level “impurities”) is envisioned for a steady-state reactor.

FTP-P

Effects of the Lithium Concentration on Tritium Release Behaviors from Advanced Tritium Breeding Material $\text{Li}_{2+x}\text{TiO}_3$

H. Uchimura¹, M. Kobayashi¹, K. Kawasaki¹, Y. Miyahara¹, T. Taguchi¹, K. Toda¹,
T. Fujii², H. Yamana², O. Yasuhisa¹, and K. Okuno¹

¹*Radioscience Research Laboratory, Faculty of Science, Shizuoka University, Shizuoka, Japan*

²*Research Reactor Institute, Kyoto University, Kyoto, Japan*

Corresponding Author: r0232002@ipc.shizuoka.ac.jp

Lithium-enriched Li_2TiO_3 , such as $\text{Li}_{2.2}\text{TiO}_3$ and $\text{Li}_{2.4}\text{TiO}_3$ ($\text{Li}_{2+x}\text{TiO}_3$), is considered as one of advanced tritium breeding materials in fusion reactors. Densities of irradiation defects in $\text{Li}_{2+x}\text{TiO}_3$ will increase with increasing lithium concentration. It is expected that tritium is trapped by irradiation defects and its release behavior will be affected by the density of the defects. Therefore, elucidation of enhancement effects of the irradiation defects on tritium release behavior in $\text{Li}_{2+x}\text{TiO}_3$ is an important issue from a viewpoint of tritium recovery.

Thermal neutron irradiation was performed for $\text{Li}_{2.0}\text{TiO}_3$, $\text{Li}_{2.2}\text{TiO}_3$ and $\text{Li}_{2.4}\text{TiO}_3$ at the Research Reactor Institute, Kyoto University. The thermal neutron flux was $5.5 \times 10^{12} \text{ n cm}^{-2} \text{ s}^{-1}$ and fluence was $3.3 \times 10^{15} \text{ n cm}^{-2}$. Thermal Desorption Spectroscopy (TDS) measurements were carried out to investigate the release behaviors of tritium generated in $\text{Li}_{2+x}\text{TiO}_3$. Electron Spin Resonance (ESR) measurements were also carried out to estimate the densities and the annihilation behaviors of irradiation defects introduced by thermal neutron irradiation.

The densities of the irradiation defects in $\text{Li}_{2+x}\text{TiO}_3$ evaluated by the peak areas of the ESR spectra were increased with increasing lithium concentrations. An X-ray diffraction (XRD) showed that the Li_4TiO_4 structure was formed in the lithium enriched samples. The Li_4TiO_4 structure may affect the enhancement to the density of defects for lithium enriched Li_2TiO_3 . It was found that the defects for $\text{Li}_{2.0}\text{TiO}_3$ observed by ESR were annihilated around 600 – 800K, although those for $\text{Li}_{2.2}\text{TiO}_3$ and $\text{Li}_{2.4}\text{TiO}_3$ were annihilated around 400 – 600K. In addition, two tritium desorption stages were observed at 450K and 600K by the TDS measurement. The tritium release in lower temperatures was enhanced with increasing lithium concentration, corresponding to the annihilation temperature region of the defects in $\text{Li}_{2.2}\text{TiO}_3$ and $\text{Li}_{2.4}\text{TiO}_3$. It was concluded that tritium release at the lower temperatures was initiated by the existence of Li_4TiO_4 structure formed in the lithium-enriched Li_2TiO_3 . These results indicate that use of lithium-enriched Li_2TiO_3 enables the recovery of tritium about lower temperature compared to $\text{Li}_{2.0}\text{TiO}_3$ and would be an advantage for the fuel recovery from the tritium breeding materials in the fusion reactors.

Progress in the Development of the ECRF System for JT-60SA

A. Isayama¹, T. Kobayashi¹, S. Moriyama¹, K. Yokokura¹, M. Shimono¹,
M. Sawahata¹, S. Suzuki¹, M. Terakado¹, S. Hiranai¹, K. Wada¹, J. Hinata¹, Y. Sato¹,
K. Hoshino¹, K. Sakamoto¹, K. Kajiwara¹, Y. Oda¹, and K. Hamamatsu¹

¹*Japan Atomic Energy Agency, Naka, Japan*

Corresponding Author: isayama.akihiro@jaea.go.jp

The electron cyclotron range of frequency (ECRF) system for JT-60SA is composed of 9 gyrotrons with the total injection power of 7 MW and the pulse duration of 100 s, transmission line with the total length of ~ 80 m, and linear-motion launchers. This paper comprehensively presents recent progress in the development of the ECRF system. Major results are

1. the extension of gyrotron output energy (60 MJ) by a factor of 2 compared with the results presented in the last IAEA FEC through the installation of a new 60.3 mm diameter transmission line,
2. successful tests on optical and mechanical characteristics of a linear-motion launcher, which enables > 1 MW, 100 s injection with a wide coverage of toroidal (typically -15 deg. to $+15$ deg.) and poloidal (-40 deg. to $+20$ deg. with respect to the horizontal plane) directions,
3. the development of a dual-frequency gyrotron which can output 110 GHz and 138 GHz ECRF at > 1 MW for 100 s for heating (ECH) and current drive (ECCD) typically around the half minor radius at the full toroidal magnetic field of 2.3 T in JT-60SA.

Feasibility and R&D Needs of a Negative Ion Based Neutral Beam System for DEMO

U. Fantz¹, P. Franzen¹

¹Max Planck Institut für Plasmaphysik, EURATOM Association, Garching, Germany

Corresponding Author: fantz@ipp.mpg.de

The R&D requirements of a heating and current drive (H&CD) system for a demonstration fusion power plant (DEMO) are presently assessed within the EFDA 3PPT activities. The requirements of the H&CD system will strongly depend on the DEMO scenario; the most demanding requirements are defined by a steady state tokamak. For such a cw CD system with several 100 MW power, the key issues are the achievement of adequate plug-in efficiency, availability and reliability. The neutral beam injection (NBI) system, at present a key system H&CD of magnetic fusion devices including ITER, is also a candidate for DEMO, due to its high current drive efficiency.

A DEMO cw CD NBI system will be based like the ITER NBI system on production, acceleration and neutralisation of negative deuterium ions. For sufficient current drive neutral particle energies of several 100 kV at minimum are required. The neutralisation efficiency of negative ions is still about 60% at these high energies whereas the efficiency of positive ions is below a few percent.

The paper concentrates on two issues which are presently addressed by IPP R&D activities:

1. The enhancement of the overall wall plug efficiency from approx. 25% for the ITER system to more than 50%; and
2. the Reliability and maintainability of the negative deuterium ion source.

At present, the only promising technology to enhance the plug-in efficiency to the required values above 50% is a laser neutraliser system with neutralisation efficiency of almost 100%. Among other benefits, a laser neutralizer does not require high heat flux components, i.e., a residual ion dump, in the beamline, so that the negative ion source and the accelerator will be the most crucial parts for the reliability of the system. Both parts are exposed to local power densities of several 10 MW/m² in the present ITER design. The operation at reduced source filling pressure (below 0.3 Pa, the ITER requirement) and a Cs-free source are identified to be very beneficial by reducing the local power loads and removing the need for a regular maintenance. On the other hand, NBI systems with energies above 1 MeV for enhanced current drive efficiency seem to be unfeasible with the present technology.

Details and concepts will be discussed in more detail in the paper, highlighting the feasibility and R&D needs from the present available ITER technology.

Progress in the Development of Long Pulse Neutral Beam Injectors for JT-60SA

M. Hanada¹, A. Kojima¹, N. Akino¹, M. Kazawa¹, M. Komata¹, K. Mogaki¹, K. Usui¹, S. Sasaki¹, N. Seki¹, H. Seki¹, T. Shimizu¹, S. Nemoto¹, Y. Endo¹, M. Ozeki¹, K. Oasa¹, T. Inoue¹, K. Watanabe¹, M. Taniguchi¹, M. Kashiwagi¹, H. Tobar¹, S. Kobayashi², Y. Yamanou², L. Grisham³, S. Jeong⁴, D. Chang⁴, B. Oh⁴, and K. Lee⁴

¹*Japan Atomic Energy Agency, Naka, Japan*

²*Saitama University, Saitama, Japan*

³*Princeton Plasma Physics Laboratory, Princeton, USA*

⁴*Korea Atomic Energy Research Institute, Daejeon, Republic Korea*

Corresponding Author: hanada.masaya@jaea.go.jp

To realize a 100 s injection of neutral beams for JT-60 Super Advanced (JT-60SA), the feasibility of the long-pulse production of the ion beams is investigated. Using the JT-60 positive ion source, the long-pulse production of the positive ion beams is confirmed to be feasible for JT-60SA by analyzing the results obtained in the productions of full power D⁺ ion beams of 85 keV, 27.5 A for 30 s and a half power H⁺ ion beams of 60 keV, 18 A for 200 s. This shows that the JT-60 positive ion source is expected to be reused in JT-60SA without modifications. To realize a stable acceleration of the high current D⁻ ion beams of 500 keV for 100 s without interruptions due to breakdowns, vacuum voltage holding capability of the multi-aperture grid designed for JT-60 SA is firstly clarified in the world. Based on results, the gap length of the accelerator was tuned for the grid area and number of the apertures for JT-60SA. As the result, high voltage holding during 100 s without breakdowns was attained at 200 kV for one acceleration gap at an optimum gap length for sufficient suppressions of the beam losses. This suggests that stable long-pulse acceleration to 500 keV could be expected for three acceleration stages in JT-60SA.

Local Current Injector System for Nonsolenoidal Startup in a Low Aspect Ratio Tokamak

R. Fonck¹, A. Redd¹, M. Bongard¹, E. Hinson¹, B. Lewicki¹, and G. Winz¹

¹*University of Wisconsin-Madison, Madison, USA*

Corresponding Author: rjfonck@wisc.edu

The Pegasus experiment is an ultralow aspect ratio spherical tokamak that is developing nonsolenoidal startup and current growth techniques. Helicity injection from localized current sources in the plasma periphery have produced plasma currents up to 0.15 MA with less than 4 kA injected, and the resulting plasmas provide stable target plasmas for further current drive. This localized helicity injection startup technique requires the development of robust, high current density sources ($\sim 1 \text{ kA/cm}^2$) that can exist in the plasma scrapeoff region during plasma initiation, growth, and possibly sustainment. An integrated assembly of active arc plasma sources and a passive electrode emitter is under development for this application to MA-class spherical tokamak applications. Compact arc plasma current sources are used for initial current injection along vacuum field lines to produce a tokamak-like plasma through null formation and Taylor relaxation. Further current growth is realized through helicity injection from these arc sources or passive electrodes in the plasma edge region. Use of passive metallic electrodes can greatly simplify the design and allow for higher injected currents to optimize the resulting plasma current. The compact, active arc sources provide an extracted current stream that appears to be governed by a double layer sheath at the arc exit region. At voltages greater than $eV/kT \sim 10$ and high currents, the extracted current scales as $V^{1/2}$, presumably due to sheath expansion or the Alfvén-Lawson current limit for electrons. Control of the arc plasma density through active gas feed control and detailed design of the arc chamber should provide active control of the effective loop voltage applied to the tokamak plasma. The arc source and electrode structures are isolated from the edge plasma by a local BN limiter and nearby scraper limiter assembly. This mitigates interactions between the injector assembly and the plasma, and resulting impurities in the plasma are negligible. High-current power supplies using IGCT solid-state switches regulate the injector current according to a pre-programmed waveform. This startup approach places minimal demands on machine design, appears scalable to MA levels in large facilities, and offers the possibility of hardware that can be withdrawn before a fusion plasma enters the nuclear burn phase.

Development of MW Gyrotrons for Fusion Devices by University of Tsukuba

R. Minami¹, T. Kariya¹, T. Imai¹, T. Numakura¹, Y. Endo¹, H. Nakabayashi¹, T. Eguchi¹, T. Shimoizuma², S. Kubo², Y. Yoshimura², H. Igami², H. Takahashi², T. Mutoh², S. Ito², H. Idei³, H. Zushi³, Y. Yamaguchi⁴, K. Sakamoto⁵, and Y. Mitsunaka⁶

¹Plasma Research Center, University of Tsukuba, Ibaraki, Japan

²National Institute for Fusion Science, Toki, Japan

³Kyusyu University, Fukuoka, Japan

⁴University of Fukui, Fukui, Japan

⁵Japan Atomic Energy Agency, Tokyo, Japan

⁶Toshiba Electron Tubes and Devices Co., Japan

Corresponding Author: minami@prc.tsukuba.ac.jp

Over-1 MW power gyrotrons for ECH have been developed in the joint program of NIFS and University of Tsukuba. The obtained maximum outputs are 1.9 MW for 0.1 s on the 77 GHz LHD tube and 1.0 MW for 1 ms on the 28 GHz one, which are the new records in these frequency ranges. In long pulse operation, 300 kW for 40 min at 77 Hz and 540 kW for 2 s at 28 GHz were achieved. Three 77 GHz gyrotrons have already been installed and operated stably in LHD. More than 3.4 MW has been injected into LHD plasma contributing to producing the electron temperature T_e of 20 keV. A new program of 154 GHz 1 MW development has started for high density plasma heating in LHD and the first tube has been fabricated. A 28 GHz gyrotron is also required at QUEST in Kyushu University, where 0.4 MW continuous wave (CW) one is needed. A few sec. with multi-MW gyrotron is useful for novel Electron Bernstein Wave (EBW) heating system of NSTX in PPPL. Based on the first 28 GHz 1 MW tube results, the design of the new 28 GHz tube has progressed, which satisfies both requirements. These lower frequency tubes like 77 GHz or 28 GHz one are also important for advanced magnetic fusion devices, which use the EBW heating / current drive.

FTP-P

Status and Plan of the Key Actuators for KSTAR Operation

H. Y. Yang¹, Y. M. Park¹, Y. S. Bae¹, H. K. Kim¹, Y. S. Kim¹, K. M. Kim¹,
 K. S. Lee¹, H. T. Kim¹, E. N. Bang¹, M. Joung¹, J. S. Kim¹, W. S. Han¹, S. I. Park¹,
 J. H. Jeong¹, H. J. Do², H. J. Lee¹, S. W. Kwag¹, Y. B. Chang¹, N. H. Song¹,
 J. H. Choi¹, D. K. Lee¹, C. H. Kim¹, J. K. Jin¹, J. D. Kong¹, S. L. Hong¹,
 H. T. Park¹, Y. J. Kim¹, S. T. Kim¹, D. S. Im¹, N. Y. Joung¹, W. Namkung²,
 M. H. Cho², H. Park², S. H. Jeong³, D. H. Chang³, J. T. Jin³, S. R. In³, S. J. Wang³,
 S. H. Kim³, K. Sakamoto⁴, K. Watanabe⁴, Y. Gorelov⁵, J. Lohr⁵, R. Ellis⁶, J. Hosea⁶,
 R. Parker⁷, L. Delpach⁸, T. Hoang⁸, X. Litaudon⁸, and J. G. Kwak¹

¹*National Fusion Research Institute, Daejeon, Republic of Korea*

²*POSTECH, Daejeon, Republic of Korea*

³*KAERI, Daejeon, Republic of Korea*

⁴*Japan Atomic Energy Agency, Naka, Japan*

⁵*General Atomic, San Diego, USA*

⁶*Princeton Plasma Physics Laboratory, Princeton, USA*

⁷*MIT, Cambridge, USA*

⁸*CEA, Cadarache, France*

Corresponding Author: hlyang@nfri.re.kr

After 1st plasma in 2008, the Korea Superconducting Tokamak Advanced Research (KSTAR) has been intensively upgraded to supply key actuators such as in-vessel components and heating system. The in-vessel components satisfactorily provided an essential condition for experiments on plasma shaping, H-mode, and edge localized mode (ELM) suppression in 2010 and 2011. There was also a big progress in upgrade of heating system. The neutral beam injection system demonstrated 1.5 MW of NB power with 95 keV of beam energy. The 170 GHz ECCD system provided an additional tool for ECH pre-ionization experiment with 0.6 MW/2 s of launched power. Upgrade of the key actuators in 2012 is mainly focused on upgrade of NBI and Lower Hybrid Current Drive (LHCD) system. After upgrade of the NBI system, available total NB power is expected to be more than 3.0 MW in 2012 campaign. LHCD system using 5 GHz is being developed with 8 arrays of 4-way splitter waveguide launcher. After minor upgrade, there will be a major change in heating system and in the diverter concept in 2nd stage of KSTAR operation from 2012 to 2016. In this period, the heating and current drive system will be extended in the deliverable power to 14 MW with 8 MW of NB and 2 MW of LHCD and ECCD.

Advances in Lower Hybrid Current Drive Technology on Alcator C-Mod

G. Wallace¹, S. Shiraiwa¹, W. Beck¹, J. Casey², J. Doody¹, I. Faust¹, H. Julien³, D. Johnson¹, A. Kanojia¹, C. Lau¹, R. Leccacorvi¹, P. MacGibbon¹, O. Meneghini¹, R. Parker¹, M. Preynas³, D. Terry¹, R. Vieira¹, J. R. Wilson⁴, and L. Zhou¹

¹*MIT Plasma Science and Fusion Center, Cambridge, USA*

²*Rockfield Research, Las Vegas, USA*

³*CEA IRFM, Saint Paul lez Durance, France*

⁴*Princeton Plasma Physics Laboratory, Princeton, USA*

Corresponding Author: wallaceg@mit.edu

Lower Hybrid Current Drive is an attractive option for non-inductive tokamak operation due to its high current drive efficiency and ability to drive current off axis. The parameters of the Alcator C-Mod LHCD system ($f = 4.6$ GHz, $B \approx 5.5$ T, $n_e \approx 10^{20} \text{ m}^{-3}$) are similar to the proposed LHCD system on ITER. The 0.5 s pulses achieved in previous operation are sufficiently long as compared to the current relaxation timescale ($\tau_R \sim 0.2$ s) for quasi-steady state non-inductive operation. Longer pulses are necessary for other plasma parameters to reach equilibrium once the current profile has been modified. Modeling of LH wave propagation indicates that the loss of LHCD efficiency at high n_e can be mitigated by enhancing the single pass power absorption. This paper will describe improvements in LHCD technology on C-Mod designed to extend pulse length (to ~ 3 s), increase power delivered to the plasma through reducing reflection coefficients (to $< 10\%$), and increase single-pass absorption at high n_e . Total net LH power with the additional antenna will be ~ 2 MW.

An off mid-plane launcher has been designed combining the 4-way poloidal splitting concept of the current LH launcher on C-Mod with a toroidal bi-junction. The new antenna was optimized to decrease reflected power and increase directivity over a broad range of plasma conditions and launched $n_{||}$ values. The four rows of the launcher are located above the mid-plane in order to exploit the poloidal upshift of $n_{||}$ as rays propagate from the antenna into the plasma. The $n_{||}$ upshift results in better wave penetration to the plasma core at high n_e ($> 10^{20} \text{ m}^{-3}$) and stronger single-pass absorption of the LH waves.

The maximum LHCD pulse length on C-Mod is limited by heating in the collector of the klystrons. Modeling shows that the klystron can operate for 5 seconds without boiling the coolant at full RF power, but the coolant will boil after 1.2 s of beam-on time with no RF power. The maximum pulse length was restricted to 0.5 s to prevent boiling. Increasing the LH pulse length to ~ 3 s will allow the LH system to remain on for $\sim 15 \times \tau_R$ and extend the I_p flattop. The Transmitter Protection System was redesigned to model the coolant temperature in real time. The electron beam is shut off if the TPS determines that the coolant boils. The TPS upgrade has been installed and operated on C-Mod.

FTP-P

Preparation of Steady State Operation of the Wendelstein 7-X Stellarator

R. Wolf¹, C. Beidler¹, H. Braune¹, A. Cardella¹, A. Dinklage¹, M. Endler¹, V. Erckmann¹, G. Gantenbein², J. Geiger¹, D. Hathiramani¹, D. Hartmann¹, B. Heinemann³, M. Hirsch¹, W. Kasperek⁴, R. König¹, P. Konejew¹, H. Lauqa¹, C. Lechte⁴, H. Maassberg¹, G. Michel¹, P. McNeely¹, J. Schacht¹, R. Schroeder¹, T. Sunn Pedersen¹, N. Rust¹, J. Svensson¹, A. Werner¹, M. Thumm², and Wendelstein 7-X Team¹

¹Max Planck Institute für Plasma Physics, EURATOM Association, Greifswald, Germany

²Karlsruhe Institute for Technology, IHM, EURATOM Association, Karlsruhe, Germany

³Max Planck Institute für Plasma Physics, EURATOM Association, Garching, Germany

⁴Institute for Plasma Research, University of Stuttgart, Stuttgart, Germany

Corresponding Author: robert.wolf@ipp.mpg.de

Wendelstein 7-X has been designed to demonstrate the steady state capability of the stellarator concept. At 10 MW of heating power a pulse duration of 30 minutes is envisaged. Short pulses of additional heating power are foreseen to access beta and equilibrium limits and study fast ion confinement and fast ion driven instabilities. The large variety of time scales is strongly affecting the design of plasma diagnostics, heating and fuelling systems, data acquisition and device control.

For steady state heating ten 1 MW continuous wave gyrotrons are foreseen, operating at 140 GHz second harmonic heating at 2.5 T. Using a system of mirrors, relaying the micro waves through air to Wendelstein 7-X, a very high transmission efficiency has been achieved. Front steering mirrors, one for each gyrotron, individually change the poloidal and toroidal launch angles, thus controlling the radial deposition and current drive. Recent modifications to the gyrotron design include an improved power handling in the collector using a rotating transverse magnetic field. The main heating scenarios are 2nd harmonic X-mode (X2) heating below the cut-off density of $1.2 \times 10^{20} \text{ m}^{-3}$ and 2nd harmonic O-mode (O2) heating at higher densities. Owing to non-absorbed power, significant levels of stray radiation are expected for O2-heating, during the transition from X2- to O2-heating, and also during plasma start-up with electron cyclotron resonance waves. Therefore all in-vessel components have to be qualified and if necessary protected to withstand up to 50 kW/m² of continuous micro-wave power flux.

Many diagnostic techniques require a specific adaptation or even new developments to cope with steady state operation. Besides the measurement of fast events, also the long times scales have to be covered. As a consequence not only data rates increase, but the total amount of data. This requires special efforts for real time plasma control, and for continuous data acquisition and data archiving, and makes new, automated concepts for data processing and analysis indispensable.

The paper summarizes the main technologies required for steady state operation of Wendelstein 7-X, including concepts for integrated data analysis and interpretation, and discusses the possible relevance for other experiments aiming at long pulse operation.

3D Particle Simulation of Neutral Beam Injector, from Extraction to Tokamak Injection

T. Minea¹, A. Lifschitz², S. Moschalsky², F. Duré², A. Revel², L. Caillault², and A. Simonin²

¹*LPGP – UMR8578: CNRS-University Paris-Sud, France*

²*CEA/IRFM, 13108 St. Paul les Durance, France*

Corresponding Author: tiberiu.minea@u-psud.fr

The heating and current drive of the future fusion machines (ITER, DEMO) require several tens MW of energetic atoms D^0 (called neutral) to be injected in the plasma core; two beamlines of 17 MW of D^0 at 1 MeV are foreseen for ITER. A Neutral Beam Injector (NBI) system is typically composed of four subsystems:

1. A large multi-ampere hydrogen negative ion (NI) source (~ 50 A of D^- for ITER).
2. A multi-grid multi-aperture (called MAMuG) accelerator generating a 1 MeV powerful NI beams (~ 40 MW of D^- at the accelerator exit).
3. The neutralizer depleting the extra-electron from the D^- beam ($\sim 55\%$ of neutralization rate on ITER).
4. the Electrostatic Residual Ion Dump (E-RID) deflecting and dumping the remaining charged ions out from the neutral beam.

Three codes — ONIX for negative ion extraction, ONAC for negative ions acceleration and OBI for the beam neutralization coupled with E-RID — compose the developed simulation package. They aim to understand the basic physics undergoing in the NBI when such intense negative ion beams are achieved. These 3D Particle-in-Cell self consistent modeling tools are dedicated to support the European experimental developments around the ITER-NBI system.

This package of self-consistent modeling tools is unique to highlight the main processes occurring along the beam line of high power NBI systems and to predict the final neutral beam features, especially in terms of NI beam aberrations (halo), magnetostatic mirror effect, partial screening of the space charge, backstreaming of ions, etc.

This package will be a centerpiece in the simulation and R&D towards a new generation of high efficiency NBI system required for DEMO.

ECH-assisted Startup using ITER Prototype of 170 GHz Gyrotron in KSTAR

J. Jeong¹, M. Joung¹, W. Han¹, S. Park¹, J. Kim¹, H. Kim¹, Y. Bae¹, H. Yang¹,
J. Kwak¹, M. Cho², H. Park², W. Namkung², K. Sakamoto³, K. Kajiwara³, Y. Oda³,
J. Hosea⁴, R. Ellis⁴, J. Doane⁵, and R. Olstad⁵

¹*National Fusion Research Institute, Daejeon, Republic of Korea*

²*Pohang University of Science and Technology, Pohang, Republic of Korea*

³*Japan Atomic Energy Agency, Naka, Japan*

⁴*Princeton Plasma Physics Laboratory, Princeton, USA*

⁵*General Atomics, San Diego, USA*

Corresponding Author: jhjeong@nfri.re.kr

The newly installed electron cyclotron heating and current drive (EC H&CD) system with a frequency of 170 GHz was successfully commissioned and used for the second-harmonic ECH-assisted startup in 2011 operational campaign of the KSTAR. As a RF power source, ITER pre-prototype of 170 GHz, 1 MW continuous-wave gyrotron was loaned from the Japan Atomic Energy Agency (JAEA). The Gaussian beam output from the gyrotron passes through an edge-cooled diamond window and is coupled to an HE11 corrugated waveguide via two phase correcting mirrors in a matching optics unit (MOU). The power coupled to the HE11 corrugated waveguide is delivered to the launcher by the transmission total length of 70 meters. For the first 1 MW EC H&CD system, 1-beam based 1 MW equatorial launcher is installed in the KSTAR Bay E-m. The launcher has been designed and fabricated in collaboration with both Princeton Plasma Physics Laboratory (PPPL) and Pohang University of Science and Technology (POSTECH). During the KSTAR 2011 campaign, 10-s pulse at 0.6 MW EC beam was reliably injected into the plasma. Also, 170 GHz second harmonic ECH-assisted start-up was successful leading to reduce the flux consumption at toroidal magnetic field of 3 T. In this experiment, the flux consumption until the plasma current flat-top was reduced from 4.13 Wb for pure Ohmic to 3.62 Wb (12% reduction) for the perpendicular injection. When the EC beam is launched with toroidal angle of 20 deg with respect to the outward radial direction at the steering mirror, more reduced magnetic flux consumption was obtained with 3.14 Wb (24% reduction) compared with pure OH plasmas. After the 2011 campaign, the gyrotron has been fully commissioned with the output power of 1 MW at the diamond window and the frequency of 170 GHz by precise alignment of the magnet to the gyrotron axis.

The Influence on System Design of the Application of Neutral Beam Injection to a Demonstration Fusion Power Plant

E. Surrey¹, C. Challis¹, I. Jenkins¹, and K. David¹

¹EURATOM/CCFE, Culham Science Centre, Abingdon, UK

Corresponding Author: elizabeth.surrey@ccfe.ac.uk

Steady state fusion power plants require significant non-inductive current drive possibly provided by neutral beam injection (NBI); in addition, NBI can be used for q -profile control for plasma stability. Economic considerations impose limitations on the necessary current drive and electrical efficiencies of the NBI system, with a figure of merit defined by the product of these quantities being greater than $0.25 \text{ Am}^{-2}\text{W}^{-1}$.

The impact of the plasma density profile on non-inductive current drive is assessed using the PENCIL code and the results expressed in terms of a spatial map of current drive efficiency. The effect of beam shinethrough on the far first wall is used to determine limiting tangency radius and elevation for beam injection and thus define an average current drive efficiency. This is used in conjunction with the figure of merit to define the lower limit of electrical efficiency, for a given plasma profile, that will provide an economic power plant.

A NBI system code has been developed to allow the electrical efficiency of a combination of different technologies to be calculated. Gas, plasma and photon neutralizers and energy recovery systems can be considered along with the effect of beam divergence, background gas density and DC electrical efficiency. The code is used to investigate system sensitivities and to identify strategy for reducing technical risk. The primary determinant of electrical efficiency is neutralization efficiency, followed by beam stripping and transmission losses. Despite the gas neutralizer being limited to 58% neutralization efficiency, it is shown that the figure of merit can be achieved by a combination of energy recovery and reduced stripping. For the photoneutralizer system, where the neutralization efficiency can be varied up to 95%, the range of options is greater. Adding energy recovery to the system reduces the sensitivity of electrical efficiency to the neutralization, offering reduced risk and hence improved reliability options. However, the range of options available depends on the current drive obtainable for a particular plasma density profile, thus the plasma itself influences the choice of NBI technology.

This work was funded by the RCUK under the contract of Association between EURATOM and CCFE. This work was carried out within the framework of the European Fusion Development Agreement.

Fusion Material Irradiation Test Facility at SNS

M. Wendel¹, M. Dayton¹, W. Lu¹, T. McManamy¹, P. Rosenblad¹, and R. Stoller¹

¹*Oak Ridge National Laboratory, Oak Ridge, USA*

Corresponding Author: wendelmw@ornl.gov

Computational modeling and experimental studies provide compelling evidence that displacement damage formation induced by fission neutrons and the 14.1 MeV neutrons representative of D-T fusion are quite similar. However, helium and hydrogen production levels with a D-T neutron energy spectrum are much higher. The impact of these gaseous transmutation products is a critical unresolved issue which is being addressed by combining numerical models and specialized ion and neutron irradiation experiments. Because of the uncertainties associated with both modeling and ion irradiation experiments, there is a clear need for an accessible irradiation facility that can provide near prototypic levels of helium and hydrogen. A modest range of He/dpa ratios is desirable to help calibrate and verify the modeling studies. The scientific understanding obtained would also enable more effective use of a future large-volume fusion engineering irradiation facility (such as IFMIF) when it becomes available.

A conceptual level design for a fusion materials irradiation test station (FMITS) for installation at the Spallation Neutron Source (SNS) has been completed. Samples would be located within two horizontal tubes in front of the mercury target. For these specimen locations, the back-scattering neutron flux spectra should be close to the ITER fusion spectrum. The PKA spectra at the FMITS samples were also compared to those for ITER, and the results show good agreement. Material damage rates would be 1.6 – 5.5 dpa/yr for steel, and 1.8 – 3.4 dpa/yr for SiC.

The test station would be water-cooled with a variable inert-gas blanket for temperature control. Thermal analysis shows that the sample temperatures can be maintained as high as 600°C even if average beam power varies by 50%. The FMITS assembly is designed to be installed over a target module and can be reused with multiple targets. The paper describes the design concepts for the FMITS gas system with additional hardware and controls, the mechanical layout of the FMITS assembly including an example experiment, revisions to the existing target shroud, target carriage modifications for FMITS utilities, and remote handling procedures and logistics. Safety and reliability impacts were also evaluated and appear to be acceptable.

Potential for Improvement in High Heat Flux HyperVapotron Element Performance Using Nanofluids

A. Sergis¹, T. Barrett², and Y. Hardalupas¹

¹*The Department of Mechanical Engineering, Imperial College, London, UK*

²*EURATOM/CCFE, Culham Science Centre, Abingdon, UK*

Corresponding Author: a.sergis09@imperial.ac.uk

HyperVapotron (HV) elements have been used extensively in high heat flux neutral beam stopping devices in nuclear fusion research facilities such as JET and MAST. These water-cooled heat exchangers use a cyclic boiling heat transfer mechanism to effectively handle power densities of the order of 10 – 20 MW/m², but are inherently limited by their critical heat flux. The use of a nanofluid as the coolant, instead of water, promises to enhance the heat transfer performance of the HV and increase the critical heat flux by a factor of 2 or 3. Such enhancement would produce a step-change improvement in the power handling capability of future high heat flux devices such as the divertor and heating and current drive systems. This paper describes the potential to improve HV performance using nanofluids.

A molecular dynamics simulation (MDS) code has been used to determine the existence of heat transfer mechanisms that depart from classical thermodynamics and that might explain the augmented heat transfer performance of nanofluids. A basic nanofluid is synthesised and the path of the nanoparticle along a temperature gradient is tracked and compared with a simulation of the base fluid alone. The results indicate a new type of heat transfer mechanism in which the nanoparticle exhibits greater thermal diffusion, with an optimum particle size manifesting in the data.

Experiments have been conducted in which the flow field in a full-scale HV model is visualised and measured using particle image velocimetry (PIV). The experimental rig design is supported by computational fluid dynamics (CFD) analysis. Relevant past studies have yielded qualitative experimental results, but the PIV results reported here provide quantitative data to aid the understanding of the preliminary flow field inside the HV (i.e., before a heat flux is applied) and to assist CFD validation. Further, using both water and Al₂O₃ nanofluid as the flow medium, the PIV observed flow structures are compared to allow an assessment of the effect on heat transfer performance. Thus, these PIV measurements offer the first evidence for enhanced heat transfer in HV devices when nanofluids are used as the coolant. The improved understanding of the cooling advantage of nanofluids and their effect on the HV flow regime facilitates the design of advanced high heat flux systems of future fusion machines.

Work was funded by the RCUK Energy Programme and EURATOM. The views and opinions expressed herein do not necessarily reflect those of the European Commission.

Overview on CEA Contributions to the Broader Approach Projects

P. Bayetti¹, S. Chel², F. Robin³, R. Gondé¹, O. Baulaigue¹, P. Brédy², J. David⁴,
P. Decool¹, L. Genini², R. Gobin², J.-F. Gournay², J. Marroncle², F. Michel⁵,
P. Nghiem², J. Noé³, F. Orsini², and J.-C. Vallet¹

¹CEA, IRFM, St-Paul-Lez-Durance, France

²CEA, IRFU, Gif sur Yvette, France

³CEA, DSM/DIR, Gif sur Yvette, France

⁴CEA, DEN/DPIE, St-Paul-lez-Durance, France

⁵CEA, INAC, Grenoble, France

Corresponding Author: pascal.bayetti@cea.fr

France is participating to the joint Europe-Japan so-called “Broader Approach Activities” in support of ITER and DEMO activities, consisting in 3 projects: The Engineering Design and Validation of a 14 MeV neutrons irradiation facility (IFMIF/EVEDA), the building of an International Fusion Research Center (IFERC) and the ITER Satellite Tokamak Programme (STP – JT-60SA).

For IFMIF/EVEDA activities, CEA is in charge of the high intensity Injector, the first part of the Superconducting RF Linac, the Cryoplant, the Accelerator Control System, the delivery of specific Beam Diagnostics and RF power tubes. This activity covers the fabrication of the systems, test of most critical components, installation and commissioning at the Japanese site.

For IFERC, in 2011, CEA contracted with Bull the procurement of the “Helios” computer which reached a performance of 1.5 Petaflop/s peak, making it, with its 70000 compute cores, the largest supercomputer dedicated to a single scientific community. It is complemented by large high bandwidth storage, pre/post processing, visualization systems and services for 5 years. The work started in Sept. 2007. In Jan. 2012, first users started to work. Helios was inaugurated in March 2012.

For JT-60SA tokamak, CEA is responsible for providing the Cryoplant System (CS), 9 of the 18 Toroidal Field Coils and supporting structures, the TF Coils Test Facility (CTF) and cold tests, and 5 Magnet Power Supplies (MPS). CEA is also participating to the JT-60SA Research Plan update. TF coil activities started in 2007; a manufacturing contract was placed to Alstom in July 2011. The last coil will be delivered to Japan in late 2016. Prior shipment, coils will be tested in the CTF at CEA-Saclay. The CS was optimized to smooth the transient heat loads during plasma operation. For CS and MPS contract are expected to be placed in June and Dec. 2012 respectively.

This paper gives an overview of present status of these projects since 2007.

Fusion Technology Facility — Key Attributes and Interfaces to Technology and Materials

C. P. Wong¹

¹*General Atomics, San Diego, USA*

Corresponding Author: wongc@fusion.gat.com

On the way to a Demonstration Fusion Power Plant (DEMO), a number of fusion technology issues will need to be resolved including the long burn or steady state DT operation, net tritium breeding ratio of > 1 and the application of the Fusion Technology Facility (FTF) as a material and component testing vehicle. This paper focuses on four interface areas between physics and technology that will have significant impacts on the design of FTF. For the interface area of divertor peak heat flux, both water and helium-cooled divertor designs are projected to be able to handle a maximum heat flux of 10 MW/m^2 . When extended to the FTF, both mantle and divertor radiation will be needed including an innovative snowflake or super-X divertor concept. For a robust divertor design, based on results from edge localized mode (ELM) and disruption simulation experiments, both high power ELMs and disruptions will have to be avoided; otherwise the surface material will suffer significant damage. For the interface area of uniform chamber wall surface heat flux, 1-D estimates were performed and, due to the minimum and maximum temperature limits of $> 350^\circ\text{C}$ and $< 550^\circ\text{C}$ for the selected RAFM steel structural material, the maximum heat flux that the design can handle is $< 1 \text{ MW/m}^2$. For the area of robust chamber wall surface material, presently W is the favored surface material for the chamber wall and divertor. Recent vertical displacement event exposures to Si-W samples in DIII-D indicated the formation of the lower melting point eutectic tungsten silicide, which forms when the surface temperature reached 1400°C . The intent was for silicon to protect the tungsten by the vapor shielding effect. For the area of low activation structural material, recent boron-doped RAFM steel results indicate the possible increase of the minimum operating temperature of RAFM steel to higher than 350°C . This could significantly narrow the operating temperature window of the RAFM steel at higher neutron fluence, leading to the need for development of ODS and nano-ferritic-alloys. These areas of plasma edge physics, chamber surface and divertor materials and advanced structural material interactions and the associated necessary research directions for both tokamak and stellerator approaches are discussed in this paper.

FTP-P

This work was supported by the US Department of Energy under DE-FG02-09ER54513.

Plasma Jets for Runaway Electron Beam Suppression

I.-N. Bogatu¹, J. R. Thompson¹, S. A. Galkin¹, J.-S. Kim¹, and
HyperV Technologies Corp. Team²

¹*FAR-TECH, Inc., San Diego, USA*

²*HyperV Technologies Corp., Virginia, USA*

Corresponding Author: nbogatu@far-tech.com

Multi-MA relativistic ($\sim 10\text{--}20$ MeV) runaway electrons (REs), likely to be produced during disruptions in ITER, are a major threat. Dissipation of the REs energy through collisions requires reaching the Rosenbluth critical electron density ($4.2 \times 10^{22} \text{ m}^{-3}$) by impurity injection, which is extremely challenging. Sufficient impurity mass, very short reaction and delivery time, deep penetration to RE beam location, and efficient ablation and assimilation into the post-current quench plasma are key parameters, whose values are very difficult to be achieved simultaneously on the required time scale for ITER safe and fast shutdown (~ 1.2 ms). Complex plasma jets with nanoparticles are an attractive candidate for a REs suppression technique with real-time capability because:

1. They carry a large mass as compared to common gases.
2. Can be accelerated to several km/s as a plasma slug in a plasma gun.
3. The resulting plasma jet has a sufficiently high ram pressure to overcome the magnetic field pressure.
4. Ablation and assimilation are much enhanced due to their very large surface-to-volume ratio.
5. Expanding plasma jet facilitates achieving toroidal uniformity of electron density.

FAR-TECH has been developing a coaxial plasma gun prototype with a solid state $\text{TiH}_2/\text{C}_{60}$ pulsed power injector, capable of producing a hyper-velocity (> 4 km/s), high-density ($> 10^{17} \text{ cm}^{-3}$), C_{60} nanoparticle plasma jet in ~ 0.5 ms, with an overall reaction-to-delivery time of $\sim 1\text{--}2$ ms. We present a comprehensive characterization of the $\text{TiH}_2/\text{C}_{60}$ cartridge, which produced ~ 180 mg of C_{60} molecular gas by explosive sublimation of C_{60} powder, and the first results for a coaxial plasma gun producing a hyper-velocity C_{60} plasma jet. In the next step, the prototype system is proposed for a small scale proof-of-principle REs suppression experiment on DIII-D, which has carbon tiles, can produce and control RE beams, and has a broad range of diagnostics. As injection time is ~ 1 ms, the nanoparticle plasma jet can be used during the thermal quench to remove RE “seeds”, the current quench to stop the REs “avalanche”, or the RE current plateau, to dissipate the REs energy.

This work was supported by the US Department of Energy under DE-FG02-08ER85196 SBIR grant.

Advances in the Electrical , Control Systems, General Analysis of the Coils Design in the Mexican Tokamak Experimental Facility

M. Salvador¹, A. E. Tapia¹, J. Martínez², J. González¹, J. R. Morones¹, S. Martínez¹,
S. Sanna³, F. J. Almaguer¹, M. A. Alcorta¹, J. A. González¹, O. A. Muñoz¹,
V. M. Arredondo¹, R. M. Chávez¹, A. Nieto¹, C. U. Acosta¹, E. J. Jasso¹, and
I. U. Liñan¹

¹*Facultad de Ingeniería Mecánica y Eléctrica – Universidad Autónoma de Nuevo León, Nuevo León, México*

²*Comisión Federal de Electricidad, Nuevo León, México*

³*Dipartimento di Fisica “A. Volta”, Università degli Studi di Pavia, Pavia, Italy*

Corresponding Author: max.salvadorhr@uanl.edu.mx

The Fusion Research Group of the Autonomous University of Nuevo Leon (UANL, Spanish acronyms) presents its advances into the electrical, control systems and its coils design developed toward the Tokamak Experimental Facility [1]. This Research and Development Project (R+D) was approved from the Mexican Education Ministry (UANL-EXB-156). The present electrical and control systems studies are mainly oriented to establish our Magnetic Confinement Facility into our University Campus, with a D-shaped tokamak design with the next main characteristics: major radius $R = 41$ cm, minor radius $a = 18.5$ cm, aspect ratio $A = 2.2162$, safety factor $q = 1.9552$, plasma current $I_p = 277$ kA , toroidal field $B_t = 1.3$ T, electronic plasma density $n_e = 2 - 3 \times 10^{13} \text{ cm}^{-3}$.

The present study at this time is an effective electrical engineering proposal to our University involving studies over the electrical power quality provided by Federal Electricity Commission. We define our parameters in voltage, current, frequency, to implement the correct strategies of electrical supplies in order to protect our facility. The analysis was performed measuring in the five domestic circuits of the University Campus: phase imbalances (current and voltage), harmonic distortion total and individual (voltages and currents of 1 – 50), transient capture, presentation of the power factor, registration of electrical interruptions and reclosing, measuring and recording quality power systems, crest factors (voltage and current), accurate RMS measurements of voltage and current, presentation of phasor diagrams.

Our tokamak design contains a proposal coils arrangement capable for generate 1.6 T, with a coil current range (10,000 – 30,000 A), short circuit times from 0.3 s to 1 s. The entirely systems uses Cu like first analysis material. The coils are designed with 3D CAD modeling and after, we apply finite element analysis through the software COMSOL Multiphysics. Our numerical calculus programs run under our SGI Altix XE250 GNU/Linux Platform.

Our computational resources can give us an absolute develop systems involved in our magnetic confinement fusion research line, focused in the stronger application of engineering, technology and science concepts, developing systems and devices into this new form of energy generation.

References

[1] Mexican Design of a Tokamak Experimental Facility, FTP/P6-36, IAEA FEC 2010.

An Advanced Plasma-material Test Station for R&D on Materials in a Fusion Environment

J. Rapp¹, T. Biewer¹, J. Canik¹, J. Caughman¹, G. Chen¹, S. Diem¹, R. Goulding¹,
D. Hillis¹, A. Lumsdaine¹, W. McGinnis¹, S. Meitner¹, L. Owen¹, M. Peng¹, and
S. Milora¹

¹*Oak Ridge National Laboratory, Oak Ridge, USA*

Corresponding Author: rappj@ornl.gov

A new era of fusion research has started with ITER under construction and DEMO for power demonstration on the horizon. However, the related fusion reactor material science requires further development before DEMO can be designed. One of the most crucial and most complex outstanding science issues to be solved is the plasma surface interaction (PSI) in the hostile environment of a nuclear reactor. Not only are materials exposed to unprecedented steady-state and transient power fluxes, but they are also exposed to unprecedented neutron fluxes. Both the ion fluxes and the neutron fluxes will change the properties and the micro-structure of the plasma-facing materials (PFM) significantly, even to the extent that their structural integrity is compromised.

A new PMTS (Plasma Material Test Station) is proposed to address these challenges, utilizing a new high-intensity plasma source concept. This device will be well suited to test toxic, as well as irradiated material samples. The advanced plasma source is based on an RF based plasma production and heating system. The source is electrode-less, so that impurity generation in the source region that could invalidate the interpretation of PSI processes will be minimized. This is especially important for high fluence experiments, accelerated lifetime studies and reduced maintenance in a radiological managed environment. B2-Eirene simulations demonstrate that ion fluxes in excess of $10^{24} \text{ m}^{-2}\text{s}^{-1}$ should be achievable at the target delivering power fluxes of $> 30 \text{ MW/m}^2$. Upstream temperatures at the exit of the source system should be high enough ($T_e > 30 \text{ eV}$) to study also radiative dissipation of heat fluxes in this device. The RF source system consists of a helicon antenna for plasma production and additional electron as well as ion heating to increase electron and ion temperature separately. A pre-prototype helicon antenna has been tested at moderate magnetic fields. A maximum electron density of $n_e = 4.0 \times 10^{19} \text{ m}^{-3}$ has been achieved in deuterium discharges. Electron heating has been investigated in a separate experiment. Electron temperatures in excess of 10 eV have been measured in the device.

The roadmap for the source development to provide the prototype plasma source for PMTS will be presented.

Overview and Status of the Linear IFMIF Prototype Accelerator

P. Cara¹, P.-Y. Beauvais², B. Branas³, P. Brédy², J.-M. Carmona³, S. Chel²,
M. Comunian⁴, M. Desmons², A. Facco⁴, P. Gastinel², D. Gex¹, R. Gobin²,
J.-F. Gournay², R. Heidinger¹, J. Knaster⁷, S. Maebara⁵, J. Marroncle², V. Massaut⁶,
H. Matsumoto⁷, P. Mendez³, P.-A.-P. Nghiem², C. Oliver³, J. Molla³, F. Orsini²,
A. Pisent⁴, I. Podadera³, G. Pruneri⁷, H. Shidara⁷, K. Shinto⁵, M. Sugimoto⁵,
H. Suzuki⁵, H. Takahashi⁵, D. Vandeplasse⁶, and C. Vermare⁷

¹*Fusion for Energy, Garching, Germany*

²*CEA, Saclay, France*

³*CIEMAT, Madrid, Spain*

⁴*INFN, Legnaro, Italy*

⁵*JAEA, Rokkasho, Japan*

⁶*SCK-CEN, Mol, Belgium*

⁷*IFMIF/EVEDA Project Team, Rokkasho, Japan*

Corresponding Author: philippe.cara@f4e.europa.eu

Under the framework of the Broader Approach (BA) Agreement, the Linear IFMIF Prototype Accelerator (LIPAc) has been launched with the objective to validate the low energy part (\sim MeV) of the two IFMIF linacs (40 MeV, 125 mA of D⁺ beam in continuous wave). Starting in mid-2007, the project is managed by two Home Teams (JA-HT and EU-HT) and coordinated by the Project Team at the BA site in Rokkasho with the aim to complete the validation activity with the commissioning and operating the whole LIPAc by June 2017.

This paper describes the activities underway with a view to the arrival of the first components in Rokkasho at the beginning of 2013, following prior testing in Europe.

IFMIF: Overview of the Validation Activities

R. Heidinger¹, H. Matsumoto², M. Sugimoto³, A. Ibarra⁴, A. Mosnier¹, F. Arbeiter⁵, G. Micciche⁶, V. Heinzel⁵, P. Cara¹, S. Chel⁷, A. Facco⁸, V. Massaut⁹, and J. Theile¹⁰

¹*Fusion for Energy, Garching, Germany*

²*IFMIF/EVEDA Project Team, Rokkasho, Japan*

³*Japan Atomic Energy Agency, Rokkasho, Japan*

⁴*CIEMAT, Madrid, Spain*

⁵*KIT, Karlsruhe, Germany*

⁶*ENEA, Brasimone, Italy*

⁷*CEA, Saclay, France*

⁸*INFN, Legnaro, Italy*

⁹*SCK-CEN, Mol, Belgium*

¹⁰*CRPP, Lausanne, Switzerland*

Corresponding Author: roland.heidinger@f4e.europa.eu

The International Fusion Materials Irradiation Facility (IFMIF) Engineering Design and Engineering Validation Activities (EVEDA), which started in 2007 under the framework of the Broader Approach (BA) Agreement between EU and Japan, are coming to the final stage with the exception of the Accelerator Prototype Validation subproject (running till 2017). By June 2013, the engineering design of IFMIF will be completed by delivering an Interim IFMIF Engineering Design Report (IIEDR) together with the final reporting for the majority of the validation activities.

IFMIF/EVEDA consists of the following sub projects:

- The engineering design of IFMIF providing all the necessary information to take decisions for its construction, operation and decommissioning.
- The validation of the main challenging technologies of IFMIF through the design, construction and tests of:
 - An Accelerator Prototype, fully representative of the IFMIF low energy (9 MeV) accelerator (125 mA of D⁺ beam in continuous wave) to be completed in June 2017.
 - A Lithium Test Loop, integrating all elements of the IFMIF lithium target facility, already commissioned in February 2011.
 - The High Flux Test Module (different designs) and its internals to be irradiated in a fission reactor and tested in the helium loop HELOKA-LP.

An overview of the engineering design will be reported together with the outcome of the validation activities already achieved and still expected. In particular, the present status of the Accelerator Prototype (LIPAc) Validation activities ahead of the start of the installation of sub-subsystems in Rokkasho BA Site in early 2013 will be a highlight of these validation activities.

Feasibility of a Fusion Hybrid Reactor Based on the Gasdynamic Mirror

T. Kammash¹

¹*University of Michigan, Ann Arbor, USA*

Corresponding Author: tkammash@umich.edu

A Comprehensive analysis of the feasibility of a fusion hybrid reactor whose fusion component is the gasdynamic mirror (GDM) is presented. Since the primary role of the fusion component is to supply neutrons to a blanket laden with fertile material, it can operate at or near “breakeven” condition which is a much less stringent condition than that required for a pure fusion reactor. As a high beta device, with demonstrated MHD and kinetic stability, the GDM is chosen for utilization in such a reactor because it can also operate in steady state. Using extensive multigroup neutronic analysis, we show that such a reactor is capable of breeding fissile material and burning it to produce tens to hundreds of megawatts of thermal power per centimeter of length “safely” since it will be “subcritical”, and “securely” because of the use of a thorium fuel cycle which is known to be resistant to “proliferation” and clandestine operations. Moreover, we demonstrate that D-D fusion reactions are more suitable for use in a hybrid reactor since the energy of the neutrons produced by these reactions is closer to “thermalization” than those produced by D-T leading to a much more manageable waste disposal problem. Finally, since the reactor in question is “self-fueling” it can be designed to operate for an extensive period of time without refueling.

A 14 MeV Fusion Neutron Source for Material and Blanket Development and Fission Fuel Production

T. Simonen¹, R. Moir², A. Molvik³, and D. Ryutov³

¹*University of California, Berkeley, USA*

²*Vallecitos Molten Salt Research, Livermore, USA*

³*Lawrence Livermore National Laboratory, Livermore, USA*

Corresponding Author: simonen42@yahoo.com

Fusion Development will require materials capable of withstanding extensive harsh bombardment by energetic neutrons and plasma. The plasma based Gas Dynamic Trap neutron source concept is capable of testing and qualifying materials and fusion blanket sub modules for eventual deployment in fusion energy systems. In this paper we describe new results on the suitability of this source to assess thermal fatigue in fusion blanket components caused by the small normal variability of neutron flux inherent in fusion energy concepts. A second part of the paper considers the requirements for a hybrid fusion-fission hybrid suitable for producing fissile fuel. Both solid and molten salt fuel form blanket designs are described that emphasize non-proliferation and passive safety.

Work at LLNL performed under DoE Contract DE-AC52-07NA27344.



Radiation Damage Studies on a Laser Fusion Reactor

S. Sahin¹, H. M. Sahin², and A. Acir²

¹*ATILIM University, Faculty of Engineering, Ankara, Turkey*

²*Faculty of Technology, Gazi University, Ankara, Turkey*

Corresponding Author: ssahin@atilim.edu.tr

A laser fusion-fission (hybrid) has been investigated with a multi-layered spherical blanket, composed of a first wall made of oxide dispersed steel (ODS, 2 cm); neutron multiplier and coolant zone made of LiPb; ODS-separator (2 cm); a molten salt Flibe coolant and fission zone; ODS-separator (2 cm); graphite reflector. In the second phase, LiPb coolant zone behind the first wall has been removed. But instead, a flowing liquid protective first wall is included of in front of the solid first wall in order to reduce material damage and residual radioactivity after final disposal of the latter.

Tritium breeding ratio (TBR) has been calculated as $TBR > 1.05$ over 8 to 9 years of continuous plant operation period, which would supply fusion fuel for self-sustaining fusion reactor operation. Blanket energy multiplication factor (M) remains nearly stable between 2.4 to 6.8 over 10 years for TRISO fractions 2 to 8 vol-% in the coolant.

Without an internal liquid wall protection, major damage mechanisms have been calculated as $DPA = 50$ and $He = 170$ appm/year at the ODS first wall. It faces directly to the fusion chamber, and will be the primary component subject to material damage. This will oblige to change the ODS first wall every ~ 3 years. Hydrogen production is calculated as 650 appm/year. Hydrogen will not reside permanently in the metallic lattice as helium atoms, but diffuse out of the structure by high operation temperatures. The alternative version to include a Flibe zone of ~ 50 cm thickness as flowing wall liquid protection in front of the solid ODS first wall reduces material damage below permissible limits. It allows shallow burial of structure after final reactor decommissioning.

Calculations have yielded very high burn up grades ($> 400\,000$ MW.D/MT) for the fissionable RG-PuC/ThC fuel without fuel change, making the LIFE engine a sustainable power source. Peach Bottom experiments have shown that TRISO fuel particles can withstand burn ups of 740 000 and 650 000 MW.D/MT). Such high burn ups would reduce final disposed nuclear waste mass per unit energy production drastically.

A Feasibility Study on a Clean Power Fusion Fission Hybrid Reactor

T. Siddique¹, M. H. Kim¹

¹*Department of Nuclear Engineering, Kyung Hee University, Republic of Korea*

Corresponding Author: mtariq@khu.ac.kr

In this paper, a design concept of fusion-fission hybrid reactor for the purpose of high level radioactive waste transmutation was investigated. A concept of fusion based trans-uranium isotope (TRU) burner reactor (FTBR) was based on a low power tokamak (150 MW max) and annular ring shaped TRU core with metallic fuel (TRU 60 w/o, Zr 40 w/o) and adjacent fission product (FP) zone. Composition data for TRU and FP are assumed to be the same with those in spent fuel from 1,000 MWe PWR with 10 years decay cooling. Calculation for blanket part were performed using MCNP-X 2.6. Irradiation (burn) cycle was chosen to be 1,100 days (3 years). The power level of TRU core was set to be 2,000 MW and k_{eff} at BOC was calculated as 0.97979 and at EOC 0.85049. Calculated TBR value was 1.49 representing a self-sufficiency of fusion fuel.

TRU burning was analyzed by calculating TRU mass burned per full power year ($M_{\text{TRU}}/\text{fpy}$), support ratio (SR) and percentage of TRU mass burned per year (%TRU/fpy). Same parameters were also used to analyze the FP transmutation. To account for the FP produced in TRU core the net M_{FP}/fpy and net %FP/fpy was also calculated. For toxicity analysis of long lived TRU and FP the percentage reduction of long lived inhalation toxicity (LLIhT) and long lived ingestion toxicity (LLIgT) were also calculated.

$M_{\text{TRU}}/\text{fpy}$ was 747.11 kg with 14.25 MT of initial TRU mass loading, %TRU/fpy was 5.24% and SR was 2.24. FP mass produced in TRU core per fpy was 162.25 kg. LLIhT and LLIgT of TRU's were reduced by 9% and 6% respectively over the burn cycle. FP depletion calculations were performed for two different thicknesses of FP zone 30 cm and 50 cm to evaluate the FP loading effect on FP transmutation performance.

TRU transmutation performance of FTBR was also compared with Subcritical Advance Burner Reactor (SABR) design. The comparison showed good TRU transmutation performance of FTBR with a small scaled fusion facility but it still can be improved by utilizing two or three batch fuel cycle configurations and modeling the TRU core in detailed geometry. This preliminary study shows that a clean plant concept has a good potential for waste transmutation.

Neutronic Calculation of Radiation Damage in First Wall of a Fusion-Fission Reactor

H. Şahin¹

¹Gazi University, Faculty of Technology, Ankara, Turkey

Corresponding Author: mesahin@gazi.edu.tr

A fusion-fission (hybrid) is a combination of the fusion and fission processes. The fusion plasma is surrounded with a multi-layered cylindrical blanket made of the fertile materials (^{238}U or ^{232}Th) to convert them into fissile materials (^{239}Pu or ^{233}U) by transmutation through the capture of the high-yield fusion neutrons and neutron multiplier and coolant zone made of LiPb. A hybrid reactor is based on either magnetic fusion energy (MFE) or inertial fusion energy (IFE). The neutron source is volumetric in MFE systems, whereas the target represents a point neutron source in IFE plants.

In this study, the (D, T) fusion neutron driver of MFE for the hybrid reactor has been carried out. The temporal neutronic performance of the hybrid blanket have been evaluated for the NWL of 2.25 MW/m^2 by full reactor power (plant factor $\text{PF} = 100\%$). Hence, this corresponds to the fusion neutron flux of 10^{14} (14.1 MeV) $\text{n/cm}^2\text{s}$ at FW for conventional (D,T) driven hybrid reactor. Neutronic calculations were performed by Monte Carlo Neutron-Particle Transport code MCNP5 version 1.40 in three-dimensions using three different data libraries; ENDF/B-V, ENDF/B-VI and CLAW-IV for comparing neutronic parameters. The nuclear heat deposition in the first wall (FW), tritium breeding ratio (TBR) in the blanket and radiation damage such as displacement per atom (DPA), He-production (n, α), H-production (n, p); (n, d); (n, t) for composed of FW made of different materials, namely, ferritic/martensitic steels, vanadium alloy, silicon carbide, copper alloy, and stainless steel as a lifetime of one full power year (FPY) have been calculated based on different data libraries.

In this concept, a line neutron source in a cylindrical cavity simulates the fusion plasma chamber. The latter is surrounded by a FW which various materials will be used for investigation. In this study, some different materials were considered as FW and fuel clad material. The fissile zone is composed of typical LWRs spend fuel which contain natural uranium dioxide (UO_2) in hexagonal geometry as 10 rows having pitch length = 1.25 cm in the radial direction.

Neutronic Analysis of a Thorium-uranium Fueled Fusion-fission Hybrid Energy System

S. Xiao¹, Z. Zhou¹, and Y. Yang¹

¹*Institute of Nuclear and New Energy Technology, Tsinghua University, Beijing, China*

Corresponding Author: endeavorone@163.com

In this paper, a thorium-uranium based fusion-fission hybrid reactor (FFHR) aiming at efficiently utilizing natural uranium and thorium resources is presented. The major objective is to study the feasibility of this new concept with multi-purposes, including energy gain, tritium breeding ratio (TBR) and ^{233}U breeding rate. The basic logic of this concept is to use the excess neutrons generated in the natural uranium fuel region to breed fissile fuel ^{233}U in the thorium fuel region, while maintaining high energy amplifying factor (M) and tritium self-sufficiency. The guiding principle for the blanket design is to obtain a good neutron economy. The main method is to maximize the available neutrons and optimally distribute them in the blanket via competing processes of fission, tritium breeding and fissile fuel breeding by adjusting the neutron spectrum and system's geometry. The COUPLE code developed by INET of Tsinghua University is used to simulate the neutronic behavior in the blanket. The simulation results show that a combined soft and hard neutron spectrum could yield $M > 15$ while maintaining $\text{TBR} > 1.10$ and conversion ratio of fissile materials (including ^{239}Pu and ^{233}U) $\text{CR} > 1.0$ in a reasonably long refueling cycle (about 5 years). The results also demonstrates that due to the poor neutron economy with thorium, better utilization of thorium, which means high ^{233}U fuel breeding capability, can only be achievable with the costs of system's M and/or TBR performances. And the compromised solution between fission suppressed (fissile fuel breeding) and energy production oriented choices should be found under the hybrid system operating goals and the FFHR's long-term nuclear development strategy.

Conceptual Design Requirements and Solutions for MW-Range Fusion Neutron Source FNS-ST

B. Kuteev¹, P. Alexeev¹, V. Chernov¹, B. Chukbar¹, A. Bykov¹, A. Frolov¹, A. Golikov¹, P. Goncharov¹, M. Gryaznevich¹, M. Gurevich¹, A. Dnestrovskij¹, A. Dudnikov¹, R. Khayrutdinov¹, V. Khripunov¹, A. Klischenko¹, B. Kolbasov¹, V. Lukash¹, S. Medvedev¹, V. Petrov¹, A. Sedov¹, A. Spitsyn¹, S. Subbotin¹, A. Shimkevich¹, Y. Shpansky¹, and A. Zhirkin¹

¹National Research Centre "Kurchatov Institute", Moscow, Russian Federation

Corresponding Author: kuteev@nfi.kiae.ru

Development of the demonstration fusion neutron source FNS-ST for the nuclear fuel production and the nuclear waste transmutation on the basis of a spherical tokamak with the MW power of deuterium and tritium fusion has reached the stage of technical requirements for conceptual design.

The concept of a FNS-ST has been proposed and developed in details (plasma current 1.5 MA, magnetic field 1.5 T, major radius 0.5 m, aspect ratio 1.67 and auxiliary heating power up to 15 MW). A comparison of physical plasma parameters and the economics for an FNS-ST and a conventional tokamak will be presented. It suggests the feasibility to reach 1 – 10 MW of the Fusion power for a conventional or low aspect ratio. It will be shown that the ST economics is better. Zero and one-dimensional plasma models have been developed and used in this analysis. The necessary operation characteristics of the plasma confinement, stability and current drive have been determined. Scenarios to reach and maintain the steady state operation are considered and optimized.

Perspective technical solutions for technology systems have been validated, and choices of enabling technologies and materials of the basic FNS have been made. The best characteristics both for the neutronics and the power consumption for the toroidal magnet system suggest Be-made toroidal coils, cooled to the liquid nitrogen temperature. A conceptual design of a thin-wall water cooled vacuum chamber for the heat load up to 6 MW/m² will be presented. The chamber consists of 2 mm Be tiles, pre-shaped CuCrZr 1 mm shell and a 1 mm stainless steel shell as a structural material. A concept of the double-null divertor for the FNS-ST will be suggested that is capable to withstand heat fluxes up to 6 MW/m². Lithium dust injection technology is proposed to use for control of the border plasma radiation and plasma-surface interaction in the scrape-off layer.

Concepts of the FNS-ST blankets for the pure thermal neutron production and for the development of a thorium fuel cycle for fission reactors will be considered. It is shown that thermal neutron fluxes as large as 10¹⁵ n/cm²s are feasible in the FNS with Be coils. The radial structure, neutronics and thermal hydraulic characteristics as well as the U233-production rate and opportunities to self-breed tritium will be discussed.

Deterministically Safe Highly Sub-Critical Fission-Fusion Hybrid Reactors

M. Kotschenreuther¹, P. Valanju¹, S. Mahajan¹, B. Covele¹, and D. Raj²

¹ *University of Texas at Austin, Austin, USA*

² *Bhabha Atomic Design Division, Mumbai, India*

Corresponding Author: mtk@mail.utexas.edu

Fusion Fission Hybrids present a much less technically demanding, nearer term, application of fusion research. Pre-conceptual designs of Fission-Fusion Hybrids are based on conventional tokamaks and spherical tokamaks are presented and compared. The designs have multiple unique features, relative to other hybrid approaches. The worst of nuclear accidents — the criticality accidents — are deterministically excluded, even for a worst case core rearrangement in an extreme accident. This feature is unique to a Hybrid driven by a relatively strong neutron source, with a judiciously chosen fission blanket and fuel cycle. Nuclear fuel reprocessing is minimized or avoided entirely if possible. For waste incineration or fuel production, high support ration fuel cycles are examined where a single hybrid can support many more fission reactors of the same power. Incremental waste incineration rates are several times faster than for fission-only or accelerator approaches. The fission and fusion blankets are physically separate to insure safety, and to allow a maximum utilization of existing technology. The fusion driver is a replaceable module that allows the use of two fusion modules to achieve high system availability, when a single module has availability of only $\sim 40\%$. Detailed neutronic calculations demonstrate the waste incineration, fuel production and direct energy production capabilities of these hybrids. Fuel breeding for Light Water Reactors (LWRs) is possible with no fuel reprocessing, in which, a single hybrid can support about 4 LWRs of comparable power.

Behaviors of Hydrogen Isotopes in Silicon Carbide for Evaluation of Hydrogen Permeability and Retention in Nuclear Fusion Systems

S. Nagata¹, T. Shikama¹, H. Katsui¹, Y. Hatano², M. Matsuyama², Y. Oya³,
K. Okuno³, Y. Katoh⁴, M. Shimada⁵, Y. Nakashima⁶, and T. Imai⁶

¹*Institute for Materials Research, Tohoku University, Sendai, Japan*

²*Hydrogen Isotope Research center, Toyama University, Toyama, Japan*

³*Radiation Research Laboratory, Shizuoka University, Shizuoka, Japan*

⁴*Oak Ridge National Laboratory, Oak Ridge, USA*

⁵*Idaho National Laboratory, Idaho Falls, USA*

⁶*Plasma Research Center, University of Tsukuba, Tsukuba, Japan*

Corresponding Author: nagata@imr.tohoku.ac.jp

Silicon Carbide (SiC) has some attractive material properties such as a low-Z, low induced radioactivity, high strength, good radiation resistance, and refractoriness, and is a strong candidate for nuclear fusion materials in several applications such as thermal and tritium barriers, and as a plasma facing material. There, the mobility and the retention behavior of the hydrogen isotopes injected into SiC are very important engineering factors. The SiC would not work as a tritium barrier if the mobility is high, and the tritium inventory will be seriously high if the retention is high.

Behaviors of hydrogen isotopes in the silicon carbide are studied after hydrogen isotopes are injected into the SiC, by exposing SiC to the hydrogen plasma of the fusion plasma machine of the GAMMA-10, irradiating SiC in the high flux fission reactor of HFIR with lithium containing oxides (tritium injection through (n, α) nuclear reaction of lithium), and ion accelerator irradiation with hydrogen and deuterium. The GAMMA-10 exposure showed high retention of tritium in the SiC of about 5×10^{20} H/m² even after a short period exposure of about 30 seconds. The HFIR irradiation revealed that the retention of tritium in the SiC is substantial and the mobility of the tritium is limited even at 800°C, while the accelerator irradiation with 10 keV deuterium showed that the deuterium will have a good mobility at about 800°C. The comparison among data obtained is showing the importance of trapping of hydrogen isotopes by the radiation induced defects.

FTP-P

Performances of Helium, Neon and Argon Glow Discharges for Reduction of Fuel Hydrogen Retention in Tungsten, Stainless Steel and Graphite

T. Hino¹, Y. Yamauchi¹, Y. Kimura¹, A. Matasumoto¹, K. Nishimura², and Y. Ueda³

¹*Laboratory of Plasma Physics, Hokkaido University, Sapporo, Japan*

²*National Institute for Fusion Science, Toki, Japan*

³*Osaka University, Osaka, Japan*

Corresponding Author: tomhino@qe.eng.hokudai.ac.jp

It is quite important to investigate the performance of glow discharge conditionings for controls of in-vessel tritium inventory and hydrogen recycling. For this purpose, first, the deuterium retentions in tungsten (W), graphite (C) and stainless steel (SS) were measured. The retention in W was not small as expected, several times larger than that of SS, although the retention in SS was one order smaller than that of C. Such the large retention in W is owing to the growth of rough surface structure produced by the plasma irradiation. For reduction of deuterium retention in W, SS and C, second, inert gas (He, Ne, Ar) glow discharges were conducted and these performances were compared. The removal ratio was highest in He discharge, and lowest in Ar discharge. These values are well explained by the numerical analyses using SRIM code. The removal ratios for SS and C were significantly large, but the ratio for W was quite small. This reason is owing to the rough surface structure in W. For W, thirdly, the hydrogen isotope exchange and the wall baking experiments were conducted. It is found that the wall baking with a temperature higher than 700K can well reduce the retention, and the hydrogen isotope exchange using glow discharge is also useful to replace the fuel hydrogen retention in the wall. The present results significantly contribute to evaluate the fuel hydrogen retention and to reduce the in-vessel tritium inventory in fusion reactors.

Development of W Based Materials for Fusion Power Reactors

M. Battabyal¹, M. Q. Tran¹, P. Spaetig¹, N. Baluc¹, and L. Veleva¹

¹*Centre de Recherches en Physique des Plasmas, Ecole Polytechnique Fédérale de Lausanne, Villigen-PSI, Switzerland*

Corresponding Author: manjusha.battabyal@psi.ch

Due to the superior thermophysical properties, tungsten (W) materials are candidates for plasma facing applications for ITER and DEMO. W-base materials are being developed on the basic idea that alloys and nano-grained materials should be more ductile than pure W and standard grain-sized materials, and that oxide or carbide dispersion strengthened materials should be more radiation resistant than pure W and standard grain-sized materials. A variety of materials are being produced using standard powder metallurgy (PM) methods including mechanical alloying (MA), hot isostatic pressing (HIPping) and thermo-mechanical treatment.

The goal of this work is to develop W-base materials by standard PM, which include mostly pure W and W-Y, W-Y₂O₃, W-TiC, W-Ta and W-Re-TiC alloys. For instance, W-(0.3-1.0-2.0)Y, W-(0.3-1.0-2.0)Y₂O₃, and W-(0.3-0.9-1.1-1.5-1.7)TiC (in wt.%) were produced by MA followed by HIPping. From X-ray diffraction and scanning electron microscopy studies on one powder with different milling time, it was shown that the particles are uniformly distributed in the W matrix and crystallite size decreases with time. All the materials are made of small grains, 20 and 500 nm, and contain a high density of nano-sized Y₂O₃ or TiC particles. For W-Y materials, Y transformed into Y₂O₃ during MA, due to the high amount of O present in the milled powders. All the materials contain a residual porosity of a few percents (1 – 3%). They exhibit high strength but they show no ductility. In collaboration with the Plansee Company, a more promising W-2Y₂O₃ material was produced by sintering and hot forging. The density of the ingot was 99.3%. The material appears to be composed of grains with a mean size around 1 μ m and also contains nano-sized Y₂O₃ particles. Three-point bending (3PB) tests showed that the material is brittle at 25°C and ductile above 400°C. The bending stress shows that the mechanical property is improved in W-2Y₂O₃ material with respect to pure W and W-1Y₂O₃. 3PB tests also show that the increase in the grain size improves the ductility of the material. This improvement outbalances the degradation of the fracture properties due to the increase of the particle size. Correlation between the mechanical properties and their respective microstructures resulting from various production routes will be discussed.

FTP-P

Self-healing of Radiation Damage by Coupled Motion of Grain Boundaries in Tungsten Divertor Plates under Reactor Conditions

V. Borovikov¹, X.-Z. Tang¹, D. Perez¹, X.-M. Bai¹, B. Uberuaga¹, and A. Voter¹

¹*Los Alamos National Laboratory, Los Alamos, USA*

Corresponding Author: valery@lanl.gov

Radiation damage by fusion neutrons can significantly degrade material properties. In a fusion reactor, long-lasting radiation-induced defects such as vacancies, vacancy clusters, and voids introduce additional nuclear safety complication in terms of tritium retention. This is especially true in the divertor/first wall of a tokamak like ITER, where extreme thermal stress is also present. Here we use molecular dynamics simulations to elucidate a self-mitigating mechanism in which the large thermal stress can facilitate the recombination of the neutron-collision-cascade-induced vacancies and interstitials through coupled grain boundary (GB) motion in a bcc tungsten under fusion reactor conditions. Specifically, our simulations reveal that for a number of tungsten GBs, absorbing the fast-moving interstitials can help activate coupled GB motion at reduced mechanical stress; the migrating GB then sweeps up the less-mobile vacancies, facilitating vacancy-interstitial recombination inside the GB. We examine the stress-induced mobility characteristics of a number of GBs in W to investigate the likelihood of this scenario.



Research on Tritium/Heat Transfer and Irradiation Synergism for First Wall and Blanket in the TITAN Project

T. Muroga¹, D.-K. Sze², K. Okuno³, T. Terai⁴, A. Kimura⁵, R. Kurtz⁶, A. Sagara¹,
R. Nygren⁷, Y. Ueda⁸, R. Doerner², B. Merrill⁹, T. Kunugi⁵, S. Smolentsev¹⁰,
Y. Hatano¹¹, M. Sokolov¹², T. Yamamoto¹³, A. Hasegawa¹⁴, and Y. Katoh¹³

¹*National Institute for Fusion Science, Toki, Japan*

²*UCSD, San Diego, USA*

³*Shizuoka University, Shizuoka, Japan*

⁴*University of Tokyo, Tokyo, Japan*

⁵*Kyoto University, Uji, Japan*

⁶*Pacific Northwest National Laboratory, Richland, USA*

⁷*SNL, Albuquerque, USA*

⁸*Osaka University, Suita, Japan*

⁹*Idaho National Laboratory, Idaho Falls, USA*

¹⁰*UCLA, Los Angeles, USA*

¹¹*Toyama University, Toyama, Japan*

¹²*Oak Ridge National Laboratory, Oak Ridge, USA*

¹³*UCSB, Santa-Barbara, USA*

¹⁴*Tohoku University, Sendai, Japan*

Corresponding Author: muroga@nifs.ac.jp

The research in Japan-USA fusion cooperation program TITAN (Tritium, Irradiation, and Thermofluid for America and Nippon, from April 2007 to March 2013) is highlighted by tritium transfer in PFM exposed to tritium-plasma, effects of neutron irradiation on deuterium retention in PFM, MHD flow of Li-Pb in magnetic fields, synergistic neutron irradiation and helium injection effects for structural materials, and irradiation effects on advanced materials including joints and coatings. These unique results were obtained through unprecedented experiments using a nuclear reactor (HFIR), a tritium-plasma test facility (TPE), a thermofluid test facility with a magnet (MTOR) and so forth, including their combined use.

Tritium concentration was measured by Tritium Imaging Plates for W and RAFM Steel (F82H) after exposure to D +0.2%T plasma at 200°C. The cross sectional detection clearly showed higher tritium diffusion into bulk (~ 3 mm) in F82H.

Deuterium depth profiles in W were obtained by NRA after deuterium plasma exposure at 100, 200 and 500°C with and without prior neutron irradiation to 0.025 dpa at 50°C. A high deuterium concentration was detected only in neutron-irradiated specimens in the case of deuterium plasma exposure at 500°C, showing that the defects formed by neutron irradiation captured deuterium in the specimen and significantly increased the deuterium retention at 500°C.

Joint samples of F82H with NiAl alloy (He implanter) were irradiated in HFIR. During the neutron irradiation, He produced by transmutation of Ni with thermal neutrons was injected into F82H. A comparison was carried out for microstructures at 480°C to 10 dpa and 380 ppm He by this technique and those obtained by Ni/He dual ion irradiation, respectively. Large voids were observed only by neutron irradiations. The difference would be attributed to the large difference in damage production rate between neutron and ion irradiations.

Modeling studies for tritium and heat transfer, thermofluid in magnetic fields, and materials performance have been enhanced in the project keeping close connections with the experimental studies, for the purpose of increasing contributions to the integration modeling and the MFE/IFE reactor designs.

FTP-P

Development of Small Specimen Test Techniques for the IFMIF Test Cell

E. Wakai¹, B. Kim¹, T. Nozawa¹, T. Kikuchi¹, M. Hirano¹, A. Kimura², R. Kasada², T. Yokomine², T. Yoshida², S. Nogami³, H. Kurishita⁴, Y. Itoh⁴, K. Abe⁴, M. Saito⁴, A. Nishimura⁵, K. Kondo⁶, F. Arbeiter⁶, V. Heinzl⁶, P. Jacquet⁷, V. Massaut⁷, M. Sugimoto¹, and T. Nishitani¹

¹Japan Atomic Energy Agency, Ibaraki, Japan

²Kyoto University, Kyoto, Japan

³Tohoku University, Tohoku, Japan

⁴College of Hachinohe, Aomori, Japan

⁵National Institute for Fusion Science, Toki, Japan

⁶Karlsruhe Institute of Technology, Karlsruhe, Germany

⁷SCK-CEN, Mol, Belgium

Corresponding Author: wakai.eiichi@jaea.go.jp

Recent progress of small specimen test technique (SSTT) for the IFMIF (International Fusion Materials Irradiation Facility) test cell is mainly evaluated in this paper. The engineering designs and validations of high flux test module (HFTM) are performed by JAEA, Japanese Universities, and Karlsruhe Institute of Technology (KIT) in the IFMIF/EVEDA (Engineering validation and engineering design activities) projects under Broader Approach (BA) Agreement between EURATOM and Japan. The optimization of shape and size of specimen and the arrangement are under evaluating and present plan is summarized. Effects of specimen size on mechanical properties such as impact properties and ductile-to-brittle transition temperature (DBTT) are known to occur in ferritic/martensitic steels, and some parts of them have been prepared in the guideline and standard of mechanical tests by ASTM-international and ISO. However, our research of ferritic/martensitic steel F82H shows that it does not match with our data, i.e., master curve method for fracture transition behaviors of F82H steel. Accordingly, we have to modify and develop these standards for the tests including small size specimens in IFMIF. Test methodologies are evaluated for the tests of fracture toughness, fatigue, crack growth rate, tensile, and creep for IFMIF, and the irradiation conditions are analyzed in HFTM of IFMIF.

In the design of HFTM, two types are proposed for RAF/M steels by EU KIT team and for the advanced materials by JA team, respectively. The former type has 12 or 24 rigs instrumented inside HFTM, and liquid NaK is used as a heat medium for small size specimens, and the upper limitation temperature would be up to 823K. If it needs to test at higher temperatures than 823K, we would have to use helium gas as a heat medium. The latter type of HFTM has been developed by JA team for use at temperatures up to 1,273K, and the module design with 9 set-capsules (3 sets \times 3 layers) is set in horizontal direction. The size of one capsule is 15 mm in height and 200 mm in width, and the regime of the capsules in HFTM just corresponds to the foot print size of neutron beam. For validation tests and engineering design, W-3%Re alloy and SiC_f/SiC composites were selected as heater materials and the type R (Pt-Rh alloy and Pt) was chosen as thermocouples because of their phase stability during irradiation.

Research of Low Activation Structural Material for Fusion Reactor in SWIP

J. Chen¹, P. Wang¹, H. Fu¹, and Z. Xu¹

¹*Southwestern Institute of Physics, Chengdu, China*

Corresponding Author: chenjm@swip.ac.cn

Development of low activation structural materials is a critical path to fusion power plant. This paper briefly reviews the strategies for structural materials development in Southwestern Institute of Physics (SWIP) and the current status of the materials under investigation.

To provide material database for the China Helium-cooled ceramic breeder TBM, several 1000 kg heats of CLF-1 RAFM steel have been produced with the chemical composition of Fe-8.5Cr-1.5W-0.25V-0.5Mn-0.1Ta-0.1C-0.03 N (wt.%). The material has a fully martensitic microstructure without either Laves phase or delta ferrite phases after an optimized normalizing and tempering heat treatment. A large number of material properties were evaluated, including mechanical properties and physical properties. Studies on the thermal ageing showed no obvious degradation in tensile properties even after ageing at 550°C and 600°C for 6000 h. Various joining technologies were investigated, such as TIG welding, electron beam welding and hot isostatic pressing bonding. In addition, researches on the influence of magnetic fields on mechanical properties were carried out for understanding the applicability of the RAFM steel in fusion reactors.

A 30 kg V-4Cr-4Ti alloy ingot and various Ti₃SiC₂ particle dispersion strengthened vanadium alloys (PDS) were developed. For SWIP-30 good control of impurities was achieved with the sum of C, N, and O less than 430 wppm. Thermo-mechanical Treatment has been investigated, which increases the alloy's tensile strength significantly. The ultimate tensile strength can reach 562 MPa with 7% total elongation at 700°C. Cold working before aging manifests better strengthening effect due to the strong interaction of dislocations and precipitations. PDS-vanadium alloys have much higher mechanical strength. After vacuum annealing at 1000 – 1200°C, the alloy can achieve 1108 MPa in RT ultimate tensile strength, and total elongation of 16.8%. The alloy has ultra-fine grain of 0.5 – 1.5 μm with < 100 nm dispersing Ti₃SiC₂ particle and ~ 50 nm Y₂O₃ or YN.

A neutron irradiation campaign has been planned by SWIP for the CLF-1 steel and the irradiation will be performed. Post-irradiation properties and microstructure of the steel will be studied using miniature specimens. In 2013, the target dose level for the irradiation is up to 1 dpa and the nominal irradiation temperature is 300°C.

Research and Development Status of Reduced Activation Ferritic/Martensitic Steels Corresponding to DEMO Design Requirement

H. Tanigawa¹, M. Ando², S. Nogami², T. Hirose¹, D. Hamaguchi¹, T. Nakata¹,
H. Sakasegawa¹, M. Enoda¹, Y. Someya¹, H. Utoh¹, K. Tobita¹, K. Ochiai¹,
C. Konno¹, R. Kasada³, A. Möslang⁴, E. Diegele⁵, M. A. Sokolov⁶, L. L. Snead⁶,
Y. Katoh⁶, R. E. Stoller⁶, and S. Zinkle⁶

¹Japan Atomic Energy Agency, Naka, Japan

²Tohoku University, Sendai, Japan

³Institute of Advanced Energy, Kyoto University, Uji, Japan

⁴Karlsruhe Institute of Technology, Eggenstein-Leopoldshafen, Germany

⁵Fusion For Energy, Barcelona, Spain

⁶Oak Ridge National Laboratory, Oak Ridge, USA

Corresponding Author: tanigawa.hiroyasu@jaea.go.jp

Crucial issues on the path to fusion power are the development of plasma facing and breeding blanket materials which are capable of withstanding high neutron fluences and high heat fluxes. Reduced activation ferritic/martensitic (RAFM) steels are now considered to be the candidates for structural applications in the fusion demonstration reactor, DEMO, because they have a sound engineering basis. But it is also well recognized that the severe DEMO operating conditions, especially 14 MeV fusion neutron irradiation, could cause extra degradation of mechanical properties, such as the loss of plastic deformability which is not covered by current design codes. Thus, estimation methods of materials behavior under 14MeV fusion neutron irradiation and a design methodology for highly irradiated structure have become indispensable elements in DEMO developments.

A critical issue is the materials loss of ductility under irradiation. This loss of plasticity could finally result in unstable crack propagation, when fracture or fatigue crack propagation is the failure mode. 14 MeV fusion neutron irradiation effects, especially helium effects, are anticipated to enhance this irradiation induced loss of plasticity. Reports of helium effects such as extra hardening, increment of fatigue crack propagation rate, or increased ductile-brittle transient temperature shift indicate that a certain amount of helium could increase the possibility of unstable fracture. These results are based on simulation irradiation experiments, thus a mechanistic understanding of these property changes based on microstructural analyses is essential.

As of today, there are indications from many studies and helium effects can be modeled or estimated, however, it is mandatory to verify fusion neutron irradiation effects at an early date with 14 MeV neutron irradiation. Above all else, the estimation and early experimental verification of the critical condition is found to be essential, up to the condition where no significant 14 MeV fusion neutron irradiation effects are expected and fission irradiation data can be used for design activity, regarding to the fact that an intense 14 MeV neutron source – IFMIF – will not be available before 2020', and only the fission irradiation database and complementary modeling is available for design activity until that time.

Simulation of Defects in Fusion Materials Containing Hydrogen and Helium

T. Troev¹, E. Popov¹

¹*Institute for Nuclear Research and Nuclear Energy, Bulgarian Academy of Science, Sofia, Bulgaria*

Corresponding Author: troev@inrne.bas.bg

Simulations of damages in beryllium, alpha-iron and tungsten, irradiated by fusion neutrons have been performed using molecular dynamics (MD). We applied three codes MCNP5, GEANT4 and FLUKA for simulation of 14 MeV neutron interactions in beryllium, iron and tungsten lattices. The displacement cascades induced by the Primary Knocked-on Atoms (PKA), produced by the bombardment of fast neutrons destroys locally the crystalline structure. The displacement cascades efficiency has been calculated using the Norgett-Robinson-Torrens (NRT) formula, the pair potential of Ziegler-Biersack-Littmark (ZBL) and the more realistic EAM interatomic potential.

The second part of the study has covered the positron lifetime computer simulations for 14 MeV neutron irradiated Be, alpha-Fe and W samples, containing hydrogen and helium. The positron lifetimes calculated by TCDFE correlate with the magnitude of electron density of targets. The positron is bound to a mono-vacancy even it contains hydrogen or helium atoms. The vacancy-clusters without helium are active positron traps, if once they are bound with helium or hydrogen, they become less effective in the trapping of positrons. The lattice relaxation of atoms around vacancy, reduce the effective vacancy volume, which decreases the positron lifetime at a vacancy location. Positron lifetime is proportional to the increasing of the nano-void size while an increase the number of helium atoms into nano-void decrease the lifetime. The model calculated positron lifetimes of nano-void containing gases atoms are shorter than in the empty nano-void of the same size.

KIT Fusion Neutronics R&D Activities and Related Design Applications

U. Fischer¹, G. Dennis¹, K. Kondo¹, D. Leichtle¹, M. Majerle², P. Pereslavytsev¹,
A. Serikov¹, and S. Simakov¹

¹Association KIT-Euratom, Karlsruhe Institute of Technology, Eggenstein-Leopoldshafen,
Germany

²Nuclear Physics Institute of the Czech Academy of Science, Rez, Czech Republic

Corresponding Author: ulrich.fischer@kit.edu

The availability of suitable computational methods, tools, models and data, qualified for design applications, is a pre-requisite to enable reliable nuclear design and performance analyses of future fusion devices. Various efforts are being conducted worldwide to develop and extend the capabilities of the neutronics simulation tools including the capabilities to model the problem geometry in true 3D representation and taking advantage of the high performance parallel computing resources available nowadays.

At the Karlsruhe Institute of Technology (KIT), Institute for Neutron Physics and Reactor Technology (INR), the efforts focus on the development of various computational schemes based on the Monte Carlo technique for the particle transport simulation, by adapting and coupling available codes, and extending their capabilities to specific application requirements. This includes, among others, a coupled programme system for the Monte Carlo based calculation of shut-down dose rate distributions in full 3D geometry, and an enhanced version of the MCNP code, called McDeLicious, with the ability to sample in the transport calculation the generation of d-Li source neutrons on the basis of tabulated cross-section data. A dedicated effort is being conducted on the development of the in-house geometry conversion software tool McCad to enable the automatic generation of MCNP models from available CAD geometry data.

The objective of this paper is to present the progress achieved recently in the development of the mentioned computational tools and demonstrate their suitability for fusion neutronics calculations in applying them to specific design and performance analyses of the ITER device and the IFMIF neutron source facility.

Manufacturing and Development of JT-60SA Vacuum Vessel and Divertor

A. Sakasai¹, K. Masaki¹, Y. Shibama¹, S. Sakurai¹, T. Hayashi¹, S. Nakamura¹,
H. Ozaki¹, K. Yokoyama¹, Y. Seki¹, and K. Shibamura¹

¹*Naka Fusion Institute, Japan Atomic Energy Agency, Naka, Japan*

Corresponding Author: sakasai.akira@jaea.go.jp

The JT-60SA vacuum vessel (VV) and divertor are key components for the performance requirements. Therefore the manufacturing and development of VV and divertor are in progress by the first priority, inclusive of the superconducting magnets. The vacuum vessel has a double wall structure in high rigidity to withstand electromagnetic force at disruption and to keep high toroidal one-turn resistance. In addition, the double wall structure fulfills originally two functions.

1. The remarkable reduction of the nuclear heating in the superconducting magnets is made by boric-acid water circulated in the double wall.
2. The effective baking is enabled by nitrogen gas flow of 200°C in the double wall after draining of water.

Three welding types were chosen for the manufacturing of the double wall structure VV to minimize deformation by welding. Trial manufacturing of the 20-degree upper half segment was carried out with three welding types in order to investigate welding deformation, to verify a manufacturing procedure and to design constraint jigs for the welding. The manufacturing of the first VV 40-degree sector was completed after the inboard and outboard connection on Naka site in May 2011.

Divertor cassettes with fully water cooled plasma facing components are designed to realize the JT-60SA lower single null closed divertor. The divertor cassettes in the radio-active VV are especially developed to ensure compatibility with remote handling (RH) maintenance in order to allow long pulse high performance discharges with high neutron yield. Trial manufacturing of divertor cassette with typical precision of ± 1 mm has been successfully completed and the real manufacturing has started. Brazed CFC (carbon fiber composite) monoblock targets for a divertor target have been successfully manufactured by precise control of tolerances inside CFC blocks. The first CFC monoblock target delivered in March 2011. The heat removal performance of the CFC monoblock target was successfully demonstrated on the JAEA Electron Beam Irradiation Stand. The surface temperature of the CFC monoblock target was able to keep around 1700°C against heat load of 15 MW/m². Infrared thermography test of real monoblock targets by using hot and cold water was also carried out to construct database for acceptance inspection of 1000 monoblock targets.

Radiological Dose Rate Mapping of D-D/D-T Neutron Generator Facilities

S. Panchapakesan¹, S. Priya¹, S. Bishnoi², T. Patel¹, R. K. Gopalakrishnan¹, and D. N. Sharma¹

¹*Radiation Safety Systems Division, Bhabha Atomic Research Centre, Mumbai, India*

²*Neutron & X-Ray Physics Facilities, Bhabha Atomic Research Centre, Mumbai, India*

Corresponding Author: praka17@yahoo.com

DD/DT reaction neutron generators are used as sources of 2.5 MeV/14 MeV neutrons in laboratories for various purposes. 14 MeV neutron generators are proposed to be located at several positions in the ITER vessel for calibrating neutron/gamma diagnostic systems. Detailed knowledge of the radiation dose rates around the neutron generators is essential to obtain data on personnel exposures, calibration time, optimizing the number of calibration points with accuracy and radiological protection of the personnel involved with operation of 2.5 MeV and 14 MeV neutron sources. This work describes the studies carried out towards verifying the neutron and gamma dose rates near DD/DT neutron sources and the adequacy of bulk shielding to meet the stipulated dose limits in personnel occupancy areas of a neutron generator lab. Shielding adequacy was verified by experimental measurements at various locations inside and outside the neutron generator hall during different conditions. The experimental measurements were validated by Monte Carlo simulation code FLUKA, taking into account the geometry and structural details of source and the surrounding materials. Ambient neutron and gamma dose rate profiles and dose rate spectra at various locations are presented in this work. Measurements show a good agreement (up to 20% deviation) with FLUKA simulations. This study has served in generating detailed radiological dose rate maps around 2.5 MeV and 14 MeV neutron generators for various source neutron yields and also in benchmarking the Monte Carlo simulation methods adopted for dose rate evaluations and shield design of such facilities. This study has also yielded valuable information on the response of the various radiological monitoring instruments and the recently procured personnel neutron/gamma dosimeters (MGP-make) for use in mixed neutron and gamma fields in the vicinity of D-D (2.5 MeV) and D-T (14 MeV) generator based neutron sources.

FTP-P

Work supported by the Health Safety and Environment Group and Neutron and X Ray Physics Facilities, Physics Group, Bhabha Atomic Research Centre, Department of Atomic Energy, INDIA.

The support and guidance offered by IAEA and ITER publications are gratefully acknowledged for completing this work.

Optimization of JT-60SA Plasma Operational Scenario with Capabilities of Installed Actuators

S. Ide¹, N. Aiba¹, T. Bolzonella², C. Challis³, T. Fujita¹, G. Giruzzi⁴, E. Joffrin⁴,
K. Hamamatsu¹, N. Hayashi¹, M. Honda¹, H. Kawashima¹, G. Kurita¹,
G. Matsunaga¹, Y. Miyata¹, T. Nakano¹, K. Shimizu¹, J. Shiraishi¹, T. Suzuki¹,
M. Takechi¹, and H. Urano¹

¹*Japan Atomic Energy Agency, Naka, Japan*

²*CONSORZIO RFX, Padova, Italy*

³*Culham Centre for Fusion Energy, Abingdon, UK*

⁴*French Alternative Energies and Atomic Energy Commission, Gif-sur-Yvette, France*

Corresponding Author: ide.shunsuke@jaea.go.jp

Assessment of plasma operation scenarios and possible operation spaces in JT-60SA has been carried out with emphasis on controllability with actuators, including not only heating and current drive but also fueling and pumping system. The main target of this assessment is high normalized pressure (β_N) steady-state scenario, which requires careful control. It is confirmed that the safety factor profile, which is believed to play an important role for confinement improvement, can be prepared appropriately at the plasma current (I_p) ramp-up phase in a wide extent within capability of the installed ECRF system. At the flat-top of a high normalized pressure and high bootstrap current plasma, it is also confirmed that the installed NB system can modify the safety factor profile and the confinement property within the planned capabilities. It is confirmed that impurity seeding in the SOL and the divertor region can maintain the heat flux within the divertor heat tolerance keeping the separatrix density level acceptable.

SST-1 Magnet System Progress Towards Device Assembly

A. Sharma¹, S. Pradhan¹, U. Prasad¹, K. Doshi¹, Y. Khristi¹, P. Varmora¹, D. Patel¹,
S. Jadeja¹, and P. Gupta¹

¹*Institute for Plasma Research, Bhat, Gandhinagar, India*

Corresponding Author: ansharma@ipr.res.in

Steady State Superconducting (SST-1) Magnet system comprises of sixteen superconducting Toroidal Field (TF) Magnets, nine superconducting Poloidal Field (PF) Magnets, resistive central solenoid (CS) and compensating magnets, resistive Vertical Field (VF) equilibrium magnets, resistive in-vessel feedback coils and radial control coils. The magnet system could only be partially commissioned in 2006 because of leaks appearing at cold in the helium circuit of magnets. Since then, under the SST-1 Mission mandate, all sixteen TF magnets have been completely refurbished with modified leak-tight joints, enhanced insulation resistances, new manifolds and case cooling shields. To validate the integrated performance of these modifications, each TF magnet was tested in its self field in representative helium flow conditions (4 bar, 4.5K, 16 g/s at the inlet) with full transport currents of 10 kA (2.2 T self field). The normal zone propagation characteristics of the winding packs, electronics for fail-proof quench detection and magnet protection aspects were also experimentally established in these campaigns. Following these successful validations, all TF magnets have been assembled on the SST-1 machine shell. All superconducting PF magnets have also been suitably modified and assembled. Refurbishment and testing of damaged divertor coil using bridge type joints and modifications of all joints in the outer PF magnets are some of the important experimental and process modifications carried out on the PF magnet system. The central solenoid was also successfully tested for representative operational scenarios of SST-1. A pair of single turn radial control coils meant for controlling the null during the plasma break-down and for providing radial control to the plasma has also been designed and would be installed shortly inside the SST-1 vacuum vessel. The integrated engineering commissioning and testing of the entire magnet system of SST-1 is envisaged during the “engineering validation phase” of the SST-1 towards the middle of 2012.

Lessons Learned from EAST's Failures

J. Li¹, Y. Wan¹, B. Wan¹, P. Fu¹, and EAST Team¹

¹*Institute of Plasma Physics, Chinese Academy of Sciences, Hefei, China*

Corresponding Author: j_li@ipp.ac.cn

Significant progresses have been obtained on EAST tokamak partially based on lessons from its failures marked by more than 20 times leakages from PFC and 1.6 ton water inside of vacuum chamber. Lessons learned from major failures in EAST have been summarized in this paper. Major failures came from design, construction, commissioning and operation phases have been described which have been classified as imperfect design, QA control, failure of components and lack of understanding. Predictions for further risks and possible ways to mitigating these risks have been given in this paper.

Neutronic Evaluation of a Power Plant Conceptual Study considering Different Modelings

C. E. Velasquez¹, C. Pereira¹, M. A. F. Veloso¹, and A. L. Costa¹

¹ *Universidade Federal de Minas Gerais, Belo Horizonte, Brazil*

Corresponding Author: carlosvelcab@eng-nucl.mest.ufmg.br

Three different models of Power Plant Conceptual Study (PPCS) are considered maintaining some conditions as the volume of the vacuum chamber (VC) based on the ITER parameters, in order to study the effect of the neutron flux related to the shape of each VC. Using MCNP, three surfaces were simulated: plane, cylindrical and torus. One of the geometries is made considering the intersection of cylinders and tori, another one with cylinders and planes and the last one just with tori. The walls along the radial axis are located at the same distance and all were filled with the same order of materials. The geometries have symmetry and then the reactor could be divided into four perpendicular parts from the top view of the reactor. In this way, it is possible to follow the flux along different trajectories. The point detector would follow the neutron flux until it gets lost. The detectors are located starting from the first wall until the last one and surrounding each wall. In addition, it is tallying the flux over each volume that surrounds the vacuum chamber. The data from these tallies would give different types of information, such as the flux through each volume and the reactions rate over the volume. Particularly, this study will identify which isotopes from the material composition might have significant values of neutrons capture, absorption, and production cross sections. Such results allow assessment of its composition along the time and the possible impact of changes in the neutronic behavior of the material.

The results give information about the behavior of each modeling, from the point of view of neutron flux shielding, neutronic activation from the materials and the possibility of a transmutation blanket.



First Results from Tests of High Temperature Superconductor Magnets on Tokamak

M. Gryaznevich¹, V. Svoboda², J. Stockel³, A. Sykes⁴, T. T. Todd¹, D. Kingham⁴, Z. Melhem⁵, S. Ball⁵, S. Chappell⁵, I. Duran³, K. Kovarik³, T. Markovic², G. Ondrej², M. K. Lilley⁶, P. de Grouchy⁶, and H.-T. Kim⁶

¹*Euratom/CCFE Fusion Association, Culham Science Centre, Abingdon, UK*

²*Czech Technical University, Prague, Czech Republic*

³*IPP Prague, Czech Technical University, Prague, Czech Republic*

⁴*Tokamak Solutions, Culham Science Centre, Abingdon, UK*

⁵*Oxford Instruments, Abingdon, UK*

⁶*Imperial College, London, UK*

Corresponding Author: mikhail.gryaznevich@ccfe.ac.uk

It has long been known that high temperature superconductors (HTS) could have an important role to play in the future of tokamak fusion research. Here we report on first results of the use of HTS in a tokamak magnet and on the progress in design and construction of the first fully-HTS tokamak. In the experiment, the two copper vertical field coils of the small tokamak GOLEM were replaced by two coils each with 6 turns of HTS (Re)BCO tape. Liquid nitrogen was used to cool the coils to below the critical temperature at which HTS becomes superconducting. Little effect on the HTS critical current has been observed for perpendicular field up to 0.5 T and superconductivity has been achieved at $\sim 90.5\text{K}$ during bench tests. There had been concerns that the plasma pulses and pulsed magnetic fields might cause a “quench” in the HTS, i.e., a sudden and potentially damaging transition from superconductor to normal conductor. However, many plasma pulses were fired without any quenches even when disruptions occurred with corresponding induced electrical fields. In addition, experiments without plasma have been performed to study properties of the HTS in a tokamak environment, i.e., critical current and its dependence on magnetic and electrical fields generated in a tokamak both in DC and pulsed operations, maximum current ramp-up speed, performance of the HTS tape after number of artificially induced quenches etc. No quench has been observed at DC currents up to 200 A (1.2 kA-turns through the coil). In short pulses, current up to 1 kA through the tape (6 kA-turns) has been achieved with no subsequent degradation of the HTS performance with a current ramp rate up to 0.6 MA/s. In future experiments, increases in both the plasma current and pulse duration are planned. Considerable experience has been gained during design and fabrication of the cryostat, coils, isolation and insulation, feeds and cryosystems, and GOLEM is now routinely operated with HTS coils. The construction of a small fully-HTS low aspect ratio tokamak has started at the Tokamak Solutions UK premises in the Culham Science Centre. It is planned to operate a small tokamak with $A = 2$ and circular cross section in steady state with plasma currents of 10 – 20 kA driven by Electron Bernstein Wave current drive. In parallel, the design and manufacture of a high-field (5 T) HTS TF coil for a spherical tokamak is carried out.

FTP-P

Analysis of Consequences in the Loss-of-Coolant Accident in Wendelstein 7-X Experimental Nuclear Fusion Facility

E. Uspuras¹

¹*Laboratory of Nuclear Installations Safety, Lithuanian Energy Institute, Kaunas, Lithuania*
Corresponding Author: algis@mail.lei.lt

Fusion is the energy production technology, which could potentially solve problems with growing energy demand of population in the future. Starting 2007, Lithuanian energy institute (LEI) is a member of European Fusion Development Agreement (EFDA) organization. LEI is cooperating with Max Planck Institute for Plasma Physics (IPP, Germany) in the frames of EFDA project by performing safety analysis of fusion device W7-X. Wendelstein 7-X (W7-X) is an experimental stellarator facility currently being built in Greifswald, Germany, which shall demonstrate that in the future energy could be produced in such type of fusion reactors.

The W7-X facility divertor cooling system consists of two coolant circuits: the main cooling circuit and the so-called “baking” circuit. Before plasma operation, the divertor and other in-vessel components must be heated up in order to “clean” the surfaces by thermal desorption and the subsequent pumping out of the released volatile molecules. The rupture of pipe, providing water for the divertor targets during the “baking” regime is one of the critical failure events, since primary and secondary steam production leads to a rapid increase of the inner pressure in the plasma (vacuum) vessel. Such initiating event could lead to the loss of vacuum condition up to overpressure of the plasma vessel, damage of in-vessel components and bellows of the ports.

In this paper the safety analysis of 40 mm inner diameter coolant pipe rupture in cooling circuit and discharge of steam-water mixture through the leak into plasma vessel during the W7-X no-plasma “baking” operation mode is presented. For the analysis the model of W7-X cooling system (pumps, valves, pipes, hydro-accumulators, and heat exchangers) and plasma vessel was developed by employing system thermal-hydraulic state-of-the-art RELAP5 Mod 3.3 code. This paper demonstrated, that the developed RELAP5 model allows to analyze the processes in divertor cooling system and plasma vessel. The results of analysis demonstrated that proposed burst disk, connecting the plasma vessel with torus hall, opens and pressure inside plasma vessel do not exceed the limiting 1100 kPa absolute pressure. Thus, the plasma vessel remains intact after loss-of-coolant accident during no-plasma operation of Wendelstein 7-X experimental nuclear fusion facility.

Progress in Developing a High-Availability Advanced Tokamak Pilot Plant

T. Brown¹, A. Costley², R. Goldston¹, L. El-Guebaly³, C. Kessel¹, G. Neilson¹,
S. Malang⁴, J. Menard¹, S. Prager¹, S. Scott¹, P. Titus¹, L. Waganer⁵, and
M. Zarnstorff¹

¹*Princeton University, Princeton Plasma Physics Laboratory, Princeton, USA*

²*Consultant, former Head of Diagnostics in ITER, Henley on Thames, UK*

³*University of Wisconsin, Madison, USA*

⁴*Consultant, Fusion Nuclear Technology Consulting, Linde, Germany*

⁵*Consultant, formerly with The Boeing Company, St. Louis, USA*

Corresponding Author: tbrown@pppl.gov

A fusion pilot plant study was initiated to clarify the development needs in moving from ITER to a first of a kind fusion power plant, following a path similar to the approach adopted for the commercialization of fission. The mission of the pilot plant was set to encompass component test and fusion nuclear science missions yet produce net electricity with high availability in a device designed to be prototypical of the commercial device. The objective of the study was to evaluate three different magnetic configuration options, the advanced tokamak (AT), spherical tokamak (ST) and compact stellarator (CS) in an effort to establish component characteristics, maintenance features and the general arrangement of each candidate device. With the move to look beyond ITER the fusion community is now beginning to embark on DEMO reactor studies with an emphasis on defining configuration arrangements that can meet a high availability goal. In this paper the AT pilot plant design will be presented. The selected maintenance approach, the device arrangement and sizing of the in-vessel components and details of interfacing auxiliary systems and services that impact the ability to achieve high availability operations will be discussed. Efforts made to enhance the interaction of in-vessel maintenance activities, the hot cell and the transfer process to develop simplifying solutions will also be addressed.

Benchmarking Reactor Systems Studies by Comparison of EU and Japanese System Code Results for Different DEMO Concepts

R. Kemp¹, M. Nakamura², D. J. Ward¹, K. Tobita², and G. Federici³

¹EURATOM/CCFE Association, Culham Centre for Fusion Energy, Abingdon, UK

²Japan Atomic Energy Agency, Rokkasho, Japan

³EFDA Garching, Max Planck Institut für Plasmaphysik, Garching, Germany

Corresponding Author: richard.kemp@ccfe.ac.uk

Recent systems studies work within the Broader Approach framework has focussed on benchmarking the EU systems code PROCESS against the Japanese code TPC for conceptual DEMO designs. This paper describes benchmarking work for a conservative, pulsed DEMO and an advanced, steady-state, high-bootstrap fraction DEMO. The resulting former machine is an $R_0 = 10$ m, $a = 2.5$ m, $\beta_N < 2.0$ device with no enhancement in energy confinement over IPB98. The latter machine is smaller ($R_0 = 8$ m, $a = 2.7$ m), with $\beta_N = 3.0$, enhanced confinement, and high bootstrap fraction $f_{BS} = 0.8$. These options were chosen to test the codes across a wide range of parameter space. While generally in good agreement, some of the code outputs differ. In particular, differences have been identified in the impurity radiation models and flux swing calculations. The global effects of these differences are described and approaches to identifying the best models, including future experiments, are discussed. Results of varying some of the assumptions underlying the modelling are also presented, demonstrating the sensitivity of the solutions to technological limitations and providing guidance for where further research could be focussed.

Steady State versus Pulsed Tokamak DEMO

F. P. Orsitto¹, T. Todd²

¹*Associazione EURATOM-ENEA Unità Tecnica Fusione, Frascati, Italy*

²*CCFE/Fusion Association, Culham Science Centre, Abingdon, UK*

Corresponding Author: francesco.orsitto@enea.it

The present report deals with a Review of problems for a Steady state(SS) DEMO, related argument is treated about the models and the present status of comparison between the characteristics of DEMO pulsed versus a Steady state device. The studied SS DEMO Models (SLIM CS , PPCS model C EU-DEMO, ARIES-RS) are analyzed from the point of view of the similarity scaling laws and critical issues for a steady state DEMO. A comparison between steady state and pulsed DEMO is therefore carried out: in this context a new set of parameters for a pulsed (6 – 8 hours pulse) DEMO is determined working below the density limit, peak temperature of 20 keV, and requiring a modest improvement in the confinement factor($H_{IPB\gamma 2} = 1.1$) with respect to the H-mode. Both parameters density and confinement parameter are lower than the DEMO models presently considered. The concept of partially non-inductive pulsed DEMO is introduced since a pulsed DEMO needs heating and current drive tools for plasma stability and burn control. The change of the main parameter design for a DEMO working at high plasma peak temperatures $T_e \sim 35$ keV is analyzed: in this range the reactivity increases linearly with temperature, and a device with smaller major radius ($R = 7.5$ m) is compatible with high temperature. Increasing temperature is beneficial for current drive efficiency and heat load on divertor, being the synchrotron radiation one of the relevant components of the plasma emission at high temperatures and current drive efficiency increases with temperature. Technology and engineering problems are examined including efficiency and availability R&D issues for a high temperature DEMO. Fatigue and creep-fatigue effects of pulsed operations on pulsed DEMO components are considered in outline to define the R&D needed for DEMO development.

Critical Design Factors for Sector Transport Maintenance in DEMO

H. Utoh¹, Y. Someya¹, K. Tobita¹, N. Asakura¹, K. Hoshino¹, and M. Nakamura¹

¹*Japan Atomic Energy Agency, Rokkasho, Japan*

Corresponding Author: uto.hiroyasu@jaea.go.jp

Maintenance is a critical issue for fusion DEMO reactor because the design conditions and requirements of DEMO maintenance scheme are different from that of ITER remote handling. The sector transport maintenance scheme has advantages to maintain blankets and divertors without the use of sophisticated remote handling devices including sensitive devices to radiation in the reactor. SlimCS designed in JAEA adopts the sector transport maintenance scheme in which every sector is pulled out horizontally through a port between TF coils. A critical design issue for the horizontal sector transport maintenance scheme is how to support an enormous turnover force of the toroidal field (TF) coils. We propose following two options; first option is the horizontal transport maintenance scheme in which every sector is pulled out through four horizontal ports connected with the corridor. Second option is the vertical sector transport maintenance scheme with small vertical maintenance ports (total: 6 ports). The new horizontal sector transport limited in the number of maintenance ports is a more realistic maintenance scheme, and the key engineering issue is the transferring mechanism of sector in the vacuum vessel.

In the maintenance scenario, the key design factors are the cool down time in reactor and the cooling method in maintenance scheme for keeping components under operation temperature. By one-dimensional heat conduction analysis, the sector should be transported to hot cell within 40 hours in the case the cool down time is one month. In the horizontal sector transport maintenance, the maintenance time including removal of cooling piping, drain of cooling water and sector transport to hot cell is about 32 hours. Furthermore, the tritium release in the sector transport can be suppressed because the components temperature drops by forced-air cooling system.

This paper mainly focuses on a sector transport maintenance scheme from the aspects of high plant availability. This design study clarifies critical design factors and key engineering issues on the maintenance scheme, that is:

1. How to support an enormous turnover force of the toroidal field (TF) coils in the large open port for sector transport.
2. The transferring mechanism of sector in the vacuum vessel.

In addition, maintenance scenario under the high decay heat is proposed for the first time.

Divertor Design and Physics Issues of Huge Power Handling for SlimCS Demo Reactor

N. Asakura¹, K. Shimizu², K. Hoshino¹, K. Tobita¹, Y. Someya¹, H. Utoh¹,
M. Nakamura¹, and T. Takizuka³

¹ *Japan Atomic Energy Agency, Rokkasho, Japan*

² *Japan Atomic Energy Agency, Naka, Japan*

³ *Osaka University, Osaka, Japan*

Corresponding Author: asakura.nobuyuki@jaea.go.jp

Power exhaust scenario for a 3 GW class fusion reactor with the ITER-size plasma has been developed with enhancing the radiation loss from seeding impurity. Transport of plasma, impurity and neutrals was simulated self-consistently, for the first time, under the Demo divertor condition using an integrated divertor simulation code SONIC. The total heat load, q_{target} , was evaluated including radiation power load and neutral load, in addition to the plasma heat load. It was found that heat and particle diffusion coefficients significantly affect the plasma detachment. For the case of increasing the coefficients by the factor of two, peak q_{target} is reduced from 18 MW/m² to below the engineering design level of 10 MW/m², while the characteristic width of the heat flux at the midplane SOL increases slightly from 2.2 to 2.7 mm. It was also found that that enhancement of the local χ and D at the outer SOL affects a reduction in the peak q_{target} near the separatrix. Effects of the divertor geometry such as the divertor leg were investigated. Outer divertor leg length was extended to 2.7 m, while the magnetic flux expansion at the target is reduced to a half compared to the reference case of 1.8 m. Large radiation volume is shifted further upstream from the target due to a reduction in T_e . The peak q_{target} decreases to 10 MW/m² due to reduction in both the plasma heat load and the radiation power load.

A Feasible DEMO Blanket Concept Based on Water Cooled Solid Breeder

Y. Someya¹, K. Tobita¹, H. Utoh¹, K. Hoshino¹, N. Asakura¹, M. Nakamura¹,
H. Tanigawa¹, E. Mikio¹, H. Tanigawa¹, M. Nakamichi¹, and T. Hoshino¹

¹*Japan Atomic Energy Agency, Rokkasho, Japan*

Corresponding Author: someya.yoji@jaea.go.jp

JAEA has conducted the conceptual design study of blanket for a fusion DEMO reactor SlimCS. Considering DEMO specific requirements, we place emphasis on a blanket concept with durability to severe irradiation, ease of fabrication for mass production, operation temperature of blanket materials, and maintainability using remote handling equipment. This paper presents a promising concept satisfying these requirements, which is characterized by minimized welding lines near the front, a simplified blanket interior consisting of cooling tubes and a mixed pebble bed of breeder and neutron multiplier, and approximately the same outlet temperature for all blanket modules. Neutronics calculation indicated that the blanket satisfies a self-sufficient production of tritium. An important finding is that little decrease is seen in tritium breeding ratio even when the gap between neighboring blanket modules is as wide as 0.03 m. This means that blanket modules can be arranged with such a significant clearance gap without sacrifice of tritium production, which will facilitate the access of remote handling equipment for replacement of the blanket modules and improve the access of diagnostics.



Multifarious Physics Analyses of the Core Plasma Properties in a Helical DEMO Reactor FFHR-d1

J. Miyazawa¹, M. Yokoyama², Y. Suzuki², Y. Masaoka², S. Murakami², S. Satake¹, T. Goto¹, R. Seki¹, M. Nunami¹, H. Funaba¹, I. Yamada¹, C. Suzuki¹, R. Sakamoto¹, G. Motojima¹, H. Yamada¹, and A. Sagara¹

¹*National Institute for Fusion Science, Toki, Japan*

²*Department Nuclear Engineering, Kyoto University, Kyoto, Japan*

Corresponding Author: miyazawa@lhd.nifs.ac.jp

Theoretical analyses on the MHD equilibrium, the neoclassical transport, and the alpha particle transport, etc., are being carried out for a helical fusion DEMO reactor named FFHR-d1, using radial profiles extrapolated from LHD. FFHR-d1 is a heliotron type DEMO reactor of which the conceptual design activity has been launched since 2010. It is possible to sustain the burning plasma without auxiliary heating (i.e., self-ignition) in FFHR-d1, since there is no need of plasma current drive in heliotron plasmas. The device size is 4 times enlarged from LHD, i.e., the major radius of helical coil center is 15.6 m, the magnetic field strength at the helical coil center is 4.7 T, and the fusion output is ~ 3 GW. One of the distinguished subjects in FFHR-d1 compared with the former FFHR design series is the robust similarity with LHD. The arrangement of superconducting magnet coils in FFHR-d1 is similar to that of LHD, except a pair of planar poloidal coils omitted to maximize the maintenance ports. This makes reasonable to assume a similar MHD equilibrium as observed in LHD for FFHR-d1, as long as the beta profiles in these two are similar. In FFHR-d1, radial profiles of density and temperature are determined by multiplying proper enhancement factors on those obtained in LHD, according to the DPE (Direct Profile Extrapolation) method. The enhancement factors are calculated consistently with the gyro-Bohm model. Therefore, the global confinement properties as expressed in ISS95 or ISS04 are kept in FFHR-d1. A large Shafranov shift is foreseen in FFHR-d1 due to its high-beta property. This leads to deterioration in the neoclassical transport and alpha particle confinement. Effectiveness of plasma position control and/or magnetic configuration optimization has been examined to solve this problem and to check the validity of extrapolated profiles. According to these analyses, it is concluded that the self-ignition condition can be achieved in FFHR-d1 by mitigating the Shafranov shift. Plasma position control by the vertical magnetic fields is effective for the Shafranov shift mitigation and will improve both the neoclassical transport and alpha heat deposition properties.

FTP-P

A Fast-Track Path to DEMO Enabled by ITER and FNSF-AT

A. M. Garofalo¹, V. S. Chan², J. M. Canik², M. Choi¹, D. A. Humphreys¹,
J. E. Kinsey¹, L. L. Lao¹, M. E. Sawan³, P. B. Snyder¹, H. E. St. John¹,
P. C. Stangeby⁴, A. D. Turnbull¹, and T. S. Taylor¹

¹General Atomics, San Diego, USA

²Oak Ridge National Laboratory, Oak Ridge, USA

³University of Wisconsin, Madison, USA

⁴University of Toronto Institute for Aerospace Studies, Toronto, Canada

Corresponding Author: garofalo@fusion.gat.com

A Fusion Nuclear Science Facility based on the Advanced Tokamak concept (FNSF-AT) [1] is a key element of a fast track plan to a commercially attractive fusion DEMO. The next step forward on the path towards fusion commercialization must be a device that complements ITER in addressing the community identified science and technology gaps to DEMO, and that enables a DEMO construction decision triggered by the achievement of $Q = 10$ in ITER, presently scheduled for the year 2030. This paper elucidates the logic flow leading to the FNSF-AT approach for such a next step forward, and presents the results of recent analysis resolving key physics and engineering issues.

A FNSF-AT will show fusion can make its own fuel, provide a materials irradiation facility, show fusion can produce high-grade process heat and electricity. In order to accomplish these goals, the FNSF has to operate steady-state with significant duty cycle and significant neutron fluence. In FNSF-AT, advanced tokamak physics enables steady-state burning plasmas with the high fluence required for FNSF's nuclear science development objective, in the compact size required to demonstrate Tritium fuel self-sufficiency using only a moderate quantity of the limited supply of Tritium.

Physics based integrated modeling has found a steady-state baseline equilibrium with good stability and controllability properties. 2-D analysis assuming ITER heat and particle diffusion coefficients in the SOL predicts peak heat flux $< 10 \text{ MW/m}^2$ at the outer divertor targets. High fidelity and high-resolution 3D neutronics calculations have also been carried out, showing acceptable cumulative end-of-life organic insulator dose levels in all the device coils, and $\text{TBR} > 1$ for two blanket concepts considered. This FNSF-AT baseline plasma scenario has significant margin to meet the FNSF nuclear science mission. Moreover, the facility allows the development of more advanced scenarios to close the physics gaps to DEMO. Because its design can already start now, FNSF-AT can enable a DEMO construction decision triggered by the achievement of $Q = 10$ in ITER.

References

[1] V. S. Chan, R. D. Stambaugh, A. M. Garofalo, *et al.*, Fusion Sci. Technol. **57** (2010) 66.

This work was supported in part by General Atomics IR&D funding, and the U.S. Department of Energy under DE-FC02-04ER54698, DE-FG02-95ER54309, DE-AC05-00OR22725 and DE-FG02-09ER54513.

Neutronics Design of Helical Type DEMO Reactor FFHR-d1

T. Tanaka¹, A. Sagara¹, T. Goto¹, N. Yanagi¹, S. Masuzaki¹, H. Tamura¹,
J. Miyazawa¹, and T. Muroga¹

¹*National Institute for Fusion Science, Toki, Japan*

Corresponding Author: teru@nifs.ac.jp

Neutronics design study has been performed in a newly started conceptual design activity for a helical type DEMO reactor FFHR-d1. Features of the FFHR-d1 design are enlargement of the basic configurations of reactor components and extrapolation of plasma parameters from those of the helical type plasma experimental machine Large Helical Device (LHD) to achieve the highest feasibility. From the neutronics point of view, a blanket space of FFHR-d1 is severely limited at the inboard of the torus. This is due to the core plasma position shifting to the inboard side under the confinement condition extrapolated from LHD.

The first step of the neutronics investigation using the MCNP code has been performed with a simple torus model simulating thin inboard blanket space. A Flibe+Be/Ferritic steel breeding blanket showed preferable performances for both tritium breeding and shielding, and has been adapted as a reference blanket system for FFHR-d1. The investigations indicate that a combination of a 15 cm thick breeding blanket, 55 cm thick WC+B4C shield, i.e., the blanket space of 70 cm, could suppress the fast neutron flux and nuclear heating in the helical coils to the design targets for the neutron wall loading of 1.5 MW/m². Since the outboard side can provide a large space for a 60 cm thick breeding blanket, a fully-covered tritium breeding ratio (TBR) of 1.31 has been obtained in the simple torus model.

The neutronics design study has proceeded to the second step using a 3-D helical reactor model. The most important issue in the 3-D neutronics design is a compatibility with the helical divertor design. To achieve a higher TBR and shielding performance, the core plasma has to be covered by the breeding blanket layers as possible. However, the dimensions of the blanket layers are limited by magnetic field lines connecting an edge of the core plasma and divertor pumping ports. After repeating modification of the blanket configuration, the global TBR of 1.08 has been obtained. Sufficient radiation shielding for the helical coils has also been confirmed in the 3-D model.

The neutronics design studies have been conducted while keeping compatibilities also with in-vessel design, core plasma distribution etc. Optimization of the helical divertor configuration without significant degradation of shielding performance for coil systems is being investigated at present.

FTP-P

Divertor Heat Flux Reduction by Resonant Magnetic Perturbations in the LHD-Type Helical DEMO Reactor

N. Yanagi¹, A. Sagara¹, T. Goto¹, S. Masuzaki¹, and J. Miyazawa¹

¹*National Institute for Fusion Science, Toki, Japan*

Corresponding Author: yanagi@lhd.nifs.ac.jp

The conceptual design studies of the LHD-type helical fusion DEMO reactor, FFHR-d1, are progressing steadfastly. The LHD-type heliotron magnetic configuration equipped with the built-in helical divertors has a potential to realize low divertor heat flux in spatial average. However, the toroidal asymmetry may give more than a couple of times higher peak heat flux at some locations, as has been experimentally observed in LHD and confirmed by magnetic field-line tracing. By providing radiation dispersion accompanied with a plasma detachment, the heat flux may decrease significantly though the compatibility with a good core plasma confinement is an important issue to be explored. Whereas the engineering difficulties for developing materials to be used under the neutron environment require even further decrease of the heat flux (even though the heliotron is a unique configuration that divertor plates be largely shielded from the direct irradiation of neutrons by breeder blankets). In this respect, we proposed, in the last IAEA FEC, a new strike point sweeping scheme using a set of auxiliary helical coils, termed helical divertor (HD) coils. The HD coils carrying a few percent of the current amplitude of the main helical coils sweep the divertor strike points without altering the core plasma. Though this scheme is effective in dispersing the heat flux in the poloidal direction, the toroidal asymmetry still remains. The AC operation may also give unforeseen engineering difficulties. We here propose that the peak heat flux be mitigated using RMP fields in steady-state. The magnetic field-lines are numerically traced in the vacuum configuration and their footprints coming to the divertor regions are counted. Their fraction plotted as a function of the toroidal angle indicates that the peak heat flux be mitigated to ~ 20 MW per square meters at 3 GW fusion power generation without having radiation dispersion when an RMP field is applied. We note that the magnetic surfaces at the core region are not significantly affected by the RMP field. The poloidal sweeping by HD coils (with quasi-steady-state AC operation) should mitigate the erosion of divertor plates. We propose that these coils be fabricated using YBCO high-temperature superconductors operated at > 20 K.

Innovative Confinement Concepts



Progress on HIT-SI and Imposed Dynamo Current Drive

T. Jarboe¹, C. Akcay¹, D. Ennis¹, C. Hansen¹, A. Hossack¹, G. Marklin¹, B. Nelson¹,
R. Smith¹, and B. Victor¹

¹ *University of Washington, Seattle, USA*

Corresponding Author: jarboe@aa.washington.edu

Efficient current drive and profile control are primary goals of the Helicity Injected Torus (HIT) current drive program. With the achievement of greatly improved parameters on HIT-SI came the discovery of Imposed Dynamo Current Drive (IDCD) a method of efficiently sustaining a stable equilibrium with the possibility of current profile control. A model of IDCD, which predicts the current ramp up, the injector impedance, and the current profile in HIT-SI is presented. The model indicates that dynamo current drive does not need plasma generated fluctuations and a stable equilibrium with profile control through fluctuation profile control can be sustained, a major advance. Applying IDCD to ARIES-AT and ITER at 80 kHz gives injector powers less than 10 MW, $\delta B/B = 10^{-4}$ and fluctuation amplitudes of plasma and flux about the mean flux surface of a few ion gyro radii, indicating the effect on confinement may be acceptable. Since very low fluctuation, in the reactors, can provide current drive for the entire plasma the effect of fluctuations on the plasma current profile is extremely important.

On HIT-SI two injectors, with $n = 1$ symmetry and oscillating 90° out of phase, inductively sustain an $n = 0$ spheromak ($R_o = 0.34$ m, $a = 0.2$ m) by IDCD. Very good progress, since the last meeting, on the HIT-Steady Inductive (HIT-SI) experiment includes: achieving 55 kA of toroidal current, 40 kA of separatrix current, a current gain of 3 (the spheromak record) [1], measuring the relaxation time, discovering IDCD, and observing and simulating a new three phase evolution to the higher currents. The simulations are 3D two-fluid MHD and are done using NIMROD. This research addresses the issues that conventional RF and neutral beam current drive are very power-inefficient, leading to high recirculating power fraction in a reactor, and that lack of profile control causes disruptions.

References

- [1] B. S. Victor *et al.*, Phys. Rev. Lett. **107** (2011) 165005.

Flow and Magnetic Field Profiles in the HIST Spherical Torus Plasmas Sustained by Double Pulsing Coaxial Helicity Injection

M. Nagata¹, Y. Kikuchi¹, T. Kanki², N. Fukumoto¹, T. Higashi¹, M. Ishihara¹,
T. Hanao¹, K. Ito¹, and K. Matumoto¹

¹*University of Hyogo, Himeji, Japan*

²*Japan Coast Guard Academy, Hiroshima, Japan*

Corresponding Author: nagata@eng.u-hyogo.ac.jp

The double pulsing Coaxial Helicity Injection (CHI) on HIST has regenerated toroidal currents up to 80 kA against resistive decay. The internal magnetic field measurements have verified the flux amplification and the formation of the closed flux surfaces after the second CHI pulse. The poloidal flux increases proportionally with the toroidal current as increasing the toroidal field coil current. We have studied characteristics of the plasma flow and the magnetic field structures during the sustainment. The observed poloidal shear flow could be explained in terms of the ion diamagnetic drift that is responsible for the steep density gradient between the central open flux column and the closed flux region. These results are confirmed with help of 3D-MHD computational simulation.

ICC-P

Magnetic System for the Upgraded Spherical Tokamak Globus-M2

V. B. Minaev¹, V. K. Gusev¹, N. Sakharov¹, Yu. V. Petrov¹, E. Bondarchuk²,
A. Arneman², A. Kavin², S. Krasnov², G. Kurskiev¹, A. Malkov², A. B. Mineev²,
A. Novokhatsky¹, I. Yu. Senichenkov³, V. Tanchuk², V. I. Varfolomeev¹, and
E. G. Zhilin⁴

¹*Ioffe Physical-Technical Institute of the Russian Academy of Sciences, St. Petersburg, Russian Federation*

²*D. V. Efremov Scientific Research Institute of Electrophysical Apparatus, St. Petersburg, Russian Federation*

³*Saint Petersburg State Polytechnical University, St. Petersburg, Russian Federation*

⁴*Ioffe Fusion Technology Ltd., St. Petersburg, Russian Federation*

Corresponding Author: vladimir.minaev@mail.ioffe.ru

The necessity of toroidal magnetic field increase for further gain in plasma parameters is evident from experiments conducted on the spherical tokamaks. Modernization of the machines is planned for NSTX (US), MAST (UK) and Globus-M (Russia) and aimed at toroidal magnetic field magnification. For the upgraded spherical tokamak Globus-M2 it means toroidal magnetic field (TF) increase from the present value of 0.4 T up to 1 T as well as the plasma current rise up to 0.5 MA. The vacuum vessel stays unchanged in order to reduce project costs. Present parts of the magnetic system also will be used as far as possible. The key point of the design is the novel central stack with the inductor winded above. In the current report conception of tokamak upgrade is discussed and mechanical and thermal stress analysis results for the magnets under increased field and plasma current are presented.

Stability and Confinement Improvement of Oblate Field-Reversed Configuration by Neutral Beam Injection

T. Ii¹, M. Inomoto¹, K. Gi¹, T. Umezawa¹, S. Kamio¹, A. Kuwahata¹, Q. Cao¹, H. Itagaki¹, T. Watanabe¹, B. Gao¹, K. Takemura¹, K. Yamasaki¹, E. Kawamori², T. Asai³, S. Okada⁴, and H. Zushi⁵

¹*The University of Tokyo, Tokyo, Japan*

²*National Cheng Kung University, Tainan, Taiwan*

³*Nihon University, Tokyo, Japan*

⁴*Osaka University, Osaka, Japan*

⁵*Kyushu University, Fukuoka, Japan*

Corresponding Author: ii@ts.t.u-tokyo.ac.jp

The first experimental investigation of tangential neutral beam injection (NBI) application on oblate field-reversed configurations (FRCs) has been conducted in the TS-4 plasma merging device. The low- n modes are responsible for the short discharge duration of the oblate FRCs formed from light gases. The co-NBI with injection power of 0.6 MW largely extended the magnetic energy decay time of oblate FRCs, while no improvement was observed in the counter-NBI case in which the fast ions are not confined inside the separatrix. These results indicate that the NB fast ions stabilized the low- n global modes and prolonged the discharge duration. Oblate FRCs produced from heavier gases such as argon and xenon show better stability against the low- n modes due to kinetic or two-fluid effects. The argon FRC without NBI shows a degraded confinement state with flux decay time of ~ 0.03 ms. The NBI significantly extended the flux decay time to ~ 0.2 ms while the injection power is much smaller than the maximal loss power of 11 MW. The reduced total loss power of less than 5 MW indicates that NBI not only heats FRC plasma but also changes the equilibrium and transport properties. The observed thermal pressure outside of the magnetic axis in the case with NBI shows significant increment from the case without NBI, as expected from the orbit calculation of NB fast ions. The expected NB power deposition density of 8.5 MW/m^3 will be large enough to modify the pressure profile locally since the volume averaged loss power density of the FRC was 10 MW/m^3 . The current density profile outside of the magnetic axis was also changed to satisfy pressure balance, suggesting that the diamagnetic plasma current is spontaneously driven by the modified pressure profile in the NB-injected FRC. Though these modifications were localized outside the magnetic axis, the flux decay was suppressed in a wide area of the FRC. These results indicate that the utilization of NBI might bring about improvement of FRC confinement by active control of pressure and current profiles as well as electron heating.

ICC-P

This work was partially supported by a Grant-in-Aid for JSPS Fellows 23-2462 and the Core-to-Core Program No. 22001.

A New High Performance Field Reversed Configuration Regime Through Edge Biasing and Neutral Beam Injection

M. Binderbauer¹

¹ *Tri Alpha Energy, Inc., Rancho Santa Margarita, USA*

Corresponding Author: michl@trialphaenergy.com

Field Reversed Configurations (FRCs) with high confinement are obtained in the C-2 device by combining plasma gun edge biasing and neutral beam injection. The plasma gun inward radial electric field counters the usual FRC spin-up and mitigates the $n = 2$ rotational instability without applying quadrupole magnetic fields. The FRCs are nearly axisymmetric, which enables fast ion confinement. The plasma gun also produces $\mathbf{E} \times \mathbf{B}$ shear in the FRC edge layer, which may explain the observed improved particle transport. The combined effects of the plasma gun and of neutral beam injection yield a new High Performance FRC regime with confinement times improved by factors 2 to 4 and FRC lifetimes extended from 1 to 3 ms.

Results from LTX with Lithium-Coated Walls

R. Majeski¹, T. Abrams¹, L. Baylor², L. Berzak¹, T. Biewer², D. Bohler¹,
D. P. Boyle¹, M. Cassin³, E. Granstedt¹, T. Gray², J. Hare¹, C. M. Jacobson¹,
M. Jaworski¹, R. Kaita¹, T. Kozub¹, B. LeBlanc¹, D. P. Lundberg¹, M. Lucia¹,
R. Maingi², E. Merino¹, A. Ryou⁴, E. Shi¹, J. Schmitt¹, J. Squire¹, D. Stotler¹,
C. E. Thomas⁵, K. Tritz⁶, and L. Zakharov¹

¹*Princeton Plasma Physics Laboratory, Princeton, USA*

²*Oak Ridge National Laboratory, Oak Ridge, USA*

³*Bucknell University, Lewisburg, USA*

⁴*University of Pennsylvania, Philadelphia, USA*

⁵*Third Dimension Technologies, Oak Ridge, USA*

⁶*Johns Hopkins University, Baltimore, USA*

Corresponding Author: rmajeski@pppl.gov

The Lithium Tokamak experiment (LTX) is a low aspect ratio tokamak with $R = 0.4$ m, $a = 0.26$ m, and $\kappa = 1.5$. Typical discharge parameters are now: Toroidal field of 2.1 kG, plasma current less than 100 kA, and discharge duration less than 25 msec. LTX is fitted with a conformal 1 cm thick heated copper liner or shell. The plasma-facing surface of the shell is clad with stainless steel, and is conformal to the last closed flux surface (a close-fitting wall). The shell can be heated to 300–400°C, and coated with lithium. LTX was designed to investigate the modifications to tokamak equilibrium with low recycling walls of liquid or solid lithium. With a close-fitting high-Z wall, discharges are strongly affected by wall conditioning. In LTX, the only wall conditioning technique used is lithium coating. Discharges without lithium wall coatings are limited to plasma currents of 15 kA, and discharge durations of order 5 msec. With lithium coatings discharge currents exceed 70 kA, and discharge durations exceed 20 msec, a factor of 4–5 increase in both peak current and duration. Peak electron temperatures, from preliminary Thomson scattering measurements, range from 100–200 eV. Electron temperature profiles for lithium-wall discharges will be presented. Preliminary estimates of local recycling using an extensive set of Lyman-alpha detectors will be discussed. Other spectroscopic diagnostics include edge measurements of impurity lines, and a scanning VUV spectrometer. Discharge fueling employs gas injection. We have studied the fueling efficiency of a number of different gas injection techniques, including supersonic gas injection, and molecular cluster injection. The use of highly directed gas jets results in the highest fueling efficiencies, up to 0.35. A system to fill each of the two the lower shell segments with up to 50 g of liquid lithium has been constructed and is now undergoing testing. Experiments will begin in early spring 2012, and results will be presented. Spectroscopic measurements of the Doppler shifted emission of Li ions have been made to estimate the ion temperature and rotation profiles of LTX discharges. Detailed analysis is in progress and preliminary results will be reported.

This work was supported by USDoE contracts DE-AC02-09CH11466 and DE-AC05-00OR22725.

The Finite Element Analysis of an Inertial Electrostatic Confinement Unit

E. Kurt¹, S. Arslan²

¹*Gazi University, Faculty of Technology, Department of Electrical and Electronics Engineering, Ankara, Turkey*

²*Harran University, Birecik Vocational School, Birecik, Sanliurfa, Turkey*

Corresponding Author: ekurt52tr@yahoo.com

A new inertial electrostatic confinement (IEC) fusion unit was designed via finite element analysis (FEA) in a 3D electrostatic frame. Finite element method (FEM) was applied to the unit in order to identify the potential and electrical fields inside the spherical reaction chamber. Different material types and cathode geometries were tested, theoretically and the electrostatic responses of the central cathode were determined in the cases of different dielectric materials. The effects of cathode geometries were explored in order to identify the minimal and maximal field values at the vicinity of the cathode and inside the vertical and horizontal rings of the cathode structure. It was found that the number of vertical rings plays an important role to produce circular potential wells near the vertical rings. The increment of vertical rings on the cathode affects the bottom corner of electrical potential, thereby ions may be scattered to the entire region of the cathode. In fact, there should be an optimal number of vertical rings so that a better ion core can be obtained at the middle of the central grid for the confinement. Parallel to our earlier study, the dielectric materials surrounding the cathode also affect the field structure near the cathode rods, too. The dielectric thickness was changed in the entire study and some materials were found to be better in order to form homogeneous field inside the cathode for the ion dynamics.

Recent Magneto — Inertial Fusion Experiments on FRCHX

J. Degnan¹, D. Amdahl¹, M. Domonkos¹, C. Grabowski¹, R. Edward¹, W. White¹,
T. Intrator², G. Wurden², J. Sears², W. Waganaar², M. Frese³, S. Frese³,
F. Camacho³, S. Coffey³, V. Makhin³, N. Roderick³, D. Gale⁴, M. Kostora⁴,
W. Sommars⁴, G. Kiuttu⁵, B. Bauer⁶, S. Fuelling⁶, and A. Lynn⁷

¹*Air Force Research Laboratory, Kirtland Air Force Base, New Mexico, USA*

²*Los Alamos National Laboratory, Los Alamos, USA*

³*NumerEx, LLC, Albuquerque, USA*

⁴*SAIC, Albuquerque, USA*

⁵*VariTech Services, Albuquerque, USA*

⁶*University of Nevada, Reno, USA*

⁷*University of New Mexico, Albuquerque, USA*

Corresponding Author: james.degnan@kirtland.af.mil

Magneto-Inertial Fusion (MIF) approaches take advantage of embedded magnetic field to improve plasma energy confinement by reducing thermal conduction relative to conventional inertial confinement fusion (ICF). MIF reduces required precision in the implosion and the convergence ratio. Since 2008 [1], AFRL and LANL have developed one version of MIF. We have:

1. Reliably formed, translated, and captured Field Reversed Configurations (FRCs) in magnetic mirrors inside metal shells or liners in preparation for subsequent compression by liner implosion.
2. Imploded a liner with interior magnetic mirror field, obtaining evidence for compression 1.36 T field to 540 T
3. Performed a full system experiment of FRC formation, translation, capture, and imploding liner compression operation.
4. Identified by comparison of 2D-MHD simulation and experiments factors limiting the closed-field lifetime of FRCs to about half that required for good liner compression of FRCs to multi-keV, 10^{19} ion/cm³, high energy density plasma (HEDP) conditions.
5. Designed and prepared hardware to increase that closed field FRC lifetime to the required amount. Those lifetime extension experiments are now underway, with the goal of at least doubling closed-field FRC lifetimes and performing FRC implosions to HEDP conditions this year.

These experiments have obtained imaging evidence of FRC rotation, and of initial rotation control measures slowing and stopping such rotation.

References

- [1] G. A. Wurden, T. P. Intrator, *et al.*, LA-UR-08-0796, "FRCHX Magnetized Target Fusion Experiments", IC/P4-13, IAEA 2008 Fusion Energy Conference, Geneva, Switzerland, Oct. 13-18, 2008.

Dynamics of Open-field-line MHD Experimental Configurations and Theoretical Investigation of Action Integrals as Effective Hamiltonians

P. Bellan¹, A. Moser¹, E. Stenson¹, R. Perkins^{1,2}, D. Kumar^{1,3}, and T. Shikama^{1,4}

¹*Caltech, Pasadena, USA*

²*Current address: Princeton Plasma Physics Laboratory, Princeton, USA*

³*Current address: Johns Hopkins University, Baltimore, USA*

⁴*Permanent address: Kyoto University, Kyoto, Japan*

Corresponding Author: pbellan@caltech.edu

The Taylor relaxation theory prediction that there exists a unique minimum-energy state towards which a magnetized plasma invariably relaxes has applicability to magnetic fusion confinement (spheromaks and RFP's), the solar corona, and certain astrophysical plasmas. While Taylor theory predicts the minimum-energy end state reasonably well, it does not even attempt to describe what actually happens, i.e., does not predict the dynamics underlying relaxation. Furthermore, Taylor theory assumes zero beta whereas actual plasmas have finite beta. The actual dynamics underlying self-organization of a magnetized plasma has been investigated using two related devices, a coaxial magnetized plasma gun and a bipolar magnetized plasma gun. Experimental observations using high speed imaging that resolves sub-Alfvén time scales have given insights into what happens during Taylor relaxation and also have revealed unexpected and altogether new phenomena. Measurements revealed that a highly collimated MHD-driven plasma flow, i.e., a magnetized plasma jet, is a critical feature of the dynamics. The jet velocity is found to be in good agreement with an MHD acceleration model. These MHD jets are self-collimating as a result of interaction between the magnetic pinch force and jet stagnation. Depending on the flaring of the flux tube radius, open flux tubes can have jets flowing into the flux tube from both ends or from just one end. Jets kink when the Kruskal-Shafranov stability limit is breached; the effective gravity resulting from the acceleration of a sufficiently strong kink can cause a fine-scale, extremely fast Rayleigh-Taylor instability that erodes the current channel to be smaller than the ion skin depth. This cascade from the ideal MHD scale of the kink to the non-MHD ion skin depth scale results in a fast magnetic reconnection whereby the jet breaks off from its source electrode. A multi-channel time- and space-resolved polarimeter has measured the internal magnetic fields of the jet spectroscopically. Theoretical consideration of particle orbits motivated a model showing that adiabatic invariants (action integrals) act as effective Hamiltonians for orbit-averaged motion. This has the consequence that particle drifts can be obtained by taking partial derivatives of adiabatic invariants with respect to their arguments.

Supported by USDOE, NSF, AFOSR.

Observation of Magnetic Fluctuations and Disruption of Magnetospheric Plasma in RT-1

H. Saitoh¹, Z. Yoshida¹, Y. Yano¹, J. Morikawa¹, M. Furukawa¹, H. Mikami¹,
N. Kasaoka¹, W. Sakamoto¹, T. Harima¹, Y. Kawazura¹, Y. Kaneko¹, S. Emoto¹,
S. Iizuka¹, and Y. Goto¹

¹ Graduate School of Frontier Sciences, University of Tokyo, Chiba, Japan

Corresponding Author: saito@ppl.k.u-tokyo.ac.jp

The Ring Trap 1 (RT-1) device is a magnetospheric levitated dipole field configuration constructed for the study of high- β plasma suitable for burning advanced fuels. As observed in planetary magnetospheres, dipole plasmas can be stable against MHD interchange and ballooning instabilities even in bad curvature regions, due to the effects of field lines compressibility. In the first series of experiments in RT-1, plasma is generated and maintained by using electron cyclotron resonance heating (ECH) at 2.45 and 8.2 GHz, and high- β (local $\beta \sim 70\%$) hot-electron plasma that sustained for more than 1 s has been realized. In the presence of intense energetic charged particles in plasmas, emergence of several kinds of fluctuations and instabilities are widely known. Understanding of the stability limit and fluctuation properties is very important for the stable operation of high- β fusion plasma in the magnetospheric configuration. In this study, we report the emergence of magnetic fluctuations and disruptive rapid loss of RT-1 plasma observed in the presence of intense hot electrons. At low neutral gas pressure operation, very intense hot electrons are generated by ECH in the plasma. In such cases, the plasma sometimes becomes unstable and the excitation of MHz-range magnetic fluctuations was observed. Magnetic fluctuations were measured with pickup coils located at different toroidal and poloidal positions. The fluctuations rotate in the electron curvature drift direction and have no clear phase difference along field lines, and disruptive loss of plasma was simultaneously observed. The onset of instability has a strong correlation with the ratio of hot electron component in the plasma. The destructive magnetic fluctuations were observed when the hot electron ratio was above $\sim 40\%$. Kinetic effects due to the intense hot electrons may provide an energy source to induce the disruption, restricting the stability conditions of magnetospheric plasmas. Stabilization of the fluctuations is realized by reducing the ratio of hot electron component with optimized formation conditions, realizing the formation of stable high- β plasma.

Inertial Fusion Experiments and Theory



Diagnosing Implosion Performance at the National Ignition Facility by Means of Advanced Neutron-Spectrometry and Neutron-Imaging Techniques

J. Frenje¹, R. Ashabrunner², R. Bionta², E. Bond², J. Caggiano², A. Carpenter²,
 D. Casey¹, C. Cerjan², T. Clancy², J. Edwards², M. Eckart², M. Farrell³,
 D. Fittinghoff², S. Friedrich², V. Glebov⁴, S. Glenzer², G. Grim⁵, S. Haan²,
 R. Hatarik², S. Hatchett², M. Gatu-Johnson¹, O. Jones², J. Kilkenny³, J. Knauer⁴,
 O. Landen², R. Leeper⁶, S. Le Pape², R. Lerche², C. Li¹, E. Loomis⁵, A. Mackinnon²,
 J. Magoon⁴, M. McKernan², J. McNaney², F. Merrill⁵, M. Moran², G. Morgan⁵,
 D. Munro², T. Murphy⁵, R. Paguio³, R. Petrasso¹, R. Rygg², T. Sangster⁴, F. Séguin¹,
 S. Sepke², M. Shoup⁴, B. Spears², P. Springer², C. Stoeckl⁴, N. Guler⁵, W. Carl⁵, and
 D. Wilson⁵

¹*Massachusetts Institute of Technology, Cambridge, USA*

²*Lawrence Livermore National Laboratory, Livermore, USA*

³*General Atomics, San Diego, USA*

⁴*Laboratory for Laser Energetics, University of Rochester, Rochester, USA*

⁵*Los Alamos National Laboratory, Albuquerque, USA*

⁶*Sandia National Laboratory, Albuquerque, USA*

Corresponding Author: jfrenje@psfc.mit.edu

Proper assembly of capsule mass, as manifested through the evolution of fuel areal density, is essential for achieving hot-spot ignition planned at the National Ignition Facility (NIF). Experimental information about areal density and areal-density asymmetries, hot-spot ion temperature (T_i) and yield (Y_n) are therefore critical for understanding the assembly of the fuel. To obtain this information, a suite of neutron Time-of-Flight (nTOF) spectrometers and a Magnetic Recoil Spectrometer (MRS) has been commissioned and extensively used on the NIF for measurements of the neutron spectrum in the energy range from 1.5 to 20 MeV. This range covers all essential details of the neutron spectrum, allowing for the determination of areal density, Y_n , and T_i . The spectrometers are fielded at different locations around the implosion for directional measurements of the neutron spectrum, also allowing for determination of areal-density asymmetries and possible kinetic effects. The data obtained from these diagnostics have been essential to the progress of the National Ignition Campaign (NIC), indicating that the implosion performance, characterized by the Experimental Ignition Threshold Factor (ITFx), has improved about two orders of magnitude since the first cryogenic shot taken in September 2010. Areal-density values greater than 1 g/cm² are now readily achieved. By combining the areal-density data with information about the spatial extent of the high-density region obtained from Neutron Imaging System (NIS), it has been demonstrated that densities above 500 g/cc and pressure-time (P_τ) products in excess of 10 atm s have been achieved, which are according to HYDRA simulations about a factor of three from ignition conditions.

Progress toward Polar-Drive Ignition for the NIF

R. L. McCrory¹, D. Meyerhofer¹, R. Betti¹, T. Boehly¹, D. Casey², T. Collins¹,
 S. Craxton¹, J. Delettrez¹, D. Egdel¹, R. Epstein¹, J. Frenje², D. Froula¹,
 M. Gatu-Johnson², V. Gelbov¹, D. Harding¹, M. Hohenberger¹, S. Hu¹,
 V. Goncharov¹, I. Igumenshev¹, T. Kessler¹, J. Knauer¹, C. Li², J. Marozas¹,
 F. Marshall¹, P. McKenty¹, T. Michel¹, J. Myatt¹, P. Nilson¹, S. Padalino³,
 R. Petrasso², P. Radha¹, S. Regan¹, C. Sangster¹, F. Séguin², W. Seka¹, R. Short¹,
 A. Shvydky¹, S. Skupsky¹, J. Soures¹, C. Stoeckl¹, W. Theobald¹, B. Yaakobi¹, and
 J. Zuegel¹

¹Laboratory for Laser Energetics, University of Rochester, Rochester, USA

²Plasma Science Fusion Center, Massachusetts Institute of Technology, Cambridge, USA

³State University of New York, Geneseo, USA

Corresponding Author: rmcc@lle.rochester.edu

The Omega Laser Facility at the Laboratory for Laser Energetics (LLE) is used to study direct-drive inertial confinement fusion (ICF) ignition concepts. The baseline ignition target design for this research, using symmetric irradiation, consists of a 1.5-MJ multiple-picket laser pulse that generates four shock waves [similar to the National Ignition Facility (NIF) baseline indirect-drive design] and produces a 1-D gain of 48. Re optimized for polar-drive (PD) illumination (with beams in the x-ray drive configuration), the predicted 2-D gain for this design is ~ 32 , including all known sources of nonuniformities. Verification of the physics base of these simulations is a major thrust of implosion experiments on both OMEGA and the NIF. Many physics issues can be examined with symmetric beam irradiation. OMEGA cryogenic-DT target experiments with symmetric irradiation have produced areal densities of $\sim 0.3 \text{ g/cm}^2$. Physics issues unique to PD are being examined on OMEGA by turning off the equatorial beams and closely approximating the polar-illumination geometry on the NIF. Initial PD “exploding-pusher” experiments on the NIF, designed and tested on OMEGA, have produced neutron yields up to 6×10^{14} and are a critical facet in the testing of diagnostics required for the ignition campaign on the NIF.

This talk describes progress in direct-drive central hot-spot ICF in both symmetric and PD configurations. The current research program is comprised of three segments:

1. Validation of direct-drive, symmetric, cryogenic target performance on the OMEGA Laser System.
2. Demonstration of a viable polar-drive-ignition platform using experiments on the OMEGA Laser System.
3. Definition and execution of a polar-drive-ignition campaign on the NIF.

Each of these segments has seen significant progress since the 2010 IAEA FEC, enhancing our confidence in achieving polar-drive ignition on the NIF.

This work was supported by the U.S. Department of Energy Office of Inertial Confinement Fusion under Cooperative Agreement No DE-FC52-08NA28302, the University of Rochester, and the New York State Energy Research and Development Authority. The support of DOE does not constitute an endorsement by DOE of the views expressed in this article.

Fast Ignition Integrated Experiments with Gekko-XII and LFEX Lasers

H. Shiraga¹, S. Fujioka¹, M. Nakai¹, T. Watari¹, H. Nakamura¹, Y. Arikawa¹,
 H. Hosoda¹, T. Nagai¹, M. Koga¹, K. Shigemori¹, H. Nishimura¹, Z. Zhang¹,
 M. Tanabe¹, Y. Sakawa¹, T. Ozaki², K. Tanaka³, H. Habara³, H. Nagatomo¹,
 T. Johzaki¹, A. Sunahara⁴, M. Murakami¹, H. Sakagami², T. Taguchi⁵, T. Norimatsu¹,
 H. Homma¹, Y. Fujimoto¹, A. Iwamoto², N. Miyanaga¹, J. Kawanaka¹, T. Jitsuno¹,
 Y. Nakata¹, K. Tsubakimoto¹, K. Sueda³, N. Sarukura¹, T. Shimizu¹, K. Mima¹, and
 H. Azechi¹

¹*Institute of Laser Engineering, Osaka University, Osaka, Japan*

²*National Institute for Fusion Science, Toki, Japan*

³*Graduate School of Engineering, Osaka University, Osaka, Japan*

⁴*Institute for Laser Technology, Osaka, Japan*

⁵*Faculty of Science and Engineering, Setsunan University, Neyagawa, Japan*

Corresponding Author: shiraga@ile.osaka-u.ac.jp

Implosion and heating experiments of Fast Ignition (FI) targets for FIREX-1 project have been performed with Gekko-XII and LFEX lasers at the Institute of Laser Engineering, Osaka University. The goal of the project is to achieve fast heating of the imploded fuel plasma up to 5 keV by injection of the heating laser beam. After the first integrated experiments of Fast Ignition with LFEX laser in 2009, in which we concluded that the existence of the prepulse in the heating laser may have affected the heating efficiency by modifying the hot electron spectrum to unexpected higher energy range, we tried to significantly improve the pulse contrast of the LFEX laser beam. Also we have much improved the plasma diagnostics to be able to observe the plasma even in the hard x-ray harsh environment. In 2010-2011 experiment after the previous IAEA/FEC-23, a plastic (CD) shell target with a hollow gold cone was imploded with Gekko-XII laser. LFEX laser beams were injected into the cone at the time around the maximum implosion. We have successfully observed neutron enhancement up to 3.5×10^7 with total heating energy of 300 J, which is higher than the yield obtained in the experiment with previous heating laser, PW, in 2002. We found the estimated heating efficiency assuming a uniform temperature rise is at a level of 10 – 20%. Fuel heating up to 5 keV is expected with full-spec output of LFEX.

Inertial Fusion Energy with Direct Drive and Krypton Fluoride Lasers

J. Sethian¹, S. Obenschain¹, A. Schmitt¹, J. Weaver¹, V. Serlin¹, R. Lehmberg²,
M. Karasik¹, J. Oh², Y. Aglitsky³, D. Kehn¹, M. Wolford¹, F. Hegeler⁴, M. Myers¹,
A. Velikovich¹, L. Y. Chan¹, and S. Zalesak²

¹*Plasma Physics Division, Naval Research Laboratory, Washington, USA*

²*Research Support Instruments Inc., Lanham, USA*

³*Science Applications International Corporation, Mclean, USA*

⁴*Commonwealth Technology Inc., Alexandria, USA*

Corresponding Author: john.sethian@nrl.navy.mil

We are developing the science and technologies needed for a practical fusion energy source using direct drive targets driven by electron beam pumped krypton fluoride (KrF) lasers. The direct drive approach:

1. Allows higher target energy gain.
2. Simplifies target fabrication.
3. Reduces the complexity of target material recycling.

The advantages of KrF include:

1. Very uniform target illumination, thus reducing the seeds for hydrodynamic instability;
2. Shorter wavelength, which allows higher ablation pressures and helps suppress laser-plasma instabilities;
3. Ready capability for zooming, to decrease the diameter of the focal spot to follow the imploding pellet and thereby improve the coupling efficiency by as much as 30%.

Simulations indicate the unique qualities of KrF should substantially reduce the laser energy required to obtain the high gains needed for fusion power plants. High resolution 2-dimensional simulations predict directly-driven shock ignited designs can achieve gains above 150 with KrF energies at and possibly below 1 megajoule. Present research is evaluating the effects of the deeper UV. Experiments on the Nike KrF laser are consistent with the theoretically expected increase in 2-plasmon decay threshold.

We have similarly advanced the laser technology. We predict, based on demonstrations with the individual components, that a KrF laser should have the efficiency needed for a power plant. We have run the Electra as an integrated laser for long runs at 5 Hz. And we have built an all solid state sub scale demonstrator pulsed power supply that has operated for 11 000 000 shots continuously at 10 Hz (319 hours) with an efficiency exceeding 80%. The Orestes KrF physics code, has been developed and benchmarked against experiments on Nike, Electra, and other KrF experiments. Based on this, we have a predictive capability to design future KrF systems, including the required pulse shape.

We will discuss progress in all these areas and our vision for a path forward to develop fusion energy based on this approach.

IFE-P

Approach to Power Plant Physics and Technology in Laser Fusion Energy Systems under Repetitive Operation

J. M. Perlado¹, J. Sanz^{1,2}, J. Alvarez¹, D. Garoz¹, R. González-Arrabal¹, N. Gordillo¹, C. Guerrero¹, O. Peña¹, A. Rivera¹, E. del Río¹, D. Cereceda¹, J. Fernández^{1,3}, A. Fraile¹, R. Juárez¹, N. Moral¹, R. Suárez¹, C. Sánchez², G. Vallés¹, M. Velarde¹, M. Victoria¹, B. Rus⁴, B. Le Garrec⁵, M. Tyldsley³, C. Edwards³, and J. Collier³

¹*Instituto de Fusión Nuclear, (DENIM)/ETSII/Universidad Politécnica, Jose Gutierrez, Madrid, Spain*

²*Departamento Ingeniería Energética, ETSII, UNED, Madrid, Spain*

³*STFC Rutherford Appleton Laboratory, Didcot, UK*

⁴*Academy of Science-PALS, Czech Republic*

⁵*Commissariat à l'Energie Atomique et aux Energies Alternatives, France*

Corresponding Author: josemanuel.perlado@upm.es

Different proposals of Laser Fusion Energy have been envisioned in the last years. Those concepts cover Engineering Facility at large scale in Energy, to Power Prototyping and final DEMO Reactors. HiPER (Europe), extended two years as ESFRI Project, LIFE in USA and LIF-T in Japan, and other initiatives, are entering a new phase where is critical the integration of systems (lasers, target manufacturing and injection, chamber and blanket, tritium handling and Power cycles). The decision to start studies for a Engineering Burst (in HiPER) facility with a repetitive laser operation, with realistic burst mode of hundreds to thousands of shots at 5 – 10 Hz rate, and small gain under continuous (24/7) repetition (Prototype) or final high gain Demo Reactor will be of critical importance. It is very important to consider this difference between Prototype and Demo, because the different target energy gains could have consequences in the first wall and optics. The Engineering Test Bed results will be able to demonstrate with the lowest risk, repetitive laser-injection systems in an already defined model of Chamber. Assuming those conditions, it could be possible to accommodate Experiments in Technology relevant for Prototype and Reactor. This paper shows the differences in designing the chamber for single shot operation (NIF or LMJ Ignition/Gain machines), or repetitive systems, from Laser requirements to Chamber area, activation and damage in optics, wall and structural materials and also dose assessment. A summary of the differences in new designs from Engineering, Prototyping and Demonstration approaches will be the key goal. This paper will presents integration of the various systems needed for an early demonstration of laser-driven power production, including the requirements of tritium and neutron breeding, use of existing reactor-capable materials and considerations of plant safety. Our approach uses two levels: research in each one of the key questions from fundamental to applied physics and technology; and integration of our available answers into a Power Plant System for defining progressive designs from burnup: to thermo-mechanical responses of materials; fluidynamics; tritium generation and cycle; accident analysis after evaluation of activation and radionuclide concentrations, safety and radioprotection.

Particle Simulation of Fusion Ignition

R. More¹, J. Barnard¹, F. Graziani¹, and E. Henestroza¹

¹*Lawrence Berkeley National Laboratory, Berkeley, USA*

Corresponding Author: rmore2262@sbcglobal.net

A new molecular dynamics (MD) particle simulation code has been developed to study inertial fusion ignition physics including effects of a non-Maxwellian ion velocity distribution. 10,000 DT ions at density 100 g/cc and temperatures of several keV are followed for 10 to 20 psec. The simulation includes ion-ion collisions, electron-ion coupling and emission and absorption of radiation. Fusion reactions produce energetic alphas which deposit energy to electrons and ions and the plasma self-heats to 20 – 30 keV.

This simulation using realistic particles and interactions poses the scientific challenge of including quantum processes (fusion, radiation) in a classical particle simulation and the computational challenge of following the calculation for long enough to see significant plasma self-heating. The paper gives a detailed discussion of special physical and numerical techniques which make it possible to do such a simulation.

The molecular dynamics is carefully compared to hydrodynamic simulations of small plasma volumes to test both codes. The most important new physics in MD simulations is the possibility to include a non-Maxwell ion velocity distribution $f(v)$; fusion reaction rates are very sensitive to the high-energy tail of $f(v)$, which depends delicately on plasma transport and equilibration processes.

Although equilibrium ion-pair correlation is not strong in multi-keV plasmas we find substantial dynamical correlations caused by alpha-particle energy transfers. It is found that calculations starting from a variety of initial conditions evolve to follow a unique self-heating trajectory, an ignition attractor.

Calculations starting with 3 keV DT heat to ignition within a few psec after a pulse of energetic ions are injected; this shows that fast ions are quite effective for fast ignition of pre-compressed DT. A series of such calculations are performed to determine the threshold ion deposition heating required to ignite DT fuel within the short time of peak target compression.

This work was supported in part by Department of Energy under Contract DE-AC02-05CH11231 at the Lawrence Berkeley National Laboratory and under Contract DE-AC52-07NA27344 at the Lawrence Livermore National Laboratory.

Application of Radiative Cooling to ICF Ignition

Y.-M. Wang¹

¹*Los Alamos National Laboratory, Albuquerque, USA*

Corresponding Author: ymwang@lanl.gov

Achieving ignition of ICF capsule is the ultimate goal of ICF research. As demonstrated by recent experimental results from NIF, one of the greatest challenges is to achieve the necessary areal density, ρR , in both the fuel and hot-spot regions so that a self-sustained thermonuclear burn can be initiated and maintained by the deposition of 3.5-MeV alpha particles in both regions. Unfortunately, the results of recent ignition shots indicate that the equivalent ρR necessary for a self-sustained thermonuclear burn was not reached at ignition time. In this presentation, I propose a novel approach to increase ρR in the main fuel and especially the hot spot by introducing a radiative cooling mechanism at the end of the implosion phase. The idea is to give both the hot spot and fuel an additional push so that a higher ρR can be reached just before ignition. The proposal of radiative cooling is counterintuitive at first. In the past, it was thought that radiative cooling caused by mixing of high- Z material into the gas cavity could only degrade the performance of inertial-confinement-fusion capsules. However, in this presentation, I demonstrate that radiative cooling properly implemented during the final implosion phase will enhance the performance margin dramatically. The two immediate benefits of such radiative cooling are (a) cooling of the fuel in the final implosion phase to reduce the pressure of the fuel so that a better compression can be achieved, and (b) a momentary decrease in the ion temperature of the fuel and gas, which in turn delays thermonuclear burn ignition, providing a few more picoseconds to further implode the capsule. Importantly, this new approach simply adds a high- Z dopant in the gas region, so that all the previous research and development efforts of the NIF campaign can be fully utilized, for example, laser pulse shaping, holhraum physics, laser-plasma interaction, and even capsule design. Detailed simulation results will be presented to demonstrate the effectiveness of this approach on thermonuclear burn performance and the dramatically increased chance of ignition using the current NIF point ignition design. The simulations show that adding a high- Z dopant (Kr) increases the hot-spot ρR by 38% and the energy production rate by 50% compared with the NIF baseline point design (Rev. 5B) at identical drive conditions.

Shock Studies in Nonlinear Force Driven Laser Fusion with Ultrahigh Plasma Block Acceleration

H. Hora¹, P. Lalouis², S. Moustazis³, I. Földes⁴, G. H. Miley⁵, X. Yang⁵, and X. He⁶

¹*University of New South Wales, Sydney, Australia*

²*Institute of Electronic Structure and Laser FORTH, Heraklion, Greece*

³*Technical University of Crete, Science Department, Crete, Greece*

⁴*Wigner Research Center, Institute for Particle and Nuclear Physics Association EURATOM, Budapest, Hungary*

⁵*Department of Nuclear, Plasma and Radiological Engineering, University of Illinois, Urbana, USA*

⁶*Institute of Applied Physics and Computation Mathematics, Beijing, China*

Corresponding Author: herbitz@yahoo.com

Sauerbrey's measurement [1] of ultrahigh acceleration of plasma blocks by 10^{20} cm/s² with ps laser pulses at very high intensity — confirmed by Földes *et al.* [2] — are 10,000 times higher than any acceleration with ns laser pulses. At ns, thermal pressure with losses and delays dominates the interaction, while the ps case is dominated by the instantly acting nonlinear (ponderomotive) force. The ps acceleration of 10^{20} cm/s² was theoretically and numerically predicted in 1978 [3] (see p. 179). The mechanism is different from electron acceleration in vacuum, first derived against preceding knowledge 1988 [4] as a nonlinear interaction process, and is different from acceleration of ion beams due to relativistic self-focusing [5].

Based on the measurements [1,2] the mechanism of the ps acceleration in contrast to that with ns pulses can now be understood as the non-thermal > 99% efficient transfer of optical energy into macroscopic motion of the irradiated electron cloud in the space charge neutral plasma, where the inertia is determined by the cloud of the attracted ions. The sufficient small Debye length is essential in the high density plasma blocks. It is not trivial to distinguish the acceleration mechanisms of electrons in vacuum [4] of ion beams up to GeV [5] and that of space charge quasi-neutral plasma blocks [6] which were mostly interrelated and rather complicated. The clarification is shown how the block acceleration with full agreement between measurements [1] and the nonlinear force theory [6] led now to realize the fundamental difference to the thermokinetic processes with ns pulses. This is guided by the measurements of the ultrahigh block accelerations with consequences to a new scheme of fast ignition of laser fusion [7].

References

- [1] R. Sauerbrey, *Physics of Plasmas* **3** (1996) 4712.
- [2] I. B. Földes, J. S. Bakos, K. Gal, *et al.*, *Laser Physics* **10** 264.
- [3] H. Hora *Physics of Laser Driven Plasmas*, New York: John Wiley (1981).
- [4] H. Hora *Nature* **333** (1988) 337; H. Hora, M. Hoelss, W. Scheid *et al.*, *Laser & Part. Beams* **18** (2000) 135.
- [5] H. Hora *J. Opt. Soc. Am.* **65** (1975) 228; Cicchitelli *et al.*, *Phys. Rev. B* **A41** (1990) 3727; T. Häuser *et al.*, *Phys. Rev.* **A45** (1992) 1278.
- [6] H. Hora *Laser & Part. Beams* (2012) doi:10.1017/S0263034611000784.
- [7] H. Hora, G. H. Miley *et al.*, *Energy & Environm. Science* **3** 479.

Status of Fast Ignition Point Design

P. Patel¹, F. N. Beg², C. Bellei¹, S. Chawla², C. Chen¹, B. Cohen¹, L. Divol¹, D. P. Higginson², L. C. Jarrott², A. Kemp¹, E. Kemp¹, M. Key¹, D. Larson¹, A. Link¹, T. Ma¹, M. Marinak¹, H. McLean¹, Y. Ping¹, F. Perez¹, H. Sawada², H. Shay¹, A. Sorokovikova², R. Stephens³, D. Strozzi¹, M. Tabak¹, B. Westover², M. Wei³, and S. Wilks¹

¹*Lawrence Livermore National Laboratory, Livermore, USA*

²*University of California, San Diego, CA*

³*General Atomics, San Diego, USA*

Corresponding Author: patel9@llnl.gov

The fast ignition (FI) approach to inertial confinement fusion offers the prospect for achieving the high target gains necessary for an attractive inertial fusion energy system. In the FI scheme a two step approach is used to reach the conditions required to initiate fusion and burn: firstly, a DT-filled capsule is compressed to form a dense core (300 g/cc); secondly, a small region of the core is heated rapidly to ignition temperature (12 keV) with a high-power laser-generated electron beam. A major challenge for FI target design has been the complexity in modeling both the compression and ignition phases self-consistently and at full-scale.

We report on progress in the design of a high gain FI target using an integrated suite of codes capable of simulating all aspects of an FI implosion, including fuel compression, ignitor pulse laser-plasma interaction, fast electron generation and transport, core heating, ignition, and burn. We use a cone-in-shell target with an indirect-drive irradiation scheme compatible with the 1.8 MJ National Ignition Facility (NIF) at LLNL. Two-dimensional hohlraum and capsule simulations are performed with the radiation-hydrodynamics code, HYDRA, to optimize the peak density, areal density, and spatial uniformity of the compressed fuel around the cone tip, whilst maintaining its physical integrity. The ultrashort-pulse laser-plasma interaction and fast electron generation is simulated with a three-dimensional explicit particle-in-cell (PIC) code. The subsequent transport of the electrons through the imploding plasma and their heating of the dense core is modeled with a hybrid-PIC electron transport code coupled to the HYDRA code. The PIC calculations predict an over-energetic and divergent electron source that results in low energy coupling to the compressed core and reduced gain. We describe techniques to improve energy coupling and gain through the use of both azimuthal and axial magnetic fields generated through gradients in material resistivity and magnetic compression of initially imposed seed fields. Integrated calculations are used to design and optimize these schemes and determine ignition energy requirements for achieving high fusion gain.

IFE-P

This work performed under the auspices of the U.S. Department of Energy by Lawrence Livermore National Laboratory under Contract DE-AC52-07NA27344.

Computational Study of the Strong Magnetic Field Generation in Non-Spherical Cone-Guided Implosion

H. Nagatomo¹, T. Johzaki², A. Sunahara², K. Mima³, H. Sakagami⁴, S. Fujioka¹,
H. Shiraga¹, and H. Azechi¹

¹*Institute of Laser Engineering, Osaka University, Osaka, Japan*

²*Institute for Laser Technology, Osaka, Japan*

³*Graduate School for the Creation of New Photonics Industries, Hamamatsu, Shizuoka, Japan*

⁴*National Institute for Fusion Science, Toki, Japan*

Corresponding Author: naga@ile.osaka-u.ac.jp

The magnetic field in non-spherical cone-guided implosion is simulated using temporal evolution equations of the magnetic field coupled with simulated result of 2-D radiation hydrodynamic simulation for Fast Ignition as the first attempt. We have found that the magnetic field is generated by $\nabla \mathbf{T}_e \times \nabla \mathbf{N}_e$ term, and it is compressed by the implosion. In the result, it reaches 5 MG at maximum compression, which was not considered before. Also, high Hall parameter region is appeared between cone tip and core plasma. This magnetic field is strong enough to affect the implosion dynamic and hot electron transport, therefore it should be paid attention in these simulations for Fast Ignition.

Study of Fast Electron Generation and Transport for Fast Ignition

M. Wei¹, R. Mishra², S. Chawla², A. Sorokovikova², F. N. Beg², C. Chen³, H. Chen³, R. Fedosejevs⁴, J. Jaquez¹, L. C. Jarrott², G. Kemp⁵, M. Key³, J. Kim², A. Link⁵, H. McLean³, A. Morace², V. M. Ovchinnikov⁵, P. K. Patel³, Y. Ping³, B. Qiao², H. Sawada², Y. Sentoku⁶, C. Stoeckl⁷, W. Theobald⁷, and R. B. Stephens¹

¹General Atomics, San Diego, USA

²University of California San Diego, La Jolla, USA

³Lawrence Livermore National Laboratory, Livermore, USA

⁴University of Alberta, Edmonton, Canada

⁵The Ohio State University, Columbus, USA

⁶University of Nevada, Reno, USA

⁷Laboratory for Laser Energetics, University of Rochester, Rochester, USA

Corresponding Author: weims@fusion.gat.com

In cone-guided fast ignition (FI), a high intensity short pulse laser interacts with the cone tip to generate relativistic electrons that travel through the cone tip and deposit their energy in a preassembled high density fuel outside the tip to initiate the fusion spark. Energy coupling to the fuel depends on laser-plasma-interaction (LPI) produced electron source characteristics (laser-to-electron energy conversion, electron energy and divergence). A series of experiments evaluated the energy coupling dependence on target material, geometry, preformed plasma scale length, and laser pulse length using the Titan laser (150 J, 0.7 ps) at LLNL and the OMEGA EP laser (300 – 1500 J, 1 – 10 ps) at LLE. Targets were multilayered foils in both planar and buried cone geometries consisting of Au or Al (either as the transport material or as the cone tip material) and a Cu layer buried 100 μm deep in the target. Fast electrons were characterized by measuring the induced Cu K_{α} radiation, bremsstrahlung x-rays, and the escaped electron spectrum at various angles.

Important findings include:

1. Buried cone geometry improved energy coupling by 2X compared to the flat, however with an increased electron divergence. High Z Au cone resulted in a large diverged electron beam, which we attribute to the extended preplasma inside the Au cone.
2. Electron divergence is reduced (for 1 ps pulse) with a thin high-Z transport layer a few μm beneath the Al front layer compared to the pure Al transport target. 2D collisional particle-in-cell (PIC) modeling including dynamic ionization and radiation cooling suggest strong resistive B -fields in the high-Z transport target collimate fast electron beam.
3. Preliminary experiments with 10 ps pulses showed irregular, variable shapes in the electron beam; 2 – 3 distinct spots were observed with a separation distance of $\sim 100 \mu\text{m}$, which suggest the growth, over a few ps, of widely separated, stable filaments either in the LPI region or inside the solid target.

The experiments are modeled using collisional PIC and hybrid PIC codes. Detailed experimental and simulations results will be discussed. Understanding of these dependences is important for optimization of FI cone target design to achieve high energy coupling to the fuel core.

Work supported by the US DOE under contracts DE-FG02-05ER54834, DE-AC52-07NA27344, and NA0000870.

Self-consistent Integrated Modeling for Proton Fast Ignition

B. Qiao¹, M. E. Foord², R. B. Stephens³, M. S. Wei³, P. K. Patel², H. S. McLean²,
M. H. Key², and F. N. Beg¹

¹*Center for Energy Research, University of California San Diego, La Jolla, USA*

²*Lawrence Livermore National Laboratory, Livermore, USA*

³*General Atomics, San Diego, USA*

Corresponding Author: bqiao@ucsd.edu

The demonstration of the efficient energy conversion from laser to electrons then to protons via the Target Normal Sheath Acceleration (TNSA) mechanism on the Nova PW laser experiments [1] has opened a door to new regimes of high energy density sciences with the laser produced high energy proton beams either as heating sources or probes. One of the most important potential applications is to use proton beams as an ignitor [2,3] to initiate fusion spark in the fast ignition (FI) scheme [4] of inertial fusion energy. Large-scale hybrid particle-in-cell (PIC) simulations using the LSP code [5] with self-consistent laser-plasma interaction (LPI) package have been carried out in an integrated fashion for the proton FI scheme. Unlike modeling previously considered [6], the environment has been included; the thin hemispherical target is attached to the inside of a conical structure, which in turn is surrounded by an imploded fuel configuration for the DT plasma. The respective physical processes occurring in the proton FI scheme, including the proton beam source production, focusing and transport of proton beam from the proton source foil into dense plasma, stopping and deposition of the proton beam energy in hot spot of DT fuel, have been analyzed. The energy delivered by the proton beam to the DT fuel will be compared to Atzeni's ignition conditions [7] and to current results on electron-driven fast ignition scheme. This work also has important implication to other applications of laser produced proton beams because the proton beam dynamics during transitions analyzed here — of a high current proton beam transitioning from the source foil into vacuum and further towards the solid (cone tip), — is of critical importance to virtually all uses of proton beams, whether as probes or heaters.

References

- [1] R. A. Snavely *et al.*, Phys. Rev. Lett. **85** (2000) 2945.
- [2] M. Roth *et al.*, Phys. Rev. Lett. **86** (2001) 436.
- [3] M. H. Key, Phys. Plasmas **14** (2007) 055502.
- [4] M. Tabak *et al.*, Phys. Plasmas **1** (1994) 1626.
- [5] D. R. Welch *et al.*, Nucl. Instrum. Methods Phys. Res. Sect. A **464** (2001) 134.
- [6] M. Temporal, J. J. Honrubia and S. Atzeni, Phys. Plasmas **9** (2002) 3098.
- [7] S. Atzeni, Phys. Plasmas **6** (1999) 3316.

The work was performed under the auspices of the U.S. DOE contract DE-SC0001265.

IFE-P

Focusing Protons Beams for Fast Ignition

C. McGuffey¹, T. Bartal Hughes^{1,2}, M. E. Foord², C. Bellei², M. S. Wei³, M. H. Key²,
P. K. Patel², L. C. Jarrott¹, D. P. Higginson¹, R. B. Stephens³, and F. N. Beg¹

¹*Center for Energy Research, University of California, San Diego, USA*

²*Lawrence Livermore National Laboratory, Livermore, USA*

³*General Atomics, San Diego, USA*

Corresponding Author: cmcguffey@ucsd.edu

The Fast Ignition (FI) concept [1] has the potential for higher gains and smaller energy requirements as compared to conventional central hot spot (CHS) IFE. A hollow cone inserted in the side of the compressed fuel may be used to maintain a clear path for an ultra-short-pulse ignition laser to generate energetic particles that travel into and ignite the dense fuel. In the proton/ion FI concept [2], the ignition laser impinges upon a hemispherical target inside the cone, which generates a proton plasma jet with multi-MeV proton energies that is focused to a spot in the fuel. Optimizing the target's conversion efficiency and beam focus are key issues. Focusing has been demonstrated and studied using freestanding curved targets [3-5]. However, integration into full FI geometry will require the understanding of additional effects including interaction with fields associated with charging of surrounding structures, such as the cone. Experiments were conducted to examine these effects using curved targets with and without surrounding structure [6]. The focused waist diameter was found to be 50% smaller for the structured cases as compared to the freestanding cases. It was $< 40 \mu\text{s}$ for all measured energies. The focal position was also deeper for the conical structure case, but conversion efficiency was lower. Hybrid Particle-In-Cell (PIC) simulations identified connections between structure charging, beam focusing, and conversion efficiency [7] that can explain the focusing behavior observed experimentally in [6] and the conversion efficiency trends in subsequent experiments. Our findings show that targets with a cone structure result in non-ballistic focusing of proton beams to the diameter required for proton FI experiments. This effect could play an important role in controlling proton focusing and conversion efficiency in full-scale proton FI studies.

References

- [1] M. Tabak, *et al.*, Phys. Plasmas **1** (1994) 1626-1634.
- [2] M. Roth, *et al.*, Phys. Rev. Lett. **86** (2001) 436-439.
- [3] P. K. Patel, *et al.*, Phys. Rev. Lett. **91** (2003) 125004.
- [4] R. Snavely, *et al.*, Phys. Plasmas **14** (2007) 092703.
- [5] S. Kar, *et al.*, Phys. Rev. Lett. **106** (2011) 225003.
- [6] T. Bartal, *et al.*, Nature Physics **8** (2011) 139-142.
- [7] M. E. Foord, invited talk submitted to Phys. Plasmas, APS DPP Meeting, (2011).

This work was performed under the auspices of the U.S. DOE contract DE-SC0001265.

Improvement of Characteristics of Laser Source of Ions by Changing the Interaction Angle of Laser Radiation

R. Khaydarov¹, H. Beisinbaeva¹, G. Berdierov¹, and A. Kholbaev¹

¹*Institute of Applied Physics, National University of Uzbekistan, Tashkent, Uzbekistan*

Corresponding Author: rkhaydarov@yahoo.com.ph

Increased effort has been given in the past to improve the parameters of laser-source of ions [1], which can be done either by changing the parameters of the laser itself (intensity, frequency, laser pulse duration) or by modifying the target (target composition, structure, density) [2,3]. We have shown that [3] the intensity of the ions can be increased by varying the concentration of the light element in PbMg targets, due to the energy exchange between the plasma ions. We also found that [4] structural changes in the crystal structure of slid targets during the neutron irradiation have significant influence not only to the efficiency of the process of material evaporation and emission of plasma ions, but also on the efficiency of ionization and recombination processes.

Here, we report our investigations of the effect of the interaction angle of the laser radiation with the target (θ) on the parameters of plasma ions using the mass-spectrometric method. We found that for certain parameters of the laser radiation and geometry of the experiment, the electric field in the plasma region with a critical density sharply increase and oscillation in the electron density takes place. The electrons in this critical region accelerate and collection of high-energy electrons is formed. The emission of these electrons is restricted by the self-consistent electric field generated due to electron-ion separation. Taking into account the effect of the increase of the longitudinal component of the electric field in the region of the critical density we expect that for certain values of θ the parameters of the laser-produced plasma can be improved.

References

- [1] I. G. Brown, J. E. Galvin *et al.*, Appl. Phys. Let. **49** (1986) 1019-1021.
- [2] B. Yu. Sharkov, S. Kondrashev *et al.*, Rev. Scie. Instrum. **69** (1998) 1035-1039.
- [3] R. T. Khaydarov, G. R. Berdiyev *et al.*, Laser and Particle Beams **23** (2005) 521-526.
- [4] R. T. Khaydarov, H. B. Beisinbaeva *et al.*, Nucl. Fusion **50** (2010) 025024(5pp).

Proton Imaging of Hohlraum Plasma Stagnation in Inertial Confinement Fusion Experiments

C. Li¹, F. Séguin¹, J. Frenje¹, M. Rosenberg¹, H. Rinderknecht¹, A. Zylstra¹,
R. Petrasso¹, P. Amendt², O. Landen², A. Mackinnon², R. Town², S. Wilks²,
R. Betti³, D. Meyerhofer³, J. Soures³, J. Hund⁴, J. Kilkenny⁴, and A. Nikroo⁴

¹*Plasma Science and Fusion Center, Massachusetts Institute of Technology, Cambridge, USA*

²*Lawrence Livermore National Laboratory, Livermore, USA*

³*Laboratory for Laser Energetics, University of Rochester, Rochester, USA*

⁴*General Atomics, San Diego, USA*

Corresponding Author: ckli@mit.edu

We report the first time-gated proton radiography of the spatial structure and temporal evolution of how the fill gas compresses the wall blow-off, inhibits plasma jet formation, and impedes plasma stagnation in the hohlraum interior. Interpenetration of the two materials occurs due to the classical Rayleigh-Taylor instability as the lighter, decelerating ionized fill gas pushes against the heavier, expanding gold wall blow-off. The important roles of spontaneously generated electric and magnetic fields in the hohlraum dynamics and capsule implosion are demonstrated. The heat flux is shown to rapidly convect the magnetic field due to the Nernst effect. This experiment provides novel physics insight into the effects of fill gas on x-ray-driven implosions, and will have important impact on the ongoing ignition experiments at the National Ignition Facility.



Study on the Energy Transfer Efficiency in the Fast Ignition Experiment

Y. Arikawa¹, H. Hosoda¹, T. Nagai¹, T. Johzaki², N. Sarukura¹, M. Nakai¹,
S. Takehiro¹, Y. Ishii¹, Z. Zhang¹, M. Koga¹, S. Fujioka¹, H. Nishimura¹, H. Shiraga¹,
and H. Azechi¹

¹*Institute of Laser Engineering, Osaka University, Suita, Osaka, Japan*

²*Institute for Laser Technology, Suita, Osaka, Japan*

Corresponding Author: arikawa-y@ile.osaka-u.ac.jp

Accuracy of the energy transfer efficiency evaluation for fast ignition laser fusion at GEKKO XII and LFEX facility was improved to a great extent by newly developed x-ray spectrometer, time-resolving x-ray imager, and a fast-response gated neutron detector. Energy transfer efficiency from heating laser to hot electrons through an Au cone attached on a CD shell target was diagnosed from absolute yield measurement of Au K_{α} line with a newly developed Laue-type x-ray spectrometer to be 11 – 27% on the assumption of hot electron temperatures derived by widely used scaling-laws.

Imploding shell dynamics, self-emission image, and electron temperature were measured with a multi-imaging x-ray streak camera. In some shots enhancement of the emission after heating were observed.

Relationship between the neutron yield and the heating time relative to the time of density peak diagnosed with multi imaging x-ray streak camera is compared. Significant increase in neutron yield was obtained only when the core is heated within ± 25 ps of the maximum compression. This time-window is comparable to the retaining time of dense compression. This fact indicates the neutron enhancement was induced by fast heating. Maximum neutron yield in the present experiment was revealed to be 3.5×10^7 in the shot with the 301 J heating, which was the highest value ever reported. In this shot, the energy transfer efficiency from laser to core plasma was estimated to be 10 – 20% with the assumption of typical density profile and uniform heating model. The ion temperatures for this shot and the shot without heating were estimated, by assuming the core having density profile previously reported was heated uniformly, to be 0.7 keV and 0.5 keV, respectively. This energy transfer efficiency successfully promises the core can be heated up to the 5 keV required for ignition with 10 kJ heating which is designed value of LFEX laser.

Fast Ignition Scheme Fusion Using High-Repetition-Rate Laser

Y. Kitagawa¹, Y. Mori¹, O. Komeda¹, K. Ishii¹, R. Hanayama¹, K. Fujita¹,
S. Okihara¹, T. Sekine², N. Satoh², T. Kurita², T. Kawashima², H. Kan²,
N. Nakamura³, T. Kondo³, M. Fujine³, H. Azuma⁴, T. Motohiro⁴, T. Hioki⁴,
M. Kakeno⁴, Y. Nishimura⁵, A. Sunahara⁶, and Y. Sentoku⁷

¹*The Graduate School for the Creation of New Photonics Industries, Japan*

²*Hamamatsu Photonics, K.K., Japan*

³*Advanced Material Engineering Div., TOYOTA Motor Corporation, Japan*

⁴*TOYOTA Central Research and Development Laboratories, Inc., Japan*

⁵*Toyota Technical Development Corp., Japan*

⁶*Institute for Laser Technology, Japan*

⁷*University of Nevada, Reno, USA*

Corresponding Author: kitagawa@gpi.ac.jp

Using a high-repetition-rate laser for the first time, we have performed a compact fast ignition experiment to initiate a fusion reaction and to clarify its dynamics.

A 4 J/0.4-ns output of an LD-pumped high-repetition laser HAMA is divided into the imploding and heating beams, which are illuminated on double deuterated polystyrene foils separated by 100 μm . The heating pulses heat the imploded core, emitting X-ray radiations and yielding 1000 thermal neutrons. Once heated, the core plasma maintains a temperature of few tens eV as long as the core stagnates. The result that the heating pulse transports its energy to the core plasma, is promising for promoting the fast ignition scheme laser fusion.

10-J Green DPSSL-pumped Laser System HAMA for High-repetitive Counter Irradiation Fast Heating Fusion Demonstration

Y. Mori¹, O. Komeda¹, K. Ishii¹, R. Hanayama¹, K. Fujita¹, S. Okihara¹,
Y. Kitagawa¹, T. Sekine², N. Satoh², T. Kurita², T. Kawashima², H. Kan²,
N. Nakamura³, T. Kondo³, M. Fujine³, H. Azuma⁴, T. Hioki⁴, T. Motohiro⁴,
Y. Nishimura⁵, A. Sunahara⁶, and Y. Sentoku⁷

¹*The Graduate School for the Creation of New Photonics Industries, Kurematsuchou, Hamamatsu, Japan*

²*Hamamatsu Photonics, K. K. Kurematsuchou, Hamamatsu, Japan*

³*Advanced Material Engineering Div., Toyota Motor Corporation, Shizuoka, Japan*

⁴*Toyota Central Research and Development Laboratories Inc., Aichi, Japan*

⁵*Toyota Technical Development Corp., Aichi, Japan*

⁶*Institute for Laser Technology, Osaka, Japan*

⁷*Department of Physics, University of Nevada, Reno, USA*

Corresponding Author: ymori@gpi.ac.jp

The achievement of controlled fusion burn and gain with single-shot mega-joule-class laser such as National Ignition Facility (NIF) is scheduled within a few years. Following this scientific proof of ignition, inertial fusion energy (IFE) needs to start engineering development based on repetitive mode experiment. In this engineering phase, development of IFE driver has the first priority because energy or power of IFE driver decides the design and size of IFE experiment machine. A diode pumped solid-state laser (DPSSL) is a promising candidate of the reactor driver for IFE because we can operate it at a high repetition rate (> 10 Hz) with high efficiency ($> 10\%$). Based on available DPSSL represented by HALNA and Mercury, we can develop a repetitive IFE experiment machine by including the other indispensable IFE technologies of target injection and energy conversion system in hand. This is the promising pass to realize the power plant step by step. Here, we developed a DPSSL-pumped laser HAMA to demonstrate repetitive fast heating ICF fusion in which both implosion and heating pulse are required. Demonstration of fast heating scheme requires an ultra-intense laser around 10^{18} W/cm². The present DPSSL provide energy around 10-J class, however, they are not high intense to demonstrate the heating. Applied DPSSL as Ti:Sapphire pumping is a convenient way to demonstrate implosion and heating because it can activate short pulse duration. To demonstrate a counter irradiation fast heating fusion scheme, amplified chirped pulse of 4 J/0.4 ns is divided into four beams, two for imploding and the others for heating the imploded core. The energy is 0.5 J each and intensities are 5.9×10^{13} and 1.9×10^{17} W/cm², respectively. These intensities are within the scope of fast heating fusion experiments. HAMA succeeded in generation of 10^3 DD neutrons/shot by fast heating scheme in repetitive experiments. This is the first demonstration that 10-J class DPSSL is adapted to repetitive ICF experiments. Based on HAMA, we can construct a repetitive ICF experiment machine by including target injection and tracking. In this presentation, we will describe the detail setup of HAMA including laser irradiation system.

IFE-P

Highly Repetitive Laser Inertial fusion driver with Tiled Coherent Beam Combination Laser using Stimulated Brillouin Scattering Phase Conjugation Mirrors

H. J. Kong¹, S. Cha¹, and M. Kalal²

¹*KAIST, Daejeon, Republic of Korea*

²*Czech Technical University, Prague, Czech Republic*

Corresponding Author: hjkong@kaist.ac.kr

In these days, the energy problem is serious in the world. It is necessary to develop a new source of the sustainable energy. In these sustainable energy sources, fusion energy is the most promised energy source. Especially, the laser inertial fusion energy is easy to maintain and easy to increase its scale. However, there are 3 hot problems to achieve the laser inertial fusion energy. To achieve the LIFE, it is necessary to develop 2.5 kJ/10 ns at 10 Hz laser. The Second problem is target injection with high repetition rate and high accuracy. We need to inject the fuel target to the centre of a chamber with accuracy to 20 μm after the fusion reaction. The third problem is the target window coating due to debris from the target implosion. The first and the second problems can be resolved simply by coherent beam combination laser using Stimulated Brillouin Scattering Phase Conjugation Mirrors (SBS-PCM).

The 4-beam combination system is built to prove its feasibility to laser inertial fusion energy driver. The input energy of the each sub-beam is 1.032 ± 0.027 mJ, and the output energy of sub-beam is 402.3 ± 1.21 mJ. The standard deviations of the phase differences between the reference beam and other beams were measured to be less than $\lambda/13$, during 2,500 shots (250 s), and we will get it better than $\lambda/20$ soon.

The coherent beam combination using SBS-PCM has additional advantages in LIFE reactor system. In the fusion reaction, target injection is one of the serious problems. The repetition rate of the target injection is ~ 10 Hz, and the target speed is around 400 m/s. We need the accuracy of target position to 20 μm . Because of the turbulent flow after the prior fusion reaction, it is impossible to inject the target with the accuracy to more than 20 μm . This method can give the accuracy to less than 1 μm even when the turbulence exists in the reactor chamber.

In this paper, the authors introduce the tiled coherent beam combining laser using SBS-PCMs and the self-navigation techniques. With the SBS-PCMs, the authors constructed a tiled-aperture coherent beam combination laser system successfully. The 4-beam coherent combination laser shows the possibility of the practical LIFE driver with the self-navigation techniques.

Overview and Latest Proposals in SBS PCM Based IFE Technology Featuring Self-navigation of Lasers on Injected Direct Drive Pellets

M. Kalal¹, O. Slezak¹, H. J. Kong², and N. B. Alexander³

¹*Czech Technical University, Faculty of Nuclear Sciences and Physical Engineering, Prague, Czech Republic*

²*Korea Advanced Institute of Science and Technology, Daejeon, Republic of Korea*

³*General Atomics, San Diego, USA*

Corresponding Author: kalal@fjfi.cvut.cz

The current status will be reviewed of a recently proposed novel approach to inertial fusion energy (IFE) technology, where phase conjugating mirrors (PCM) generated by stimulated Brillouin scattering (SBS) are employed in combination with a special target displacement compensation system to implement an automatic self-navigation of every individual laser beam onto injected IFE pellets. This novel technology is of a particular importance to the direct drive schemes of pellet irradiation, which is the basis of a number of IFE project (e.g., HiPER). If successful in its full scale realization, this aiming scheme would greatly reduce the technical challenges of adjusting large and heavy optical elements during each shot in an IFE reactor, where a typical repetition rates are several Hertz. Featuring no moving parts, this technology would allow for a high number of laser drivers to be employed. Operating with lower energies (< 1 kJ — thus avoiding the optics damage caused by perpendicular SBS) such laser drivers would be easier to design for the required repetition rate. The latest achievement in the gradual step-by-step development of this technology is a conceptual design for the removal of the unconverted basic laser harmonic. This is needed since, the corresponding schemes already developed to deal with this issue, e.g., for Laser MegaJoule (LMJ–France) or National Ignition Facility (NIF–USA) are not applicable in the SBS PCM IFE technology, so a special Faraday isolator is proposed. For the basic harmonic propagating in both directions (to be removed during its second pass) it will work in its classical configuration. The higher harmonic (propagating only in the backward direction) will be allowed to pass through. Having the unconverted harmonic removal problem solved, a serious development of the SBS PCM based laser driver can be started to establish an upper limit of energy at which the required laser beam parameters would be still acceptable. This energy limit comes from the use of SBS PCMs to self-navigation steering of the laser beams to the target, which means that spatial filtering cannot be employed to take care of the laser beam quality. The value of the upper energy level obtained would determine the number of laser drivers needed for a direct drive fusion facility working in the expected 5 – 10 Hz repetition regime of an IFE power plant.

IFE-P

Summary of Progress in US Heavy Ion Fusion Science Research

J. Kwan¹, E. Henestroza¹, S. Lidia¹, G. Logan¹, P. Ni¹, P. Roy¹, P. Seidl¹,
W. Waldron¹, J. Barnard², R. Cohen², A. Friedman², D. Grote², S. Lund², R. More²,
J. Perkins², W. Sharp², M. Terry², R. Davidson³, P. Efthimion³, E. Gilson³,
L. Grisham³, I. Kaganovich³, H. Qin³, and E. Startsev³

¹*Lawrence Berkeley National Laboratory, Berkeley, USA*

²*Lawrence Livermore National Laboratory, Livermore, USA*

³*Princeton Plasma Physics Laboratory, Princeton, USA*

Corresponding Author: jwkwan@lbl.gov

Construction of the Neutralized Drift Compression eXperiment (NDCX-II), a new high-current, moderate-kinetic-energy accelerator facility at LBNL, is being completed in the spring of 2012. The machine will produce a nanosecond Li^+ ion beam bunch at ~ 2 MeV energy for volumetric heating of thin foils. Extensive simulations using the Warp code led to a physics design with specialized acceleration voltage waveforms that can achieve > 500 -fold longitudinal beam compression. Planned experiments on NDCX-II to study warm dense matter include: measuring equation of state and phase transitions, conductivity, opacity and shock generation. Theoretically, we have:

1. Studied transverse and longitudinal beam compression on two-stream interactions of an intense ion beam in plasma.
2. Studied transverse gradients and profile shapes on beam-plasma instabilities.
3. Identified a class of self-consistent periodic kinetic “equilibria” for intense beams in alternating-gradient focusing systems, and extended nonlinear perturbative particle simulations to such focusing systems.
4. Investigated nonlinear effects of beam-plasma instabilities on beam current neutralization.
5. Proposed a Rayleigh-Taylor instability mechanism for droplet formation in expanding warm dense matter.
6. Carried out theoretical studies of using a beam “wobbler” (periodic deflector) as a beam smoothing technique.

Using HYDRA simulations to design the novel Heavy Ion Fusion X-target, it was found that, by adding an aluminum pusher and radial tamping, the fusion gain can be increased from 50 to 300, and the stagnation fuel density doubled to 100 g/cm^3 at peak compression, with a $\rho_r \sim 2 \text{ g/cm}^2$. The X-target has a simple cylindrical metal case filled with DT fuel and a conical insert with an “X” shaped cross-section. Using multiple heavy ion beams to illuminate the target axially from only one side, the fuel can be compressed and ignited at the X-vertex. The simulations showed negligible RT growth leaving a central clean DT ignition zone. We have also developed a directly driven, spherical, tamped, hot-spot ignited target that has high hydrodynamic efficiency while relaxing accelerator phase-space constraints. This target is driven by a combination of an exploding pusher followed by radiation driven ablation.

Axial Magnetic Field Compression Studies Using Gas Puff Z-pinches and Thin Liners on COBRA

P. Gourdain¹, I. Blesener¹, K. Blesener¹, A. Cahill¹, M. Evans¹, J. Greenly¹, D. Hammer¹, C. Hoyt¹, B. Kusse¹, S. Pikuz¹, P. Schrafel¹, C. Seyler¹, T. Shelkovenko¹, Z. Xuan¹, E. Kroupp², G. Rosenzweig², A. Fisher², Y. Maron², and N. Qi³

¹*Laboratory of Plasma Studies, Cornell University, Ithaca, USA*

²*Weizmann Institute of Science, Rehovot, Israel*

³*L3 Pulsed Sciences, San Leandro, USA*

Corresponding Author: pag89@cornell.edu

The MagLIF concept proposes to reach fusion parameters by imploding a cylindrical liner onto fusion fuel on the 27 MA Z machine at Sandia National Laboratories. The concept relies on plasma preheating using a laser and magnetic confinement with an axial magnetic field. The success of this scheme depends upon the compression of the magnetic field by the plasma to limit electron losses to the liner. The work presented here addresses magnetic field compression in hydrogen gas puff and thin liner Z-pinches. The principal goal of this research is to understand the development of gas and liner Z-pinch instabilities and investigate the possibility that axial magnetic fields can mitigate them while obtaining the largest possible compression ratios. The axial magnetic field time evolution will be measured using miniature Bdot probes. We will compare experimental results to the newly developed three-dimensional extended MHD PERSEUS code to assess the validity of numerical tools and the importance of the Hall effect in plasma implosion.

FIREX Foam Cryogenic Target Development: Attempt of Residual Voids Reduction with Solid Hydrogen Refractive Index Measurement

A. Iwamoto¹, H. Sakagami¹, T. Fujimura², M. Nakai², T. Norimatsu², H. Shiraga², and H. Azechi²

¹*National Institute for Fusion Science, Toki, Japan*

²*Institute of Laser Engineering, Osaka University, Osaka, Japan*

Corresponding Author: iwamoto.akifumi@lhd.nifs.ac.jp

To develop a Fast Ignition Realization EXperiment (FIREX) target, we have two strategies: a foam shell method and a cone guide heating technique for a Polystyrene (PS) shell. In this paper, the former method is focused. A target consists of a 500 micron foam shell with a ~ 20 micron foam layer, a gold cone guide and a glass fill tube. A Resorcinol/Formalin (RF) material is utilized to create the foam shell. A foam layer is formed with aggregations of tiny cells. The porous foam material has the advantage to form a uniform liquid layer by capillarity. In the liquid-solid transition of fuel, however, their different densities would cause void spaces in each cell. Preventing the residual voids is one of important issues. The voids must come from random solidification. Continuous liquid fuel supply to a controlled solidification front would reduce the residual voids formation. We apply the effect of capillary attraction of the porous foam in a liquid state as the driving force of the continuous liquid fuel supply. Monotonic temperature gradient along a foam layer would realize the controlled solidification front. We demonstrate it in two steps. The first step is a basic study to lower the void fraction in formed solid hydrogen using a triangular prism shape foam plate. Eventually, the direction of a moving solidification front could be controlled by temperature gradient control along the plate. Based on hydrogen refractive index measurements, the residual void fraction was estimated less than $\sim 2\%$. (The void fraction of $\sim 11\%$ is calculated from the density gap.) Our proposed method was proved to be effective. Then the valid technique applies to FIREX foam shell target layering. For a real target, cone guide heating is useful to control the ideal temperature gradient in a foam shell. The controlled solidification front was successfully simulated using ANSYS code (ANSYS, inc.). We are going to experimentally demonstrate FIREX foam shell target layering.

Mass-Fabrication of Targets for Inertial Fusion Energy

N. B. Alexander¹, R. W. Petzoldt¹, E. I. Valmianski¹, G. E. Lee¹, D. T. Frey¹, and
J. T. Bousquet¹

¹*General Atomics, San Diego, USA*

Corresponding Author: alexande@fusion.gat.com

The ability to economically fabricate large quantities of targets is a key feasibility issue for inertial fusion energy. There exist numerous targets designs in support of various concepts for inertial fusion energy power plants. Common to all is the need to fabricate numerous targets to supply the plant. Most (but not all) plants also require targets to be injected rather than placed into a reactor chamber where the driver meets the targets. Targets can be as simple as a capsule to contain DT fuel. However, many targets are an assembly of parts. The tolerance required of parts and assemblies is high. General Atomics is developing technologies for IFE target production and injection. We report on the development of production methods for hohlraums, and P2 shields. A robot target assembly station was built and we discuss its ability to build high tolerance target assemblies. A six degree of freedom ballistics code was implemented to model the trajectory of targets injected into an IFE target chamber. We use this model to examine issues affecting the accuracy of the injection of the target, including the tolerance with which targets are assembled and the effect of gas in the chamber.

This work supported by General Atomics internal funding.

ITER Activities

ITER

Scaling of the Tokamak near Scrape-off Layer H-mode Power Width and Implications for ITER

T. Eich¹, R. Goldston², A. Kirk³, A. Kallenbach¹, A. S. Kukushkin⁴, R. Maingi⁵,
M. A. Makowski⁶, J. Terry⁷, A. W. Leonard⁸, R. Pitts⁴, W. Fundamenski³,
A. Herrmann¹, O. J. Kardaun¹, A. Scarabosio¹, B. Sieglin¹, T. Andrew³,
B. LaBombard⁷, and T. Gray⁵

¹Max-Planck-Institute für Plasma Physics, Garching, Germany

²Princeton Plasma Physics Laboratory, Princeton, USA

³Culham Centre for Fusion Energy, EURATOM-Association, Culham Science Centre, Abingdon, UK

⁴ITER Organization, Saint Paul Lez Durance, France

⁵Oak Ridge National Laboratory, Oak Ridge, USA

⁶Lawrence Livermore National Laboratory, Livermore, USA

⁷MIT-PSFC, Cambridge, USA

⁸General Atomics, San Diego, USA

Corresponding Author: teich@ipp.mpg.de

The presence of a steep edge pedestal gradient in H-mode divertor plasmas implies that strong gradients should also exist across the separatrix, forcing most of the $P_{\text{SOL}} \sim 100$ MW of power arriving in the SOL at $Q_{\text{DT}} = 10$ in ITER to flow inside a narrow channel on open field lines connecting to the divertor target plates. Recent results (coordinated in part through ITPA DivSOL group) indicate that the ITER assumed value is too large. Scaling from the new database provides a clear dependence on the poloidal magnetic field, little variation with other key variables found in previous scalings and suggests $\lambda_{\text{SOL}} \cong 1$ mm for ITER. Measurements from DIII-D, C-Mod and NSTX indicate a systematic narrowing of the inter-ELM divertor heat flux width with plasma current in H-mode plasmas. For the near SOL power width, the data indicate

$$\lambda_{\text{SOL}} \propto \left(\frac{q_{95}}{B_{\text{tor}}} \right)^{\sim 1} \sim \frac{a}{I_p} \propto \frac{1}{B_{\text{pol}}}, \quad (1)$$

with little or no dependence on P_{SOL} or R (major radius). Analysis of data obtained in the same way from JET and ASDEX Upgrade yields

$$\lambda_{\text{SOL}} \text{ (mm)} = 0.73 B_t^{-0.78} q_{\text{cyl}}^{1.2} P_{\text{SOL}}^{0.1} R^0, \quad (2)$$

again with no dependence on R . Data are consistent in absolute magnitude with a recent heuristic drift-based theory. These new findings are based on IR analysis of strongly attached H-mode discharges. Key improvements here have been the avoidance of ELM effects, accounting for changes in the deposition profile due to heat diffusion across the divertor legs into the private flux region. Experimentally, essentially the full operational range of plasma current and toroidal field in each device was scanned. The value of $\lambda_{\text{SOL}} \cong 1$ mm obtained jointly from these scalings for ITER at 15 MA in the Baseline Inductive Scenario, is about a factor 3 shorter than the lowest values predicted on the basis of earlier studies. Such narrow power channels are a concern for ITER, though preliminary SOLPS simulations indicate that they could be tolerated, since volumetric power dissipation in the divertor can still be sufficient to maintain heat flux densities at acceptable levels provided the outer divertor leg is partially detached. Simple estimates show that for ITER, if $\lambda_{\text{SOL}} \leq 2$ mm the implied upstream pedestal pressure gradient would exceed ideal ballooning stability by some margin, assuming that the SOL pressure width is a measure of that in the pedestal. This issue will be examined in the context of the current database.

Progress on the Application of ELM Control Schemes to ITER

A. Loarte¹, G. Huijsmans¹, S. Futatani¹, Y. Gribov¹, M. Becoulet², D. Campbell¹, T. Casper¹, R. Pitts¹, L. R. Baylor³, T. Evans⁴, D. Orlov⁵, A. Wingen⁶, O. Schmitz⁷, H. Frerichs⁷, A. Kirschner⁷, P. Cahyna⁸, R. Laengner⁷, and G. Saibene⁹

¹ITER Organization, St Paul-lez-Durance, France

²CEA/IRFM, Cadarache, St Paul-lez-Durance, France

³Oak Ridge National Laboratory, Oak Ridge, USA

⁴General Atomics, San Diego, USA

⁵University of California, San Diego, USA

⁶Institut für Theoretische Physik, Heinrich-Heine-Universität, Düsseldorf, Germany

⁷Forschungszentrum Jülich GmbH, Association EURATOM-FZJ, Jülich, Germany

⁸Czech Institute of Plasma Physics, Prague, Czech Republic

⁹Fusion for Energy Joint Undertaking, Barcelona, Spain

Corresponding Author: alberto.loarte@iter.org

High fusion performance DT operation in ITER is based on the achievement of the H-mode confinement regime with $H_{98} \geq 1$ and an edge transport barrier that is expected to lead to the quasi-periodic triggering of ELMs. Operation of ITER with H-mode plasmas is also foreseen during the non-active (H & He) and DD operation allowing the development of ELM control schemes before DT operation.

The non-linear MHD evolution of the plasma during ELMs in ITER has been modelled with the JOREK code which shows that the non-linear MHD growth during the ELM causes a temporary ergodisation of the plasma edge leading to the appearance of striations in the ELM power flux at the divertor target. On the contrary, power fluxes to the first wall are expected to be dominated by the convection of energy by the radial propagation of plasma filaments produced during the ELM crash. JOREK has also been applied to investigate the capabilities of the ITER pellet injection system to meet the requirements for ELM control following its validation with DIII-D experimental results.

The application in-vessel coils to create edge magnetic field perturbations for ELM control and the associated power/particle fluxes to PFCs have been studied for ITER. Evaluations of the edge magnetic field perturbation by in-vessel coils show that the toroidal symmetry of the applied currents in the coils ($n = 3$ or $n = 4$ symmetry) can have a significant impact on the level of current required (up to 50% current level reduction) to achieve a given level of edge ergodisation. Optimization of the relative toroidal phasing of the currents applied to the 3 rows of coils shows that there is an appropriate margin (factor of $\sim 1.5 - 2$) in coil current magnitude required to achieve the design criterion (vacuum approximation) for the 15 MA $Q_{DT} = 10$ scenario. Power and particle fluxes in the perturbed edge magnetic field have been evaluated in the vacuum field approximation and including plasma response. The application of edge magnetic field perturbations leads to the appearance of non-toroidally symmetric divertor power/particle fluxes extending up to ~ 50 cm from the separatrix but also to a reduction of the peak heat flux by a factor of 2 – 3. The inclusion of plasma response decreases transport of energy/particles from the main plasma and the detrimental effects on plasma energy/particle confinement.

ITR

Design of the MITICA Neutral Beam Injector: From Physics Analysis to Engineering Design

P. Sonato¹, D. Boilson², T. Bonicelli³, A. Chakraborty⁴, C. Day⁵, F. Peter⁶,
G. Gorini⁷, T. Inoue⁸, J. Milnes⁹, and T. Minea¹⁰

¹*Consorzio RFX, Euratom-ENEA Association, Padova, Italy*

²*ITER Organization, St Paul Lez Durance, France*

³*Fusion for Energy, Barcelona, Spain*

⁴*Iter India, Gandhinagar, Gujarat, India*

⁵*Karlsruhe Institute of Technology, Eggenstein-Leopoldshafen, Germany*

⁶*Max-Planck-Institut für Plasmaphysik, Garching, Germany*

⁷*Università degli Studi di Milano-Bicocca, Milano, Italy*

⁸*Naka Fusion Institute, Ibaraki, Japan*

⁹*Culham Centre for Fusion Energy, Culham Science Centre, Abingdon, UK*

¹⁰*Université de Paris Sud, Orsay, France*

Corresponding Author: piergiorgio.sonato@igi.cnr.it

For ITER heating and current drive, two neutral beam injectors (NBIs) are planned, delivering a total of 33 MW in stationary conditions up to one hour; each injector will accelerate a 40 A negative deuterium ion current up to 1 MV. Such requirements have never been achieved simultaneously. Hence the PRIMA (Padova Research on ITER Megavolt Accelerator) facility is under construction at Consorzio RFX in Padua, Italy. PRIMA will include a test bed named MITICA (Megavolt ITeR Injector and Concept Advancement), with the aim of meeting the ITER beam requirements in terms of negative ion yield, beam uniformity, high voltage holding, operation of beam line components and power supplies, overall reliability of the NBI.

The present contribution describes the current status of numerical simulations, devoted to the optimisation of MITICA, providing the main inputs for the design of accelerator, beam line components, diagnostics and power supplies. Physics and engineering aspects include: beam optics, dumping of co-extracted and stripped electrons, thermo-mechanical behaviour of grids and beam line components during long pulse operation, voltage holding capabilities. The optimised geometry of the accelerator is characterised by equal acceleration gaps (increased voltage holding capability) and a combination of horizontal and vertical magnetic fields in the accelerator (reducing heat loads and electrons exiting the accelerator); the gas pressure profile is also simulated in the accelerator and in the injector.

The design of the accelerator power supplies has been supported by simulations of static and dynamic performances, including the investigation of overvoltages by a sophisticated fast transient model and the modelling of matching network and RF systems.

Moreover the signals expected from the diagnostic systems have been simulated, with realistic beam features, providing prescriptions for the design of diagnostics, like beam emission spectroscopy, beam tomography and neutron diagnostic.

Most of the design of MITICA plants and components are well developed and close to finalisation.

Development in Russia of Megawatt Power Gyrotrons for Fusion

A. Litvak¹, G. Denisov¹, and V. Myasnikov²

¹*Institute of Applied Physics of Russian Academy of Sciences, Nizhny Novgorod, Russian Federation*

²*GYCOM Ltd., Novgorod, Russian Federation*

Corresponding Author: litvak@appl.sci-nnov.ru

During last years several new gyrotrons were designed and tested in Russia. Main efforts were spent for development 170 GHz/1 MW/50%/CW gyrotron for ITER and multifrequency gyrotrons. Additionally other new gyrotrons were shipped and installed at running plasma installations. The industrial production prototypes of the ITER gyrotron were tested at power 1.0 MW in 400 – 500 second pulses and 0.8 – 0.9 MW in 1000 second pulses. For 1 MW power regime the gyrotron efficiency is 55%. The last gyrotron versions operate in LHe-free magnet. It is important that two last gyrotrons (V-10 and V-11) demonstrate very similar output parameters. Time traces for the main gyrotron parameters are stable and confirm possibility of the gyrotron operation even in longer pulses. Detail analysis of the test results showed that a slightly modified ITER gyrotron prototype is capable to operate at power 1.2 MW. First tests of the modified tube are rather encouraging: microwave power 1.2 MW at MOU output was demonstrated in 100 second pulses with efficiency of 53%. Additionally two gyrotron models with TE28.12 operating mode were tested in short-pulse experiments.

The use of step-tunable gyrotrons can greatly enhance performance of ECRH/ECCD systems due to larger accessible radial range, possible replacement of steerable antennas, higher CD efficiency for NTM stabilization. The main problems in development of multifrequency gyrotrons are to provide: efficient gyrotron operation at different modes, efficient conversion of the modes into a Gaussian beam, reliable operation of broadband or tuneable window. Considering this three key problems one can say that first two of them are solved, but realization of a CVD diamond window for a megawatt power level multi-frequency gyrotron met real difficulties. Now a new tuneable window concept is under consideration.

ITER Diagnostics — Technology and Integration Challenges

D. Johnson¹

¹*Princeton Plasma Physics Laboratory, Princeton, USA*

Corresponding Author: djohnson@pppl.gov

Diagnostics play a vital role in controlling the plasma and optimizing its behavior. The higher temperatures and densities of the burning plasma drive the need for advances in diagnostic technology. Discussion of such needs is part of a conceptual design review activity in progress at ITER, and supported by experts from the ITER parties. The front-ends of most of these diagnostics will be housed in massive port plugs, which also shield the machine from radiation, and supply cooling to the first wall. Many diagnostics are housed in a single equatorial port plug, presenting new and interesting technical and organizational challenges for developers. Front-end components must tolerate thermally-induced stresses, disruption-induced mechanical loads, stray ECH radiation, radiation damage, and degradation due to plasma-induced coatings. Challenges are amplified due to the difficulty in performing maintenance on these large structures, particularly once they are activated. In the active phase, port plug removal and maintenance will be performed robotically. Such activities benefit from a standardized approach to diagnostic packaging. Motivated by needs to minimize disruption loads on the plugs, to standardize the handling of diagnostic shield modules, and to decouple the parallel design efforts of the many parties developing ITER diagnostics, the packaging of diagnostics has recently focused on 3 vertical shield modules inserted from the plasma side into each equatorial port plug structure. The dimensions and attachment features of these modules are standardized. At the front of each is a detachable first wall element with customized apertures. Examples of developmental needs identified in the conceptual design phase will be given. Progress on front-end integration into port plugs will be described, including qualification test plans. Also discussed will be measures for coping with the neutron loads, the thermal and electromagnetic loads, the ECH loads, and the first-mirror vulnerabilities.



Imaging Challenges for the ITER Plasma Facing Components Protection

J.-M. Travere¹, M.-H. Aumeunier^{1,2}, M. Joanny¹, T. Loarer¹, V. Martin¹,
V. Moncada¹, L. Marot³, D. Chabaud², E. Humbert², J.-J. Fermé⁴, and C. Thellier⁴

¹*CEA, IRFM, Saint-Paul-lez-Durance, France*

²*OPTIS, Toulon, France*

³*University of Basel, Department of Physics, Basel, Switzerland*

⁴*THALES-SESO, Aix en Provence, France*

Corresponding Author: jean-marcel.travere@cea.fr

The ITER actively cooled tokamak is the next-generation fusion device which will allow studying the burning plasma during hundreds of seconds. ITER plasma facing components (PFCs) real-time protection will be mandatory to minimize operational risks as critical heat flux leading to degradation of PFCs and eventually to water leak. Thanks to Tore Supra expertise in actively cooled tokamak and long pulse operation, urgent research and development actions are presented and discussed addressing the feasibility and the performances of the PFCs protection function foreseen in ITER using a network of wide angle visible and IR imaging systems (VIS/IR WAVS). Three major steps addressing PFCs protection have been reached. First, the contribution of reflected light that could disturb the measurement of surface temperature has been taken into account through an industrial physic-based Monte Carlo ray-tracing method. Secondly, an integrated software and hardware framework validated on existing fusion devices has been proposed. In addition, extended functionalities to analyze and understand in real-time the huge volume of images produced by the VIS/IR WAVS have also been developed. Finally prototypes of ITER first mirrors have been built and tested with successful first results. These results demonstrate that a more precise definition of the functional specifications of the entire imaging system can be obtained addressing both machine protection and plasma performance.

Technology R&D Activities for the ITER Full-tungsten Divertor

P. Lorenzetto¹, F. Escourbiac², T. Hirai², M. Merola², R. Pitts², M. Bednarek¹,
P. Gavila¹, B. Riccardi¹, G. Saibene¹, S. Suzuki³, and I. Mazul⁴

¹*Fusion for Energy, Barcelona, Spain*

²*ITER Organization, St Paul-lez-Durance, France*

³*JAEA, Ibaraki, Japan*

⁴*Efremov Institute, St.Petersburg, Russian Federation*

Corresponding Author: patrick.lorenzetto@f4e.europa.eu

The current ITER Baseline foresees the use of carbon fibre composite (CFC) as armour material in the high heat flux strike point regions and tungsten (W) elsewhere in the divertor for the initial non-active phase of operation with hydrogen and helium plasmas. This divertor would then be replaced with a full-W divertor for the nuclear phase with deuterium and deuterium-tritium plasmas. To reduce costs the ITER Organization (IO) has proposed to install a full-W divertor from start of operations and to implement a work programme to develop a full-W divertor design, qualify the corresponding fabrication technology and investigate critical physics and operational issues with support from the R&D fusion community.

An extensive R&D programme has been implemented over more than 15 years to develop fabrication technologies for the procurement of ITER divertor components. Significant effort has been devoted to the development of reliable armour/heat sink joining techniques such as Hot Isostatic Pressing (Europe), Hot Radial Pressing (Europe) or brazing (Japan, Russia). In this development programme, established for the CFC/W divertor variant, the design solution for W-armoured components was optimized for the divertor baffle and dome regions, namely for steady state operation conditions at heat flux values of typically 5 MW/m² and for slow transient events at heat flux values up to 10 MW/m².

A very positive outcome of this R&D work has been that some fabrication technologies mentioned above can achieve much higher performances, close to the expected slow transient conditions for the strike point region (20 MW/m² for 10 s). To prepare for the procurement of a full-W divertor, a development work programme has been launched including in particular the manufacturing and high heat flux testing of small-scale mock-ups with improved monoblock geometries and full-W pre-qualification prototypes, and the manufacturing and testing of qualification full-size full-W vertical target prototypes. Further important R&D activities will study the behaviour of W-armoured components under combined normal (e.g., thermal fatigue) and off-normal heat loads (e.g., disruptions and ELMs) and the behaviour of recrystallized surfaces under combined plasma and thermal shock loading.

This paper will present the status of progress of this development work programme.

ITER Magnet Systems — from Qualification to Full Scale Construction

H. Nakajima¹

¹*Japan Atomic Energy Agency, Ibaraki, Japan*

Corresponding Author: nakajima.hideo@jaea.go.jp

The ITER requires superconducting magnet systems, which consist of 18 Toroidal Field (TF) coils, one Central Solenoid (CS), and 6 Poloidal Field (PF) coils, 18 (9 pairs) Correction Coils (CC), and additional components such as feeders, current leads, and instrumentation feedthroughs, and so on. Six Domestic Agencies (DAs), EURATOM (EU), China (CN), Japan (JA), Korea (KO), Russian Federation (RF), and United States of America (US), are involved in the procurement sharing of the components of the ITER magnet systems and their constructions have been implemented under more than 20 Procurement Arrangements (PAs) signed between the ITER Organization (IO) and 6 DAs.

During recent years, qualification activities have good progress and full scale constructions have been started in TF conductors. Four jacketing lines have been set-up and qualified in EU, CN, JA, and RF, and one jacketing line has been constructed in US. The JA, RF, CN, and KO/EU has already started full scale construction of TF conductors, especially, JA has completed 25 conductors by the end of March 2012. The latest topic is the delivery of the 660-m dummy conductor manufactured by CN to JA. It is the first ITER component completed in CN and also first shipment between DAs under cooperation with the IO, CN, and JA.

The qualification of radial plate manufacture has almost completed in both EU and JA, and both DAs are ready for full scale construction. JA has also qualified full manufacturing processes such as winding, heat treatment, insulation, and impregnation with a 1/3 prototype prior to the qualification by the full scale prototype. Two full scale mock-ups of basic segments of TF coil structure were manufactured in Phase II to optimize and industrialize manufacturing process of TF coil structure. A preparation of the full scale construction of TF coil winding is under way in EU manufacturer, and contracts for full scale construction of TF coil and structure will be placed in JA in July 2012.

A building for PF coil manufacture has been constructed in the ITER site in February 2012. The US and JA have started to manufacture dummy CS conductors with a collaborative work for trial winding in US. The constructions of other components of the ITER magnet systems are also going well toward to the first plasma in 2020.

Test Results of ITER Conductors in the SULTAN Facility

P. Bruzzone¹, B. Stepanov¹, R. Wesche¹, N. Mitchell², A. Devred², Y. Nunoya³,
V. Tronza⁴, K. Kim⁵, T. Boutboul⁶, N. Martovetsky⁷, and Y. Wu⁸

¹*Ecole Polytechnique Fédérale de Lausanne, Centre de Recherches en Physique des Plasmas,
Association EURATOM-Confédération Suisse, Villigen, Switzerland*

²*ITER Organization, St Paul Lez Durance, France*

³*Japan Atomic Energy Agency, Ibaraki, Japan*

⁴*ITER Centre, Moscow, Russian Federation*

⁵*National Fusion Research Institute, Daejeon, Republic of Korea*

⁶*Fusion for Energy, Barcelona, Spain*

⁷*Oak Ridge National Laboratory, Oak Ridge, USA*

⁸*Institute of Plasma Physics, Chinese Academy of Sciences, Hefei, China*

Corresponding Author: pierluigi.bruzzone@psi.ch

Starting March 2007, over 60 ITER cable-in-conduit conductors (CICC) have been tested in the SULTAN test facility in Villigen, Switzerland, including TF, CS, PF and busbars samples. The conductors are supplied by the ITER Domestic Agencies (DAs) and assembled into SULTAN samples at CRPP. The test reproduces the actual operating conditions in the ITER coils, except for the hoop load and the CS maximum field. Depending on the stage of the procurement, the SULTAN samples are categorized into Design Verification, Supplier Qualification, Process Qualification and Series Production. The number of remaining samples to be tested during the ITER construction phase is about 40.

For the NbTi CICC, the results confirm the prediction from the strand data, which are made taking the peak field over the conductor cross section as operating field. At low current density, where the n -index of the transition is measurable, the NbTi CICC and the NbTi strand have the same n -index. All the NbTi samples passed the supplier qualification phase.

For the Nb₃Sn CICC, the performance prediction is hindered by the irreversible degradation caused by filament damage occurring during cyclic loading. At the first run of the test campaign, the performance of all the Nb₃Sn samples largely meets the target. Contrary to the NbTi CICC case, the n -index of the transition is substantially lower than in the strands. The performance loss upon load cycles and thermal cycles has a broad range. All the TF conductor samples passed the supplier qualification phase. For the CS conductors, the supplier qualification phase will be finalized in 2012.



The ITER Blanket System Design Challenge

A. R. Raffray¹, B. Calcagno¹, P. Chappuis¹, F. Zhang¹, J. Chen², D.-H. Kim³,
S. Khomiakov⁴, A. Labusov⁵, A. Martin¹, M. Merola¹, R. Mitteau¹, S. Sadakov¹,
M. Ulrickson⁶, and F. Zacchia⁷

¹ITER Organization, St. Paul lez Durance, France

²Southwestern Institute of Physics, Chengdu, China

³ITER Korea, NFRI, Republic of Korea

⁴NIKIET, RF Domestic Agency, Russian Federation

⁵Efremov, RF Domestic Agency, Russian Federation

⁶Sandia National Laboratory, Livermore, USA

⁷Fusion for Energy, EU Domestic Agency, Barcelona, Spain

Corresponding Author: rene.raffray@iter.org

The blanket system is one of the most technically challenging components of the ITER machine, having to accommodate high heat fluxes from the plasma, large electromagnetic loads during off-normal events and demanding interfaces with many key components (in particular the vacuum vessel and in-vessel coils) and the plasma. Plasma scenarios impose demanding requirements on the blanket in terms of heat fluxes on various areas of the first wall during different phases of operation (inboard and outboard midplane for start-up/shut-down scenarios and the top region close to the secondary X-point during flat top) as well as large electro-magnetic (EM) loads and transient energy deposition during off-normal plasma events (such as disruptions and vertical displacement events (VDE)). The high heat fluxes resulting in some areas have necessitated the use of “enhanced heat flux” panels capable of accommodating an incident heat flux of up to 5 MW/m² in steady state. The other regions utilize “normal heat flux” panels, which have been developed and tested for a heat flux of the order of 1 – 2 MW/m². The FW shaping design requires a compromise between the conflicting requirements for accommodation of steady state and transient loads (energy deposition during off-normal events). A shaped surface increases the heat loads which are due to plasma particles following the field lines compared to a perfectly toroidal surface. The blanket provides a major contribution to the shielding of the vacuum vessel and coils. A challenging criterion is the need to limit the integrated heating in the toroidal field coil (TFC) to ~ 14 kW. This is particularly severe on the inboard leg where approximately 80% of the total nuclear heat on the TFC is deposited. Several design modifications were considered and analyzed to help achieve this, including increasing the inboard blanket radial thickness and reducing the assembly gaps. This paper summarizes the latest progress in the blanket system design as it proceeds through its final design phase, focusing in particular on the challenge of accommodating demanding and sometime conflicting design and interface requirements.

Commissioning and First Results of the ITER-Relevant Negative Ion Beam Test Facility ELISE

P. Franzen¹, B. Heinemann¹, U. Fantz¹, D. Wunderlich¹, W. Kraus¹, M. Frösche¹,
C. Martens¹, R. Riedl¹, B. Ruf¹, L. Schiesko¹, and C. Wimmer¹

¹*Max-Planck-Institut für Plasmaphysik, EURATOM Association, Garching, Germany*
Corresponding Author: peter.franzen@ipp.mpg.de

For heating and current drive the ITER NBI system requires a negative hydrogen ion source capable of delivering above 40 A of D^- ions for up to one hour pulses with an accelerated current density of 200 A/m². In order to limit the power loads and ion losses in the accelerator, the source must be operated at a pressure of 0.3 Pa at maximum and the amount of co-extracted electrons must not exceed the amount of extracted negative ions. As presently these parameters have not yet been achieved simultaneously, also due to a lack of adequate test facilities, the European ITER domestic agency F4E has defined an R&D roadmap for the construction of the neutral beam heating systems. An important step herein is the new test facility ELISE (Extraction from a Large Ion Source Experiment) for a large-scale extraction from a half-size ITER RF source which was constructed in the last 2 years at IPP Garching. The early experience of the operation of such a large RF driven source (1×1 m² with an extraction area of 0.1 m²) will give an important input for the design of the Neutral Beam Test Facility PRIMA in Padova and the ITER NBI systems and for their commissioning and operating phases. PRIMA consists of the 1 MeV full power test facility MITICA, operational 2017, and the 100 kV ion source test facility SPIDER, operational 2015.

The aim of the design of the ELISE source and extraction system was to be as close as possible to the ITER design; it has however some modifications allowing a better diagnostic access as well as more flexibility for exploring open questions. The extraction system is designed for the acceleration of 20 A of negative hydrogen ions of up to 60 kV. Plasma operation of up to one hour is foreseen; but due to the limits of the IPP HV system, pulsed extraction only is possible.

ELISE went into operation in spring 2012 with first plasma and beam pulses. The paper discusses critical issues of the manufacturing and describes the commissioning phases of the different subsystems with a special emphasis on the HV conditioning of the large grids. First results of the dependence of the plasma homogeneity on the magnetic filter field, measured by optical emission spectroscopy, are shown and compared with beam homogeneity measurements by calorimetry and beam emission spectroscopy.

Nuclear Analyses For ITER NB System

S. Sato¹, K. Ochiai¹, C. Konno¹, H. Morota², H. Nasif², M. Tanaka³, E. Polunovskiy³,
and M. Loughlin³

¹*Japan Atomic Energy Agency, Naka, Japan*

²*MHI Nuclear Engineering Company Ltd., Tokyo, Japan*

³*ITER Organization, Saint Paul Lez Durance, France*

Corresponding Author: sato.satoshi92@jaea.go.jp

Detailed nuclear analyses for the latest ITER NB system are required to ensure that NB design conforms to the nuclear regulations and licensing. A variety of nuclear analyses was conducted for the NB system including a tokamak building and outside the building by using Monte Carlo code MCNP5.14, activation code ACT-4 and Fusion Evaluated Nuclear Data Library FENDL-2.1. A special “Direct 1-step Monte Carlo” method is adopted for the shutdown dose rate calculation. The NB system and the tokamak building are very complicated, and it is practically impossible to make geometry input data manually. We used the automatic converter code GEOMIT from CAD data to MCNP geometry input data. GEOMIT was improved for these analyses, and the conversion performance was drastically enhanced. Void cells in MCNP input data were generated by subtracting solid cells data from simple rectangular void cells. The CAD data were successfully converted to MCNP geometry input data, and void data were also adequately produced with GEOMIT. The effective dose rates at external zones (non-controlled areas) should be less than 80 $\mu\text{Sv}/\text{month}$ according to French regulations. Shielding structures are under analysis to reduce the radiation streaming through the openings. We are confirming that the criterion is satisfied for the NB system. The effective dose rate data in the NB cell after shutdown are necessary to check the dose rate during possible rad-works for maintenance. Dose rates for workers must be maintained as low as reasonably achievable, and at locations where hands-on maintenance is performed should be below a target of 100 $\mu\text{Sv}/\text{h}$ at 12 days after shutdown. We are specifying the adequate zoning and area where hands-on maintenance can be allowed, based on the analysis results. The cask design for transport activated NB components is an important issue, and we are calculating the effective dose rates. The target of the effective dose rate from the activated NB components is less than 25 $\mu\text{Sv}/\text{h}$ at 30 cm from the outer surface of the iron cask.

Status of the Negative Ion Based Diagnostic Neutral Beam for ITER

B. Schunke¹, D. Bora¹, D. Boilson¹, J. Chareyre¹, H. Decamps¹, F. Geli¹,
R. Hemsworth¹, J. Graceffa¹, M. Urbani¹, D. Lathi¹, A. K. Chakraborty², U. Baruah²,
I. Ahmed², M. Bandyopadhyay², G. R. Nair², C. Rotti², S. Shah², M. Singh²,
N. P. Singh², A. Krylov³, and A. Panasenkov³

¹ITER Organization, St Paul lez Durance, France

²ITER-India, GIDC Electronic Estate, Gandhinagar, India

³Russian Research Centre, Kurchatov Institute, Moscow, Russian Federation

Corresponding Author: beatrice.schunke@iter.org

In ITER a dedicated 100 keV Diagnostic Neutral Beam (DNB) based on negative ion technology will be injecting 18 – 20 A of hydrogen to provide helium ash measurements via Charge Exchange Recombination Spectroscopy (CXRS). The CXRS diagnostics will also provide measurements of ion temperatures and other essential plasma parameters and the DNB will also be used for Beam Emission Measurements (BES). Recently on-axis Motional Stark Effect (MSE) has been proposed as an additional complementary diagnostics. Reliable DNB performance predictions are essential input parameters for the design of the diagnostic systems which will pass the conceptual design stage this year. They also assure the correct characterization of all ITER interfaces to allow safe operation of the ITER plant. The expected performance parameters of the system will be critically re-assessed taking into account the recently increased neutral edge density predictions in the plasma chamber. The DNB duty cycle will be discussed in detail, indicating all operational limitations identified in the design phase.

An overview of the current status of the DNB system and the interface constraints will be given. The consolidated design, including the recently updated magnetic field reduction system, will be presented and the most challenging design features highlighted. While the performance of the RF ion source — identical to the one used in the Heating Neutral Beams but operated at much more challenging current densities — will be demonstrated in the dedicated Ion Source Test Bed SPIDER in Padua, the full DNB Beamline will be demonstrated in the Indian Test Facility (INTF). The INTF will specifically allow far-field measurements to confirm the beam divergence and allow reliable predictions of the DNB power delivered to the plasma. This parameter is essential for obtaining dependable signal to noise estimates for the design of the diagnostic systems.

Procurement of the DNB Beamsources, part of the DNB power supplies and the proto-type DNB beamline components will start in 2012, while the INTF building premises are already available. The availability of the DNB as a diagnostic tool in the hydrogen/helium phase will be discussed shortly looking both at the shine through limitations and the commissioning planning to identify the earliest date the DNB will be available for CXRS measurements.

EU Development of the ITER Neutral Beam Injector and Test Facility

A. Masiello¹, G. Agarici¹, T. Bonicelli¹, F. Paolucci¹, M. Simon¹, D. Boilson²,
H. Decamps², J. Graceffa², B. Heinemann³, R. Hemsworth², M. Kuriyama²,
B. Schunke², L. Svensson², A. Luchetta⁴, P. Sonato⁴, V. Toigo⁴, and P. Zaccaria⁴

¹*Fusion for Energy, Barcelona, Spain*

²*ITER, ITER Joint Work Site, CEA Cadarache, St. Paul Lez Durance, France*

³*IPP, Garching, Germany*

⁴*Consorzio RFX, Padova, Italy*

Corresponding Author: antonio.masiello@f4e.europa.eu

The activities towards the establishment of the NB Test Facility (NBTF) in Padova Italy and those related to the procurement of the heating neutral beams for ITER have recently reached a good level of progress thanks to the finalization of the agreements on the NBTF between F4E (the EU Domestic Agency for ITER), Consorzio RFX (the host of the NB test facility) and the ITER organization. This paper presents the status of the design of the various components within the EU scope of procurement, with a focus on the modifications implemented in the last years as a result of intense R&D activity undertaken in EU.

Development of ITER Equatorial EC Launcher

K. Takahashi¹, K. Kajiwara¹, Y. Oda¹, N. Kobayashi¹, K. Sakamoto¹, T. Omori², and M. Henderson²

¹*Japan Atomic Energy Agency, Naka, Japan*

²*ITER Organization, St. Paul lez Durance, France*

Corresponding Author: takahashi.koji@jaea.go.jp

The present day EC launcher typically injects a few MW power and the pulse length is 10–20 s. On the other hand, the ITER equatorial EC launcher is making an advanced technology to injecting ≥ 20 M and CW operation. The ITER equatorial EC launcher consists of an unique blanket shield structure and a port plug installing millimeter (mm) wave components, neutron shields, cooling water lines and so on. The design of the blanket shield structure that tolerates thermal and electromagnetic load is attained. The mm-wave design that enables to guide the wave power of 20 MW into plasma with toroidal steering capability of $20^\circ - 40^\circ$ and efficiency of 98.4–99% assuming HE11 fundamental wave mode + TEM000 gaussian mode are described. Reduction of the heat load to 2.1 MW/m² on the steering mirror and the optimization of beam radius at plasma, 16–22 cm that satisfies the requirement, are attained. The mock-up of the mm-wave launching system and the subcomponents are fabricated to investigate the design availability. High power (0.5 MW) experiment of the mock-up confirmed the expected wave beam propagation and steering capability.

Optimization of the EC Heating and Current Drive Capabilities

M. Henderson¹, Fusion for Energy Collaborators², and JA-DA, IN-DA, USIPO³

¹ITER Organization, Saint Paul Lez Durance, France

²Fusion for Energy, EU Associations, EU

³Japan Atomic Energy Agency, Naka, Japan

Corresponding Author: mark.henderson@iter.org

A 24 MW CW Electron Cyclotron Heating and Current Drive (EC H&CD) system operating at 170 GHz is to be installed for the ITER tokamak. The ITER EC system will represent a large step forward in the use of microwave systems for plasma heating and current drive applications. Present day systems are operating in relatively short pulses (≤ 10 s) and installed power levels of ≤ 4.5 MW, while the ITER EC system parameters are CW operation and 20 MW injected power. The technical challenge facing the development and installation of the EC system is further complicated due to the harsh ITER in-vessel environment and complicated procurement strategy. The ITER EC international community has confronted these challenges, aiming at integrating the modifications proposed from the 2007 ITER design review and further enhancing the EC system capabilities. These changes have not only simplified the technical design, but have also simplified the procurement interfaces and increased the functional capabilities for plasma heating and current drive applications. The functional improvements include increasing the access of the EC power from $\sim 50\%$ to nearly $\sim 90\%$ of the plasma cross section. In particular the UL has been modified to allow power deposition over the range of $\sim 0.3 \leq \rho_T \leq 0.9$ compared to previous access of $\sim 0.55 \leq \rho_T \leq 0.85$ (where ρ_T is the square root of the normalized toroidal flux). This allows the UL to be applicable for a broader access for stabilization of neoclassical tearing modes (NTMs) and sawtooth instability. The EC heating is functionally limited in magnetic field region depending on the resonant harmonic. The heating access in ITER was assumed to be applicable over $\sim 33\%$ of the range from 2.3 T to 5.3 T, regions of fundamental and second harmonics. Recent analysis associated with the EL has demonstrated that the EC system is applicable over a much broader range: $\sim 75\%$ for central heating ($\rho_T \leq 0.5$) and $\sim 90\%$ for L to H-mode assist ($\rho_T \leq 0.85$). Further improvements to the EC system are now being considered, which include adapting the PS to accommodate future higher power gyrotrons (≥ 1.2 MW) and modifying the sweeping direction of the EL from a toroidal to poloidal steering more than doubling the driven current in the region of $0.4 \leq \rho_T \leq 0.6$. These and other improvements under study will be reviewed in this paper.

Validation of the RF Properties and Control of the ITER ICRF Antenna

P. Dumortier¹, F. Durodié¹, D. Grine¹, V. Kyrtsya¹, F. Louche¹, A. Messiaen¹,
M. Vervier¹, and M. Vrancken¹

¹*LPP-ERM/KMS, Brussels, Belgium*

Corresponding Author: pierre.dumortier@rma.ac.be

One ITER ICRF antenna consists of a close-packed array of 24 straps arranged in a 6 poloidal by 4 toroidal array. Three poloidally adjacent straps (a “triplet” of straps) are fed in parallel from one single feeding line through a 4-port junction. A shunt service stub is inserted on the feeding line inside the antenna. It has been optimized to provide a broad-band RF frequency response of the array. Load tolerance is achieved by feeding each pair of two poloidal triplets through a 3dB hybrid coupler. The array has to radiate 20 MW of RF power (with a 45 kV limit on the system) in quasi-CW operation for frequencies ranging from 40 MHz to 55 MHz and different toroidal phasings to provide a wave spectrum appropriate for both heating and current drive. Two identical ICRF antennas are foreseen on ITER.

In order to gain confidence in the design options the RF properties of the ITER ICRH antenna array are experimentally validated on reduced-scale mock-ups of part or of the whole antenna array. Experimental measurements allow to check the optimization of the antenna front-end geometry, to confirm the RF frequency response of the antenna array and hence the expected performance of the antenna for the different proposed phasings, to verify the impact of critical parameters as the vertical septum recess on the coupling properties of the antenna as well as on the mutual coupling terms and finally to test and validate the proposed grounding options to the vessel.

An overview of the experimental measurement results on the different mock-ups is given. Comparisons with simulations performed by various codes (Topica, CST MWS and ANTITER II) are given together with the expected performance on plasma deduced from measurements with dielectric load. The effect of limitations (voltage, current) on the maximum total radiated power is discussed. The importance of a good decoupling network and of grounding is emphasized.

Finally the control of the antenna wave spectrum and of the matching is performed by implementing a feedback control of the matching-decoupling system close to the one foreseen for ITER on a low-power reduced-scale mock-up of the whole ITER ICRH antenna array. It uses 23 feedback loops simultaneously operated. Control algorithms are developed and tested together with the stability of the system.

This work was performed under the F4E grant F4E-2009-GRT-026.

RF Optimization of the Port Plug Layout and Performance Assessment of the ITER ICRF Antenna

F. Durodié¹, M. Vrancken¹, R. Bamber², P. Dumortier¹, D. Hancock², D. Lockley²,
R. Maggiora³, F. Louche¹, A. Messiaen¹, D. Milanese³, M. Nightingale², M. Shannon²,
P. Tigwell², M. Van Schoor¹, D. Wilson², K. Winkler⁴, and CYCLE Team^{1,2,3,4,5}

¹LPP/ERM-KMS, Association EURATOM-Belgian State, Brussels, Belgium

²EURATOM/CCFE Association, Culham Science Centre, Abingdon, UK

³Associazione EURATOM-ENEA, Politecnico di Torino, Torino, Italy

⁴IPP-MPI, EURATOM-Assoziation, Garching, Germany

⁵Association EURATOM-CEA, DSM/IRFM, Cadarache, France

Corresponding Author: frederic.durodie@rma.ac.be

ITER ICRF antenna's capability to couple power to plasma is determined by the plasma Scrape-Off Layer (SOL) profiles, shaping of the front strap array, organized as a 6 poloidal by 4 toroidal array of short straps, overall layout of the feed network and detailed design of its RF components. The first two factors are taken into account in the TOPICA [1] calculated strap array 24×24 S/Z -matrices. This data is coupled to a RF circuit model of the strap feeding circuit of which the components are S/Z matrices calculated with CST Microwave Studio (MWS) [2], such as the 4 Port Junction (4PJ) which combines 3 poloidally adjacent straps so as to obtain a 2 poloidal by 4 toroidal array of triplets, or simple Transmission Line (TL) sections for the rest of the Removable Vacuum Transmission Line (RVTL) which include the Service Stub tee (SST) and Vacuum Ceramic Windows (VCW).

The RF feeding circuit inside the port plug is optimized in order to maximize the power coupled to the plasma for the various phasings considered for operation. This takes into account geometrical constraints, assembly requirements and RF quantities (E-field less than 2 kV/mm along the magnetic field in the torus vacuum areas and less than 3 kV/mm perpendicular to the magnetic field and private vacuum areas, voltages less than 45 kV and currents through RF contacts less than 2 kA).

The ITER-Like Antenna on JET results obtained in 2008-9 [3] support the proposed design by having validated the TOPICA coupling estimations as well as demonstrated that there were no unforeseen difficulties in operating at 42 kV and power densities in the range required by ITER in terms of reliability and possible ICRF impurity production.

The effect of the RF grounding of the Front Housing Module, carrying 2 toroidally adjacent triplets, as well as the grounding of the whole antenna port plug to the vessel is analyzed as well in conjunction with the Blanket Shielding Modules surrounding the antenna.

References

- [1] V. Lancellotti *et al.*, "TOPICA: an Accurate and Efficient Numerical Tool for Analysis and Design of ICRF Antennas", Nuclear Fusion, Vol. 46 (2006) S476-S499.
- [2] CST GmbH, CST Microwave Studio, User Manual (2011).
- [3] F. Durodié *et al.*, "Latest Achievements of the JET ICRF Systems in View of ITER", 23rd IAEA FEC, Daejeon, Republic of Korea, (2010).

On the Use of Lower Hybrid Waves at ITER Relevant Density

A. A. Tuccillo¹, V. Pericoli Ridolfini¹, Y. Baranov², R. Cesario¹, M. Goniche³,
A. E. Hubbard⁴, L. Amicucci¹, J. F. Artaud³, S. G. Baek⁴, E. Barbato¹, V. Basiuk³,
G. Berger-By³, P. Bonoli⁴, G. Calabro¹, A. Cardinali¹, C. Castaldo¹, S. Ceccuzzi¹,
J. Decker³, F. Di Napoli¹, B. J. Ding⁵, A. Ekedahl³, J. Gunn³, J. Hillairet³, K. Kirov²,
J. Mailloux², O. Meneghini⁴, F. C. Mirizzi¹, R. Parker⁴, Y. Peysson³, F. Santini¹,
S. Shiraiwa⁴, G. Wallace⁴, and B. N. Wan⁵

¹Associazione EURATOM-ENEA, CR ENEA-Frascati, Roma, Italy

²Euratom/CCFE Fusion Association, Culham Science Centre, Abingdon, UK

³CEA, IRFM, St-Paul-Lez-Durance, France

⁴MIT, Cambridge, USA

⁵Institute of Plasma Physics, Chinese Academy of Science, Hefei, China

Corresponding Author: angelo.tuccillo@enea.it

Collisional Absorption (CA), Parametric Instabilities (PI) and Scattering from Density Fluctuations (SDF) can preclude the penetration of Lower Hybrid (LH) waves, dissipating the power in the plasma periphery. A multi-machine assessment started at the end of 2009 under the coordination of ITPA-IOS group. It aims at understanding the complex physics underlying the phenomenon and increasing confidence in LH modeling for ITER's advanced scenarios. Results from C Mod, FTU, HT-7, JET and Tore Supra will be reported, while results from EAST are expected in the near future. The reported experiments have relevant plasma and waves parameters that encompass ITER's. Limiter and divertor operations are included, as well as operation with metallic and carbon walls, with plasma edge conditioned by wall boronisation and, on FTU, by using liquid lithium. Experiments on FTU show that LH waves at 8 GHz does penetrate bulk plasmas, with density profiles even higher than those expected in ITER, only if operating with the increased edge electron temperature provided by operating with lithized walls. The reduced broadening of the launched spectrum, as detected by loop antennas, suggests a PI influence. C-Mod detects an improved penetration of LH waves at 4.6 GHz, at relatively high density, when edge electron temperature is higher and absorption condition is closer to single-pass. This trend is qualitatively reproduced in both ray tracing and full wave model as reduced effect of CA due to increased single pass absorption. A gradual shift of 3.7 GHz LH power deposition to the periphery, is observed in JET with increasing density. Reduced density and increased pedestal temperature lead to broader but still very peripheral absorption. Decrease of LH effects, at 3.7 GHz in Tore Supra, correlates with increasing edge fluctuations, suggesting a role of SDF. LH experiments at the lowest frequency of 2.45 GHz on HT-7 did not find anomalies, at moderate density, in discharges with Li and B coatings. From the available information a preliminary conclusion on encouraging trend can be inferred for ITER. There will be a high edge temperature that helps avoid PI and SDF while LH waves will clearly be in single pass regime, minimising CA. A strong modelling effort is nevertheless progressing to reproduce the experimental evidence with physics models to strengthen the prediction for ITER.

Self-consistent Simulation of Plasma Scenarios for ITER Using a Combination of 1.5 D Transport Codes and Free Boundary Equilibrium Codes

V. Parail¹, D. McDonald¹, R. Albanese², R. Ambrosino², J. F. Artaud³, K. Besseghir⁴,
M. Cavinato⁵, G. Corigan¹, L. Garzotti¹, Y. Gribov⁶, F. Imbeaux³, J. Garcia³,
F. Koechl⁷, C. Labate², J. Lister⁴, X. Litaudon³, A. Loarte⁶, P. Maget³, E. Nardon³,
G. Saibene⁵, R. Sartori⁵, and J. Urban³

¹Euratom/CCFE Fusion Association, Culham Science Centre, UK

²Association EURATOM-ENEA-CREATE, Padova, Italy

³CEA, IRFM, St Paul-Lez-Durance, France

⁴Association EURATOM-Confédération Suisse, Lausanne, Switzerland

⁵Fusion for Energy, Barcelona, Spain

⁶ITER Organisation, St Paul-Lez-Durance, France

⁷Association EURATOM-ÖAW/ATI, Atominstitut, TU Wien, Austria

Corresponding Author: vassili.parail@ccfe.ac.uk

Self-consistent transport simulation of ITER scenarios is an important tool for the exploration of the operational space and for scenario optimisation. It also provides an assessment of the compatibility of developed scenarios (which include fast transient events) with machine constraints, in particular with the poloidal field (PF) coil system, heating and current drive (H& CD), fuelling and particle and energy exhaust systems. Credible prediction of the plasma and plasmas systems behaviour can only be achieved when the best combination of high quality transport codes, using the most advanced theory-based transport models, are combined with state of the art free boundary equilibrium codes.

This paper summarises results of predictive modelling of all reference ITER scenarios with two EU suites of transport and free boundary codes. Modelling of 15 MA baseline DT scenario with $Q = 10$ and its variants was mostly based on GLF23 for the H-mode part of scenario, combined with the explicit modelling of edge barrier and type-I ELMs. The L-mode phase was simulated with Bohm/gyroBohm model. One of the novel elements was predictive modelling of fast transient phenomena, such as L-H and H-L transitions as well as predictive modelling of D and T densities and He ash accumulation. Self-consistent simulations of fast transients revealed potential difficulty for ITER PF position control system to maintain the plasma-inner wall distance during fast uncontrolled H-L transition, due to voltage saturation in the CS.

Since Hybrid and Steady State (SS) scenarios have less established theoretical and experimental basis, their predictive simulation rely more on ad-hoc assumptions about heat and particle transport inside the edge barrier. It was assumed that hybrid scenario has heat transport which ensures energy confinement time with $H_{98}(y, 2) = 1.3$ during the flat top burn. The main emphasis of the simulation was on the selection of the heating and current drive scheme to ensure that q_{\min} stays above 1 for at least 1000 s. Also, the ability of ITER PF system to sustain fast transient phenomena (such as sudden loss of the internal transport barrier in SS scenario) as well as the control of MHD stability was studied.

Demonstrating the ITER Baseline Operation at $q_{95} = 3$

A. C. C. Sips^{1,2}, G. Jackson³, J. Schweinzer⁴, S. Wolfe⁵, J. Hobirk⁴, H. Hoehnle⁶,
A. Hubbard⁵, E. Joffrin⁷, C. Kessel⁷, P. Lomas⁸, T. Luce³, I. Nunes⁹, J. Stober⁴,
JET EFDA Contributors¹⁰, DIII-D Team³, ASDEX Upgrade Team⁴, and
Alcator C-Mod Team⁵

¹JET-EFDA, Culham Science Centre, Abingdon, UK

²European Commission, Brussels, Belgium

³General Atomics, San Diego, USA

⁴Max-Planck-Institut für Plasmaphysik, EURATOM-Association, Garching, Germany

⁵Massachusetts Institute of Technology, Plasma Science and Fusion Center, Cambridge, USA

⁶Institut für Plasmaforschung, University Stuttgart, Stuttgart, Germany

⁷Association Euratom-CEA, Cadarache, Saint Paul Lez Durance, France

⁸EURATOM/UKAEA Fusion Association, Culham Science Centre, Abingdon, UK

⁹Euratom/IST Fusion Association, Centro de Fusao Nuclear, Lisboa, Portugal

¹⁰JET-EFDA, Culham Science Centre, Abingdon, UK

Corresponding Author: george.sips@jet.efda.org

ITER requires robust operation of various plasma scenarios within the hardware constraints of the device. Operation in H-mode at 15 MA and $q_{95} = 3$ is planned to achieve $Q = 10$ in deuterium-tritium mixtures. The Integrated Operation Scenario Topical Group of the ITPA has coordinated experiments in C-Mod, ASDEX Upgrade, DIII-D and JET to obtain optimum data assessing H-mode scenarios at $q_{95} \sim 3$. Previous results for the plasma formation at low loop voltage and the ramp-up phase were reported.

Recent joint studies on the flat top and ramp down phase show that entering H-mode is generally observed at $P_{\text{tot}}/P_{\text{L-H}} \sim 1$. Regular ELMing H-modes achieving $H_{98} \sim 1$ require $P_{\text{tot}}/P_{\text{L-H}} = 1.3 - 2$ at JET, for I_p up to 4.5 MA, in DIII-D regular ELMing H-modes are only achieved at higher plasma β ($\beta_N = 2.0$), while in C-Mod $P_{\text{tot}}/P_{\text{L-H}} \sim 1$ is only achieved in stationary H-modes at high input power and higher radiation fraction using seeding. JET data show no significant difference in plasma performance or temperature and density profile shapes when using ion cyclotron heating compared to neutral beam heating, despite the rotation profile changing dramatically when the co-neutral beam is reduced to zero. For H-modes at high plasma current, some experiments only reach $n_e/n_{\text{GW}} \sim 0.65 - 0.7$ using gas fuelling. At DIII-D the stability of long pulse operation at $q_{95} = 3$, shows susceptibility to $n = 1$ tearing modes. The current ramp down requires H-mode combined with a reduction in plasma elongation to control the plasma inductance excursion without additional flux consumption, for ohmic or L-mode discharges a stronger reduction in elongation would be required.

The experimental data presented provide important input for benchmarking integrated code simulations using sophisticated models for transport and heating or current drive systems; moreover they give additional confidence and insight into the possible operation domain of the baseline plasma scenario in ITER.

JET EFDA Contributors: See the Appendix of F. Romanelli *et al.*, Proceedings of the 23rd IAEA Fusion Energy Conference 2010, Daejeon, Republic of Korea

Modelling of ITER Plasma Shutdown with Runaway Mitigation Using TSC

I. Bandyopadhyay¹, M. Sugihara², S. C. Jardin³, and A. K. Singh¹

¹*ITER-India, Institute for Plasma Research, Gandhinagar, India*

²*ITER International Organisation, Saint Paul Lez Durance, France*

³*Princeton Plasma Physics Laboratory, Princeton, USA*

Corresponding Author: indranil.bandyopadhyay@iter-india.org

Fast shutdown of an ITER plasma discharge without generating large runaway current has been an area of active research over the past several years. In ITER, during the thermal quench preceding the current disruption, the toroidal electric field can resistively grow to values about 50 times the critical electric field for runaway current generation, which can give rise to avalanche generation of runaway electrons with energies up to 15 MeV and currents of unprecedented magnitude of more than 10 MA, causing potential damage to the ITER first wall. Such a scenario can be avoided by rapidly increasing the plasma electron density by about 50 – 60 times, close to Rosenbluth density values, by which the toroidal electric field remains lower than the critical electric field. In this case, the runaway electrons are slowed down through collisional processes, suppressing the runaway current. In this paper we have carried out simulations for ITER plasma shutdown using both impurity doped deuterium pellets using the TSC code. The pellet model of TSC is also extended to approximately model massive gas injection into ITER plasmas. Using pellet initial radius of 5 mm and initial pellet velocity of 500 m/s and repetition frequency of around 100 Hz launched from the outboard mid-plane, we have explored possibilities of safe plasma shutdown without large runaway current generation. The MGI is modeled in TSC by a train of 3 – 5 large pellets of pure neon with total number of atoms equal to that in a gas jet cartridge is injected with velocity of 500 m/s. The major difference between a pellet and a gas jet in the low ablation rate of the pellets, especially at low target T_e , is overcome by artificially increasing the ablation rate to such an extent that the entire pellet atoms are ablated by the time it crosses the $q = 2$ surface. We are carrying out detailed parametric study of the ITER plasma shutdown in the wide parameter space of pellet impurity content, number of injected pellets, radius of the pellets etc. The relative merits and issues with the different options will be discussed.

CORSICA Modelling of ITER Hybrid Mode Operation Scenarios

S. H. Kim¹, T. A. Casper¹, D. J. Campbell¹, J. A. Snipes¹, L. L. LoDestro²,
W. H. Meyer², and L. D. Pearlstein²

¹ITER Organization, St Paul lez Durance, France

²Lawrence Livermore National Laboratory, Livermore, USA

Corresponding Author: sunhee.kim@iter.org

The hybrid mode operation observed in several tokamaks is characterized by further enhancement over the high plasma confinement (H-mode) associated with reduced MHD instabilities linked to a stationary flat safety factor (q)-profile in the core region. The proposed ITER hybrid mode is currently aiming at operating for a long burn duration (> 1000 s) with a moderate fusion power multiplication factor, Q , of at least 5. This paper presents candidate ITER hybrid mode operation scenarios developed using a free-boundary transport modelling code, CORSICA, taking relevant physics and engineering constraints into account. First, we have developed a 12.5 MA ITER hybrid mode operation scenario by tailoring the 15 MA ITER inductive H-mode scenario. Second, we have studied accessible operation conditions and achievable range of plasma parameters. ITER operation capability for avoiding the poloidal field (PF) coil current, field and force limits are examined by applying different current ramp rates, flat-top plasma currents and densities, and pre-magnetization of the PF coils. Various combinations of heating and current drive (H&CD) schemes have been applied to investigate several physics issues, such as the plasma current density profile tailoring, enhancement of the plasma energy confinement and fusion power generation. A parameterized edge pedestal model based on EPED1 was recently added to the CORSICA code and applied to hybrid scenarios. Finally, fully self-consistent free-boundary transport simulations have been performed to provide information on the PF coil voltage demands and to study the controllability with the ITER controllers.



Disruption Impacts and their Mitigation Target Values

M. Sugihara¹, S. Putvinski¹, D. Campbell¹, S. Carpentier-Chouchana¹, F. Escourbiac¹,
S. Gerasimov², Y. Gribov¹, T. Hender², T. Hirai¹, K. Ioki¹, R. Khayrutdinov³,
H. Labidi¹, V. Lukash³, S. Maruyama¹, M. Merola¹, R. Mitteau¹, S. Miyamoto⁴,
J. Morris², G. Pautasso⁵, R. Pitts¹, R. Raffray¹, V. Riccardo², R. Roccella¹,
G. Sannazzaro¹, T. Schioler¹, J. Snipes¹, and R. Yoshino¹

¹ITER Organization, St. Paul lez Durance, France

²CCFE, Culham Science Centre, Abingdon, UK

³NRC "Kurchatov Institute", Moscow, Russian Federation

⁴Japan Atomic Energy Agency, Naka, Japan

⁵Max-Planck-Institut für Plasmaphysik, Garching, Germany

Corresponding Author: masayoshi.sugihara@iter.org

Major disruptions (MD) and vertical displacement events (VDE) in ITER will be the cause of a variety of deleterious impacts due to the high stored thermal and magnetic energy. Extrapolation from the disruption database obtained on current tokamaks and the results of numerical simulations, demonstrate that the thermal loads which will be produced during the thermal quench (TQ) of MD and VDEs in ITER, will lead to large scale macroscopic melting of metallic plasma-facing components (PFC). During the current quench (CQ) phase, runaway electrons (RE) are expected to deposit severe thermal loads on PFCs. The electromagnetic (EM) loads due to halo and eddy currents during the CQ are a critically important factor in the mechanical design of the vacuum vessel (VV) and in-vessel components (IVC).

For reliable operation and machine protection in ITER, mitigation of these heat and EM loads and REs during MDs and VDEs is mandatory. It is essential to realize high performance in the following three elements simultaneously for reliable mitigation:

1. High mitigation performance factor (high reduction of impact).
2. High prediction performance (high success rate simultaneously with low false rate).
3. Low disruptivity (by passive and active disruption avoidance).

Proper target values of each element are of primary importance to achieve the overall mitigation performance required in ITER and to promote the physics R&D for the development of mitigation, prediction and avoidance systems and algorithms. In this paper, we will quantify proper target values for each element of mitigation based on the assessment of the impacts by heat and EM loads and REs using physics databases and modeling for the present ITER design. Key components like VV, IVC and PFC will be carefully examined to quantify these requirements.

Development of ITER Scenarios for Pre-DT Operations

T. Casper¹, D. Campbell¹, V. Chuyanov¹, Y. Gribov¹, T. Oikawa¹, A. Polevoi¹,
J. Snipes¹, R. Budny², I. Voitsekhovitch³, and P. Bonoli⁴

¹ITER Organization, St. Paul-lez-Durance, France

²Princeton University, Princeton, USA

³Euratom-CCFE, Culham Science Center, Abingdon, UK

⁴Massachusetts Institute of Technology, Cambridge, USA

Corresponding Author: thomas.casper@iter.org

In preparation for the full deuterium-tritium (DT) operation in ITER, a significant period of experimentation will be dedicated to plasma operations that generate no or minimal activation products. This operation would utilize plasmas with helium (He) or hydrogen (H) gas species since these generate no fusion reactions producing tritium or neutrons that result in materials activation. Present planning also includes consideration for deuterium (D) operation with possibly short pulse duration to limit the production of tritium and activation from DD fusion reaction neutrons. Low-activation operation is needed to qualify all major mechanical and electrical subsystems before reliance on remote handling capability. Access to and sustainment of the high-confinement mode (H-mode) must be demonstrated with sufficient control of edge localized modes to limit the power flow to the divertor. Results from time-dependent 2-dimensional equilibrium with 1-dimensional transport predictive simulations explore possible operating scenarios. Simulations in current flat top evaluate steady performance to determine the parameter operating space at full plasma current $I_P = 15$ MA and magnetic field $B_T = 5.3$ T and for reduced performance at 7.5 MA and 2.65 T. In addition to baseline neutral beam injection and electron cyclotron heating, techniques for application of ion cyclotron heating under steady conditions are presented. Full duration time-dependent simulations with start-up limited on the inside wall, I_P ramp up to full current, flat top burn, and I_P ramp down to develop controllable operating scenarios in H and D are presented. With present understanding of H-mode threshold scaling, the proposed auxiliary heating power level of 63 MW (nominal) should allow access to H-mode operation in helium at 7.5 MA/2.65 T. Access to H-mode in pure H-plasmas would be, at best, marginal. Time-dependent free-boundary equilibrium simulations using controllers for the baseline operation indicate there is sufficient capability in the coil system to produce and control short pulse flat top plasmas suitable to validate physics and engineering systems before DT operation. These simulations are completed under a joint modeling effort in the Integrated Operations Scenarios (IOS) group of the International Tokamak Physics Activity (ITPA).

ITER Plasma Position Control System and Scenario Optimization

M. Cavinato¹, G. Ambrosino², R. Ambrosino³, Y. Gribov⁴, F. Koechl⁵, M. Mattei⁶,
A. Pironti², G. Saibene¹, R. Sartori¹, and L. Zabeo⁴

¹*Fusion For Energy, Barcelona, Spain*

²*CREATE/ENEA/Euratom Association, Università di Napoli, Naples, Italy*

³*CREATE/ENEA/Euratom Association, Università di Napoli Parthenope, Naples, Italy*

⁴*ITER Organization, St Paul Lez Durance, France*

⁵*Association EURATOM-ÖAW/ATI, Atominstitut, Wien, Austria*

⁶*CREATE/ENEA/Euratom Association, Seconda Università di Napoli, Naples, Italy*

Corresponding Author: mario.cavinato@f4e.europa.eu

The ITER machine is reaching a stage in which the design is in large part frozen. Nevertheless design changes are necessary in the procurement phase due to additional constraint linked to manufacturing techniques and/or cost containment. In this framework, the reference ITER scenario and the control system strategy are in continuous evolution. The aim is preserving the final goal of a 15 MA $Q = 10$ burning plasma in ITER, which will require a careful optimization of the scenario in order to fully exploit the machine capabilities within the engineering limits which define and restrict the operational space available.

This paper presents a summary of the activities carried out within the EU-DA on the engineering optimization of the ITER plasma scenarios and of the magnetic plasma position control system strategy.

Integrated Modelling of ITER Hybrid Scenarios Including Momentum Transport, NTMs, and ELMs in Preparation for Active Control

Y. S. Na¹, H. S. Kim¹, K. Kim¹, W. Lee¹, J. Lee¹, L. Terzolo², O. Kwon³, and T. S. Hahm¹

¹*Seoul National University, Seoul, Republic of Korea*

²*National Fusion Research Institute, Daejeon, Republic of Korea*

³*Daegu University, Gyungbuk, Republic of Korea*

Corresponding Author: ysna@snu.ac.kr

Hybrid scenario is an operational regime designed to achieve a long pulse operation with a combination of inductive and non-inductive current drive. It was suggested for the operation of ITER to allow high fusion power in long pulse operations over 1000 s at a plasma current lower than the inductive reference scenario. Engineering tests of reactor-relevant components, such as breeding blankets are planned to perform in this scenario.

Here, we report integrated simulation results of ITER hybrid scenario including momentum transport, neoclassical tearing mode (NTM), and edge localised mode (ELM). In this work, ASTRA is used for integrated simulations of plasma equilibrium, transport, heating and current drive, and magnetic island evolution, self-consistently. Firstly, the effect of toroidal rotation to confinement is addressed by solving the momentum transport equation including inward pinch, turbulent transport and residual stress. Secondly, the ELM activities are simulated and the pedestal height of ITER hybrid scenario is predicted. Lastly, the NTM activities are simulated and the capability of the ECH upper launcher is evaluated. The methodology of simulations presented can be applied to design feedback controllers for ELMs and NTMs in ITER.

Challenges in Burning Plasma Physics: the ITER Research Plan

D. Campbell¹, ITER Collaborators¹

¹*ITER Organization, St-Paul-lez-Durance, France*

Corresponding Author: david.campbell@iter.org

Following First Plasma, currently scheduled for late 2020, the ITER project aims to develop the capability for DT operation as rapidly as possible in order to address the key mission goal of demonstrating long pulse operation at $Q \geq 10$ with approximately 500 MW of fusion power. The ITER Research Plan (IRP) has been developed to analyze the experimental programme necessary to develop ITER's operational capability from First Plasma to the achievement of the $Q \geq 10$ mission goal. It integrates the experimental activities required to develop a robust capability for high current (15 MA) H-mode operation using DT fuel and, incorporating the planned schedule for the installation and commissioning of ITER auxiliary and plant systems, develops a schedule to allow full DT operation in late 2027 and the exploration of high fusion gain DT plasmas in 2028.

The experimental programme is foreseen to develop through 3 phases: H/He (non-active), D and DT (nuclear). During the first phase, all systems necessary for operation at full technical performance (15 MA/ 5.3 T) will be commissioned and integrated into plasma operation to establish the plasma operating regimes and the plasma control capability required to provide a robust basis for the transition to DT Operation. A second, relatively short, phase in deuterium completes the plasma commissioning activities, allows H-mode operation to be extended to high current and DT relevant parameters, and initiates the transition to full DT operation via a series of "trace tritium" experiments.

The experimental programme on high fusion power DT scenarios to be explored in the third phase of operations must address several challenges in burning plasma physics to achieve and sustain the necessary level of fusion performance to satisfy the $Q \geq 10$ mission goal. The paper will discuss the key physics issues to be resolved, the elements of the experimental programme foreseen to address them and the opportunities for burning plasma research which the experimental programme will provide.

Tokamak Experiments to Study the Parametric Dependences of Momentum Transport

T. Tala¹, R. McDermott², J. Rice³, A. Salmi¹, W. Solomon⁴, C. Angioni², G. Chi³,
C. Giroud⁵, J. Ferreira⁶, S. Kaye⁴, P. Mantica⁷, G. Tardini², Y. Podpaly³, F. Ryter²,
M. Yoshida⁸, JET EFDA Contributors⁹, ASDEX Upgrade Team⁹, DIII-D Team⁹,
Alcator C-Mod Team⁹, and NSTX Research Team⁹

¹Association Euratom-Tekes, VTT, Finland

²Max-Planck-Institut für Plasmaphysik, EURATOM-Association, Garching, Germany

³MIT, Plasma Science and Fusion Center, Cambridge, USA

⁴Princeton Plasma Physics Laboratory, Princeton University, Princeton, USA

⁵EURATOM/CCFE Fusion Association, Culham Science Centre, Abingdon, UK

⁶Associação EURATOM/IST, Instituto de Plasmas e Fusão Nuclear, Lisbon, Portugal

⁷Istituto di Fisica del Plasma CNR-EURATOM, Milano, Italy

⁸Japan Atomic Energy Agency, Naka, Japan

⁹JET-EFDA, Culham Science Centre, Abingdon, UK

Corresponding Author: tuomas.tala@vtt.fi

Momentum transport and plasma rotation have been studied extensively on many tokamaks in recent years. Numerous experimental results have been reported on individual devices — yet no dedicated multi-machine momentum transport experiments have been performed. This paper reports dedicated scans to study momentum transport that have been carried out on JET, DIII-D, AUG, NSTX and C-Mod within the ITPA framework.

NBI modulation technique to create a periodic rotation perturbation has been exploited on JET, DIII-D and AUG from which the convective velocity v_{pinch} and diffusion coefficient χ_ϕ profiles are determined. On NSTX, 50 ms pulses of $n = 3$ non-resonant magnetic fields were applied to extract v_{pinch} and χ_ϕ profiles. On C-Mod, either ICRH modulation or septum sweeping between the lower and upper null configurations was applied to create the rotation perturbation.

A 3-point collisionality ν^* scan by varying collisionality by a factor of 4 – 5 while keeping the other dimensionless quantities, such as ρ^* , β_N , q , R/L_n and T_i/T_e , as constant as possible (10 – 20% variation), has been performed independently both on JET and DIII-D in L-mode plasmas. Neither the pinch nor the Prandtl number depends on collisionality on JET or on DIII-D. On NSTX, no clear trend between the pinch number and ν^* was found either.

The dependence of the Prandtl and pinch numbers on R/L_n obtained from JET, DIII-D and AUG NBI modulation shots indicates that P_r does not depend on R/L_n although JET plasmas tend to have higher values in general. On the contrary, the pinch number shows a clear dependence on R/L_n in each device separately and also as a joint database. This increase in the pinch number with increasing R/L_n is qualitatively consistent with theory and gyro-kinetic simulations.

Based on the results from these multi-tokamak parametric scans, one can conclude that the inward pinch will have a significant impact on the rotation profile in ITER provided that the density profile is at least moderately peaked ($R/L_n \geq 1$) and some rotation source is available at the edge of the plasma. In all these analyses, the possible intrinsic torque has not been taken into account.

JET EFDA Contributors: See the Appendix of F. Romanelli *et al.*, Proceedings of the 23rd IAEA Fusion Energy Conference 2010, Daejeon, Korea.

Integrated Magnetic and Kinetic Control of Advanced Tokamak Scenarios Based on Data-Driven Models

D. Moreau¹, E. Schuster², M. Walker³, J. R. Ferron³, D. Humphreys³, J. E. Barton², M. D. Boyer², K. H. Burrell³, S. Flanagan³, P. Gohil³, R. Groebner³, A. W. Hyatt³, R. D. Johnson³, R. La Haye³, F. Liu¹, J. Lohr³, T. Luce³, B. Penaflor³, W. Shi², F. Turco³, and W. Wehner²

¹CEA/DSM/IRFM, Saint-Paul-lez-Durance, France

²Lehigh University, Bethlehem, USA

³General Atomics, San Diego, USA

Corresponding Author: didier.moreau@cea.fr

The first real-time profile control experiments integrating magnetic and kinetic variables in tokamaks are described. Parameters such as the current, toroidal rotation and pressure profiles play a crucial role in governing plasma confinement and stability and their control is important for extrapolating advanced tokamak scenarios to future tokamaks. The integrated model-based approach presented here is being developed under the framework of the International Tokamak Physics Activity for Integrated Operation Scenarios and was initially explored on JET for current profile control. A generic method to identify device-specific, control-oriented models from experimental data was validated on JET, JT-60U and DIII-D. Such data-driven models were used to synthesize integrated magnetic and kinetic profile controllers with different levels of model integration. Closed-loop experiments were performed on DIII-D for the regulation of:

1. The poloidal flux profile, $\psi(x)$.
2. The inverse of the safety factor profile, $\iota(x) = 1/q(x)$.
3. Either the poloidal flux profile or the inverse of the safety factor profile together with the normalized pressure parameter, β_N .

The neutral beam injection (NBI) and electron cyclotron current drive (ECCD) systems provided the heating and current drive sources for these experiments. Available beamlines and gyrotrons were grouped to form, together with the plasma surface loop voltage, V_{ext} , or current, I_p , five independent heating and current drive actuators:

- Co-current NBI power, P_{CO} .
- Counter-current NBI power, P_{CNT} .
- Balanced NBI power, P_{BAL} .
- Total ECCD power from all gyrotrons in an off-axis current drive configuration, P_{EC} .
- V_{ext} or I_p .

Control of $\iota(x)$ or $\psi(x)$ and simultaneous control of $\iota(x)$ or $\psi(x)$ together with β_N were performed through a mixed-sensitivity robust control algorithm and a near-optimal proportional-plus-integral control algorithm, respectively. With the same approach, closed-loop control simulations have been performed for ITER. The nonlinear burning plasma evolution and closed-loop response to the specific ITER actuators under the controller action are modelled. Results for various control configurations and targets are discussed.

Work supported by the US DOE under DE-FG02-09ER55064, DE-FG02-92ER54141, and DE-FC02-04ER54698, and by the European Fusion Development Agreement.

Stability and Performance of ITER Steady State Scenarios with ITBs

F. Poli¹, C. Kessel¹

¹*Princeton Plasma Physics Laboratory, Princeton, USA*

Corresponding Author: fpoli@pppl.gov

Steady state scenarios envisaged for ITER aim at optimizing the bootstrap current drive, while maintaining sufficient confinement and stability to provide the necessary fusion yield. Non-inductive steady state scenarios on ITER will need to operate with Internal Transport Barriers (ITBs) in order to reach adequate fusion gain at typical currents of 9 MA. We have analyzed the ideal MHD stability of steady state scenarios that use 8 – 33 MW of Neutral Beam with addition of different mixtures of external heating, namely 20 – 40 MW of EC, 20 – 40 MW of LH and 5 – 20 MW of IC. Target plasmas have $H_{98} \sim 1.6$, which is necessary to access 100% non-inductive current in the range of 7 – 10 MA and fusion yield of $Q \sim 3 - 6$ [1]. These configurations are established as relaxed flattop states with time-dependent transport simulations, which have been run with TSC [2]. The sensitivity of $n = 1, 2$ kink (with and without a wall) and $n = \infty$ ballooning instabilities has been analyzed against variations of the pressure profile peaking between 2.3 and 2.9, and of the Greenwald fraction up to 1.2.

It is found that LH heating is desirable to maintain the safety factor profile above 1.5. By operating with broad pressure profiles and ITBs at 2/3 of the minor radius, plasmas with 33 MW of NB and 40 MW of LH have $q_{\min} > 2$, are ideal MHD stable and can achieve $\beta_N > 4l_i$ with an ideal wall. The EC provides localized heating and current drive profiles, but 40 MW of EC raise the self-inductance and drive q_{\min} down below 1.5, driving $n = 1$ and $n = 2$ kinks instabilities. The stability of these configuration can be improved for deposition outside $\rho(q_{\min}) = 0.35$. The trade-off of current drive efficiency vs ideal MHD stability with $\rho(q_{\min})$ will be discussed, with focus on the effectiveness of the upper launcher in controlling the current profile.

References

[1] Kessel CE *et al.*, Development of ITER Advanced Steady State and Hybrid Scenarios, IAEA Fusion Energy Conference 2010.

This work was supported by the US Department of Energy under DE-AC02-CH0911466.



Non-linear MHD Modelling of ELM Triggering by Pellet Injection in DIII-D and Implications for ITER

S. Futatani¹, G. Huijsmans¹, A. Loarte¹, L. Baylor², N. Commaux², T. Jernigan²,
M. Fenstermacher^{3,4}, C. J. Lasnier^{3,4}, T. Osborne⁴, and B. Pégourié⁵

¹ITER Organization, Saint Paul lez Durance, France

²Oak Ridge National Laboratory, Oak Ridge, USA

³Lawrence Livermore National Laboratory, Livermore, USA

⁴General Atomics, San Diego, USA

⁵CEA/IRFM, St Paul-lez-Durance, France

Corresponding Author: shimpei.futatani@iter.org

ITER operation in its high fusion performance DT scenarios (inductive, hybrid and steady-state) relies on the achievement of the H-mode confinement regime, which is expected to lead to the quasi-periodic triggering of ELMs. Extrapolation of measurements of ELM energy fluxes to plasma facing components (PFCs) in present devices to ITER indicates that, for naturally occurring ELMs (or “uncontrolled”), these will produce an unacceptably low PFC lifetime because of excessive erosion and/or superficial surface damage. Controlled triggering of ELMs by the injection of small pellets has been demonstrated in present experiments as a viable technique to reduce ELM energy fluxes. The application of this technique to ITER requires frequencies exceeding (by typically more than one order of magnitude) those of uncontrolled ELMs. Thus, significant uncertainties remain for its practical application to ITER regarding both the optimization of the pellets for efficient triggering as well as of the associated fuel throughput required by this technique.

In order to provide a firmer physics basis to the triggering of ELMs by pellet injection, and to reduce the uncertainties with regards to its application in ITER, non-linear MHD modelling of ELM triggering by pellet injection in DIII-D experiments has been carried out with the JOREK code. The modelling results show that the triggering of ELMs is associated with the pressure (and its gradient) in the pedestal region of the plasma reaching a critical value during the pellet ablation process. As a consequence, a minimum pellet size for ELM triggering (for given pellet velocity and injection geometry) has been identified. Modelling of the effect of pellet injection location (outer midplane, X-point region, high field side) and of the details of the ablation profile on ELM triggering by pellets at DIII-D, as well as of the power fluxes to PFCs during pellet triggered ELMs, are in progress and will be reported in the paper. Comparison between simulations for DIII-D and experimental measurements will be used to validate and refine modelling assumptions. Predictions of the pellet requirements for optimum ELM triggering in ITER will be carried out with the validated model and implications for the requirements and implications for pellet pacing as a technique for ELM control in ITER will be drawn.

Non-linear MHD Simulation of ELM Energy Deposition

G. Huijsmans¹, A. Loarte¹

¹*ITER Organization, Saint Paul Lez Durance, France*

Corresponding Author: guido.huijsmans@iter.org

Measurements of the power deposition profile on the divertor target due to ELMs show that the wetted area during the ELMs increases significantly with the amplitude of the ELM energy losses. Taking the broadening into account in the estimates for the allowable ELM size in ITER leads to a larger operating window in plasma current (up to ~ 8 MA) where natural ELMs can be tolerated. The allowable ELM sizes for the high performance DT scenario at 15 MA are very small and thus no significant broadening is expected for tolerable ELMs in this scenario.

Non-linear MHD simulations of ELMs have previously shown good qualitative agreement on features like the formation of filaments and their propagation speed and the fine structure in the power deposition profile during ELMs. The next step towards a quantitative validation of MHD simulations of ELMs is to compare observed trends in the experimental data with results from nonlinear MHD simulations. Here, the non-linear MHD code JOREK is used to study the origin of the observed broadening of the wetted area as a function of the ELM size, and to provide a physics basis for the expected ELM power losses in ITER.

MHD simulations of ELMs for JET-scale plasmas show a significant broadening of the power deposition profiles at the divertor targets during ELMs. The broadening is a function of the ELM amplitude, the dependence being in reasonable agreement with experimental observations. The broadening is due to the ergodisation of the magnetic field due to the magnetic perturbation of the unstable ballooning mode. The ergodised field shows the characteristic homoclinic tangles which lead to filamentary structures on the divertor target with multiple strike points. The broadening of the power deposition varies during the temporal evolution of the ELM itself, which is correlated with the amplitude of the magnetic perturbation.

Simulations of ELMs in the ITER 15 MA, $Q = 10$ reference scenario, including the ITER divertor and first wall geometry, show significant broadening due to the ELM magnetic perturbation on the outer vertical target, less on the inner target. The paper will describe in detail the influence of the various MHD and transport processes occurring during an ELM on the modelled ELM heat flux pattern.

Three-dimensional Fluid Modeling of Plasma Edge Transport and Divertor Fluxes during RMP ELM Control at ITER

O. Schmitz¹, M. Becoulet², P. Cahyna³, T. Evans⁴, Y. Feng⁵, H. Frerichs¹,
D. Harting¹, A. Kirschner¹, A. Kukushkin⁶, R. Laengner¹, A. Loarte⁶, T. Lunt⁵,
R. Pitts⁶, G. Saibene⁷, D. Reiter¹, D. Reiser¹, and S. Wiesen⁷

¹*Forschungszentrum Jülich, IEK-4, Association EURATOM-FZJ, Jülich, Germany*

²*IRFM/CEA, St. Paul-lez-Durance, France*

³*IPP AS CR, Prague, Czech Republic*

⁴*General Atomics, La Jolla, CA, USA*

⁵*Max-Planck-Institut für Plasmaphysik, Greifswald, Germany*

⁶*ITER Organization, Saint Paul Lez Durance, France*

⁷*Fusion for Energy Joint Undertaking, Barcelona, Spain*

Corresponding Author: o.schmitz@fz-juelich.de

Application of resonant magnetic perturbation (RMP) fields is one option for control of edge-localized modes (ELMs) at ITER. During RMP ELM suppression at DIII-D the measured heat and particle fluxes are rearranged into a three-dimensional (3D) pattern. In this contribution, the consequences of this 3D boundary formation on the divertor heat and particle loads during RMP application at ITER are studied. We use EMC3-Eirene, a 3D fluid plasma and kinetic neutral transport code. An $n = 3$ RMP field at 90 kAt maximum coil current was applied in:

1. The vacuum limit.
2. Including plasma response from non-linear MHD.

A low recycling divertor regime is addressed at an input power of $P_H = 100$ MW without impurity radiation losses. This represents an extreme case to test the upper bound for the 3D heat fluxes. A clear reduction of the electron temperature T_e field is seen with vacuum RMP field. The outer boundary of the temperature field is set by the perturbed separatrix, which forms a finger like 3D boundary structure. These fingers reach out to the divertor target and the divertor fluxes are not axisymmetric anymore but deposited in a helical pattern reaching out as far as 70 cm from the unperturbed strike line. This yields spreading of the heat flux with a reduction of the peak heat flux from $q_{\text{peak}} = 28$ MW/m² without RMP field to $q_{\text{peak}} = 9$ MW/m² with RMP where the integral heat flux is reduced by 30%. This is induced by an increase of the divertor recycling flux by a factor of 10, which is necessary to maintain the density with RMPs applied. The increasing divertor density and enhanced ionization power losses reduce the divertor heat load. A comparison of these ionization losses with impurity radiation shows that they determine the actual divertor heat fluxes.

The plasma response to the $n = 3$ field applied was investigated based on a non-linear MHD plasma response modeling. For the case studied, all modes inside normalized flux of $\Psi_N < 0.96$ are shielded out while in the edge for $\Psi_N > 0.96$ a vacuum like penetration is predicted. This has a strong impact on the modeling result. The electron temperature is restored to the no-RMP value and the extension of the finger like structure at the separatrix is reduced. The maximum reach out of the helical heat fluxes are reduced to 30 cm and the heat flux deposition is more localized with increasing peak heat flux to $q_{\text{peak}} = 17$ MW/m².

3D Vacuum Magnetic Field Modeling of the ITER ELM Control Coils during Standard Operating Scenarios

T. E. Evans¹, D. M. Orlov², A. Wingen³, W. Wu¹, A. Loarte⁴, T. A. Casper⁴,
O. Schmitz⁵, G. Saibene⁶, and M. J. Schaffer¹

¹General Atomics, San Diego, USA

²University of California San Diego, La Jolla, USA

³Institut für Theoretische Physik, Heinrich-Heine-Universität, Düsseldorf, Germany

⁴ITER Organization, St Paul lez Durance, France

⁵Forschungszentrum Jülich, Jülich, Germany

⁶JET Joint Undertaking, Barcelona, Spain

Corresponding Author: evans@fusion.gat.com

ITER edge localized mode (ELM) coil current optimization and failure studies have been completed for nine standard operating scenarios using an automated program that calculates the vacuum island overlap width (VIOW) and compares the results to a criterion that has been correlated with ELM suppression in DIII-D. The analysis was done, using $n = 3$ and 4 perturbation fields, by varying the spatial phase of a cosine waveform approximated by the currents in the 9 coils making up each of the three rows of ELM coils. Results from the cases studied show that the minimum ELM coil current needed to satisfy the DIII-D correlation criterion varies from 20 kAt to 50 kAt depending on the operating scenario and that the available phase angle operating space increases rapidly with coil current above the minimum. It is also found that the DIII-D correlation criterion can be satisfied in the most demanding ITER scenario with $n = 3$ perturbation fields and with failures in up to 8 of the full 27 coil set although the available phase angle operating space is reduced from 79% with no failures to 27% with eight failures using a maximum ELM coil operating current of 90 kAt. Details of these results will be discussed along with plans to extend the analysis to include the plasma response to the perturbation field.

This work was supported in part by the US Department of Energy under DE-FG02-05ER54809, DE-FG02-07ER54917, and ITER Task Agreement C19TD42FU.

Analysis of Tungsten Dust Generation under Powerful Plasma Impacts Simulating ITER ELMs and Disruptions

I. Garkusha¹, N. Aksenov¹, B. Bazylev², A. Chuvilo¹, V. Chebotarev¹, I. Landman², M. Sadowski³, V. Makhlai¹, S. Pestchanyi², E. Skladnik-Sadowska³, and Y. Morgal³

¹NSC KIPT, Institute of Plasma Physics, Kharkov, Ukraine

²Karlsruhe Institute of Technology, Karlsruhe, Germany

³National Centre for Nuclear Research in Otwock-Świerk, Poland

Corresponding Author: garkusha@ipp.kharkov.ua

In this paper, experimental simulations of ITER transient events with relevant surface heat load parameters (energy density $0.45 - 1.1 \text{ MJ/m}^2$ and the pulse duration of 0.25 ms) as well as particle loads (varied in wide range of $10^{23} - 10^{27} \text{ ion/m}^2\text{s}$) were carried out with a quasi-stationary plasma accelerator QSPA Kh-50. Particular attention is paid to the material erosion due to particles ejection from the tungsten surfaces both in the form of droplets and solid dust. The erosion products flying from the tungsten target have been registered using high-speed 10 bit CMOS digital camera. Traces of particles ejected from the tungsten surface allow calculation of the particles velocity and the time moment when it started from the target surface. Additionally the mass loss of the target was measured after several shots. Erosion products ejected in the form of droplets and solid dust were also collected and examined with microscopy. Several mechanisms of dust generation under the transient energy loads to the tungsten surfaces have been identified. Dust particles with sizes up to tens microns are ejected from the surface due to the cracking development and major cracks bifurcation. Fatigue cracks after a large number of transient impacts to the preheated W surface became a source of smaller dust. Surface modification of tungsten material after the repetitive plasma pulses with development of ordered submicron cellular structures contributes significantly to the nm-dust generation. It is shown that majority of generated dust nano-particles, generated due to cells evolutions, are deposited back to the surface by a plasma pressure, in contrast to micrometer-size dust. For plasma exposures with energy loads above the melting threshold both droplets splashing and solid dust ejection is observed. Analytical estimations of dust production rate have been performed, and the results are verified with experiments in plasma guns having typical for ITER ELMs.

Narrow Heat Flux Widths and Tungsten: SOLPS Studies of the Possible Impact on ITER Divertor Operation

A. S. Kukushkin¹, H. D. Pacher², G. Pacher³, V. Kotov⁴, R. A. Pitts¹, and D. Reiter⁴

¹ITER Organization, St. Paul-lez-Durance, France

²INRS EMT, Varennes, Québec, Canada

³St. Bruno, Québec, Canada

⁴FZ Jülich, Jülich, Germany

Corresponding Author: andre.kukushkin@iter.org

Recent experimental observations of a very narrow SOL for energy flow in the inter-ELM H-mode have raised a concern for the consequences for target heat loading if it were to occur in ITER. Simulations using SOLPS4.3 for a carbon divertor have shown that because of the energy dissipation by impurity radiation in the divertor, the peak divertor power load could be maintained at an acceptable level even if the SOL width were reduced down to 1 mm instead of the 5 mm resulting from current transport assumptions. In other words, partial detachment of the divertor can counteract the effect of narrowing the SOL in ITER. However, the reduced radial transport in the narrow SOL case leads to relatively high separatrix density. Whereas this should not be a problem during the burn phase in ITER, low line average densities will almost certainly be necessary to obtain an acceptably low power threshold for the L-H transition, and this may be incompatible with high separatrix density. Investigations using the integrated core-pedestal-SOL model are underway to explore the expected plasma response around the L-H transition. In this study, we initially consider a carbon divertor with two sets of boundary conditions corresponding to the wide (L-mode) and narrow (H-mode) SOL and switch between them when the core plasma matches the usual criterion for the L-H transition (the transport reduction in the pedestal area is also applied at this point).

An initial simulation study is also underway to investigate divertor performance during the burn phase in the case of W targets, using seeded Ne impurity to replace the naturally produced C radiation in the C divertor case. Since the transport and radiation properties of the seeded impurity differ from those of C, this can affect the controllability of the discharge and the divertor plasma conditions, as well as the distribution of radiative power loading on divertor components. As an example, initial modelling runs already available indicate that the radiation contribution to the peak power load on targets is lower for the W divertor than for C, since Ne radiates further upstream than C. A beneficial effect is a factor 2 reduction of the maximum radiation power loads in the gaps between the cassettes, where the heat removal can be critical.

Multi-machine Comparisons of Divertor Heat Flux Mitigation by Radiative Cooling

A. Kallenbach¹, M. Bernert¹, T. Eich¹, C. Giroud², A. Herrmann¹, J. Hughes³,
B. Lipschultz³, T. W. Petrie⁴, A. Loarte⁵, G. Maddison², F. Reimold¹, M. Reinke³,
J. Schweinzer¹, B. Sieglin¹, M. Wischmeier¹, and S. Wolfe³

¹*Max-Planck-Institut für Plasmaphysik, Garching, Germany*

²*CCFE, Abingdon, UK*

³*MIT, Cambridge, UK*

⁴*General Atomics, San Diego, USA*

⁵*ITER Organization, Saint Paul Lez Durance, France*

Corresponding Author: arne.kallenbach@ipp.mpg.de

Due to the absence of carbon as intrinsic low- Z radiator, and tight limits for the acceptable power load on the divertor target, ITER will rely on impurity seeding for radiative power dissipation. Partial detachment of the outer divertor needs to be achieved and integrated with an ELM mitigation technique. This contribution reports about cross-machine studies of impurity seeded scenarios initiated by the ITPA group for integrated operational scenarios (IOS-1.2).

In current devices, the plasma response to impurity seeding reveals a quite broad phenomenology. In Alcator C-Mod, energy confinement degrades when the power flux through the separatrix is reduced towards the L-H threshold power, P_{LH} , under EDA H-mode conditions. In AUG, improvement of confinement is seen during nitrogen seeding at higher values of P_{sep}/P_{LH} , correlating with increasing Z_{eff} due to N seeding. In JET, degradation of normalized confinement was usually obtained during seeding. Different responses of the pedestal on the increased impurity level is supposed to be the main origin of the observed behaviour. To allow the comparison of different experiments with regard to the heat flux reduction, an analytical scaling relation for the normalized divertor power load has been developed, based on the main plasma Z_{eff} and the divertor neutral pressure. Higher divertor neutral pressures and higher heating powers in terms of P/R will be required to approach ITER divertor conditions in present day devices. No issues are foreseen for the combination of impurity seeding with ELM mitigation by pellet ELM pacing. Regarding ELM mitigation by magnetic perturbations, the quite different responses of the plasma in AUG, DIII-D and JET do not allow a clear forecast for ITER. So far, no negative effects of magnetic perturbations on the radiative efficiency or core impurity penetration have been observed in DIII-D and AUG. On the technical side, possible sensors and combined control schemes for the facilitation of partial detachment in ITER will be discussed based on recent tokamak experience.

PTRANSP Tests of TGLF and Predictions for ITER

R. Budny¹, X. Yuan¹, S. Jardin¹, G. Hammett¹, and G. Staebler²

¹*Princeton University, Princeton, USA*

²*General Atomics, San Diego, USA*

Corresponding Author: budny@princeton.edu

Time-dependent integrated predictive modeling is important for helping ITER achieve the physics goals of studying reactor-relevant burning plasmas. The PTRANSP code is being used to generate time-dependent integrated predictions. These are self-consistent in that the heating, current-drive, torques and equilibria are calculated using predicted plasma profiles, and vice versa.

Predictions for ITER have incorporated physics-based models such as GLF23. An improved Trapped gyro-Landau Fluid model TGLF contains physics not included in GLF23 such as realistic shaped finite aspect ratio flux geometry, and collisionality. TGLF achieves more accurate predictions of temperatures measured in L-mode, H-mode and hybrid discharges than does GLF23. This paper describes a major upgrade to PTRANSP which implements TGLF. The upgrade uses a new robust solver for stiff transport models.

Both GLF23 and TGLF are incorporated. The solver has both standalone and PTRANSP-coupled modes. The implementation of TGLF is verified by comparing results derived using the XPTOR code, and is tested using H-mode ITER-like plasmas. Predictions for ITER plasmas are given and compared with predictions using GLF23.

ITER Implications of the Beta Scaling of Energy Confinement

C. C. Petty¹, W. Guttenfelder², C. Holland³, S. Kaye², J. E. Kinsey¹,
D. C. McDonald⁴, G. R. McKee⁵, L. Vermare⁶, C. Angioni⁷, C. Bourdelle⁸, G. Hoang⁸,
F. Imbeaux⁸, F. Ryter⁸, H. Urano⁹, and M. Valovic⁴

¹General Atomics, San Diego, USA

²Princeton Plasma Physics Laboratory, Princeton, USA

³University of California San Diego, La Jolla, USA

⁴JET-EFDA, Culham Science Centre, Abingdon, UK

⁵University of Wisconsin-Madison, Madison, USA

⁶École Polytechnique, Palaiseau, France

⁷Max-Planck-Institut für Plasmaphysik, Garching, Germany

⁸Associatione Euratom CEA, Cadarache, France

⁹Japan Atomic Energy Agency, Naka, Japan

Corresponding Author: petty@fusion.gat.com

There is emerging evidence that the variation in the measured beta dependence of confinement in H-mode plasmas is due in part to different turbulent modes being dominant, with ITG modes being important in weak beta scaling cases and micro-tearing modes being potential candidates explaining strong beta degradation. Additionally, the normalized H-mode pedestal height may not be constant over a beta scan, which affects core transport and global confinement. Determining the beta scaling of transport helps to differentiate between various proposed theories of turbulent transport that are primarily electrostatic or primarily electromagnetic. Initial experiments on JET, DIII-D and NSTX found a weak dependence of confinement on beta; however, this picture of primarily electrostatic transport was brought into question by experiments on JT-60U and ASDEX Upgrade that observed a strong unfavorable beta scaling.

The ITPA topical group on Transport and Confinement has coordinated experimental and modeling activity to better understand the origin of these different beta scalings. An important factor that can impact scaling results is experimental imperfections in the beta scans. For some experiments the normalized H-mode pedestal height decreases with higher beta, which can result in an unfavorable beta scaling even if core transport is primarily electrostatic. A DIII-D experiment with joint participation by the ASDEX Upgrade team found no beta dependence in the local thermal diffusivities outside of the $\approx 15\%$ error bars, and the magnitude and trend with beta of density fluctuations were in reasonable agreement with GYRO simulations for electrostatic ITG-mode turbulence. In contrast, turbulence modeling of ASDEX Upgrade experiments using GS2 found that micro-tearing modes are unstable in the high beta cases but their contribution to the beta degradation remains to be assessed quantitatively. Micro-tearing modes should be important for high collisionality and flat density profiles, which were the conditions for ASDEX Upgrade and JT-60U. Therefore, the disparate beta scalings may be explained by either different dominant turbulence modes or experimental imperfections such as changes in the H-mode pedestal height during the beta scan.

Supported in part by the US DOE under DE-FC02-04ER54698, DE-AC02-09CH11466, DE-FG02-07ER54917, DE-FG02-89ER53296, and DE-FG02-08ER54999.

Assessing the Power Requirements for Sawtooth Control in ITER through Modelling and Joint Experiments

I. Chapman¹, J. P. Graves², V. Igoshine³, R. La Haye⁴, O. Sauter², O. Asunta⁵,
S. Coda², G. Giruzzi⁶, T. Goodman², T. Johnson⁷, M. Lennholm⁸,
ASDEX Upgrade Team⁸, DIII-D Team⁸, MAST Team⁸, TCV Team⁸,
Tore Supra Team⁸, and JET EFDA Contributors⁸

¹*CCFE, Abingdon, UK*

²*CRPP, Lausanne, Switzerland*

³*MPI für Plasmaphysik, Garching, Germany*

⁴*General Atomics, San Diego, USA*

⁵*Aalto University, Aalto, Finland*

⁶*IRFM, CEA, St Paul-Lez-Durance, France*

⁷*Euratom/VR Association, EES, KTH, Stockholm, Sweden*

⁸*JET-EFDA, Culham Science Centre, Abingdon, UK*

Corresponding Author: ian.chapman@ccfe.ac.uk

Recent advances in theoretical understanding and numerical modelling of sawtooth oscillations have allowed the invention and application of experimental control techniques. This enhanced understanding, coupled with demonstration of control techniques in ITER-relevant plasmas and using real-time feedback, has facilitated prediction of control actuator requirements for ITER. The control of sawteeth is important for baseline scenario operation of burning plasmas, since plasmas with long sawtooth periods are empirically more susceptible to neoclassical tearing modes, which result in substantial confinement degradation. The stabilising effects of alpha particles are likely to exacerbate this, so recent experiments have identified methods for amelioration. Sawtooth control using electron cyclotron current drive has been demonstrated in ITER-like plasmas with a large fast ion fraction, wide $q = 1$ radius and long uncontrolled sawtooth period in DIII-D and ASDEX Upgrade. Operation at $\beta_N = 3$ without NTMs has been achieved in ITER demonstration plasmas in DIII-D using only modest ECCD power for sawtooth control. Further, real-time ECCD control techniques have been developed in TCV and Tore Supra. Numerical modelling suggests that the achieved driven current changes the local magnetic shear sufficiently to compensate for the stabilising influence of the fast particles. Extrapolating this to ITER, transport modelling coupled to ray-tracing predictions and using the linear stability thresholds for sawtooth onset suggests that 13 MW of ECCD could be sufficient to reduce the sawtooth period by 30%, and this being the case, dropping it below the NTM triggering threshold. However, since the ECCD control scheme is solely predicated upon changing the local magnetic shear, it is prudent to plan for 10 MW off-axis ICRH using ^3He minority as a complementary scheme which directly damps the internal kink potential energy drive responsible for trapped fast ion stabilisation. Experimental evidence from JET plasmas heated with toroidally propagating ICRH using a ^3He minority exhibited sawtooth control avoiding NTMs in H-mode, as predicted by drift-kinetic modelling. Such modelling suggests that 10 MW of ICRH in ITER will negate the stabilising effect of alphas.

Work funded by RCUK Energy Programme and EURATOM.

JET EFDA Contributors: See the Appendix of F. Romanelli *et al.*, Proceedings of the 23rd IAEA Fusion Energy Conference 2010, Daejeon, Republic of Korea.

Observation of Localized Fast-Ion Induced Heat Loads in Test Blanket Module Simulation Experiments on DIII-D

G. J. Kramer¹, A. G. McLean², N. H. Brooks³, R. V. Budny¹, R. Ellis¹,
W. W. Heidbrink⁴, T. Kurki-Suonio⁵, R. Nazikian¹, T. Koskela⁵, M. J. Schaffer³,
K. Shinohara⁶, J. A. Snipes⁷, D. A. Spong⁸, and M. A. Van Zeeland³

¹*Princeton Plasma Physics Laboratory, Princeton, USA*

²*Lawrence Livermore National Laboratory, Livermore, USA*

³*General Atomics, San Diego, USA*

⁴*University of California Irvine, Irvine, USA*

⁵*Helsinki University of Technology, Helsinki, Finland*

⁶*Japan Atomic Energy Agency, Naka, Japan*

⁷*ITER Organization, St. Paul lez Durance, France*

⁸*Oak Ridge National Laboratory, Oak Ridge, USA*

Corresponding Author: gkramer@pppl.gov

Heat loads on the first wall of ITER can potentially be very high in localized regions such as the divertor or in regions on the first wall where magnetic field perturbations can channel energetic ions to create localized hot spots. One area where hot spots can be created in ITER is on the Test Blanket Modules (TBMs) because of the ferritic steel required for these components and their effect on the distortion of the poloidal and toroidal magnetic field near the modules. Simulating the level of those heat loads is important for assessing their effects on the ITER first wall. It is therefore essential that the codes that perform such assessments are validated against experimental results using configurations similar to those expected in ITER. The development of the mock-up ITER-like TBM on DIII-D allows just such a validation to be carried out on DIII-D for the case of neutral beam ions. An important new capability in the last run period was the direct infra-red imaging of the front surface of the protective TBM tiles and the calibration of the images to infer heat loads induced by the localized deposition of deuterium beam ions. A key result of the experiments is that the detailed simulations using a variety of particle following codes reproduce well the heat loads observed using the infra-red camera.

This work was supported supported in part by the US DOE under DE-AC02-09CH11466, DE-AC52-07NA27344, DE-FC02-04ER54698, SC-G903402, and DE-AC05-00OR22725.

Fast Ion Power Loads on ITER First Wall Structures in the Presence of ELM-mitigation Coils and MHD Modes

T. Kurki-Suonio¹, E. Hirvijoki¹, T. Koskela¹, A. Snicker¹, O. Asunta¹, S. Sipilä¹, and S. Äkäslompolo¹

¹*Aalto University, Aalto, Finland*

Corresponding Author: taina.kurki-suonio@aalto.fi

The new physics introduced by ITER operation, of which there is very little prior experience, is related to the large number of fast ions: fusion alphas, NNBI deuterons and multi-MeV minority ions from ICRH. These particles present a potential hazard to the surrounding material structures. Assuming axisymmetry and neoclassical transport only, the fast ion wall power loads are found tolerable in all scenarios and for all particle species.

However, in ITER the axisymmetry is destroyed by several mechanisms: Finite number of TF coils causes toroidal ripple, the field is further perturbed by the test blanket modules, and the proposed ELM control coils (ECC) cause a field modulation at their own periodicity. All the deviations can cause significant fast ion leakage, leading to localized power loads on the walls. Furthermore, it is highly unlikely that ITER plasmas will be MHD quiescent: the massive fast ion population can drive energetic particle modes that act back to the fast ion population. ITER is also prone to NTM islands. All these MHD phenomena can increase fast ion population at the edge, where transport due to the field aberrations can lead to unacceptably high peak power loads on some first wall components.

In this contribution we address these issues: the effect non-axisymmetry on NBI power loss, and the effect of NTM islands and Alfvénic modes (AEs) on fast ion distribution. Non-axisymmetry: we use the 5D Monte Carlo orbit-following code ASCOT to simulate fast ions in the presence of all relevant mechanisms perturbing the edge magnetic field. The fast ion power loads are found tolerable as long as the edge magnetic field does not become stochastic. The very high NBI power losses, reported earlier, can also be reproduced, but are found to correspond to stochastic edge field that does not support the NBI source profile assumed for the simulations.

MHD effects: we have developed a model applicable for both stationary (NTMs) and rotating (AEs) MHD modes. The island structures are included in the equations of motion, expressed in vector form. Thus the allows arbitrary coordinate system and simulations all the way to the wall, and permits the use of 3D fields. We use the model for ITER to:

1. Determine the critical NTM island size not be exceeded from the fast ion confinement point-of-view.
2. Estimate the effect of AEs on the fast ion losses.



Benchmark of Gyrokinetic, Kinetic MHD and Gyrofluid Codes for the Linear Calculation of Fast Particle Driven TAE Dynamics

A. Könies¹, S. Briguglio², N. Gorelenkov³, T. Fehér¹, M. Isaev⁴, P. Lauber¹,
A. Mishchenko¹, D. Spong⁶, Y. Todo⁷, W. Cooper⁸, R. Hatzky⁵, R. Kleiber¹,
M. Borchardt¹, and G. Vlad²

¹Max-Planck-Institut für Plasmaphysik, Greifswald, Germany

²Associazione EURATOM-ENEA sulla Fusione, Rome, Italy

³Princeton Plasma Physics Laboratory, Princeton University, Princeton, USA

⁴Tokamak Physics Institute, NRC Kurchatov Institute, Moscow, Russian Federation

⁵Max-Planck-Institut für Plasmaphysik, EURATOM-Association, Garching, Germany

⁶Oak Ridge National Laboratory, Oak Ridge, USA

⁷National Institute for Fusion Science, Toki, Japan

⁸École Polytechnique Fédérale de Lausanne, Centre de Recherches en Physique des Plasmas, Lausanne, Switzerland

Corresponding Author: axel.koenies@ipp.mpg.de

Fast particles in ITER may originate from the fusion process itself or from external heating, as Neutral Beam Injection (NBI). It is well known that those non-thermal populations of fast particles may interact with otherwise stable Alfvén waves in the bulk plasma driving them unstable. This process takes place as a resonance phenomenon that requires a kinetic treatment of the fast particles but not necessarily a kinetic treatment of the bulk plasma. The rising amplitude of the oscillating electro-magnetic field in the plasma may lead to a redistribution or a loss of supra-thermal particles. In consequence, a degradation of the heating efficiency or even hazards for in-vessel components of the machine are possible.

In the last decades, much effort has been invested in the development of theory and codes that can be used to describe and explain the related phenomena. However, up to now, there is no well-understood standard case that these models have been tested against quantitatively. Providing the first quantitative code comparison, the ITPA Energetic particle Topical Group is contributing to the design activity on the ITER operation scenario. The benchmark of the codes for the energetic ion driven modes is necessary for the accurate prediction of plasma behavior in ITER. The international benchmarking effort between a variety of codes shall ensure scientific quality and reliability when predictions for ITER will be made.

Comparisons will be made between the different codes at different levels of approximation for growth rates, frequencies and eigenfunctions. While the limit of zero orbit width has been well met by all codes, the spread of the results in the zero Larmor radius case illustrates the necessity of a quantitative comparison. Furthermore, the importance of finite Larmor radius (FLR) effects is shown which lower the growth rates considerably. The benchmark will provide codes capable of predicting Alfvén eigenmode physics in ITER reliably.

Effects of ELM Control Coil on Fast Ion Confinement in ITER H-mode Scenarios

T. Oikawa¹, K. Tani², K. Shinohara³, A. Loarte¹, S. Putvinski¹, T. Casper¹,
Y. Gribov¹, M. J. Schaffer⁴, J. Snipes¹, D. Campbell¹, T. Sugie³, and Y. Kusama⁴

¹*ITER Organization, Saint Paul Lez Durance, France*

²*Nihon Advanced Technology, Naka, Japan*

³*Japan Atomic Energy Agency, Naka, Japan*

⁴*General Atomics, San Diego, USA*

Corresponding Author: toshihiro.oikawa@iter.org

This paper reports the effects of the ELM control coil on fast ion confinement in ITER H-mode plasmas. The effects of the ELM coil on the loss of NBI-produced fast ions and fusion-produced alpha particles have been investigated using an orbit following Monte-Carlo code for an ITER 9 MA non-inductive plasma, where the simulations have been performed for the vacuum fields produced by the ELM coils and then magnetic screening effects could influence the numerical conclusions. The effect of the ELM coil field dominates the loss of NBI-produced fast ions over the effect of magnetic field ripple by the toroidal field coils and the test blanket modules, leading to a significant loss of fast ions on the order of 16–17%. A significant transit particle loss occurs in the cases of the toroidal mode number $n = 4$ in which magnetic surfaces are ergodic near the plasma periphery. Concerning the resonance of fast-ion trajectories, the anti-resonant surfaces of the main mode $n = 4$ are very close to the resonant surfaces of the complementary mode $n_c = (9 - 4) = 5$ and vice versa. Since the effect of resonance on fast-ion trajectories dominates that of anti-resonance, a synergy effect of the main and complementary modes enlarges the resonant regions. The simulations also shows that the optimization of current phase of the ELM coils is not effective for the loss of fast ions for the $n = 4$ case in this plasma.

The two-dimensional heat load on the first wall due to the NBI ion loss was evaluated. With a stationary magnetic field pattern the peak heat load near the upper ELM coils due to the NBI ion loss is as high as 1.0–1.5 MW/m², which exceeds the allowable level in ITER. The peak heat load can be reduced to 0.2–0.25 MW/m² by rotation of the ELM coil field pattern, a feature foreseen in the design of the ELM control system. Most loss particles hit the inner side of the torus of the dome in the ITER divertor, and the peak heat load averaged over the 9 toroidal sectors of ELM coils is in a range of 0.3–0.5 MW/m², which is in the acceptable level again. Simulations have been done also for 3.5 MeV alpha particles. The loss of alpha particles also increases due to the ELM coil field. However, the loss is still acceptably low at less than 1.0%.

Assessment of the H-mode Power Threshold Requirements for ITER

P. Gohil¹, D. J. Battaglia², E. de la Luna³, M. E. Fenstermacher⁴, J. W. Hughes⁵,
S. M. Kaye², A. Kirk⁶, Y. Ma⁵, R. Maingi⁷, Y. Martin⁸, D. C. McDonald⁶, H. Meyer⁶,
and F. Ryter⁹

¹General Atomics, San Diego, USA

²Princeton Plasma Physics Laboratory, Princeton, USA

³JET-EFDA-CSU Culham Science Center, Abingdon, UK

⁴Lawrence Livermore National Laboratory, Livermore, USA

⁵Massachusetts Institute of Technology, Cambridge, USA

⁶Culham Science Centre for Fusion Energy, Abingdon, UK

⁷Oak Ridge National Laboratory, Oak Ridge, USA

⁸Centre de Recherches en Physique des Plasmas, Lausanne, Switzerland

⁹Max-Planck-Institut für Plasmaphysik, Garching, Germany

Corresponding Author: gohil@fusion.gat.com

This paper contains a comprehensive multi-machine assessment on accessing and maintaining H-mode plasmas in ITER. The results from these joint experiments address L-H transition power threshold issues, which are not adequately included in the scaling from the ITPA H-mode power threshold database. Consequently, these results affect the ability to make accurate predictions for the H-mode threshold in ITER using the presently available H-mode scaling relationships and can be used to improve and reduce the uncertainty in these predictions. For the non-nuclear operational phase in ITER with H and/or He plasmas, experiments have been performed in ASDEX Upgrade (AUG), C-Mod, DIII-D, JET, NSTX, and MAST. The ratio of $P_{\text{TH}}(\text{H})/P_{\text{TH}}(\text{D})$ appears to be relatively consistent at about a value of 2. However, for helium there is a large variation in $P_{\text{TH}}(\text{He})/P_{\text{TH}}(\text{D})$ from 1.0 – 2.0. On detailed examination of the results from the many devices, the ratio of $P_{\text{TH}}(\text{He})/P_{\text{TH}}(\text{D})$ decreases towards unity with increasing L-mode (or target) electron density, which is a favorable trend for ITER operational scenarios at relatively higher target densities. The application of resonant magnetic perturbation (RMP) fields can lead to significant increases in the H-mode power threshold as has been determined in AUG, DIII-D, MAST and NSTX. Multi-machine results will also be presented on the H-mode confinement in He and also on modeling of ITER scenarios, based on the above results, and the predictions and implications for accessing H-mode plasmas in ITER.

This work was supported in part by the US Department of Energy under DE-FC02-04ER54698, DE-AC52-07NA27344, DE-FC02-99ER54512, and DE-AC02-09CH11466.

A Model for the Power Required to Access the H-mode in Tokamaks and Projections for ITER

R. Singh¹, P. Kaw¹, A. Loarte², D. Campbell², D. Bora², and H. Nordman³

¹*Institute for Plasma Research India, Gandhinagar, India*

²*ITER Organization, Saint Paul Lez Durance, France*

³*Department of Earth and Space Sciences, Chalmers University of Technology, Göteborg, Sweden*

Corresponding Author: rsingh129@yahoo.co.in

We describe a new model for the L-H transition which, in common to other models, determines the physics requirements to stabilize turbulent transport by $\mathbf{E} \times \mathbf{B}$ shear but also derives the required edge power flow to achieve these physics requirements. Plasma transport in the L-mode plasma edge (typically from $\Psi = 0.95 - 1.0$) is assumed to be dominated by resistive ballooning turbulence. Because of the access of an H-mode transport barrier, the scale length of the edge plasma density (L_n) is expected to be set by ionization balance and to be smaller than that of the temperature (L_T). The power out flux from the core plasma is transported through the edge by conduction, convection and part of it is also radiated by impurities in this edge region before reaching the separatrix. Under the assumptions of dominant resistive ballooning transport the edge power balance is derived. Suppression of resistive ballooning transport is assumed to occur when the $\mathbf{E} \times \mathbf{B}$ rotational shear exceeds the typical autocorrelation time of the turbulence. This condition is used to evaluate the H-mode power threshold. It is shown that the H-mode power threshold for the existing tokamaks found to be in reasonable agreement with the measurements and predictions for ITER is shown. Power threshold can also be used to identify the physics processes leading to the increase of the H-mode threshold at low density:

1. The scale length of density profile becomes longer than that of the temperature.
2. The ratio of ion to electron temperature decreases for electron heated plasmas because of the inefficiency of equipartition at these densities as found in experiments.



Studying the Capabilities of Be Pellet Injection to Mitigate ITER Disruptions

S. Konovalov¹, V. Leonov¹, R. Khayrutdinov², V. Lukash¹, S. Medvedev¹,
S. Putvinski³, V. Zhogolev¹, P. Aleynikov¹, and A. Kavin⁴

¹*NRC "Kurchatov Institute", Moscow, Russian Federation*

²*RF SRC TRINITI, Troitsk, Russian Federation*

³*ITER IO, St. Paul-lez-Durance, France*

⁴*Efremov Institute of Electrophysical Apparatus, St. Petersburg, Russian Federation*

Corresponding Author: konoval@nfi.kiae.ru

Principal goal of the ITER disruption mitigation system (DMS) is retention of the heat and electro-mechanical loads on the machine components during disruption within the tolerable limits. This includes heat loads on divertor and plasma facing components during thermal quench (TQ), electromagnetic forces on vacuum vessel and other constructive elements during current quench (CQ) and heat loads due to the loss of runaway electron (RE) beam to the wall.

Capabilities of the Be pellet injection to meet the goals of the ITER DMS are studied in the present report using the set of numerical codes providing integrated simulation of ITER disruptions with RE generation.

Simulations of the TQ with ASTRA code demonstrated a principle possibility of re-radiation of more than 80% of plasma thermal energy with injection of about 2×10^{23} Be atoms. Subsequent simulation of the CQ with DINA code showed that the duration of CQ is close to, but exceeds the engineering limit of 36 ms, especially in the case of most probable Upward vertical displacement events (VDE). The RE generation in the plasma with Be impurity was found to be strongly suppressed. However, at the CQ stage of simulations it was found that even very small RE seed current of about 100 A would be sufficient to convert up to the half of the pre-disruption plasma current into RE one. Maximum electromagnetic forces on the VV of order of 100 MN were found in DINA simulations of the Downward VDE with RE. Possibilities of the mitigation of the RE current and energy by means of the Be pellet injection at the CQ stage are discussed.

Modelling of Material Damage and High Energy Impacts on Tokamak PFCs during Transient Loads

B. Bazylev¹, I. Landman¹, S. Pestchanyi¹, Y. Igitkhanov¹, R. Pitts², S. Putvinski², G. Arnoux³, S. Brezinsek⁴, A. Huber⁴, M. Lehnen⁴, J. W. Coenen⁴, G. Saibene⁵, and P. C. Stangeby⁶

¹Karlsruhe Institute of Technology, Karlsruhe, Germany

²ITER Organization, Saint Paul Lez Durance, France

³Euratom/CCFE Association, Culham Science Centre, Abingdon, UK

⁴Forschungszentrum Jülich, Jülich, Germany

⁵Fusion for Energy Joint Undertaking, Barcelona, Spain

⁶University of Toronto, Toronto, Canada

Corresponding Author: boris.bazylev@kit.edu

Tungsten (divertor) and beryllium (first wall) will be the plasma-facing components used on ITER. In reactor-scale tokamaks using metallic PFCs, transient events such as ELMs, VDEs and disruptions will produce strong vaporization and surface melting. Likewise, intense heat loads due to the impact of runaway electrons (RE) generated during the current quench phase of disruptions become a major issue in devices operating at high plasma current. Even if the thermal quench energy of major disruptions is expected to be successfully dissipated by mitigation using massive gas injection (MGI), the resulting photonic radiation loads on the ITER Be wall can be very intense. Unfortunately, no existing tokamak or laboratory device can simultaneously match all the conditions of ITER transients and so estimates of expected damage to ITER PFCs can only be provided by numerical simulations, supported by benchmarking on existing experiments. This paper describes a series of applications of the codes MEMOS, ENDEP and TOKES, developed at the Karlsruhe Institute of Technology, to specific ITER transient loading on both W and Be surfaces in the case of W divertor PFC melting due to disruptions (MEMOS), RE impact on Be first wall panels (MEMOS and ENDEP) and estimates of MGI driven photon radiation flash first wall heating (TOKES). An account is also given of benchmarking studies in which these codes have been compared with results obtained on the JET and TEXTOR tokamaks.

Control of Major Disruptions in ITER

A. Sen¹

¹*Columbia University, New York, USA*

Corresponding Author: amiya@ee.columbia.edu

It is argued that major disruptions in ITER can be avoided by the feedback control of the causative MHD precursors. The sensors will be 2D-arrays of ECE detectors and the suppressors will be modulated ECH beams injected radially to produce non-thermal radial pressures to counter the radial dynamics of MHD modes. The appropriate amplitude and phase of this signal can stabilize the relevant MHD modes and prevent their evolution to a major disruption. For multimode MHD precursors, an optimal feedback scheme with a Kalman filter is discussed.

Progress on Manufacturing of the ITER Vacuum Vessel Equatorial and Lower Ports in Korea

J. W. Sa¹, H. Kim¹, C. Park¹, K. Hong¹, Y. Lee¹, B. Kim¹, H. Ahn¹, J. G. Bak¹,
K. Jung¹, C. Choi², Y. Utin², and K. Ioki²

¹*National Fusion Research Institute, Daejeon, Republic of Korea*

²*ITER Organization, Saint Paul Lez Durance, France*

Corresponding Author: jwsa@nfri.re.kr

Korea is responsible for procuring all port components at the equatorial and lower level including the VV (vacuum vessel) supports, NB (neutral beam) duct liners, and sealing flanges. Since procurement arrangement in late 2008, the contract for the main port components was signed in early 2010 and activities are going on in preparation of product fabrication. Major activities for main port are creation of drawings, material procurement, structural/welding distortion analysis, qualification/documentation, and checks on manufacturing feasibility through mock-up fabrication. Analysis will be focused on fabrication related work such as structural assessment for shell thickness reduction effect and welding distortion. Also in-wall shield design of the NB port has been developed. Major activities for VV gravity support are to perform detail design including coupon test to verify performance of friction surface. The fabrication feasibility study for neutral beam duct liner has been carried out. This paper presents the status on fabrication preparation and design activity for port components.

Quench Detection in ITER Superconducting Magnet Systems

J. L. Duchateau¹, M. Coatanea¹, B. Lacroix¹, S. Nicollet¹, D. Ciazynski¹, and P. Bayetti¹

¹CEA, St-Paul-lez-Durance, France

Corresponding Author: jean-luc.duchateau@cea.fr

The quench of one of the ITER magnet systems is an irreversible transition of the conductor from superconducting to normal resistive state. The normal zone propagates along the cable in conduit conductor, dissipating a large power. The detection has to be fast enough (2 – 3 s) to initiate the dumping of the magnetic energy and avoid irreversible damage of the systems.

The experience of CEA is based on the operation of the superconducting tokamak TORE SUPRA for more than 20 years. In support to ITER, CEA was also very involved during these last 3 years in quench detection investigations, in the framework of ITER contracts.

The primary quench detection in ITER is based on voltage detection, which is the most rapid detection. The very magnetically disturbed environment during plasma scenario makes the voltage detection particularly difficult, inducing large inductive components across the pulsed coils (10 kV) or coil subcomponents. Voltage compensations have therefore to be designed to discriminate the resistive voltage associated with the quench.

A conceptual design of the quench detection based on voltage measurements is discussed for the main ITER magnet systems and a clear methodology is developed. It includes the analysis of the main phases of the quench detection, given below with typical orders of magnitude:

- The propagation phase characterized by the time τ_P (~ 1 s).
- The filtering time characterized by the time τ_H (~ 1 s).
- The opening time of the current breakers τ_{CB} (~ 0.5 s).
- The total allowable detection and action time (hot spot criterion) τ_{DA} (~ 3 s).

Based on this analysis it is possible to propose for each ITER magnet system the two main parameters of the quench detection which are V_t and τ_H . V_t (0.1 – 0.5 V) is the voltage triggering the current breaker opening after the filtering time τ_H .

A secondary detection based on thermohydraulic signals system has also to be investigated to protect the environment in case of a non detected quench, especially for the largest ITER system which is the TF system with a stored energy of 40 GJ.

Simulation of Eddy Current and Electromagnetic Loads in ITER Conducting Structures

V. Belyakov¹, A. Alekseev², Z. Andreeva¹, A. Belov¹, D. Campbell², O. Filatov¹, Y. Gribov², K. Ioki², V. Kukhtin¹, A. Labusov¹, E. Lamzin¹, B. Lyublin¹, A. Malkov¹, I. Mazul¹, M. Merola², M. Sugihara², and S. Sychevsky¹

¹*D. V. Efremov Scientific Research Institute, St. Petersburg, Russian Federation*

²*ITER Organization, St. Paul-Lez-Durance, France*

Corresponding Author: [syтч@sintez.niiefa.spb.su](mailto:sytch@sintez.niiefa.spb.su)

A modelling technique has been developed to efficiently predict EM loads in conducting structures. A set of models that integrally covers the structures has been developed in the course of activities requested and supervised by the IO ITER. Reasoning from the simulation efficiency, a local model based either on the 3D solid body or shell approximation is applied. Detailed models were built for the system “vacuum vessel (VV), cryostat, and thermal shields (TS)” which enable description of its complex multiply connected thin-walled structures with required accuracy. The EM transients are simulated through the space and time variations of the toroidal plasma current, halo current, the toroidal magnetic flux, and the coil currents, that covers practically all field sources. These data are derived from results of MHD simulations. This enables simulations for all plasma scenarios and operating modes. At the first step, induced eddy currents are simulated in the system “VV + TS + Cryostat” that has crucial EM effect on other structures. A shell model of the system implements an integral-differential formulation, and a single unknown is determined in terms of the vector electric potential taken at the nodes of a FE mesh on a shell surface. EM loads on massive in-vessel and out-vessel structures and thin-walled components are simulated with the use of local FE models. In-time field sources can be described via a set of basic functions. As an alternative to direct integration over the entire operation scenario, a generalized solution for any scenario is obtained as a superposition of individual solutions. The mathematical formulation is implemented in terms of vector potentials or through a field vector. In the Cartesian coordinates, a separation of variables (vector components) is applicable. Parallel computations enable solving the problem in both formulations during the same runtime. An efficiency of these solutions is compared. Combined computations with different models provide cross-checking within common procedures. Integration with other computer codes is feasible that improves reliability of simulations. The proposed computational technique has been applied to EM analyses to support ITER design activities. The results have been included in the project documentation. Developed models enable cost-and time effective computations at further activity.

Transient Electromagnetic Analysis of the ITER Blanket System

M. Ulrickson¹, J. Kotulski¹, R. Coats¹, R. Roccella², M. Sugihara², and S. Sadakov²

¹*Sandia National Laboratories, Albuquerque, USA*

²*ITER Organization, St. Paul le Durance, France*

Corresponding Author: maulric@sandia.gov

The design of the ITER Blanket System is controlled by three main considerations. Two of these considerations, plasma heat flux to the surface and nuclear heating, determine the cooling requirements and coolant distribution to control thermal stress in the modules. Electromagnetic forces due to off-normal events like disruptions must be controlled to be within the strength of the supports on the vacuum vessel and determine the mechanical stress in the blanket components. First, electromagnetic forces are generated by three different causes during an off-normal event. The shift in plasma paramagnetism during thermal quench generates eddy currents due to the change in toroidal field. Second the changing plasma current during current quench generates eddy currents due to the change in poloidal field. Finally, halo currents flow from the plasma to the wall due to plasma motion during current quench. The analyses conducted are based on disruption simulations, performed using the DINA code. The DINA output includes information on toroidal flux change during thermal quench, plasma shape, current, and position during current quench, and halo current flow to the plasma-facing surface. Raw DINA output was processed to reduce the plasma current temporal and spatial variation to time dependent current in a fixed set of 64 conductors that surround the plasma volume. The OPERA code was used to simulate the transient eddy currents in, and current flow through the complex 3D blanket components. Forces and moments were calculated from the current distribution and the local magnetic field. We studied numerous options for slits to control eddy currents in the shield blocks, electrical connections between the first wall and shield, fault scenarios for insulators in the support system between the blanket and the vessel, and variations on two different types of first wall panels (lower and higher heat flux rating). The support system between the first wall and shield block and between the shield block and vessel contains several insulators to control the flow of halo or eddy currents among the various components. We have examined the consequence of failure of one or more insulators by replacing the insulator with a controlled electrical contact. Insulator failure creates additional conducting loops or current paths. These studies led to revision of the design of the mounts.

Results of ITER TF Coil Sub and Full Scale Trials Performed in Japan

K. Matsui¹, N. Koizumi¹, T. Hemmi¹, K. Takano¹, H. Kajitani¹, M. Iguchi¹,
Y. Chida¹, H. Nakajima¹, J. Knaster², and A. Foussat²

¹Japan Atomic Energy Agency, Naka, Japan

²ITER Organization, St Paul lez Durance, France

Corresponding Author: matsui.kunihiro@jaea.go.jp

Japan Atomic Energy Agency (JAEA) is responsible for the procurement of 9 Toroidal Field (TF) coils as Japanese Domestic Agency. The TF coil consists of 7 double-pancakes (DPs), a DP consists of radial plates (RPs) which are mechanical structure supporting large electromagnetic force, and a TF conductor using Nb₃Sn cable-in-conduit superconductor. In manufacturing the TF coil, heat-treated TF conductor whose length varies due to heat treatment shall be inserted in the groove of the RP. There are some technical issues for the TF coil manufacture as follows:

1. The winding with the accuracy of 0.01%.
2. Evaluation of the conductor elongation due to heat treatment.
3. Development of insulation/impregnation procedure using the newly developed resin which has high resistance to irradiation.
4. Manufacturing RP satisfying tight tolerances of a few mm in flatness and in-plane displacement.

JAEA had started reduced and full-scale trials to develop technologies for the TF coil manufacture with resolving above-mentioned technical issues, from March 2009 to March 2011, prior to series production of the TF coils. In this activity, JAEA performed one-third scale trials for the DP fabrication and full-scale trial for the RP fabrication. One of one-third scale DPs was made by using the copper dummy to demonstrate winding and insulation/impregnation procedure and, in addition, the other is fabricated using TF conductor to demonstrate heat treatment technology. The findings from these trials are follows:

1. The accuracy of 0.011% in the conductor length was achieved, resulting in enabling to insert the conductor into the RP groove.
2. The conductor elongation of the one-third scale DP due to heat treatment was evaluated as 0.073% due to heat treatment. This conductor elongation should be taken into account in the fabrication of the TF coils.
3. The one-third scale DP was successfully impregnated with the CE resin.

In the full-scale trial, a RP was fabricated from 10 segmented RP subsections, which were machined SS316LN hot rolled plates in parallel. These subsections were joined by the laser welding and the flatness and in-plane displacement of fabricated RP within 2 mm were achieved.

These trials indicate feasibilities of the TF coil manufacture. After final qualification by manufacturing a dummy DP, JAEA will start series production of the TF coils.

Progress of Manufacturing and Quality Testing of the ITER Divertor Outer Vertical Target in Japan

Y. Seki¹, K. Ezato¹, S. Suzuki¹, K. Yokoyama¹, K. Mohri¹, and M. Enoda¹

¹Japan Atomic Energy Agency, Naka, Japan

Corresponding Author: seki.yohji@jaea.go.jp

Japan Domestic Agency (JADA) has started to manufacture 11 plasma facing units of an outer vertical target full-scale prototype which is just the same as those of a half cassette of ITER divertor. At the beginning of this activity, a joint technology and quality control for an interface between a plasma-facing material and a heat-sink material became key issues in the manufacturing process of the plasma facing units. In consequence of research and development, JADA achieved to increasing the success rate of the joint by improvements which are to metalize the joint surface of a carbon fiber composite by the use of Ti-coating with accurate thickness controlling, and also to change a buffer layer material from a soft copper to a Cu-W alloy. Moreover, JADA solved the problems of the quality control of joint interface by improved a system of an infrared thermography inspection which provides quick feedback to the manufacturing process about the presence of defect in the joint.

In the staged procurement of the plasma facing units for the full-scale prototype, a pre-prototype was manufactured as a final exercise toward the manufacturing. The result of the infrared thermography inspection indicates a good performance. Based on the result from the pre-prototype, the first 6 plasma facing units were manufactured at the end of June 2012. The manufacturing of the rest is scheduled in 2013.

In parallel to above development, research and development of the W monoblocks enough to endure the repetitive heat load of more than 20 MW per square meter has been started. JADA successfully completed the high heat flux testing of two mock-ups which are manufactured by using a non defect bonding. The result indicates that the soundness of the non defect bonding is sufficient against the repetitive heat flux of 20 MW per square meter for 1,000 cycles except for the recrystallization.

This paper presents the overview of achievements and clarifications of technical and quality issues for the manufacturing activity and the quality control of the divertor in Japan.

Developments Toward Fully Metallic Actively Cooled Plasma Facing Components for ITER divertor

X. Courtois¹, J. Bucalossi¹, M. Missirlian¹, M. Richou¹, D. Serret¹, M. Firdaouss¹,
P. Gavila², A. Grosman², T. Loarer², and P. Magaud²

¹*CEA, IRFM, Saint-Paul-Lez-Durance, France*

²*Fusion for Energy, Barcelona, Spain*

Corresponding Author: xavier.courtois@cea.fr

On the road toward fusion energy, a significant threshold to step over is giving up the use of carbon (CFC) for plasma-facing components (PFC) armour. Since years, laboratories and industries have carried out studies and experiments to make possible the use of tungsten as main PFC armour in the near future. This is now mainly driven by the use of W for the ITER divertor and can be divided in two lines: on the one hand, the technological development of relevant PFC, aiming at withstanding very high heat fluxes up to 20 MW/m² and, on the other hand, integrated operational implementation of W PFCs in present tokamaks such as JET and ASDEX Upgrade. CEA/IRFM has been active for the last two years in both lines by participating in the qualification of the development achieved by Fusion for Energy to procure the European part of the ITER divertor and also by the preliminary studies launched in the frame of the WEST project (Tungsten Environment for Steady State Tokamak) [1]. This project aims at installing a W divertor in Tore Supra, in order to operate the 1st tokamak with a full W actively cooled divertor in long plasma discharged.

The paper describes the main studies and their results, which have been performed at IRFM within the last 2 years, in the field of W PFC: heat removal capabilities and thermal fatigue testing of the latest monoblock designed for ITER divertor targets and also foreseen for WEST, components surface shaping to take into account local particles flux orientations and leading edges effect, transient (ELMs) and steady state cumulated loads and their link with the issue of W recrystallization, and finally the acoustic monitoring of the cooling regimes to prevent critical heat flux events.

References

[1] J. Bucalossi, *et al.*, Fusion Engineering and Design **86** (2011) 684-688.

Effort on Design of a Full Tungsten Divertor for ITER

F. Escourbiac¹, T. Hirai¹, S. Carpentier-Chouchana¹, A. Fedosov¹, L. Ferrand¹,
T. Jokinen¹, V. Komarov¹, A. Kukushkin¹, M. Merola¹, R. Mitteau¹, R. A. Pitts¹,
P. C. Stangeby², and M. Sugihara¹

¹ITER Organization, St. Paul lez Durance, France

²University of Toronto, Toronto, Canada

Corresponding Author: frederic.escourbiac@iter.org

This paper will report on the results of the design efforts which have been launched at the IO following a recent decision to develop the option to start with W Divertor targets.

According to the current ITER physics Research Plan, the first divertor installed will be exposed to two helium/hydrogen campaigns, a single deuterium campaign and one full DT campaign, at the end of which the first mission goal of long pulse operation at fusion gain ($Q \geq 10$) would be achieved.

Amounts of stationary heat fluxes of $\sim 10 \text{ MWm}^{-2}$ and of slow transient heat flux expected to reach as much as 20 MWm^{-2} for transient periods of a few seconds were estimated and will be used as a basis to define the technology qualification programme.

Lifetime is determined as well by thermal transients resulting, for example, from vertical displacement events (VDE) and major disruptions. It was found from new analyses of VDE undertaken with the DINA code that, at the moment of the thermal quench, the inner vertical target and divertor dome areas appear to be extremely rarely impacted and thus do not require particular design modifications compared with the existing CFC variant. On the other hand, for most of the downward VDE events, the plasma becomes limited by the outer divertor baffle for which the same “roof-shaping” principle used in the ITER First Wall panel design will be implemented. Toroidal “set-backs” (typically 20 mm) are proposed on each side of the baffle to completely shadow any direct leading edge whilst optimizing the load spreading over the remaining wetted surface.

Regards to the strike point region, in addition with the PFCs tilt when assembled onto the CB, ensuring protection of leading edges, introducing W also requires the systematic shadowing of monoblock edges at the PFU scale, for this a simple “fish-scaling” solution is foreseen.

Designing in this way introduces the need for a transition from global roof-shaping to local fish-scale shaping in the HHF regions. That is one of the main difficulties of the current full-W design. The reality is that a compromise must be sought between perfect shadowing protecting all possible misalignments and the increase of manufacturing costs due to complex shapes.

Supporting analysis is being performed in parallel with the evolving full-W design and will be briefly discussed in the paper.

Experimental Simulation of Beryllium Armour Damage Under ITER-like Intense Transient Plasma Loads

I. Kupriyanov¹, E. Basaleev¹, G. Nikolaev¹, L. Kurbatova¹, V. Podkovyrov²,
A. Zhitlukhin², and L. L. Khimchenko³

¹*A. A. Bochvar High Technology Research Institute of Inorganic Material, Moscow, Russian Federation*

²*SRC RF TRINITI, Troitsk, Russian Federation*

³*Project Centre of ITER, Moscow, Russian Federation*

Corresponding Author: igkupr@gmail.com

Beryllium will be used as a plasma facing material in the next generation of tokamaks such as ITER. During plasma operation in ITER, the plasma facing materials and components will be suffered by different kinds of loading which may affect their surface or their joint to the heat sink. In addition to quasi-stationary loadings which are caused by the normal cycling operation, the plasma facing components and materials may also be exposed to the intense short transient loads like disruptions, ELMs. All these events may lead to beryllium surface melting, cracking, evaporation and erosion. It is expected that the erosion of beryllium under transient plasma loads such as ELMs and disruptions will mainly determine a lifetime of ITER first wall. To obtain the experimental data for the evaluation of the beryllium armor lifetime and dust production under ITER-relevant transient loads, the advanced plasma gun QSPA-Be facility has been constructed in Bochvar Institute.

This paper presents recent results of the experiments with Russian beryllium of TGP-56FW ITER grade. The mock-ups of a special design armored with two beryllium targets ($80 \times 80 \times 10 \text{ mm}^3$) were tested by hydrogen plasma streams (5 cm in diameter) with pulse duration of 0.5 ms and heat load of 0.5 and 1.0 MJ/m². Experiments were performed at RT temperature. The evolution of surface microstructure and profile, cracks morphology and mass loss/gain under erosion process on the beryllium surface exposed to up to 250 shots will be presented and discussed.

Status & Progress of the R&D Work for ITER Magnet Supports

P. Li¹, B. Hou¹, M. Liao¹, S. Han¹, Z. Sun¹, D. Kang¹, C. Pan¹, B. Zhang², Y. Fu³,
and F. Arnaud³

¹*Southwestern Institute of Physics, Chengdu, China*

²*China International Nuclear Fusion Energy Program Executive Center, Beijing, China*

³*Tokamak Department, ITER Organization, St. Paul-Lez-Durance, France*

Corresponding Author: lipy@swip.ac.cn

Magnet supports is designed as class A quality components, because these components should sustain all the dead weight of magnet coils, thermal load, electromagnetic forces, and seismic loads if occur. China will supply all the supports for ITER construction. First of all, selection the suitable technical road for the final high quality components is important. It is estimated that several thousand tons of various type 316LN stainless steel including hot-rolled plate, forged blocks and pipes, is needed for all the magnet supports. Last year, the large-size forged block for PFS6 (total weight up to 10 T) was developed domestically. Both the plate and the forged block showed high strength and good elongation at room temperature and 4.2K. In addition, almost no ferritic phase could be seen. Furthermore, we have developed a special NDT (non-destructive test) method to detect the defects for more than half meter thick 316LN austenitic block. A new design for GS manufacture without welding was put out, the static stress analysis using three-dimensional finite element model (FEM), was developed to analyze the redesigned structure. It can be known that the stress in the present load condition/combination is under the stress limitation of the material. In order to further check the engineering stability of this support under various possible work condition, a special test platform, which can simulate all forces during ITER operation, to check the prototype TF pedestal was designed and constructed. Various cooling pipe is needed for maintaining the low temperature of the magnet supports. We develop laser brazing method to reduce the heat input and then improve the connection, and the microstructure observation shows that almost no microcrack could be found. In the ITER magnet system, more than 10 000 various bolts and tie rods will be used, the material include Inconel 718, A286 and 316LN. We have successfully developed the fastener fabrication technology. The fastener qualification is an important work to guarantee the structure safety of magnet supports. The engineering test of the fastener, for instance, tensile strength, fatigue at 77K is developed in our institute. The further test is in schedule.

Feedback of the Licensing Process of the First Nuclear Installation in Fusion, ITER

C. Alejaldre¹, J. Elbez-Uzan¹, and ITER Collaborators¹

¹*ITER Organization, St-Paul-lez-Durance, France*

Corresponding Author: carlos.alejaldre@iter.org

After the submission of Preliminary Safety Report (PSR) in March 2010 by the ITER Organization, the safety French authorities started an intensive and detailed examination led by its technical support IRSN (Institut de Radioprotection et de Sûreté Nucléaire). Sixteen months later, in December 2011, the standing group (composed by expert members in different field of nuclear safety) concluded that the measures elaborated by IO in their PSR are satisfactory on the whole and therefore gave a favourable advice for the creation of the Installation. The IO must still consolidate the design of some equipment and provide further information on various issues within a period of two years. The standing group would thus like to examine the additional information provided before the start of the tokamak equipment assembly phase.



ITER Machine Assembly — Challenges and Progress

K. Blackler¹, V. Bedakihale¹, K. Im², B. Macklin¹, P. Petit¹, R. Shaw¹, D. Wilson¹,
and K. Yamaura¹

¹*ITER Organization, St. Paul lez Durance, France*

²*ITER Korea, Daejeon, Republic of Korea*

Corresponding Author: ken.blackler@iter.org

The basic ITER machine has around 1 million parts which must be successfully integrated and assembled. This complex and challenging task requires robust planning, processes, heavy lifting, welding and precise alignment and tolerance control.

The ITER Organization (IO) is responsible for the assembly of the ITER Tokamak machine from components delivered in-kind from each of the Domestic Agencies. IO is currently undertaking detailed design and planning for the assembly of the machine, to define the sequence and kinematics of each operation.

This poster will present the current status of the design and planning for ITER Machine Assembly and will describe the overall strategy, schedule and critical technical challenges and ways they are being mitigated.

In addition to technical descriptions and diagrams, this poster shall show the progress and challenges of the Phase 1 Tokamak Assembly, through a 5 minute high definition animated video based on actual CAD data, with audio commentary. This video shows actual CAD data taken from assembly studies and allows viewers to better understand the scale and complexity of the assembly process.

Activation Analyses of Lead Lithium Cooled Ceramic Breeder Test Blanket Module in ITER

C. Danani¹, H. L. Swami¹, A. K. Shaw¹, V. Chaudhari¹, and E. R. Kumar¹

¹*Institute for Plasma Research, Bhat, Gandhinagar, India*

Corresponding Author: chandanipr@gmail.com

India has proposed a test blanket module (TBM) to be placed in ITER equatorial port for testing Lead-Lithium cooled Ceramic Breeder (LLCB) concept. The LLCB blanket concept consists of lithium titanate as ceramic breeder (CB) material in the form of packed pebble beds and Pb-Li eutectic as multiplier, breeder, and coolant for the CB zones. The blanket module structure will be cooled by helium. RAFMS will be used as a structural material and tritium produced in ceramic breeder will be purged by Helium gas. A electrical insulation of Alumina is being considered presently for reduction in MHD effects. The LLCB TBM will face the neutron flux and will be irradiated during the ITER operations. A data base of activation characteristics is required for safety analyses of LLCB TBM. The activation analyses has been carried out assuming the irradiation scenario given in ITER TBM safety guidelines using EASY-2007. The radioactive inventory, decay heat and dose-rate have been calculated at the shutdown and several post-irradiation times following the pulsed operation scheme of ITER. In this paper we present the main results of the activation analyses of LLCB TBM.

Preliminary Corrosion Studies on Structural Materials in Lead-Lithium for Indian LLCB TBM

S. S. Atchutuni¹, T. Kamble¹, H. Agravat¹, P. Chakraborty², R. Fotedar²,
R. K. Ellappan¹, and A. Suri²

¹*Institute for Plasma Research, Bhat, India*

²*Bhabha atomic Research centre, Mumbai, India*

Corresponding Author: sarada.sree@gmail.com

Liquid Lead-Lithium (Pb-Li) eutectic is considered as one of the promising candidates of tritium breeder materials for fusion reactors. Several experiments have been conducted to study the corrosion of different structural materials with Lead Lithium eutectic Pb-Li. Series of experiments on compatibility of candidate structural materials such as P-91 (9Cr, 1Mo Ferritic Steel) and Indian specific RAFMS with Pb-Li are being attempted under Indian TBM R&D program. Two parallel experiments were conducted in Pb-Li buoyancy loop and in a electromagnetic pump driven loop, in the presence and absence of magnetic field.

In buoyancy loop, hot leg is maintained at a temperature of 550°C and cold leg is maintained at a temperature of 465°C. Typical liquid metal velocity was ~ 8 cm/sec. Flat and tensile sample chains of Indian specific RAFMS were kept in both hot and cold legs. This experiment was carried out for 1900 hours.

A experiment in pump driven loop was performed in the set-up at IPUL, Latvia, to study the corrosion of Ferritic Martensitic steel P91 (9% Chromium and 1% Molybdenum) with/without the presence of magnetic field (1.7 T). Flat and tensile samples were exposed to flowing Lead Lithium at a velocity of 15 cm/sec. In the test section, samples are mounted in three regions:

1. Before magnetic field.
2. Within magnetic field.
3. After magnetic field.

Temperature is maintained at 550°C in the test section. This experiment was carried out for 1000 hours. In the same setup and configuration, another experiment was carried out at higher flow rate, 30 cm/sec, maintaining 550°C in the test section for a duration of 2700 hours.

The specimens were characterized using analytical tools such as Optical microscopy, Scanning electron microscopy, energy dispersive X- ray (SEM/EDX), EPMA (Electron probe micro analyser). Hardness measurement, tensile strength measurement and fractography would also be carried out on the samples.

This paper presents the preliminary results obtained from the corrosion experiments with IN-RAFMS samples and P-91 samples along with the magnetic effects on corrosion.

Progress in the EU Test Blanket Systems Safety Studies

D. Panayotov¹, Y. Poitevin¹, J. Furlan¹, M. T. Porfiri², T. Pinna², and M. Iseli³

¹*Fusion For Energy, Barcelona, Spain*

²*ENEA UTFUS-TEC Frascati, Rome, Italy*

³*ITER Organization, Saint Paul Lez Durance, France*

Corresponding Author: dobromir.panayotov@f4e.europa.eu

The European Joint Undertaking for ITER and the Development of Fusion Energy (“Fusion for Energy”- F4E) provides the European contributions to the ITER international fusion energy research project. Among others it includes also the development, design, technological demonstration and implementation of the European Test Blanket Systems (TBS) in ITER. An overview of the ITER TBS program has been presented recently at ISFNT-10.

Currently two EU TBS designs are in the phase of conceptual design — Helium-Cooled Lithium-Lead (HCLL) and Helium-Cooled Pebble-Bed (HCPB). Safety demonstration is an important part of the work devoted to the achievement of the next key project milestone the Conceptual Design Review.

The paper will reveal the details of the work on EU TBS safety performed in the last couple of years in the fields of update of the TBS safety demonstration file; TBS Safety approach, design principles, requirements, features and safety functions; detailed TBS components classifications; Radiation Shielding and Protection; Potential Hazards and adopted safety measures; Selection of reference accidents scenarios and Accidents analyses; and TBS Safety requirements and fulfillments matrix.

Finally the authors will share the planning of the future EU TBS safety activities.

Transient Thermal-hydraulic Modeling and Analysis of Chinese HCSB TBM

Y. Zhang¹, Z. Zhou¹, T. Peng¹, and X. Sheng¹

¹INET Tsinghua University, Beijing, China

Corresponding Author: zhangyl03@gmail.com

The Chinese helium-cooled solid breeder (CH-HCSB) test blanket module (TBM) is designed to be tested in ITER, aiming to validate the feasibility of a DEMO fusion reactor with helium-cooled solid tritium breeders. Safety analysis is part of the TBM design process ensuring that the TBM does not adversely affect the safety of ITER. Transient thermal-hydraulic analysis was performed to testify that TBM and its helium cooling system will not impact the safety of ITER under both normal and accidental conditions. The latest design of TBM was introduced in the paper, and its transient thermal-hydraulic modeling and analysis were performed using RELAP5/MOD3 code. As the peak temperature of lithium pebble bed inside the sub-module is very high, detailed modeling of sub-module was proposed and verified. According to the accident sequences of Accident Analysis Specification for TBM, design basis accidents were investigated. The influences of different break locations, leak areas and plasma termination behavior were analyzed comprehensively. The results showed that the design of the CH-HCSB TBM could be further modified in order to assure the safety of the TBM to be tested in ITER.

ITER-P

Experimental Assessment of Materials Exposed to Coolant Water under ITER Relevant Operational Conditions

S. Wikman¹, J. Eskhult², A. Molander², and J. Öijerholm²

¹*Fusion for Energy, Barcelona, Spain*

²*STUDSVIK, Nyköping, Sweden*

Corresponding Author: stefan.wikman@f4e.europa.eu

The ITER Vacuum Vessel materials that are exposed to the coolant water consist of mechanically strained structural materials, joints and bolts along with non-loaded parts. The complex geometries result in high amount of crevices. Therefore, it is important to map the formation of corrosion products (impurities) susceptibility to stress corrosion cracking and surface effects such as pitting to determine the engineering margins and the operational lifetime. Taking into account highlighted corrosion issues along with results from initial activities and presently ongoing work it was possible to setup exposure experiments simulating ITER relevant operational conditions comprising exposure, drainage and drying cycles. The drying step was performed with hot nitrogen and superheated steam in two separate test systems. Studsvik performed the presented work organized by F4E via a task agreement with ITER IO. The exposure was repeated during 38 cycles to allow for accumulation of impurities. The water chemistry, using degassed ultrapure water, was maintained at 1 ppm hydrogen peroxide and 10 ppb chloride. Material specimens were manufactured from the steel grades 316L(N)-IG, 304B4, 304B6, 304B7, 430, 304 and XM-19. The susceptibility to crevice corrosion was evaluated using crevice corrosion specimens. The susceptibility to stress corrosion cracking was evaluated using the Crevice Bent Beam (CBB) method with graphite wool as crevice former. A purpose-built conductivity cell to simulate capillary condensation in crevices was employed to register the progress of drying. The results show that impurities are concentrated in the creviced area after each cycle. The ferritic stainless steel Type 430 showed the lowest corrosion resistance, followed by the borated stainless steels 304BX. Welded 316L(N)-IG also showed lower resistance. The 316L(N)-IG and reference material type 304 were the most resistant. Microscopy of the loaded CBB specimens revealed short surface cracks for both XM-19 and 316L(N)-IG. Short straight cracks with a depth less than 6 μm evolved in a crackled surface zone and the cracks stopped when reaching the unaffected base material. In summary, during the test conditions used, the crevice corrosion attacks were relatively small in both drying environments. The CBB method on XM-19 and 316L(N)-IG only exhibited short surface cracks in both drying environments

Development and Testing of Plasma Disruption Mitigation Systems Applicable for ITER

S. Combs¹, L. Baylor¹, S. Meitner¹, C. Foust¹, T. Jernigan¹, N. Commaux¹, P. Parks², S. Maruyama³, and D. Rasmussen¹

¹*Oak Ridge National Laboratory, Oak Ridge, USA*

²*General Atomics, San Diego, USA*

³*ITER Organization, Saint Paul Lez Durance, France*

Corresponding Author: combsk@ornl.gov

Disruptions on large tokamaks present challenges to handle the intense heat flux, the large forces from halo currents, and the potential first wall damage from multi-MeV runaway electrons. Injecting large quantities of material into the plasma during the disruption can reduce the plasma energy and increase its resistivity and electron density to mitigate these effects. Developing the technology to inject sufficient material deeply into the plasma for a rapid shutdown and runaway electron collisional suppression is an important capability needed for maintaining successful operation of ITER and future reactors. The initial system developed for this application at Oak Ridge National Laboratory (ORNL) made use of a fast acting solenoid valve designed and routinely used for pneumatic pellet injection systems. The prototype valve equipped with a relatively large supply cylinder (0.3 ℓ) was tested in the lab with various gases (Ar, Ne, He, and hydrogen) at pressures up to 70 bar and then used in experiments on DIII-D to inject gases to mitigate some of the deleterious effects of disruptions on the tokamak [1]. The prototype was later replaced with a multi-valve system that can accommodate up to six valves. This system allowed experiments with much higher gas injection rates. The prototype was provided to C-Mod and used for successful disruption mitigation experiments [2]. A second ORNL system was recently provided to C-Mod, and initial experiments have been carried out. An alternative technique, injection of a relatively large (~ 16 mm diameter) shattered pellet, for rapidly getting sufficient material into the plasma was more recently developed at ORNL and successfully tested in plasma disruption experiments on DIII-D [3]. With the large pellets proving to be very effective, we are evaluating different techniques to shatter the pellet and direct the debris stream. Here we present the status/progress on the development of these systems and the potential of these techniques to provide reliable disruption mitigation on ITER.

References

- [1] D. G Whyte *et al.*, Phys. Rev. Lett. **89** (2002) 055001-1.
- [2] R. Granetz *et al.*, Nucl. Fusion **46** (2006) 1001.
- [3] N. Commaux *et al.*, Nucl. Fusion **51** (2011) 103001.

ITER Fuelling and Glow Discharge Cleaning System Overview

S. Maruyama¹, Y. Yang¹, G. Kiss¹, M. O'Connor², M. Sugihara¹, P. Sergei¹,
S. Michiya¹, R. Pitts¹, L. Bo³, L. Wei³, Y. Pan³, M. Wang³, L. Baylor⁴, S. Meitner⁴,
and D. Douai⁵

¹ITER Organization, St. Paul lez Durance, France

²Babcock International, Oxfordshire, UK

³Southwestern Institute of Physics, Chengdu, China

⁴Oak Ridge National Laboratory, Oak Ridge, USA

⁵CEA-IRFM, Cadarache, France

Corresponding Author: so.maruyama@iter.org

The ITER Fuelling and Wall Conditioning System plays a key role in plasma operation. It consists of 4 major sub-systems:

1. The Gas Injection System (GIS).
2. Pellet Injection System (PIS).
3. Disruption Mitigation System (DMS).
4. Glow Discharge Cleaning System (GDC).

This paper describes the design status of these four systems and the challenges associated with each.

The ITER fuelling system is capable of delivering fuel particles (H_2 , D_2 and T_2) at average and peak throughputs of $200 \text{ Pam}^3\text{s}^{-1}$ and $400 \text{ Pam}^3\text{s}^{-1}$ respectively in the form of gas or pellets, as well as impurities such as Ne, Ar and N_2 with average and peak throughputs of $10 \text{ Pam}^3\text{s}^{-1}$ and $100 \text{ Pam}^3\text{s}^{-1}$. The DMS injects particles (e.g., Ne and/or D_2) into the plasma preemptively or repetitively to mitigate thermal and electromagnetic loads onto the in-vessel components and to suppress runaway electrons. The GDC reduces and controls impurity (e.g., oxygen) and hydrogenic fuel out-gassing from plasma-facing components.

The GIS and GDC will be procured by the Chinese Domestic Agency (CN DA) and the PIS and DMS by the United States Domestic Agency (US DA).

Scientific Computing for Real Time Data Processing and Archiving for ITER Operation

S. Simrock¹, A. Aallekar², M. Walsh¹, L. Bertalot¹, M. Cheon³, C. Hansalia¹,
D. Joonekindt¹⁰, G. Jablonski⁴, Y. Kawano⁵, W. D. Klotz¹, T. Kondoh⁵, T. Kozak⁴,
P. Makijarvi¹, D. Makowski⁶, M. Annigeri⁶, A. Mielczarek⁴, A. Napieralski⁴,
M. Orlikowski⁴, M. Park³, P. Perek⁴, S. Petrov⁴, P. Predki⁴, R. Reichle¹, I. Semenov⁷,
D. Shelukhin⁷, F. Tomi⁸, V. Udintsev¹, G. Vayakis¹, A. Wallander¹, A. Winter¹,
S. Wu⁹, Q. Yang⁹, I. Yonekawa¹, and K. Zagar¹¹

¹ITER Organization, St. Paul-lez-Durance, France

²TCS, Bangalore, India

³National Fusion Research Institute, Daejeon, Republic of Korea

⁴DMCS, Lodz, Poland

⁵Japan Atomic Energy Agency, Naka, Japan

⁶TCS, Pune, India

⁷Kurchatov Institute, Moscow, Russian Federation

⁸ENSEA, Cergy-Pontoise, France

⁹ITER, Beijing, China

¹⁰ATOS Origin, Meylan, France

¹¹COSYLAB, Ljubljana, Slovenia

Corresponding Author: stefan.simrock@iter.org

The operation of the ITER tokamak imposes significant demands on the instrumentation and control (I&C) section of its 170 plant systems in terms of data acquisition, data processing and data transport via networks. The plant I&C systems must support the operational needs for machine protection, plasma operation and physics exploitation. The most stringent requirements are found in the more than 50 diagnostics measurement systems in terms of high performance data acquisition, data processing and real-time data streaming from distributed sources to the plasma control system as well as large amounts of raw data streaming to scientific archiving. While most of these requirements have been achieved individually the challenge for ITER will be the integration of these state-of-the-art technologies in a coherent design while maintaining all of the performance aspects simultaneously.

Status of R&D on In-Vessel Dust&Tritium Management in ITER

F. Le Guern¹, S. Ciattaglia², G. Counsell¹, E. Veshchev², M. Walsh², A. Denkevits⁵,
E. Gauthier³, W. Jacob⁴, and V. Rohde⁵

¹*Fusion for Energy Joint Undertaking, Barcelona, Spain*

²*ITER Organization, St Paul lez Durance, France*

⁵*KIT, Institut für Kern- und Energietechnik, Eggenstein-Leopoldshafen, Germany*

³*CEA, IRFM, Centre de Cadarache, St Paul lez Durance, France*

⁴*Max-Planck-Institut für Plasmaphysik, Garching, Germany*

Corresponding Author: frederic.leguern@f4e.europa.eu

In a tokamak, plasma-surface interactions can produce dust. During operation, tritium present in the Vacuum Vessel (VV) can be trapped in VV materials and particularly in dust and co-deposited layers accumulating in the divertor area.

In event of an accident involving ingress of steam into the VV, hydrogen could be produced by chemical reaction with hot metal and dust, particularly Beryllium. In case of ingress of air into the VV, reaction of air with hydrogen and/or dust cannot be completely excluded and could lead to a possible explosion which could challenge the VV (first confinement barrier) tightness. To prevent such accidents and their radiological consequences, limitations on in-VV accumulation of dust and tritium and on air ingress are imposed. Correlatively, ITER has defined a strategy for the control of in-VV dust and tritium inventories based on both measurement and removal techniques. In this context, this paper gives the status of tasks aiming at developing some of the measurement systems and necessary R&D for ITER strategy validation.

In a first part, this paper will provide outcomes of tasks on in-VV dust measurement diagnostics:

1. On Divertor Erosion Monitor aiming at measuring erosion and deposition on divertor vertical targets: A detailed optical path was defined and an outline design produced.
2. On Capacitive Diaphragm Monitor (gauges) allowing direct measurement of dust:
 - Extensive characterization and calibration of gauges in laboratory conditions were done.
 - An enhanced electronics and an housing were developed for in-VV tests.
 - Gauges were tested in AUG to check their behaviour under harsh conditions (radiation, electromagnetic field).
 - An outline design for integration in ITER was produced, together with recommendations for operation in ITER.
3. On feasibility of measuring the quantity of “hot dust” using steam injection:
 - A dedicated set-up was assembled and commissioned.
 - An experimental matrix based on key relevant parameters (dust mean size, steam pressure, temperature) has been defined and tests performed.

In a second part, the status of experiments on effectiveness of desorption of tritium from Be co-deposits baked at 350°C will be detailed. The paper will focus on:

1. Manufacture and characterization of prototypic set of layers.
2. The release rates of deuterium during baking of the layers.

Challenges of Integrating a Typical Diagnostics Port Plug in ITER

S. Salasca¹, A. Grosman¹, B. Cantone¹, M. Dapena¹, B. Esposito², D. Marocco², F. Moro², R. Villari², M. Angelone², E. Rincon³, C. Hidalgo³, D. Nagy⁴, G. Kocsis⁴, P. Varela⁵, G. Porempovics⁶, G. Perrollaz⁷, K. Patel⁸, Y. Krivchenkov⁸, and M. Walsh⁹

¹CEA, IRFM, Saint-Paul-lez-Durance, France

²ENEA, C. R. Frascati, Roma, Italy

³CIEMAT, Madrid, Spain

⁴WIGNER RCP Budapest, Hungary

⁵IST, Lisbon, Portugal

⁶BME-MM, Budapest, Hungary

⁷AMETRA, Venelles, France

⁸CCFE, Culham Science Centre, Abingdon, UK

⁹ITER Organization, Saint-Paul-lez-Durance, France

Corresponding Author: sophie.salasca@cea.fr

Diagnostics in ITER are mandatory to characterize the parameters of plasma and study its interactions with plasma-facing components. They thus play a crucial role for both the tokamak operation and protection.

Diagnostics components closest to the plasma are supported by big metallic structures called port plugs, located within the vacuum vessel. At the tokamak mid-plane, these components are installed in port plugs through intermediate structures called drawers. Indeed, apart from hosting the diagnostics, the port plugs act as shielding against neutrons and gammas, in order to limit the nuclear loads in crucial components (such as diagnostics and superconducting coils) as well as the dose levels in the controlled zones of the tokamak. The radiation shielding function of the port plugs is ensured through an optimized mixture of heavy metallic materials and water, forming shielding blocks surrounding the diagnostics.

The integration of diagnostics in ITER appears quite challenging. The major issue stems from the RAMI aspects (Reliability, Availability, Maintainability, Inspectability). Diagnostics maintenance will be exclusively performed in hot cell with a frequency of only 4 years, through remote handling devices. The diagnostics design must thus be compatible with such maintenance constraints. Another issue is relative to the consistency of the diagnostics with the neutron shielding efficiency of the port plugs. Indeed, to maximize the view towards the plasma, diagnostics need large fields of view, inducing big apertures in the shielding blocks and degrading their screen efficiency. Another issue is the perennity of diagnostics performance in ITER severe environment. Components in the plasma vicinity are submitted to high thermal loads requiring an active cooling. They are also subject to great electromagnetic loads, which can be prejudicial if they cause failures of cooling channels or irreversible displacement of sensitive objects. The design of diagnostics will inevitably result from a trade-off between integration constraints and performance requirements.

This paper presents an overview of the complex issues linked to the diagnostics integration in ITER, providing preliminary guidelines to address them. These issues have been recently tackled in the frame of a study performed in Europe regarding a specific port plug, the Equatorial Port Plug 1.

ITR-P

Assessing the Nuclear Environment for ITER Port Plugs and Port-based Diagnostics

R. Feder¹, M. Youssef², and S. Pitcher³

¹*Princeton Plasma Physics Laboratory, Princeton, USA*

²*University of California, Los Angeles, USA*

³*ITER Organization, Saint Paul Lex Durance, France*

Corresponding Author: rfeder@pppl.gov

ITER diagnostic systems will operate in a harsh nuclear environment. Component protection and nuclear shielding is realized by housing diagnostics inside massive steel port plug structures. The diagnostic port plugs must be optimized to provide adequate diagnostic throughput while minimizing the flux of escaping nuclear radiation and staying under a total dry weight of 45 metric tons. Most diagnostic systems are in the conceptual design phase and the optimization of this balance between performance, weight and shielding has not yet been realized. Sophisticated analysis tools are needed to predict the performance of components in ITER since actual measurements of the environment may not be realized for some time. The commercially available discrete-ordinates code Attila has been used for the conceptual phase analysis of several ITER diagnostics and diagnostic port plugs. Assessment of the diagnostic port plug nuclear environment with Attila is essentially a 3-step process involving a neutron transport run, a calculation of the activation and depletion in steel structures and finally the transport of the activated steel gamma rays.

This paper will survey current neutronics results for a selection of Upper and Equatorial port plugs and the diagnostic systems in these ports. General port plug neutronics results like total nuclear heating and general shielding issues will be described. Specific diagnostic design studies will also be presented with a focus on meeting diagnostic measurement requirements while achieving adequate shielding. For example, the Core Imaging X-Ray Spectrometer diagnostic cannot use labyrinths to mitigate neutron and gamma flux. A multi-faceted solution approach was needed. This includes the use of radial baffles to limit streaming to only collimated neutrons and the narrowing of apertures that limits streaming while still allowing for minimum system performance. Many diagnostics have mirrors and shutters in the very front of the port plugs where nuclear heating is on the order of 6 W/cc. This paper will summarize the current diagnostic first wall and shield block neutronics around these “first mirrors”.

This work is supported by DOE contract numbers DE-AC02-09CH11466 (PPPL) and DE-AC05-00OR22725 (UT-Battelle, LLC). The views and opinions expressed herein do not necessarily reflect those of the ITER Organization.

Error Fields Expected in ITER and their Correction

Y. Gribov¹, V. Amoskov², E. Lamzin², N. Maximenkova², J. E. Menard³, J. K. Park³,
V. Belyakov², J. R. Knaster¹, and S. Sytchevsky¹

¹ITER Organization, St Paul Lez Durance, France

²Efremov Scientific Research Institute, St. Petersburg, Russian Federation

³Princeton Plasma Physics Laboratory, Princeton, USA

Corresponding Author: yuri.gribov@iter.org

This paper summarises the present status in the study of error fields expected in ITER ($n = 1$ modes) and their correction. Two approaches were used in the study of ITER error fields: analysis of the “3-mode” error fields and analysis of the “overlap” error fields. Since the earliest phase of the ITER design activity, the “3-mode” error field criterion on the weighted averaged amplitude of the (1, 1), (2, 1) and (3, 1) Fourier modes of the component of magnetic field normal to the $q = 2$ surface has been used to determine the allowable level of error fields. The newly developed criteria on “overlap” error fields and algorithm for calculation of the “overlap” error field has been derived from analysis performed with the IPEC code for three fiducial ITER plasmas. The IPEC code calculates those components of the external error fields which are most efficient at driving the growth of a magnetic island, taking into account the perturbation to the plasma equilibrium associated with the external fields.

Error fields expected in ITER from different sources are analysed:

1. The main contributor to the error fields — misalignments of TF, CS and PF coils.
2. TF, CS and PF coils joints and busbars.
3. Ferromagnetic structures of the six test blanket modules.
4. Irregularity of the ferromagnetic inserts located near NBI ports and scattering in the values of the steel plate thicknesses and saturated magnetization.
5. Magnetic field reduction system of NBIs.
6. Ferromagnetic elements of the bioshield and tokamak complex (rebar in concrete).
7. Scattering in weak magnetic permeability of the austenitic steel from which the cryostat, the cryostat thermal shield and the vacuum vessel thermal shield are made.

The main actuator for error field correction in ITER is the correction coils (CC). The analysis performed has shown that CC are capable to reduce the expected error fields below the present criteria. The primary objective of the ELM coils is the control of Edge Localized Modes with the goal of avoiding excessive heat loads on the plasma facing components of the tokamak. However, in combination with CC, ELM coils can be used in some experiments for identification of the error fields and for study of how they should be reduced. Capability of ELM coils to correct error fields has been analyzed.

Status of Thomson Scattering in ITER Divertor

E. Mukhin¹, A. Razdobarin¹, V. Semenov¹, S. Tolstyakov¹, M. Kochergin¹,
G. Kurskiev¹, S. Masyukevich¹, A. Berezutsky¹, P. Chernakov¹, A. Koval¹, and
P. Andrew²

¹*Ioffe Physical Technical Institute, St. Petersburg, Russian Federation*

²*ITER Organization, Saint Paul Lez Durance, France*

Corresponding Author: e.mukhin@mail.ioffe.ru

Detailed measurements of electron parameters in the ITER divertor will be an important part of the experimental program and will be used to study the divertor's ability to adequately deal with plasma position during disturbances and adequately screen impurities released by intense plasma-surface interaction. The divertor Thomson scattering (TS) system is well suited for this purpose. Although TS for ITER will be nominally similar to those used on previous devices, its implementation will be quite different. The large scale of the ITER vacuum vessel and the long distance from the vacuum boundary to plasma boundary (5 – 10 m) necessitates including in-vessel diagnostic components in the ITER design. The in-vessel diagnostic component design has to take into account the nuclear nature of the ITER device as well as the presence of intensive erosion and redeposition. In addition, the in-vessel diagnostic components have to withstand possible mechanical deformations, displacements during cooling/heating procedures as well as powerful electromagnetic forces generated by the interaction between eddy currents induced during disruptions and the strong magnetic field (~ 5 T). The main difficulties and challenges for the divertor TS and many other ITER diagnostics are the operability of the components located close to the first wall. The diagnostics has to provide reliable data on the electron parameters near the ionization front characterized by very steep gradients of n_e and $T_e = n_e$ in the range of $10^{19} - 10^{21} \text{ m}^{-3}$ and T_e from several ten's of eV to extra-low values around 1 eV. Additional challenges include a limited diagnostic access to the plasma and a weak laser scattering signal to be detected against intense background radiation.

System-Level Optimization of ITER Magnetic Diagnostics: Preliminary Results

G. Ambrosino¹, S. Arshad², G. Vayakis³, R. Albanese¹, V. Coccoresse¹, A. Pironti¹,
G. Rubinacci¹, L. Appel⁴, T. Hender⁴, M. Ariola⁵, P. Bettini⁶, M. Brombin⁶,
R. Delogu⁶, S. Peruzzo⁶, L. Zabeo³, C. Cianfarani⁷, F. Crisanti⁷, V. Fusco⁷,
P. Micozzi⁷, G. Ramogida⁷, O. Tudisco⁷, G. Vlad⁷, M. Mattei⁸, and F. Villone⁸

¹ *Università di Napoli Federico II, Naples, Italy*

² *Fusion for Energy (F4E), Barcelona, Spain*

³ *ITER Organization, Saint Paul Lez Durance, France*

⁴ *EURATOM/CCFE Fusion Association, Culham Science Centre, Abingdon, UK*

⁵ *CREATE/ENEA/Euratom Association, Università di Napoli Parthenope, Naples, Italy*

⁶ *Consorzio RFX, EURATOM/ENEA Association, Padova, Italy*

⁷ *ENEA/EURATOM Association, Centro Ricerche Frascati, Frascati, Italy*

⁸ *CREATE/ENEA/Euratom Association, Seconda Università di Napoli, Naples, Italy*

Corresponding Author: ambrosin@unina.it

The present accuracy requirements on ITER parameters to be obtained primarily from magnetic measurements are demanding and, in many situations, they might be not achieved. As a consequence, in specifying the diagnostic, either the requirements should be qualified or the overall process for the estimation of each parameter should be modified.

Although previous work in this area has been reported this is the first study combining the complete baseline diagnostic with a realistic and detailed description of the ITER machine, in 3D.

The paper considers two different estimation problems:

1. Reconstruction of plasma equilibrium (plasma current and plasma-wall gaps).
2. Identification of n and m of TAE perturbations.

As far as the first problem is concerned, we firstly give an estimation of the parameter reconstruction errors obtainable with standard axisymmetric 2D equilibria using the EFIT++ reconstruction code. In particular the analyses have been carried out on an ITER equilibrium database composed of 322 axis-symmetric static plasma equilibria (with no eddy currents) and 150 axis-symmetric perturbed plasma equilibria (in the presence of eddy currents). The first set of analyses assumed ideal sensors. Additional analyses to account for the sensor measurement errors are also presented. The main conclusion is that, even ignoring additional sources of uncertainty, considered in the next section, the accuracy requirements are not met under all conditions. Successively, we evaluate the pick-up on magnetic sensors and the impact on the gap reconstruction accuracy due to three different sources:

- 3D non-axisymmetric eddy currents induced by the plasma and actuator coils.
- Non-axisymmetric in-vessel actuator coils (ELM coils) for plasma control.
- 3D non-axisymmetric ferritic materials.

The analysis of the TAE perturbations is carried out using a new approach proposed by the authors. It is based on the use of MARS code to generate the magnetic field perturbation due to a given TAE on the plasma boundary, in presence of a fictitious ideal wall, and on the determination of a current-carrying sheet, sufficiently inside the plasma surface, providing approximately the same field on the plasma boundary. This current distribution is then used to determine the propagation of the magnetic field to the sensors, using the CARIDDI code.

Electron Kinetic Effects on Interferometry, Polarimetry and Thomson Scattering in Burning Plasmas

V. Mirnov¹, D. Brower², D. Den Hartog¹, W. Ding², J. Duff¹, and E. Parke¹

¹*University of Wisconsin-Madison, Madison, USA*

²*University of California, Los Angeles, USA*

Corresponding Author: vmirnov@wisc.edu

Several major optical diagnostics are under development for plasma parameters, magnetic field and current control in ITER: Thomson scattering (TS), toroidal interferometer/polarimeter (TIP) and poloidal polarimeter (PP). Since these diagnostics are needed for basic machine operation as well as physics studies, accurate measurements are required to meet the ITER goals. Each of these measurements is based on the electron response to laser light propagating in plasma. At anticipated ITER plasma conditions, the effects of electron thermal motion will be significant and must be accurately treated or the diagnostics will fail to meet the measurement requirements for ITER operation. The primary focus of our work is to examine the effects of electron thermal motion on the refractive indices and polarization of high-frequency electromagnetic waves (specifically laser light, both directed and scattered). We calculate:

1. Thermal corrections to the interferometric phase and polarization state of the wave propagating in the direction of the incident laser beam (Faraday and Cotton-Mouton polarimetry).
2. Perform analysis of the degree of polarization for incoherent TS.

Our earlier linear in electron temperature T_e calculations predicted 10 – 30% corrections for the interferometric phase, Faraday rotation, and Cotton-Mouton effect at $T_e = 30$ keV. Knowing electron temperature from the Thomson scattering, the thermal effects can be corrected. This has already been included in the error analysis and design projections of the ITER TIP and PP systems. The new findings are:

1. The precision of the previous lowest order linear in T_e model may be insufficient; we present a more precise model with quadratic corrections to satisfy the high accuracy required for ITER TIP and PP diagnostics. The importance of these results and their practical application for the ITER TIP and PP systems are discussed.
2. The degree of polarization of incoherent Thomson scattered laser light is calculated accurately without approximation for the full range of incident polarizations, scattering angles, and electron thermal motion from non-relativistic to ultra-relativistic.

The results are discussed in the context of the possible use of the polarization properties of Thomson scattered light as a method of T_e measurement relevant to ITER operational scenarios.

Work supported by USDOE and NSF.

ITPA Assessment of ITER Microwave Diagnostic Design Issues

G. Conway¹, G. Vayakis², V. Udintsev², M. Austin³, G. Hanson⁴, A. Stegmeir¹,
T. Peebles⁵, V. Petrov⁶, and T. Estrada⁷

¹*Max-Planck-Institut für Plasmaphysik, Garching, Germany*

²*ITER Organization, St Paul Lez Durance, France*

³*Institute for Fusion Studies, University of Texas, Austin, USA*

⁴*Oak Ridge National Laboratory, Oak Ridge, USA*

⁵*University California Los Angeles, Los Angeles, USA*

⁶*TRINITI, Moscow, Russian Federation*

⁷*Laboratorio Nacional de Fusión, Asociación Euratom-CIEMAT, Madrid, Spain*

Corresponding Author: garrard.conway@ipp.mpg.de

The microwave-based diagnostic suite proposed for ITER includes Electron Cyclotron Emission, Reflectometry, Collective Thomson Scattering and Refractometry. Their common feature is the use of simple in-vessel metallic antennas and waveguide transmission lines (front-end components) which are relatively insensitive to radiation damage. However, once installed they will be difficult to replace or modify, hence, their careful design is a pressing issue. In contrast, the back-end microwave transceivers (which are well developed and can employ the latest technology) will be accessible and less problematic. Here, several topics critical to the overall diagnostic designs and component selection are assessed. These include the provision for in-situ component and system calibration. E.g., initial performance measurements (losses, reflections, mode-conversion) are required to allow identification of component degradation. All the microwave diagnostics will be susceptible to stray radiation damage from non-absorbed ECRH and CTS gyrotron beams or from fast electron generated Bremsstrahlung. Various options and techniques, such as combinations of fast acting shutters, waveguide filters, fuses etc. have been identified to protect the sensitive diagnostic electronics and TL components, such as polarization splitters etc. The Low-Field-Side Reflectometer system is at a crucial design phase — systematic studies of the design drivers as well as the placement and alignment of the antennas using beam-tracing codes have been performed. A major issue is the sensitivity of the probing beam to vertical movements of the plasma column, which is linked to the selection of antenna gain and placement, monostatic vs bistatic antenna arrangements, and fixed antenna alignments vs steerable antennas. The timely assessment of these diagnostic issues has directly impacted the detailed diagnostic designs — which will shortly be placed in the hands of the respective ITER domestic agencies.

Mirrors for ITER Optical Diagnostics

A. Razdobarin¹, E. Mukhin¹, V. Semenov¹, S. Tolstyakov¹, M. Kochergin¹,
G. Kurskiev¹, A. Berezutsky¹, D. Kirilenko¹, A. Sitnikova¹, S. Masyukevich¹,
P. Chernakov¹, V. Voitsenya², V. Bondarenko², V. Konovalov², I. Ryzhkov²,
O. Skorik², A. Gorodetsky³, V. Bukhovets³, R. Zalavutdinov³, A. Zakharov³,
I. Arkhipov³, A. Smirnov⁴, T. Chernoziumskaya⁴, E. Khilkevitch⁴, K. Vukolov⁵,
I. Orlovskiy⁵, A. Alekseev⁵, and P. Andrew⁶

¹*Ioffe Physical Technical Institute of the Russian Academy of Sciences, St. Petersburg, Russian Federation*

²*National Science Centre, Kharkov Institute of Physics and Technology, Kharkov, Ukraine*

³*Frumkin Institute of Physical Chemistry and Electrochemistry, Moscow, Russian Federation*

⁴*Saint-Petersburg State Polytechnic University, St. Petersburg, Russian Federation*

⁵*National Research Centre "Kurchatov Institute", Moscow, Russian Federation*

⁶*ITER Organization, Saint Paul Lez Durance, France*

Corresponding Author: aleksey.razdobarin@mail.ioffe.ru

The large distance between ITER vacuum windows and the plasma boundary necessitates the use of in-vessel optical diagnostic components. High particle fluxes, temperature and radiation level expected inside ITER imposes considerable limitations on mirrors design. The choice of FM (First Mirrors) structure and material depends on the mirror location and on the diagnostic needs.

The presentation covers the most general approaches to the FM problem in ITER and demonstrates the implantation of basic concepts in the design of FM in the divertor Thomson scattering system. The FM design options and their advantages and disadvantages in different operation conditions expected in ITER are discussed along with new results on the development of optics cleaning and deposition-mitigating techniques. The focus is on the efficiency of plasma cleaning combined with blowing out contaminations. The impact of plasma treatment on the mirror surface is also discussed. The parameters of cleaning capacitively-coupled discharge in working ITER gas — deuterium were calculated within the hydrodynamic model and experimentally verified. The blowing-out efficiency has been estimated for the prototype of the divertor laser launcher duct. The implementation of other protection and cleaning techniques, like laser cleaning, heating and shutters is considered.



Progress on Design and R&D for ITER Diagnostic Systems in Japan Domestic Agency

Y. Kawano¹, Y. Kusama¹, T. Kondoh¹, T. Hatae¹, K. Sato¹, H. Ogawa¹, M. Ishikawa¹,
T. Sugie¹, E. Yatsuka¹, R. Imazawa¹, M. Takeuchi¹, T. Shimada¹, T. Hayashi¹,
T. Yamamoto¹, T. Ono¹, Y. Seki¹, S. Suzuki¹, L. Bertalot², G. Vayakis², C. Watts²,
R. Barnsley², P. Andrew², R. Reichle², A. Encheva², C. Walker², S. Pitcher²,
V. Udintsev², and M. Walsh²

¹Japan Atomic Energy Agency, Naka, Japan

²ITER Organization, Saint Paul Lez Durance, France

Corresponding Author: kawano.yasunori@jaea.go.jp

Japan Domestic Agency (JADA) has been conducting the design and R&D for six ITER diagnostic systems that JADA is responsible for. In summary: For the Microfission Chambers, the prototyping of the vacuum tight triaxial connector has indicated that it could be used in the ITER environment, and a neutron transport analysis has shown that the cooling water pipe in the blanket module should be filled with water for in-situ calibration of the diagnostic. For the Edge Thomson Scattering System, the stray light level can be reduced by a factor of 10 by a new beam dump design with chevron shaped fins. The target performance of the prototype YAG laser system, i.e., 5 J of output energy and 100 Hz repetition rate, has been successfully achieved. A novel in-situ calibration method has been proposed based on the detection of bremsstrahlung emissions. For the Poloidal Polarimeter, a new design of robust mirror modules in the port plugs has been developed, in which the plasma facing mirrors and mirror support structure are unified. Optical analyses of the retroreflectors, which are deformed by nuclear heating, have indicated that about 50 – 70% of the laser power can be returned to the diagnostic hall. For the Divertor Impurity Influx Monitor, the detected signal would increase by a factor of 10 using a new design of equatorial port optics with components which are tolerant to gamma-ray irradiation. The bidirectional reflectivity distribution function of the tungsten block has been measured for the first time to study the surface reflection effect. For the Divertor Thermocouples (Outer Target), an R&D result indicated that a metal foil could be bonded to the divertor target as an attachment point for the thermocouples. Finally, for the Divertor IR-Thermography, the requirement specifications for the optics have been studied using estimated spectral radiance of the target.

Reconstruction of Distribution Functions of Fast Ions and Runaway Electrons in ITER Plasmas Using Gamma-Ray Spectrometry

A. Shevelev¹, I. Chugunov¹, V. Kiptily², D. Doinikov¹, D. Gin¹, E. Khilkevitch¹, and V. Naidenov¹

¹*Ioffe Physical-Technical Institute of the Russian Academy of Sciences, St. Petersburg, Russian Federation*

²*EURATOM/CCFE Fusion Association, Abingdon, UK*

Corresponding Author: shevelev.cycla@mail.ioffe.ru

Vertical Gamma-Ray Camera (VGC) system of ITER is being designed in Ioffe Institute. Using gamma-ray spectrometers allows solving one of the most important issues for the safe tokamak operations — the runaway electrons diagnostics. Monte-Carlo model calculations of bremsstrahlung fluxes in the place of the VGC detectors installation were carried out for different ITER plasmas and plasma impurities. Tomographic measurements of the HXR emission profile can provide important information on runaway beam location in the ITER plasmas and allow estimating the value of the runaway current in the MeV energy range.

Code DEGAS has been developed for deconvolution of gamma-ray spectra emitted from plasmas. The code can be applied to reconstruct the runaway electrons energy distribution basing on the recorded HXR spectra. Results of Monte-Carlo modeling of the gamma-ray spectrometers response functions and bremsstrahlung spectra calculated for electrons in wide energy range are used in the DEGAS code. Deconvolution of gamma-ray and HXR spectra allows identifying nuclear reactions, which take place during plasmas discharge, calculating their gamma-ray lines intensities and determining the maximal energy of runaway electrons with accuracy satisfied to the ITER Project Requirements. Using the DEGAS code during processing of the spectra recorded at JET experiments increased the peak-to-background ratio in 2 – 3 times. Application of the deconvolution technique during tomographic measurements of gamma-ray emission profiles can facilitate the reconstruction of spatial distributions of different fast ions in ITER plasmas.

This work was supported by RF State contracts N.4k.52.90.11.1094 and N.4k.52.90.11.1151.



Evolution of the ITER Diagnostic Set Specifications

G. Vayakis¹, C. Watts¹, R. Reichle¹, M. Walsh¹, R. Barnsley¹, L. Bertalot¹,
S. Pitcher¹, V. Ushintsev¹, E. Veshchev¹, P. Andrew¹, R. Bouhamou¹, and J. Snipes¹

¹ITER Organization, Saint Paul lez Durance, France

Corresponding Author: george.vayakis@iter.org

The ITER diagnostic set [1] and proposed specifications, developed jointly with the ITPA [2], were formally reviewed together in 2007. Key results of this process were presented in Ref. [3]. Since then, ITER diagnostic designs have progressed [4] and been taken through their conceptual design reviews (CDRs), a process that is about 2/3 complete. In the process of arriving at a diagnostic specification for each CDR, the ability of a diagnostic to meet its contribution to the project measurement requirements (PR, [5]) is also reviewed. In turn, this allows a review of the justification of these requirements. To ensure consistency, and to ensure that the integrated diagnostic set performance meets ITER needs and, in particular, the needs for plasma control, a parallel process of recording the rationale behind the measurement parameter specifications, expanding the specification to deal with specific conditions and justifying the diagnostic roles is underway. Parameters that have already undergone extensive review include most the density-related parameters and all of the parameters with a primary contribution from magnetic diagnostics as well as the current profile. A complete update will be included in the contributed paper, together with key implications for the ITER diagnostic set.

References

- [1] A. Costley *et al.*, (IT/1-5) The design and implementation of diagnostic systems on ITER, Proc. 21st IAEA FEC, Chengdu (2006), IAEA-CN-149.
- [2] A. J. H. Donné *et al.*, Chapter 7: Diagnostics, Nucl. Fusion **47** (2007) S 337 ff.
- [3] A. Costley *et al.*, (IT/P6-21) Measurement Requirements and the Diagnostic System on ITER: Modifications Following the Design Review, Proc. 22nd IAEA FEC, Geneva (2008), IAEA-CN-165.
- [4] M. J. Walsh *et al.*, (ITR/P1-07) Overview of high priority ITER Diagnostic systems status, Proc. 23rd IAEA FEC, Daejeon (2010), IAEA-CN-180.
- [5] ITER Organization, Project Requirements version 4.6 (2010), internal document.

Analysis of Current Profile Measurement Capability on ITER

R. Imazawa¹, Y. Kawano¹, M. De Bock², F. Levinton³, N. Hawkes⁴, M. Beurskens⁴,
P. McCarthy⁵, C. Watts⁶, R. Barnsley⁶, M. Von Hellermann⁷, H. Park⁸, G. Vayakis⁶,
R. Boivin⁹, D. Johnson¹⁰, Y. Kusama¹, and M. Walsh⁶

¹Japan Atomic Energy Agency, Naka, Japan

²Eindhoven University of Technology, Eindhoven, Netherlands

³Nova Photonics, Princeton, USA

⁴Culham Centre for Fusion Energy, Culham Science Centre, Abingdon, UK

⁵University College Cork, Cork, Ireland

⁶ITER Organization, St. Paul lez Durance, France

⁷Dutch Institute for Fundamental Energy Research, Nieuwegein, Netherlands

⁸Pohang University of Science and Technology, Pohang, Republic of Korea

⁹General Atomics, San Diego, USA

¹⁰Princeton Plasma Physics Laboratory, Princeton, USA

Corresponding Author: imazawa.ryota@jaea.go.jp

In this study, the CUPID (Current Profile Identification) code is applied for the first time to assess

1. the accuracy of q profile measurement utilizing both the poloidal polarimeter and motional Stark effect (MSE) diagnostic,
2. influence of the tilted heating neutral beam (HNB) for the q profile measurement, and
3. the accuracy of q profile measurement during the start-up phase.

CUPID determines a current profile consistent with the measurement data from the poloidal polarimeter, MSE, the position and shape of the last closed flux surface, the total plasma current and the electron density and temperature measured by Thomson scattering. We added random errors to the input data and ran CUPID 40 times in order to obtain the cumulative distribution function (CDF) of the maximum error of the identified q -value. The measurement data of the poloidal polarimeter are orientation, θ , and ellipticity angle, ε , of the polarization state of the probe laser beam. The measurement data of MSE is pitch angle, γ . We estimate the maximum error (evaluated as the error of the q -value when the value of CDF equals to 0.954) of q -identification with varying standard deviation of θ , ε , and γ (σ_θ , σ_ε), and (σ_γ) and several conditions of HNB. The analysis results suggest that at least one of σ_θ or σ_γ , with 0.1 degree or less is needed to satisfy the required accuracy of q (10 %) at start-of-burn phase of S2 and S4. The error of q profile measurement by the poloidal polarimeter and MSE with the off-axis HNB is not significantly different from that by the poloidal polarimeter and MSE with the on-axis HNB. Therefore, even though the information around the magnetic axis lacks, MSE with the off-axis HNB is informative for the q -profile identification. It is recommended that both σ_θ and σ_γ , are 0.1 degree or less to keep redundancy in diagnostics. The analysis results of the start-up phase suggest that the accuracy of q identified by only the poloidal polarimeter could be less than 10 % when σ_θ is less than 0.1 degree.

ITER High Resolution Gamma Spectrometry

D. Gin¹, I. Chugunov¹, A. Shevelev¹, M. Petrov¹, S. Petrov¹, V. Afanasyev¹,
M. I. Mironov¹, V. Kiptily², A. Pasternak¹, E. Khilkevitch¹, and V. Naidenov¹

¹*Ioffe Physical-Technical Institute of the Russian Academy of Sciences, St. Petersburg,
Russian Federation*

²*EURATOM-CCFE Fusion Association, Abingdon, UK*

Corresponding Author: pipha@mail.ru

Gamma-ray spectrometric systems on tokamaks provide means for fast ions and runaway electrons diagnostics. High resolution of HPGe detectors allows registering shapes of gamma lines. Analysis of Doppler broadened lineshapes (LS) can be used for obtaining parameters of fast ions distribution functions (DF) as it was proved in JET experiments. Recent progress in ITER diagnostics development includes adding to the NPA (neutral particles analyzer) project the high resolution gamma-detector (HRGD). Common viewable volume of plasma makes joint analysis of diagnostics data notably more convenient. Indeed, information on lines intensities can be used for deducing the relative plasma components densities, particularly D/T ratio — which is one of the main tasks for NPA. High resolution of the HRGD allows obtaining anisotropy parameters of DF, which are complimentary to NPA data on distribution of perpendicular to magnetic field component of particles speeds. Even more complete data can be obtained using gamma- and neutron- tomography under development for ITER.

At the moment conceptual design of the new NPA diagnostic complex is under development. Using MCNP calculations:

1. Feasibility of the concept demonstrated.
2. Parameters of the shield and ⁶LiH attenuator to be placed in front of detector formulated.
3. Estimated expected detector loads and neutron and gamma fields in diagnostic room and behind it.

Monte-Carlo codes are developed and under further improvement for establishing connection between DFs and LSs. Additional semi- analytical models suggested for corresponding data cross-checking. Finally, application of different signal processing techniques including deconvolution and trapezoidal codes have been analyzed. Mentioned techniques were found being able to ensure higher detection efficiency (up to 10⁶ counts/sec) than available stock solutions.

Overview of the ITPA R&D Activities for Optimizing ITER Diagnostic Performance

H. K. Park¹, Y. Kawano², G. Vayakis³, M. Beurskens⁴, G. Conway⁵, N. Hawkes⁴,
S. Popovichev⁴, B. Stratton⁶, and C. Skinner⁶

¹*POSTECH, Pohang, Republic of Korea*

²*Japan Atomic Energy Agency, Naka, Japan*

³*ITER Organization, St Paul Lez Durance, France*

⁴*CCFE, Culham Science Centre, Abingdon, UK*

⁵*MPI für Plasmaphysik, Garching, Germany*

⁶*PPPL, Princeton, USA*

Corresponding Author: hyeonpark@postech.ac.kr

The research and development activity of the International Tokamak Physics Activity Topical Group (ITPA TG) on Diagnostics is focused on identification and solutions for diagnostic techniques, which are critical for ITER scientific goals. While majority of diagnostic systems has been developed and integrated with the main body, several issues related to ITER environment are still outstanding and R&D efforts on these issues are progressing. In order to demonstrate reheating of fusion products, the measurement of escaping alpha particles, which may lead to excess erosion and damages on the first wall, is critical in addition to the measurement of confined alphas. An accurate confirmation of the fusion energy gain entirely relies on the precise neutron (from DD and DT reactions) measurement and its calibration. Life time issue of the plasma facing mirror for all optical diagnostics is critical due to the degraded reflectivity of these mirrors over the operation period. Safety requirements demand an accurate assessment on dust and erosion of the first wall material and divertor plate. Impacts of the reflected plasma emission from the in-vessel wall are critical for the performance of diagnostic system. Diagnostic issues for plasma initiation and ramp-down phases are critical for monitoring and controlling the plasmas. Impact of in-vessel stray microwave radiation even in moderate level can be detrimental for the microwave based diagnostic systems.

Exploring Measurement Capabilities of ITER ECE System

V. Udintsev¹, G. Vayakis¹, M. Walsh¹, M.-F. Drez¹, J. Snipes¹, C. Watts¹, K. Patel¹,
M. Austin², H. Pandya³, R. Feder⁴, D. Johnson⁴, P. Vasu³, A. Hubbard⁵, W. Rowan²,
and P. Phillips²

¹*ITER Organization, Saint Paul Lez Durance, France*

²*University of Texas at Austin, Austin, USA*

³*ITER-India, Institute for Plasma Research, Bhat, India*

⁴*Princeton Plasma Physics Laboratory, Princeton, USA*

⁵*Massachusetts Institute of Technology, Plasma Science and Fusion Center, Cambridge, USA*

Corresponding Author: victor.udintsev@iter.org

The Electron Cyclotron Emission diagnostic provides essential information for plasma operation and for establishing performance characteristics in ITER [1]. The ECE diagnostic design has to address the specifications in the ITER project measurement requirements. The different requirements are specified with different spatial, temporal and spectral resolutions and accuracy.

The relativistic downshift at high temperatures, which in ITER is substantial, will strongly influence the access to the plasma for ECE. Integrated performance for the temperature measurement is, however, adequate when all T_e systems (ECE and two Thomson scattering systems) are considered together. A prioritization has been given to the core electron temperature measurement and to NTM detection. For the characterization of the temperature perturbation caused by NTMs, ECE is the only diagnostic that can deliver this measurement.

However, there are other measurements that can be exploited by ECE, thus increasing significantly the contribution of the diagnostic to the scientific and operational program of ITER. There is a functional requirement for the broadband measurement system to measure the total radiated power due to ECE. The specified frequency for the broadband measuring system is from 70 GHz up to 1 THz. The diagnostic capability to measure the spectra at these frequencies has to be assessed during the detailed design phase, taking into account the physics and technical constraints the layout of the transmission line, the back-end instrumentation and the performance of the system for priority measurements.

The present design of the system permits measurements of both the X and O mode radiation simultaneously along two lines-of-sight, one perpendicular to the plasma and another at the slightly oblique (toroidal) angle of about 10 degrees. In scenarios with strong additional heating (radio frequency, neutral beam and possibly alpha heating), deformations of the electron distribution function can occur. Simultaneous observation of several ECE harmonics, together with oblique ECE, can provide some important information for modeling the velocity distribution.

A complete update on the ITER ECE measurement capabilities and their impact on the system design will be included in the contributed paper.

References

- [1] A. E. Costley, *Fus Sci Technol.* **55** (2009) 1.

First Studies of ITER Diagnostic Mirrors in a Tokamak with All-metal Interior: Results of First Mirror Test in ASDEX Upgrade

A. Litnovsky¹, M. Matveeva¹, A. Herrmann², V. Rohde², V. Voitsenya³, G. Vayakis⁴,
A. E. Costley⁴, P. Wienhold¹, G. de Temmerman⁵, S. Richter⁶, U. Breuer⁷,
B. Luxherta⁸, S. Möller¹, V. Philipps¹, U. Samm¹, and ASDEX Upgrade Team¹

¹*Forschungszentrum Jülich, Jülich, Germany*

²*Max-Planck-Institut für Plasmaphysik, Garching, Germany*

³*IPP, NSC Kharkov Institute of Physics and Technology, Kharkov, Ukraine*

⁴*ITER Organization, St. Paul Lez Durance, France*

⁵*Dutch Institute For Fundamental Energy Research, Nieuwegein, Netherlands*

⁶*Central Facility for Electron Microscopy, Aachen, Germany*

⁷*Central Division of Analytical Chemistry, Forschungszentrum Jülich, Jülich, Germany*

⁸*Department of Applied Physics, Ghent University, Ghent, Belgium*

Corresponding Author: a.litnovsky@fz-juelich.de

In ITER, mirrors will be used as plasma-viewing elements in all optical and laser diagnostics. In the harsh environment mirror performance will degrade hampering the operation of respective diagnostics. The most adverse effect on mirrors is caused by the deposition of impurities and it is expected that the most challenging situation will occur in the divertor. With envisaged changes to all-metal plasma-facing components (PFCs) in ITER, an assessment of mirror performance in the existing divertor tokamak with all-metal PFCs is urgently needed. Such an experiment was made in the ASDEX Upgrade with all-tungsten PFCs as proposed by the International Tokamak Physics Activity (ITPA) Topical Group on Diagnostics, supported by the Specialists Working Group on First Mirrors and carried out in the frame of collaboration between Forschungszentrum Jülich and IPP Garching.

Four molybdenum and four copper mirrors were mounted at the inner wall, in the dome facing the inner and outer divertor targets and in the pump-duct and exposed for seven months in ASDEX Upgrade. After exposure, degradation of the reflectivity was detected on all mirrors. The mirrors in the pump duct almost preserved their reflectivity unlike the mirrors in the dome facing the outer divertor which suffered from highest deposition and the strongest reflectivity degradation. Remarkably, only on the mirror facing the inner divertor and having very thin deposition layer of 15 nm, the carbon fraction was about 50 at.%. On all other mirrors this fraction did not exceed 20 at.%.

The exposure of diagnostic mirrors in the tokamak with all-metal PFCs demonstrated a positive trend to a reduction of net deposition and minor changes in the reflectivity of mirrors located in the pump-duct far away from divertor plasmas. However, the degradation of all exposed mirrors underlines the necessity of an active mirror recovery. Urgent R&D is needed to address the lifetime issues of mirrors in ITER divertor.

Exploring the Engineering Performance Limits of DNB

C. Rotti¹, A. K. Chakraborty¹, M. Bandyopadhyay¹, M. Singh¹, R. Gangadharan¹,
I. Ahmed¹, S. Shah¹, C. Julien², B. Schunke², D. Boilson², J. Graceffa²,
R. Hemsworth², and L. Svensson²

¹ITER-India, Institute for Plasma Research, Gandhinagar, India

²ITER Organisation, St Paul Lez Durance, France

Corresponding Author: crotti@iter-india.org

Amongst the two Neutral Beam systems for ITER, the Diagnostic Neutral Beam (DNB) system has a special operational mandate to provide a 100 keV, ~ 20 A beam to ITER, with a modulation frequency of 5 Hz having duty cycle of 3 s ON – 20 s OFF for 3600 s. The modulation of beam is realised by the application of modulating acceleration and extraction voltage levels; thereby leading to a modulation of power density incident on the beam facing heat flux receiving components — accelerator & electron dumps system, neutraliser, residual ion dump (RID), calorimeter, exit scraper and duct liner. The design requirements have been generated taking into consideration the ITER needs and engineering design of these components has been carried out considering modulated high heat flux and the corresponding thermal hydraulic engineering. Different scenarios such as operational, test, handling, emergency and faulted conditions are considered and the analysis have been performed by FEA software- ANSYS. Both monotonic as well as cycle type structural damage verifications were performed using ITER SDC-IC. Final designs of all components have been arrived at after different stress intensities conformed to the criterion levels of SDC-IC. The BTP specifications for DNB components take into account this conformity and incorporate adequate safety margin.

While this design meets the requirements of the mandate for DNB, there is a need to assess the limits of operation of DNB in terms of the following:

1. The maximum length of time, beyond 3 s for with the modulation can be sustained.
2. The maximum pulse length for which the beam can be operated without modulation.

These inputs will help CXRS, BES diagnosticians to design their diagnostic setup for the maximum level of performance. The performance characterisation of DNB to be carried out in the Indian-Test Facility (INTF), which include provisions to tests those above mentioned limits. The paper presents the results of assessments that have been carried out and provides recommendations for the maximum operation limits.

Theoretical Issues of High Resolution H- α Spectroscopy Measurements in ITER

A. B. Kukushkin¹, V. S. Lisitsa¹, M. B. Kadomtsev¹, M. G. Levashova¹,
V. A. Shurygin¹, V. Kotov², A. S. Kukushkin³, S. Lisgo³, A. G. Alekseev¹,
A. V. Gorshkov¹, D. K. Vukolov¹, K. Y. Vukolov¹, V. S. Neverov¹, and E. Veshchev³

¹*NRC "Kurchatov Institute", Moscow, Russian Federation*

²*Forschungszentrum Jülich, Jülich, Germany*

³*ITER Organization, Saint Paul Lez Durance, France*

Corresponding Author: kuka@nfi.kiae.ru

A survey of theoretical issues of high resolution H-alpha spectroscopy measurements in ITER, which have been under consideration at the stage of the H- α (and Visible Light) Spectroscopy Diagnostic Conceptual Design Review, is given. These include:

1. Comparative analysis of predictive numerical modeling of 2D spatial distributions of plasma parameters (densities and temperatures) in the divertor and scrape-off layer (SOL) at a steady-state stage of discharge in ITER with the SOLPS4.3 (B2-EIRENE) code.
2. Semi-analytic, 1D model of neutral atoms velocity distribution function (VDF) in the SOL and its comparison with the EIRENE stand-alone simulations of neutral deuterium VDF, applied on the plasma background calculated by the SOLPS4.3 (B2-EIRENE) code.
3. Semi-analytic model for the spectra of the light emitted in the Balmer lines in divertor and taken by spectrometers after diffusive or multiple mirror reflections from all-metal first wall (divertor stray light (DSL) problem).
4. Formulation of an inverse problem for assessment of tritium-to-deuterium ratio and total neutral density recovery in the SOL from high resolution H- α spectroscopy measurements.
5. Assessment of the above measurements' accuracy under condition of a substantial dominance of DSL spectral intensity over that for the Balmer-alpha emission from the SOL for a number of lines of sight in ITER.

Safety, Environmental and Economic Aspects of Fusion

SEE

International Perspectives on a Path to a Magnetic Fusion Energy DEMO

G. Neilson¹, M. Abdou², G. Federici³, A. Garafalo⁴, R. Kamendje⁵, P. K. Kaw⁶,
K. Kim⁷, R. Kurtz⁸, B. Kuteev⁹, D. Ward¹⁰, H. Yamada¹¹, and H. Zohm¹²

¹*Princeton Plasma Physics Laboratory, Princeton, USA*

²*University of California at Los Angeles, USA*

³*European Fusion Development Agreement, Garching, Germany*

⁴*General Atomics, San Diego, USA*

⁵*International Atomic Energy Agency, Vienna, Austria*

⁶*Institute for Plasma Research, Bhat, India*

⁷*National Fusion Research Institute, Daejeon, Republic of Korea*

⁸*Pacific Northwest National Laboratory, Richland, USA*

⁹*RRC Kurchatov Institute, Moscow, Russian Federation*

¹⁰*Culham Centre for Fusion Energy, Abingdon, UK*

¹¹*National Institute for Fusion Science, Toki, Japan*

¹²*Max-Planck Institut für Plasmaphysik, Garching, Germany*

Corresponding Author: hneilson@pppl.gov

Nations engaged in magnetic fusion R&D are now examining the needed programmes to move toward DEMO, i.e., a practical demonstration of electricity generation on a power plant scale, also satisfying a range of socio-economic goals. The path to DEMO will include major fusion nuclear facilities and their accompanying programmes to develop the various technologies needed to harness fusion energy for peaceful purposes. An IAEA “consultancy meeting” was held in January 2012 to discuss possibilities and opportunities for a coordinated international approach to addressing the critical issues for DEMO. Three findings resulted:

1. The scientific and technical issues for fusion development are known.
2. There is no single roadmap.
3. International collaboration on promoting a coordinated DEMO programme would be beneficial to all parties.

Concerning the third finding, it was concluded that the best way to move forward is to institute a DEMO Programme Workshop Series under the auspices of the IAEA.

The Long-term Impact of the Fukushima on the Prospect of the Fusion Power in Korea: TIMES Model Approach for the Electricity Sector

H. Chang¹, W.-J. Choi¹, H. Tho¹, D.-Y. Kang¹, and Y.-G. Park²

¹*National Fusion Research Institute, Daejeon, Republic of Korea*

²*Ajou University, Su-won, Republic of Korea*

Corresponding Author: jjang@nfri.kr

Until the Fukushima disaster of March 2011, the recent history of nuclear power has been relatively uneventful. About 440 power reactors in 30 countries have been operating for almost 25 years without a catastrophic accident, and this relative uneventfulness and encouraging safety record led many to believe in the viability of a large-scale global nuclear expansion or renaissance. Post-Fukushima, the relative economics of nuclear power compared with other generating technologies may deteriorate. Finance providers may demand tougher financing conditions, driving up the cost of capital, and some may decide to discontinue investing in nuclear projects altogether. More stringent safety regulations may lengthen lead times for construction and increase construction and operating costs, as could more vigorous action by opponents of nuclear power. In view of these uncertainties, we examine the potential of fusion power by assuming that no more reactors are built beyond those already under construction and government confirmed plants in the TIMES (The Integrated MARKAL EFOM System) model. The TIMES model maps the Korean electricity energy system from 2010 to 2050 in five year time steps, modeling in detail the primary energy supply and electricity generation sectors. To examine the potential of fusion power, three scenarios (base, no more nuke and high carbon) are adopted to estimate the long-term role of fusion power. In the “no more nuke” scenario, fusion power takes a substantial share of the market in 2040 and 2050 compared to the “base” case. The goals of carbon mitigation have a critical role in the degree of penetration by fusion power. Higher carbon constraints, lead to more fusion power to generate electricity.

Economic, CO₂ Emission and Energy Assessments of Fusion Reactors

K. Yamazaki¹, K. Ban¹, T. Oishi¹, and H. Arimoto¹

¹*Graduate School of Engineering, Nagoya University, Nagoya, Japan*

Corresponding Author: yamazaki@ees.nagoya-u.ac.jp

Global warming due to rapid greenhouse gas (GHG) emission is a serious environmental problem, and fusion reactors are expected as one of safe and abundant electric power generation systems to reduce GHG emission amounts. To search for economic, environment-friendly and energy-efficient fusion reactors, system studies have been done using PEC (Physics-Engineering-Cost) code taking care of life-cycle cost of electricity (COE), CO₂ gas emission rate equivalently including other GHG emission, and energy payback ratio (EPR), for magnetic fusion reactors (tokamak (TR), spherical tokamak (ST) and helical (HR)) and inertial fusion reactors (IR).

At first, reactor system modeling is described and typical design parameters are derived. The magnetic fusion reactor designs strongly depend on achievable plasma beta value and permissible magnetic field strength, and inertial fusion designs depend on the driver energy and driver repetition rate.

Using the PEC code, COE, CO₂ emission rate and EPR can be analyzed. The former two indices were previously evaluated by the authors, and the latter parameter EPR is defined here as a ratio of electric output energy to input energy investments required for construction, operation, fuel, replacement and decommissioning. Especially, as for TR design to reduce COE and to raise EPR, high plasma-current-drive efficiency is required for low-beta (normalized $\beta_N < 4$) reactor designs.

In these extensive assessment studies, we clarify typical scaling formulas for COE, GHG emissions and EPR of various magnetic and inertial fusion reactors with respect to key design parameters; such as electric power at $P_e = 1 - 3$ GW, plant availability $f_{\text{avail}} = 0.65 - 0.85$, normalized $\beta_N = 3 - 5$ or averaged beta (3 - 5%), maximum magnetic field strength $B_{\text{max}} = 10 - 16$ T, thermal efficiency $f_{\text{th}} = 0.37 - 0.59$, operation year (20 - 40 Years) and isentropic parameter $\alpha_F = 2 - 4$. These formulas might be important for making a strategy of fusion research development.

As future assessments, the accident risk probability and related accident settlement expenditures should be included in COE, in addition to CO₂ environmental tax and nuclear fuel tax, for the comparisons with other electric power generation systems such as oil-fired, nuclear fission and solar power systems.

Index by contribution number

EX/1-1	34	EX/P2-08.....	82	EX/P4-04.....	130
EX/1-2	35	EX/P2-09.....	83	EX/P4-05.....	131
EX/1-3	36	EX/P2-10.....	84	EX/P4-06.....	132
EX/1-4	37	EX/P2-11.....	85	EX/P4-07.....	133
EX/1-5	38	EX/P2-12.....	86	EX/P4-08.....	134
EX/10-1	68	EX/P2-13.....	87	EX/P4-09.....	135
EX/10-2	69	EX/P2-14.....	88	EX/P4-10.....	136
EX/10-3	70	EX/P2-15.....	89	EX/P4-11.....	137
EX/11-1	71	EX/P2-16.....	90	EX/P4-12.....	138
EX/11-2	72	EX/P2-17.....	91	EX/P4-13.....	139
EX/11-3	73	EX/P3-01.....	92	EX/P4-14.....	140
EX/11-4	74	EX/P3-02.....	93	EX/P4-15.....	141
EX/2-1	39	EX/P3-03.....	94	EX/P4-17.....	142
EX/2-2	40	EX/P3-04.....	95	EX/P4-18.....	143
EX/2-3	41	EX/P3-05.....	96	EX/P4-19.....	144
EX/2-4	42	EX/P3-06.....	97	EX/P4-20.....	145
EX/2-5	43	EX/P3-07.....	98	EX/P4-21.....	146
EX/3-1	44	EX/P3-08.....	99	EX/P4-22.....	147
EX/3-2	45	EX/P3-09.....	100	EX/P4-23.....	148
EX/3-3	46	EX/P3-10.....	101	EX/P4-24.....	149
EX/3-4	47	EX/P3-11.....	102	EX/P4-25.....	150
EX/4-1	48	EX/P3-12.....	103	EX/P4-26.....	151
EX/4-2	49	EX/P3-13.....	104	EX/P4-27.....	152
EX/4-3	50	EX/P3-14.....	105	EX/P4-28.....	153
EX/4-4	51	EX/P3-15.....	106	EX/P4-29.....	154
EX/5-1	52	EX/P3-16.....	107	EX/P4-30.....	155
EX/5-2	53	EX/P3-17.....	108	EX/P4-31.....	156
EX/5-3	54	EX/P3-18.....	109	EX/P4-32.....	157
EX/6-1	55	EX/P3-19.....	110	EX/P4-33.....	158
EX/6-2	56	EX/P3-20.....	111	EX/P4-34.....	159
EX/6-3Ra.....	57	EX/P3-21.....	112	EX/P4-35.....	160
EX/6-3Rb.....	58	EX/P3-22.....	113	EX/P4-36.....	161
EX/7-1	59	EX/P3-23.....	114	EX/P5-01.....	162
EX/7-2Ra.....	60	EX/P3-24.....	115	EX/P5-02.....	163
EX/7-2Rb.....	61	EX/P3-25.....	116	EX/P5-03.....	164
EX/8-1	62	EX/P3-26.....	117	EX/P5-04.....	165
EX/8-2	63	EX/P3-27.....	118	EX/P5-05.....	166
EX/8-3	64	EX/P3-28.....	119	EX/P5-06.....	167
EX/9-1	65	EX/P3-29.....	120	EX/P5-07.....	168
EX/9-2	66	EX/P3-30.....	121	EX/P5-08.....	169
EX/9-3	67	EX/P3-31.....	122	EX/P5-09.....	170
EX/P2-01.....	75	EX/P3-32.....	123	EX/P5-10.....	171
EX/P2-02.....	76	EX/P3-33.....	124	EX/P5-11.....	172
EX/P2-03.....	77	EX/P3-34.....	125	EX/P5-12.....	173
EX/P2-04.....	78	EX/P3-35.....	126	EX/P5-13.....	174
EX/P2-05.....	79	EX/P4-01.....	127	EX/P5-14.....	175
EX/P2-06.....	80	EX/P4-02.....	128	EX/P5-15.....	176
EX/P2-07.....	81	EX/P4-03.....	129	EX/P5-16.....	177

EX/P5-17.....	178	EX/P7-03.....	232	FTP/4-6.....	437
EX/P5-18.....	179	EX/P7-04.....	233	FTP/P1-01.....	438
EX/P5-19.....	180	EX/P7-05.....	234	FTP/P1-02.....	439
EX/P5-21.....	181	EX/P7-06.....	235	FTP/P1-03.....	440
EX/P5-22.....	182	EX/P7-07.....	236	FTP/P1-04.....	441
EX/P5-23.....	183	EX/P7-08.....	237	FTP/P1-05.....	442
EX/P5-24.....	184	EX/P7-09.....	238	FTP/P1-06.....	443
EX/P5-25.....	185	EX/P7-10.....	239	FTP/P1-07.....	444
EX/P5-26.....	186	EX/P7-11.....	240	FTP/P1-08.....	445
EX/P5-27.....	187	EX/P7-12.....	241	FTP/P1-09.....	446
EX/P5-28.....	188	EX/P7-13.....	242	FTP/P1-10.....	447
EX/P5-29.....	189	EX/P7-14.....	243	FTP/P1-11.....	448
EX/P5-30.....	190	EX/P7-16.....	244	FTP/P1-12.....	449
EX/P5-31.....	191	EX/P7-17.....	245	FTP/P1-13.....	450
EX/P5-32.....	192	EX/P7-18.....	246	FTP/P1-14.....	451
EX/P5-33.....	193	EX/P7-19.....	247	FTP/P1-15.....	452
EX/P5-34.....	194	EX/P7-20.....	248	FTP/P1-16.....	453
EX/P5-35.....	195	EX/P7-21.....	249	FTP/P1-17.....	454
EX/P5-36.....	196	EX/P7-22.....	250	FTP/P1-18.....	455
EX/P5-37.....	197	EX/P7-23.....	251	FTP/P1-19.....	456
EX/P5-38.....	198	EX/P7-24.....	252	FTP/P1-20.....	457
EX/P5-39.....	199	EX/P8-01.....	253	FTP/P1-21.....	458
EX/P5-40.....	200	EX/P8-02.....	254	FTP/P1-22.....	459
EX/P6-01.....	201	EX/P8-03.....	255	FTP/P1-23.....	460
EX/P6-02.....	202	EX/P8-04.....	256	FTP/P1-24.....	461
EX/P6-03.....	203	EX/P8-05.....	257	FTP/P1-25.....	462
EX/P6-04.....	204	EX/P8-06.....	258	FTP/P1-26.....	463
EX/P6-05.....	205	EX/P8-07.....	259	FTP/P1-27.....	464
EX/P6-06.....	206	EX/P8-08.....	260	FTP/P1-28.....	465
EX/P6-07.....	207	EX/P8-09.....	261	FTP/P1-29.....	466
EX/P6-08.....	208	EX/P8-10.....	262	FTP/P1-30.....	467
EX/P6-09.....	209	EX/P8-11.....	263	FTP/P1-31.....	468
EX/P6-10.....	210	EX/P8-12.....	264	FTP/P1-32.....	469
EX/P6-11.....	211	EX/P8-13.....	265	FTP/P1-33.....	470
EX/P6-12.....	212	EX/P8-14.....	266	FTP/P1-34.....	471
EX/P6-13.....	213	EX/P8-15.....	267	FTP/P1-35.....	472
EX/P6-14.....	214			FTP/P7-01.....	473
EX/P6-15.....	215	FTP/1-1.....	420	FTP/P7-02.....	474
EX/P6-16.....	216	FTP/1-2.....	421	FTP/P7-03.....	475
EX/P6-17.....	217	FTP/1-3Rb.....	422	FTP/P7-04.....	476
EX/P6-18.....	218	FTP/2-1Rb.....	423	FTP/P7-05.....	477
EX/P6-19.....	219	FTP/3-1.....	424	FTP/P7-06.....	478
EX/P6-20.....	220	FTP/3-2.....	425	FTP/P7-07.....	479
EX/P6-21.....	221	FTP/3-3.....	426	FTP/P7-08.....	480
EX/P6-22.....	222	FTP/3-4.....	427	FTP/P7-09.....	481
EX/P6-23.....	223	FTP/3-5.....	428	FTP/P7-10.....	482
EX/P6-24.....	224	FTP/4-1.....	429	FTP/P7-11.....	483
EX/P6-25.....	225	FTP/4-2.....	430	FTP/P7-12.....	484
EX/P6-26.....	226	FTP/4-3.....	431	FTP/P7-14.....	485
EX/P6-27.....	227	FTP/4-4Ra.....	432	FTP/P7-15.....	486
EX/P6-28.....	228	FTP/4-4Rb.....	433	FTP/P7-16.....	487
EX/P6-29.....	229	FTP/4-4Rc.....	434	FTP/P7-17.....	488
EX/P7-01.....	230	FTP/4-5Ra.....	435	FTP/P7-18.....	489
EX/P7-02.....	231	FTP/4-5Rb.....	436	FTP/P7-19.....	490

FTP/P7-20.....	491	ITR/1-2.....	549	ITR/P5-06.....	603
FTP/P7-21.....	492	ITR/1-3.....	550	ITR/P5-07.....	604
FTP/P7-22.....	493	ITR/1-4Ra.....	551	ITR/P5-08.....	605
FTP/P7-23.....	494	ITR/2-1.....	552	ITR/P5-09.....	606
FTP/P7-24.....	495	ITR/2-2Ra.....	553	ITR/P5-10.....	607
FTP/P7-25.....	496	ITR/2-3.....	554	ITR/P5-11.....	608
FTP/P7-26.....	497	ITR/2-4.....	555	ITR/P5-12.....	609
FTP/P7-27.....	498	ITR/2-5.....	556	ITR/P5-14.....	610
FTP/P7-28.....	499	ITR/2-6.....	557	ITR/P5-15.....	611
FTP/P7-29.....	500	ITR/P1-01.....	558	ITR/P5-16.....	612
FTP/P7-30.....	501	ITR/P1-02.....	559	ITR/P5-18.....	613
FTP/P7-31.....	502	ITR/P1-03.....	560	ITR/P5-22.....	614
FTP/P7-32.....	503	ITR/P1-04.....	561	ITR/P5-23.....	615
FTP/P7-33.....	504	ITR/P1-05.....	562	ITR/P5-24.....	616
FTP/P7-34.....	505	ITR/P1-06.....	563	ITR/P5-25.....	617
FTP/P7-35.....	506	ITR/P1-07.....	564	ITR/P5-26.....	618
FTP/P7-36.....	507	ITR/P1-08.....	565	ITR/P5-27.....	619
FTP/P7-37.....	508	ITR/P1-09.....	566	ITR/P5-28.....	620
		ITR/P1-10.....	567	ITR/P5-29.....	621
ICC/1-1Ra.....	510	ITR/P1-11.....	568	ITR/P5-30.....	622
ICC/1-1Rb.....	511	ITR/P1-12.....	569	ITR/P5-31.....	623
ICC/P1-01.....	512	ITR/P1-13.....	570	ITR/P5-32.....	624
ICC/P3-01.....	513	ITR/P1-14.....	571	ITR/P5-33.....	625
ICC/P3-02.....	514	ITR/P1-15.....	572	ITR/P5-34.....	626
ICC/P5-01.....	515	ITR/P1-16.....	573	ITR/P5-35.....	627
ICC/P6-01.....	516	ITR/P1-17.....	574	ITR/P5-36.....	628
ICC/P6-02.....	517	ITR/P1-18.....	575	ITR/P5-37.....	629
ICC/P8-01.....	518	ITR/P1-19.....	576	ITR/P5-38.....	630
ICC/P8-02.....	519	ITR/P1-20.....	577	ITR/P5-39.....	631
IFE/1-1.....	522	ITR/P1-21.....	578	ITR/P5-40.....	632
IFE/1-2.....	523	ITR/P1-22.....	579	ITR/P5-41.....	633
IFE/1-3.....	524	ITR/P1-23.....	580	ITR/P5-42.....	634
IFE/1-4.....	525	ITR/P1-24.....	581	ITR/P5-43.....	635
IFE/1-5.....	526	ITR/P1-25.....	582	ITR/P5-44.....	636
IFE/P6-01.....	527	ITR/P1-26.....	583		
IFE/P6-02.....	528	ITR/P1-27.....	584	OV/1-1.....	2
IFE/P6-03.....	529	ITR/P1-28.....	585	OV/1-2.....	3
IFE/P6-04.....	530	ITR/P1-29.....	586	OV/1-3.....	4
IFE/P6-05.....	531	ITR/P1-30.....	587	OV/1-4.....	5
IFE/P6-06.....	532	ITR/P1-31.....	588	OV/2-1.....	6
IFE/P6-07.....	533	ITR/P1-32.....	589	OV/2-2.....	7
IFE/P6-08.....	534	ITR/P1-33.....	590	OV/2-3.....	8
IFE/P6-09.....	535	ITR/P1-34.....	591	OV/2-4.....	9
IFE/P6-10.....	536	ITR/P1-35.....	592	OV/2-5.....	10
IFE/P6-11.....	537	ITR/P1-36.....	593	OV/3-1.....	11
IFE/P6-12.....	538	ITR/P1-37.....	594	OV/3-2.....	12
IFE/P6-13.....	539	ITR/P1-38.....	595	OV/3-3.....	13
IFE/P6-14.....	540	ITR/P1-39.....	596	OV/3-4.....	14
IFE/P6-15.....	541	ITR/P1-40.....	597	OV/4-1.....	15
IFE/P6-16.....	542	ITR/P5-01.....	598	OV/4-2.....	16
IFE/P6-17.....	543	ITR/P5-02.....	599	OV/4-3.....	17
IFE/P6-18.....	544	ITR/P5-03.....	600	OV/4-4.....	19
IFE/P6-19.....	545	ITR/P5-04.....	601	OV/4-5.....	20
ITR/1-1.....	548	ITR/P5-05.....	602	OV/5-1.....	21

OV/5-2Ra	22	TH/P2-24	309	TH/P4-17	364
OV/5-2Rb	23	TH/P2-25	310	TH/P4-18	365
OV/5-3	24	TH/P2-26	311	TH/P4-19	366
OV/5-4	25	TH/P2-27	312	TH/P4-20	367
OV/P-01	26	TH/P2-28	313	TH/P4-21	368
OV/P-02	27	TH/P2-29	314	TH/P4-22	369
OV/P-03	28	TH/P2-30	315	TH/P4-23	370
OV/P-05	29	TH/P3-01	316	TH/P4-24	371
OV/P-06	30	TH/P3-02	317	TH/P4-25	372
OV/P-07	31	TH/P3-03	318	TH/P4-26	373
OV/P-08	32	TH/P3-04	319	TH/P4-27	374
SEE/1-1	638	TH/P3-05	320	TH/P4-28	375
SEE/P7-01	639	TH/P3-06	321	TH/P6-01	376
SEE/P7-02	640	TH/P3-07	322	TH/P6-02	377
		TH/P3-08	323	TH/P6-03	378
TH/1-1	270	TH/P3-09	324	TH/P6-04	379
TH/2-1	271	TH/P3-10	325	TH/P6-05	380
TH/3-1	272	TH/P3-11	326	TH/P6-06	381
TH/3-2	273	TH/P3-12	327	TH/P6-08	382
TH/4-1	274	TH/P3-13	328	TH/P6-09	383
TH/4-2	275	TH/P3-14	329	TH/P6-10	384
TH/5-1	276	TH/P3-16	330	TH/P6-11	385
TH/5-2Ra	277	TH/P3-17	331	TH/P6-12	386
TH/5-2Rb	278	TH/P3-18	332	TH/P6-13	387
TH/5-3	279	TH/P3-19	333	TH/P6-14	388
TH/6-1	280	TH/P3-20	334	TH/P6-16	389
TH/6-2	281	TH/P3-21	335	TH/P6-17	390
TH/6-3	282	TH/P3-22	336	TH/P6-18	391
TH/6-4	283	TH/P3-23	337	TH/P6-19	392
TH/7-1	284	TH/P3-24	338	TH/P6-20	393
TH/7-2	285	TH/P3-25	339	TH/P6-21	394
TH/8-1	286	TH/P3-26	340	TH/P6-22	395
TH/8-2	287	TH/P3-27	341	TH/P6-23	396
TH/P2-01	288	TH/P3-28	342	TH/P6-24	397
TH/P2-02	289	TH/P3-29	343	TH/P6-25	398
TH/P2-03	290	TH/P3-30	344	TH/P6-26	399
TH/P2-04	291	TH/P3-31	345	TH/P6-27	400
TH/P2-05	292	TH/P3-32	346	TH/P6-28	401
TH/P2-06	293	TH/P3-34	347	TH/P6-29	402
TH/P2-08	294	TH/P4-01	348	TH/P6-30	403
TH/P2-09	295	TH/P4-02	349	TH/P7-01	404
TH/P2-10	296	TH/P4-03	350	TH/P7-02	405
TH/P2-11	297	TH/P4-04	351	TH/P7-03	406
TH/P2-12	298	TH/P4-05	352	TH/P7-04	407
TH/P2-13	299	TH/P4-06	353	TH/P7-05	408
TH/P2-14	300	TH/P4-07	354	TH/P7-06	409
TH/P2-15	301	TH/P4-08	355	TH/P7-07	410
TH/P2-16	302	TH/P4-09	356	TH/P7-08	411
TH/P2-17	303	TH/P4-10	357	TH/P7-09	412
TH/P2-18	304	TH/P4-11	358	TH/P7-10	413
TH/P2-19	305	TH/P4-12	359	TH/P7-11	414
TH/P2-21	306	TH/P4-13	360	TH/P7-12	415
TH/P2-22	307	TH/P4-14	361	TH/P7-13	416
TH/P2-23	308	TH/P4-15	362	TH/P7-14	417
		TH/P4-16	363	TH/P7-15	418

Index by author

— A —	
Aallekar, A.	617
Abdou, M.	638
Abe, K.	486
Abiteboul, J.	28, 412
Abrams, T.	191, 515
Achard, J.	224
Acir, A.	475
Acosta, C. U.	469
Adámek, J.	251
Afanasyev, V.	631
Agarici, G.	561
Aglitsky, Y.	525
Agostini, P.	438
Agravat, H.	611
Agullo, O.	356
Ahmed, I.	560, 635
Ahn, H.	598
Ahn, J. W.	57, 138, 187, 193 , 200, 247, 451
Aho-Mantila, L.	194
Aiba, N.	52, 279, 324, 333, 390, 493
Aiello, G.	433
Airoidi, A.	27
Äkäslompolo, S.	203, 590
Akcay, C.	289, 510
Akers, R.	206, 230, 347
Akino, N.	455
Akio, S.	192
Akiyama, T.	51, 136, 139, 149, 232
Aksenov, N.	583
Albanese, R.	27, 49, 567, 623
Albergante, M.	284
Alcator C-Mod Team,	8, 568, 576
Alcorta, M. A.	469
Alejaldre, C.	608
Alekseev, A.	600, 626
Alekseev, A. G.	636
Alessi, E.	204
Alexander, N. B.	541, 545
Alexander, P.	357
Alexeev, P.	479
Aleynikov, P.	595
Alimov, V.	429
Allain, J. P.	191, 451
Allan, S.	178
Almagri, A.	22, 296
Almagri, A. F.	99, 107
Almaguer, F. J.	469
Almaviva, S.	175
Alonso, A.	113
Alper, B.	17, 248
Altukhov, A.	233, 282
Alvarez, J.	526
Alves, L.	288
Ambo, T.	85
Ambrosino, G.	573, 623
Ambrosino, R.	567, 573
Amdahl, D.	517
Amendt, P.	536
Amicucci, L.	229, 566
Amoskov, V.	156, 621
Anderson, D.	285
Anderson, D. T.	121
Anderson, F. S. B.	121
Anderson, J.	22, 107 , 108, 404, 407
Anderson, K.	24
Ando, M.	488
Andre, R.	125
Andreeva, T.	439
Andreeva, Z.	600
Andrew, P.	622, 626, 627, 629
Andrew, T.	548
Andruczyk, D.	428
Angelini, S.	144
Angelone, M.	619
Angioni, C.	37, 39, 127, 248, 306 , 426, 576, 587
Angus, J. R.	273
Aniel, T.	288
Annigeri, M.	617
Aoyama, M.	94
Apicella, M. L.	255
Appel, L.	623
Apruzzese, G.	255
Arai, S.	98
Arbeiter, F.	472, 486
Arevalo, J.	105
Argouarch, A.	210
Arikawa, Y.	524, 537
Arimoto, H.	640
Ariola, M.	623
Arkhipov, I.	626
Arnaud, F.	607
Arneman, A.	512
Arnoux, G.	65, 184, 190, 197 , 257, 423, 596
Arredondo, V. M.	469
Arshad, S.	623

Arslan, S.	516	Barnes, M.	283
Artaserse, G.	255	Barnsley, R.	627, 629, 630
Artaud, J. F.	221, 288, 290, 292, 566, 567	Barr, J.	161
Arvin, R.	253	Barrera Orte, L.	47
Arzhannikov, A.	120	Barrera, L.	37
Asai, T.	151, 513	Barrett, T.	465
Asakura, N.	448, 502, 503 , 504	Barsukov, A.	211
Ascasíbar, E.	53, 69, 105, 143, 196	Bartal Hughes, T.	534
ASDEX Upgrade Team,	7, 194, 568, 576, 588, 634	Barton, J. E.	83 , 577
Ashabraner, R.	522	Baruah, U.	560
Ashikawa, N.	118, 170, 179, 192	Baruzzo, M.	34, 290
Askinazi, L.	211	Basaleev, E.	606
Asunta, O.	50, 203, 588, 590	Basiuk, V.	221, 288, 310, 566
Atchutuni, S. S.	611	Bass, E. M.	381
Atrey, P.	91	Batchelor, D. B.	385
Aumeunier, M.-H.	553	Battabyal, M.	483
Auphan, T.	373	Battaglia, D.	181, 188
Auriemma, F.	22, 201	Battaglia, D. J.	593
Austin, M.	625, 633	Bauer, B.	517
Austin, M. E.	66	Baulaigue, O.	466
Avino, F.	228	Baumgaertel, J.	232
Avrorov, A. P.	120	Baumgarten, N.	65
Aydemir, A.	360	Bayetti, P.	466 , 599
Azechi, H.	16 , 524, 531, 537, 544	Baylor, L.	515, 579, 615, 616
Azizov, E.	185, 437 , 438	Baylor, L. R.	56 , 549
Azuma, H.	538, 539	Bazylev, B.	257, 583, 596
<hr/>			
— B —			
Baciero, A.	97	Beauvais, P.-Y.	471
Bader, A.	92, 382	Beck, W.	459
Bae, Y.	41, 73, 81, 138, 462	Becoulet, A.	20
Bae, Y. S.	57, 224, 247, 458	Becoulet, M.	271 , 549, 581
Baek, S. G.	90, 566	Bedakihale, V.	609
Bai, X.-M.	484	Bednarek, M.	554
Bak, J. G.	46, 57, 138 , 209, 598	Beg, F. N.	530, 532, 533, 534
Balakirev, V.	196	Behn, R.	96
Balasubramanian, K.	441	Beidler, C.	105, 460
Baldwin, M.	164	Beisinbaeva, H.	535
Baldzuhn, J.	105	Bell, M.	67, 72, 84, 158, 191, 451
Ball, S.	497	Bell, R.	67, 72, 130, 158, 188, 191, 200, 205, 244, 246, 249, 259, 280, 451
Baluc, N.	435, 483	Bell, R. E.	59, 93, 125, 181, 202
Bamber, R.	565	Bellan, P.	518
Ban, K.	640	Bellei, C.	530, 534
Bandyopadhyay, I.	569	Belli, E. A.	280, 353 , 354
Bandyopadhyay, M.	560, 635	Belli, F.	255
Bang, E. N.	458	Belo, J.	224
Banks, J.	48	Belo, P.	48, 292
Banon Navarro, A.	283	Belov, A.	600
Barabaschi, P.	15	Belova, E.	389
Baranov, Y.	566	Belyakov, V.	600 , 621
Barbato, E.	566	Benkadda, S.	207, 356
Barnard, J.	527, 542	Bensiali, B.	373
		Berdierov, G.	535
		Berezutsky, A.	622, 626
		Berger-By, G.	566

Bergerson, W.	22, 201	Bombarda, F.	27
Berionni, V.	298	Boncagni, L.	204, 255
Berk, H.	17, 274	Bond, E.	522
Berk, H. L.	389	Bondarchuk, E.	512
Berkery, J.	67, 81, 259	Bondarenko, V.	626
Bernard, J. M.	210	Bonfiglio, D.	302
Bernert, M.	129, 194, 264, 585	Bongard, M.	161, 456
Bertalot, L.	617, 627, 629	Bonicelli, T.	550, 561
Bertram, J.	223	Bonoli, P.	90, 270, 385 , 566, 572
Berzak, L.	515	Bonoli, P. T.	382
Bespamyatnov, I.	119	Boom, J.	133, 203
Bessegghir, K.	567	Boozzer, A.	67, 312, 417
Betti, R.	24 , 259, 523, 536	Boozzer, A. H.	156
Bettini, P.	623	Bora, D.	362, 560, 594
Beurskens, M.	34, 106, 128, 166, 190, 248 , 303, 325, 630, 632	Borba, D.	17
Beurskens, M. N. A.	55, 148, 272	Borchardt, M.	22, 321, 591
Beyer, P.	356	Borisov, M.	241
Bhatt, S. B.	91	Bornschein, B.	446
Bialek, J.	81, 144, 259	Borovikov, V.	484
Bierwage, A.	390	Borschegovskij, A.	101
Biewer, T.	470, 515	Bortolon, A.	205
Bilanceri, M.	373	Boscary, J.	439
Bin, W.	204, 255	Bosch, H.-S.	424
Binderbauer, M.	514	Botrugno, A.	204, 207, 255
Bindslev, H.	315	Bottollier-Curtet, H.	210
Bionta, R.	522	Bouhamou, R.	629
Bird, T.	283	Bourdelle, C.	34, 248, 298, 362, 587
Bishnoi, S.	492	Bousquet, J. T.	545
Biswas, P.	425	Boutboul, T.	556
Bitter, M.	41, 123, 140, 219	Bovet, A.	228
Bizarro, J.	288, 292	Boyer, M. D.	83, 577
Blackler, K.	609	Boyle, D. P.	72, 515
Blackwell, B.	53, 223	Bozhenkov, S.	139
Blanco, E.	69	Branas, B.	471
Blazevski, D.	314	Braun, F.	180
Blesener, I.	543	Braune, H.	460
Blesener, K.	543	Brédy, P.	466, 471
Blokhin, A.	436	Breizman, B.	17, 274, 347, 360
Blokhin, D.	436	Brémond, S.	170, 210, 258
Bo, L.	616	Breslau, J.	316
Bobkov, V.	37, 50, 106, 170, 180	Breslau, N.	319
Boboc, A.	48	Breuer, U.	634
Bodi, K.	373	Brezinsek, S.	34, 48 , 65, 106, 148, 165, 166, 170, 184, 190, 248, 272, 596
Boedo, J. A.	66, 70, 234, 353	Briesemeister, A. R.	121
Boehly, T.	24, 523	Briguglio, S.	378, 394, 396, 591
Boerner, P.	369	Brix, M.	190, 197, 272
Bogatu, I.-N.	468	Brombin, M.	623
Bogomolov, A.	133	Brooks, J. N.	172
Bohler, D.	515	Brooks, N. H.	56, 66, 172, 589
Boilson, D.	550, 560, 561, 635	Brosset, C.	168
Boivin, R.	630	Brotankova, J.	223
Bolourian, H.	253	Brower, D.	22, 201, 624
Bolzonella, T.	290, 493	Brower, D. L.	99

Brown, T.	427, 499	Cannas, B.	256
Bruce, L.	36	Cantone, B.	619
Brun, S.	412	Cao, G.	429
Brunetti, D.	284	Cao, J.	111, 154, 237
Brunner, D.	164	Cao, J. Y.	212
Brunner, S.	283	Cao, Q.	434, 513
Brunsell, P.	146	Cao, Z.	137
Bruschi, A.	204	Capes, H.	369
Bruzzo, P.	556	Cappa, A.	97
Bu, J.	126	Cappello, S.	22, 201, 302
Bucalossi, J.	34, 48, 106, 168, 186, 258, 373, 604	Cara, P.	471 , 472
Buchenauer, D. N.	172	Carati, D.	283
Budny, R.	299, 395, 572, 586	Cardella, A.	460
Budny, R. V.	305, 589	Cardinali, A.	27, 229, 383, 566
Budyln, N.	436	Carl, W.	522
Bufferand, H.	197, 373	Carmody, D.	22, 296
Bukhovets, V.	626	Carmona, J.-M.	471
Bulanin, V. V.	64, 282	Carpenter, A.	522
Buldakov, M.	241	Carpentier-Chouchana, S.	571, 605
Buratti, P.	26 , 145, 207, 248, 255	Carraro, L.	95
Burckhart, M.	129	Carreras, B.	113
Burdakov, A.	31, 120	Carreras, B. A.	329
Burke, M. G.	161	Carter, T.	239
Burrell, K. H.	109, 110, 134 , 238, 245, 331, 577	Cary, J.	354, 357
Bush, C. E.	249	Cary, J. R.	397
Buttery, R. J.	44, 75, 82, 156 , 173, 235, 284, 368	Casey, D.	24, 522, 523
Bykov, A.	479	Casey, J.	459
Byrne, P.	144	Casner, A.	24
— C —		Caspary, K. J.	22, 107
Cabral, J.	32	Casper, T.	292, 325, 549, 572 , 592
Cachon, L.	433	Casper, T. A.	570, 582
Caggiano, J.	522	Cassin, M.	515
Cahill, A.	543	Casson, F.	39, 306
Cahyna, P.	45, 374 , 549, 581	Castaldo, C.	229, 255, 566
Cai, L. Z.	61	Castejón, F.	21
Caillault, L.	461	Caughman, J.	470
Calabro, G.	34, 190, 207, 248, 255, 444, 566	Cavinato, M.	567, 573
Calcagno, B.	557	CEA-IRFM Team,	20
Callen, J. D.	354, 367	Cecconello, M.	206, 347
Camacho, F.	517	Ceccuzzi, S.	566
Camenen, Y.	303, 304, 306	Celso, R.	313
Campbell, D.	362, 549, 571, 572, 575 , 592, 594, 600	Cenacchi, G.	27
Campbell, D. J.	570	Cereceda, D.	526
Canal, G.	35, 157, 182	Cerjan, C.	522
Candy, J.	104, 114, 238, 280, 331, 353	Cesario, R.	229 , 566
Caneve, L.	175	Cha, S.	540
Canik, J.	72, 173, 178, 187, 193, 244 , 427, 439, 451, 470	Chabaud, D.	553
Canik, J. M.	506	Chacon, L.	302, 314
		Chakraborty Thakur, S.	61
		Chakraborty, A.	550
		Chakraborty, A. K.	560, 635
		Chakraborty, P.	611
		Challis, C.	17, 34, 50, 206, 248, 463, 493
		Champeaux, S.	212

Chan, L. Y.	525	Choe, G. H.	57
Chan, V. S.	506	Choe, W.	359
Chandra, D.	334	Choi, C.	598
Chang, C.	28, 354, 375	Choi, J. H.	458
Chang, C. S.	74, 130, 188, 359 , 416	Choi, M.	73, 265, 506
Chang, D.	455	Choi, M. J.	57
Chang, D. H.	458	Choi, W.-J.	639
Chang, H.	639	Chowdhury, J.	403
Chang, Y. B.	458	Chrzanowski, J.	427
Chapman, B.	22, 201	Chu, M. S.	351
Chapman, B. E.	107	Chugunov, I.	628, 631
Chapman, I.	45, 325, 374, 588	Chugunov, I. N.	64
Chapman, I. T.	152, 284	Chukbar, B.	479
Chappell, S.	497	Chung, J.	440
Chappuis, P.	557	Chung, K.-S.	440
Chareyre, J.	560	Churchill, R.	78, 141
Chaudhari, V.	445 , 610	Chuvilo, A.	583
Chaudhuri, P.	445	Chuyanov, V.	572
Chauhan, A.	425	Ciaccio, G.	302
Chávez, R. M.	469	Cianfarani, C.	255, 623
Chávez-Alarcon, E.	313	Ciattaglia, S.	618
Chawla, S.	530, 532	Ciazynski, D.	599
Chebotarev, V.	583	Ciracolo, G.	373
Chel, S.	466, 471, 472	Cirant, S.	145, 204
Chen, C.	100, 137, 237, 267, 530, 532	Ciric, D.	50
Chen, C. Y.	57, 58	Citrin, J.	100, 283, 292
Chen, G.	470	Clairret, F.	186, 233
Chen, H.	532	Clancy, T.	522
Chen, J.	319, 385, 397, 399, 449, 487 , 557	Classen, I.	17, 133
Chen, L.	89, 111, 174, 275, 384, 396, 449	Classen, I. G. J.	203
Chen, Q.	341	Clever, M.	34, 48, 165, 166, 184, 190, 272
Chen, R.	132, 174, 243	Coatanea, M.	599
Chen, S.	214, 215	Coats, R.	601
Chen, S. Y.	54	Coccorese, V.	623
Chen, W.	54 , 111, 150, 212–215	Cocilovo, V.	255
Chen, X.	203	Coda, S.	19 , 35, 96, 103, 160, 182, 208, 284, 380, 588
Chen, Y.	225, 359, 434	Coelho, R.	288, 310
Chen, Z.	30	Coenen, J.	34, 148
Cheng, J.	54, 57, 58, 60, 61, 70, 111, 112, 236, 243, 252 , 371	Coenen, J. W.	48, 50, 106, 165 , 166, 184, 190, 272, 596
Cheng, Z.	30	Coffey, I.	48, 49, 106, 165, 190
Cheon, M.	617	Coffey, S.	517
Cherkasov, S.	241	Cohen, B.	365, 530
Chernakov, P.	622, 626	Cohen, R.	365, 542
Chernoiziumskaya, T.	626	Cohen, R. H.	350, 353
Chernov, V.	436 , 479	Colao, F.	175
Chernyshev, F. V.	64, 211	Colas, L.	50, 186, 210
Chi, G.	576	Cole, A. J.	284, 367
Chiavassa, G.	373	Colella, P.	350, 353
Chida, Y.	602	Collier, J.	526
Chistiakov, V.	241	Collins, T.	24, 523
Cho, M.	462	Combs, S.	261, 615
Cho, M. H.	458	Combs, S. K.	56
Cho, S.-G.	440		

- Commaux, N. 56, 66, 579, 615
 Compton, J. C. 350
 Comunian, M. 471
 Conway, G. 129, 251, **625**, 632
 Conway, G. D. 203
 Cooper, W. **284**, 591
 Coppi, B. **27**, **311**
 Corbel, E. 224
 Corigan, G. 567
 Corre, Y. 186, 210
 Corrigan, G. 272
 Costa, A. L. 496
 Costa, E. 27
 Coster, D. 194, 288, 310
 Costley, A. 499
 Costley, A. E. 634
 Counsell, G. 618
 Courtois, X. **604**
 Covele, B. 480
 Craig, D. 22, 107
 Craxton, S. 24, 523
 Crisanti, F. **444**, 623
 Crocker, N. 158, **202**, 205, 249
 Cui, C. 137
 Cui, X. 450
 Cui, Z. 111, **112**, 154, 179
 Cunningham, G. 250
 CYCLE Team, 565
 Czarnecka, A. 50, 106, 175
 Cziegler, I. 40, 70, 199, 420
- D —
- da Silva Aresta Belo, P. 190, 272
 Dachicourt, R. 186
 DaGraca, S. 129
 Dairaku, M. 421
 Dal Bello, S. 162
 Danani, C. 445, **610**
 Danilov, A. 241
 Dannert, T. 283
 D'Antona, G. 204
 Dapena, M. 619
 D'Arcangelo, O. 204
 Darrow, D. 205
 David, J. 466
 David, K. 463
 David, P. 92
 Davidson, R. 542
 Davis, E. 141
 Davis, W. M. 370
 Davydenko, V. I. 22, 107
 Day, C. **446**, 550
 Day, I. 50
 Daybelge, U. **372**
 Dayton, M. 464
 De Baar, M. 103
 De Bock, M. 630
 De Dinechin, G. 433
 de Grassie, J. S. 44, 122
 de Grouchy, P. 497
 de la Luna, E. 34, **55**, 106, 248, 593
 de Marné, P. 251
 de Temmerman, G. 182, 634
 de Vries, P. 34, 65, 122, 133, 166, 190, 248, 257, 303, 423
 de Vries, P. C. **49**
 DeBono, B. 144
 DeBoo, J. C. 109, 238
 Decamps, H. 560, 561
 Decker, J. 207, 208, 221, 224, 335, 380, 566
 Decool, P. 466
 Degnan, J. **517**
 Degtyarev, N. 436
 Deguchi, K. 149
 Deichuli, P. 22
 Dejarnac, R. 186
 del-Castillo-Negrete, D. **314**
 Delabie, E. 55
 Delettrez, J. 24, 523
 Delgado-Aparicio, L. F. 40, **140**, 344
 Delogu, R. 623
 Delpech, L. 224, 458
 del Río, E. 526
 Demange, D. 446
 Demers, D. 22
 Den Hartog, D. 22, **108**, 149, 201, 624
 Den Hartog, D. J. 99, 107
 Deng, W. 150, **212**, 390
 Denisov, G. 551
 Denkevits, A. 618
 Denner, P. 45, 148
 Dennis, G. 490
 Desmons, M. 471
 Detragiache, P. 27
 Devaux, S. 184, 190, 197, 423
 DeVellis, A. 27
 Devred, A. 556
 Devynck, P. 186
 Dewar, R. 223
 Di Napoli, F. 566
 Di Troia, C. 378, **394**, 396
 Diallo, A. 59, 72, 93, **130**, 181, 188, 191, 200, 205, 246, 249, 259
 Diamond, P. 71, 278, 295, 298, 405
 Diamond, P. H. 14, **28**, 40, 41, 57, 60, 61, 70, 100, 234, 236, 281, 348, **349**, 388, 409, 412, 415, 416

Dickinson, D.	276, 325
Diegele, E.	488
Diem, S.	470
Dif-Pradalier, G.	14, 28, 271, 298, 412, 416
DIII-D Team,	2, 568, 576, 588
Dimatteo, L.	255
Dimits, A.	278
Ding, B.	221
Ding, B. J.	566
Ding, S.	115, 132, 451
Ding, W.	22, 107, 201, 323, 624
Ding, W. X.	99
Ding, X.	13, 14, 100, 111, 112, 154, 214, 215, 236, 237, 242, 267
Ding, X. T.	54, 57, 60, 61, 252
Ding, Y.	30, 151
Dinklage, A.	105, 460
D'Ippolito, D.	370
Direz, M.-F.	633
Ditenberg, I.	436
Dittmar, T.	168, 190
Divol, L.	530
Djigailo, N.	185
Dnestronskii, Y.	241
Dnestrovskij, A.	479
Do, H. J.	458
Doane, J.	462
Dodt, D.	55
Doerk, H.	283, 411
Doerner, R.	164, 485
Doerner, R. P.	273
Doinikov, D.	628
Domier, C.	73, 126, 133, 231
Dominguez, A.	36
Dononkos, M.	517
Dong, C.	179
Dong, J.	13, 14, 60, 70, 79, 111, 137, 154, 214, 215, 236, 237, 243, 345, 346
Dong, J. Q.	54, 57, 61, 252
Dong, Y.	111, 150, 213, 214, 242
Dong, Y. B.	212
Donné, A.	73
Donne, T.	133
Doody, J.	459
Dorf, M. A.	350, 353
Dormido-Canto, S.	256
Dorner, J.	429
Dorr, M.	350
Dorr, M. R.	353
Dorris, J.	104
Doshi, K.	425, 494
Douai, D.	48, 170, 190, 442, 616
Doyle, E. J.	38, 82, 109, 117, 238, 245
Drake, J.	146
Drenik, A.	150
Dreval, M.	151
Drevlak, M.	352
Drewelow, P.	139
Drobyshev, V.	436
Du, X.	136
Duan, X.	13, 111, 112, 137, 154, 213–215, 236, 237, 242, 267, 443, 449
Duan, X. R.	54, 58, 60, 61, 212, 252
Duan, Y.	115
Dubuit, N.	207
Duchateau, J. L.	599
Dudarev, S.	430
Dudek, L.	427
Dudnikov, A.	479
Dudson, B.	278
Duff, J.	22, 624
Dumont, R.	210, 412
Dumortier, P.	210, 564, 565
Dunai, D.	230, 250
Dunne, M.	128
Duran, I.	497
Duré, F.	461
Durodié, F.	564, 565
Duval, B.	35, 103, 157, 182
Duval, B. P.	96, 284
Dux, R.	34, 39, 106, 165, 166, 180, 306
Dyachenko, V. V.	.64
<hr/>	
EAST Team,	
Ebrahimi, F.	10, 495
Eckart, M.	108
Eckart, M.	522
ECRH Team,	26
Edgell, D.	24
Edward, R.	517
Edwards, C.	526
Edwards, J.	522
Efthimion, P.	542
Egdell, D.	523
Eguchi, T.	457
Eich, T.	47, 148, 184, 190, 251, 272, 548, 585
Eidietis, N. W.	466
Eilerman, S.	22, 107
Ejiri, A.	85, 149
Ekedahl, A.	50, 221, 224, 566
El-Guebaly, L.	427, 499
Elbez-Uzan, J.	608
Elbeze, D.	207
Elder, D.	177
Elder, J. D.	172
Elgriw, S.	151
Ellappan, R. K.	445, 611

- Ellis, R. 458, 462, 589
 Elmore, S. 178
 Emoto, S. 519
 Encheva, A. 627
 Endler, M. 460
 Endo, Y. 455, 457
 England, A. 138, 227
 Ennever, P. 40, 104
 Ennis, D. 510
 Enoeda, M. 488, 603
 Epstein, R. 24, 523
 Erckmann, V. 460
 Eriksson, L. G. 122, 310
 Ernst, D. 40, 104, 114
 Ernst, D. R. 119
 Escande, D. 302, **304**
 Escourbiac, F. 554, 571, **605**
 Esipov, L. 282
 Eskhult, J. 614
 Esposito, B. 145, 255, 619
 Esser, H. G. 48, 442
 Estrada, T. 14, 53, **69**, 262, 625
 Ethier, S. 403, 417, 418
 Evans, M. 543
 Evans, T. 549, 581
 Evans, T. E. 44, 56, 66, 117, 235, 284, 368, **582**
 Ezato, K. 603
- F —
- Fable, E. 37, 39, 77, 292
 Facco, A. 471, 472
 Faelli, G. 27
 Faganello, M. 356
 Falchetto, G. **310**
 Falkowski, A. 22
 Fanni, A. 256
 Fantz, U. **454**, 558
 Farengo, R. **379**
 Farina, D. 204, 288, 290, 310
 Farley, T. 197, 423
 Farrell, M. 522
 Fasoli, A. 17, **228**, 361
 Faugel, H. 180
 Faust, I. 420, 459
 Faust, I. C. 90
 Feder, R. **620**, 633
 Federici, G. 426, 500, 638
 Federspiel, L. 157
 Fedorczak, N. 28, 61, 70, 186, 349
 Fedosejevs, R. 532
 Fedosov, A. 605
 Fehér, T. 321, 591
 Felici, F. 35, **103**, 160, 208
 Felton, R. 48
 Feng, B. 100, 112, 137, 150, 214, 215, 237, 267
 Feng, B. B. 57, 58, 212
 Feng, C. 226
 Feng, K. **434**, 450
 Feng, Y. 51, 105, 434, 581
 Feng, Z. 154, 237
 Fenstermacher, M. 172, 579
 Fenstermacher, M. E. 56, 134, 173, 593
 Fermé, J.-J. 553
 Fernandes, A. 257
 Fernandes, H. J. **32**
 Fernández, J. 526
 Ferrand, L. 605
 Ferrari, A. 27
 Ferrari, H. 379
 Ferraro, N. 319
 Ferraro, N. M. 44, 156, **368**
 Ferreira Nunes, I. M. 34, 190, **423**
 Ferreira, J. 288, 292, 576
 Ferreira, J. A. 196
 Ferrero, R. 204
 Ferri, S. 183
 Ferron, J. R. . . 38, 52, 75, 82, 83, 87, 173, 284, 577
 Field, A. 14, **230**, 250
 Figini, L. 204, 288, 290
 Figueiredo, A. 288
 Figueiredo, H. 113
 Fikar, J. 435
 Fiksel, G. 99, 107
 Filatov, O. 600
 Fimognari, P. 22
 Fiore, C. 104, **119**, 270
 Firdaouss, M. 197, 210, 423, 604
 Firpo, M. C. 379
 Fischer, R. 37, 47, 127, 129, 251
 Fischer, U. **490**
 Fisher, A. 543
 Fisher, R. K. 203
 Fishpool, G. 45, **178**
 Fittinghoff, D. 522
 Fitzgerald, M. 223
 Fitzpatrick, R. **322**
 Flanagan, J. 65, 248, 272
 Flanagan, S. 577
 Fogaccia, G. 378, 394, 396
 Földes, I. 529
 Fonck, R. 161, 246, **456**
 Fonck, R. J. 234
 Foord, M. E. 533, 534
 Forest, C. 22, 108
 Forest, C. B. 107
 Forest, L. 433

Fotedar, R.	611
Foussat, A.	602
Foust, C.	615
Fraile, A.	526
Franz, D.	285
Franz, P.	22, 201
Franzen, P.	454, 558
Frassinetti, L.	34, 146 , 148, 190, 248, 325
Frattolillo, A.	27
Fredrickson, E.	17, 67, 158, 205
Fredrickson, E. D.	202, 389
Frenje, J.	24, 522 , 523, 536
Frerichs, H.	549, 581
Frese, M.	517
Frese, S.	517
Fresinger, M.	48
Frey, D. T.	545
Friedman, A.	542
Friedman, B.	239
Friedrich, S.	522
Frigione, D.	48, 197, 255
Frolov, A.	479
Fröschle, M.	558
Frosi, P.	27
Froula, D.	24, 523
FTU Team,	26
Fu, G.	346, 395
Fu, G. Y.	17
Fu, H.	487
Fu, J.	219
Fu, P.	495
Fu, Y.	607
Fuchs, C.	251
Fuchs, J. C.	47, 127
Fuelling, S.	517
Fuhr, G.	356
Fujii, K.	179
Fujii, T.	452
Fujimoto, Y.	16, 524
Fujimura, T.	544
Fujine, M.	538, 539
Fujioka, S.	16, 524, 531, 537
Fujisawa, A.	60, 68
Fujita, K.	538, 539
Fujita, T.	42, 290, 300, 493
Fukahori, D.	149
Fukumoto, M.	169
Fukumoto, N.	447, 511
Fukunaga, T.	218
Fukuyama, A.	270, 290, 387
Fülöp, T.	320, 352
Fulton, D.	406
Funaba, H.	189, 505
Fundamenski, W.	178, 548
Fünfgelder, H.	180
Furlan, J.	612
Furno, I.	228, 361
Furui, H.	85
Furukawa, M.	519
Furukawa, T.	431
Furuta, T.	448
Fusco, V.	378, 444, 623
Fusion for Energy Collaborators,	563
Futagami, N.	429
Futatani, S.	549, 579
Futtersack, R.	373
G	
Gabellieri, L.	255
Gabriel, F.	433
Gal, K.	264, 288
Gale, D.	517
Galkin, S. A.	342, 468
Galli, A.	229
Galperti, C.	204
Gan, C.	397
Gan, K.	174, 193
Ganesh, R.	403, 418
Gangadharan, R.	635
Gantenbein, G.	426, 460
Gao, B.	513
Gao, C.	40
Gao, J. M.	212
Gao, L.	30
Gao, Q.	305
Gao, W.	163
Gao, X.	116 , 126, 174, 221, 240
Gao, Y.	112
Gao, Z.	226, 399 , 400
Garafalo, A.	638
Garavaglia, S.	204
Garbet, X.	207, 298, 335 , 356, 362, 412
García, L.	113
Garcia, J.	290, 292, 567
Garcia-Martinez, P.	379
Garcia-Munoz, M.	17, 50, 203 , 315
Garkusha, I.	583
Garofalo, A. M.	75, 134, 506
Garoz, D.	526
Garrett, M.	199, 420
Garrido, I.	160
Garzotti, L.	288, 292, 567
Gasior, P.	175
Gassner, T.	17, 301
Gastinel, P.	471
Gates, D.	140, 153, 259, 285, 344
Gatu-Johnson, M.	522, 523

- Gauthier, E. 168, 618
 Gavila, P. 554, 604
 Geiger, B. 203, 306, 315
 Geiger, J. 105, 439, 460
 Gelbov, V. 523
 Gelfusa, M. 303
 Geli, F. 560
 Genesio, P. 369
 Genini, L. 466
 Gennrich, F. 251
 Gentle, K. 30
 Gerasimov, S. 148, 571
 Gerasimov, S. N. 65
 Gerhardt, S. 59, 72, 84, 125, 153, 188, 191,
 200, 205, 259, 427, 451
 Gerhardt, S. P. **67**, 181
 Gex, D. 471
 Ghantous, K. 17, 274
 Ghendrih, P. 298, **373**, 412
 Ghim, Y. C. 230
 Ghoranneviss, M. 253
 Ghosh, J. 91
 Gi, K. 513
 Giammanco, F. 27
 Giannone, L. 180
 Giegerich, T. 446
 Gierse, N. 175
 Gilbert, M. **430**
 Gilson, E. 542
 Gin, D. 628, **631**
 Giovannozzi, E. 248, 255, 310
 Girard, C. 433
 Giroud, C. 34, 50, 55, 122, 166, **190**, 248, 272,
 303, 576, 585
 Giruzzi, G. **290**, 493, 588
 Giuliana, S. 256
 Gladush, G. 437
 Glasser, A. 289
 Glebov, V. 24, 522
 Glenzer, S. 522
 Gobin, R. 466, 471
 Godbert-Mouret, L. 183, 369
 Goerler, T. 283
 Goetz, J. 22
 Gohil, P. 234, 577, **593**
 Goldston, R. 158, **366**, 499, 548
 Golikov, A. 479
 Goloborodko, V. 17, 301
 Gonçalves, B. 113
 Goncharov, P. 479
 Goncharov, V. 24, 523
 Gondé, R. 466
 Gong, X. 10, **80**, 163, 174, 225
 Gong, X. Z. 221
 Goniche, M. 50, 224, 566
 González, J. 469
 González, J. A. 469
 González-Arrabal, R. 526
 Goodman, T. 35, 103, **208**, 588
 Goodman, T. P. 96
 Gopalakrishnan, R. K. 492
 Gorbunov, E. 101, 241
 Gordillo, N. 526
 Gorelenkov, N. 17, 205, 274, 591
 Gorelenkov, N. N. 202, 389
 Gorelenkova, M. 395
 Gorelov, Y. 458
 Gorini, G. 550
 Gorodetsky, A. 626
 Gorshkov, A. V. 636
 Goto, M. 43, 51, 136, 179, 183, 189
 Goto, T. 505, 507, 508
 Goto, Y. 519
 Gouard, P. 210
 Goulding, R. 470
 Gourdain, P. **543**
 Gournay, J.-F. 466, 471
 Grabowski, C. 517
 Graceffa, J. 560, 561, 635
 Graham, M. 50, 170
 Grandgirard, V. 271, 298, 412
 Granetz, R. 140, 147, **261**
 Granstedt, E. 515
 Granucci, G. 145, 255
 Grashin, S. 159, 241
 Grasso, G. 27
 Graves, J. P. 284, 588
 Gray, T. 72, **187**, 191, 193, 200, 451, 515, 548
 Graziani, F. 527
 Green, D. 200
 Greenly, J. 543
 Greenwald, M. **8**, 36, 40, 104, 114, 140
 Gribov, Y. 156, 549, 567, 571–573, 592, 600,
621
 Grierson, B. **110**
 Grim, G. 522
 Grine, D. 564
 Grisham, L. 455, 542
 Groebner, R. **74**, 128, 141, 354, 357, 577
 Groebner, R. J. 173, 234, 245, 331
 Groeschel, F. 431
 Grosman, A. 604, 619
 Grosso, A. 204
 Grote, D. 542
 Groth, M. 34, 48, 165, 166, 184, 197, 248, **272**
 Grünhagen, S. 48
 Gryaznevich, M. 17, 148, 479, **497**
 Guerrero, C. 526

Gui, B.	277, 278	Han, X. Y.	212
Guilhem, D.	210, 224	Hanada, K.	217
Guillard, H.	373	Hanada, M.	421, 455
Guillemaut, C.	373	Hanao, T.	511
Guillerminet, B.	310	Hanatani, K.	53, 98, 142, 262
Guimarães-Filho, Z. O.	26, 207	Hanayama, R.	538, 539
Guirlet, R.	335	Hancock, D.	565
Guler, N.	522	Hansalia, C.	617
Gunn, J.	197, 210, 566	Hansen, C.	289, 510
Gunn, J. P.	186	Hanson, G.	625
Günter, S.	128	Hanson, J.	152, 285
Guo, H.	10, 70, 71, 132, 163, 174, 176	Hanson, J. M.	38, 75, 135
Guo, H. Y.	221	Hao, G.	341, 346
Guo, S.	302	Hao, Y. M.	209
Guo, Z.	363	Happel, T.	69, 203
Gupta, C. N.	91	Hara, M.	429
Gupta, M. K.	91, 425	Hardalupas, Y.	465
Gupta, N. C.	425	Harding, D.	24, 523
Gupta, P.	494	Hare, J.	515
Gürçan, Ö.	28, 298 , 349, 405	Harima, T.	519
Gurchenko, A.	233, 282	Harris, J.	285, 439
Gurevich, M.	479	Harrison, J.	45, 178, 374
Gusakov, E.	233, 282 , 391	Harting, D.	55, 148, 272, 581
Gusev, V. K.	64 , 512	Hartmann, D.	460
Gustafson, K.	228	Hartmann, T.	426
Gustavo, G.	204	Harvey, R.	326, 377
Guterl, J.	273	Harvey, R. W.	22, 90, 382 , 385
Guttenfelder, W.	59, 72, 125, 130, 231, 232, 244, 280 , 451, 587	Hasegawa, A.	485
— H —		Hasegawa, M.	88
Haan, S.	522	Hashimoto, K.	142
Habara, H.	524	Hashimoto, T.	85
Hacquín, S.	17	Haskey, S.	223
Hahm, T.	28, 409	Hasuo, M.	179
Hahm, T. S.	14, 349, 415 , 417, 574	Hatae, T.	627
Hahn, S.	81, 138	Hatakeyama, M.	429
Hahn, S. H.	57, 195	Hatano, Y.	429 , 481, 485
Hakim, A.	354, 357	Hatarik, R.	522
Hakola, A.	175	Hatayama, A.	448
Hallatschek, K.	413	Hatch, D.	283, 411
Halpern, F.	284, 335, 361	Hatchett, S.	522
Hamaguchi, D.	488	Hathiramani, D.	460
Hamamatsu, K.	453, 493	Hatzky, R.	321, 591
Hammer, D.	543	Havlickova, E.	178
Hammett, G.	232, 280, 586	Hawkes, N.	55, 630, 632
Han, H.	138	Hayashi, K.	422
Han, H. S.	266	Hayashi, N.	42, 279 , 290, 300, 493
Han, S.	607	Hayashi, R.	218
Han, W.	462	Hayashi, T.	491, 627
Han, W. S.	458	Hayashi, Y.	63
Han, X.	79, 111, 116, 126, 137	Hazeltine, R.	360
Han, X. F.	221	He, H.	341, 345, 346 , 450
		He, X.	529
		He, Z.	345, 346
		Hegeler, F.	525

Hegna, C.	283, 318, 367	Hoehnle, H.	568
Heidbrink, B.	17	Hogeweyj, G.	292
Heidbrink, W. W.	52, 87, 110, 203, 222 , 315, 589	Hogeweyj, G. M. D.	100
Heidinger, R.	471, 472	Hohenberger, M.	24, 523
Heikkinen, J.	282, 408	Holcomb, C. T.	38 , 52, 75, 87, 173
Heim, B.	191	Hole, M. J.	209 , 223
Heinemann, B.	460, 558, 561	Holland, C.	61, 70, 109, 235, 238 , 587
Heinzel, V.	472, 486	Hollmann, E. M.	66
Held, E.	289, 326	Holly, D.	22
Hellesen, C.	17	Holod, I.	406
Hellsten, T.	122	Homma, H.	16, 524
Hemmi, T.	602	Hommen, G.	103
Hemsworth, R.	560, 561, 635	Honda, M.	300 , 493
Hender, T.	257, 571, 623	Hong, K.	598
Hender, T. C.	65	Hong, S. H.	170, 195, 440
Henderson, M.	562, 563	Hong, S. L.	458
Henestroza, E.	527, 542	Hong, W.	70, 236, 243
Hennequin, P.	298	Hong, W. J.	61
Herrera-Velázquez, J.	313	Hong, W. Y.	60, 252
Herrmann, A.	180, 251, 264, 548, 585, 634	Hooper, E.	84
Heuraux, S.	233	Hopf, C.	37, 77
Hidalgo, C.	14, 69, 113 , 619	Hora, H.	529
Higashi, T.	511	Horacek, J.	197, 251
Higginson, D. P.	530, 534	Horiike, H.	431
Hill, D. N.	2 , 173	Horton, W.	356
Hill, K.	41, 123, 140, 219	Hosea, J.	200, 458, 462
Hill, P.	230	Hoshino, K.	453, 502–504
Hillairet, J.	224 , 420, 566	Hoshino, T.	504
Hillesheim, J. C.	238, 245	Hosoda, H.	524, 537
Hillis, D.	138, 470	Hosoi, K.	448
Himura, H.	149, 340	Hossack, A.	510
Hinata, J.	453	Hou, B.	607
Hino, T.	482	Howard, J.	223
Hinson, E.	161, 456	Howard, N.	36, 40, 92, 114
Hioki, T.	538, 539	Howard, N. T.	119
Hirai, T.	554, 571, 605	Hoyt, C.	543
Hiranai, S.	453	Hsu, C. T.	351
Hirano, M.	486	Hu, G.	434
Hirata, M.	94, 220, 448	Hu, H. C.	221
Hiratsuka, J.	85	Hu, J.	163
Hirooka, Y.	448, 451	Hu, L.	126, 163, 225
Hirose, A.	151	Hu, L. Q.	221
Hirose, T.	488	Hu, S.	24, 523
Hirota, M.	324	Hu, X.	30
Hirsch, M.	460	Huang, H.	30, 126
Hirshman, S.	285	Huang, M.	111, 212, 214, 215
Hirvijoki, E.	590	Huang, X.	100, 111, 112, 242
Hittinger, J. A.	350, 353	Huang, X. L.	212
Hizanidis, K.	402	Huang, Y.	54, 60, 61, 111, 137, 154 , 214, 215, 237
HL-2A Team,	13	Huang, Z.	236, 251
Hoang, G.	587	Huang, Z. H.	60, 252
Hoang, T.	210 , 224, 458	Hubbard, A.	36 , 40, 78, 90, 92, 104, 140, 141, 568, 633
Hobirk, J.	34, 48, 77, 248, 283, 292, 568		

Hubbard, A. E.	385, 566	In, S. R.	458
Hubeny, M.	151	In, Y.	38, 52, 75, 135, 152
Huber, A. 48, 65, 165, 171, 175, 184, 190, 257, 272, 596		Inagaki, S.	14, 60, 62, 68 , 118, 232
Hughes, J.	36, 40, 78, 92, 141 , 585	Innocente, P.	22, 95, 201
Hughes, J. W.	74, 76, 119, 593	Inomoto, M.	513
Hughes, P.	144	Inoue, T.	421 , 455, 550
Huijsmans, G.	271, 325, 549, 579, 580	Intrator, T.	517
Humbert, E.	553	Ioki, K.	571, 598, 600
Humphreys, D.	153, 577	Ionita, C.	251
Humphreys, D. A.	66, 83, 506	Irzak, M. A.	64
Hund, J.	536	Isaev, M.	241, 591
Hutchinson, I. H.	76, 92	Isayama, A.	453
Huynh, P.	221, 288	Iseli, M.	612
Hwang, C. K.	227	Ishida, S.	15
Hwang, Y. S.	195	Ishiguro, M.	88
Hyatt, A. W.	38, 82, 173, 577	Ishihara, M.	511
HyperV Technologies Corp. Team,	468	Ishii, K.	118, 538, 539
Hyungho, L.	43	Ishii, Y.	324, 537
— I —		Ishikawa, M.	390, 627
Iannone, F.	204	Ishizawa, A.	286, 308
Ibarra, A.	472	Isobe, M.	54, 136, 213
Ichiguchi, K.	329 , 340	Itagaki, H.	513
Ichihiro, Y.	232	Itagaki, N.	192
Ichimura, K.	448	ITER Collaborators,	575, 608
Ichimura, M.	94, 220 , 448	Ito, K.	511
Ida, K. 14 , 28, 41, 43, 62, 68, 105, 136, 138, 155, 216, 232, 263, 285		Ito, S.	457
Ida, M.	431	Itoh, K.	14, 60, 68, 236, 270, 307
Ide, S.	290, 493	Itoh, S. I.	14, 60, 68
Idei, H.	86, 216, 217 , 457	Itoh, Y.	486
Ido, T.	43, 68, 118	Iuchi, H.	431
Idomura, Y.	410	Ivanov, A.	22, 31, 107
IFERC Project Team,	29	Ivanov, N.	336
IFERC-Home Team, EU,	29	Ivanova, D.	165, 171
IFERC-Home Team, JA,	29	Ivanova-Stanik, I.	288, 364
Igami, H.	43, 86, 216, 457	Iwai, T.	220
Igitkhanov, Y.	596	Iwamoto, A.	16, 524, 544
Igochine, V.	203, 588	Iwamoto, D.	447
Iguchi, M.	602	Izzo, V. A.	66, 328
Igumenshev, I.	24, 523	— J —	
Ii, T.	513	JA-DA, IN-DA, USIPO,	563
Imura, T.	220	Jablonski, G.	617
Iizuka, S.	519	Jachmich, S. 48, 65, 148, 184, 190, 197, 257, 272	
Ikeda, K.	43	Jackson, G.	568
Ikezoe, R.	94, 220, 448	Jackson, G. J.	87
Ilgisonis, V.	343	Jackson, G. L.	52, 75, 82
Im, D. S.	458	Jacob, E.	17
Im, K.	609	Jacob, W.	618
Imai, T.	94, 220, 448, 457, 481	Jacobson, C. M.	515
Imazawa, R.	627, 630	Jacquet, P.	50, 486
Imbeaux, F.	221, 288, 292, 310, 567, 587	Jacquot, J.	210
		Jadav, H. M.	91

Jadeja, S.	494	Joung, N. Y.	433
Jaeger, E. F.	200, 382	Jourdheuil, L.	433
Jakubowski, M.	105, 139	JT-60SA Team,	15
James, A. N.66	Ju, S.	225
Janhunen, J. S.	408	Juárez, R.	526
Janhunen, S.	282	Juhn, J. W.	195
Jaquez, J.	532	Julien, C.	635
Jarboe, T.	84, 289, 510	Julien, H.	459
Jardin, S.	84, 316, 586	Jung, K.	598
Jardin, S. C.	319 , 385, 569	Jung, M.	57
Jarrott, L. C.	530, 532, 534		
Jasso, E. J.	469		
Jaworski, M. . 72, 158, 187, 191 , 200, 451, 515			
Jenkins, I.	50, 463		
Jenkins, T.	326		
Jenko, F.	283 , 411		
Jeon, Y.	73, 81, 138, 375		
Jeon, Y. M.	46 , 247, 265, 415		
Jeong, J.	462		
Jeong, J. H.	458		
Jeong, S.	455		
Jeong, S. H.	458		
Jernigan, T.	579, 615		
Jernigan, T. C.	56, 66		
JET EFDA Contributors, . 257, 568, 576, 588			
Jha, R.	91		
Jhang, H.	28, 278, 281 , 415		
Ji, J. Y.	289		
Ji, X.	111, 150 , 154, 213–215		
Ji, X. Q.	54, 60, 212		
Jiang, M.	131, 132, 163, 174		
Jiaqi, D.	371		
Jie, Y.	116		
Jiménez-Gómez, R.	53		
Jin, J. K.	458		
Jin, J. T.	458		
Jitsuno, T.	16, 524		
Joanny, M.	553		
Joffrin, E. . 34 , 49, 50, 106, 170, 190, 248, 290, 292, 493, 568			
Johnson, D.	459, 552 , 630, 633		
Johnson, R. D.	83, 577		
Johnson, T.	122, 588		
Johzaki, T.	16, 524, 531, 537		
Joisa, S.	91		
Jokinen, T.	605		
Jolliet, S.	361		
Jones, O.	522		
Jones, T.	50		
Jonsson, T.	288, 310		
Joonekindt, D.	617		
Joseph, I.	278, 354		
Joshi, R.	91		
Joung, M.	458, 462		

	K	
Kadia, B. R.	91	
Kado, S.	98, 448	
Kadomtsev, M. B.	636	
Kadowaki, K.	63	
Kagan, G.	354	
Kaganovich, I.	542	
Kagawa, T.	98, 262	
Kaita, R. 72, 125, 181, 187, 191, 451, 515		
Kajita, S.	169	
Kajitani, H.	602	
Kajiura, K.	422 , 453, 462, 562	
Kakeno, M.	538	
Kakuda, H.	85	
Kakurin, A.	336	
Kalal, M.	540, 541	
Kalinnikova, E.	217	
Kallenbach, A.	77, 180, 251, 548, 585	
Kallman, J.	191, 451	
Kalupin, D.	288 , 310	
Kamada, Y.	15 , 42	
Kamataki, K.	192	
Kamble, T.	611	
Kamendje, R.	638	
Kamino, Y.	63	
Kamio, S.	513	
Kamiya, K.	14, 62	
Kammash, T.	473	
Kan, H.	538, 539	
Kaneko, O.	6 , 43, 86	
Kaneko, Y.	519	
Kanemitsu, T.	218	
Kanemura, T.	431	
Kang, D.	607	
Kang, D.-Y.	639	
Kanki, T.	511	
Kanno, M.	118	
Kanno, R.	309	
Kanojia, A.	459	
Kantor, M.	282	
Karasik, M.	525	
Kardashev, B.	436	

Kardaun, O. J.	127, 548	Khirwadkar, S.	441
Kariya, T.	94, 448, 457	Khitrov, S. A.	64
Karpushov, A.	96, 157	Kholbaev, A.	535
Kasada, R.	486, 488	Khomiakov, S.	557
Kasahara, H.	43, 85, 86, 225	Khorshid, P.	253
Kasaoka, N.	519	Khripunov, V.	479
Kashiwagi, M.	421, 455	Khristi, Y.	425, 494
Kasperek, W.	460	Khromov, N. A.	64
Kasugai, A.	422	Kikuchi, T.	486
Kasuya, N.	68	Kikuchi, Y.	447 , 511
Katanuma, I.	94, 327 , 448	Kilkenny, J.	522, 536
Kato, D.	179	Kim, B.	486, 598
Kato, K.	85	Kim, C.	289, 393
Katoh, Y.	481, 485, 488	Kim, C.-B.	414
Katsui, H.	481	Kim, C. H.	458
Katsuma, J.	218	Kim, D.	157
Katsuro-Hopkins, O.	259	Kim, D.-H.	557
Kauffmann, K.	321	Kim, H.	46, 138, 462, 598
Kavin, A.	512, 595	Kim, H.-S.	415
Kaw, P.	407, 594	Kim, H.-T.	497
Kaw, P. K.	91, 334, 362 , 638	Kim, H. K.	57, 458
Kawahata, K.	68, 136, 149, 232	Kim, H. S.	247 , 265, 574
Kawamori, E.	513	Kim, H. T.	49, 57, 458
Kawanaka, J.	16, 524	Kim, J. ...	22, 57, 81, 138, 203, 209, 266 , 375, 411, 462, 532
Kawano, Y.	617, 627 , 630, 632	Kim, J.-S.	468
Kawasaki, K.	452	Kim, J. H.	201
Kawashima, H.	493	Kim, J. S.	458
Kawashima, T.	538, 539	Kim, J. Y.	203, 263
Kawazura, Y.	519	Kim, K.	265 , 312 , 556, 574, 638
Kaye, S. ...	72, 84, 125, 181, 188, 231, 246, 249, 280, 427, 451, 576, 587	Kim, K.-R.	440
Kaye, S. M.	59 , 593	Kim, K. M.	458
Kazawa, M.	455	Kim, K. P.	57
Kazuyoshi, W.	431	Kim, M. H.	476
Kehn, D.	525	Kim, S.	28, 278
Keller, D.	433	Kim, S. H.	170, 227 , 458, 570
Kemp, A.	530	Kim, S. K.	227
Kemp, E.	530	Kim, S. S.	281, 415
Kemp, G.	532	Kim, S. T.	458
Kemp, R.	500	Kim, W.	46, 138
Kempenaars, M.	190, 248	Kim, W. C.	57, 81, 100, 247, 440
Kengoh, K.	218	Kim, Y. J.	458
Kenzhin, E.	438	Kim, Y. S.	123, 458
Kessel, C.	36, 76 , 84, 427, 499, 568, 578	Kimura, A.	485, 486
Kessel, C. E.	385	Kimura, Y.	482
Kessler, T.	523	King, D.	50
Key, M.	16, 530, 532	King, J.	22, 323, 326
Key, M. H.	533, 534	King, R.	50
Khan, W.	146	Kingham, D.	497
Khan, Z.	425	Kinsey, J. E.	109, 238, 287, 506, 587
Khaydarov, R.	535	Kiptily, V.	17, 50, 257, 628, 631
Khayrutdinov, R.	479, 571, 595	Kirilenko, D.	626
Khilkevich, E.	257	Kirk, A. ...	45 , 178, 206, 250, 276, 325, 374, 548, 593
Khilkevitch, E.	626, 628, 631		

- Kirneva, N. **96**, 101
Kirov, K. 50, 122, 566
Kirschner, A. 549, 581
Kisaki, M. 43
Kiss, G. 616
Kitagawa, Y. 447, **538**, 539
Kitajima, S. **118**
Kiuttu, G. 517
Kiviniemi, T. 282, 408
Kleiber, R. **321**, 591
Klepper, C. 50, 210
Klingshirn, H. J. 310
Klischenko, A. 479
Klotz, W. D. 617
Kluchnikov, L. 101, 241
Knaster, J. 471, 602
Knaster, J. R. 621
Knauer, J. 24, 522, 523
Knipe, S. 48
Knowlton, S. 285
Ko, J. 22
Ko, W. 41, 46, 81, 138
Ko, W. H. 57, 123, 247, 263, 415
Kobayashi, M. **51**, 112, 139, 179, 189, 429, 452
Kobayashi, N. 562
Kobayashi, S. 53, 98, 142, 262, 455
Kobayashi, T. 68, 232, 453
Kocan, M. 47, 180, **251**
Kohergin, M. 622, 626
Kocsis, G. 127, 619
Kodama, R. 16
Koechl, F. 55, 292, 567, 573
Koga, K. **192**
Koga, M. 16, 524, 537
Koh, S. 359
Kohagura, J. 94, 220, 448
Koike, F. 179
Koizumi, N. 602
Kojima, A. 421, 455
Kolbasov, B. 479
Kolemen, E. 67, **153**, 181, 365, 427
Koliner, J. J. 22, 107
Komarov, V. 605
Komata, M. 455
Komeda, O. 538, 539
Kominis, Y. 402
Komm, M. 251
Komori, A. 86, 189
Kondo, H. **431**
Kondo, K. 16, 486, 490
Kondo, T. 538, 539
Kondoh, T. 617, 627
Konejew, P. 460
Kong, D. 236, **243**
Kong, D. F. 252
Kong, E. H. 221
Kong, H. J. **540**, 541
Kong, J. D. 458
Könies, A. 223, 321, **591**
König, R. 460
Konno, C. 488, 559
Konoshima, S. 53, 98, 142, 262
Konovalov, S. 336, **595**
Konovalov, V. 626
Konz, C. 288, 310
Kornev, V. 211
Korobov, K. 241
Korpilo, T. 282, 408
Korsholm, S. B. 315
Koskela, T. 589, 590
Kosolapova, N. **233**
Kostora, M. 517
Kosuga, Y. 28, 349, **405**
Kotov, V. 584, 636
Kotschenreuther, M. 337, 427, **480**
Kotulski, J. 601
Koubiti, M. **183**, 369
Koval, A. 622
Kovari, M. 446
Kovarik, K. 497
Kozak, T. 617
Kozub, T. 515
Kramer, G. 17, 200, 205, 312
Kramer, G. J. 130, 389, **589**
Krashenninnikov, S. **273**
Krasnov, S. 512
Kraus, W. 558
Kreter, A. 170, **442**
Krieger, K. 165, 166
Krikunov, S. 211
Kritz, A. **294**, 299, 354
Krivchenkov, Y. 619
Kroupp, E. 543
Kruezi, U. 48, 65, 190, 257
Kruger, S. **326**, 354, 357
Kruglyakov, E. **31**
Krupin, V. 101, 241
Krylov, A. 560
Krylov, S. 101, 241
KSTAR Team, 9
Ku, S. 28, 359
Ku, S. H. 130, 188, **416**
Kubic, M. 210
Kubkowska, M. 175
Kubo, S. 43, 68, 86, 216, 457
Kubota, S. 158, 202, 205, 244, **249**
Kugel, H. 72, 191, 244, 451
Kukhtin, V. 600

Kukushkin, A.	398 , 581, 605	Lake, R.	347
Kukushkin, A. B.	636	Lakhin, V.	343
Kukushkin, A. S.	548, 584 , 636	Lalousis, P.	529
Kuleshin, E.	241	Lamzin, E.	156, 600, 621
Kulkarni, S.	91	Lan, T.	243, 252
Kulsartov, T.	438	Lanctot, M. J.	38, 75, 152, 260, 368
Kumar, D.	518	Landen, O.	522, 536
Kumar, E. R.	610	Landman, I.	583, 596
Kumar, S.	22, 91, 201	Lang, J.	416
Kumar, S. T. A.	107	Lang, P.	127
Kumazawa, R.	43, 85, 86, 216, 225	Languille, P.	168
Kunugi, T.	485	Lao, L. L.	284, 285, 368, 506
Kuprienko, D.	282	Larson, D.	530
Kupriyanov, I.	606	Lashkul, S.	282
Kurbatova, L.	606	Lasnier, C. J.	56, 172, 173, 177, 579
Kurishita, H.	429, 486	Lathi, D.	560
Kurita, G.	493	Latu, G.	271, 412
Kurita, T.	538, 539	Lau, C.	199, 420, 459
Kuriyama, M.	561	Lauber, P.	17, 591
Kurki-Suonio, T.	203, 589, 590	Lauqa, H.	460
Kurskiev, G.	512, 622, 626	Lauro Taroni, L.	444
Kurskiev, G. S.	64	Lawson, K.	106, 165, 190
Kurt, E.	516	Lazanyi, N.	203
Kurtz, R.	485, 638	Lazarev, V.	185
Kurzan, B.	37, 127–129	Lazarus, E.	284, 285, 317
Kusama, Y.	592, 627, 630	Lazerson, S.	285
Kusse, B.	543	Lazzaro, E.	157 , 204
Kuteev, B.	437, 479 , 638	Le Garrec, B.	526
Kuwahata, A.	513	Le Guern, F.	618
Kwag, S. W.	458	Le Pape, S.	522
Kwak, J.	81, 138, 462	Le, H. B.	160
Kwak, J. G.	9 , 46, 57, 100, 123, 247, 458	Lebedev, S.	211
Kwan, J.	542	LeBlanc, B.	72, 130, 158, 188, 191, 200, 205, 244, 246, 259, 280, 451, 515
Kwon, J.	28, 41	LeBlanc, B. P.	59, 67, 93, 125, 181, 202, 249
Kwon, J. M.	57, 123, 412, 415	Leccacorvi, R.	459
Kwon, O.	325, 574	Lechte, C.	460
Kyrytsya, V.	564	Leconte, M.	348
<hr/> <p style="text-align: center;">— L —</p>		Lee, D. K.	458
L. Khimchenko, L.	606	Lee, G. E.	545
La Haye, R.	577, 588	Lee, H.	98, 138, 263
La Haye, R. J.	38, 75, 82, 152, 156, 260	Lee, H. H.	123
Laan, M.	175	Lee, H. J.	458
Labate, C.	567	Lee, H. Y.	53, 142, 262
Labidi, H.	571	Lee, J.	41, 73, 119, 138, 325, 415, 574
Labit, B.	96, 182, 284	Lee, J. D.	22
LaBombard, B.	36, 78, 164, 370, 548	Lee, K.	41, 46, 81, 138, 231, 455
Labusov, A.	557, 600	Lee, K. D.	46, 57, 247, 263, 265
Lackner, K.	128, 426	Lee, K. S.	458
Lacroix, B.	599	Lee, S.	41, 81, 219
Laengner, R.	549, 581	Lee, S. G.	46, 57, 100, 123 , 263, 266
Lafon, M.	24	Lee, W.	73, 415, 574
Lahazi, A.	253	Lee, W.-L.	418
		Lee, Y.	598

Lee, Y. S.	227	Liniers, M.	97
Leeper, R.	522	Link, A.	530, 532
Leerink, S.	282, 408	Lipschultz, B.	141, 164, 420, 585
Lehmberg, R.	525	Lisak, M.	17
Lehnen, M.49, 65 , 106, 184, 190, 257, 272, 596		Lisgo, S.	636
Lei, G.	111	Lisitsa, V. S.	636
Leichtle, D.	490	Lister, J.	567
Leipold, F.	315	Litaudon, X. 210, 224, 290, 292 , 310, 458, 567	
Lennholm, M.	588	Litnovsky, A.	634
Leonard, A. W.	172, 173, 177, 331, 548	Litvak, A.	551
Leonov, V.	297 , 595	Liu, A.	243
Lerche, E.	50	Liu, A. D.	252
Lerche, R.	522	Liu, C.	154, 237
Lesur, M.	388	Liu, D.	22, 107
Leuterer, F.	37	Liu, F.	292, 577
Levashova, M. G.	636	Liu, F. K.	221
Levesque, J.	144	Liu, H.	116
Levinton, F.	205, 630	Liu, L.	221
Lewicki, B.	456	Liu, P.	131, 132, 174
Leyland, M.	248, 325	Liu, S.	131, 132, 174, 277
LHD Experiment Group,	6	Liu, W.	243
Lho, T.-H.	440	Liu, X.	449
Li Puma, A.	433	Liu, Y.	13, 45, 54, 60, 61, 111, 126, 137, 150–152, 154, 156, 212 , 213 , 214, 215, 226, 236, 237, 242, 252, 267, 341, 374, 443
Li, C.	24, 522, 523, 536	Liu, Y. Q.	52
Li, E.	126	Liu, Z.	111, 115, 116, 240 , 277
Li, H.	243	Loarer, T.	48, 168, 553, 604
Li, J. . 10, 80, 89, 111, 163, 176, 225, 240, 277, 371 , 495		Loarte, A.	55, 56, 66, 325, 362, 549 , 567, 579–582, 585, 592, 594
Li, J. G.	221	Lockley, D.	565
Li, M. H.	221	LoDestro, L. L.	570
Li, P.	607	Logan, G.	542
Li, Q.	60	Loginov, N.	436
Li, W.	54	Lohr, J.	458, 577
Li, X.	267	Loizu, J.	228, 361
Li, Y.	112, 163, 219	Lomas, P.	34, 55, 148, 190, 197, 248, 568
Li, Y. G.	212, 252	Lomas, P. J.	49, 184, 423
Li, Z.	434	Lombard, G.	170, 210
Lian, Y.	449	Longwen, Y.	371
Liang, Y.	10, 45, 148 , 176, 338	Lönroth, J.	292
Liao, M.	607	Loomis, E.	522
Liao, W.	116	López-Bruna, D.	105, 143
Lidia, S.	542	López-Fraguas, A.	105, 143
Lifschitz, A.	379, 461	Lore, J.	193, 439
Liger, K.	433	Lorenzetto, P.	554
Likin, K. M.	121	Lorenzini, R.	22, 201
Lilley, M.	17, 274, 347	Louche, F.	564, 565
Lilley, M. K.	497	Loucks, S.	24
Lin, L.	22, 99, 107, 201	Loughlin, M.	559
Lin, Y.	36, 76, 92, 122, 147 , 199, 225, 420	Lowrie, W.	289
Lin, Z.	332, 406	Lowry, C.	272
Liñan, I. U.	469	Lu, B.	219
Lindl, J.	5		
Linez, F.	168		
Ling, B.	126		

Lu, G.	345, 346	Majerle, M.	490
Lu, W.	464	Majeski, R.	515
Lu, Z.	383	Makhin, V.	517
Luce, T.	568, 577	Makhlai, V.	583
Luce, T. C.	38, 52, 75, 82, 83, 109, 173	Makijarvi, P.	617
Luchetta, A.	561	Makino, R.	216
Lucia, M.	291, 515	Makowski, D.	617
Luciani, J. F.	335	Makowski, M. A.	177, 365, 548
Luhmann, N.	73, 126, 133, 203	Makwana, K.	411
Lukash, V.	479, 571, 595	Malang, S.	499
Lukin, V.	289	Malaquias, A.	175
Lumsdaine, A.	439, 470	Malkov, A.	512, 600
Lund, S.	542	Malkov, M.	349
Lundberg, D. P.	515	Maltsev, S.	101
Lunt, T.	47, 203, 251, 581	Manduchi, G.	310
Luo, G.	174, 449	Manickam, J.	67, 72, 259, 403, 418
Luo, T.	434	Mank, K.	264
Lütjens, H.	335	Mansfield, D.	72, 451
Luxherta, B.	634	Mansfield, D. K.	273
Lynn, A.	517	Mantica, P.	122, 248, 283, 444, 576
Lyssoivan, A.	170, 442	Mantovani, S.	27
Lyublin, B.	600	Manz, P.	61, 70
Lyublinski, I.	185, 438	Mao, S.	260
— M —			
Ma, S.	223	Mao, Y.	225
Ma, T.	530	Maqueda, R. J.	249
Ma, Y.	76, 78, 104, 119, 593	Marandet, Y.	168, 183, 369, 373
Maassberg, H.	105, 460	Maraschek, M.	127, 133, 203, 251
MacGibbon, P.	459	Marchenko, V.	376
Mackinnon, A.	522, 536	Marchetto, C.	204
Macklin, B.	609	Marcotte, F.	50
Maday, M.-F.	435	Marcus, A.	356
Maddaluno, G.	175, 184	Marenkov, E. D.	273
Maddison, G.	34, 166, 190, 585	Marinak, M.	530
Madeleine, S.	433	Marinoni, A.	109
Maebara, S.	471	Marinucci, M.	255
Maekawa, T.	218	Marklin, G.	510
Maeyama, S.	286, 308	Markovic, T.	497
Magaud, P.	604	Marmar, E.	40, 78, 104, 140
Magee, R.	22	Marocco, D.	145, 255, 619
Maget, P.	207, 271, 567	Maron, Y.	543
Maggi, C.	34, 50, 55, 248	Marot, L.	553
Maggi, C. F.	272	Marozas, J.	24, 523
Maggiore, R.	565	Marrelli, L.	198, 285
Magne, R.	224	Marroncle, J.	466, 471
Magoon, J.	522	Marsen, S.	106, 165, 166, 184, 190, 197, 272
Mahajan, S.	480	Marshall, F.	24, 523
Mahdavi, M. A.	173	Martens, C.	558
Maier, H.	184	Martin, A.	557
Mailloux, J.	34, 50, 106, 122, 566	Martin, C.	168
Maingi, R.	59, 67, 72, 74, 130, 138, 158, 181, 187, 188, 191, 193, 200, 244, 246, 249, 427, 451, 515, 548, 593	Martin, D.	350
		Martin, G.	258
		Martin, P.	23, 444
		Martin, V.	553
		Martin, Y.	593

Martin-Rojo, A.	190	McGarry, M.	22
Martin-Rojo, A. B.	196	McGinnis, D.	439
Martin-Solis, J. R.	66	McGinnis, W.	470
Martines, E.	22, 201, 254, 255	McGuffey, C.	534
Martínez, J.	469	McKee, G. R. 44, 109, 117, 234, 235 , 238, 246, 395, 413, 587	
Martínez, S.	469	McKenty, P.	24, 523
Martovetsky, N.	556	McKernan, M.	522
Marushchenko, N.	262	McLean, A.	67, 187, 191, 193, 200, 451
Maruyama, S.	571, 615, 616	McLean, A. G.	172, 181, 589
Masaki, K.	491	McLean, H.	530, 532
Masamune, S.	149 , 340	McLean, H. S.	533
Masand, H.	425	McManamy, T.	464
Masaoka, Y.	505	McMillan, B.	230
Masiello, A.	561	McNaney, J.	522
Maslov, M.	248, 303	McNeely, P.	460
Massaut, V.	471, 472, 486	Medley, S. S.	389
MAST Team,	12, 588	Medvedev, S.	479, 595
Masuda, K.	262	Mehlmann, F.	251
Masuzaki, S. . 51, 118, 136, 139, 169, 179, 189, 192, 448, 507, 508		Meier, E.	181, 289
Masyukevich, S.	622, 626	Meigs, A.	48, 106, 148, 165, 166, 190, 272
Maszl, C.	251	Meitner, S.	470, 615, 616
Matasumoto, A.	482	Meitner, S. J.	56
Matsui, K.	602	Mekkaoui, A.	369
Matsumoto, H.	471, 472	Melhem, Z.	497
Matsunaga, G.	52 , 390, 493	Mellera, V.	204
Matsuoka, S.	43, 286	Mellet, N.	271
Matsushita, I.	431	Melnik, A. D.	64, 211
Matsuura, H.	448	Menard, J. . 67, 72, 84, 153, 156, 158, 188, 191, 259, 312, 365, 427 , 451, 499	
Matsuyama, M.	481	Menard, J. E.	181, 202, 621
Mattei, M.	573, 623	Mendez, P.	471
Matthews, G. . . 34, 48, 50, 166, 197, 248, 423		Meneghini, O.	90, 420, 459, 566
Matthews, G. F.	65, 184	Menmuir, S.	146
Matumoto, K.	511	Mentrelli, A.	373
Matveeva, M.	634	Meo, F.	315
Mauel, M.	144	Merino, E.	515
Mauzaki, S.	86	Merle, A.	207, 335
Mavigilia, F.	49	Merola, M.	554, 557, 571, 600, 605
Maximenkova, N.	621	Merrill, B.	485
Mayoral, M.	34	Merrill, F.	522
Mayoral, M. L.	50 , 106, 122, 170, 248	Mertens, P.	184
Mazul, I.	554, 600	Messiaen, A.	210, 564, 565
Mazzitelli, G.	255, 438	Meyer, H.	12 , 250, 593
Mazzotta, C.	255	Meyer, O.	210
Mazzucato, E.	231	Meyer, W. H.	570
McCarthy, P.	630	Meyerhofer, D.	24, 523, 536
McCollam, K.	22, 201	Micciche, G.	472
McCorquodale, P. W.	350, 353	Michael, C.	230, 232, 347
McCorry, R. L.	24, 523	Michel, F.	466
McDermott, R. . 37, 39 , 47, 77, 127, 129, 306, 576		Michel, G.	460
McDevitt, C.	28, 298	Michel, T.	523
McDonald, D.	55, 567	Michelsen, P.	315
McDonald, D. C.	587, 593	Michiya, S.	616

Micozzi, P.	623	Moir, R.	474
Mielczarek, A.	617	Molander, A.	614
Migliori, S.	27	Molchanov, P.	178
Mikami, H.	519	Molla, J.	471
Miki, K.	349	Mollard, P.	210
Mikio, E.	504	Mollén, A.	320
Mikkelsen, D.	114, 119, 232, 280	Möller, S.	442, 634
Mikkelsen, D. R.	76	Molvik, A.	474
Milanesio, D.	50, 210, 565	Momo, B.	22, 201
Miley, G. H.	529	Monaco, F.	37
Militello, F.	178	Monakhov, I.	50
Milnes, J.	550	Moncada, V.	553
Milora, S.	470	Monier-Garbet, P.	186
Milroy, R.	289	Monnier, A.	356
Mima, K.	16, 524, 531	Morace, A.	532
Minaev, V. B.	64, 512	Moradi, S.	320
Minami, R.	94, 448, 457	Moral, N.	526
Minami, T.	53, 98, 142, 262	Moran, M.	522
Minashin, P.	398	Mordijck, S.	117, 235
Minea, T.	461 , 550	More, R.	527 , 542
Mineev, A. B.	64, 512	Moreau, D.	292, 577
Minelli, D.	204	Moreau, P.	258
Mirizzi, F. C.	566	Morel, P.	283, 298
Mirnov, S.	185	Moret, J. M.	35, 103, 160
Mirnov, V.	22, 323, 624	Morgal', Y.	583
Mirnov, V. V.	107	Morgan, G.	522
Mironov, M. I.	64, 631	Mori, Y.	538, 539
Mironova, E.	436	Morikawa, J.	519
Miroshnikov, I. V.	64	Morin, A.	433
Mishchenko, A.	321, 591	Morisaki, T.	105, 118, 136, 139, 189
Mishra, K.	91	Morita, S.	43, 51, 112, 136, 179 , 183
Mishra, R.	532	Morita, Y.	192
Missirlian, M.	604	Moriyama, S.	453
Mitchell, N.	556	Moro, A.	204
Mitsunaka, Y.	457	Moro, F.	619
Mitteau, R.	557, 571, 605	Morones, J. R.	469
Miyahara, Y.	452	Morota, H.	559
Miyamoto, S.	571	Morris, J.	65, 571
Miyamoto, T.	167	Morrison, P.	324
Miyanaga, N.	16, 524	Moschalskyy, S.	461
Miyata, Y.	94, 493	Moseev, D.	315
Miyato, N.	333	Moser, A.	518
Miyazawa, J.	189, 505 , 507, 508	Moses, E.	5
Mizoguchi, H.	218	Mosetto, A.	361
Mizuguchi, M.	94	Moskvitin, A.	358, 401
Mizuguchi, N.	149, 340	Moskvitina, Y.	358 , 401
Mizuno, K.	98, 262	Möslang, A.	25, 488
Mizuuchi, T.	53, 98 , 142, 262	Mosnier, A.	472
Mlynar, J.	256, 257	Motohiro, T.	538, 539
Mlynek, A.	37, 127, 264	Motojima, G.	189, 216, 262, 505
Moeller, C.	85	Motojima, O.	3
Mogaki, K.	455	Moulton, D.	373
Mohammadi, S.	253	Moustaizis, S.	529
Mohri, K.	603	Moyer, R. A.	44, 56, 66, 117, 172, 173, 235, 368

- Mueller, D. 67, 84, 153, 181, 451
 Mueller, S. 37, 70
 Muenich, M. 37
 Mukai, K. 53, 98, 142, 262
 Mukhin, E. **622**, 626
 Müller, H. W. 180, 194
 Müller, S. 251
 Müller, W. 251
 Muñoz, O. A. 469
 Munoz-Burgos, J. M. 66
 Munro, D. 522
 Muraglia, M. 356
 Murakami, I. 179
 Murakami, M. 16, 87, 524
 Murakami, S. 43, 105, **270**, 387, 505
 Murari, A. **256**
 Muroga, T. 25, **485**, 507
 Murphy, T. 522
 Muto, S. 43
 Mutoh, T. 43, 85, **86**, 216, 457
 Myalton, T. 101, 241
 Myasnikov, V. 551
 Myatt, J. 523
 Myers, M. 525
 Mynick, H. **291**
 Myra, J. **370**
- N —
- Na, D. 265, 415
 Na, Y. 138, 325
 Na, Y. S. 123, 247, 265, 415, **574**
 Nabais, F. 17
 Nagae, Y. 262
 Nagai, K. 16
 Nagai, T. 524, 537
 Nagaoka, K. 43, 53, 62
 Nagasaki, K. 53, 62, 98, 142, **262**
 Nagashima, Y. 60, 85
 Nagata, M. 447, **511**
 Nagata, S. 448, **481**
 Nagatomo, H. 16, 524, **531**
 Nagayama, Y. 68, 94, 118
 Nagy, D. 619
 Naidenov, V. 628, 631
 Nair, G. R. 560
 Nakabayashi, H. 457
 Nakai, M. 16, 524, 537, 544
 Nakajima, H. **555**, 602
 Nakajima, N. **29**, 308, 339
 Nakaki, S. 149
 Nakamichi, M. 504
 Nakamura, H. 16, 524
 Nakamura, M. 500, 502–504
 Nakamura, N. 538, 539
 Nakamura, S. 491
 Nakamura, T. 16
 Nakamura, Y. 53, 86, 98, 262
 Nakanishi, H. 94
 Nakano, H. 43
 Nakano, T. 42, 169, 493
 Nakao, Y. 16
 Nakashima, Y. 94, 98, **448**, 481
 Nakata, M. **410**
 Nakata, T. 488
 Nakata, Y. 524
 Nakazato, T. 16
 Nam, Y. 41, 46, 138
 Nam, Y. U. 57, 195, 440
 Namkung, W. 224, 458, 462
 Napieralski, A. 617
 Napoli, F. 229
 Nardon, E. 45, 271, 374, 567
 Narihara, K. 43, 136, 155, 232
 Narushima, Y. 51, 62, 136, 139, 155
 Nasif, H. 559
 Naulin, V. 71, 131, 132, 355
 Nave, M. F. 48, **122**
 Navratil, G. A. 152
 Navratil, G. A. 144
 Nazikian, R. 17, 44, 235, 331, 395, 589
 Neilson, G. 499, **638**
 Nelson, B. 84, 289, 510
 Nemoto, S. 455
 Nesterenko, V. 185
 Neu, R. 34, 48, 50, 106, 165, 166, 180, 184, 190, 248
 Neumeyer, C. 427
 Neverov, V. S. 636
 Nevins, W. 280, 411
 Nghiem, P. 466
 Nghiem, P.-A.-P. 471
 Ni, P. 542
 NIC Team, 5
 Nicolai, A. 372
 Nicolas, T. 335
 Nicollet, S. 599
 Nie, L. 154, 237
 Nielsen, A. H. 310
 Nielsen, S. K. 315
 Nieto, A. 469
 Nightingale, M. 50, 565
 Nikmohammadi, A. 253
 Nikolaev, G. 606
 Nikroo, A. 536
 Nilson, P. 24, 523
 Nishihara, K. 16
 Nishimura, A. 486

Nishimura, H.	16, 524, 537	Ohno, N.	51, 167, 169, 448
Nishimura, K.	118, 192, 482	Ohshima, S.	53, 142 , 262
Nishimura, Y.	538, 539	Öijerholm, J.	614
Nishino, N.	98, 448	Oikawa, T.	572, 592
Nishitani, T.	486	Oishi, T.	640
Nishiura, M.	43, 216	Okabayashi, M.	38, 52, 75, 135, 152
Nishiyama, K.	192	Okada, H.	53, 98, 142, 262
Noé, J.	466	Okada, S.	513
Nogami, S.	486, 488	Okamoto, A.	118, 172
Noguchi, Y.	218	Okamoto, M.	155
Nold, B.	251	Oki, K.	149, 340
Nonn, P.	22	Okiharu, S.	538, 539
Nora, R.	24	Oksiuta, Z.	435
Nordman, H.	362, 404, 407, 594	Okuno, K.	429, 452, 481, 485
Norimatsu, T.	16, 524, 544	Okuyama, Y.	327
Nornberg, M.	22, 201	Oldenbürger, S.	14
Nornberg, M. D.	107	Oliva, S.	22
Norreys, P.	16	Oliver, C.	471
Noterdaeme, J. M.	170, 180, 225	Olofsson, E.	146
Novokhatsky, A.	512	Olstad, R.	462
Novokhatsky, A. N.	64	Olynyk, G.	261
Nowak, S.	145 , 157, 204, 255, 288, 290	Omi, S.	218
Nozawa, T.	486	Omori, T.	562
NSTX Research Team,	11, 451, 576	O'Mulane, M.	49
Nuga, H.	387	Onchi, T.	151
Nührenberg, C.	223	Ondrej, G.	497
Numakura, T.	94, 448, 457	Ongena, J.	50, 122, 170
Nunami, M.	43, 286, 505	Ono, M.	72, 84, 158, 191, 427, 451
Nunes, I.	48, 49, 148, 248, 568	Ono, T.	627
Nunoya, Y.	556	Ono, Y.	63
Nygren, R.	191, 451, 485	Oosako, T.	85
Nyqvist, R.	17, 274	Orain, F.	271
<hr/> O <hr/>		Orlikowski, M.	617
Oasa, K.	455	Orlov, D.	331, 549
Obenschain, S.	525	Orlov, D. M.	44, 368, 582
Oberkofler, M.	190	Orlovskiy, I.	626
O'Bryan, J.	289	Orsini, F.	466, 471
Ochando, M. A.	143, 196	Orsitto, F. P.	501
Ochiai, K.	488, 559	Osakabe, M.	43
Ochoukov, R.	199, 420	Osborne, T. ...	72, 128, 130, 141, 187, 244, 248, 579
O'Connor, M.	616	Osborne, T. H. ...	38, 56, 87, 134, 177, 234, 331
Oda, T.	429	Oshima, S.	98
Oda, Y.	422, 453, 462, 562	Ottaviani, M.	310
Odstrcil, M.	256	Ovchinnikov, V. M.	532
Ogasawara, S.	216	Owen, L.	470
Ogawa, H.	627	Oya, Y.	429, 481
Ogawa, K.	62, 136	Oyama, N.	42, 135, 279
Oh, B.	455	Oyarzabal, E.	196
Oh, J.	525	Ozaki, H.	491
Oh, Y.	81, 138	Ozaki, T.	16, 524
Oh, Y. K.	46, 57, 123, 263	Ozeki, M.	455
Ohdachi, S. ...	62, 136, 155, 189, 212, 216, 329		

— P —

- Pablant, N. 140, 285
 Pablant, N. A. 110
 Paccagnella, R. 149, 310, 316
 Pace, D. 203
 Pace, D. C. 87
 Pacher, G. 584
 Pacher, H. D. 584
 Packer, L. 430
 Padalino, S. 523
 Paguio, R. 522
 Paley, J. 160
 Pan, C. 443, 607
 Pan, Y. 30, 450, 616
 Panasenkov, A. 211, 560
 Panasenkov, A. A. 64
 Panayotis, S. 168
 Panayotov, D. **612**
 Panchapakesan, S. **492**
 Pandya, H. 633
 Panek, R. 374
 Panella, M. 204
 Pankin, A. 294, 299, **354**, 357
 Paolucci, F. 561
 Papp, G. **352**
 Parail, V. 55, 292, **567**
 Paredes, A. 373
 Parekh, T. 425
 Parihar, M. 91
 Park, B. H. 263
 Park, C. 598
 Park, E.-K. 440
 Park, G. 278, 354, **375**
 Park, H. 81, 133, 203, 440, 458, 462, 630
 Park, H. K. 57, **73**, **632**
 Park, H. T. 458
 Park, J. 81
 Park, J.-W. 415
 Park, J. K. 46, 134, 135, 156, **158**, 249, 309, 312, 621
 Park, J. M. 38, **87**
 Park, M. 227, 617
 Park, S. 138, 263, 265, 462
 Park, S.-J. 440
 Park, S. I. 57, 224, 458
 Park, Y. 138
 Park, Y.-G. 639
 Park, Y. M. 458
 Park, Y. S. **81**, 259, 265
 Parke, E. 22, 201, 624
 Parker, R. 420, 458, 459, 566
 Parker, R. R. 90, 385
 Parker, S. 359
 Parks, P. 615
 Parks, P. B. 56, 66, 328
 Parmar, K. 91
 Parra, F. I. 122
 Pascal, J. Y. 168
 Pasley, J. 16
 Pasquetti, R. 373
 Passeron, C. 271
 Pasternak, A. 631
 Patel, A. 250
 Patel, D. 494
 Patel, H. 425
 Patel, K. 619, 633
 Patel, P. **530**
 Patel, P. K. 532–534
 Patel, T. 492
 Patrov, M. I. 64
 Pau, A. 256
 Paul, S. 187, 191, 451
 Paul, S. F. 181
 Pautasso, G. **264**, 571
 Pavageau, J. 433
 Pavlov, Y. 101
 Peacock, A. 439
 Pearlstein, L. D. 570
 Pearson, J. 148
 Pedrosa, M. A. 113
 Peebles, T. 625
 Peebles, W. A. 117, 202, 245, 249
 Peeters, A. 306
 Pégourié, B. 168, 170, 579
 Peña, O. 526
 Penaflo, B. 577
 Penaflo, B. G. 83
 Peng, M. 470
 Peng, Q. 144
 Peng, T. 613
 Peng, X. 213, 341, 346
 Pereira, C. 496
 Pereira, R. 257
 Perek, P. 617
 Pereslavitsev, P. 490
 Pereverzev, G. 288, 310
 Perez von Thun, C. 17
 Perez, D. 484
 Perez, F. 530
 Pericoli Ridolfini, V. 444, 566
 Perkins, J. 24, 542
 Perkins, R. **200**, 518
 Perlado, J. M. **526**
 Perrollaz, G. 619
 Peruzzo, S. 623
 Pestchanyi, S. 583, 596
 Peter, F. 550
 Peterka, M. 374

— Q —

Q

Qi, N.	543
Qian, J.	80, 115, 225
Qiao, B.	532, 533
Qin, C.	225
Qin, H.	542
Qiu, X.	341
Qiu, Z.	384

R

Raburn, D.	387
Rack, M.	148
Radha, P.	24, 523
Raffray, A. R.	557
Raffray, R.	571
Rafiq, T.	294, 299 , 354
Raj, D.	480
Rajendrakumar, E.	432
Ram, A.	402
Ramaiya, N.	91
Raman, R.	67, 72, 84 , 181, 249, 427, 451
Ramirez, J. M.	256
Ramogida, G.	27, 255, 623
Ramos, J.	326

Rampal, G.	433	Rognlien, T. D.	181, 353
Ramponi, G.	204	Rohde, V.	170, 251, 618, 634
Rao, J.	89, 111, 214, 215, 242	Romanelli, F.	4
Rapp, J.	470	Romano, A.	145, 255
Rasmussen, D.	615	Romanov, V.	436
Rath, N.	144	Romero, J. A.	160
Rathgeber, S.	37, 47, 129	Roquemoire, A. L.	181, 273
Ratnani, A.	271	Roquemoire, L.	72, 191, 193, 200
Raval, D.	425	Rosato, J.	183, 369
Razdobarin, A.	622, 626	Rosenberg, M.	536
Razumenko, D.	211	Rosenblad, P.	464
Read, J.	223	Rosenzweig, G.	543
Redd, A.	161 , 456	Rossel, J.	35, 157, 284
Regan, S.	24, 523	Rost, J. C.	104, 109
Regaña, J.	321	Roth, J.	429
Reichle, R.	617, 627, 629	Rott, M.	47
Reimerdes, H.	135 , 152, 157, 182, 284	Rotti, C.	560, 635
Reimold, F.	194, 585	Roubin, P.	168
Reinke, M. 36, 40, 92 , 104, 114, 147, 261, 420, 585		Rowan, W.	40, 633
Reinke, M. L.	76, 119, 140	Rowan, W. L.	119
Reiser, D.	581	Roy, I.	101
Reiter, D.	369, 581, 584	Roy, P.	542
Ren, Y.	72, 231 , 244, 249, 280, 296, 451	Rozhansky, V.	178
Reusch, J.	22, 108, 201	Rozhansky, V. A.	64
Reux, C.	65, 257, 423	Rozhdestvensky, V.	211
Revel, A.	461	Rubel, M.	171 , 175
Reznik, S.	376	Rubinacci, G.	27, 623
RFX-mod Team,	23	Rudakov, D. L.	66, 172 , 234
Rhee, T.	28, 41, 57, 278	Ruf, B.	558
Rhodes, D.	144	Rus, B.	526
Rhodes, T. L.	38, 117, 203, 235, 238, 245	Ruset, C.	184
Ribeiro, T.	251	Russell, D.	370
Ribeyre, X.	24	Rust, N.	460
Riccardi, B.	554	Ruzic, D.	428
Riccardo, V.	50, 65, 184, 257, 423, 571	Ryan, P.	200
Ricci, P.	228, 361	Rygg, R.	522
Rice, J. 14, 28, 36, 40 , 92, 104, 140, 147, 270, 576		Ryjakov, D.	241
Rice, J. E.	119	Ryou, A.	515
Richou, M.	604	Ryter, F.	37, 39, 47, 129 , 576, 587, 593
Richter, S.	634	Ryu, C. M.	209
Riedl, R.	558	Ryutov, D.	182, 365 , 474
Rigal, E.	433	Ryutov, D. D.	181
Rimini, F.	34, 49, 50, 55, 106, 190	Ryzhkov, I.	626
Rincon, E.	619		
Rinderknecht, H.	536		
Rivera, A.	526		
Roach, C.	230, 276 , 325		
Robin, F.	466		
Roccella, R.	571, 601		
Roderick, N.	517		
Rogers, B.	361		
Rognlien, T.	182, 273, 350, 354, 357, 365		

— S —

Sa, J. W.	598
Saarelma, S.	45, 148, 230, 248, 276, 325
Sabbagh, S. 67, 72, 81, 138, 191, 200, 259, 427, 451	
Sabbagh, S. A.	11 , 351
Sabot, R.	207, 233, 335
Sadakov, S.	557, 601
Sadowski, M.	583

Sagara, A.	401, 448, 485, 505, 507, 508
Şahin, H.	477
Sahin, H. M.	475
Sahin, S.	475
Saibene, G.	55, 549, 554, 567, 573, 581, 582, 596
Saint-Laurent, F.	258
Saito, K.	43, 85, 86
Saito, M.	486
Saito, Y. K.	220
Saitoh, H.	519
Sakagami, H.	16, 524, 531, 544
Sakakibara, S.	62, 136, 155 , 216, 232, 285, 329
Sakamoto, K.	262, 421, 422, 453, 457, 458, 462, 562
Sakamoto, M.	94, 448
Sakamoto, R.	189, 505
Sakamoto, T.	85
Sakamoto, W.	519
Sakamoto, Y.	14, 290
Sakasai, A.	491
Sakasegawa, H.	488
Sakaue, H.	179
Sakawa, Y.	16, 524
Sakharov, N.	512
Sakharov, N. V.	64
Sakuma, I.	447
Sakurai, S.	491
Salasca, S.	619
Salavy, J. F.	433
Salewski, M.	315
Salmi, A.	122, 135, 303, 304, 576
Salvador, M.	469
Samm, U.	48, 442, 634
Samuli, S.	250
Sánchez, C.	526
Sanchez, J.	21
Sangaroon, S.	206
Sangster, C.	523
Sangster, T.	24, 522
Sanna, S.	469
Sannazzaro, G.	571
Sano, F.	53, 98, 142, 262
Sanpei, A.	149, 340
Santini, F.	566
Sanz, J.	526
Sarazin, Y.	28, 298, 412
Sardain, P.	433
Sarff, J.	22 , 99, 201, 296, 323
Sarff, J. S.	107
Sarichev, D.	159
Sartori, R.	55, 567, 573
Sarukura, N.	16, 524, 537
Sasaki, S.	455
Sasao, M.	118
Sassi, M.	27
Satake, S.	43, 118, 286, 309 , 505
Satio, K.	225
Sato, K.	51, 627
Sato, M.	339
Sato, S.	327, 559
Sato, T.	220
Sato, Y.	118, 453
Satoh, N.	538, 539
Sattin, F.	302, 304
Sauppe, J.	323
Sauter, O.	35, 96, 103, 157, 283, 284, 288, 426, 588
Sauter, P.	129
Saveliev, A.	391
Saveliev, A. N.	64
Savrukhnin, P.	159
Sawada, H.	530, 532
Sawahata, M.	453
Sawan, M. E.	506
Sayer, R.	316
Scannell, R.	45, 250 , 276
Scarabosio, A.	548
Schacht, J.	460
Schaffer, M. J.	134, 135, 156, 582, 589, 592
Schaffner, D.	239
Schettini, G.	229
Schiesko, L.	558
Schioler, T.	571
Schlossberg, D.	161
Schmitt, A.	525
Schmitt, J.	285, 515
Schmitt, J. C.	121
Schmitz, L.	238, 245
Schmitz, O.	44, 235, 284, 331, 374, 549, 581 , 582
Schnack, D.	108, 326
Schneider, M.	288, 290, 292
Schneider, P. A.	128
Schoepf, K.	17, 301, 358
Schrafel, P.	543
Schrittwieser, R.	251
Schroeder, R.	460
Schubert, M.	37
Schuetz, H.	37
Schulz, C.	442
Schunke, B.	560 , 561, 635
Schurtz, G.	24
Schuster, E.	83, 577
Schwander, F.	373
Schweer, B.	171, 175
Schweinzer, J.	77 , 283, 568, 585
Scott, B.	251, 288, 310

- Scott, S. 140, 499
 Scotti, F. 93, **125**, 181, 187, 191, 193, 451
 Sears, J. 517
 Sedov, A. 479
 Séguin, F. 24, 522, 523, 536
 Seidl, P. 542
 Seka, W. 24, 523
 Seki, H. 455
 Seki, N. 455
 Seki, R. 43, 62, 105, 505
 Seki, T. 43, 85, 86, 225
 Seki, Y. 491, **603**, 627
 Sekine, T. 538, 539
 Seltzman, A. 22
 Semenov, I. 617
 Semenov, V. 622, 626
 Sen, A. **334**, 356, **597**
 Senichenkov, I. Yu. 64, 512
 Sentoku, Y. 532, 538, 539
 Seo, H. 192
 Seol, J. **263**
 Sepke, S. 522
 Sergeev, D. 101, 241
 Sergei, P. 616
 Sergienko, G. 170, 272, 442
 Sergis, A. **465**
 Serikov, A. 490
 Serlin, V. 525
 Serre, E. 373
 Serret, D. 604
 Sertoli, M. 34, 106, 165, 306
 Sethian, J. **525**
 Severo, J. H. F. 122
 Sevillano, G. 160
 Seyler, C. 543
 Shah, S. 560, 635
 Shaing, K. C. 263, 338, **351**
 Shan, J. F. 221
 Shannon, M. 565
 Shao, L. 131, 132, 174
 Shapovalov, G. 438
 Sharapov, S. **17**, 301, 347
 Sharma, A. 425, **494**
 Sharma, D. N. 492
 Sharma, P. 224
 Sharp, W. 542
 Shasharina, S. 357
 Shaw, A. K. 610
 Shaw, R. 609
 Shay, H. 530
 Shcherbinin, O. N. 64
 Shelkovenko, T. 543
 Shelukhin, D. 101, 241, 617
 Shen, H. 243
 Shen, J. 116
 Shen, Y. 212, 345
 Sheng, X. 613
 Shestakov, E. 159
 Shevelev, A. 257, **628**, 631
 Shevelev, A. E. 64
 Shi, E. 515
 Shi, J. 429
 Shi, W. 83, 577
 Shi, Y. **41**, 123, 219, 263
 Shi, Z. 14, 100, 111, 112, 137, 214, 215, 237, **242**
 Shi, Z. B. 54, 57, 61
 Shi, Z. H. 58
 Shibama, Y. 491
 Shibanuma, K. 491
 Shidara, H. 471
 Shigemori, K. 16, 524
 Shikama, T. 179, 448, 481, 518
 Shima, Y. 220
 Shimada, M. 170, 429, 481
 Shimada, T. 627
 Shimizu, A. 43, 68, 118
 Shimizu, K. 493, 503
 Shimizu, T. 16, 455, 524
 Shimkevich, A. 479
 Shimono, M. 453
 Shimozuma, T. 43, 68, 86, 216, 457
 Shino, R. 85
 Shinohara, K. 17, 52, 203, 390, 589, 592
 Shinto, K. 471
 Shinya, T. 85
 Shiraga, H. 16, **524**, 531, 537, 544
 Shiraishi, J. **333**, 493
 Shiraiwa, S. **90**, 385, 420, 459, 566
 Shiraki, D. 144
 Shiratani, M. 192
 Shoda, K. 447
 Shoji, M. 118, 189, 448
 Short, R. 24, 523
 Shoup, M. 522
 Shpansky, Y. 479
 Shumlak, U. **289**
 Shurygin, V. A. 636
 Shvarts, D. 24
 Shvydky, A. 24, 523
 Shyshkin, O. 358, **401**
 Siddique, T. **476**
 Siegl, G. 180
 Sieglin, B. 34, 65, 148, 184, 190, 272, 548, 585
 Silva, C. 32, 113, 197, 272
 Silva, M. 96, 208
 Simakov, S. 490
 Simon, H. 433

Simon, M.	561	SONG, X. M.	61
Simonen, T.	474	Song, X. M.	54, 252
Simonetto, A.	204	Song, Y.	225
Simonin, A.	461	Sontag, A.	285
Simrock, S.	617	Sorokovikova, A.	530, 532
Singh, A. K.	569	Soukhanovskii, V.	67, 72, 84, 181 , 187, 191, 193, 244, 365, 427, 451
Singh, M.	560, 635	Soukhanovskii, V. A.	125
Singh, N. P.	560	Soures, J.	24, 523, 536
Singh, R.	28, 362, 404, 407, 594	Sovinec, C.	22, 289, 318, 323
Singh, R. K.	445	Sozzi, C.	204 , 290
Sipilä, S.	590	Spaetig, P.	483
Sips, A. C. C.	49, 190, 568	Spatig, P.	435
Sips, G.	34, 166	Spears, B.	522
Sirinelli, A.	190, 272	Spineanu, F.	293
Sitnikova, A.	626	Spitsyn, A.	479
Sivak, A.	436	Spizzo, G.	302
Sivak, P.	436	Spolaore, M.	22, 201
Skinner, C.	72, 191, 451, 632	Spong, D.	22, 53, 392 , 591
Skinner, C. H.	273	Spong, D. A.	107, 589
Skladnik-Sadowska, E.	583	Springer, P.	522
Skorik, O.	626	Squire, J.	515
Skosyrev, Y.	241	Srinivas, Y.	91
Skupsky, S.	24, 523	Srivastav, A.	425
Skyman, A.	404 , 407	St. John, H. E.	506
Slezak, O.	541	Staebler, G.	104, 280, 586
Smirnov, A.	626	Staebler, G. M.	109, 117, 238, 287
Smirnov, A. P.	90	Stamm, R.	183, 369
Smirnov, R. D.	273	Stamp, M.	48, 49, 106, 165, 166, 190, 197
Smith, D.	130, 246	Stamp, M. F.	272
Smith, R.	48, 510	Stangeby, P. C.	172, 173, 177, 506, 596, 605
Smith, S. P.	109, 238	Stankiewicz, R.	288, 364
Smolentsev, S.	485	Startsev, E.	542
Smolyakov, A.	343, 356	Stegmeir, A.	625
Snead, L. L.	488	Steinbuch, M.	103
Snicker, A.	590	Stejner, M.	315
Snipes, J.	571, 572, 592, 629, 633	Stenson, E.	518
Snipes, J. A.	135, 570, 589	Stepanov, B.	556
Snyder, P.	36, 72, 141, 278, 292	Stephens, H.	22, 108
Snyder, P. B.	44, 74, 109, 128, 134, 238, 248, 331 , 353, 354, 368, 506	Stephens, R.	530
Sokolov, M.	429, 485	Stephens, R. B.	532–534
Sokolov, M. A.	488	Stevenson, B.	285
Solano, E. R.	55	Stevenson, T.	427
Solomon, W.	28, 135, 287, 576	Stoaf, C.	144
Solomon, W. M.	52, 75 , 82, 109, 110, 134, 152, 245	Stober, J.	37 , 77, 568
Someya, Y.	488, 502, 503, 504	Stockel, J.	497
Sommars, W.	517	Stoeckl, C.	24, 522, 523, 532
Sommer, F.	37	Stoller, R.	464
Sonato, P.	550 , 561	Stoller, R. E.	488
Sonehara, M.	85	Stone, D.	22
Song, J. I.	57	Storelli, A.	298
Song, N. H.	458	Stotler, D.	191, 416, 515
Song, X.	89 , 100, 111, 154, 214, 215, 267	Strachan, J.	50
		Strait, E. J.	52, 56, 66, 135, 152, 156, 260

Strand, P.	288, 310, 404	Tabares, P.	190
Stratton, B.	246, 632	Tachibana, J.	118
Strauss, H.	316	Tafalla, D.	196
Stroth, U.	7 , 14, 251	Taguchi, T.	16, 452, 524
Strozzi, D.	530	Tailor, G.	126
Strugarek, A.	412	Takagi, I.	429
Strykowski, R.	427	Takahashi, H.	43 , 86, 118, 216, 457, 471
Stupishin, N.	22, 107	Takahashi, K.	422, 562
Suárez, R.	526	Takamura, S.	167 , 169
Subbotin, G.	241	Takano, K.	602
Subbotin, S.	479	Takase, Y.	85
Sublet, J.-C.	430	Takayama, M.	118
Sudo, S.	68	Takechi, M.	493
Sueda, K.	524	Takeda, H.	448
Sugama, H.	286, 308, 309	Takehiro, S.	537
Sugie, T.	592, 627	Takeiri, Y.	43
Sugihara, M.	569, 571 , 600, 601, 605, 616	Takemoto, J.	421
Sugimoto, M.	471, 472, 486	Takemura, K.	513
Sugiyama, K.	429	Takemura, Y.	62, 155, 232
Sugiyama, L.	140, 316	Takeri, Y.	86
Sun, A.	79	Takeuchi, M.	98, 142, 627
Sun, H.	14, 40, 242	Takizuka, T.	42, 279, 300, 503
Sun, H. J.	100	Tal, B.	182
Sun, P.	112	Tala, T.	122, 135, 303, 304, 576
Sun, T.	150	Talmadge, J. N.	121
Sun, Y.	338 , 351, 355	Tamain, P.	197, 373
Sun, Z.	163, 607	Tamura, H.	507
Sunahara, A.	16, 524, 531, 538, 539	Tamura, N.	14, 43, 51, 68
Sunn Pedersen, T.	460	Tan, Y.	226
Suri, A.	611	Tanabe, H.	63
Surla, V.	451	Tanabe, M.	524
Surrey, E.	50, 463	Tanaka, H.	189, 218
Sushkov, A.	101, 159	Tanaka, K.	16, 43, 51, 68, 105, 116, 136, 139, 155, 189, 216, 232 , 286, 524
Suttrop, W.	47 , 127, 129, 133, 203, 251	Tanaka, M.	559
Suzuki, C.	43, 105, 179, 216, 505	Tanaka, T.	507
Suzuki, H.	471	Tanchuk, V.	512
Suzuki, S.	447, 453, 554, 603, 627	Tang, W.	416
Suzuki, T.	290, 493	Tang, W. M. T.	417
Suzuki, Y.	62 , 105, 118, 136, 155, 232, 285, 339, 505	Tang, X.	363
Svensson, J.	460	Tang, X.-Z.	484
Svensson, L.	561, 635	Tani, K.	592
Svoboda, V.	497	Tanigawa, H.	25, 488 , 504
Swami, H. L.	610	Taniguchi, M.	421, 455
Sychevsky, S.	600	Tank, J.	425
Sykes, A.	497	Tanna, R.	91
Sytchevsky, S.	621	Tanna, V.	425
Sze, D.-K.	485	Tapia, A. E.	469
Szepesi, T.	127	Tardini, G.	77, 127, 283, 315, 426, 576
		Tashima, S.	88
		Tavani, M.	27
		Taylor, C.	191, 451
		Taylor, G.	200
		Taylor, T. S.	506
Tabak, M.	530		
Tabares, F.	196		

— U —

Uspuras, E. **498**
 Usui, K. 455
 Utin, Y. 598
 Utoh, H. 488, **502**, 503, 504

— V —

Valanju, P. 337, 427, 480
 Valisa, M. **102**, 444
 Vallés, G. 526
 Vallet, J.-C. 466
 Valmianski, E. I. 545
 Valovic, M. 587
 Van Dam, J. 270
 van der Meiden, H. 175
 Van Eester, D. 50
 van Milligen, B. 113
 Van Oost, G. 124
 van Rooij, G. 34, 49, 50, 106, 165, **166**, 184,
 190, 272
 Van Schoor, M. 565
 van Zeeland, M. 17, 274, 284, 395
 Van Zeeland, M. A. 66, 87, 203, 589
 Vandeplassche, D. 471
 Varadarajalu, A. 425
 Varandas, C. A. F. 32
 Varela, P. 619
 Varfolomeev, V. I. 64, 512
 Varia, A. 91
 Varmora, P. 494
 Vartagnian, S. 48
 Vasu, P. 633
 Vayakis, G. 617, 623, 625, 627, **629**, 630,
 632–634
 Vdovin, V. **386**
 Vega, J. 256
 Velarde, M. 526
 Velasco, J. L. 105
 Velasquez, C. E. **496**
 Veleva, L. 483
 Velikovich, A. 525
 Veloso, M. A. F. 496
 Veranda, M. 302
 Verdoolaege, G. 124
 Vermare, C. **471**
 Vermare, L. 298, 587
 Vershkov, V. 101, **241**
 Vertkov, A. 185, 196, 438
 Vervier, M. 564
 Veshchev, E. 618, 629, 636
 Veth, C. 306
 Vianello, N. **254**
 Vicente, J. 129
 Victor, B. 510

Victoria, M. 526
 Vieira, R. 459
 Vierle, T. 47
 Viezzer, E. 37, 39, 47, 129
 Vijvers, W. 166
 Vijvers, W. A. J. **182**
 Vildjunas, M. 211
 Villard, L. 283
 Villari, R. 619
 Villone, F. 27, 444, 623
 Vitale, V. 204
 Vlad, G. 310, **378**, 394, 396, 444, 591, 623
 Vlad, M. O. 293
 Voitsekhovitch, I. 17, 288, 292, 299, 310, 572
 Voitsenya, V. 626, 634
 Volk, A. 283
 Volpe, F. A. **260**
 Von Hellermann, M. 630
 Voorhoeve, R. 103
 Voronin, A. V. 64
 Voss, G. 427
 Voter, A. 484
 Vrancken, M. 564, 565
 Vukolov, D. K. 636
 Vukolov, K. 626
 Vukolov, K. Y. 636
 Vyacheslavov, L. 232

— W —

Wada, K. 453
 Wada, Y. 98
 Wade, M. R. **44**, 82, 235, 331, 368
 Waelbroeck, F. 356
 Waganaar, W. 517
 Waganer, L. 499
 Wagner, D. 37, 157
 Wagner, F. 64
 Wagrez, J. 433
 Wakai, E. 431, **486**
 Wakasa, A. 43, 105, 387
 Wakatsuki, T. 85
 Waksman, J. 22, 107
 Waldron, W. 542
 Walk, J. 141
 Walker, C. 627
 Walker, M. 153, 577
 Walker, M. L. 83
 Wallace, G. 420, **459**, 566
 Wallace, G. M. 90
 Wallander, A. 617
 Walsh, M. 617–619, 627, 629, 630, 633
 Waltz, R. 104
 Waltz, R. E. 238, 287, 381

Wampler, W. R.	172	Wesley, J. C.	66
Wan, B. 10 , 70, 71, 80, 115, 131, 132, 174, 176, 219, 225, 243, 355, 495		Westover, B.	530
Wan, B. N.	221, 566	Weyssow, B.	446
Wan, W.	359	White, A.	36, 114
Wan, Y.	495	White, A. E.	109, 238
Wang, A.	341	White, R.	205
Wang, D. S.	174	White, W.	517
Wang, E.	179	Whyte, D.	36, 141, 164, 199, 261, 420
Wang, F.	174, 219, 355, 434	Wienhold, P.	634
Wang, G.	238, 245, 274	Wiesen, S.	106, 190, 272, 581
Wang, H. 70, 71, 131, 132 , 174, 212, 225, 393		Wikman, S.	614
Wang, J. Q.	150	Wilks, S.	530, 536
Wang, L. 131, 132, 174 , 225, 226, 295 , 346, 405		Willensdorfer, M.	129, 203
Wang, M.	221, 616	Wilson, D.	522, 565, 609
Wang, P.	434, 487	Wilson, H.	276, 325
Wang, Q.	154, 434, 449	Wilson, H. R.	331
Wang, S. J.	170, 227, 263, 458	Wilson, J.	200
Wang, W.	28, 226, 403	Wilson, J. R.	90, 459
Wang, W. W.	417	Wilson, R.	140, 420
Wang, X.	150, 378, 396	Wimmer, C.	558
Wang, X. G.	212	Wingen, A.	549, 582
Wang, X. Q.	212	Winkler, K.	565
Wang, Y.	126	Winter, A.	617
Wang, Y.-M.	528	Winz, G.	456
Wang, Z.	30, 100, 302, 346	Wischmeier, M.	194 , 426, 585
Wang, Z. X.	60	Wodniak, I.	206
Ward, D.	426, 638	Wolf, R.	105, 139, 446, 460
Ward, D. J.	500	Wolfe, S.	40, 140, 141, 147, 568, 585
Watada, H.	98	Wolfe, S. M.	76
Watanabe, F.	136, 218	Wolford, M.	525
Watanabe, K.	62, 155, 339, 421, 455, 458	Wolfrum, E. . .	47, 128, 129, 133, 203, 251, 283
Watanabe, O.	85	Wong, C. P.	172, 467
Watanabe, T.	308, 513	Wright, G.	164
Watanabe, T. H.	286 , 409	Wright, J. C.	385
Watari, T.	524	Wu, S.	617
Watkins, J. G.	172, 173	Wu, W.	582
Watts, C.	627, 629, 630, 633	Wu, Y.	556
Wauters, T.	170, 442	Wu, Z.	163, 174
Weaver, J.	525	Wukitch, S.	36, 92, 140, 147, 199, 225, 420
Wehner, W.	577	Wukitch, S. J.	76
Wehner, W. P.	83	Wunderlich, D.	558
Wei, L.	60, 616	Wurden, G.	517
Wei, M.	530, 532		
Wei, M. S.	533, 534		
Wei, W.	221		
Weir, G. M.	121		
Weisen, H.	303		
Welander, A. S.	75, 153, 260		
Wendel, M.	464		
Wendelstein 7-X Team,	460		
Werner, A.	460		
Wesche, R.	556		

— X —

Xanthopoulos, P.	283, 291
Xi, P.	278
Xia, F.	111
Xia, T.	277 , 278
Xia, Z. W.	54, 212
Xiang, B.	434
Xiang, N.	397
Xiao, C.	151
Xiao, S.	478

Xiao, W.	73, 111	Yang, H.	462
Xiao, W. W.	57	Yang, H. Y.	46, 458
Xiao, Y.	332	Yang, J.	267
Xie, H.	226	Yang, Q.	111, 112, 137, 150, 154, 214, 215, 236, 242, 267, 617
Xie, L.	226	Yang, Q. W.	54, 58, 60, 61, 252
Xie, T.	346	Yang, X.	226, 529
Xiong, H.	131, 132, 174, 355	Yang, Y.	116, 148, 221, 478, 616
Xu, G.	10, 70, 71, 131, 132, 163, 174, 176, 219, 243, 349, 355	Yang, Z.	30
Xu, G. S.	221	Yano, Y.	519
Xu, H.	237	Yao, K.	154, 237
Xu, H. D.	221	Yao, L.	100, 137, 237, 267
Xu, M.	57, 60, 61, 70, 71, 236, 243, 252	Yao, L. H.	57, 58
Xu, W.	428	Yarim, C.	372
Xu, X.	141, 240, 277, 278, 365	Yashin, A. Yu.	64
Xu, X. Q.	74	Yashiro, H.	98
Xu, Y.	111, 112, 150, 348	Yasuaki, K.	371
Xu, Z.	443, 449, 487	Yasuda, K.	53
Xuan, Z.	543	Yasuhara, R.	136, 232
Xue, D.	225	Yasuhisa, O.	452
		Yasushi, H.	431
		Yatsuka, E.	627
		Yavorskij, V.	17, 301, 358
		Ye, X.	434
		Yi, S.	28, 41, 412
Yaakobi, B.	24, 523	Yokokura, K.	453
Yadav, B.	445	Yokomine, T.	486
Yadikin, D.	310	Yokoyama, K.	491, 603
Yagi, M.	324, 333, 390	Yokoyama, M.	43, 105, 118, 232, 505
Yamada, H.	43, 62, 68, 86, 105, 136, 139, 155, 189, 216, 505, 638	Yokoyama, T.	220
Yamada, I.	43, 51, 136, 155, 189, 505	Yonekawa, I.	617
Yamada, T.	63	Yoo, J. W.	123, 227, 263, 266
Yamaguchi, N.	179	Yoo, M. G.	265
Yamaguchi, T.	85	Yoon, S.	41, 46, 73, 81, 100, 138
Yamaguchi, Y.	457	Yoon, S. W.	57, 247, 266
Yamamoto, K.	98	Yoshida, M.	300, 576
Yamamoto, N.	179	Yoshida, N.	169, 429
Yamamoto, S.	53, 98, 142, 262	Yoshida, T.	486
Yamamoto, T.	485, 627	Yoshida, Z.	519
Yamana, H.	452	Yoshikawa, M.	94, 220, 448
Yamanaka, H.	421	Yoshimura, Y.	43, 86, 216, 262, 457
Yamanou, Y.	455	Yoshino, R.	571
Yamaoka, N.	431	Yoshinuma, M.	43, 62, 105, 136, 155, 216
Yamasaki, K.	63, 513	You, K. I.	81, 263, 266
Yamashita, D.	192	Youssef, M.	620
Yamauchi, Y.	482	Yu, C.	243
Yamaura, K.	609	Yu, D.	111, 137, 154, 237
Yamazaki, K.	640	Yu, D. L.	57, 58
Yan, L.	13, 70, 111, 112, 137, 154, 214, 215, 236, 237, 243, 267	Yu, J. H.	61, 66
Yan, L. W.	54, 57, 60, 61, 252	Yu, L.	213, 214, 215
Yan, N.	131, 132, 174, 355	Yu, L. M.	54
Yan, Q.	449	Yu, Y.	195
Yan, Z.	109, 234, 235, 238	Yuan, B.	150
Yanagi, N.	401, 507, 508	Yuan, G.	267

Yuan, S.	225	Zhao, Y.	225
Yuan, X.	586	Zhao, Y. P.	221
Yuh, H.	67, 202, 205, 259, 280	Zhao, Z.	434
Yun, G.	46, 73, 81, 265	Zheng, G.	346, 450
Yun, G. S.	57, 263	Zheng, L.	270, 337
— Z —			
Zabeo, L.	573, 623	Zheng, S.	430
Zaccaria, P.	561	Zhilin, E. G.	64, 512
Zacchia, F.	557	Zhirkin, A.	479
Zacharias, O.	321	Zhitlukhin, A.	606
Zagar, K.	617	Zhogolev, V.	595
Zagorski, R.	364 , 444	Zhong, W.	111 , 137, 237, 242
Zakharov, A.	626	Zhong, W. J.	58
Zakharov, L.	342 , 451, 515	Zhong, W. L.	57, 61
Zalavutdinov, R.	626	Zhong, Y.	434
Zalesak, S.	525	Zhou, H.	112, 179
Zanca, P.	22, 201	Zhou, J.	89, 100, 111, 137, 154, 212, 214, 215, 242, 267
Zang, L.	53, 98, 142, 262	Zhou, K.	70
Zarnstorff, M.	499	Zhou, L.	459
Zarzoso, D.	210, 412	Zhou, T.	311
Zastrow, K.-D.	423	Zhou, Y.	54, 58, 100, 111, 137, 214, 215, 237, 242
Zeng, L.	38, 44, 109, 116, 117, 148, 238, 245, 255	Zhou, Z.	478, 613
Zeus, F.	180	Zhu, G.	154, 237
Zhai, K.	121	Zhu, J. Z.	409
Zhang, B.	607	Zhu, P.	318
Zhang, F.	557	Zhu, Y.	38
Zhang, G.	434	Zhuang, G.	30
Zhang, J.	89	Zhubr, N.	211
Zhang, L.	163 , 221, 434	Zielinski, J.	182
Zhang, M.	30, 434	Zinkle, S.	25 , 488
Zhang, S.	126	Zlobinski, M.	171, 175
Zhang, T.	126	Zohm, H.	37, 127, 128, 180, 426 , 638
Zhang, W.	131, 132, 174, 243	Zoletnik, S.	250
Zhang, X.	30, 115, 225, 443	Zolfaghari, A.	427
Zhang, Y.	111, 213, 267 , 613	Zonca, F.	207, 275 , 378, 383, 384, 394, 396
Zhang, Z.	524, 537	Zou, X.	111
Zhao, A.	400	Zou, X. L.	14, 57
Zhao, F.	434	Zuegel, J.	523
Zhao, H.	71, 243	Zuin, M.	255
Zhao, K.	236	Zurro, B.	97
Zhao, K. J.	60 , 61, 252	Zushi, H.	88 , 217, 457, 513
Zhao, L.	295	Zweben, S.	78, 199, 370
Zhao, L. M.	221	Zweben, S. J.	249
		Zwingmann, W.	310
		Zylstra, A.	536